CHAPTER 11

LATERAL EARTH PRESSURE

11-1 THE LATERAL EARTH PRESSURE PROBLEM

Lateral earth pressure is a significant design element in a number of foundation engineering problems. Retaining and sheet-pile walls, both braced and unbraced excavations, grain in silo walls and bins, and earth or rock contacting tunnel walls and other underground structures require a quantitative estimate of the lateral pressure on a structural member for either a design or stability analysis.

The method of plastic equilibrium as defined by the Mohr rupture envelope of Figs. 2-24 and 11-1*a* is most generally used for estimating the lateral pressure from earth and other materials such as grain, coal, and ore. On occasion one may use the finite-element (of the elastic continuum) method but this has several distinct disadvantages for most routine design. The FEM has more application for estimating pressure on tunnel liners and large buried conduits than for most lateral pressure analyses.

Earth pressures are developed during soil displacements (or strains) but until the soil is on the verge of failure, as defined by the Mohr's rupture envelope (see Fig. 11-1*a*), the stresses are indeterminate. They are also somewhat indeterminate at rupture since it is difficult to produce a plastic equilibrium state in a soil mass everywhere simultaneously—most times it is a progressive event. Nevertheless, it is common practice to analyze rupture as an ideal state occurrence, both for convenience and from limitations on obtaining the necessary soil parameters with a high degree of reliability.

Referring to Fig. 11-1*a*, we see two circles that are common to point A and tangent to the rupture line. Both these circles represent a state of plastic equilibrium in plane strain. One of the other circles such as EA or AF would be a steady-state K_o condition depending on the overconsolidation ratio (OCR) defined by Eq. (2-13) (with discussion in Sec. 2-8).

11-2 ACTIVE EARTH PRESSURE

Active earth pressure refers to the plastic equilibrium state defined by rupture circle AC of Fig. 11-1*a*. This equilibrium state is obtained from Fig. 11-1*b* and *c* as follows. First apply

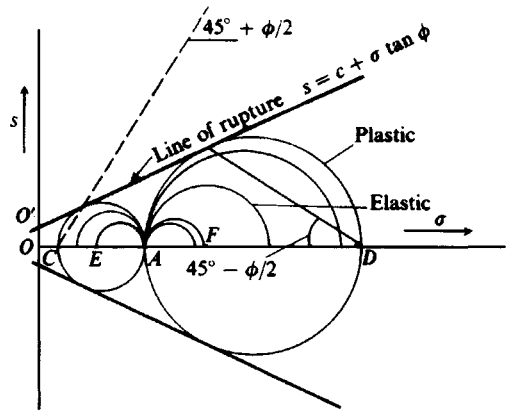

(*a*) Mohr's circles for the K_o and at plastic equilibrium (or rupture).

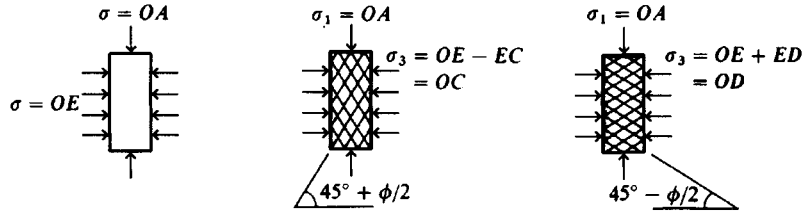

(*b*) Initial K_o state. (*c*) Active pressure. (*d*) Passive pressure.

Figure 11-1 Illustration of the concept of elastic and plastic equilibrium. Note in both (*c*) and (*d*) the slip lines are highly idealized. The stresses in (*b*), (*c*), and (*d*) such as *OA*, *OE*, *EC* are identified on the Mohr's circles of (*a*).

stresses *OA* and *OE* such that the initial K_o condition is obtained. Next gradually decrease *OE* to failure at *OC*. Stresses *OA* (maximum) and *OC* (minimum) can be used to plot a Mohr's circle. The difference between *OA* and *OC* is the circle diameter and is also the deviator stress as might be obtained in a laboratory CK_oUE triaxial test (see Fig. 2-40, case 2). The slip lines form as shown, since the horizontal and vertical planes defining the soil element in Fig. 11-1*b* are principal planes when the K_o state is developed. The latter is based on mechanics of materials and is independent of material; however, observations of model walls in sand indicates the slip-line angle of $45° + \phi/2$ shown is approximately developed.

The minimum principal stress $OC = \sigma_3$ is termed the *active earth pressure* and can be computed using Eq. (2-55), repeated here for convenience:

$$\sigma_3 = \sigma_1 \tan^2\left(45° - \frac{\phi}{2}\right) - 2c \tan\left(45° - \frac{\phi}{2}\right) \qquad (2\text{-}55)$$

This equation was developed by Coulomb about 1776 in a considerably different form; Bell (1915) appears to be the first published source of the equation in the above form. This equation is often written in European literature with the following trigonometric relationships for the tangent function:

$$\tan^2\left(45° - \frac{\phi}{2}\right) = \frac{1 - \sin\phi}{1 + \sin\phi} \qquad \tan\left(45° - \frac{\phi}{2}\right) = \frac{1 - \sin\phi}{\cos\phi}$$

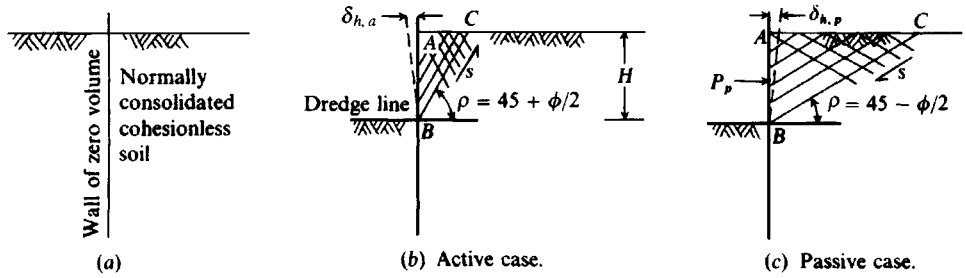

Figure 11-2 Idealization of active and passive earth pressure from a K_o developed by inserting a wall of zero thickness (and volume) into a soil mass as in (*a*).

It is also usual to use K_a for the $\tan^2$ term as shown previously in Fig. 4-2 and regularly used in this chapter. For the $\tan(45° + \phi/2)$ (passive) values of the next section, reverse the signs of the sine ratio terms.

Let us investigate the practical implications of Fig. 11-1 by using Fig. 11-2. In Fig. 11-2 we have inserted a wall of zero thickness into a normally consolidated; isotropic, cohesionless soil mass (we could use any soil but this simplifies the discussion). At this point we have a K_o stress state on the wall; and the lateral (soil-to-wall or wall-to-soil) pressure is, from the definition of K_o,

$$\sigma_3 = K_o \sigma_1$$

and is triangular since at any depth z the vertical pressure $\sigma_1 = \gamma z$. If we assume the soil is normally consolidated, K_o can be defined by one of the qualitative stress ratios of Fig. 11-1*a* as

$$K_o = \frac{OE}{OA}$$

Now let us excavate the soil on the left side of the wall of Fig. 11-2*a* to the depth H in Fig. 11-2*b* and *c*. If the wall does not shear off at point B (termed the *dredge line*) the wall will do one of the following:

1. Deflect laterally under the cantilever beam loading causing slip planes to form in the soil as in Fig. 11-1*c*. The lateral pressure $\sigma_h = \sigma_3$ on the Mohr's circle plot moves from E toward O. The Fig. 11-1*c* case develops since the K_o pressure exerted on the wall decreases as it deflects away from (but is followed by) the soil behind the wall.

   If the wall displacement is sufficient, the lateral pressure reaches plastic equilibrium at OC and the wall pressure is a minimum (termed *active pressure case*) defined from Eq. (2-55) as

   $$\sigma_h = \sigma_1 K_a \qquad (\text{since } c = 0)$$

   This minimum pressure case can be explained from observing that the slip wedge is a minimum volume at $45° + \phi/2$ from the horizontal. That is, the slope of the line from C to the point of tangency of Fig. 11-1*a* is also the slope of line BC of Fig. 11-2*b*. The shear resistance developed on line BC of Fig. 11-2*b* also reduces the tendency of the wedge ABC to push against the wall.

   If the lateral displacement ($\delta_{h,a}$) is limited (by a brace, prop, or wall stiffness), the wall pressure becomes indeterminate but is intermediate between the K_o and K_a pressures

(pressures OE and OC of Fig. 11-1a). The reason is that soil requires some limiting strain to mobilize the maximum shear resistance on the slip planes. This active pressure case is approximately illustrated as case 2 of Fig. 2-40 since Fig. 11-2b shows the wall rotating about the base B, whereas Fig. 2-40 shows a wall translation. Wall pressures depend on both wall movement and mode of movement.

2. Not deflect at all if the wall is sufficiently rigid and in this case the lateral pressure remains at

$$\sigma_h = \gamma z K_o$$

Since a lateral displacement of the wall produces a state of active earth pressure at the point where the wall pressure reduces to a minimum, we might ask what happens if there is no wall. In this case we have $\sigma_3 = \sigma_h = 0$, and it is evident that if the soil resistance mobilized on the slip plane (as BC of Fig. 11-2b) is not sufficient to satisfy statics of the wedge ABC the soil will slip into the excavation. This action can be readily observed in a small excavation in dry sand where the sides form slopes at some angle with the horizontal.

It should also be evident that as a hole is opened the surrounding soil will immediately displace laterally along similar slip planes into the cavity. When this shift happens, any device inserted into the hole must first "push" this displaced soil back to its original location before the in situ state is reproduced. It turns out that pushing the soil back to its original location is nearly impossible and, additionally, we introduce changes in the soil structure. This makes it very difficult to measure K_o in any excavated hole—including boreholes.

Since the wall must displace/rotate laterally away from the soil being retained to produce active (or K_a) earth pressure conditions, the question is, how much rotation is necessary? This has been modestly investigated and the following may be used as a guide:

Soil and condition	Amount of translation, $\delta_{h,a}$
Cohesionless, dense	0.001 to 0.002H
Cohesionless, loose	0.002 to 0.004H
Cohesive, firm	0.01 to 0.02H
Cohesive, soft	0.02 to 0.05H

As previously stated, if there is not sufficient lateral displacement, the wall pressure is indeterminate between K_o and K_a. Most walls are designed for resisting active earth pressure since any rotation that tends to produce failure is usually large enough to allow the active (or minimum) pressure to develop. If the wall is rigid or if top rotation may be undesirable for aesthetic reasons, the wall is designed for higher (usually for K_o) wall pressures. Even in this case if the wall starts into failure mode some rotation/translation will take place and the lateral pressure will start a reduction toward the K_a state. Failures of structural walls are most likely to occur during backfilling where compaction of the backfill with heavy rollers may induce a lateral pressure too large for the wall to support. Only in excavations do the conditions approximate Fig. 11-2a, b. In these cases the wall is usually installed then excavated to some depth. Lateral bracing is then installed and the excavation continued to another depth, bracing installed, etc. The lateral pressure retained by the wall should be at least K_o or somewhat larger; otherwise the ground around the excavation sinks and if structures are in the settling zone they crack and lawsuits result.

11-3 PASSIVE EARTH PRESSURE

The *passive earth pressure state* is given by the larger Mohr's circle of Fig. 11-1*a*. This state is developed by obtaining K_o conditions of Fig. 11-1*b* and holding OA constant while increasing the lateral pressure from OE to the plastic equilibrium failure at OD (and the case 4 situation of Fig. 2-40). The slip planes in the soil now make angles that are $45° - \phi/2$ with the horizontal and are ϕ from the active state. This slip angle orientation is shown by the line from D to the point of tangency of the large Mohr's circle of Fig. 11-1*a*.

The major principal stress $OD = \sigma_1$ can be computed from the geometry of Mohr's circle similarly as for the active pressure case to obtain Eq. (2-54) of Sec. 2-11:

$$\sigma_1 = \sigma_3 \tan^2\left(45° + \frac{\phi}{2}\right) + 2c \tan\left(45° + \frac{\phi}{2}\right) \tag{2-54}$$

Passive earth pressure developed by increasing the lateral pressure from OE to OD of Fig. 11-1*b* and *d* is analogous to pushing the wall of Fig. 11-2*c* into the soil. Again the soil undergoes deformation and with sufficient deformation the maximum shear resistance is mobilized; however, note these points:

1. The resisting passive wedge volume is substantially larger.
2. The mobilized shear resistance s reverses direction to *increase* the wall force. The shear direction of the active case assists in reducing the wall force.

The change in the resisting wedge ABC of Figs. 11-2*b*, *c* is the principal reason why a wall that moves forward to the minimum active pressure case cannot be pushed back to its original position.

Figure 11-3 illustrates the relative movements and order of magnitude of the lateral earth pressure coefficients defined by the trigonometric ratios of Eqs. (2-54) and (2-55). Typically, passive earth pressure is developed by anchor plates or blocks embedded in the soil with a tension rod or cable oriented so that the cable pulls the block against the soil. Another case of passive pressure is the soil below the dredge line of Fig. 11-2, which must resist the wall

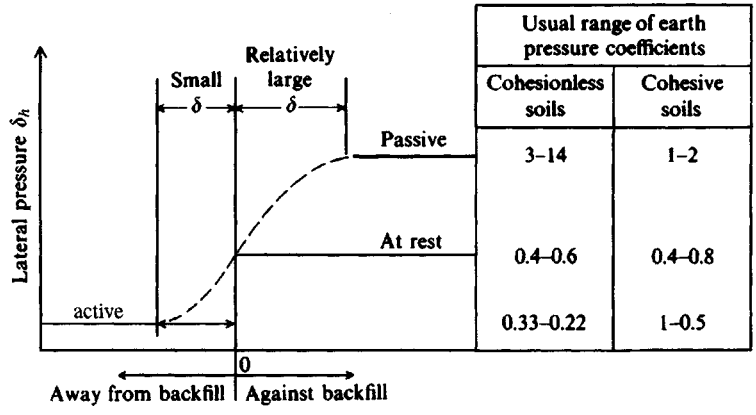

Usual range of earth pressure coefficients	
Cohesionless soils	Cohesive soils
3–14	1–2
0.4–0.6	0.4–0.8
0.33–0.22	1–0.5

Figure 11-3 Illustration of active and passive pressures with usual range of values for cohesionless and cohesive soil.

moving forward from point B down so that active pressure can develop behind the wall from the soil wedge defined by line BC.

This discussion has been theoretical to this point. We must now develop a means to apply these principles in a general way to evaluate what the earth pressure will be for specific applications. There are currently two general procedures for soil masses and a theory of elasticity method for loads on the soil mass that is to be resisted by the wall. These methods will be considered in the following several sections.

11-4 COULOMB EARTH PRESSURE THEORY

One of the earliest methods for estimating earth pressures against walls, credited to C. A. Coulomb (ca. 1776), made a number of assumptions as follows:

1. Soil is isotropic and homogeneous and has both internal friction and cohesion.
2. The rupture surface is a plane surface (as BC of Fig. 11-2*b*) and the backfill surface is planar (it may slope but is not irregularly shaped).
3. The friction resistance is distributed uniformly along the rupture surface and the soil-to-soil friction coefficient $f = \tan\phi$.
4. The failure wedge is a rigid body undergoing translation.
5. There is wall friction, i.e., as the failure wedge moves with respect to the back face of the wall a friction force develops between soil and wall. This friction angle is usually termed δ.
6. Failure is a plane strain problem—that is, consider a unit interior slice from an infinitely long wall.

The principal deficiencies in the Coulomb theory are the assumptions that the soil is ideal and that the rupture zone is a plane (although for clean sand in the *active pressure* case, photographs of model walls indicate the rupture zone is very nearly a plane as BC of Fig. 11-2*b*).

The equations based on the Coulomb theory for a cohesionless soil can be derived from Figs. 11-4 and 11-5, using a large number of trigonometric relationships. The weight of the soil wedge ABE, for a unit thickness perpendicular to the drawing, of Fig. 11-4 is

$$W = \gamma A(1) = \frac{\gamma H^2}{2\sin^2\alpha}\left[\sin(\alpha+\rho)\frac{\sin(\alpha+\beta)}{\sin(\rho-\beta)}\right] \qquad (a)$$

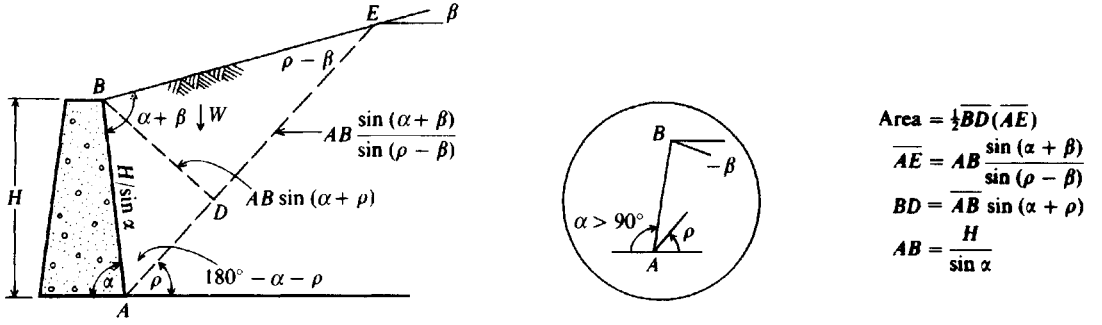

Figure 11-4 Failure wedge used in deriving the Coulomb equation for active pressure. Note β may be $\pm$ (− in inset) and $0 < \alpha < 180°$ (> 90° in inset).

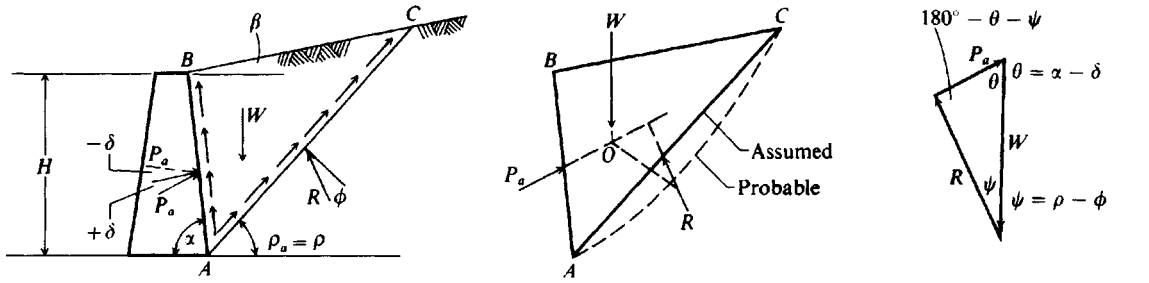

(*a*) Assumed conditions for failure

(*b*) Indication that all force vectors may not pass through point *O*; hence static equilibrium is not satisfied

(*c*) Force triangle to establish P_a

Figure 11-5 Coulomb active pressure wedge.

The active force P_a is a component of the weight vector as illustrated in Fig. 11-5*c*. Applying the law of sines, we obtain

$$\frac{P_a}{\sin(\rho - \phi)} = \frac{W}{\sin(180^\circ - \alpha - \rho + \phi + \delta)}$$

or

$$P_a = \frac{W \sin(\rho - \phi)}{\sin(180^\circ - \alpha - \rho + \phi + \delta)} \tag{b}$$

From Eq. (*b*) we see that the value of P_a depends on angle ρ; that is, all other terms for a given problem are constant, and the value of P_a of primary interest is the largest possible value. Combining Eqs. (*a*) and (*b*), we obtain

$$P_a = \frac{\gamma H^2}{2 \sin^2 \alpha} \left[\sin(\alpha + \rho) \frac{\sin(\alpha + \beta)}{\sin(\rho - \beta)} \right] \frac{\sin(\rho - \phi)}{\sin(180^\circ - \alpha - \rho + \phi + \delta)} \tag{c}$$

The maximum active wall force P_a is found from setting $dP_a/d\rho = 0$ to give

$$P_a = \frac{\gamma H^2}{2} \frac{\sin^2(\alpha + \phi)}{\sin^2 \alpha \sin(\alpha - \delta) \left[1 + \sqrt{\dfrac{\sin(\phi + \delta) \sin(\phi - \beta)}{\sin(\alpha - \delta) \sin(\alpha + \beta)}} \right]^2} \tag{11-1}$$

If $\beta = \delta = 0$ and $\alpha = 90^\circ$ (a smooth vertical wall with horizontal backfill), Eq. (11-1) simplifies to

$$P_a = \frac{\gamma H^2}{2} \frac{(1 - \sin \phi)}{(1 + \sin \phi)} = \frac{\gamma H^2}{2} \tan^2 \left(45^\circ - \frac{\phi}{2} \right) \tag{11-2}$$

which is also the Rankine equation for the active earth pressure considered in the next section. Equation (11-2) takes the general form

$$P_a = \frac{\gamma H^2}{2} K_a$$

where

$$K_a = \frac{\sin^2(\alpha + \phi)}{\sin^2 \alpha \sin(\alpha - \delta) \left[1 + \sqrt{\dfrac{\sin(\phi + \delta) \sin(\phi - \beta)}{\sin(\alpha - \delta) \sin(\alpha + \beta)}} \right]^2} \tag{11-3}$$

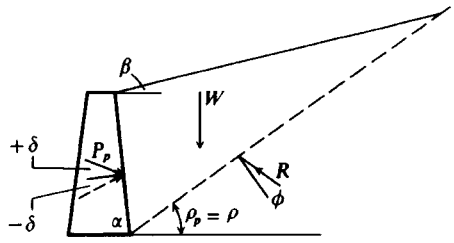

(*a*) Failure wedge and forces acting on it for passive earth pressure

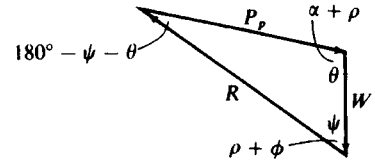

(*b*) Force polygon for graphical computation of passive earth force, note $\rho_p = \rho_a$ of Fig. 11-5

Figure 11-6 Coulomb passive pressure wedge.

and K_a is a coefficient that considers α, β, δ, and ϕ, but is independent of γ and H. Table 11-1 gives values of K_a for selected angular values, and computer program FFACTOR on your diskette can be used to obtain values of K_a for other angle combinations.

Passive earth pressure is derived similarly except that the inclination at the wall and the force triangle will be as shown in Fig. 11-6.

From Fig. 11-6 the weight of the assumed failure mass is

$$W = \frac{\gamma H^2}{2} \sin(\alpha + \rho) \frac{\sin(\alpha + \beta)}{\sin(\rho - \beta)} \tag{d}$$

and from the force triangle, using the law of sines,

$$P_p = W \frac{\sin(\rho + \phi)}{\sin(180^\circ - \rho - \phi - \delta - \alpha)} \tag{e}$$

Setting the derivative $dP_p/d\rho = 0$ gives the minimum value of P_p as

$$P_p = \frac{\gamma H^2}{2} \frac{\sin^2(\alpha - \phi)}{\sin^2 \alpha \sin(\alpha + \delta) \left[1 - \sqrt{\dfrac{\sin(\phi + \delta)\sin(\phi + \beta)}{\sin(\alpha + \delta)\sin(\alpha + \beta)}}\right]^2} \tag{11-4}$$

For a smooth vertical wall with horizontal backfill ($\delta = \beta = 0$ and $\alpha = 90°$), Eq. (11-4) simplifies to

$$P_p = \frac{\gamma H^2}{2} \frac{1 + \sin\phi}{1 - \sin\phi} = \frac{\gamma H^2}{2} \tan^2\left(45^\circ + \frac{\phi}{2}\right) \tag{11-5}$$

Equation (11-4) can also be written

$$P_p = \frac{\gamma H^2}{2} K_p$$

where

$$K_p = \frac{\sin^2(\alpha - \phi)}{\sin^2 \alpha \sin(\alpha + \delta) \left[1 - \sqrt{\dfrac{\sin(\phi + \delta)\sin(\phi + \beta)}{\sin(\alpha + \delta)\sin(\alpha + \beta)}}\right]^2} \tag{11-6}$$

Table 11-2 gives values for K_p for selected angular values of ϕ, α, δ, and β. Use program FFACTOR for other values and $\alpha \neq 90°$.

TABLE 11-1
Coulomb active earth pressure coefficients K_a using Eq. (11-3)

ALPHA = 90 BETA = −10

δ	ϕ = 26	28	30	32	34	36	38	40	42
0	0.354	0.328	0.304	0.281	0.259	0.239	0.220	0.201	0.184
16	0.311	0.290	0.270	0.252	0.234	0.216	0.200	0.184	0.170
17	0.309	0.289	0.269	0.251	0.233	0.216	0.200	0.184	0.169
20	0.306	0.286	0.267	0.249	0.231	0.214	0.198	0.183	0.169
22	0.304	0.285	0.266	0.248	0.230	0.214	0.198	0.183	0.168

ALPHA = 90 BETA = −5

δ	ϕ = 26	28	30	32	34	36	38	40	42
0	0.371	0.343	0.318	0.293	0.270	0.249	0.228	0.209	0.191
16	0.328	0.306	0.284	0.264	0.245	0.226	0.209	0.192	0.176
17	0.327	0.305	0.283	0.263	0.244	0.226	0.208	0.192	0.176
20	0.324	0.302	0.281	0.261	0.242	0.224	0.207	0.191	0.175
22	0.322	0.301	0.280	0.260	0.242	0.224	0.207	0.191	0.175

ALPHA = 90 BETA = 0

δ	ϕ = 26	28	30	32	34	36	38	40	42
0	0.390	0.361	0.333	0.307	0.283	0.260	0.238	0.217	0.198
16	0.349	0.324	0.300	0.278	0.257	0.237	0.218	0.201	0.184
17	0.348	0.323	0.299	0.277	0.256	0.237	0.218	0.200	0.183
20	0.345	0.320	0.297	0.276	0.255	0.235	0.217	0.199	0.183
22	0.343	0.319	0.296	0.275	0.254	0.235	0.217	0.199	0.183

ALPHA = 90 BETA = 5

δ	ϕ = 26	28	30	32	34	36	38	40	42
0	0.414	0.382	0.352	0.323	0.297	0.272	0.249	0.227	0.206
16	0.373	0.345	0.319	0.295	0.272	0.250	0.229	0.210	0.192
17	0.372	0.344	0.318	0.294	0.271	0.249	0.229	0.210	0.192
20	0.370	0.342	0.316	0.292	0.270	0.248	0.228	0.209	0.191
22	0.369	0.341	0.316	0.292	0.269	0.248	0.228	0.209	0.191

ALPHA = 90 BETA = 10

δ	ϕ = 26	28	30	32	34	36	38	40	42
0	0.443	0.407	0.374	0.343	0.314	0.286	0.261	0.238	0.216
16	0.404	0.372	0.342	0.315	0.289	0.265	0.242	0.221	0.201
17	0.404	0.371	0.342	0.314	0.288	0.264	0.242	0.221	0.201
20	0.402	0.370	0.340	0.313	0.287	0.263	0.241	0.220	0.201
22	0.401	0.369	0.340	0.312	0.287	0.263	0.241	0.220	0.201

ALPHA = 90 BETA = 15

δ	ϕ = 26	28	30	32	34	36	38	40	42
0	0.482	0.440	0.402	0.367	0.334	0.304	0.276	0.251	0.227
16	0.447	0.408	0.372	0.340	0.310	0.283	0.258	0.234	0.213
17	0.447	0.407	0.372	0.339	0.310	0.282	0.257	0.234	0.212
20	0.446	0.406	0.371	0.338	0.309	0.282	0.257	0.234	0.212
22	0.446	0.406	0.371	0.338	0.309	0.282	0.257	0.234	0.212

TABLE 11-2
Coulomb passive earth pressure coefficients K_p using Eq. (11-6)

ALPHA = 90 BETA = −10

δ	ϕ = 26	28	30	32	34	36	38	40	42
0	1.914	2.053	2.204	2.369	2.547	2.743	2.957	3.193	3.452
16	2.693	2.956	3.247	3.571	3.934	4.344	4.807	5.335	5.940
17	2.760	3.034	3.339	3.679	4.062	4.493	4.983	5.543	6.187
20	2.980	3.294	3.645	4.041	4.488	4.997	5.581	6.255	7.039
22	3.145	3.490	3.878	4.317	4.816	5.389	6.050	6.819	7.720

ALPHA = 90 BETA = −5

δ	ϕ = 26	28	30	32	34	36	38	40	42
0	2.223	2.392	2.577	2.781	3.004	3.250	3.523	3.826	4.163
16	3.367	3.709	4.094	4.529	5.024	5.591	6.243	7.000	7.883
17	3.469	3.828	4.234	4.694	5.218	5.820	6.516	7.326	8.277
20	3.806	4.226	4.704	5.250	5.879	6.609	7.462	8.468	9.665
22	4.064	4.532	5.067	5.684	6.399	7.236	8.222	9.397	10.809

ALPHA = 90 BETA = 0

δ	ϕ = 26	28	30	32	34	36	38	40	42
0	2.561	2.770	3.000	3.255	3.537	3.852	4.204	4.599	5.045
16	4.195	4.652	5.174	5.775	6.469	7.279	8.229	9.356	10.704
17	4.346	4.830	5.385	6.025	6.767	7.636	8.661	9.882	11.351
20	4.857	5.436	6.105	6.886	7.804	8.892	10.194	11.771	13.705
22	5.253	5.910	6.675	7.574	8.641	9.919	11.466	13.364	15.726

ALPHA = 90 BETA = 5

δ	ϕ = 26	28	30	32	34	36	38	40	42
0	2.943	3.203	3.492	3.815	4.177	4.585	5.046	5.572	6.173
16	5.250	5.878	6.609	7.464	8.474	9.678	11.128	12.894	15.076
17	5.475	6.146	6.929	7.850	8.942	10.251	11.836	13.781	16.201
20	6.249	7.074	8.049	9.212	10.613	12.321	14.433	17.083	20.468
22	6.864	7.820	8.960	10.334	12.011	14.083	16.685	20.011	24.352

ALPHA = 90 BETA = 10

δ	ϕ = 26	28	30	32	34	36	38	40	42
0	3.385	3.712	4.080	4.496	4.968	5.507	6.125	6.840	7.673
16	6.652	7.545	8.605	9.876	11.417	13.309	15.665	18.647	22.497
17	6.992	7.956	9.105	10.492	12.183	14.274	16.899	20.254	24.633
20	8.186	9.414	10.903	12.733	15.014	17.903	21.636	26.569	33.270
22	9.164	10.625	12.421	14.659	17.497	21.164	26.012	32.601	41.863

ALPHA = 90 BETA = 15

δ	ϕ = 26	28	30	32	34	36	38	40	42
0	3.913	4.331	4.807	5.352	5.980	6.710	7.563	8.570	9.768
16	8.611	9.936	11.555	13.557	16.073	19.291	23.494	29.123	36.894
17	9.139	10.590	12.373	14.595	17.413	21.054	25.867	32.409	41.603
20	11.049	12.986	15.422	18.541	22.617	28.080	35.629	46.458	62.759
22	12.676	15.067	18.130	22.136	27.506	34.930	45.584	61.626	87.354

Figure 11-1 displays that earth pressure is dependent on the *effective* stresses in the soil and not total stresses. It necessarily follows that the wall pressure below the water table is the sum of the hydrostatic pressure and the *effective* lateral earth pressure from using the *effective* unit weight γ' of the soil.

Example 11-1. What is the total active force per meter of wall for the soil-wall system, shown in Fig. E11-1, using the Coulomb equations? Where does P_a act?

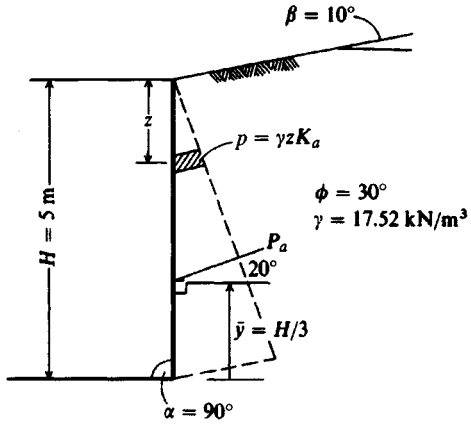

Figure E11-1

Solution. Take the wall friction $\delta = 2\phi/3 = 20°$ (a common estimate). For $\phi = 30°$ obtain $K_a = 0.34$ from Table 11-1:

$$p_a = \gamma z K_a$$

$$P_a = \int_0^H \gamma z K_a \, dz = \frac{1}{2}\gamma H^2 K_a$$

$$P_a = \tfrac{1}{2}(17.52)(5)^2(0.34) = \mathbf{74.5}\ \text{kN/m}$$

Summing moments about the top, we have

$$P_a \bar{y}' = \int_0^H \gamma z K_a z \, dz = \frac{\gamma H^3}{3} K_a$$

Using the symbolic P_a and equating, we obtain

$$\bar{y}' = \frac{2\gamma H^3 K_a}{3\gamma H^2 K_a} = \frac{2}{3}H \qquad \text{from top or}$$

$$\bar{y} = H - \frac{2H}{3} = \frac{\mathbf{H}}{\mathbf{3}} \qquad \text{from bottom (value usually used)}$$

For $\delta = 20°$ a force polygon would show that P_a will act on the wall as shown in Fig. E11-1.

////

Example 11-2. What is the total active force/unit width of wall and what is the location of the resultant for the system shown in Fig. E11-2*a*? Use the Coulomb equations and take a smooth wall so $\delta = 0°$.

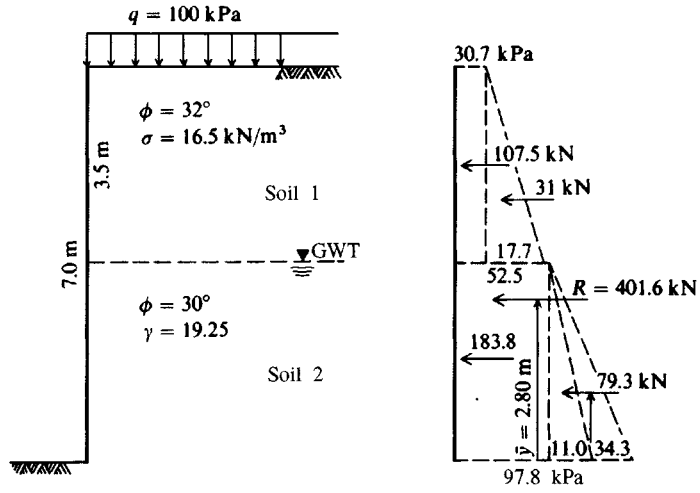

Figure E11-2

Solution. We have a surcharge, which is seen by the wall at $z = 0$ as a pressure q (which could be caused by a fictitious soil depth of γz_o). There will be K_a values for each soil of

$$K_{a1} = 0.307 \qquad K_{a2} = 0.333 \qquad \text{(Table 11-1 and } \alpha = 90°\text{)}$$

At $z = 0$ (top of wall where surcharge acts) we have

$$p_1 = \gamma z_o K_a = qK_a = 100(0.307) = \mathbf{30.7}\ \text{kPa}$$

At the interface (interpreted as $z - dz$) of top stratum $z_1 = 3.5$ m and noting the surcharge q carries through to give the effect of $q_z = \gamma z_o + \gamma z_1$, we have

$$\begin{aligned} p_2 = (q + \gamma z_1)K_a &= [100 + 16.5(3.5)]0.307 \\ &= 30.7 + 17.7 = \mathbf{48.4}\ \text{kPa} \end{aligned}$$

It is often convenient to retain the several effects separately. Here we see that q gives a rectangular (constant) wall pressure whereas the increasing depth of soil gives a triangular pressure diagram with 17.7 kPa at the base.

Continuing for soil 2, at depth $z + dz = 3.5$ m we are into soil 2 and since that is the location of the water table we will have to use $\gamma' = 19.25 - 9.81 = 9.44\ \text{kN/m}^3$.

Just at the interface we have

$$\begin{aligned} p_2' &= [q + 16.5(3.5) + 9.44\,dz]K_{a2} \\ &= [100 + 16.5(3.5) + 0]0.333 = \mathbf{52.5}\ \text{kPa} \end{aligned}$$

Note we have an abrupt discontinuity in the pressure diagram of 48.4 kPa and at $3.5 + dx$ a pressure of 52.5 kPa. At the bottom of the wall we have

$$p_3 = [100 + 16.5(3.5) + 9.44(3.5)]K_{a2}$$

which is the same as

$$\begin{aligned} p_3 &= 52.5 + 9.44(3.5)0.333 \\ &= 52.5 + 11.0 = \mathbf{63.5}\ \text{kPa} \qquad \text{(again the 11.0 is a triangle)} \end{aligned}$$

The water also contributes lateral pressure and has $K_a = K_p = 1$ since $\phi_w = 0°$. Thus,

$$p_w = \gamma_w z_w = 9.807(3.5) = \mathbf{34.3}\ \text{kPa}$$

These pressure values are plotted on Fig. E11-2*b* so the several pressure areas can be numerically integrated to obtain the total wall force. By using triangles and rectangles as shown, the total wall force is the sum from the several areas and the forces act through the centroids of the areas as shown so that we can easily sum moments about the base to obtain

$$R\bar{y} = \sum P_i y_i$$

$$P_1 = 30.7(3.5) = 107.5\ \text{kN} \qquad y_i = 3.5 + \frac{3.5}{2} = 5.25\ \text{m}$$

$$P_2 = 17.7\left(\frac{3.5}{2}\right) = 31.0\ \text{kN} \qquad y_2 = 3.5 + \frac{3.5}{3} = 4.67\ \text{m}$$

$$P_3 = 52.5(3.5) = 183.8\ \text{kN} \qquad y_3 = \frac{3.5}{2} = 1.75\ \text{m}$$

Include water with P_4 since both areas are triangles:

$$P_4 = (34.3 + 11.0)\left(\frac{3.5}{2}\right) = 79.3\ \text{kN} \qquad y_4 = \frac{3.5}{3} = 1.17$$

$$R = \sum P_i = 107.5 + 31.0 + 183.8 + 79.3 = \mathbf{401.6}\ \text{kN}$$

Now sum the moments for $\bar{y}$:

$$401.6\bar{y} = 107.5(5.25) + 31.0(4.67) + 183.8(1.75) + 79.3(1.17)$$

$$\bar{y} = \frac{1123.6}{401.6} = \mathbf{2.80}\ \text{m} \qquad \text{(above wall base)}$$

////

11-5 RANKINE EARTH PRESSURES

Rankine (ca. 1857) considered soil in a state of plastic equilibrium and used essentially the same assumptions as Coulomb, except that *he assumed no wall friction or soil cohesion.* The Rankine case is illustrated in Fig. 11-7 with a Mohr's construction for the general case shown in Fig. 11-8. From Fig. 11-8 we can develop the Rankine active and passive pressure cases by making substitution of the equation for r (shown on the figure) into the equations for EF (and FG) (also shown on the figure). Then substitution into the expression for K'_a (with OB canceling and using $\sin^2\beta = 1 - \cos^2\beta$) gives the pressure ratio acting parallel to backfill slope β as

$$K'_a = \frac{\cos\beta - \sqrt{\cos^2\beta - \cos^2\phi}}{\cos\beta + \sqrt{\cos^2\beta - \cos^2\phi}} \tag{11-7}$$

We note that the *horizontal component* of active earth pressure is obtained as

$$\sigma_{a,\text{hor}} = \sigma_a \cos\beta \qquad (= OE\cos\beta = OA \text{ of Fig. 11-8}b)$$

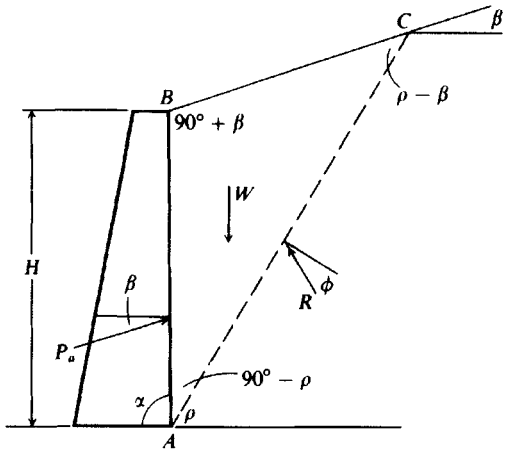

(*a*) Soil-structure system for the Rankine solution for $\alpha = 90°$

$$\text{Area } ABC = \frac{1}{2}H^2 \frac{\sin(90° - \rho)\sin(90° + \beta)}{\sin(\rho - \beta)}$$

$$(1)\quad W = \frac{1}{2}\gamma H^2 \frac{\cos\rho\cos\beta}{\sin(\rho - \beta)}$$

$$(2)\quad P_a = W \frac{\sin(\rho - \phi)}{\sin(90° - \rho + \phi + \beta)}$$

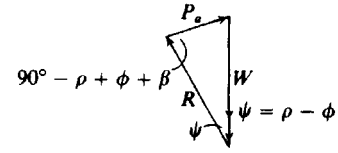

(*b*) Force triangle in the Rankine solution

Figure 11-7 Rankine active earth pressure wedge.

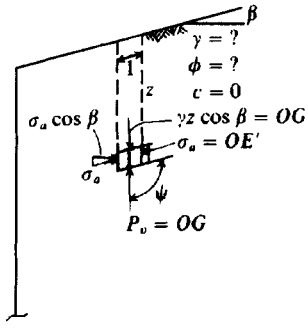

(a) General case: only for $+\beta$ as shown.

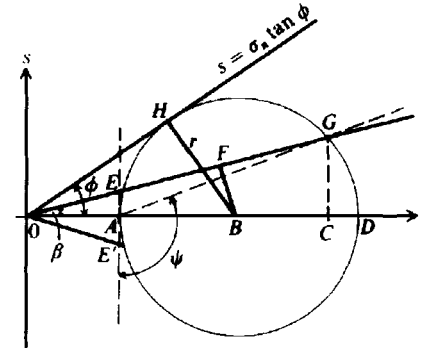

(*b*) Mohr's circle.

$$OG = \gamma z \cos\beta$$

$$K'_a = \frac{OE}{OG} = \frac{OF - EF}{OF + FG} = \frac{OE'}{OG}$$

$$K'_p = \frac{OF + FG}{OF - EF}$$

$$OF = OB\cos\beta$$

Since BF bisects EG,

$$EF = FG = \sqrt{r^2 - BF^2}$$

$$BF = OB\sin\beta$$

$$r = OB\sin\phi$$

Figure 11-8 General conditions and Mohr's circle to derive the Rankine earth pressure equations.

By analogy (and referring again to Fig. 11-8) we obtain the pressure ratio for K'_p in a similar manner:

$$K'_p = \frac{\cos\beta + \sqrt{\cos^2\beta - \cos^2\phi}}{\cos\beta - \sqrt{\cos^2\beta - \cos^2\phi}} \tag{11-8}$$

Noting that the ratio of $K'_a = \sigma_a/(\gamma z\cos\beta)$ is for an earth pressure parallel to β and that the vertical pressure on a horizontal plane at depth z is $\gamma z\cos\beta$, we have

$$\sigma_a = \gamma z\cos\beta K'_a$$

TABLE 11-3
Rankine active earth pressure coefficients K_a using Eq. (11-7*a*)

β	ϕ = 26	28	30	32	34	36	38	40	42
0	0.3905	0.3610	0.3333	0.3073	0.2827	0.2596	0.2379	0.2174	0.1982
5	0.3959	0.3656	0.3372	0.3105	0.2855	0.2620	0.2399	0.2192	0.1997
10	0.4134	0.3802	0.3495	0.3210	0.2944	0.2696	0.2464	0.2247	0.2044
15	0.4480	0.4086	0.3729	0.3405	0.3108	0.2834	0.2581	0.2346	0.2129
20	0.5152	0.4605	0.4142	0.3739	0.3381	0.3060	0.2769	0.2504	0.2262
25	0.6999	0.5727	0.4936	0.4336	0.3847	0.3431	0.3070	0.2750	0.2465
30	—	—	0.8660	0.5741	0.4776	0.4105	0.3582	0.3151	0.2784
35	—	—	—	—	—	0.5971	0.4677	0.3906	0.3340
40	—	—	—	—	—	—	—	0.7660	0.4668

Since $\cos\beta$ is a permanent entry it is convenient to include it with K_a' of Eq. (11-7) or K_p' of Eq. (11-8), giving, e.g.,

$$K_a = \cos\beta \frac{\cos\beta - \sqrt{\cos^2\beta - \cos^2\phi}}{\cos\beta + \sqrt{\cos^2\beta - \cos^2\phi}} \tag{11-7a}$$

and similarly for K_p. These latter values are given in Tables 11-3 and 11-4 to use in active and passive pressure computations (use program FFACTOR for intermediate values). Using these pressure ratios, one obtains the lateral pressure and force as follows:

$$\begin{aligned} p_a &= \gamma z K_a \qquad P_a = \int_0^H \gamma z K_a \, dz = \frac{1}{2}\gamma H^2 K_a \\ p_p &= \gamma z K_p \qquad P_p = \int_0^H \gamma z K_p \, dz = \frac{1}{2}\gamma H^2 K_p \end{aligned} \tag{11-9}$$

which is applicable for cohesionless soils. Again note that the γz term represents *effective* stresses. The horizontal and vertical components of P_a and P_p are usually required for design, giving

$$\begin{aligned} P_{a,h} &= P_a \cos\beta \qquad P_{a,v} = P_a \sin\beta \\ P_{p,h} &= P_p \cos\beta \qquad P_{p,v} = P_p \sin\beta \end{aligned}$$

Figure 11-9 gives typical lateral pressure profiles for backfill conditions shown.

TABLE 11-4
Rankine passive earth pressure coefficients K_p

β	ϕ = 26	28	30	32	34	36	38	40	42
0	2.5611	2.7698	3.0000	3.2546	3.5371	3.8518	4.2037	4.5989	5.0447
5	2.5070	2.7145	2.9431	3.1957	3.4757	3.7875	4.1360	4.5272	4.9684
10	2.3463	2.5507	2.7748	3.0216	3.2946	3.5980	3.9365	4.3161	4.7437
15	2.0826	2.2836	2.5017	2.7401	3.0024	3.2926	3.6154	3.9766	4.3827
20	1.7141	1.9176	2.1318	2.3618	2.6116	2.8857	3.1888	3.5262	3.9044
25	1.1736	1.4343	1.6641	1.8942	2.1352	2.3938	2.6758	2.9867	3.3328
30	—	—	0.8660	1.3064	1.5705	1.8269	2.0937	2.3802	2.6940
35	—	—	—	—	—	1.1239	1.4347	1.7177	2.0088
40	—	—	—	—	—	—	—	0.7660	1.2570

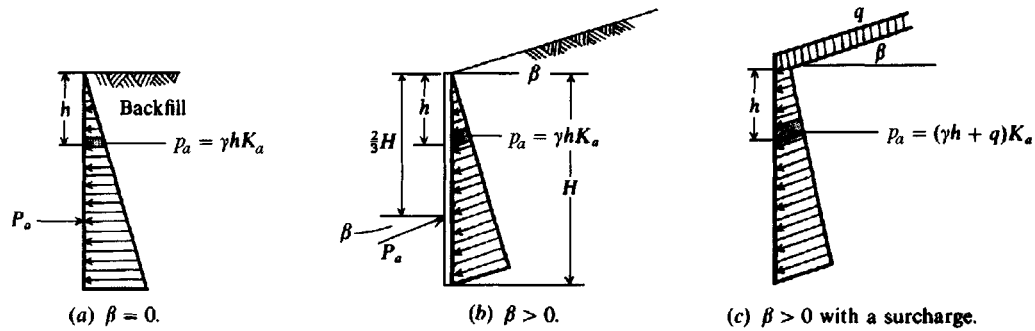

Figure 11-9 Rankine active earth pressure diagrams in a cohesionless soil.

Example 11-3. What is the total active earth force per meter of wall for the wall system shown in Example 11-1 using the Rankine equation?

Solution. For $\beta = 10°$ and $\phi = 30°$ we obtain $K_a = 0.3495$ from Table 11-3. Directly substituting into Eq. (11-9), we may write

$$P_a = \tfrac{1}{2}\gamma H^2 K_a = \tfrac{1}{2}(17.52)(5)^2 0.350 = \mathbf{76.6}\ \text{kN/m}$$

This value compares with 74.5 kN/m by the Coulomb equation, for a difference of about 2 percent, but acts here at a wall angle of $\beta = \delta = 10°$ as shown on Fig. E11-3 instead of $\delta = 20°$ of Fig. E11-1. The horizontal and vertical force components are

$$P_{a,h} = P_a \cos 10° = 76.6 \cos 10° = \mathbf{75.4}\ \text{kN}$$
$$P_{a,v} = P_a \sin 10° = 76.6 \sin 10° = \mathbf{13.3}\ \text{kN}$$

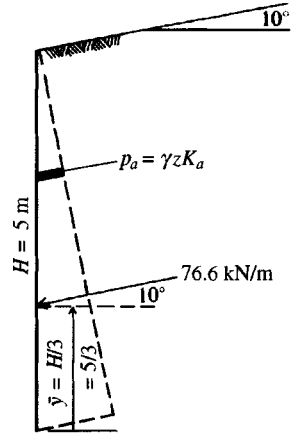

Figure E11-3

////

11-6 GENERAL COMMENTS ABOUT BOTH METHODS

One should not use the Rankine method for K_p when $\beta > 0$, since an inspection of Table 11-4 shows that it decreases with increasing β. This is clearly not correct—K_a does properly increase. Note also that one can use a $(-)$ β in the Rankine equations, but the computed coefficients are those of $(+)$ β.

The Coulomb equations are valid for both (+) and (−) β. That is, K_p increases with increasing β and decreases with (−) β values.

SOIL WITH COHESION. Neither the Coulomb nor Rankine method explicitly incorporated cohesion as an equation parameter in lateral earth pressure computations. Bell (1915) seems to be the first person to publish a solution to this problem. Bell's equations are actually Eqs. (2-54) and (2-55) and were directly obtained from Mohr's circle. With these equations for the pressure the wall force is obtained as in Eqs. (11-9) for the cohesionless case by integrating between limits over the depth increment dz. Modifications to these equations might include using the Coulomb or Rankine K factors in lieu of the tangent factors.

Example 11-4. Draw the active earth pressure diagram for a unit width of wall for the conditions shown in Fig. E11-4*a*. Compare the several possible alternatives that are produced from this problem (tension crack, how the diagram might be modified, and water in tension crack).

At top: $z = 0$

$$p_a = \gamma z K_a - 2c\sqrt{K_a} = -2(10.5)(0.84) = \mathbf{-17.64}\ \text{kPa}$$

At $p = 0$:

$$\gamma z K_a - 2c\sqrt{K_a} = 0 \qquad [\text{Set Eq. (2-55)} = 0]$$

and

$$z = \frac{2c\sqrt{K_a}}{\gamma K_a} = \frac{2c}{\gamma\sqrt{K_a}} = \frac{2(10.5)}{17.52(0.84)} = \mathbf{1.43}\ \text{m}$$

Note: This value of z is the depth of a potential tension crack, since (−) p = tension stresses that the soil cannot carry. At base, the lateral pressure [from Eq. (2-55)] is

$$p_a = 17.52(6.5)(0.704) - 2(10.5)(0.84) = \mathbf{62.53}\ \text{kPa}$$

The resultant force is found as $\sum F_h = R$. The location of the resultant may be found by summing moments at the base or by inspection, depending on the complexity of the pressure diagram. The tension zone $\overline{ab}$ is usually neglected for finding the magnitude and location of the resultant.

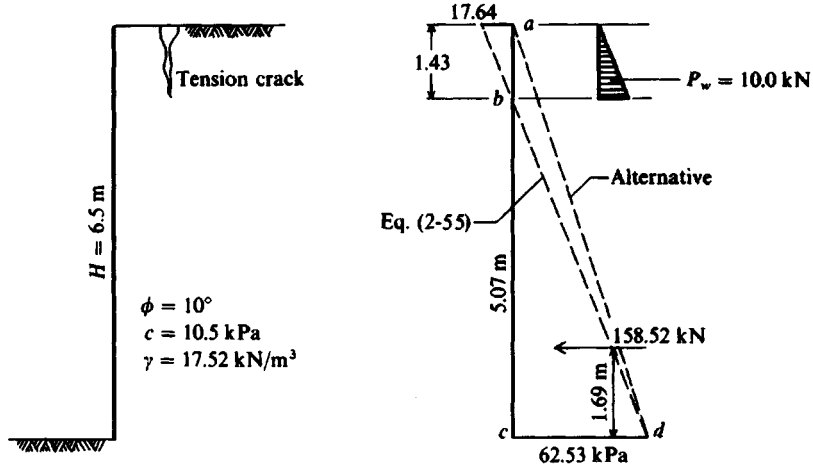

(*a*) Given. (*b*) Computed.

Figure E11-4

Neglecting the tension zone	**Using alternative pressure diagram *acd***
$R = 62.53\left(\frac{5.07}{2}\right) = \mathbf{158.5}$ kN/m	$R = 62.53\left(\frac{6.5}{2}\right) = \mathbf{203.2}$ kN/m
$\bar{y} = \frac{5.07}{2} = \mathbf{1.69}$ m above c	$\bar{y} = \frac{6.5}{3} = \mathbf{2.17}$ m (by inspection)

With water in the tension crack,

$$R = 158.5 + \frac{9.807(1.43)^2}{2} = \mathbf{168.5} \text{ kN/m}$$

and the overturning moment including water in the tension crack is

$$M_o = 158.5(1.69) + 10.0\left(5.07 + \frac{1.43}{3}\right) = \mathbf{323.3} \text{ kN} \cdot \text{m/m}$$

$$\bar{y} = \frac{323.3}{168.5} = \mathbf{1.92} \text{ m above } c$$

In this case the water-in-crack solution is between the two previous solutions, from which it appears that the alternative pressure diagram *acd* provides a conservative solution.

////

Example 11-5. Plot the active earth pressure diagram and compute the resultant R and its location $\bar{y}$ for the wall system shown in Fig. E11-5. This type of problem is often encountered in excavations for large structures where there may be two or more basement levels. The soil parameters ϕ, c may be estimated or else be obtained from performing consolidated isotropically undrained (CIU) tests on good-quality tube samples. The major approximation is defining the several strata by abrupt discontinuities (using lines as shown to delineate layers). In most real situations the soil type grades through a finite length from one to the next.

Solution. We should plot the soil and pressure profiles adjacent to each other as in Fig. E11-5. The Rankine equations for active earth pressure coefficients K_a will be used [use program FFACTOR since these small ϕ angles are not in Table 11-3, or use Eq. (11-7*a*)].

For instance, for $\phi = 32°$, use Table 11-3, obtain $K_a = 0.307$ and $\sqrt{0.307} = 0.554$, etc.

Typical computations for $\Delta p'_o$ are as follows:

Depth, m	**$\Delta p'_o$, kPa**
0	100 kPa (surcharge)
1.80	$100 + 1.80(17.30) = 131.4$ kPa
2.40	$131.4 + 0.6(19.60 - 9.807) = 131.4 + 0.6(9.79)$ $= 137.02$ kPa
5.15	$137.02 + 2.75(9.89) = 164.22$ etc.

It will be convenient to tabularize the computations as in Table E11-5 following.

Notice that at the interface between two soils we use the interface pressure two times: first with $-dz$ and the upper K coefficients, and second with $+dz$ and the K coefficients of the lower soil. Note also that the $2c\sqrt{K_a}$ term can be simplified for the second use.

To find the resultant we must divide the pressure profile into rectangles and triangles as shown on Fig. E11-5*b*. The water pressure is included ($K_a = K_p = K_w = 1$) if the water cannot drain

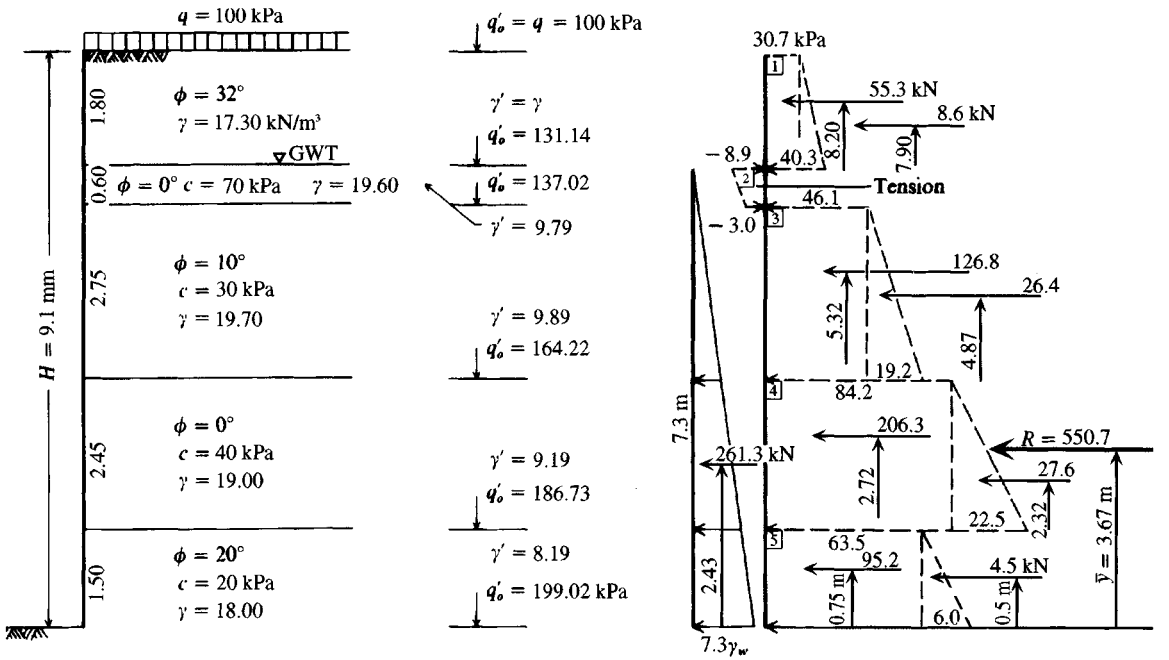

(*a*) Soil profile.

(*b*) Pressure profile.

Figure E11-5

TABLE E11-5

Soil	Depth, m	K_a	$\sqrt{K_a}$	$\Delta P'_o$, kPa	Wall pressure, q_h, kPa	
1	0	0.307	0.554	100.	100(0.307)	= 30.7
	1.80−dz			131.14	(131.14)(0.307)	= 40.3
2	1.80+dz	1.000	1.000	131.14	(131.14)(1.00) − 2(70)(1.00)	= −8.9
	2.40−dz			137.02	(137.02)(1.00) − 2(70)(1.00)	= −3.0
3	2.40+dz	0.704	0.839	137.02	(137.02)(0.704)−2(30)(0.839)	= 46.1
	5.15−dz			164.22	(164.22)(0.704) − 60(0.839)	= 65.3
4	5.15+dz	1.000	1.000	164.22	(164.22)(1.000) − 2(40)(1.00)	= 84.2
	7.60−dz			186.73	(186.73)(1.000) − 80(1.00)	= 106.7
5	7.60+dz	0.490	0.700	186.73	(186.73)(0.490)−2(20)(0.700)	= 63.5
	9.1			199.02	(199.02)(0.490) − 40(0.700)	= 69.5

through the wall or away by other means. Since the water contribution is significant, it is obvious that drainage should be allowed if possible.

The tension zone (−) q_h is a problem. Should it be included to reduce the wall force or neglected, as it may pull away from the wall? A more conservative case is made if the tension zone is neglected, which we will do here—so *neglect tension zone.*

There is much busywork with this type of problem—particularly to get the pressure profile—so that a computer program such as B-25 should be used if possible.

Computations for finding the resultant are as follows:

1. Compute the force P_i for each geometric area (rectangle or triangle) and locate its resultant $\bar{y}$ from the base as partially shown on Fig. E11-5*b*:

$$P_1 = 30.7(1.80) = 55.3 \text{ kN}$$
$$P_2 = (40.3 - 30.7)1.80/2 = 8.6 \text{ kN}$$
$$P_3 = 46.1(2.75) = 126.8 \text{ kN} \quad \text{etc.}$$

2. Sum the horizontal forces $\sum F_h = R$

$$R = 55.3 + 8.6 + 126.8 + 26.4 + 206.3 + 27.6 + 95.2 + 4.5$$
$$= \mathbf{550.7} \text{ kN}$$

The water $P_w = 7.3(9.807)(7.3/2) = \mathbf{261.3}$ kN.
Compute y_i for each P:

$$y_1 = 1.5 + 2.45 + 2.75 + 0.60 + 1.80/2 = 8.20 \text{ m}$$
$$y_2 = 7.3 + 180/3 = 7.9 \text{ m}$$
$$y_3 = 1.5 + 2.45 + 2.75/2 = 5.32 \text{ m}$$
$$y_4 = 3.95 + 2.75/3 = 4.87 \text{ m} \quad \text{etc.}$$

Compute $\bar{y}$:

$$R\bar{y} = \sum_1^n P_i y_i$$
$$550.7\bar{y} = 55.3(8.20) + 8.6(7.90) + 126.8(5.32) + 26.4(4.87)$$
$$+ 206.3(2.72) + 27.6(2.32) + 95.2(0.75) + 4.5(0.50)$$
$$\bar{y} = \frac{2023.36}{550.7} = \mathbf{3.67} \text{ m} \quad \text{(above base of wall)}$$

The soil pressure resultant and corresponding $\bar{y}$ are shown on Fig. E11-5*b* (and *this calculation does not include water*).

////

11-7 ACTIVE AND PASSIVE EARTH PRESSURE USING THEORY OF PLASTICITY

The Coulomb and Rankine passive earth pressure methods consistently overestimate the passive pressure developed in field and model tests for ϕ much over 35°. This estimate may or may not be conservative, depending on the need for the passive pressure value. Because of the problem of overestimation, Caquot and Kerisel (1948) produced tables of earth pressure based on nonplane-failure surfaces; later Janbu (1957) and then Shields and Toluany (1973) proposed an approach to the earth pressure problem similar to the method of slices used in slope-stability analyses. Sokolovski (1960) presented a finite-difference solution using a highly mathematical method. All these methods give smaller values for the passive earth pressure coefficient. None of these methods significantly improves on the Coulomb or Rankine active earth pressure coefficients.

Rosenfarb and Chen (1972) developed a closed-form earth pressure solution using plasticity theory that can be used for both active and passive earth pressure computations. The closed-form solution requires a computer program with an iteration routine, which is not particularly difficult. This method is included here because of the greater clarity over the alternative methods.

Rosenfarb and Chen considered several failure surfaces, and the combination of a so-called *log-sandwich* mechanism gave results that compared most favorably with the Sokolovski solution, which has been accepted as correct by many persons. Figure 11-10 illustrates the passive log-sandwich mechanism. From this mechanism and appropriate consideration of its velocity components the following equations are obtained.

Cohesionless Soil

For a smooth wall ($\delta < \phi$)*:*

$$\begin{Bmatrix} K_{a\gamma} \\ K_{p\gamma} \end{Bmatrix} = \frac{\mp \sec\delta}{\mp \sin\alpha + \tan\delta\cos\alpha - [\tan\delta\cos(\alpha-\rho)/\cos\rho]} \times \left(\frac{\tan\rho\cos(\rho \pm \phi)\cos(\alpha-\rho)}{\sin\alpha\cos\phi} + \frac{\cos^2(\rho\pm\phi)}{\cos\rho\sin\alpha\cos^2\phi(1+9\tan^2\phi)} \times \left\{ \cos(\alpha-\rho)[\pm 3\tan\phi + (\mp 3\tan\phi\cos\psi + \sin\psi) \times \exp(\mp 3\psi\tan\phi)] + \sin(\alpha-\rho)[1 + (\mp 3\tan\phi\sin\psi - \cos\psi) \times \exp(\mp 3\psi\tan\phi)] \right\} + \frac{\cos^2(\rho\pm\phi)\sin(\alpha-\rho-\psi+\beta)\cos(\alpha-\rho-\psi)\exp(\mp 3\psi\tan\phi)}{\cos\phi\sin\alpha\cos(\alpha-\rho-\psi\mp\phi+\beta)\cos\rho} \right) \tag{11-10}$$

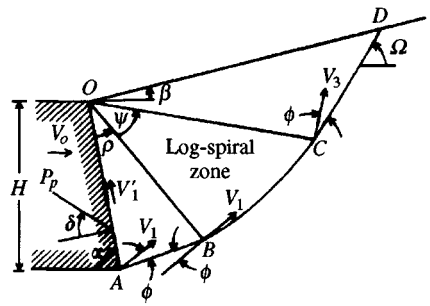

(*a*) Passive log-sandwich mechanism with $V_3 = V_1 \exp(\psi \tan\phi)$.

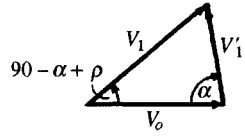

(*b*) Velocity diagram for a smooth wall $\delta < \phi$.

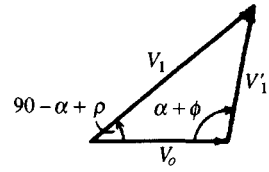

(*c*) Velocity diagram for a rough wall $\delta = \phi$.

Figure 11-10 Plastic stress fields for earth pressure using the theory of plasticity. [*Rosenfarb and Chen (1972).*]

For a rough wall ($\delta = \phi$)*:*

$$\begin{Bmatrix} K_{a\gamma} \\ K_{p\gamma} \end{Bmatrix} = \frac{\mp \sec\delta}{\mp \sin\alpha + \tan\delta\cos\alpha}\left(\frac{\sin^2\rho\cos(\rho \pm \phi)\cos(\alpha - \rho)\sin(\alpha \mp \phi)}{\sin^2\alpha\cos\phi\cos(\rho \mp \phi)}\right.$$

$$\mp \frac{\cos^2(\rho \pm \phi)\sin(\alpha \mp \phi)}{\sin^2\alpha\cos^2\phi(1 + 9\tan^2\phi)\cos(\rho \mp \phi)}$$

$$\times\left\{\cos(\alpha - \rho)[\pm 3\tan\phi + (\mp 3\tan\phi\cos\psi + \sin\psi)\exp(\mp 3\psi\tan\phi)]\right.$$

$$\left.+ \sin(\alpha - \rho)[1 + (\mp 3\tan\phi\sin\psi - \cos\psi)\exp(\mp 3\psi\tan\phi)]\right\}$$

$$\left. + \frac{\cos^2(\rho \pm \phi)\sin(\alpha - \rho - \psi + \beta)\cos(\alpha - \rho - \psi)\sin(\alpha \mp \phi)\exp(\mp 3\psi\tan\phi)}{\sin^2\alpha\cos\phi\cos(\alpha - \rho - \psi + \beta \mp \phi)\cos(\rho \mp \phi)}\right) \tag{11-11}$$

Cohesive Soil

For a smooth wall ($\delta < \phi$)*:*

$$\begin{Bmatrix} K_{ac} \\ K_{pc} \end{Bmatrix} = \frac{\sec\delta}{\mp \sin\alpha + \tan\delta\cos\alpha - [\tan\delta\cos(\alpha - \rho)/\cos\rho]}$$

$$\times\left\{\tan\rho + \frac{\cos(\rho \pm \phi)\sin(\alpha - \rho - \psi + \beta)\exp(\mp\psi\tan\phi)}{\cos\rho\cos(\alpha - \rho - \psi \mp \phi + \beta)}\right.$$

$$\left.\mp \frac{\cos(\rho \pm \phi)[\exp(\mp 2\psi\tan\phi) - 1]}{\sin\phi\cos\rho}\right\} \tag{11-12}$$

For a rough wall ($\delta = \phi$):

$$\begin{Bmatrix} K_{ac} \\ K_{pc} \end{Bmatrix} = \frac{\sec\delta}{\mp\sin\alpha + \tan\delta\cos\alpha}\left\{\frac{\cos\phi\cos(\alpha-\rho)}{\sin\alpha\cos(\rho\mp\phi)} + \frac{\sin\rho\sin(\alpha\mp\phi)}{\sin\alpha\cos(\rho\mp\phi)}\right.$$
$$+\frac{\cos(\rho\pm\phi)\sin(\alpha-\rho-\psi+\beta)\sin(\alpha\mp\phi)\exp(\mp\psi\tan\phi)}{\sin\alpha\cos(\alpha-\rho-\psi\mp\phi+\beta)\cos(\rho\mp\phi)}$$
$$\left.\mp\frac{\cos(\rho\pm\phi)\sin(\alpha\mp\phi)[\exp(\mp 2\psi\tan\phi)-1]}{\sin\phi\sin\alpha\cos(\rho\mp\phi)}\right\} \tag{11-13}$$

In solving Eqs. (11-10) through (11-13), it is necessary to solve for the maximum value of K_p or K_a. The maximizing of these equations depends on the two variables ρ and ψ. This requires a search routine in computer program B-23. The values of the two dependent variables are initialized to approximately

$$\rho \cong 0.5(\alpha + \beta)$$
$$\psi \cong 0.2(\alpha + \beta)$$

With these initial values, the search routine is used to revise the values until convergence is obtained. In most cases values from which K_p is computed are found after not more than 20 iterations. A computer program should shut off after 46 to 50 iterations. In a few cases the program may not find a solution using the above initial values because of the programming search routine. For these cases, one must change the initial values and retry as necessary to obtain the solution. Table 11-5 gives selected values of K_p for cohesionless soils. Note that these equations correctly give K_p increasing with β. Values of $\beta = \delta = 0$ are not shown, as they are identical to the Coulomb or Rankine solution.

The "smooth" wall solution is used for wall friction $\delta < \phi$; when $\delta = \phi$ the "rough" wall equation is used. Equations (11-12) and (11-13) can readily be programmed, using the same routines to solve an equation for minimum or maximum with two dependent variables, to obtain passive pressure coefficients for cohesive soil. This solution does not give greatly different values from the Coulomb passive pressure theory until the ϕ angle becomes larger than 35° and with δ on the order of $\phi/2$ or more and $\beta \neq 0°$ (since the back slope can have $\pm\beta$).

11-8 EARTH PRESSURE ON WALLS, SOIL-TENSION EFFECTS, RUPTURE ZONE

The Rankine or Coulomb earth pressure equations can be used to obtain the force and its approximate point of application acting on the wall for design. Soil-tension concepts can also be investigated. These will be taken up in the following discussion.

11-8.1 Earth Forces on Walls

From Eq. (2-55) and temporarily considering a soil with $c = 0$, γ constant with depth z and referring to Fig. 11-9*a*, we can compute the wall force as

$$P_a = \int_0^H \sigma_3 K_a\, dz = \int_0^H \gamma z K_a = \frac{\gamma z^2 K_a}{2}\Bigg|_0^H = \frac{\gamma H^2}{2}K_a \tag{a}$$

from which it is evident that the soil pressure diagram is hydrostatic (linearly increases with depth) as shown in the figure. If there is a surcharge q on the backfill as shown in Fig. 11-9*c* (other surcharges will be considered in Sec. 11-13), the wall force can be computed as

TABLE 11-5
Selected values of K_p using limit analysis for $\alpha = 90°$ (vertical wall) for a granular soil. Values same as in Table 11-2 for $\beta = 0°$. Intermediate values may be obtained by plotting K_p

β	$\phi = 30°$	35°	40°	45°
		$\delta = 0$		
−10	2.21	2.65	2.68	3.90
10	4.01	5.20	6.68	8.93
20	5.25	7.03	9.68	13.8
30	6.74	9.50	14.0	21.5
		$\delta = 10$		
−10	2.77	3.44	4.3	5.5
10	5.70	7.61	10.4	14.9
20	7.79	10.9	15.9	24.4
30	10.3	14.7	23.6	39.6
		$\delta = 20$		
−10	3.56	4.61	6.1	8.2
10	7.94	11.2	16.3	24.9
20	11.2	16.5	25.6	42.4
30	15.1	23.2	41.0	70.2
		$\delta = 30$		
−10	4.5	6.2	8.6	12.4
10	10.6	15.8	24.6	40.7
20	15.2	23.2	39.5	70.3
30	20.8	34.8	62.0	0*

*No solution after 46 iterations.

$$P_a = \int_0^H (\gamma z + q) K_a \, dz = \left(\frac{\gamma H^2}{2} + qH\right) K_a \tag{b}$$

The point of application requires taking moments about a convenient point, and for the case with surcharge and from the top of the wall we have

$$P_a y = \int_0^H (\gamma z + q) K_a z \, dz = \left(\frac{\gamma H^3}{3} + \frac{qH^2}{2}\right) K_a \tag{c}$$

and, inserting the value of P_a from Eq. (*b*), the distance from the top of the wall is

$$\bar{y}_t = \frac{1}{3} \frac{2\gamma H^2 + 3qH}{\gamma H + 2q}$$

and from the bottom of the wall $\bar{y} = H - \bar{y}_t$

$$\bar{y} = \frac{H}{3} \frac{3q + \gamma H}{2q + \gamma H} \qquad (\text{for } c = 0) \tag{11-14}$$

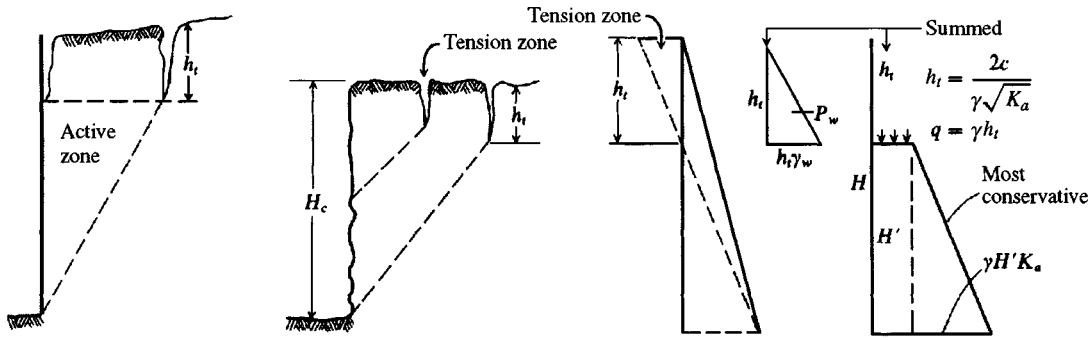

(*a*) Behind walls. (*b*) Open cuts. (*c*) Suggested pressure diagrams (solid) in cohesive soil

Figure 11-11 Tension crack and critical depth of an unbraced excavation. Tension cracks are often readily visible adjacent to excavations.

When the surcharge $q = 0$, we obtain $\bar{y} = H/3$; for $c > 0$ locate $\bar{y}$ using Example 11-4 or Fig. 11-11*c* as a guide. It is not correct to convert the surcharge to an equivalent additional wall height and use $\bar{y}$ to the centroid of a triangle, because the surcharge effect is rectangular against the wall.

A number of researchers using both models and fairly large retaining walls have found that the wall force resultant seldom acts at the distance $\bar{y} = H/3$ from the wall base. This implies that the wall pressure diagram is not triangular. Williams (1989, with a number of references) derived equations that tend to produce a somewhat parabolic pressure distribution, which may or may not coincide with the Coulomb pressure profile near the top.

In any case, the resultant of the lateral pressure is commonly taken as $H/3$ and the pressure diagram is assumed to be triangular (if there is no surcharge), including cases where the backfill slope angle $\beta \neq 0$. Some evidence exists that, because the wall rotates about its base, the pressure diagram is not triangular and that the resultant is somewhere in the middle one-third of the wall height—about the $0.4H$ point above the base.

Most walls are constructed with a void on the backfill side, which is then stage-filled and compacted (that is, add a layer, compact it, add another layer, compact it, etc.) until the surface is reached. This method also tends to increase the wall pressure—particularly near the bottom—and more particularly for clay backfills (which may be necessary if granular backfill is not available). The lower compacted soil produces lateral displacements in the upper wall zone, so soil later compacted in this area may not produce enough additional deflection to reduce the lower wall pressure to an active state.

Clayton et al. (1991) measured compaction pressures against a wall from a clay backfill. They found that compaction pressures did not become significant until the air-void content (difference between the zero-air-voids curve and the maximum dry density) was less than 15 percent and that the pressures could be expressed as a percentage of s_u, ranging from about 20 to 40 percent. Also they found that the lateral pressure, partially produced by compaction, tended to reduce with time. The question is, what to do?

CHOOSE A *K* VALUE. Overdesign the wall by using a K intermediate between K_a and K_o.

MAKE ASSUMPTIONS. Assume the computed soil pressure resultant is above the usual point of application (the one-third point for no surcharge). If the pressure resultant (no

surcharge) is assumed to be at a point above the one-third point, the only way this can be achieved is to force a trapezoidal pressure diagram into the model. This can substantially increase the bending moments for structural walls, but the shear (and soil pressure resultant R) remains the same, unless R is increased by some uncertainty factor, such as 1.1, 1.4, 1.5, and so forth.

We can derive a general equation for locating the pressure resultant and the pressure at the top of the wall necessary to define a trapezoidal pressure diagram. We already know that the bottom pressure $q_b = \gamma_s H$. From a trapezoid pressure diagram with q_t and q_b and height H and the pressure resultant located at kH we can obtain two equations. The resultant R = area of a trapezoid, giving

$$R = Hq_t + (q_b - q_t)\frac{H}{2} \rightarrow q_t + q_b = \frac{2R}{H} \qquad (a)$$

Use Eq. (9-2) (the location of the center of a trapezoid) as the second equation and substituting q_t and q_b for a and b, obtain

$$\bar{y} = \frac{H}{3}\left(\frac{2q_t + q_b}{q_t + q_b}\right) = kH \qquad (b)$$

Now substitute Eq. (a) into Eq. (b) and simplify to obtain

$$\left.\begin{aligned} q_t &= \frac{2R}{H}(3k - 1) \\ q_b &= \frac{2R}{H}(2 - 3k) \end{aligned}\right\} \quad \text{valid from } \frac{1}{3} \leq k < \frac{2}{3} \qquad (11\text{-}15)$$

For $q_{b,\text{init}} = 40$ kPa, $H = 10$, compute $R = 40 \times 10/2 = 200$. For $k = \frac{1}{3}$ we have $q_t = 0$; $q_b = q_{b,\text{init}} = 40$. For $k = 0.5$ we have $q_t = q_b = 20$ {and the new $R = [(20 + 20)/2](10) = 200$ as before} but now $\bar{y} = 5$ instead of $\frac{10}{3}$. Before computing the new top and base pressures we may increase (or decrease) R as deemed necessary for the given wall.

One should adjust R with care—probably it is best to increase the earth pressure coefficient—since available evidence indicates the initial resultant R_{init} is about that from the Coulomb/Rankine equation but the location is not. Make the reduction as follows.

Although it is not unreasonable to put the location of the resultant above the one-third point, one must decide what the minimum pressure will be that the wall must resist before failure. A high pressure above the minimum active value may reduce to the minimum active value as the wall starts to rotate forward under the higher pressure. This movement decreases the pressure, but the wall may rotate further still under the reduced lateral pressure. The wall either breaks or shears off or reaches some equilibrium resisting lateral pressure, and movement stops.

11-8.2 Soil-Tension Effects on Backfill and Open Trenches

Visible tension cracks usually develop where

1. Cohesive soil is used for backfill.
2. A trench or basement excavation is made in cohesive soil.

In the excavation case the cracks form parallel to the excavation and if under pavements and structures can produce damage. We may use Eq. (2-55), slightly modified and repeated here as

$$\sigma_3 = (q + \gamma z)K_a - 2c\sqrt{K_a} \tag{c}$$

where the quantity $(q + \gamma z) = \sigma_1$. Tension exists in a cohesive soil to some depth $z = h_t$ until the stress $\sigma_3 = 0$ (after that the stress is compression). This depth is estimated from Eq. (*c*) by rearranging, replacing z with h_t, and solving to obtain

$$h_t = \frac{2c\sqrt{K_a} - qK_a}{\gamma K_a} \tag{11-16}$$

Note the inclusion of the surcharge q makes this equation general. The equation is most often seen without the surcharge term as follows:

$$h_t = \frac{2c}{\gamma\sqrt{K_a}} \tag{11-16a}$$

The tension crack can form at the wall-soil interface and/or at some distance back from the wall (see Figs. 11-11*a*, *b*). It is not unusual for several approximately parallel tension cracks to form.

Another value of interest is the theoretical depth an excavation can stand without lateral bracing. The key words here are the *theoretical depth.* Building codes and governmental safety divisions (OSHA in the United States) usually give limitations on unbraced excavation depths. In any case the theoretical value is computed by integrating Eq. (*d*) and using $z = H_c$ = theoretical or critical depth to obtain:

$$P = \int_0^{H_c} \left[(q + \gamma z)K_a - 2c\sqrt{K_a}\right] dz$$

Integrating (constant = 0), inserting the limits, setting the horizontal force $P = 0$, and simplifying, we obtain

$$H_c = \frac{4c}{\gamma\sqrt{K_a}} - \frac{2q}{\gamma} \tag{11-17}$$

There may be some question of what to use for K_a in Eqs. (11-16) and (11-17) when $\beta > 0$, since Eq. (2-55) as developed was for a horizontal ground surface. In the absence of any better information use the Coulomb values from Table 11-3 with $\delta = 0$.

One should not rely on the tension zone (see Fig. 11-11*c*) to reduce lateral pressures. Instead one should assume that it can form and will possibly fill with water.[1] The depth of water (not the quantity) can increase the overturning pressure against the wall considerably owing to both the hydrostatic force of $\gamma_w h_t$ and the larger moment arm caused by combining the hydrostatic force with the already existing lateral pressure.

[1]If the crack fills with water it will usually close with time as the soil swells. The soil-excavation system must, however, survive during this time, so it is conservative to consider a crack filled with water as a worst case.

It is suggested that when there is a wall tension zone you use either of the two alternatives of Fig. 11-11*c*, together with the water pressure profile shown, if the tension crack can fill with water. Treating the tension block as a surcharge is probably more nearly correct and gives a more conservative (larger) wall force and overturning moment.

One cannot rely on Eq. (11-17) to predict the critical embankment height accurately for several reasons:

1. Once the tension crack forms, Eq. (2-55) is not valid for the full depth of the excavation.
2. Cohesive soils tend to lose cohesion when exposed in excavations as a result of moisture adsorption and/or shrinkage cracks.
3. A surcharge effect results from equipment and materials piled on the ground adjacent to the excavation.

Because of these several factors, Eq. (11-17) should include a safety factor for design to obtain a design depth H_c', as

$$H_c' = \frac{1}{\text{SF}}\left[\frac{4c}{\gamma\sqrt{K_a}} - \frac{2q}{\gamma}\right] \qquad (11\text{-}17a)$$

Of course, if local authorities require a lesser value of H_c', that should be used.

11-8.3 Rupture Zone

The solution of the Rankine equations as shown by the Mohr's circle of Fig. 11-1*a* gives the rupture slope ρ in the backfill as

$$\rho = 45 \pm \frac{\phi}{2} \qquad (+) = \text{active pressure case}$$

for horizontal ($\beta = 0$) ground. For the general case of sloping ground and/or wall friction the ρ angle is not that given above. For these cases it is recommended to use the trial wedge computer program B-7 on your diskette to obtain the critical ρ angle (so as to locate the potential slip zone) since it is given as part of the output for hand checking. There are closed-form solutions as in Jumikis (1962); however, they are complicated and subject to error in either derivation or typesetting so that they should be used very cautiously if at all.

11-9 RELIABILITY OF LATERAL EARTH PRESSURES

Several sets of wall tests have been performed to check the validity of the Coulomb and Rankine active and passive earth pressure methods. These include the tests of Terzaghi (1934), Peck and Ireland (1961), Rowe and Peaker (1965), Mackey and Kirk (1967), James and Bransby (1970), Rehnman and Broms (1972), and Coyle et al. (1972). Field and model tests [as by Fang and Ishibashi (1986)] tend to confirm the active earth pressure concept reasonably well if the backfill is carefully placed so that compaction effects do not create excessive stresses and if the wall rotates and/or translates sufficiently to mobilize the maximum shearing resistance in the soil. Often the top of the wall translates/rotates adequately while near the stem base it does not so that the pressure near the base is larger than predicted by theory—particularly if some compaction of the backfill has been done. Regardless, the total wall force from numerically integrating the pressure profile is usually close to the theoretical "active"

value and the resultant is usually at or above the lower one-third point (often closer to 0.4 or $0.45H$).

The active zone rupture surface is also fairly close to that predicted by theory and close to being a plane. The passive zone, however, often is not in close agreement and the rupture surface is closer to being a spiral. This latter gives additional cause for suggesting the use of Sec. 11-7 with computer program B-23 (or similar) for the passive earth pressure case.

11-10 SOIL PROPERTIES FOR LATERAL EARTH PRESSURE COMPUTATIONS

It is evident from the use of the Mohr's circle as a starting point for earth pressure coefficients that *effective* stresses together with any hydrostatic water pressure are used to compute the wall force. The usual condition of soil behind walls is as shown in Fig. 11-12. We have excavated a vertical or sloping space for the wall, poured the wall footing and wall and then backfilled the zone previously excavated, usually with some compaction. We then have to idealize the model somewhat to compute the earth force that the wall must resist.

11-10.1 Soil Parameters

These soil parameters are used in computing lateral earth pressure:

1. Drained values for sand are used for reasons cited in Chap. 2. Ideally, plane strain ϕ values as obtained from direct shear, direct simple shear, or from triaxial values that have

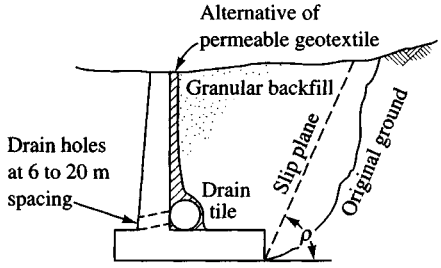

(*a*) Backfill Rankine zone with select backfill. Use vertical geotextile for poor-quality backfill.

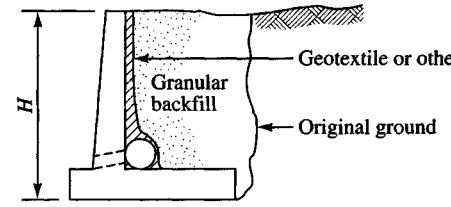

(*b*) Backfill-limited zone. Use geotextile for poor-quality backfill.

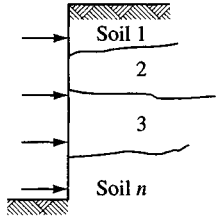

(*c*) Usual conditions of braced excavations.

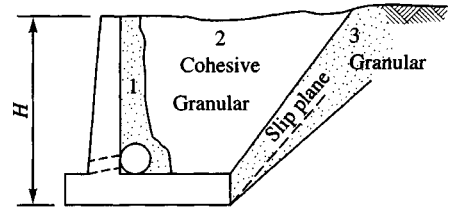

(*d*) Backfill where select material is limited. Zone 3 should be sufficient to account for extra weight due to cohesive backfill and allow slip in this fill material. Zone 1 may be omitted if geotextile is used.

Figure 11-12 Various backfill conditions. The longitudinal collector (or drain) pipe is optional.

been adjusted to plane strain values are employed. However, very commonly a ϕ value is estimated from visual examination of the sand and using a conservative value from 30 to 34°.

2. For cohesive soils s_u values are commonly used and are generally adequate for normally and lightly overconsolidated soil.
3. For overconsolidated soil we may use these:
   a. A drained strength parameter with ϕ' obtained from a drained shear test, using Fig. 2-25 as a test guide (not often), or estimated from one of the correlations given on Figs. 2-35 or 2-36.
   b. The undrained shear strength at the creep threshold.
   c. A drained ϕ angle between peak and residual strength.

In cohesive soil a wall designed using almost any set of reasonable design strength parameters is likely to have an adequate risk factor if the following conditions are met:

1. Wall excavation did not cave during wall construction.
2. Excavated zone is backfilled and compacted using a freely draining soil.
3. If backfill is cohesive, increase the k-factor of Eq. (11-15) to 0.40 to 0.50.

The risk factor is likely adequate even if the excavation/backfill zone is fairly limited since a cave-in would have occurred if the retained soil were inherently unstable.

11-10.2 Water in Backfill

Water in the backfill soil is particularly undesirable since it increases the unit weight and lateral pressure. If a water table can form (or stabilize), the effect is considerably worse since the ϕ angle of water is zero, giving $K_a = K_p = 1$ as used earlier. A further undesirable side effect in cold climates is that the backfill water may freeze and greatly increase the lateral pressure, causing the wall to displace forward. This displacement is usually not fully recovered when thawing occurs.

Most of the water problem can be avoided by constructing drain (or weep) holes through the wall base or using lateral drain pipes. The major problem here is to ensure that the backfill does not erode through the weep holes or clog the lateral drain pipes. If sand is used it should be properly graded, with coarse material adjacent to the drainage device and finer material over the coarse. Currently a more reliable method is to face the backfill side of the wall with a geotextile especially fabricated to allow vertical drainage. The backfill adjacent to the geotextile does not have to be carefully graded for the geotextile prevents soil erosion. It can be placed vertically and draped over the lateral drains to avoid clogging. This material will allow the use of either granular (always preferable) or cohesive backfill.

Although a geotextile material is ideal for allowing backfill drainage it is initially more costly and requires care in placing and backfilling. Offsetting the higher initial cost is the savings accrued from reduced maintenance, i.e., regular inspections and recovering eroded material (refer to Fig 12-18*b*) from the weep hole exits and putting it back behind the wall (often in vertical "pipes" formed by erosion down to the weep holes).

11-10.3 Angle of Wall Friction δ

Wall friction apparently depends not only on the soil properties but also on the amount and direction of wall movement [see Sherif et al. (1982)]. Indications are that maximum wall friction may not occur simultaneously with maximum shearing resistance along the rupture surface and that wall friction is not a constant along the wall—probably because the relative soil-wall movement is not constant.

Considerable engineering judgment must be applied to obtain realistic values of wall friction since they are pressure-dependent. Values of $\delta = 0.6$ to 0.8ϕ are reasonable for concrete walls where forms are used giving a relatively smooth backface. Table 11-6 gives several values of δ for other wall-to-soil materials. For steel, concrete, and wood the values shown are for a normal pressure σ_n of about 100 kPa. Decrease the values about 2 degrees for each 100 kPa increase in sand [see Acar et al. (1982) and Fig. 2-31].

Rankine earth pressure is commonly used for the structural design of low- and medium-height walls, since a larger wall pressure is obtained from not including any wall friction angle δ. For high walls (say more than about 6 m) one should consider using the Coulomb

TABLE 11-6
Friction angles δ between various foundation materials and soil or rock*

Interface materials	Friction angle, δ, degrees†
Mass concrete or masonry on the following:	
Clean sound rock	35°
Clean gravel, gravel-sand mixtures, coarse sand	ϕ
Clean fine to medium sand, silty medium to coarse sand, silty or clayey gravel	ϕ
Clean fine sand, silty or clayey fine to medium sand	ϕ
Fine sandy silt, nonplastic silt	ϕ
Very stiff and hard residual or preconsolidated clay	ϕ
Medium stiff and stiff clay and silty clay	ϕ
Steel sheet piles against the following:	
Clean gravel, gravel-sand mixture, well-graded rock fill with spalls	22°
Clean sand, silty sand-gravel mixture, single-size hard rock fill	17
Silty sand, gravel, or sand mixed with silt or clay	14
Fine sandy silt, nonplastic silt	11
Formed concrete or concrete sheetpiling against the following:	
Clean gravel, gravel-sand mixtures, well-graded rock fill with spalls	22–26
Clean sand, silty sand-gravel mixture, single-size hard rock fill	17–22
Silty sand, gravel, or sand mixed with silt or clay	17
Fine sandy silt, nonplastic silt	14
Various structural materials	
Masonry on masonry, igneous and metamorphic rocks:	
Dressed soft rock on dressed soft rock	35°
Dressed hard rock on dressed soft rock	33
Dressed hard rock on dressed hard rock	29
Masonry on wood (cross grain)	26
Steel on steel at sheet-pile interlocks	17
Wood on soil	14–16‡

*May be stress-dependent (see text) for sand.

†Single values ±2°. Alternate for concrete poured on soil is $\delta = \phi$.

‡May be higher in dense sand or if sand penetrates wood.

earth pressure (with some estimated wall friction angle δ), as the Rankine pressure is likely to produce too much wall overdesign.

11-10.4 Wall Adhesion

Wall adhesion develops from any cohesion in the soil. In the upper region it is expected a tension crack may form (or form during dry periods as the ground naturally shrinks). The value of adhesion c_a below the tension crack is usually taken at from 0.5 to $0.7s_u$ with a maximum value not much over 50 kPa. There is some opinion to neglect the tension zones along a wall (see Examples 11-4 and 11-5). One may need to investigate both the total stress case [with cohesion (s_u)] and the drained (effective) stress case using only ϕ', depending on the particular problem parameters.

11-11 EARTH-PRESSURE THEORIES IN RETAINING WALL PROBLEMS

Both the Rankine and Coulomb methods are widely used to compute the lateral earth pressure on retaining walls. The Rankine solution is often used because the equations are simple and are somewhat more conservative than the Coulomb equations, that is, they compute a larger lateral pressure.

The Rankine (and Coulomb) equation for cohesionless soil and no surcharge has the same form as for hydrostatic problems, that is,

$$P_a = \frac{H}{2}\sigma_h = \frac{H}{2}(\gamma H K_a)$$

where the γK_a term is the equivalent unit weight of some fluid. Values in the range of 5 to 8 kN/m^3 are given in some handbooks, and when these values are used, the resulting design is termed the *equivalent fluid method.* This procedure is not generally recommended, partly because one can simply select some value and not really analyze the problem.

In using either the Rankine or Coulomb solutions, no part of the wall should interfere with the formation of the approximate rupture surface (line BC of Fig. 11-2). Generally for cantilever retaining walls (walls with a heel projection as in Fig. 11-13*b*) one must make two solutions:

1. At the back face of the wall using $H = AB$ of Fig. 11-13*b* so the stem can be designed to resist shear and moment.
2. At the heel point C using $H = A'C$ for overall wall sliding and overturning stability.

11-11.1 Walls with Limited Backfill Zones

A major consideration in wall design is whether the idealized rupture zone can form as illustrated in Fig. 11-12. In Fig. 11-12*a* the backfill zone is large enough that the *"Rankine" zone* can develop in soil of known properties. In Fig. 11-12*b* the backfill zone is limited and the Rankine zone (if one develops) will be in the original ground—the granular backfill only provides free drainage so hydrostatic water pressure does not form. Obviously, if the existing ground has been standing for some time it will contribute little—if any—lateral pressure to the wall and the principal wall pressure will be from compacting the backfill in the limited zone; however, lateral pressure from compaction may be substantial and even exceed any computed active pressure.

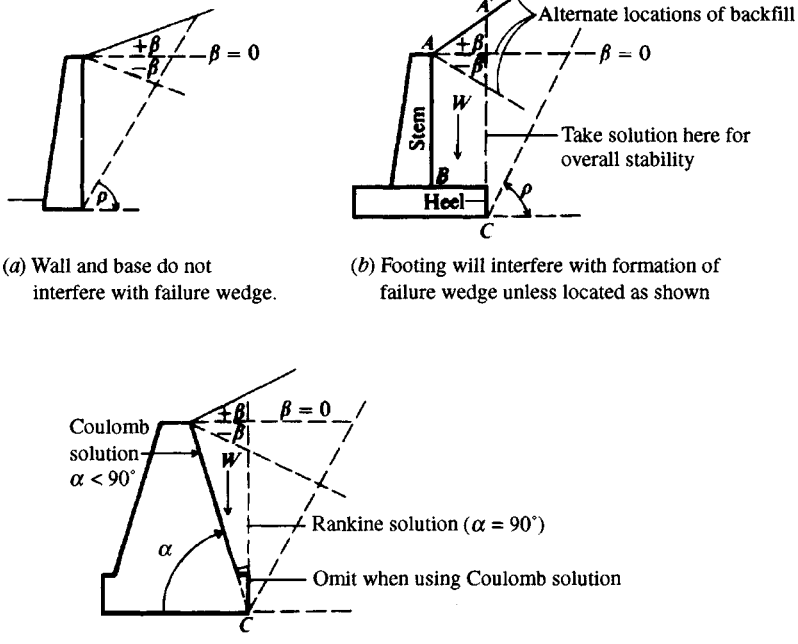

(*a*) Wall and base do not interfere with failure wedge.

(*b*) Footing will interfere with formation of failure wedge unless located as shown

(c) Backslope and footing will interfere with failure wedge unless located as indicated.

Figure 11-13 Rankine wedge locations for valid solutions. In (*b*) and (*c*) include weight W in stability computations.

The actual wall pressure in this case depends on wall rigidity (in terms of displacement) and compaction effort. Usually compaction-induced wall pressures produce a resultant wall force close to midheight versus the one-third height for the active pressure case. This problem was discussed in Sec. 11-8.1, where it was given that one may use a lateral earth pressure coefficient

$$K_a \leq K \leq K_o$$

and either locate the resultant at the one-third point or use Eq. (11-15) to locate the resultant higher along the wall.

Figure 11-12*b* represents a common field situation where considerable engineering judgment is required to estimate the wall pressures. Considerable opinion holds that, when the b dimension shown on the figure is so narrow that the Rankine wedge does not form, some kind of arching action occurs. Handy (1985) considered arching in some detail and later Frydman and Keissar (1987) suggested that one might estimate the lateral pressure using a modification of Eq. (11-24) of Sec. 11-16 to read

$$\sigma_h = \frac{\gamma b}{2 \tan \delta} \left[1 - \exp(-2K \frac{z}{b} \tan \delta \right] \tag{11-18}$$

where γ = unit weight of backfill
b = backfill zone width

$\tan \delta$ = coefficient of friction
z = depth from top to where the lateral pressure σ_h is computed
K = lateral pressure coefficient

The value of K is critical—some use $K = K_a$, others use $K = K_o$, and still others use some intermediate value. It would appear reasonable to use K_a if the wall can rotate and K_o if the wall is rigid. Frydman and Keissar (1987) also give an equation for estimating K that depends on ϕ and δ as follows:

$$K = \frac{(\sin^2 \phi + 1) - \sqrt{(\sin^2 \phi + 1)^2 - (1 - \sin^2 \phi)(4 \tan^2 \delta - \sin^2 \phi + 1)}}{(4 \tan^2 \delta - \sin^2 \phi + 1)} \tag{11-19}$$

For $\phi = 32°$ and $\delta = 18°$ one obtains $K = 0.329$. The Rankine $K_a = 0.307$ but it has no provision for including the wall friction angle δ. This equation is somewhat sensitive to δ, so one should exercise care to try to estimate a "best" value. Equation (11-19) is programmed into program FFACTOR as option 8 on your program diskette.

Figure 11-12*d* presents a method where granular backfill is limited in availability, so some is placed to locate the "Rankine" zone adequately and then poor material is used in the region where it is not critical. The limited back face zone is for drainage and could be eliminated by using a vertical drainage geotextile against the wall. Here one would use the ϕ angle of the granular soil but a unit weight that is an average for the backfill. Since this backfill geometry requires careful field control, its use is a last resort.

11-11.2 Sloping and Irregular Backfill Surface

When the backfill is smooth or even, it may either be horizontal or have a $\pm\beta$ angle as illustrated in Fig. 11-13. The Rankine equations see only a (+) β angle, but the Coulomb equations recognize the β angle and its sign.

Additionally we may have a sloping dredge line (of Fig. 11-2). We would intuitively expect a (+) slope to increase the wall pressure and a (−) to decrease the pressure. This expectation is reflected in the Coulomb and Theory of Elasticity methods for both (+) and (−) β values and in the Rankine method for (+) values. The (−) values have particular value for walls using passive pressure in the soil below the dredge line. Occasionally walls supporting coal piles and the like may have a negative slope as the stored material is depleted.

Where the ground is irregular, we may estimate the exit of the Rankine zone (line AC of Fig. 11-7) and in region BC treat the irregular surface as either a best-fit slope or as a uniform surcharge and use the equations for the case; for example in Fig. 11-14*a* we might smooth out the irregular slope $B'FE$, measure the resulting β angle, and use either the Rankine or Coulomb equation to obtain a lateral pressure coefficient.

Alternatively, we may also use the trial wedge method in Sec. 11-11.3, particularly if we want a better estimate of the location of the rupture line.

11-11.3 Surcharges on Backfill

Surcharges such as point, line, strip, or finite area loads may be on the backfill and increase the lateral pressure. Neither the Coulomb nor the Rankine equations have provision for these types of surcharges. The graphical and computer methods of the next section and the Theory of Elasticity method of Sec. 11-13 are often used to obtain lateral earth pressures for backfill loads.

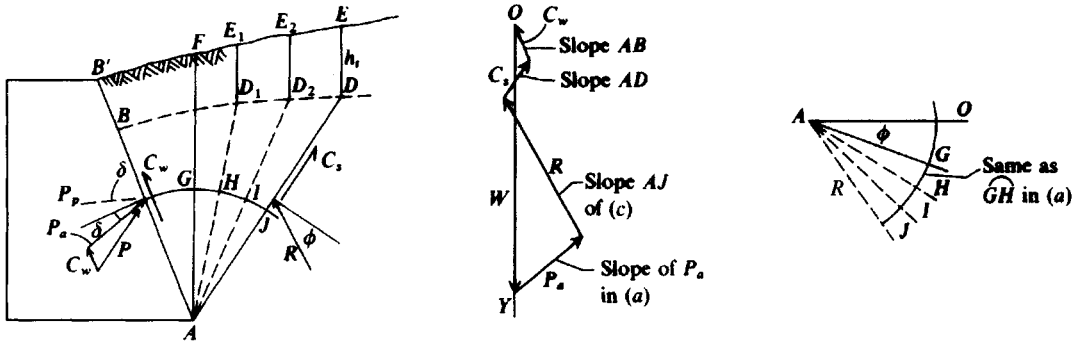

(*a*) Forces acting on a trial wedge *AB'ED*

(*b*) Forces acting on *AB'ED* formed into the force polygon

(*c*) Rapid method of establishing the slope of *R*

C_w = *AB* · cohesion (direction and magnitude known)
C_s = *AD* · cohesion (direction and magnitude known)
W = weight of trial wedge (direction and magnitude known)

R = known in direction
P_a = known in direction

Figure 11-14 The trial wedge active force solution. For passive force slope of P_p is shown; slope *R* changes, C_s, C_w reverse directions.

From the several solutions by these methods shown in Table 11-7 (Sec. 11-13), it is suggested that the Rankine or Coulomb solution may be better than the graphical methods for surcharges located within the Rankine wedge defined by the angle ρ (Slope of *AC* shown on Fig. 11-7*a*).

If the surcharge is located within this zone, simply convert the surcharge to a vertical load, divide by the distance *BC* (see also the figure on Table 11-7), and treat the result as a surcharge *q*.

If the surcharge lies outside the distance *BC* the best solution is generally the Coulomb or Rankine method plus the contribution from using the Theory of Elasticity of Sec. 11-13.

A special case of backfill surcharge is one located a distance *d* from the back face of the wall. Motta (1994) has produced a closed-form solution but the equations are difficult. They have been programmed in subroutine MOTTAKA in program FFACTOR as option 9; data are input using screen prompts. All the values in MOTTAKA have been previously used (i.e., consistent notation).

11-12 GRAPHICAL AND COMPUTER SOLUTIONS FOR LATERAL EARTH PRESSURE

There are graphical solutions for estimating lateral forces when the backfill is irregular-shaped or loads are concentrated. Neither of these cases is consistent with the Rankine or Coulomb theories. Among the several solutions are Culmann's (ca. 1886), the trial wedge method (ca. 1877), and the logarithmic spiral.

An analytical solution based on the Theory of Elasticity can also be used. This is particularly suited for computer use.

The Culmann and trial wedge methods are very similar except for the general orientation of the force polygons. Both methods rely on computing the known forces on a trial wedge, which include any external load on the backfill, the weight of the trial wedge, and the shear force on the tentative (or trial) rupture surface, and, from known slopes of the unknown wall force vector P_a (or P_p) and the unknown resultant force *R* on the rupture surface, plotting

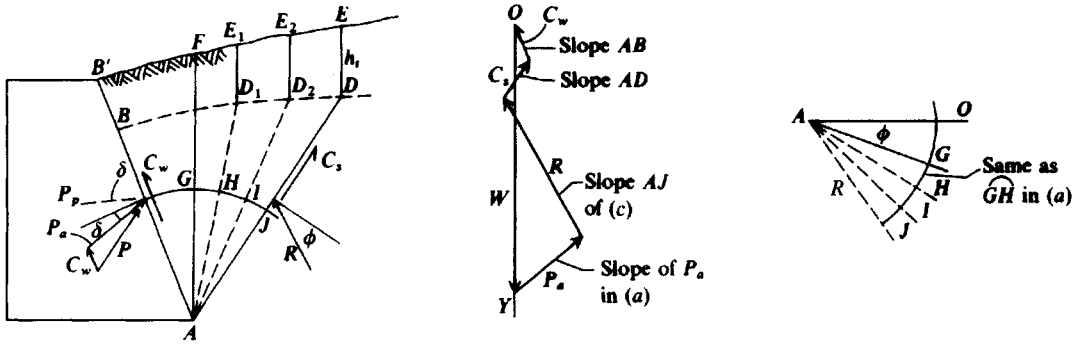

(*a*) Forces acting on a trial wedge *AB'ED*

(*b*) Forces acting on *AB'ED* formed into the force polygon

(*c*) Rapid method of establishing the slope of *R*

C_w = *AB* · cohesion (direction and magnitude known)
C_s = *AD* · cohesion (direction and magnitude known)
W = weight of trial wedge (direction and magnitude known)

R = known in direction
P_a = known in direction

Figure 11-14 The trial wedge active force solution. For passive force slope of P_p is shown; slope *R* changes, C_s, C_w reverse directions.

From the several solutions by these methods shown in Table 11-7 (Sec. 11-13), it is suggested that the Rankine or Coulomb solution may be better than the graphical methods for surcharges located within the Rankine wedge defined by the angle ρ (Slope of *AC* shown on Fig. 11-7*a*).

If the surcharge is located within this zone, simply convert the surcharge to a vertical load, divide by the distance *BC* (see also the figure on Table 11-7), and treat the result as a surcharge *q*.

If the surcharge lies outside the distance *BC* the best solution is generally the Coulomb or Rankine method plus the contribution from using the Theory of Elasticity of Sec. 11-13.

A special case of backfill surcharge is one located a distance *d* from the back face of the wall. Motta (1994) has produced a closed-form solution but the equations are difficult. They have been programmed in subroutine MOTTAKA in program FFACTOR as option 9; data are input using screen prompts. All the values in MOTTAKA have been previously used (i.e., consistent notation).

11-12 GRAPHICAL AND COMPUTER SOLUTIONS FOR LATERAL EARTH PRESSURE

There are graphical solutions for estimating lateral forces when the backfill is irregular-shaped or loads are concentrated. Neither of these cases is consistent with the Rankine or Coulomb theories. Among the several solutions are Culmann's (ca. 1886), the trial wedge method (ca. 1877), and the logarithmic spiral.

An analytical solution based on the Theory of Elasticity can also be used. This is particularly suited for computer use.

The Culmann and trial wedge methods are very similar except for the general orientation of the force polygons. Both methods rely on computing the known forces on a trial wedge, which include any external load on the backfill, the weight of the trial wedge, and the shear force on the tentative (or trial) rupture surface, and, from known slopes of the unknown wall force vector P_a (or P_p) and the unknown resultant force *R* on the rupture surface, plotting

a force polygon and graphically obtaining the wall force P_a or P_p. The log spiral method is similar but uses a log spiral segment to define the rupture surface, whereas the Culmann and trial wedge methods use a plane surface.

Current analysis trends are to use a computer as much as practical, and for this reason the only methods considered by the author are the trial wedge method (which can be programmed for an irregular-shaped backfill and any number of surcharge loads) and the Theory of Elasticity method. For the interested reader the third edition of this book contains adequate descriptions of both the Culmann and logarithmic spirals.

Computations using the trial wedge method can produce greatly different lateral pressures from those resulting from the Theory of Elasticity (or Boussinesq) method. It is probable that the trial wedge is overly conservative, whereas the Theory of Elasticity method may be slightly unsafe. In any case we will look at the two procedures, recognizing that there will be cases where one procedure may be preferable.

11-12.1 The Trial Wedge Method

As previously noted, the trial wedge and Culmann procedures are identical except for orientation of the force polygon. The trial wedge also has an advantage over the Culmann solution since one can have cohesion as a soil parameter. Figure 11-14 illustrates the general procedure, which may be outlined as follows:

1. Draw the wall and ground surface to a scale that is as large as possible and compute the depth of the tension crack as

$$h_t = \frac{2c}{\gamma \sqrt{K_a}}$$

   This value of h_t is then plotted at sufficient points to establish the tension-crack profile (dashed line BD_1D_2D of Fig. 11-14*a*).
2. Lay off trial wedges as $AB'E_1D_1$, $AB'E_2D_2$, ..., and compute the weight of the corresponding wedges as $w_1, w_2, \ldots, w_n$. With a tension crack it may be preferable to compute the weights as the sum of the tension block plus the weight of the triangle (as in Ex. 11-6).
3. Compute C_w and C_s (note that C_w is a constant) and lay off C_w as indicated in Fig. 11-14*b* to the wall slope and to the appropriate force scale. As a tension crack can form along the wall, the length AB (and not AB') should be used to compute C_w. Also draw the weight vectors $\mathbf{w}_1, \mathbf{w}_2, \ldots, \mathbf{w}_n$ along the line OY. Note that the slopes are transferred from the wedge to the force polygon.
4. From the terminus of C_w lay off C_s at the slope of the assumed trial failure wedges.
5. Through points $w_1, w_2, \ldots, w_n$ established in step 3, lay off a vector P_a to the correct slope. Note that the slope of P_a (or P_p) is constant.
6. Through the terminus of C_s lay off the vector R to the appropriate slope. The slope is at the angle ϕ to a perpendicular to the assumed failure surfaces $AD_1, AD_2, AD_3, \ldots$.
7. The intersection of the R and P_a vectors establishes a locus of points, through which a smooth curve is drawn.
8. Draw a tangent to the curve obtained in step 7, parallel to the weight vector, and draw the vector P_a through the point of tangency. As with the Culmann solution, several maximum values may be obtained. The largest possible value of P_a is the design value.

The slope of the R vector (step 6 preceding) can be established conveniently (Fig. 11-14*c*) as follows:

1. To some radius r draw the arc GJ from the vertical line AF in Fig. 11-14*a*.
2. Draw a horizontal line AO and lay off the angle ϕ as shown. With the same r used in step 1, draw arc OJ using A as the center.
3. Then AG is the slope of the vector R to failure plane AF.
4. Now lay off arcs GH, HI, IJ in Fig. 11-14*c* to the same arc length used in step 1.
5. The slopes of lines AH, AI, and AJ of Fig. 11-14*c* are the corresponding slopes of the vector R to failure surface AD_1, AD_2, ...

In cohesionless materials the values C_w and C_s are zero, and the trial wedge solution is the same as the Culmann solution except for the orientation of the force polygon.

There are a number of alternative methods of plotting the force polygon. These came about because of the great difficulty in transferring the slope of the wedge line (AD, AD_2, AD_1 of Fig. 11-14*a*) and the slope of the R vector. The slope of R can be obtained from the method shown as Fig. 11-14*c* but must then be transferred to the force polygon of Fig. 11-14*b*. Accurate slope transfer requires using as large a scale for the plots as possible and careful attention to detail. If the force scale is too small or the slope transfer (usually using two triangles) includes any slip, the measured value of P_a (or P_p) can be in error by 10 to 20 percent or more. For these reasons a computer program with sufficient output to reproduce the "failure" wedge is much preferred.

Example 11-6. Solve the soil-wall system of Fig. E11-6 using the trial wedge method.

Solution.

1. The problem is plotted to scale as shown with line AB drawn vertically through the heel of the wall. Locate the ground surface and plot concentrated loads as shown. Also plot the tension crack profile at depth $z_t = 1.5$ m.
2. We will assume $\mathbf{P}_a$ acts horizontally as shown (although a friction angle of $\delta = \phi$ might be a better assumption for soil-to-soil on vertical face AB).
3. Compute adhesion on vertical face AB using an effective distance of

$$z_e = H - h_t = 6.1 - 1.5 = 4.6 \text{ m}$$

   Use full cohesion along z_e for soil-to-soil.
4. Next lay off a trial wedge such as $ABCI$ and compute weight. Also compute cohesion C_s = distance $AI \times$ cohesion, etc.
5. Draw arc XY from A and similarly in the small inset (at same scale), and from AX of inset lay off $\phi = 20°$ and then locate points 1 through 7 as shown. $A1$ = slope of first R, $A2$ = slope of second R, etc., which are directly transferred to the force polygon as extended lines that are intersected by P_a from the $\mathbf{W}$ vector to complete the force polygon for any given trial wedge.

////

Calculate $h_t = \frac{2c}{\gamma\sqrt{K_a}}$ $\frac{20}{19.0 \times 0.70} = 1.50$ m

Calculate cohesion C_i:

$C_w = 4.6(10) = 46$ kN
$C_1 = 5.7(10) = 57$ kN
$C_2 = 6.0(10) = 60$ kN
$C_3 = 6.4(10) = 64$ kN
$C_4 = 7.0(10) = 70$ kN
$C_5 = 7.6(10) = 76$ kN
$C_6 = 8.35(10) = 84$ kN
$C_7 = 9.1(10) = 91$ kN

W_i	= Triangle crack block + Triangle i		$+W_{i-1}$	$\Sigma = W$
W_1	$1.2 \times 34.2 \times 19 + \frac{1}{2}(5.7 \times 0.97)(19)$ =	86.7	0	86.7
W_2	$1 \times 28.5 \times 19 + \frac{1}{2}(6.0 \times 0.93)(19)$ =	81.5	86.7	168.2
W_3	$28.5 + \frac{1}{2}(6.4 \times 0.86)(19)$ =	80.8	168.2	249.0
W_{4L}	$28.5 + \frac{1}{2}(7.0 \times 0.80)(19)$ =	81.7	249.0	330.7
W_{4R}	35.0 =		330.7	365.7
W_5	$28.5 + \frac{1}{2}(7.6 \times 0.72)(19)$ =	80.5	365.7	446.2
W_{6L}	$28.5 + \frac{1}{2}(8.4 \times 0.67)(19)$ =	82.0	446.2	528.2
W_{6R}	40 =		528.2	568.2
W_7	$1 \times 28.5 \times 19 + \frac{1}{2}(9.1 \times 0.61)(19)$ =	81.2	568.2	649.4

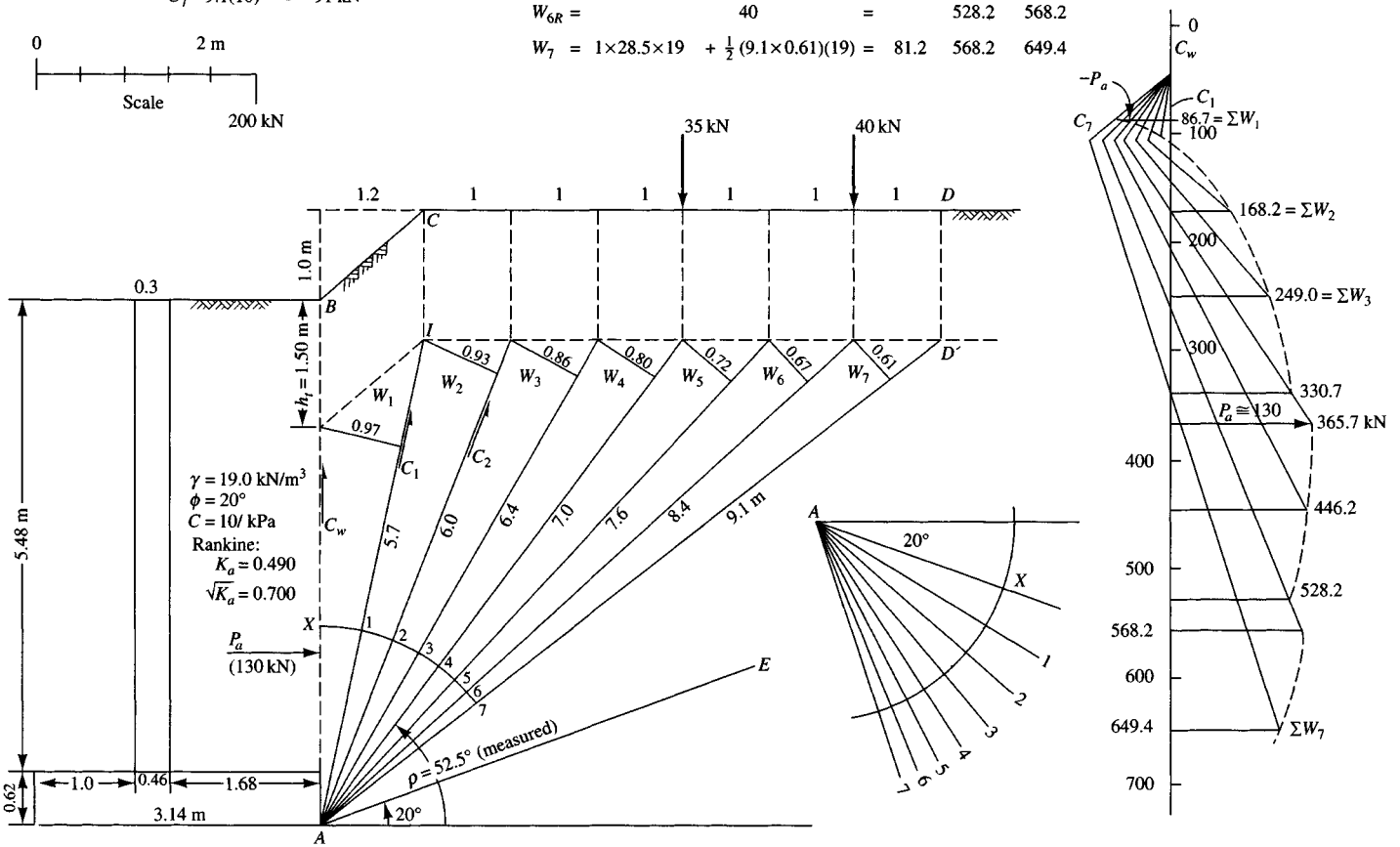

Figure E11-6

11-12.2 Computer Solution of Trial Wedge

The simplest method of solving the trial wedge (or Culmann) method is to use a computer solution, for which it is necessary to do the following:

1. Draw the wall-soil geometry to scale and obtain coordinates for sufficient points to plot the ground profile and to locate any loads on the backfill. If a plotter is available and one desires to plot the output, enough additional coordinates must be obtained and input to plot the wall geometry.
2. Program a solution of the force triangle of Fig. 11-14*b* for P_i. This involves two unknown variables: the wall force P_i and the wedge resultant, labeled R, at the orientations (or slopes) shown on Fig. 11-14*a*. Since the force polygon must close and we know the slopes of the unknown vectors, a direct analytical solution for P_i can be made.
3. Initialize the computations by using a starting soil wedge, say AFE_1D_1 with angle FAD_1 of about 5° (depending on whether AF is vertical), and increment the wedge angle in 1° increments. Solve the soil wedge twice at all point loads (dx to left and dx to right).
4. Sort the P_i values computed from steps 3 and 4 until all concentrated loads have been accounted for and P_i has decreased at least two consecutive times. Stop the computations and print out the maximum P_i and the corresponding ρ angle. This procedure allows for study of parametric effects (ϕ, δ, c, and γ) much more easily than with the graphical procedures previously discussed (and illustrated in Example 11-6).

Example 11-7. Redo Example 11-6 using computer program SMTWEDGE (B-7) provided on your program diskette.

Solution. Refer to Fig. E11-6 for general geometry. Arbitrarily set the coordinates at the wall heel (point A) at $X = 1.68$, $Y = 0.0$ m. There are two lines defining the backfill, so we give coordinates at point B as $X = 1.68$, $Y = 6.10$ (consistent with coordinates at point A). At point C, $X = 1.88$, $Y = 7.10$. Give coordinates at D a large value ($X = 10.00$, $Y = 7.10$). In a similar manner the coordinates for the two loads can be obtained (see computer output sheet Fig. E11-7 on next page).

The above dimensions allow us to develop the input data set (given on your diskette as TWEDGE.DTA, which you can print for inspection). All of the input data are shown on the output sheet but not in a format suitable for program execution. It is necessary to specify a tension crack using parameter ITENCR = 1, otherwise the cohesion is not used. Also specify IHEEL = 1 to increment at 1° trial wedges. From the output we obtain $P_a = \mathbf{130.8}$ kN (versus 130 kN of hand solution). It took 34 trials and $\rho = 53.1°$ from the horizontal.

////

11-12.3 Point of Application of Wall Force P_a

The following procedure to find the point of application of the wall force P_a was suggested by Terzaghi (1943). This procedure for case 1 (following) for a sloping or horizontal backfill with no concentrated loads gives the point as $H/3$ as from the theoretical case. For the other cases the user will have to decide if the procedure is valid. Note that case 3 is highly speculative since it is questionable that a concentrated load outside the failure wedge contributes much (if any) increase in P_a.

CASE 1. There are no concentrated loads (Fig. 11-15*a*), but there may be other surcharges.

a. Find the center of gravity of the failure wedge graphically or by trimming a cardboard model and hanging it by a thread at two or three points.

```
EXAMPLE 11-7.  REDO EXAMPLE 11-6 TO CHECK GRAPHIC SOLUTION

          ++++ DATA FILE NAME FOR THIS EXECUTION:  TWEDGE.DTA

          TYPE OF EARTH PRESSURE PROB = ACTIVE

LINE NOS AND END COORDS LEFT END FIRST
LINE NO      X1          Y1          X2          Y2
  1        1.6800      6.1000      2.8800      7.1000
  2        2.8800      7.1000     10.0000      7.1000

        NO OF LINES =    2   NO OF CONC LOADS =    2
    UNIT WT OF SOIL = 19.000 KN/M**3
ANGLES:  SOIL (PHI) = 20.000 DEG
               WALL = 90.000 DEG
              DELTA =   .000 DEG
      SOIL COHESION =  10.000 KPA     WALL ADHES FACTOR = 1.000
INITIAL COORDINATES:
 XSTART =    1.680    YSTART =     .000  M
   XTOP =    1.680      YTOP =    6.100  M


THE CONC LOADS AND COORDS:

  1        35.000      5.880      7.100
  2        40.000      7.880      7.100


   HT OF TENSION CRACK =   1.5033
 ORIGINAL AND REVISED Y-COORDS:

I =   1  Y(I,J) =    6.100    7.100    YP(I,J) =    4.597    5.597
I =   2  Y(I,J) =    7.100    7.100    YP(I,J) =    5.597    5.597


 THE MAXIMUM VALUE OF ACTIVE EARTH PRESSURE =  130.804   KN ++++
                   THE RHO ANGLE FROM HORIZ =   53.115 DEG
                           NO OF ITERATIONS =   34
```

Figure E11-7

---

b. Through the center of gravity and parallel to the failure surface draw a line of action for P_a until it intercepts AB (wall or plane through the heel of the cantilever wall). P_a acts at an angle of δ or β to a perpendicular to AB.

CASE 2. There is a concentrated load or line load within the failure wedge (Fig. 11-15*b*).

a. Parallel to AC draw line Pc', and parallel to AC_f draw PC'_f.

b. Take one-third of distance $c'c'_f$ from c' for the point of application of P_a.

CASE 3. There is a concentrated load or line load outside the failure wedge (Fig. 11-15*c*).

a. Draw a line from the concentrated load to $A(PA)$.

b. Draw Pc' parallel to AC.

c. Take one-third of $c'A$ from c' for the point of application of P_a.

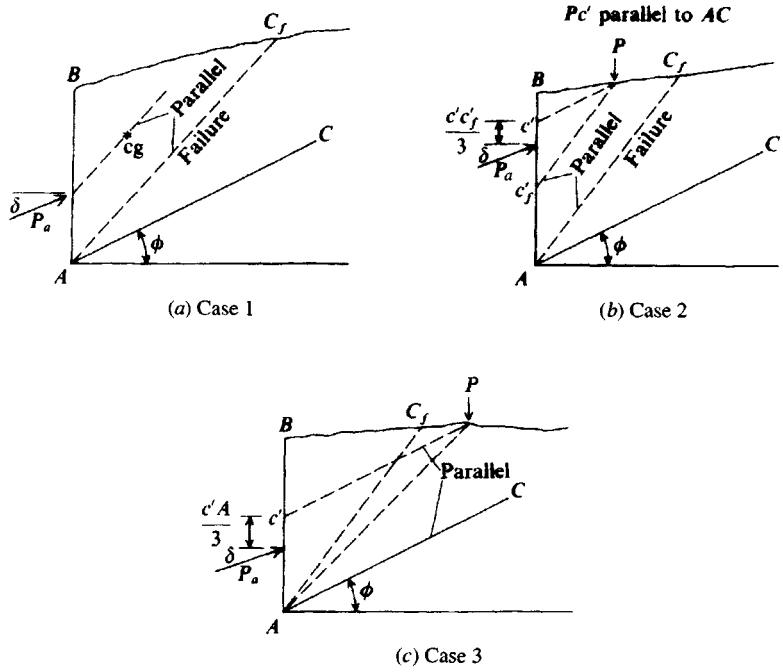

Figure 11-15 Procedures for location of point of application of P_a for (*a*) irregular backfill; (*b*) concentrated or line load inside failure zone; (*c*) concentrated or line load outside failure zone (but inside zone *ABC*).

The author suggests the best solution for total wall force and point of application when there are backfill loads of any type and location is to use one of the following:

1. If the backfill load is inside the Rankine zone, convert it to an equivalent surcharge over the Rankine zone, then obtain the wall pressure and resultant using either the Coulomb or Rankine equations.
2. If the backfill load is either inside or outside the Rankine zone, use the Coulomb or Rankine equations for the soil wedge with no backfill load. Next use the Theory of Elasticity equations given in Sec. 11-13 to find the wall forces from the backfill loads. Then to find total force and point of application use $\sum P = R = \sum P_i$ and $R\bar{y} = \sum P_i y_i$.

11-13 LATERAL PRESSURES BY THEORY OF ELASTICITY

The Boussinesq Equation

The trial wedge method seems to be too conservative in estimating the lateral force against a wall when there are surcharges (or loads) on the backfill—particularly outside the Rankine zone. For this reason, at present this procedure does not seem to be used much. The Theory of Elasticity method can be used to compute the lateral pressure profile against the wall from the surface surcharge (point, line, strip) loading. The Boussinesq equation—or some variation of it—is commonly used. The equation form usually credited to Boussinesq is

$$\sigma_r = \frac{P}{2\pi z^2}\left[3\sin^2\theta\cos^3\theta - \frac{(1-2\mu)\cos^2\theta}{1+\cos\theta}\right] \tag{11-20}$$

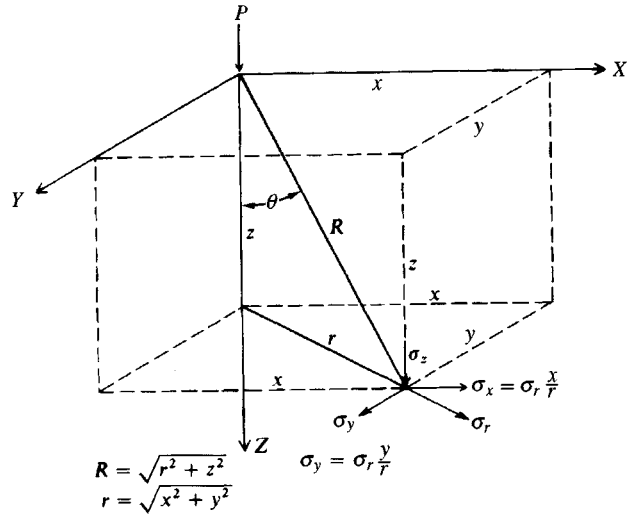

Figure 11-16 Identification of terms used in the Boussinesq equation [Eq. (11-20)] for lateral pressure.

Equation (11-20) can also be written as

$$\sigma_r = \frac{P}{2\pi}\left[\frac{3r^2 z}{R^5} - \frac{1-2\mu}{R(R+z)}\right] \tag{11-20a}$$

where the several terms including θ, z, r, and R are identified on Fig. 11-16. This form of the equation is particularly suitable for programming on a small calculator, since the point load P is usually fixed with given x, y coordinates and we want to vary z to obtain the wall pressure profile.

The computer programming of this equation allows one to solve any of the given backfill surcharge loads of Fig. 11-17 defined as follows:

1. Point load. Use the equation in the given form.
2. Line load. Treat as either one load or a series of concentrated loads along a line of unit width acting on unit areas.
3. Strip load. Treat as a series of parallel line loads acting on strips of some unit width.
4. Loaded area. Treat as a series of parallel line loads acting on strips of finite length.

We can easily analyze a constant uniformly loaded area (say, the interior part of an embankment) or one with a linear varying load (say, the embankment side slopes). In either of these cases the loaded area is divided into strips with some load intensity q and some small "unit" width B, on the order of 0.25 to 0.5 m. These strips are then subdivided into "unit" areas of some length L also on the order of 0.25 to 0.50 m. These "unit" areas are treated as a series of point loads of $Q = qBL$ acting at the center of each of the unit areas. The several "unit" area contributions making up the total loaded area are then summed to obtain the total lateral pressure acting at some point at the depth of interest (either in the soil or on a wall). This is the procedure used in program SMBLP1 (B-8) on your program diskette.

The general validity of using a form of Eq. (11-20) for surcharges was established in several publications, including the work of Spangler (1936), Spangler and Mickle (1956), Rehnman and Broms (1972), and others.

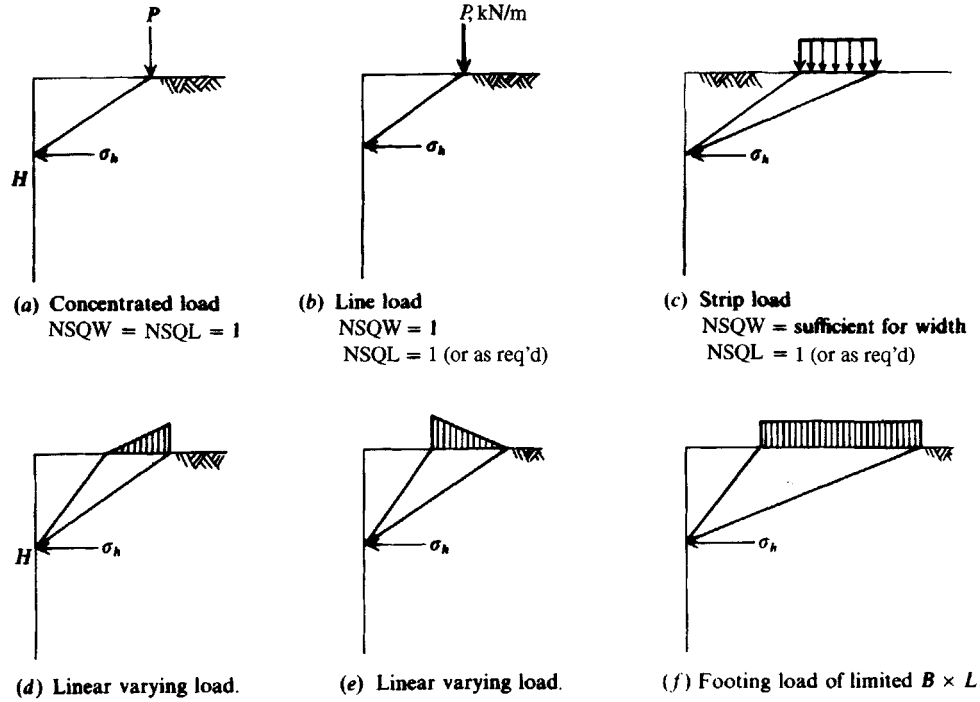

Figure 11-17 Surcharge loads that can be used with the computer program SMBLP1 (B-8) on your program diskette. NSQW, NSQL = number of unit elements away from wall and parallel to wall, respectively, as used in the computer program.

The early work of Spangler and Spangler and Mickle introduced an error into the general application of the equations; however, that can be avoided by direct use of Eq. (11-20) and an appropriate value for Poisson's ratio μ.

When the work of Spangler was first published, he used $\mu = 0.5$ [and later in Spangler and Mickle (1956)], which substantially simplifies Eq. (11-20)—but may not be correct. Spangler's work consisted of trying to measure the lateral pressure against a 1.829 m (2.134 m total height) high × 4.572 m wide retaining wall with a constant stem thickness of 0.150 m. He used metal ribbons (since earth-pressure cells were not readily available in the early 1930s) and simply dumped a granular ($w_L = 17.5$, $w_P = 13.2\%$) backfill behind the wall with no compaction at all to produce an extremely loose state. After a time, he had a truck backed onto the loose backfill so that the rear wheels could simulate two concentrated loads. To simulate a line load he laid a railroad crosstie parallel to the wall, onto which the rear wheels (a single axle with dual tires) of a loaded truck were backed. Since the wall was only 4.572 m long and a railroad crosstie is about 3 m long, a strip model was not very likely to have been produced.

From these efforts Spangler (both references) found that the measured lateral pressure was about twice that predicted by Eq. (11-20) with $\mu = 0.5$. From the reported results, Mindlin (1936*a*), in discussing Spangler's (1936) work suggested that the factor of 2 could be explained by a rigid wall producing the effect of a mirror load placed symmetrically in front of the wall (Fig. 11-18*a*). The author began looking at this problem more closely and decided that the mirror load is not an explanation. As shown in Fig. 11-18*b*, a mirror load on a rigid

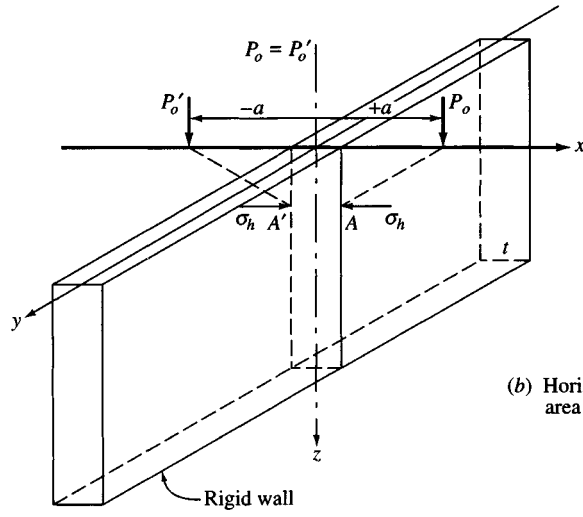

(*a*) Mirrored loads on rigid wall.

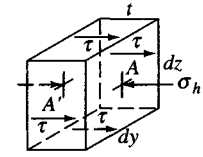

(*b*) Horizontal stress σ_h on differential area $dy\,dz$.

Figure 11-18 The case for lateral pressure on a rigid wall.

wall would simply cancel the lateral shear stresses in the wall and certainly not double the horizontal pressure. A flexible wall could possibly double the lateral pressure but would have to be extremely flexible (and have the loads applied sequentially). Referring to Fig. 11-18*b*, we see that the horizontal pressure σ_h produced by P_o (applied first) acting on a rigid area of $dy\,dz$ would develop shear resistance τ such that $\tau t(2dz+2dy) = \sigma_h$. When mirror load P_o' is applied, a second shear stress τ would develop on the element but in the opposite direction, so the shear stress would cancel and we would simply have on each side of the wall a horizontal stress σ_h (not $2\sigma_h$). If the wall is flexible and little shear stress develops, the element would (if the loads were applied sequentially) displace laterally toward the $-a$ direction to produce a resisting soil stress on the $-a$ side of $\sigma_h' = \sigma_h - \tau(2dz + 2dy)$. Since this would become locked in when P_o' is applied, the stress on the left would become $\sigma_h + \sigma_h'$, and since σ_h' is transmitted through the wall, the right side would also have the existing σ_h+ transmitted σ_h' value from load P_o'. If the loads were applied simultaneously the stresses would simply be σ_h on each side (and not $2\sigma_h$).

Mindlin got around this complication by inserting a statement that the wall was rigid but could not carry shear. There is no such wall type known to the author.

Because the Spangler work was done in the early 1930s, it is difficult to speculate on the cause of the high stresses except to note that the wall had rather finite dimensions. The surcharge load was caused by a truck backing onto the backfill. When it stopped at the desired position it would have produced an inertial force that was amplified because the fill was not well compacted. The backfill probably was of limited extent, so that it is also possible some type of arching occurred that increased the lateral pressure.

More recently Rehnman and Broms (1972) showed (using modern earth-pressure cells) that when the soil behind the wall was dense the lateral pressure from point loads was much less than when the soil was loose. They also found that gravelly backfill produced larger lateral pressures than finer-grained materials. This observation indicates that both soil state and Poisson's ratio are significant parameters.

Theory of elasticity gives the limiting range of Poisson's ratio as

$$-1 \leq \mu \leq 0.5$$

Also note that, strictly, there is a sign with μ, so that (+) means an elongation strain with lateral contraction, as for a tensile steel test that gives $\mu = 0.3$, and a compression strain with lateral expansion, as for a concrete test cylinder giving $\mu \approx 0.15$. No engineering material is known that might give a (−) ratio where there is lateral expansion with elongation or lateral contraction with compression.

In Chap. 2 it was stated that for soils, values of μ can be greater than 0.5 with values of 0.6 and 0.7 fairly common because soil is only pseudoelastic.

Equation (11-20) and similar expressions do not compute reliable wall pressures for surcharge loads (point, strip, or line) unless the loads are located beyond some critical distance from the wall. Laba and Kennedy (1986) suggested this distance might be $0.4H$. Terzaghi (1954) had also suggested $0.4H$ might be the critical distance and provided two equations, based on Eq. (2-20) but with $\mu = 0.5$: one for the surcharge distance $< 0.4H$ from the wall and a second for the surcharge distance $> 0.4H$.

With this background, it is clear that approximations to using Eq. (11-20) should be used cautiously. There are a number of closed-form solutions for select cases of backfill loads; however, the author has found substantial differences, particularly for variable intensity loading. For these several reasons, and because Eq. (11-20) can be easily programmed *for all the cases,* it is the only method recommended by the author. Comparison with closed-form solutions indicates almost no error from using discrete methods for continuous loadings.

There is some misuse of Eq. (11-20) or its equivalent caused by setting $\mu = 0.5$ so the μ term disappears. For example, line and strip loads of infinite length should be treated as plane strain problems. That is, take a unit length parallel to the wall similar to the procedure for surcharges.

For both line and strip surcharges, Terzaghi (1943) performed integrations on the modified Eq. (11-20) using $\pm\infty$ for the limits—but stated that these loadings were plane strain problems. In using Eq. (11-20) one should be using a plane strain μ' [see Eq. (2-65)] instead of the triaxial value (or a value estimated at around 0.3 to 0.4). Note the following short table for the plane strain μ' versus triaxial μ:

μ =	0.3	0.33	0.35	0.40	0.45	0.50	0.60
μ' =	0.42	0.50	0.54	0.67	0.82	1.00	1.50

Table 11-7 illustrates the case of a small retaining wall with a concentrated load at varying distance, using a range of Poisson's ratio. This wall also includes the trial wedge solution for the several load positions and the Rankine lateral pressure computed for no surcharge. From this table several conclusions can be drawn:

1. The trial wedge method gives the Coulomb (or Rankine if $\delta = 0$) wall force for a horizontal backfill and correctly locates the failure surface using angle ρ measured from the horizontal. For concentrated surcharges on the backfill, much larger wall forces are obtained than by any other method.
2. Poisson's ratio $\mu = 1$ gives a substantial increase in wall pressure versus $\mu = 0.3$ to 0.5. A plane strain $\mu' = 1.00$ may be possible for soil in a very loose state.

TABLE 11-7

Comparison of trial wedge and Boussinesq wall forces computed using Eq. (11-20).

Also shown is the Coulomb active pressure force.

						2.217 m				
Load position from wall, m	**0**	**0.3**	**0.6**	**1.0**	**1.3**	**1.6**	**2.0**	**2.3**	**2.6**	**3.0 m**
Trial wedge, kN		65.0	65.0	65.0	65.0	64.8	63.4	61.6	59.3	55.5
Coulomb $P_a = \frac{1}{2}(17.30)(4)^2(0.276) = 38.2$ kN (vs. 38.1 of trial wedge)										
Boussinesq					Inside			Outside		
$\mu = 0.3$	—	8.8	8.3	5.3	4.1	3.3	2.5	2.1	1.8	1.4
0.5	—	13.1	11.5	7.5	5.8	4.6	3.6	3.0	2.5	2.1
0.7	—	18.0	14.8	9.7	7.5	6.0	4.6	3.9	3.3	2.7
1.0	—	25.3	19.9	13.0	10.0	8.1	6.2	5.2	4.5	3.7

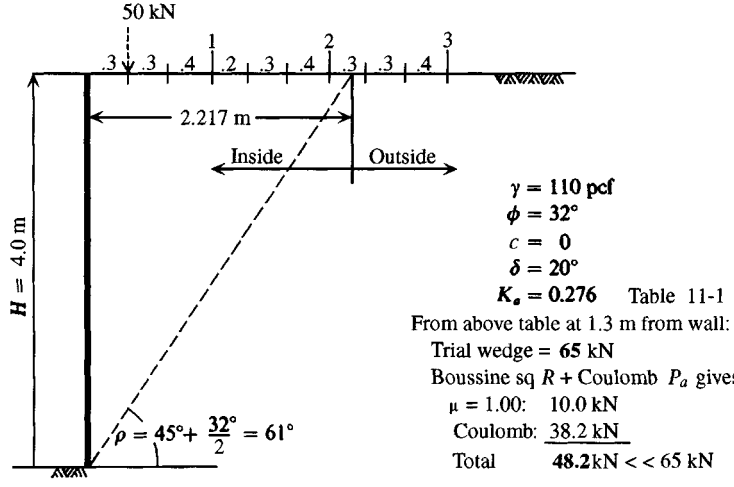

3. Concentrated loads well outside the Rankine zone contribute to P_a in the trial wedge case, leading one to the opinion that the trial wedge is not correct, but conservative.
4. Since Eq. (11-20) gives small lateral pressures when the load is very close to the wall, this result may mean either that the surcharge load is being carried downward by vertical wall friction rather than by lateral pressure or that Eq. (11-20) is not valid for a load close to such a massive discontinuity in the elastic half-space.
5. Wall pressures computed by Eq. (11-20) are rather small once the wall-to-load distance is greater than the Rankine zone.

Computer Program for Lateral Pressure

Computer program SMBLP1 (B-8) on your program diskette can be used for all the lateral pressure problems shown on Fig. 11-17. By superposition, almost any conceivable surcharge load can be analyzed, quite rapidly in most cases.

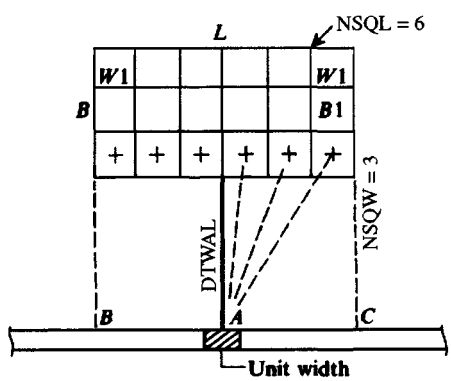

(*a*) Plan dimensions. DOP is perpendicular to DTWAL and there are three cases shown
At A: DOP = $L/2$ (can use + or –)
B: DOP = $+L$
C: DOP = $-L$

Note accumulation at point on wall from element centroids.

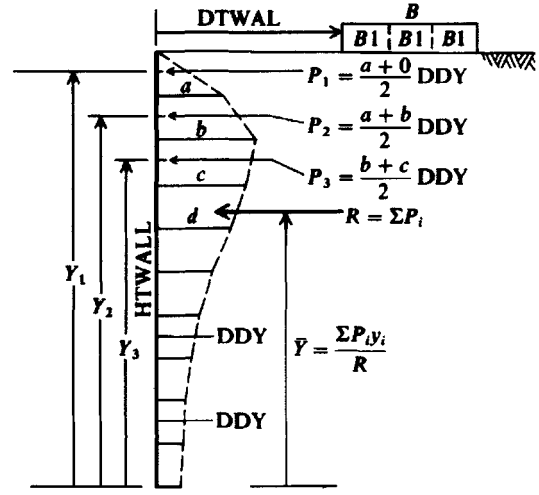

(*b*) Elevation showing HTWALL. Here the wall uses 10 elements with 11 points (NVERT = 11). Also shown is method used by computer (slightly approximate) to compute wall resultant and $\bar{y}$.

Figure 11-19 General method used in computer program to obtain wall pressure profile, wall resultant R, and point of application $\bar{y}$. Variables used in computer program are shown to identify dimensions required for analysis.

The program is written to solve Eq. (11-20) for a uniform or strip load modeled as a series of point loads located at the centroid of a small area. The area should be on the order of 0.3×0.3 m (1×1 ft) but does not have to be square (use 0.2×0.3, 0.3×0.4, etc.).

For a line load with the plane strain assumption, use a single point load perpendicular to the wall location where the pressure profile is wanted and use μ'. For a strip use a unit width opposite the wall, divided into as many unit areas as necessary to define the strip width, and again use μ'. For a finite-loaded area divide the load into as many unit areas as necessary and use μ (not μ'), but it can be > 0.5 based on your analysis of the soil state. The computer program also allows one to input a factor such as 2.0, 1.4, 1.2, 1.0, etc. to "adjust" the pressure for close proximity to the wall.

Note that Fig. 11-16 shows the lateral stress as a radial value. The program, however, uses the horizontal component, always assuming the distance to the load DTWAL is perpendicular to the wall face. Refer to Fig. 11-19 for select program variable identification and the method used to compute the wall force resultant and location $\bar{y}$.

Program SMBLP1 will be used to solve the following two examples. The first example illustrates the effect of μ on the lateral pressure and the second example examines the linear varying load and how to check certain types of problems.

Examples 11-8 and 11-9 show that the lateral pressure is heavily dependent on Poisson's ratio μ. Any lateral pressure equation that does not include Poisson's ratio has probably used $\mu = 0.50$, which may not be a bad estimate if it is used as a plane strain value since it corresponds to a triaxial type μ of about $\frac{1}{3}$.

Example 11-8. Find the lateral force against a 7.5 m wall from a 2×4 m loaded area that is 3 m from the wall as in Fig. E11-8*a*.

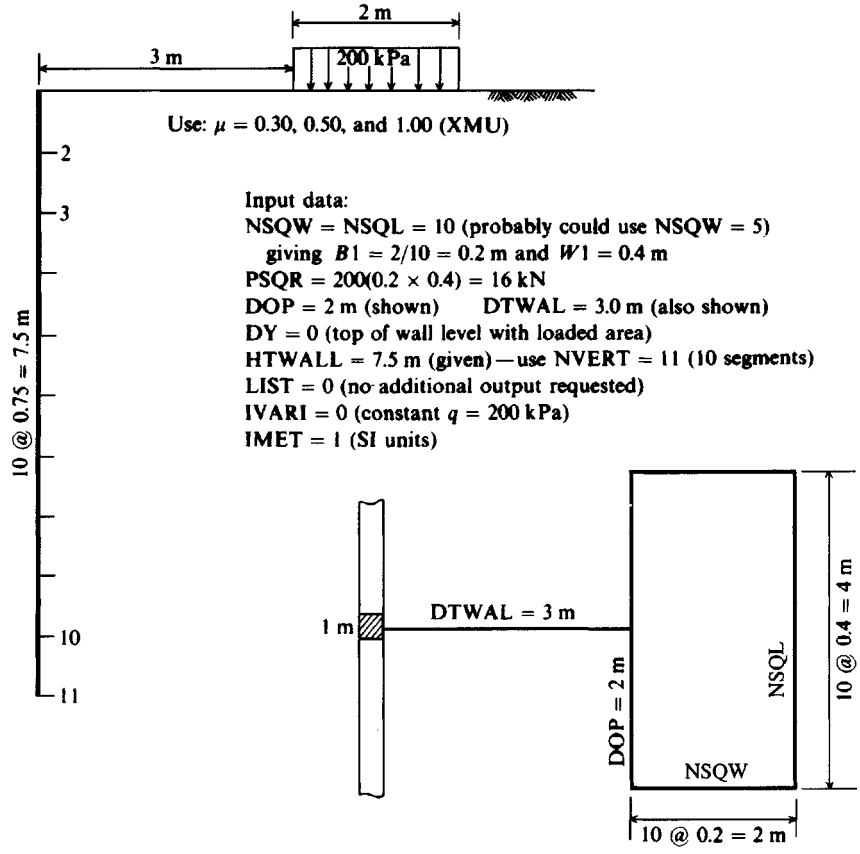

Figure E11-8*a*

Solution. We will use $\mu = 0.3, 0.5$, and 1.0.

Since the center of the loaded area will cause the greatest possible wall pressure, we will center the base on the wall point of interest.

From the sketch we see that the length is parallel to the wall, so we will use NSQW = NSQL = 10, giving unit areas that are $B1 = 0.2$ m × $W1 = 0.40$ m. The equivalent concentrated load on this unit area is

$$200 \text{ kPa} \times 0.2 \times 0.4 = 16 \text{ kN (input as PSQR since it is constant)}$$

For the text we will restrict the listing to only the input data and the solution.

Using 11 points on the wall gives DDY = 7.5/(NVERT − 1) = 0.75 m, which is computed in the program. With PSQR = constant, use IVARI = 0, DOP = 2 m since the wall is centered and DTWAL = 3.0 m (given data). Building a data file, we obtain Fig. E11-8*b* as I/O. We see that varying μ from 0.3 to 1.00 nearly triples the wall force and from 0.5 to 1.0 nearly doubles the wall force. Of interest in the next example is the wall force for $\mu = 0.50$ for resultant $R = 52.672$ kN shown on Fig. E11-8*b*.

Figure E11-8*b*

```
      +++ NAME OF DATA FILE FOR THIS EXECUTION:  LPRESS2.DTA

  EXAMPLE 11-8 USING POISSON'S RATIO = 0.3--1 POINT

     POISSON'S RATIO, XMU =    .30
NO OF CONTRIBUTING POINTS, NPTS =  1
   NO OF VERT INCREMENTS, NVERT = 11
     LIST = 0      IMET (SI > 0) = 1
          HEIGHT OF WALL,HTWALL =  7.500 M
   VERTICAL WALL INCREMENT, DDY =  .750 M
WALL PRESS INCREASE FACTOR, FAC = 1.000
FOR POINT NO =  1
NO SQUARES NSQW:  WIDTH = 10   LENGTH, NSQL = 10
    ELEMENT SIZE: B X W =     .200     .400 M
TOTAL LOAD ON UNIT AREA = 16.000 KN
 DOP =     2.000        DTWAL =  3.000 M
DIST OF WALL BELOW LOAD, DY =  .000 M
RESULTANT (TOTAL) HORIZONTAL FORCE =  36.967 KN
     DIST BOTTOM OF WALL UP TO RESULT, YBAR =  4.258 M


  EXAMPLE 11-8 USING POISSON'S RATIO = 0.5--1 POINT

     POISSON'S RATIO, XMU =    .50
NO OF CONTRIBUTING POINTS, NPTS =  1
   NO OF VERT INCREMENTS, NVERT = 11
     LIST = 0      IMET (SI > 0) = 1
          HEIGHT OF WALL,HTWALL =  7.500 M
   VERTICAL WALL INCREMENT, DDY =  .750 M
WALL PRESS INCREASE FACTOR, FAC = 1.000
FOR POINT NO =  1
NO SQUARES NSQW:  WIDTH = 10   LENGTH, NSQL = 10
    ELEMENT SIZE: B X W =     .200     .400 M
TOTAL LOAD ON UNIT AREA = 16.000 KN
 DOP =     2.000        DTWAL =  3.000 M
DIST OF WALL BELOW LOAD, DY =  .000 M
RESULTANT (TOTAL) HORIZONTAL FORCE =  52.672 KN <-- See Ex. 11 - 9
     DIST BOTTOM OF WALL UP TO RESULT, YBAR =  4.401 M


  EXAMPLE 11-8 USING POISSON'S RATIO = 1.0--1 POINT

     POISSON'S RATIO, XMU =  1.00
NO OF CONTRIBUTING POINTS, NPTS =  1
   NO OF VERT INCREMENTS, NVERT = 11
     LIST = 0      IMET (SI > 0) = 1
          HEIGHT OF WALL,HTWALL =  7.500 M
   VERTICAL WALL INCREMENT, DDY =  .750 M
WALL PRESS INCREASE FACTOR, FAC = 1.000
FOR POINT NO =  1
NO SQUARES NSQW:  WIDTH = 10   LENGTH, NSQL = 10
    ELEMENT SIZE: B X W =     .200     .400 M
TOTAL LOAD ON UNIT AREA = 16.000 KN
 DOP =     2.000        DTWAL =  3.000 M
DIST OF WALL BELOW LOAD, DY =  .000 M
RESULTANT (TOTAL) HORIZONTAL FORCE =  91.935 KN
     DIST BOTTOM OF WALL UP TO RESULT, YBAR =  4.544 M
```

////

Example 11-9. For the linear loaded area shown in Fig. E11-9*a* compute the wall force.

Solution. Since the general data are identical to Example 11-8 the only additional input is to use IVARI = 1 and then input a series of element loads PSQL(I) for the 10 strips parallel to the wall. The strip element loads are computed as shown on Fig. E11-9*a* and are output with the other input data on Fig. E11-9*b*.

Comments. This problem is self-checking by solving the problem with the load linearly increasing and then linearly decreasing [which simply reverses the order of PSQL(I)]. The sum of the two solutions should equal the 52.672 kN of Example 11-8.
Here the sum is

$$23.898 + 28.774 = 52.672 \text{ kN} \qquad \text{(vs. 52.672 previous)}$$

Also

$$52.672\bar{y} = 23.898(4.247) + 28.774(4.528)$$

$$\bar{y} = \frac{231.783}{52.672} = \mathbf{4.401\ m} \qquad \text{(versus 4.401 m)}$$

From the check it would appear that the program is correct and that the sloping surcharge has been correctly modeled.

Figure E11-9*a*

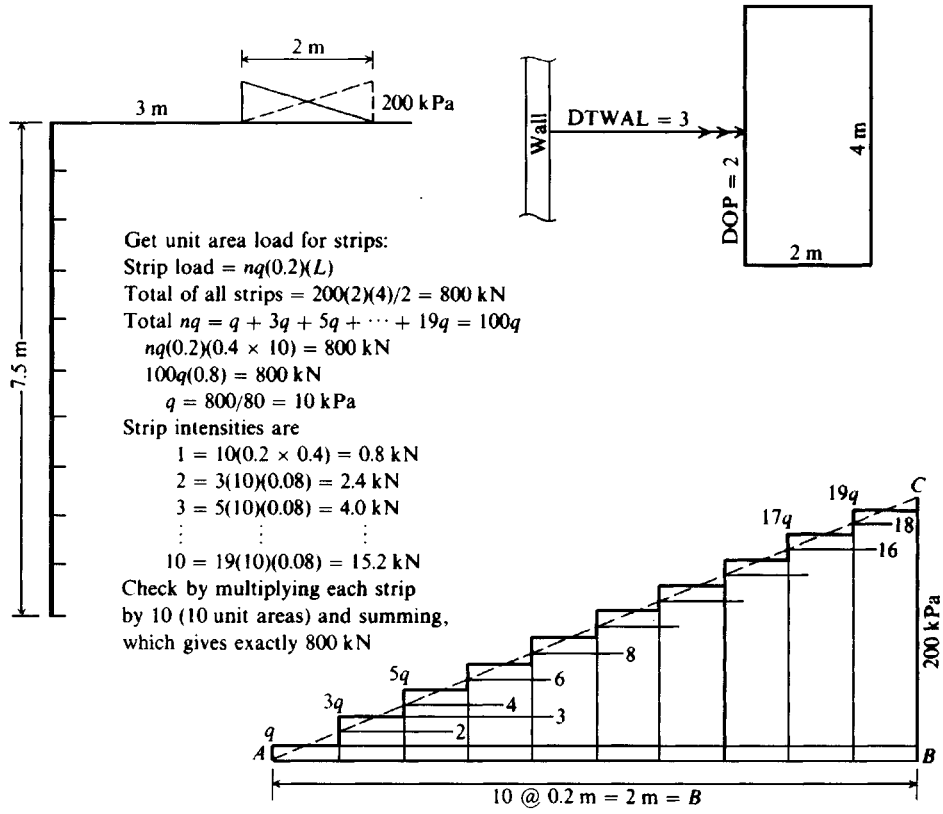

Figure E11-9*b*

```
      +++ NAME OF DATA FILE FOR THIS EXECUTION:  LPRESS3.DTA

   EXAMPLE 11-9--POISSON'S RATIO = 0.5--INCREASING Q

     POISSON'S RATIO, XMU =    .50
NO OF CONTRIBUTING POINTS, NPTS =  1
   NO OF VERT INCREMENTS, NVERT = 11
     LIST = 0      IMET (SI > 0) = 1
          HEIGHT OF WALL,HTWALL =  7.500 M
   VERTICAL WALL INCREMENT, DDY =  .750 M
WALL PRESS INCREASE FACTOR, FAC = 1.000
FOR POINT NO =  1
NO SQUARES NSQW:  WIDTH = 10   LENGTH, NSQL = 10
    ELEMENT SIZE: B X W =     .200     .400 M
TOTAL LOAD ON UNIT AREA =    .000 KN
 DOP =     2.000        DTWAL =  3.000 M
DIST OF WALL BELOW LOAD, DY =  .000 M
STRIP LOAD INCREMENTS ARE:
PSQL(I) =    .800  2.400  4.000  5.600  7.200
            8.800 10.400 12.000 13.600 15.200

RESULTANT (TOTAL) HORIZONTAL FORCE =  23.898 KN
     DIST BOTTOM OF WALL UP TO RESULT, YBAR =  4.247 M


  EXAMPLE 11-9--POISSON'S RATIO = 0.5--DECREASING Q

     POISSON'S RATIO, XMU =    .50
NO OF CONTRIBUTING POINTS, NPTS =  1
   NO OF VERT INCREMENTS, NVERT = 11
     LIST = 0      IMET (SI > 0) = 1
          HEIGHT OF WALL,HTWALL =  7.500 M
   VERTICAL WALL INCREMENT, DDY =  .750 M
WALL PRESS INCREASE FACTOR, FAC = 1.000
FOR POINT NO =  1
NO SQUARES NSQW:  WIDTH = 10   LENGTH, NSQL = 10
    ELEMENT SIZE: B X W =     .200     .400 M
TOTAL LOAD ON UNIT AREA =    .000 KN
 DOP =     2.000        DTWAL =  3.000 M
DIST OF WALL BELOW LOAD, DY =  .000 M
STRIP LOAD INCREMENTS ARE:
PSQL(I) = 15.200 13.600 12.000 10.400  8.800
            7.200  5.600  4.000  2.400   .800

RESULTANT (TOTAL) HORIZONTAL FORCE =  28.774 KN
     DIST BOTTOM OF WALL UP TO RESULT, YBAR =  4.528 M
```

Comment. The lateral pressure problem has a number of solutions in the literature for linearly varying surcharges but the author has found the only consistent answers are from the computer program.

////

One can model a strip or line load, as previously stated, but the model is probably not correct since these types of loadings are properly plane strain cases. If one elects to use the infinite strip one can model it using a finite number of unit areas—say, about 40 or 50 depending on the distance from the wall. Also use one-half the length and double the computed force or pressures. One can determine whether there are enough unit areas by making two

runs with, say, 40 areas in one and 50 in the other, and seeing whether there is any significant change in the computed wall force resultant.

11-14 OTHER CAUSES OF LATERAL PRESSURE

Ice Formation

Lateral pressures can be developed when pore water in the backfill freezes. This problem is minor in an unsaturated soil unless ice lenses form. The problem can be eliminated by using granular backfill and/or providing a drainage system, as illustrated in Fig. 11-12, of drain (or weep) holes and longitudinal collector drains with or without a vertical geotextile drain.

Swelling Pressure

If the retaining wall backfill is an expansive clay whose water content increases beyond that at the time of placement, it can expand and produce very large lateral wall pressures. The problem can be somewhat alleviated by placing the clay under carefully controlled conditions of no lumps and at a water content considerably above optimum (> OMC). The problem can be considerably alleviated by using granular backfill; however, this is not always possible. Lateral pressure is not likely to be developed when one is building against overconsolidated clay, for the high initial K_o stresses will be lost as soon as the excavation is opened. Vertical rather than lateral expansion is more likely to be a problem in overconsolidated clay.

Thrust Due to Temperature

Walls providing restraint to members that can undergo thermal expansion and contraction may develop unwanted stresses. This problem can be solved by minimizing the restraint with rollers, hinges, or expansion joints. Typically this type of action occurs in bridge abutments and such.

Lateral Pressure Due to Compaction

A number of studies have been made in an effort to estimate the lateral wall pressure due to compaction of the backfill. Not much success has been had except to ascertain that compaction does generally increase the wall pressure. The problems are these:

1. Width of backfill zone
2. Type of backfill
3. Type—weight and method—of compaction equipment used

Because of these several variables designers have the options of ignoring compaction pressures or raising the pressure resultant location from about $H/3$ to 0.4 or $0.5H$. Those who ignore the compaction pressure assume the wall, being somewhat flexible, will rotate sufficiently to produce active pressure conditions regardless of the initial pressures.

11-15 LATERAL WALL PRESSURE FROM EARTHQUAKES

Field observations and model studies indicate that earthquake and machinery vibrations will increase the wall pressure/force. The earthquake acceleration a produces an inertial force in the active, passive, and wall masses (see Fig. 11-20) according to

$$F = ma \qquad (a)$$

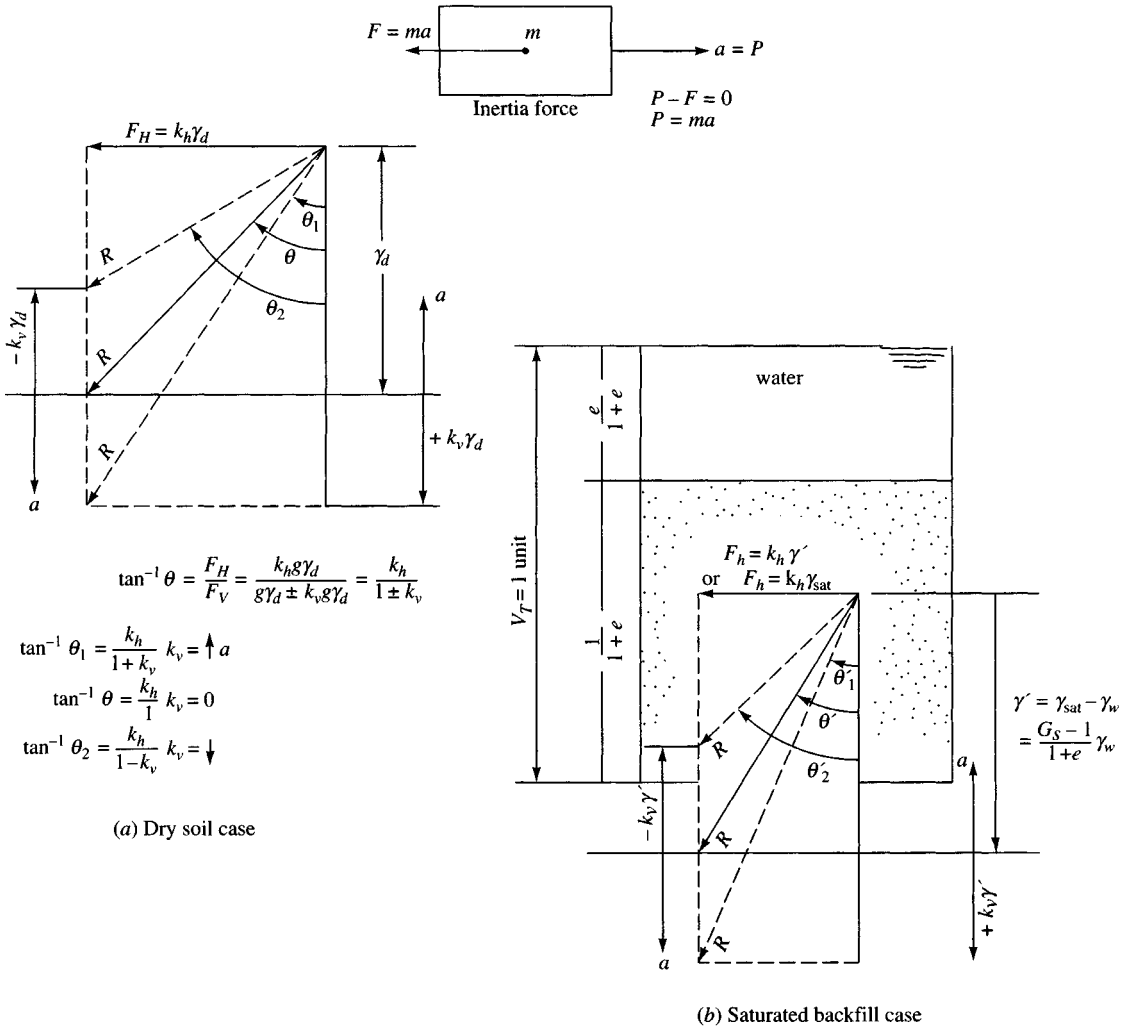

Figure 11-20 Definition of θ in the Mononobe-Okabe earthquake equation dynamic coefficient K_{ae} or K_{pe}.

where $m = W/g$ = mass of soil or wall

a = some fraction of the acceleration of gravity g (such as 0.1, 0.2, 0.3, etc.)

From this we obtain from Eq. (*a*)

$$F_h = ma_h = \frac{\gamma_1}{g}(k_h \times g) = \gamma_i k_h \qquad (b)$$

$$F_v = k_v(\gamma_d \text{ or } \gamma') \qquad (c)$$

as shown on Fig. 11-20.

We can define the angle of the earthquake resultant (see Fig. 11-20, which includes both the net gravity force of the soil wedge and the lateral earthquake force) as an angle θ defined as

$$\tan^{-1}\theta = \frac{F_h}{F_v} = \frac{k_h}{1 \pm k_v} \quad \text{(rads)} \qquad (d)$$

for a dry soil using the substitution of values shown on Fig. 11-20*a*. For a submerged soil there are two cases to consider (see Fig. 11-20*b*).

Case I. The soil is saturated but **relatively impervious**, so that the water essentially moves with the soil giving $F_h = k_h \gamma_{sat}$; however, the *vertical component is always the submerged* $\gamma' = \gamma_{sat} - \gamma_w$. With suitable manipulations using methods and soil definitions given in Sec. 2-3, we obtain

$$\tan^{-1}\theta = \frac{F_h}{F_v} = \frac{k_h \gamma_{sat}}{k_v \gamma'}$$

which can be transformed to a new value, say θ', of

$$\theta' = \frac{G_s + e}{G_s - 1} \tan^{-1}\theta = M_e \tan^{-1}\theta$$

In this case with a soil of low permeability (clays, silts, and very fine sand) the θ angle to be used is about twice as large as for a dry soil.

Case II. For soils with **large permeability** such as coarse sands and gravels we use the alternative form shown on Fig. 11-20*b* to obtain

$$\tan^{-1}\theta = \frac{F_h}{F_v} = \frac{k_h \gamma'}{\gamma' \pm k_v \gamma'}$$

which can be transformed into a new value, say θ'', of

$$\theta'' = \frac{G_s}{G_s - 1} \tan^{-1}\theta = M_e \tan^{-1}\theta$$

In the case of a soil with $G_s = 2.65$ and a high permeability (coarse sands, etc.) the θ-angle to be used is about 1.6 times as large as a dry soil.

The foregoing values for the angle θ can be used in the Mononobe-Okabe equations for the dynamic active and passive earth pressure coefficients K_{ae}, K_{pe}—if you use program FFACTOR you will be asked if you want to input one of the forms of the multiplier M_e given above.

The Mononobe-Okabe equations were developed in Japan ca. 1926 (and the original reference is probably no longer available[2]). Referring to Fig. 11-21*a*, we see that a passive zone may assist in resisting wall movement. The active and passive forces at an angle of δ normal to the wall face can be computed in general (including dynamic water pressure P_{wd}) using

$$\begin{Bmatrix} P_{ae} \\ P_{pe} \end{Bmatrix} = \frac{1}{2}(1 \pm k_v)\left(\gamma' + \frac{2q_s \sin\alpha}{\sin(\alpha + \beta)}\right) H^2 \begin{Bmatrix} K_{ae} \\ K_{pe} \end{Bmatrix} + P_{wd} + P_w \qquad (11\text{-}21)$$

This equation requires some discussion:

1. The $(1 \pm k_v)$ term depends on the sign of k_v and not on P_{ae} or P_{pe}.

---

[2]The most readily available reference is probably Matsuzawa et al. (1985). Almost all the equations found in several reference sources include one or more errors. The equations as programmed in program FFACTOR give values that are similar to those from several graphs found in the literature.

2. For the Mononobe-Okabe earthquake coefficients, use subscript a for the active K_{ae} and p for K_{pe}. The dynamic water pressure term P_{wd} is generally that given by Westergaard (1933, closure p. 472) for a large body of free water,

$$P_{wd} = 0.583\gamma_w H^2 \qquad \text{(kN/m or kips/ft of wall)}$$

This equation for P_{wd} (at $\bar{y} = 0.4H$) is not applicable if the pore water is not free to move. When the permeability is low the dynamic water force will have to be estimated in some other manner, or simply use γ_{sat} in the appropriate equation for θ above and neglect the P_{wd} term.

Use P_{wd} only on the backfill side of the wall.

3. The surcharge term q_s was added by Matsuzawa et al. (1985).
4. The static water force P_w term is optionally used for the passive side of the wall when there is water on both sides of the wall. It may be used on the backfill side if you do not use P_{wd}, but do not use it on both sides at the same time.
5. The original equations were for a *dry* sand backfill with the resultant at $H/3$ above the base. Current opinion, based on laboratory shaking table experiments [see Sherif et al. (1982)], is to put the resultant $\bar{y}$ at between 0.45 and $0.63H$. Whitman (1990) suggests using $\bar{y} = 0.6H$. For an equivalent trapezoidal pressure profile use the resultant earth force and its $\bar{y}$ location; refer to Eq. (11-15).
6. If you have a stratified backfill (as for anchored sheet piling of Chap. 13) along a waterfront you should use *averaged* soil properties for the full length of the piling for H—not the height above the dredge line—with the resultant force placed at $0.6H$ above the pile tip.
7. The dynamic ρ_i defining the failure wedges (of Fig. 11-21*a*) is not the Rankine value of $45° \pm \phi/2$. If $K_{ae} < 1$ you might obtain a ρ_a of $45° - \phi'/2$, where you find a pseudo ϕ' by trial using the Coulomb equation in FFACTOR and smaller ϕ angles until the value of K_a computed is approximately that of K_{ae}. Note that $\rho_i = 0$ if $K_{ae} \geq 1$ or if $K_{pe} \leq 1$.

Davies et al. (1986) suggest the ρ angle for dry soil has an approximate parabolic variation from the static case ($k_h = 0$) to zero as $k_h \to 0.6$. The value of k_h producing $\rho = 0$ is termed the *critical acceleration* and is approximately

$$k_h = (1 \pm k_v)\tan\phi$$

The following Mononobe-Okabe dynamic earth pressure coefficients are not exactly as given in Mononobe-Okabe but have been modified to be similar to the Coulomb equations and to use the Coulomb definition of wall angle α_i:

$$\begin{Bmatrix} K_{ae} \\ K_{pe} \end{Bmatrix} = \frac{\sin^2(\alpha_i \pm \theta \mp \phi)}{\cos\theta \sin^2\alpha_i \sin(\alpha_i \pm \theta \pm \delta)\left[1 \pm \sqrt{\dfrac{\sin(\phi + \delta)\sin(\phi \mp \beta_i - \theta)}{\sin(\alpha_i \pm \theta \pm \delta)\sin(\alpha_i - \beta_i)}}\right]^2} \tag{11-22}$$

with terms as previously used and as illustrated on Fig. 11-21 and with subscript $i = a$ or p. Owing to the difficulties of typesetting and using this equation, it is in program FFACTOR as option 7 on your program diskette. *Carefully note that the foregoing*

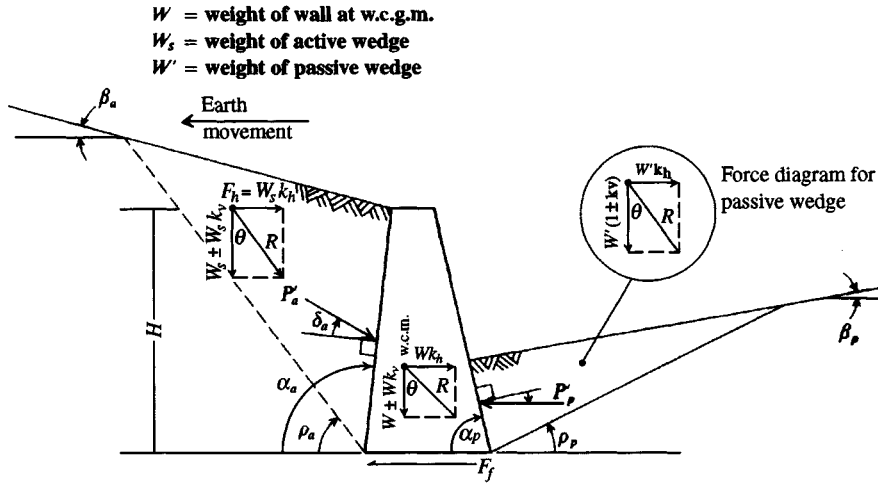

(*a*) Sign convention and definition of terms for the equations with (+) signs as shown

Figure 11-21 For passive force slope of P_p is shown; slope R changes, C_s, C_w reverse directions.

coefficients include both the static and earthquake-induced earth pressure at an angle of $\pm\delta$ *to the normal vector to the wall.* The sign with δ depends on the direction of relative earth-to-wall movement and is influenced by the sign of any assumed k_v. This relationship is shown to be true from the use of the weight vector resultant defined by the θ angle shown on Fig. 11-21*a*. Note that if you use $k_h = 0$ you get the Coulomb values of Tables 11-1 and 11-2.

When the $\sqrt{}$-term of Eq. (11-22) is (−) it should be set to 0 [as is done in program FFACTOR—output ROOT1 or ROOT2 = (−)]. It is often negative when using the θ multiplier M_e of θ' or θ'' previously given.

The horizontal earth force is usually required; however, this should be a trivial exercise if you draw the system to a reasonable scale (see Fig. 11-21*b*) showing the wall angles α_i and earth-pressure vectors P_{ae}, P_{pe} at the correct δ against the wall.

Whitman (1990) suggests that one might approximate K_{ae} as

$$K_{ae} = K_a + 0.75k_h$$

If you compute K_{ae} using Eq. (11-22), you might check whether the value $K_{ae}(1 \pm k_v)$ is in the range Whitman suggested to avoid any large error in K_{ae}. The value of K_a is the Coulomb value from Table 11-1. The following short tabulation lists several values of K_a, K_p, and K_{ae}, K_{pe} as well as the Whitman (1990) approximation:

Values shown from using program FFACTOR with $k_h = 0.30$; $k_v = 0$

ϕ	β	δ	α_a	α_p	K_a	K_p	K_{ae}	K_{pe}	K^*_{ae}
32	10	20	95	85	0.273	17.606	0.791	13.602	0.498
32	10	20	90	90	0.313	12.733	0.713†	10.060	0.538
32	10	20	85	95	0.357	9.862	0.646	7.960	0.582

*Using the Whitman (1990) approximation of $K_a + 0.75k_h$.
†If we use $M_e = 2.65/(1 + 0.6) = 1.66$ we obtain $K_{ae} = 2.149$; $K_{pe} = 7.948$.

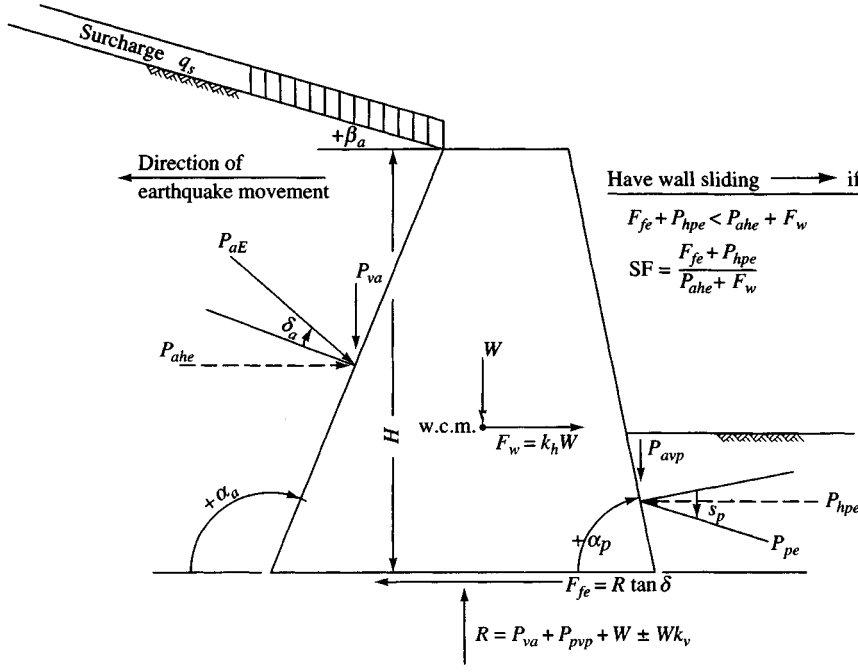

(*b*) General wall forces for dry backfill

Figure 11-21

The table shows that the dynamic active earth pressure K_{ae} is considerably larger than the Coulomb value of K_a and the dynamic passive earth pressure K_{pe} is substantially smaller than the Coulomb K_p. These observations should not be unexpected. The Whitman (1990) suggestion does not appear to be valid—possibly because $k_h = 0.3$ may be too large and in any case should only be used for the *dry* soil case.

Some problems associated with using the Mononobe-Okabe equation include the following:

1. Identification of k_h and k_v. Often k_v will be zero (no vertical acceleration—or very small). Note k_v has a sign as shown on Fig. 11-20 and, depending on direction, can either increase or decrease the vertical (gravity) force F_v. In most cases k_v can be neglected; however, both the 1994 Northridge (California) and the 1995 Kobe (Japan) earthquakes had upward vertical components, with the result that the upward acceleration increased the downward gravity force by the inertial force, causing the ground floor of a number of multistory structures to be squashed.
2. What to use for wall friction δ. Seed and Whitman (1970) suggested $\delta \approx \phi/2$ and Matsuzawa et al. (1985) suggested $\delta \approx 2\phi/3$.
3. What soil parameters to use for stratified soils in both the active and passive zones.

Since one must estimate the earthquake fraction ($a = k_h$ or $k_v \times g$) it is obvious a solution that is about as reliable as any would be to use the Rankine equations together with perhaps an additional horizontal force of from 0.2 to $0.4W_R$, where W_R = weight of the Rankine wedge + any surcharge and any other soil that might push against the wall

(or stem) during the earthquake. Any passive pressure could be reduced about 10 percent for each 0.1 of g used. Apply the driving earthquake force at about $0.5H$ in addition to the Rankine force applied at $H/3$.

11-16 PRESSURES IN SILOS, GRAIN ELEVATORS, AND COAL BUNKERS

Lateral pressure of agricultural products against the walls of grain storage containers (typically as in Fig. 11-22*a*) is similar to lateral earth-pressure problems earlier in this chapter. It is necessary to obtain the internal and wall friction angles of the material. The ϕ values depend on the material being contained, its water content, and its density. Wall friction δ depends on the wall material used and the factors cited earlier for soil. Table 11-8 gives representative values for several agricultural grains for which containment structures may be required. Grain is often measured in terms of bushels; a bushel is approximately 0.0352 m^3 (1.24 ft^3).

The grain (or other stored material) pressure for relatively shallow containment structures, say, under about 7 m in height, and with a height/width ratio ≤ 2 (see also Fig. 11-22*c*), can be computed using the Rankine or Coulomb earth-pressure equation with β = angle of repose of material (ϕ is also often taken as the angle of repose). The Rankine solution will tend to be somewhat more conservative than the Coulomb method since wall friction angle $\delta = 0$ in the Rankine case.

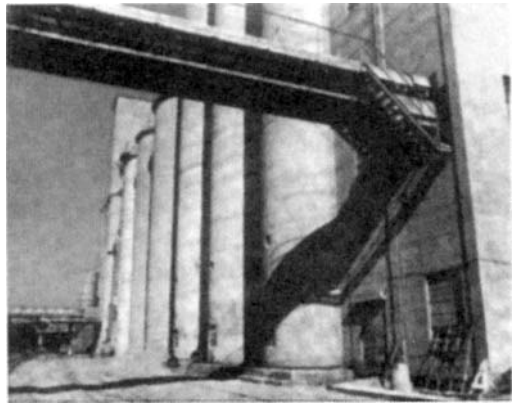

(*a*)

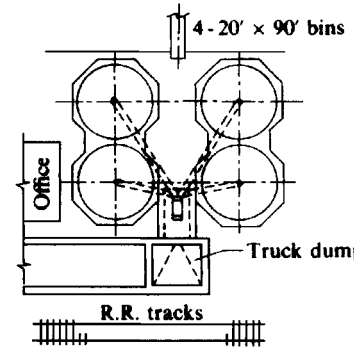

(*b*)

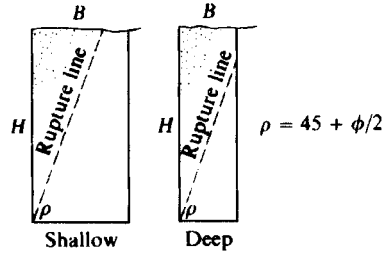

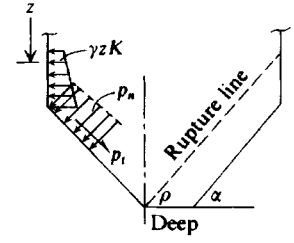

(*c*)

Figure 11-22 Grain elevators. (*a*) Photograph of typical elevator; (*b*) general layout of small four-silo group; (*c*) condition for shallow or deep silo analysis—if potential material-rupture line intersects wall, silo is "deep."

TABLE 11-8
Angle of internal friction and other data for selected grain and other bulk storage materials. Values shown are representative; actual values should be obtained from tests.

Material being stored	ϕ†	ϕ_r‡	δ for wall material*			ρ, g/cm³¶
			Concrete	Wood	Brick	
Agricultural products						
Wheat	28°	25°	28°	25°	26°	0.75–0.85
Rye	29	24	25	25	27	0.72–0.82
Barley	32	30	29	26	27	0.65–0.75
Oats	33	29	28	26	28	0.42–0.55
Corn	35	32	28	25	28	0.65–0.79
Beans	33	27	28	25	27	0.83–0.88
Peas	34	30	27	24	27	0.70–0.80
Flour		40	17	17		0.60–0.70
Sugar		35	23	22		0.95–1.05
Coal	35	35	30		35	0.75–1.10
Cement	38	42	22			1.01–1.60
Iron ore		40	26	26		2.55–2.75
Lime		35	26	26		0.70–0.96

*For metal walls use 16–18°; use 17–20° for coal.

†±2° for grain based on water content w percent.

‡Angle of repose also ±2°.

¶kN/m³ = 9.807 × g/cm³; pcf = 62.4 × g/cm³.

Use plane strain ϕ for long rectangular bunkers and triaxial ϕ values for square and round storage shapes.

Coal bunkers often have sloping hopper bottoms as in Fig. 11-22*c*, which require obtaining the normal and tangential components of pressure on their slopes. These values can be obtained from the geometry of the problem and an ellipse of stress analysis [see Rogers (1952)] to obtain (in units of $z\gamma$ of kPa or ksf)

$$\left.\begin{aligned} &\text{Tangential stress:} \quad p_t = z(\gamma - yK_a)\sin\alpha\cos\alpha \\ &\text{Normal stress:} \quad p_n = \gamma z\cos^2\phi + \gamma z K_a \sin^2\phi \end{aligned}\right\} \tag{11-23}$$

where terms are as defined on Fig. 11-22*c* or previously used and K_a is either the Rankine or Coulomb (or at-rest) lateral pressure coefficient.

Grain elevators, silos, and deep storage bunkers (for coal, cement, lime, etc.) are deep bins and require a modified analysis for the lateral and vertical wall pressure for design. When grain elevators (Fig. 11-22*a*) are emptied, dynamic pressures can develop that have caused walls to split. These overpressures are caused by the funneling action of the falling material which produces a lateral wall-bursting pressure similar to flowing water in a tapered conduit. Currently there is no precise method of evaluating these forces, since the material drop speed and taper diameter vary from the upper region to the exit point.

There is opinion that in the transition zone of Fig. 11-23*b* the lateral wall pressure transitions from an active case to a passive pressure case at the hopper (or other exit level). If this situation occurs, it would certainly produce some very large pressures since K_p is substantially larger than K_a. Passive pressure formation is not illogical since the flow of Fig. 11-23*a*

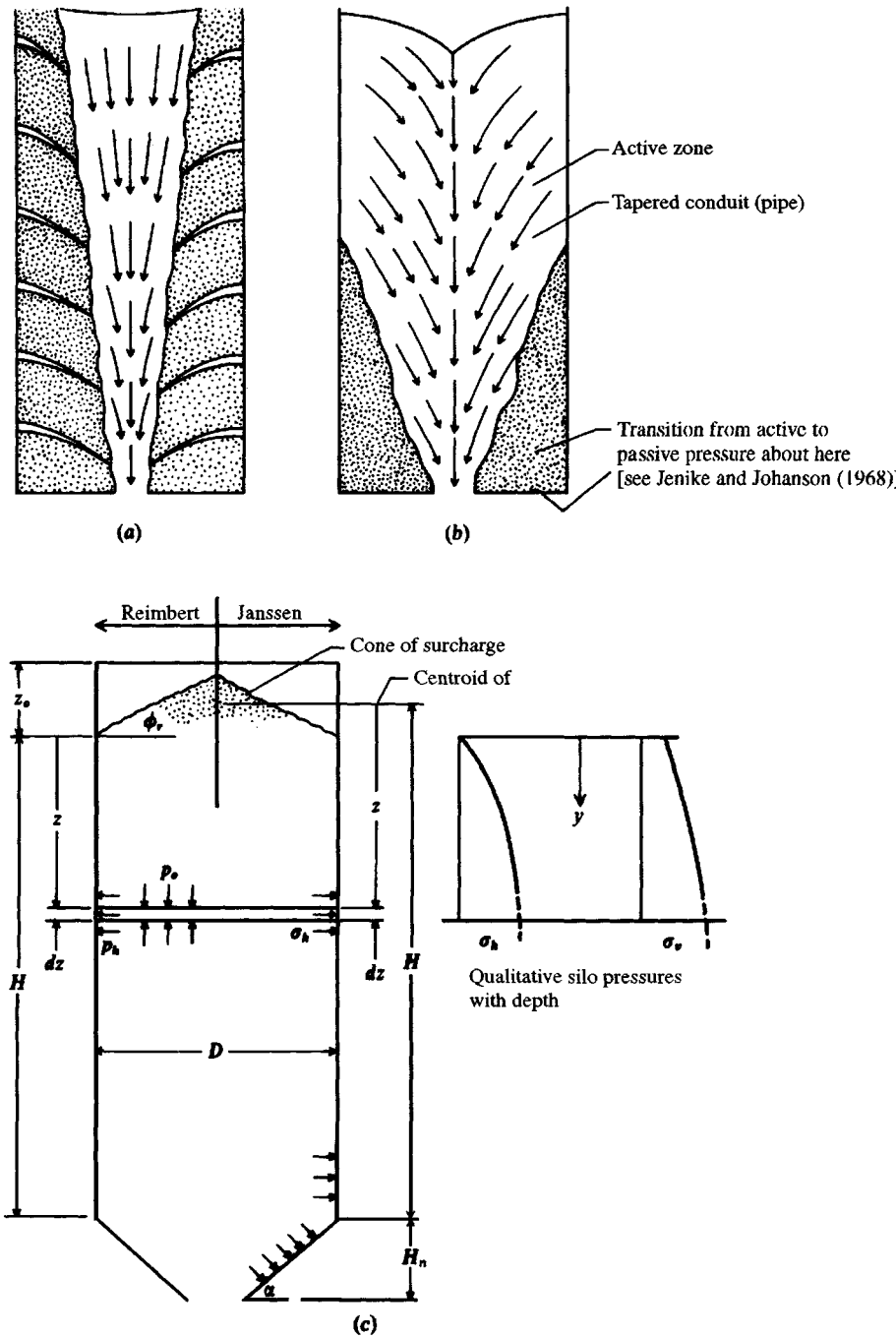

Figure 11-23 (*a*) Nondynamic silo flow conditions; (*b*) dynamic flow conditions; (*c*) identification of terms in the Reimbert and Janssen pressure equations.

and b essentially represents a plug of material flowing downward in the "pipe" formed by the nonflowing material. From this concept, it follows that the minimum overpressure is likely to occur if the draw-off orifice is centered in the middle third of the bin and would be a maximum when it is located to one side.

The pressures generated by storage of granular materials in deep containment structures such as silos, bins, etc. are generally determined by either the Janssen or Reimbert method. The procedure currently recommended by ACI 313 (1991) suggests these two methods for the static pressure analysis and overpressure factors for dynamically dumping material into the bin or for outflow based on estimates of ratio of dumped material to bin size or for the height/diameter ratio for outflow.

The Janssen method [Briassoulis (1991), Safarian (1969), ACI (1977)] computes the static pressures at any depth z measured from the centroid of z_o (see the right side of Fig. 11-23c) as

$$\text{Vertical pressure:} \qquad p_o = \frac{\gamma R}{K_a \tan\delta}\left[1 - \exp\left(-K_a \cdot \frac{z}{R} \cdot \tan\delta\right)\right] \tag{11-24}$$

$$\text{Lateral pressure:} \qquad p_h = p_o K_a \tag{11-25}$$

The total vertical force on a unit strip of wall perimeter from friction, producing compression in the wall, is

$$P_z = (\gamma z - 0.8 p_o)R \tag{11-26}$$

The Reimbert method computes the static pressures at any depth z (see left side of Fig. 11-23c) as

$$\text{Vertical pressure:} \qquad p_o = \gamma\left[z\left(\frac{z}{C} + 1\right)^{-1} + \frac{z_o}{3}\right] \tag{11-27}$$

$$\text{Lateral pressure:} \qquad p_h = \frac{\gamma R}{\tan\delta}\left[1 - \left(\frac{z}{C} + 1\right)^{-2}\right] \tag{11-28}$$

where

$$C = \frac{R}{K_a \tan\delta} - \frac{z_o}{3}$$

The total vertical force on a unit strip of wall perimeter is

$$P_z = (\gamma z - p_o)R \tag{11-29}$$

where terms not previously defined or used are as follows:

R = hydraulic radius = area/perimeter = $D/4$ for circular walls
z = depth to point where pressure is computed as on Fig. 11-23c
z_o = cone of surcharge = $(D/2)\tan\phi_r$ where ϕ_r = angle of repose of material (also often used for ϕ)
D = internal diameter of round container (for rectangular bins use equivalent diameter unless L/B is large)

Mackey and Mason (1972) proposed an analysis based on Fig. 11-24. The bottom *dead* zone of height $1.75D$ is designed based on the Janssen equations. The *pipe* zone is designed based on lateral pressures to hold an arch ring in place by friction where the ring is $0.6D$

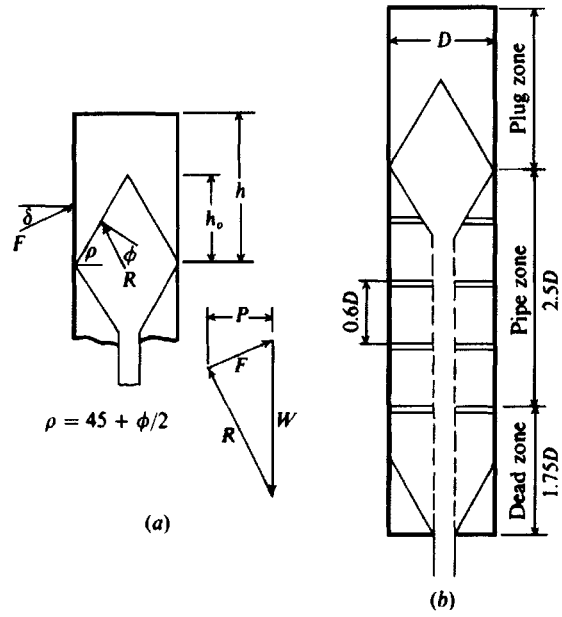

Figure 11-24 Alternative method of computing bursting pressure in silos. (*a*) Force polygon in plug zone; (*b*) zones for analysis in silo. [*After Mackey and Mason (1972).*]

thick. The remainder of the wall height is computed using a wedge theory as shown in the figure. The angle ρ shown in the figure is computed as $45° + \phi/2$.

The Mackey and Mason method gives higher computed pressures than the static values of either Janssen's or Reimbert's method so overburden pressure factors are not needed to account for dynamic pressures during bin emptying.

Table 11-9 gives the ACI recommended overpressure factors for use with the Janssen and Reimbert methods to increase the static pressures computed from Eqs. (11-24) through (11-29) to design (dynamic) values.

TABLE 11-9
Overpressure factors C_d for increasing the static pressures computed by the Janssen (J) or Reimbert (R) equations to design values*

	$\frac{H}{D} < 2$		$2 \le \frac{H}{D} < 3$		$3 \le \frac{H}{D} < 4$		$4 \le \frac{H}{D} < 5$		$\frac{H}{D} > 5$	
	J	R	J	R	J	R	J	R	J	R
$z = z_o$	1.35	1.10	1.45	1.20	1.50	1.25	1.60	1.30	1.65	1.35
$= z_1$	1.45	1.20	1.55	1.30	1.60	1.35	1.70	1.40	1.75	1.50
$= z_2$	1.55	1.45	1.65	1.55	1.75	1.60	1.80	1.70	1.90	1.75
$= z_3$	1.65	1.65	1.75	1.75	1.85	1.85	1.90	1.90	2.00	2.00
$= z_4$	1.65	1.65	1.75	1.75	1.85	1.85	1.90	1.90	2.00	2.00

where $z_i = \frac{H - z_o}{4}$ (see Fig. 11-23*c*)

Notes: z_o = base of surcharge cone
z_4 = at junction of hopper or other outlet orifice

*After ACI (1991).

Example 11-10. Compute the pressures acting on a wheat storage elevator that is 5 m diameter × 28.6 m high. Use all three methods presented. Use $\gamma_{wheat} = 0.8(9.807) = 7.846$ kN/m^3; $\phi = 28°$; $\delta = 24°$; $z_o = 0$ m.

Solution. We will make a table of p_o and p_h for each 5 m of depth.

1. By Janssen's method: Use Eqs.(11-24) and (11-25):

$$p_o = \frac{\gamma R}{K_a \tan\delta}\left[1 - \exp\left(-K_a \cdot \frac{z}{R} \cdot \tan\delta\right)\right] \qquad (11\text{-}24)$$

$$p_h = p_o K_a$$

For $\phi = 28°$, $K_a = 0.361$ (Table 11-3). Then

$$\tan\delta = \tan 24 = 0.445 \qquad \text{for circle } R = \frac{D}{4} = \frac{5}{4} = 1.25$$

With these data, program a computer and obtain the data shown in Table E11-10 for each 5 m of depth at the base.

We will check the base pressure as follows [and using Eq. (11-24)]:

$$P_v = (\gamma z - 0.8p_o)R = [7.846(28.6) - 0.8(59.50)]1.25 = 221 \text{ kPa}$$

using p_o at 28.6 m from Table E11-10.

The total perimeter force $= \pi D P_v = \pi(5)(221) = 3471$ kN.

The total wheat weight $= 0.7854D^2H\gamma_{wheat}$

$= 0.7854(5^2)(28.6)(7.846) = 4406$ kN

The base must carry the difference between total weight and the perimeter friction giving

$$\Delta P = 4406 - 3471 = 935 \text{ kN}$$

$$p_o = \frac{\Delta P}{\text{Area of base}} = \frac{935}{0.7854(5^2)} = \mathbf{47.6} \text{ vs. } 59.5 \qquad \text{(but O.K.)}$$

This difference in p_o versus Table E11-10 is due to the approximation using $0.8p_o$ in Eq. (11-24) (47.6/0.8 = 59.5).

2. By Reimbert's method (note $z_o = 0$ here also): Rearranging Eq. (11-25) with $z_o = 0$, we obtain

$$p_o = \frac{\gamma z C}{C + z}$$

$$p_h = \frac{\gamma R}{\tan\delta}\left[1 - \left(\frac{C}{C+z}\right)^2\right]$$

$$C = \frac{R}{K_a \tan\delta}$$

where $K_a = 0.361$

$\tan\delta = 0.445$

$R = D/4 = 1.25$ as for the Janssen method

Programming p_o and p_h on a computer and incrementing z by 5 m and the base $z = 28.6$, we obtain the additional data shown in Table E11-10.

Make an approximate check:

P_v per meter of wall = area of lateral pressure diagram × $\tan\delta$

TABLE E11-10

		Janssen		Reimbert	
h, m		P_h	P_o	P_h	P_o, kPa
0	Top	0	0	0	0
5		10.45	28.94	13.87	23.88
10		15.94	44.16	17.81	34.33
15		18.83	52.17	19.47	40.20
20		20.35	56.38	20.31	43.95
25		21.15	58.59	20.80	46.56
28.6	Bottom	21.48	59.50	21.03	47.99

Using the average end area formula for the area of pressure diagram, we write

$$A = \frac{p_1 + p_2}{2} z_z + \frac{p_2 + p_3}{2} z_2 + \cdots 17.81$$

$$= \frac{0 + 13.87}{2}(5) + \frac{13.87 + 1281}{2}(5) + \cdots = 486.4 \text{ kN/m}$$

$$\text{Total } P_v = \pi DA \tan\delta = \pi(5)(486.4)(0.445) = \mathbf{3387} \qquad (< 4406)$$

Comments

1. We have checked the computations for statics and to see if the pressures are reasonable.
2. For design we would divide the silo height into four sections and recompute the pressures p_o and p_h and, based on $H/D = 28.6/5 = 5.72$, use the appropriate overpressure factors from Table 11-9 to factor the static pressures to design values as $p_{h(\text{des})} = p_h C_d$, etc.
3. By the Mackey and Mason method (Fig. 11-23):

In bottom $1.75D = 1.75(5) =$	8.75 m	use Janssen pressure distribution
In next (pipe) zone $2.5(5) =$	12.5 m	use arching
In top $28.6 - 12.5 - 8.75 =$	7.35 m	use wedge (plug zone)

In considering any ring arch in the pipe zone, the weight of an arch ring of height $z = 0.6D$ is

$$W = \gamma Az$$

$$= 7.846(0.7854)(5)^2(0.6) \times (5) = 462.17 \text{ kN}$$

$$\text{Friction resistance} = 0.5\gamma z^2 K(\tan\phi')\pi D$$

$$= 0.5(7.846)(0.6 \times 5)^2(\tan 28°)\pi(5) = 246.8K = W$$

Solving, we find

$$K = \frac{462.17}{246.8} = 1.87$$

The lateral pressure for each ring arch (varying from 0 at top to maximum at $0.6D$) is

$$\sigma_h = \gamma z K = 7.846(0.6 \times 5)(1.87) = \mathbf{44.01} \text{ kPa}$$

This value compares with values of 15.94 and 17.81 kPa of previous methods indicating that the Mackey values do not require "factoring" up for design.

In the top plug zone the weight of the plug is

$$W = 0.7854D^2\gamma\left(h_o - \frac{z_o}{3}\right)$$

$$\theta = 45° + \phi/2 = 59° \qquad z_o = 2.5\tan 59° = 4.16 \text{ m} \qquad h_o = 7.35 \text{ m}$$

$$W = 0.7854(5)^2(7.846)\left(7.35 - \frac{4.16}{3}\right) = \mathbf{918.65} \text{ kN}$$

The active earth wedge can be solved directly for P_a to give

$$P_a = \frac{W}{\sin\phi' + \cos\phi' \tan(45° + \phi/2)}$$

$$= \frac{918.65}{0.407 + 0.914(1.664)} = \mathbf{476.44} \text{ kN}$$

If we assume average lateral pressure on plug height,

$$P_a = p_h A = p_h \pi D h_o = 476.44 \text{ kN}$$

Rearranging and solving for the lateral pressure p_h we obtain

$$p_h = \frac{476.44}{\pi(5)(7.35)} = \mathbf{4.13} \text{ kPa}$$

////

PROBLEMS

11-1. Find the active lateral force/unit of width and the point of application for a retaining wall with the following data:
$\gamma = 17.30$ kN/m^3; $\phi = 36°$; $c = 0$ kPa; $H = 5.10$ m; $\delta = 20°$.

a. Using the Coulomb equation and $\beta = 0°$

b. For backfill slope $\beta = 10°$

c. For backfill slope $\beta = -10°$

Answer: (*a*) $P_a = 58.5$ kN/m at 1.7 m above base

(*b*) $P_a = 64.3$ kN/m (*c*) $P_a = 53.8$ kN/m

11-2. Do Prob. 11-1 using the Rankine equations for active earth pressure.
Answer: (*a*) $P_a = 58.4$ kN/m;
(*b*) = (*c*) $P_a = 60.6$ kN/m; all act at $H/3$ above the wall base.

11-3. Redo Prob. 11-1 for Coulomb passive earth pressure.

11-4. What is the percent increase in the wall force of Prob. 11-2*a* if H increases from 5.1 to 5.7 m?
Answer: About 25 percent

11-5. Compute the lateral force/unit of width and locate the resultant for the following data: $\gamma = 17.50$ kN/m^3; $\phi = 26°$; $c = 10$ kPa; $\beta = 0$; and $H = 6.5$ m. Neglect the tension zone and use the Rankine method.
Answer: $R = 63.2$ kN/m at $\bar{y} = 4.65/3$ m

11-6. Do Prob. 11-5 if there is a surcharge of 100 kPa on the backfill. Use the Coulomb method with $\delta = 16°$.
Answer: $R = 315.3$ kN/m at $\bar{y} = 2.76$ m above base

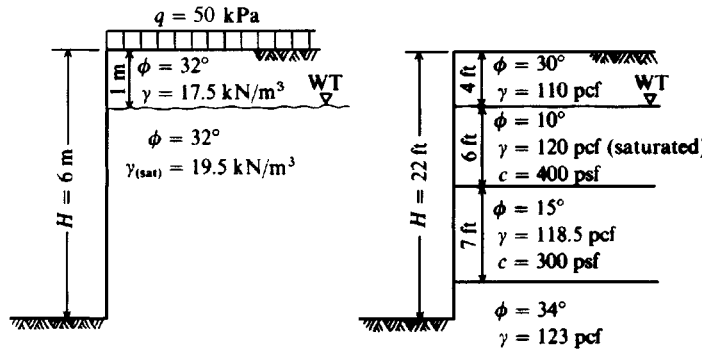

Figures P11-8 and P11-9

11-7. Do Prob. 11-5 with the tension crack zone replaced as in the left figure of Fig. 11-11*c*.
Answer: $R = 103.3$ kN/m at $\bar{y} = 2.17$ m above base

11-8. Compute the lateral force and show the location of the resultant using the Rankine equations for the wall-soil system of Fig. P11-8.

11-9. Compute the lateral force and show the location of the resultant for the wall-soil system of Fig. P11-9.

11-10. What is the depth of tension crack and critical depth for the wall-soil system of Fig. P11-8 if, in addition to the soil parameters shown, there is cohesion of $c = 20$ kPa both above and below the water table?

For the following problems use computer program SMTWEDGE or SMBLP1 on your program diskette as required. On the output sheet draw a neat sketch of the problem and highlight the answer (force P_a and ρ angle).

For Probs. 11-11 through 11-16 take the pressure on a vertical line through the heel at point *A*.

11-11. For the conditions given in Fig. P11-10 find the active earth pressure and estimate its point of application.

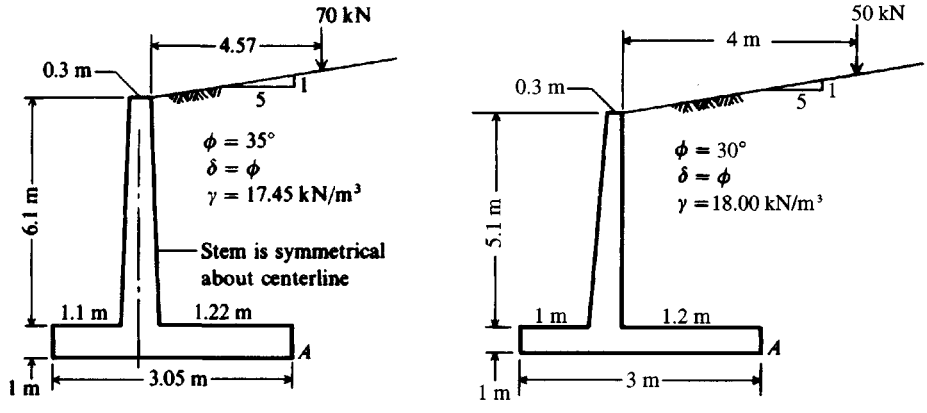

Figures P11-10 and P11-11

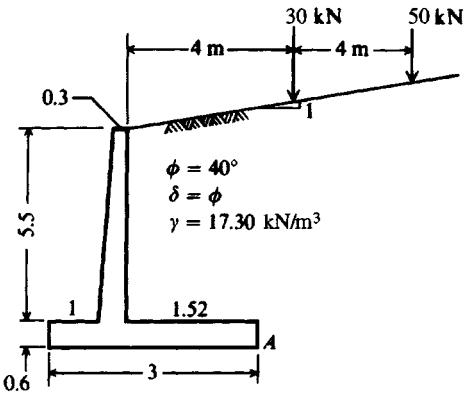

Figure P11-12

11-12. For the conditions given in Fig. P11-11, find the active pressure and estimate its point of application.

11-13. For the cantilever retaining wall shown in Fig. P11-12 find the active earth pressure and point of application.

11-14. Find the active earth pressure of Prob. 11-10 if there is cohesion of $c = 5$ kPa and all other data are the same.

11-15. Find the active earth pressure of Prob. 11-11 if the soil parameters are as given on the sketch but in addition the tension crack depth $h_t = 1.2$ m; $c_a = c$; and $\delta = \phi$.

11-16. Find the active earth pressure of Prob. 11-12 if the soil parameters are $\phi = 20°$; $c = c_a = 7.17$ kPa; $\delta = \phi$; and $\gamma = 17.30$ kN/m^3.

11-17. Estimate the lateral pressure for the wall of Fig. 11-12*b* if $H = 6$ m; $\phi = 36°$; $\delta = 24°$; and the distance $b = 3$ m. *Hint*: Use Eqs. (11-18) and (11-19).

11-18. Estimate the lateral pressure for the wall of Fig. 11-12*b* if $H = 6$ m; $b = 3$ m; $\phi = 0°$; $c = 300$ kPa (a stiff sandy clay).

11-19. Using the data set LPRESS2.DTA and program SMBLP1 on your diskette, output the pressure profile for the data for $\mu = 0.5$, and by hand verify the horizontal force and $\bar{y}$. Refer to Fig. 11-19.

11-20. Using the data set LPRESS3.DTA and program SMBLP1 output the pressure profile for whichever of the two subsets you are assigned and by hand verify the horizontal force and $\bar{y}$.

11-21. Redo Example 11-8 with a base of 3×4 m instead of 2×4 m.

11-22. Redo Example 11-9 with a base of 3×4 m instead of 2×4 m.

11-23. What is the resultant wall force for an infinitely long line load (0.3 m wide) loaded with $q = 50$ kN/m if the strip is located 1.2 m from the wall (DTWAL) for a soil with $\mu = 0.3$ and 0.6?

11-24. What is the resultant wall force for an infinitely long strip load of width = 1.0 m with a pressure intensity of 100 kPa, located 1.5 m from the wall (DTWAL)?

11-25. Compare K_a and K_p of Eq. (11-22) with the Coulomb values for a vertical wall (both faces vertical so $\alpha = \beta = 0$; $\phi = 36°$; $\delta = 24°$ for $k_v = 0.0$ and 0.2 and $k_h = 0.3$ and 0.5). There will be four different values each of K_a and K_p.

11-26. Compute the "active" earthquake pressure against the wall of Example 11-1. Note that α in Eq. (11-22) is 90°. Make a plot of P_a versus $k_h = 0.1$, 0.2, 0.5, and 1.0 and take $k_v = 0$.

11-27. Redo Example 11-10 using either the Janssen or Reimbert method as assigned with a bin diameter of 8 m and height of 32 m.

11-28. Establish dimensions and plot the pressure profile for a 30,000-bushel wheat silo. Use an *H/D* ratio between 4 and 5 and the Janssen method.

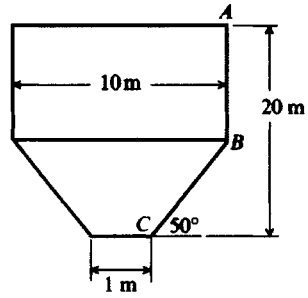

Figure P11-29

11-29. A steel plate coal bunker is 20 m deep; the hopper slope $\rho = 50°$ as shown in Fig. P11-29. Plot the normal pressure profile along ABC when the bunker is full of coal of $\gamma = 7.9\ \text{kN/m}^3$. What is the "hoop" tension force at B for design? Should one use a dynamic overpressure factor c_d for this example?

CHAPTER 12

MECHANICALLY STABILIZED EARTH AND CONCRETE RETAINING WALLS

12-1 INTRODUCTION

Retaining walls are used to prevent retained material from assuming its natural slope. Wall structures are commonly used to support earth, coal, ore piles, and water. Most retaining structures are vertical or nearly so; however, if the α angle in the Coulomb earth-pressure coefficient of Eq. (11-3) is larger than 90°, there is a reduction in lateral pressure that can be of substantial importance where the wall is high and a wall tilt into the backfill is acceptable.

Retaining walls may be classified according to how they produce stability:

1. Mechanically reinforced earth—also sometimes called a "gravity" wall
2. Gravity—either reinforced earth, masonry, or concrete
3. Cantilever—concrete or sheet-pile
4. Anchored—sheet-pile and certain configurations of reinforced earth

At present, the mechanically stabilized earth and gravity walls are probably the most used—particularly for roadwork where deep cuts or hillside road locations require retaining walls to hold the earth in place. These walls eliminate the need for using natural slopes and result in savings in both right-of-way costs and fill requirements.

Cantilever walls of reinforced concrete are still fairly common in urban areas because they are less susceptible to vandalism and often do not require select backfill. Typically they compete well in costs where the wall is short (20 to 50 m in length) and not very high (say, under 4 m). They are also widely used for basement walls and the like in buildings.

This chapter will investigate the basic principles of the reinforced earth, gravity, and concrete cantilever wall; the sheet-pile cantilever and anchored walls will be considered separately in the next two chapters.

12-2 MECHANICALLY REINFORCED EARTH WALLS

The mechanically reinforced earth wall of Fig. 12-1 uses the principle of placing reinforcing into the backfill using devices such as metal strips and rods, geotextile strips and sheets and grids, or wire grids. There is little conceptual difference in reinforcing soil or concrete masses—reinforcement carries the tension stresses developed by the applied loads for either material. Bond stresses resist rebar pullout in concrete; soil relies on friction stresses developed based on the angle of friction δ between soil and reinforcement or a combination of friction and passive resistance with geo- and wire grids.

The principle of reinforced earth is not new. Straw, bamboo rods, and similar alternative materials have long been used in technologically unsophisticated cultures to reinforce mud bricks and mud walls. Nevertheless, in spite of this long usage French architect H. Vidal was able to obtain a patent (ca. mid-1960s) on the general configuration of Fig. 12-1, which he termed "reinforced earth." We see three basic components in this figure:

1. The earth fill—usually select granular material with less than 15 percent passing the No. 200 sieve.
2. Reinforcement—strips or rods of metal, strips or sheets of geotextiles, wire grids, or chain link fencing or geogrids (grids made from plastic) fastened to the facing unit and extending into the backfill some distance. Vidal used only metal strips.
3. Facing unit—not necessary but usually used to maintain appearance and to avoid soil erosion between the reinforcements.

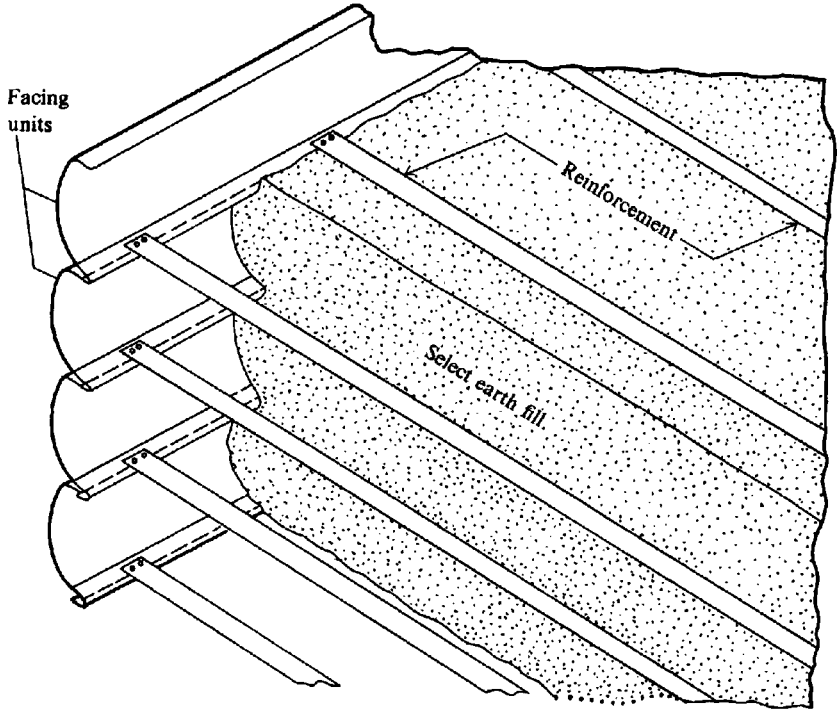

Figure 12-1 The reinforced earth concept. [After Vidal (1969).]

These three components are combined to form a wall whose side view is shown in Fig. 12-2*a*. The facing units may be curved or flat metal plates or precast concrete strips or plates (see Fig. 12-2*b*). Where geotextiles are used the sheet may lap, as in Fig. 12-3, to produce the facing unit.

When wire mesh or or other reinforcement with discontinuities (grid voids) is used, a portion may be bent, similar to the sheet of Fig. 12-3, to form a facing unit. Grid-type

Figure 12-2 Reinforced earth walls.

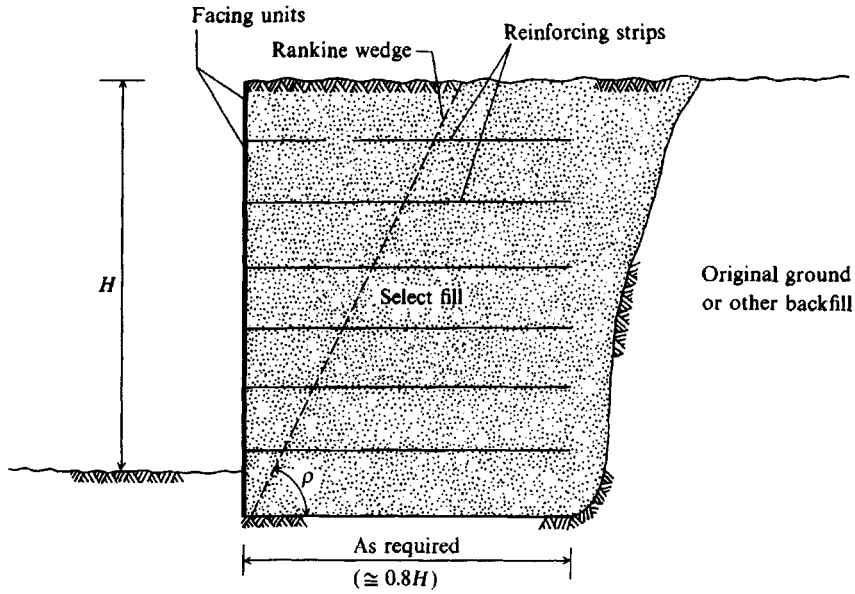

(*a*) Line details of a reinforced earth wall in place

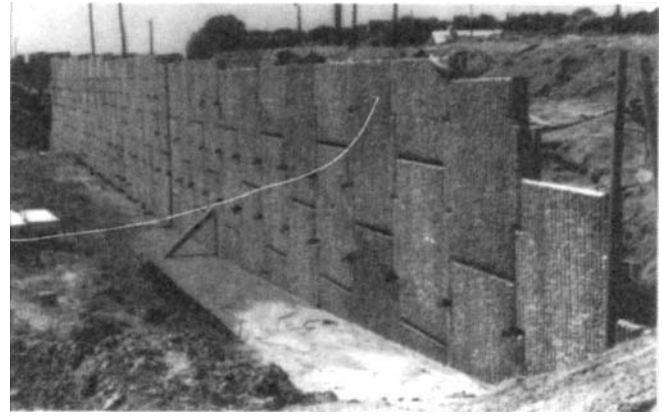

(*b*) Front face of a reinforced earth wall under construction for a bridge approach fill using patented precast concrete wall face units

(*c*) Backside of wall in (b), which shows the reinforcing strips attached to the wall face units. Note the drain pipe to carry runoff from the future road surface. Recent rain has eroded soil beneath reinforcement strips at wall, which will have to be carefully replaced. Also shown are interlocking dowels and lifting devices (D rings), which weigh around 2 kips each.

(*d*) A low reinforced earth wall showing a different concrete facing unit pattern (also patented). Note top cap includes a drainage depression that empties into a drop inlet barely seen at forward end.

reinforcements strengthen the soil through a combination of friction and passive pressure pullout resistance. The bent-up portion used as a facing piece provides some erosion control until the wall is completed.

The exposed reinforcements are usually sprayed with concrete mortar or gunite (material similar to mortar) in lifts to produce a thickness on the order of 150 to 200 mm. This is both to improve the appearance and to control erosion. For metals this covering also helps

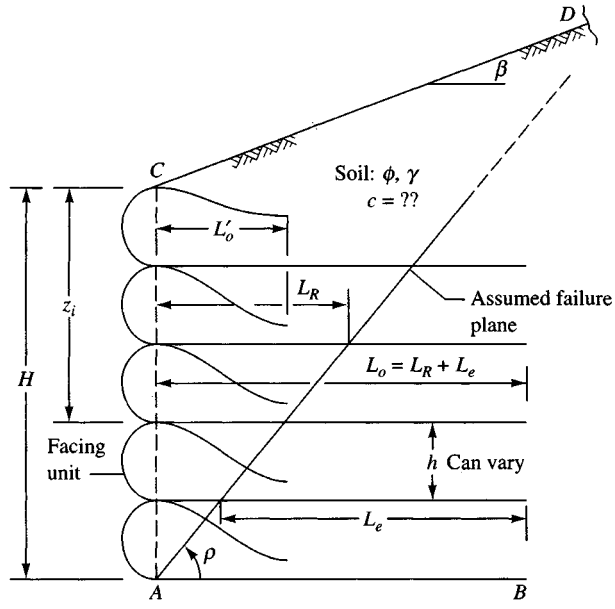

Figure 12-3 Using geotextile sheets for reinforcement with the facing unit formed by lapping the sheet as shown. Critical dimensions are L_e, L'_o, and L_o. Distances L_e and L_o are variable but for this wall produce a constant length $L_{con} = L_o + L_e$. The Rankine $\rho \neq 45° + \phi/2$ for backfill β as shown. Use your program SMTWEDGE (B-7) to find ρ, and make a scaled plot to check computed lengths.

control rust, and for geotextiles it provides protection from the ultraviolet rays[1] in sunlight and discourages vandalism.

The basic principle[2] of reinforced earth is shown in Fig. 12-4 where we see a wall acted on by either the Rankine or Coulomb active earth wedge. Full-scale tests have verified that the earth force developed from the active earth wedge at any depth z is carried by reinforcing strip tension.

Strip tension is developed in the zone outside the active earth wedge from the friction angle δ between strip and soil and the vertical earth pressure γz on the strip. With no lateral earth pressure left to be carried by the wall facings they can be quite thin and flexible with the principal functions of erosion control and appearance.

The following several factors enter into the design of a reinforced earth wall:

1. Backfill soil is usually specified to be granular; however, recent research indicates that we can use cohesive soil if a *porous* geotextile is used for reinforcement to allow backfill drainage. This allows one to use the drained friction angle ϕ' to calculate friction between the soil and reinforcing.

   For cohesive materials, either use a narrow vertical back face zone of granular material or, alternatively, use strips of a permeable geotextile for vertical drainage.

[1]Most geotextiles have a rating of strength loss versus amount of ultraviolet exposure. ASTM D 4355 gives a standard in which geotextile strength loss is reported for 150 hours of exposure.

[2]An extensive literature survey along with a number of applications, primarily in Europe, is given by Ingold (1982).

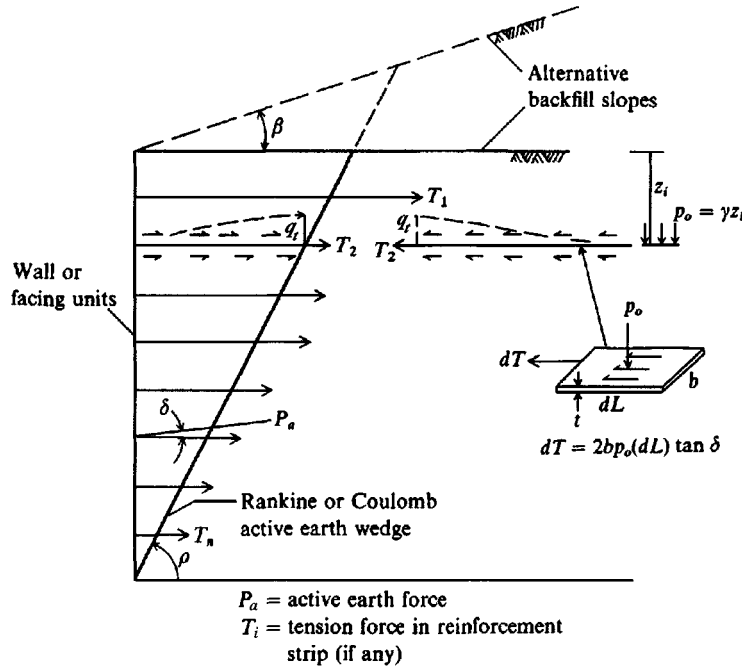

Figure 12-4 The general concept of reinforced earth is that $\sum T_i = P_a \cos \delta$, so the earth force against the wall (or facing units) = 0.

2. Backfill soil should be compacted, taking care not to get equipment too close to the facing unit, so that it is not pulled from the reinforcement.

   It is also necessary to exercise care with geotextile fabrics not to tear the fabric in the direction parallel to the wall. A partial tear of this type would reduce the amount of tension the fabric can carry.
3. Tests with experimental walls indicate that the Rankine wedge (of angle $\rho = 45° + \phi/2$) adequately defines the "soil wedge." This angle should be routinely checked using the trial wedge method (or computer program) for large backfill β angles.
4. The wall should be sufficiently flexible that the active earth pressure wedge forms and any settlement/subsidence does not tear the facing unit from the reinforcement.
5. It is usual to assume all the tension stresses are in the reinforcement outside the assumed soil wedge zone—typically the distance L_e of Fig. 12-5.
6. The wall failure will occur in one of three ways:
   a. Tension in the reinforcements
   b. Bearing-capacity failure of the base soil supporting the wall, as along the baseline *AB* of Figs. 12-3 and 12-6.
   c. Sliding of the full-wall block (*ACDB* of Fig. 12-6) along base *AB*.
7. Surcharges (as in Fig. 12-6) are allowed on the backfill. These require analysis to ascertain whether they are permanent (such as a roadway) or temporary and where located. For example:
   a. Temporary surcharges within the reinforcement zone will increase the lateral pressure, which in turn increases the tension in the reinforcements but does not contribute to reinforcement stability.

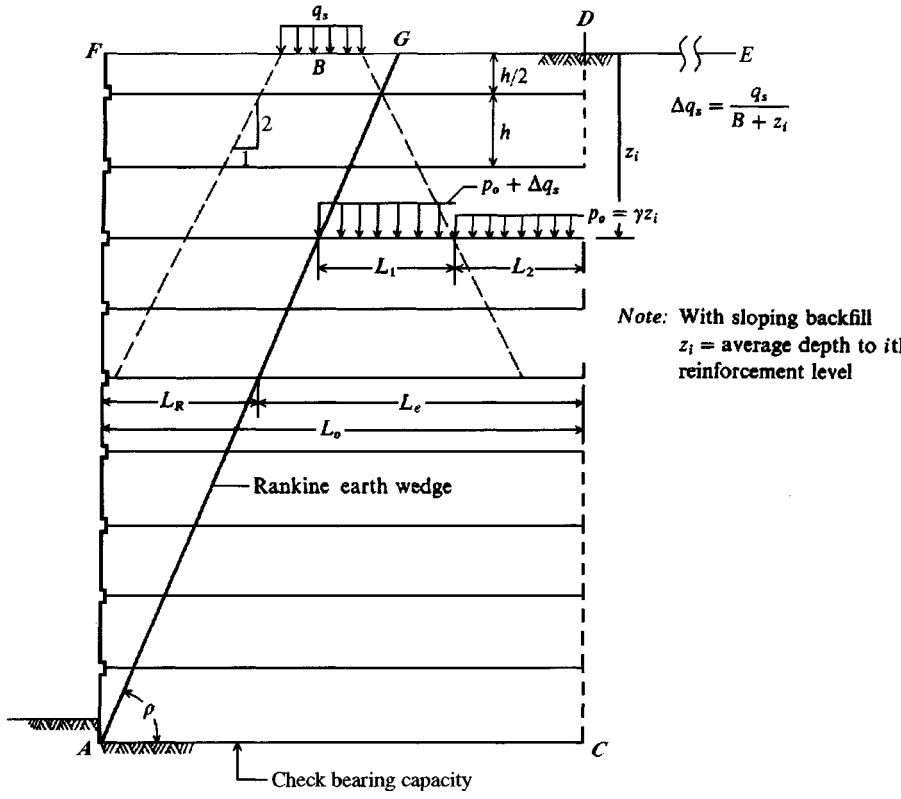

Figure 12-5 Length of reinforcements $L_o = L_R + L_e$ as required but must extend beyond Rankine/Coulomb earth-pressure wedge.

b. Permanent surcharges within the reinforcement zone will increase the lateral pressure and tension in the reinforcements and will contribute additional vertical pressure for the reinforcement friction.

c. Temporary or permanent surcharges outside the reinforcement zone contribute a lateral pressure, which tends to overturn the wall.

In most cases the lateral pressure from a backfill surcharge can be estimated using the Theory of Elasticity equation [Eq. (11-20)]. One can also use the Boussinesq equation for vertical pressure, but it may be sufficiently accurate to use the 2 : 1 (2 on 1) method [Eq. (5-2)] adjusted for plane strain to give

$$q_v = \frac{Q}{B + z}$$

where $Q = Bq_o$ for the strip width (side view) and average contact pressure produced by the surcharge; for point loads use either a unit width (0.3 m or 1 ft) or Eq. (5-3). Since these two methods give greatly differing vertical pressures (the 2 : 1 is high and Eq. (5-3) is very low) you may have to use some judgment in what to use—perhaps an average of the two methods.

B = strip width; you are implicitly using $L = 1$ unit of width.

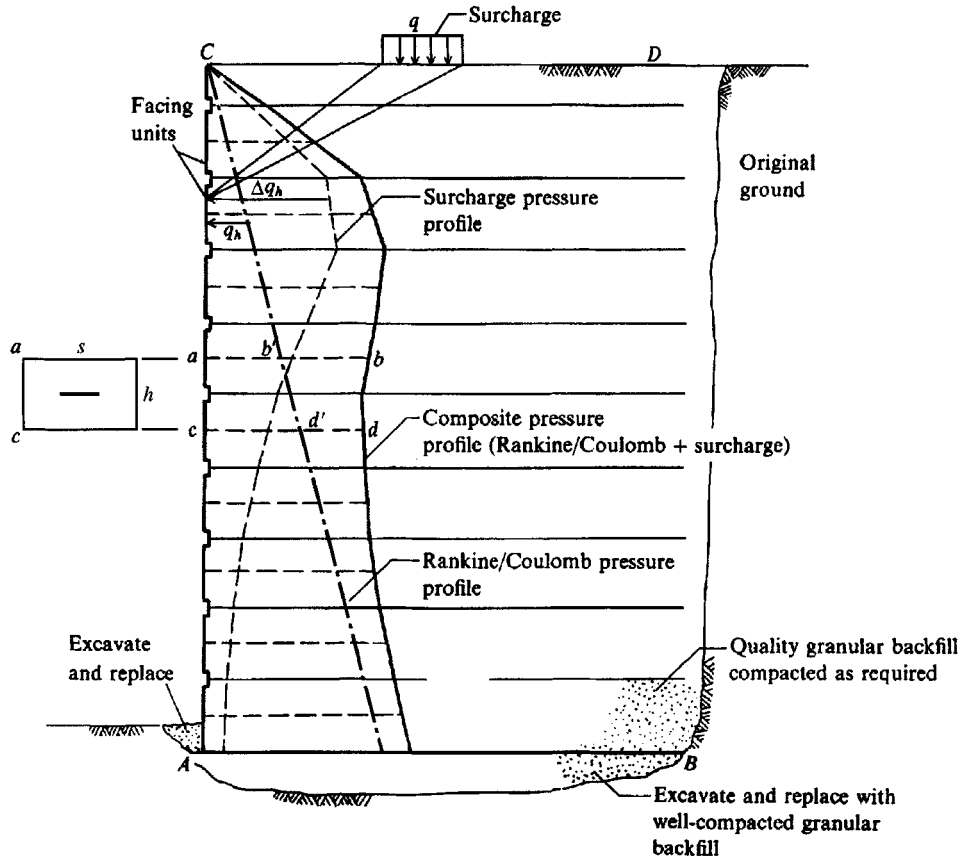

Figure 12-6 General wall case with surcharge on backfill as from a road or other construction. Linearizing the surcharge pressure profile as shown is sufficiently accurate.

Laba and Kennedy (1986) used the 2:1 vertical pressure method [Eq. (5-2)] as shown in Fig. 12-5 with reasonably good results. In this figure Eq. (5-2) is being used to get a pressure increase in the zone L_1 so that the friction resistance F_R for the effective lengths ($L_e = L_1 + L_2$) is

$$F_r = \tan\delta[(\gamma z + \Delta q)L_1 + \gamma z L_2]$$

where terms are identified in Fig. 12-5.

8. Corrosion may be a factor where metal reinforcements are used. It is common to increase the theoretical strip thickness somewhat to allow for possible corrosion within the design period, which may be on the order of 50 to 100 years.
9. Where aesthetics is critical, a number of concrete facing unit configurations are available in a wide range of architecturally pleasing facades, which can either outline the wall or blend it into the landscape (Figs. 12-2*b*, *d*).
10. There will be two safety factors SF involved. One SF is used to reduce the ultimate strength of the reinforcements to a "design" value. The other SF is used to increase the computed length L_e required to allow for any uncertainty in the backfill properties and soil-to-reinforcement friction angle δ.

12-3 DESIGN OF REINFORCED EARTH WALLS

The design of a reinforced earth wall proceeds basically as follows:

1. Estimate the vertical and horizontal spacing of the reinforcement strips as in Fig. 12-7. Horizontal spacing s is meaningless for both wire grids and geotextile sheets but one must find a suitable vertical spacing h for those materials. The vertical spacing may range from about 0.2 to 1.5 m (8 to 60 in.) and can vary with depth; the horizontal strip spacing may be on the order of 0.8 to 1.5 m (30 to 60 in.). The lateral-earth-pressure diagram is based on a unit width of the wall but is directly proportional to horizontal spacing s.
2. Compute the tensile loads of the several reinforcements as the area of the pressure diagram contributing to the strip. This calculation can usually be done with sufficient accuracy by computing the total lateral pressure at the strip (see Fig. 12-6) level,

$$q_{h,i} = q_h + \Delta q_h \tag{12-1}$$

where q_h = Rankine or Coulomb lateral earth pressure, taking into account backfill slope and any uniform surcharge

Δq_h = lateral pressure from any concentrated backfill surcharge; obtain using your computer program SMBLP1

With the average pressure obtained from Eq. (12-1), the strip tensile force can be computed as

$$T_i = A_c q_{h,i} \tag{12-1a}$$

where A_c = contributory area, computed (including the horizontal spacing s) as

$$A_c = \frac{h_i + h_{i+1}}{2} s$$

One should routinely make a computational check:

$$\sum T_i = s \times (P_{ah} + \text{area of } \Delta q \text{ diagram}) \tag{12-1b}$$

Figure 12-7 Typical range in reinforcement spacing for reinforced earth walls.

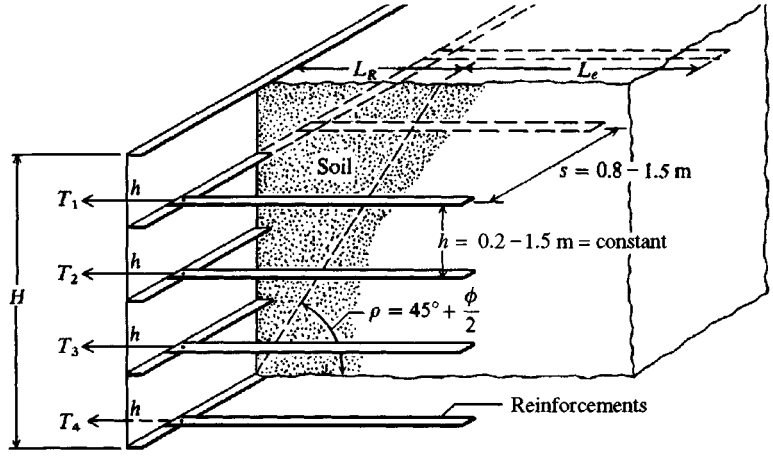

That is, the sum of the several tensile reinforcement forces should equal the lateral-earth-pressure diagram ratioed from a unit width to the actual reinforcement spacing s.

Although Fig. 12-6 does not show the correct pressure profile for a surcharge q_o and $\beta > 0$ (for that case refer to Fig. 11-9*c* and use K_a, which includes the effect of β), it is a common case. The other common case is a sloping backfill (Fig. 11-9*b*) but no concentrated surcharge.

3. Compute the strip lengths L_e of Fig. 12-5 that are required to develop a friction resistance $F_r = T_i \times \text{SF}$ (or $L_{e,\text{design}} = L_{e,\text{computed}} \times \text{SF}$). From these lengths and the Rankine wedge zone we can then determine the overall strip length L_o to use. It is common to use a single length for the full wall height so that the assembly crew does not have to be concerned with using an incorrect length at different elevations; however, this choice is a designer's prerogative. The friction length is based on soil-to-strip friction of $f = \tan\delta$, where δ = some fraction of ϕ such as 1.0, 0.8, 0.6ϕ. What to use depends on the roughness of the strip (or geotextile sheet). For rough materials use $\delta = \phi$; for smooth metal strips use $\delta \approx 20$ to 25°.

   For strips of $b \times L_e$ or geotextile sheets of base width $\times L_e$, both sides resist in friction. For round bars the perimeter resists friction. In both cases friction is the product of $f \times$ normal pressure on the reinforcement, computed as $p_o = \gamma z_i$ where z_i = *average* depth from ground surface to reinforcement. Using consistent units, this approach gives the following reinforcements:

$$\text{Strip:} \quad F_r = 2(\gamma z_i)(b \times L_e)\tan\delta \geq T_i \times \text{SF} \tag{12-2a}$$

$$\text{Rod:} \quad F_r = \pi D(\gamma z_i)L_e \tan\delta \geq T_i \times \text{SF} \tag{12-2b}$$

$$\text{Sheet:} \quad F_r = 2(\gamma z_i)(1 \times L_e)\tan\delta \geq T_i \times \text{SF} \tag{12-2c}$$

   where b = strip width, D = rod diameter, and 1 = unit sheet width. Manufacturers provide geotextiles in rolls of various lengths and widths.[3] For the year 1993 and earlier, the *Specifier's Guide* of fabric specifications listed roll dimensions of geotextiles the given manufacturer could supply. For 1994 and later, the roll dimensions are no longer supplied. The supplier should be contacted prior to design to see what fabric dimensions can be provided.

4. Next compute the reinforcement area for strips $b \times t$ and for rods with bar diameter D. For wire and geotextile grids, obtain the tension force per some unit of width. For geotextile sheets look in the manufacturer's catalog to find a fabric with a suitable strength.

   For these materials a suitable SF must be used to reduce the ultimate tensile strength of metal strips and bars to a design value or the geotextile strength (which is, by the way, orientation-sensitive) to a design value. For metals it is common to use some SF such as 1.5 to 1.67; however, for both metals and geotextiles we can compute an SF based on partial safety factors as follows:

$$T_{\text{allow}} = T_{\text{ult}}\left(\frac{1}{\text{SF}_{\text{id}} \times \text{SF}_{\text{cr}} \times \text{SF}_{\text{cd}} \times \text{SF}_{\text{bd}} \times \text{SF}_{\text{if}} \times \text{SF}_{\phi}}\right) \tag{12-3}$$

[3]The Industrial Fabrics Association International, 345 Cedar St., Suite 800, St. Paul, MN, 55101, Tel. 612-222-2508, publishes a quarterly magazine *Geotextile Fabrics Report* and an annual *Specifier's Guide,* which tabulates available geotextile fabrics and select engineering properties such as tensile strength and permeability.

where T_{allow} = allowable tensile stress
T_{ult} = ultimate tensile stress
SF_{id} = installation damage factor, 1.1 to 1.5 for geotextiles; 1 for metal
SF_{cr} = creep factor (1.0 to 3.0 for geotextiles; 1 for metal)
SF_{cd} = factor for chemical damage or corrosion (about 1.0 to 1.5 for geotextiles; 1.0 to 1.2 for metal)
SF_{bd} = factor for biological degradation (about 1.0 to 1.3 for geotextiles; 1.0 to 1.2 for metal)
SF_{if} = importance factor (1.0 to 1.5)
SF_{ϕ} = general factor; (about 1.0 for geotextiles; about 1.3 to 1.4 for metal)

Koerner (1990 in Table 2-12, p. 115) gives some ranges for the partial factors of safety. The preceding values (not all are in his table) can be used, since you have to estimate them anyway.

Let us compute an allowable tensile stress f_a for a steel strip based on 350 MPa steel (factors not shown are 1.0) as

$$f_a = 350\frac{1}{1.1 \times 1.2 \times 1.3} = \frac{350}{1.716} = 204 \rightarrow \mathbf{200}\ \text{MPa}$$

Let us now consider a geotextile example. From the 1995 *Specifier's Guide* we find an Amoco 2044 woven (W) geotextile with a wide-width tensile strength, using the ASTM D 4595 method, of 70.05 kN/m in both the MD (along the roll) and XD (across the roll) directions. The allowable tensile strength is computed using Eq. (12-3). Substituting some estimated values, we obtain

$$T_{allow} = 70.05\frac{1}{1.5 \times 2.0 \times 1.2 \times 1.1 \times 1.1 \times 1.0} = \frac{70.05}{4.356}$$
$$= 16.08 \rightarrow \mathbf{16.0}\ \text{kN/m}$$

12-3.1 General Comments

For geotextiles we have a problem in that the fabric strength varies

1. Between manufacturers.
2. With fabric type and grade. For example, woven fabric is usually stronger than film fabric and additionally has a larger coefficient of friction.
3. With direction. The MD direction (*machine direction,* also *warp;* that is, with the roll) is stronger than (or as strong as) the XD direction (*cross-machine,* or *fill;* that is, across the roll—transverse to the roll length). Sometimes the strength difference is on the order of XD $\approx$ 0.5MD. This means that attention to the strength direction during placing may be critical.

We must test (or have tested by the mill, or use an independent testing laboratory) the fabric to obtain the strength, usually in kN/m (or lb/in.) of width. From the several choices we choose a strip so that

$$\text{Strip width b} \times \textit{design}\ \text{strength/unit width} \geq T_i$$

Strip design may require several iterations to set the horizontal and vertical reinforcement spacing. Since fabric cost is relatively small compared with other costs (engineering time, backfill, etc.) and since there is some uncertainty in this type of analysis, a modest amount of overdesign is acceptable.

Metal reinforcement strips currently available are on the order of $b = 75$ to 100 mm and t on the order of 3 to 5 mm, with 1 mm on each face excluded for corrosion. Concrete reinforcing rods are often used for their roughness, but with one end prepared for attachment to the face piece—by welding or threads. Rod diameters should be at least three times larger than the average (D_{50}) particle diameters of the granular backfill so adequate friction contact is developed. Particle diameter is less critical with wire grids since the grid bars perpendicular to the tension rods provide considerable additional pullout resistance.

The pullout forces and resistance are assumed to be developed as shown in Fig. 12-4 where a tension from the wall face to the Rankine/Coulomb rupture zone defined by the angle ρ develops to a maximum at the wedge line. Even with a sloping backfill and/or surcharges the Rankine wedge shown is generally used. This tension is resisted by the friction developing outside the zone along length L_e of Fig. 12-5, so we can write, from the differential equation shown on Fig. 12-4,

$$T = \int_0^{L_e} 2b(p_o \tan \delta)\, dL$$

This expression may be somewhat of a simplification, and $2b$ must be replaced with the perimeter (πD) for round bars, but it seems to allow an adequate wall design.

Most of the construction technology currently used for reinforced earth walls is under patent protection; however, it is important to understand the principles involved and methods of analysis both in order to make a reasonable decision on the best system for a site and because the patents on some of the walls will expire shortly and the method(s) will transfer to the public domain.

12-3.2 Soil Nailing

Using "nails" to reinforce the earth is a relatively recent (about 20 years old) method for soil reinforcement. Basically this consists in either driving small-diameter rods (on the order of 25 to 30 mm) into the earth or drilling holes on the order of 150 to 200 mm, inserting the required diameter (again 25- to 30-mm) rod, and filling the remainder of the hole with grout (usually a cement-sand mixture with a low enough viscosity that it can be pumped).

The essential difference between soil nailing and tieback walls (of Chap. 14) is that there is little prestress applied to the soil nails, whereas the tieback wall requires prestressing the rods.

Soil nailing has the advantage of being suitable both for walls and for excavation support. For walls one starts the wall upward and at specified levels inserts "nails" into the backfill. The wall then proceeds and the nail is attached to the wall (often through a prepared hole with a face plate and a nut for fastening). In excavations some depth is excavated, the nails are inserted, and wall is added and attached as for the retaining wall. The next level is excavated, nails are inserted, wall facing is added and attached, etc.

The rods are usually inserted or drilled at a slope from the horizontal of about 15°, but near the upper part of the wall the slope may be larger (20 to 25°) to avoid underground utilities.

The latest soil nail insertion technique consists in using a compressed-air driver that fires (or launches) the nail at high velocity into the soil. The tip is the launch point, so the nail rod is pulled rather than driven into position. Pulling avoids rod buckling, since the nail diameters for current air launchers are on the order of 25 to 40 mm for depths of 3 to 6 m—larger diameters may be used but smaller penetration depths result. This type of device can fire a nail at any orientation and at a rate of up to 15 per hour. The nail head is normally prefitted with a threaded portion or prefastened to an arresting collar so that it is not fired too far into the ground for accessibility.

Rod spacing varies between 1 and 4 m^2 of wall surface area depending on factors such as type of retained soil, wall height, available space behind the wall for rod penetration, rod diameter, and designer caution.

Although the analysis is somewhat similar to other reinforced earth walls there are some differences. Usually the analysis consists in a global stability analysis using a slope stability program. The slope stability program must be specifically modified to allow locating the rods (if they protrude through the trial circle arc).

It may also require modification to use a portion of a logarithmic spiral as the failure surface rather than part of a circle. A rod stability analysis for both tension (or pullout) and bending (on the potential slip plane) is also required—but often just for pullout.

One can make a reasonable wall design with reference to Fig. 12-8 as follows:

1. Estimate the rod tension T_i using the appropriate pressure diagram of Fig. 12-8*b* (see similarity with Fig. 14-5), the position of the rod (upper $\frac{1}{4}$, middle $\frac{1}{2}$, or lower $\frac{1}{4}$), and the spacing. Use the equation shown on the figure for T_i. You should compute a table with the several values of T_i. Since all the rods should be the same diameter D, select the largest T_i.

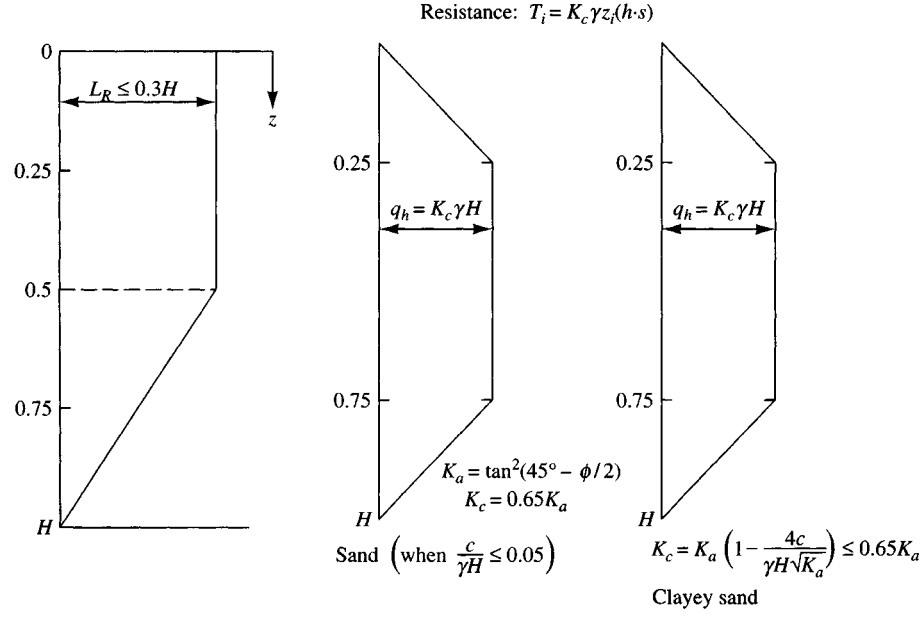

(*a*) Modified Rankine failure wedge. Note that it roughly approximates a logarithmic spiral.

(*b*) Approximate soil pressure diagrams with pressure intensities and soil types

Figure 12-8 Failure wedge and approximate pressure diagrams for soil nailing.

2. Compute the required rod diameter D for this tension using a suitable SF so that $f_a = f_y/\text{SF}$ of rod steel (or other rod material). With T_i and f_a, compute

$$D = \sqrt{\frac{T_i}{0.7854 f_a}}$$

3. Estimate the nail friction resistance (outside the modified Rankine wedge zone of Fig. 12-8*a*) using Eq. (12-2*b*). Use the actual rod diameter if the rod is driven, but use the grouted diameter if the rod is put in a drilled hole and grouted. Use $\tan\delta$ = estimated value for soil-metal interface based on metal roughness. Use $\delta = \phi$ for grouted rods. For sloping rods use an average depth z_i in the length outside the wedge zone. One must use a trial process for finding the computed distance $L_{e,\text{comp}}$—that is, assume a length and compute the resistance $F_r \geq T_i$. Several values may be tried, depending on whether all rods are to be the same length, or variable lengths (depending on wall location) are to be used. In any case increase the computed length as

$$L_{e,\text{des}} \geq \text{SF} \cdot L_{e,\text{comp}}$$

Compute the total rod (nail) length L_{tot} at any location as the length just computed for pull-out resistance $L_{e,\text{des}}$ + length L_R to penetrate through the Rankine wedge zone, giving the following:

$$L_{\text{tot}} = L_{e,\text{des}} + L_R$$

It will be useful to make a table of nail lengths L_{tot} versus depth z to obtain the final design length(s). One has the option of either using a single nail length or of locating elevations where the nail length changes occur if different nail lengths are used.

4. Make a scaled plot of the wall height, modified Rankine wedge, rod locations, and their slopes and lengths. Use this plot to make your slope stability analysis. Clearly one possibility is to use a regular slope stability computer program and ignore the "nails."

There is already an enormous amount of literature as well as at least three separate design procedures for nailed walls. The reader is referred to Jewell and Pedley (1992), Juran et al. (1990) and ASCE Geotechnical SP No. 12 (1987) for design information sources or to build confidence in the procedure outlined above.

12-3.3 Examples

We will examine the reinforced earth methodology further in the following three examples.

Example 12-1. Analyze the wall of Fig. E12-1 using strip reinforcement. The strips will be tentatively spaced at $s = 1$ m and $h = 1$ m and centered on the concrete wall facing units. We will use interlocking reinforced concrete facing units, shaped as indicated, that are 200 mm thick (with a mass of about 1000 kg or 9.807 kN each). A wall footing will be poured to provide alignment and to spread the facing unit load somewhat, since their total mass is more than an equivalent volume of soil. A 150-mm thick reinforced cap will be placed on top of the wall to maintain top alignment and appearance.

Required. Analyze a typical interior vertical section and select tension strips based on $f_y = 250$ MPa and $f_a = 250/1.786 = 140$ MPa. Other data: $\phi = 34°$; $\gamma = 17.30$ kN/m^3; and assume $\delta = 0.7 \times 34 = 24°$.

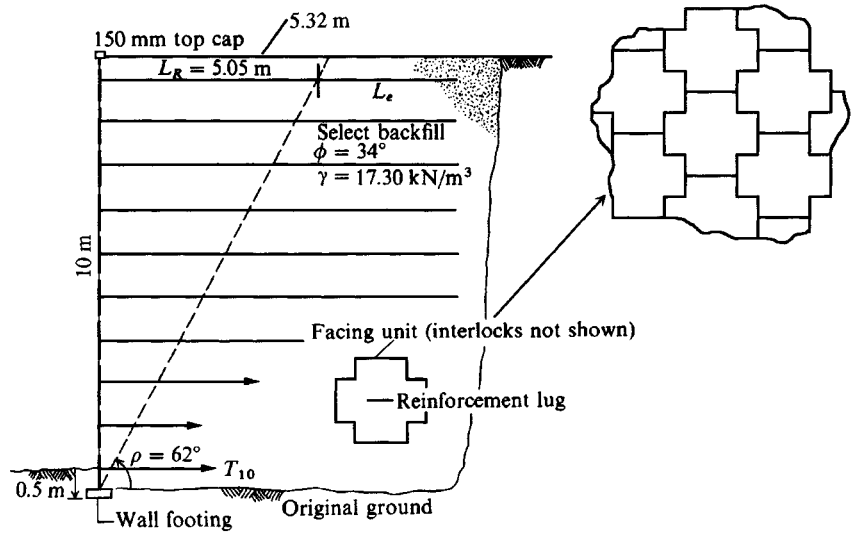

Figure E12-1

Solution. From Table 11-3 obtain $K_a = 0.283$

$$f = \tan\delta \rightarrow \tan 24° = 0.445$$

Set up the following table from wall data (L_e is computed after T_i and strip width b are computed):

Strip no.	z_i, m	$T_i = \gamma z_i(1 \times 1)K_a$, kN	$L_e = \dfrac{T_i \times \text{SF}}{2b\tan\delta(\gamma z_i)}$, m
1	0.5	2.45	4.77
2	1.5	7.34	↑
3	2.5	12.24	|
4	3.5	17.14	|
5	4.5	22.03	|
6	5.5	26.93	|
7	6.5	31.82	|
8	7.5	36.72	|
9	8.5	41.62	↓
10	9.5	46.51	4.77
		$\sum T_i = 244.80$ kN	

Check:

$$P_a = \tfrac{1}{2}\gamma H^2 K_a \qquad \text{[Eq. (11-9) and } s = 1 \text{ m} = \text{unit width]}$$

$$P_a = \tfrac{1}{2}(17.30)(10^2)(0.283) = \mathbf{244.80}\ \text{kN/m}$$

Next we find the cross section of the reinforcement strips. Tentatively try $b = 100$ mm since the wall is 10 m high.

$$b \times t \times f_a = T_i \qquad \text{(a SF is already on } f_a\text{)}$$

The largest T_i is strip 10, so for T_{10} we have

$$0.100(t)(140) = \mathbf{46.51}\ \text{kN} \qquad \text{(using meters)}$$

Solving (and inserting 1000 to convert MPa to KPa), we obtain

$$t = \frac{46.51}{0.10(140)1000} = 0.003\,32 \text{ m} \rightarrow 3.32 \text{ mm, so use } t = \mathbf{5.0} \text{ mm}$$

This value allows a little less than 1-mm loss on each side for corrosion. Next find the strip length for T_i and total strip length L_o. We equate $\tan\delta \times$ vertical pressure p_o on both sides of strip of width $b \times L_e$ to the strip tension $T_i \times$ SF. Get T_i from the preceding table and use an SF = 1.5:

$$2b(\tan\delta)(\gamma z_i)L_e = T_i(\text{SF})$$

Rearranging into solution form for L_e, we have

$$L_e = \frac{(\text{SF})T_i}{2b(\tan\delta)(\gamma z_i)} = \frac{1.5T_i}{2(0.10)(0.445 \times 17.30z_i)}$$

This equation can be programmed. The first value (for $z_i = 0.50$ m) is

$$L_e = \frac{1.5(2.45)}{1.5397(0.50)} = \mathbf{4.77} \text{ m}$$

Other values for $z_i = 1.5, 2.5, 3.5, \ldots, 9.5$ are similarly computed and we find them constant as shown in the preceding table. We now find total strip lengths L_o as follows:

$$\rho = 45° + \phi/2 = 45° + 34°/2 = 62°$$

The Rankine zone at 9.5 m (strip 1) is

$$L_R = 9.5 \times \tan(90° - 62°) = 9.5 \times \tan 28° = 5.05 \text{ m}$$
$$L_o = L_R + L_e = 5.05 + 4.77 = \mathbf{9.82} \text{ m}$$

We can use this length for all of the strips or, noting that the Rankine zone has a linear variation, we can use a linear variation in the strip lengths and apply careful construction inspection to ensure the correct strip lengths are used. This wall is high, so considerable savings can be had by using variable strip lengths. Do it this way:

At 0.5 m above base: $L_o = 0.5 \times \tan 28° + 4.77 = \mathbf{5.04}$ m

At 4.5 m above base: $L_o = 4.5 \times \tan 28° + 4.77 = \mathbf{7.16}$ m

At 9.5 m above base (top strip): $L_o = \mathbf{9.82}$ m

As a check, plot the wall to scale, plot these three strip lengths, connect them with a line, and read off the other strip lengths.

Bearing capacity. We should check the bearing capacity for a unit width strip with a footing width B of either 9.82 or 5.04 m depending on strip configuration. Take all shape, depth, and inclination factors = 1.0. The poured footing for the concrete facing units will have a unit length but should have a B that is wide enough (greater than the 200-mm thickness of the wall units) that the bearing pressures for backfill and facing units are approximately equal to avoid settlement of the facing units and possibly tearing out the reinforcement strips.

Sliding resistance. The wall should resist sliding. Assuming a linear variation of reinforcement strips, we will have a block of soil that is one unit wide of weight $W = \gamma H B_{\text{av}}(1.0)$. Note that sliding is soil-to-soil, so take $\tan\delta = \tan\phi$. Inserting values, we have

$$W = 17.30(10)\frac{9.82 + 5.04}{2} \times 1 = 1286 \text{ kN}$$

$$F_R = W\tan\phi = 1286\tan 34° = \mathbf{867} \text{ kN} \gg P_a = 244.8 \text{ kN}$$

$$\text{Sliding stability} = \frac{867}{244.8} = \mathbf{3.5}$$

The wall should be drawn to a reasonable scale with all critical dimensions shown to complete the design. Owing to limited text space this figure is not included here.

////

Example 12-2. Compute the reinforcement tension and friction resistance to obtain a tentative strip length L_o for the wall of Fig. E12-2 with a surcharge on the backfill. Check the strip at the 1.5-m depth (T_5) to illustrate the general procedure with a surcharge.

Soil data: $\gamma = 17.30$ kN/m^3; $\phi = 32°$ (backfill); take $f = \tan\delta = 0.4$ as the coefficient of friction between backfill soil and strip.

Strip data: $h = 0.30$ m; $s = 0.60$ m; width $b = 75$ mm; SF $= 2.0$ on steel of $f_y = 250$ MPa; SF $= 2.0$ on soil friction.

Solution. Obtain Rankine $K_a = 0.307$ from Table 11-3. Use your computer program SMBLP1 to obtain the lateral pressure profile for the surcharge. Assume plane strain, the B dimension of 1.5 m as shown, and a length of 1 m consistent with the Rankine wall pressures. A good approach is to use unit areas of 1.5/5 = 0.3 (NSQW = 5) and 1.0/4 = 0.25 (NSQL = 4) so that PSQR = $100(0.3 \times 0.25) = 7.5$ kN. When requested by the program, have the wall pressure profile output along with the total wall force so you can compare these to the values plotted on Fig. E12-2. You can use a "point" load at 2.25 m from wall with $P = 150$ kN and obtain almost "exact" pressures from 1.5 m down to the 6.0 m depth, but in the upper 1.5 m the pressures are somewhat in error.

At the 1.5-m depth the Rankine earth pressure is

$$q_R = \gamma z_i K_a = 17.30(1.5)(0.307) = \mathbf{8.0}\ \text{kPa}$$

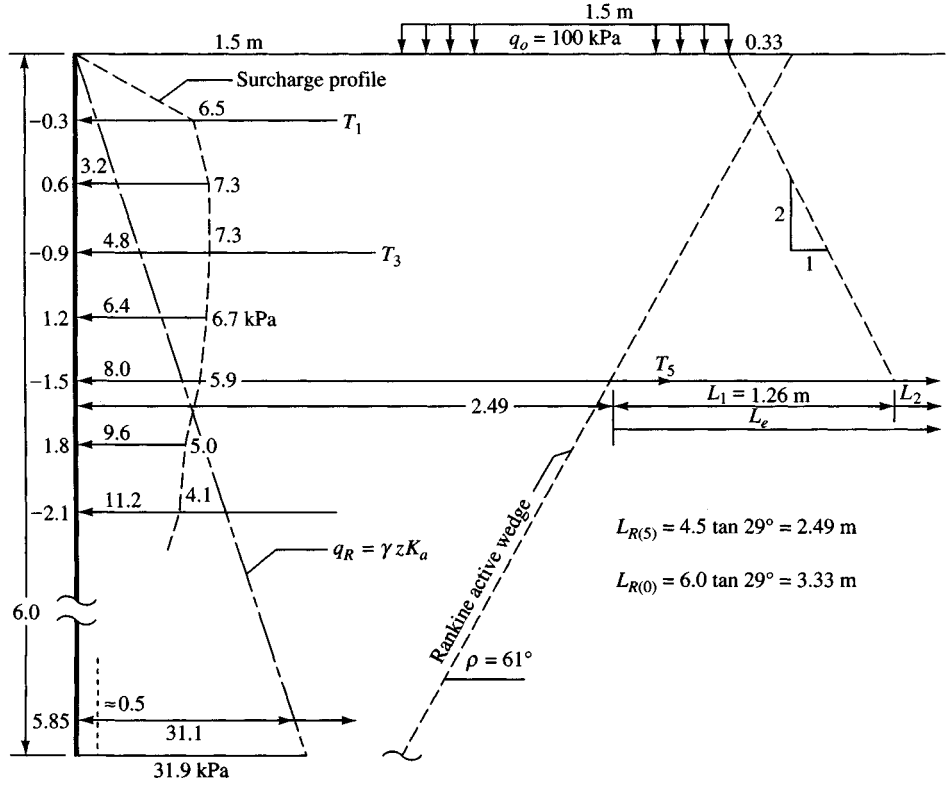

Figure E12-2

At this depth (also 4.5 m above base) program SMBLP1 gives

$$\Delta q = \mathbf{5.9}\ \text{kPa}$$

The design pressure is the sum of the two pressures, giving

$$q_{\text{des}} = q_R + \Delta q = 8.0 + 5.9 = 13.9\ \text{kPa}$$

The strip design force is

$$\begin{aligned} T_5 = F_{\text{des}} &= q_{\text{des}}(h \times s) \\ &= 13.9(0.30 \times 0.60) = \mathbf{2.50}\ \text{kN/strip} \end{aligned}$$

The allowable strip tension $f_a = f_y/\text{SF} = 250/2 = 125$ MPa. The strip cross section of $b \times t$ with $b = 75$ mm is

$$b(t) f_a = T_5 \rightarrow t = \frac{F_{\text{des}}}{b f_a}$$

Inserting values, we obtain

$$t = \frac{2.5}{0.075 \times 125 \times 1000} = 0.000\,27\ \text{m} \rightarrow 0.27\ \text{mm}$$

Use $t = \mathbf{3}$ mm (to allow for corrosion)

The force $F_{\text{des}} = T_5$ must be resisted by friction developed on both sides of the strip of length L_e outside the Rankine wedge zone. This force will be assumed to be made of two parts, so $L_e = L_1 + L_2$.

From the sketch drawn to scale we can scale the length L_1 or directly compute it as follows:

$$\text{Distance to right edge of surcharge} = 1.5 + 1.5 = 3\ \text{m}$$

$$\begin{aligned} \text{Distance from wall} &= L_R + L_1 \\ &= \text{distance to right of surcharge} + 1.5/2 \\ L_R + L_1 &= 3.0 + 1.5/2 = 3.75\ \text{m} \\ L_1 &= 3.75 - L_R \\ L_1 &= 3.75 - 4.5\tan(90^\circ - \rho) \\ &= 3.75 - 2.49 = \mathbf{1.26}\ \text{m} \qquad (L_R = 2.49\ \text{m}) \end{aligned}$$

In this region the vertical pressure is

$$p_o = \gamma z_i + \frac{Q}{B + z_i}$$

$$p_o = 17.30(1.5) + \frac{1.5(100)}{1.5 + 2(0.75)} = 26 + 50 = \mathbf{76}\ \text{kPa}$$

Now equating friction resistance to tension and using the given SF = 2 we have

$$2b[(p_o \tan\delta)L_1 + (\gamma z_i \tan\delta)L_2] = 2.50(\text{SF})$$

Inserting values (remember that $\tan\delta$ was given as 0.4), we obtain

$$2(0.075)[(76)(0.4)L_1 + 17.30(1.5)(0.4)L_2] = 2.50(2)$$

Thus, we have

$$4.56L_1 + 1.56L_2 = 5.0$$

It appears we do not need an L_2 contribution. If on solving for L_1 we obtain a value > 1.26, we will set $L_1 = 1.26$ and solve for the L_2 contribution,

$$L_1 = \frac{5.0}{4.56} = \mathbf{1.09}\ \text{m} \qquad \text{(less than 1.26 m furnished, so result is O.K.)}$$

The total length at this point is

$$L_o = L_R + L_1 \rightarrow 2.49 + 1.09 = \mathbf{3.58}\ \text{m}$$

To complete the design, we must check other strip locations. Again one can use one length for all strips or use variable strip lengths, or use one strip length for the lower half of the wall and a different strip length for the upper half.

The remaining steps include the following:

1. Find the strip thickness based on the largest T_i. The Rankine earth pressure at $z_i = H = 5.85$ m is

$$q_R = 17.30 \times 5.85 \times 0.307 = \mathbf{31.1}\ \text{kPa}$$

and for the strip (including 0.5 for surcharge) is

$$T_{21} = (31.1 + 0.5)(0.3 \times 0.6) = \mathbf{5.7}\ \text{kN}$$

2. Check bearing capacity.
3. Check sliding stability.

////

Example 12-3. This example illustrates using geotextiles instead of strips for the wall design. The author's computer program GEOWALL will be used, since a substantial output is provided in a compact format and there is much busywork in this type of wall design. Refer to Fig. E12-3*a* and the following data:

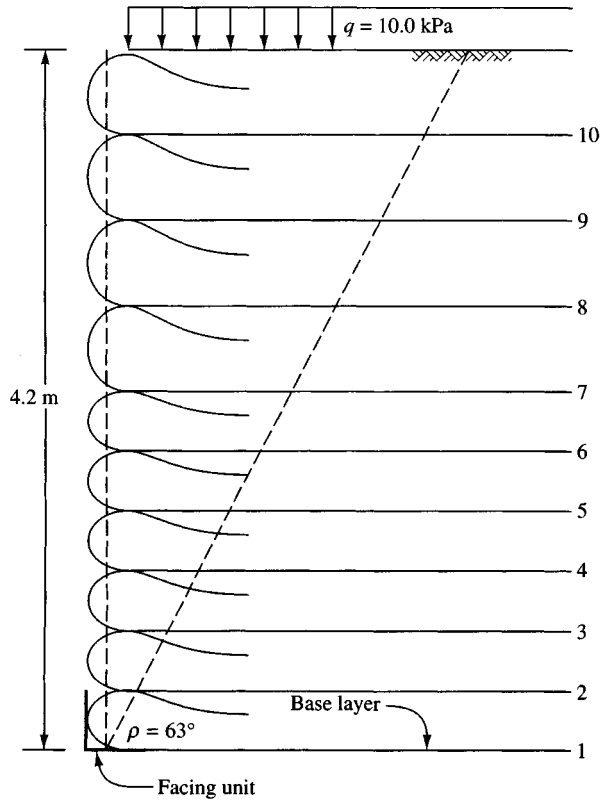

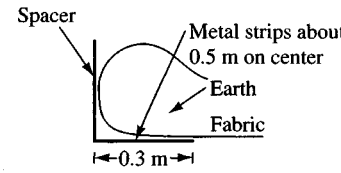

Facing form: 2–3 m long × 0.3 m legs
It is pulled and reused for next layer and so on.

Figure E12-3*a*

Backfill soil: $\gamma = 17.10\ \text{kN/m}^3$; $\phi = 36°$; $c = 0.0\ \text{kPa}$;
backfill slope $\beta = 0°$; Poisson's ratio $\mu = 0.0$
These are the input data here but the program also allows a concentrated backfill surcharge.

Base soil: $\gamma = 18.10\ \text{kN/m}^3$; $\phi = 15°$; $c = 20\ \text{kPa}$;
$\delta = 12°$ (soil to fabric); cohesion reduction factor $\alpha = 0.8$
(so $c_\alpha = 0.8 \times 20 = 16\ \text{kPa}$)

Note all these data are shown on the output sheets (Fig. E12-3*b*).

The geotextile will be tentatively selected from the 1994 *Specifier's Guide* published annually by the Industrial Fabrics Association International in the "Geotextiles" section as a Carthage Mills 20 percent fabric with a wide-width tensile strength of 32.4 kN/m. It has a permeability of 0.55 L/min/m^2, which should be adequate for a sandy backfill.

A geotextile wall design consists in obtaining an optimum balance between fabric weight (a function of strength), spacing, and length. This can be done in a reasonable amount of time only by using a computer. What does the computer program do that otherwise one would do by hand?

1. Compute the Rankine wall pressures and any Boussinesq surcharge pressures (here there are no Boussinesq-type surcharges, but there is a uniform surcharge of 10 kPa). These are always output in the first listed table using equal spacings of 0.3 m (or 1 ft) down the wall (Fig. E12-3*b*). The Rankine and Boussinesq values are summed, as these would be used to compute fabric tensile force at these locations. Note that $10K_a = 10(0.2597) = 2.597$ kPa as top table entry.

   Also found at this initial spacing are the total wall resultant (RFORC = **50.074** kN) for any surcharges + Rankine resultant and the location YBAR1 = $\bar{y}$ = **1.552** m above the base.
2. Next the program checks sliding stability based on asking for an input value for N_s (usual range between 2 and 3—the author used 2). For this value of N_s a base fabric length of 3.0 m is required.
3. The program then outputs to the screen the first table shown and asks whether the user wants to change any of the vertical spacings. The author did, and elected to use 0.4-m (16-in.) layers for the upper 3.6 m of wall height and 0.3-m (12-in.) layers for the last 0.6 m (3.6 + 0.6 = 4.2). These values were chosen to give a reasonable balance between number of sheets and excessively thick soil layers. One could obtain a solution using 0.6 m for six layers and 0.3 m for two layers at the bottom for some savings; however, although 0.6 m (24-in.) might produce a more economical wall, the facing part may be at risk, and if one of the geotextile layers went bad, the internal spacing would be unacceptable in that region.
4. The program recomputes the earth pressures, the backfill, and any surcharges at the new spacing (the spacings can be changed any number of times—or repeated) and outputs this spacing (nine at 0.4 m and two at 0.3 m) to screen and asks whether this is O.K. or to change it. The author answered O.K., and this was used.
5. Next compute the fabric lengths for tension. This result is also output in a table as shown. The program has a preset SF = 1.4 here but also requires a preset minimum distance for fabric lengths L_e:
   a. If the computed $L_e < 0.5$ m (18 in.) use 0.5 m.
   b. If the computed L_e is $0.5 < L_e < 1$ m use 1.0 m.
   c. If the computed $L_e > 1.0$ m use the computed value.

   We need 3.00 m for the first layer—not for tension but for the sliding SF computed earlier. The top layer (layer 11) requires

$$L_{\text{tot}} = L_e + L_R = 0.500 + 1.936 = \mathbf{2.436}\ \text{m}$$

The program does not make "exact" computations here. It takes the distance from layer $i-1$ to layer $i \times q_{h,i} \times \text{SF} = 1.4$ to compute sheet tension. Strictly, the tension force should use a zone centered (or nearly so) on the sheet, but the error from not doing this is negligible. In this example the preset minimum $L_e = 0.500$ m controls for the full wall height.

The required sheet length L_e is computed using the vertical distance from the backfill surface to the ith layer to compute the vertical sheet pressure. Both sides are used and with $\sigma_v \tan \delta$ and (if applicable) adhesion c_a.

On the basis of a screen display of this table the program asks what lengths the user wants to use. A single length or up to five different lengths can be used. From the table the author elected to use a single length for all layers of 3.00 m. This is less confusing to the construction crews, and besides in the upper several layers there are not much savings.

6. With the length selected the program next computes bearing capacity along AB of Fig. E12-3*c* using the length of layer 1 as B. It presents to the screen the stability number based on $\text{SF} = q_{\text{ult}}/q_v$, where $q_v = \gamma H + q_{\text{surcharge}}$. Shown on the output, the SF = **3.985**.

7. On the basis of the length and any surface surcharges, the program computes the overturning stability about point A of Fig. E12-3*c* (the toe). This is far from a rigid body, but conventional design makes a rigid body assumption. Here use block $ADCB$ with a surcharge on DC. This gives a block of width = 3.0 m and height = 4.2 m. The overturning moment from the horizontal force is

$$P_h \bar{y} = M_o = 50.074(1.552) = 77.71 \text{ kN} \cdot \text{m}$$

The resisting moment consists of two parts—one is the block mass and the other is block friction. Block friction is based on the concept that the the block cannot turn over without developing a vertical friction force on its back face of $P_{ah} \tan \phi$ (it is soil-to-soil), and the block has a moment arm that equals block width (here 3.0 m):

$$M_r = W\bar{x} = [4.2(3.0)(17.1) + 3.0(10)]1.5 = 368.19 \text{ kN} \cdot \text{m}$$

The program asks whether this is satisfactory, and it is.

8. As a final step the program produces the last table shown. It uses the vertical spacing, assumes an overlap of 1 m, and obtains the length of fabric to be ordered. For example for layer 11 we have space = 0.40 m + lap = 1.00 + required L_e = 3.00 m, or

$$L_{\text{tot}} = 0.40 + 1.00 + 3.00 = \mathbf{4.40} \text{ m (as shown in the table)}$$

At the bottom, $L_{\text{tot}} = 0.30 + 1.00 + 3.00 = \mathbf{4.30}$ m (also as shown).

9. In the last column the actual geotextile stress f_r is shown, which varies with Rankine tension stress. The f_a is computed using the input partial SF values listed on output sheet 1 [Eq. (12-3), which is programmed into this program]. From the output sheet we find that the partial SF_i in combination gives SF = 2.265 and

$$f_a = \frac{f_{\text{ult}}}{\text{SF}} = \frac{34.4}{2.265} = \mathbf{14.3} \text{ kPa (shown)}$$

From inspection of f_r we see the following stresses for layers 1, 3, and 4:

Layer	f_r, kPa	f_a, kPa
1	14.44	14.30
3	16.84	14.30
4	15.23	14.30

What do we do? Use this fabric-soil combination, or a stronger fabric, or a closer spacing. We probably would not want to use a closer spacing, so that leaves either using this fabric or a

Figure E12-3*b*

```
   PARTIAL EXAMPLE OF REINFORCED EARTH WALL USING GEOTEXTILE SHEETS

++++++++++ NAME OF DATA FILE USED FOR THIS EXECUTION:  EXAM123.DTA

NO OF CONC LOADS ON BACKFILL =  0
              IMET (SI > 0) =  1

WALL HEIGHT =   4.200  M   BACKFILL SURCHARGE =  10.000 KPA
BACKFILL SOIL:
                              UNIT WEIGHT =  17.100 KN/M^3
                 ANGLE OF INT FRICT, PHI1 =  36.000 DEG
                        BACKFILL COHESION =    .000 KPA
                    BACKFILL SLOPE, BETA1 =    .000 DEG
                          POISSON'S RATIO =    .000
BASE SOIL:
                              UNIT WEIGHT =  18.100 KN/M^3
                 ANGLE OF INT FRICT, PHI2 =  15.000 DEG
                       BASE SOIL COHESION =  20.000 KPA
   EFF ANGLE OF INT FRIC TO FABRIC, EPHI2 =  12.000
  EFF BASE SOIL COHESION TO FABRIC, ECOH2 =  16.000 KPA (   .80)

GEOTEXTILE TENSILE STRENGTH PERPENDICULAR TO WALL =    32.400 KN/M

BASED ON THE INPUT ULTIMATE GEOTEXTILE TENSION, GSIG =     32.40
AND USING THE FOLLOWING SAFETY FACTORS:
                        INSTALL DAMAGE, FSID =  1.10
                                 CREEP, FSCR =  1.20
               CHEMICAL DEGRADATION, FSCD =  1.30
             BIOLOGICAL DEGRADATION, FSBD =  1.20
               SITE SPECIFIC FACTOR, FSSS =  1.10
              COMBINED SF PRODUCT, FSCOMB = 2.265
      THE ALLOWABLE FABRIC TENSION, ALLOWT =   14.3039 KN/M

     RANKINE HORIZ. FORCE RESULTANT, RFORC =  50.074 KN
               LOCATION ABOVE BASE, YBAR1 =   1.552  M
        HORIZ FORCE BASED ON USING KA*COSB =   .2597  (   .2597)


THIS SET OF PRESSURES FOR EQUAL SPACINGS DOWN WALL
I      DDY(I)     QH(I)      BOUSQ QH   TOT QH, KPA
1       .0000    2.5969       .0000     2.5969
2       .6000    5.2614       .0000     5.2614
3       .9000    6.5936       .0000     6.5936
4      1.2000    7.9258       .0000     7.9258
5      1.5000    9.2580       .0000     9.2580
6      1.8000   10.5903       .0000    10.5903
7      2.1000   11.9225       .0000    11.9225
8      2.4000   13.2547       .0000    13.2547
9      2.7000   14.5869       .0000    14.5869
10     3.0000   15.9191       .0000    15.9191
11     3.3000   17.2514       .0000    17.2514
12     3.6000   18.5836       .0000    18.5836
13     3.9000   19.9158       .0000    19.9158
14     4.2000   21.2480       .0000    21.2480

FOR SLIDING STABILITY:
            REQUIRED BASE FABRIC LENGTH =   3.00  M
            BASED ON USING A SLIDING SF =   2.00
   AND USING AVERAGE WALL HEIGHT, HAVGE =   4.20  M
```

Figure E12-3*b* (*continued*)

THIS SET OF PRESSURES FOR MODIFIED VERTICAL SPACINGS

I	DDY(I)	QH(I)	BOUSQ QH	TOT QH, KPA
1	.0000	2.5969	.0000	2.5969
2	.4000	4.3732	.0000	4.3732
3	.8000	6.1495	.0000	6.1495
4	1.2000	7.9258	.0000	7.9258
5	1.6000	9.7021	.0000	9.7021
6	2.0000	11.4784	.0000	11.4784
7	2.4000	13.2547	.0000	13.2547
8	2.8000	15.0310	.0000	15.0310
9	3.2000	16.8073	.0000	16.8073
10	3.6000	18.5836	.0000	18.5836
11	3.9000	19.9158	.0000	19.9158
12	4.2000	21.2480	.0000	21.2480

SOIL-TO-FABRIC FRICTION FACTORS:
DELTA = 24.00 DEG
ALPHA = 1.00 (ON COHESION)

FABRIC LENGTH SUMMARY--ALL DIMENSIONS IN M

LAYER NO	DEPTH DDY	VERT SPACING	LE	LR	LFILL LE+LR
11	.40	.40	.500	1.936	2.436
10	.80	.40	.500	1.733	2.233
9	1.20	.40	.500	1.529	2.029
8	1.60	.40	.500	1.325	1.825
7	2.00	.40	.500	1.121	1.621
6	2.40	.40	.500	.917	1.417
5	2.80	.40	.500	.713	1.213
4	3.20	.40	.500	.510	1.010
3	3.60	.40	.500	.306	.806
2	3.90	.30	.500	.153	.653
1	4.20	.30	.500	.000	3.000

COMPUTED BEARING CAPACITY = 326.04 KPA
COMPUTED VERTICAL PRESSURE = 81.82 KPA
GIVES COMPUTED SAFETY FACTOR SF = 3.985
***BEARING CAPACITY BASED ON B = 3.00 M
INITIAL BASE WIDTH = 3.00 M

EXTRA DATA FOR HAND CHECKING
NC, NG = 12.9 2.5 FOR PHI-ANGLE = 15.00 DEG
FOR VERTICAL PRESSURE USED AVERAGE WALL HEIGHT = 4.20 M

OVERTURNING STABILITY BASED ON USING:
BASE FABRIC LENGTH = 3.00 M
AVERAGE WALL HEIGHT = 4.20 M
THE COMPUTED O.T. STABILITY = 6.14

FABRIC LENGTH SUMMARY--ALL DIMENSIONS IN: M

LAYER #	DEPTH DDY	VERT SPACING ACTUAL	VERT SPACING MAXIMUM	OVERLAP LO	FILL LE+LR* ROUND	FILL LE+LR* (REQ'D)	TOT L**	REQ'D GSIG,KN/M
11	.40	.400	3.271	1.000	3.00	(2.44)	4.40	3.962
10	.80	.400	2.326	1.000	3.00	(2.23)	4.40	5.572
9	1.20	.400	1.805	1.000	3.00	(2.03)	4.40	7.181
8	1.60	.400	1.474	1.000	3.00	(1.82)	4.40	8.791
7	2.00	.400	1.246	1.000	3.00	(1.62)	4.40	10.400
6	2.40	.400	1.079	1.000	3.00	(1.42)	4.40	12.009
5	2.80	.400	.952	1.000	3.00	(1.21)	4.40	13.619
4	3.20	.400	.851	1.000	3.00	(1.01)	4.40	15.228
3	3.60	.400	.770	1.000	3.00	(.81)	4.40	16.838
2	3.90	.300	.718	1.000	3.00	(.65)	4.30	13.534
1	4.20	.300	.673	1.000	3.00	(3.00)	4.30	14.439

* = ROUNDED FILL Le + Lr AND ACTUAL (REQ'D) LENGTHS
** = TOTAL REQUIRED FABRIC LENGTH = Le + Lr + Lo + SPACING

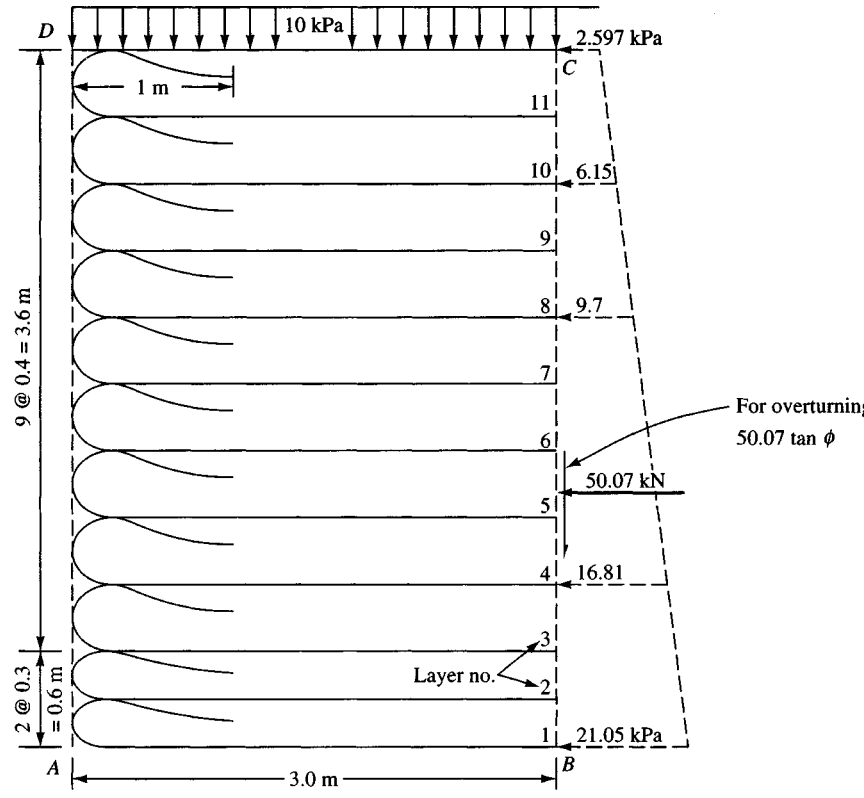

Figure E12-3*c*

stronger one (which will cost more). Let us look again at the partial SF_i. Near the base, chemical degradation could be 1.2 instead of 1.3—this change gives SF = 2.09 instead of 2.265 and an allowable f_a = 34.4/2.09 = **16.4** kN/m.

Since the required f_r is computed using the same SF as on the geotextile we have in general,

$$f_r = \text{vertical space} \times q_R \times \text{SF}$$

and before adjusting the SF,

$$f_R = 0.4(18.58)(2.265) = \mathbf{16.83}\ \text{kN/m (as on output sheet)}$$

After adjusting SF,

$$f_R = 0.4(18.58)(2.09) = \mathbf{15.53}\ \text{kN/m} < 16.4 \qquad \text{(O.K.)}$$

10. All that is left is to draw a neat sketch so the construction crew can build the wall. Next determine the wall length (we would use one width of 4.40 m) and determine the number of rolls of geotextile needed, and the project is designed.

Comment. This geotextile may not be available in a **4.40** m width. If there is a large enough quantity, the mill might set up a special run to produce the desired (or a slightly larger) width. Otherwise it will be necessary to search the catalog for another producer. Since part of the design depends on

available widths, it should be evident that a highly precise design is not called for. Also, the Rankine zone appears to be more of a segment of a log spiral than the wedge shown, so it may not exceed $0.3H$ in any case. The reason for this statement is that we would search for an available fabric of width between **4.1** and **4.6** m with a strength $\geq$ **32.4** kN/m as satisfactory.

////

12-4 CONCRETE RETAINING WALLS

Figure 12-9 illustrates a number of types of walls of reinforced concrete or masonry. Of these, only the reinforced concrete cantilever wall (*b*) and the bridge abutment (*f*) are much used at present owing to the economics of reinforced earth.

The reinforced earth configuration produces essentially the gravity walls of Fig. 2-9*a* and the crib wall of Fig. 12-9*d*. The "stretcher" elements in the crib wall function similarly to the reinforcement strips in reinforced earth walls.

The counterfort wall (*c*) may be used when a cantilever wall has a height over about 7 m. Counterforts (called buttresses if located on the front face of the wall) are used to allow a reduction in stem thickness without excessive outward deflection. These walls have a high labor and material cost, so they do not compete economically with reinforced earth. They may be used on occasion in urban areas where aesthetics, space limitations, or vandalism is a concern.

There are prefabricated proprietary (patented) walls that may compete at certain sites with other types of walls. Generally the producer of the prefabricated wall provides the design procedures and enough other data so that a potential user can make a cost comparison from the several alternatives.

Cantilever and prefabricated retaining walls are analyzed similarly, so a basic understanding of the cantilever procedure will enable a design review of a prefabricated wall for those cases where a cost comparison is desired.

The focus of the rest of this chapter is on the design of reinforced concrete cantilever retaining walls (as shown in Fig. 12-9*b*).

For reinforced concrete, the concept of *Strength Design* (USD) was used in Chaps. 8 through 10 for foundations. In those chapters multiple load factors were used, but they did not overly complicate the design. In wall design the use of load factors is not so direct, and, further, the ACI 318- does not provide much guidance—that is, the Code user must do some interpretation of Code intent.

When the USD was first introduced in the mid-1960s, it was common to use a single load factor (1.7 to 2.0) applied to any load or pressure to obtain an "ultimate" value to use in the USD equations. However, there is some question whether the use of a single load factor is correct, and ACI 318- is of no help for this. Retaining wall design procedures are often covered in reinforced concrete (R/C) design textbooks and range from using a single load factor to using multiple load factors—but only with USD since R/C design textbooks are based on this method.

For these and other reasons stated later the author has decided there is considerable merit in using the *Alternate Design Method* (ADM). This was the only method used prior to the mid-1960s, but it is still considered quite acceptable by both ACI 318- and AASHTO.

The ACI 318- places more emphasis on the USD because of claimed economies in building construction, but the AASHTO bridge manuals (including the latest one) give about equal consideration to both methods.

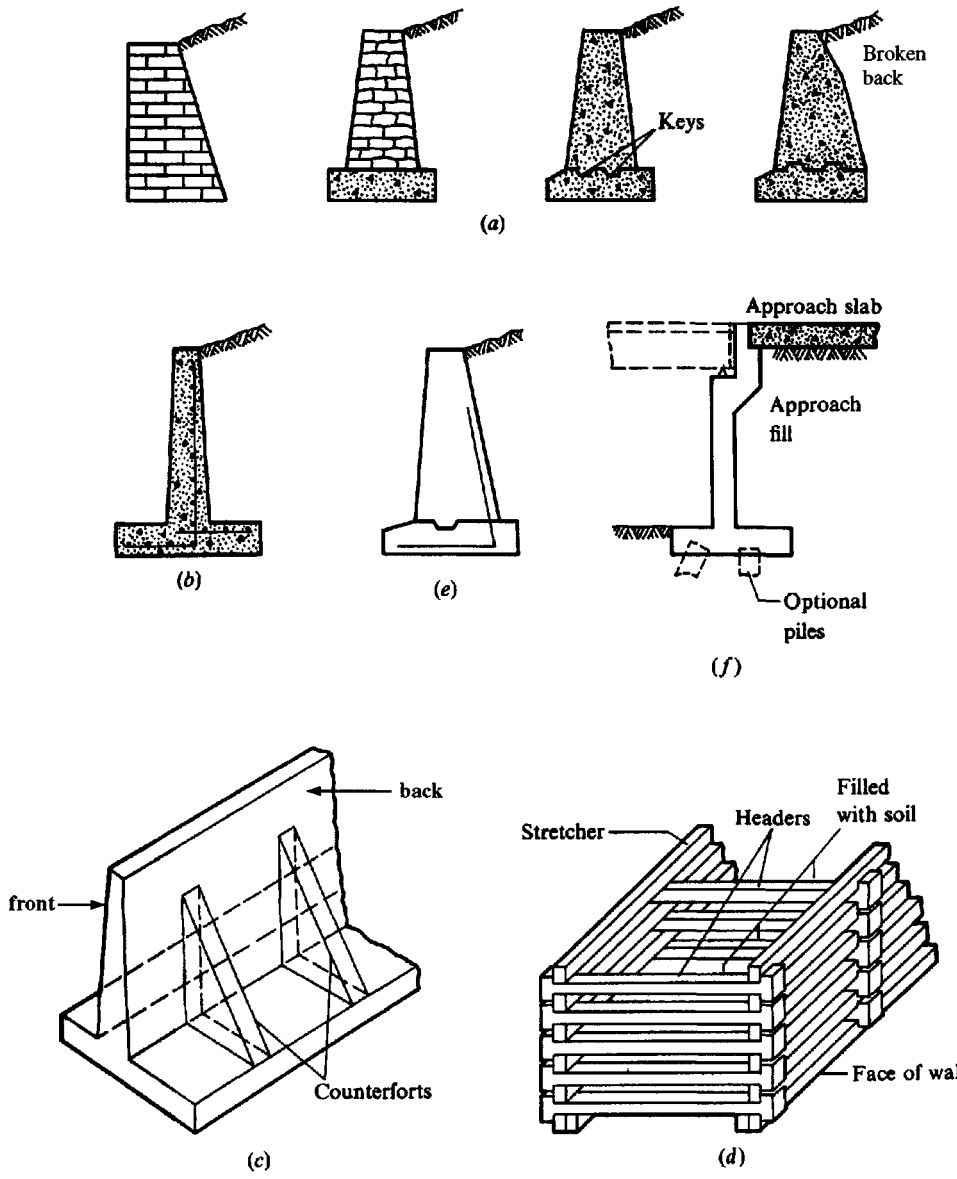

Figure 12-9 Types of retaining walls. (*a*) Gravity walls of stone masonry, brick, or plain concrete—weight provides stability against overturning and sliding; (*b*) Cantilever wall; (*c*) Counterfort, or buttressed wall—if backfill covers the counterforts the wall is termed a counterfort; (*d*) Crib wall; (*e*) Semigravity wall (uses small amount of steel reinforcement); (*f*) Bridge abutment.

The ADM procedure will be used here so that we can avoid the use of multiple load factors and the associated problems of attempting to mix earth pressures (LF = 1.7) with vertical soil and wall loads (LF = 1.4) and surcharge loads (some with LF = 1.4 and others with LF = ?). For retaining walls the ADM has two advantages:

1. The resulting wall design may (in some cases) be slightly more conservative than *strength design* unless load factors larger than the minimum are used.
2. The design is much simpler since all LF = 1 and thus less prone to error than the *strength design* method. Aside from this, the equations for design depth d and required steel area A_s are also easier to use.

12-5 CANTILEVER RETAINING WALLS

Figure 12-10 identifies the parts and terms used in retaining wall design. Cantilever walls have these principal uses at present:

1. For low walls of fairly short length, "low" being in terms of an exposed height on the order of 1 to 3.0 m and lengths on the order of 100 m or less.
2. Where the backfill zone is limited and/or it is necessary to use the existing soil as backfill. This restriction usually produces the condition of Fig. 11-12*b*, where the principal wall pressures are from compaction of the backfill in the limited zone defined primarily by the heel dimension.
3. In urban areas where appearance and durability justify the increased cost.

In these cases if the existing ground stands without caving for the depth of vertical excavation in order to place (or pour) the wall footing and later the stem, theoretically there is no lateral earth pressure from the existing backfill. The lateral wall pressure produced by the limited backfill zone of width b can be estimated using Eqs. (11-18) or (11-19)—this latter is option 8 in your program FFACTOR. There is a larger lateral pressure from compacting the backfill (but of unknown magnitude), which may be accounted for by raising the location of the resultant from $H/3$ to 0.4 to $0.5H$ using Eq. (11-15). Alternatively, use K_o instead of K_a with the $H/3$ resultant location.

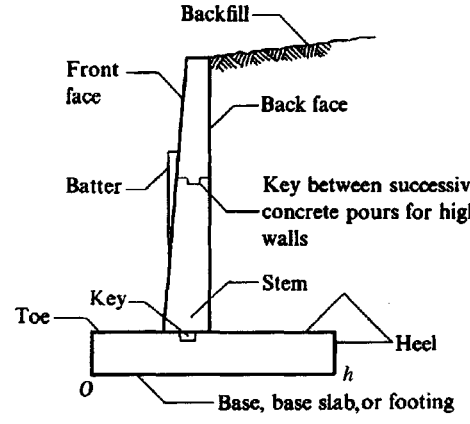

Figure 12-10 Principal terms used with retaining walls. Note that "toe" refers to both point O and the distance from front face of stem; similarly "heel" is point h or distance from backface of stem to h.

It is common for cantilever walls to use a constant wall thickness on the order of 250 mm to seldom over 300 mm. This reduces the labor cost of form setting, but some overdesign should be used so that the lateral pressure does not produce a tilt that is obvious—often even a few millimeters is noticeable.

You can use your program FADBEMLP to compute an estimate of the tilt by using fixity at the stem base and loading the several nodes down the wall with the computed pressure diagram converted to nodal forces using the average end area method. Of course, it is possible to build a parallel-face wall with an intentional back tilt, but there will be extra form-setting costs.

Figure 12-11 gives common dimensions of a cantilever wall that may be used as a guide in a hand solution. Since there is a substantial amount of busywork in designing a retaining wall because of the trial process, it is particularly suited to a computer analysis in which the critical data of γ, ϕ, H, and a small base width B are input and the computer program (for example, the author's B-24) iterates to a solution.

The dimensions of Fig. 12-11 are based heavily on experience accumulated with stable walls under Rankine conditions. Small walls designed for lateral pressures from compaction, and similar, may produce different dimensions.

It is common, however, for the base width to be on the order of about $0.5H$, which depends somewhat on the toe distance ($B/3$ is shown, but it is actually not necessary to have any toe). The thickness of the stem and base must be adequate for wide-beam shear at their intersections. The stem top thickness must be adequate for temperature-caused spalls and impacts from equipment/automobiles so that if a piece chips off, the remainder appears safe and provides adequate clear reinforcement cover.

The reinforcement bars for bending moments in the stem back require 70 mm clear cover[4] (against ground) as shown in Fig. 12-12*a*. This requirement means that, with some T and S bars on the front face requiring a clear cover of 50 mm + tension rebar diameter + 70 mm and some thickness to develop concrete compression for a moment, a **minimum** top thickness of about 200 mm is automatically mandated.

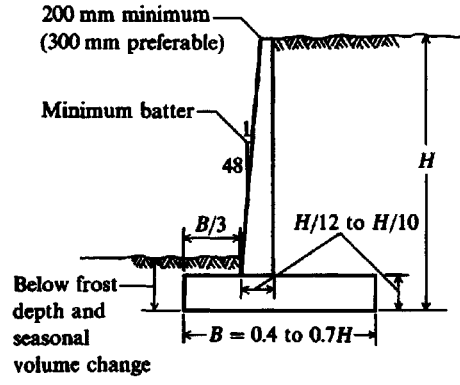

Figure 12-11 Tentative design dimensions for a cantilever retaining wall. Batter shown is optional.

[4]Actually the ACI Code Art. 7-7.1 allows 50 mm when the wall stem is built using forms—the usual case. The code requires 70 mm only when the stem (or base) is poured directly against the soil.

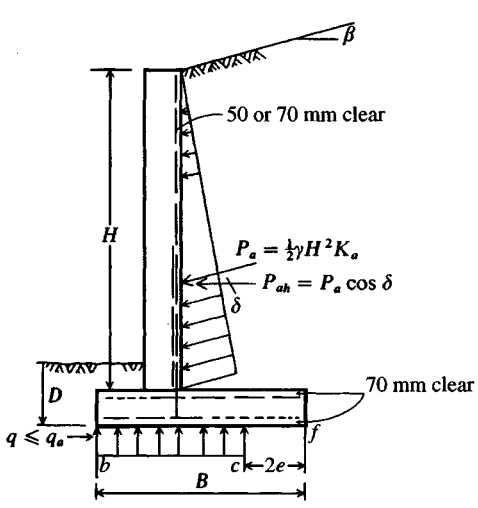

(*a*) Wall pressure to use for shear and bending moment in stem design. Also shown is bearing capacity pressure diagram based on Fig. 4-4 using $B' = b - 2e$ and $L = L' = 1$ unit.

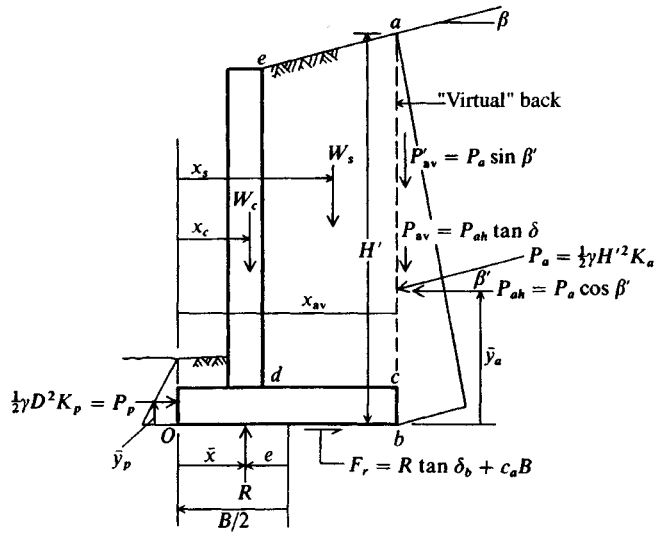

(*b*) Wall pressure for overall stability against overturning and sliding. W_c = weight of all concrete (stem and base); W_s = weight of soil in zone *acde*. Find moment arms x_i any way practical – usually using parts of known geometry. Use this lateral pressure for base design and bearing capacity.

Figure 12-12 General wall stability. It is common to use the Rankine K_a and $\delta = \beta$ in (*a*). For β' in (*b*) you may use β or ϕ since the "slip" along *ab* is soil-to-soil. In any case compute $P_{av} = P_{ah} \tan\phi$ as being most nearly correct.

Walls are designed for wide-beam shear with critical locations as indicated in ACI 318-. The author suggests, however, taking the wide-beam shear at the stem face (front and back) for the base slab as being more conservative and as requiring a negligible amount of extra concrete. For the stem one should take the critical *wide-beam* location at the top of the base slab. The reason is that the base is usually poured first with the stem reinforcement set. Later the stem forms are set and poured, producing a discontinuity at this location.

Formerly, a wood strip was placed into the base slab and then removed before the stem was placed. This slot or *key* provided additional shear resistance for the stem, but this is seldom done at present. Without the key at this discontinuity, the only shear resistance is the bonding that develops between the two pours + any friction from the stem weight + reliance on the stem reinforcement for shear. ACI Art. 11.7.5 with the reduction given in Art. A.7.6 gives a procedure for checking *shear friction* to see if shear reinforcement is required at this location. The required ACI equation seems to give adequate resistance unless the wall is quite high.

12-6 WALL STABILITY

Figure 12-12 illustrates the general considerations of wall stability. The wall must be structurally stable against the following:

1. Stem shear and bending due to lateral earth pressure on the stem. This is a separate analysis using the stem height.

2. Base shear and bending moments at the stem caused by the wall loads producing bearing pressure beneath the wall footing (or base). The critical section for shear should be at the stem faces for both toe and heel. Toe bending is seldom a concern but for heel bending the critical section should be taken at the approximate center of the stem reinforcement and not at the stem backface.

   The author suggests that for base bending and shear one use the rectangular bearing pressure (block *abde*) given on Fig. 12-12*a* in order to be consistent with bearing-capacity computations (see Fig. 4-4) for q_a. A trapezoidal diagram *(acf)* is also used but the computations for shear and moment are somewhat more complicated.

12-6.1 Sliding and Overturning Wall Stability

The wall must be safe against sliding. That is, sufficient friction F_r must be developed between the base slab and the base soil that a safety factor SF or stability number N_s (see Fig. 12-12*b*) is

$$\text{SF} = N_s = \frac{F_r + P_p}{P_{ah}} \geq 1.25 \text{ to } 2.0 \tag{12-4}$$

All terms are illustrated in Fig. 12-12*b*. Note that for this computation the total vertical force R is

$$R = W_c + W_s + P'_{av}$$

These several vertical forces are shown on Fig. 12-12*b*. The heel force P'_{av} is sometimes not included for a more conservative stability number. The friction angle δ between base slab and soil can be taken as ϕ where the concrete is poured directly onto the compacted base soil. The base-to-soil adhesion is usually a fraction of the cohesion—values of 0.6 to 0.8 are commonly used. Use a passive force P_p if the base soil is in close contact with the face of the toe. One may choose not to use the full depth of D in computing the toe P_p if it is possible a portion may erode. For example, if a sidewalk or roadway is in front of the wall, use the full depth (but not the surcharge from the sidewalk or roadway, as that may be removed for replacement); for other cases one must make a site assessment.

The wall must be safe against overturning about the toe. If we define these terms:

$\bar{x}$ = location of R on the base slab from the toe or point O. It is usual to require this distance be within the middle $\frac{1}{3}$ of distance Ob—that is, $\bar{x} > B/3$ from the toe.

P_{ah} = horizontal component of the Rankine or Coulomb lateral earth pressure against the vertical line ab of Fig. 12-12*b* (the "virtual" back).

$\bar{y}$ = distance above the base Ob to P_{ah}.

P_{av} = vertical shear resistance on virtual back that develops as the wall tends to turn over. This is the only computation that should use P_{av}. The δ angle used for P_{av} should be on the order of the residual angle ϕ_r since the Rankine wedge soil is in the state of Fig. 11-1*c* and "follows" the wall as it tends to rotate.

We can compute a stability number N_o against overturning as

$$N_o = \frac{M_r}{M_o} = \frac{\sum W_i \bar{x} + P_{av} B}{P_{ah} \bar{y}} \geq 1.5 \text{ to } 2.0 \tag{12-5}$$

In both Eqs. (12-4) and (12-5) the stability number in the given range should reflect the importance factor and site location. That is, if a wall failure can result in danger to human life

or extensive damage to a major structure, values closer to 2.0 should be used. Equation (12-5) is a substantial simplification used to estimate overturning resistance. On-site overturning is accompanied by passive resistances at (1) the top region of the base slab at the toe, (2) a zone along the heel at *cb* that tends to lift a soil column along the virtual back face line *ab*, and (3) the slip of the Rankine wedge on both sides of *ab*. Few walls have ever overturned—failure is usually by sliding or by shearoff of the stem.

The $\sum(W_c + W_s)$ and location $\bar{x}$ are best determined by dividing the wall and soil over the heel into rectangles and triangles so the areas (and masses) can be easily computed and the centroidal locations identified. Then it becomes a simple matter to obtain

$$(W_c + W_s + P'_{av})\bar{x} = P_{ah}\bar{y} - P_p\bar{y}_p$$

$$\bar{x} = \frac{M_o - P_p\bar{y}_p}{W_c + W_s + P'_{av}}$$

If there is no passive toe resistance (and/or P'_{av} is ignored) the preceding equations are somewhat simplified.

12-6.2 Rotational Stability

In Fig. 12-13 we see that in certain cases a wall can rotate as shown—usually when there are lower strata that are of poorer quality than the base soil. This failure is similar to a slope stability analysis using trial circles. These computations can be done by hand. Where several circles (but all passing through the heel point) are tried for a minimum stability number N_r, though, the busywork becomes prohibitive; and a computer program (see author's B-22) for slope stability analysis—adjusted for this type of problem as an option—should be used. This procedure is illustrated later in Example 12-4.

12-6.3 General Comments on Wall Stability

It is common—particularly for low walls—to use the Rankine earth-pressure coefficients K_a and K_p (or Table 11-5), because these are somewhat conservative. If the wall angle α of Fig. 11-4 is greater than 90°, consider using the Coulomb equations with $\delta \geq 0$.

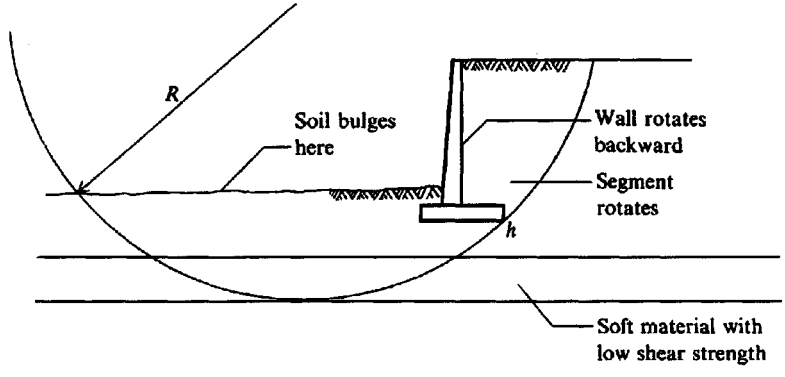

Figure 12-13 Wall-soil shear failure may be analyzed by the Swedish-circle method. A "shallow" failure occurs when base soil fails. A "deep" failure occurs if the poor soil stratum is underlying a better soil, as in the figure.

For stem analysis the friction angle δ of Fig. 12-12*a* is taken as the slope angle β in the Rankine analysis. The friction angle is taken as some fraction of ϕ in a Coulomb analysis, with 0.67ϕ commonly estimated for a concrete wall formed using plywood or metal forms so the back face is fairly smooth.

For the overall wall stability of Fig. 12-12*b* the angle β' may be taken as β for the Rankine method, but for the Coulomb analysis take $\beta' = \phi$. This value then is used to obtain the horizontal component of P_a as shown. For the vertical friction component P_{av} resisting overturning take

$$P_{av} = P_{ah} \tan \phi_r \tag{12-6}$$

since the δ angle shown on Fig. 12-12*b* is always soil-to-soil, but the soil is more in a "residual" than a natural state.

The Rankine value for K_p (or see Table 11-5) is usually used if passive pressure is included. If there is uncertainty that the full base depth D is effective in resisting via passive pressure, it is permissible to use a reduced value of D' as

$$D' = D - \text{potential loss of depth}$$

The potential loss of depth may be to the top of the base or perhaps the top 0.3^+ m, depending on designer assessment of how much soil will remain in place over the toe. Note that some of this soil is backfill, which must be carefully compacted when it is being replaced. Otherwise full passive pressure resistance may not develop until the wall has slipped so far forward that it has "failed."

12-6.4 Base Key

Where sufficient sliding stability is not possible—usually for walls with large H—a base key, as illustrated in Fig. 12-14, has been used. There are different opinions on the best location for a key and on its value. It was common practice to put the key beneath the stem as in Fig. 12-14*a*, until it was noted that the conditions of Fig. 12-14*b* were possible. This approach was convenient from the view of simply extending the stem reinforcement through the base and into the key. Later it became apparent that the key was more effective located as in Fig. 12-14*c* and, if one must use a key, this location is recommended. The increase in H by the key depth may null its effect.

12-6.5 Wall Tilt

Concrete retaining walls have a tendency to tilt forward because of the lateral earth pressure (Fig. 12-15*a*), but they can also tilt from base slab rotation caused by differential settlement. Occasionally the base soil is of poor quality and with placement of sufficient backfill (typically, the approach fill at a bridge abutment) the backfill pressure produces a heel settlement that is greater than at the toe. This difference causes the wall to tilt into the backfill as shown in Fig. 12-15*b*.

If the Rankine active earth pressure is to form, it is necessary that the wall tilt forward as noted in Sec. 11-2. A wall with a forward tilt does not give an observer much confidence in its safety, regardless of stability numbers. Unless the wall has a front batter, however, it is difficult for it to tilt forward—even a small amount—without the tilt being noticeable. It may be possible to reduce the tilt by overdesigning the stem—say, use K_o instead of K_a pressures and raise the location of the resultant. When one makes this choice, use a finite-element program such as your B-5 to check the wall movements. Although this type of analysis may not be completely accurate, there is currently no better way of estimating wall tilt.

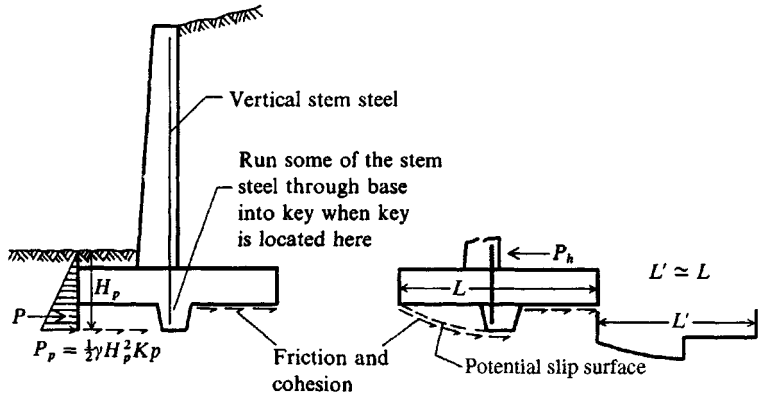

(*a*) Base key near stem so that stem steel may be extended into the key without additional splicing or using anchor bends.

(*b*) Potential sliding surface using the key location of *a*. There may be little increase in sliding resistance from this key, if the slip surface develops as shown.

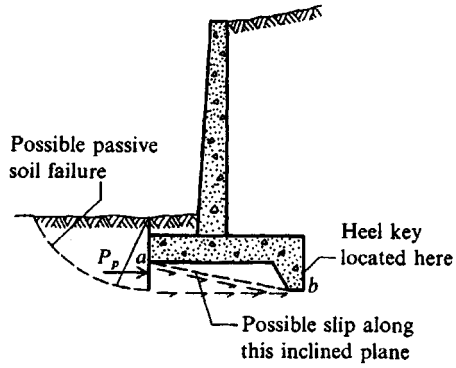

(*c*) Possible sliding modes when using a heel key.

Figure 12-14 Stability against sliding by using a base key.

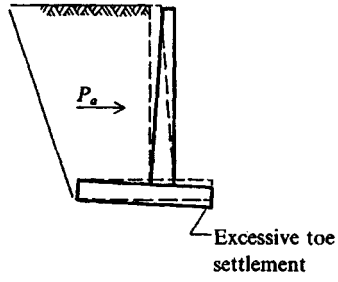

(*a*) High toe pressure.

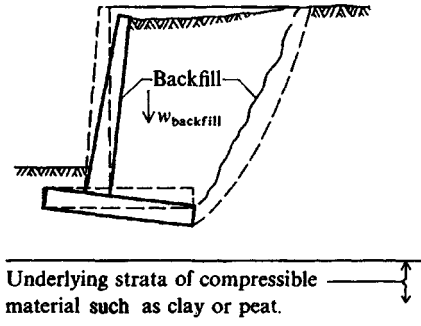

(*b*) Excessive heel zone settlement (from back fill).

Figure 12-15 Causes of excessive wall tilting.

12-6.6 Other Considerations in Retaining Wall Design

When there is a limited space in which to place the wall base slab and the sliding stability number N_s is too small, what can be done? There are several possible solutions:

1. Look to see if you are using a slab-soil friction angle δ that is too small—for concrete poured on a compacted soil it can be $\delta = \phi$. Are you using any P'_{av} contribution? Can you?
2. Consider placing the base slab deeper into the ground. At the least, you gain some additional passive resistance.
3. Consider using short piles, on the order of 2 to 2.5 m in length, spaced about 1.5 to 2.0 m along the wall length. These would be for shear, i.e., laterally loaded.
4. Consider improving the base soil by adding lime or cement to a depth of 0.3^+ m just beneath the base.
5. Consider sloping the base, but keep in mind that this is not much different from using a heel key. Considerable hand work may be needed to obtain the soil slope, and then there is a question of whether to maintain the top of the base horizontal or slope both the top and bottom. You may get about the same effect by increasing the base-to-soil δ angle 1 or 2°.
6. Sloping the heel as shown in Fig. 12-16 has been suggested. This solution looks elegant until one studies it in depth. What this configuration hopes to accomplish is a reduction in lateral pressure—the percentage being

$$R = 100.0 - \left(\frac{H_s}{H}\right)^2 100 \qquad (\%)$$

   Note that because of the natural *minimum energy law* a soil wedge will form either as $A'C'D'$ or as $BCDA$. $A'C'D'$ is the Rankine wedge, so if this forms the heel slope BA is an unnecessary expense.

   If the wedge $BCDA$ forms, the net gain (or loss) is trivial. We can obtain the value from plotting two force diagrams—one for wedge $AC'D$, which is in combination with the force diagram from block $BCC'A$ as done in the inset of Fig. 12-16.

   Keep in mind that if this slope is deemed necessary, the reason is that the base slab is narrow to begin with. By being narrow, the overturning moment from P_{ah} may tend to lift the heel away from the underlying soil, so the value of R_2 may be close to zero. If the heel slope compresses the soil, friction may be so large that wedge $A'C'D'$ is certain to form. Walls built using this procedure may be standing but likely have a lower than intended SF. Their current safety status may also be due to some initial overdesign.
7. It has been suggested that for high walls Fig. 12-17 is a possible solution—that is, use "relief shelves." This solution has some hidden traps. For example, the soil must be well compacted up to the relief shelf, the shelf constructed, soil placed and compacted, etc. In theory the vertical pressure on the shelf and the lateral pressure on the wall are as shown. We can see that the horizontal active pressure resultant P_{ah} is much less than for a top-down pressure profile—at least for the stem.

   What is difficult to anticipate is the amount of consolidation that will occur beneath the shelves—and it will—regardless of the state of the compaction. This tends to cantilever the shelves down, shown as dashed lines in the pressure profile diagram. When this occurs, either the shelf breaks off or the wall above tends to move into the backfill and develop

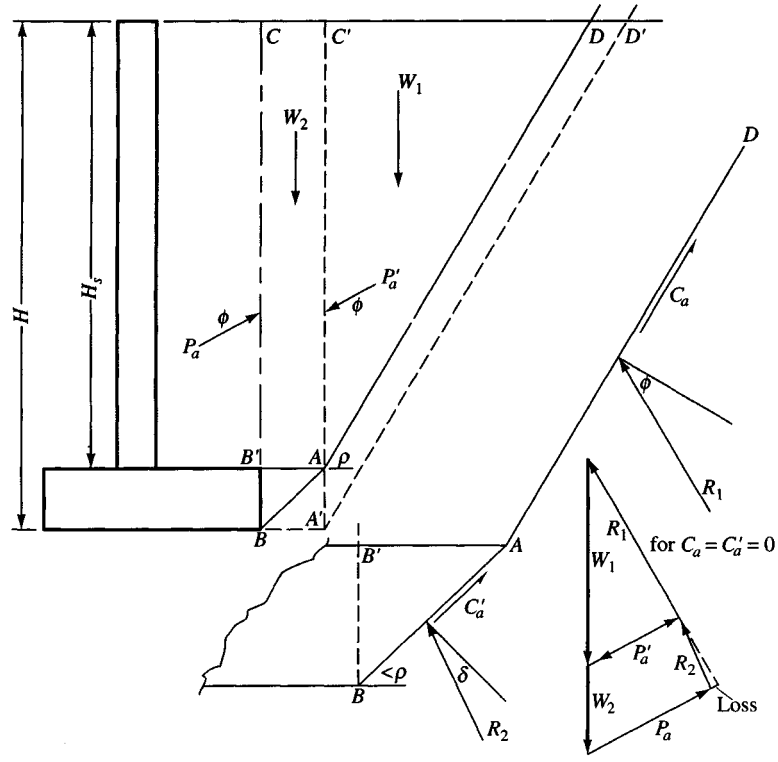

Figure 12-16 A suggested method to increase the sliding stability number.

passive pressure. The wall therefore must be well reinforced on both faces and of sufficient thickness to carry this unanticipated shear and moment.

There is also the possibility of a Rankine wedge forming on line *GH* (overall wall stability). In this case the relief shelves have only increased the design complexity of the project.

12-7 WALL JOINTS

Current practice is to provide vertical *contraction joints* at intervals of about 8 to 12 m. These are formed by placing narrow vertical strips on the outer stem face form so that a vertical groove is developed when the concrete hardens. The groove produces a plane of weakness to locate tension cracks (so they are less obvious) from tensile stresses developing as the concrete sets (cures) or from contraction in temperature extremes.

Joints between successive pours are not currently identified—the new concrete is simply poured over the old (usually the previous day's pour) and the wall continued. When the forms are stripped, any obvious discontinuities are removed in the wall finishing operation.

Very large walls previously tended to be made with vertical *expansion joints* at intervals of 16 to 25 m. Current practice discourages[5] their use, since they require a neat vertical joint

[5]Formerly it was considered good practice to require expansion joints in concrete walls at a spacing not to exceed 27 m (about 90 ft).

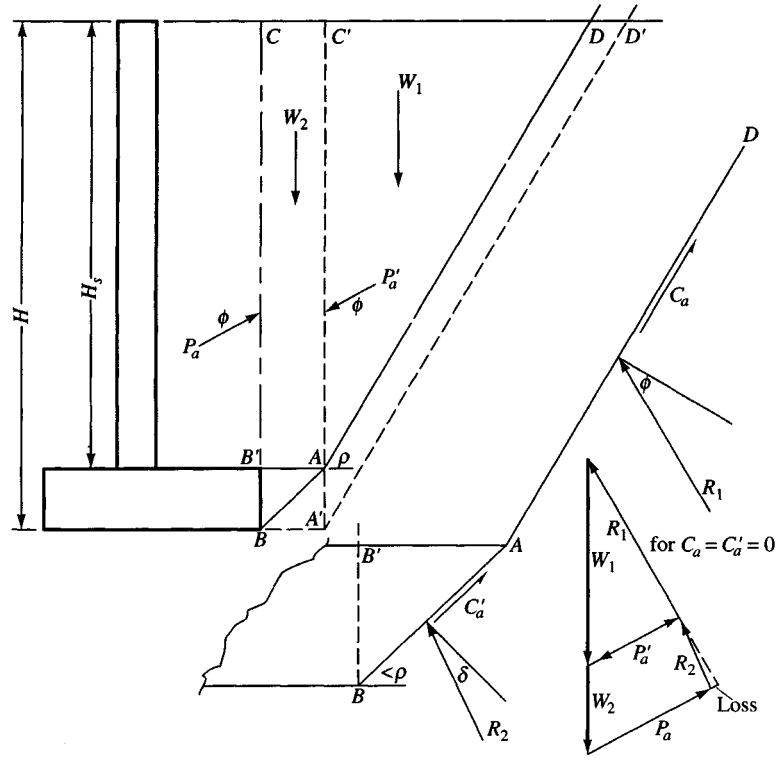

Figure 12-16 A suggested method to increase the sliding stability number.

passive pressure. The wall therefore must be well reinforced on both faces and of sufficient thickness to carry this unanticipated shear and moment.

There is also the possibility of a Rankine wedge forming on line *GH* (overall wall stability). In this case the relief shelves have only increased the design complexity of the project.

12-7 WALL JOINTS

Current practice is to provide vertical *contraction joints* at intervals of about 8 to 12 m. These are formed by placing narrow vertical strips on the outer stem face form so that a vertical groove is developed when the concrete hardens. The groove produces a plane of weakness to locate tension cracks (so they are less obvious) from tensile stresses developing as the concrete sets (cures) or from contraction in temperature extremes.

Joints between successive pours are not currently identified—the new concrete is simply poured over the old (usually the previous day's pour) and the wall continued. When the forms are stripped, any obvious discontinuities are removed in the wall finishing operation.

Very large walls previously tended to be made with vertical *expansion joints* at intervals of 16 to 25 m. Current practice discourages[5] their use, since they require a neat vertical joint

[5]Formerly it was considered good practice to require expansion joints in concrete walls at a spacing not to exceed 27 m (about 90 ft).

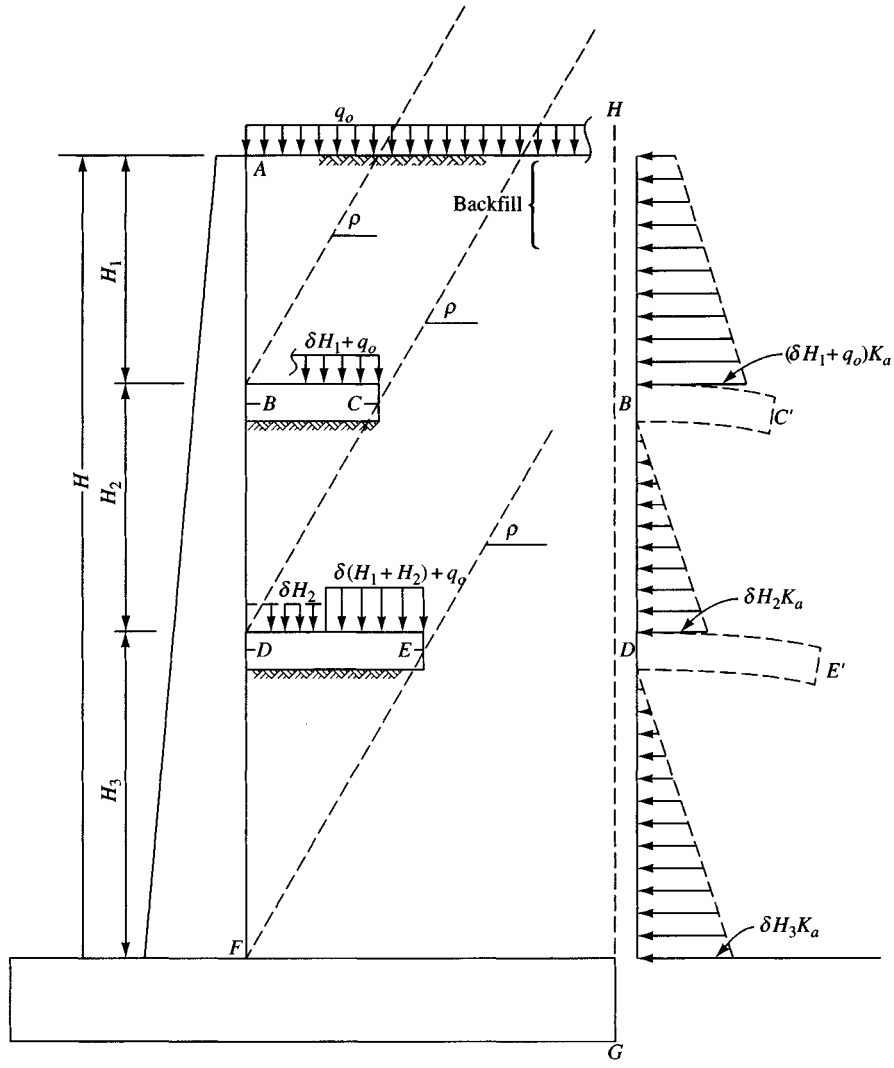

Figure 12-17 Using "relief shelves" to give an apparent reduction in the lateral wall (stem) pressure.

filled with an asphaltic spacer and dowels through the joint with the ends on one side greased or sheathed to allow expansion/contraction.

Current thinking is that with the large shear resistance to expansion/contraction on the back face from the lateral pressure + the friction resistance of the base, the joint is useless. Also, whereas joints are common for concrete roads, these are exposed to more sunlight than a wall, which (at most) would be exposed for only about half a day.

12-8 WALL DRAINAGE

It was pointed out in Chap. 11 that it is preferable to provide backfill drainage rather than to design the wall for the large lateral pressure that results from a saturated backfill.

Drainage can be accomplished by providing a free-draining material at the back face (or entire Rankine zone) and longitudinal collector drains along the back face as in Fig. 12-18*a*. At intervals drain pipes (about 75 to 100 mm in diameter) called *weep holes* are run through the wall to carry away the accumulated water from the horizontal collector pipe, unless it can discharge naturally from one end of the wall. Where the base is well into the ground, it may only be practical to use weep holes close to the ground surface in front of the wall, to drain the backfill to that level. Below this level the ground would saturate on both sides; the hydrostatic pressure would cancel and not be highly objectionable.

A major problem with any drainage system is to provide some kind of filter material around the entrance on the backfill side so loss of fines does not occur. One may use a porous geotextile wick material along the vertical face of the wall and over the weep holes (with or without a granular backfilled zone). This allows water to penetrate the geotextile and travel vertically (and horizontally) to the weep holes while preventing the large loss of backfill fines shown in Fig. 12-18*b*.

If a geotextile is not used, one should use very coarse gravel in the vicinity of the weep holes (and around any horizontal collector drain) that gradually grades to the backfill sieve size. If only a medium coarse sand is used, it will nearly always wash through the weep holes after several heavy rains. Here again, project inspection is critical, for it is much easier (and cheaper) for the builder simply to dump sand behind the wall with little regard that it will leach through the weep holes later than to locate the weep holes, backfill around them with gravel, then dump the sand. For sand backfill and a water source, a common "compaction" procedure is to saturate the sand until there is visible surface water. This can be done only if the saturation water does not damage the surrounding soil.

12-9 SOIL PROPERTIES FOR RETAINING WALLS

It is evident that we will need the backfill parameters γ and ϕ for the earth-pressure computation. It is implicit that in at least a limited zone behind the wall a granular backfill will be used.

As previously noted, we may use K_o for all or part of the wall—especially if the backfill zone is limited and/or we use compaction equipment on clayey backfill. Here K_o is computed using Eq. (2-18*a*):

$$K_o = 1 - \sin\phi \qquad (2\text{-}18a)$$

Unless the backfill soil parameters are provided by the geotechnical consultant it is common to estimate them conservatively as follows:

$$\phi = 30 \text{ to } 36^\circ \qquad \text{(usually 32 to 34°)}$$

$$\gamma = 16.5 \text{ to } 17.5 \text{ kN/m}^3 \qquad (105 \text{ to } 110 \text{ lb/ft}^3)$$

One should have values of ϕ, γ, and cohesion c for the original ground (where it will be excavated vertically to make space for a wall). Direct shear or direct simple shear (DSS) tests on good-quality tube samples provide the best soil parameters, since a retaining wall is a plane strain case. Most testing is triaxial (if any is done) and either unconsolidated or consolidated-undrained. Many test laboratories do not have DSS test equipment. The base soil plane strain parameters of ϕ, γ, and cohesion c must be obtained (or estimated) so that sliding stability and bearing capacity can be computed.

Figure 12-18 Wall drainage.

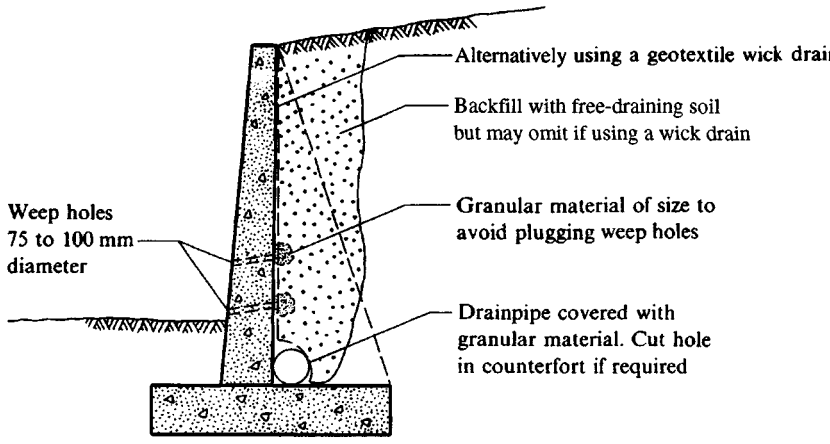

If weep holes are used with a counterfort wall at least one weep hole should be located between counterforts

(*a*) Retaining wall drainage alternatives of granular backfill or geotextile wick drain. Note weep holes (as upper line) may cause staining of wall face from oxides in backfill. Do not use a longitudinal wall drain unless it can empty.

(*b*) Poorly designed weep holes showing loss of granular backfill. Pile of sand in foreground has washed through and now completely submerges weep hole at that location. More distant holes marked with white tape also show loss of backfill. Sidewalk joints at 1.5-m spacing show weep hole spacing is about 3.0 m. Top white tape marks vertical settlement cracks.

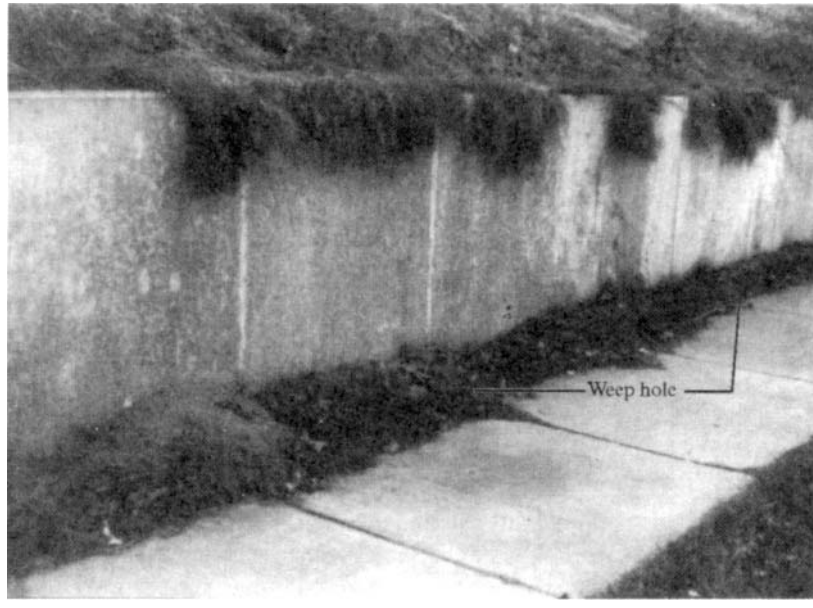

It is common practice, however, to obtain $s_u = q_u/2$ for any cohesive soil, where q_u is obtained as outlined in Chap. 3 from SPT data and using either compression machine testing or a pocket penetrometer (or in combination).

This type of soil data has a history of success. The principal deficiencies (wall failures) derive from inadequate drainage of the backfill zone, so that a large hydrostatic pressure develops, and/or from excessive saturation of the base soil, so that s_u reduces from the softening that occurs when a cohesive soil becomes saturated.

12-10 GENERAL CONSIDERATIONS IN CONCRETE RETAINING WALL DESIGN

Retaining walls may be designed for the active soil pressure case when the wall is sufficiently flexible that it will rotate enough to allow the active earth-pressure wedge to form. In other cases, the wall may be somewhat overdesigned where the backfill is in a limited zone and/or compaction pressures may develop. Several methods have been presented in Chap. 11 and in this chapter for taking into account pressures in excess of the active value.

There is some opinion that the active earth pressure is appropriate for all walls since a failure of the stem always involves sufficient movement to initiate the active earth-pressure wedge. More conservative opinion, however, holds that this may not always be the case—particularly for walls where the backfill zone is limited as shown in Fig. 11-12*b*. Bear in mind that if a wall is designed for an active pressure and the soil becomes saturated, the additional hydrostatic lateral pressure may shear the stem[6]—or produce excessive sliding.

Figure 11-12*b* is a common situation for basement walls and some bridge abutments. In neither of these cases do we want the excessive deflections necessary to produce active earth pressure to occur.

In passing, note that even in cohesionless soils where the Rankine active wedge can form, it is likely to do so only in the upper part of the wall; the lower (approximately one-fourth) part is somewhat restrained by the base and other factors so that the Rankine wedge does not fully form. Large-scale walls instrumented to record pressure, as reported by Coyle et al. (1972) and Prescott et al. (1973) consistently measured earth pressures in the lower part of the wall that were higher than either the Rankine or Coulomb active values.

Some pressure measurements were as much as 2.5 times the "theoretical" values. In a number of cases the "average" wall force was reasonably close to the "active" value but the location of the resultant seemed to be consistently higher—on the order of 0.4 to 0.45H (instead of $H/3$). An extensive survey of compaction-induced pressures and methods for analysis is given by Ingold (1979).

Finally, note that if a retaining wall is backfilled with a cohesive material and compacted, very high lateral pressures will be developed. These are not predictable either by the Rankine or Coulomb earth-pressure equations or by Eq. (2-55) or the like. Clayton et al. (1991) suggest that in compacted clay fills the lateral pressure at the end of backfilling is likely to be on the order of $0.2s_u$ for intermediate and $0.4s_u$ for highly plastic clays, with some reduction with elapsed time. You might use the following:

---

[6]Hydrostatic pressure does not decrease with wall translation, and the active pressure is a limiting soil state.

Clay	I_p, %
Intermediate plasticity	20 to 35
Highly plastic	> 35

When one is using a clay backfill, swelling is less likely, according to the Clayton et al. study, if $I_P < 30$. For $I_P < 40$ swelling could be avoided by using a compaction moisture content greater than the OMC. In any case many existing walls have been constructed using cohesive backfills.

12-11 ALLOWABLE BEARING CAPACITY

Stability of the base against a bearing-capacity failure is achieved by using a suitable safety factor with the computed ultimate bearing capacity, where the safety factor is usually taken as 2.0 for granular soil and 3.0 for cohesive soil.

The allowable soil pressure can be computed using the Hansen bearing-capacity equation (from Table 4-1) with the shape factors deleted:

$$q_{ult} = cN_c d_c i_c + \gamma D N_q d_q i_q + \tfrac{1}{2}\gamma B' N_\gamma i_\gamma$$

where d_i = depth factors and i_i = inclination factors, which are based on the load inclination since there is both a vertical and horizontal load. It is suggested to use the Hansen inclination factors of Table 4-5*b* with an exponent of $\alpha_1 = 2$ for i_q and $\alpha_2 = 3$ for i_γ. This approach is approximately the same as using the Vesić exponent m (and $m + 1$) for the inclination factors in that table. These reduced exponents can be somewhat justified on the basis that the wall footing often has a considerable depth of embedment and the earth pressure in front of the wall stem is neglected in computing the horizontal force $P_{ah} = H$ in the equations for the inclination factors. The shape factors are not used since the wall footing is classified as a strip, so that all $s_i = 1$.

The above bearing-capacity equation computes the rectangular bearing-capacity profile as given in Fig. 4-4*a* and Fig. 12-12*a*, and for consistency the base design should use that profile (the L dimension = 1 unit). The base width B should be such that $\bar{x} \leq B/3$ of Fig. 12-12*b* so that the toe pressure is not excessive for any type of base soil pressure profile.

The base depth D must place the footing below topsoil and frost depth. It also must be deep enough to be stable against scour/erosion and to allow adequate development of bearing capacity and sliding resistance.

When the soil is of low bearing capacity and/or it is not practical to use a larger base slab, it will be necessary to use a pile foundation to support the base slab, which in turn supports the wall. For bridge abutments this is a common procedure used to control settlements at the junction of the approach fill and the bridge deck.

12-12 WALL SETTLEMENTS

Settlements are usually finished by the time a wall has been completed on granular base soil. If the base soil is a saturated, cohesive material (or there is a deeper layer of cohesive soil in the stress influence zone) consolidation settlements will occur over time. In any of these cases

there may be differential settlements between the toe and heel if there is a large difference in pressure between the two locations.

Heel settlement larger than the toe occurs primarily when there is a substantial increase in backfill, e.g., in the backfill zones of Figs. 11-12*a*, *b*, and *d* and Fig. 12-15*b*, which represents an increase in load on the soil. If this zone has been excavated, the wall built, and then soil replaced, there will be very little settlement because the replacement of soil with concrete in the wall volume represents only a small increase in load. A new soil pressure resulting from perhaps 2 to 3 m of backfill that did not previously exist is an increase that can produce substantial long-term settlements in cohesive soils and at least some settlement (immediate) in cohesionless soils.

A more critical situation, however, occurs where the soil is excavated for the footing using power equipment and the rough base is then covered with a thin layer of sand, raked smooth, and the footing poured. This is almost certain to cause settlements and cracks in the wall as in Fig. 12-19 (also in Fig. 12-18*b*)—often shortly after it is completed. Settlement cracks in the wall can be nearly eliminated with adequate construction inspection and by having and enforcing compaction specifications before the base slab is poured.

Toe settlements are more difficult to control since they are produced (assuming adequate base compaction) by lateral soil pressure. They can be somewhat hidden by using a batter on the front face of the wall. They can be somewhat controlled by using a wider base slab so the base pressure is reduced (but the bearing stresses will penetrate further into the ground). If toe settlements are to be eliminated, one can strengthen the soil to a depth using sand piles, rock columns, grouting, or structural piles.

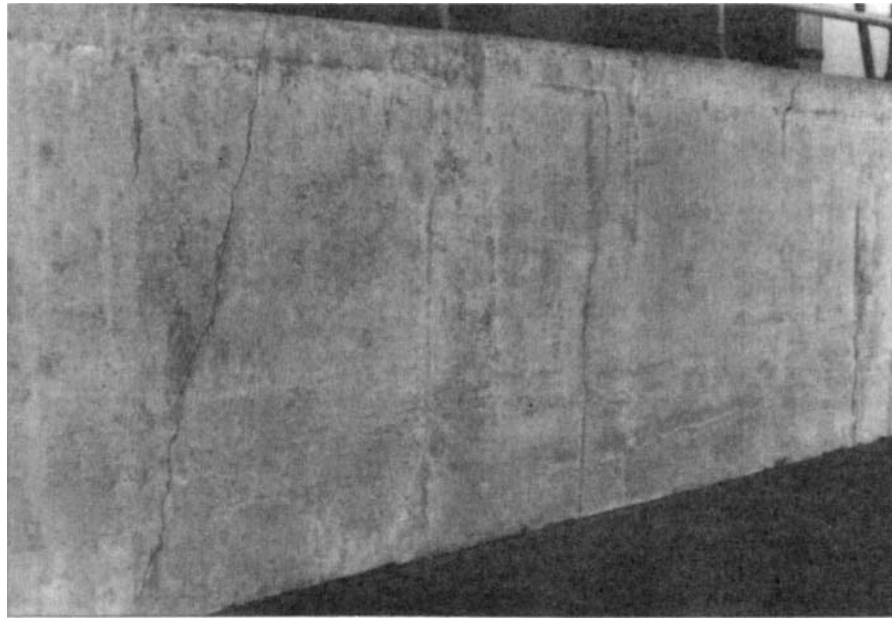

Figure 12-19 Settlement cracks. Three vertical cracks about 1.5 m apart in this wall section were caused by placing base on loose soil. Sidewalk joints are on 1.5 m spacing. Wall cracks developed about 1 week after forms were stripped. Upper level supports a small parking lot. *This is not the wall designed in Example 12-6.*

12-13 RETAINING WALLS OF VARYING HEIGHT; ABUTMENTS AND WINGWALLS

Seldom does a long retaining wall have constant height except possibly when used in hydraulic structures. In cold climates with a deep frost depth there may be as much of the wall below ground as above, or even more.

Conventional wall analysis considers a constant height on a strip of unit width. If the wall is long, two or three typical sections with different heights but using the same stem thickness might be analyzed for reinforcing bar changes. In construction the same stem thickness is used; the amount of reinforcing bars projecting out of the base slab for dowels may be left constant to the next section analyzed and then either the size or number reduced (or not reduced but not spliced since the wall is shorter). Where welded wire fabric is used for reinforcement it is usually just cut to a shorter height, because that is usually less costly than having a number of different fabrics on site to sort through.

Where the wall varies in height, both nonplane strain conditions and wall twist are assumed to develop. For the usual conditions of a change in wall height developed gradually, using a uniform slope, the wall is overdesigned sufficiently to absorb the twist both because the wall thickness is held constant and because the temperature and shrinkage (T and S) steel requirements in the stem will carry some twist moment. Where abrupt changes in wall height occur, one probably should increase the T and S steel in the transition zone—perhaps 10 to 25 percent (depending on the importance factor for the site).

Abutments and wingwalls are commonly used for bridge structures. There is at present little guidance on the design of these members. The principal design considerations in AASHTO (1990) Sec. 3-20 are to use an earth pressure based on an equivalent fluid (γKa) of not less than 4.75 kN/m^3 (30 pcf). The design requirements are given in AASHTO Sec. 7-4:

1. Abutments shall be designed to withstand the earth pressure of AASHTO Sec. 3-20.
2. Abutments shall be designed to be safe against overturning about the toe of the footing and against sliding on the base, and for bearing capacity.
3. The backfill vertically over the base can be considered a part of the effective weight of the abutment.

For wingwalls the requirements are these:

1. They shall be of sufficient length to retain the roadway embankment.
2. Reinforcing bars or suitable rolled sections shall be spaced across the junction between wingwalls and abutments to tie them together. The bars will be extended sufficiently to develop bond for the bar strength and vary in length so that a plane of weakness is not formed vertically.

From a careful study of the AASHTO specifications we see that abutment and wingwalls are designed as cantilever (or gravity) retaining walls with account taken in the abutment for the bridge seat (see Fig. 12-9*f*), which may apply a horizontal thrust, a vertical weight, and top moment (if the bearing device is not in the stem axis) in addition to the lateral earth pressure. There may be some question of how much design force (shear, tension, and moment) is

produced at the junction of the wingwall and abutment; however, the AASHTO specification further states (sec. 7.4.3.2):

> If bars are not used, an expansion joint shall be provided and the wing wall shall be keyed into the body of the abutment.

From this it appears that the specification writers assume that there is negligible force transfer.

From inspection of Fig. 12-20 we see that if the walls carry the forces P_{ab} and P_{ww} there is in fact little for the junction to carry, and shrinkage and temperature (or some similar approximation) reinforcement would be sufficient.

The only item in the design that appears not to be conservative is the "equivalent fluid" value of 4.75 kN/m^3. In the limited backfill zone defined by an abutment and wingwalls (that is, a compacted zone), it would appear that the equivalent fluid should be a minimum of 8 to 12 kN/m^3. For a granular soil of unit weight $\gamma = 17.30$ kN/m^3 (110 pcf) and an equivalent fluid of 4.75 kN/m^3 the active earth-pressure coefficient can be backcomputed as

$$K_a = 4.75/17.30 = \mathbf{0.275}$$

The corresponding ϕ angle is $\phi \approx 34.7°$. For this ϕ angle

$$K_o = 1 - \sin 34.7° = \mathbf{0.431}$$

The resulting "equivalent fluid" = 17.30(0.431) = 7.46 kN/m^3. Since many abutment fills are clayey and are compacted—often in a fairly limited zone—it would appear that the

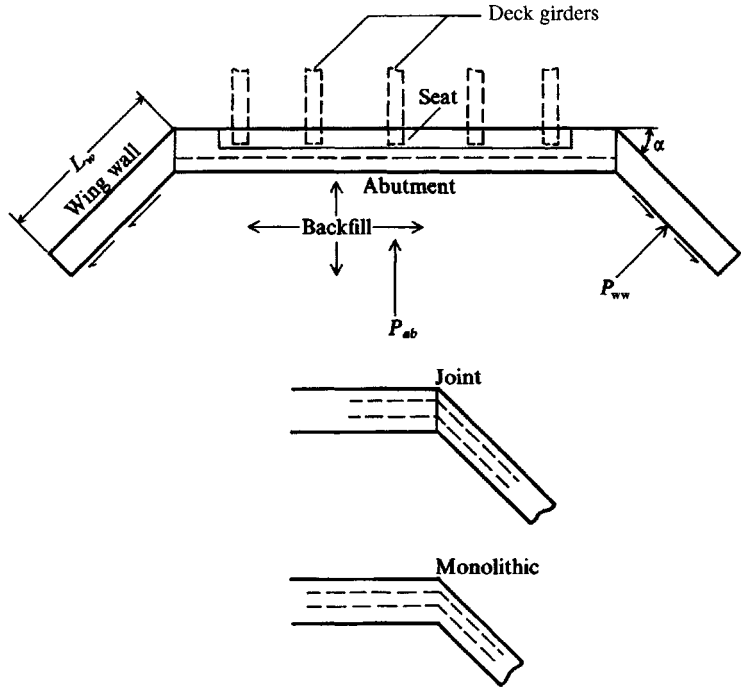

Figure 12-20 Bridge abutment and wingwall earth pressures and methods of construction. As abutment tilts forward, friction develops on wingwalls as shown if wall is rigidly attached.

AASHTO procedure would be somewhat unsafe were it not that rather large load factors are used elsewhere in the design.

12-14 COUNTERFORT RETAINING WALLS

Prior to reinforced earth, when the cantilever retaining wall reached a height of about 7 m, it became economical to consider a counterfort wall (Fig. 12-9*c*). There may be a rare occasion where this is still a practical (but not an economical) solution, so the basic elements of counterfort wall design are presented. Note in Fig. 12-9*c* that if the counterforts are in front of the wall (exposed), the structure is a *buttressed* wall.

The counterfort wall base dimensions tend to range from 0.5 to 0.7H as for the cantilever wall, and the toe and heel dimensions similarly as shown on Fig. 12-11. Counterfort spacings (Fig. 12-21) are commonly on the order of 0.3 to 0.5H, and the counterforts are on the order of 300 mm thick, so reinforcement (as a **T** beam) can be placed with 70 mm clear cover on each side. The trial wall slab (or stem) dimensions may be approximated as for the cantilever stem.

The design proceeds by selecting trial dimensions and making a cantilever retaining wall–type analysis for overturning, sliding, and bearing capacity. When these proportions are approximately adequate, the design may proceed.

The counterfort wall is at least partially a plate fixed on three edges, and one may approximate a solution in that manner. In fact, modern practice and wide availability of computers and computer programs (such as FADMAT on your diskette) almost mandate this method of analysis, especially when taking into account that a counterfort wall is very costly.

For use in program FADMAT (and for other similar computer programs) grid the mat as a plate fixed on three edges as shown in Fig. 12-21. Input is the active lateral pressure converted

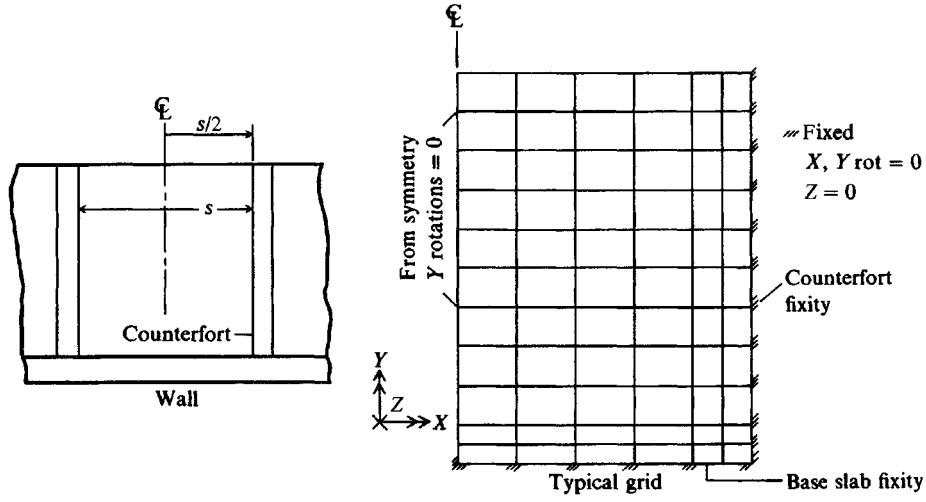

Figure 12-21 Typical layout for using program FADMAT on your program diskette to solve a plate fixed on three edges. Note use of closer grid spacing at fixed edges the better to develop plate curvature and use of one-half the plate and of a large number of boundary conditions of zero rotation.

to nodal forces. There is no resisting soil force but, by using the boundary conditions of no translation at the fixed nodes, structural stability is obtained. Also, inspect the grid and input select boundary conditions of zero rotation for vertical NP along the axis of symmetry and for both horizontal and vertical NP at the fixed edges. From the element output one can obtain the shear at the node points for a wide-beam type of analysis to check the stem thickness; and from the moments at the nodes one can select the necessary stem reinforcement. At this stage several trials may be necessary to somewhat optimize the stem thickness.

From the shears at the counterfort nodes one can design the reinforcement to attach the counterfort to the wall.

A similar plate-fixed-on-three-edges analysis can be done for the heel (or toe, if a buttress-type wall). The free toe (or heel) is similar to the cantilever retaining wall and does not require a computer analysis.

The bearing capacity is computed as for a regular cantilever retaining wall.

The counterforts are analyzed as **T** beams to provide sufficient reinforcement to carry the tension between counterfort and heel and between stem and counterfort. For buttressed walls the counterfort (or buttress) is in compression and only requires sufficient dowels to avoid separation of components. The tensions are obtained from the node shears based on the elements framing into the node.

12-15 BASEMENT OR FOUNDATION WALLS; WALLS FOR RESIDENTIAL CONSTRUCTION

Walls for building foundations, and basement walls for both residential construction and larger structures, require the same design considerations. It is very common (but certainly not recommended) for the basement walls of residential dwellings to be backfilled with excavated earth (also construction debris and anything else lying on the earth piled around the wall and left for backfill) with little regard to its quality. It is pushed into the *b* zone cavity (see Fig. 11-12*b*) behind the wall using a front-end loader or the like and seldom is compacted. Compaction, except using hand equipment, would be difficult because the *b* zone is seldom over 0.6 m and because unreinforced concrete block and mortar walls are often used. It is also not unusual in these cases after an intense rain to observe props against the walls (still under construction) to keep them from caving—and sometimes they do; and sometimes several years after construction. Collapse would not be a problem if

1. A perimeter drain has been installed; and
2. A granular, freely draining material is used for backfill. A perimeter drain is of diminished value if the backfill is not freely draining—but it will usually drain enough water to maintain a dry basement.

A propped wall will always have a bulged region, since propping does not start until the wall starts to show distress. After the building is finished and the site landscaped so that surface water drains away from the structure, these wall problems usually stop.

The tops of these walls are usually restrained from lateral movement by attachment to the superstructure floor, so earth pressures larger than active are likely. If the floors are not strongly attached to the basement walls, the building may shift off of the foundation in a

high wind or during a mild earthquake. Since basement walls for residential construction are seldom over 2.5 m high, earth pressures larger than the active value can usually be tolerated.

Backfill for residential basement walls should be carefully placed and of good quality and preferably granular. The wall should be provided with a perimeter drain placed either on the wall footing or in the wall footing trench. This type of construction will nearly always ensure a dry basement and is more economical than later having to dry the basement by excavating and replacing the fill with quality material and/or installing a perimeter drain.

A perimeter drain is especially important when there is an underground aquifer in which the ground water table varies with rainfall and the basement floor can intercept the GWT. If there is the potential for a GWT-basement interception it is good practice for both residental and commercial construction to grade the subsoil with a slope to one corner of the building, place a 150-mm maximum depth horizontal granular layer on this, compact it, and pour the floor. Later, if the basement becomes wet, a sump hole can be dug in the low corner to drain the subsoil around the building. This is seldom done unless water appears in the subsoil during construction.

In closing this section, observe that all of these suggested practices would substantially (but not visibly) increase the quality of the construction. Their implementation should seldom increase building costs over 1 to 2 percent, and despite any claims to the contrary, no builder can produce a building estimate any closer than this.

12-16 ELEMENTS OF ACI 318- ALTERNATE DESIGN METHOD

Since the ACI 318- Alternate Design Method (ADM) is being used to design retaining walls, select elements will be presented in this section for the reader not familiar with the procedure. For this method the most used design stresses are given in Table 12-1.

TABLE 12-1
Allowable stress values for the ACI 318- Alternate Design Method (ADM)

Stress type	SI	Fps
Flexure	$0.45f'_c$	$0.45f'_c$
Shear		
Two-way	$\left(1+\frac{2}{\beta}\right)\frac{\sqrt{f'_c}}{12} \le \frac{\sqrt{f'_c}}{6}$	$\left(1+\frac{2}{\beta}\right)\sqrt{f'_c} \le 2\sqrt{f'_c}$
Wide-beam	$\frac{\sqrt{f'_c}}{11}$	$1.1\sqrt{f'_c}$
With axial compression (stem)	$0.09\sqrt{f'_c}$	$1.1\sqrt{f'_c}$
Steel		
Grades 40, 50 (f_y = 40, 50)	140 MPa	20 ksi
Grade 400+ (f_y = 60+)	170	24
For splices use Strength Design methods.		
	$E_c = 4700\sqrt{f'_c}$, MPa	$57\,000\sqrt{f'_c}$ psi
	$n = E_s/E_c$ = nearest integer ≥ 6	
All ϕ = 1.0; All Load Factors LF = 1.0.		

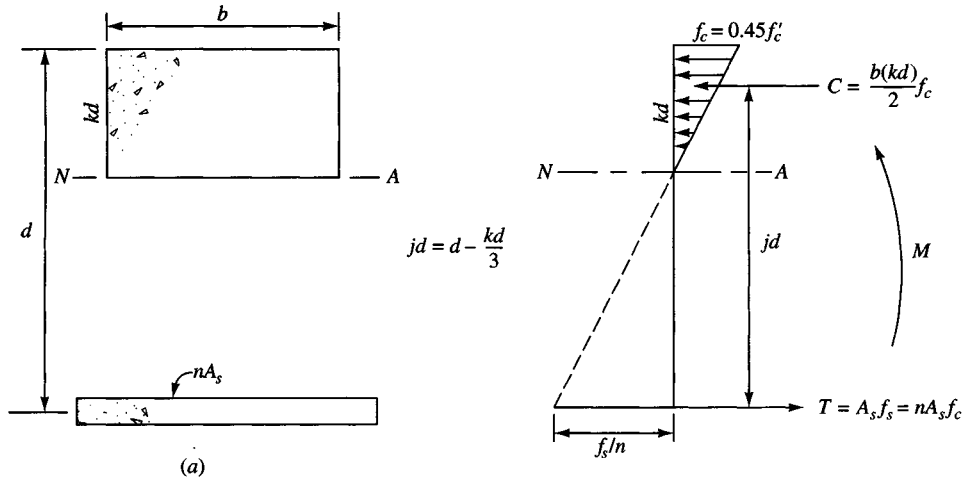

$$Cjd = M = Tjd$$

$$\frac{b(kd)}{2} f_c jd = M = A_s f_s jd$$

By proportion:

$$\frac{kd}{d} = \frac{f_c}{f_c + f_s/n}$$

For $f_c = 21$ MPa, $f_s = 140$ MPa

$$n = E_s/E_c = 9$$

and $$\frac{kd}{d} = \frac{0.45(21)}{9.45 + 140/9} = \mathbf{0.378}$$

$$j = 1 - 0.378/3 = \mathbf{0.874}$$

(b)

Figure 12-22 Balanced design concepts using the ACI 318- Alternate Design Method. (*a*) Shows cracked cross section (assume crack from bottom to neutral axis (*N*-*A*)). (*b*) Assumed stress profile for a beam of width *b* in bending. Equations derived for flexure and a sample computation for *k* in *kd* and *j* in *jd* are shown.

Figure 12-22 displays the usual assumptions in this design method, and the required equation for *balanced design* is developed for bending. For shear the critical sections are the same as for Strength Design. Here one computes the shear force V at the critical section with

$$v_c \geq \frac{V}{bd}$$

where b, d are defined on Fig. 12-22 and v_c is allowable concrete shear stress for the analysis, two-way, wide-beam, etc.

It is convenient when using the flexure equation shown on Fig. 12-22 to tabulate the most used values of k and j so these stress ratios do not have to be computed for each design.

This method is somewhat simpler than the Strength Design method—particularly if d is given and the *balanced* conditions apply. When additional steel is required to meet ACI

TABLE 12-2
Select coefficients for use in the ADM in *balanced design*

			f_s, MPa (ksi)			
			140 (20)		170 (24)	
f'_c	E_c	n	k	j	k	j
3000 psi	3 122 000	10	0.403	0.866	0.360	0.880
21 MPa	21 500	9	0.378	0.874	0.333	0.889
4000	3 605 000	8	0.474	0.842	0.375	0.875
28	24 800	8	0.419	0.860	0.372	0.876

Code minimum requirements, the design is no longer balanced. When this occurs, one should equate

$$C = T \rightarrow bkd\frac{kd}{2}f_c = A_s f_s$$

and see if the new kd is within the section depth. If it is not, the depth d will have to be increased or the steel area reduced if possible. This is illustrated in Example 12-6 in Sec. 12-17.

12-17 CANTILEVER RETAINING WALL EXAMPLES

The several concepts discussed will now be incorporated into three illustrative examples.

Rotational Stability

This example illustrates a general method to analyze the rotational stability of a wall where a base failure that is not identified by bearing capacity may occur. The procedure makes use of the slope stability analysis as given in most introductory courses in geotechnical engineering. If your textbook does not give the procedure, see Bowles (1984) Chap. 16. Because of the large amount of busywork it is preferable to use a slope stability computer program[7] as follows:

1. Draw the wall-soil system and soil layers to a convenient (and fairly large) scale.
2. Compute all the forces acting against the vertical plane through the heel point and their moment arms with respect to the trial circle center. There is usually only P_a, but this may be at a slope to the horizontal.
3. Divide the wall and all contributing backfill zones into geometric shapes so that you can easily compute their weights and moment arms with respect to the toe. Find the total

[7]A number are available commercially—the author uses his own, which has a specific routine for this type of analysis and is listed in your README.DOC diskette file as SMSLOPE (B-22).

weight and its location $\bar{x}'$ from the toe. This weight will be used as a surcharge on a small width (say 0.3 m) so that it is seen as essentially a "point" load. This weight and its location will replace the wall just as the active earth force replaces the backfill outside the "virtual wall" plane through the heel. You cannot combine the lateral and vertical forces for a resultant $\bar{x}$ as in Fig. 12-12*b*, but you can ignore any P_p lateral force on the toe depth, since that will be internal to the circle boundaries.

4. With most computer programs the next step is to identify the several lines that make up the slope (not wall) geometry, identify the several soils, and identify which lines enclose the several soils. For this you do not need a scaled drawing.
5. Number the lines and line ends in the order required by the program. Program B-22 requires that you number the top slope lines in sequence of increasing x coordinate before numbering the interior lines. It requires the line ends also be numbered in order of increasing x coordinate.
6. Next set the line end coordinates. This step requires consistency but usually you can use relative values. If the actual $y = 120$ m, use a relative value of possibly $y = 10$ m—but take off 110 m from all other y coordinates as well.
7. Now tentatively locate the several trial circle centers you want to investigate and locate the entrance coordinates. The entrance coordinates must by definition of this analysis be taken through the heel point of the wall.
8. After finding the minimum safety factor you will need to revise the wall geometry if N_r = SF is too small (usually less than 1.5). If after several wall revisions are done the stability number N_r is still too small, you will have to consider some other solution—perhaps using piles or soil improvement.

Note that although a cantilever retaining wall is shown for this example, this analysis is also applicable to a reinforced earth wall.

Example 12-4. The retaining wall shown in Fig. E12-4*a* overlies a soft clay deposit that may produce a rotational instability. It is required to determine the minimum N_r (or SF) against this type of failure. Refer to the figure for soil properties and critical dimensions.

Solution. Since it is necessary to investigate several trial circles the *only* practical means is to use a slope stability program. Even with this as an aid a substantial amount of preliminary work is involved.

1. The wall geometry and soil lines are drawn to approximate scale as in Fig. E12-4*a*. The wall is critical, but the remainder is less so. Since all slope stability programs require you to input lines to define the slope and soil, their end coordinates must be obtained. Scale them from the drawing, or make up a set of relative values as in Fig. E12-4*a*. Where two lines intersect, be sure they have the same input coordinates with a precision of at least 0.01.
2. Number the lines with the outside top lines first; also number line ends and intersections based on increasing x coordinate. Some of the numbers are shown on Fig. E12-4*a* and a table of input line coordinates is on the output sheet (Fig. E12-4*b*).
3. The Rankine active earth pressure using $K_a = 0.2948$ (from program FFACTOR since 33° is not in Table 11-3) is computed as

$$P_{ah} = \tfrac{1}{2}\gamma H^2 K_a = \tfrac{1}{2}(\mathbf{17.29})(\mathbf{6.7^2})\mathbf{0.2948} = \mathbf{114.4}\ \text{kN/m}$$

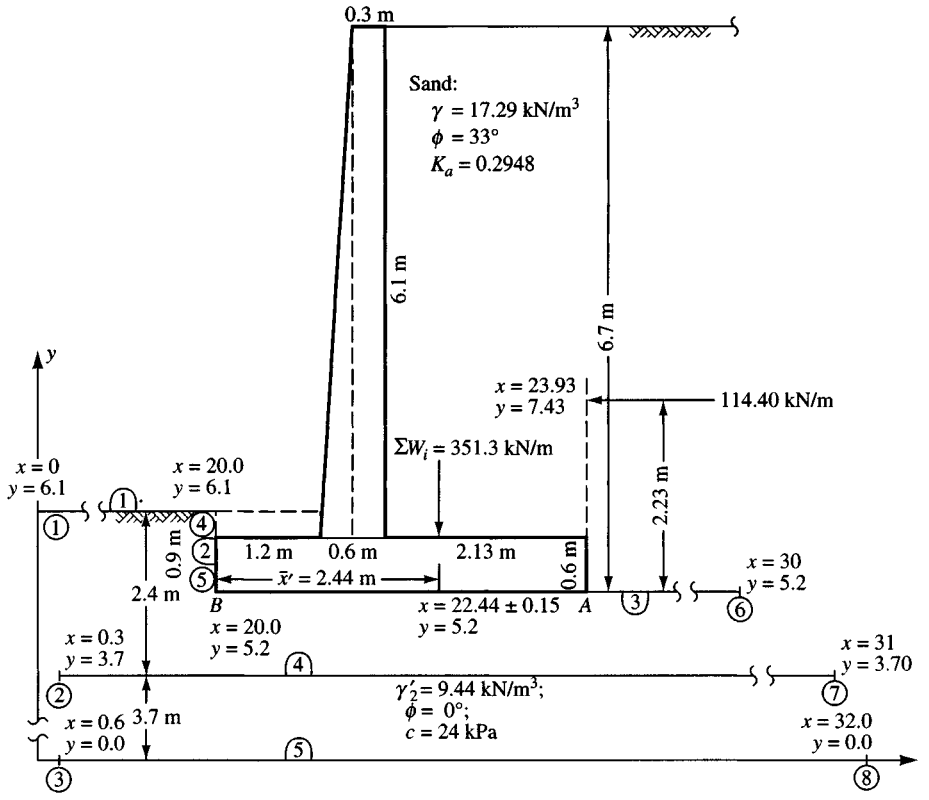

Figure E12-4*a*

It is located at a zero slope to the horizontal of

$$x = 20.0 + 3.93 = 23.93 \text{ m}$$

$$y = 5.2 + 6.7/3 = 7.43 \quad \text{m (also on output sheets)}$$

4. The two soils are enclosed by lines—the base soil is enclosed by lines 1, 2, 3, and 4. The soft clay is enclosed by lines 4 and 5 and the effective unit weight $\gamma' = 9.44$ kN/m^3 is used.

Comments. (Refer to output sheets Fig. E12-4*b* following obtained from using program B-22).

1. Line 1 on Fig. E12-4*a* starts from point 1 at $x = 0$, $y = 6.1$ m. The lower two lines have these features: Line 4 has $x = 0.3$ m, and line 5 has $x = 0.6$ m (so we do not encounter problems of two coordinates with the same x value). Line 1 stops at intersection 4 with $x = 20.0$ m and $y = 6.1$ m.
2. Line 2 starts at point 4 and ends at 5 (or *B*) with $x = 20.0$ m and $y = 5.20$ m. The vertical distance is 0.9 m and is given a small program-defined (−) slope with the value shown (0.100 E+11 on Fig. E12-4*b*) so there is "no divide by zero" error. The slope sign is computed by the program.
3. Line 3 starts at *B* and is arbitrarily extended beyond *A* to x coordinate = 30.0 m and $y = 4.90$ m. We will locate the wall weight as a surcharge on this line, but we only have to specify the surcharge Q, the x coordinate at the left where it starts, and the x coordinate on the right. Here we used $Q = 351.3/0.3$ kN/m on a width of 0.3 m. First we had to locate the x coordinate of Q using the several parts making up the wall and backfill on the heel of Fig. E12-4*a*. Note that a small triangular zone in the toe region is neglected as not being worth the computation effort.

Figure E12-4*b*

```
 RETAINING WALL STABILITY--EXAMPLE 12-4  FOUND ANALY & DESIGN 5/E--SI


 ++++ DATA FILE NAME FOR THIS EXECUTION:  EXAM124.DTA


NO OF LINES =  5          NO OF LINE INTERSECT =  8
NO OF SOILS =  2     NO OF EXTERNAL SOIL LINES =  3
 NO OF X-INCREMENTS =  3    NO OF Y-INCREMENTS =  3
             DIMEN = 25          RET WALL CODE =  1
    TENS CRACK CODE =  0   SOIL FOR TENS CRACK =  0
WATER IN TENS CRACK =  0             EXTRA LIST =  0

                  INITIAL SLICE WIDTH =   1.5  M
          SLID BLOCK SOIL LINE, FALLIN =  0
                  TAILWATER ELEVATION =     .00  M
 EXCESS PORE PRESSSURE PIEZOMETRIC HEAD =     .00  M


 SURCHARGE =  1171.0000   X-LEFT =    22.2900   X-RIGHT  =    22.5900


 RETAINING WALL SOLUTION:  PA =  114.400
       XPA =   23.930    YPA =    7.430   SLOPE OF PA =      .000

 THE LINE END COORD MATRIX
LINE NO     X1        Y1        X2        Y2        SLOPE        LINE INTER NO
  1.        .00      6.10     20.00      6.10     .000000          1    4
  2.      20.00      6.10     20.00      5.20    -.100000E+11      4    5
  3.      20.00      5.20     30.00      5.20     .000000          5    6
  4.        .30      3.70     31.00      3.70     .000000          2    7
  5.        .60       .00     32.00       .00     .000000          3    8


 LINE INTERSECTION ARRAY
INT NO      X             Y
   1          .00         6.10
   2          .30         3.70
   3          .60          .00
   4        20.00         6.10
   5        20.00         5.20
   6        30.00         5.20
   7        31.00         3.70
   8        32.00          .00


 SOIL # =    1  LINE NOS =    1    2    3    4
 SOIL # =    2  LINE NOS =    4    5


 SOIL DATA ARRAY
SOIL NO  UNIT WT    PHI, DEG    COHESION     SAT CODE
     1   17.290       33.00        .000          .0
     2    9.440         .00      24.000          .0

 +++ UNITS:  IF GAM = LBS/CU FT---COHES = PSF
             IF GAM = K/CU FT---COHES = KSF
             IF GAM = KN/CU M---COHES = KPA


 COORDINATES OF PERPENDICULAR FROM CENTER TO PA:
    X =   17.450    Y =    7.430    PERP DIST =    2.910
```

Figure E12-4*b* (*continued*)

```
 ON SLICE # = 11  SURCHARGE LENGTH D1 =     .300
  SLICE WT INCREASE D1*Q = 351.299


 SURCHARGE LENGTH DX =     .300   SURCHARGE Q =1171.000
 TOTAL ACCUMULATED SURCHARGE WEIGHT DX*Q =  351.299


COORDINATES OF PERPENDICULAR FROM CENTER TO PA:
   X =   17.750    Y =    7.430    PERP DIST =    2.910


COORDINATES OF PERPENDICULAR FROM CENTER TO PA:
   X =   18.050    Y =    7.430    PERP DIST =    2.910


COORDINATES OF PERPENDICULAR FROM CENTER TO PA:
   X =   17.450    Y =    7.430    PERP DIST =    3.210


COORDINATES OF PERPENDICULAR FROM CENTER TO PA:
   X =   17.750    Y =    7.430    PERP DIST =    3.210


COORDINATES OF PERPENDICULAR FROM CENTER TO PA:
   X =   18.050    Y =    7.430    PERP DIST =    3.210


COORDINATES OF PERPENDICULAR FROM CENTER TO PA:
   X =   17.450    Y =    7.430    PERP DIST =    3.510


COORDINATES OF PERPENDICULAR FROM CENTER TO PA:
   X =   17.750    Y =    7.430    PERP DIST =    3.510


COORDINATES OF PERPENDICULAR FROM CENTER TO PA:
   X =   18.050    Y =    7.430    PERP DIST =    3.510


SUMMARY OF SF FOR THIS TRIAL SET OF ENTX, ENTY =   23.9300    4.9000
PT NO      CX        CY     RADIUS        SF
  1       17.45     10.34     8.461     1.7826    10.128     6.100
  2       17.75     10.34     8.233     1.7261    10.692     6.100
  3       18.05     10.34     8.010     1.8462    11.254     6.100
  4       17.45     10.64     8.657     1.7795    10.079     6.100
  5       17.75     10.64     8.434     1.8589    10.642     6.100
  6       18.05     10.64     8.217     2.0722    11.201     6.100
  7       17.45     10.94     8.858     1.8802    10.031     6.100
  8       17.75     10.94     8.641     2.0709    10.591     6.100
  9       18.05     10.94     8.429     2.2926    11.149     6.100

          FOR TRIAL NO =  1   MINIMUM SAFETY FACTOR SF =    1.7261
               AND OCCURS AT GRID POINT JJ =   2  +++++++++
```

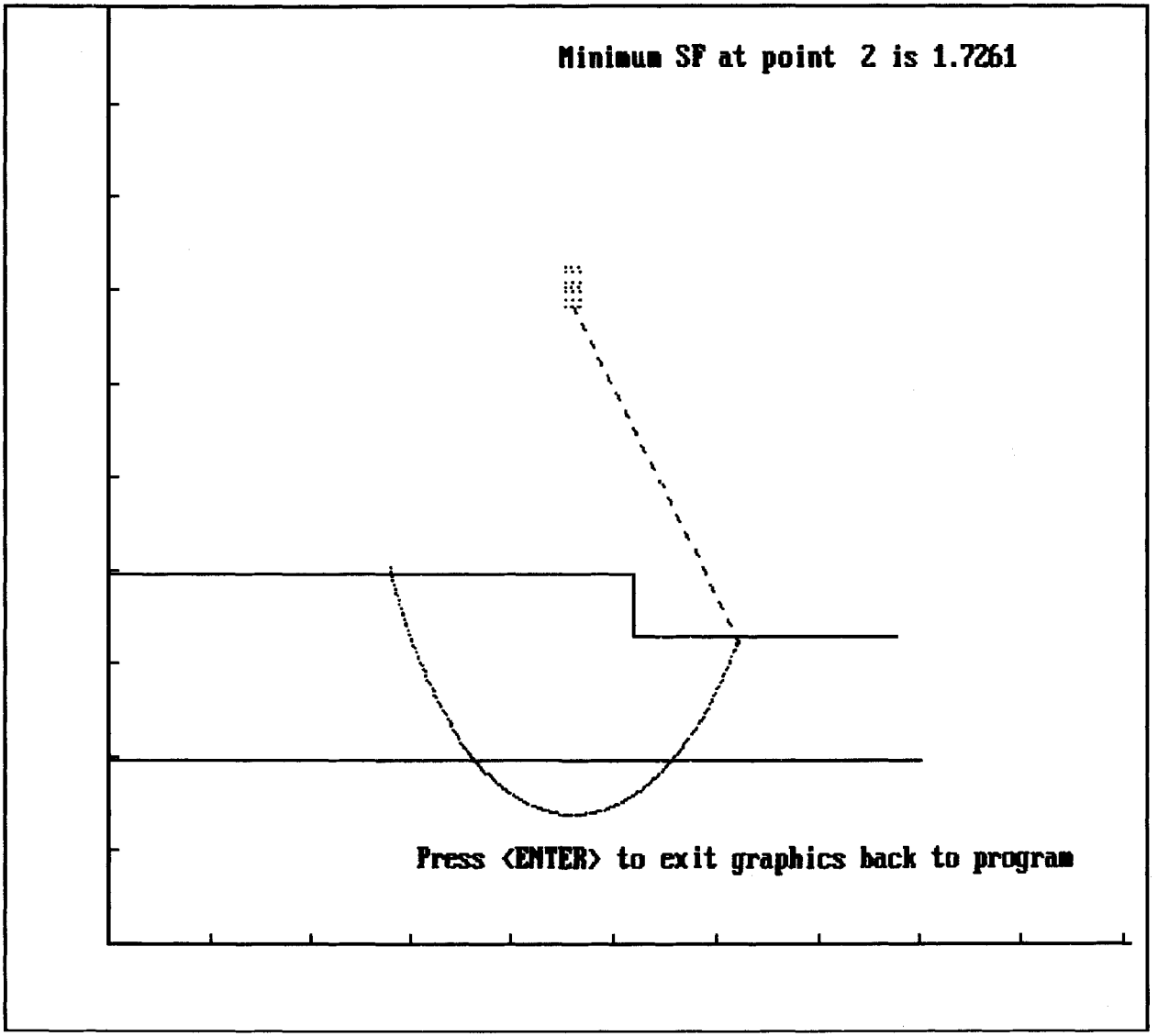

Figure E12-4*c*

From the $\sum W_i = 351.3$ kN and the moment arms x_i referenced to point B, a moment of 858.19 kN · m/m is computed and the location is found as

$$\bar{x}' = \frac{858.19}{351.3} = \mathbf{2.44}\text{ m} \qquad \text{(shown on Fig. E12-4}a\text{)}$$

4. Note that the output sheet shows the perpendicular distance to P_a for each trial circle. You can see after the first three trials the y distance increased 0.3 m (the vertical grid spacing) and another 0.3 m again after the first six trials. This is a small output check and clutters the output sheet somewhat, but remember, you need all the checks you can get for complicated programs.

   The program tabulates data on the several trial circles tried (using a center point grid of nine points at a spacing of 0.3 m each way starting from the lower left). The minimum SF for nine trials is found to be 1.7261 and is found at center grid point 2. Refer also to Fig. E12-4*c*. Note that the center coordinates for all the nine entrance points used, the trial circle radius (through the ENTX, ENTY point) and SF are output in a table (Fig. E12-4*b*). Clearly from this table we see that the SF is sensitive to the center coordinates.

5. A rough plot is produced on screen, if requested, (*a*) to check if the lines meet (bad input coordinates) and (*b*) to see if the minimum trial circle is reasonable. If it were all in the base soil, it would not be considered a solution. The program has some internal checks to output a large SF if the circle is below the clay soil (y coordinate < 0) or to the left (x coordinate < 0).

   This plot is reproduced on paper using the <Print Screen> function but is not to scale, since screen pixels are not well-scaled. To get a scaled drawing, the output can be directed to a disk file for later use with a plotting program.

   The screen plot is particularly useful for more general types of slope analyses where the user may want to change the entrance coordinates. Here they must always pass through the heel at point A of Fig. E12-4*a*, but it is useful here to see if the minimum SF is partly in the clay.

6. The program also outputs the slice location and surcharge data. We see it finds the surcharge on slice 11 and, with a 0.3-m width, the product of Q × D1 = 1171.0 × 0.3 = 351.299 (351.3 is input). This result also somewhat clutters the output sheet, but again remember that the more self-checks are in a program, the higher is the user confidence level. Here the slice number without the program is of little value, but the remainder shows that the surcharge Q was used. In the program there is an input switch that allows output of slice locations giving the x coordinate of each slice (by the way, there are two slices with the same x coordinates at the vertical line) so one can obtain sufficient data to reproduce the complete trial circle for hand-checking including slice weights, pore pressure head (if applicable), or any upstream tailwater heads.

   One probably should make several more trials to see if the minimum SF = **1.7261** or if a smaller value can be found that has part of the trial circle in the clay soil.

////

Retaining Wall Stability

The next example will illustrate the method of analyzing a retaining wall for overturning and sliding stability. The general stability considerations are shown in Fig. 12-12*b*. The mechanical details involve finding the several weight vectors and moment arms x_i with respect to overturning. A substantial amount of busywork is involved and it may be convenient (if you do not use a computer program) to draw the system to a large scale and measure the required dimensions.

We note that with several weight vectors, and if the backfill has a β angle and the wall has a batter, the computations become especially involved. A tabulation of data is necessary so that quantities are not overlooked.

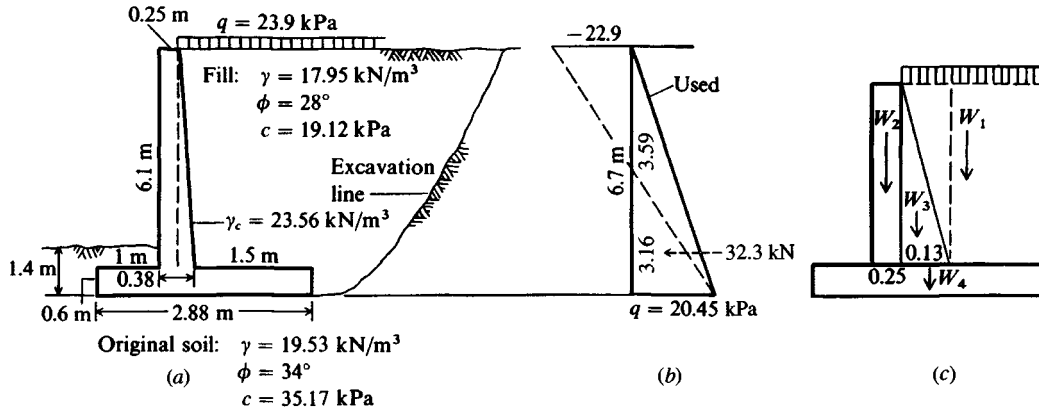

Figure E12-5

Example 12-5. Analyze the retaining wall shown in Fig. E12-5 for overturning and sliding stability. Note that this wall is backfilled in a limited zone with a cohesive soil. The batter is on the back face, as used by some transportation departments. Most of the output was obtained from using the author's computer program B-24. Dimensions shown were optimized by the program to satisfy both strength and stability requirements (usually wide-beam shear for member thickness and bearing capacity for dimension B).

Solution.

Step 1. Find the ϕ' angle for an equivalent cohesionless soil (see Fig. E12-5*b*):

$$q = \gamma H K_a - 2c\sqrt{K_a} = \gamma H K_a'$$

Rankine $K_a = 0.361$ for $\phi = 28°$ (Table 11-3)

$$q = 17.95(6.7)(0.361) - 2(19.12)(0.601)$$
$$= 43.42 - 22.97 = 20.45 \text{ kPa}$$

$$K_a' = \frac{20.45}{(6.7)(17.95)} = 0.170$$

$$45° - \frac{\phi}{2} = 22.42°$$

$$\phi = 45.16° \qquad \text{Use } \phi' = 45° \qquad K_a' = 0.171$$

This value of ϕ', as well as $\gamma = 17.95$ kN/m³, was used in the computer program.

Step 2. Compute P_a:

$$P_a = (0.5\gamma H^2 + qH)K_a'$$
$$= [0.5(17.95)(6.7)^2 + 23.90(6.7)](0.171)$$
$$= 96.28 \text{ kN} \qquad (\text{vs. } 20.45 \times 3.16/2 = 32.3 \text{ kN at } \bar{y} = 3.16/3 = 1.05 \text{ m})$$

Step 3. Compute overturning stability. Set up a table and refer to Fig. E12-4*c*.
The location of P_a is at $\bar{y}$:

$$P_a\bar{y} = M_o$$
$$\bar{y} = \frac{68.89(6.7/3) + 27.38(6.7/2)}{96.28} = \frac{245.58}{96.28} = \mathbf{2.55} \text{ m}$$

Part	Weight of part, kN		Arm, m	Moment, kN·m
1	1.5(23.9)+6.1(1.5)(17.95)	= 200.09	2.130	426.19
2	23.56(0.25)(6.1)	= 35.93	1.125	40.43
3	0.13[(0.61)(23.56+17.95)0.5+23.90]	= 19.57	1.315*	25.73
4	23.56(0.6)(2.88)	= 40.71	1.440	58.62
P_{av}†	$= P_{ah}\tan\phi = 96.28[\tan 0.8(28)]$	= (39.70)	2.880	(114.30)
		$\sum F_v$ = 296.30 kN‡		$\sum M_r$ = 550.97¶

*To center; value is slightly approximate.
†Neglect cohesion and only for overturning—not for $\sum F_v$ and bearing capacity. Use $\phi_r = 0.8\phi$.
‡Sum does not include 39.7 kN.
¶Does not include 114.30 kN · m.

The overturning stability number is (and including P_{av} but using 0.8ϕ)

$$N_o = \frac{M_r}{M_o} = \frac{550.97 + 114.3}{245.58} = \frac{65.27}{245.58} = \mathbf{2.71} \gg 1.5 \qquad \text{(O.K.)}$$

Step 4. Compute the sliding stability number N_s but do not include P_{av}. Use base soil parameters and

$$\begin{aligned} c' &= 0.67c = 0.67(35.17) = 23.56 \text{ kPa} \\ \tan\delta &= \tan\phi = \tan 34^\circ = 0.675 \\ F_r &= c'B + F_v \tan\delta \\ &= 23.56(2.88) + 296.3(0.675) = 267.86 \text{ kN} \\ N_s &= \frac{F_r}{F_d} = \frac{267.86}{96.28} = \mathbf{2.78} > 2.0 \qquad \text{(O.K.)} \end{aligned}$$

Step 5. Locate the resultant on the base of the footing. From rigid body statics a moment summation can be taken at any location. Use the toe, as we already have most of the moments computed, but do not include P_{av}:

$$\begin{aligned} \sum M &= M_r - M_o = 550.97 - 245.58 = 305.40 \text{ kN} \cdot \text{m} \\ X &= \frac{\sum M}{\sum F_v} = \frac{305.4}{296.3} = 1.03 \text{ m from toe } (> 2.88/3) \\ e &= \frac{B}{2} - X = 1.44 - 1.03 = 0.41 \text{ m} \\ \frac{L}{6} &= \frac{2.88}{6} = \mathbf{0.48} > 0.41 \end{aligned}$$

Therefore, the resultant is in the middle one-third of base.

Step 6. Compute passive pressure in front of wall and recompute N_s of Step 4. (This calculation is for illustrative purposes, as N_s is already O.K.)

$$\begin{aligned} K_p &= \tan^2\left(45^\circ + \frac{\phi}{2}\right) = \tan^2 62^\circ = 3.537 \\ P_p &= 0.5(19.53)(1.4)^2(3.537) = 67.7 \text{ kN} \end{aligned}$$

Now, how do we apply P_p?

(1) P_p = −driving force

$$N_s = \frac{267.86}{96.28 - 67.7} = 9.37$$

(2) P_p = resisting force

$$N_s = \frac{267.86 + 67.7}{96.28} = 3.48$$

At least two other ways of computing N_s exist, including 267.86 taken as a (−) driving force and 96.28 considered as a (−) resisting force.

////

Retaining Wall Design

This example will go through the complete design of a small retaining wall. In general, the wall design involves tentatively selecting stem and base dimensions, checking them for stability, and resizing as necessary. Next the allowable bearing capacity is computed, and the base shear and moments at the stem faces are computed. If the base shear is too large, the base depth is increased and the problem is recycled. When increasing the base depth, it is best to reduce the stem height the same amount so the overall wall height remains constant. When the base thickness is found adequate, the base toe and heel steel requirements are computed.

Since there is much busywork involved, a computer program that finds the required stem and base dimensions is useful. The program is of even more value if it also produces a rebar schedule and outputs material quantities.

Figure 12-23 illustrates the critical sections for structural design of the wall elements. Stem moment steel is on the backfill side of the wall. Since the wall face is exposed, it is required to place T and S bars longitudinally as shown. The principal toe reinforcement is in the bottom with one or more bars extended the full base width and the others bent 90° and extended (a short distance or the full stem height) above the base slab when it is poured so any needed stem steel bars can be spliced. The principal heel bars are in the top as shown in the figure and one or more might extend the full base width. Those cut (toe or heel) must extend at least a distance D_c of the stem or $12d_b$ beyond the front or back stem faces. Clear cover of 70 mm (3 in.) is required on all sides for the base. If the stem back face is formed (and it usually is), a clear cover of 50 mm can be used.

Minimum T and S steel and flexural steel requirements are as follows (see ACI 318-, Appendix A: Commentary, Articles RA.1-RA.1.4):

	Grade 300 (f_y = **40 or 50 ksi**)		**Grade 400** ($f_y \geq$ **60 ksi**)
T and S	0.002		0.0018
Flexural	$1.4/f_y$ (MPa)		$200/f_y$ (psi)
Alternative		$A_s' = 1.33A_s$	

The preceding ratios are multiplied by the gross concrete area (A_g = full thickness including clear cover × width); the one-third increase in computed steel area A_s is self-explanatory.

Longitudinal T and S steel is always required in the stem but may be optional for the base slab, which is covered with soil. Give consideration to its use in the base slab for some longitudinal settlement crack control.

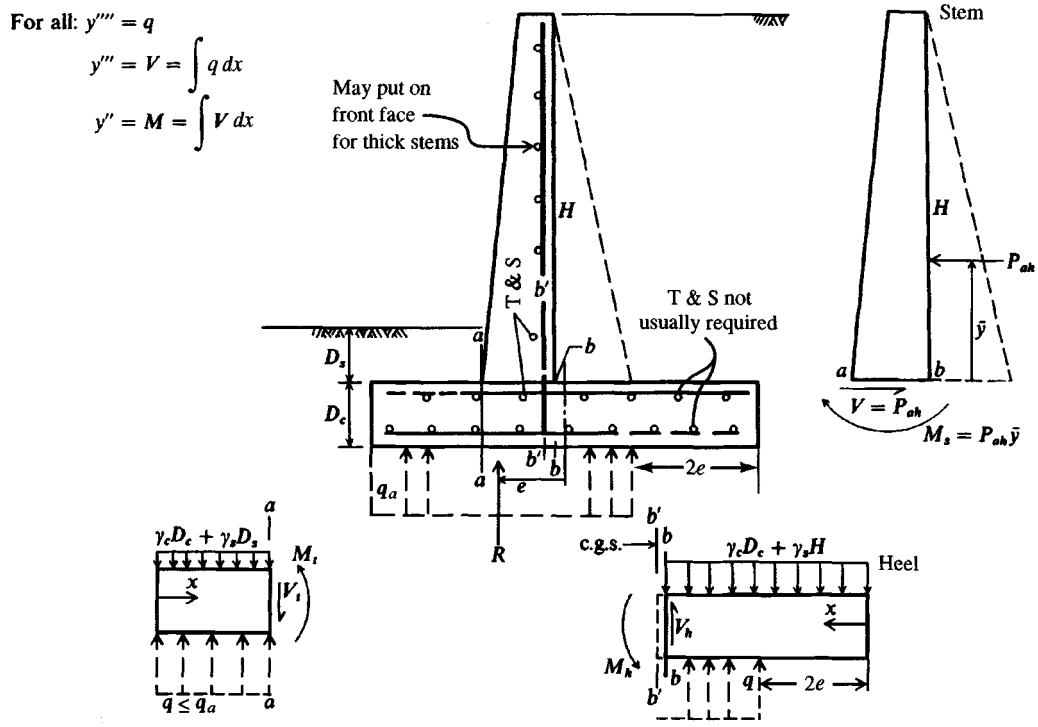

Figure 12-23 Critical sections for retaining wall design. Use the differential equations shown for stem shear and moment. Also use these equations if a linear variable base pressure diagram is used. The rectangular base pressure diagram shown is preferred and is consistent with the method used to obtain the allowable bearing capacity.

With high walls it is a common practice to cut the stem bars (cutoff points) when the stem moment is small enough that the bar(s) are no longer needed or the diameter(s) can be reduced to save steel weight, since the moment in the upper half of the stem is quite low. For small walls the extra design and labor costs for cutting and splicing may far outweigh the savings in material.

Example 12-6. Design the retaining wall of Fig. E12-6*a* to provide lateral support for an existing parking lot adjacent to a new sidewalk in a road-widening project. The wall height will range from about 0.3 to 1.7 m above the sidewalk grade in the required 92.2 m of wall length. For frost and bearing the base will be placed at $D = 1.22$ m. A typical section appears in Fig. E12-6*a*, which also displays the ground before and after the wall is built.

We will generally follow the ACI specifications; AASHTO specifications are similar, but allowable stresses are 10 to 15 percent lower (more conservative) because of the additional environment exposure.

Other information. We will specify granular backfill in the limited zone over the heel as shown, which will be compacted to $\gamma = 17.30$ kN/m^3 and an estimated $\phi = 36°$. The original soil will be excavated 50 mm below the footing grade, and the resultant space will be backfilled with 65 mm of granular soil (as in backfill) that is then compacted to grade prior to pouring the footing. It is assumed in the stability analysis, however, that the footing is on clay, for the sand will probably become well mixed with the site soil from using equipment for excavation and from spreading and compacting.

One end of the wall exits in such a manner that a longitudinal drain pipe can be used for drainage; however, a drain is optional since the backfill is paved.

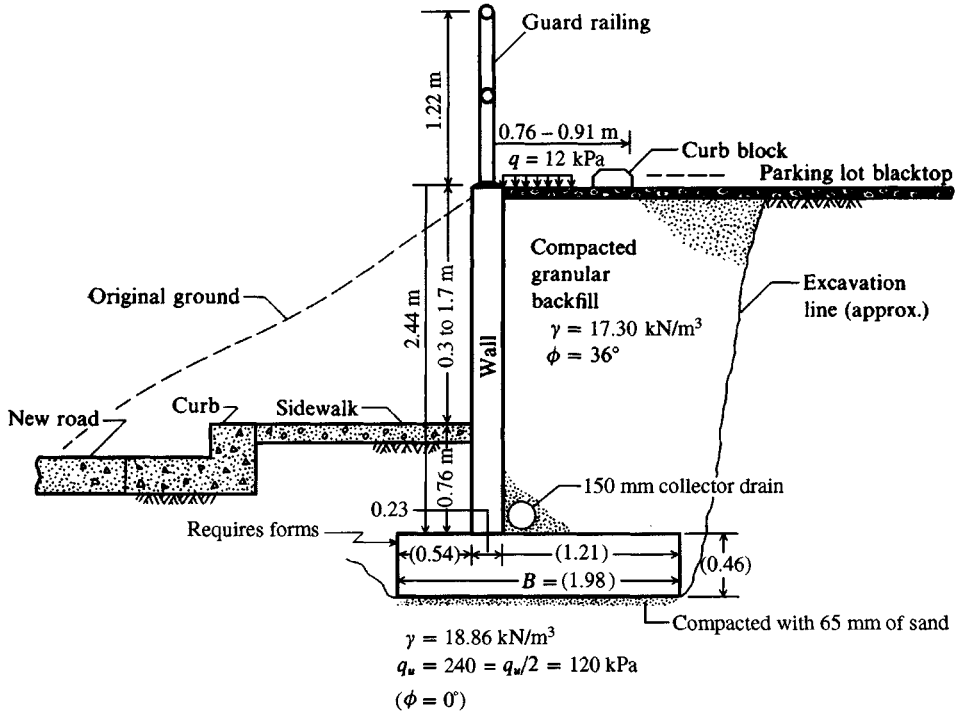

Figure E12-6*a*

With this background and the given soil data, several trial computer runs are made using the largest wall height (of 2.44 m) to obtain the wall dimensions shown on Fig. E12-6*a*. These data seem reasonable and will be used in the design steps following to illustrate the general procedure without having to iterate dimensions. In actual practice, of course, the computer output sheets would be checked for input and spot-checked for output and the data then provided either to a draftsperson or to a plot routine for plotting.

Solution. The initial design includes the following considerations:

1. Use a fictitious surcharge of 12 kPa to partially model the parking lot pavement and wheel loads in the proximity of the parking curb to the wall.
2. Ignore the guard rail. Its mass per meter is negligible and would only occasionally have a lateral load from persons leaning against it. Guard rail force contributions will be somewhat accounted for by using a larger earth-pressure coefficient.
3. Use an earth-pressure coefficient of $K_a = K_o = 1 - \sin\phi$ for the reasons in the preceding item and to account for compaction-induced lateral pressures and the probability that a Rankine active wedge will not form in the limited backfill zone. This gives

$$K_a = 1 - \sin 36^\circ = \mathbf{0.412}$$

   The Rankine K_a from Table 11-3 is 0.260.
4. We will arbitrarily use a wall of constant thickness to save on forming costs. The wall has a variable height ranging from about 1.07 to 2.44 m, so tilt is not so likely as for a much higher wall. Figure E12-6*a* shows that a substantial amount of the wall height is effectively embedded.

5. We will not specify the particular reinforcing bars but rather specify the amounts and let the contractor élect whether to use rebars or welded wire fabric.
6. Use $f'_c = 21$ MPa and $f_y = 400$ MPa. Most transportation departments do not allow using f'_c as low as 21 MPa because of the hostile environment, but this concrete strength is acceptable here. For the Alternate Design Method (ADM) these choices give working stresses of

$$f_c = 0.45f'_c = 0.45(21) = 9.45 \text{ MPa} \quad (9450 \text{ kPa}) \quad \text{(flexural)}$$

$$v_c = \frac{\sqrt{f_c}}{11} = \frac{\sqrt{21}}{11} = 0.417 \text{ MPa} \quad (417 \text{ kPa}) \quad \text{(wide-beam shear)}$$

$$f_s = 170 \text{ MPa} \quad \text{(see Table 12-1)}$$

Also $k = 0.360$; $j = 0.880$; and $n = 10$ (see Table 12-2).

We will now proceed to analyze the wall.

Step 1. Using earth pressure principles of Chap. 11, obtain the vertical stem pressure profile of the wall as

$$q = (q_s + \gamma z)K_a$$
$$= (12.0 + 17.30z)(0.412)$$
$$\text{At top:} \quad q = (12.0 + 17.30 \times 0.0)(0.412) = \mathbf{4.94} \text{ kPa}$$
$$\text{At base:} \quad q = (12.0 + 17.30 \times 2.44)(0.412) = \mathbf{22.34} \text{ kPa}$$

The total lateral wall force is the area of the pressure diagram,

$$P_a = \frac{(a+b)}{2}H = \frac{4.94 + 22.34}{2} \times 2.44 = \mathbf{33.28} \text{ kN/m}$$

Obtain its location using Eq. (11-14):

$$\bar{y} = \frac{H}{3}\frac{3q + \gamma H}{2q + \gamma H} = \frac{2.44}{3}\frac{(3 \times 12 + 17.30 \times 2.44)}{(2 \times 12 + 17.30 \times 2.44)} = 0.961 \text{ m} \quad (\text{which is} > 2.44/3)$$

$$\text{The stem shear } V = P_a = 33.28 \text{ kN}$$

$$\text{The stem base stem moment} = P_a\bar{y} = 33.28 \times 0.961 = \mathbf{31.98} \text{ kN} \cdot \text{m/m}$$

These data are summarized on Fig. E12-6*b*.

Since we will use a constant amount of reinforcing steel for moment based on the largest H it is only necessary to investigate the stem base. For high walls it would be worthwhile to investigate other points and perhaps use cutoff points at about $H/4$ intervals vertically. (Computer program B-24 checks the 0.1 points.)

Step 2. Using the shear V and moment M from step 1 check wide-beam shear at the stem base and find the amount of vertical reinforcement per meter of wall length.

Take 50 mm of clear cover and about 20-mm diameter reinforcing bars; the stem depth d = D − clear cover − bar diameter/2 = 230 − 50 − 10 = **170** mm.

$$\text{Allowable } V_a = 170(417)/1000 = \mathbf{70.9} \text{ kN} \gg 33.28 \quad \text{(O.K.)}$$

Check shear friction since the wall is built after the base has been poured and partially cured. Shear friction is governed by ACI 318- Art. 11-7-5 with a 55 percent reduction for using the ADM method (use $\phi = 0.85$):

$$V_n = 0.55(0.2\phi f'_c A_g)$$
$$= 0.55[(0.2 \times 0.85 \times 21\,000)(0.23 \times 1.0)] = 451.6 \text{ kN/m} \gg 33.28$$

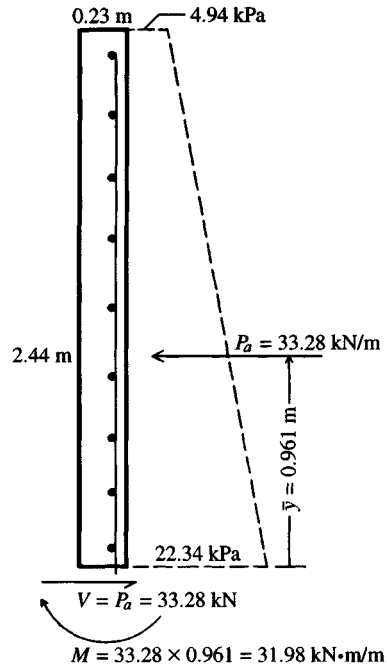

Figure E12-6*b*

From this computation it would appear that shear friction seldom controls except possibly for a very high wall with a thin stem. The stem appears somewhat overdesigned, but we will use this wall thickness because it is not difficult to construct the formwork, and there is adequate space to place the reinforcement and necessary top width to secure the guard railing adequately.

The area of reinforcement/meter of wall is computed using the equations shown on Fig. 12-22. The determination is quite simple when d is known as here:

$$b\frac{(kd)}{2}f_c jd = M = A_s f_s jd$$

Taking $d = 0.170$ m and $j = 0.880$, we obtain

$$A_s(170 \times 1000)(0.880 \times 0.170) = 31.98 \text{ kN} \cdot \text{m}$$

$$A_s = \frac{31.98}{(170\,000)(0.880 \times 0.170)} = 0.001\,2575 \text{ m}^2/\text{m} \rightarrow \mathbf{1257} \text{ mm}^2/\text{m}$$

The minimum for flexure $= 1.4/f_y = 1.4/400 = 0.0035$.

$$A_{s,\min} = 0.0035A_g = 0.0035(1000 \times 230) = 805 \text{ mm}^2/\text{m} < 1257$$

For T and S we have

$$A_{s,\text{TS}} = 0.0018(A_g) = 0.0018(1000 \times 230) = \mathbf{414} \text{ mm}^2/\text{m} < 1257$$

Let us summarize:

Vertical stem reinforcement requires **1257** mm^2/m.
Longitudinal stem T and S requires **414** mm^2/m.
We have a "balanced" design for the stem.

If we were selecting reinforcing bars (using the table inside the front cover of this text), we would use four No. 20, giving $4 \times 300 = 1200 \approx 1257$ (about 5 percent overstressed) and for longitudinal T and S use four No. 10 bars per meter, giving $4 \times 100 = 400 \approx 414$ (about 3 percent under). The stem bars require an embedment of at least d_{base} of base ($12 \times 20 = 240 < d_{base}$). One would likely either use some toe steel bent up for dowels or bend the stem steel 90° to wire to the toe bars.

Step 3. Check wall stability for overturning and sliding and that the resultant R is in the middle third of base width B. For these computations refer to Fig. 12-12*b* but use dimensions from Fig. E12-5*a*.

a. First we must compute the active earth pressure at the heel through line *ba* of Fig. 12-12*b*, except here the backfill slope angle $\beta = 0°$. Compute the following:

$$H = 2.44 + 0.46 = \mathbf{2.90}\text{ m}$$

$$\text{Lateral pressure } q_{top} = 4.94\text{ kPa} \qquad \text{(as for stem)}$$

$$\text{Lateral pressure } q_{base} = (12. + 17.30 \times 2.9)0.412 = 25.61\text{ kPa}$$

$$\text{Horizontal force} = P_a = \frac{4.94 + 25.61}{2} \times 2.9 = \mathbf{44.30}\text{ kN/m}$$

Find $\bar{y}$ as for stem using Eq. (11-14):

$$\bar{y} = \frac{2.9}{3}\frac{(3 \times 12.0 + 17.3 \times 2.9)}{(2 \times 12.0 + 17.3 \times 2.9)} = \mathbf{1.123}\text{ m}$$

To compute the resultant vertical force we will divide the wall geometry into rectangles since the stem has a different γ from the soil, etc. It is convenient to use Table E12-6, where the parts are labeled, weights computed, moment arms given, etc. For this, first observe that the soil weight W_s includes the 12 kPa surcharge. Also take $\gamma_c = 23.6\text{ kN/m}^3$.

TABLE E12-6

Part	Weight, kN	Arm, m, $\bar{x}$	Moment, kN · m/m
W_s	$1.21(12 + 17.30 \times 2.44) = 65.59$	1.375	90.18
Stem	$23.6(0.23)(2.44) = 13.24$	0.655	8.67
Base slab	$23.6(0.46)(1.98) = 21.49$	0.99	21.28
	$P_{av} = 0 \quad (\beta = 0)$		0.00
	$P'_{av} = 33.28 \tan(0.8 \times 36) = (18.30)$	1.98	(36.23)
	$\sum W_i = \mathbf{100.32}$ kN		$\sum M_r = \mathbf{156.36}$ kN · m/m

b. Compute the overturning stability:

$$\text{Overturning moment } M_o = P_a\bar{y} = 44.30 \times 1.123 = 49.75\text{ kN/m}$$

The resisting moment M_r (includes P'_{av} of 36.23) is the sum shown in Table E12-6.

$$\text{Stability number } N_o = \frac{M_r}{M_o} = \frac{156.36}{49.75} = \mathbf{3.14} > 1.5 \qquad \text{(O.K.)}$$

c. Now check that the location of the resultant R on base is inside the middle third. The net overturning moment (excluding any passive pressure and friction P'_{av} on the vertical plane through the heel) is:

$$M_{\text{net}} = M_r - M_o = 156.36 - 36.23 - 49.75 = \mathbf{70.38}\ \text{kN} \cdot \text{m/m}$$

$$\bar{x} = \frac{M_{\text{net}}}{R} = \frac{70.38}{100.32} = 0.70\ \text{m from toe} (> 1.98/3)$$

$$e = B/2 - \bar{x} = 1.98/2 - 0.70 = \mathbf{0.29}\ \text{m}$$

$$B/6 = 1.98/6 = 0.33 > 0.29 \qquad \text{so resultant is in middle 1/3}$$

d. Compute the sliding stability (we needed to compute the eccentricity e so the effective base width B' can be computed). For sliding, the resistance is

$$F_r = R \tan \delta + c_a B' + P_p$$

From soil data $\delta = 0°$. Take $c_a = 0.7c = 0.7 \times 120 = 84.0$ kPa. Do not use P_p unless necessary. So

$$F_r = 84(1.98 - 2 \times 0.29) = \mathbf{117.60}\ \text{kN}$$

The resulting sliding stability number is

$$N_s = \frac{F_r}{P_a} = \frac{117.6}{44.3} = \mathbf{2.65} > 1.5 \qquad \text{(O.K.)}$$

We do not need any passive pressure, but if it were used we could probably use the full embedment depth but not include the sidewalk as a surcharge (it may need future repairs).

Let us summarize:

$$N_o = \mathbf{3.14} \qquad N_s = \mathbf{2.65}$$

$$\text{Eccentricity } e = \mathbf{0.29}\ \text{m}$$

Step 4. Compute bearing capacity. Use the Hansen bearing-capacity equation with all shape factors $s_i = 1.0$; there will be depth d_i and inclination factors i_i. Since $\phi = 0$ for base soil, we will use the modified equation:

$$q_{\text{ult}} = cN_c(1 + d'_c - i'_c) + \bar{q}N_q d_q i_q$$

Here $N_c = 5.14$ and $N_q = 1.0$ from Table 4-4. Compute factors as follows ($c_a = 84.0$ kPa);

$$d'_c = \frac{0.4D}{B} = \frac{0.4 \times 1.22}{1.98} = 0.246$$

$$i'_c = 0.5 - 0.5\sqrt{1 - \frac{H}{c_a A_f}} = 0.5 - 0.5\sqrt{1 - \frac{44.3}{84.0(1.98 - 2(0.29))(1)}} = 0.105$$

(unit width ↗)

For $\phi = 0°$, $d_q = i_q = 1.0$. Substituting, we find

$$q_{\text{ult}} = 120(5.14)(1.000 + 0.246 - 0.105) + 17.30(1.22)(1)(1)$$
$$= 724.9\ \text{kPa}$$

For a cohesive soil using SF = 3.0 gives the allowable soil pressure as

$$q_a = 724.9/3.0 = 241.6 \rightarrow \mathbf{225}\ \text{kPa}$$

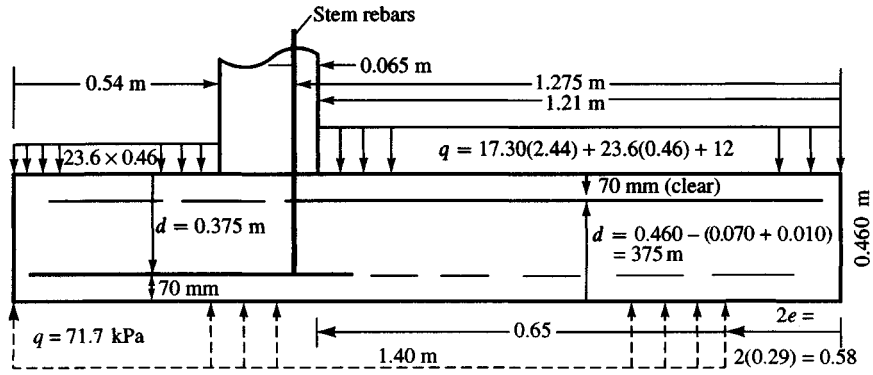

Figure E12-6*c*

The actual soil pressure is

$$q = \frac{V}{B' \times 1.0} = \frac{100.32}{1.4 \times 1.0} = 71.7 \text{ kPa} \ll 225$$

This wall design is now substantially completed.

Step 5. Find the reinforcing needed for the toe and heel. For this refer to Fig. E12-6*c*.

For the *toe* (neglect backfill soil over the toe as being conservative) the net soil pressure is

$$q_{\text{net}} = 71.7 - 0.46(23.6) = 60.8 \text{ kPa}$$

The shear force at the stem face (toe distance = 0.54 m) is

$$V_{\text{toe}} = 60.8(0.54) = \mathbf{32.8} \text{ kN}$$

Thus, we estimate $d = D_c - 70 - \text{No. 30 bar}/2 = 460 - 70 - 30/2 = 375$ mm. Also, we have

$$b = 1.0 \text{ m} \qquad f_c = 417 \text{ kPa}$$

$$V_c = f_c d b = 417(0.375)(1.0) = 156.4 \text{ kN} \gg 32.5 \qquad \text{(OK)}$$

The toe bending moment is

$$M_t = V_{\text{toe}} \times \text{Toe}/2$$
$$= 32.8(0.54/2) = 8.86 \text{ kN} \cdot \text{m/m}$$

The maximum toe bending moment, based on concrete strength f_c and depth d, is

$$M_{\max} = f_c b \frac{(kd)}{2} jd = 9450(1.0)\frac{(0.36 \times 0.375)}{2}(0.880 \times 0.375) = 210.5 \text{ kN} \cdot \text{m/m}$$

The base depth d is more than adequate ($210.5 \gg 8.86$), now find the required amount of steel area for balanced design:

$$A_s f_s jd = M_t$$

$$A_s = \frac{M_t}{f_s jd} = \frac{8.86}{170\,000 \times 0.880 \times 0.375} = 0.000\,1579 \text{ m}^2/\text{m}$$
$$= 158 \text{ mm}^2/\text{m}$$

$$A_s' = 1.33(158) = 211 \text{ mm}^2/\text{m} \qquad \text{(Code } \tfrac{1}{3} \text{ increase)}$$

$$A_f' = \frac{1.4}{f_y} A_g = 0.0035(1000 \times 460) = 1610 \text{ mm}^2/\text{m}$$

$$A_{s,\text{TS}} = 0.0018(1000 \times 460) = 828 \text{ mm}^2/\text{m} \qquad \text{(T and S)}$$

Which steel area do we use? Both the ACI and AASHTO have these requirements. Since 211 mm^2/m is 1.33×158, we can use that instead of the minimum flexural requirement of $1.4/f_y$. The slab is far enough in the ground that the T and S requirement is not needed. We will examine the possibility of using one No. 20 bar giving

$$A_s = \mathbf{300}\ mm^2/m > 211$$

on a spacing of 500 mm (less than 3 × base slab thickness) per ACI Art. 7.6.5. Since this is not a balanced design, check steel and concrete stresses.

Summing moments about the neutral axis of Fig. 12-22*a*, we obtain

$$kd \cdot \frac{kd}{2} \cdot 1 = nA_s(d - kd)$$

$$n = 10 \qquad A_s = 300\ mm^2 = 0.0003\ m^2 \qquad d = 0.375m$$

Substituting we find:

$$\frac{(kd)^2}{2} = 10 \times 0.0003(0.375 - kd)$$

$$kd = 0.044\,53\ m \qquad jd = d - kd/3 = 0.360\ m$$

$$Tjd = M \rightarrow A_s f_s jd = M$$

Solving for f_s, we find

$$f_s = \frac{8.86}{0.0003 \times 0.360 \times 1000} = \mathbf{82.04}\ MPa$$

$$T = A_s f_s = 0.0003(82.04) = 0.024\,61\ MN$$

Now $C = f_c kd/2 = T$, which leads to

$$f_c = \frac{2 \times 0.024\,61}{0.044\,53} = 1.1\ MPa < 0.45\sqrt{21} = 2.06$$

If we were selecting bars, we would use

$$1\ \text{No. 20 bar, giving } A_s = 300 = 300\ mm^2/m > 211$$

We could also use one No. 15 = 200 and one No. 10 = 100 for 300 mm^2, but this choice mixes bar sizes and is not desirable.

We could, of course, use any A_s between 211 and 828 mm^2/m and be in code compliance—but the closer to 211 mm^2 the closer to balanced design. Welded wire fabric should definitely be a contractor option, as it may give the most economical steel mass and labor costs.

For the **heel** there is a rectangular pressure block of $q = 71.7$ kPa on part of the base. There is a vertical downward pressure from backfill, surcharge, and base of

$$q_{down} = 17.30 \times 2.44 + 12.0 + 23.6(0.46) = \mathbf{65.1}\ kPa$$

Shear at the stem back face (from toe computations the allowable shear force = 156.4 kN) is

$$V_{s,b} = 1.21 \times 65.1 - 0.65 \times 71.7 = \mathbf{32.17}\ kN\downarrow \ll 156.4\ kN$$

The moment at the approximate center of the stem steel is

$$M_h = 65.1(1.21)(1.21/2 + 0.065) - 71.7(0.65 + 0.065)^2/2$$

$$= 52.78 - 18.33 = \mathbf{34.45}\ kN \cdot m/m$$

$$A_s = \frac{M}{f_s jd} = \frac{34.45}{170\,000 \times 0.880 \times 0.375} = 0.000\,614\ m^2/m \rightarrow \mathbf{623}\ mm^2/m$$

From the just-completed toe computations we know that increasing this value by one-third will control (but not quite a balanced design) so

$$A_s' = 1.33(623) = \mathbf{828.6}\ \text{mm}^2/\text{m}$$

We could use three No. 20 bars, giving $3(300) = 900 > 828$.
Let us summarize the base slab:

$A_{s,\text{toe}} = \mathbf{300}\ \text{mm}^2/\text{m}$
$A_{s,\text{heel}} = \mathbf{900}\ \text{mm}^2/\text{m}$
Depth is adequate for shear.
No T and S reinforcement for base slab.

If we use the No. 20 rebars and cut part of them, the lengths (the stem has a thickness of 230 mm) are as follows:

Toe: $540 - 70 + 12(20) = 710$ mm (0.71 m)
Heel: $1210 - 70 + 12(20) = 1380$ mm (1.38 m)

Since the base is 1.98 m and with clear cover full-length bars $= 1980 - 2(70) = 1840$ mm (1.84 m), it may not be worth the effort to cut the heel bars.

Step 6. Make the final design sketch of Fig. E12-6*d* to summarize the design. *Note*: We should not select reinforcing bars at this point since any reasonable selection (presented here) is substantially in excess of that required. Welded wire fabric may provide a suitable alternative that does not provide excessive amounts of extra steel.

////

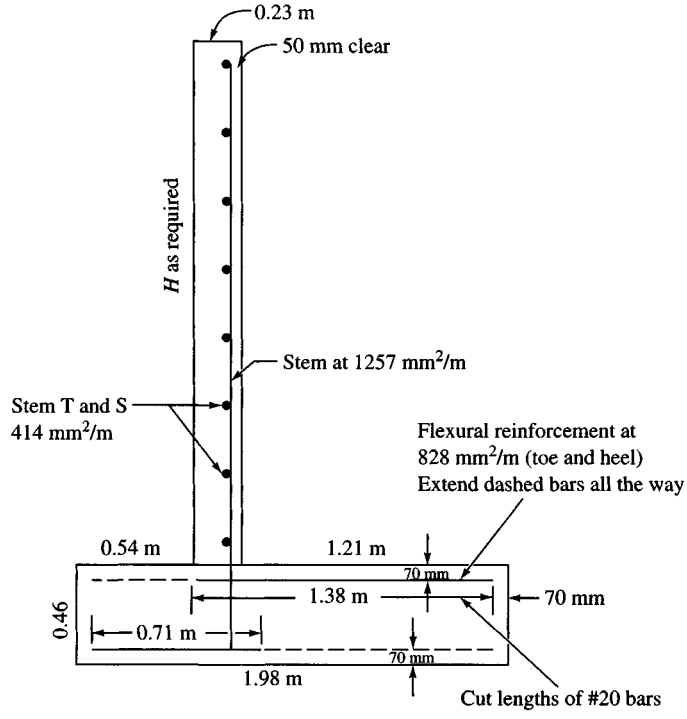

Figure E12-6*d*

PROBLEMS

12-1. Why is L_e a constant in Example 12-1?

12-2. Redo Example 12-1 if $\phi = 32°$, $\gamma = 17.8$ kN/m^3, and friction angle δ between strip and soil $= 20°$.

12-3. Redo Example 12-1 if the unit weight of the backfill is $\gamma = 16.95$ kN/m^3.

12-4. Use your program SMBLP1 and plot a complete pressure profile for Example 12-2. Use this profile to find the largest possible tension force for the reinforcement. If this T_i is below 1.5 m from surface, neglect the additional vertical pressure from the surcharge and find the required strip length L_e and total strip length L_o. For any needed data refer to Example 12-2.

12-5. Verify the required fabric lengths for strips 4 and 5 of Example 12-3.

12-6. Verify that the required fabric length for the base of 3.0 m is correct for Example 12-3 using SF = 2.0.

12-7. What is the required fabric length for Example 12-3 if the base cohesion is 18.0 kPa? What effective soil-to-fabric friction angle is required in this case to keep the required fabric length $L_e = 3.0$ m?

12-8. Verify the location of the vertical forces on the base of Example 12-4. Is the horizontal pressure and its point of application $\bar{y}$ correct?

12-9. What are the four values of N_s for Example 12-5 when using passive resistance in front of the wall P_p, and which value do you think is correct? Why?

12-10. If we use a Load Factor LF = 1.8 and USD, are the stem, toe, and heel d of Example 12-6 adequate?

12-11. Redo Example 12-6 if the stem $H = 3.05$ m and all other data and trial dimensions are the same. Use passive resistance P_p for a depth of 1.22 m in front of the wall.

12-12. If you have a computer program, check Example 12-3 for other circle centers to search for a minimum SF. You should use the listed trial centers as a guide. Do not obtain a minimum SF in the upper base soil and state why.

12-13. Revise Example 12-6 to use the minimum thickness base and stem and see if the revised values produce justifiable savings over using the values in the example.

12-14. Compute the approximate required volume (m^3) of granular backfill required in Example 12-6 assuming that site soil will be used to fill over the toe.

12-15. For the assigned retaining wall problems listed in Table P12-15 and referring to Fig. P12-15, analyze the following as assigned:

a. Draw shear and moment diagrams for the stem and compute the required stem thickness and obtain the amount of reinforcing steel A_s/unit width. Note there is a limited backfill space.

b. Analyze the wall for overturning and sliding stability and bearing capacity.

c. Find the toe and heel shears and moments for base depth and rebars. Also find the required steel area/unit width.

TABLE P12-15

Problem	H	γ_1	ϕ_1	$\beta°$	D
a	2.50 m	17.30 kN/m^3	32°	10°	1.2 m
b	3.00 m	18.00	34	10	1.2
c	3.25 m	18.00	34	0	1.2
d*	3.25 m	16.80	36	0	1.4
e†	10.0 ft	112.0 lb/ft^3	34	0	3.5 ft

*Use backfill surcharge $q_s = 40$ kPa.

†Use backfill surcharge $q_s = 0.5$ ksf.

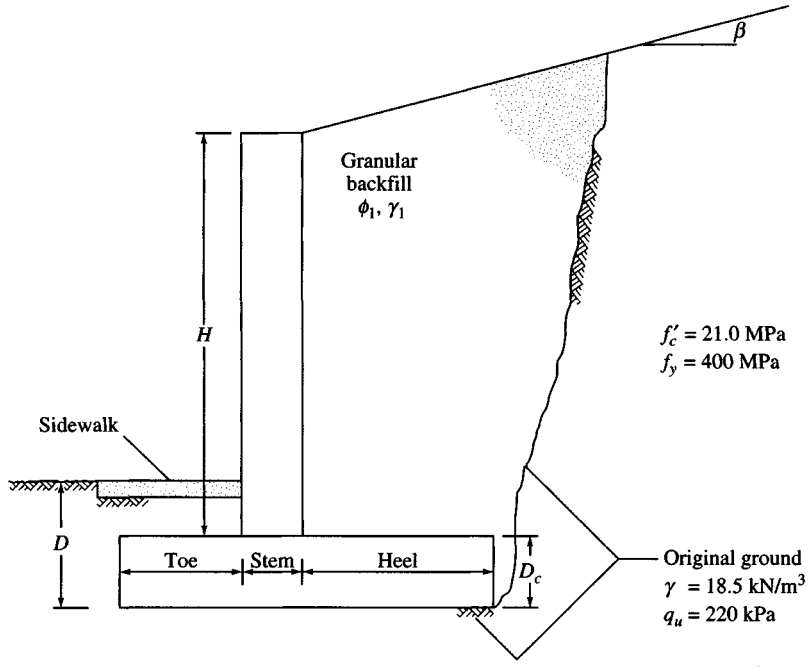

Figure P12-15

CHAPTER 13

SHEET-PILE WALLS: CANTILEVERED AND ANCHORED

13-1 INTRODUCTION

Sheet-pile walls are widely used for both large and small waterfront structures, ranging from small pleasure-boat launching facilities to large dock structures where ocean-going ships can take on or unload cargo. A pier jutting into the harbor, consisting of two rows of sheetpiling to create a space between that is filled with earth and paved, is a common construction.

Sheetpiling is also used for beach erosion protection; for stabilizing ground slopes, particularly for roads (instead of using the walls of Chap. 12); for shoring walls of trenches and other excavations; and for cofferdams. When the wall is under about 3 m in height it is often cantilevered (Fig. 13-1*a*); however, for larger wall heights it is usually anchored using one or more anchors. The resulting wall is termed an *anchored sheet-pile wall* or *anchored bulkhead*. Several of the more common wall configurations are illustrated in Fig. 13-1. The alternative shown in Fig. 13-1*d* of using continuous rods for parallel sheet-pile walls may be considerably more economical than driving pile anchorages—even for tie rod lengths of 30 to 40 m.

There are several methods of analyzing cantilever and anchored sheet-pile walls. Two of the early methods were (*a*) the *free-earth* support and the (*b*) *fixed-earth* support, as shown in Fig. 13-2 along with the simplified assumptions of active (from filled side) and passive pressure on the free side below the dredge line. The design was based primarily on taking moments about the anchor rod, increasing the depth of embedment D until $\sum F_h$ was satisfied, and then computing the resulting bending moments in the piling. A safety factor was incorporated by using a reduced K_p for passive pressure or by increasing the embedment depth D some arbitrary amount such as 20 or 30 percent. Two of the simplifications could result in errors:

1. Unless the anchor rod elongates sufficiently, the active pressure may not fully develop, resulting in a computed anchor rod force that is too small.

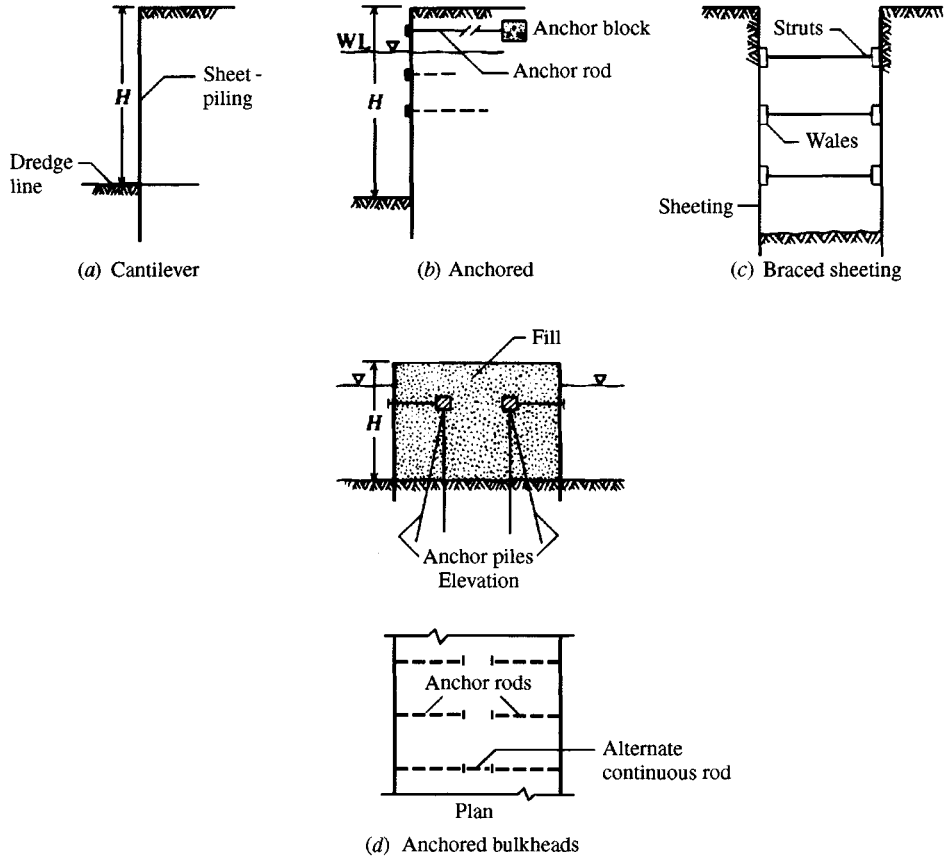

Figure 13-1 Sheet-pile structures.

2. The center of pressure below the dredge line is qualitatively shown by the dashed lines of Fig. 13-2*c* and *d* and is closer to the dredge line than assumed using the passive pressure profiles shown. The erroneous location of the center of pressure usually results in moments that are too large.

Cantilever sheet-pile walls were analyzed similarly to anchored walls, except the soil pressure profiles were slightly different and moments were usually taken about the base since there was no anchor rod.

These were the only methods used in the United States and elsewhere until the mid-1960s when Haliburton (1968) described a finite-difference method he and his coworkers had developed. Bowles (1974*a*, and included in the second and later editions of this textbook) used the finite-element method (FEM) for sheet-pile wall analysis. As of this edition the *free-* and *fixed-earth* support methods will no longer be presented.[1] Although these two methods were widely used, so many of the author's FEM programs are available (worldwide) and use of personal computers is so widespread their continued inclusion is no longer warranted.

[1]The reader can still access them in the first through fourth editions of this text.

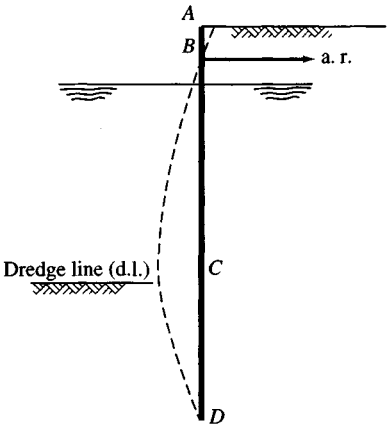

(*a*) Free-earth support deflection line (qualitative).

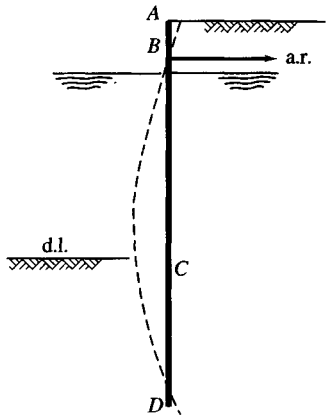

(*b*) Fixed-earth support deflection line (qualitative).

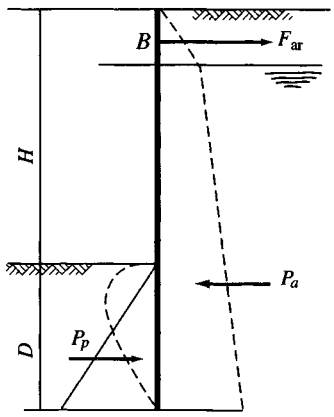

All cohesionless

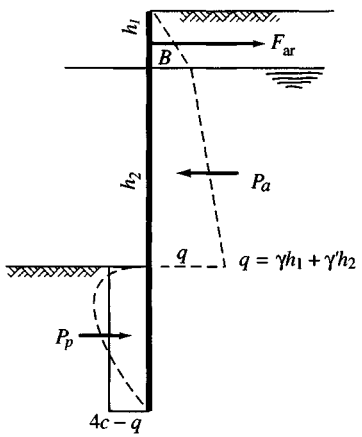

Cohesive below d.l.

(*c*) Assumed and probable (dashed) soil resistance and active earth pressure profile for "*free-earth*" support method.

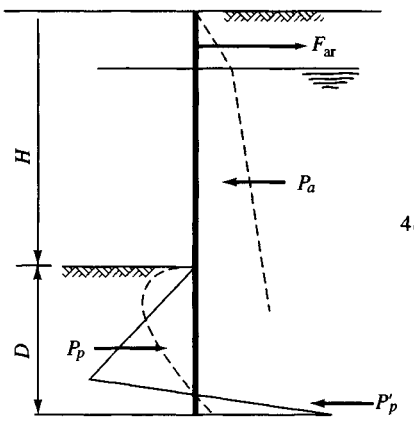

All cohesionless

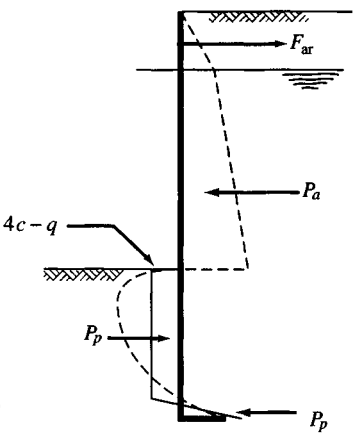

Cohesive below d.l.

(*d*) Assumed and probable (dashed) soil resistance and active earth pressure profile for "*fixed earth*" support method.

Figure 13-2 General assumptions and earth pressure profiles for anchored walls. Essential difference between anchored and cantilevered walls is there is no anchor rod in the cantilever wall design. Active and passive pressure profiles are similar (but not exactly same).

There is no "exact" method to analyze/design a sheet-pile type of wall. Both field observations and laboratory model tests show that there is a complex interaction of (as a minimum) construction method (install and backfill, or install and excavate the free side), excavation depth, stiffness of wall material, type and state of retained soil, and passive pressure resistance. With anchored walls there is also the anchor geometry, initial anchor prestress (or load), construction stage when anchor rod is installed, and behavior of that part of the wall above the anchor rod (into or away from the backfill).

The two original methods named were oversimplifications of an extremely complex problem, relied totally on rigid body statics, and were based entirely on the assumptions of an active earth pressure above the dredge line and passive earth pressure below. Wall and anchor rod stiffness did not enter into the equation. As a result of substantial overdesign, few walls failed.

The FEM is somewhat less of an approximation. Additionally, it allows for better modeling of the problem and gives more useful design information as part of the output. It requires a computer program, but this is provided as program B-9 (FADSPABW) on your computer diskette. Section 13-6 will present considerable detail on this method so it can be used in design with reasonable confidence.

The finite-difference method (FDM) is not considered further because it offers no advantage over the FEM and is more difficult to use. Indeed, it has these disadvantages: Constant-length elements are required over the full pile length; the stiffness matrix cannot be banded; and modeling boundary conditions of zero displacement and rotation is difficult.

The several materials and material configurations used for sheet piles will be given in Sec. 13-2 since they are used for walls in both this and the next two chapters.

13-2 TYPES AND MATERIALS USED FOR SHEETPILING

Sheetpiling materials may be of timber, reinforced concrete, or steel. Allowable design stresses are often higher than in general building construction and may be from about 0.65 to $0.90 f_y$ for steel[2] and wood. Reinforced concrete design stresses may be on the order of $0.75 f_c'$ for unfactored loads. The design stress actually used will depend on engineering judgment, effect of wall failure (site importance factor), and the local building code.

13-2.1 Timber Sheetpiling

Timber piling is sometimes used for free-standing walls of $H < 3$ m (see Fig. 13-1*a*). It is more often used for temporarily braced sheeting to prevent trench cave-ins (see Fig. 13-1*c*) during installation of deep water and sewer lines. If timber sheeting is used in permanent structures above water level, preservative treatment is necessary, and even so the useful life is seldom over 10 to 15 years. At present timber is little used except in temporary retaining structures owing to both the scarcity of timber—particularly of large cross section—and cost.

Several timber piling shapes are shown in Fig. 13-3, of which the Wakefield and **V** groove piling have been and are the most used. Dimensions shown are approximate and you will have to use what is currently available.

[2]Value recommended by Bethlehem Steel Corporation, the principal producer of rolled sheetpiling in the United States at present.

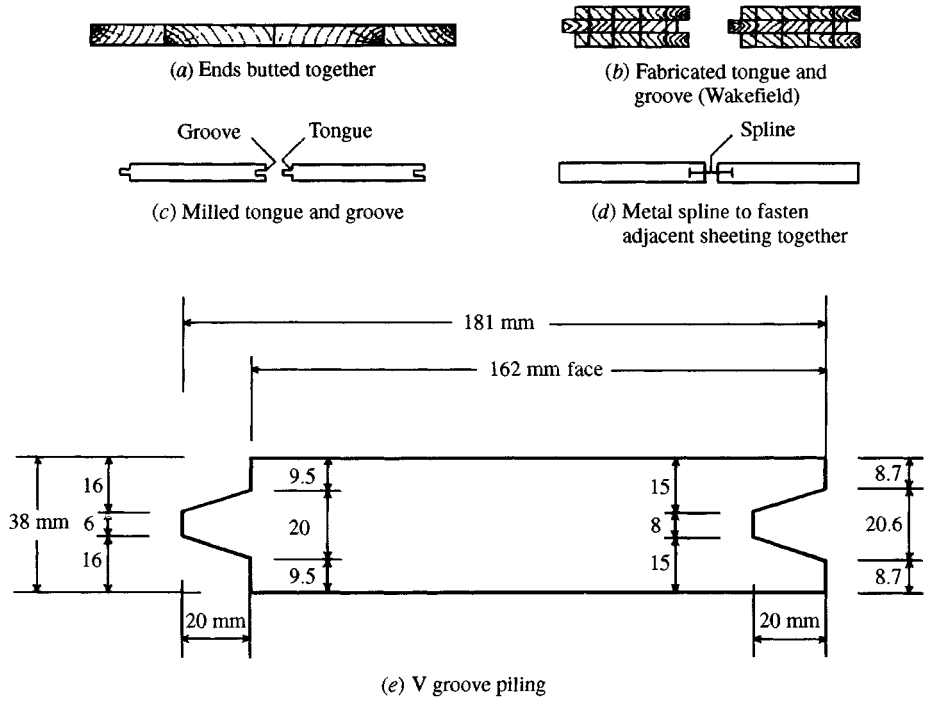

Figure 13-3 Wood sheet piles.

It is common to see low timber walls treated with wood preservative in use along waterfronts. A substantial amount of timber piling—mostly fast-growing pine—is still used for protection where the piling is driven, then surrounded with stabilizing blocks or boulders (termed *groins*) to catch sand from the ocean side to maintain beaches. Here the intent is for the wall eventually to become covered with sand from tidal action. Strength is not the primary concern for this use, so if the wood lasts long enough to become buried, the purpose of the wall has been accomplished.

If wood sheetpiling is being considered, the soil type is a major factor. Almost any driving requires interfacing the pile hammer with a driving cap over the timber to minimize top damage. Driving in hard or gravelly soil tends to damage or even split the pile tip. Damage can sometimes be avoided by driving and pulling a steel mandrel or the like or by using a water jet to create a "predrilled" hole to reduce the driving resistance. The sheeting may be pointed, generally as shown in Fig. 13-4, and placed so that the pile being driven tends to wedge against the previously driven pile.

13-2.2 Reinforced Concrete Sheetpiling

These sheet piles are precast concrete members, usually with a tongue-and-groove joint. Even though their cross section is considerably dated (see Fig. 13-4), this form is still used. They are designed for service stresses, but because of their mass, both handling and driving stresses must also be taken into account. The points are usually cast with a bevel, which tends to wedge the pile being driven against the previously driven pile.

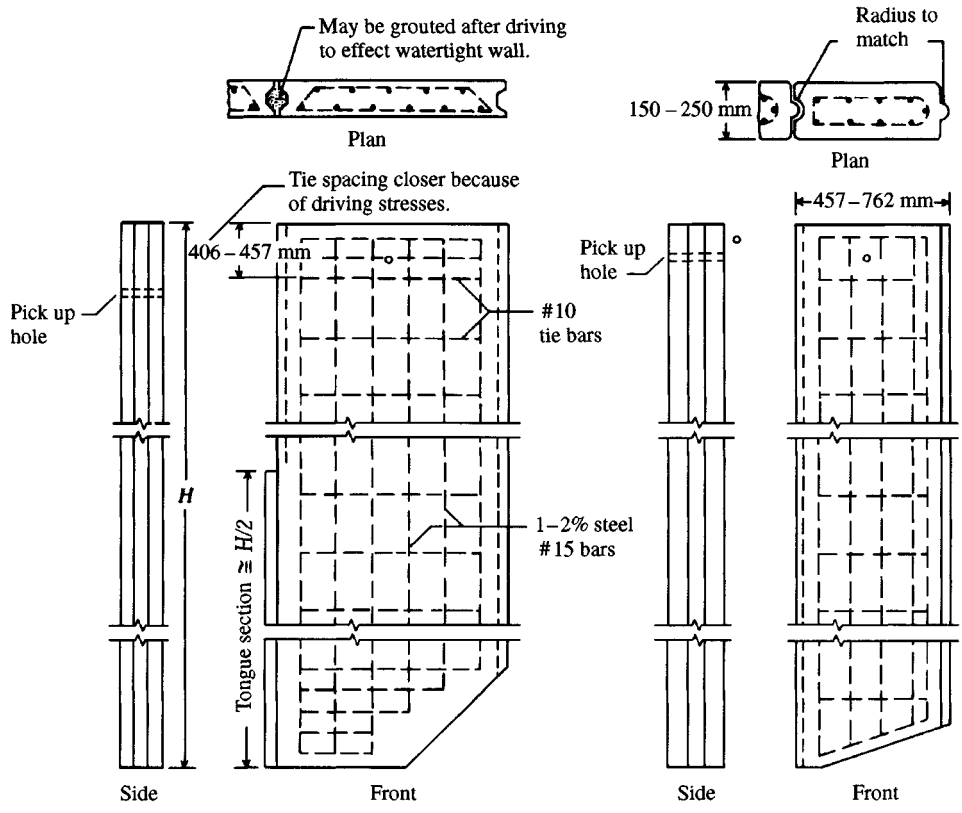

Figure 13-4 Typical details of reinforced concrete sheet piles. [*After PCA (1951).*]

The typical dimensions[3] shown in Fig. 13-4 indicate the piles are relatively bulky. During driving they will displace a large volume of soil for an increase in driving resistance. The relatively large sizes, coupled with the high unit weight (γ_c = 23.6 kN/m^3) of concrete, mean that the piles are quite heavy and may not be competitive with other pile types unless they are produced near the job site.

Dimensions and reinforcing bars shown in Fig. 13-4 are typical, but currently produced piles will contain bars that are available to the producer at casting time.

If the joints are cleaned and grouted after they have been driven, a reasonably watertight wall may be obtained. However, if the wall is grouted, expansion joints may be required along the wall at intervals that are multiples of the section width.

13-2.3 Steel Sheetpiling

Steel sheetpiling is the most common type used for walls because of several advantages over other materials:

[3]Soft-converted since only Fps units were used by U.S. industry in 1951.

1. It is resistant to the high driving stresses developed in hard or rocky material.
2. It is relatively lightweight.
3. It may be reused several times.
4. It has a long service life either above or below water if it is provided with modest protection according to NBS (1962), which summarizes data on a number of piles inspected after lengthy service. Watkins (1969) provides some guidance for considering corrosion of sheetpiling in sea water. There is no available information on corrosion of steel piling in chemically contaminated soil. There is a resistance probe [see Roy and Ramaswamy (1983)] utilizing a set of electrodes, one of which is magnesium and the other is steel, that can measure the resistance of the soil between them. The soil resistance is related to the amount (in terms of "high" or "low" amount/likelihood) of expected steel pile corrosion.
5. It is easy to increase the pile length by either welding or bolting. If the full design length cannot be driven, it is easy to cut the excess length using a cutting torch.
6. Joints are less apt to deform when wedged full with soil and small stones during driving.
7. A nearly impervious wall can be constructed by driving the sheeting with a removable plug in the open thumb-and-finger joint. The plug is pulled after the pile is driven, and the resulting cavity is filled with a plastic sealer. The next pile section is then driven with the intersecting thumb or ball socket displacing part of the plastic sealer from the prefilled cavity. When the piling is driven in pairs, sealing the intermediate joint by prefilling may not provide a 100 percent impervious joint. Sellmeijer et al. (1995) describe an experimental wall project using this general approach but with European-produced piling, which has a slightly different joint configuration than the standard "thumb-and-finger" or "ball-and-socket" interlocks of piling produced in the United States (see Fig. 13-5).

Figure 13-5 illustrates several angle sections and joints that can be fabricated from cut pieces of sheetpiling; these are for illustration, as other joints can be produced. The crosses and wyes shown are used in cellular cofferdams (of Chap. 15); the angles and bends are used for direction changes in the wall.

Several steel sheet-pile cross sections currently available are given in Tables A-3*a* and A-3*b* in the Appendix. The straight-web sections are used in situations where the web is in tension; the **Z** sections are used where large bending moments require a substantial moment of inertia or section modulus.

When the stiffness capacity of the available **Z** piles is insufficient, the box sections of Table A-3 (also as Fig. 13-6*a*) or the soldier-**Z**-pile combination of Fig. 13-6*b* might be used.

13-2.4 Composite Sheet-Pile Walls

Walls may be constructed using composite construction. The soldier beam–wood lagging combination of Chap. 14 (Fig. 14-1*a*) is an example.

Other examples include use of soldier beams[4] on some spacing with sheetpiling used between the spacings. For corrosion protection one might encase the upper part of steel sheetpiling in concrete after it is driven, with the concrete extending from below the water line

[4]Rolled pile or structural sections with a moment of inertia I_p that is several times the moment of inertia I_{sp} of the sheetpiling ($I_p \gg I_{sp}$).

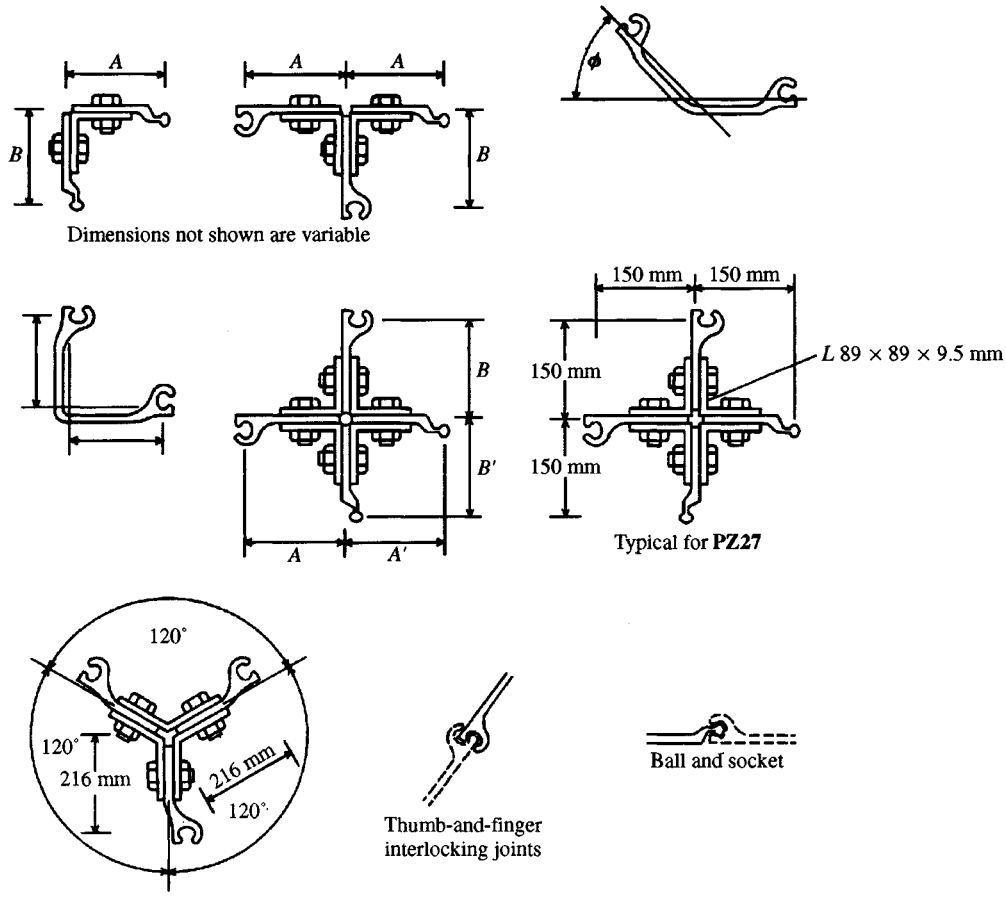

Figure 13-5 Typical fabricated or rolled sheet-pile joints. All dimensions shown are millimeters. Bolts are high-strength 22-mm diameter on 150-mm centers except at end 610-mm where they are on 75-mm centers.

to the pile top. A wood facing might also be used, or the lower part of the sheeting could be made of steel and the upper part of a different material—wood or concrete.

Since steel is relatively durable in most waterfront installations, the principal composite construction consists in using a mix of soldier beams and sheet piles or built-up box pile sections.

13-3 SOIL PROPERTIES FOR SHEET-PILE WALLS

Referring to Fig. 13-2, we see that lateral earth pressures are involved with active pressures approximately developed behind the walls from the fill (or backfill) and passive pressures in front of the wall below the dredge line. Either the Rankine or Coulomb lateral earth-pressure coefficients may be used for the earth pressures, however, the Coulomb values are generally preferred. Because a sheet-pile wall is not very rigid, relatively large lateral displacements (and resulting relative movement between soil and wall) often occur between points of assumed fixity. Relative soil-wall movement produces adhesion and/or friction depending upon

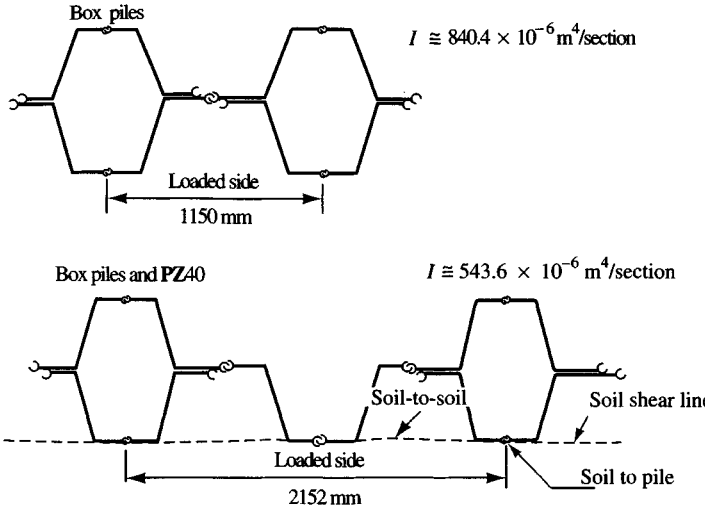

(*a*) Bethlehem Steel sections.

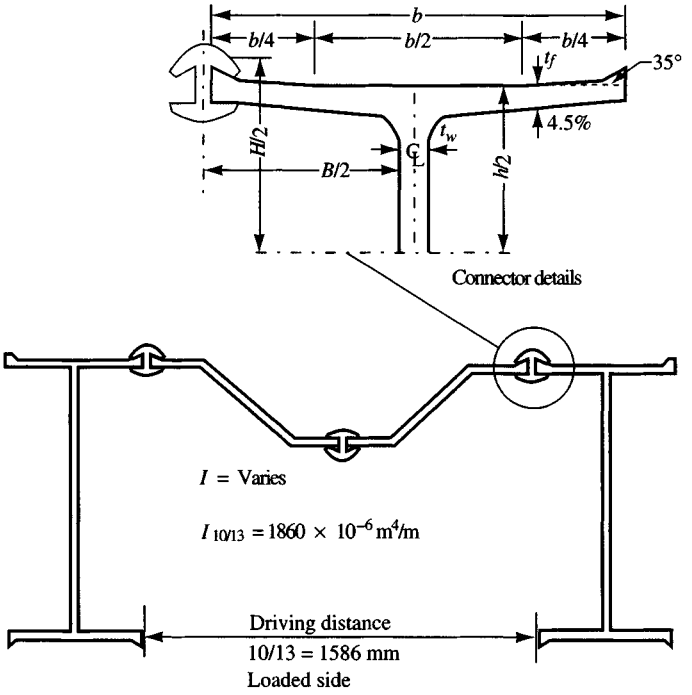

(*b*) Arbed steel (European) sections using special pile sections with upset edges and special connector.

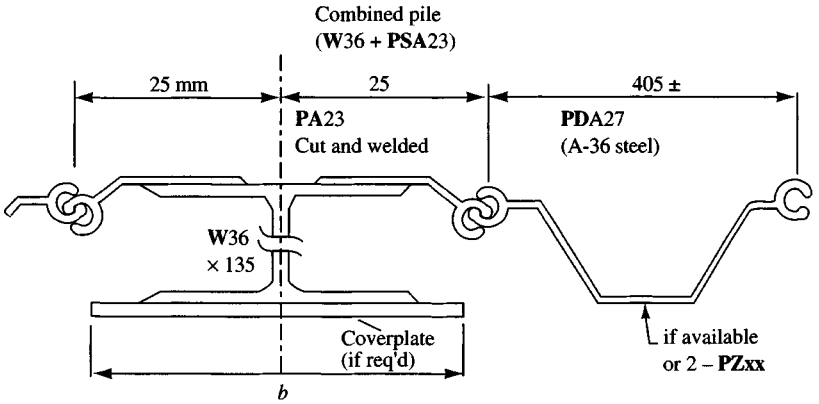

(*c*) Locally fabricated pile section. Any **W** section can be used. [From Munfakh (1990).]

Figure 13-6 Built-up pile sections used where standard rolled shapes do not have adequate bending stiffness. The Bethlehem Steel Corporation box sections of (*a*) and the Arbed sections of (*b*) can be obtained directly from the producers. The section shown in (*c*) can be fabricated locally to meet the required bending stiffness. The principal precaution in fabricating this section is that the interlocks be compatible.

the soil. Friction can be approximately accounted for by use of the Coulomb earth-pressure coefficient. If the backfill is cohesive, you have to do the best you can. You might use Fig. 11-11*c* and Example 11-4 as a guide with a Coulomb K_a. You might also consider programming Eq. (11-12) to give reduced values to account for cohesion. In this latter case obtain the lateral pressure as

$$\sigma_h = \gamma z K_{a,\phi} + c K_{a,c}$$

For passive pressure use the $K_{p,i}$-coefficients.

Any backfill cohesion would appear to reduce the lateral pressure; however, give consideration to a wall-soil tension crack, which would produce a surcharge effect on the soil below the tension crack depth and negate most of its beneficial effect.

Even though it is known that wall friction develops, the Rankine earth-pressure coefficients are often used for K_a, with the rationale being that they are slightly more conservative.

For the finite-element procedure it is necessary to use active earth-pressure coefficients behind the wall and the concept of the modulus of subgrade reaction k_s for the soil below the dredge line. The use of k_s allows one to model the dredge line soil as a series of nodal springs on the wall to assist in resisting lateral displacement.

From this discussion it is evident that we need soil parameters of γ, ϕ, and *cohesion* for both the wall backfill and the base soil. Because the wall must survive the initial loading as well as long-term loading, the undrained strength parameters are usually used. In the case of waterfront structures the soil below the water line will always be in an undrained state, but close to the wall a small zone may be in a consolidated undrained state. For on-shore retaining structures the dredge line soil is exposed to the weather and the state varies from saturated to dry. Since the undrained state is usually the worst case, it is appropriate to use that for design.

Seldom are laboratory tests performed to obtain these parameters. It is common to use CPT or SPT data and/or simply estimate ϕ and γ. The retained material is often backfill with little to no compaction; if it is hydraulically dredged silty sand, precise soil parameters are extremely difficult to obtain. The base soil into which the sheet pile is driven is more amenable to laboratory tests on recovered samples. However, in nearly all cases either SPT or CPT data are all that are taken. When one is using the SPT in cohesive soil, field q_u tests are routinely performed on recovered (but highly disturbed) samples. In this case the values for $s_u = c = q_u/2$ are obtained for cohesive soils, and the SPT or CPT data are converted to an estimate of ϕ and γ for cohesionless soils using correlations such as those given in Chap. 3. The unit weight of cohesive soils can be obtained using the procedure of Example 2-1. For loose sand backfill a γ of 12.5 to 14 kN/m^3 (80–90 pcf) might be used, but exercise care in using these values, for sand in this state may consolidate over time and produce a great increase in the lateral pressure/force.

If the equipment is available, one should perform laboratory tests of the direct shear or direct simple shear type to obtain an approximation of the plane strain ϕ angle. In most cases, as previously stated, the angle of internal friction is simply "estimated" with conservative values in the range of 28 to 32° commonly used; any testing is likely to be isotropically consolidated compression (CIUC) triaxial tests.

13-3.1 Drained Conditions

When the dredge line soil is cohesive and **not submerged**, particularly if some soil is excavated to produce the dredge line, one should use both undrained (total stress) and drained

(effective stress) strength conditions for the dredge line s_u. Cohesive soil under long-term loading tends to a drained state above the water table.

When soil is excavated to produce the dredge line, unloading occurs. For cohesive soil above the GWT this produces an initial increase in s_u as a result of negative pore pressures, but over time the suction disappears and a drained state may develop (or alternate between a total and drained state with rainfall). Figure 2-28*b* indicates that there can be a substantial decrease in shear strength in transition from the total to an effective stress state.

For **submerged** cohesive soil below the dredge line, excavation also produces soil suction, but with water available the water content slightly increases with a resulting loss in strength s_u. In this case one should use consolidated-undrained tests, which give both a small total stress ϕ and cohesion c. Below the water surface the soil consolidates under lateral pressure to a consolidated-undrained state. This might be approximated in a laboratory shear test by consolidating a sample to in situ pressure in the presence of water, then unloading it to represent the final overburden state with the water available to allow an increase in water content. When one believes enough time has passed (several days) to allow for stabilization one should perform the test without allowing drainage.

Daniel and Olson (1982) thought the use of total instead of effective strength parameters caused a major bulkhead failure. In this case one can question the conclusion that not using drained strength parameters caused the failure. Here the dredge line soil was permanently below the water table, where all that could develop is a consolidated undrained state. The dredging that took place in front of this wall after it was constructed produced a sloping dredge line. One can speculate that unloading the soil of overburden produced some expansion and an increase in water content from *suction,* causing a strength reduction. This wall was constructed in the late 1970s, and the designer used the classical method of analysis. Thus, not a great deal of design information would have been obtained to provide guidance in the design compared with using the FEM. Although Daniel and Olson (1982) also stated that there was no way to ascertain exactly what caused the wall failure, their description of the bulging (lateral wall deformation away from the backfill) before failure makes it evident that there was an increase in lateral pressure in the backfill. This may have been accompanied by some loss of dredge line soil strength (or carrying capacity) as a result of sloping the dredge line and/or soil suction.

13-3.2 Angle of Wall Friction δ

The angle of wall friction δ can be estimated from Table 11-6 or directly measured for important projects. Any direct measurements between the soil and wall material should use a pressure that is on the order of what is expected in the prototype, since δ is somewhat pressure-dependent. If $\phi < \delta$, you assume a frictionless interface (but there may be adhesion, since a $\phi < \delta$ soil would have cohesion).

For metal sheetpiling of **Z** and deep web shapes, the unit width of wall will include a minimum slip zone, part of which is soil-to-soil and part soil-to-steel as in Fig. 13-5*a*. In this case one can use an average (or weighted average) value for δ as

$$\tan \delta' = \frac{\tan \delta + \tan \phi}{2} \qquad \text{(weighting factors not included)}$$

where ϕ = angle of internal friction of contact soil and δ = the friction angle from Table 11-6 or measured in a laboratory test.

13-3.3 Modulus of Subgrade Reaction, k_s

The finite-element method uses k_s in the passive pressure region below the dredge line in front of the wall. The author has shown [Bowles (1974*a*)] that this model is reasonably correct by using it to analyze full-scale field walls and to reanalyze large model sheet-pile walls reported by Tschebotarioff (1949) and small models used by Rowe (1952). Estimates of k_s can be made using the procedures given in Sec. 9-6; however, we need the equation given there that has a depth parameter Z as

$$k_s = A_s + B_s Z^n \tag{9-10}$$

Alternative equation forms (which are in your computer program B-9) are

$$k_s = A_s + B_s \tan^{-1}(Z/D)$$
$$k_s = A_s + B_s(Z/D)^n$$

with the restriction that the exponent $n > 0$ [cannot be 0 or (−)].

We can approximate these equations by using

$$k_s = C(\text{SF})q_a \qquad \text{or} \qquad k_s = Cq_{\text{ult}}$$

where q_a = bearing capacity computed at several depths in the likely range of pile embedment depth D and $q_a = q_{\text{ult}}/\text{SF}$. The C factor is

$$C = \frac{1}{0.0254 \text{ m}} \quad \text{(SI)}; \qquad \frac{1}{1/12 \text{ ft}} \quad \text{(Fps)}$$

This expression gives $C = 40$ for SI and $C = 12$ for Fps. The safety factor is SF = 3 for cohesive soil and SF = 2 for cohesionless soils. We can then plot the several values of k_s versus depth Z and obtain a best fit for the foregoing equation.

Alternatively one might use one of the bearing-capacity equations from Table 4-1, simplified (no shape, depth, inclination, **base**, or **ground** factors) to read

$$k_s = \frac{q_{\text{ult}}}{\Delta H} = C(cN_c + \bar{q}N_q + 0.5\gamma BN_\gamma)$$

where ΔH = is an *assumed* displacement of 0.0254 m ($\frac{1}{12}$ ft) when the ultimate bearing pressure q_{ult} is developed (and gives $C = 1/0.0254 \cong 40$ or 12). Separating terms, we have the following:

$$\left.\begin{aligned} A_s &= C(cN_c + 0.5\gamma \times 1 \times N_\gamma) \\ B_s Z^n &= C(\gamma N_q Z^1) \end{aligned}\right\} \tag{13-1}$$

The use of 1 in the equation for A_s is for B = unit width of wall. An upper limit can be placed on k_s by using something other than $n = 1$ in Eqs. (13-1) or using one of the previously given alternatives. We do not want k_s to become unreasonably large because driving difficulties generally limit sheet-pile embedment depths D to 5 to 6 m.

Some persons have suggested an upper limit on k_s be the passive pressure. Since there are difficulties with computing σ_p for small ϕ angles one might use computer program WEDGE on your diskette (see also Sec. 13-5) to obtain P_p. Compare this result to the sum of the computed (+) node forces [do not include any (−) values] below the ground line, and if

$$\sum F_{\text{node}} > P_p$$

arbitrarily increase the depth of embedment 0.3 to 0.6 m and make another analysis.

Using the FEM and computer program B-9 allows you to make a parametric study rapidly (vary pile section I, k_s, embedment depth D, anchor rod location, and so on). You will generally find that the preceding suggestions for k_s will give reasonable values for pile bending and node soil pressure. Deflections are highly dependent on the flexural rigidity EI of the pile *and* k_s, so if you want a reliable dredge line value you have to input a carefully chosen k_s. Keep in mind that exact values are not possible, for too many variables are beyond the designer's control. What is desired is enough output data to make a design with reasonable confidence that the wall will serve its intended purpose.

The FEM allows you to consider nonlinear effects using the term $X_{\max}$ identified in Sec. 9-6 and used in Example 13-1 following. A program should do these things (as incorporated into B-9):

1. Allow adjustment of the dredge line springs to account for driving or excavation damage to the soil
2. Remove node springs when the computed $X_i > X_{\max}$ and recycle

13-4 STABILITY NUMBERS FOR SHEET-PILE WALLS

13-4.1 Stability Numbers and Safety Factors

The concept of stability number (or safety factor) for sheet-pile walls is somewhat a misnomer, since it is not clear just what it means. For this discussion it is more convenient to use the term *safety factor* (SF) rather than *stability number*, which implies the ratio of system resistance/system failure effects. In classical sheet-pile wall design it has been common to do one of the following:

1. Divide the Rankine (or Coulomb) K_p by a SF for the soil below the dredge line. Some designers might use K_a larger than the Rankine or Coulomb value as well.
2. Arbitrarily increase the computed embedment depth by some factor, say, 1.2 to 1.3.

The author suggests that a more rational method is needed to estimate probable wall safety. This is done as follows:

1. Do a wall analysis using the existing conditions to find the depth required such that any depth increase does not change the dredge line deflection (at least within some tolerance of, say, 2 to 3 mm). This depth D_1 is all that is required for stability for the given load conditions.
2. Next make trial runs with the depth increased several arbitrary amounts (perhaps 0.5, 1.0, 1.5 m). Make additional analyses and make a table of dredge line displacements versus these depths and the depth from step 1.
3. From an inspection of the table from step 2, choose an arbitrary new depth of embedment D_{new}. Assume a loss of dredge line so the new depth is more than the dredge line loss, or

$$D_{\text{new}} > D_1 + \text{dredge line loss}$$

4. Now revise a copy of the original FEM data set to show the new dredge line location and new depth (compute additional active pressure values that are in the dredge line soil). Because the dredge line loss is probably attributable to erosion, it may not be necessary to reduce k_s of the first one or two nodes for driving or other damage but look at the

conditions. Make the computer analysis with this new data set. Do not recycle for depth, but do a *nonlinear* check.

5. Check this output to see if the bending moment can be carried by the sheet-pile section chosen. If not, increase the section. Also check if the toe node moves forward and how much. A large forward movement represents a soil shear failure and the embedment depth would have to be increased. If you change sheet-pile sections recycle to step 1. If you increase D recycle to step 4.
6. When step 5 is adequate, make another copy of this data set with the dredge line reset to the original location. Now add a backfill surcharge (or increase any existing surcharge) and recompute the active earth-pressure profile. Make the FEM analysis and see whether the section can carry this bending moment—if not, increase the section. Check whether the toe tends to kick out (translate forward). If it does, increase the pile embedment depth. If you change sections recycle to step 1; if you increase the embedment depth recycle to step 2.

When you have obtained satisfactory solutions from steps 3, 4, and 6, you have a suitable design. Now, what is the resulting safety factor? One possibility is that the maximum increase in depth D_{new} from steps 3 and 6 might be divided by the required depth D_1. Probably the best solution is to give the client a compact report showing the pile section and embedment depth and to indicate what loss of dredge line may produce a failure or what the maximum allowable surcharge is. File a copy and the computer printouts in case problems develop later; put the data sets on a diskette.

The finite-element method provides a relatively rapid means to analyze changed field conditions. The classical methods are much less amenable to these types of analyses and thus encourage use of an SF. If you do the analysis as outlined above and compare it to a classical design, you may find that a SF of 1.2 to 1.3 does not provide the required margin of safety for certain changed field conditions, particularly loss of dredge line.

13-4.2 Moment Reduction

From your computer output you will see that the soil node reactions below the dredge line produce a center of pressure that is closer to the dredge line than indicated by the linear Rankine/Coulomb profiles shown on Fig. 13-2*c* and *d*. This center of pressure results in computed moments that are less than those computed from the classical theories but have been confirmed by the small-scale model tests of Rowe (1952, 1957) and the larger-scale model tests of Tschebotarioff (1949). To account for this moment reduction, Rowe introduced the concept of *moment reduction* as a means to reduce moments computed by classical methods so the design would not be overly conservative (at least for bending). It is evident that the FEM directly gives the "reduced" design moment—applying Rowe's moment reduction method is not easy.

13-5 SLOPING DREDGE LINE

In many sheet-pile wall configurations the dredge line is not horizontal ($\beta = 0°$) but rather slopes away from the wall ($\beta < 0°$). How should we treat this situation? There are two cases:

1. The soil below the dredge line is a sand with $\phi > 28$ to 30°.
2. The soil below the dredge line is a cohesive material with a small ϕ angle and cohesion c.

In case 1 we can use the Coulomb equation [Eq. (11-6)] to compute two values of K_p: one for a horizontal dredge line $K_{p,h}$ using $\beta = 0$, the other for a sloping dredge line $K_{p,s}$ using a $(-)$ β. We can use these values to obtain a reduced $k_{s,s}$ for program input as

$$k_{s,s} = k_{s,h}\frac{K_{p,s}}{K_{p,h}} \tag{13-2}$$

where $k_{s,h}$ is your best estimate of a horizontal value that will be reduced to take into account the sloping dredge line.

For case 2 we cannot get a valid K_p from Eq. (11-6), so we will rely on the trial wedge method of Sec. 11-12.1 to obtain passive forces[5] P_p. For this, use program WEDGE on your program diskette. This program is specifically written to obtain the *passive earth force* for either a horizontal or sloping dredge line. It uses the embedment depth D for the "wall" H. We make two trials:

Trial 1: Dredge line horizontal (use only a single line) as in Fig. 13-7*a*, obtain $P_{p,h}$, and
Trial 2: Dredge line sloping as in Fig. 13-7*b* and obtain $P_{p,s}$.

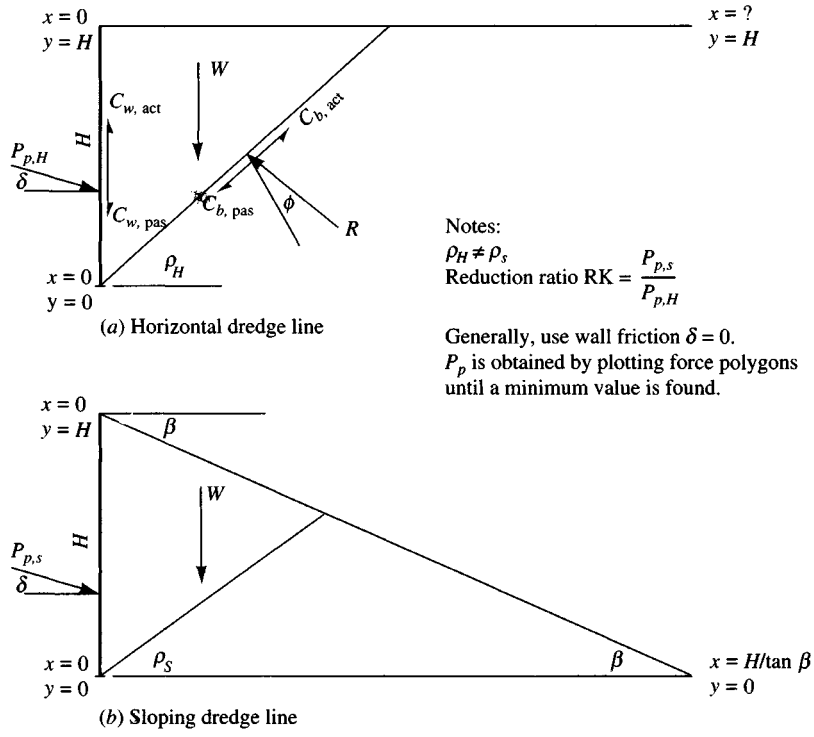

Figure 13-7 The case of sloping dredge line. Use program WEDGE from your diskette and solve both cases to obtain $P_{p,H}$ and $P_{p,s}$. Note coordinates to use. For X = ? use a value of about 4 to 5H.

[5]Terzaghi (1954) indicated that passive earth force is a factor but did not elaborate on how to apply its effect for the sloping dredge line.

Next Page

From these two values we can compute a *reduction factor* (RF) for the several values of k_s below the sloping dredge line using

$$\text{RF} = \frac{P_{p,s}}{P_{p,h}} \qquad \text{and} \qquad k_{s,s} = \text{RF} \times k_{s,h} \tag{13-3}$$

where $k_{s,s}$ = sloping value
$k_{s,h}$ = best estimate of a horizontal value

For this case you must be able to input node values of k_s as a program option (allowed with program B-9).

As outlined in Sec. 13-4.1 you initiate the design of a wall for a sloping dredge line by going through design steps 1 and 2. At this point you make an initial embedment depth selection D_{init}. Now you use that D_{init} and the $k_{s,s}$ and check if D_{init} is adequate. Next check for loss of dredge line and increased surcharge.

When you check the computer output for each of the foregoing cases, you will notice that the moments are larger than for the horizontal ground case. You will also note that the nodal soil reactions will be larger near the dredge line and decrease with depth (this is similar to the horizontal case). There may even be negative values if the embedment depth is larger than needed for this analysis (but you increased it for other reasons).

Nevertheless, we need to check whether the computer program output is a possible solution and this can be determined as follows:

1. Sum by hand the node spring forces (tabulated in a table on the output sheets) and compute the passive force for the sloping dredge line as $P_{p,\text{sdl}}$.

$$P_{p,c} = \sum F_{\text{springs}} \qquad \text{then} \qquad \text{Check } P_{p,\text{sdl}} \geq P_{p,c}$$

   If you have a cohesionless dredge line soil, compute $P_{p,\text{sdl}}$ for use in the preceding as $P_{p,\text{sdl}} = \frac{1}{2}\gamma D^2 K_{p,\text{sdl}}$; if cohesive, use program WEDGE. This check assumes the limiting wall resistance is the passive force for a wall whose height is the embedment depth. The limiting passive force must be larger than that computed in the analysis [the sum of the (+) node reactions].

2. If $P_{p,c} > P_{p,\text{sdl}}$ you initially have three options to try:
   a. Try a larger pile section, because a stiffer section may even out the nodal reactions somewhat.
   b. Increase the embedment depth. [Note: This step will not improve the solution if the bottom soil nodes have (−) reactions.]
   c. Try a lower node location for the anchor rod.

If none of these produces $P_{p,\text{sdl}} \geq P_{p,c}$ consult with the geotechnical engineer who provided the soil data. It may be necessary to build up or modify the dredge line slope or use one of the walls of Chap. 12.

Schroeder and Roumillac (1983) conducted a model wall study in sand that showed that the sloping dredge line case produced less passive resistance than for horizontal ground; however, this result could have been predicted prior to any testing. Their tests showed that as the slope increased, so did the bending moments in the sheet pile. The FEM analysis using the foregoing k_s reductions does precisely that.

13-6 FINITE-ELEMENT ANALYSIS OF SHEET-PILE WALLS

The finite-element method presented in the following material is the most efficient and rational method for the design of sheet-pile wall design/analysis currently available. The same program is applicable for both cantilever (Fig. 13-1*a*) and anchored (Fig. 13-1*b*) walls and, with some adjustment, can be used for the braced walls of Fig. 13-1*c*. It directly gives the lateral displacement profile (valid for that set of soil parameters and pile stiffness) as well as nodal pressures in the passive zone in front of the wall, bending moments at nodes, and force(s) in the anchor rod(s). Multiple anchor levels can be as readily accommodated as a single anchor; and parametric studies for optimum anchor location can be made very easily, for data copies can be made and edited with the new location.

Any wall material can be analyzed—we are not limited to sheet piles as given in Sec. 13-2. You can use the program for composite sheet piles (part is one material with E_1 and part has an E_2). In this case it is only necessary to adjust the input so that the program computes EI correctly. For example, if E_1 is the base material and you use a second material of E_2, simply adjust the moments of inertia I_m so that you have

$$E_1 I_m = E_2 I_2 \rightarrow I_m = \frac{E_2 I_2}{E_1} \tag{13-4}$$

where I_m = adjusted value of actual moment of inertia for material m.

The FEM analysis finds the center of pressure to sustain the wall in a soil-pile interaction mode rather than making arbitrary assumptions about passive pressure as in the classical methods. Another particular advantage is that the same method of developing the stiffness matrix used for the beam-on-elastic foundation of Sec. 9-8 can be used for sheet-pile walls, so very little new material has to be learned.

The finite-element method uses the same equations as given in Chap. 9 and repeated here for convenience:

$$P = \mathbf{A}F \qquad e = \mathbf{A}^{\mathrm{T}}X \qquad F = \mathbf{S}e$$

and substituting, we obtain

$$F = \mathbf{S}\mathbf{A}^{\mathrm{T}}X \qquad P = \mathbf{A}\mathbf{S}\mathbf{A}^{\mathrm{T}}X$$
$$X = (\mathbf{A}\mathbf{S}\mathbf{A}^{\mathrm{T}})^{-1}P$$

which are the wall deflections consisting of translations and rotations of the several nodes. With the deflections at each node known, the bending moments are computed using the element $\mathbf{E}\mathbf{S}\mathbf{A}^{\mathrm{T}}$ as

$$F = \mathbf{E}\mathbf{S}\mathbf{A}^{\mathrm{T}}X$$

The element shear is computed from the element bending moments, but the node reactions and anchor rod force are directly computed using the spring equation of

$$F = K(I)X(I)$$

Study Fig. 13-8 carefully, for it illustrates the sheet-pile wall and *P–X* coding, the element forces, soil node springs, and the *sign convention*—this last is absolutely essential to interpret output. The problem is actually the beam-on-elastic-foundation problem turned 90° with the soil springs removed above the dredge line.

Anchor rods are allowed for by considering that an anchor rod will consist in a member of cross section A, modulus of elasticity E, and some length L. Now, the axial displacement in

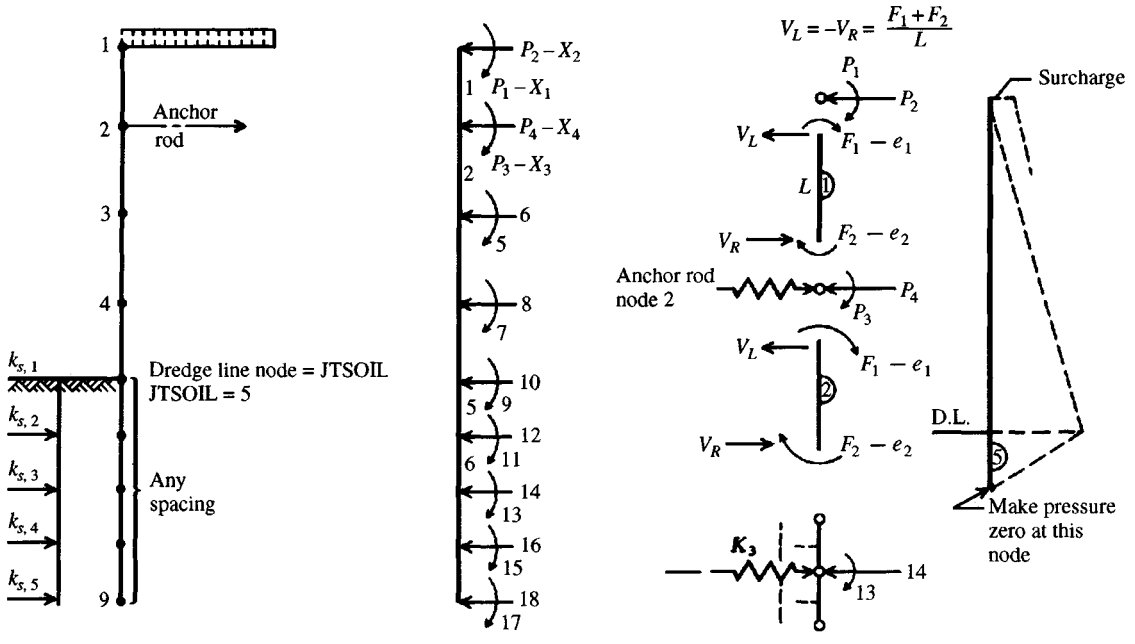

(*a*) Wall system with nodes selected. (*b*) Global *P*–*X* coding. (*c*) Node spring based on contributory length of two adjacent elements. (*d*) Coulomb pressure diagram.

Figure 13-8 Finite-element model for either a cantilever or anchored (including multiple anchors) sheet-pile wall. Both soil k_s and anchor rod springs are input as nodal entries. Here the anchor is identified with node 2, and the program computes soil springs (K_3 shown) for nodes 5 through 9, which are then added at NP locations of 4 (anchor rod), 10, 12, 14, 16, and 18 (soil springs) in the stiffness matrix [STIFF(I)].

this type of member is similar to the bar of a truss and is given in any Mechanics of Materials text as

$$e = \frac{FL}{AE} = X \qquad \text{and obtain} \qquad F = P = \frac{AE}{L}X$$

where X = nodal displacement computed from inverting the $\mathbf{ASA}^{\mathrm{T}}$ matrix
P = anchor rod force

To obtain the anchor rod force, one must place the anchor rod at a node. The anchor rod spring(s) AE/L (where force/length = units of a spring) are part of the input data required by the program. Earth anchors used in tieback construction (Chap. 14) usually slope from the horizontal, but we can input the horizontal component of the spring and obtain the horizontal component of force. It is then a trivial computation to obtain the axial force in the tieback or anchor rod. Since we always analyze a unit width of wall, the AE/L of the anchor rod is prorated based on the anchor rod spacing s [which is often more than a unit width—say, 1.5 to 2.0 m (5 to 6 ft)]. For spacing s (Fig. 13-9*c*) and defining η = slope with horizontal (Fig. 13-9*e*), the input anchor rod spring is

$$K(I)_{\mathrm{ar}} = \frac{AE}{sL}\cos\eta \tag{13-5}$$

For each anchor rod the preceding computation for its spring is made by hand and input into the data set. An input program parameter identifies the number of springs used, and other input identifies their node locations.

Soil springs are computed by the program in a subroutine and saved into an array for recycling as necessary. Similarly the program builds the banded stiffness matrix (always four entries wide × NP).

GENERAL PROGRAM OVERVIEW. This program uses a large number of subroutines so that any program modifications can be isolated for easier debugging.

The first subroutine that might be used is a universal subroutine DATAIN, which allows you to create a data file that is always saved to disk on program exit. Since you have only the compiled program the first time you use this program, to create a data file you should do a series of <PRT-SCREEN> keypresses to obtain a paper listing of the several lines of input data. You do not have to use this routine if you already have a data file on disk.

There is a USERMANL.DOC file on your diskette that both identifies and gives the order of input for selected data for applicable programs; you should print and file this for a convenient reference when using that program. You should print one data set and write in the variable names so that, when you want to do parameter studies, you can quickly identify the applicable control parameters. The element and most other data are readily identified by looking at the data set.

In subroutine INPUT the element lengths are read from the input file, and on any recycling the element lengths below the dredge line are increased by the input parameter DEPINC. This approach allows us to find the optimum embedment depth by starting with a small value of DEMB and incrementing it using DEPINC. In previous versions of this program the elements were of constant length below the dredge line—this version allows variable lengths initially but all added increments are the value of DEPINC.

The node NPs are computed in subroutine INPUT, so they do not have to be input by hand.

Incrementing depth of embedment. When the depth is incremented, the program increases NP by 2. Under these initial conditions,

$$\text{DEPINC} = 0.3 \qquad \text{DEMB} = 1.5 \text{ m}$$
$$15 \text{ elements (16 nodes)} \qquad \text{and} \qquad \text{NP} = 32$$

the first depth increment gives

$$\text{DEMB} = 1.5 + 0.3 = 1.8 \text{ m} \qquad 16 \text{ elements (17 nodes)}$$
$$\text{NP} = 32 + 2 = 34 \qquad \text{and so on}$$

If an equation is used to compute k_s and additional nodes are created using DEPINC, the program automatically computes k_s for the new node. If you input values of k_s for each node, you must assume that the program may increment the depth NCYC times. Thus, it is necessary to input sufficient *additional* node k_s values so that there is a value for any new node produced. The number NK of k_s to input is as follows:

$$\text{NCYC} = 1: \qquad \text{NK} = \text{NM} - \text{JTSOIL} + 2$$
$$\text{NCYC} > 1: \qquad \text{NK} = \text{NM} - \text{JTSOIL} + \text{NCYC} + 2$$

If you do not input enough k_s values according to the preceding, the program will output a message and stop. If this happens, use your DOS editor to recover the disk file and insert the additional k_s entries as required.

Subroutine LOAD allows us to input the node pressures from the top node to the first node below the dredge line (1 to JTSOIL + 1). One must input a value of 0.0 for the first node below the dredge line, as the program uses the pressure profile illustrated in Fig. 13-8*d* to compute node forces at nodes 1 through JTSOIL + 1 using the average end area method. This subroutine also allows input of node **P** matrix entries using NNZP > 0, so a strut/anchor rod can be modeled as either a force or a spring. The load (**P**) matrix is saved for reuse when NCYC > 1.

Subroutine SPRING computes both the node k_s (if an equation is used) and the soil springs below the dredge line. If an equation is used for the soil below the dredge line to obtain node k_s the program allows the use of two reduction factors, FAC1 and FAC2. Factor FAC1 is used to reduce the k_s values as follows:

```
SK(JTSOIL) = FAC1*SK(JTSOIL)
SK(JTSOIL+1) = FAC2*SK(JTSOIL+1)
```

In earlier editions of this text a single factor REDFAC was used to reduce the dredge line soil spring for driving and other disturbance. It has since been found that it is more realistic to reduce the soil modulus. The preceding reductions will affect the top three node springs by varying amounts. Since FAC1, FAC2 are not specified, they can be 1.0, but their relationship must be FAC2 ≥ FAC1. Usually, take FAC1 on the order of 0.6 to 1.0 and FAC2 on the order of 0.7 to 1.0.

If node k_s values are input, any reductions for dredge line damage or for other causes are made before their entry so that the control parameter to input soil node springs will be input as NRC = 0.

It is in this subroutine that the anchor rod springs are input using IAR = number of anchor rods. We input all springs via node identification (J) and spring value (SPRNG).

Subroutine BSTIF is then called to build the element stiffness matrix ESAT and EASAT for each element in turn. This routine calls subroutine BANDM to band the global ASAT. The result is a rectangular matrix four columns wide × NP rows, a particularly attractive feature of this program over a finite-difference method. This is saved in a single array STIFF(I) to save memory. The ESAT is saved in this routine so that it can be used later to compute the element bending moments. This routine is used each time the depth is incremented.

Subroutine MODIF is next called so that the stiffness matrix can be modified to add the previously computed soil (and anchor) springs to the appropriate diagonal nodes. This routine also allows input of boundary conditions based on NZX > 0. Those NP values that have known displacements (say, zero translation and/or rotation) are input in array NXZERO(I) and the known displacements input in array XSPEC(I) and in the same order. This procedure allows us, for example, to fix the top of the wall (or any other node location). Although the program allows nonzero XSPEC(I) values, seldom will we know any boundary displacements other than zero.

LISTB allows you to write the band matrix so that you can check whether the boundary cases were correctly identified. At a boundary location there should be a 1.0 in the first column (the diagonal) and three horizontal and diagonal 0.0s from that position.

Subroutine SOLVI is called next to reduce the band matrix, and in the process it replaces the **P** matrix with the displacement matrix. This is the reason for saving the original **P** matrix when NCYC > 1.

Subroutine CONVER is called if NCYC > 1, and in this case the program always does at least two cycles so that the current and previous dredge line displacements can be compared.

When two successive values are within the range of the input value CONV (usual range of 0.002 to 0.003 m) recycling stops.

In case convergence is not obtained in NCYC iterations, inspect the last output (also check for any input errors) and/or increase the initial depth of embedment DEMB and rerun.

Subroutine CHECK is called after dredge line convergence if NONLIN > 0 to see if any dredge line displacements X(I) > XMAX(I). For a valid check, short element lengths should be used in a zone near the dredge line, since it is nodes in that zone that will have any X(I) > XMAX(I). When a node displacement is larger than XMAX(I), a node force is computed as follows:

$$F = -K(I) * XMAX(I) \tag{13-6}$$

This force (with sign) is inserted into the **P** matrix and spring K(I) is set to 0.0, and the problem is recycled until the number of springs set to zero equals the number required to be set to zero. More than one spring may be zeroed on any cycle.

Setting a spring to zero can produce a substantial discontinuity in the soil-pile model. The effect is reduced by using closer-spaced nodes.

It is also necessary to recycle when making a nonlinear check. Since the negative force K(I) * XMAX(I) is less than was required by the previous analysis, the node displacement will increase. This change may result in the next lower node having X(I) > XMAX(I), and so on; if this were to occur for all the nodes the system would be unstable and you might get a halt in execution with an *exponent overflow* error reported. Otherwise, you get very large displacements in the soil below the dredge line, which indicate a shear failure.

When the program recycles for nonlinear effects the embedment depth is not incremented.

The nonlinear check is a reasonably realistic procedure for this model and usually produces three items of considerable interest:

1. Dredge line zone displacements are increased.
2. Bending moments in the pile are slightly increased.
3. Anchor rod force increases.

Subroutine FORCE is called when convergence and displacement criteria (or NCYC = 1) are met. By using the last-computed displacement matrix, the element end moments, shears, the anchor rod force, and the soil spring reactions (forces) $R(I)$ and the soil pressures $Q(I)$ are computed. These soil values are computed as

```
R(I) = X(I)*K(I)      and      Q(I) = X(I)*SK(I)
```

The program uses SK(I) for k_s; Q(I) for soil pressure q; and I for the translation NP-value.

Steps in a sheet-pile wall design. Steps in making a finite-element solution should include at least the following:

1. Assemble available site (importance factor) and soil information.
2. Draw the soil-wall system to a reasonable scale and decide on node locations. Tentatively locate anchor rod node(s) since a search may be made for a best node location. Both bending moments and rod forces are sensitive to location of the anchor rod node.

Locate nodes where soil stratum changes occur and at the GWT. Try to keep the ratio of adjacent element lengths under 5 and preferably under 3. Element lengths do not have to be constant, as for the finite-difference method. Where output is not limited (as it is in the following text examples, to save text pages) lengths should be on the order of 0.4 to 0.6 m with some as short as 0.3 m in critical regions.

3. Compute the lateral soil pressure from ground surface to the dredge line using K_a from the Coulomb (preferably) or Rankine equations; however, it may be appropriate to use a larger value if site conditions warrant. Where the strata change, use an average pressure value, which will introduce a small computational error for the node force unless the two contributing elements are equal in length. There can be much busywork in this step, so a program such as B-25 is recommended.
4. Estimate k_s below the dredge line. For depths up to about 5 m there should not be a great difference between the value for the dredge line and that for lower nodes; for clay a constant value based on the upper soil may be adequate. For sand there would be a small increase with depth.
5. Locate any nodes where you will input soil springs (NRC > 0) to replace program-computed values. These may be where marked differences in adjacent strata occur, soft lenses or thin strata of poor soil have been identified, cavities are known, and similar. *Note:* It may be preferable to input all node k_s values (an equation would probably not apply in this case anyway). That way, node springs that would give an incorrect soil pressure would not have to be input.
6. Select a tentative wall section and obtain the moment of inertia/unit width and section modulus/unit width so that the output moments can be checked for actual bending stresses. It is a trivial task to edit a copy of the data file to use a stiffer (or less stiff) section.
7. Select a tentative anchor rod cross section A, length L, and spacing s so the anchor rod spring can be computed using Eq. (13-5). It is a trivial task to edit the data file to input a larger- (or smaller-) diameter anchor rod. It is possible, however, to use other sections such as double angles, small **I** or **W** sections, square rods, etc. for the anchor "rod." Rods are usually more practical.
8. You have the option of either inputting an anchor rod force or a spring—the spring is usually preferable. You also have the option of inputting either node forces or node earth-pressure values—pressure is usually preferable. If you input a node force for the anchor rod, use IAR = 0 (no rod) and use NNZP = 1 to input the force. If you input node forces in lieu of the wall pressures input IPRESS = 0 and NNZP = IPRESS.
9. Check the output for overstress or excessive displacements. The largest element moment, anchor rod force, and soil pressure are checked by the user for

$$f_s = \frac{M}{\mathbf{S}} \le f_a \qquad f_s = \frac{F_{\text{ar}}}{A} \le f_a \qquad \text{and} \qquad Q(I) \le q_a$$

You will have allowable stress values f_a for the piling and anchor rod but you may not have a q_a for the soil. Even so, you can still check if the node soil pressures are reasonable or possible. They probably should not exceed the vertical bearing capacity or the passive earth pressure (or force using program WEDGE) at about the middepth of embedment.

Finally, check the node displacements below the dredge line. If they are all forward and sufficiently large, it is evident that a slip failure has formed. For example, if the

bottom node has a $+X$ displacement of 0.002 m (about 2 mm) this is negligible; however, if the $+X$ displacement is 0.003 to 0.010 m this may be large enough for a slip failure in the base soil. The embedment depth should be increased and the entire design recycled.

Depending on anchor rod location, wall height, and stiffness, one or more of the nodes above the top anchor rod may have a $(-)$ displacement, indicating the development of passive pressure. You might approximate this by rerunning the data set with the active pressure entries increased by using a small surcharge whose magnitude depends on the type of backfill and the $(-)$ displacement—perhaps 10 kPa for a dense sandy backfill when the $(-)$ X is on the order of 0.006 m.

10. The overall wall stability must be checked when a design has been produced for which statics are satisfied, none of the elements are overstressed, and displacements are not deemed excessive. The overall stability is considered in some detail in Sec. 13-9.

13-7 FINITE-ELEMENT EXAMPLES

The following examples will illustrate the FEM in a general manner and can be reproduced using program FADSPABW (B-9) on your diskette with the included data sets. Expertise can only be gained by making a number of computations in parametric studies, which are beyond the scope of a textbook. Also it is not possible to show the iterations necessary to optimize any of these examples because there is too much output for a textbook. The data sets are included so that you can do this without much effort.

Example 13-1. Anchored sheet-pile walls (or anchored bulkheads).

Given. the soil-wall system in a silty cohesionless material as in Fig. E13-1*a*. The initial location of the wall line is such that about half the depth shown is initially retained and material is to be dredged from the front. This location allows the piling to be driven and the anchors set. Then the remaining front soil is excavated and mixed with imported sand to produce a backfill with properties estimated as shown. The top will be paved so that boats can load and unload. We will account for those activities with a 25 kPa surcharge. The soil below the dredge line is a silty clay with some sand, and the average of consolidated-undrained tests on several tube samples gives the properties shown.

Required. Find a suitable rolled sheet-pile section and anchor rod for the system.

Solution. Estimate $\gamma = 16.50\ \text{kN/m}^3$ above and below the water line. The angle of internal friction ϕ may be on the order of 34 to 36°, but we will conservatively use $\phi = 30°$ since the dredged soil will be somewhat loose—at least initially.

With the same water level on both sides of the wall (the interlocks are seldom watertight unless sealed as noted in Sec. 13-2.3) the water pressure is ignored. We must, however, use $\gamma' = 6.70\ \text{kN/m}^3$ in computing the lateral earth pressure below the water line. The dredge line γ_{sat} is obtained by trimming a sample and performing a direct measurement as in Example 2-1.

Step 1. Draw Fig. E13-1*a* based on the given data and tentative node locations; plot Fig. E13-1*b* to keep track of the initial P–X coding. Plot the lateral earth-pressure profile of Fig. E13-1*c* for reader convenience. The pressure profile uses the Coulomb $K_a = 0.3$ shown since there was little variation for any reasonable δ angle. The information to plot the node forces of Fig. E13-1*d* was obtained from outputs of an initial trial program execution. They can also be computed from the pressure profile of Fig. E13-1*c* using the average end area method, and nodes 1 and 2 are hand-computed (for illustration) as follows:

Node 1:
$$\text{P(2)} = \frac{7.5 \times 1.2}{2} + (13.4 - 7.5) \times \frac{1.2}{2} \times \frac{1}{3} = \mathbf{5.7}\ \text{kN}$$

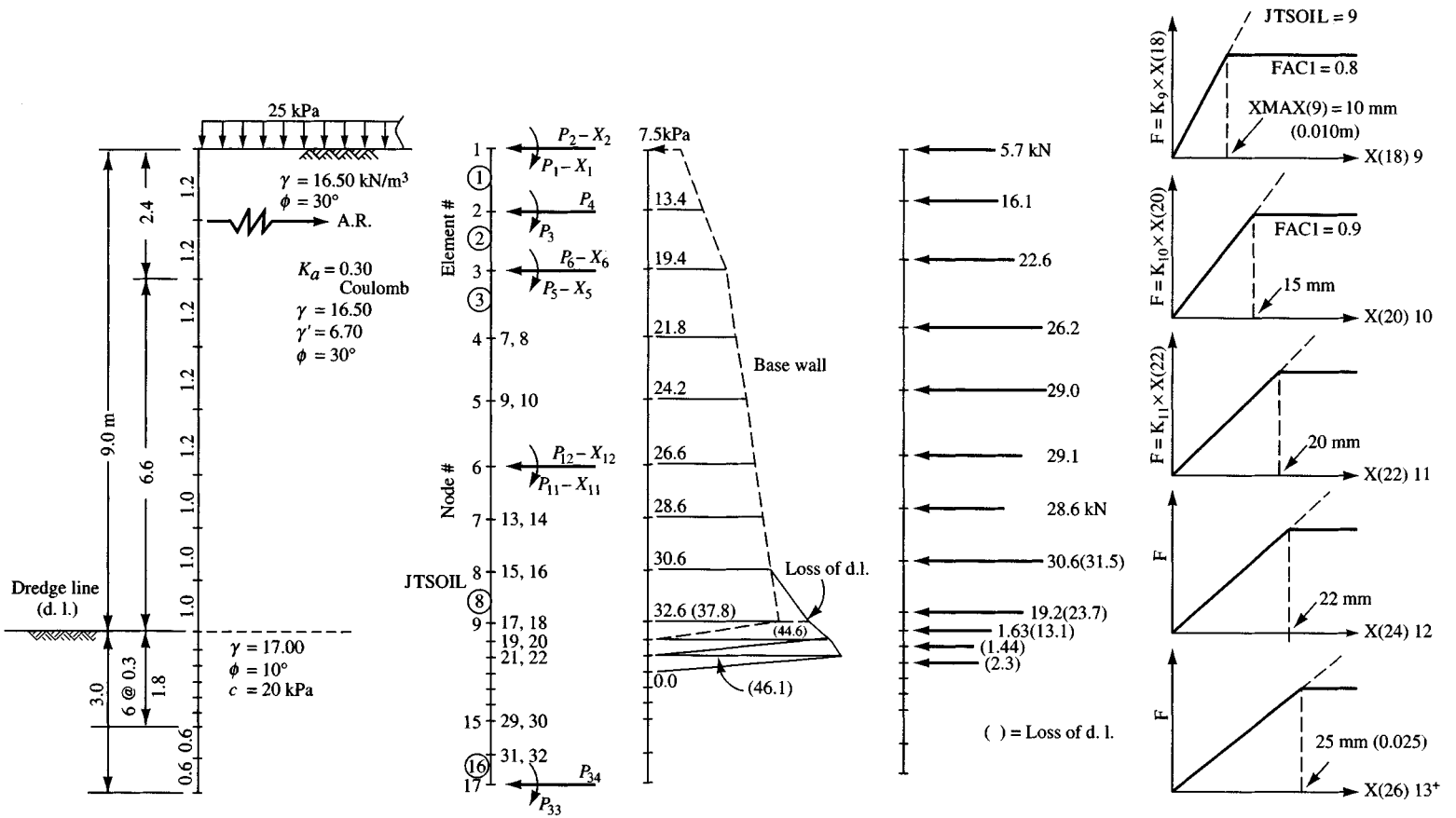

(*a*) Wall profile. (*b*) *P*–*X* coding. (*c*) Pressure profile. (*d*) Node forces. (*e*) XMAX(I) definition.

Figure E13-1*a–e*

Required. Find a suitable rolled sheet-pile section and anchor rod for the system.

Node 2: $$P(4) = \frac{1.2}{2}(7.5 + 13.4 + 13.4 + 19.4) = \mathbf{16.1}\ \text{kN}$$

Figure E13-1*e* illustrates the significance of using a different XMAX(I) for the top several nodes below the dredge line.

Comments

1. The node spacing above the dredge line is as shown to save space. Ideally a node spacing of 0.6 (instead of 1.2) and 0.5 (instead of 1.0) would be used. The element length transition ratio at the dredge line is 1.0/0.3 = 3.333, and 0.5/0.3 would be much preferred.
2. As part of this design, additional nodes are shown below the 1.8-m initial embedment depth. You will see their purpose later.
3. The node forces of Fig. E13-1*d* are from computer output sheets and would not usually be shown like this. A better location is on the output sheets beside their listing—or not at all.

Step 2. From the *initial P–X* coding and general node configuration for the total depth of 9.0 + 1.8 = 10.8 m, obtain the following initial values (the text output sheets will use slightly different values in some cases):

NM = 14 (initial count of 8 above and 6 below the dredge line)
NP = 30 [2 × (NM + 1)]
There are no input forces → NNZP = 0
Use 1 load case → NLC = 1
For a sheet-pile wall, ITYPE = 1
We do not need a listing of the band matrix → LISTB = 0
Recycle limit → NCYC = 5
No soil springs to input → NRC = 0

The foregoing eight parameters are the first line of input in the given sequence after the project TITLE. The next line in order is as follows:

Dredge line soil starts at node 9 by count → JTSOIL = 9
Activate the nonlinear routine → NONLIN = 1
Anchor rod at node 2 → IAR = 2
No known displacements → NZX = 0
There are JTSOIL + 1 pressure entries → IPRESS = 10
We are using SI units → IMET = 1

The next line of input contains the following (in order):

E = modulus of elasticity of steel pile = 200 000 MPa
DEMB = initial embedment depth = 6 × 0.3 = 1.8 m
CONV = dredge line displacement convergence = 0.002 m (2 mm)
DEPINC = depth increment for recycling = 0.3 m
BSHP = width used (usually 1 unit) = 1.0 m

Sheet-pile and anchor rod sections must be selected and later revised as necessary. For the initial trial let us use an anchor rod with these properties:

$$\text{Diam} = 55 \text{ mm} \qquad \text{Spacing } s = 1.83 \text{ m} \qquad \text{Length } L = 10.83 \text{ m}$$
$$\text{Steel grade} = 250 \text{ (A-36 with } f_y = 250 \text{ MPa)}$$
$$f_{a,\text{ar}} = 0.6 f_y = 0.6\,(250) = \mathbf{150} \text{ MPa}$$

The anchor rod area is $A = 0.7854(0.055)^2 = \mathbf{2.3758 \times 10^{-3}}$ m^2 and the spring [using Eq. (13-5) with $\eta = 0°$] is

$$\text{ARSPG} = \frac{AE}{sL}\cos\eta = \frac{2.3758^{-3} \times 200\,000 \times 10^{-3}}{1.83 \times 10.83}(1) = \mathbf{23\,974.0} \text{ kN/m}$$

Try a PZ32 pile section using A-328 steel (Grade 250) with $f_y = 250$ MPa and

$$f_{a,p} = 0.6 f_y = 0.6(250) = \mathbf{150} \text{ MPa}$$

and convert table values for I and **S** for pile width to values per 1 meter of wall width, giving

$$\text{Moment of inertia } I = \frac{I_{\text{table}}}{\text{Width}} = \frac{283.7 \times 10^{-6}}{0.575} = 0.4934 \times 10^{-3} \text{ m}^4/\text{m}$$

$$\text{Section modulus } S = \frac{S_{\text{table}}}{\text{Width}} = \frac{1.498 \times 10^{-3}}{0.575} = 2.605 \times 10^{-3} \text{ m}^3/\text{m}$$

We will use an approximate equation for k_s. From Table 4-4 we obtain Hansen bearing-capacity factors of 8.34, 2.5, and 0.4 at $\phi = 10°$ and compute

$$\text{AS} = 40[cN_c + 0.5\gamma(1)(N_\gamma)]$$
$$= 40[20 \times 8.34 + 0.5(17.0 - 9.81)(1)(0.4)] = 6673$$
$$\text{BS} = 40(7.19)(2.5) = 719$$

Round and use AS = **7000** BS = **1000** (equation is approximate)

Since the dredge line will be excavated, use soil modulus reduction factors (but not for the case of lost dredge line depth) as

$$\text{FAC1} = 0.80 \qquad \text{FAC2} = 0.90$$

We do not want k_s to increase much with depth, so use the following equation form (a program option) instead of Z[1]:

$$k_s = \text{SK(I)} = 7000 + 1000 \tan^{-1}(Z/D)$$

where D = embedment depth on any cycle
Z = depth from dredge line to the current node

Referring to Fig. E13-1*a*, *b*, and *c*, we will make a program execution using DEMB = 1.8 m; NCYC = 5; NONLIN = 1; and setting all XMAX(I) = 0.5 m.

From this output the nodal displacements XMAX(I) are revised to those shown on the output sheets (0.010, 0.015, 0.020, 0.022, and the remainder at 0.025). Their significance is shown on Fig. E13-1*e*.

Let us somewhat arbitrarily make some additional executions using NCYC = 1; NONLIN = 1; **and** for DEMB = 1.8, 2.4, 3.0, and 3.6 m. These executions are summarized in the following table:

	Trial					
	1	2	3	4	5	Units
$DEMB_i$	1.8	1.8	2.4	3.0	3.6	m
$\delta_{D.L.}$	13.4	13.6	13.5	13.7	13.6	mm
Mom_{max}	228.1	226.7	227.2	221.7	212.7	kN · m
F_{ar}	108.0	107.7	107.8	106.6	104.8	kN
q_{max}	75.0	76.8	75.3	76.6	76.8	kPa
$DEMB_f$	2.1	1.8	2.4	3.0	3.6	m

From the output sheets for each trial, the maximum moment occurs at node 6; q_{max} occurs at node 10. From the preceding table tentatively select an embedment depth DEMB = 3.0 m. This gives a reasonable driving depth, and we will consider in the stability analysis a loss of dredge line of 0.6 m (leaving only 2.4 m—for a 1.8-m initial depth the dredge line converged at 2.1 m, which is very close to 2.4 m). We will also consider the possibility of the surcharge somehow becoming doubled (from 25 kPa as used above to 50 kPa). Part of this effect might derive from an actual surcharge increase that increases the lateral pressure; another possibility is that the active pressure might not fully develop if the anchor rod spring does not stretch sufficiently.

With these considerations a copy of the initial data file is made and named EX131.DTA, (on your diskette). It was edited for depth of embedment DEMB = 3.0, NM = 16 (two bottom elements of 0.6 m added), and NCYC = 1 (we do not want to increment since we already know from using the 1.8-m depth that convergence is obtained on the first cycle). Use NONLIN = 1 (we do want to check the dredge line for possible X(9) > XMAX(9) = 0.010 m (10 mm). This set of output is shown as Fig. E13-1*f*.

We make copies of file EX131.DTA as EX131A.DTA and EX131B.DTA (all on your diskette) and edit them. EX131A.DTA is edited for a 0.6-m loss of dredge line so that for DEMB = 3.0 − 0.6 = 2.4, we use FAC1, FAC2 = 1.0 (not 0.8 and 0.9 of EX131.DTA). We must recompute the dredge line soil pressure and include nodes 10 and 11. The clay below node 9 produces a discontinuity as shown in Fig. E13-1*c* and the two values are "averaged." The other two nodes have values as shown.

For the surcharge increase from 25 to 50 kPa we edit file EX131B.DTA for the new pressure profile (not shown; but at node 1 it is 15.0 instead of 7.5 kPa). Refer to the data file for the pressure profile if you wish to check it—actually, all values merely increased by 7.5 kPa.

These files were executed and the data are summarized in the following table:

For:	Design		D.L. loss of 0.6 m		Surcharge = 50 kPa	
	JTSOIL = 9 IPRESS = 10 DEMB = 3.0		JTSOIL = 11 IPRESS = 12 DEMB = 3.0		JTSOIL = 9 IPRESS = 10 DEMB = 3.0	
	Value	Increase, %	Value	Increase, %	Value	Increase, %
$\delta_{D.L.}$, mm	13.7		16.7		17.8	
Mom_{max}, kN · m/m	213.1	1.0	270.9	1.27	286.2	1.34
F_{ar}, kN	106.6	1.0	116.9	1.10	148.2	1.39
δ_{ar}, mm	4.4		4.9		6.2	
q_{max}, kPa	76.6	1.0	102.8	1.34	96.3	1.26
δ_{max}, mm	23.7		31.5		30.9	
$D(D/2.1)$, %		1.42		1.42		1.42

A check of the pile (**PZ**35) and anchor rod (diam. = 50 mm) stresses yields the following (for anchor rod include the spacing s):

$$f_{s,\text{ar}} = \frac{sF}{A} = \frac{1.83 \times 148.2}{2.3758 \times 10^{-3} \times 10^3} = 114.1 < 150 \text{ MPa} \qquad \text{(O.K.)}$$

$$f_{s,\text{pile}} = \frac{M}{\mathbf{S}} = \frac{286.2}{2.605 \times 10^{-3} \times 10^3} = 109.9 \ll 150 \text{ MPa} \qquad \text{(also O.K.)}$$

From the stresses this section appears somewhat overdesigned, however, several considerations should be made. First, it is a trivial matter to edit the three data files (EX131.DTA, EX131A.DTA, EX131B.DTA) to use a different section (perhaps a **PZ**27). Second, note the maximum node displacement above the dredge line from the design case of 23.7 (say, 24 mm or 1 in.) is 31.5 (say, 31 mm or 1.25 in.). These displacements are below the water line but may be noticeable. From the information tabulated, one can say with certainty, without changing sections and making additional trials, that the displacements would increase with a smaller pile section.

What one should do is to create a more realistic P–X coding using 0.6-m and 0.5-m elements above the dredge line, and try moving the anchor rod to the new node 4 or 5, and make new executions.

One might try using either a 35- or 40-mm diameter anchor—but a small diameter rod will increase the lateral displacements above the dredge line. This modification clearly has merit, since the current rod elongation of 4.4 mm may not be enough to allow active earth pressure, using as a guide that the wall should translate about $0.001H$, giving $0.001(9.0 - 2.4) = 0.001(6.6 \times 1000) = 6.6 \text{ mm} > 4.4 \text{ mm}$. Be careful when considering anchor rod diameter. If the rod is normally threaded, the actual area is less than the nominal area because the area is calculated to the thread root (see Table 8-4). If the threads are upset, the actual rod area can be safely used, but a rod with upset threads costs more.

There is some opinion that the anchor rod force will increase with time as the soil settles from beneath the rod. The rod then becomes a beam supported at the wall and at the anchorage, and in addition to the axial anchor rod load it now carries the depth of soil above + its self-weight as a uniform loading along the rod length. It has been suggested that this long-term loading can nearly double the initial anchor rod force—in this case from 106.6 to 213 kN—and the allowable stress would be exceeded.

For the design case we use FAC1 = 0.8 and FAC2 = 0.9 and calculate the following (note the use of DEMB = D = 3.0 here):

$$\begin{aligned}
\text{SK(9)} &= 0.8[7000 + 1000\tan^{-1}(0.0/3.0)] = 5600. \text{ kN/m}^3 \\
\text{SK(10)} &= 0.9[7000 + 1000\tan^{-1}(0.3/3.0)] = 6389.702 \\
\text{SK(11)} &= 7000 + 1000\tan^{-1}(0.6/3.0) = 7197.396\ldots \text{ and so on}
\end{aligned}$$

For the dredge line loss we use the same equation, but there is a design question of whether it should have been adjusted for the depth lost—I arbitrarily decided not to since FAC1, FAC2 are taken as 1.0. In this case k_s is computed as

$$\begin{aligned}
\text{SK(JTSOIL)} &= \text{SK(11)} = (7000 + 0) = 7000. \text{ kN/m}^3 \\
\text{SK(12)} &= 7000 + \tan^{-1}(0.3/2.4) = 7124.35 \\
\text{SK(13)} &= 7000 + \tan^{-1}(0.6/2.4) = 7294.979 \\
&\vdots \\
\text{SK(17)} &= 7000 + \tan^{-1}(2.4/2.4) = 7785.398
\end{aligned}$$

The computer output sheets of Fig. E13-1*f* show the final design choice using data set EX131.DTA with DEMB = 3.0. Thus, there are several changes from the initial input (different NP, NM). You should identify the changes from the original input data used for the preliminary trial (not shown).

EXAMPLE 13-1 OF FOUND ANALY & DESIGN 5/E--USE 3.0 M AS DESIGN--SI UNITS

++++++++++++++ THIS OUTPUT FOR DATA FILE: EX131.DTA

SOLUTION FOR SHEET PILE WALL--CANTILEVER OR ANCHORED ++++++++++++++ ITYPE = 1

NO OF NP =	34	NO OF MEMBERS =	16
NO OF LOAD CONDITIONS =	1	NO OF BOUNDARY CONDITIONS, NZX =	0
MAX NO OF ITERATIONS, NCYC =	1	NONLIN CHECK (IF > 0) =	1
NO OF NODE MODULUS TO INPUT, NRC =	0	NODE SOIL STARTS, JTSOIL =	9
LIST BAND MATRIX, LISTB (IF >0) =	0	NO OF ANCHOR RODS, IAR =	1
INPUT NODE PRESSURES, IPRESS =	10	NO OF NON-ZERO P-MATRIX ENTRIES =	0
		IMET (SI > 0) =	1

MODULUS OF ELASTICITY = 200000.0 MPA

SOIL MODULUS = 7000.00 + 1000.00*ATAN(Z/D) KN/M**3
NODE Ks REDUCTION FACTORS: JTSOIL = .80 JSTSOIL + 1 = .90

SHEET PILE AND CONTROL DATA:

WIDTH =	1.000	M
INITIAL EMBED DEPTH, DEMB =	3.000	M
DEPTH INCR FACTOR, DEPINC =	.300	M
DREDGE LINE CONVERGENCE, CONV =	.002000	M

ANCHOR RODS LOCATED AT NODE NOS = 2

MEMBER AND NODE DATA FOR WALL WIDTH = 1.000 M

MEMNO	NP1	NP2	NP3	NP4	LENGTH M	INERTIA M*4
1	1	2	3	4	1.2000	.0004934
2	3	4	5	6	1.2000	.0004934
3	5	6	7	8	1.2000	.0004934
4	7	8	9	10	1.2000	.0004934
5	9	10	11	12	1.2000	.0004934
6	11	12	13	14	1.0000	.0004934
7	13	14	15	16	1.0000	.0004934
8	15	16	17	18	1.0000	.0004934
9	17	18	19	20	.3000	.0004934
10	19	20	21	22	.3000	.0004934
11	21	22	23	24	.3000	.0004934
12	23	24	25	26	.3000	.0004934
13	25	26	27	28	.3000	.0004934
14	27	28	29	30	.3000	.0004934
15	29	30	31	32	.6000	.0004934
16	31	32	33	34	.6000	.0004934

NODE	KS KN/M*3	SPRINGS SOIL/A.R.	XMAX M	NODE Q KPA	NODE P KN
1	.000	.000	.0000	7.5000	5.6800
2	.000	23974.000	.0000	13.4000	16.1000
3	.000	.000	.0000	19.4000	22.5600
4	.000	.000	.0000	21.8000	26.1600
5	.000	.000	.0000	24.2000	29.0400
6	.000	.000	.0000	26.6000	29.1133
7	.000	.000	.0000	28.6000	28.6000
8	.000	.000	.0000	30.6000	30.6000
9*	5600.000	879.485	.0100	32.6000	19.2267
10*	6389.702	1917.810	.0150	.0000	1.6300
11	7197.396	2123.537	.0200		
12	7291.457	2187.187	.0220		
13	7380.506	2213.857	.0250		
14	7463.647	2238.776	.0250		
15	7540.419	3402.782	.0250		
16	7674.741	4602.478	.0250		
17	7785.398	2324.554	.0250		

* = Ks REDUCED BY FAC1 OR FAC2

+++NON-LINEAR CHECK: CURRENT CYCLE, ICYC = 0 CURRENT SPRGS ZEROED = 1 PREVIOUS COUNT = 0
CURRENT D.L. X(I) = .01341 PREVIOUS D.L. X(I) = .01341

Figure E13-1*f*

```
+++NON-LINEAR CHECK: CURRENT CYCLE, ICYC =  1   CURRENT SPRGS ZEROED =  1   PREVIOUS COUNT =  1
          CURRENT D.L. X(I) =  .01366  PREVIOUS D.L. X(I) =    .01341
```

MEMBER MOMENTS, NODE REACTIONS, DEFLECTIONS, SOIL PRESSURE, AND LAST USED P-MATRIX FOR LC = 1

MEMNO	MOMENTS--NEAR END 1ST, KN-M		NODE	SPG FORCE, KN	ROT, RADS	DEFL, M	SOIL Q, KPA	P-, KN-M	P-, KN
1	.000	6.816	1	.0000	.00560	-.00349	.000	.000	5.680
2	-6.816	-95.015	2	106.6387	.00564	.00445	.000	.000	16.100
3	95.015	-169.774	3	.0000	.00611	.01222	.000	.000	22.560
4	169.772	-213.139	4	.0000	.00450	.01867	.000	.000	26.160
5	213.139	-221.655	5	.0000	.00217	.02272	.000	.000	29.040
6	221.656	-199.637	6	.0000	-.00048	.02375	.000	.000	29.113
7	199.637	-149.017	7	.0000	-.00261	.02219	.000	.000	28.600
8	149.016	-67.797	8	.0000	-.00438	.01865	.000	.000	30.600
9	67.797	-40.297	9	8.7949	-.00548	.01366*	56.000	.000	10.432
10	40.305	-19.203	10	22.9880	-.00564	.01199	76.591	.000	1.630
11	19.206	-4.638	11	21.8288	-.00573	.01028	73.985	.000	.000
12	4.645	4.309	12	18.7086	-.00577	.00855	62.369	.000	.000
13	-4.313	8.726	13	15.1051	-.00577	.00682	50.357	.000	.000
14	-8.723	9.713	14	11.4076	-.00575	.00510	38.031	.000	.000
15	-9.712	4.799	15	11.4856	-.00572	.00338	25.452	.000	.000
16	-4.799	.000	16	-.1912	-.00568	-.00004	-.319	.000	.000
			17	-7.9985	-.00566	-.00344	-26.789	.000	.000

```
   SUM SPRING FORCES =    208.77 VS SUM APPLIED FORCES =    208.71   KN
    (*) = SOIL DISPLACEMENT > XMAX(I) SO SPRING FORCE AND Q = XMAX*VALUE ++++++++++++
    NOTE THAT P-MATRIX ABOVE INCLUDES ANY EFFECTS FROM X > XMAX ON LAST CYCLE ++++
```

```
DATA FOR PLOTTING IS SAVED TO DATA FILE: WALL.PLT
   AND LISTED FOLLOWING FOR HAND PLOTTING
```

NODE	DEPTH	KS	COMP X,MM	XMAX	SHEAR V(I,1),V(I,2) LT OR T	RT OR B	MOMENT MOM(I,1),MOM(I,2) LT OR TOP	RT OR BOT
1	.000	.0	-3.489	.000	.00	5.68	.00	.00
2	1.200	.0	4.448	.000	5.68	-84.86	6.82	6.82
3	2.400	.0	12.221	.000	-84.86	-62.30	-95.01	-95.02
4	3.600	.0	18.673	.000	-62.30	-36.14	-169.77	-169.77
5	4.800	.0	22.724	.000	-36.14	-7.10	-213.14	-213.14
6	6.000	.0	23.749	.000	-7.10	22.02	-221.66	-221.66
7	7.000	.0	22.188	.000	22.02	50.62	-199.64	-199.64
8	8.000	.0	18.651	.000	50.62	81.22	-149.02	-149.02
9	9.000	5600.0	13.656	10.000	81.22	91.67	-67.80	-67.80
10	9.300	6389.7	11.987	15.000	91.67	70.34	-40.30	-40.31
11	9.600	7197.4	10.279	20.000	70.34	48.56	-19.20	-19.21
12	9.900	7291.5	8.554	22.000	48.56	29.85	-4.64	-4.64
13	10.200	7380.5	6.823	25.000	29.85	14.71	4.31	4.31
14	10.500	7463.6	5.095	25.000	14.71	3.30	8.73	8.72
15	10.800	7540.4	3.375	25.000	3.30	-8.19	9.71	9.71
16	11.400	7674.7	-.042	25.000	-8.19	-8.00	4.80	4.80
17	12.000	7785.4	-3.441	25.000	-8.00	.00	.00	.00

Figure E13-1*f* (*continued*)

The final design clearly needs refinement but this will not be done here because of space limitations.

Discussion of computer output.

1. The program informs you of any recycling based on both NCYC and NONLIN with adequate identification so you can see what was done.
2. The program puts an * beside any SK(I) that have been reduced (FAC1, FAC2 < 1.0). If FAC1 = 1 then FAC2 should also equal 1.0, but if either value is 1.0 the * is not printed for that node.
3. The program puts an * beside nodes where X(I) > XMAX(I) so you can verify (if desired) that the node reaction is computed as

$$\text{R} = \text{XMAX(I)} * \text{K(I)} \qquad q = \text{XMAX(I)} * \text{SK(I)}$$

4. The revised P matrix is output so you can see the effect of inserting the (−) spring force when X(I) > XMAX(I).
5. The program sums the node soil reactions together with the anchor rod and outputs this value along with a sum of the active earth node forces so you can make a visual check of $\sum F_h = 0$.
6. The moment table is output along with the spring forces and other data so you can make a visual check that at the ends the element moment is nearly 0 (Node 1 should always be 0 unless the top is embedded in a concrete slab, as in a pier) and is restrained. Computer round-off error using single precision may give small nonzero values (exactly 0.000 is shown on the output sheet but this is unusual).

   You can make an instant visual moment check since the far-end moment of element I should equal the near-end moment of element $I + 1$ with a sign change. For element 1 the near-end moment = 0.000; the far-end moment = 6.816; the near-end moment of element 2 = −6.816. This means that the $\sum M$ for node 2 = 0(6.816 − 6.816 = 0)$\cdots$ and so on.
7. The output sheet lists a table for plotting. These data are saved to a disk file if specified at the beginning of program execution. It is always output, however, so you can plot the displacement profile and superimpose on it the XMAX(I) profile below the dredge line. *This file is also useful to make a quick handplot of the shear and moment diagrams as shown in Fig. E13-1g.* These diagrams may require interpretation, but this should not be a problem. You know that between the anchor rod and dredge line the piling bulges outward creating compression on the backfill side.

   The shear (and direction) for node 1 is

$$V = \frac{F_1 + F_2}{L} = \frac{0.000 + 6.816}{1.2} = 5.68 \leftarrow$$

The direction derives from using element moment sign conventions. At node 2 (the anchor rod) we have

$$V_{\text{top}} = 5.68 \qquad \text{and from element 2}$$

$$V_{\text{bot}} = \frac{-6.816 + (-95.015)}{1.2} = -84.859 \rightarrow$$

Check this statement as

$$\text{To left } \overleftarrow{5.68} + \overleftarrow{16.01} - \overrightarrow{106.639} = \overrightarrow{-84.859}$$

This expression says the sum of node forces from the top to node 2− the anchor rod force is the shear. It is much easier, however, to get the shears directly from $V = (F_1 + F_2)/L$ but you need the sign convention for the F_i (element moments), which is shown on Fig. 13-8*c*.

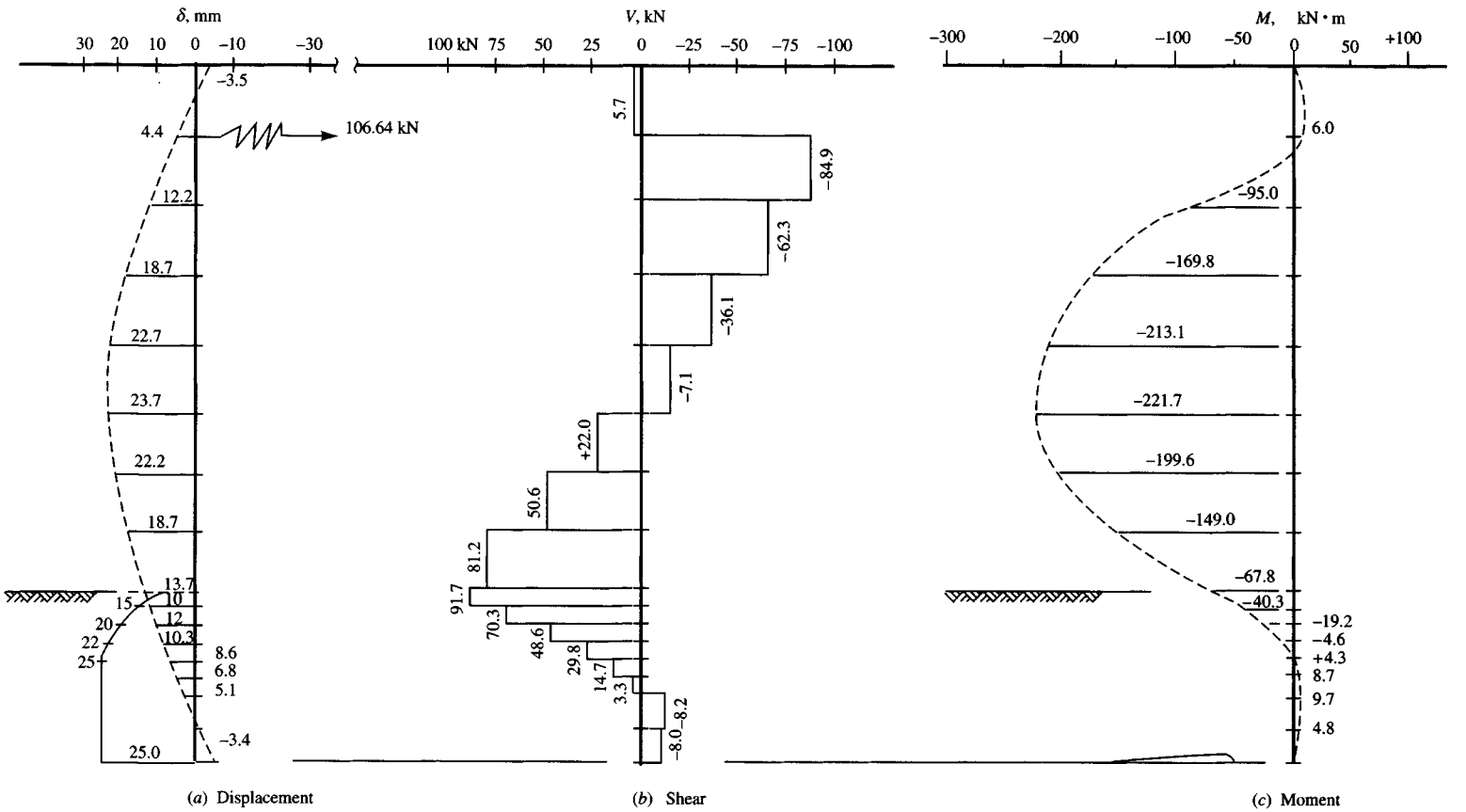

Figure E13-1*g*

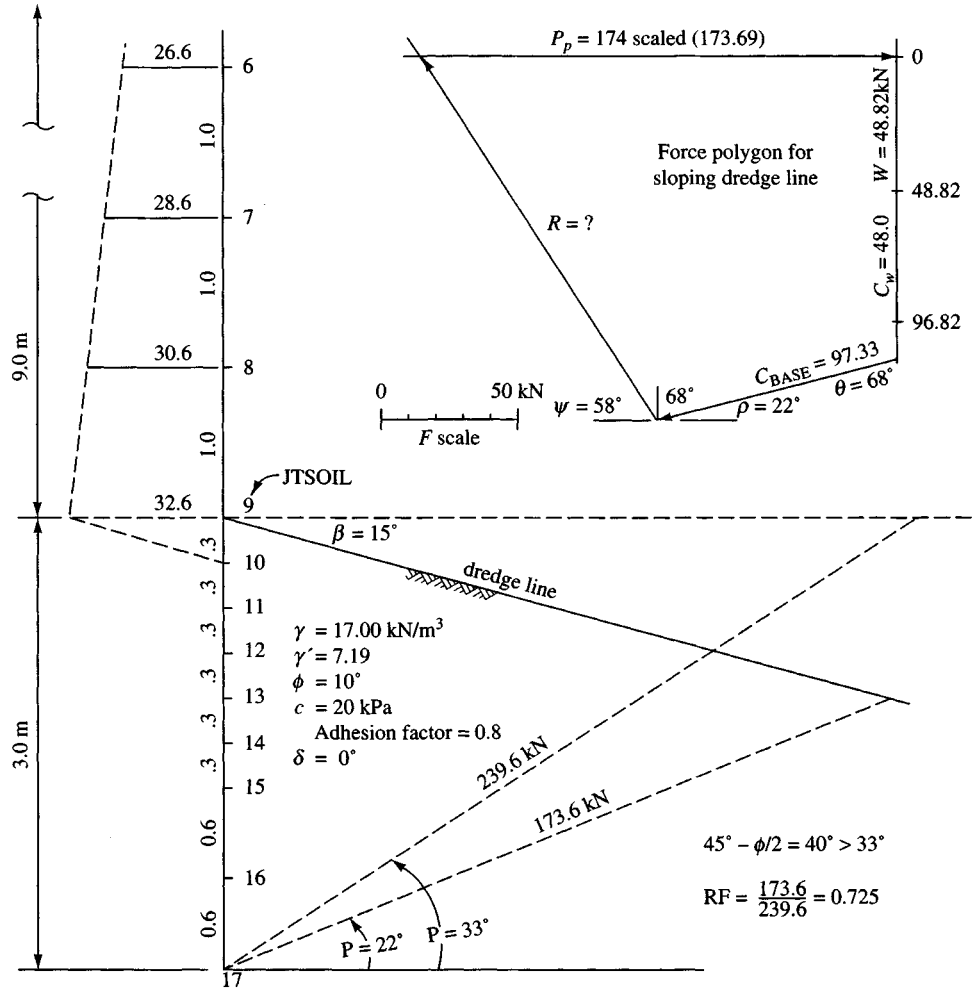

Figure E13-2*a* Given wall and soil data.

Example 13-2. It is required to find the embedment depth, anchor rod force, and an adequate sheet pile section if the dredge line of Example 13-1 has the slope $\beta = -15°$ as shown in Fig. E13-2*a*. The figure has been reversed to look from the left, whereas in Fig. 13-1*a* we look from the right side of the wall and parallel along it. The view here matches the profile used in program WEDGE.

Solution. From the several trial runs of Example 13-1 we will tentatively try the embedment depth of 3 m, use NCYC = 5, and activate NONLIN = 1. We will use FAC1 = 0.8 and FAC2 = 0.9 for dredge line damage and the same XMAX(I) values.

We must also adjust k_s for the sloping dredge line. For this we will use data sets WDG132A.DTA and WDG132B.DTA, provided on your program diskette, with program WEDGE to obtain $P_{p,h}$ = 239.6 kN (horizontal dredge line) and $P_{p,s}$ = 173.6 kN (sloping dredge line) shown on Fig. E13-2*a* as well as the force polygon used to find the passive force P_p. Passive force P_p is horizontal since $\phi = 10°$, and for this small angle $\delta = 0$. The resulting reduction factor of 0.725 is

EXAMPLE 13-2 SHEET-PILE WALL OF EXAMPLE 13-1--WITH SLOPING DREDGE LINE

++++++++++++++ THIS OUTPUT FOR DATA FILE: EX132.DTA

SOLUTION FOR SHEET PILE WALL--CANTILEVER OR ANCHORED ++++++++++++++ ITYPE = 1

NO OF NP =	34	NO OF MEMBERS =	16
NO OF LOAD CONDITIONS =	1	NO OF BOUNDARY CONDITIONS, NZX =	0
MAX NO OF ITERATIONS, NCYC =	5	NONLIN CHECK (IF > 0) =	1
NO OF NODE MODULUS TO INPUT, NRC =	14	NODE SOIL STARTS, JTSOIL =	9
LIST BAND MATRIX, LISTB (IF >0) =	0	NO OF ANCHOR RODS, IAR =	1
INPUT NODE PRESSURES, IPRESS =	10	NO OF NON-ZERO P-MATRIX ENTRIES =	0
		IMET (SI > 0) =	1

MODULUS OF ELASTICITY = 200000.0 MPA

SHEET PILE AND CONTROL DATA:

WIDTH =	1.000	M
INITIAL EMBED DEPTH, DEMB =	3.000	M
DEPTH INCR FACTOR, DEPINC =	.300	M
DREDGE LINE CONVERGENCE, CONV =	.003000	M

ANCHOR RODS LOCATED AT NODE NOS = 2

MEMBER AND NODE DATA FOR WALL WIDTH = 1.000 M

MEMNO	NP1	NP2	NP3	NP4	LENGTH M	INERTIA M*4	NODE	KS KN/M*3	SPRINGS SOIL/A.R.	XMAX M	NODE Q KPA	NODE P KN
1	1	2	3	4	1.2000	.0004934	1	.000	.000	.0000	7.5000	5.6800
2	3	4	5	6	1.2000	.0004934	2	.000	23974.000	.0000	13.4000	16.1000
3	5	6	7	8	1.2000	.0004934	3	.000	.000	.0000	19.4000	22.5600
4	7	8	9	10	1.2000	.0004934	4	.000	.000	.0000	21.8000	26.1600
5	9	10	11	12	1.2000	.0004934	5	.000	.000	.0000	24.2000	29.0400
6	11	12	13	14	1.0000	.0004934	6	.000	.000	.0000	26.6000	29.1133
7	13	14	15	16	1.0000	.0004934	7	.000	.000	.0000	28.6000	28.6000
8	15	16	17	18	1.0000	.0004934	8	.000	.000	.0000	30.6000	30.6000
9	17	18	19	20	.3000	.0004934	9	4060.000	637.650	.0100	32.6000	19.2267
10	19	20	21	22	.3000	.0004934	10	4633.000	1390.500	.0150	.0000	1.6300
11	21	22	23	24	.3000	.0004934	11	5218.000	1539.550	.0200		
12	23	24	25	26	.3000	.0004934	12	5286.000	1585.650	.0220		
13	25	26	27	28	.3000	.0004934	13	5351.000	1605.050	.0250		
14	27	28	29	30	.3000	.0004934	14	5411.000	1623.100	.0250		
15	29	30	31	32	.6000	.0004934	15	5467.000	2467.050	.0250		
16	31	32	33	34	.6000	.0004934	16	5564.000	3336.700	.0250		
							17	5644.000	1685.200	.0250		

Ks REDUCED WHEN YOU INPUT ALL VALUES

CURRENT CYCLE NO = 1 D.L. DEFL: PREVIOUS = .00000 CURRENT = .01559 FOR EMBED DEPTH = 3.000 M

++++ NEW NP = 36
NEW NM = 17

Figure E13-2*b*

MEMBER AND NODE DATA FOR WALL WIDTH = 1.000 M

MEMNO	NP1	NP2	NP3	NP4	LENGTH M	INERTIA M*4
1	1	2	3	4	1.2000	.0004934
2	3	4	5	6	1.2000	.0004934
3	5	6	7	8	1.2000	.0004934
4	7	8	9	10	1.2000	.0004934
5	9	10	11	12	1.2000	.0004934
6	11	12	13	14	1.0000	.0004934
7	13	14	15	16	1.0000	.0004934
8	15	16	17	18	1.0000	.0004934
9	17	18	19	20	.3000	.0004934
10	19	20	21	22	.3000	.0004934
11	21	22	23	24	.3000	.0004934
12	23	24	25	26	.3000	.0004934
13	25	26	27	28	.3000	.0004934
14	27	28	29	30	.3000	.0004934
15	29	30	31	32	.6000	.0004934
16	31	32	33	34	.6000	.0004934
17	33	34	35	36	.3000	.0004934

NODE	KS KN/M*3	SPRINGS SOIL/A.R.	XMAX M	NODE Q KPA	NODE P KN
1	.000	.000	.0000	7.5000	5.6800
2	.000	23974.000	.0000	13.4000	16.1000
3	.000	.000	.0000	19.4000	22.5600
4	.000	.000	.0000	21.8000	26.1600
5	.000	.000	.0000	24.2000	29.0400
6	.000	.000	.0000	26.6000	29.1133
7	.000	.000	.0000	28.6000	28.6000
8	.000	.000	.0000	30.6000	30.6000
9	4060.000	637.650	.0100	32.6000	19.2267
10	4633.000	1390.500	.0150	.0000	1.6300
11	5218.000	1539.550	.0200		
12	5286.000	1585.650	.0220		
13	5351.000	1605.050	.0250		
14	5411.000	1623.100	.0250		
15	5467.000	2467.050	.0250		
16	5564.000	3336.700	.0250		
17	5644.000	2533.550	.0250		
18	5679.000	850.100	.0250		

Ks REDUCED WHEN YOU INPUT ALL VALUES

D. L. DEFL CONVERGED ON CYCLE = 2
DEFLS ARE: PREVIOUS = .01559 CURRENT = .01565 FOR EMBED DEPTH = 3.300 M

+++NON-LINEAR CHECK: CURRENT CYCLE, ICYC = 2 CURRENT SPRGS ZEROED = 1 PREVIOUS COUNT = 0
CURRENT D.L. X(I) = .01565 PREVIOUS D.L. X(I) = .00000

+++NON-LINEAR CHECK: CURRENT CYCLE, ICYC = 3 CURRENT SPRGS ZEROED = 1 PREVIOUS COUNT = 1
CURRENT D.L. X(I) = .01599 PREVIOUS D.L. X(I) = .01565

MEMBER MOMENTS, NODE REACTIONS, DEFLECTIONS, SOIL PRESSURE, AND LAST USED P-MATRIX FOR LC = 1

MEMNO	MOMENTS--NEAR END 1ST, KN-M		NODE	SPG FORCE, KN	ROT, RADS	DEFL, M	SOIL Q, KPA	P-, KN-M	P-, KN
1	.000	6.816	1	.0000	.00708	-.00398	.000	.000	5.680
2	-6.816	-97.178	2	108.4413	.00712	.00452	.000	.000	16.100
3	97.178	-174.100	3	.0000	.00657	.01286	.000	.000	22.560
4	174.101	-219.628	4	.0000	.00492	.01985	.000	.000	26.160
5	219.628	-230.307	5	.0000	.00252	.02437	.000	.000	29.040
6	230.306	-210.092	6	.0000	-.00021	.02577	.000	.000	29.113
7	210.092	-161.274	7	.0000	-.00244	.02443	.000	.000	28.600
8	161.274	-81.854	8	.0000	-.00432	.02100	.000	.000	30.600
9	81.859	-54.172	9	6.3765	-.00556	.01599*	40.600	.000	12.850
10	54.170	-31.955	10	19.8757	-.00576	.01429	66.224	.000	1.630
11	31.962	-15.523	11	19.3118	-.00589	.01254	65.453	.000	.000
12	15.521	-4.189	12	17.0673	-.00597	.01076	56.896	.000	.000
13	4.187	2.812	13	14.3948	-.00600	.00897	47.990	.000	.000
14	-2.812	6.324	14	11.6358	-.00600	.00717	38.791	.000	.000
15	-6.326	5.411	15	13.2512	-.00598	.00537	29.365	.000	.000
16	-5.411	.907	16	5.9787	-.00595	.00179	9.970	.000	.000
17	-.907	.001	17	-4.4846	-.00593	-.00177	-9.990	.000	.000
			18	-3.0167	-.00593	-.00355	-20.152	.000	.000

SUM SPRING FORCES = 208.83 VS SUM APPLIED FORCES = 208.71 KN
(*) = SOIL DISPLACEMENT > XMAX(I) SO SPRING FORCE AND Q = XMAX*VALUE ++++++++++++
NOTE THAT P-MATRIX ABOVE INCLUDES ANY EFFECTS FROM X > XMAX ON LAST CYCLE ++++

Figure E13-2*b* (*continued*) Plot file for Fig. E13-2 is not shown.

computed as shown on Fig. E13-2*a*. From this and other WEDGE trials, for horizontal dredge lines it is evident that the ρ angle for the passive pressure failure surface is $\rho_p \neq 45° - \phi/2$ except for horizontal, *cohesionless* backfills with wall $\delta = 0$. By analogy the active earth-pressure failure surface is only defined by $\rho_a = 45° - \phi/2$ for horizontal, *cohesionless* backfills also with $\delta = 0$.

The reduction factor RF = 0.725 is applied to values 9 through 17 obtained from a listing of k_s = SK(I) from the output sheet given in Fig. E13-1*f*. We must input 22 values to allow for NCYC = 5, so the last five values are computed by hand based on the depth increment DINCR = 0.3 m. With this calculation we have the following (edited input):

Node	Original k_s, kN/m³	Revised k_s, kN/m³
9	5600.	× 0.725 = 4060 (rounded)
10	6389.7	4633
11	7197.4	5218
⋮		
17	7785.4	5644
⋮		
22	7982.8	5788

These several node values are input by hand. One could have simply multiplied AS = 7000 × FAC1 × RF and BS = 1000 × FAC2 × RF and used the equation; however, the preceding table illustrates the program option for inputting node values. Actually, considerable efficiency could be obtained by editing a copy of the data set EX131.DTA to create the data set EX132.DTA for this example.

The output is shown in Fig. E13-2*b*, from which we can see the dredge line converged on the second cycle of NCYC, producing a final embedment depth of 3.0 + 0.3 = 3.3 m. The nonlinear check also cycled two times: On the first time ICYC = NCYC = 2, and for the second ICYC = 3 since only node 9 displaced such that X(9) > 0.01 m and is marked with an ∗. The dredge line displacement stabilized at X(9) = 15.99 mm > XMAX(9) = 10, which is larger than the value obtained in Example 13-1 of X(9) = 13.7 mm. We would expect that the dredge line displacement would be larger. It would be even larger for a 20° dredge line slope.

Now one can ask, is this a solution? We look at P_p from the WEDGE program and see it is 173.6 kN. The sum of the node soil reactions that are (+) is written as

$$6.41 + 19.91 + 19.34 + \cdots + 5.91 = \mathbf{107.93}\ \text{kN} < 173.6$$

This result indicates the embedment depth for this loading case is satisfactory. In fact, it might be satisfactory if the sum of soil reactions were larger than 173.6 kN since the bottom two nodes had (−) displacements (and reactions). The wall could hardly fail in a passive pressure mode (by toe kickout) with negative node displacements. If all the nodes below the D.L. were (+), we would have to look at the toe displacement and, if it were more than 1 or 2 mm, increase the embedment depth DEMB, but this depth appears adequate for this case.

Since the dredge line displacement is larger, the anchor rod force is larger (108.44 vs. 106.64 kN) than in Example 13-1. The maximum bending moment is also larger (−230.3 vs. −221.7 kN · m).

There is nothing unexpected in this analysis.

Problems occur if there a loss of dredge line or an increase in backfill surcharge. Both of these situations may call for an embedment depth larger than the current value of 3.0 m. The analysis is left as an exercise for the reader.

////

Example 13-3.

Given. The sheet-pile wall system of Fig. E13-3*a*, which is supporting 5 m of sand backfill overlying 6 m of clay. Sand data are estimated as shown, and q_u was obtained from SPT tests. We will use two anchor rods: one is placed above the water level; the lower one uses a drilled tie-back system and can be installed at low tide. From trials not shown, we tentatively choose a **PZ**40 sheet-pile section.

Required. Design the wall (at least the first cycle of the iterative design process).

Solution.

Step 1. Locate the nodes as in Fig. E13-3*b*; from these we can readily establish NP, NM, node soil starts JTSOIL, etc. as shown.

Step 2. Compute the earth-pressure profile using the Coulomb K_a, with $\delta = 17°$, and $\beta = 0$. This calculation gives $K_a = 0.277$ (from Table 11-1). The value of δ is an engineering estimate and generally ranges from about 0.5 to 0.7ϕ. We use a 17° value here because only the upper 5 m of wall is sand. A larger friction value may not develop because of the deeper clay backfill. Also K_a only varies from 0.278 to 0.275 as δ varies from 16 to 22°, so is not very sensitive in the likely range of wall friction angle.

However, there is wall adhesion in the underlying 6 m of clay, both from its being below the water table and because there is the sand acting as a surcharge to keep the clay squeezed against the wall.

Using the methods given in Chap. 11 for lateral pressure computations, we obtain the pressure profile of Fig. E13-3*c* with the following supplemental explanation. At the junction of the sand and clay layers at the water line,

$$\sigma_{a,s} = [20 + 17.9(5)]0.277 = 30.33 \text{ kPa}$$

In the clay $K_a = 1.0$, so we have

$$\sigma_{a,c} = [20 + 17.9(5)]1.0 - 2c\sqrt{1.} = 48.5 \text{ kPa}$$

Averaging for input gives

$$\sigma_a = \frac{30.3 + 48.5}{2} = 39.4 \text{ kPa}$$

Below the water line for the rest of clay,

$$\sigma_{a,c} = 48.5 + \gamma' z K_a = 48.5 + 11.0z$$

At the dredge line

$$\sigma_{a,c} = 48.5 + 11(6) = \mathbf{114.5} \text{ kPa}$$

Step 3. Obtain the moment of inertia per meter of wall width for the **PZ**40 section. From Appendix A-3*a*, we find

$$I = 335.23 \times 10^{-6} \text{ m}^4 \qquad \text{for } w = 500 \text{ mm}:$$

$$I = \frac{335.23}{0.50} = 670.0 \times 10^{-6} \text{ m}^4/\text{m}$$

$$E = 200\,000 \text{ MPa}$$

Step 4. Compute anchor rod springs per meter of wall width from the spacing of 3 m and using a rod length so the anchor is out of "active" zone (and from Example 13-2 we found we do not really know where this zone is when there is cohesive soil involved). What we will do is use program WEDGE, a wall height from the dredge line to the top of the clay, an adhesion factor of 0.8, and the sand calculated as a surcharge of

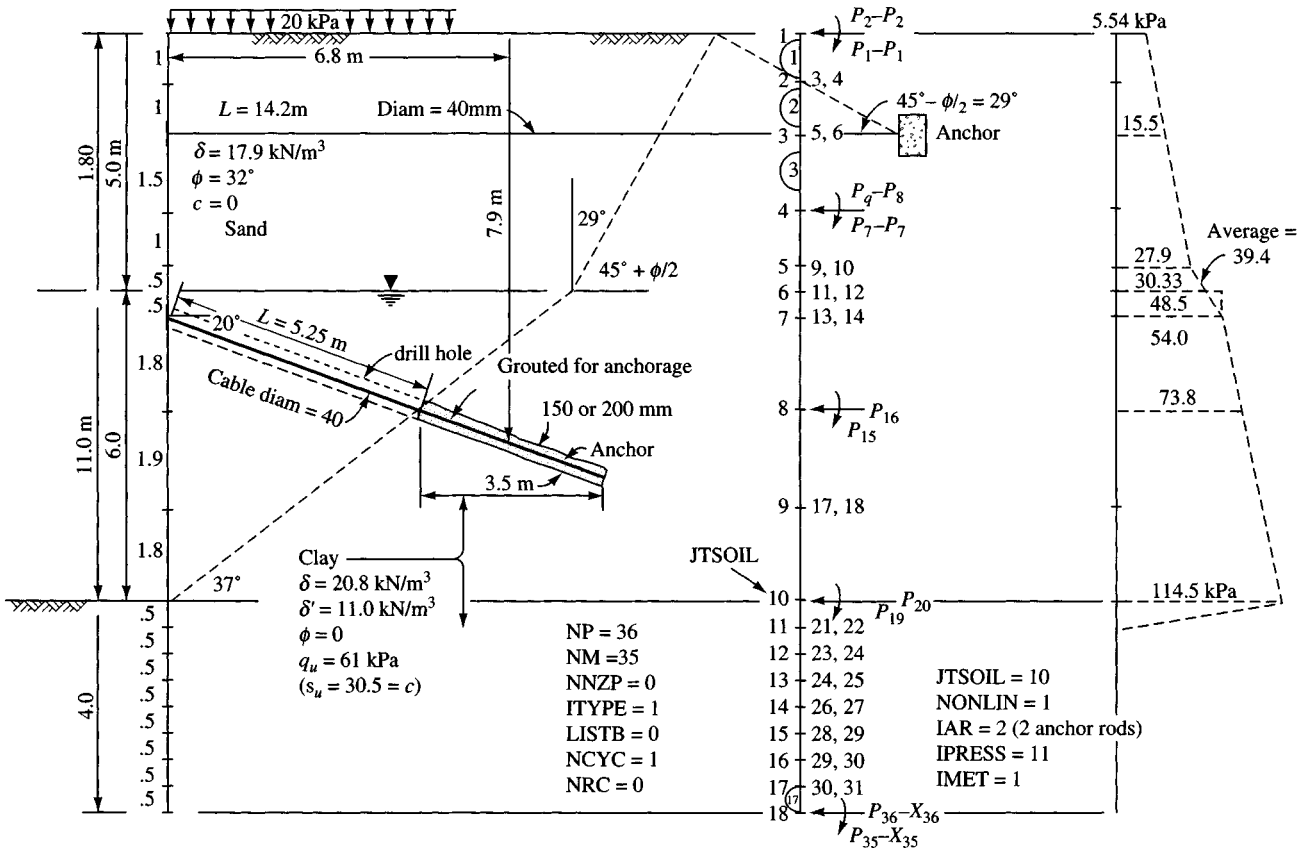

(*a*) Given condition and selected other date — tentative anchor rods and locations (nodes).

(*b*) *P*–*X* coding.

(*c*) Pressure profile.

Figure E13-3*a–c*

$$q = \text{SURCHG} = 20.0 + 5(17.9) = \mathbf{109.50}\ \text{kPa}$$

We now have a dilemma. If we directly compute the active force, we have

$$\sigma_a = (q_s + 11z) - 2c$$

$$P_p = \int_0^6 \sigma_a\, dz$$

Integrating and inserting limits, we have

$$P_p = 109.5(6) + 11(6)^2/2 - 2(30.5)(6) = \mathbf{489}\ \text{kN}$$

If we use program WEDGE, we obtain this value exactly at the Rankine $\rho = 45° + 0°/2 = 45°$. On the other hand, if we use a wall adhesion of $0.8c$, we obtain

$$P_p = 363.93\ \text{kN at}\ \rho = 37°$$

This latter value is probably more nearly correct and is used to plot the ρ angle of Fig. E13-3*a* for the clay. The conventional value of $\rho = 45° + 32°/2 = 61°$ is used for the sand. This ρ value is necessary to locate the anchor block.

The anchor block for anchor rod 1 must be located far enough from the wall so that the passive wedge ($\rho = 45° - 32°/2 = 29°$) does not intersect the active wedge from the wall. A scaled drawing should be made so that the several control dimensions can be plotted and required distances scaled. This approach tends to reduce computation errors. This plotting is shown on Fig. E13-3*a*. The design of the anchor block is considered in the next section.

Anchor 2 uses a drilled hole with grout in the zone outside the active wedge zone. The hole diameter and grout length are design parameters taken up in Sec. 13-8.

The rod diameter can be set here. After several trials, we select tentative anchor rod diameters of 40 mm for each. From scaling the drawing one obtains these lengths for the anchors:

No. 1 = 14.2 m

No. 2 = 5.25 m (only the ungrouted length that is free to elongate in the drill hole)

From these lengths and using 40-mm rod diameters ($A_r = 0.7854(0.040)^2 = 0.001\,257\ \text{m}^2$) we obtain

$$\text{ARSPRG(1)} = \frac{A_r E}{sL} = \frac{0.001\,257 \times 200 \times 10^6}{3 \times 14.2} = 5901.4\ \text{kN/m/m}$$

$$\text{ARSPRG(2)} = \frac{0.001\,257 \times 200 \times 10^6}{3 \times 5.25} \cos 20° = 14\,999.3\ \text{kN/m/m}$$

Step 5. Take $k_s = 40(\text{SF})q_a$; it was shown in Chap. 4 that within reasonable accuracy $q_a = q_u$ with SF = 3. Thus, $k_s = 40(3)(61) = 7320 \rightarrow 7300\ \text{kN/m}^3$. Use this value in the equation format of AS = 7300; BS = 0; and arbitrarily use FAC1 = 0.70 and FAC2 = 0.85.

Step 6. With these data a file EX133.DTA is built (and on your diskette) and executed to obtain the output shown on Fig. E13-3*d*.

Perform an output check as follows.

1. Sum of spring forces = 607.41 kN versus input forces computed from the input soil pressures of 607.39 kN $\rightarrow \sum F_h = 0$.
2. Dredge line node 10 (JTSOIL), node 11, and node 12 all have displacements as follows:

Node	Displ δ, mm	XMAX(I), mm
10	26.578	10.0
11	23.096	12.0
12	19.276	14.0
13	15.274	16.0

```
 DATA FOR EXAMPLE 13-3--ANCHORED WALL PZ-40 W/SURCHARGE AND 2 ANCHORS--SI

     +++++++++++++++ THIS OUTPUT FOR DATA FILE:  EX133.DTA

 SOLUTION FOR SHEET PILE WALL--CANTILEVER OR ANCHORED +++++++++++++++     ITYPE =  1

                          NO OF NP =  36                  NO OF MEMBERS = 17
              NO OF LOAD CONDITIONS =  1       NO OF BOUNDARY CONDITIONS, NZX =  0
        MAX NO OF ITERATIONS, NCYC =  1              NONLIN CHECK (IF > 0) =  1
 NO OF NODE MODULUS TO INPUT, NRC =  0            NODE SOIL STARTS, JTSOIL = 10
   LIST BAND MATRIX, LISTB (IF >0) =  0             NO OF ANCHOR RODS, IAR =  2
     INPUT NODE PRESSURES, IPRESS = 11      NO OF NON-ZERO P-MATRIX ENTRIES =  0
                                                          IMET (SI > 0) =  1

      MODULUS OF ELASTICITY =  200000.0  MPA

               SOIL MODULUS =    7300.00 +       .00*Z**EXPO      KN/M**3
   NODE Ks REDUCTION FACTORS:  JTSOIL =   .70   JSTSOIL + 1 =   .85

 SHEET PILE AND CONTROL DATA:
                        WIDTH =     1.000  M
    INITIAL EMBED DEPTH, DEMB =     4.000  M
    DEPTH INCR FACTOR, DEPINC =      .500  M
 DREDGE LINE CONVERGENCE, CONV =   .003000  M

 ANCHOR RODS LOCATED AT NODE NOS =   3   7

 MEMBER AND NODE DATA FOR WALL WIDTH =   1.000  M

                                    LENGTH    INERTIA                    KS        SPRINGS      XMAX      NODE Q    NODE P
MEMNO   NP1   NP2   NP3   NP4         M         M*4      NODE        KN/M*3       SOIL/A.R.        M         KPA       KN
   1     1     2     3     4     1.0000   .0006700        1          .000            .000       .0000    5.5400    3.5967
   2     3     4     5     6     1.0000   .0006700        2          .000            .000       .0000   10.5000   10.5067
   3     5     6     7     8     1.5000   .0006700        3          .000        5901.400       .0000   15.5000   20.3917
   4     7     8     9    10     1.0000   .0006700        4          .000            .000       .0000   22.9000   27.6083
   5     9    10    11    12      .5000   .0006700        5          .000            .000       .0000   27.9000   21.0500
   6    11    12    13    14      .5000   .0006700        6          .000            .000       .0000   39.4000   19.9583
   7    13    14    15    16     1.8000   .0006700        7          .000       14999.300       .0000   54.0000   66.8233
   8    15    16    17    18     1.9000   .0006700        8          .000            .000       .0000   73.8000  137.2083
   9    17    18    19    20     1.8000   .0006700        9          .000            .000       .0000   94.7000  174.5167
  10    19    20    21    22      .5000   .0006700       10*    5110.000        1368.750       .0100  114.5000  116.1933
  11    21    22    23    24      .5000   .0006700       11*    6205.000        3102.500       .0120     .0000    9.5417
  12    23    24    25    26      .5000   .0006700       12     7300.000        3558.750       .0140
  13    25    26    27    28      .5000   .0006700       13     7300.000        3650.000       .0160
  14    27    28    29    30      .5000   .0006700       14     7300.000        3650.000       .0180
  15    29    30    31    32      .5000   .0006700       15     7300.000        3650.000       .0200
  16    31    32    33    34      .5000   .0006700       16     7300.000        3650.000       .0200
  17    33    34    35    36      .5000   .0006700       17     7300.000        3650.000       .0200
                                                         18     7300.000        1825.000       .0200

       * = Ks REDUCED BY FAC1 OR FAC2

  +++NON-LINEAR CHECK: CURRENT CYCLE, ICYC =  0   CURRENT SPRGS ZEROED =  3   PREVIOUS COUNT =  0
            CURRENT D.L. X(I) =  .02290  PREVIOUS D.L. X(I) =   .02290
```

Figure E13-3*d*

```
+++NON-LINEAR CHECK: CURRENT CYCLE, ICYC =  1   CURRENT SPRGS ZEROED =  3   PREVIOUS COUNT =  3
          CURRENT D.L. X(I) =  .02658  PREVIOUS D.L. X(I) =    .02290


  MEMBER MOMENTS, NODE REACTIONS, DEFLECTIONS, SOIL PRESSURE, AND LAST USED P-MATRIX FOR LC =  1
MEMNO  MOMENTS--NEAR END 1ST, KN-M    NODE   SPG FORCE,   KN   ROT, RADS    DEFL,  M   SOIL Q, KPA
   1          .000        3.597        1         .0000        .00435       -.00204          .000
   2        -3.597       17.700        2         .0000        .00436        .00231          .000
   3       -17.700       10.153        3       39.5263        .00444        .00670          .000
   4       -10.153       32.728        4         .0000        .00459        .01348          .000
   5       -32.726       54.531        5         .0000        .00475        .01814          .000
   6       -54.533       86.318        6         .0000        .00492        .02056          .000
   7       -86.322     -301.951        7       346.1120       .00518        .02308          .000
   8       301.952     -451.100        8         .0000        .00373        .03188          .000
   9       451.099     -278.270        9         .0000       -.00161        .03423          .000
  10       278.269     -179.012       10       13.6875       -.00651        .02658*       51.100
  11       179.014      -93.591       11       37.2300       -.00736        .02310*       74.460
  12        93.593      -33.075       12       49.8225       -.00787        .01928*      102.200
  13        33.084        -.444       13       55.7492       -.00810        .01527       111.498
  14          .445       11.756       14       40.8830       -.00817        .01120        81.766
  15       -11.752       10.957       15       25.9906       -.00815        .00712        51.981
  16       -10.957        4.579       16       11.1635       -.00810        .00306        22.327
  17        -4.580        -.001       17       -3.5953       -.00807       -.00099        -7.191
                                       18       -9.1605       -.00807       -.00502       -36.642

    SUM SPRING FORCES =    607.41 VS SUM APPLIED FORCES =    607.39   KN
     (*) = SOIL DISPLACEMENT > XMAX(I) SO SPRING FORCE AND Q = XMAX*VALUE ++++++++++++
     NOTE THAT P-MATRIX ABOVE INCLUDES ANY EFFECTS FROM X > XMAX ON LAST CYCLE ++++


  DATA FOR PLOTTING IS SAVED TO DATA FILE: WALL.PLT
     AND LISTED FOLLOWING FOR HAND PLOTTING
                                                    SHEAR V(I,1),V(I,2)    MOMENT MOM(I,1),MOM(I,2)
 NODE   DEPTH        KS      COMP X,MM   XMAX      LT OR T    RT OR B      LT OR TOP   RT OR BOT
   1      .000        .0       -2.041    .000         .00       3.60           .00         .00
   2     1.000        .0        2.308    .000        3.60      14.10          3.60        3.60
   3     2.000        .0        6.698    .000       14.10      -5.03         17.70       17.70
   4     3.500        .0       13.482    .000       -5.03      22.57         10.15       10.15
   5     4.500        .0       18.142    .000       22.57      43.61         32.73       32.73
   6     5.000        .0       20.556    .000       43.61      63.57         54.53       54.53
   7     5.500        .0       23.075    .000       63.57    -215.71         86.32       86.32
   8     7.300        .0       31.877    .000     -215.71     -78.50       -301.95     -301.95
   9     9.200        .0       34.229    .000      -78.50      96.02       -451.10     -451.10
  10    11.000     5110.0       26.578  10.000       96.02     198.51       -278.27     -278.27
  11    11.500     6205.0       23.096  12.000      198.51     170.85       -179.01     -179.01
  12    12.000     7300.0       19.276  14.000      170.85     121.03        -93.59      -93.59
  13    12.500     7300.0       15.274  16.000      121.03      65.28        -33.08      -33.08
  14    13.000     7300.0       11.201  18.000       65.28      24.40          -.44        -.45
  15    13.500     7300.0        7.121  20.000       24.40      -1.59         11.76       11.75
  16    14.000     7300.0        3.058  20.000       -1.59     -12.76         10.96       10.96
  17    14.500     7300.0        -.985  20.000      -12.76      -9.16          4.58        4.58
  18    15.000     7300.0       -5.019  20.000       -9.16        .00           .00         .00
```

Figure E13-3*d* (*continued*)

Nodes 10, 11, and 12 are marked with an asterisk (*) on Fig. E13-3*d* for rapid identification that X > XMAX(I). The anchor rod forces and pile moments include the effect of this nonlinear check.

3. The maximum sheet-pile moment of 451.10 kN·m occurs at node 9, and the bending stress is computed as

$$f_s = M/S = 451.10/S$$

$$S = \frac{1.632 \times 10^{-3}}{0.50} = 0.003\,264\ \text{m}^3/\text{m}$$

and inserting values (10^3 converts kN to MN) obtain

$$f_s = \frac{451.1}{0.003\,264 \times 10^3} = \mathbf{138.2}\ \text{MPa} < f_a$$

This stress is satisfactory for A328 steel with $f_y = 250$ MPa and an allowable bending stress of $f_a = 0.65 f_y = 160$ MPa.

4. The anchor rod stresses (based on the 3-m spacing s) are next checked:

Rod 1: $A_r = 0.001\,257\ \text{m}^2$ $\quad P = 39.53s = 39.53 \times 3.0 = 118.59$ kN

$$f_s = \frac{P}{A_r} = \frac{118.59}{1.257} = \mathbf{94.34}\ \text{MPa (since } 10^{-3} \times 10^3 = 1.0\text{)}$$

(O.K. for $f_y = 250$ MPa grade steel)

Rod 2: $P = P_h/\cos 20^\circ = 346.11 \times 3/\cos 20^\circ = 1105.0$ kN

$$f_s = \frac{P}{A_r} = \frac{1105.0}{1.257} = \mathbf{879.1}\ \text{MPa}$$

The stress in anchor 2 is so high it would require using either a larger rod diameter or using high-strength rods or cables as used for prestressed concrete. If you try a larger rod diameter, you must recompute the spring and rerun the problem.

5. Check the computed soil pressures. The output sheet shows the soil pressures for critical nodes as follows:

Node	q, kPa	q_a, kPa
11	74.5	61
12	102.2	61
13	111.5	61
14	81.8	61

These soil pressures are not failure values, for q_{ult} is theoretically on the order of $3 \times 61 = 183$ kPa. Also the passive earth force is 415.4 kN, which is greater than the sum of the (+) soil reactions from the dredge line of 234.5 kN. Note that the bottom two nodes kick back [(−) X(I)] into the backfill. Considering these two data items, the wall should be stable for this load case. The only problem is that anchor rod No. 2 may require a larger diameter rod and/or use of prestressed steel cables.

Summary

1. The dredge line soil appears adequate.
2. The sheet-pile section seems satisfactory.

3. Anchor rod No. 2 may be overstressed. It may require a larger diameter rod or use of very-high-strength steel cable. Another possibility is to see if it can be relocated to a lower depth.
4. Anchor rod No. 1 appears overdesigned, but you can check by using a 30-mm diameter rod to see what happens.

////

The next example is a cantilever retaining wall. The basic difference between the anchored and cantilever wall is that the latter does not use an anchor rod. Another difference is that the cantilever wall is usually limited in height to about 3 to 4 m because without an anchor very large translation X(I) values result, that produce large bending moments. The principal advantage in not using an anchor is economy since the anchor, anchorage, and installation costs are considerable. Adjacent property owners may not allow entry to install anchorage. In those cases where a cantilever wall is higher than 3 to 4 m it may be necessary to use some of the special sections shown in Fig. 13-6. Since some of these built-up sections are more than 1 m in width, it is necessary to divide by their width to obtain the unit width values for use in these analyses.

Example 13-4. Make a tentative design for the cantilever wall shown in Figs. E13-4*a*, *b*, and *c*.

Solution.

Step 1. Do the necessary coding and compute the node pressures to the dredge line as shown in the figures. Note that several preliminary executions were made so that the output could be minimized. From the preliminary trials it appears that a PZ27 section can be used. The resulting moment of inertia is

$$I = \frac{115.0 \times 10^{-6}}{0.460} = 0.2500 \times 10^{-3} \text{ m}^4/\text{m}$$

Step 2. An initial embedment depth DEMB = 4.0 m is chosen (based on previous trials) with NCYC = 1 and NONLIN = 1 so the embedment depth is not increased. The soil below the dredge line is checked for any X(I) > XMAX(I). Most cantilever walls will require an embedment depth $D \approx$ height of wall above the D.L.

Step 3. Obtain the modulus of subgrade reaction k_s. Since the soil is layered it will be best to input node values that are hand-computed. The first two nodes will be reduced by FAC1, FAC2 as shown following.

For the sand, we use the bearing-capacity equation and obtain from Table 4-4 for Hansen's equation the following:

$$\text{For } \phi = 32^\circ : N_q = 23.2; N_\gamma = 20.8$$
$$k_s = 40[16.50(23.2)Z^1 + 0.5(16.5)(1.0)(20.8)]$$
$$k_s = \text{SK(I)} = 6864 + 15\,312Z^1 \rightarrow 6800 + 15\,300Z \qquad \text{(rounding)}$$

Using these values we obtain the following (Note: The first two nodes are reduced using FAC1, FAC2):

For node 1: $\text{SK(1)} = 0.7(6800 + 0.) = \mathbf{4760}$ kN/m^3

node 2: $\text{SK(2)} = 0.8[6800 + 15\,300(0.5)] = \mathbf{11\,560}$

node 3: $\text{SK(3)} = 6800 + 15\,300(1) = \mathbf{22\,100}$

node 4: $\text{SK(I)} = 6800 + 15\,300(1.5) = \mathbf{29\,750}$

but node 4 is interfaced with the clay.

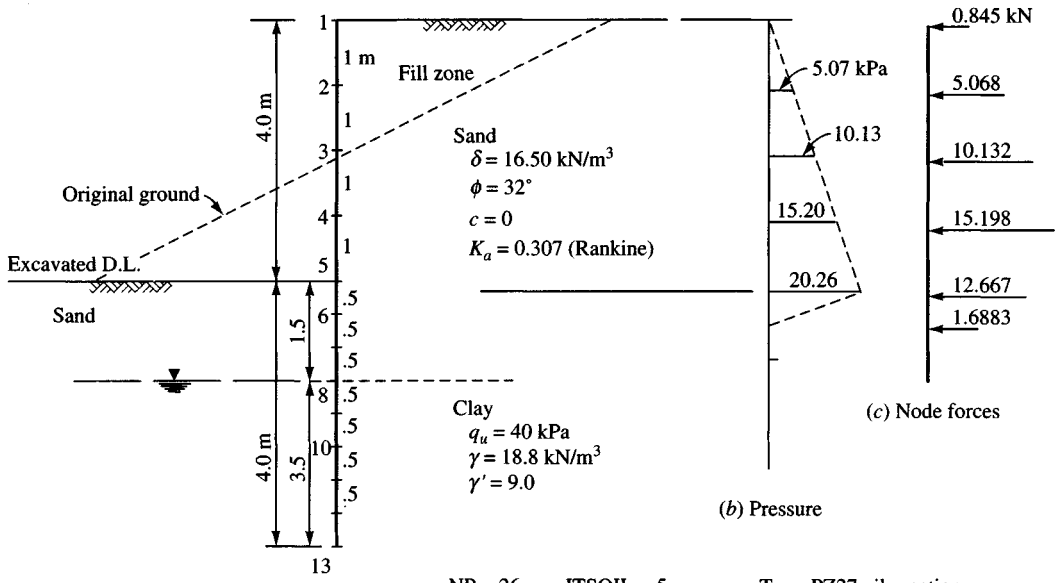

NP = 26	JTSOIL = 5	Try a PZ27 pile section
NM = 12	NONLIN = 1	
NNZP = 0	IAR = 0 (no anchor)	$E = 200\,000$ MPa $f_y = 250$ MPa
NLC = 1	NZX = 0	$\text{DEMB}_{\text{initial}} = 4.0$ m
ITYPE = 1	IPRESS = 6	
LISTB = 0	IMET = 1	
NCYC = 1		
NRC = 0	Input SK (I) = NM – JTSOIL + 2 = 9	
	Input XMAX (I) = SK (I) = 9	
	FAC1 = 0.7; FAC2 = 0.8 and used on SK (I) before input	

Figure E13-4*a–c*

For the clay use $k_s = 40(\text{SF})q_a$, but $q_a = q_u$ with SF = 3.0. With these values we find

$$k_s = \text{SK(I)} = 40(3)(40) = \mathbf{4800}\ \text{kN/m}^3$$

We calculate an average SK(3) as

$$(29\,750 + 4800)/2 = \mathbf{17\,275}\ \text{kN/m}^3$$

For SK(4) through end of SK(I) the value is 4800 kN/m^3.

Step 4. With the preceding data for moment of inertia XI(I), SK(I), and the control parameters shown on the figure, data file EX134.DTA is created (also on your diskette). The execution gives Fig. E13-4*d* from which we can make the following observations:

a. The final depth $D_f = D_i = 4.0$ m, which appears adequate. Five nodes have (−) displacement toward the backfill side. Three nodes have a (+) displacement, and node 5 has X(5) = 7.9 mm > XMAX(5) of 6.0 mm—it is marked with an * for rapid notice.

b. The displacement of the top (node 1) is 33.983 mm, which may be noticeable. It can only be reduced by using a stiffer section or by using an anchorage of some type.

c. The maximum bending moment occurs at node 7 (not at dredge line node 5) and is 72.18 kN·m. For $f_y = 250$ MPa the allowable stress $f_a = 0.65f_y = 0.65(250) = 162.5$ MPa. The section modulus of the **PZ**27 is

$$S = \frac{0.742 \times 10^{-3}}{0.460} = 1.620\ \text{m}^3/\text{m}$$

EXAMPLE 13-4 CANTILEVER SHEET-PILE WALL USING A PZ-27 SECTION 4-M HIGH--SI

++++++++++++++++ THIS OUTPUT FOR DATA FILE: EX134 DTA

SOLUTION FOR SHEET PILE WALL--CANTILEVER OR ANCHORED ++++++++++++++ ITYPE = 1

NO OF NP =	26	NO OF MEMBERS =	12
NO OF LOAD CONDITIONS =	1	NO OF BOUNDARY CONDITIONS, NZX =	0
MAX NO OF ITERATIONS, NCYC =	1	NONLIN CHECK (IF > 0) =	1
NO OF NODE MODULUS TO INPUT, NRC =	9	NODE SOIL STARTS, JTSOIL =	5
LIST BAND MATRIX, LISTB (IF >0) =	0	NO OF ANCHOR RODS, IAR =	0
INPUT NODE PRESSURES, IPRESS =	6	NO OF NON-ZERO P-MATRIX ENTRIES =	0
		IMET (SI > 0) =	1

MODULUS OF ELASTICITY = 200000.0 MPA

SHEET PILE AND CONTROL DATA:

WIDTH =	1.000	M
INITIAL EMBED DEPTH, DEMB =	4.000	M
DEPTH INCR FACTOR, DEPINC =	.500	M
DREDGE LINE CONVERGENCE, CONV =	.003000	M

MEMBER AND NODE DATA FOR WALL WIDTH = 1.000 M

MEMNO	NP1	NP2	NP3	NP4	LENGTH M	INERTIA M*4	NODE	KS KN/M*3	SPRINGS SOIL/A.R.	XMAX M	NODE Q KPA	NODE P KN
1	1	2	3	4	1.0000	.0002500	1	.000	.000	.0000	.0000	.8450
2	3	4	5	6	1.0000	.0002500	2	.000	.000	.0000	5.0700	5.0683
3	5	6	7	8	1.0000	.0002500	3	.000	.000	.0000	10.1300	10.1317
4	7	8	9	10	1.0000	.0002500	4	.000	.000	.0000	15.2000	15.1983
5	9	10	11	12	.5000	.0002500	5	4760.000	1756.667	.0060	20.2600	12.6633
6	11	12	13	14	.5000	.0002500	6	11560.000	6091.667	.0100	.0000	1.6883
7	13	14	15	16	.5000	.0002500	7	22100.000	9769.583	.0150		
8	15	16	17	18	.5000	.0002500	8	17275.000	8000.000	.0200		
9	17	18	19	20	.5000	.0002500	9	4800.000	3439.583	.0250		
10	19	20	21	22	.5000	.0002500	10	4800.000	2400.000	.0250		
11	21	22	23	24	.5000	.0002500	11	4800.000	2400.000	.0250		
12	23	24	25	26	.5000	.0002500	12	4800.000	2400.000	.0250		
							13	4800.000	1200.000	.0250		

Ks REDUCED WHEN YOU INPUT ALL VALUES

+++NON-LINEAR CHECK: CURRENT CYCLE, ICYC = 0 CURRENT SPRGS ZEROED = 1 PREVIOUS COUNT = 0
CURRENT D.L. X(I) = .00759 PREVIOUS D.L. X(I) = .00759

Figure E13-4*d*

```
+++NON-LINEAR CHECK: CURRENT CYCLE, ICYC =  1   CURRENT SPRGS ZEROED =  1   PREVIOUS COUNT =  1
          CURRENT D.L. X(I) =  .00793  PREVIOUS D.L. X(I) =    .00759

  MEMBER MOMENTS, NODE REACTIONS, DEFLECTIONS, SOIL PRESSURE, AND LAST USED P-MATRIX FOR LC =  1
MEMNO  MOMENTS--NEAR END 1ST, KN-M    NODE   SPG FORCE,   KN   ROT, RADS    DEFL,  M   SOIL Q, KPA    P-, KN-M      P-,   KN
   1          .000         .846        1         .0000        -.00675       .03398          .000         .000         .845
   2         -.845        6.759        2         .0000        -.00674       .02723          .000         .000        5.068
   3        -6.758       22.804        3         .0000        -.00667       .02052          .000         .000       10.132
   4       -22.803       54.047        4         .0000        -.00637       .01397          .000         .000       15.198
   5       -54.046       70.730        5       10.5400        -.00560       .00793*       28.560         .000        2.123
   6       -70.730       72.178        6       32.1572        -.00498       .00528        61.024         .000        1.688
   7       -72.178       59.132        7       28.9872        -.00427       .00297        65.573         .000         .000
   8       -59.132       42.071        8        8.0328        -.00361       .00100        17.346         .000         .000
   9       -42.070       26.155        9       -2.2927        -.00310      -.00067        -3.199         .000         .000
  10       -26.155       12.791       10       -5.1022        -.00276      -.00213       -10.204         .000         .000
  11       -12.791        3.569       11       -8.2857        -.00257      -.00345       -16.571         .000         .000
  12        -3.569         .000       12      -11.3074        -.00248      -.00471       -22.615         .000         .000
                                      13       -7.1375        -.00247      -.00595       -28.550         .000         .000

   SUM SPRING FORCES =     45.59 VS SUM APPLIED FORCES =     45.60   KN
    (*) = SOIL DISPLACEMENT > XMAX(I) SO SPRING FORCE AND Q = XMAX*VALUE ++++++++++++
    NOTE THAT P-MATRIX ABOVE INCLUDES ANY EFFECTS FROM X > XMAX ON LAST CYCLE ++++


  DATA FOR PLOTTING IS SAVED TO DATA FILE: WALL.PLT
     AND LISTED FOLLOWING FOR HAND PLOTTING
                                                  SHEAR V(I,1),V(I,2)    MOMENT MOM(I,1),MOM(I,2)
  NODE   DEPTH        KS      COMP X,MM   XMAX     LT OR T   RT OR B      LT OR TOP   RT OR BOT
    1     .000         .0       33.983    .000        .00       .85           .00         .00
    2    1.000         .0       27.234    .000        .85      5.91           .85         .84
    3    2.000         .0       20.518    .000       5.91     16.05          6.76        6.76
    4    3.000         .0       13.971    .000      16.05     31.24         22.80       22.80
    5    4.000      4760.0        7.932   6.000      31.24     33.37         54.05       54.05
    6    4.500     11560.0        5.279  10.000      33.37      2.90         70.73       70.73
    7    5.000     22100.0        2.967  15.000       2.90    -26.09         72.18       72.18
    8    5.500     17275.0        1.004  20.000     -26.09    -34.12         59.13       59.13
    9    6.000      4800.0        -.667  25.000     -34.12    -31.83         42.07       42.07
   10    6.500      4800.0       -2.126  25.000     -31.83    -26.73         26.16       26.16
   11    7.000      4800.0       -3.452  25.000     -26.73    -18.44         12.79       12.79
   12    7.500      4800.0       -4.711  25.000     -18.44     -7.14          3.57        3.57
   13    8.000      4800.0       -5.948  25.000      -7.14       .00           .00         .00
```

Figure E13-4*d* (*continued*)

$$f_s = \frac{72.18}{1.620} = \mathbf{44.55}\ \text{MPa} \ll 162.5$$

Is this wall overdesigned? If the client will accept a much larger displacement at node 1, it may be possible to use a **PZ**22. It probably is not necessary to increase the embedment depth. It may be prudent to place a surcharge on the backfill of about 20 kPa and rerun the program to see if the embedment depth and section are still adequate. If they are not it may be necessary to increase the embedment by another 0.5 m and/or use a stiffer section. This latter check is your *stability* analysis.

////

13-8 ANCHOR RODS, WALES, AND ANCHORAGES FOR SHEETPILING

This section will consider additional factors in the design of anchored sheet-pile walls.

13-8.1 Anchor Rods

The FEM analysis for the anchored sheet-pile walls of Examples 13-1, 13-2, and 13-3 illustrated that the design of the anchor rods is closely associated with the total design. That is, we must assume some size rod[6] and its length. From this an anchor rod spring (AE/L) is computed as part of the input data.

The program output gives an anchor force for that anchor section used, and the following criteria must be met:

1. The anchor node displacement must be large enough that active earth pressure can develop behind the wall. This δ is usually on the order of $0.001H$, where H is the free height from the dredge line to the anchor rod node.
2. The allowable tensile stress

$$f_s = \frac{F_{\text{ar}}}{A_r} \le f_a$$

where $f_a = 0.6$ to $0.75 f_y$. The factors to reduce f_y to the allowable stress f_a are the necessary rod safety factor for that anchor rod force F_{ar}.

The force (and the pile bending moment) also depends on anchor rod location (analyses not shown). Thus, in a design one must first try a given node as in Example 13-1 until a reasonable solution seems to be found. Then one shifts the anchor rod location *if this is possible* and makes additional trials to attempt to find the lightest pile section and smallest-diameter anchor rod consistent with the given wall specifications + any stability cases checked.

There are several complications to consider in addition to the foregoing two basic considerations:

1. If the soil beneath the anchor settles away from the rod it becomes unsupported and must carry its self-weight + any fraction of the upper soil assigned to the rod as a strip load.

[6]Although the term *rods* is used and implies a round solid bar, in practice the rod may be either a rod or a large wire strand cable.

Usually there is some arching, so the full column of soil over the rod may not bear on it; however, a small-diameter rod in a long span can develop significant bending moments just from self-weight. A small-diameter rod will have a very small section modulus S, so the increase in the tension stresses from bending can be substantial.

2. It has been suggested that one should put a negative camber into the rod, using seating blocks (or props), in anticipation of rod sag from item 1. This may be difficult to do since backfill placed over the rod and the several seating blocks would cause settlement of both the underlying soil and the blocks themselves. Seating blocks may be practical in original ground, but this is seldom where the anchor rod is located.
3. Some persons suggest placing the anchor rod in a hollow tube that is supported by the backfill so that the rod is initially unsupported. This method is a solution only if the tube containing the rod does not settle into (or with) the fill.

13-8.2 Wales

Wales are longitudinal members running parallel with and in close contact with the wall, as shown in Fig. 13-9. They may be located on either the front or back face of the wall. The back face location is desirable in certain cases for both appearance and clearance, but it will require both a work space and adequate attachment to the wall by bolting or welding to support the anchor rod pull. Back face wales are most often attached by field-welding.

Bolting is difficult for either face location, since bolt holes shop-drilled in the sheetpiling by the steel fabricator seldom align with the wale after the piles are driven. On the other hand it is very difficult to field-drill large-diameter bolt holes in the driven piles using hand drills.

Wales on the front face are somewhat easier to install but also require a hole through the wall for the anchor rod—usually made by burning with an acetylene torch. Again, shop holes for bolting are not practical; however, here the wale usually covers the hole, so ragged edges of burned holes are not noticeable.

Wales are usually made from a pair of back-to-back channels with spacing for the anchor rod. Sometimes a pair of I beams is used; however, **W** shapes having wide flanges are not suitable unless the flanges are braced so they do not bend.

It is usually permissible to use large bending stresses—as much as $0.9f_y$ in the wales; however, the wales must be sufficiently rigid to transfer the anchor force laterally over the anchor spacings s (of Fig. 13-9*c*) to satisfy the mathematical model. If there is very much lateral displacement between anchor spacings, most of the anchor force will be concentrated at the anchor. At best, this effect produces an unsightly wall, but more importantly soil moves into those "bulged" regions and backfill settlements occur. This causes pavement cracks; and if structures are near the wall they may crack and even collapse. Thus, anchor rod spacing s is a significant design parameter.

Since wale fixity is fairly certain only at the anchor points, it is usual to use the assumptions shown in Fig. 13-9*c*. The wales are assumed to carry a uniform load w of intensity shown, and if we assume an approximate fixed end beam the bending moment at any anchor point (which will be the maximum) is

$$M \approx \frac{ws^2}{10} \quad \text{or} \quad \frac{ws^2}{12}$$

Usually the larger of the two approximations is used.

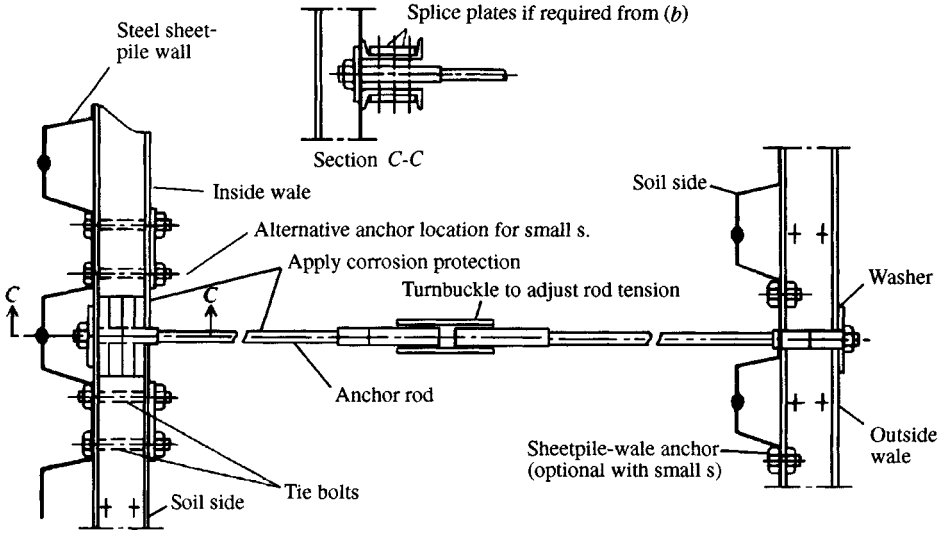

(*a*) Front of wall or back of wall

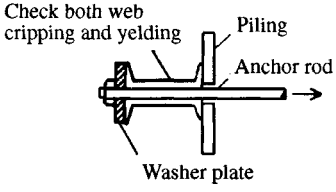

(*b*) Web cripping check

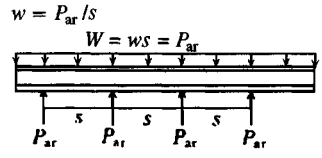

(*c*) Wale design for bending assuming a uniform pressure from anchor rods.

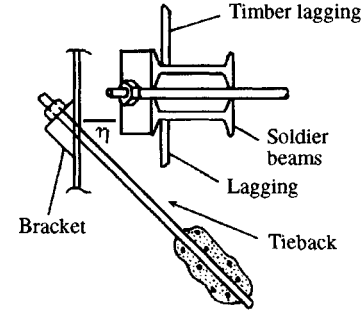

(*d*) Paired soldier beams used in a tieback anchor system without using wales.

Figure 13-9 Wale location and design.

Web crippling should be checked at the anchor locations as shown in Fig. 13-9*b*, for very high stresses can develop from the anchor rod force. Web crippling can be checked using the procedure given by the AISC (1989 or later) *ASD* manual.

Example 13-5. Tentatively design wales for the lower anchor rod of Example 13-3 assuming the output is satisfactory. Consider a typical wale section on an *interior* span of $s = 3$ m as in Fig. E13-5. Try to use a pair of channels back to back with $f_y = 250$ MPa (A-36). From the computer output (Fig. E13-3*d*) the axial anchor rod force per meter was found to be

$$F_{ar} = 346.11/\cos 20^\circ = \mathbf{368.32}\ \text{kN/m}$$

Solution. The anchor rod force per meter is the uniform pressure on the wale. Using the previously given moment approximation, compute the following

$$M = \frac{ws^2}{10} = \frac{368.32 \times 3^2}{10} = \mathbf{331.49}\ \text{kN} \cdot \text{m}$$

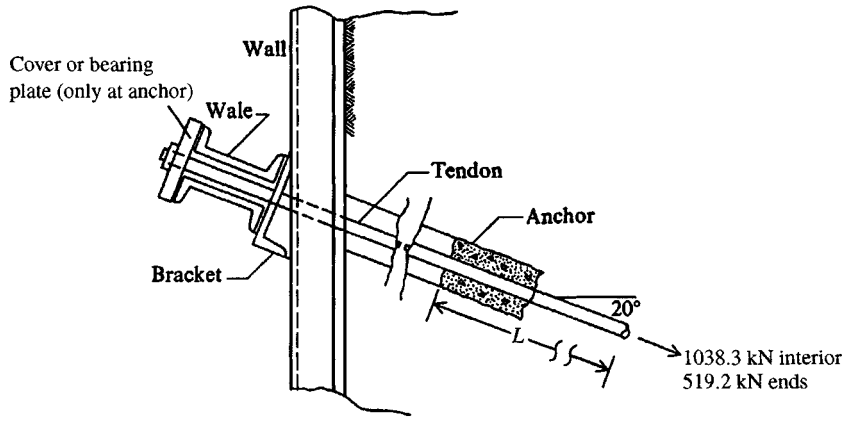

Figure E13-5

Using an allowable bending stress of $0.75f_y$ provides a nominal SF = 1/0.75 = 1.33 and f_a = 0.75(250) = **190** MPa. The required section modulus for two channels is

$$f_a = \frac{M}{S} \rightarrow S = \frac{M}{f_a}$$

$$S_x = \frac{331.49}{190\,000} = 1.745 \times 10^{-3}\ \text{m}^3$$

For a single channel

$$S_x = \frac{1.745 \times 10^{-3}}{2} = 0.8723 \times 10^{-3}\ \text{m}^3$$

From tables of rolled sections in metric units in the AISC (1992) manual we find the largest available channel is the only section that can be used:

Use **C**380 × 74 : d = 381 mm b_f = 94.4 mm t_w = 18.2
(**C**15 × 50) : t_f = 16.5 k = 37.0 mm

$$S_x = 0.882 \times 10^{-3}\ \text{m}^3 \qquad I_x = 168 \times 10^{-6}\ \text{m}^4$$

1. Find the approximate deflection between two anchor points for the wale assuming a *fixed end* beam with an L = 3 m:

$$\Delta_c = \frac{wS^4}{384EI} \qquad \text{(AISC (1989) handbook equation)}$$

Inserting values (E = 200 000 MPa), we find the deflection (using 2 channels) is

$$\Delta_c = \frac{368.32 \times 3^4}{384 \times 200 \times 10^6 \times (2 \times 168 \times 10^{-6})} = 1.16 \times 10^{-3} = 1.16\ \text{mm}$$

This displacement is quite adequate.

2. Check web yielding and crippling under the anchor plate, which is somewhat limited in area. To cover the two channel flanges and leave a 45-mm space for the 40-mm diameter anchor rods assumed in Example 13-3, a cover plate width (Fig. E13-5) will have to be

$$w_p = 2b_f + 45 = 2 \times 94.4 + 45 = 233.8 \rightarrow \mathbf{235}\ \text{mm}$$

Make the plate length $L_p = w_p = 235$ mm as well.

For channel web yield, check an end anchor where the contributory length = $s/2 = 3/2 = 1.5$ m and

$$F_{ar} = 368.32 \times 1.5 = \mathbf{552.5}\ \text{kN}$$

The AISC [9th ed., *ASD*, Eq. (*K*1-3)] equation is

$$\frac{P}{2} = 0.66 f_y t_w (N + 2.5k)$$

Substituting values ($N = w_p = 235$ mm; from above, $k = 37$ mm; $t_w = 18.2$ mm; and previously $f_y = 250$ MPa) we obtain

$$\frac{P}{2} = 0.66 \times 250 \times 10^3 \times 0.0182(0.235 + 2.5 \times 0.037) = \mathbf{983.5}\ \text{kN} > 552.5$$

Web yielding in the channel is clearly adequate.

3. Check channel web crippling using AISC [9th ed., *ASD*, Eq. (*K*1-5)]. The equation is

$$\frac{P}{2} = C t_w^2 \left[1 + 3\left(\frac{N}{d}\right)\left(\frac{t_w}{t_f}\right)^{1.5}\right] \sqrt{f_y t_f / t_w} \qquad \text{(per channel)}$$

where $C = 89$ for ends and 176.7 for interior nodes. Since the end node is more critical, use $C = 89$ and substitute (1000 kN/MN) to obtain

$$\frac{P}{2} = 34 \times 0.0182^2 \left[1 + 3\left(\frac{235}{381}\right)\left(\frac{18.2}{16.5}\right)^{1.5}\right] \sqrt{250(16.5/18.2)} \times 1000$$

$$P = 89 \times 0.0182^2 [3.14] \times 15.05 \times 1000 \times 2 = \mathbf{2986} \gg 2(552.5)$$

For interior nodes $P = 2786(176.7)/89 = 5531 \gg 2(552.5)$.
Web crippling is not a critical design item here.

////

13-8.3 Sheet-Pile Anchorages

Anchorage for sheet piles may be obtained from large cast-in-place concrete blocks (usually square and of necessary length) or precast concrete blocks that are embedded in the soil some depth (Fig. 13-10*a*). Instead of using a concrete block of some length, a row of sheetpiling that is similar to the supported wall but of shorter length may be driven, as in Fig. 13-10*d*; alternate pairs may be driven deeper for additional stability. As shown, a wale is used to carry the anchor rod force.

Piles may be driven as in Fig. 13-10*b* and *c*, and some authorities suggest these are the most reliable of the several anchorages. A surface paved with concrete may be extended (with edge thickened and reinforced) to provide an encasement for the top node region of the sheet pile instead of using a top anchor. This generally fixes the top against both translation and displacement and is efficiently handled with the FEM program using boundary conditions. Top fixity may reduce the pile bending moments, but the results depend on an interaction of wall height, pile stiffness, and whether the node is both fixed for no rotation and translation or just fixed for no translation.

TIEBACKS. One of the most popular anchorage methods presently used is the *tieback* of Fig. 13-10*e*. These are essentially small piles oriented at about $\eta = 15$ to 25° from the horizontal.

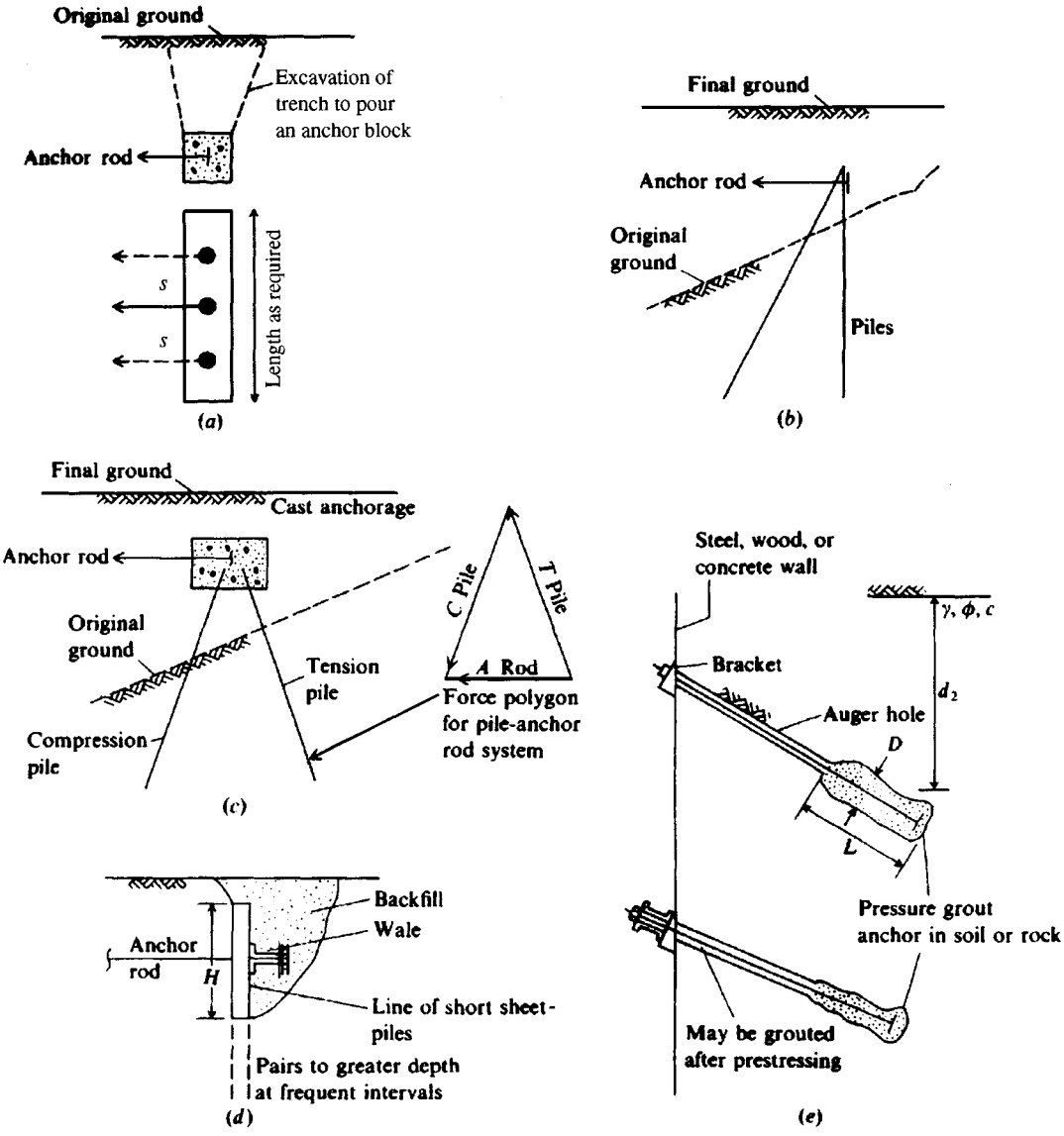

Figure 13-10 Sheet pile anchorages: (*a*) Cast-in-place anchor block; (*b, c*) pile configurations used as anchorages; (*d*) short sheet-pile wall used as anchorage; (*e*) tie-back anchor.

By using small slopes the vertical stress component on the wall can be neglected. Tiebacks are constructed by drilling a hole on the order of 150 to 375 mm in diameter using a hollow-stem auger. The anchor cable or rod, with an expandable end plate (or toggle), is pushed or carried in the hollow stem of the auger and at the design depth is extruded. Then the end plate/toggle is expanded. The end plate greatly increases the pull-out resistance of the anchor from the concrete shaft. The auger is slowly withdrawn, and simultaneously concrete or sand-cement grout (with either material containing appropriate admixtures), usually of about $f_c' \approx 21$ MPa, is forced through the hollow stem. The concrete/grout is under a pressure of from 75 to 225 kPa so that it expands around the cable/rod for bond and against the soil to produce

an irregular surface for friction/adhesion. A grouting pressure is used to approximate K_o^+ conditions so that the soil-anchor friction angle $\delta \rightarrow \phi$ or, if cohesive, an adhesion such that $c_a \rightarrow c$.

High-strength steel (f_y on the order of 1000 to 14 000 MPa) tendons or rods are generally used for tieback anchors because they are usually prestressed to a design force computed using methods of the next chapter. High-strength steel is used instead of regular structural steel with an $f_y = 250$ MPa (A36) so that after soil creep and steel relaxation occur there is a substantial holding force remaining in the "tieback."

Tieback walls are often used in deep excavations where it is essential that lateral wall movements and subsequent perimeter settlements be minimized. An advantage of these walls is they can be constructed from the top down (built as excavation proceeds). Another advantage is they do not produce obstructions in the construction area. Often these walls are left in place and become part of the final construction.

They have the disadvantages that adjacent property owners must give permission and that underground utilities must not be encountered.

Only a part of the drilled depth is backfilled with concrete. A part must be left free so that the anchor cable can elongate (with no length in which to develop $e = PL/AE$, it would pull apart). The force used to develop the prestress is always larger than the design force (the designer knows the soil will creep and the steel will relax), so effectively the anchor is *proof* tested during installation. If the rod or cable does not pull apart or the assembly pull out, the design is adequate.

The tieback anchor design can be made with reference to Fig. 13-10*e* as

$$P_{ar} = \pi DL[\gamma d_2 K \tan \delta + c_a] \tag{13-7}$$

where D = average shaft diameter; compute based on volume of concrete pumped, together with the original and final hole depths, m or ft

L = length of cement/grout; compute based on original and final hole depth, m or ft

K = soil coefficient—between K_a and K_o

d_2 = average depth of grouted length L, m or ft

δ = soil-cement friction coefficient and $\rightarrow \phi$

c_a = adhesion to cement zone—0.7 to 1.0c, kPa or ksf

If the anchorage is belled, you can use Eq. (4-25).

Additional details on prestressed anchors may be found in PCI (1974), Ware et al. (1973), and Oosterbaan and Gifford (1972). The methodology is well-established, so there is a scarcity of very recent publications.

Example 13-6. Tentatively size the concrete shaft of the tie-back anchor of Example 13-3 for the anchor force of 3(368.32) = 1104.96 kN (refer to Figs. E13-3*a* and E13-5 for other data).

Solution. Try a 350-mm nominal anchor shaft diameter. Take adhesion as $0.8s_u$($s_u = q_u/2 = 61/2 = 30.5$ kPa). Assume that CU conditions will be obtained around the shaft perimeter from the pressure grouting. This state will produce a small angle of internal friction of about $\phi = 20°$. We will also assume the grout pressure produces K_o conditions so that $K = K_o = 1 - \sin 20° = 0.66$ and the friction angle $\delta = \phi = 20°$.

We are making this design with less than ideal soil data—often the case in practice. In the absence of better data we do the best we can. Proof loading of the anchor will quickly indicate if the design is inadequate. With these estimates we will use Eq. (13-7):

$$P_{ar} = \pi DL[\gamma d_2 K \tan\delta + c_a]$$

From a scale drawing of Fig. E13-3*a* we obtain a tentative vertical average distance $d_2 \approx 10$ m (we may have to make more than one trial to obtain compatible d_2 and embedment length L). Five meters of this depth is sand to the water line; the remaining 5 m is clay soil below the water line, requiring using $\gamma' = 20.8 - 9.8 = 11.0$ kN/m^3. Substituting values into Eq. (13-7) we obtain

$$\begin{aligned} P_{ar} &= L(\pi \times 0.350)[(5 \times 17.9 + 5.0 \times 11)(0.66 \times \tan 20°) + 0.8 \times 30.5] \\ &= L(1.10)[(144.5)(0.2402) + 24.4] \\ &= L(1.10)(34.7 + 24.4) = L(65.01) \end{aligned}$$

Since axial $P_{ar} = 3(368.32) = 1104.96$ kN, solving for L gives

$$L = \frac{1104.96}{65.01} = \mathbf{17.00}\text{ m}$$

The total anchor rod/cable Ltot $= 5.25 + 17.00 = \mathbf{22.2}$ m. The vertical force/meter of wall $F_v = 368.32 \sin 20° = \mathbf{126.0}$ kN. This value of L is reasonably consistent with d_2 used, so we may take this as a valid solution—unless the anchor fails during installation.

////

BLOCK[7] ANCHORS. The block anchor is a cast-in-place or precast concrete member that may be square or rectangular in section with the necessary length to develop adequate passive resistance for one or more anchor rods/cables attached along its length.

A general equation can be developed for a block anchor using Fig. 13-11*b* and noting that P'_a may not fully develop unless the anchor translates toward the wall a small amount, and P'_p similarly may not fully develop unless there is sufficient translation. For these reasons the values are given primed superscripts. With this understood, we obtain the general equation as follows:

$$\sum F_h = F_{ar} - L(P'_p - P'_a + F_{top} + F_{bot})$$

Solving and including an SF, we obtain

$$F_{ar} = \frac{L(P'_p + F_{top} + F_{bot} - P'_a)}{SF} \tag{13-8}$$

Use an SF of about 1.2 to 1.5 in this equation, depending on the importance factor. Assuming that P'_p, P'_a should be collinear, we can take $\sum M_{P_p} = 0$, giving

$$B'LP' + B'LF_R + (H - \bar{y})LF_{top} = F_{ar}e + \bar{y}LF_{bot}$$

Rearranging and solving for vertical corner force P', we obtain

$$P' = \frac{F_{ar}e}{BL} + \frac{\bar{y}F_{bot}}{B} - \frac{(H - \bar{y})F_{top}}{B} - F_R \tag{13-8a}$$

[7]The block anchor is also called a "deadman." Rather than amending that term to "deadperson," this text will call these members "block anchors."

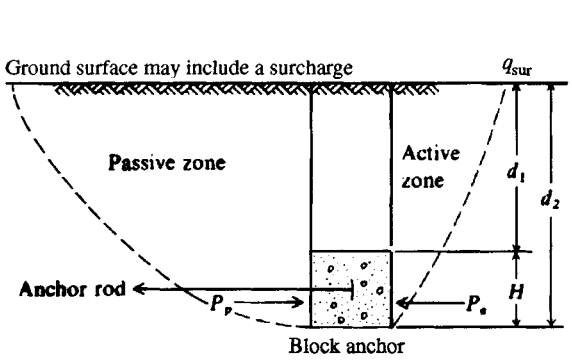

(*a*) Block anchor located at $d_1/H \leq 0.5$ to $0.7H$.

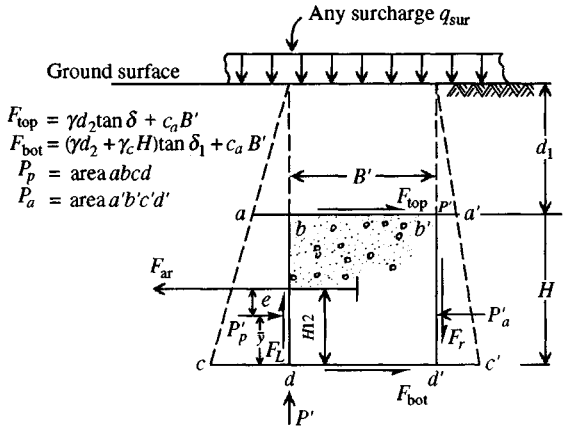

(*b*) Complete set of forces, not including q_{sur}, acting on any anchor block.

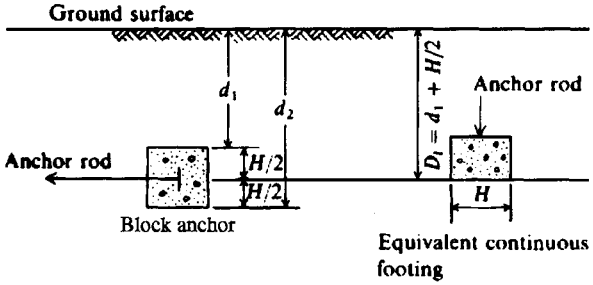

(*c*) Block anchor at substantial $d_1/H > 3$.

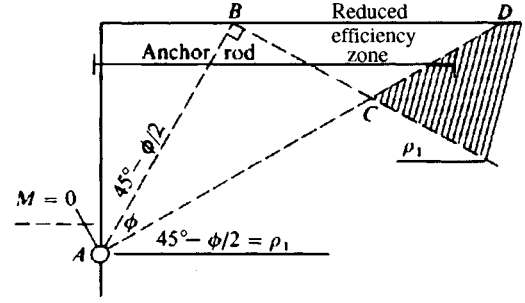

(*d*) Locating anchor so active and passive zones do not intersect gives maximum efficiency.

Figure 13-11 Block anchorage with terms used in Eqs. (13-8) through (13-11). Note L is perpendicular to paper.

and the force P' located at point b' must be

$$P' \leq (q_{sur} + \gamma d_1)L$$

Refer to Fig. 13-11*b* for identification of terms used in the preceding equations and note that F_{ar} = total anchor rod force based on spacing s and that F_L, F_R = side friction ($F_R = P'_a \tan\delta$) forces. For the preceding equations use $L = s$ for anchorages that are continuous for the total wall length—the usual case. Earth pressures are usually calculated for a unit width so they must be multiplied by L to obtain forces consistent with the anchor rod.

When using Eq. (13-8), one should locate the anchorage so that the passive zone of Fig. 13-11*d* and Example 13-3 is outside the active wedge. Actually the anchorage can be in the *reduced efficiency zone* of Fig. 13-11*d* but with a passive pressure computed using d_1 reduced by the depth of the intersection of the passive and active zones (similar to point C of Fig. 13-11*d*). For this case the top and bottom friction/adhesion components must provide the principal anchor rod resistance.

Regardless of anchorage location the anchorage must be carefully backfilled both around the sides and on top so that the assumed passive condition with friction and/or adhesion can develop. There may be a question of using an SF on the active pressure component of Eq. (13-8), but this is a conventional procedure that has generally proved satisfactory.

A few verification tests have been made—primarily on small models but a few on full-scale anchorages [see Smith (1957) and Tschebotarioff (1962)]. From these the following semi-empirical equations were produced:

1. If the anchorage is a short rectangular (or square) block of $L \leq 1.5H$, the anchor resistance can be computed (see Fig. 13-11*a* or *c*) as

$$P_{ar} = \frac{C\gamma d_2^2 L K_p + q_u H^2}{SF} \tag{13-9}$$

In this equation take K_p = Rankine value from Table 11-4. Use a SF = 1.2 to 1.5. Take $C \approx 0.65$ for concrete; for steel plates or sheetpiling use $C \approx 0.5$.

2. For a cohesive soil ($\phi = 0°$) compute the anchorage resistance as

$$P_{ar} = \frac{MHLs_u}{SF} \tag{13-10}$$

where $M = 9$ for $\frac{d_2}{H} \geq 3$ (9 = bearing capacity factor for a deep footing)

$= 9\frac{d_2}{H}$ for $\frac{d_2}{H} < 3$ (using linear interpolation)

d_2 = block depth shown on Fig. 13-11*a*

3. For $\phi - c$ soil and $L > 1.5H$ use Eq. (13-8) with the active and passive earth forces computed using Eqs. (2-54) and (2-55); for short anchor blocks use

$$P_{ar} = \frac{P_p L}{SF} \tag{13-11}$$

When the anchor block is very deep, say $d_2/H \geq 6.5$, one may compute the anchor resistance by Eq. (13-9) for all values of L.

Example 13-7. Design a concrete anchorage for the anchor rod force and its location of Example 13-1.

Given. $F_{ar} = 106.6$ kN on $s = 3$ m (see Fig. E13-1*f*)

Depth $d_1 = 1.2$ m (see Fig. E13-1*a*)

$\gamma = 16.50$ kN/m^3 $q_{sur} = 25$ kPa (see Fig. E13-1*a*)

$\phi = 32°$ Concrete: $f'_c = 21$ MPa

Solution. We know that a soil with $\phi = 32°$ will have a reasonably large passive earth and friction resistance. Let us try a block of 0.6 × 0.6 m × length of the wall; but for any interior anchorage the effective length $L = 3$ m and is 1.5 m for the two ends (but the two ends will also have end friction). We will look at a typical interior section having these properties:

Dimensions = 0.6 × 0.6 × 3.0 m length

Anchor rod force = $sF_{ar} = 3 \times 106.6 =$ **319.8** kN

For friction we will use $\delta = 25°$ for top

$\delta = \phi = 32°$ for base

Using a smaller δ for the block top is justified on the basis that it will not be so rough as the sides, which are cast against the soil; also top will be backfill. With these data we compute block friction resistance as follows:

$$F_{top} = L(q_{sur} + \gamma d_1)\tan 25°$$
$$= 3(25 + 16.5 \times 1.2)\tan 25° = 3(20.9) = 62.7 \text{ kN}$$
$$F_{bot} = 3(25 + 16.5 \times 1.8)\tan 32° = 3(34.2) = 102.5 \text{ kN}$$

Using the Coulomb (same as Rankine) pressure coefficients with $\delta = 0$ and $\phi = 32°$, we obtain, from Table 11-1, $K_a = 0.307$; from Table 11-2, $K_p = 3.25$.

The active and passive earth forces on the block can be computed from the average block pressure as follows:

$$\sigma_{av} = (q + h_{av}\gamma)K_i: \qquad \sigma_a = (25 + 1.5 \times 16.5)0.307 = \mathbf{15.3} \text{ kPa}$$
$$\sigma_p = (25 + 1.5 \times 16.5)3.25 = \mathbf{161.7} \text{ kPa}$$
$$P_i = L \times \sigma_{i,av} \times H \qquad \text{where } L = 3 \text{ m}, H = 0.6 \text{ m}$$
$$P_a = 3 \times 15.3 \times 0.6 = \mathbf{27.5} \text{ kN}$$
$$P_p = 3 \times 161.7 \times 0.6 = \mathbf{291.1} \text{ kN}$$

The total resisting force is

$$F_R = F_{top} + F_{bot} + P'_p - P'_a$$
$$= 62.7 + 102.5 + 291.1 - 27.5 = \mathbf{428.8} \text{ kN}$$

and the resulting SF is

$$\text{SF} = \frac{F_R}{F_{ar}} = \frac{428.8}{319.8} = \mathbf{1.34} \qquad \text{(probably O.K.)}$$

We do not check the eccentricity of the anchor rod with P'_p but it is probably rather small. Instead, this question is left as a reader exercise (Prob. 13-16).

////

13-9 OVERALL WALL STABILITY AND SAFETY FACTORS

A sheet-pile wall can fail in one of four basic modes as shown in Fig. 13-12:

1. Sheet-pile bending. Using the maximum design moment M from the analysis with $f_a \approx 0.60$ to $0.65 f_y$ gives an apparent SF = 1.66 to 1.54, which is usually adequate. One may, of course, use a smaller or larger f_a based on site conditions and the importance factor. Safety factors much smaller than 0.5 are not recommended.

   If there is enough lateral displacement (or bending) the pile may pull out of the ground, for it cannot elongate.
2. Anchor rod or anchorage failure. This may be by the anchor rod pulling apart either along its length or failing at its anchor point(s). For the anchor rod one should limit the allowable stress so that a SF on the order of 1.5 to 2.0 is obtained.

   Anchorage failure can occur if passive pressure and friction resistance is inadequate. This would occur from placing the block too close to the wall, combined with inadequate backfilling procedures.
3. A toe (or kickout) failure. This may occur if the embedment depth is not adequate. This failure mode is usually checked by taking a moment summation about one of the anchor

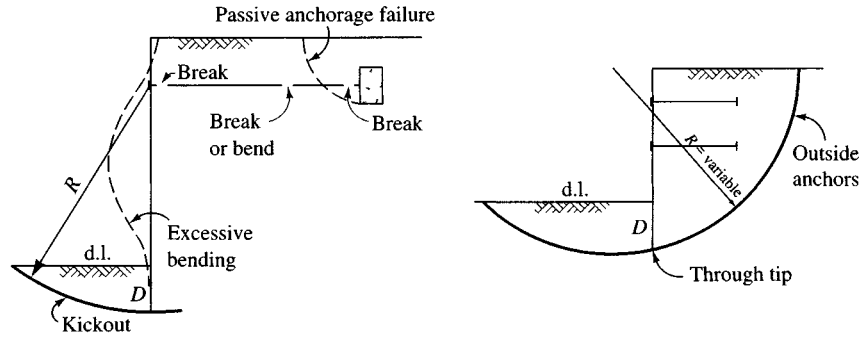

(*a*) Rod failure, anchor failure, bending/pullout failure, or toe kickout.

(*b*) Rotational instability.

Figure 13-12 Sheet-pile wall failure modes.

rods. When this is done the $\sum M_{ar}$ should be for a worst case, not for the basic design case. Actually, this check is not required in the FEM since it is automatically satisfied for any design case checked.

4. A system (see Fig. 13-12*b*) failure. This failure mode is usually checked using a slope stability program with trial circles located such that they are outside the anchorages for the anchor rods and pass either through or just below the pile tip. A minimum recommended SF for this mode is 1.2^+.

The zone between the active earth-pressure wedge and the anchorage is similar to a reinforced earth system. The major difference is the use of only one or two anchor rods versus a number of reinforcement strips. Thus, it would appear that no slip circles would form in this region.

Some persons suggest that a vertical or "plunging" failure by excessive pile penetration be investigated when the anchor rod slopes. It is not likely that the active pressure would force the piling further into the ground; however, when the anchor uses a prestress tendon that is tensioned to a high value, a fairly large vertical force can be developed. The problem with this type of analysis is that, as the large vertical force develops, there is also an increase in the horizontal force and in the friction component and (depending on the soil) there is additional adhesion, so it is nearly impossible to make any kind of analysis. If plunging is a problem, it will be discovered during the application of the proof load—one can see the wall moving vertically and stop operations for a redesign. Probably the best solution is to increase the embedment depth, since that zone has friction and/or adhesion on both sides of the piling.

PROBLEMS

13-1. Use your FEM program FADSPABW (B-9) and find an embedment depth for an HP pile section (see Table A-1 of Appendix A) for the "flagpole" problem summarized in Table P13-1 and illustrated in Fig. P13-1. After the program finds a depth, indicate what you recommend for the depth and your reasons. In this case input IPRESS = 0, NNZP = 1, BSHP = width of HP, m, and the horizontal load P at NP = 2.

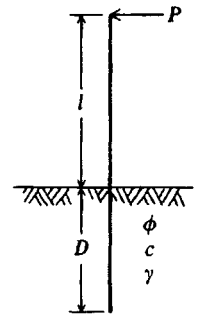

Figure P13-1

TABLE P13-1

No.	l, m	P, kN	γ, kN/m^3	ϕ, degrees	c, kPa
1	8.0	45	17.30	32	60
2	6.5	60	17.50	34	20
3	7.0	40	18.20	20	30

Note: In the following problems, if you input something that does not produce a stable structural system, the program will likely cancel, and you will not get all of the output. If this occurs, you must edit the change to something larger or stiffer or increase the embedment depth.

13-2. Redo Example 13-1 with 0.6- and 0.5-m element lengths above the dredge line and see if there are any major differences in nodal output compared with Fig. E13-1*f*.

13-3. Make a stability analysis of Example 13-1 using data sets EX131A.DTA and EX131B.DTA. Using the worst-case anchor rod load, check if the anchor rod is adequate. Using the largest moment, check if the bending stress is satisfactory.

13-4. Using data set EX131C.DTA (it is already set to fix node 1 and remove the anchor rod), make an analysis and compare the output to that from using data set EX131.DTA. Draw a sketch showing the bending moment caused by fixity (and sign) and compute the equivalent anchor force produced by fixing the node.

13-5. Redo Example 13-2 (sloping dredge line) but take the dredge line slope as 25°. Use program WEDGE and data sets WDG132A.DTA and WDG132B.DTA (with WDG132B.DTA revised for the new slope angle). Recompute the SK(I) values below the dredge line and make an analysis using program B-9. Compare the output from your analysis with the execution using data set EX132.DTA.

13-6. Redo Example 13-2 using a revised copy of data set EX132.DTA for a surcharge of 50 kPa on the backfill. Check whether the bending moment stress and anchor stress are satisfactory. If they are not try these:

a. A stiffer sheet-pile section

b. A larger-diameter anchor rod

13-7. Redo Example 13-2 using a revised copy of data set EX132.DTA. Move the anchor rod to the water line node (be sure that you are using 0.6- and 0.5-m nodes above the dredge line) and see if there is sufficient improvement to warrant movement. Be sure to check the new anchor and bending stresses.

13-8. Redo Example 13-3 using a copy of data set EX133.DTA, edited to use a larger-diameter rod for the top anchor. Compare these results to your execution of the original data set and note whether there is any improvement.

13-9. Redo Example 13-3 using a copy of data set EX133.DTA but with the rod springs reversed (i.e., just switch the two K values). Compare this output to your execution of the original data set.

13-10. Redo Example 13-3 using a copy of data set EX133A.DTA that fixes the top node (NZX = 2) and uses only the lower anchor. Compare this output to that from using the original data set. Are any bending moments too large? Is the anchor rod overstressed?

13-11. Redo Example 13-3 using a copy of data set EX133.DTA and increase the surcharge to 40 kPa. Check if the bending and anchor stresses are adequate.

13-12. Redo Example 13-4 using a copy of data set EX134.DTA and the next larger sheet-pile section. How much does this larger section reduce the top node displacement?

13-13. Redo Example 13-4 using a copy of data set EX134.DTA and adding a surcharge of 20 kPa to the backfill. By trial find a section that limits the top node deflection to not more than 35 mm.

13-14. Redo Example 13-5 with a diameter of 375 mm and see if there is any significant change in anchor elongation.

13-15. Design the wales for the anchor rod of Example 13-1 using the data in Fig. E13-1*f*. You should obtain a regular copy using data set EX131.DTA, which will be easier to read and work with. Use a pair of back-to-back channels with adequate spacing for the anchor rod to fit between in a loose fit.

13-16. For Example 13-6, find the eccentricity e and compute the vertical force P' (at b'). Use $F_R = P'_a \tan 32°$, note there is a surcharge on the backfill, and be sure to include L.

CHAPTER 14

WALLS FOR EXCAVATIONS

14-1 CONSTRUCTION EXCAVATIONS

It is a legal necessity with any new construction to provide protection to the adjacent structures when excavating to any appreciable depth. Without adequate lateral support the new excavation will almost certainly cause loss of bearing capacity, settlements, or lateral movements to existing property.

New construction may include cut-and-cover work when public transportation or public utility systems are installed below ground and the depth is not sufficient to utilize tunneling operations. The new construction may include excavation from depths of 1 to 20^+ m below existing ground surface for placing any type of foundation from a spread footing to a mat, or for allowing one or more subbasements.

All of this type of construction requires installation of a lateral retaining system of some type before excavation starts.

Current practice is to avoid clutter in the excavation by using some kind of tieback anchorage (if required). The older methods of Fig. 14-1*b* and *c* produced substantial obstructions in the work area. Accidental dislodgement of these obstructions (struts and rakers) by equipment could cause a part of the wall to collapse. This mishap could be hazardous to the health of anyone in the immediate vicinity and to the contractor's pocketbook shortly afterward.

14-1.1 Types of Walls

Until the late 1960s basically two types of walls were used in excavations. These are shown in Fig. 14-1*b* and *c*. Since then there has been a veritable explosion of wall types and/or materials used for the wall. We might group these walls as follows:

Braced walls using wales and struts
Soldier beam and lagging
Braced sheeting

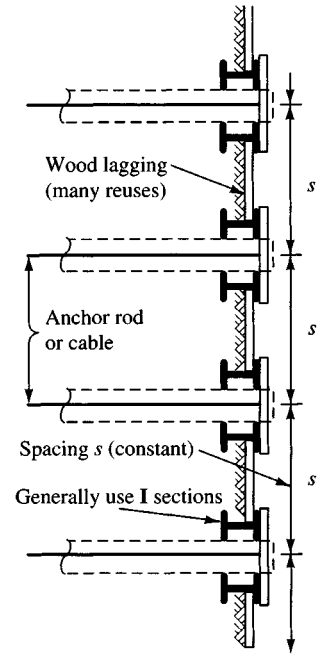

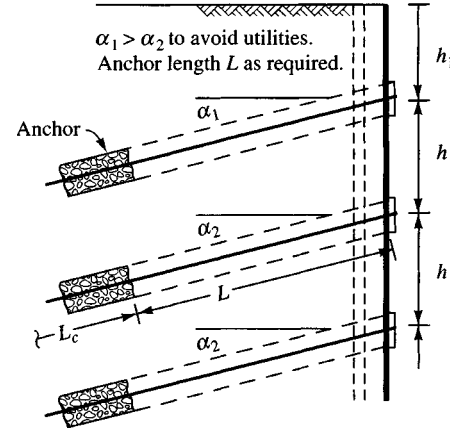

(*a*) Tieback construction

Figure 14-1*a* Three methods for providing lateral support for excavations. Method (*a*) is most popular in urban areas if trespass for anchorages is allowed.

Bored-pile walls

Diaphragm-slurry walls

Braced walls using struts or rakers as shown in Fig. 14-1*b*, *c* were widely used up to the mid-1960s. They are seldom used today except in small projects such as bracing for water and sewer line trenches that are over about 2.5^+ m deep. They are not much used for large excavations in urban areas since the struts and rakers produce too much clutter in the excavated area and increase both the labor cost and the possibility of accidents.

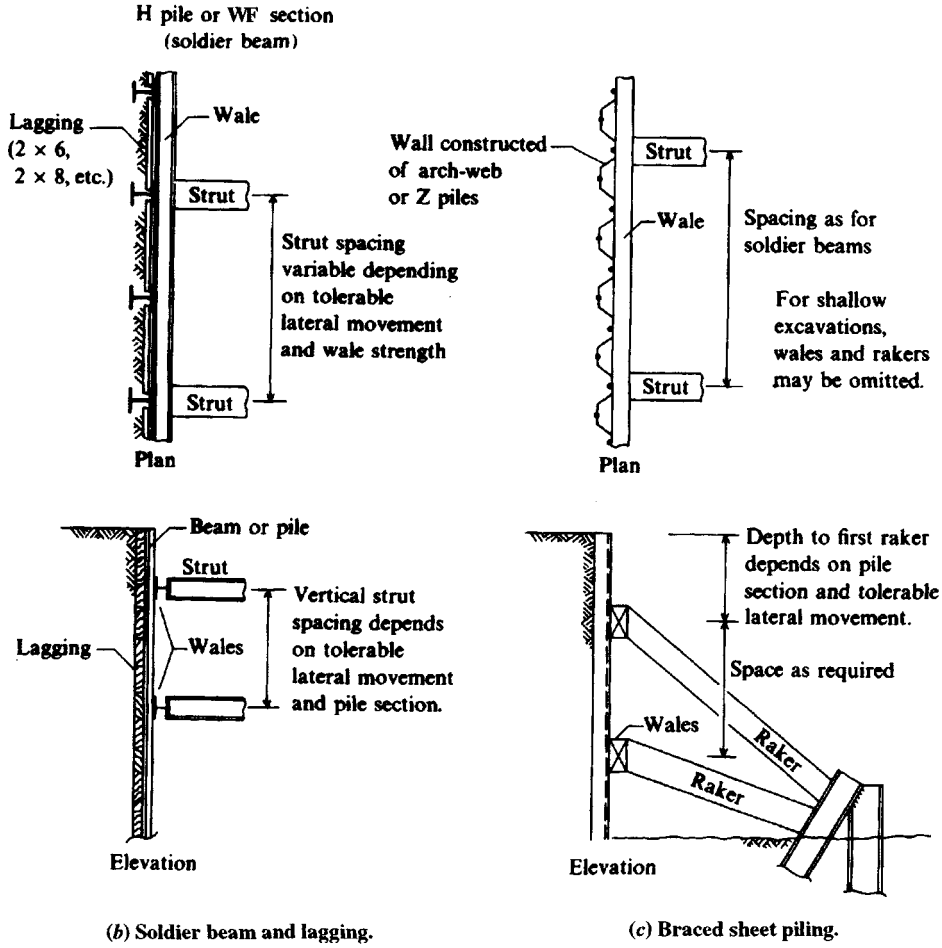

(*b*) Soldier beam and lagging.

(*c*) Braced sheet piling.

Figure 14-1*b, c*

The *soldier beam and lagging* system of Fig. 14-1*a* is popular for temporary construction. That is, pairs of rolled steel sections (the soldier beams) are driven to a depth slightly below the final excavation. Their spacing s is on the order of 2 to 4 m so that available timber can be used for lagging. The lagging timbers, which are slightly shorter than the spacing but on the order of 50 to 100 mm thick, are installed behind the front flanges (or clipped to the front flanges using proprietary clips) to retain the soil as excavation proceeds. If the lagging is behind the flange, some hand excavation is usually required to get the lagging into place.

At depths specified by the foundation engineer—usually computed using empirical methods—excavation halts and a drill rig is used to drill the anchor holes for tiebacks. These are installed using bearing plates on the soldier beam flanges and tack welded for the vertical force component from the anchor; additional welding may be needed to hold the beams in alignment. The plates may be tilted to accommodate sloping anchorages (see Fig. E13-5 and Fig. 13-10*d*). It is usually more economical when using tieback slopes in the range of 15° to 20° to shop-drill the holes for the anchor rods at approximately that slope (the hole

must be slightly oversize anyway) in the plate to produce an anchor point that costs less than cutting a channel to produce a slope. Alternatively, the anchor plate may have two holes for bolting to holes field-drilled into the outer flanges of the soldier beams in lieu of welding for easier wall disassembly.

Braced sheeting is essentially the anchored sheet-pile wall of Chap. 13 but with multiple levels of tiebacks or anchors. Construction is similar to the soldier beam lagging system in that the sheeting is driven and at selected excavation depths the wales and tiebacks are installed. When using this system it may also be necessary to tilt the anchorage assembly as shown in Fig. 13-10*d*.

Advantages of both the soldier beam and lagging and the braced sheeting systems are that they are easy to install (unless the excavation zone is rocky) and to remove and that the materials can be reused a number of times. The principal disadvantage is that the adjacent property owner may not allow encroachment (or request a royalty payment deemed too high) to install the anchorage. Since anchorages are not removed they represent permanent obstacles in the underground area around the perimeter of the construction site.

When the soil is rocky or the excavation is into rock, one only needs to drive the piling to the rock interface. Sometimes—especially with sheetpiling—it is impossible to drive the piling the full depth of the excavation. When this situation occurs, it may be possible to step the construction as shown in Fig. 14-2. An equation for the sheeting depth for each stage is given on the figure.

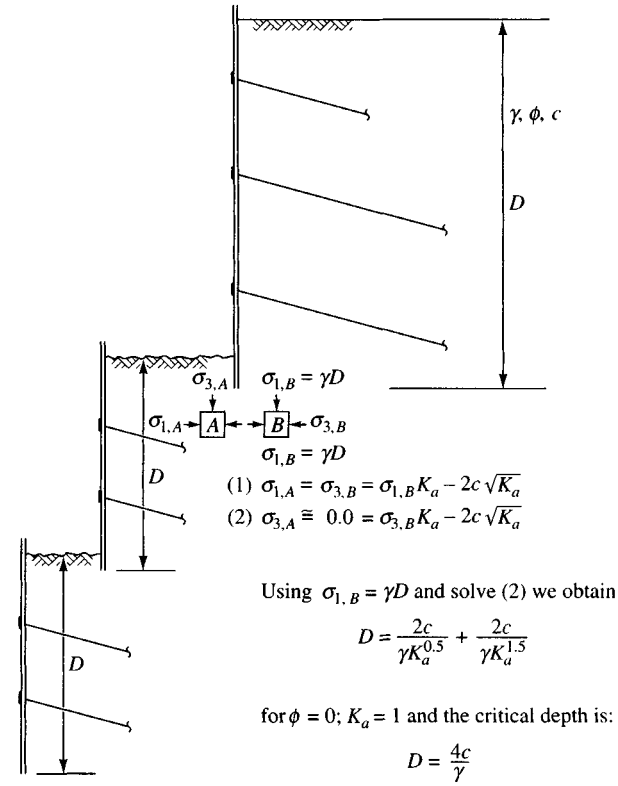

Figure 14-2 Critical depth D (SF = 1) when soil conditions do not allow sheetpiling to be driven the full depth of excavation and it is possible to reduce lower work areas.

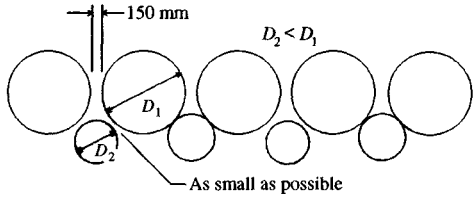

(*a*) Using two rows of bored piles to produce a relatively watertight wall (may require some grouting).

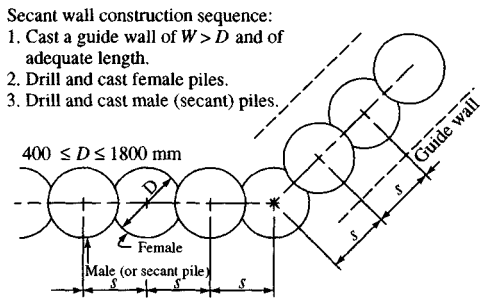

(*b*) Secant pile method for a watertight excavation support.

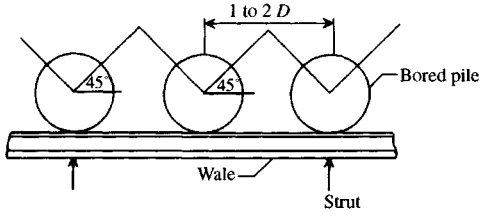

(*c*) Single row of closely spaced piles so arching between piles retains the soil.

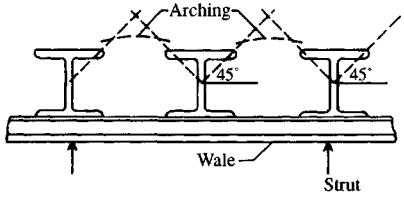

(*d*) Using **H** piles instead of bored piles of (*a*) or (*c*).

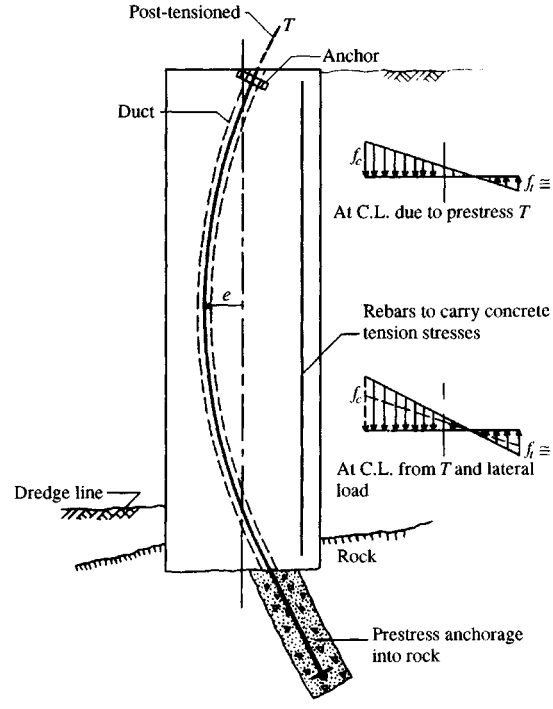

(*e*) Using a line of closely spaced prestressed piles to maintain vertical alignment of excavation.

Figure 14-3 Bracing systems for excavations.

Pile walls are used in these circumstances:

a. It is too difficult to drive soldier beams or sheetpiling.

b. It is necessary to have a nearly watertight wall so as not to lower the GWT outside the construction perimeter.

c. The retaining wall is to be used as a permanent part of the structural system (e.g., the basement walls).

d. It is necessary to use the full site space, and adjacent owners disallow using their underground space to install tieback anchors (or there are already existing obstructions such as tunnels or basement walls).

There are a large number of pile wall configurations or modifications of existing methodology, of which Fig. 14-3 illustrates several. The diaphragm-slurry wall is shown in Fig. 14-16 and will be considered in Sec. 14-9. The particular wall configuration used may depend on available equipment and contractor experience. Terms used in the construction of these walls are shown on the appropriate figures.

When the wall must be watertight, the *secant wall,* consisting of interlocking piles (available in diameters ranging from 410 to 1500 mm), is most suited. This wall is constructed by first casting a concrete guide wall about 1 m thick and of a width 400 to 600 mm larger than the pile diameters and preferably with the casing preset for the primary piles. The primary (or female) piles are then drilled (they may be cased, but the casing must be pulled) and the piles cast using any required reinforcement. After hardening, the secant (or male) piles (of the same or smaller diameter) are drilled; during this process the drilling removes segments of the primary piles so an interlock is obtained as shown (Fig. 14-3*b*). The secant piles may also be cased, but here the casing does not have to be removed. They also may be reinforced—either with reinforcing bar cages or **W**, **H**, or **I** sections placed in the cavity before the concrete is placed. This pile configuration is possible because of the more recent development of high-torque drilling equipment capable of cutting hard materials such as rock and concrete with great efficiency.

Secant pile walls can also be constructed using a cement slurry for the primary piles so that the cutting for the secant piles is not quite so difficult.

Tiebacks may be used with the pile walls. If the piles are in fairly close lateral contact, the tiebacks will require wales. For the secant-type piles, the tiebacks are simply drilled through the pile (although if this is known in advance it might be practical to preset the top one or two anchor holes in place using large-diameter pieces of plastic tubing cut to size and inserted into the hole and held in place by some means).

Slurry walls will be considered in Sec. 14-9.

14-1.2 Drilled-in-Place Piles

Where pile-driving vibrations using either pile hammers or vibratory drivers may cause damage to adjacent structures or the noise is objectionable, some type of drilled-in-place piles are required.

Where the soil to be retained contains some cohesion and water is not a factor, the soldier beam or drilled-in-place pile spacing may be such that lagging or other wall supplement is not required, because *arching,* or bridging action of the soil from the lateral pressure developed by the pile, will retain the soil across the open space. This zone width may be estimated roughly as the intersection of 45° lines as shown in Fig. 14-3*c, d.* The piles will, of course, have to be adequately braced to provide the necessary lateral soil resistance. This kind of construction can only be used for a very short time period, because soil chunks will slough off from gravity and/or local vibrations as drying of the exposed surfaces takes place.

Where sufficient anchorage is available at the pile base (perhaps socketed into rock) and with an adequate diameter, one method is to design the pile as a prestressed beam (see Fig. 14-3*e*). After installation the tendon, cast in a conduit, is tensioned to a preset load and anchored at the top. The prestress load produces a qualitative stress as shown at various sections along the pile depending on the eccentricity. The pile tends to deflect toward the backfill/original ground with the tendon installed as shown, but this deflection is resisted by the soil so that the final result is a nearly vertical pile and (one hopes) no loss of ground from any deflection toward the excavation side.

Placing the prestress tendon with e on the right side of the vertical pile axis would tend to deflect the pile away from the backfill. Although this deflection would more efficiently utilize the concrete strength f_c' in bending, the lateral displacement into the excavation would encourage additional ground loss.

Where both the earth and water must be retained, the system will have to be reasonably watertight below the water table and be capable of resisting both soil and hydrostatic pressures. Lowering the water table is seldom practical for environmental reasons but, additionally, it will produce settlement of the soil (and of any structures on that soil). If there is a high differential water head (the construction area must be kept dry), sheetpiling joints cannot be relied on to retain water without adequate sealing and/or pumping the infiltration so the retaining wall solutions may become limited to the secant or slurry wall.

It is evident that uplift or buoyancy will be a factor for those structures whose basements are below the water table. If uplift is approximately equal to the weight of the structure, or larger, it will be necessary to anchor the building to the soil. This can be done using anchor piles to bedrock. Two other alternatives are belled piles (tip enlarged) or vertical "tiebacks."

When making excavations where adjacent property damage can occur from pile driving or excavation vibrations, one should take enough photographs of the surrounding structures to establish their initial condition so that future claims can be settled in a reasonable manner.

A select number of ground elevation control stations should be established around the perimeter of the excavation to detect whether ground loss damage claims are real or imagined.

Ground loss is a very serious problem around excavations in built-up areas. It has not been solved so far with any reliability; where the ground loss has been negligible, it has been more a combination of overdesign and luck rather than rational analysis.

14-2 SOIL PRESSURES ON BRACED EXCAVATION WALLS

The braced or tieback wall is subjected to earth-pressure forces, as are other retaining structures, but with the bracing and/or tieback limiting lateral wall movement the soil behind the wall is not very likely to be in the *active* state. The pressure is more likely to be something between the active and at-rest state.

With tiebacks (and bracing) the wall is pressed against the retained earth, meaning the lateral pressure profile behind the wall is more trapezoidal than triangular. Figure 14-4 idealizes the development of wall pressures behind a braced wall.

In stage 1 of Fig. 14-4 the wall is subjected to an active earth pressure, and wall displacement takes place. The lateral deformation depends on cantilever soil-wall interaction as would be obtained by the finite-element program FADSPABW (B-9) of Chap. 13. Next a strut force is applied to obtain stage 2. No matter how large the strut force (within practical limitations), the wall and earth are not pushed back to their original position, but the strut[1] force, being larger than the active pressure, causes an increase in the wall pressure.

The integration of the pressure diagram at the end of stage 2 would be approximately the strut force. It is not exactly that amount of force since inevitably there is soil and anchor creep and much uncertainty in earth-pressure distribution. As shown for the end of stage 2 the excavation causes a new lateral displacement between b and c and probably some loss of

[1] For convenience the term *strut force* will be used for any kind of restraint—from struts, tiebacks, or whatever.

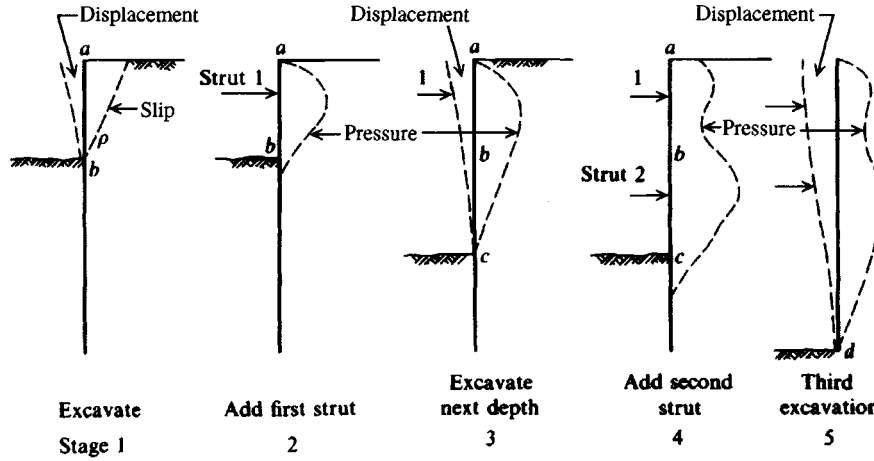

Figure 14-4 Qualitative staged development of earth pressure behind an excavation. The strut force produces lateral pressures that generally are larger than the active values. The strut force generally changes with time and installation method.

strut force (as soil moves out of the zone behind the first strut into the displacement between *b* and *c*) as well as soil creep. The application of the second strut force and/or tightening up of the first strut results in the qualitative diagram at the beginning of stage 4 and the excavation and additional ground loss due to lateral movement at the end of stage 4 when excavation proceeds from *c* to *d*. Thus, it is evident that if one measures pressures in back of this wall *they will be directly related to the strut forces* and have little relation to the actual soil pressures involved in moving the wall into the excavation.

Peck (1943) [using measurements taken from open cuts in clay during construction of the Chicago, IL, subway system (ca. 1939–41)] and later in the Terzaghi and Peck (1967) textbook, proposed apparent pressure diagrams for wall and strut design using measured soil pressures obtained as from the preceding paragraph. The apparent sand pressures of Fig. 14-5 were based primarily on their interpretation of those reported by Krey (in the early 1930s) from measurements taken in sand cuts for the Berlin (Germany) subway system.

These apparent pressure diagrams were obtained as the envelope of the maximum pressures that were found and plotted for the several projects. The pressure envelope was given a maximum ordinate based on a portion of the active earth pressure using the Coulomb (or Rankine) pressure coefficient.

The Peck pressure profiles were based on total pressure using γ_{sat} (and not $\gamma' = \gamma_{sat} - \gamma_w$), and it was never clearly explained how to treat the case of both γ_s and γ_{sat} being retained.

These diagrams have been modified several times, with the latest modifications [Peck (1969)] as shown in Fig. 14-5. When the *Peck pressure diagrams* were initially published, Tschebotarioff and coworkers [see Tschebotarioff (1973)] noted that Peck's initially proposed clay profiles could produce $K_a = 0.0$ for certain combinations of $s_u/\gamma H$, so a first modification was made to ensure that this did not occur.

Tschebotarioff observed that for most cohesionless soils $0.65K_a \approx 0.25$ for all practical purposes, since ϕ is usually approximated. On this basis he drew some slightly different suggested pressure profiles that have received some use.

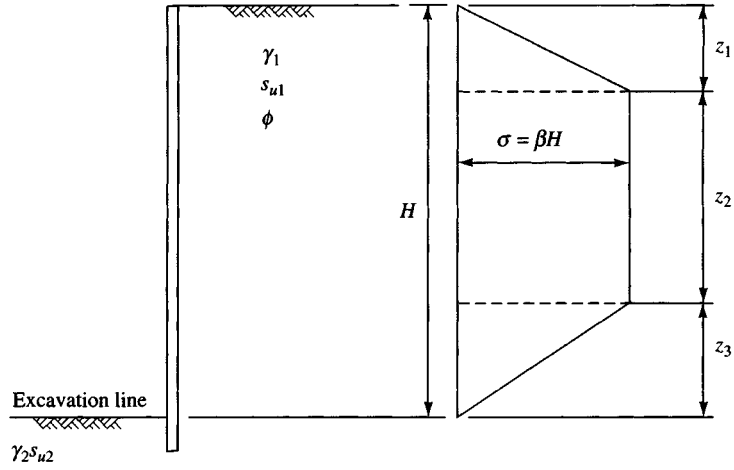

Soil Type	Author	z_1	z_2	z_3	β
Sand	P	0	1.0	0	$0.65_\lambda K_a$
Sand	T	0.	0.7	0.2	0.25_λ
Soft-to-Medium Clay	P	0.25	0.75	0	λK_{ap}*
Temp. Support Medium Clay	T	0.6	0	0.4	0.3λ
Stiff fissured Clay	P	0.25	0.50	0.25	K_{ap}†
Perm. Support Medium Clay	T	0.75	0	0.25	0.375λ

* K_{ap} = 0.4 to 1.0
† K_{ap} = 0.2 to 0.4
Source: P = Peck (1969); T = Tschebotarioff (1973).

Figure 14-5 Summary of the Peck (1969) and Tschebotarioff (1973) apparent lateral pressure diagrams for braced excavations.

The figure and table shown in Fig. 14-5 allow use of either the Peck or Tschebotarioff apparent (*total*) pressures or any others by suitable choice of the z_i values.

If one designs a strut force based on the apparent pressure diagram *and* uses simply supported beams for the sheeting as proposed by Terzaghi and Peck, the strut force will produce not more than the contributory area of that part of the apparent pressure diagram. The sheeting may be somewhat overdesigned, because it is continuous and because simple beam analysis always gives larger bending moments; however, this overdesign was part of the intent of using these apparent pressure diagrams.

That these apparent pressure diagrams produce an overdesign in normally consolidated soils was somewhat verified by Lambe et al. (1970) and by Golder et al. (1970), who predicted loads up to 50 percent smaller than measured strut loads. This difference is not always the case, however, and if ground conditions are not exactly like those used by Peck in developing his apparent pressure profiles, the error can sometimes be on the unsafe side.

For example, Swatek et al. (1972) found better agreement using the Tschebotarioff apparent pressures for clayey soils in designing the bracing system for a 21.3-m deep excavation in Chicago, IL. Swatek, however, used a "stage-construction" concept similar to Fig. 14-4 along with the Tschebotarioff pressure diagram. In general, the Tschebotarioff method may be more nearly correct in mixed deposits when the excavation depth exceeds about 16 m.

A major shortcoming of all these apparent pressure diagrams is what to do when the retained soil is stratified. In this case it would be reasonable [see also suggestions by Liao and Neff (1990)] to do the following:

1. Compute two Rankine-type pressure diagrams using the Rankine K_a and $K_o(= 1 - \sin\phi)$ *and* using *effective* unit weights. Make a second pressure diagram for the GWT if applicable.
2. Plot the two pressure diagrams [use 0 for any (−) pressure zones] on the same plot.
3. Compute the resultant R_a and R_o for the two pressure plots.
4. Average the two R values, and from this compute an apparent pressure diagram. Take a rectangle ($\sigma = R/H$) or a trapezoid. For example if you use $z_1 = z_3 = 0.25H$, the average pressure σ is

$$R_{av} = \frac{H + 0.5H}{2}\sigma \rightarrow \sigma = \frac{2R_{av}}{1.5H}$$

5. Include the water pressure as a separate profile that is added to the preceding soil pressures below the GWT depending on the inside water level.
6. Instead of using an average of the two R values from step 3, some persons simply multiply the active pressure resultant R_a by some factor (1.1, 1.2, 1.3) and use that to produce the apparent soil pressure diagram. It may be preferable to factor R_a and compare this diagram to the "average" pressure diagram (using unfactored R_a and R_o) and use the larger (or more conservative) value.

14-2.1 Soil Properties

The soil properties to use for design will depend on whether the wall is temporary or permanent and on the location of the GWT behind the wall.

If the ground is reasonably protected and above the water table, drained soil parameters would be appropriate (or at least parameters determined from consolidated undrained tests at the in situ water content). If the retained soil is partly above and partly submerged, the drained parameters would apply to the region above the water table.

For retained soil below the water table, consolidated-undrained tests would be appropriate. The lateral pressure from the tieback or bracing would tend to put the soil below the GWT into a consolidated-undrained condition, but this state would depend on how long the wall is in place and the permeability of the retained soil. If the wall is in place only a week or so, undrained strength parameters should be used. Keep in mind that pore water drainage in cohesionless soils is rapid enough that the drained ϕ angle can be used.

The interior zone of the wall is in a plane strain condition whereas the ends or corners are in more of a triaxial state. When the angle of internal friction ϕ is not measured or is taken (estimated) as less than about 35°, it is not necessary to adjust for plane strain conditions.

14-2.2 Strength Loss with Elapsed Time

Bjerrum and Kirkedam (1958) measured strut forces in an excavation from September through November that indicated the lateral earth pressure increased from 20 to 63 kPa owing to an apparent loss of cohesion. This observation was based on back-computing using consolidated-undrained strength values of both ϕ and c and later assuming only a drained

ϕ angle. Ulrich (1989) observed that tieback and/or strut loads increased with time in overconsolidated clays. Others have also reported that tieback or strut loads increase with time but not in a quantitative manner. It appears, however, that 20 to 30 percent increases are not uncommon. These increases seldom result in failure but substantially reduce the SF.

Cohesion is often reduced in cuts because of changes in moisture content, oxidation, tension cracks, and possibly other factors, so that on a long-term basis it may not be safe to rely on large values of cohesion to reduce the lateral pressure. Temporary strut load increases may also result from construction materials and/or equipment stored on the excavation perimeter.

Where the cut is open only 2 to 5 days, soil cohesion is relied upon extensively to maintain the excavation sides.

14-3 CONVENTIONAL DESIGN OF BRACED EXCAVATION WALLS

The conventional method of designing walls (but not pile walls) for excavations consists in the following steps:

1. Sketch given conditions and indicate all known soil data, stratification, water level, etc.
2. Compute the lateral pressure diagram using Peck's method, Tschebotarioff's method, or the procedure outlined in the preceding section, depending on the quality (and quantity) of soil data and what is to be retained. In the case of a cofferdam in water for a bridge pier or the like, the lateral pressure is only hydrostatic pressure.
3. Design the sheeting, wales, and struts or tiebacks; in the case of a bridge pier cofferdam, the *compression ring.*

   The sheeting making up the wall can be designed either as a beam continuous over the several strut/tieback points or (conservatively) as a series of pinned beams as in Fig. 14-6. For continuous sheeting a computer program[2] is the most efficient means to obtain bending moments.

The *wales* can be designed similarly to those for anchored sheetpile walls. They may be conservatively taken as pin-ended; however, where a computer program is available, they can be taken as continuous across the anchor points. Alternatively, we can estimate the fixed-end moments (fem) conservatively as $wL^2/10$ (true fem are $wL^2/12$) as was done in Example 13-5. The wale system for a braced cofferdam for a bridge pier and the like, where the plan area is small, may be designed primarily for compression with the wales across the ends accurately fitted (or wedged) to those along the sides so that the effect is a compression ring (even though the plan is rectangular). In this case there may be some struts across the width, but the end wale loads will be carried into the side wales as an axial compression force.

If tiebacks cannot be used and piles or a slurry wall would be too costly, the only recourse is to use wales with either struts or rakers as shown in Fig. 14-1*b* and *c*.

Struts and rakers are actually beam-columns subjected to an axial force such as R_n of Fig. 14-6 and bending from member self-weight. Since the strut is a column, the carrying capacity

[2]You can use your program B-5 as follows: JTSOIL = node where soil starts, k_s = ?, NZX = no. of brace points if x = 0.0 m; convert pressure diagram to node forces and input NNZP values. Input E and I for a unit width (1 m or 1 ft) of sheeting. Make similar adjustments for wales.

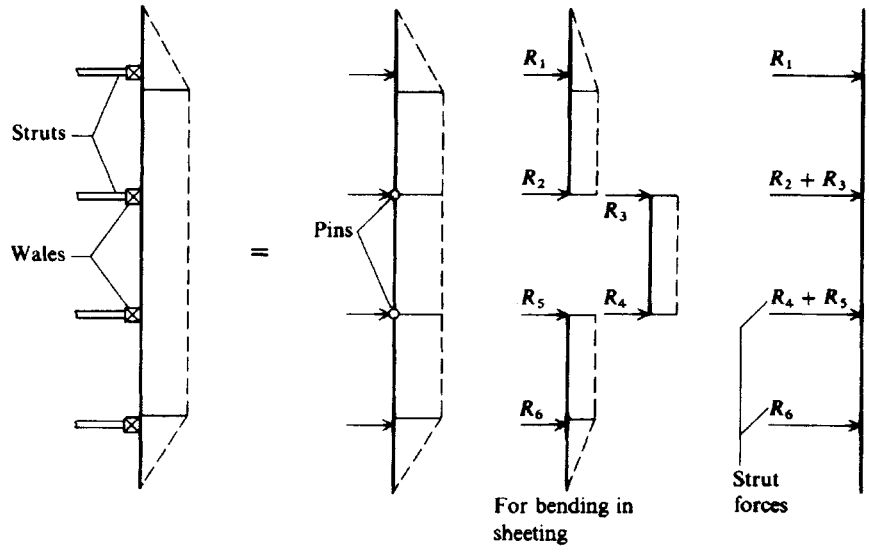

Figure 14-6 Simplified method of analyzing the sheeting and computing the strut forces. This method of using a *simple beam* for strut forces is specifically required if you use the Peck apparent pressure profiles.

is inversely proportional to the ratio $(L/r)^2$. The only means to reduce the L/r ratio is to use intermediate bracing. These might be struts used for the end walls; if so, they will greatly increase the construction area obstructions and will require design of the framing.

Usually vertical supports will be required for horizontal struts unless the unsupported span is relatively short.

The intended purpose of the struts and rakers (and tiebacks) is to restrain the wall against lateral movement into the excavation. Any inward movement that takes place must be tolerated, for forcing the wall back to the original position is impossible.

Because lateral movement of the wall is associated with a vertical ground settlement in a perimeter zone outside the excavation (termed *ground loss*), the following are essential:

1. The wall must fit snugly against the sides of the excavation.This criterion is critical with soldier beam and lagging or when the wall is placed against the earth face after some depth of excavation.
2. The struts, rakers, or tiebacks must allow a very limited amount of lateral displacement. These are all elastic members with an AE/L, so some movement toward the excavation always occurs as the equivalent "spring" stretches or compresses under the wall load.
3. The wales must be sufficiently rigid that displacements interior from the anchor points are not over 1 to 3 mm more than at the anchors. This criterion assumes the wales are in close contact with the wall sheeting, so the assumption of a uniform wall pressure computed as $w = F_{ar}/s$ is valid.
4. The bracing must be located vertically so that large amounts of wall bulging into the excavation do not occur between brace points. This restriction either puts minimum limits on the stiffness of the wall facing (or sheeting) or limits the vertical spacing of the wales—or both.

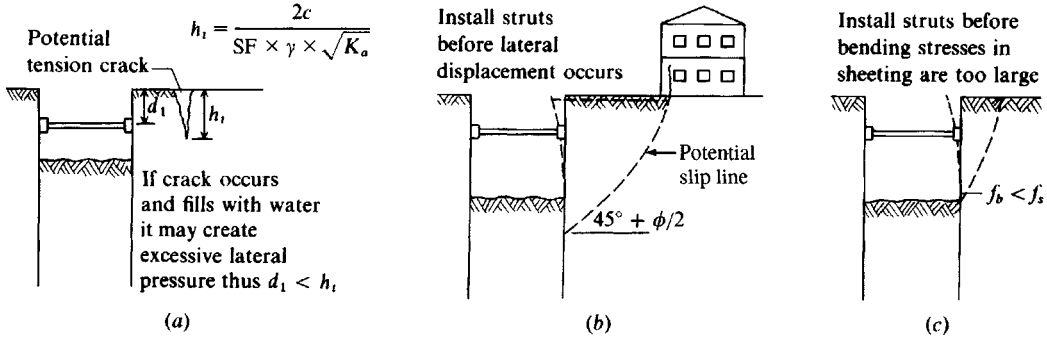

Figure 14-7 Depth of first wale and struts (or rakers) in a braced wall system.

5. The struts or rakers are slightly prestressed by constructing the brace point so that a hydraulic jack and/or wedges can be driven between the wale and strut both to force the wales against the wall and to compress the strut or raker. The system of jacking and/or wedges usually requires periodic adjustments during construction to maintain the necessary strut prestress.

The location of the first wale can be estimated by making a cantilever wall analysis using program FADSPABW (B-9) and several trials for the dredge line location and by inspecting the output for lateral movement into the excavation. This approach is applicable for all soils; however, in cohesive soils, the depth should not exceed the depth of the potential tension crack h_t (see Fig. 14-7*a*) obtained from using a suitable SF.

The formation of this tension crack will increase the lateral pressure against the lower wall (it now acts as a surcharge), and if the crack fills with water the lateral pressure increases considerably. Also, this water will tend to soften the clay in the vicinity for a reduction in shear strength s_u.

The choice of the first wale location should also consider the effect of the location of successive Rankine active earth wedges as in Fig. 14-7*b*, since they will develop at approximate zero moment points from the wall slightly below the excavation line. Note, however, the wedge angle ρ is not always $\rho = (45° + \phi/2)$—it depends on the cohesion, wall adhesion, and backfill surcharges. Program SMTWEDGE or WEDGE may be used to approximately locate the wedge angle ρ.

Where lateral movement and resulting ground subsidence can be tolerated, the depth to the first strut in sandy soils may be where the allowable bending stress in the sheeting is reached from a cantilever wall analysis as in Fig. 14-7*c*.

Example 14-1. Make a partial design for the braced sheeting system shown in Figs. E14-1*a,b* using **PZ** footprint 27 sheet-pile sections for the wall. Use either a pair of channels back to back or a pair of **I** sections for wales and **W** sections for struts. The struts will use lateral bracing at midspan for the weak axis of the struts (giving 2.5 m of unbraced length) as shown by the dotted lines in the plan view of Fig. E14-1*a*.

Horizontal and vertical construction clearances require the strut spacing shown. The water level near the bottom of the excavation will be controlled by pumping so that there is no water head to consider. We will make only a preliminary design at this point (design should be cycled in a computer program to see if lateral movements are satisfactory for controlling ground loss outside the perimeter). Use the apparent lateral pressure diagrams of Fig. 14-5 and check using a K_o pressure.

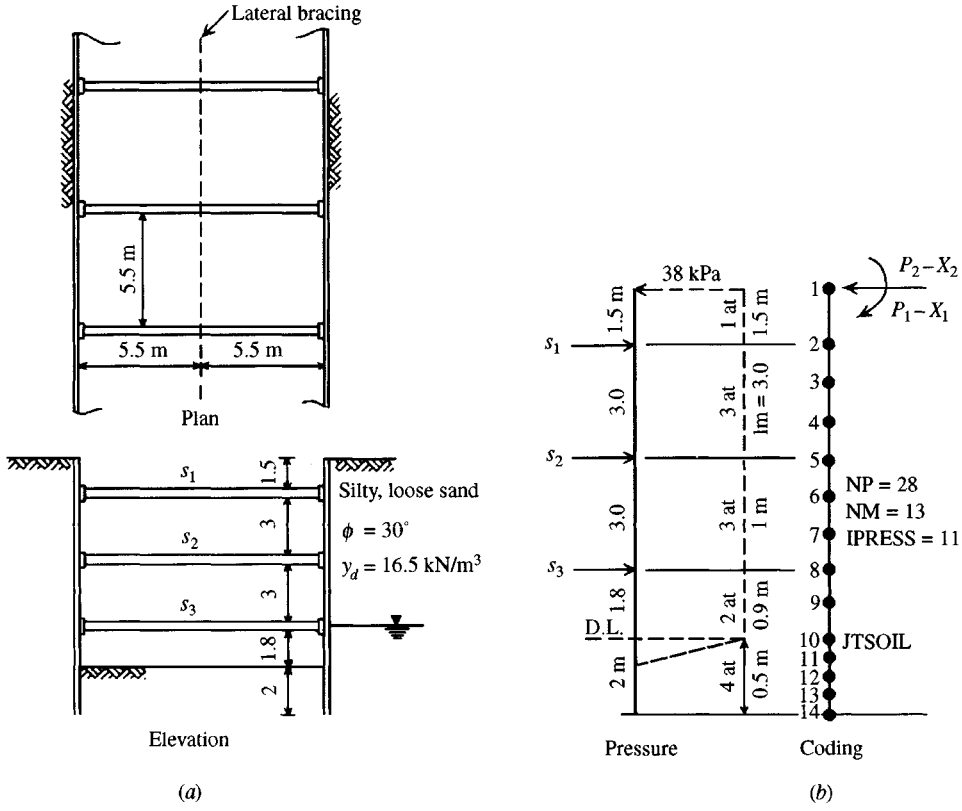

Figure E14-1*a, b*

Required. Draw pressure diagram, code the problem, create a data set, and use computer program FADSPABW (B-9) to analyze strut forces and bending; check bending in sheeting and axial force in the critical strut.

Solution.

Step 1. Obtain the pressure diagram using Fig. 14-5. For loose sand we have $z_1 = z_3 = 0$ and $z_2 = H = 9.3$ m. The lateral pressure for the resulting rectangle shown dashed in Fig. E14-1*b* is

$$\sigma_h = 0.65\gamma H K_a = 0.65 \times 16.5 \times 9.3 \times 0.333 = 33.2 \text{ kPa}$$

This value will be increased 15 percent to allow for water or other uncertainties, giving for design

$$\sigma_{\text{des}} = 1.15 \times 33.2 = \mathbf{38.2} \text{ kPa} \rightarrow \text{use } \mathbf{38} \text{ kPa (Fig. E14-1}b\text{)}$$

What would be the design pressure if we used k_o for the pressure coefficient? $K_o = 1 - \sin 30° = 0.50$ and the total wall force is

$$R_o = \tfrac{1}{2} \times 16.5 \times 9.3^2 \times 0.5 = 357 \text{ kN}$$

Dividing by wall height, we obtain

$$\sigma_o = 357/9.3 = 38.38 \text{ kPa} \qquad \text{(very close, so use } \mathbf{38} \text{ kPa)}$$

Step 2. Code wall as shown in Fig. E14-1*b* and set up data file EX141.DTA (on your diskette) for using computer program FADSPABW. Use the following input control parameters:

NP = 28		JTSOIL = 10	
NM = 13		NONLIN = 0	(no check)
NNZP = 0	(no node forces)	IAR = 3	(the struts)
NLC = 1	(1 load case)	NZX = 0	(no B.C.)
ITYPE = 0	for sheet pile wall	IPRESS = 11	(11 node pressures input)
LISTB = 0	(no band matrix list)	IMET = 1	(SI units)
NCYC = 1	(embedment depth fixed)		
NRC = 0	(input equation for k_s)		

Step 3. Estimate the modulus of subgrade reaction k_s for the base 2 m of embedment depth using Eq. (9-10) with the bearing capacity equation as previously used in Chap. 13:

$$k_s = 40(\gamma N_q Z + 0.5\gamma B N_\gamma)$$

From Table 4-4 obtain $N_q = 18.4$ and $N_\gamma = 15.1$ (Hansen values), which give

$$k_s = 4983 + 12\,144Z^1 \qquad \text{(use AS = } \mathbf{5000}\text{; BS = } \mathbf{12\,000}\text{; EXPO = } \mathbf{1}\text{)}$$

To keep k_s from increasing significantly in the 2-m depth we will use an EXPO value of 0.5 instead of 1.0. The value of NRC initially input (and on the data file) informs the program of the type of equation that will be used. During program execution a "beep," followed by a screen request to input EXPO, alerts the user to input the value. The EXPO value is output with the equation so you can check that the correct value was input.

Since the sheeting is continuous, we can use any value for moment of inertia I; however, we will make a side run (not shown) and try a **PZ**22, which is the smallest **Z** section in Table A-3 (Appendix A). Compute for the **PZ**22 section the following:

$$I/\text{m} = 64.39/0.560 = 114.98 \times 10^{-6}\ \text{m}^4/\text{m}$$
$$S/\text{m} = 0.542/0.560 = 0.9679 \times 10^{-3}\ \text{m}^3/\text{m}$$

We must estimate a **W** section for the strut so that we can compute the spring AE/L (struts are horizontal). From previous runs (not shown) we will try to use a

$$\mathbf{W}200 \times 52 \qquad f_y = 250\ \text{MPa} \quad (\text{Fps}: \mathbf{W}8 \times 35 \qquad f_y = 36\ \text{ksi})$$
$$A = 6.65 \times 10^{-3}\ \text{m}^2 \qquad \text{and} \qquad L = 5.5\ \text{m about } x \text{ axis}$$

Since the strut spans the excavation and is compressed from both ends we will use half the spring for each wall, and for spacing $s = 3$ m the input spring K is

$$K_{\text{strut}} = \frac{AE}{L} = \frac{6.65 \times 200\,000}{3 \times 2 \times 5.5} = \mathbf{40\,300}\ \text{kN/m}$$

The spring is slightly rounded,[3] consistent with the accuracy of the other data.

The y axis has lateral bracing to give an unbraced length L_u of 2.75 m; also

$$r_x = 89\ \text{mm} \qquad r_y = 52\ \text{mm}$$

[3]Note that in SI when $\mathbf{10^{-3}}$ and $\mathbf{10^3}$ are used and cancel they are not shown—this is one of the major advantages of using SI.

giving $r_x/r_y = 1.71 < 2$ so the x axis controls the column stress. Thus,

$$S_x = 0.51 \times 10^{-3}\ \text{m}^3$$

From these data, using the rectangular pressure diagram of Fig. E14-1*b* we create a data file EX141.DTA and use it to produce the output sheets shown as Fig. E14-1*c*.

Step 4. Make an output check and design the members.

a. First check $\sum F_h = 0$. Output is 362.9 kN. Using the formula for the area of a trapezoid (and noting the bottom triangle with a length of 0.5 m), we find the pressure diagram gives

$$R = \frac{9.8 + 9.3}{2} \times 38 = \mathbf{362.9} \qquad \text{(O.K.)}$$

b. A visual examination of the near-end and far-end moments in the output tables shows $\sum M_{\text{nodes}} = 0$.

c. Check if the strut is adequate. The largest strut force is at $S_1 = 120.4$ kN. The self-weight of the strut over a 5.5-m span is 52 kg × 9.807 N/kg × 0.001 kN/N = 0.51 kN/m. The resulting maximum bending moment is

$$M_{\max} = \frac{wL^2}{8} = \frac{0.51 \times 5.5^2}{8} = 1.93\ \text{kN} \cdot \text{m}$$

The stress is

$$f_s = \frac{M}{S} = \frac{1.93}{0.51} = 3.8\ \text{MPa} \qquad \text{(insignificant)}$$

The allowable axial load for a **W**200 × 52 section (in column load tables provided by AISC (1989) or elsewhere) is

$$P_{\text{allow}} = 553\ \text{kN} \gg 361.2 \qquad [3 \times 120.4 \qquad \text{(may be overdesigned)}]$$

$$f_s = \frac{P_{\text{allow}}}{A} = \frac{553}{6.65} = 83.2\ \text{MPa} \qquad \text{(bending can be neglected)}$$

Now the question is whether we should use this section or one much smaller. This is answered by looking at the displacements at the strut nodes. We find these values:

Node	Displacement, mm	Strut force, kN
2	2.987	120.4
5	2.712	109.3
8	2.703	108.9

Consider the following:

1. These are theoretical displacements, and the actual displacements will probably be larger.
2. When jacking or wedging the struts against the wales, axial loads that are greater than the computed strut loads might be developed.
3. The strut forces are nearly equal; the strut displacements are nearly equal, which is ideal.

Considering these several factors, we find the struts appear satisfactory. Keep in mind this is not a very large rolled **W** section.

```
 EXAMPLE 14-1  FOUND. ANALYSIS & DESIGN 5/E--PZ-22 SHEETPILE; W200 X 52--SI

     ++++++++++++++ THIS OUTPUT FOR DATA FILE:  EX141.DTA


 SOLUTION FOR SHEET PILE WALL--CANTILEVER OR ANCHORED ++++++++++++++    ITYPE =  1

                        NO OF NP =  28                    NO OF MEMBERS = 13
          NO OF LOAD CONDITIONS =  1      NO OF BOUNDARY CONDITIONS, NZX =  0
     MAX NO OF ITERATIONS, NCYC =  1            NONLIN CHECK (IF > 0) =  0
 NO OF NODE MODULUS TO INPUT, NRC =  0          NODE SOIL STARTS, JTSOIL = 10
  LIST BAND MATRIX, LISTB (IF >0) =  0           NO OF ANCHOR RODS, IAR =  3
    INPUT NODE PRESSURES, IPRESS = 11  NO OF NON-ZERO P-MATRIX ENTRIES =  0
                                                    IMET (SI > 0) =  1

      MODULUS OF ELASTICITY =  200000.0  MPA

              SOIL MODULUS =    5000.00 +  12000.00*Z**  .50  KN/M**3
   NODE Ks REDUCTION FACTORS:  JTSOIL =   .70   JTSOIL+1 =   .90

 SHEET PILE AND CONTROL DATA:
                      WIDTH =     1.000  M
    INITIAL EMBED DEPTH, DEMB =     2.000  M
    DEPTH INCR FACTOR, DEPINC =      .500  M
 DREDGE LINE CONVERGENCE, CONV =  .050000  M


 ANCHOR RODS LOCATED AT NODE NOS =   2   5   8

 MEMBER AND NODE DATA FOR WALL WIDTH =   1.000  M

                                  LENGTH    INERTIA                    KS        SPRINGS     XMAX     NODE Q    NODE P
MEMNO   NP1   NP2   NP3   NP4       M         M*4        NODE       KN/M*3      SOIL/A.R.      M        KPA       KN
   1     1     2     3     4     1.5000   .0001150       1          .000          .000       .0000   38.0000   28.5000
   2     3     4     5     6     1.0000   .0001150       2          .000     40300.000       .0000   38.0000   47.5000
   3     5     6     7     8     1.0000   .0001150       3          .000          .000       .0000   38.0000   38.0000
   4     7     8     9    10     1.0000   .0001150       4          .000          .000       .0000   38.0000   38.0000
   5     9    10    11    12     1.0000   .0001150       5          .000     40300.000       .0000   38.0000   38.0000
   6    11    12    13    14     1.0000   .0001150       6          .000          .000       .0000   38.0000   38.0000
   7    13    14    15    16     1.0000   .0001150       7          .000          .000       .0000   38.0000   38.0000
   8    15    16    17    18      .9000   .0001150       8          .000     40300.000       .0000   38.0000   36.1000
   9    17    18    19    20      .9000   .0001150       9          .000          .000       .0000   38.0000   34.2000
  10    19    20    21    22      .5000   .0001150      10*    3500.000      1594.729       .0100   38.0000   23.4333
  11    21    22    23    24      .5000   .0001150      11*   12136.750      5753.917       .0150     .0000    3.1667
  12    23    24    25    26      .5000   .0001150      12     17000.000      8319.475       .0200
  13    25    26    27    28      .5000   .0001150      13     19696.940      9813.193       .0250
                                                        14     21970.560      5303.172       .0250

       * = Ks REDUCED BY FAC1 OR FAC2
```


Figure E14-1*c*

MEMBER MOMENTS, NODE REACTIONS, DEFLECTIONS, SOIL PRESSURE, AND LAST USED P-MATRIX FOR LC = 1

MEMNO	MOMENTS--NEAR END 1ST, KN-M		NODE	SPG FORCE, KN	ROT, RADS	DEFL, M	SOIL Q, KPA	P-, KN-M	P-, KN
1	.000	42.750	1	.0000	-.00221	.00560	.000	.000	28.500
2	-42.750	-1.616	2	120.3660	-.00081	.00299	.000	.000	47.500
3	1.616	-7.982	3	.0000	.00008	.00278	.000	.000	38.000
4	7.982	23.652	4	.0000	-.00013	.00278	.000	.000	38.000
5	-23.652	-15.988	5	109.2735	.00021	.00271	.000	.000	38.000
6	15.988	-17.627	6	.0000	.00038	.00315	.000	.000	38.000
7	17.627	18.733	7	.0000	-.00035	.00317	.000	.000	38.000
8	-18.733	-14.091	8	108.9314	-.00033	.00270	.000	.000	36.100
9	14.091	-16.134	9	.0000	-.00024	.00255	.000	.000	34.200
10	16.134	-7.207	10	3.3081	-.00083	.00207	7.260	.000	23.433
11	7.207	-1.270	11	9.1457	-.00108	.00159	19.291	.000	3.167
12	1.270	.421	12	8.4922	-.00117	.00102	17.353	.000	.000
13	-.421	.000	13	4.2252	-.00118	.00043	8.481	.000	.000
			14	-.8426	-.00118	-.00016	-3.491	.000	.000

SUM SPRING FORCES = 362.90 VS SUM APPLIED FORCES = 362.90 KN
(*) = SOIL DISPLACEMENT > XMAX(I) SO SPRING FORCE AND Q = XMAX*VALUE ++++++++++++
NOTE THAT P-MATRIX ABOVE INCLUDES ANY EFFECTS FROM X > XMAX ON LAST CYCLE ++++

DATA FOR PLOTTING IS SAVED TO DATA FILE: wall.plt
AND LISTED FOLLOWING FOR HAND PLOTTING

NODE	DEPTH	KS	COMP X,MM	XMAX	SHEAR V(I,1),V(I,2) LT OR T	RT OR B	MOMENT MOM(I,1),MOM(I,2) LT OR TOP	RT OR BOT
1	.000	.0	5.599	.000	.00	28.50	.00	.00
2	1.500	.0	2.987	.000	28.50	-44.37	42.75	42.75
3	2.500	.0	2.782	.000	-44.37	-6.37	-1.62	-1.62
4	3.500	.0	2.783	.000	-6.37	31.63	-7.98	-7.98
5	4.500	.0	2.712	.000	31.63	-39.64	23.65	23.65
6	5.500	.0	3.152	.000	-39.64	-1.64	-15.99	-15.99
7	6.500	.0	3.173	.000	-1.64	36.36	-17.63	-17.63
8	7.500	.0	2.703	.000	36.36	-36.47	18.73	18.73
9	8.400	.0	2.546	.000	-36.47	-2.27	-14.09	-14.09
10	9.300	3500.0	2.074	10.000	-2.27	17.85	-16.13	-16.13
11	9.800	12136.8	1.589	15.000	17.85	11.87	-7.21	-7.21
12	10.300	17000.0	1.021	20.000	11.87	3.38	-1.27	-1.27
13	10.800	19696.9	.431	25.000	3.38	-.84	.42	.42
14	11.300	21970.6	-.159	25.000	-.84	.00	.00	.00

Figure E14-1c (*continued*)

Step 5. Check the sheet-pile bending stresses. From the output sheet the largest bending moment is 42.75 kN · m and occurs at node 2:

$$f_s = \frac{M}{S} = \frac{42.75}{0.9679} = 44.2 \text{ MPa} \qquad \text{(well under 0.6 or 0.65}f_y\text{)}$$

In summary, it appears this is a solution. It may not be the absolute minimum cost, but it is both economical and somewhat (but not overly) conservative. Remember: Before the wales and struts are installed, excavation takes place to a depth that allows adequate workspace for the installation. That is, already some lateral displacement has not been taken into account here (we will make an estimate in Example 14-3).

Also, although it is self-evident that we could use two lines of struts (instead of the three shown), the vertical spacing would be such that the lateral movement in the region between struts could represent unacceptable perimeter ground loss.

////

14-4 ESTIMATION OF GROUND LOSS AROUND EXCAVATIONS

The estimation of ground loss around excavations is a considerable exercise in engineering judgment. Peck (1969) gave a set of nondimensional curves (Fig. 14-8) that can be used to obtain the order of magnitude. Caspe (1966, but see discussion in November 1966 critical of the method) presented a method of analysis that requires an estimate of the bulkhead deflection and Poisson's ratio. Using these values, Caspe back-computed one of the excavations in Chicago reported by Peck (1943) and obtained reasonable results. A calculation by the author indicates, however, that one could carry out the following steps and obtain results about equally good:

1. Obtain the estimated lateral wall deflection profile.

Figure 14-8 Curves for predicting ground loss. [*After Peck (1969).*]

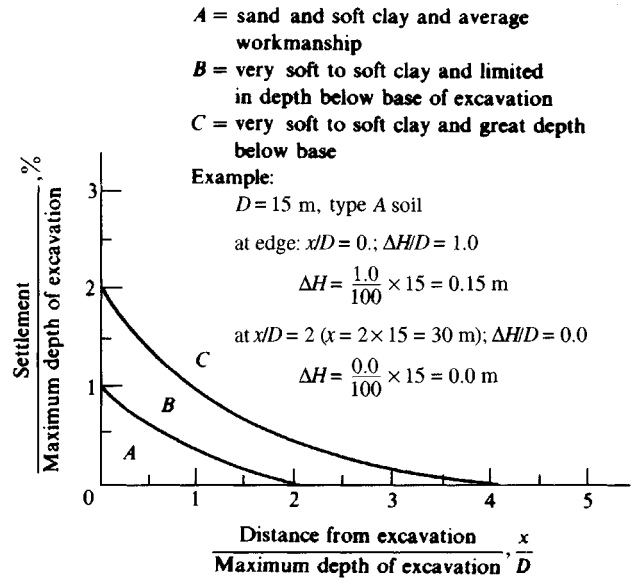

2. Numerically integrate the wall deflections to obtain the volume of soil in the displacement zone V_s. Use average end areas, the trapezoidal formula, or Simpson's one-third rule.
3. Compute or estimate the lateral distance of the settlement influence. The method proposed by Caspe for the case of the base soil being clay is as follows:
   a. Compute wall height to dredge line as H_w.
   b. Compute a distance below the dredge line

Soil type	Use $H_p \approx$
$\phi = 0$	B
ϕ–c	$0.5B \tan\left(45 + \frac{\phi}{2}\right)$

   where B = width of excavation, m or ft. From steps (*a*) and (*b*) we have

$$H_t = H_w + H_p$$

   c. Compute the approximate distance D from the excavation over which ground loss occurs as

$$D = H_t \tan\left(45° - \frac{\phi}{2}\right)$$

4. Compute the surface settlement at the edge of the excavation wall as

$$s_w = \frac{2V_s}{D}$$

5. Compute remaining ground loss settlements assuming a parabolic variation of s_i from D toward the wall as

$$s_i = s_w\left(\frac{x}{D}\right)^2$$

Example 14-2. Using the values provided by Caspe, verify the method just given. Figure E14-2 displays data from Caspe and as plotted on Peck's settlement curve. The excavation was 15.85 m (52 ft) wide and 11.58 m (38 ft) deep. The upper 4.25 m was sand backfill with the remaining depth being a soft to stiff clay with an undrained $\phi = 0°$. Displacements were taken on 1.2-m (4-ft) distances down the wall to the dredge line, and Caspe estimated the remaining values as shown on the displacement profile.

Solution. Caspe started by computing the total settlement depth based on $H_w = 11.58$ m + $H_p = B = 15.85$ m ($\phi = 0°$) = 27.43 m = D. Integrating the wall profile from 0.6 m to −26.83 m (27.43 − 0.6) using the average end area formula, we obtain

$$V_s = \left(\frac{30.5 + 5.0}{2} + 33.0 + 35.6 + 49.6 + 45.7 + \cdots + 18.0 + 12.7\right) \times 1200$$

$$= 807\,900 \text{ mm}^3 \rightarrow 0.8079 \text{ m}^3 \qquad \text{(per meter of wall width)}$$

At the wall face the vertical displacement is

$$s_w = \frac{2 \times 0.8079}{26.23} = 0.0616 \text{ m} \rightarrow \mathbf{62} \text{ mm} \qquad \text{(Peck} \approx 50 \text{ mm)}$$

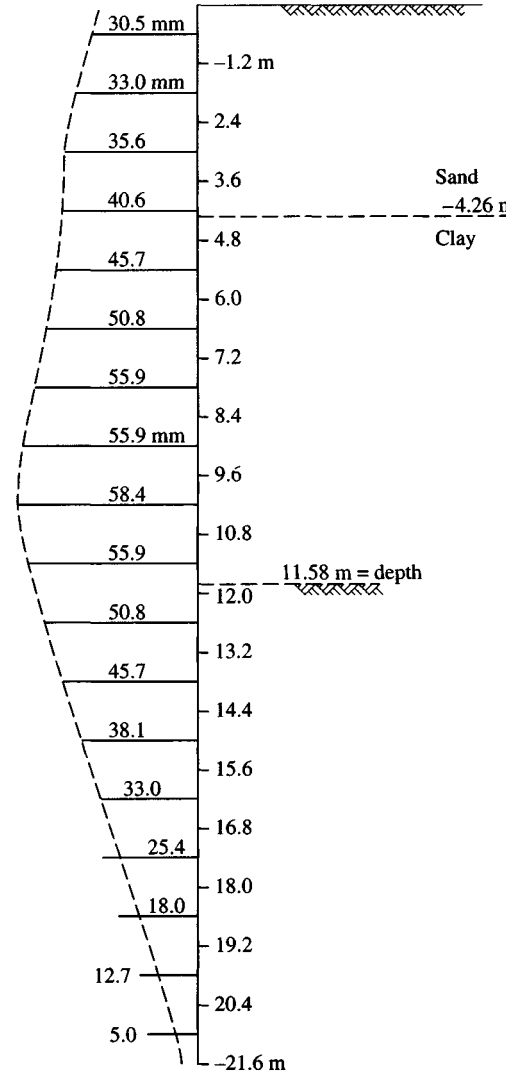

Figure E14-2*a*

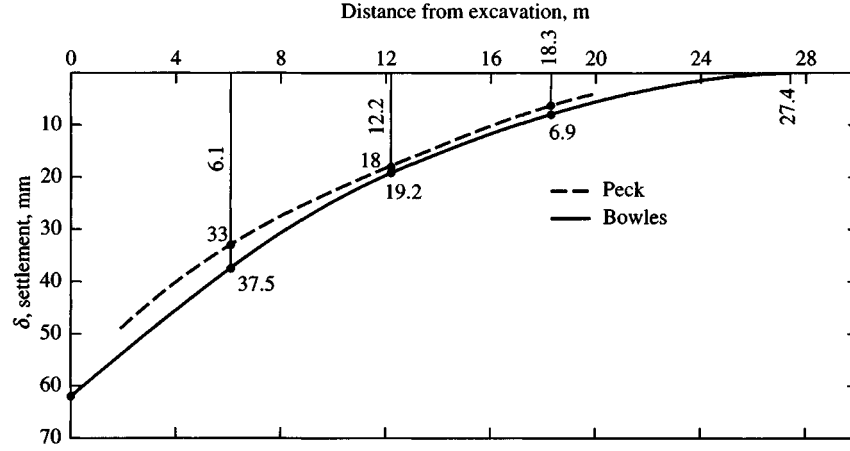

Figure E14-2*b*

At distances from the wall of 6.1, 12.2, and 18.3 m the distances from D are 21.3, 15.24, and 9.1 m, giving a parabolic variation of

$$\sigma_{6.1} = 62\left(\frac{21.3}{27.4}\right)^2 = 37.5 \text{ mm} \qquad (\text{Peck} \approx 33.0 \text{ mm})$$

$$\sigma_{12.2} = 62\left(\frac{15.24}{27.4}\right)^2 = 19.2 \text{ mm} \qquad (\text{Peck} \approx 18.0 \text{ mm})$$

$$\sigma_{18.3} = 62\left(\frac{9.1}{27.4}\right)^2 = 6.9 \text{ mm} \qquad (\text{Peck} \approx 7.6 \text{ mm})$$

These displacements are shown on the settlement versus excavation distance plot on Fig. E14-2.

////

Several factors complicate the foregoing calculations. One is the estimation of displacements below the excavation line. However, satisfactory results would probably be obtained by integrating the soil volume in the lateral displacements to the dredge line. The displacements shown here below the dredge line are an attempt to account somewhat for soil heave (which also contributes to ground loss) as well as lateral wall movement.

14-5 FINITE-ELEMENT ANALYSIS FOR BRACED EXCAVATIONS

The finite-element method (FEM) can be used to analyze a braced excavation. Either the finite element of the elastic continuum (Fig. 14-9) using a program such as FEM2D (noted in the list of programs in your README.DOC file) or the sheet-pile program FADSPABW (B-9) can be used.

14-5.1 Finite-Element Method for the Elastic Continuum

The FEM2D program (or similar) uses two-dimensional solid finite elements (dimensions of $a \times b \times$ thickness) of the elastic continuum. These programs usually allow either a plane-stress ($\sigma_x, \sigma_y > 0$; $\sigma_z = 0$) or plane-strain ($\epsilon_x, \epsilon_y > 0$; $\epsilon_z = 0$) analysis based on an input control parameter. They usually allow several soils with different stress-strain moduli (E_s) and μ values for Poisson's ratio.

For us to use these programs, it is helpful if they contain element libraries (subroutines) that can compute stiffness matrix values for solids, beam-column elements (element axial forces and bending moments), and ordinary column (AE/L) elements. Some programs allow additional elements, but for two-dimensional analyses of both walls and tunnel liners, these are usually sufficient and are a reasonable balance between program complexity and practical use.

In an analysis for an excavation with a wall one would develop a model somewhat as shown in Fig. 14-9. Initially it would be rectangular, but one should try to take advantage of symmetry so that only the excavation half shown is analyzed to reduce input and computational time (and round-off errors). The cross section represents a unit thickness, although FEM2D allows a thickness to be input such that shear walls, which are often one concrete block thick, can be analyzed.

It would be necessary to estimate the lateral and vertical dimensions of the model. Lateral fixity is assumed along the vertical line of symmetry (the C.L.). It is convenient to model the other two cut boundaries with horizontal and vertical columns or struts as shown.

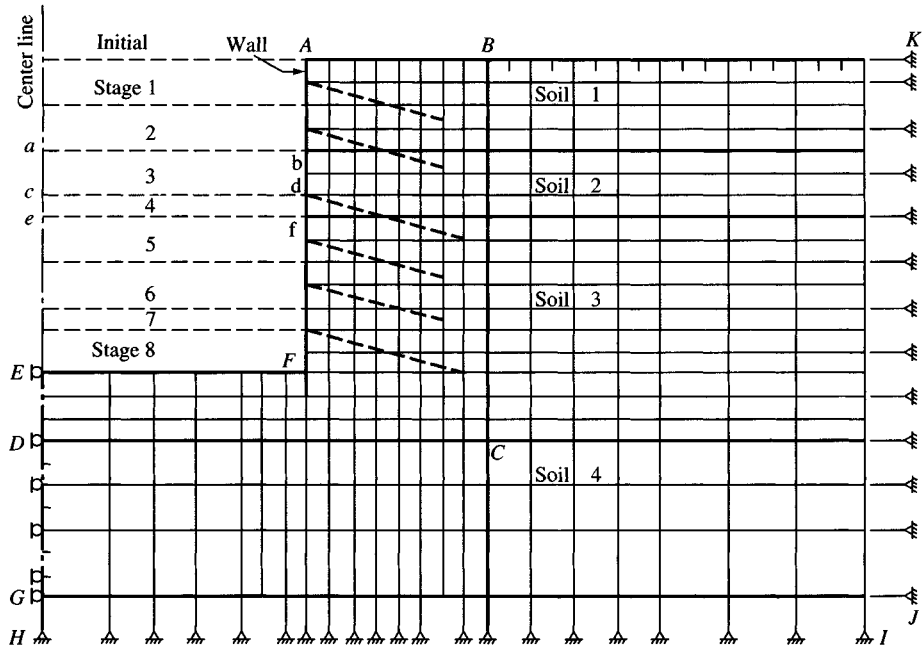

Figure 14-9 A grid of the elastic continuum for using a FEM for estimating excavation movements.

The use of strut-supported boundaries allows a quick statics check, since the sum of the axial forces in the bottom vertical struts is the weight of the block at any stage. The horizontal struts on the right side provide a structurally stable soil block. If the right-side nodes are fixed, they tend to attract stresses unless a very large model is used. By using struts, their EI/L can be varied so that they provide structural stability without attracting much stress. If there are large axial loads in the horizontal struts, for any EI/L, the model is too small. If large axial loads occur, either additional elements must be added to the right or the element x coordinates of several of the right-side nodes must be increased to produce wider elements and a larger model.

Wall bracing (or struts) can be modeled by inputting either lateral node forces or springs; tiebacks can be modeled by inputting AE/L-type elements defined by end coordinates. The node spacing should be such that any interior tiebacks lie along corner nodes, or so the horizontal component of AE/L is colinear with a node line. This methodology also allows modeling the vertical force component if desired.

Node spacing should be closer (as shown in Fig. 14-9) in critical regions, with larger element spacing away from the critical zone. Node spacing can be somewhat variable using more recent FEM that employ isoparametric elements; there is less flexibility with the older FEM programs, which used triangular nodes (rectangles are subdivided into triangles, manipulated, and then converted back). The trade-off, since either model computes about the same results, is to use the method with which you are most familiar.

Model soil excavation in stages as:

1. Vertical—nodal concentration of removed soil *weight* overlying a node as a ↑ force.
2. Horizontal—nodal concentration of $K \times$ removed soil weight overlying the node as a horizontal node force toward the excavation.

The finite-element analysis for an excavation involves several steps [see also Chang and Duncan (1970)], as follows:

1. Grid and code a block of the elastic continuum, taking into account excavation depth and any slopes. It is necessary that the several excavation stages coincide with horizontal grid lines.
2. Make an analysis of the unexcavated block of step 1 so that you can obtain the node stresses for the elements in the excavation zone.
3. Along the first excavation line of the finite-element model, obtain the stresses from step 2 and convert them to nodal forces of opposite sign as input for the next analysis, which will be the excavation of stage 1. Remove all the elements above the excavation outline.
4. Execute the program with the new input of forces and the model with the elements that were removed in step 3. From this output, obtain the node stresses along the next excavation line. Also, remove all the elements above the current excavation line.
5. Repeat steps 3 through 4 as necessary.

It requires clever node coding to produce an initial data set that can be reused in the several excavation stages by removing a block of elements for that stage. It may be preferable to use some kind of element data generator for each stage; some programs have this program built in and call it a "preprocessor."

There are major problems with using the FEM of the elastic continuum for excavations, including at least the following:

1. A massive amount of input data is required. Several hundred elements may be required for each stage plus control parameters and other data.
2. Obtaining soil parameters E_s and μ for the several strata that may be in the model is very difficult.
3. Most critical is the change in the elastic parameters E_s and Poisson's ratio μ when the soil expands laterally toward the excavation or against the excavation wall and vertically upward (heaves) from loss of overburden pressure. If these values are not reasonably correct, one does a massive amount of computation to obtain an estimate that may be as much as 100 percent in error.

Clough and coworkers at Virginia Polytechnic Institute claim modest success using this procedure and have published several papers in support of these claims—the latest is Clough and O'Rourke (1990), but there were several earlier ones [Clough and Tsui (1974); Clough et al. (1972)]. Others have used this method in wall analysis, including Lambe (1970), but with questionable success.

14-5.2 The Sheet-Pile Program to Estimate Lateral Wall Movements

The sheet-pile program FADSPABW can be used to make a wall movement estimate as follows:

1. Locate the nodes at convenient spacings. You will want to locate nodes at all tiebacks or struts. Also locate nodes about 0.5 m below where any tiebacks or struts are to be installed so there is room for their installation.

2. Code the full wall depth including to the dredge line and the depth of embedment for stage 1. You do this so that most of the element and other data can be reused in later stages by editing copies of the initial data file. Use NCYC = 1 and probably NONLIN = 0 to avoid excessive refinement.
3. Referring to Fig. 14-4, make a number of trials using the conventional lateral pressure profile and including any surcharge. Do not use a pressure diagram such as in Fig. 14-5 at this point. These several trials are done to find a reasonable depth of excavation so that the first strut can be installed without excessive lateral deflection of the wall top. Depending on the situation, this displacement probably should be kept to about 25–30 mm.
4. Copy the foregoing data set and edit it to install the first strut and excavate to the next depth. You can now continue using the conventional lateral pressure profile or some kind of diagram of Fig. 14-5. The following program parameters are changed: JTSOIL; IAR = 1 (first strut); and IPRESS [to add some PRESS(I) values]; and reduce XMAX(I) entries.
5. Now copy this data set at a second strut; change JTSOIL; IAR = 2; IPRESS [and PRESS(I)]; and again reduce the number of XMAX(I) entries.
6. Make a copy of this data set, add the next strut, and so forth.

The displacement profile is the sum of the displacements with the sign from the preceding sequence of steps.

Example 14-3. Make an initial estimate of the lateral movements of the braced excavation for which the sheeting and struts were designed in Example 14-2. The data sets for this problem are on your program diskette as EX143A, EX143B, EX143C, and EX143D.DTA, so you can rapidly reproduce the output.

Solution.

Stage 1. Draw the full wall height of 11.3 m as shown in Fig. E14-3*a* and locate nodes at strut points and other critical locations. For struts S1, S2, additional nodes of 0.5 m are added below the strut to give enough room for its installation. The 1.8 m depth below strut S3 is only divided into two 0.9-m elements. From this information the initial input is

NP = 34 (17 nodes—we are using more than in Example 14-2)
NM = 16
IAR = 0
JTSOIL = 4

The soil pressure diagram used is shown in Fig. E14-3*b*, and the last (4th node value) nonzero entry = 16.5 kPa = $16.5zK_o$ = 16.5(2.0)(0.5). Note use of K_o and not K_a to give a somewhat more realistic model.

Refer to data set EX143A.DTA for the rest of the input and use it to make an execution for a set of output.

Stage 2. Make a copy of EX143A.DTA as EX143B.DTA (on your diskette) with the strut installed IAR = 1, JTSOIL, IPRESS, PRESS(I), and XMAX(I) reduced. Refer to the pressure profile for the additional PRESS(I) entries.

Make an execution of this data set to obtain a second set of output. You have at this point excavation to node 8 with strut S1 installed at node 3.

Stage 3. Make a copy of EX143B.DTA as EX143C.DTA (on your diskette). Now install strut S2 using IAR = 2. Use JTSOIL = 12 and adjust IPRESS, PRESS(I), and XMAX(I).

Make an execution of this data set to obtain a third set of output.

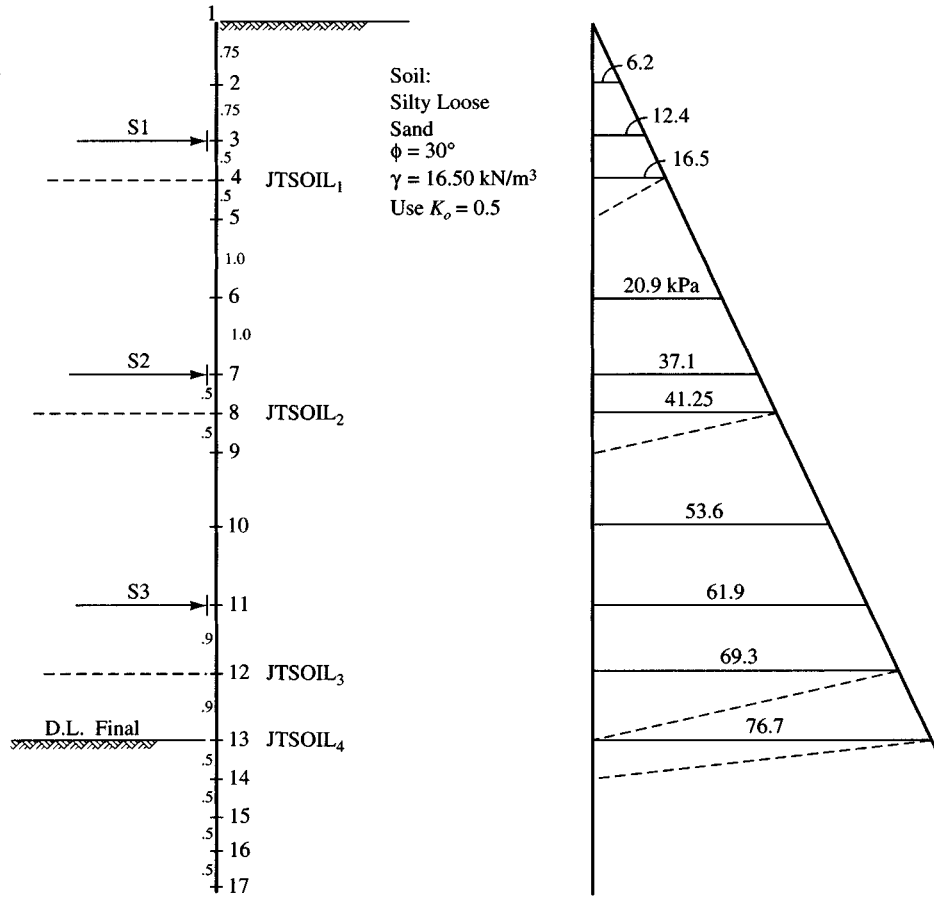

(*a*) *P–X* & nodes. (*b*) Pressure profile.

Figure E14-3

Stage 4. Make a copy of EX143C.DTA as EX143D.DTA (on your diskette). Now install strut S3 using IAR = 3. Use JTSOIL = 13 (will excavate to bottom of excavation) and adjust IPRESS, PRESS(I), and XMAX(I).

Make an execution of this data set to obtain a fourth set of output, etc. (takes 8 data sets).

A partial output summary follows:

		Stage 1	Stage 2	Stage 3	Stage 4	
			Excavate to			
Node		2.0 m	5.0 m	8.4 m	9.3 m	$\sum \delta_h$
	1	7.0 mm	−3.1	−0.5	−0.6	2.8 mm
S1	3	3.7	1.4	0.4	0.8	6.3
	5	1.7	4.2	1.2	1.8	8.9
S2	7	—	5.3	4.8	3.0	13.1
	9	—	3.3	9.5	4.0	16.8
S3	11	—	0.2	13.5	4.3	18.0
B.E.	13	—	−0.2	6.1	3.9	9.8

The total node displacements $\sum \delta_h$ look reasonable for this type of excavation. It is not unreasonable that there could be 18.0 mm of displacement at strut S3. If the value is deemed high, one can do some adjusting, but basically this procedure gives you an estimate of what the lateral movements might be. They could be less than this but are not likely to be more unless there is extremely poor workmanship.

The strut forces and wales were designed in Example 14-2. This example is only to give an estimate of lateral displacements. If you work with copies of the data sets you might be able to improve the displacements, but keep in mind that no matter how you manipulate the numbers the actual measured values are what count.

////

Example 14-3 gives a fairly simple means to make an estimate of lateral wall movement into an excavation. Notice that the first set of data (EX143A.DTA) is the most difficult. Beyond that only a few values are changed. Actually, to avoid confusing the user the data sets have generally been edited more than actually required for all but the last one. Note also that a backfill surcharge or some earth pressure factor other than K_o can be used to produce a number of different earth pressure and displacement profiles.

In any case this procedure is about as accurate (in advance of construction) as any other procedure and far simpler than the FEM of the elastic continuum.

14-6 INSTABILITY DUE TO HEAVE OF BOTTOM OF EXCAVATION

When a braced excavation (sometimes called a cofferdam) is located either over or in a soft clay stratum as in Fig. 14-10*a*, the clay may flow beneath the wall and into the excavation, producing *heave* if sufficient soil is removed that the resisting overburden pressure is too small.

The pressure loss from excavation results in a base instability, with the soil flow producing a rise in the base elevation commonly termed *heave,* which can range from a few millimeters to perhaps 300 mm. This case can be analyzed from Mohr's circle using Eqs. (2-54) and (2-55) as done in Fig. 14-2 or as the bearing failure of Fig. 4-1.

There are two general cases to consider:

Case 1. In this instance the goal is to provide sufficient depth of the piling of Fig. 14-10 to prevent the soft underlying clay from squeezing into the excavation. For this case and

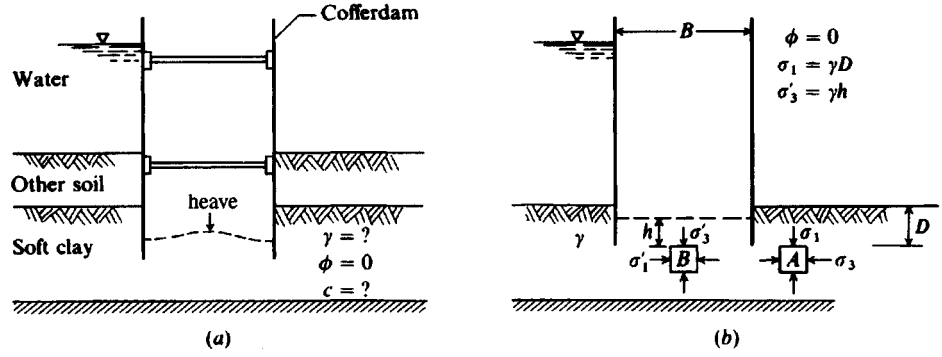

Figure 14-10 (*a*) Cofferdam on soft clay; (*b*) theoretical solution.

referring to Fig. 14-10 for identification of terms we have (noting $K_a = \sqrt{K_a} = 1$) for element A

$$\sigma_3 = \gamma D - 2s_u \tag{a}$$

and for element B we have

$$\sigma_1' = \gamma h + 2s_u \tag{b}$$

since $\sigma_1' = \sigma_3$ and $\sigma_3' = \gamma h = \sigma_1' - 2s_u$. Substituting values, we find that

$$\gamma h = \gamma D - 2s_u - 2s_u$$

Solving for the critical depth $D = D_c$ and inserting an SF we obtain the desired equation:

$$D_c = \frac{\gamma h + 4s_u}{\gamma(\text{SF})} \quad (\phi = 0°) \tag{14-1}$$

Case 2. This is a general analysis for excavation depth where the depth of excavation is limited such that the effective bearing capacity of the base soil can be utilized.

This more general analysis is as follows (refer to Fig. 14-11). Block $OCBA$ produces a net vertical pressure σ_v on OA of

$$\sigma_v = \gamma D + q_s - \frac{F_f - Dc_a}{r} \tag{a}$$

where terms not shown on Fig. 14-11 are

$F_f = \frac{1}{2}\gamma D^2 K_a \tan\phi$
ϕ = friction angle of soil above dredge line
c = cohesion of soil above dredge line
c_a = wall adhesion as fraction of c
c' = base soil cohesion
q_s = any surcharge
$r = 0.707B$

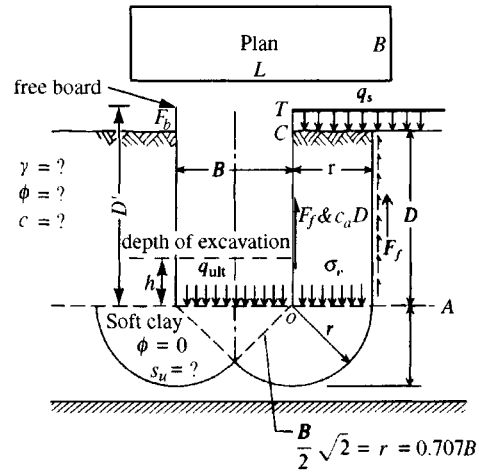

Figure 14-11 Stability of excavation against bottom heave using bearing capacity fundamentals.

Substitution for F_f into Eq. (*a*) and equating $\sigma_v = q_{ult}$ (at the same depth on either side of the wall) we obtain

$$\frac{\gamma Dr + q_s r - \left(\frac{1}{2}\gamma D^2 K_a \tan\phi + c_a D\right)}{r} = q_{ult}$$

where $q_{ult} = c'N'_c + \gamma h N_q$.

TABLE 14-1

Bearing capacity factor N'_c for square and circular bases and for strip bases

Interpolate table or plot N'_c (ordinate) versus D/B (abscissa) for intermediate values. Tabulated values are similar to those given by Skempton (1951) [see also Meyerhof (1972)] and later on the Bjerrum and Eide (1956) curves. Values for N'_c can be obtained from Hansen's bearing capacity equation of $N'_c = 5.14(1 + s'_c + d'_c)$ shown in Table 4-1 and Table 4-5*a*. The Hansen values are compared to Skempton's, which are given in parentheses. In general, N_c for a rectangle is computed as

$$N'_{c,\text{rect}} = N_c(0.84 + 0.16B/L);$$

For a strip, $B/L \to 0$.

D/B	$(1 + s'_c + d'_c)$	N'_c	$N'_{c,\text{strip}}$
0	$5.14(1 + 0.2 + 0)$	= 6.2 (6.2)	$\pi + 2 = 5.14$
0.25	$(1 + 0.2 + 0.1)$	= 6.7 (6.7)	$\times 0.84 = 5.6$
0.50	$(1 + 0.2 + 0.2)$	= 7.2 (7.1)	$\times 0.84 = 6.0$
0.75	$(1.2 + 0.4 \times 0.75)$	= 7.7 (7.4)	= 6.5
1.0*	$(1.2 + 0.4\tan^{-1} 1)$	= 7.8 (7.7)	= 6.6
1.5	$(1.2 + 0.4\tan^{-1} 1.5)$	= 8.2 (8.1)	= 6.9
2.0	$(1.2 + 0.443)$	= 8.4 (8.4)	= 7.1
2.5	$(1.2 + 0.476)$	= 8.6 (8.5)	= 7.2
3.0	$(1.2 + 0.500)$	= 8.7 (8.8)	= 7.3
4.0	$(1.2 + 0.530)$	= 8.9 (9.0)**	= 7.5
5.0	$(1.2 + 0.549)$	= 9.0 (9.0)	= 7.5

*Discontinuous at $D/B = 1$ (from $0.4D/B$ to $0.4\tan^{-1} D/B$).

**Limiting value of $N'_c = 9.0$.

Examples

Given. Square footing on soft clay with a $D/B = 2$. Obtain N_c.
Solution. At D/B above obtain directly $N'_c = \mathbf{8.4}$.

Given. Rectangular footing on soft clay. $B = 2$ m, $L = 4$ m and embedment depth $D = 1$ m. Obtain N_c.
Solution. Compute

$$B/L = 2/4 = 0.5; \qquad D/B = 1/2 = 0.5$$

At $D/B = 0.5$ obtain

$$N'_c = 7.2$$

and

$$N'_{c,\text{rect}} = N_c(0.84 + 0.16B/L) = 7.2(0.84 + 0.16 \times 0.5) = \mathbf{6.6}$$

Substituting and simplifying, we obtain the maximum depth of wall D' (including any freeboard depth F_b) as

$$D' = \frac{r(c'N_c' + \gamma h N_q - q_s)}{\gamma r - \frac{1}{2}\gamma D K_a \tan\phi - c_a} + F_b \tag{14-2}$$

For the case of $\phi = 0$ *above the base of the wall,* Eq. (14-2) reduces to

$$D' = \frac{c'N_c' + \gamma h N_q - q_s}{\gamma - c_a/r} + F_b \tag{14-2a}$$

In these equations use an SF on the order of 1.2 to 1.5 (i.e., $d'_{\text{des}} = D'/\text{SF}$); use the upper range of around 1.4 to 1.5 for anisotropic soils [see Mana and Clough (1981)]. Carefully note that the inside depth h above the wall base is a factor, and if the upper soil has a ϕ angle, the critical depth is found by trial using Eq. (14-2). Equation (14-2*a*) contains a bearing capacity factor N_c'. This value is obtained from Table 14-1, and one uses either N_c' or $N'_{c,\text{rect}}$ depending on whether the excavation is square or has $B/L < 1$. The values in Table 14-1 were given as curves by Skempton (1951), who plotted them from work by Meyerhof in the late 1940s. Bjerrum and Eide (1956) are usually incorrectly credited with the curves. The author has elected to provide tabulated values so that users can either compute values or draw curves to a useful scale.

Bjerrum and Eide (1956) used the N_c' bearing-capacity factors from Table 14-1 to analyze the base stability of 14 deep excavations and found a very reasonable correlation of ±16 percent. Later Schwab and Broms (1976) reanalyzed the Bjerrum and Eide excavations plus two others and concluded that the correlation might have been improved if anisotropy had been considered.

Example 14-4. Refer to Fig. E14-4. Can an excavation be made to 18 m, and if so what depth of sheeting is required to avoid a bottom heave (or soil flow into the excavation) based on using an SF of at least 1.25? Note that this problem formulation is the usual situation, and Eqs. (14-1) and (14-2) are of little value, but the derivation procedure is valuable since we have to use some of the parts.

Solution. Let us use these estimates:

$$\gamma_{\text{sand}} = 17.00 \text{ kN/m}^3$$
$$\gamma_{\text{clay}} = 18.00 \text{ kN/m}^3$$

Consider the 3 m of sand as a surcharge, giving

$$q_s = 3 \times 17.00 = \mathbf{51} \text{ kPa}$$

Take an unweighted[4] average of the undrained shear strength of the clay for design, so that

$$s_{u,\text{av}} = \frac{40 + 60}{2} = \mathbf{50} \text{ kPa}$$

[4]An unweighted average is acceptable if no strength value in the region from B above to $2B$ below the base depth is smaller than 50 percent of the average strength. If any strength values are smaller than 50 percent of the average, then you should weight the strength as $s_{u,\text{av}} = \sum s_{u,i} \times H_i / \sum H_i$.

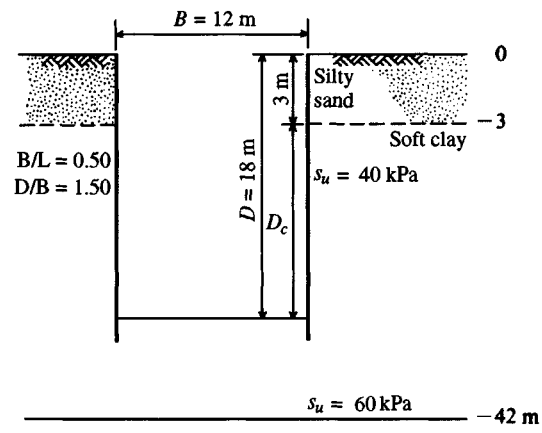

Figure E14-4

Assume that there will be wall adhesion of $0.8c$. We will try an initial depth of $D = 18 + 1 = 19$ m. This gives the depth of interest as

$$D' = 19 - 3 \text{ m (of sand)} = \mathbf{16} \text{ m}$$

The dimension $r = 0.707B = 0.707 \times 12 = \mathbf{8.5}$ m. For this state we have

$$\sigma_v = -D'c_a/r + \gamma D' + q_s$$

and substitution gives

$$\begin{aligned}\sigma_v &= -16(0.8 \times 50/8.5) + 16(18.0) + 51 \\ &= -75.3 + 288.0 + 51 = \mathbf{263.7} \text{ kPa}\end{aligned}$$

The bearing-pressure resistance $q_{ult} = cN'_{c,rect} + \gamma h$ $(h = 1$ m). Thus,

$$\begin{aligned}N'_c &= (5.14 \times 1.2)(1 + 0.4 \cdot \tan^{-1} 1.5)(0.84 + 0.16 \times 0.50) \quad \text{(see Table 14-1)} \\ &= 6.17 \times 1.39 \times 0.92 = \mathbf{7.89}\end{aligned}$$

This result gives $q_{ult} = 50(7.89) + 18(1) = 412.5$. The resulting safety factor is

$$\text{SF} = \frac{412.5}{263.7} = \mathbf{1.56} \qquad \text{(O.K.)}$$

Note: The wall sheeting would have to be at least 18 m, but 19 m gives some base restraint as well as a slight increase in the SF.

////

14-7 OTHER CAUSES OF COFFERDAM INSTABILITY

A bottom failure in cohesionless soils may occur because of a piping, or *quick,* condition if the hydraulic gradient h/L is too large. A flow net analysis may be used as illustrated in Fig. 2-12 (it does not have to be highly accurate) to estimate when a quick condition may occur. Possible remedies are to drive the piling deeper to increase the length of the flow path L of Fig. 14-12*a* or to reduce the hydraulic head h by less pumping from inside the cell. In a few cases it may be possible to use a surcharge inside the cell.

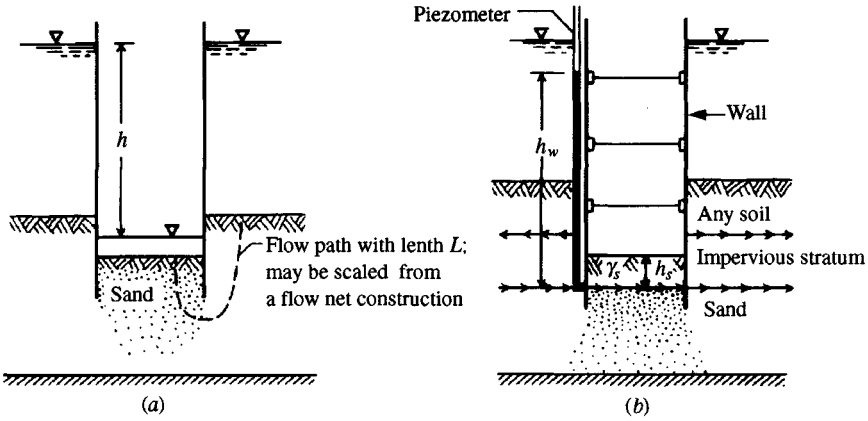

Figure 14-12 (*a*) Conditions for piping, or quick, conditions; (*b*) conditions for a *blow-in* (see also Figs. 2-10, 2-11, and 2-12).

In Fig. 14-12*b*, the bottom of the excavation may *blow in* if the pressure head h_w indicated by the piezometer is too great, as follows (SF = 1.0):

$$\gamma_w h_w = \gamma_s h_s$$

This equation is slightly conservative, since the shear, or wall adhesion, on the walls of the cofferdam is neglected. On the other hand, if there are soil defects in the impervious layer, the blow-in may be local; therefore, in the absence of better data, the equality as given should be used. The safety factor is defined as

$$\text{SF} = \frac{\gamma_s h_s}{\gamma_w h_w} > 1.25$$

14-8 CONSTRUCTION DEWATERING

Figure 14-12 indicates that water inflow into an excavation can cause a bottom failure. Where it is impractical or impossible to lower the water table, because of possible damage claims or environmental concerns, it is necessary to create a nearly impervious water barrier around the excavation. Because no barrier is 100 percent impervious, it is also necessary to provide drainage wells below the bottom of the excavation, called sump pits, that are pumped as necessary to maintain a reasonably dry work space.

The groundwater level outside the excavation will require monitoring wells to avoid real (or imagined) claims for damages from any lowering of the original groundwater level.

Where it is allowed to depress the water table in the vicinity of the excavation, a system of perimeter wells is installed. This system may consist of a single row of closely spaced wellpoints around the site. A wellpoint is simply a section of small-diameter pipe with perforations (or screen) on one end that is inserted in the ground. If the soil is pervious in the area of the pipe screen, the application of a vacuum from a water pump to the top of the pipe will pull water in the vicinity of the pipe into the system. A vacuum system will be limited in the height of water raised to about 6 m. Theoretically water can be raised higher, but this type of system is less than theoretical. More than one set of perimeter wells can be installed as illustrated in Fig. 14-13. This type of system is seldom "designed"; it is contracted by

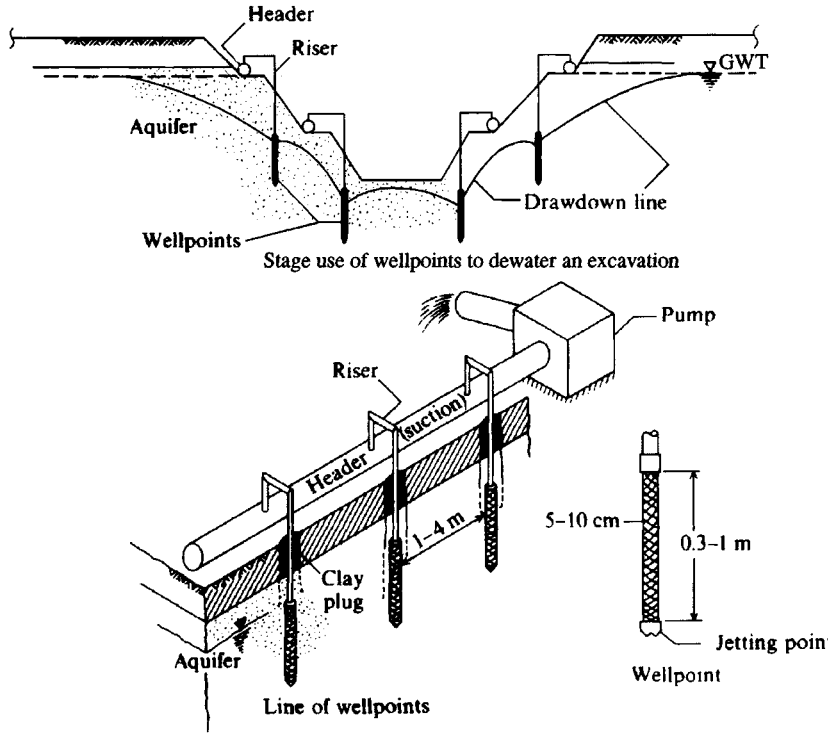

Figure 14-13 Wellpoints used for dewatering.

companies that specialize in this work. Although rough computations can be made, the field performance determines the number of wellpoints and amount of pumping required.

Where wellpoints are not satisfactory or practical, one may resort to a system of perimeter wells that either fully or partially penetrate the water-bearing stratum (aquifer) depending on site conditions and amount of pumpdown. Again, only estimates of the quantity of water can be made, as follows.

One may use a plan flow net as in Fig. 14-14 to obtain the seepage quantity. A plan flow net is similar to a section flow net as in Chap. 2. The equipotential drops are now contour lines of equal elevation intersecting the flow paths at the same angle. Sufficient contour lines must be established to represent the required amount of drawdown to provide a dry work area.

Some approximation is required, since it is not likely that the piezometric head is constant for a large distance around an excavation. Furthermore, approximation is necessary because a system of wells located around the excavation will not draw down the water to a constant contour elevation within the excavation. The water elevation will be a minimum at—and higher away from—any well. From a plan flow net the quantity of water can be estimated as

$$Q = \alpha k(\Delta H)\frac{N_f}{N_e}L \tag{14-3}$$

where N_f = number of flow paths (integer or decimal)
N_e = number of equipotential drops (always integer)

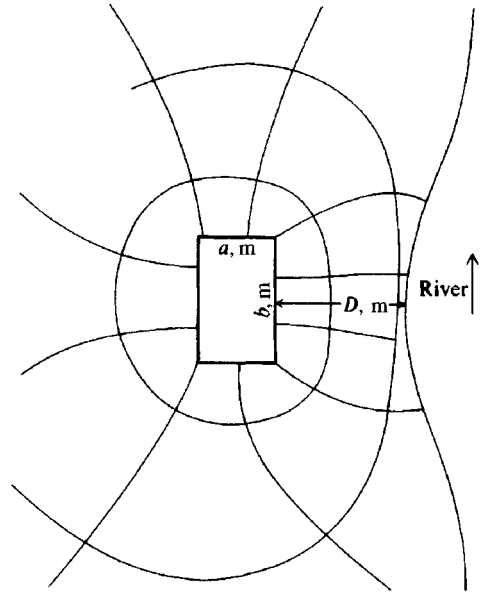

Figure 14-14 Plan flow net. Note it is only necessary to draw enough flow and equipotential lines to obtain N_f, N_e.

$\Delta H = H^2 - h^2$ for gravity flow (see Fig. 14-15)
$= H - h_w$ for artesian flow
$L = 1.0$ for gravity flow
$=$ thickness of aquifer for artesian flow
$k =$ coefficient of permeability in units consistent with H and L
$\alpha = 0.5$ for gravity flow
$= 1.0$ for artesian flow

An estimate of the number of wells and flow per well is obtained by *placing one well in the center of each flow path.* The resulting flow per well is then

$$\text{Number of wells} = N_f$$
$$\text{Flow per well} = Q/N_f$$

An estimate of the quantity of water that must be pumped to dewater an excavation can also be obtained by treating the excavation as a large well (Fig. 14-15) and using the equation for a gravity flow well,

$$q = \frac{\pi k(H^2 - h_w^2)}{\ln(R/r_w)} \tag{14-4}$$

where terms not previously defined are

$H =$ surface elevation of water at the maximum drawdown influence a distance R from well center
$h_w =$ surface elevation of water in well
$r_w =$ well radius (use consistent units of m or ft)

This equation is for *gravity wells;* that is, the piezometric head and static water level are coincident, which is the likely case for pumping down the water table for a large excavation.

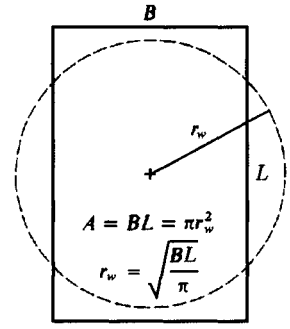

Excavation analyzed as large well of radius, r_w

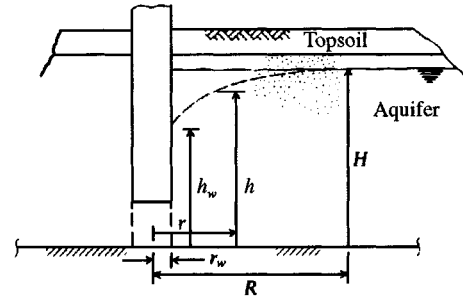

Gravity well hydraulics

Figure 14-15 Approximate computation for flow quantity to dewater an excavation.

The maximum radius of drawdown influence R is not likely to be known; however, one may estimate several values of R/r_w and obtain the corresponding probable pumping quantities Q. The value of the static groundwater level H is likely to be known, and h_w would normally be estimated at 1 to 2 m below the bottom of the excavation.

This estimate of well pumping to dewater an excavation should be satisfactory for most applications. It is not likely to be correct, primarily because the coefficient of permeability k will be very difficult to evaluate unless field pumping tests are performed. It is usually sufficient to obtain the order of magnitude of the amount of water to be pumped. This is used for estimating purposes, and the contract is written to pay for the actual quantity pumped.

Example 14-5. Estimate the flow quantity to dewater the excavation shown in Fig. 14-14. Other data are as follows:

$$H = 50 \text{ m} \qquad a = 60 \text{ m}$$
$$\Delta H = 15 \text{ m} \qquad b = 100 \text{ m}$$
$$k = 0.2 \text{ m/day} \qquad D = 100 \text{ m}$$

The soil profile is as shown in Fig. E14-5.

Solution. We will use a plan flow net (Fig. 14-14 was originally drawn to scale) and compute the quantity using Eq. (14-3) and check the results using Eq. (14-4).

Step 1. Compute Q for the plan flow net (assume gravity flow after drawdown is stabilized). From Fig. 14-14, $N_f = 10$; $N_e = 2.1$; and from Fig. E14-5 we obtain

$$H = 50 \text{ m} \qquad H^2 = 2500 \text{ m}^2$$
$$h_w = 34 \text{ m} \qquad h_w^2 = 1156 \text{ m}^2$$

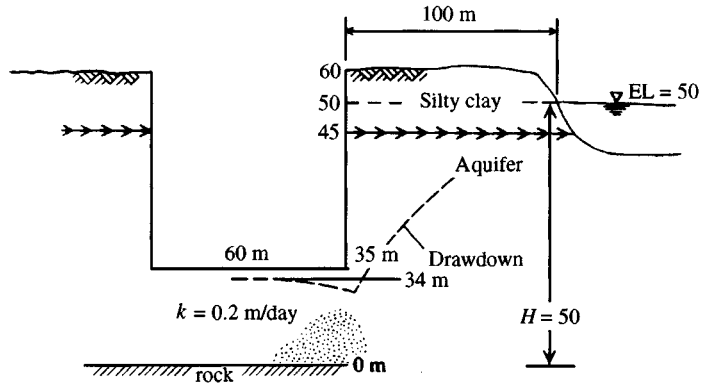

Figure E14-5

Substitution of these values into Eq. (14-3) with $\alpha = 0.5$ yields

$$Q = \alpha k(\Delta H)\frac{N_f}{N_e}L = 0.5 \times 0.2 \times (2500 - 1156)\frac{10}{2.1}(1) = \mathbf{640}\ \text{m}^3/\text{day}$$

and since $N_f = 10$ the number of wells = 10.

Step 2. Check results using Eq. (14-4):

$$Q = \frac{\pi k(H^2 - h_w^2)}{\ln(R/r_w)} \qquad \text{(may be O.K. when drawdown is stabilized)}$$

$$R = 100\ \text{m (unless we draw down the river)} + r_w$$

$$r_w = \sqrt{\frac{A}{\pi}} = \sqrt{\frac{60 \times 100}{\pi}} = 43.7 \rightarrow \text{use } \mathbf{44}\ \text{m}$$

Substitution gives

$$Q = \frac{\pi \times 0.2(2500 - 1156)}{\ln(144/44)} = \mathbf{712}\ \text{m}^2/\text{day}$$

This flow quantity compares quite well with the flow net construction, and the actual flow quantity may be on the order of 675 to 750 m^3/day.

////

14-9 SLURRY-WALL (OR -TRENCH) CONSTRUCTION

The placement of a viscous fluid, termed a slurry, in a narrow trench-type excavation to keep the ground from caving is a method in use since the early 1960s. The basic method had been (and is) used for oil well and soil exploration drilling to maintain boreholes in caving soils without casing. The large hydrostatic pressure resulting from several hundred meters of slurry allowed retention of oil or gas in oil wells until they could be capped with valving to control the fluid flow rate. The slurry used for these procedures is generally a mix of bentonite (a montmorillonitic clay-mineral-based product), water, and suitable additives.

Walls constructed in excavations where a slurry is used to maintain the excavation are termed *slurry, diaphragm-slurry,* or simply *diaphragm walls.* Figure 14-16 illustrates a

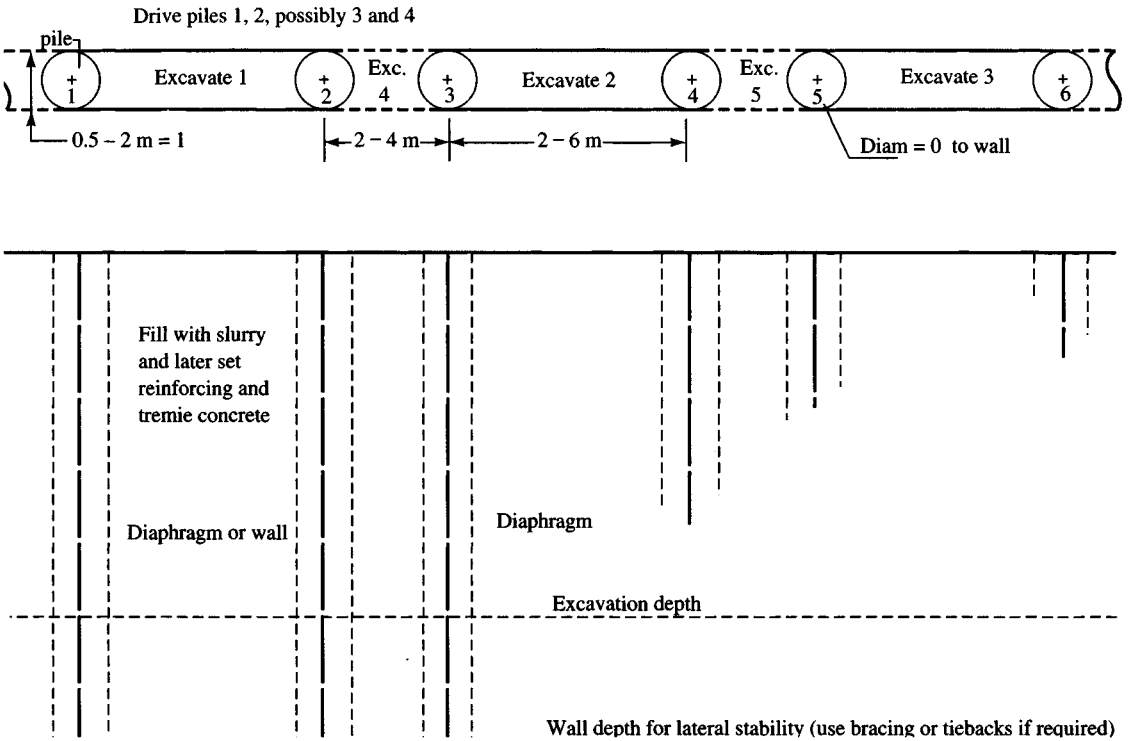

Figure 14-16 Slurry method for diaphragm wall. Drive piles for tying wall sections together. Excavate as zones 1 and 2, perhaps 3 using slurry to keep excavation open. Set rebar cages and tremie concrete for wall 1, 2, perhaps 3. Excavate zone 4, perhaps 5 using slurry, set rebar cages and tremie concrete to complete a wall section.

method of constructing a diaphragm wall. Here piles are driven on some spacing, and alternate sections are excavated, with slurry added to keep the cavity full as excavation proceeds to the desired depth. It is necessary to maintain the cavity full of slurry—and sufficiently agitated to maintain a uniform density—to keep the sides of the excavation from caving. Reinforcing bar cages are then put in place, and concrete is placed by a *tremie* (a pipe from the surface to carry the concrete to the bottom of the excavation) to fill the trench from the bottom up.

The slurry displaced by the concrete is saved in a slurry pit for use in the next section of wall, etc. The pipe piles shown (not absolutely necessary for all walls) can be pulled after the first wall sections are formed and partially cured, or they can be left in place. The purpose of the piles is to provide a watertight seal and continuity between sections. Although the piles shown are the full wall width, they can be some fraction of the width and serve equally well.

In cases where the wall depth is too great for piles to self-support the lateral pressure from outside the excavation, the walls can be braced or tiebacks used. Tiebacks require drilling through the concrete, but this is not a major task with modern equipment so long as the reinforcement cages are designed so that the drill does not intersect rebars. These types of walls are usually left in place as part of the permanent construction.

This method and similar wall construction methods are under continuous development—primarily outside the United States. Figure 14-17 illustrates one of the more recent proprietary procedures for producing a slurry-type wall, which consists of three drills aligned with mixing paddles as shown. Here a soil-cement slurry (with various additives depending on wall purpose) is used, producing what is called a soil-cement mixed wall (SMW). Wide-flange beams can be inserted into the freshly constructed SMW section for reinforcing if necessary. Wall sections can range in width from about 1.8 to 6 m and up to 61 m in depth. Taki and Yang (1991) give some additional details of installation and use. A major advantage of this type of construction is that there is very little slurry to dispose of at the end of the project.

Open trenches that are later backfilled or filled with clay, clay-soil, or lean concrete to act as cutoff walls (as for dams) and to confine hazardous wastes are termed *slurry trenches.* These are widely used with bentonite as the principal slurry additive.

Figure 14-17 New method for constructing a soil-cement mixed wall (SMW). (Courtesy Osamu Taki, SCC Technology, Box 1297, Belmont, CA 94002.)

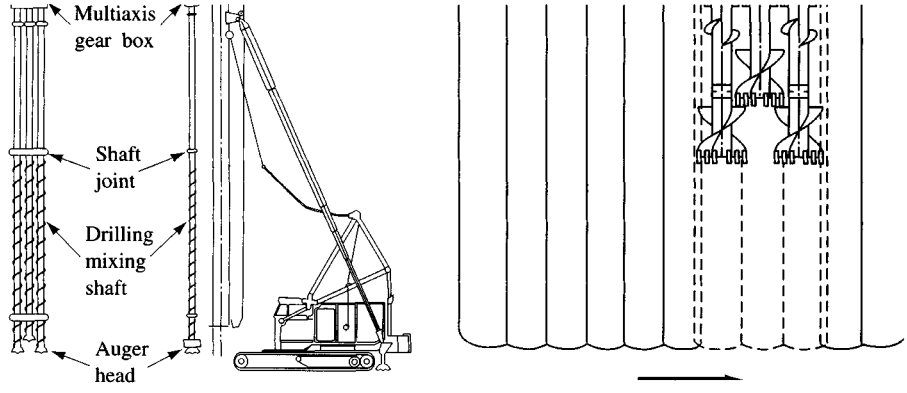

(*a*) SMW machine. (*b*) SMW installation procedure.

Concrete walls constructed using the slurry method can use wale and strut or tiebacks for additional support against lateral movement. Walls have been built with lateral displacements as low as 6 mm ($\frac{1}{4}$ in.); however, excessive lateral wall displacements can occur if the site and soil conditions are not correctly assessed.

Slurry walls are about two times as expensive (per m^2 or ft^2) as walls of sheetpiling or soldier beams and lagging. For this reason, they are used when it is essential that ground loss be kept to near zero and when the walls can be used as part of the permanent construction. They are generally more impermeable than sheetpiling when used as water barriers; however, geotextiles can be competitive for this type of construction.

Basically, slurry construction consists in making an evaluation of the required density and properties of the slurry based on the site soil profile; providing a means to develop large quantities of the water admixture; and, as the excavation proceeds, keeping the ground cavity filled to the necessary depth with the slurry. When excavation is complete, the slurry-filled cavity is periodically agitated to keep the admixture in suspension. Obviously the agitation must be carefully done to avoid wall caving. Next the cavity is filled using a tremie so that the wall is cast from the bottom up. This action ensures a solid wall and, in the case of concrete, a minimum exposure (for both strength and bonding quality) to slurry. The slurry is displaced from the top and saved for use in the next trench section if stage construction is employed. Disposal of slurry (a slime) is the greatest disadvantage of this type construction.

Slurry construction depends upon two factors for successful performance:

1. Formation of a filter skin or "cake" about 3 mm thick at the interface of the slurry and excavation via *gel action* and particulate precipitation—the primary purpose of select additives.
2. Stabilization of lateral pressure owing to the dense slurry pushing against the filter skin and sidewalls of the excavation. Slurry density is adjusted by using select additives as well.

Since field performance indicates that walls are usually (but not always) stable with a slurry pressure 65 to 80 percent of the active soil pressure, the filter cake must provide considerable stability [Gill (1980)].

The slurry must be of sufficient viscosity that it does not easily drain out through the sides of the excavation and the filter skin coat. If the filter skin forms reasonably well, exfiltration loss will likely be minimal and the filter skin penetration into the sides of the excavation may be on the order of only a few millimeters where fine-grained soils are supported. A slurry excavation in gravel was reported by La Russo (1963) to have penetrated some 16 m into the surrounding soil, but this may be considered exceptional.

Slurry construction can be used for both caving and cohesive soils and has been used for drilled piers as well as wall and trench construction [O'Neill and Reese (1972), Lorenz (1963)]. Slurry densities up to $\rho = 1.92$ g/cm^3 can be obtained using a mixture of barium sulfate (barite of specific gravity $G = 4.3$ to 4.5) and bentonite (for gel action with $G = 2.13$ to 2.18). Other materials, including silt, clay, and fine sand from the excavation, may be included in the slurry mix to reduce the quantity of commercial admixture.

Where the soil is loose, subject to caving, or gravelly, it may first be grouted to obtain some stability before constructing the slurry wall. In some cases, the grout alone may be sufficient to allow the excavation to stand long enough to place wall sections. This may be possible

owing to the strength gain from the grout and arching action of the soil. It should be evident that when this is done the wall segments must be fairly short.

Cement and finely ground slag have been used in slurry as admixtures to increase ρ. At present there are polymers based on carboxymethyl cellulose, xanthan gum, and several polyacrylates that can be used for special site conditions. Generally their costs are six to eight times that of the more common bentonite-based slurries, but if they can be reused sufficiently, their cost becomes competitive.

Commonly, slurry densities of $\rho = 1.15$ to 1.25 g/cm^3 are employed using a mixture of bentonite, barite, and a dispersing agent to reduce the tendency of the clay to floc. The gel is a natural by-product of the admixture, and the basic design element consists in determining the required density of the slurry.

The slurry mixture is a trial process in the laboratory, where water, clay, and any other admixture(s) are mixed by trial until a slurry with the desired density ρ (and gel properties) is obtained. In use it will be necessary to check the slurry density on a regular basis and either agitate or revise the basic formula as required.

Referring to Fig. 14-18*a*, for a clay excavation without a slurry, the critical depth is as computed in Chap. 11-1

$$H = \frac{4c}{\gamma \sqrt{K_a}}$$

With slurry in the trench and the GWT at the ground surface (not the general case shown), a horizontal force summation for the usual case of *undrained* conditions (terms are identified on Fig. 14-18*a*) gives

$$\begin{array}{lll} \rightarrow P_{\text{slur}} & \leftarrow P_{\text{soil}} & \leftarrow P_{\text{water}} \\ \frac{1}{2}\gamma_{\text{slur}}H^2 - [\frac{1}{2}(\gamma_s - \gamma_w)H^2 - 2s_uH] - & \frac{1}{2}\gamma_wH^2 & = 0 \end{array}$$

Solving for depth H, we obtain the following equation, which is usually used in clay:

$$H = \frac{4s_u}{\gamma_s - \gamma_{\text{slur}}}$$

And with an SF we have the resulting design equation of

$$H = \frac{4s_u}{\text{SF}(\gamma_s - \gamma_{\text{slur}})} \tag{14-5}$$

Either the safety factor or the excavation depth H can be made larger by increasing γ_{slur}. This equation was first presented by Nash and Jones (1963) and later verified by Meyerhof (1972).

In cohesionless soils (Fig. 14-18*b*) the slurry density is obtained (with the GWT at the ground surface) as

$$\frac{1}{2}\gamma_{\text{slur}}H^2 - \frac{1}{2}\gamma'_sH^2K_i - \frac{1}{2}\gamma_wH^2 = 0$$

from which we have the slurry unit weight (usually in g/cm^3) as

$$\gamma_{\text{slur}} \geq \gamma'_sK_i + \gamma_w(\text{g/cm}^3) \tag{14-6}$$

In this equation take $K_a \leq K_i \leq K_o$.

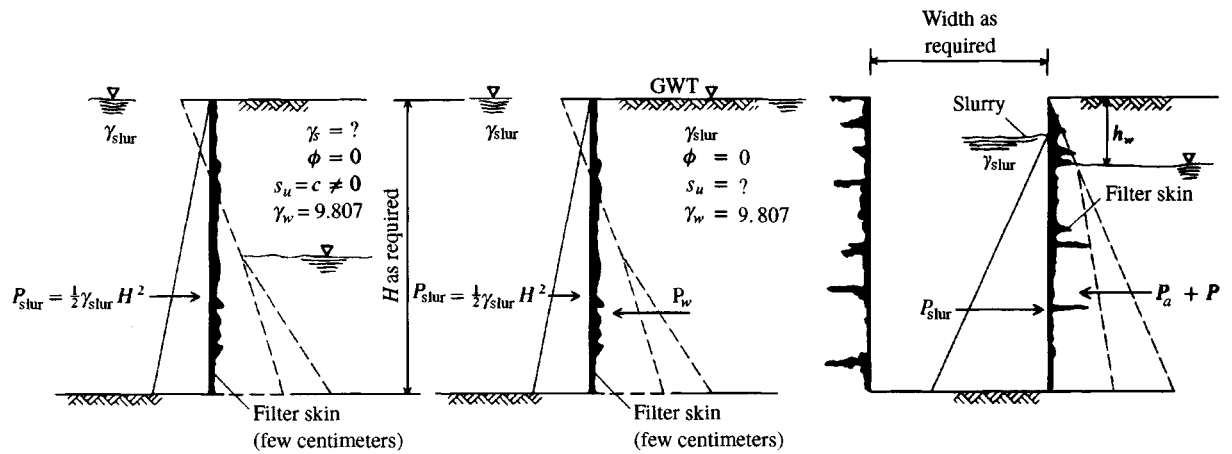

Figure 14-18 Slurry wall stability analysis.

The filter skin or cake that forms at the soil-slurry interface contributes stability to the trench; however, a reliable means of predicting its effect is not available. The beneficial effect can implicitly be allowed for by using a small factor of safety. To ensure skin formation, the slurry head should be 1 m above the water table in cohesive soils and about 1.5 m in granular soils [Gill (1980)]. Carefully note that although you can directly use Eqs. (14-5) and (14-6) for design, for the general case you must be sure the slurry is above the GWT as just noted. You may also, however, compute more accurate replacements for Eqs. (14-5) and (14-6) using a horizontal force summation that considers the actual groundwater location together with the wet γ_s and saturated γ_s' soil unit weights. This is a substantial amount of work for a doubtful increase in project confidence.

Another alternative to the use of Eqs. (14-5) and (14-6) is to use the trial wedge method to obtain a "wall force" P_w, which is resisted by P_{slur} (of Fig. 14-18). Now equate the wall force to P_{slur} and obtain the required slurry density as

$$\tfrac{1}{2}\gamma_{\text{slur}}H^2 \geq P_w$$

Depending on site geometry, you may be able to use the computer programs SMTWEDGE or WEDGE to obtain P_w.

Example 14-6. Show the effect of slurry density on excavation depth H in a cohesive soil and using an SF = 1.5. Other data for this problem are

$$s_u = 35 \text{ kPa} \qquad \gamma_s = 18.2 \text{ kN/m}^3$$

Solution. Use Eq. (14-5) with several γ_{slur} values to make a short table. Setting up Eq. (14-5) for these problem parameters, obtain

$$H = \frac{4s_u}{\text{SF}(\gamma_s - \gamma_{\text{slur}})} = \frac{4 \times 35}{1.5(18.2 - \gamma_{\text{slur}})}$$

Using this equation now create the following table:

ρ_{slur}, g/cm^3	γ_{slur}, kN/m^3	H, m
1.10	10.79	**12.6**
1.15	11.28	**13.5**
1.20	11.77	**14.5**
1.25	12.26	**15.7**

////

PROBLEMS

14-1. Reanalyze Example 14-1 for $\phi = 28°$, 32°, or 34° as assigned.

14-2. Compute the strut forces of Example 14-1 using simple beam theory (refer to Fig. 14-6) and compare your answer to those output in Example 14-1 from computer analysis.
Ans.: Strut 1: 57 kN

14-3. What is the critical depth using an SF = 1.5 for the first excavation stage of Fig. 14-2 if γ_S = 15.72, $\phi = 30°$, and cohesion = 10 kPa?
Ans.: D = 5.88 m

14-4. Using a copy of data set EX141.DTA, revise and try a **PZ**27 sheet-pile section. Comment whether this section will be satisfactory to use.

14-5. Using the output of Example 14-1, redesign the wales using the lightest pair of **I** sections you can find.

14-6. Using the data sets provided for Example 14-3, run all the stages and obtain the node displacements for each stage and the final displacement profile. Numerically integrate the displacements using the average end area method and estimate the ground loss profile. Make your best comparison with the Peck method and comment on what you would do.

14-7. Repeat Example 14-4 but revise the sheet-pile section to the next larger section. Compare the node displacement to those given in the text. If assigned by the instructor, make an estimate of ground loss.

14-8. What is the N_c factor for $D/B = 0.9$ and $B/L = 1.0$ and also for $D/B = 1.3$ and $B/L = 0.25$? What is the significance of $B/L = 0$?

14-9. What can you use for D in Example 14-4 if the excavation width B changes to 15 m? Note that B/L will also change.

14-10. Resketch the plan flow net of Fig. 14-14 so that there is at least $N_f = 11$ and recompute the flow quantity Q. Is there a significant difference?

14-11. Redo Example 14-5 if $k = 2$ m/day.

14-12. Refer to Example 14-5 and Fig. 14-14 and estimate the flow quantity for the following as assigned (use the same k, H, and h_w as in that example).

$a \times b$, m	D, m
(*a*) 75 × 110	110
(*b*) 175 × 295	300
(*c*) 65 × 95	90
(*d*) 165 × 180	240

14-13. Make a new table as in Example 14-6 if $\gamma_s = 19.25$ kN/m^3 instead of 18.2 in the example. Can you draw any conclusions?

14-14. Design the mix proportions to provide a slurry of $\rho = 1.25$ g/cm^3. Use a mixture of water, bentonite, and barite. Use 20 percent bentonite based on total mixture weight.
Partial answer: percent barite = 12.1.

14-15. Design a slurry mixture for the wall of Fig. 14-18*b* if $h_w = 2$ m, $\gamma_s = 17.9$ kN/m^3, and the trench is 10.0 m deep. *Hint:* Assume a value of G so as to compute the saturated unit weight of sand below water level or take $\gamma_s' = 9.5$ kN/m^3.

14-16. You are the project engineer on a slurry wall project. A wall segment is 3.2 m long × 1 m thick × 15 m deep, and the steel bar cage has a mass of 1508 kg. You observe that the concrete trucks deposit 47.1 m^3 into the cavity. Is this wall section satisfactory? Comment on the several factors that may account for any discrepancy so that you can justify your action either to remove or accept the wall section.

CHAPTER 15

CELLULAR COFFERDAMS

15-1 CELLULAR COFFERDAMS: TYPES AND USES

Cellular cofferdams are constructed of steel sheetpiling and used primarily as water-retaining structures. They depend for stability on the interaction of the soil used to fill the cell and the steel sheetpiling. Either material used alone is unsatisfactory; both materials in combination provide a satisfactory means to develop a dry work area in water-covered sites such as ocean- or lakefront or river area construction projects.

We will define the land, inside, or dry side of the cofferdam as the *basin side* and the outside as the *water side* since the cofferdam is usually used to keep water out of the *basin.*

Cellular cofferdams are not intended to be completely impervious but rather provide sufficient resistance to water flow that the quantity of water that does seep through can be readily pumped.

Cellular cofferdams are of three basic types: circular, diaphragm, and cloverleaf (see Fig. 15-1). These structures are usually constructed of straight-web sheetpiling since a cell full of soil and/or water tends to split so that tension stresses are produced in the web. A straight web will have essentially in-plane tension stresses; the out-of-plane thin webs of **Z** piles would develop large moments and very high bending stresses from cell-bursting forces. Tension forces would also produce large pile distortion as the pile attempted to straighten and for these two reasons **Z** piles are not used for the type of construction considered in this chapter.

Cofferdams are most commonly constructed using circular cells with smaller connecting partial cells as shown in both Figs. 15-1 and 15-4. Sometimes for waterfront structures the back side of the connecting circular cell or diaphragm (see Fig. 15-2) is omitted, however, if this is done one should consider using an anchored bulkhead.

For working out into a river or for certain types of near-shore marine work a combination of circular cells is used to create a basin as in Fig. 15-3. Figure 15-1 (see also Fig. 15-4) illustrates the usual method of joining several circular cells for this purpose. There have been a few cases where the modified full circular and diaphragm cell types of Fig. 15-2 have been successfully used.

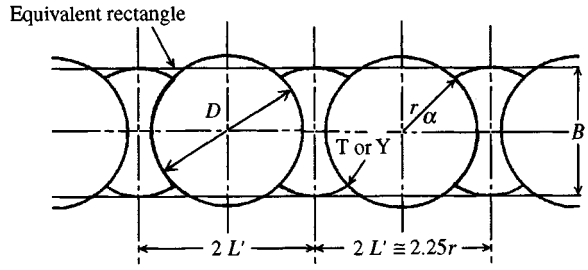

$\alpha = 30°$ $B = 0.785D$ (90°T)
$\alpha = 30°$ $B = 0.818D$ (30°Y)
$\alpha = 45°$ $B = 0.875D$ (90°T)

(a) Approximate dimensions of circular cells.

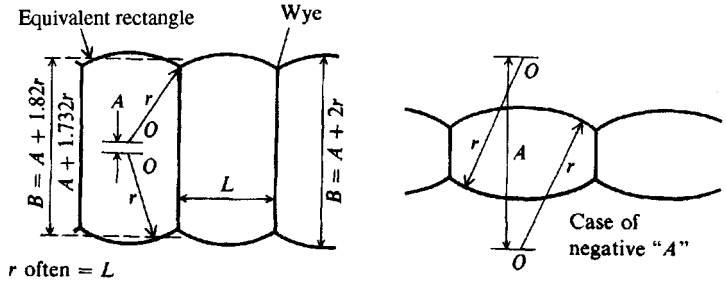

(b) Dimensions of diaphragm cofferdams.

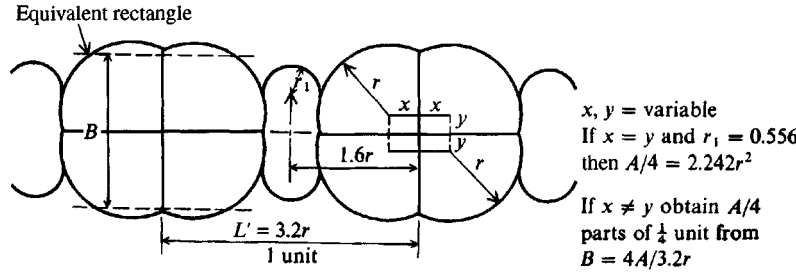

(c) Cloverleaf cell.

Figure 15-1 Types of conventional cellular cofferdams. Typical dimensions are shown for analysis. Alternative cell configurations are shown in Fig. 15-2.

River dams commonly use a form of Fig. 15-3 where approximately half the river is blocked with the cell line 1-2 and the work area enclosed by cells along lines 1-2-3-4 as shown in Fig. 15-3. A part of the dam is then built in this area and when completed, cells 3A-4 and 2A-1 are removed, leaving cell line 2-3 with the sheetpiling reused to construct a cofferdam from cell 2 to the far shore and from cell 3 to the far shore. When that section of dam is complete the cofferdam is removed and most of the piling is salvaged. The dam connection where the cell line 2-3 is located is done as most convenient to the contractor. For example an alternative line of cells might be set from 2B to 3B before removing piling from 2B to 1 and 3B to 4 and the far shore cofferdam then extended from 2B to shore and from 3B to shore, etc.

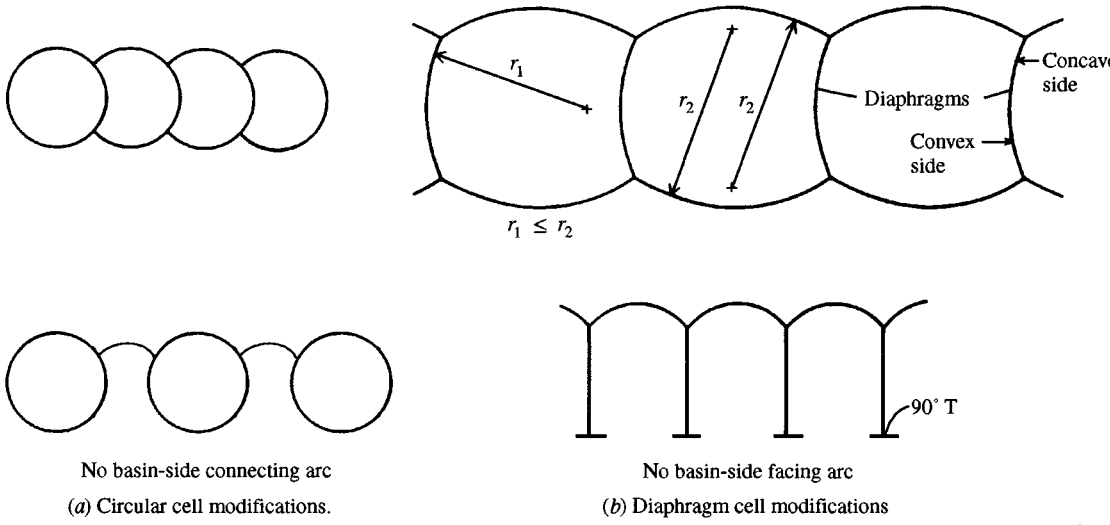

(*a*) Circular cell modifications.

(*b*) Diaphragm cell modifications

Figure 15-2 Cofferdam cell modifications. Not shown is modification of height of basin-side pilings (sometimes 1 to 2 m shorter than river-side piles).

Occasionally single cells may be used as offshore mooring structures for barges and other marine equipment. In this case extension walls to provide shore access may consist of one or more arcs of sheeting, however, again it may be more economical to use a double line of anchored walls using a common anchor rod between opposite wales as shown in Fig. 13-1*d*.

Cellular cofferdams may also be used for structures such as breakwaters and retaining walls, or the cells may be built out into the water and capped with concrete or asphalt pavement to function as piers for boats to load or unload cargo.

15-1.1 Cell Construction

Cofferdam cells are constructed by assembling the necessary number of sheet piles around a wooden template consisting of two rings (or other shape) spaced vertically about 3 m apart that have been anchored into correct position (usually with four or more steel **HP** piles). The sheetpiling is then placed into position with the pile sections, which have been fabricated[1] to connect the cells (wyes or tees), set into position first and as accurately as possible.

These become *key piles*; in deep water it may be necessary to add additional key piles made using regular sheets to which light beams or angles (or thicker plates as shown in Fig. 15-4) have been bolted to the interior part to increase their stiffness. One can also use one of the **HP** pile sections of Fig. 13-6*b*. The remainder of the piles are then set both ways from the key piles to close the cell. At this point the pile tips are resting in the overburden at the bottom of the river. If the closure piles do not slip easily in the interlocks to the bottom, the adjacent piling is picked up in multiples and "shaken out" until all the sheets in the cell perimeter are

[1]If there is sufficient quantity of intersection units it may be possible to have the producer extrude them rather than use shop fabrication.

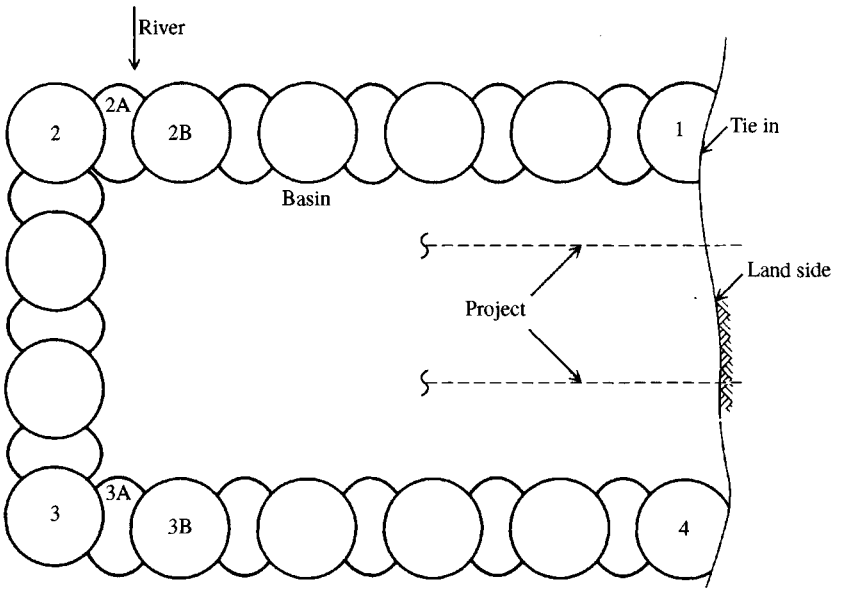

(*a*) General layout of cellular cofferdam.

(*b*) Cofferdam under construction showing initial part of cell line 1–2 with cells being partially filled for stability.

Figure 15-3 Cofferdam work (or basin) area. This "dry" area may be in the range of 5000 to 30 000 m^2.

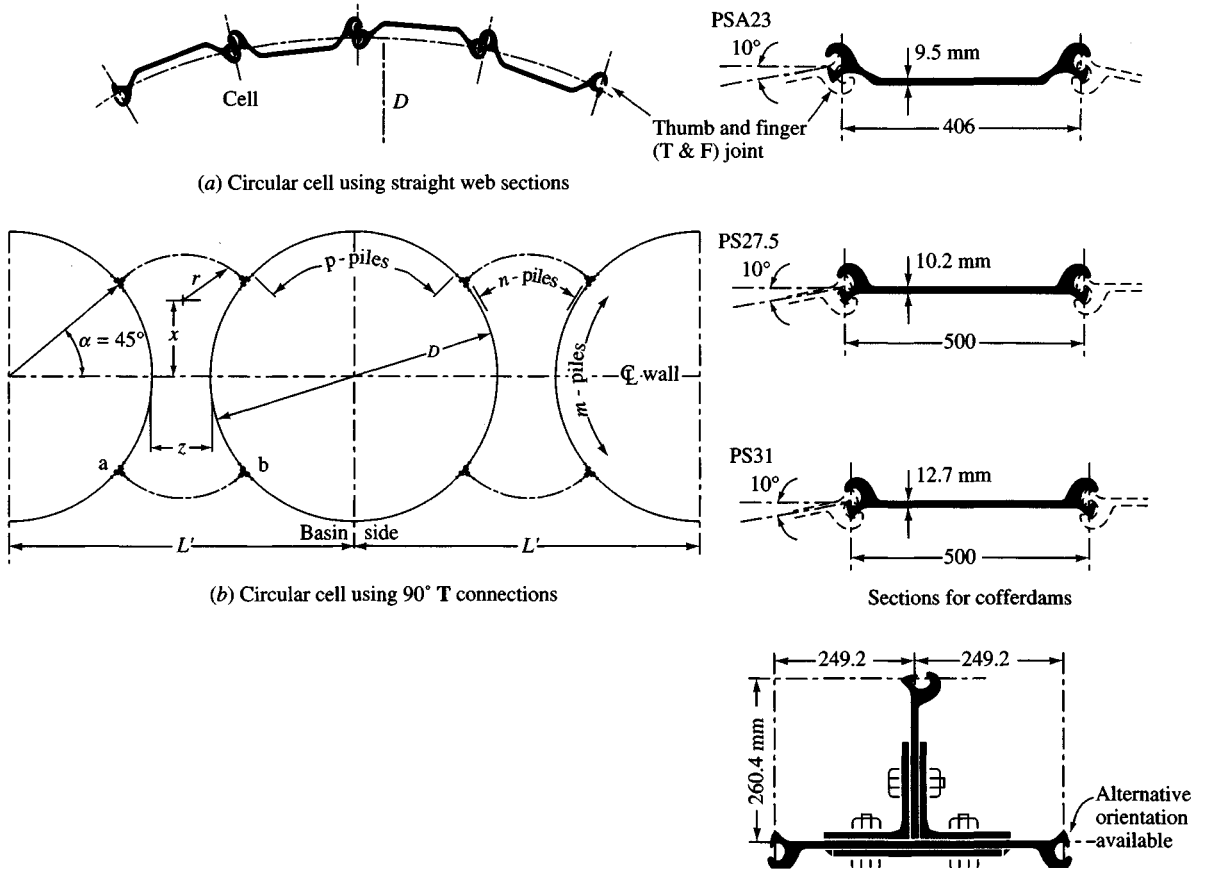

Figure 15-4 Sheetpiling and connections used in cellular cofferdam construction. Bolts are A325 with washers (usually 22-mm diam) at 115-mm spacing except 600-mm end zones where spacing is 75 mm. (Figure is a composite from Bethlehem Steel Corporation booklet No. 2001).

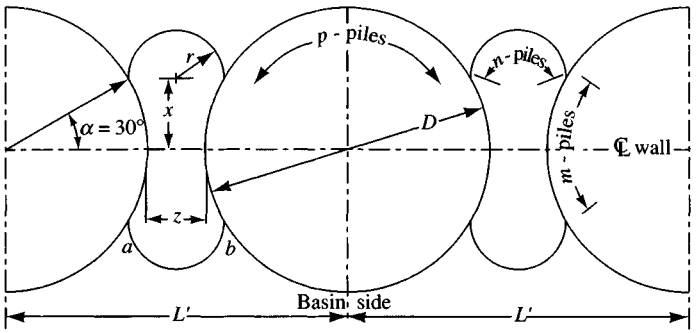

(*c*) Circular cell using 30° **Y** connections.

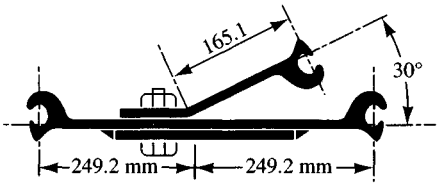

T & F joint orientations

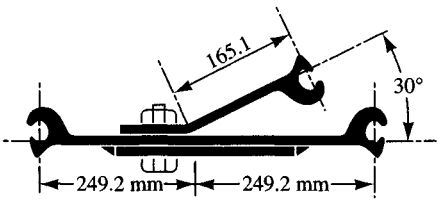

30° cell connection

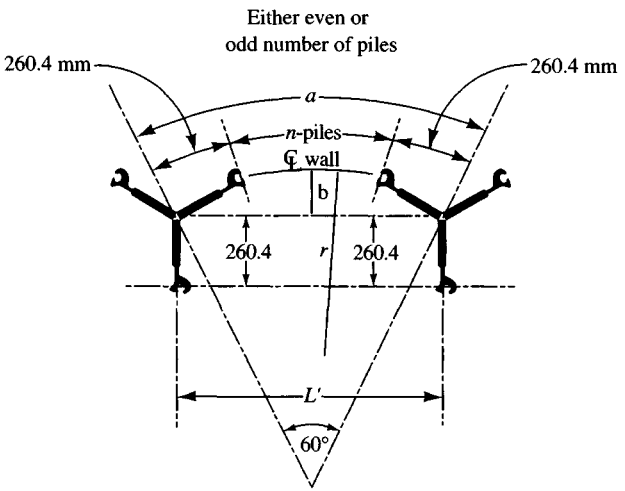

(*d*) Diaphragm cell using 120° **Y** connections.

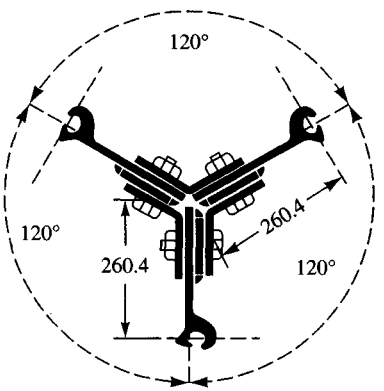

Typical **Y** connection.

Figure 15-4

free-running in the interlocks. Driving can now commence and the cell piles are driven—usually in pairs to a depth of about 1 to 2 m, then the next pair, etc., around the cell perimeter. This process requires an even multiple of piles between the key piles. The operation is then repeated, either using a new starting pair of piles or going in reverse, to avoid distortion of the cell from systematic accumulation of driving effects to one side.

Two or more piles are set for the start of the connecting arcs before the key piles are driven to final grade. Long piles may require splicing, for the driving equipment will have some kind of length limitation. Splices are made by cutting the first piles in staggers so that the splice will vary up and down some 1 to 2 m and fall above basin side cell water line and side ground level on either side.

In fast-moving water or high winds, pile-setting operations are greatly slowed as it is difficult to maintain pile alignment. A movable fender or breakwater may be used in fast water to protect the piles during driving but for wind there is little that can be done.

The cell template should be positioned within about 150 to 300 mm of alignment for circular cells and to less than 150 mm for diaphragm cells. Closer tolerance than this is not often possible and is usually unnecessary owing to cell distortion during filling and dewatering operations.

15-1.2 Cells and Number of Piles Required for a Cell

A series of connecting soil-filled cells (Fig. 15-2) around the perimeter of a work area is termed a *cofferdam.* The basin side is usually provided with a drainage ditch emptying into sump pits where the water can be pumped back to the wet side.

The circular cell cofferdam of Fig. 15-1*a* consists of circles of different radii intersecting as shown. The cell intersection angle α is usually either 30° or 45° (Fig. 15-1*a*). The joint is either a 90° **T** or a 30° **Y**, but other angles might be used for special cases. The 30° **Y** is claimed to produce smaller stresses in the connection than other angles for connecting deep, large-diameter cells.

Sheetpiling interlocks allow a maximum of about 10° deflection between pieces. This results in a minimum cell radius of

$$r \approx \frac{\text{Driving distance, m or ft}}{2 \sin 10°}$$

For a **PS**31 section, $r \approx 0.50/(2 \times \sin 10°) = 1.44$ m for a minimum cell diameter ≈ 2.88 m.

The number of sheet piles N_s in a cell (or circle) of radius r and driving distance D_d (given in sheet-pile tables such as Appendix Tables A-3*a*, A-3*b*) is

$$N_s = \frac{2\pi r}{D_d} \tag{15-1}$$

For a cell diameter of 6.05 m and using **PS**27.5 sections, we find that the driving distance (Appendix A-3*a*) $D_d = 0.500$ m requires

$$N_s = \frac{2\pi 6.05/2}{0.500} = \mathbf{38.013} \text{ piles}$$

Round off and use 38 piles. If the decimal fraction were much over 0.01 it would be necessary to round up to 40 piles (must use integer multiples of 2 for driving in pairs). Forty piles would require that the diameter be slightly increased to

$$\text{Diam} = \frac{40 \times 0.500}{\pi} = 6.37 \text{ m} \qquad \text{(vs. original 6.05 m)}$$

Pile producers generally will provide free tables for calculating the number of piles needed for cells and diaphragms of varying practical dimensions.

15-1.3 Diaphragm Cells

Diaphragm cells are made of a series of circular arcs connected by crosswalls (diaphragms) using 120° intersection pieces (Figs. 15-1*b*, 15-4*d*). The radius of the arc is often made equal to the cell width L' (Fig. 15-1*b*) so that the interlock tension in the arcs and diaphragms may be equal. The distance A shown in Fig. 15-1*b* may be either positive for high, wide cells or negative for low, narrow cells. A wide cell (large B) will be necessary for stability when a large head of water is to be resisted.

Other cell types, such as cloverleafs (Fig. 15-1*c*) and ellipsoidal shapes (Fig. 15-2*b*), may be assembled from sheetpiling shapes and fabricated connections, depending on the purpose, cell height (head of water), type of fill, amount of tolerable distortion, and location.

The cloverleaf type has been used considerably as a corner, or anchor, cell in conjunction with circular cells. This cell can also be used to reduce the effective diameter of a cell when a large cell width is required for stability against a high head of water.

15-1.4 General Cell Details

The basin-side piling may be 1 to 2 m shorter than the wet side, producing a slope across the cell top (and fill) for some savings in steel mass. It is also possible to use a **Z** pile anchored wall for the wet side of the diaphragm wall of Fig. 15-1*b* since water side piles are in compression. The anchor rods, primarily for alignment, are attached to exterior wales and extend back into the cell fill (or attach to the dry-side walls). Swatek (1967) described a wide range of cofferdam configurations and heights; one should look at this publication prior to making a design—particularly for unusual site conditions of large water head H_w or poor base soil.

The circular cell is generally preferable to the other cellular types for the following reasons:

1. It is stable as a single unit and can be filled as soon as it is constructed.
2. The diaphragm-type cell will distort unless the various units are filled essentially simultaneously with not over 0.5 to 0.75 m of differential soil height in adjacent cells; the use of a circular diaphragm cell (Fig. 15-2*b*) reduces this requirement if filling is first against the concave wall side of Fig. 15-2*b* [Cushing and Moline (1975)].
3. The collapse of a diaphragm cell may cause the entire cofferdam to fail, whereas the collapse of a circular cell is generally a local cell failure.
4. The circular cell is easier to form using templates.
5. The circular cell usually requires less sheetpiling, but this need depends somewhat on the diaphragm crosswall spacing.

Increasing the size of a circular cofferdam cell does not necessarily increase the total quantity of sheetpiling for the cofferdam, since the total number of cells will be reduced. This is not true for the diaphragm-type cell. The quantity of cell fill depends directly on the cell dimensions for all types of cofferdams.

15-1.5 Sand Islands

Sand islands are large circular cells, generally using fairly short sheetpiling, that are filled with sand and sometimes capped with concrete. They provide a dry work area where the water table is at or only 0.5–1 m above the existing ground surface.

A smaller sheeted excavation such as for a bridge pier may be constructed through this small artificial island. Sand islands are usually left in place after construction; however, most other cofferdams are removed and the sheeting stored for reuse or sold as used material.

15-1.6 Connections

The connections shown in Fig. 15-4 are all bolted. This step is necessary for economy and so that driving does not cause separation of the parts. Fillet welds tend to fracture from driving stresses and are seldom used. Fracture of built-up welded sections can be avoided by

1. Preheating the parts to be welded to about 540°C (about 1000°F) so that the parts are essentially fused together in welding. This high heat is seldom practical.
2. Using both longitudinal fillet welds and transverse slot welds. The slots should be spaced on about 1-m staggered spacings and of the filled type (not filleted). This approach is costly both because of the substantial amount of welding required and the great effort needed to achieve proper notching of pieces so the slots are staggered. The slots would tend to keep the fillet welds in joined pieces from slipping with respect to each other, and fracturing during driving.

15-2 CELL FILL

The cell fill provides mass (or weight) for stability and a reduced coefficient of permeability k for retaining water without excessive pumping. These advantages must be balanced against the lateral pressure effects of the soil-water mixture and the resulting stresses that the sheetpile interlocks must resist before rupture and/or cofferdam failure.

For mass, it would be preferable to use a soil with a high density. For permeability considerations alone, clay is the best possible fill. The earth-pressure coefficient of sand with a high angle of internal friction ϕ gives the minimum lateral pressure that must be resisted by *hoop tension* in the interlocks, which usually controls cell design. Considering all these factors, the best cell fill:

1. Is free-draining (large coefficient of permeability, k)
2. Has a high angle of internal friction, ϕ
3. Contains small amounts of No. 200 sieve material—preferably less than 5 percent
4. Is resistant to scour (nonsilty or clayey)—requires presence of some gravel

Cell fills that do not meet these criteria are sometimes used, but the closer the fill material approaches these criteria the more economical the design in terms of sheetpiling, which is usually the most expensive portion of the cofferdam.

Cell fill is often placed hydraulically; i.e., the material is obtained from the river bottom if at all possible. The material is dredged and pumped through a pipe system and discharged into the cells, which are already driven, with the river level being the inside water line. This operation may substantially reduce the fines, which are often present in river-bottom material and which are temporarily suspended in the water and wash overboard. Of course, if material is not available close by, fill may have to be brought in by barge, truck, or rail. In any case the cell fill is generally deposited under water so the angle of internal friction ϕ may not be very large. It appears that this method of soil deposition seldom produces an angle of internal friction over about $30° \pm 2°$.

Unless satisfactory drained triaxial tests can be performed on the soil and at the expected cell density, the ϕ-angle should be limited to 28 to 30° for design (or preliminary design). It is possible to increase the cell fill density and ϕ by using some type of compaction with vibratory equipment such as the Vibroflot or Terra-probe described in Sec. 6-5. If this is carefully done (*before any drawdown of water on the basin side*) relative densities D_r on the order of 0.75 to 0.85 can be obtained with ϕ-angles in the range of 35 to 40°.

15-3 STABILITY AND DESIGN OF CELLULAR COFFERDAMS

The design of a cofferdam requires providing an adequate margin of safety against the following:

1. Cell sliding (Fig. 15-5*a*)
2. Cell overturning (Fig. 15-5*b*)
3. Cell bursting of Fig 15-5*c*, which is usually critical since the interlock (thumb and finger joints) are the weakest part of the system.
4. Cell shear along the centerline and including a component of interlock friction as illustrated in Fig. 15-5*d*.
5. Bearing capacity and settlement (not shown)

There are no theoretical solutions for any of these five factors owing to the complex interaction of the cell geometry, sheet piles, and cell fill. Further complicating the analysis is the transient state of water level outside and against the cell and the saturation line inside the cell fill. Finally, in river environments there is the ever-present possibility of flooding and overtopping. As a consequence of these uncertainties, cofferdam design is semi-empirical and there are at least three design approaches to the problem, all of which have had a reasonably successful design history. These methods are as follows:

1. Former Tennessee Valley Authority (TVA) methods, also called Terzaghi's method
2. Cummings method
3. Hansen's (or Danish) method

Of these the TVA (1966, but publication now out of print) and Cummings (1960) methods are commonly used in the United States and elsewhere. The Hansen method as modified by

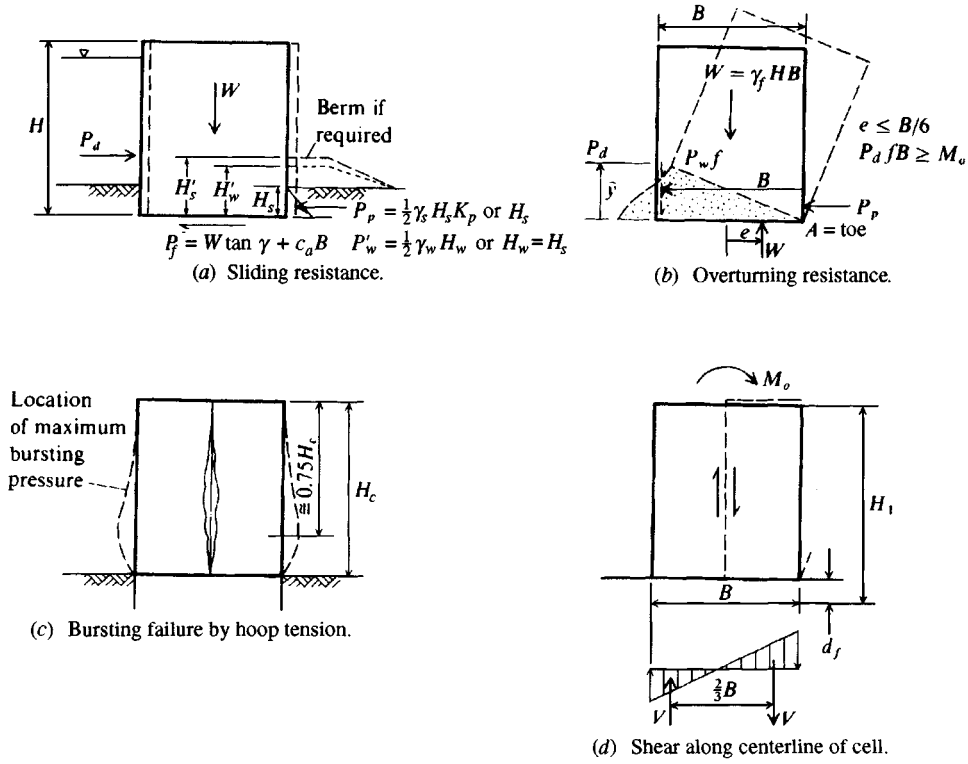

Figure 15-5 Stability of cofferdams.

Ovesen (1962) is used much less—primarily in Europe. More cofferdams have been built by TVA and the U.S. Corps of Engineers than by any others. Thus, the TVA and Cummings methods have much to commend them since, if one must use empirical methods, the simpler ones are preferable. This is a major drawback of using the Hansen method—aside from there being less construction experience to validate it. For these reasons it is not considered further in this text; however, for the interested reader the method is outlined in Lacroix et al. (1970).

Dismuke (1975) provides a summary of the several design methods in use in the United States, and Sorota and Kinner (1981) describe a recent use of the several U.S. design methods in a major cofferdam installation. This latter reference provides instrumented data comparing design to the as-built stresses and deformations; particularly valuable since there is not a great deal of published postdesign verification available.

15-3.1 TVA Method of Cellular Cofferdam Design

Terzaghi (1945) presented a paper on cellular cofferdam design in which the methods used by TVA in dam building along the Tennessee River since about 1935 were outlined. TVA (1966) later published a monograph, with the first printing in 1957 having outlined in some detail their design methods.

In the following discussion the unit weight of soil for all states will generally be used as γ_s, but its numerical value will depend on its location in Fig. 15-6 (it may be dry, damp,

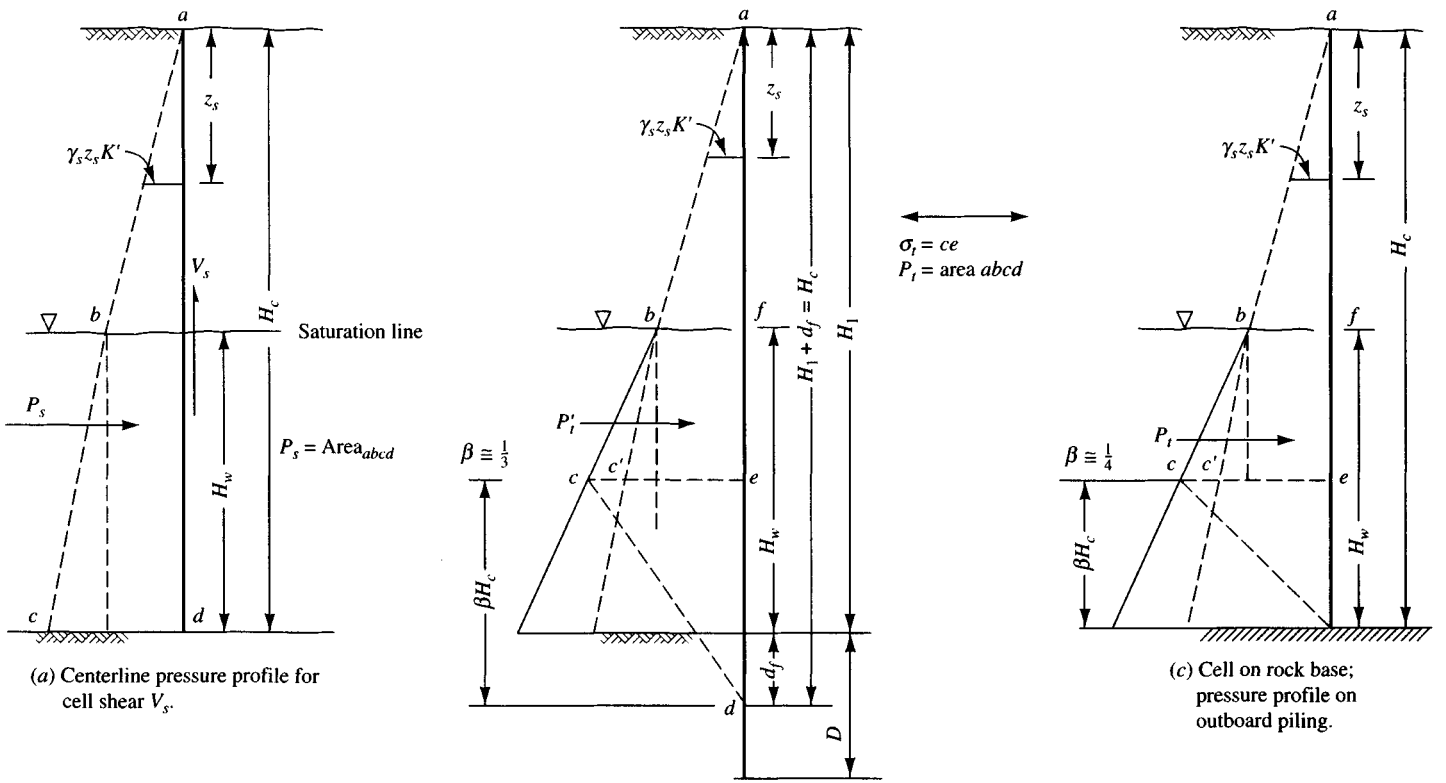

(*a*) Centerline pressure profile for cell shear V_s.

(*b*) Cell on soil base; pressure on outboard piling.

(*c*) Cell on rock base; pressure profile on outboard piling.

Figure 15-6 Cell pressure profiles for centerline shear, interlock friction, and interlock tension.

or saturated, with the effective value γ'). The TVA method considers the following (refer to Fig. 15-5 for factors and to Fig. 15-6 for terms).

SLIDING STABILITY. A cofferdam must provide adequate resistance to sliding on the base caused by the unbalanced hydrostatic pressure. A sliding stability number N_s is defined (see Fig. 15-5*a*), neglecting any active soil pressure, as

$$N_s = \frac{P_p + P_f + P'_w}{P_d} > 1.10 \tag{15-2}$$

where P_f = friction on base as $W\tan\delta + c_a B$

P_d = driving force (usually outside water with $P_w = \frac{1}{2}\gamma_w H_w^2$)

P_p = passive resistance ($\frac{1}{2}\gamma'_s H_s^2 K_p$) but may include a berm.
With a berm it is also necessary to estimate the location of the water surface since the passive pressure is an *effective* stress computation but there is also a berm water force of $\frac{1}{2}\gamma_w H_w'^2$ where H'_w = water depth on basin side (may be from near top of berm or near top of excavation of depth H_s below existing dredge line)

In this equation the active earth force P_a on the water side (not shown) is usually neglected unless the embedment depth is more than about 1.75 m.

Use a $N_s \geq 1.25$ if this analysis controls the size of the cell.

Berms (Fig. 15-5*a*) may be used to increase sliding resistance. The berm, being limited in plan, may not fully develop passive pressure, so it might be best analyzed using the trial wedge method of Sec. 11-12.1. For a sloping berm one can use the Coulomb K_p with a negative β angle. If the berm has a shelf (broken backslope) and a slope on the order of about 3H:1V or larger, the berm may be analyzed as a sliding mass of some weight and appropriate friction coefficient $\tan\delta$ between berm and base.

A problem with berms is the location of the passive resistance. Although one may take this as $H'_s/3$ or $H_s/3$ from the bottom, this is not likely correct. One might use the sheet-pile program FADSPABW to locate the center of resisting pressure and its magnitude.

It is often better to increase the cell diameter rather than to use a berm (an increase in diameter is not directly related to the increase in number of sheet piles required). The berm increases the required basin space, so some economy is achieved by increasing the cell diameter and possibly using a smaller basin.

If a berm must be used it is preferable to use the existing soil, i.e., leave that part of the basin unexcavated rather than excavating and backfilling—unless the dredged soil is totally unsuitable. If the excavation does not produce sufficient berm height, use as much of the excavated soil as practical to increase the berm height.

OVERTURNING STABILITY. The cofferdam must be stable against overturning. Two possibilities, or types of analysis, can be made when considering this type of stability. To avoid overturning, and reasoning that soil cannot take tension forces, we see that the resultant weight W should lie within the middle one-third of the base (see Fig. 15-5*b*) giving

$$e = \frac{P_d \bar{y}}{\gamma H B} = \frac{P_d \bar{y}}{W} \tag{a}$$

Thus, larger cell heights H require wider *average* cell widths B defined by the *equivalent rectangle* of Fig. 15-1. The unit weight γ used in Eq. (*a*) is understood from previous discussion as the **average** for the cell.

Alternatively, one may reason that as the cell tends to tip over, the soil will pour out at the heel. For this to occur the friction resistance between the cell fill and the water-side sheetpiling must develop from the water force $P_d = P_w$. Summing moments about the toe of the cell (point A of Fig. 15-5*b*) gives

$$BP_w \tan\delta = P_w \bar{y}$$

and the required average width B is

$$B = \frac{\bar{y}}{\tan\delta} \qquad (b)$$

where δ = angle of friction between cell fill and steel and may be estimated at about 0.6 to 0.7ϕ or from Table 11-6. The stability number N_{ot} is

$$N_{ot} = \frac{B\tan\delta}{\bar{y}} \qquad \text{(about 1.1 to 1.25)} \qquad (15\text{-}3)$$

If the sheetpiling is embedded to some depth in the soil, the effects of the active P_a and passive P_p soil pressures on the overturning moment and friction resistance should be included in summing moments about point A in Eq. (*b*).

This N_{ot} stability check is not now used by TVA (1966, see Foreword) since the mode is highly unlikely, but it is not a difficult check and probably should be continued.

CELL SHEAR. Shear along a plane through the centerline of the cell is another possible mode of failure (Fig. 15-6*a*). For stability, the shearing resistance along this plane, which is the sum of soil shear resistance and resistance in the interlocks, must be equal to or greater than the shear due to the overturning effects. Referring to Fig. 15-5*d* and assuming a linear pressure distribution across the base of the cell, we have

$$M_o = \tfrac{2}{3}BV$$

and solving for the vertical shear force V we obtain

$$V = 1.5M_o/B \qquad (15\text{-}4)$$

For stability the resisting shear $V_r \geq V$.

Since V_r depends on both interlock resistance R_{il} and cell shear along the center line V_s, it is necessary to obtain their values so that

$$V_r = V_s + R_{il} \geq V \qquad (15\text{-}5)$$

Soil shear resistance. The soil shear resistance part of the total cell shear resistance is computed from Fig. 15-6*a* as

$$V_s = P_s \tan\delta \qquad (15\text{-}5a)$$

with P_s = area of pressure profile *abcd*. The location of the resultant $\bar{y}$ is not required.

The earth-pressure coefficient K' may be computed using the Mohr's circle construction of Fig. 15-7—which may not be correct. Figure 15-7 was developed by Krynine in his discussion of Terzaghi's 1945 paper [Terzaghi (1945)] and was based on the idea that the cell centerline

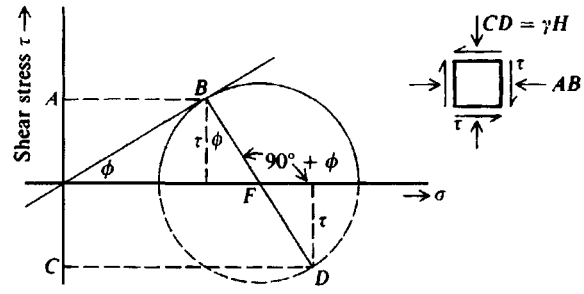

$$\tau = AB\tan\phi = AB\frac{\sin\phi}{\cos\phi} \qquad FB = \frac{\tau}{\cos\phi} = AB\frac{\sin\phi}{\cos^2\phi}$$

$$CD = AB + 2\tau\tan\phi = AB + 2AB\frac{\sin\phi}{\cos\phi}\frac{\sin\phi}{\cos\phi}$$

$$= AB\left(1 + 2\frac{\sin^2\phi}{\cos^2\phi}\right) \text{ and } \sin^2\phi = 1 - \cos^2\phi$$

$$K' = \frac{AB}{CD} = \frac{\cos^2\phi}{2 - \cos^2\phi}$$

Figure 15-7 The method suggested by Krynine in his discussion of the Terzaghi (1945) paper to compute the earth pressure coefficient K' for vertical shear along the cell centerline.

is not a principal stress plane but at any centerline depth z_i there is a vertical stress $CD = \gamma z_i$, which produces a horizontal stress of $\gamma z_i K'$ and a shear stress τ. From a Mohr's circle and using the trigonometric relationships shown in Fig. 15-7 we produce the desired equation for K' as

$$K' = \frac{\cos^2\phi}{2 - \cos^2\phi} \tag{15-6}$$

Since this equation gave $K' > K_a$ for the same angle, the readers (and Terzaghi) assumed it was correct. No one immediately noticed that although it gave $K' > K_a$ for increasing ϕ-angles, it also gave smaller K'-values for increasing ϕ-angles, which was clearly not correct. It has since been postulated that Eq. (15-6) is not correct since the lateral stress on the cell centerline was developed both by cell soil and the lateral force P_d of Fig. 15-5*a*.

The following table is instructive. It tabulates the foregoing discussion for a rapid comparison. In the table we will use a constant H, vary both ϕ and γ_s, and compute both the Rankine K_a and K' as shown:

ϕ, degrees	γ, kN/m^3	K_a	K'	$\frac{1}{2}\gamma H^2 K'$	$\frac{1}{2}\gamma H^2 K' \tan\phi$
30	15.7	0.333	0.600	$4.71H^2$	$2.72H^2$
34	16.7	0.283	0.524	$4.38H^2$	$2.95H^2$
38	17.7	0.238	0.450	$3.98H^2$	$3.11H^2$
42	18.7	0.198	0.381	$3.56H^2$	$3.21H^2$

The table uses unit weights consistent with the increase in the angle of internal friction ϕ. In the commonly used range of ϕ from 30 to 34° there is only about an 8 percent increase in shear resistance on the centerline. This table indicates that the earth-pressure coefficient K' from Eq. (15-6) is adequate if correctly used.

The use of $\phi = 30°$ is probably not realistic for a sandy soil deposited under water and given a modest amount of vibration by a Terra-probe [a round pipe firmly attached to a vibrat-

ing pile driver, which is slowly driven into the cell soil (including the base soil if possible) and pulled with a crane while still vibrating] or the like. An ordinary concrete vibrator can be used if it has a sufficiently long probe.

It is suggested that using $K' = 0.45$ to 0.50 is a good compromise instead of using Eq. (15-6). The author suggests values of K' between 0.45 and 1.0 (0.45 at 30° and 1.0 at about 40°).

Maitland and Schroeder (1979) suggested using $K' = 1$; however, the author found that using 0.56 gave the best moment resistance comparison for that case. Sorota et al. (1981) suggest $K' = 0.35$ to 0.40 for compacted well-graded granular soils, which seems somewhat low. Since there is no universal agreement on what to use for the effective cell height (see β, Fig. 15-6*b*, *c*) it is reasonable that there is no agreement on what to use for K'.

The cell environment is such that precise attempts to identify the soil state are not justified. A rain can easily saturate the top zone (unless capped). In flood stages the cells may become overtopped regardless of freeboard (see Fig. 15-11); however, overtopping may not be critical since the interior, or dry side, is likely to fill before cell saturation occurs. If it is possible that cell saturation could occur first, some systems have deliberately provided a flood gate to ensure the basin fills before the cells saturate and possibly burst.

Interlock friction/shear. Friction in the interlock joints (see Fig. 15-8) occurs simultaneously with soil shear resistance for vertical shear distortion along the centerline to take place. Conventional design uses the average interlock tension based on using P_t of Fig. 15-6*a* or *b*. Here the lateral force (for a unit of width) is

$$P_t = \text{area } abcd \tag{15-7}$$

Note the use of K_a for the lateral pressure here and not K'. The interlock friction resistance contribution is

$$R_{\text{il}} = P_t f_i \tag{15-5b}$$

Figure 15-8 Cell interlock tension force computations. Suggest using $K' = K_a$ for these computations to obtain force P_s shown in Fig. 15-6*b*, *c*.

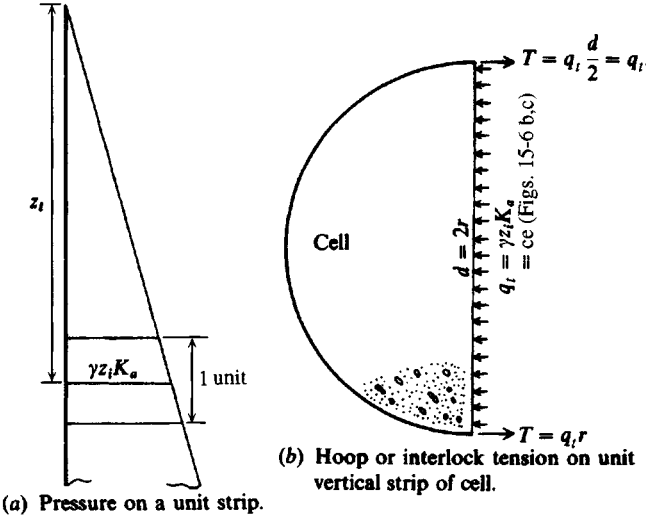

(*a*) Pressure on a unit strip.

(*b*) Hoop or interlock tension on unit vertical strip of cell.

TABLE 15-1
Sheet-pile sections commonly used for cellular cofferdams with interlock tension and suggested SF.
Recommended allowable stress for sheet pile web tension $f_a = 0.65f_y$.

AISI designation after 1971	Current* sections (1995)	Guaranteed† interlock tension, kN/m, k/in.		SF	f
PSA23, PSA28	PSA23	**2100**	(12) A328	4	0.3
PS28, PS32	PS27.5, PS31	**2800**	(16)	2	0.3
		3500	(20) A572-50	2	0.3
		4900	(24) A572-60	2	0.3

*Bethlehem Steel Corporation (only U.S. producer as of 1995).

†Normal steel grade is A328 (f_y = 270 MPa).

Notes: **1.** A572 steel grade is available in 350 and 400 MPa.

2. A690 corrosion-resistant steel grade 400 MPa.

3. Use high SF of 4 for **PSA**23 section as the web may tend to straighten under a high-tension stress.

where f_i = interlock friction coefficient, usually taken as 0.3 (values of 0.25 to 0.4 have been measured, and higher values are obtained when the steel is wet) as given in Table 15-1.

The total cell shear resistance combines Eqs. (15-5*a*) and (15-5*b*) for the *circular* cell to obtain Eq. (5-5), given earlier and repeated here:

$$V_r = V_s + R_{\text{if}} < V \tag{15-5}$$

Carefully note that V_s in Eq. (15-5) is per unit of width, and the computation for R_{if} is also in per unit of width.

The stability number against cell shear N_{cs} is defined as

$$N_{\text{cs}} = \frac{V_r}{V} = \frac{V_s + R_{\text{il}}}{V} \geq 1.1 \text{ to } 1.25 \tag{15-8}$$

BURSTING STABILITY. The cells must be stable against bursting pressures (pulling apart of the piles at the joints).

Interlock tension. Experiences at the TVA and elsewhere indicate that during filling of the cell, lateral pressures develop during filling and increase during subsequent consolidation of the fill (on the order of 10 days or so). The cell expands in proportion to the lateral pressure but expansion is dependent on the base restraint—whether the cell is founded on rock or embedded in the ground. The expanded cell takes on a modified barrel or bulged shape, and field observation finds the bulge most pronounced at from one-fifth to one-third of the free height of the cell above the dredge line or rock. On this basis the TVA uses $H_c/4$ for cells on rock to the *maximum bulge.* This point is also most critical for interlock tension.

Maitland and Schroeder (1979) suggest finding this point as one-third of the modified cell height H_1, which is based on the depth of fixity d_f below the dredge line when the cell is embedded in soil (or not driven to rock), to obtain

$$H_1 = H_c + d_f$$

where H_c = free cell height (see Fig. 15-6*b* for H_c and d_f).

The location of the depth of fixity d_f can be estimated two ways:

Method 1.

1. Compute the inside effective lateral pressure at the dredge line inside the cell as p_a.
2. Compute the estimated depth of fixity d_f *in sand* as the point of zero pressure (also zero deflection) using

$$d_f = \frac{P_a}{\gamma'(K_p - K_a)} \tag{15-9}$$

where γ' = effective unit weight below the outside dredge line

K_p, K_a = Rankine passive and active earth-pressure coefficients for the soil below the dredge line

If the dredge line soil has $\phi = 0$, use $d_f \approx 0.3$ to 0.5 m.

Method 2. Use your program FADSPABW and a pressure profile computed as $q_h = \gamma_{\text{eff}} \times z_i$ for the depth H_c. Now adjust q_h for the pile width (not a unit width); use the moment of inertia for the single sheet pile. Now code the piling (use fairly long elements above the dredge line, because they are not critical; define the JTSOIL node and use short nodes below the dredge line. Make a trial and see what you get. You may have to increase the pile depth or let the program increment it. If this analysis is done, you may find that the initial trial cell embedment depth should be increased—if so, increase the depth and try again. Now from the output sheets plot the location of zero displacement and measure this from the dredge line as d_f.

An estimate of the lateral subgrade modulus in the embedment part of the pile must be made. Note, however, that the $H_c/4$ location shown in Fig. 15-6*c* is commonly used and is probably as accurate as the ϕ and γ being used; there is not a great deal of difference in the design whether you use the $H_c/4$ or the $H_c/3$ locations. If you do not elect to find d_f, then use $H_1 = H_c$.

The pressure intensity $q_t = ce$ of Figs. 15-6*b* or 15-6*c* is used for the critical interlock tension t_i and with reference to Fig. 15-8*b* is computed as follows:

$$t_i = \frac{q_t r}{C_1} \le \frac{t_u}{\text{SF}} \tag{15-10}$$

where q_t = pressure intensity ce of Figs. 15-6*b*, *c*, kPa or k/ft^2

C_1 = constant: use 1 if q_t in kPa; use 12 if in k/ft^2

t_u = ultimate interlock value from Table 15-1, kN/m or k/in.

SF = value from Table 15-1

Appendix A Tables A-3*a* and A-3*b* give the profiles and additional section properties of the sections rolled in the United States and select sections rolled in Europe to supplement the data in Table 15-1.

The designer can, of course, use any other pressure profile deemed more suitable than those of Fig. 15-6*b*, *c* along with whatever value is selected for the earth pressure coefficient K_a. One possible choice is to use a parabolic distribution, which gives approximately a one-third increase in the hoop tension.

Both the model cells of Maitland and Schroeder (1979) and the prototype cells of Sorota et al. (1981) show that when the basin (work area) side is dewatered the interlock tensions increase in the range of 20 to 25 percent on the basin side. Simultaneously the interlock tensions decrease on the river side. The reason is probably that the cell, acting as a large gravity-retaining structure, produces a compression arch on the river side, which tends to open the basin side sheets. Since this loading stage is only one of several to which the cell is subjected, it is not generally feasible to use, say, lower strength interlocks on the river side.

The cell location during filling also affects the bursting pressure q_t; a cell near the shore will—during and shortly after filling—be subjected to both the maximum q_w and a maximum effective earth pressure q_{sh}. This increase is compensated somewhat by the near-shore cell's usually having smaller H_c. Cells in the water will undergo only active effective earth pressure until dewatering.

Most cofferdam failures result from failure of the connecting tee from either a fabrication failure or interlock failure [Swatek (1967), Grayman (1970)]. According to the TVA (1966) the interlock tension of the connection pieces can be computed from the free body of the cell as shown in Fig. 15-9. Summation of forces gives the interlock tension in the connection as

$$T_{it} = q_t L/\cos\alpha \tag{15-11}$$

In this equation $L = \frac{1}{2}L'$ of Fig. 15-1*a* and Fig. 15-9. The maximum interlock tension can be reduced by decreasing α, which may require use of a 30° **Y** instead of a 90° **T** in order to obtain a reasonable width of connecting arc.

One may obtain the maximum tension force from a free body diagram that considers hoop tension in both the main and connecting cells; however, both TVA (1966, p. 112) and Dismuke (1970) show that approximately the same value is obtained from using Eq. (15-11). Rossow (1984) made a theoretical analysis of the interlock tension at the connection joint, but the results were of little value because too many assumptions were used.

There is some opinion that Eq. (15-11) may be overly conservative, but the results reported by Sorota et al. (1981) did not indicate this. Also note that there is a wide range in possible T_{it} values, depending on what is assumed for the instant depth of water in the cell and what is used for the active earth pressure coefficient K_a. For example, using a good-quality granular cell fill with a modest amount of compaction to increase ϕ from 30 to 36° (probably more

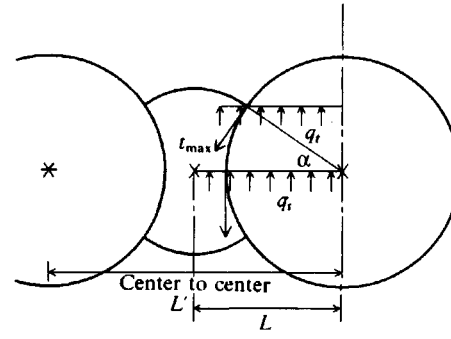

Figure 15-9 Connecting **Y** or **T** stresses according to TVA.

nearly correct) produces a 28 percent stress reduction between the Rankine K_a for 30° and K_a for 36°.

15-3.2 The Cummings Method (Currently Used by TVA)

Cummings (1960) proposed a method of analysis of cellular cofferdams based on model studies for the tilting of a cofferdam on rock, as shown in Fig. 15-10. The method provides a simple analysis; however, the models were constructed of relatively stiff material for the size of the model, which may not be realistic when related to the flexible sheetpiling sections and dimensions of a field structure.

According to TVA (1966), they had made some (unpublished) model studies similar (and prior) to Cummings and observed the same type of failures. It remained for Cummings to develop the analytical method presented here. The method has been successfully used in the design of several cofferdams and is extremely simple.

The analysis is based on the premise that the cell soil will resist lateral distortion of the cell through the buildup of soil resistance to sliding on horizontal planes (Fig. 15-10*b*). This resistance will be developed in a triangle as shown, forming an angle of ϕ to the horizontal. The triangle of soil will be in a passive pressure state and stabilized by the overlying soil, which acts as a surcharge. The weight of this soil is termed W_y. The derivation is complete when we can write an expression for the cell resistance in terms of the triangular zone of passive resistance, with shear on the horizontal planes and including the surcharge effect of W_y.

Figure 15-10 Cummings method of cell analysis. [*After Cummings (1960).*]

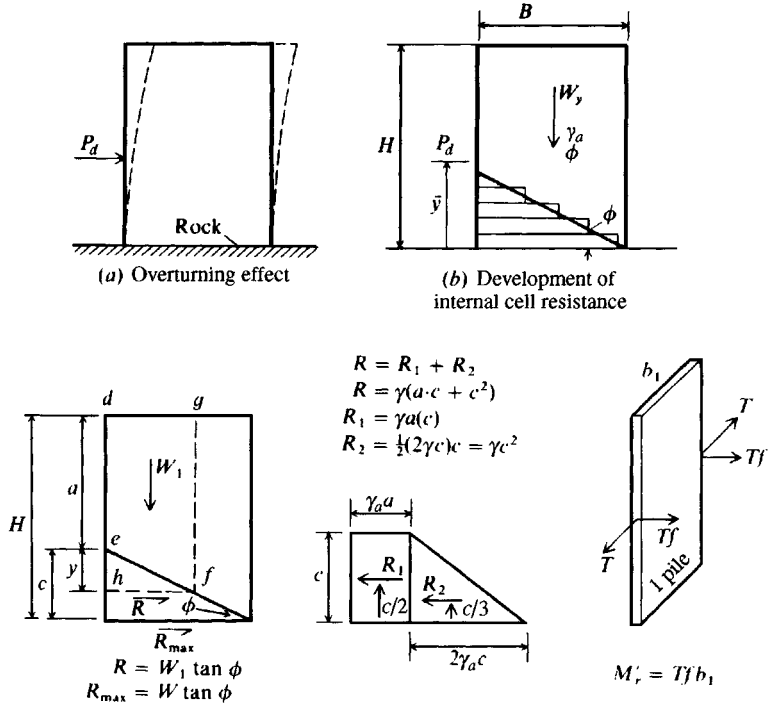

$R = W_1 \tan \phi$
$R_{max} = W \tan \phi$

(*a*) Overturning effect

(*b*) Development of internal cell resistance

(*c*) Development of sliding (friction) resistance

(*d*) Resisting moment due to cell soil

(*e*) Resisting moment due to sheet pile resistance.

Referring to Fig. 15-10*c*, we see that the weight of soil overlaying the triangle, in zone *defg*, plus the weight of the soil included in the triangle *efh* is

$$W_1 = \gamma_a(a + y)y \cot \phi \tag{a}$$

where γ_a = average effective unit weight of cell soil as a computational convenience; it can have two values if the cell is embedded in the dredge line soil (refer to Example 15-4).

The shear resistance developed by W_1 along the horizontal plane *hf* with $\delta = \phi$ is

$$R = W_1 \tan \phi = \gamma_a(ay + y^2) \tag{b}$$

The maximum value of R occurs when y is a maximum. This occurs when

$$y = c = B \tan \phi \tag{c}$$

The geometry of the problems yields, by inspection,

$$a = H - c \tag{d}$$

Now substituting the values from Eq. (*c*) for y and Eq. (*d*) for a, and Eq. (*a*) for W_1 into Eq. (*b*) and defining $R_{\max}$ = maximum force, we obtain

$$R_{\max} = \gamma_a BH \tan \phi \tag{e}$$

The force R of Eq. (*b*) can be interpreted as consisting of two parts, R_1 and R_2 (see Fig. 15-10*d*) and from Eq. (*b*) and using Eq. (*c*) for $c = B \tan \phi$ for y these two forces are

$$R_1 = \gamma_a a \cdot c \qquad R_2 = \gamma_a c^2 \tag{f}$$

The force R_1 is taken as the area of a rectangle of height c and base $\gamma_a a$. Force R_2 is the area of a triangle of height c and base $2\gamma_a c$. This concept is used so that resisting moments can be computed for these two forces as

$$M_1 = R_1 \bar{y}_1 = R_1 \frac{c}{2} \qquad M_2 = R_2 \bar{y}_2 = R_2 \frac{c}{3} \tag{g}$$

and the total soil resisting moment M_r is

$$M_r = M_1 + M_2 \tag{h}$$

Rewriting and substituting Eqs.(*f*) and (*g*) into Eq. (*h*), we find the total soil resisting moment is

$$M_r = \gamma_a c^2 \left(\frac{a}{2} + \frac{c}{3}\right) \tag{15-12}$$

The bending resistance of the piles due to interlock effects (Fig. 15-10*e*) is computed from the bursting pressure

$$T = \frac{1}{2}\gamma_a H^2 K_a r = Pr \tag{i}$$

For a unit strip (or for cell width L) the width is number of piles $n \times$ pile width b_1, giving the total resisting moment from cell fill on either a unit strip or width L as

$$M_r'' = \frac{Prf(nb_1)}{r} \qquad \text{but} \qquad nb_1 = L \qquad \text{or} \qquad B \rightarrow M_r'' = PfB$$

This expression gives the total resisting moment M_{tr} from soil and pile as

$$M_{tr} = M_r + M_r''$$
$$M_{tr} = \gamma_a c^2 \left(\frac{a}{2} + \frac{c}{3} \right) + PfB \tag{15-13}$$

The stability number against overturning N_{oc} is the ratio of the cell resisting moments to the overturning moments

$$N_{oc} = \frac{M_{tr}}{P_d \bar{y}} \rightarrow \frac{M_{tr}}{M_o} \tag{15-14}$$

Stability against sliding in the Cummings method is computed the same as by Eq. (15-2) and for interlock tension by Eqs. (15-10) or (15-11).

15-4 BEARING CAPACITY

Bearing capacity does not have to be considered when cofferdams are founded on rock. When cells are based on soil, bearing capacity may be a problem. This can be investigated as follows:

1. Convert the cofferdam to an equivalent rectangle (see Fig. 15-1).
2. Use a unit width for foundation width B ($= 1$) and an initial length L equal to *equivalent rectangle B*.
3. Using the overturning stability computations find the base eccentricity e.
4. Compute the effective foundation $L' = L - 2e$.
5. Use the Hansen bearing-capacity equations with the effective base dimensions of $B \times L'$ to compute the bearing capacity, and compare to the actual bearing pressure *under the toe half of the base.* Compute depth d_i and inclination factors i_i, but note that all $s_i = 1$.

What you are doing is computing a bearing capacity that makes some allowance for the increase in soil pressure from the overturning effect of the water.

15-5 CELL SETTLEMENT

Cells on rock do not settle. Probably cells on soil do not settle unless the base soil is extremely poor, or the cell is in place so long that consolidation settlements occur.

The apparent settlement, however, can be very large and will be illustrated by the following example.

Example 15-1. Estimate the apparent settlement of the cofferdam cell shown in Fig. E15-1. It is assumed that we can somehow measure the increases in cell diameter as given so that we can make an approximate analysis.

Solution. From the new diameters compute an average diameter and (as done in unconfined compression tests) assume the volume remains constant. The initial diameter is the as-driven cell diameter of 6.0 m and cell height $H_c = 6$ m (above dredge line). Compute the new cell diameter (after it expands from dewatering the basin side) as

$$D_{av} = \frac{6.4 + 6.6 + 6.8 + 7.0 + 7.4 + 7.5 + 6.6 + 2 \times 6.0}{9}$$
$$= 60.3/9 = \mathbf{6.7} \text{ m (average bulged diameter)}$$

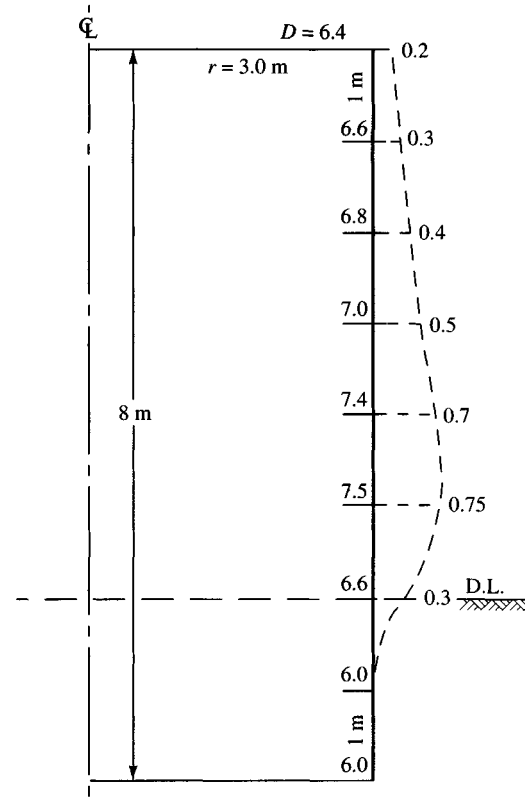

Figure E15-1

The initial cell volume based on $H = 8$ m is

$$V_i = 0.7854 \times 6^2(8) = 226.2 \text{ m}^3$$

The final volume is assumed to equal V_i or

$$0.7854 \times 6.7^2 H_f = 226.2$$

$$H_f = \frac{226.2}{0.7854 \times 6.7^2} = 6.42 \text{ m}$$

The apparent settlement is

$$\Delta H = 8.00 - 6.42 = \mathbf{1.58} \text{ m}$$

Not all of this apparent settlement would occur at once—part would occur during cell filling. It should also be evident that one could go from one cell expansion to another using the same procedure to obtain "settlements" at various stages of dewatering or other activities.

////

15-6 PRACTICAL CONSIDERATIONS IN CELLULAR COFFERDAM DESIGN

The 10-mm (0.40-in., and formerly $\frac{3}{8}$-in.) web sheetpiling is widely used for cofferdam design, providing a guaranteed tension of 2800 kN/m (16 kips/in.) and an interlock stress of 280 MPa (40 ksi)—approximately f_y for A328 steel. Using a nominal SF = 1.5 on the

interlock tension, we obtain 2800/1.5 = 1870 kN/m and the corresponding web stress = T/t_w = 1870/0.01 = 187 000 kPa = 187 MPa. The latter is close to the value of f_a = $0.65f_y$ given in the heading of Table 15-1.

For substantial embedment depths, such as for cellular cofferdams not on rock, it may be necessary to increase the web thickness to 12.7 mm. It is not usually recommended to drive sheetpiling much over 3 to 5 m (10 to 15 ft) with 6 m as an upper practical limit owing to driving damage since soil in river beds at these depths usually becomes sandy and dense so that driving becomes difficult. It is usually desirable to excavate 1 to 2 m of overburden to remove surface debris such as stumps, logs, tires, etc., which may damage the sheetpiling if large embedment depths are necessary.

Secondhand sheetpiling is widely used. It may be reused as many as four times, which represents about 25 percent loss from each use. It is for this reason that former as well as current designations for sheet-pile sections are given in Table 15-1. A major consideration with used sheetpiling is damage to the thumb and finger elements that produce the interlock groove. It is absolutely essential that the interlock be correctly done as illustrated in Fig. 15-4*a* (dashed), for a thumb reversal greatly reduces the interlock tension and may open up the groove. Other damage may also occur from rust, wedging a stone, kinking the pile, hard driving, and so forth.

For important projects it may be advisable to require either new piling or that the contractor be responsible for any cofferdam failure that arises from driving used piling.

Cofferdam dewatering is necessary to reduce the hoop tension stresses—which usually control the design—and it is standard practice to burn holes of about 35- to 50-mm diameter through several of the cell piles in each cell on the basin side. Practice is to burn the *weep* holes at about 1.5- to 2-m centers vertically on every third to sixth sheet pile (weep holes on the same pile result in maximum salvage of piling). Holes are made to the top of the berm or to the inside ground surface if no berm is used. During dewatering operations it is necessary that the drain or weep holes be systematically rodded to maintain drainage.

It appears that one cannot rely on drainage through the interlocks to dewater the cells adequately; the interlocks tend to "silt up" during the cell-filling operation. They also tighten when the cell bulges, which also reduces water flow. If the dewatering is carefully done and the cell fill is free-draining, TVA experience (1966, p. 118) indicates that it is satisfactory to assume a horizontal saturation line at one-half the free interior cell height.

Assuming a horizontal saturation line location greatly simplifies the design computations (Fig. 15-11*a*). Wells may be installed in the cells adjacent to the dry-side sheeting to collect water, which can then drain through any nearby weep holes. Alternatively, wells of 200- to 300-mm diameter (Fig. 15-9*b*) may be installed on both the river and basin side of the cell together with well pumps to aid in dewatering and to depress the saturation line further. Pump capacities on the order of 10 to 40 gal/min—depending on the drainage characteristics of the cell fill—are commonly required.

If the cells are located in very poor soils it may be possible to use stone columns (described in Sec. 6-8) to stabilize both the base and cell soil.

If cells are high, it may be possible to drive soldier piles of the type shown in Fig. 13-6*b* on a spacing to accommodate anywhere from three to six straight web piles. The cell template would have to be redesigned to accommodate the **H** pile sections.

Cell bulge may be avoided by cutting undersized circles of geogrids and using special lowering devices to position a layer until it is well-covered with fill, raising the positioning device to a higher level, installing a second geogrid, . . ., etc. If the grid openings are properly aligned, a Terra-probe or concrete vibrator may be used to densify the soil.

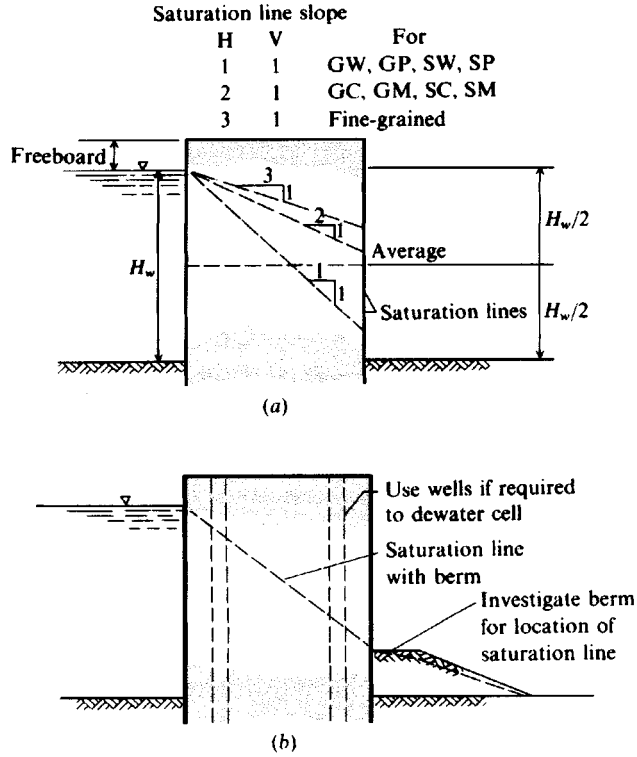

Figure 15-11 Location of the saturation (phreatic) line inside cofferdams. The average saturation line in (*a*) is probably as accurate as any, however, the alternative saturation line slopes (use an average for them also) may be required in some designs. Cell wells as in (*b*) may lower the saturation line close to the cell base if properly constructed and in sufficient number.

It was previously discussed that an inside berm may be used to obtain additional sliding resistance. It may also be used to increase the length of flow path to reduce the possibility of piping or excessive flow beneath the cofferdam. In this case, however, it is usually preferable to put wells in the cell and pump the head down so that the flow through and beneath the cofferdam is acceptable.

Cofferdams are built with a freeboard depth on the order of 1.5 to perhaps 2 m (Fig. 15-11*a*), usually based on a 5-year design period. It is usually considered more economical to allow for overtopping during an extreme flood than to design for a longer flood period (10 to 50 years).

Inclusion of overtopping considerations can quickly change design parameters unless provision is made for rapid flooding of the basin. Also overtopping can result in severe erosion of the cell fill. The cell fill may be capped with a lean (14–21 MPa) concrete mix (on the order of 150 to 200 mm thick) or with an asphalt mix. Since cell fill settlement/subsidence can approach 600 mm (or more) asphalt, being flexible, may be a better capping material than concrete to control both cracking and surface water infiltration.

Even if overtopping does not occur, the river bed tends to *scour*, or erode, during floods. If this occurs beneath the cell piling on the river side, the cell(s) tip into the river. Some means to monitor toe scour should be provided because equipment is often stored on top of the cells and could be lost if the cells tip over.

The cofferdam often will carry construction equipment such as cranes and otherwise be surcharged with stockpiles of cell fill, sheetpiling for later cells, etc. Very large surcharges should be considered in the cell design.

Most reported cofferdam failures appear due to failure of the connection element (tee or wye) between the main cell and the connecting arc. Some of the earlier failures were from using welded connections that fractured. Grayman (1970) summarized a number of cofferdam failures as to cause, and only one failure was attributed to sliding and one to overturning.

Finally, the cells cannot be aligned during driving to much more than about 150 mm owing to the flexible sheeting involved and to the problems in driving and the process of filling and dewatering. Later cell distortions may produce vertical settlement/subsidence already noted of 300 to 1000 mm or more. The system always moves into the basin some amount ranging from almost zero to perhaps 150 mm at the base and from 75 to perhaps 300+ mm at the top. Noticeable bulges nearly always develop in the cell—probably all around but visible on the basin (or cofferdam side). All of these happenings are considered acceptable practice.

COMPUTER PROGRAMMING. It should be evident that there is a substantial amount of busywork involved with a cofferdam design. Thus, there is a high possibility of errors, so a computer program should be used for the analysis if one is available. Program *COFERDAM* is one such program. These types of programs generally require an interactive mode since there are a number of options such as absence or presence of a berm, water height in berm, location of saturation line, use of passive and/or active pressures, and so on.

15-7 DESIGN OF DIAPHRAGM COFFERDAM CELL

This section will consider the design of a diaphragm cell. Both design and required as-built values and volume of cell fill are examined.

Example 15-2. Design a diaphragm cofferdam cell. Assume the cell saturation line to be at one-half the cell height from the rock base to the top. This assumption allows for a small flood rise of 0.6 m (0.6 m = freeboard) at incipient overtopping as shown in Fig. E15-2*a*. The soil data are also shown in this figure, along with select initial dimensions and depth of dredge line soil to the rock base.

Other data: Use either **PS**27.5 or **PS**31 piling of grade A 328.

f_y = 270 MPa (if possible)
Interlock tension T_i = 2800 kN/m
SF = 2.0 (Table 15-1)
Interlock friction f_i = 0.3
Friction of pile-soil f_s = 0.4 (Table 11-6)

Solution.

Step 1. Find a width B of Fig. 15-1*b* to satisfy sliding stability.

There will be a water force based on the cell height and, since the embedment depth is 5.5 m, a small active earth-pressure force. The water has K_a = 1.0; for a soil of ϕ = 30° the Rankine K_a = 0.333 (Table 11-3). The lateral forces are as follows:

$$P_w = \tfrac{1}{2}\gamma_w H_c^2(1) = \tfrac{1}{2} \times 9.807 \times 15.25^2 = \mathbf{1140.4}\ \text{kN}$$

$$\bar{y}_w = 15.25/3 = 5.08\ \text{m} \quad \text{above base}$$

$$P_a = \tfrac{1}{2}\gamma_s' H_s^2(0.333) = \tfrac{1}{2} \times 7.5 \times 5.5^2 \times 0.333 = \mathbf{37.8}\ \text{kN}$$

$$\bar{y}_s = 5.5/3 = 1.83\ \text{m} \quad \text{above base}$$

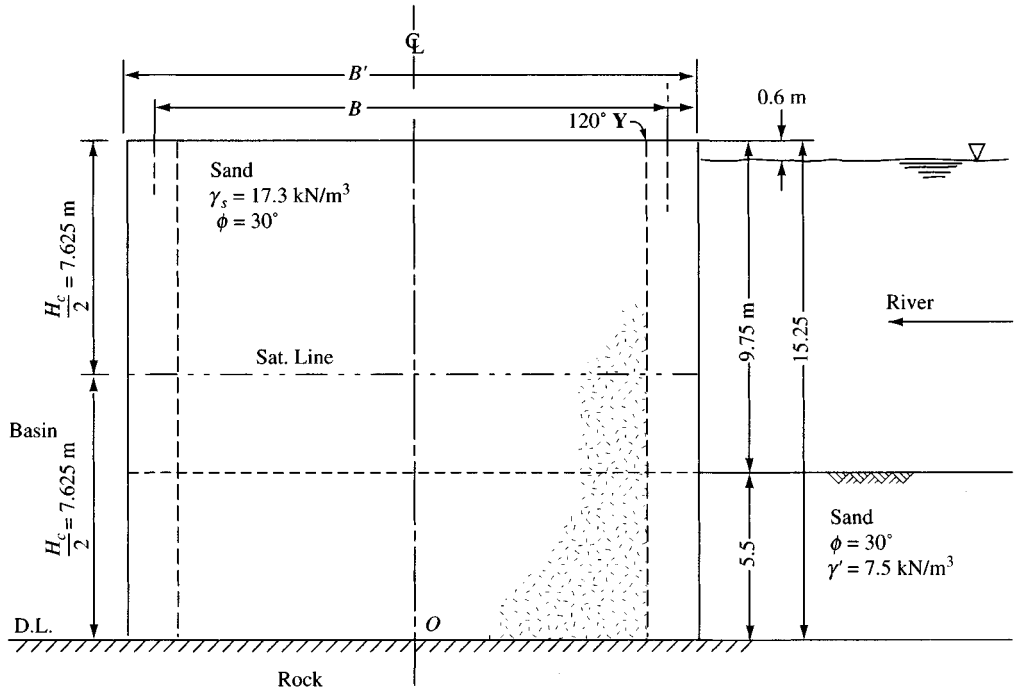

Figure E15-2*a* Diaphragm Cell.

With the saturation line at one-half the cell height, or 15.25/2 = 7.625 m, the weight W of a strip 1 unit (1 m) wide in terms of cell width B is

$$W = B\gamma_s \times 15.25/2 + B\gamma_s' \times 15.25/2$$
$$= B(17.3 + 7.5) \times 7.625 = \mathbf{189.1}B \text{ kN}$$

The sliding resistance is $W \tan\delta \rightarrow W \tan\phi$, giving

$$F_{sr}(189.1B \tan 30°) = 189.1B \times 0.577 = \mathbf{109.1}B$$

For a sliding stability number $N_s = 1.25$, we obtain the effective cell width

$$109.1B = \text{SF}(P_w + P_a)$$
$$B = \frac{1.25(1140.4 + 37.8)}{109.1} = \mathbf{13.50} \text{ m}$$

Step 2. Find the width B necessary for overturning stability. Take moments about cell base at point O:

$$M_o = P_w\bar{y}_w + P_a\bar{y}_s = 1140.4 \times 5.08 + 37.8 \times 1.83 = \mathbf{5862.4} \text{ kN} \cdot \text{m}$$

We will arbitrarily keep the base eccentricity within the middle one-third, giving

$$e = \frac{B}{6} \quad \text{and} \quad We = M_o \times \text{SF}$$

With $W = 109.1B$ and SF = 1.25, we obtain on substitution into the foregoing

$$189.1B \cdot B/6 = 5862.4 \times 1.25$$
$$B^2 = \frac{6 \times 5862.4 \times 1.25}{189.1}$$
$$B = \sqrt{232.5} = \mathbf{15.25} \text{ m} > 13.50$$

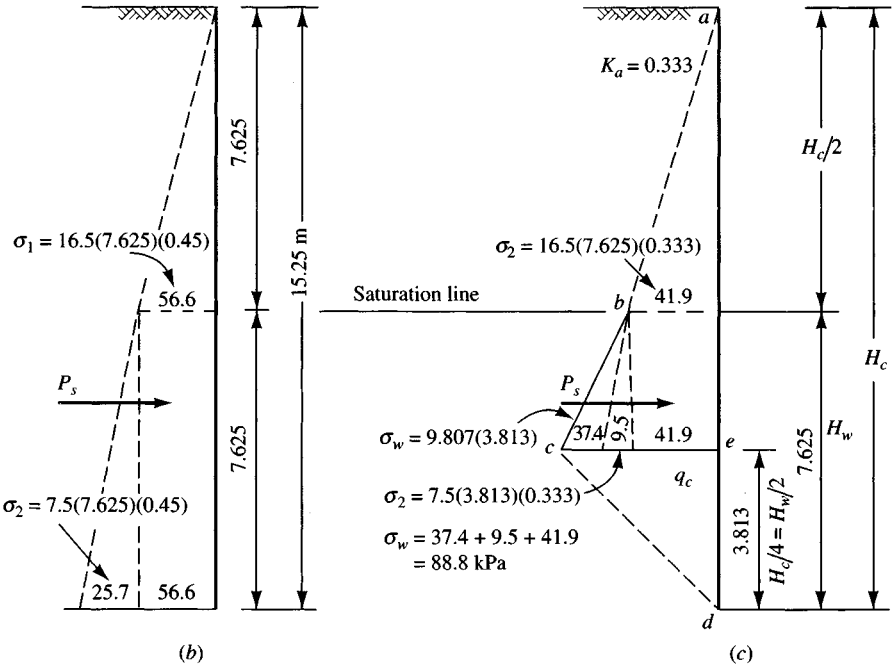

Figure E15-2*b, c*

Checking the overturning with friction on heel, we have $P_w = 1140.4$ kN, $P_a = 37.8$ kN, and $f = 0.40$, giving

$$B(P_w + P_a)f_s = M_o \times \text{SF}$$

$$B = \frac{5862.4 \times 1.25}{1178.2 \times 0.40} = \mathbf{15.55}\text{ m} > 15.29 \qquad \text{Use } \boldsymbol{B} = \mathbf{15.55}\text{ m}$$

Step 3. Check centerline shear. For this we need to refer to Fig. E15-2*b* and *c*, which gives the necessary pressure profiles for this check. We will assume $r = L$ (see Fig. 15-1*b*).

The pressure profiles show the necessary computations using the method given in Chap. 11 for pressure at critical depths. Note, however, that Fig. E15-2*b* uses a lateral earth-pressure coefficient K'. Equation (15-6) gives $K' = 0.60$ for $\phi = 30°$ [see table following Eq. 15-6]; the author suggested 0.45. The average of K' and $K_a \approx 0.45$ (a coincidence for $\phi = 30°$). We will use $K' = 0.45$ to compute the pressures in Fig. E15-2*b* (but $K_a = 0.333$ for Fig. E15-2*c*).

The centerline shear is computed using Eq. (15-4) and M_o from step two as

$$V = 1.5M_o/B = 1.5(5862.4)/15.55 = \mathbf{565.5}\text{ kN}$$

The resisting shear is made up of $P_s \tan\phi + R_{il}$. From Fig. E15-2*b* we compute P_s as follows:

$$P_s = 56.6\frac{7.625}{2} + (56.6 + \frac{25.7}{2}) \times 7.625$$

$$= 215.8 + 529.6 = 745.4\text{ kN/m}$$

$$V_s = P_s \tan\phi = 745.4 \times 0.577 = \mathbf{430.1}\text{ kN/m}$$

For the interlock resistance R_{il} we use Fig. E15-2*c* and compute the area $abcd = P_t$ so we can use Eq. (15-5*b*) [see after Eq. (15-7)]:

$$P_t = \sigma_1\frac{7.625}{2} + \frac{\sigma_t + \sigma_1}{2}\frac{7.625}{2} + \sigma_t\frac{3.813}{2}$$

Substituting values, we obtain

$$P_t = 41.9 \times 3.813 + \frac{(88.8 + 41.9)}{2} \times 3.813 + 88.8 \times 1.91$$
$$= 159.8 + 249.2 + 169.3 = 578.3 \text{ kN}$$

and using Eq. (15-5*b*), we have

$$R_{il} = P_t f_i = 578.5 \times 0.3 = \mathbf{173.6} \text{ kN}$$
$$V_r = V_s + R_{il} = 430.1 + 173.6 = \mathbf{603.6} \text{ kN} > 565.5$$

The resulting SF = 603.6/565.5 = 1.07 < 1.25

Noting the sliding and overturning stability numbers are satisfactory for the B value being used, we see that any larger B will only increase those stability numbers. Let us increase B so the cell shear stability is at least 1.25. We can do this by increasing B as follows:

$$\frac{1.5M_o}{B} = \frac{V_r}{\text{SF}} \rightarrow B = \frac{1.5 \times 5862.4 \times 1.25}{603.6} = \mathbf{18.2} \text{ m} > 15.55$$

Step 4. Check interlock tension using σ_t of Fig. E15-2*c* and Eq. (15-10). We do not need to check Eq. (15-11) since a 120° **Y** in a diaphragm cell produces the same interlock tension in any part of the cell.

Using Eq. (15-10) we will back-compute to find a suitable wall spacing $r = L$,

$$t_i = \frac{\sigma_t r}{C} = \sigma_t r \leq \frac{2800}{\text{SF}}$$

Substituting values, we obtain (σ_t = 88.8 kPa on Fig. E15-2*c*)

$$88.8r = 2800/2 \rightarrow r = 1600/88.8 = 15.8 \text{ m}$$

We will arbitrarily reduce this value and use $r = L = \mathbf{15.0}$ m.

We now have design dimensions for this cell as follows:

$$B = 18.2 \text{ m} \qquad r = L = 15.0 \text{ m} \qquad \text{Cell height } H_c = 15.25 \text{ m}$$

Step 5. Compute the required number of piles and final cell dimensions (we cannot use fractions of piles, and we must use what is available both for piles and the **Y** piece). From Fig. 13-4*d* the legs of a typical **Y** = 260.4 mm → **0.260** m. The central angle of all diaphragm cells is 60° = 1.047 radians. Both **PS**27.5 and **PS**31 piles have a driving distance (width) b_p = 500 mm (0.50 m).

a. Plot the computed dimensions to a large scale (as in Fig. E15-2*d*) and scale the wall length ≈ 17.3 m. This is reduced by two **Y** legs of 0.260 m

$$\text{No. of piles} = [17.3 - 2(0.260)]/0.5 = 16.78/0.5 = \mathbf{34} \text{ piles}$$
$$\text{Side wall } L_w = 34 \times 0.5 + 0.52 = \mathbf{17.52} \text{ m} \qquad \text{(actual distance)}$$

b. Get piles in the arc. The initial arc length is

$$L_{arc} = r\theta = 15.0(1.047) = 15.70 \text{ m}$$
$$\text{No. of piles} = (15.70 - 0.52)/0.5 = 30.36 \qquad \text{use } \mathbf{31} \text{ piles}$$
$$\text{Actual } L_{arc} = 31 \times 0.5 + 0.52 = 16.02 \text{ m}$$
$$\text{Actual } r = L_{arc}/\theta = 16.02/1.047 = \mathbf{15.3} \text{ m}$$

c. Actual effective B (refer to Fig. 15-1*b*) is approximately

$$B = A + 1.820r$$
$$L_w = A + 1.732r = 17.52 \text{ m}$$

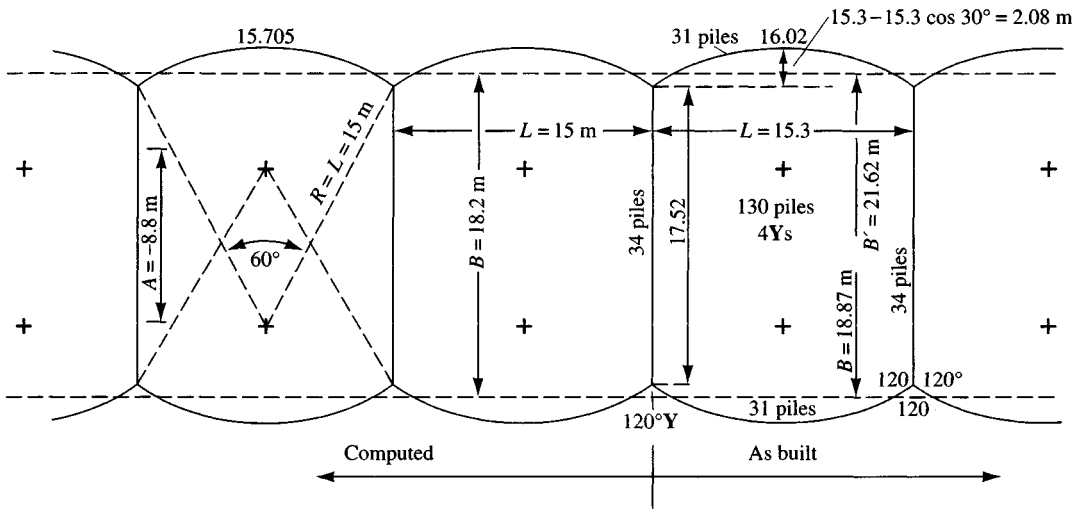

Figure E15-2*d*

Eliminating A, we obtain $0.088r = B - 17.52$. Solving, we see that

$$B = 17.52 + 0.088(15.3) = \mathbf{18.87}\text{ m}$$

Since this is larger than the last computed $B = 18.82$ it appears that the computations are satisfactory. The full cell width

$$\begin{aligned} B' &= L_w + 2(r - r\cos 30°) \\ &= 17.52 + 2(15.3 - 15.3\cos 30°) \\ &= 17.52 + 4.10 = \mathbf{21.62}\text{ m} \end{aligned}$$

d. The number of piles/cell is based on 1 side wall + 2 end arcs, giving

$$\begin{aligned} \text{Side wall} &= 34\text{ piles} \\ \text{2 end arcs} = 2 \times 31 &= \underline{62}\text{ piles} \\ \text{Total} &= 96\text{ piles} + \text{two } 120°\mathbf{Y}\text{s} \end{aligned}$$

e. The approximate cell fill volume above the dredge line is

$$V_{\text{fill}} = BrH = 18.87 \times 15.3 \times 9.75 \approx \mathbf{2815}\text{ m}^3$$

////

15-8 CIRCULAR COFFERDAM DESIGN

This section considers the design of a circular cell cofferdam on a soil base using the TVA method. The following example will illustrate both the current TVA and the Cumming's methods for analysis.

Example 15-3. Design a circular cofferdam cell resting on a riverbed sand stratum approximately 25 m thick using the current TVA method. Other data are as follows (refer also to Fig. E15-3*a*):

Cell fill: $\gamma_{\text{wet}} = 17.0\text{ kN/m}^3$ (cell fill from river bottom)
$\gamma' = 9.0\text{ kN/m}^3$

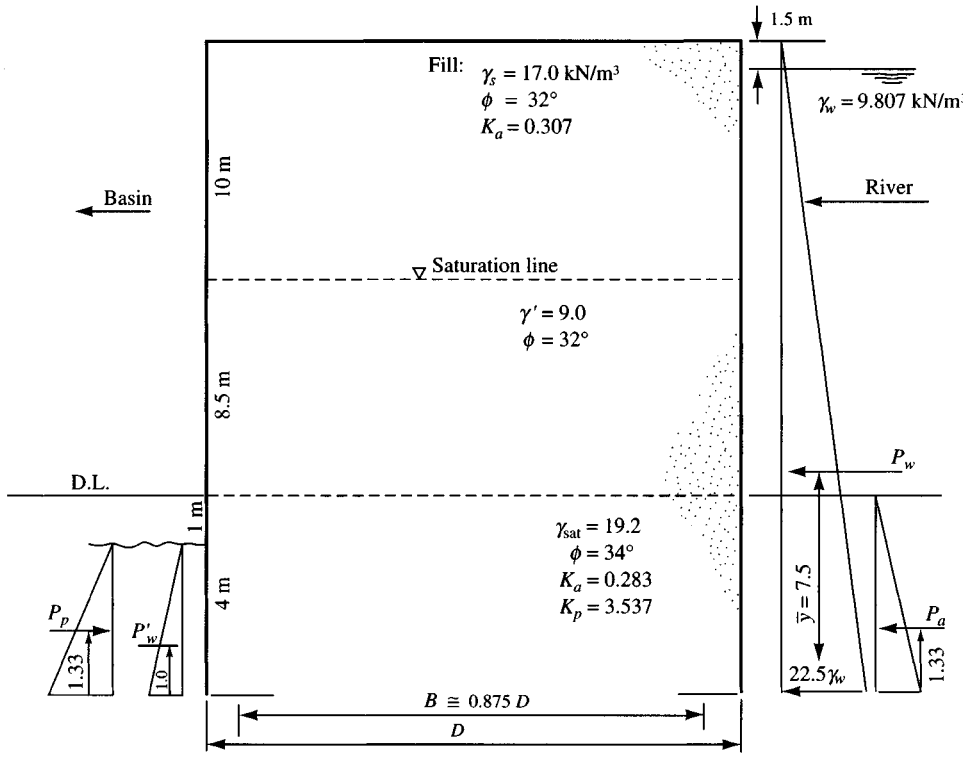

Figure E15-3*a*

Saturation line at $H_c/2$ (free-draining).
$\tan\delta = \tan 32° = 0.40$ (fill-to-pile)

Base soil: $\gamma_{sat} = 19.2$ kN/m³ $\phi = 34°$

Pile data: Use **PS**27.5 or (if required) **PS**31 piling
Interlock tension 2800 or 4900 kN/m (if required)
Interlock friction $f_i = 0.3$
Use cell $\alpha = 45°$ (see Fig. 15-1*a* with $B \approx 0.875D$)
All SF > 1.25. Neglect dynamic force of river flow.

Solution. (To minimize errors, I used the program COFERDAM to check the following computations.)

Step 1. Compute the driving forces and the overturning moment. These several forces and $\bar{y}$ locations, shown on Fig. E15-3*a*, are computed using methods given in Chap. 13:

$$P_w = \tfrac{1}{2}\gamma_w H^2 = \tfrac{1}{2} \times 9.807 \times 22.5^2 = 2482.4 \text{ kN/m} \leftarrow$$

$$P'_w = \tfrac{1}{2} \times 9.807 \times 3^2 = 44.1 \text{ kN/m} \rightarrow$$

The soil below the dredge line has $\gamma' = 19.2 - 9.807 = 9.4$ kN/m, and for $\phi = 34°$ we can look up K_i values from Tables 11-3 and 4:

$$P_a = \tfrac{1}{2}\gamma' H^2 K_a = \tfrac{1}{2} \times 9.4 \times 4^2 \times 0.283 = 21.3 \text{ kN/m} \leftarrow$$

$$P_p = \tfrac{1}{2} \times 9.4 \times 4^2 \times 3.537 = 266.0 \text{ kN/m} \rightarrow$$

Referring to directions of the arrows and (+) =←, we see that the net force is

$$P_{\text{net}} = 2482.4 + 21.3 - 44.1 - 266.0 = \mathbf{2193.6}\ \text{kN/m} \leftarrow$$

The net overturning moment M_o is computed using the foregoing forces with their $\bar{y}$ values, giving

$$\begin{aligned} M_o &= 2482.4 \times 7.5 + 21.3 \times 1.33 - 44.1 \times 1.0 - 266.0 \times 1.33 \\ &= \mathbf{18\,248.4}\ \text{kN} \cdot \text{m/m} \qquad \text{(counterclockwise } \curvearrowleft\text{)} \end{aligned}$$

Step 2. Cell centerline shear usually controls, so we will compute the B required for this (keeping the eccentricity in the middle one-third) and then check overturning and sliding stability:

$$V = 1.5M_o/B \qquad \text{[Eq. (15-4)]}$$

$$V_s = P_s \tan\delta \qquad \text{[Eq. (15-5}a\text{)]}$$

$$V = V_s + R_{\text{il}} \qquad \text{[Eq. (15-5)]}$$

$$R_{\text{il}} = P_t f_i \qquad \text{[Eq. (15-5}b\text{)]}$$

Obtain P_s from the pressure profile shown in Fig. E15-3*b* and compute R_{il} using either P_t from Fig. E15-3*c* or P_t' from Fig. E15-3*d*. Here we will compute both values of P_t and use the smaller.

For P_s it is necesssary to compute a value of K' and, based on its value, make a selection in the range of 0.45 to 1.0. Using Eq. (15-6), we obtain

$$K' = \frac{\cos^2 32^\circ}{2 - \cos^2 32^\circ} = \frac{0.719}{2 - 0.719} = 0.561$$

We will arbitrarily use $K' = 0.60$. With this the pressure profile of Fig. E15-3*b* is drawn. Select lateral pressure computations are on the diagram. Compute P_s as

$$\begin{aligned} P_s &= 102.0 \times \frac{10}{2} + \frac{(102.0 + 102.0 + 45.9)}{2} \times 8.5 \\ &= 510.0 + 1062.1 = 1572.1\ \text{kN/m} \\ V_s &= P_s \tan 32^\circ = 1572.1 \tan 32^\circ = \mathbf{982.3}\ \text{kN/m} \qquad \text{[Eq. (15-5}a\text{)]} \end{aligned}$$

The value of $P_t = \mathbf{1110.2}$ kN/m is shown on Fig. E15-3*c*, and you should be able to compute this using the pressure profile given. Let us look at Fig. E15-3*d*. This profile uses the depth of fixity suggested by Maitland and Shroeder (1979), as modified by the author.

The lateral pressure p_a is at the dredge line + dz where $\phi = 34^\circ$ so $K_a = 0.283$ and

$$\begin{aligned} p_a &= (\gamma_s \times 10 + \gamma' \times 8.5)0.283 \\ &= (17.0 \times 10 + 9.0 \times 8.5)0.283 = 69.8\ \text{kPa} \end{aligned}$$

Summing pressures, we find

$$d_f \gamma' K_p - d_f \gamma' K_a = p_a \qquad \text{[Eq. (15-9) slightly rearranged]}$$

$$d_f = \frac{p_a}{\gamma'(K_p - K_a)} = \frac{69.8}{9.4(3.537 - 0.283)} = 2.3\ \text{m}$$

The total effective pile depth $H_1 = 10 + 8.5 + 2.3 = 20.8$ m. The maximum stress is assumed to act at 20.8/3 = 6.9 m above this point, giving the dimensions and stresses shown on Fig. E15-3*d*. From the stresses and dimensions compute P_t' as

$$\begin{aligned} P_t' &= 52.2 \times 5 + \frac{(52.2 + 101.2)}{2} \times 3.9 + 101.2 \times \frac{6.9}{2} \\ &= 261.0 + 299.1 + 349.1 = 909.2\ \text{kN/m} \\ R_{\text{il}} &= P_t' f_i = 909.2 \times 0.30 = \mathbf{272.8}\ \text{kN/m} \\ V_r &= V_s + R_{\text{il}} = 982.3 + 272.8 = \mathbf{1255.1}\ \text{kN/m} \end{aligned}$$

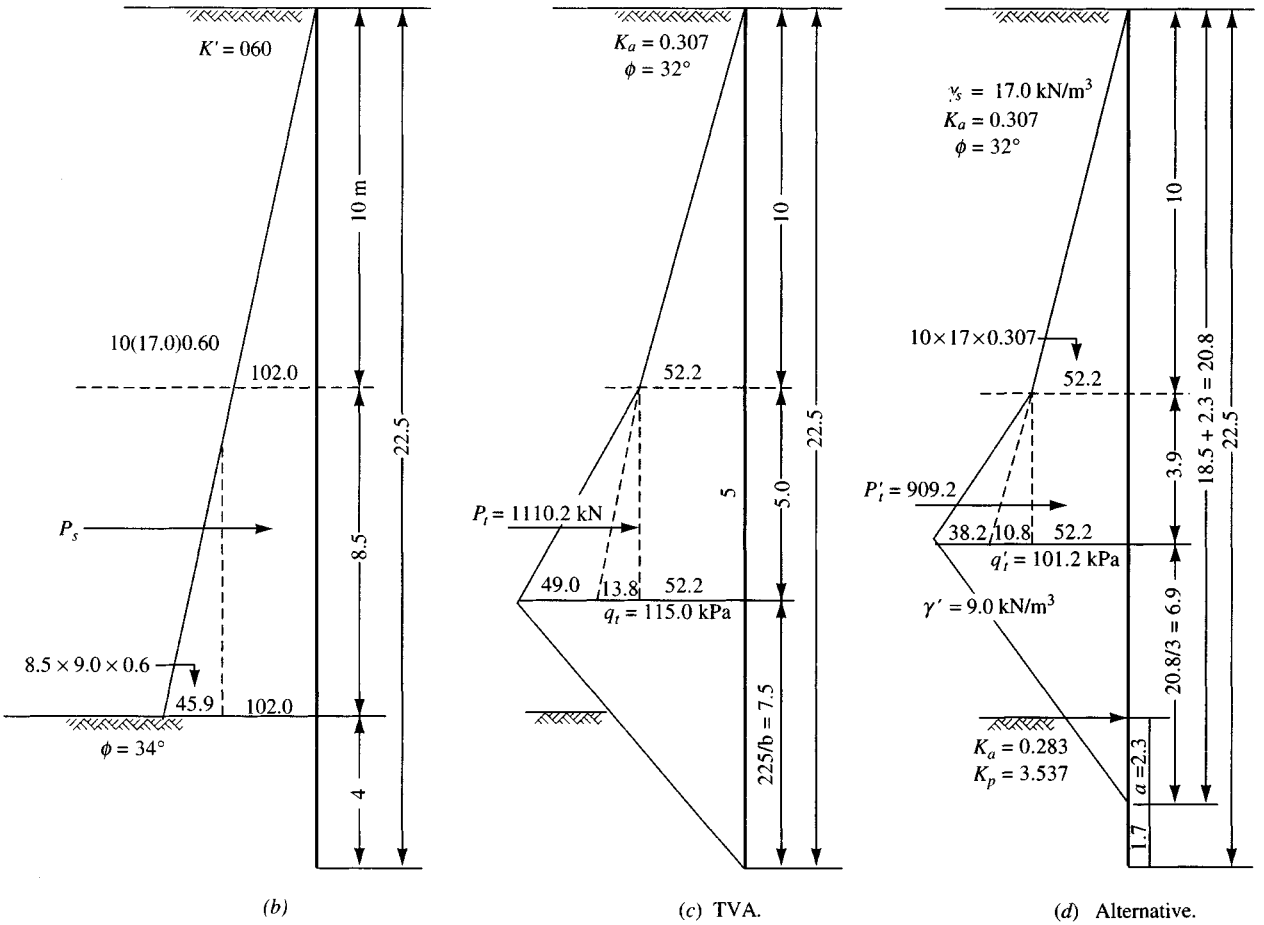

Figure E15-3*b, c, d*

We can now compute the average cell width B:

$$V = \frac{1.5M_o}{B} \leq V_r$$

Replacing the $\leq$ with an equal sign and introducing the SF = 1.25, we obtain

$$B = \frac{1.5M_o\text{SF}}{V_r} = \frac{1.5 \times 18\,248.4 \times 1.25}{1255.1} = \mathbf{27.3}\text{ m}$$

Step 3. Check sliding stability. The weight W of a unit width slice $\times$ B is

$$W = (10 \times 17.0 + 8.5 \times 9.0 + 4 \times 9.4)B = 284.1B\text{ kN/m}$$

The net driving force tending to slide the cell into the basin was computed earlier as $P_d = 2193.6$ kN/m. The resulting stability number N_s when we insert $B = 27.3$ m (just computed) is

$$N_s = \frac{P_R}{P_d} = \frac{W\tan\phi}{2193.6} = \frac{284.1 \times 27.3 \times \tan 34°}{2193.6} = 2.38 > 1.25 \qquad \text{(O.K.)}$$

Step 4. Check the interlock tension both in the cell piles and at the **T**s or **Y**s. For the cell piles use Eq. (15-10) with $C = 1$, giving

$$t_i = q_t r$$

(Obtain $q_t = 101.2$ from Fig. E15-3*d*.) The diameter $D \approx B/0.875 = 27.3/0.875 = \mathbf{31.2}$ m. Thus,

$$r = D/2 = 31.2/2 = 15.6\text{ m}$$

Substitution into Eq. (15-10) now gives

$$t_i = 101.2 \times 15.6 = \mathbf{1578.7} < 2800/2 \qquad \text{(O.K.)}$$

For Eq. (15-11) we need a value L shown on Fig. 15-1*a*: $2L = 2.25r$.

$$L' = 1.125r = 1.125 \times 15.6 = 17.55\text{ m}$$

Substitution into Eq. (15-11) with $L = L'$ gives

$$T_{iL} = q_t L/\cos\alpha = 101.2 \times 17.55/\cos 45° = \mathbf{2511}\text{ kN/m} > 2800/2$$

We might be able to use $4900/2 = 2400$ kN/m interlock. If we use $\alpha = 30°$, $T_{iL} = 2051$ kN/m.

This result is acceptable using high-strength interlocks. Alternatively, we could use a berm or install wells and lower the saturation line to near the inside dredge line. Depending on the number of cells it may be most economical to pay a premium for high-strength interlocks. These are only needed for the 30° **Y** pieces at four per cell.

Check the web tension based on using the **PS**31 pile with $t_w = 12.7$ mm (0.0127 m). Then

$$f_t = 101.2 \times 15.6/12.7 = \mathbf{124.3}\text{ MPa} \ll 0.65f_y \text{ of A328 steel}$$

Step 5. Check the bearing capacity. For the base soil $\gamma' = 9.4$; $\phi = 34°$; from Table 4-4 $N_q = 29.4$; $N_\gamma = 28.7$; depth factor = 0.262. Also $H = P_d = 2194$ kN; $V = 284.1 \times 27.3 = 7756$ kN.

The base eccentricity e is

$$We = M_o \rightarrow e = 18\,248.4/(284.1 \times 27.3) = 2.35\text{ m}$$

$$B' = B - 2 \times 2.35 = 22.6\text{ m} \qquad L = 1\text{ m}$$

$$d_q = 1 + 0.262D/B = 1 + 0.262(4/22.6) = 1.05$$

$$i_q = \left(1 - \sqrt{\frac{0.5H}{V}}\right)^{2.5} = \left(1 - \sqrt{\frac{0.5 \times 2194}{7756}}\right)^{2.5} = 0.683$$

$$i_\gamma = \left(1 - \sqrt{\frac{0.7H}{V}}\right)^{3.5} = \left(1 - \sqrt{\frac{0.7 \times 2194}{7756}}\right)^{3.5} = 0.462$$

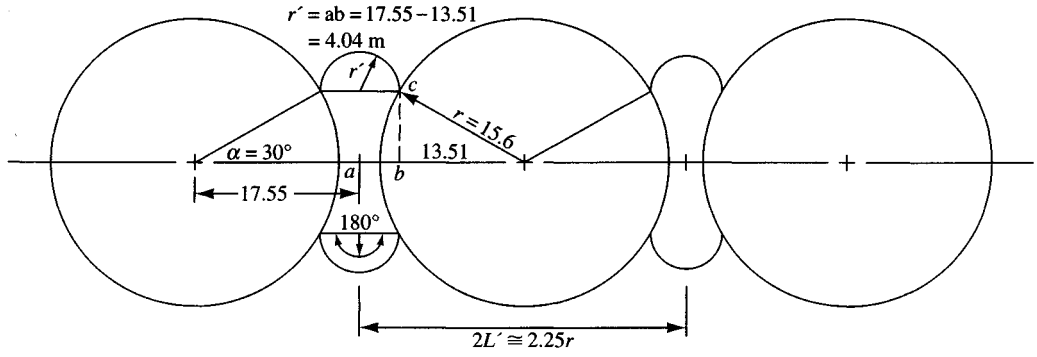

Figure E15-3*e*

The ultimate bearing capacity (cohesionless soil) is

$$\begin{aligned} q_{ult} &= \bar{q}N_q d_q i_q + \tfrac{1}{2}\gamma' B N_\gamma i_\gamma \\ &= 4 \times 9.4 \times 29.4 \times 1.05 \times 0.683 + \tfrac{1}{2} \times 9.4 \times 1 \times 28.7 \times 0.462 \\ &= 792.8 + 62.3 = 855.1 \text{ kPa} \end{aligned}$$

The bearing stability requires the actual bearing pressure computed as $q = 10 \times 17.0 + 8.5 \times 9.0 + 4 \times 9.4 = 284.1$ kPa. Therefore,

$$N_b = \frac{q_{ult}}{q} = \frac{855.1}{284.1} = \mathbf{3.0} > 2.0 \qquad \text{(O.K)}$$

Summary.

Cell $D = 31.2$ m $\quad B = 27.3$ m
Pile interlocks O.K.
Connection interlocks O.K. using 30° high-strength **Y**s
Use $\alpha = 30°$
Bearing capacity O.K.

Actual pile cell data. (refer to Fig. E15-3*e* for necessary geometric constructions in order to compute connecting arc data)

Cell:

$$\text{Circum} = \pi D = \pi \times 31.2 = 98.01 \text{ m}$$
$$N_{piles} = 98.01/0.5 = 196.03 \rightarrow \text{Use } \mathbf{196} \text{ piles}$$

Note the 30° **Y** has same length as pile.

Connecting arc:

$$\begin{aligned} r' &= \text{distance } ab = L' - r\cos 30° \\ &= 17.55 - 15.6\cos 30° = 4.04 \text{ m} \\ \text{Arc length} &= r'\theta \qquad \text{but } \theta = 180° = \pi \text{ radians} \\ &= 4.04\pi = 12.69 \text{ m (total length cell-to-cell)} \end{aligned}$$

The **Y** legs = 0.165 m each and there are two, giving 0.33 m.

$$N'_{piles} = \frac{12.69 - 0.33}{0.50} = 25.05 \rightarrow \text{Use } \mathbf{25} \text{ piles per arc}$$

Total piles:

$$\begin{aligned} \text{Cell} &= 192 + \text{four } 30^\circ \text{ Ys} \\ 2 \text{ arcs} = 2 \times 25 &= \underline{50} \\ \text{Total piles} &= \mathbf{242 + four\ 30^\circ\ Ys} \end{aligned}$$

////

Example 15-4. Use the data of Example 15-3 to analyze the cell shear stability by the Cummings method.

Fill:	$\gamma_s = 17.0$ kN/m^3	Base soil:	$\gamma_{sat} = 19.2$ kN/m^3
	$\gamma' = 9.0$ kN/m^3		$\gamma' = 9.4$ kN/m^3
	$\phi = 32^\circ$		$\phi = 34^\circ$

Solution. Refer to Fig. E15-4 (drawn from final dimensions of Example 15-3). Note the sloping line *ef* of Fig. 15-10*c* is broken here to account for two different ϕ-angles as line *BCF*. Do not use the depth of fixity concept, as that was not a part of the Cummings method.

Compute the several distances:

$$BI = \frac{4.0}{\tan 34^\circ} = 5.9 \text{ m} \qquad IJ = \frac{8.5}{\tan 32^\circ} = 13.6 \text{ m}$$

$$KL = 27.3 - 5.9 - 13.6 = 7.8 \text{ m} \qquad FL = 7.8 \tan 32^\circ = 4.9 \text{ m}$$

Step 1. Compute resistance of *DCGE* [use Eqs. (*c*) and (*d*)]:

$$c = CG \tan 32^\circ = (27.3 - 5.9) \tan 32^\circ = \mathbf{13.4} \text{ m}$$

$$a = FE = 18.5 - 13.4 = \mathbf{5.1} \text{ m}$$

Find the average unit weight γ_a of soil in the cell above dredge line:

$$\gamma_a H = W \rightarrow \gamma_a = \frac{10 \times 17.0 + 8.5 \times 9.0}{18.5} = \frac{246.5}{18.5} = \mathbf{13.3} \text{ kN/m}^3$$

$$R_1 = \gamma_a ac = 13.3(5.1)(13.4) = 909 \text{ kN} \qquad \text{[see Fig. (15-10}d\text{)]}$$

$$\bar{y}_1 = \frac{c}{2} + GH = \frac{13.4}{2} + 4.0 = 10.7 \text{ m}$$

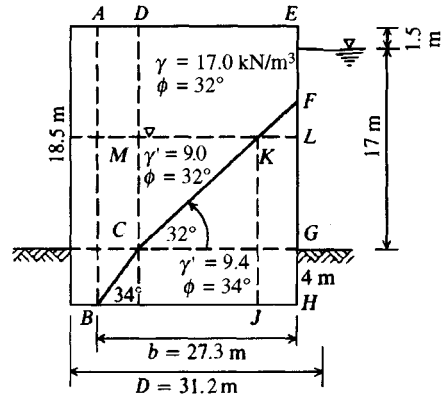

Figure E15-4

$$M_1 = R_1\overline{y_1} = 909 \times 10.7 = \mathbf{9726}\ \text{kN} \cdot \text{m}$$
$$R_2 = \gamma_a c^2 = 13.3 \times 13.4^2 = 2388\ \text{kN}$$
$$\overline{y}_2 = \frac{c}{3} + GH = \frac{13.4}{3} + 4.0 = 8.5\ \text{m}$$
$$M_2 = R_2\overline{y}_2 = 2388 \times 8.5 = \mathbf{20\ 298}\ \text{kN} \cdot \text{m}$$
$$M_T = M_1 + M_2 = 9726 + 20\ 298 = \mathbf{30\ 024}\ \text{kN} \cdot \text{m}$$

Step 2. Find M_r of zone $ABID$. First, find the average unit weight γ'_a of all the cell soil with $H = 22.5$ m:

$$\gamma'_a H = W \rightarrow \gamma'_a = \frac{10 \times 17.0 + 8.5 \times 9.0 + 4.0 \times 9.4}{22.5} = \mathbf{12.6}\ \text{kN/m}^3$$

Also,

$$a = H - GH = 22.5 - 4.0 = 18.5\ \text{m} \qquad c = 4.0\ \text{m}$$

From Eq. (15-12), we find that

$$M_r = \gamma'_a c^2\left(\frac{a}{2} + \frac{c}{3}\right) = 12.6 \times 4^2\left(\frac{18.5}{2} + \frac{4.0}{3}\right) = \mathbf{2134}\ \text{kN} \cdot \text{m}$$

Step 3. Find $M''_r = PfB$, where $B = b = 27.3$ m of Fig. E15-4; use $H = 18.5$ m. For $\phi = 32°$ the Rankine $K_a = 0.307$ from Table 11-3:

$$P = \tfrac{1}{2}\gamma_a H^2 K_a = \tfrac{1}{2} \times 13.3 \times 18.5^2 \times 0.307 = 698.7\ \text{kN}$$
$$M''_r = PfB = 698.7 \times 0.30 \times 27.3 = \mathbf{5722}\ \text{kN} \cdot \text{m}$$

Step 4. Compute stability number N_{ot} against overturning using Eq. (15-14):

$$N_{ot} = \frac{M_{tr}}{M_o} = \frac{30\ 024 + 2134 + 5722}{18\ 248.4} = \mathbf{2.08} \qquad \text{(O.K.)}$$

The remainder of the Cummings design is identical to Ex. 15-3—that is, check sliding stability and bearing capacity.

////

15-9 CLOVERLEAF COFFERDAM DESIGN

Since the cloverleaf cell contains a large amount of piling and connections it is not much used. Instead, the use of wells to dewater a circular cell to reduce the bursting pressure in the interlocks (which usually control their design) is generally more economical. When it is determined that a cloverleaf cell is required use the circular cell dimension that you will have just computed (and found inadequate) as a starting point on the cloverleaf cell dimensions.

Make an approximate scaled drawing (both plan and elevation) to select dimensions (distances x, y, and radius r). Also draw the required pressure diagrams similar to Figs. 15-6*a* and either b or c depending on whether the piling is to rock or into soil. These will not change; however, the radius may.

You will always use one 90° double **T** for the cell center and four 120° **Y**s for the cell. There will also be two, three, or four 30° **Y**s or 90° **T**s for the connecting cells. It is usual to use the dimensions of Fig. 15-1*c*—that is, $L' = 3.2r$.

The area of the cell (usually one-fourth is computed) is computed by dividing a quadrant and the connecting arc into geometrical shapes whose areas can be directly obtained and then summing the results. The equivalent width of a rectangular cell based on the total (including connecting arc) cell area is

$$B = \frac{A}{L'} = \frac{A}{3.2r}$$

Once the equivalent width B is computed, the analysis proceeds as for a circular cell, and being checked for the following:

1. Sliding stability
2. Overturning stability
3. Cell shear—when using Eq. (15-5)

$$V = V_s + R_{il}$$
$$V_s = P_s \tan \delta$$
$$R_{il} = \frac{0.94 P_t f_i}{r}$$

where select terms are identified in Fig. 15-6 or have been previously used. Note the use of δ instead of ϕ for V_s since the shear resistance is on the interior crosswalls.

PROBLEMS

15-1. What is the change in ΔH if the cell dimensions of Example 15-1 increase 10 percent (i.e., $0.2 \times 1.1 = 0.22$, $0.3 \times 1.1 = 0.33$, etc.)?

15-2. What is ΔH if the cell dimensions of Example 15-1 *decrease* 10 percent (i.e., $0.2 \times 0.9 = 0.18$, $0.3 \times 0.9 = 0.27$, etc.)?

15-3. Redesign the diaphragm cofferdam of Example 15-2 if the cell depth of embedment $D = 5.0$ m (instead of 5.5) and the total height is $H = 14$ m. Assume the saturation line is at 7 m from the top, and the freeboard distance remains at 0.6 m.

15-4. Redesign the diaphragm cofferdam of Example 15-2 if all of the soil (fill and base soil) has a ϕ-angle of 32°.

15-5. Redesign the cellular cofferdam of Example 15-3 if the saturation line is lowered to 1 m below the dredge line by using wells.

15-6. Redesign the circular cofferdam of Example 15-3 if the total $H = 20$ m with the river flood stage level = 20 m and the depth to the saturation line = 8 m (it is not 10 m). All other soil data is the same.

15-7. Redo Example 15-3 if all of the soil (cell and base) has a $\phi = 34°$.

15-8. Redo Example 15-3 using the Cummings method of Example 15-4 if the $\phi = 34°$ for all the soil (both cell and base).

15-9. Redo Example 15-3 using the given dimensions but using an inside berm as shown in Fig. P15-9. Assume the berm resistance is $R_b = W_b \tan \phi$. Note that the berm provides a surcharge for the lower passive resistance.

15-10. How many piles would be required in the diaphragm cofferdam of Example 15-2 if the $r = L = 15.5$ m (we computed 15.8 and rounded to 15 in the example)?

15-11. How many piles would be required for the cellular cofferdam of Example 15-3 if we used $\alpha = 45°$ instead of 30° used in the example?

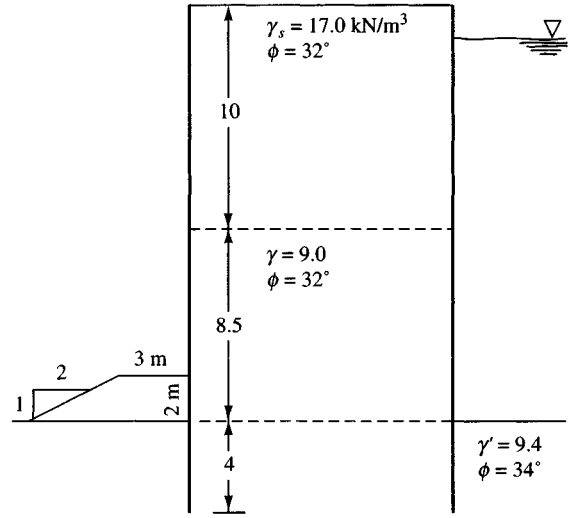

Figure P15-9

15-12. Design a cloverleaf cofferdam based on $B = 35$ m, founded on rock, and able to resist a water head $H_w = 22$ m. Neglect the embedment depth of 1.5 m. Select details are shown in Fig. P15-11.

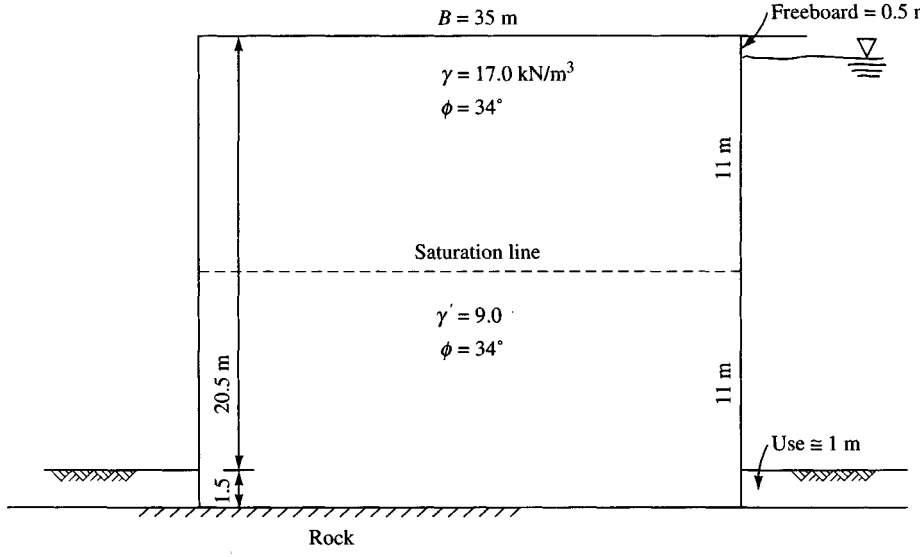

Figure P15-11

CHAPTER 16

SINGLE PILES—STATIC CAPACITY AND LATERAL LOADS; PILE/POLE BUCKLING

16-1 INTRODUCTION

Piles are structural members of timber, concrete, and/or steel that are used to transmit surface loads to lower levels in the soil mass. This transfer may be by vertical distribution of the load along the pile shaft or a direct application of load to a lower stratum through the pile point. A vertical distribution of the load is made using a *friction* (or *floating*) pile and a direct load application is made by a point, or *end-bearing*, pile. This distinction is purely one of convenience since all piles carry load as a combination of side resistance and point bearing except when the pile penetrates an extremely soft soil to a solid base.

Piles are commonly used (refer to Fig. 16-1) for the following purposes:

1. To carry the superstructure loads into or through a soil stratum. Both vertical and lateral loads may be involved.
2. To resist uplift, or overturning, forces, such as for basement mats below the water table or to support tower legs subjected to overturning from lateral loads such as wind.
3. To compact loose, cohesionless deposits through a combination of pile volume displacement and driving vibrations. These piles may be later pulled.
4. To control settlements when spread footings or a mat is on a marginal soil or is underlain by a highly compressible stratum.
5. To stiffen the soil beneath machine foundations to control both amplitudes of vibration and the natural frequency of the system.
6. As an additional safety factor beneath bridge abutments and/or piers, particularly if scour is a potential problem.
7. In offshore construction to transmit loads above the water surface through the water and into the underlying soil. This case is one in which partially embedded piling is subjected to vertical (and buckling) as well as lateral loads.

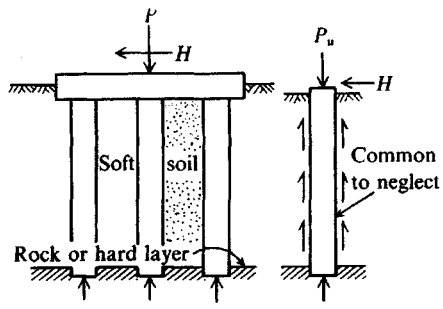

(*a*) Group and single pile on rock or very firm soil stratum.

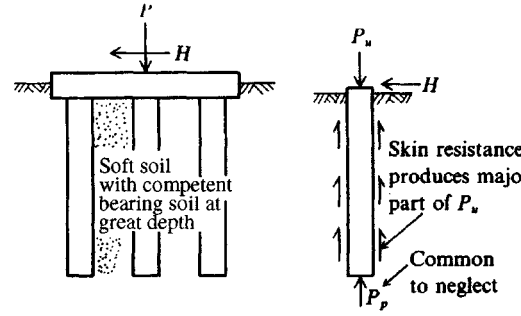

(*b*) Group or single pile "floating" in soil mass.

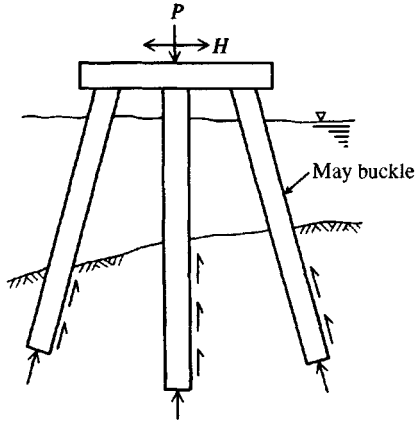

(*c*) Offshore pile group.

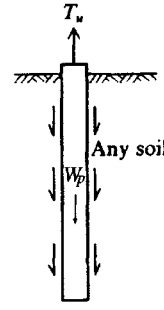

(*d*) Tension pile.

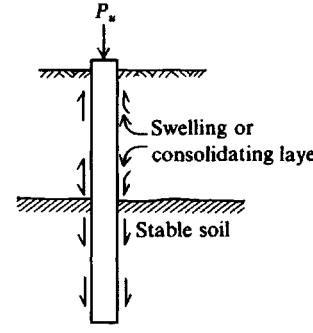

(*e*) Pile penetrating below a soil layer that swells (shown) or consolidates.

Figure 16-1 Typical pile configurations. Note that, whereas analysis is often for a single pile, there are usually three or more in a group. Typical assumptions for analysis are shown. Lateral load H may not be present in (*a*) or (*b*).

Piles are sometimes used to control earth movements (for example, landslides). The reader should note that power poles and many outdoor sign poles may be considered as partially embedded piles subject to lateral loads. Vertical loads may not be significant, although buckling failure may require investigation for very tall members.

A pile foundation is much more expensive than spread footings and likely to be more expensive than a mat. In any case great care should be exercised in determining the soil properties at the site for the depth of possible interest so that one can as accurately as possible determine whether a pile foundation is needed and, if so, that neither an excessive number nor lengths are specified. A cost analysis should be made to determine whether a mat or piles, in particular the type (steel, concrete, etc.), are more economical. In those cases where piles are used to control settlement at marginal soil sites, care should be taken to utilize both the existing ground and the piles in parallel so that a minimum number are required.

Piles are inserted into the soil via a number of methods:

1. Driving with a steady succession of blows on the top of the pile using a pile hammer. This produces both considerable noise and local vibrations, which may be disallowed by local codes or environmental agencies and, of course, may damage adjacent property.

2. Driving using a vibratory device attached to the top of the pile. This method is usually relatively quiet, and driving vibrations may not be excessive. The method is more applicable in deposits with little cohesion.
3. Jacking the pile. This technique is more applicable for short stiff members.
4. Drilling a hole and either inserting a pile into it or, more commonly, filling the cavity with concrete, which produces a pile upon hardening. A number of methods exist for this technique, and the reader is referred to Table 16-1 and Fig. 16-7 for typical installations.

When a pile foundation is decided upon, it is necessary to compute the required pile cross section and length based on the load from the superstructure, allowable stress in the pile material (usually a code value), and the in situ soil properties. These requirements allow the foundation contractor to order the necessary number and lengths of piles. Dynamic formulas, pile-load tests, or a combination are used on-site to determine if the piles are adequately designed and placed. It is generally accepted that a load test is the most reliable means of determining the actual pile capacity.

Pile capacity determinations are very difficult. A large number of different equations are used, and seldom will any two give the same computed capacity. Organizations that have been using a particular equation tend to stick with it—particularly if a successful data base has been established. It is for this reason that a number of what are believed to be the most widely used (or currently accepted) equations are included in this text. In a design situation one might compute the pile capacity by several equations using the required empirical factors suitably adjusted (or estimated) and observe the computed capacity. From a number of these computations some "feel" for the probable capacity will develop so that a design recommendation/proposal can be made.

Note that, although all the pile capacity equations are for a single pile, rarely is a single pile used; rather two or three (or more) piles are used in a group. Further note that the soil properties used in the design are those from the initial soil exploration program, and the soil properties that exist when the foundation is in service may be very different depending on how the piles have been installed and the number of piles in the group.

This chapter will be concerned with the methods of static pile capacity determination as well as an introduction to materials and methods to produce pile members. Methods to analyze lateral pile response to loads and to pile buckling will also be presented. Chapter 17 will take up the problem of estimating pile capacity based on the field driving resistance (dynamic capacity) and pile hammer energy.

16-2 TIMBER PILES

Timber piles are made of tree trunks with the branches carefully trimmed off, usually treated with a preservative, and driven with the small end as a point. Occasionally the large end is driven for special purposes as in very soft soil where the soil will flow back against the shaft and with the butt resting on a firm stratum for increased bearing. The tip may be provided with a metal driving shoe when the pile is to penetrate hard or gravelly soils; otherwise it may be cut either square or with some point.

Generally there are limitations on the size of the tip and butt end as well as on the misalignment that can be tolerated. The Chicago Building Code (in Chap. 13-132–190) requires that the tip have a minimum diameter of 150 mm and the butt 250 mm if the pile is under

TABLE 16-1
Typical pile characteristics and uses

Pile type	Timber	Steel	Cast-in-place concrete piles (shells driven without mandrel)	Cast-in-place concrete piles (shells withdrawn)
Maximum length	35 m	Practically unlimited	10–25 m	36 m
Optimum length	9–20 m	12–50 m	9–25 m	8–12 m
Applicable material specifications	ASTM-D25 for piles; P1-54 for quality of creosote; C1-60 for creosote treatment (Standards of American Wood Preservers Assoc.)	ASTM-A36, A252, A283, A572, A588 for structural sections ASTM-A1 for rail sections	ACI	ACI†
Recommended maximum stresses	Measured at midpoint of length: 4–6 MPa for cedar, western hemlock, Norway pine, spruce, and depending on Code. 5–8 MPa for southern pine, Douglas fir, oak, cypress, hickory	$f_s = 0.35$–$0.5 f_y$	$0.33 f_c'$; $0.4 f_c'$ if shell gauge ≤ 14; shell stress = $0.35 f_y$ if thickness of shell ≥ 3 mm $f_c' \geq 18$ MPa	0.25–$0.33 f_c'$
Maximum load for usual conditions	450 kN	Maximum allowable stress × cross section	900 kN	1300 kN
Optimum load range	80–240 kN	350–1050 kN	450–700 kN	350–900 kN
Disadvantages	Difficult to splice Vulnerable to damage in hard driving Vulnerable to decay unless treated Difficult to pull and replace when broken during driving	Vulnerable to corrosion HP section may be damaged or deflected by major obstructions	Hard to splice after concreting Considerable displacement	Concrete should be placed in dry More than average dependence on quality of workmanship

TABLE 16-1 (*continued*)

Pile type	Timber	Steel	Cast-in-place concrete piles (shells driven without mandrel)	Cast-in-place concrete piles (shells withdrawn)
Advantages	Comparatively low initial cost Permanently submerged piles are resistant to decay Easy to handle	Easy to splice High capacity Small displacement Able to penetrate through light obstructions	Can be redriven Shell not easily damaged	Initial economy
Remarks	Best suited for friction pile in granular material	Best suited for end bearing on rock Reduce allowable capacity for corrosive locations or provide corrosion protection	Best suited for friction piles of medium length	Allowable load on pedestal pile is controlled by bearing capacity of stratum immediately below pile

Typical illustrations

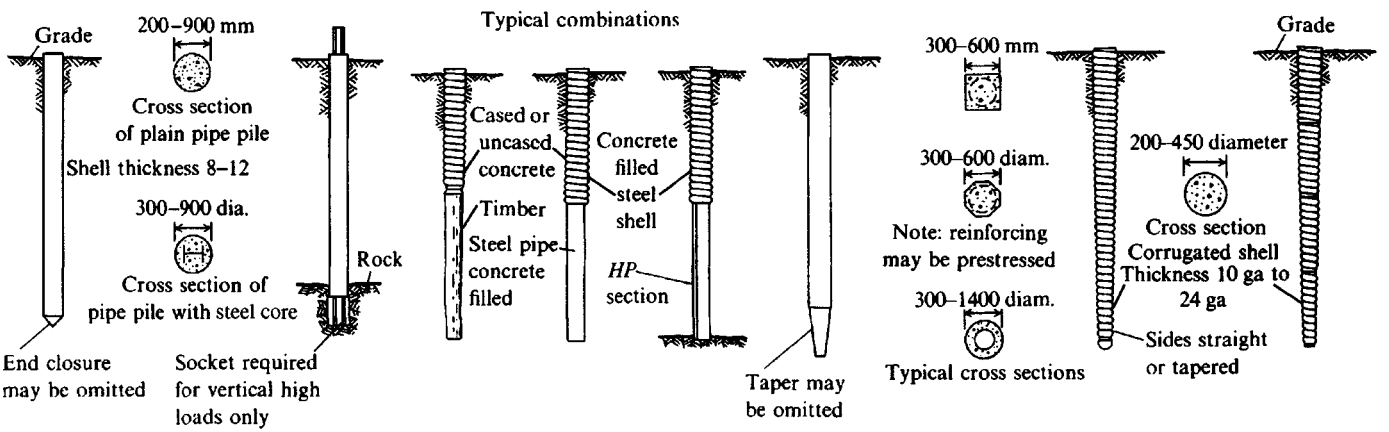

TABLE 16-1 (*continued*)

Pile type	Concrete-filled steel pipe piles	Composite piles	Precast concrete (including prestressed)	Cast in place (thin shell driven with mandrel)	Auger-placed pressure-injected concrete (grout) piles
Maximum length	Practically unlimited	55 m	10–15 m for precast 20–30 m for prestressed	6–35 m for straight sections 12 m for tapered sections	5–25 m
Optimum length	12–36 m	18–36 m	10–12 m for precast 18–25 m for prestressed	12–18 m for straight 5–12 m for tapered	10–18 m
Applicable material specifications	ASTM A36 for core ASTM A252, A283 for pipe ACI Code 318 for concrete	ACI Code 318 for concrete ASTM A36 for structural section ASTM A252 for steel pipe ASTM D25 for timber	ASTM A15 reinforcing steel ASTM A82 cold-drawn wire ACI Code 318 for concrete $f_c' \geq 28$ MPa precast $f_c' \geq 35$ MPa prestressed	ACI	See ACI
Recommended maximum stresses	$0.40f_y$ reinforcement < 205 MPa 0.35–$0.50f_y$ for shell < 175 MPa $0.33f_c'$ for concrete	Same as concrete in other piles Same as steel in other piles Same as timber piles for composite	$0.33f_c'$ unless local building code is less $0.4f_y$ for reinforced unless prestressed	$0.33f_c'$; $f_s = 0.4f_y$ if shell gauge ≤ 14 use $f_y = 0.35f_y$ if shell thickness ≥ 3 mm	$0.25f_c'$
Maximum load for usual conditions	1800 kN without cores 18 000 kN for large sections with steel cores	1800 kN	8500 kN for prestressed 900 kN for precast	675 kN	700 kN
Optimum load range	700–110 kN without cores 4500–14 000 kN with cores	250–725 kN	350–3500 kN	250–550 kN	350–900 kN
Disadvantages	High initial cost Displacement for closed-end pipe	Difficult to attain good joint between two materials	Difficult to handle unless prestressed High initial cost Considerable displacement Prestressed difficult to splice	Difficult to splice after concreting Redriving not recommended Thin shell vulnerable during driving Considerable displacement	Dependence on workmanship Not suitable in compressible soil

TABLE 16-1 (*continued*)

Pile type	Concrete-filled steel pipe piles	Composite piles	Precast concrete (including prestressed)	Cast in place (thin shell driven with mandrel)	Auger-placed pressure-injected concrete (grout) piles
Advantages	Best control during installation No displacement for open-end installation Open-end pipe best against obstruction High load capacities Easy to splice	Considerable length can be provided at comparatively low cost	High load capacities Corrosion resistance can be attained Hard driving possible	Initial economy Tapered sections provide higher bearing resistance in granular stratum	Freedom from noise and vibration Economy High skin friction No splicing
Remarks	Provides high bending resistance where unsupported length is loaded laterally	The weakest of any material used shall govern allowable stresses and capacity	Cylinder piles in particular are suited for bending resistance	Best suited for medium-load friction piles in granular materials	Patented method

Typical illustrations

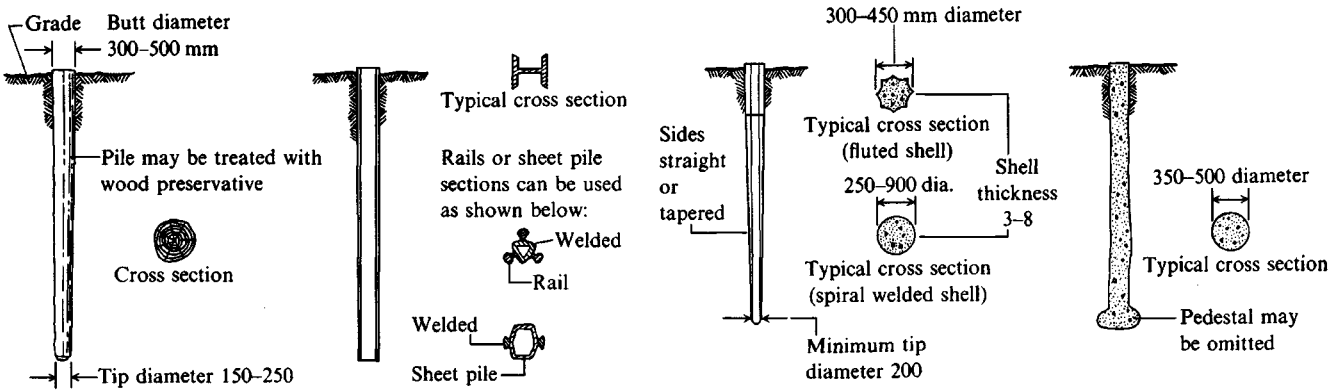

*Additional comments in *Practical Guidelines for the Selection, Design and Installation of Piles* by ASCE Committee on Deep Foundations, ASCE, 1984, 105 pages.

†ACI Committee 543, "Recommendations for Design, Manufacture, and Installation of Concrete Piles," *JACI*, August 1973, October 1974; also in ACI MCP 4 (reaffirmed 1980).

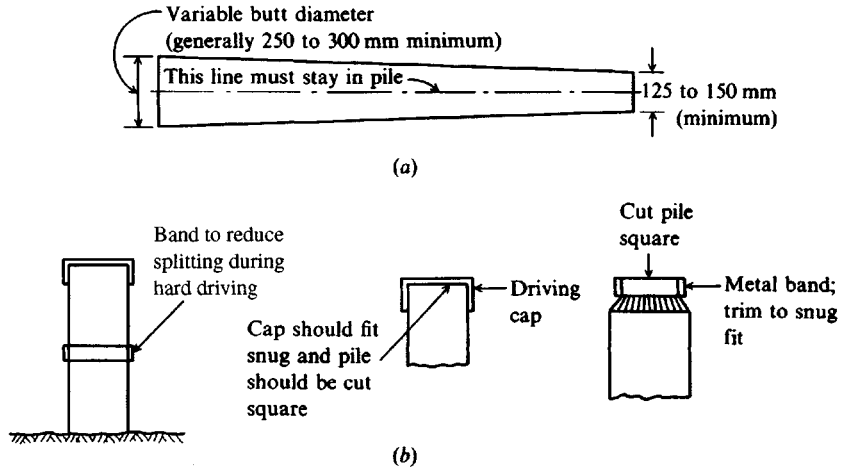

Figure 16-2 (*a*) Alignment criteria for timber piles; (*b*) devices to protect pile during driving operations.

7.6 m and have a 300-mm butt if the pile is more than 7.6 m long. The alignment requirement is that a straight line from the center of the butt to the center of the tip lie within the pile shaft (Fig. 16-2*a*).

ASCE Manual 17 [reprinted ASCE (1959) but now out of print] categorizes timber piles as follows:

Class A: To be used for heavy loads and/or large unsupported lengths. The minimum butt diameter is 360 mm.

Class B: For medium loads. Minimum butt diameter is 300 mm.

Class C: Use below the permanent water table or for temporary works. Minimum butt diameter is 300 mm. Bark may be left on this pile class.

The ASCE manual (and building codes) stipulate minimum quality of the timber concerning defects, knots, holes, and type of wood.

If a timber pile is below the permanent water table, it apparently will last indefinitely. When a timber pile is subjected to alternate wetting and drying, the useful life will be short, perhaps as little as one year, unless treated with a wood preservative. Partly embedded piles and piles above the water table are susceptible to damage from wood borers and other insects unless treated.

The driving end of a timber pile is usually damaged by fiber crushing (called brooming) from the hammer energy. This damage can be somewhat controlled by using a driving cap or metal band around the butt as illustrated in Fig. 16-2. After having been driven to the necessary penetration, the broomed end is cut square and any exposed scars, as well as the fresh end cut, should be coated with a generous application of preservative. A pile may become broken where the soil is very hard or contains boulders. Where a sudden increase in penetration occurs and a soft soil stratum is not expected, a broken pile shaft should be suspected.

Splices in timber piles are undesirable but may be effected as shown in Fig. 16-3. The splice in Fig. 16-3*b* can transmit tension. In both illustrations care should be exercised to get a maximum joint bearing area.

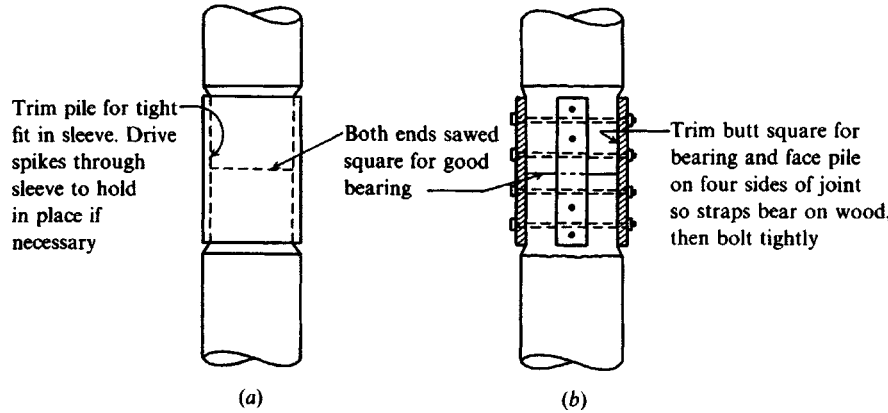

Figure 16-3 Splices in timber piles: (*a*) Using a metal sleeve with ends carefully trimmed for fit and bearing; (*b*) using splice plates. Be sure all exposed cuts are painted or sprayed with preservative.

The allowable design load based on pile material is

$$P_a = A_p f_a \tag{16-1}$$

where A_p = average pile cross-sectional area at the pile cap
f_a = allowable design stress (code) value for the type of timber

The static capacity based on the soil surrounding the pile is computed as for other pile materials and will be taken up in Sec. 16-7 and following. The principal additional factor to consider is that the coefficient of friction between wood and soil may approach tan ϕ' from a combination of soil displacement from the wood volume and from penetration of the wood by the soil grains— particularly in cohesionless soils.

Further information on timber piles may be obtained from American Wood Preservers Institute (AWPI) publications (1966, 1967, 1969, 1981) and ASTM D 25 (Vol. 4.09).

16-3 CONCRETE PILES

Table 16-1 indicates that concrete piles may be precast, prestressed, cast in place, or of composite construction.

Precast Concrete Piles

Piles in this category are formed in a central casting yard to the specified length, cured, and then shipped to the construction site. If space is available and a sufficient quantity of piles needed, a casting yard may be provided at the site to reduce transportation costs. *Precast* piles may be made using ordinary reinforcement as in Fig. 16-4 or they may be prestressed as in Fig. 16-5. Precast piles using ordinary reinforcement are designed to resist bending stresses during pickup and transport to the site and bending moments from lateral loads and to provide sufficient resistance to vertical loads and any tension forces developed during driving. The design procedures can be found in any text on reinforced-concrete design. However,

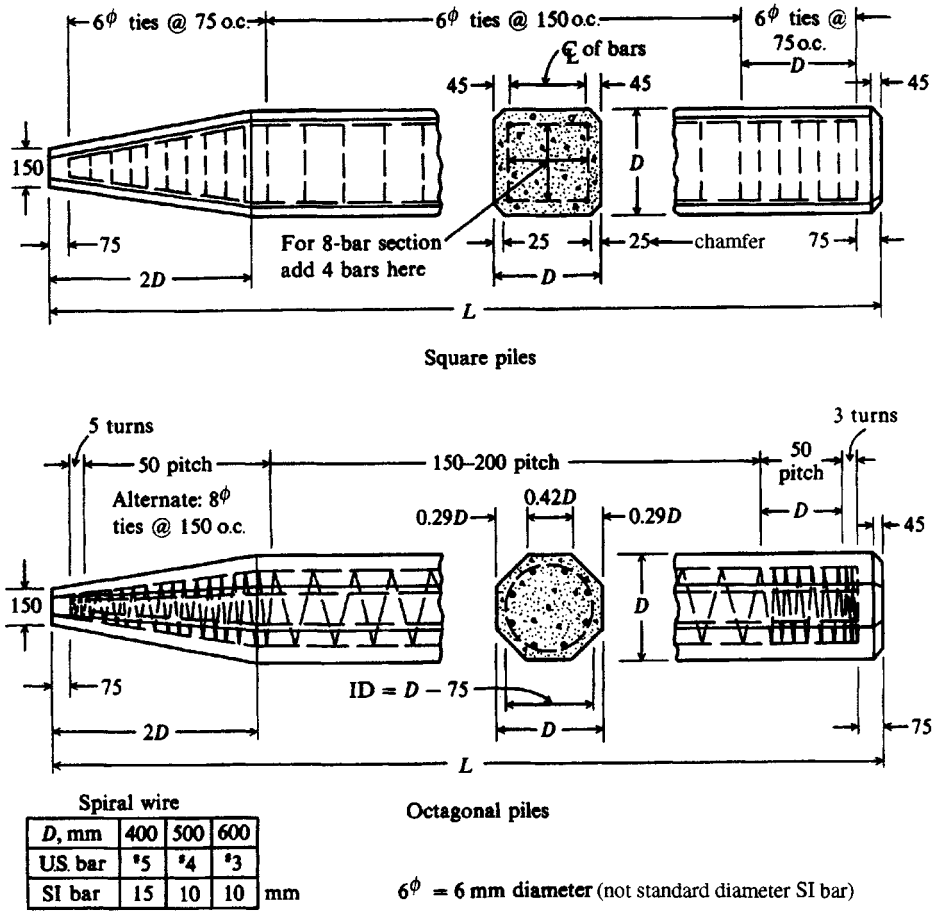

Spiral wire

D, mm	400	500	600
U.S. bar	#5	#4	#3
SI bar	15	10	10

mm

6ϕ = 6 mm diameter (not standard diameter SI bar)

Figure 16-4 Typical details of precast piles. Note all dimensions in millimeters. [*After PCA (1951).*]

temporary stresses from handling and driving (tensile) may be used that are on the order of 50 percent larger than the allowable concrete design stresses. The minimum pile reinforcement should be 1 percent.

Figure 16-6 illustrates typical bending moments developed during pickup depending on the location of the pickup point. The pickup point should be clearly marked since the bending moments depend heavily on its location.

Prestressed piles are formed by tensioning high-strength steel (f_{ult} of 1700 to 1860 MPa) prestress cables to a value on the order of 0.5 to 0.7f_{ult}, and casting the concrete pile about the cable. When the concrete hardens, the prestress cables are cut, with the tension force in the cables now producing a compressive stress in the concrete pile as the steel attempts to return to its unstretched length. The pile shortens under the prestress compression load P_i, and additionally the concrete undergoes creep, while simultaneously there is some relaxation in the steel, so the end result is an overall reduction of prestress force (and stress) that cannot be precisely evaluated. One may attempt a refined analysis of this loss, but about the same result is obtained by lumping the losses into a value of 240 MPa (i.e., $\sigma_{pf} = P_i/A - 240$). The pile will shorten some additional amount under the working load(s) to reduce the above

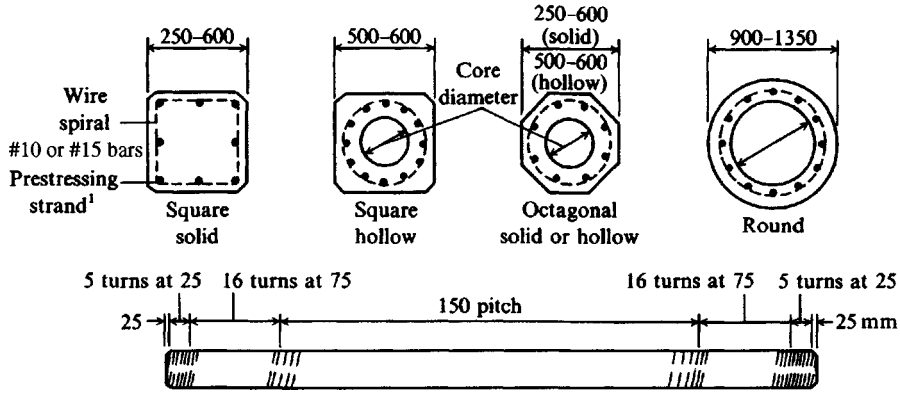

[1] Strand: 9.5–12.7 mm ($\frac{3}{8}$ to $\frac{1}{2}$ in.) nominal diam., f_u = 1860 MPa

Figure 16-5 Typical prestressed concrete piles (see also App. A, Table A-5); dimensions in millimeters.

σ_{pf} further to produce a final compressive stress σ_f in the pile. These losses in the absence of refined calculations may be taken as 240 MPa not including axial-shortening loss caused by the applied design loads. Final compressive concrete stresses from prestressing are usually on the order of 4 to 6 MPa. It is common to use higher-strength concrete (35 to 55 MPa) in prestressed piles because of the large initial compressive stresses from prestressing. A modest trade-off is obtained from the lighter-weight pile produced for the same load capacity.

The allowable design load P_a based on pile material for prestressed piles, and including prestress loss due to load and creep, can be computed as

$$P_a = A_g(0.33f'_c - 0.27f_{pe}) \tag{16-2}$$

where A_g = gross (total) concrete area
f_{pe} = effective prestress after all losses (about 5 MPa is usual)

Pickup points should be placed so that the computed bending stress has $f = M/\mathbf{S} \leq f_{pe}$, where M is from Fig. 16-6. If this is done the pile should not develop tension cracks during handling. Prestressing the pile tends to counteract any tension stresses during either handling or driving. This latter is particularly important since a pile is often placed in a hostile environment. If tension stresses during driving are large enough transient tension cracks are produced. During the time the crack is open foreign matter can enter and produce deterioration of the steel, which may not be detected for a long period of time.

Concrete piles are considered permanent; however, certain soils (usually organic) contain materials that may form acids that can damage the concrete. Saltwater may also adversely react with the concrete unless special precautions are taken when the mix proportions are designed. Additionally, concrete piles used for marine structures may undergo abrasion from wave action and floating debris in the water. Alternate freezing and thawing can cause concrete damage in any exposed situation.

Nonprestressed concrete used in marine structures should meet the following criteria:

1. Use nonreactive aggregates.
2. Use $8\frac{1}{2}$ to 10 sacks of cement per cubic meter of concrete.

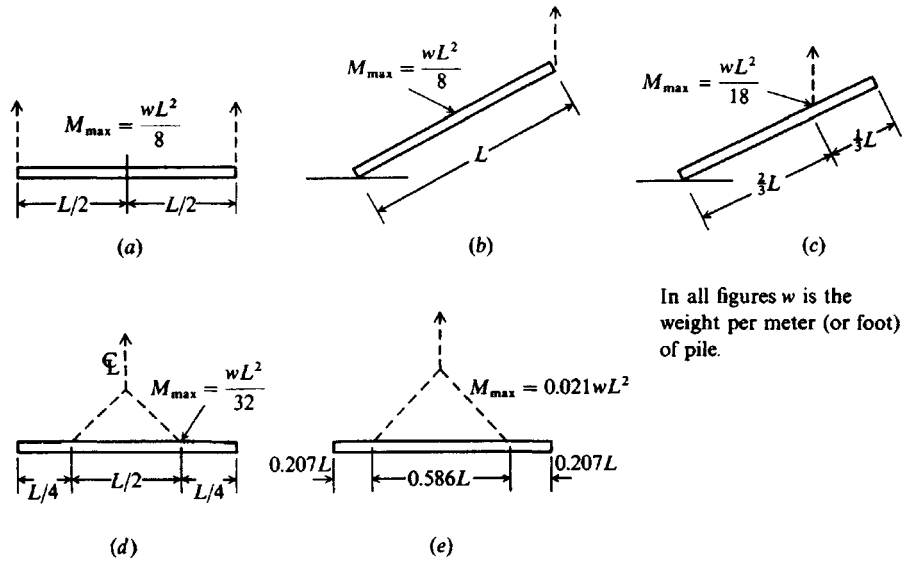

Figure 16-6 Location of pickup points for precast piles, with the indicated resulting bending moments.

3. Use type V cement (has high sulfate resistance).
4. Use a water/cement ratio ≤ 0.53 (by weight).
5. Use air-entrained concrete in temperate and cold regions.
6. Use a minimum of 75 mm of clear cover on all steel reinforcement (normal clear cover is 50 to 70 mm).

Cast-in-Place Piles

A cast-in-place pile is formed by drilling a hole in the ground and filling it with concrete. The hole may be drilled (as in caissons), or formed by driving a shell or casing into the ground. The casing may be driven using a mandrel, after which withdrawal of the mandrel empties the casing. The casing may also be driven with a driving tip on the point, providing a shell that is ready for filling with concrete immediately, or the casing may be driven open-end, the soil entrapped in the casing being jetted[1] out after the driving is completed.

Various methods with slightly different end results are available and patented. Figure 16-7 indicates some of the commonly available patented cast-in-place piles, and is intended to be representative only. Note that they are basically of three types: (1) shell or cased, (2) shell-less (uncased), or (3) pedestal types.

[1]Jetting is a common construction procedure of using a high-velocity stream of water to erode (or wash) a volume of soil into a soil-water suspension. The suspension is pumped or somehow disposed of so that an open cavity is formed. Soil cavities can be jetted into nearly all soils, including those that are very dense and hard.

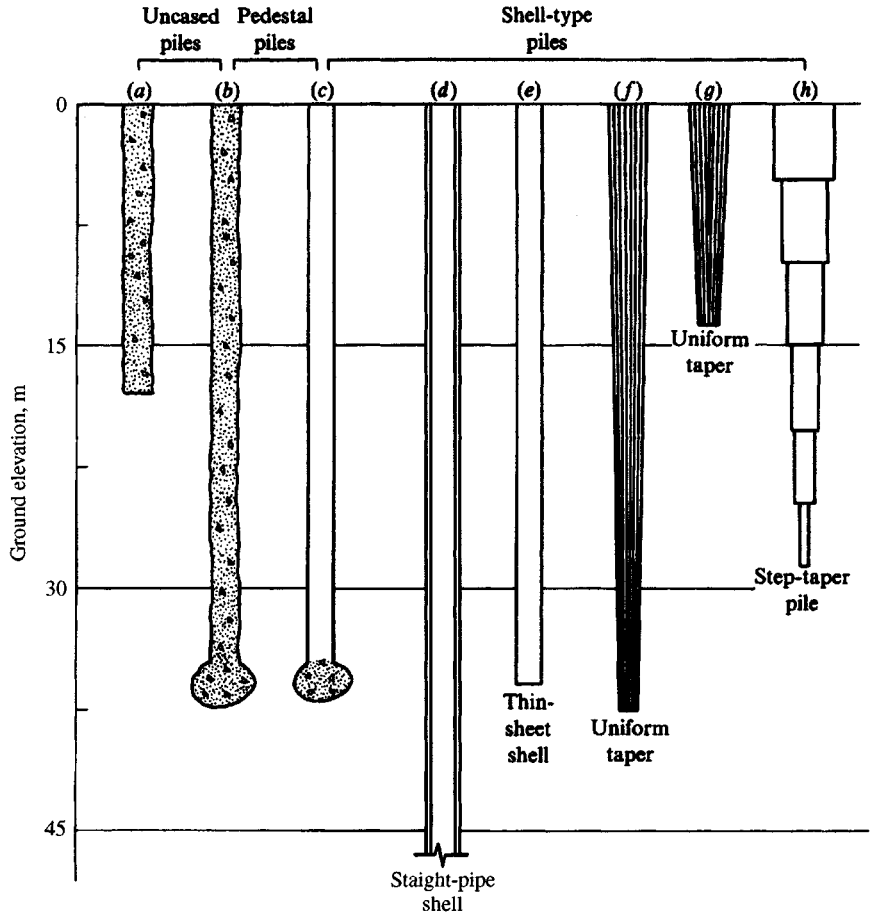

Figure 16-7 Some common types of cast-in-place (patented) piles: (*a*) Commonly used uncased pile; (*b*) Franki uncased pedestal pile; (*c*) Franki cased pedestal pile; (*d*) welded or seamless pipe; (*e*) Western cased pile; (*f*) Union or Monotube pile; (*g*) Raymond standard; (*h*) Raymond step-taper pile. Depths shown indicate usual ranges for the various piles. Current literature from the various foundation equipment companies should be consulted for design data.

The allowable design load for all concrete piles (not prestressed) is

$$P_a = A_c f_c + A_s f_s \tag{16-3}$$

where A_c, A_s = area of concrete and steel shell, respectively
f_c, f_s = allowable material stresses

Note that Eq. (16-3) does not apply for the aboveground portion of partially embedded piles. A reduction factor may be applied (to either f_c or P_a) for accidental eccentricities. Slenderness effects (l/r ratio) for that portion of the shaft length surrounded by soil are not necessary but may be required for the exposed length above ground.

A pile similar in section to that shown in Fig. 16-7*a* can be formed by using a hollow-stem continuous-flight auger with a diameter of 250 to 400 mm. The hole is excavated to

the desired elevation, a hose is connected to the auger, and cement grout (a pumpable mix of water, cement, and sand or sand and small gravel) is pumped under pressure down the auger stem and out the tip into the cavity formed as the auger is slowly withdrawn. The soil on the auger flights prevents the cement mixture from coming up the shaft and allows a modest amount of pump pressure to be exerted to reduce voids and make a solid pile-to-soil contact along the shaft.

A record should be kept of the auger depth and quantity of material pumped to ensure that the hole is filled with grout and that the auger was not withdrawn too rapidly that soil caved into the void such as to produce a discontinuous pile shaft. When the shaft has been filled, the wet concrete, having a greater density than the surrounding soil, will maintain the shaft until the concrete sets.

Reinforcement in the upper part of the shaft can be readily provided by inserting the proper number of reinforcing bars (or dowels) into the wet concrete. Where several soil layers are penetrated, the grout pressure may expand the borehole sufficiently to distort the pile shaft slightly in the soft strata; however, the principal effect of this is to increase the quantity of grout required to fill the shaft.

The Franki pile of Fig. 16-7*b* and *c* is produced by first placing very dry (zero slump) concrete in a cased shaft cavity and ramming it out of the casing base to produce an adequate-sized base enlargement. The shaft cavity is then filled with concrete to complete the pile. The casing may be pulled as the concrete is placed or left if pulling it would be difficult. Both the Franki system (which is patented) and piles formed from the continuous-flight auger method are very economical where cast-in-place procedures can be used.

16-4 STEEL PILES

These members are usually rolled **HP** shapes or pipe piles. Wide-flange beams or **I** beams may also be used; however, the **H** shape is especially proportioned to withstand the hard driving stress to which the pile may be subjected. In the **HP** pile the flanges and web are of equal thickness; the standard **W** and **I** shapes usually have a thinner web than flange. Table A-1 in App. A lists the **HP** pile sections produced in the United States and Canada. Pipe piles are either welded or seamless steel pipes, which may be driven either open-end or closed-end. Closed-end pipe piles are usually filled with concrete after driving. Open-end piles may be filled, but this is often not necessary, because there will be a dense soil plug at some depth below the top (and visible). Here it may only be necessary to jet out some of the upper soil plug to the necessary depth for any reinforcing bars required for bending (and to pump out the water used for jetting), before filling the remainder of the pile cavity with concrete. Concrete in only this shaft depth may be necessary for dowel bars.

The **HP** pile is a small-volume displacement pile since the cross-sectional area is not very large. A plug tends to form between the flanges at greater depths, however, so the bottom several meters may remold the soil on the order of the volume of the plug. An open-end pipe is also considered a small-volume displacement pile; however, a plug also forms inside with a depth one or more meters below the outside ground level—probably from a combination of inside perimeter friction and driving vibrations. From the depth at which the "plug" stabilizes (not visible during driving because of the pile cap and hammer interference) to the final driving depth, the lower soil may be remolded based on the volume of the plug and not the actual area of the pipe section.

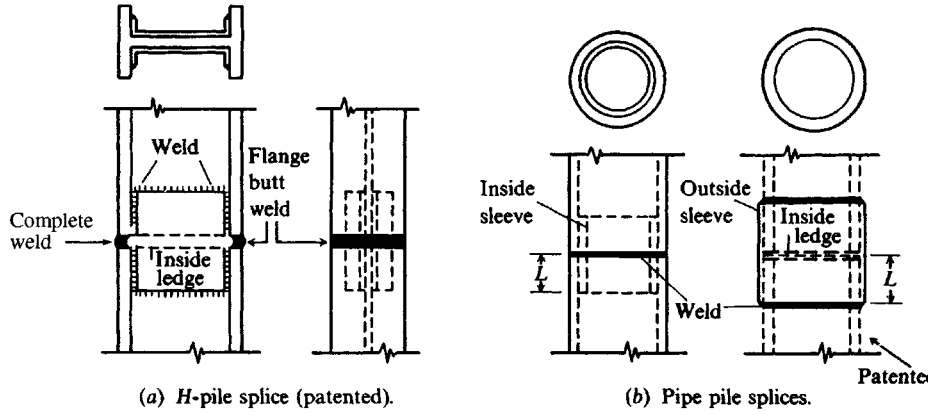

(*a*) *H*-pile splice (patented). (*b*) Pipe pile splices.

Figure 16-8 Splices for **H** and pipe piles.

HP piles have an advantage of sufficient rigidity that they will either break smaller boulders or displace them to one side. Open-end pipe piles have the advantage of surface entry to break up boulders encountered by either use of a chopping bit or drilling, blasting, and removal of the rock fragments. When large boulders are encountered one should consider the possibility of terminating the pile on (or slightly into) them.

Splices in steel piles (see Fig. 16-8) are made in the same manner as in steel columns, i.e., by welding (most common) or by bolting. Except for small projects involving only a few piles, most splices are made with prefabricated (and patented) splice connectors. For **HP** piles, splices can be prefabricated from two channels of adequate length back-to-back, with a short spacer on which the top pile section rests. The splice is then welded to the web across the ends, and the pile flanges are butt-welded to complete the splice. Pipe pile splicers consist of a ledged ring with an ID slightly larger than the pipe OD. The two sections of pipe to be joined rest against the inside ledge and an end weld is made around the pipe at both ends of the splicer. Generally these splices will develop the strength of the pile in compression, tension, bending, and shear to satisfy most building code requirements.

When a pile must be spliced to develop adequate embedment length, all the necessary equipment should be standing by so that when the hammer is shut off the splice can be quickly made. If this is not done—and sometimes if it is done—the soil tends to set or "freeze" about the pile, and resumption of driving is difficult and sometimes requires changing to a larger hammer. These larger driving stresses may cause considerable damage to the upper part of the pile. This phenomenon is independent of pile material (such as timber, concrete, or steel).

If the top of the steel pile is adequately embedded in the cap (say 150 mm or more) special load transfer plates are not necessary [Ohio (1947)]. Where embedment is limited or for special purposes, steel plates can be welded on the top of the pile to assist in load transfer and ensure that the piles and pile cap act as a unit.

In reference to Fig. 16-9*c* and Fig. 16-10*d*, there is little difference in driving resistance whether a pipe pile has a flat or conical driving point (or shoe). The reason is that a wedge-shaped zone of soil develops in front of the flat point somewhat like zone *abc* of Fig. 4-3*b* beneath a spread footing. It also appears that the later driving resistance of an open-end pipe is about that of a closed-end pile since the plug of soil inside the pipe shell (with friction developed with the wall) behaves similarly to the driving plate.

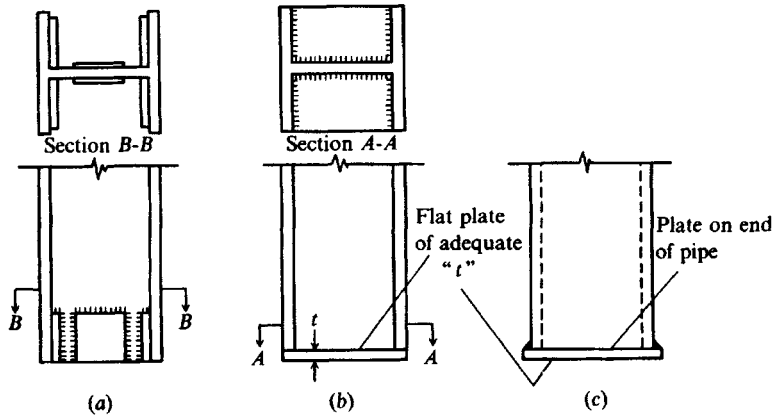

Figure 16-9 Shop- or field-fabricated driving points. Labor costs make this process generally uneconomical except for small numbers of points. Note that (*c*) will damage the perimeter soil so that skin resistance is reduced in stiff clays.

HP piles and pipe piles may require point reinforcement to penetrate hard soils or soils containing boulders without excessive tip damage. Figure 16-9 illustrates field-/shop-fabricated points, and Fig. 16-10 illustrates several that are commercially available. Those commercially available are likely to be more economical due to associated labor and fabrication costs except for isolated cases where only one or two might be needed.

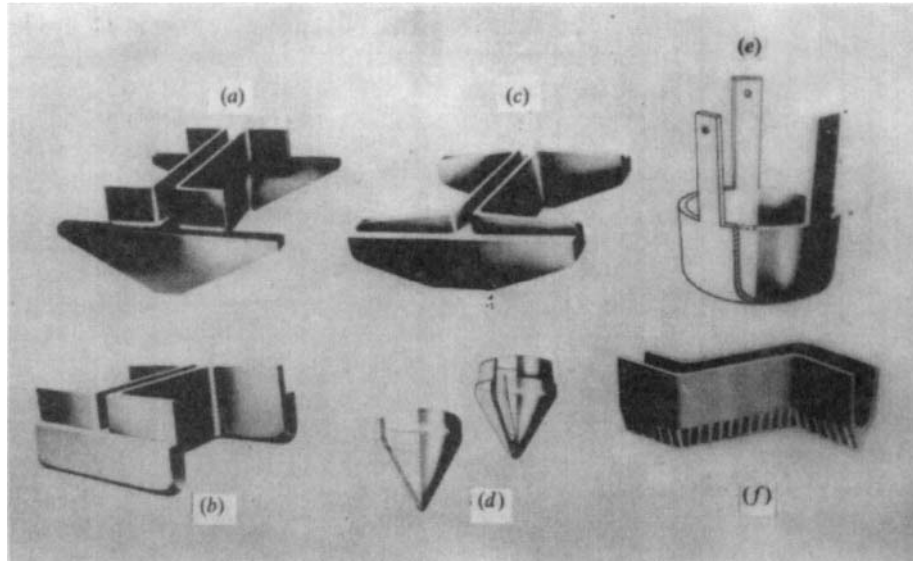

Figure 16-10 Commercially available points for several types of piles. Points are also available in higher-strength steel for very hard driving. Commercial points should be used if a large number of piles are to be driven. Parts (*a*), (*b*), and (*c*) are points for **HP** piles; (*d*) pipe-pile point; (*e*) timber-pile point; (*f*) sheet-pile point. (*Courtesy of Associated Pile and Fitting Corp.*)

The allowable design load for a steel pile is

$$P_a = A_p f_s \tag{16-4}$$

where A_p = cross-sectional area of pile at cap
f_s = allowable steel stress (code or specification); in range of 0.33 to $0.5 f_y$

16-5 CORROSION OF STEEL PILES

A corrosion study for the National Bureau of Standards [NBS (1962)] on both sheet-pile and bearing-pile substructures indicated that if piles are driven in *undisturbed natural* soil deposits, pile corrosion is not great enough to affect the strength of the piles significantly. This study encompassed soils with pH (a pH less than 7 is acidic) values from 2.3 to 8.6, and electric resistivities of 300 to 50 200 ohm · cm, from which it was further concluded that as long as the soil was undisturbed, the soil characteristics and properties are not significant. The substructures studied had been in service from 7 to 40 years. The soil resistance probe described by Roy and Ramaswamy (1983) may be used to obtain the soil resistance (ohm·cm) for estimating the probability of pile corrosion in the given site soil.

This study also indicated that piles driven in disturbed, or fill, soils will tend to undergo relatively more corrosion and may require painting (i.e., paint the pile, then construct the backfill). This observation was attributed to a higher oxygen concentration in the disturbed soil. Undisturbed soils were found to be oxygen-deficient from a few feet below the ground surface.

Piles exposed to seawater or to effluents with a pH much above 9.5 or below 4.0 will require painting or encasement in concrete to resist corrosion [Watkins (1969)]. This statement also applies to piles in general for the several feet in the zone where the water line fluctuates. As an alternative to painting or concrete encasement, a splice that uses a slightly larger section in the corrosive zone may be made.

Some of the newer grades of high-strength and copper-alloy steels are said to have substantial corrosion resistance. The A690 high-strength low-alloy steel has approximately two to three times more corrosion resistance to seawater than ordinary carbon steel of A36 grade. High-strength steel **HP** piles are seldom needed since the geotechnical considerations (bearing capacity of the rock or soil resistance) are more likely to set the structural stresses required of the steel than the structural considerations as set by codes, which may allow $f_a = 0.33$ to $0.5F_y$. For example, if the maximum allowable rock pressure for a pile founded on rock is 70 MPa, that sets a limit in the **HP** pile of 70 MPa regardless of F_y.

16-6 SOIL PROPERTIES FOR STATIC PILE CAPACITY

For *static pile* (and group) *capacity analysis* the angle of internal friction ϕ and the cohesion c of the soil are needed. Immediate controversy arises since some designers use undrained (or total) stress parameters, whereas others—particularly more recently—use effective stress values.

For *wave equation analysis* a value for the elastic recovery from deformation (quake, Q) and damping constants are needed.

Lateral pile analyses require use of the lateral modulus of subgrade reaction k_s or a lateral stress-strain modulus E_s. The context of usage determines whether the lateral or horizontal value is of interest for these latter two parameters.

The soil parameters may be determined from laboratory triaxial tests on "undisturbed" samples. These are quite satisfactory for piles installed in predrilled holes but may be considerably in error for driven piles.

Laboratory triaxial test parameters are not very reliable for driven piles since the soil in the vicinity of the pile undergoes extensive remolding, a change in water content, and usually an increase in density (or particle packing). Since these changes are highly indeterminate there is no way to duplicate them in any current laboratory test with any confidence. Thus, if laboratory tests are used, they are on the original in situ "undisturbed" samples, with experience used to extrapolate these data to obtain the design parameters. For these reasons the SPT is widely used, although there is movement to more use of CPT or PMT (the vane test is not much used) to obtain in situ parameters.

Most pile design in cohesionless materials (sands, gravelly sands, silty sands, etc.) is based on SPT N values. Pile design in cohesive deposits is usually based on unconfined compression strength q_u tests (pocket penetrometer, compression tests, the laboratory vane, hand-held pocket-sized shear strength test device called a torvane), primarily on very disturbed samples from the SPT. The CPT is, however, being used more in cohesive deposits (and in fine sands and fine silty sands) since those experienced with the procedure believe better design data are obtained.

The SPT N values should be adjusted to a standard energy—either N_{70} or N_{55} depending on the available data base and using the procedures outlined in Secs. 3-7 through 3-9.

Piles driven into the soil mass always result in remolding of the soil in the immediate vicinity of the pile (say, three to five pile diameters). At this instant, undrained soil-strength parameters are produced, which may approach remolded drained values if the degree of saturation S is low and/or the coefficient of permeability k is relatively large.

In general, however, a considerable time lapse (several months to years) occurs before the full design loads are applied. In this interval the excess pore pressures dissipate, and drained (or consolidated-undrained if below the GWT) conditions exist. For these it appears remolded (or residual) soil parameters best describe the soil behavior.

The capacity of piles in soft clays increases with time, with most strength regain occurring in from 1 to 3 months [Flaate and Selnes (1977), Orrje and Broms (1967)], **HP** piles requiring longer times. This increase in capacity is somewhat explained from the pile volume displacement producing high pore pressures that cause a more rapid drainage and consolidation of the soil very near the pile.

There is some opinion that the displaced volume of pipe and similar piles produces so much lateral compression in cohesive soils that a zone of perhaps 50 to 200 mm tends to consolidate to such a high value that the effective pile diameter is increased 5 to 7 percent over the actual value. This increase in "effective" diameter produces a corresponding increase in pile load capacity.

The reduced water content resulting from consolidation in this zone has been observed for some time [see references cited in Flaate (1972)]. The increase in "effective" pile diameter is likely to be marginal (or nonexistent) in very stiff and/or overconsolidated clays. In fact the volume displacement in these clays may produce a reduction in capacity over time as soil creep reduces the lateral pressure produced by the initial volume displacement.

Tavenas and Audy (1972) report an increase in load capacity with time for piles in sand, with the principal regain occurring in about the first month. This strength increase cannot be attributed to dissipation of excess pore pressures but may be due to *aging* from chemical contaminants (primarily carbonates) causing inter-grain and grain-to-pile adhesion. There

may be some gain in capacity from dissipation of residual driving stresses; however, this is doubtful since modern methods of driving produce a viscous semi-fluid state in a zone of 6 to 8 mm (at least) around the pile.

The pile capacity in calcareous sands may be considerably less after installation than the design value indicated by conventional design. This material (particularly if the carbonate content is greater than 50 percent) deteriorates rapidly under stress in the presence of water. Since the carbonate content is a byproduct of biological deposition (shells and such), deterioration is more likely to occur along shorelines and coral islands. Unfortunately except for performing tests (ASTM D 4373) for carbonate content (in percent) there is not much that can be done to quantify a design. Murff (1987, with a number of references) noted that some designers simply limit the skin resistance f_s (see Sec. 16.7) to some value on the order 15 to 30 kPa and point bearing q_o in the range of 4000 to 6000 kPa with smaller design values as the percent carbonates increases.

The pile literature contains a great number of conflicting conclusions obtained from both correct and incorrect interpretations of measured load test results and naturally occurring soil anomalies. As a consequence statistical correlations are particularly useful, but only on reliable data. Much of the pile literature (particularly early publications) did not provide enough data so that the reader could arrive at any kind of conclusion. Including these early data in a statistical correlation is not recommended although most publishers of correlations feel the more cases cited the better (or the more confidence the reader will have in the results).

Where piles are placed in predrilled holes, the soil state remains at nearly the existing (drained or consolidated undrained) condition. Possible deterioration of the cohesion at the interface of the wet concrete and soil may occur but this will be partially offset by the small increase in pile diameter when grains in the surrounding soil become part of the pile shaft as the cement hydrates.

The loss of K_o from soil expansion into the cavity may be partially offset by the lateral pressure developed from the wet concrete, which has a higher density than the soil.

Summarizing, for pile design we do not have a very good means to obtain soil parameters except for predrilled piles. For all cases of driven piles we have to estimate the soil parameters. In most cases if there is reasonable correlation between the design and measured load (from a load test) it is a happy coincidence.

16-7 STATIC PILE CAPACITY

All static pile capacities can be computed by the following equations:

$$\left.\begin{aligned} P_u &= P_{\text{pu}} + \sum P_{si} \\ &= P_P + \sum P_{si,u} \end{aligned}\right\} \quad \text{(compression)} \tag{16-5a}$$

$$T_u = \sum P_{si,u} + W_P \quad \text{(tension)} \tag{16-5b}$$

where P_u = ultimate (maximum) pile capacity in compression—usually defined as that load producing a large penetration rate in a load test

T_u = ultimate pullout capacity

P_{pu} = ultimate pile tip capacity—seldom occurs simultaneously with ultimate skin resistance capacity $\sum P_{si,u}$; neglect for "floating" piles (which depends only on skin resistance)

P_p = tip capacity that develops simultaneously with $\sum P_{si,u}$; neglect for "floating" piles

$\sum P_{si}$ = skin resistance developing with ultimate tip resistance P_{pu}; neglect for point bearing piles

$\sum P_{si,u}$ = ultimate skin resistance developing simultaneously with some tip capacity P_p

W = weight of pile being pulled

$\sum$ = summation process over i soil layers making up the soil profile over length of pile shaft embedment

The allowable pile capacity P_a or T_a is obtained from applying a suitable SF on the contributing parts as

$$P_a = \frac{P_{pi}}{\text{SF}_p} + \frac{\sum P_{si}}{\text{SF}_s} \qquad (a)$$

or using a single value SF (most common practice) to obtain

$$P_a = \frac{P_u}{\text{SF}} \quad \text{or} \quad T_a = \frac{T_u}{\text{SF}} \qquad (b)$$

This value of P_a or T_a should be compatible with the capacity based on the pile material (timber, concrete, or steel) considered earlier; and SF_i represents the safety factors, which commonly range from 2.0 to 4 or more, depending on designer uncertainties.

Opinion is mixed whether SF_i should be based on both load-carrying mechanisms [Eq. (*a*)] or be a single value [Eq. (*b*)]. In general, safety factors for piles are larger than for spread foundations because of more uncertainties in pile-soil interaction and because of the greater expense of pile foundations.

Although Eqs. (16-5) are certainly not highly complex in form, using them to arrive at a prediction of capacity that closely compares with a load test is often a fortunate event. A lack of correspondence is attributable to the difficulties in determining the in situ soil properties, which (as previously stated) change in the vicinity of the pile after it is has been installed. Additionally, the soil variability, both laterally and vertically, coupled with a complex pile-soil interaction, creates a formidable problem for successful analysis.

We can readily see from Eq. (16-5*a*) that the ultimate pile capacity P_u is not the sum of the ultimate skin resistance plus the ultimate point resistance but is the sum of one and a portion of the other.

Ultimate skin resistance is produced at some small value of relative slip between pile and soil, where slip is defined at any point along the pile shaft as the accumulated differences in shaft strain from axial load and the soil strain caused by the load transferred to it via skin resistance. This slip progresses down the pile shaft with increasing load.

In the upper regions the slip reaches limiting skin resistance and load is transferred to lower regions, which reach limiting skin resistance, . . . , etc., and finally to the tip, which begins to carry load. If pile penetration is rapid at this time the *ultimate* load P_u is reached. If penetration is not rapid the point load increases with further penetration until it also reaches *ultimate,* but with further penetration the slip resistance reduces to some limiting value that is less than the ultimate. We are now at the maximum pile capacity P_u.

The essential difference for tension capacity is that there is no point load, so that the force necessary to initiate a constant withdrawal rate is some limiting skin resistance, plus the pile weight W_p, plus suction at and near the point in wet soils. Suction, however, is seldom considered in design since it is transient. Again the upper pile elements reach the limiting skin resistance first.

Although it is common to compute the skin resistance contribution as an "average" value over one or two depth increments, better correlation is obtained if the summation is made for each stratum penetrated, using the best estimate of the applicable soil parameters for that stratum. The normal increase in soil density with depth will always produce several "soil layers" having values of γ, ϕ, and c that are somewhat different from those obtained using a single layer even for the same soil. It has been popular (and also convenient but not recommended) to use an average value from the several layers making up the site soil profile. A computer program (such as PILCAPAC) makes it a trivial exercise to subdivide the soil penetrated by the pile shaft into several layers for an improved analysis.

A study of load-settlement and load-transfer curves from a number of load tests indicates that slip to develop maximum skin resistance is on the order of 5 to 10 mm [Whitaker and Cooke (1966), Coyle and Reese (1966), AISI (1975)] and is relatively independent of shaft diameter and embedment length, but may depend upon the soil parameters ϕ and c. Note that sufficient slip at any point along the shaft to mobilize the limiting shear resistance is not the same as the butt movement measured in a pile-load test (as illustrated in Fig. 17-6) but is larger than the slip that produces the maximum (or ultimate) skin resistance.

Mobilization of the ultimate point resistance in any soil requires a point displacement on the order of 10 percent of the tip diameter B (see Fig. 16-11*a* for point cross section) for driven piles and up to 30 percent of the base diameter for bored piles and caissons. This is a total point displacement and when the pile point is in material other than rock may include additional point displacement caused by skin resistance stresses transferred through the soil to produce settlement of the soil beneath the point (refer to qualitative stress trajectories on right side of Fig. 16-11*a*). It is highly probable that in the usual range of working loads, skin resistance is the principal load-carrying mechanism in all but the softest of soils.

Since the pile unloads to the surrounding soil via skin resistance, the pile load will decrease from the top to the point. The elastic shortening (and relative slip) will be larger in the upper shaft length from the larger axial load being carried. Examination of a large number of load-transfer curves reported in the literature shows that the load transfer is approximately parabolic and decreases with depth for cohesive soils as shown in Fig. 16-12*a*.

The load transfer may, however, be nearly linear for cohesionless soils, and the shape may be somewhat dependent on embedment depth in all materials. Generally a short pile will display a more nearly linear load-transfer curve than a long pile; however, this conclusion is somewhat speculative since not many very long piles have been instrumented because of both expense and the poor survivability of instrumentation with increased driving effort. The more nonlinear load-transfer curves for long piles may be caused from overburden pressure increasing the soil stiffness with depth. The load-transfer curves for either short end-bearing or long friction piles may be nearly linear and vertical at the butt end where the relative slip and driving whip, or lateral shaft movement under hammer impacts (critical in stiff clays) are so large that the upper soil carries very little load. Figure 16-13 illustrates a case where the upper region also carries very little load at higher pile loads; however, this is in sand fill so that the small load is due more to relative slip than to driving whip damage.

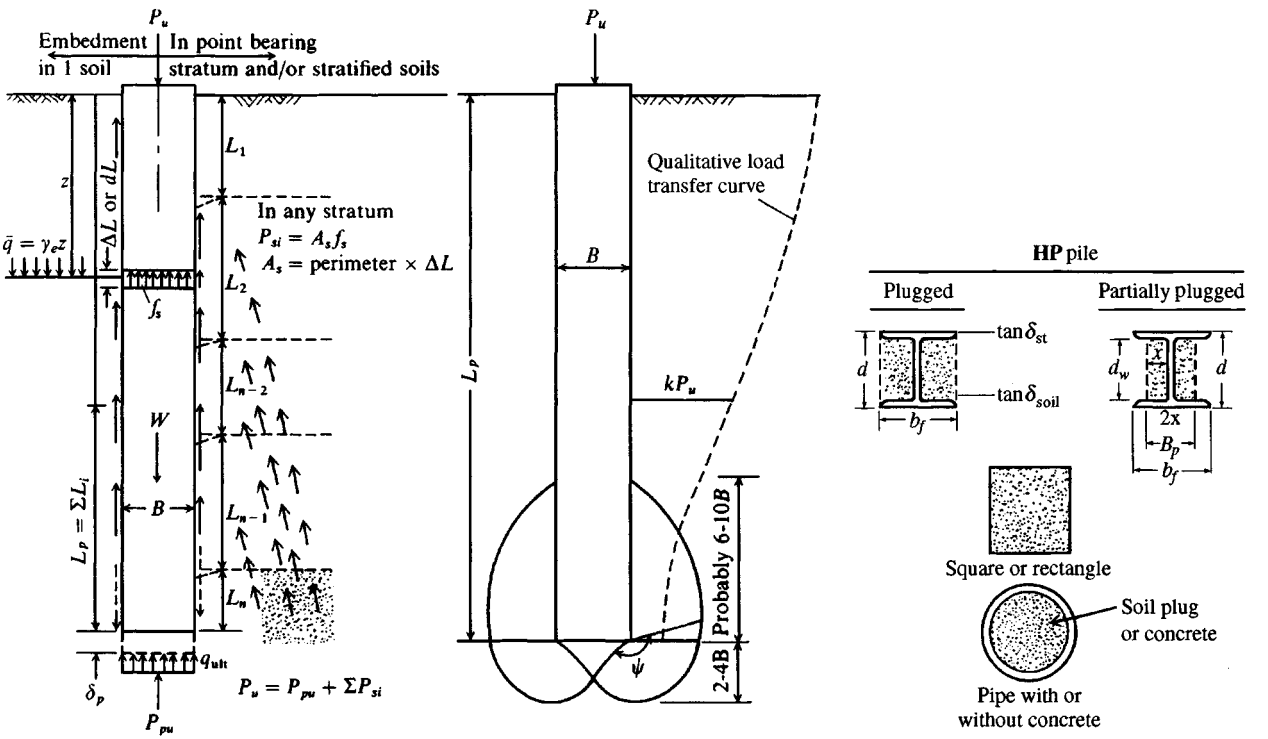

Figure 16-11 Piles in soil. Pile-to-soil friction $\tan\delta$ defined for pile perimeters shown; **HP** pile has two values; all others have a single δ value.

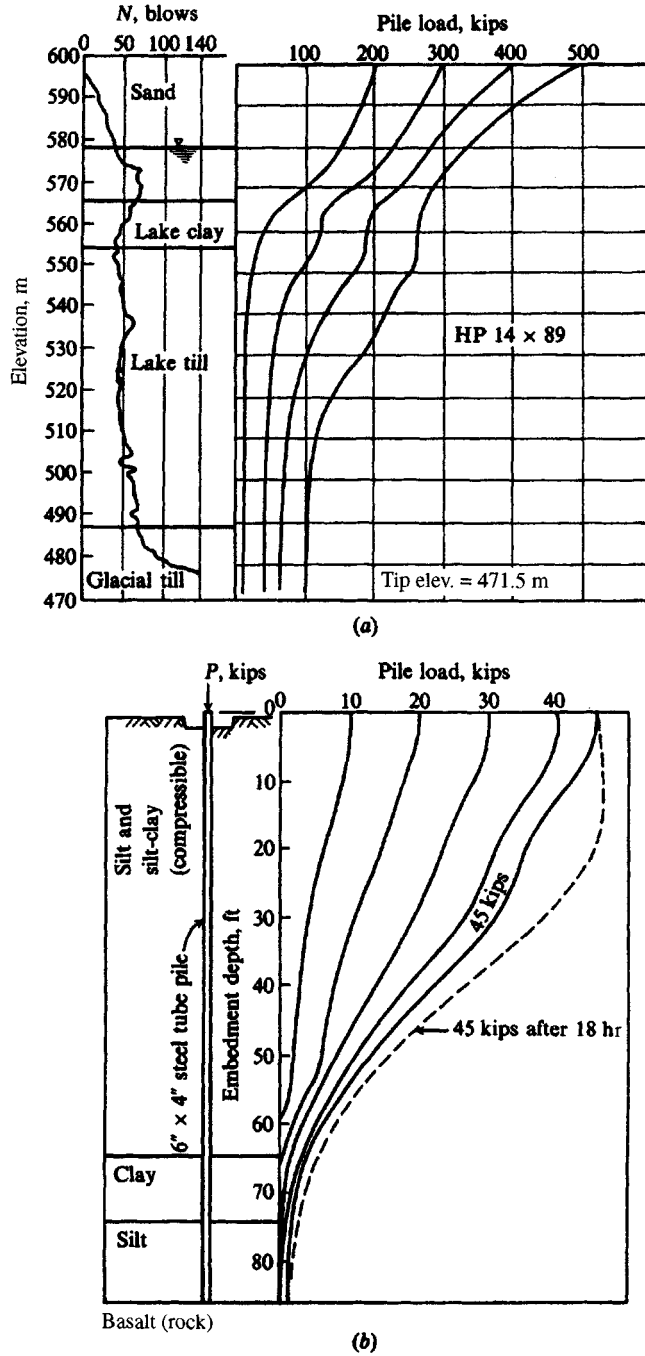

Figure 16-12 (*a*) Load-transfer curves for an **HP** pile in cohesive soil. [*From D'Appolonia and Romualdi (1963).*] (*b*) Load-transfer curves for pile in compressible soil showing transfer to be time-dependent. [*Frances et al. (1961).*]

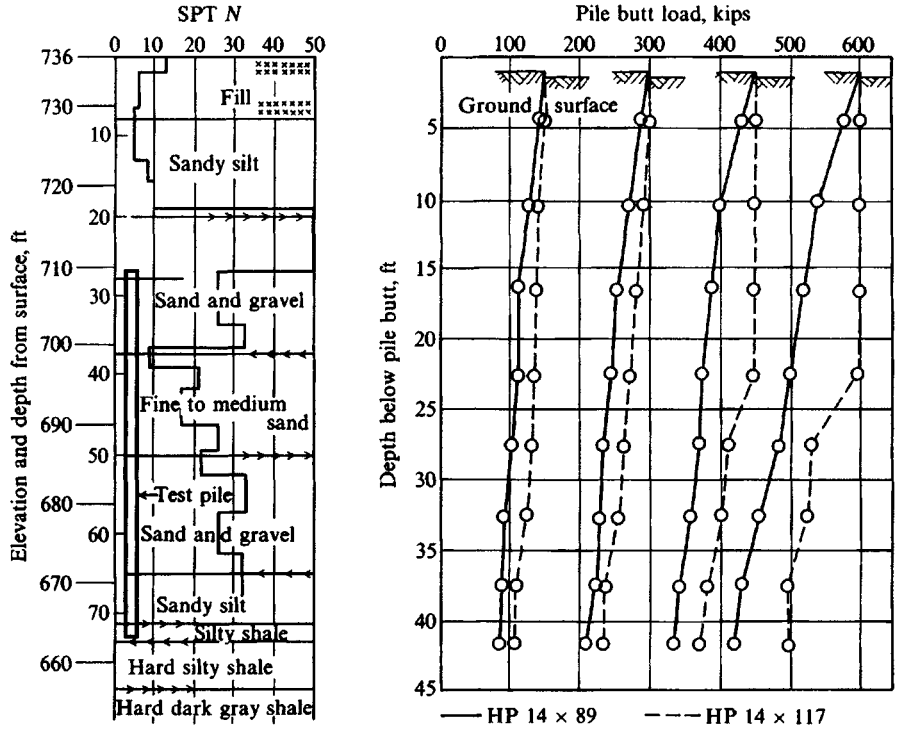

Figure 16-13 Load transfer for long **HP** piles in sand. Note that the behavior of **H** 14 × 117 is considerably different from that of the **H** 14 × 89 at higher loads. [*After D'Appolonia (1968).*]

The amount of load that is carried by the point under any butt loading depends on the surrounding soil, length and stiffness (AE/L) of the pile, and the actual load. Load duration and elapsed time before load application may also be significant factors to increase (or decrease) the point load for end-bearing piles that penetrate soft soils as shown in Fig. 16-12*b*.

Inspection of Figs. 16-12 and 16-13 indicates some interpretation is required to estimate load transfer at any depth increment. The piles of Fig. 16-13 are in the same site, but at higher loads there is little similarity in the shapes of the load-transfer curves.

When a pile is driven into a soil the response will depend upon several factors:

1. The volume of soil displaced by the pile. Concrete, closed-end pipe, and timber piles displace a large volume of soil relative to open-end pipe and **HP** piles.

   A plug forms on the inside of an open-end driven pipe pile and acts as a part of the pile cross section (including an apparent weight increase) when the friction resistance on the metal perimeter becomes larger than the weight of the plug [see Paikowsky and Whitman (1990)]. The plug is visible at some depth below the ground line in driven pipe piles. This depth represents a volume change due to driving vibrations and compression from friction between the inside pipe perimeter and the soil plug [see Eq. (17-8)].

   Two plugs (or partial plugs) usually form between the flanges of **HP** piles depending on the amount of soil-to-steel friction/adhesion along the inner faces of the two flanges

and web and on the amount of soil-to-soil friction/adhesion across the web depth. In clay the "plugged" case of Fig. 16-11*c* will generally form unless the pile is quite short. In sands the full plug may not form [see Coyle and Ungaro (1991)]. You can estimate the amount of plug formation (refer to Fig. 16-11*c*) as follows:

$$(2x_p + d_w)\gamma z K \tan\delta = d_w \gamma z K \tan\phi$$

Canceling $\gamma z K$, using $d_w = d$, and solving for x_p, we obtain

$$x_p = \frac{d}{2}\left(\frac{\tan\phi}{\tan\delta} - 1\right) < \frac{b_f}{2} \qquad \text{(partial plug forms)}$$

$$\geq \frac{b_f}{2} \qquad \text{(full plug forms)}$$

$$\text{Then } A_{\text{point}} = d \times 2x_p \qquad \text{(neglecting web thickness)}$$

$$\text{Perimeter } A_s = 2b_f + 2d \qquad \text{(neglect any inner flange width zones)}$$

The preceding roundings should give adequate computational accuracy since the x_p zone is likely curved inward from the inner flange tips and not the assumed straight line shown. You can refine the foregoing for actual web thickness if desired, but both angles ϕ and δ are usually estimated. You probably should make this check even for point bearing piles in dense sand.

Use these "plug" dimensions to compute the plug weight to add to any pile computations that include a pile weight term W_p.

2. The amount and type of overburden material. Piles penetrating a cohesionless soil into clay will tend to drag sand grains into the cohesive soil to a depth of about 20 pile diameters [Tomlinson (1971)]. This material will be trapped in the void around the perimeter caused by driving whip and tends to increase the skin resistance.
3. The fact that piles penetrating a soft clay layer into a stiffer lower layer will drag (or flow) a film of the softer material into the perimeter void to a depth of about 20 pile diameters. This dragdown may not be serious, however, for the crack closure will consolidate this material so that the resulting adhesion will be much higher than the adhesion in the upper soft layer.
4. The fact that large-volume piles penetrating a stiff clay layer tend to form large surface cracks that radiate out from the pile such that adhesion in the topmost 20 pile diameters is most uncertain. Generally the top 1.2 to 1.8 m of penetration should be neglected in computing the skin resistance in medium stiff or stiff clays and in sand.
5. The fact that soft clay tends to flow and fill any cracks that form during driving. After driving and dissipation of the excess pore pressures, the skin resistance tends to be larger than the initial values. It is believed that considerable consolidation occurs, which produces the higher skin resistances. This is the rationale that the adhesion factor α [of such as Eq. (16-11)] can be larger than 1 when s_u is under about 50 kPa.

16-8 ULTIMATE STATIC PILE POINT CAPACITY

The ultimate static pile point capacity in any soil can be computed using the bearing-capacity equations given in Table 4-1. The N_γ term is often neglected when the pile base width B_p is not large. It may not be neglected where an enlarged pile base or the *piers* of Chap. 19 are

used. The computed point bearing capacity varies widely because there is little agreement on what numerical values to use for the bearing-capacity factors N_i.

We will look at several of the more popular values, but no special recommendation is given for the "best" values since local practice or individual designer preference usually governs the values selected/used.

As previously stated, the soil parameters may be derived from laboratory tests on "undisturbed" samples but more often are unconfined compression data from an SPT or cone penetration test data. In general, the point capacity is computed as

$$P_{pu} = A_p(cN'_c d_c s_c + \eta \bar{q} N'_q d_q s_q + \tfrac{1}{2}\gamma' B_p N_\gamma s_\gamma) \tag{16-6}$$

where A_p = area of pile point effective in bearing, i.e., generally include any "plug." Use actual steel area for point bearing **HP** piles founded on rock, giving simply

$$P_{pu} = A_{steel} \times q_{ult};\ \text{see Sec. 4-16 for rock } q_{ult}$$

c = cohesion of soil beneath pile point (or s_u)

B_p = width of pile point (including "plug")—usually used only when point is enlarged

N'_c = bearing capacity factor for cohesion as previously defined in Chap. 4 but not computed the same way. Use

$$d_c = 1 + 0.4 \tan^{-1}(L/B)$$

And when $\phi = 0$; $c = s_u$; $N'_c \approx \mathbf{9.0}$

N'_q = bearing capacity factor (may include overburden effects)

$$\text{Use } d_q = 1 + 2 \tan\phi(1 - \sin\phi)^2 \tan^{-1} L/B$$

The following depth factors are representative:

L/B	d_c	d_q; $\phi = 36°$
10	1.59	$1.36 = 1 + 0.247 \tan^{-1} 10$
20	1.61	1.38
40	1.62	1.38
100	1.62	1.39

N'_γ = bearing capacity factor for base width = N_γ since it is not affected by depth

$\bar{q} = \gamma L$ = effective vertical (or overburden) pressure at pile point

η = **1.0** for all except the Vesić (1975*a*) N_i factors where

$$\eta = \frac{1 + 2K_o}{3}$$

K_o = at-rest earth pressure coefficient defined in Chap. 2.

When making point resistance computations, keep in mind that these bearing-capacity factors are based on the initial in situ soil parameters and not on any soil parameters revised to include driving effects. Initially, of course, any revised values would not be known.

Neglecting the N_γ term and making adjustment for pile weight, we may rewrite Eq. (16-6) as follows:

$$P_{pu} = A_p[cN'_c d_c + \eta\bar{q}(N'_q - 1)d_q] \tag{16-6a}$$

For $c = s_u$ and $\phi = 0$, the value of $N'_q = 1$ and

$$P_{pu} = A_p(9s_u) \tag{16-6b}$$

Most designers use N'_q, not $(N'_q - 1)$, for piles (but not piers of Chap. 19) when $\phi > 0$ since the factor reduced by 1 is a substantial refinement not justified by estimated soil parameters. The ultimate point capacity is divided by an SF on the order of 1.5 to 3.

Based on results obtained by Coyle and Castello (1981), who back-computed point capacities of a large number of piles in sand, the Hansen bearing-capacity factors of Table 4-4 can be used together with the shape and depth factors of Table 4-5 with a reliability about as good as any other procedure.

The Terzaghi bearing-capacity equation and factors (Table 4-3) are often used even though they are strictly valid only for $L \leq B$. They seem to give about the same point capacity as the Hansen equation for pile depths on the order of 10 to 20 m—probably because the Hansen $N_q d_q$ term equates to the larger Terzaghi N_q factor.

The depth factor d_c was previously shown to give a limiting value on the order of 1.62; the depth factor d_q depends on both the pile depth ratio L/B and ϕ but from the typical values previously given we see that it can be computed to give a limit on the N'_q term as well. From this we see that using any of Eqs. (16-6) gives an unlimited ultimate point resistance P_u but at a decreasing rate. The point capacity increase at a decreasing rate with increasing L/B seems to be approximately what occurs with actual piles, and for this reason *critical depth* methods such as that of Meyerhof (1976), which adjusts both bearing-capacity factors N'_c, N'_q using a critical depth ratio of L_c/B that was dependent on the ϕ angle of the soil, are not suggested for use.

The Vesić Method

According to Vesić (1975*a*) the bearing-capacity factors N'_i of Eq. (16-6) can be computed based on the following:

$$N'_q = \frac{3}{3 - \sin\phi}\left\{\exp\left[\left(\frac{\pi}{2} - \phi\right)\tan\phi\right]\tan^2\left(45° + \frac{\phi}{2}\right)I_{rr}^{\frac{1.333\sin\phi}{1+\sin\phi}}\right\} \tag{16-7}$$

The reduced rigidity index I_{rr} in this equation is computed using the volumetric strain ϵ_v [see Eq. (*d*) of Sec. 2-14] as

$$I_{rr} = \frac{I_r}{1 + \epsilon_v I_r} \tag{c}$$

The rigidity index I_r is computed using the shear modulus G' and soil cohesion and shear strength s (or τ) as

$$I_r = \frac{G'}{c + \bar{q}\tan\phi} = \frac{G'}{s} \tag{d}$$

When undrained soil conditions exist or the soil is in a dense state, take $\epsilon_v = 0.0$ so that $I_{rr} = I_r$. The value of I_{rr} depends on the soil state (loose, dense; low, medium, or high plasticity) and on the *mean normal stress* defined by $\eta\bar{q}$ with lower I_r values in sand when $\eta\bar{q}$ is low. In clay higher I_r values are used when the water content is high and/or together with a high $\eta\bar{q}$. The lowest values of $I_r \approx 10$ are obtained (or used) for a clay with high OCR and low $\eta\bar{q}$. Estimates for I_r may be made as follows:

Soil	I_r
Sand (D_r = 0.5–0.8)	75–150
Silt	50–75
Clay	150–250

Use lower I_r values with *higher* average effective mean normal stress $\eta\bar{q}$.

Since the Vesić method is based on cavity expansion theory, the pile tip behavior is similar to that of the CPT. On this basis Baldi et al. (1981) suggest the following equations for I_r:

For *Dutch cone tip* (see Fig. 3-14*a*):

$$I_r = \frac{300}{f_R} \tag{e}$$

For the *electric cone* (see Fig. 3-15*a*):

$$I_r = \frac{170}{f_R} \tag{f}$$

where f_R = friction ratio in percent given by Eq. (3-10).

The Vesić bearing-capacity factor N'_c term can be computed by one of the following equations:

$$N'_c = (N'_q - 1)\cot\phi \tag{16-7a}$$

When $\phi = 0$ (undrained conditions)

$$N'_c = \frac{4}{3}(\ln I_{rr} + 1) + \frac{\pi}{2} + 1 \tag{16-7b}$$

Janbu's Values

Janbu (1976) computes N'_q (with angle ψ in radians) as follows:

$$N'_q = \left(\tan\phi + \sqrt{1 + \tan^2\phi}\right)^2 \exp(2\psi\tan\phi) \tag{16-7c}$$

For either the Vesić or Janbu methods obtain N'_c from Eq. (16-7*a*) for $\phi > 0$, from Eq. (16-7*b*) when $\phi = 0$. The value of ψ for the Janbu equation is identified in Fig. 16-11*b* and may vary from 60° in soft compressible to 105° in dense soils. Table 16-2 gives a selected range of N'_i values, which can be used for design or in checking the Vesić and Janbu equations.

TABLE 16-2
Bearing-capacity factors N'_c and N'_q by Janbu's and Vesić's equations

A shape factor of s_c 1.3 may be used with Janbu's N'_c. Use program FFACTOR for intermediate values.

	Janbu			Vesić				
ϕ	$\psi = 75°$	90	105	$I_{rr} = 10$	50	100	200	500
0°	$N'_q = 1.00$	1.00	1.00	$N'_q = 1.00$	1.00	1.00	1.00	1.00
	$N'_c = 5.74$	5.74	5.74	$N'_c = 6.97$	9.12	10.04	10.97	12.19
5	1.50	1.57	1.64	1.79	2.12	2.28	2.46	2.71
	5.69	6.49	7.33	8.99	12.82	14.69	16.69	19.59
10	2.25	2.47	2.71	3.04	4.17	4.78	5.48	6.57
	7.11	8.34	9.70	11.55	17.99	21.46	25.43	31.59
20	5.29	6.40	7.74	7.85	13.57	17.17	21.73	29.67
	11.78	14.83	18.53	18.83	34.53	44.44	56.97	78.78
30	13.60	18.40	24.90	18.34	37.50	51.02	69.43	104.33
	21.82	30.14	41.39	30.03	63.21	86.64	118.53	178.98
35	23.08	33.30	48.04	27.36	59.82	83.78	117.34	183.16
	31.53	46.12	67.18	37.65	84.00	118.22	166.15	260.15
40	41.37	64.20	99.61	40.47	93.70	134.53	193.13	311.50
	48.11	75.31	117.52	47.04	110.48	159.13	228.97	370.04
45	79.90	134.87	227.68	59.66	145.11	212.79	312.04	517.60
	78.90	133.87	226.68	53.66	144.11	211.79	311.04	516.60

The American Petroleum Institute [API (1984)] has formulated recommendations for pile design in the form of design parameters for piles in sands, silts, sand silts, and gravels based on a soil description ranging from very loose to very dense. This publication suggests using N'_q ranging from a low of 8 for very loose sand to 50 for a dense gravel or very dense sand. The table is footnoted that the values are intended as guidelines only. These values seem rather low compared to recommendations by most authorities, particularly when considering that piles driven into loose sand will densify it a modest amount in almost all circumstances.

A study of a number of pile load tests by Endley et al. (1979) indicated the 1979 API [reissued as API (1984)] recommendations for N'_q were about 50 percent too low. Be aware that recommended values are not requirements; however, if they are not followed, one must be prepared to justify the use of any alternative values.

Using Penetration Test Data for Pile Point Resistance

For standard penetration test (SPT) data Meyerhof (1956, 1976) proposed

$$P_{pu} = A_p(40N)\frac{L_b}{B} \leq A_p(380N) \qquad \text{(kN)} \tag{16-8}$$

where N = statistical average of the SPT N_{55} numbers in a zone of about $8B$ above to $3B$ below the pile point (see Fig. 16-11*b*). Use any applicable SPT N corrections given in Chap. 3.

B = width or diameter of pile point
L_b = pile penetration depth into point-bearing stratum
L_b/B = average depth ratio of point into point-bearing stratum

According to Shioi and Fukui (1982) pile tip resistance is computed in Japan as

$$P_{pu} = q_{ult} A_p \tag{16-9}$$

with the ultimate tip bearing pressure q_{ult} computed from the SPT based on the embedment depth ratio L_b/D into the point-bearing stratum as follows:

Driven piles	$q_{ult}/N = 6L_b/D$	≤ 30 (open-end pipe piles)
	$q_{ult}/N = 10 + 4L_b/D$	≤ 30 (closed-end pipe)
Cast-in-place	$q_{ult} = 300$	(in sand)
	$q_{ult} = 3s_u$	(in clay)
Bored piles	$q_{ult} = 10N$	(in sand)
	$q_{ult} = 15N$	(in gravelly sand)

where this SPT N should be taken as N_{55}.

For *cone penetration data* with $L/B \geq 10$ the point load is estimated by the Japanese as

$$P_{pu} = A_p q_c \qquad \text{(in units of } q_c\text{)} \tag{16-9a}$$

where q_c = statistical average of the cone point resistance in a zone similar to that for N_{55} of Eq. (16-8).

Summarizing Pile Point Capacity

We can compute the ultimate pile point capacity by using Eqs. (16-6), (16-8), or (16-9), depending on the data available. The major problem in using Eq. (16-6) is having access to a reliable angle of internal friction ϕ and soil unit weight γ. We have at least three methods of obtaining the N factors: Table 4-1, Vesić, or Janbu. We should note that Fig. 2-31 indicates that ϕ is pressure-dependent, so laboratory values in the common range of triaxial cell test pressures of 70 to 150 kPa may be several degrees larger than field values at the pile point, which may be 20 or 30 meters down where there is a substantially larger effective normal stress.

In Table 4-4, N_q more than doubles going from $\phi = 34°$ to 40°; thus, even small variations of 1 or 2° can produce a significant change in the pile point capacity.

The following example will illustrate how some of the methods given here are used.

Example 16-1. The point of a pile of $L = 25$ m is founded into a dense medium-coarse sand deposit, which has an average $N_{70} = 30$ in the zone of influence of about 1.5 m above the tip to 3 m below. The pile is an **HP** 360 × 174 with $d \times b = 361 \times 378$ mm. The GWT is 5 m below the ground surface.

Required. Estimate the point capacity P_u using the several methods presented in this section.

Solution.

$$A_p = d \times b \text{ (including the plug between flanges)} = 0.361 \times 0.378 = \mathbf{0.136}\ \text{m}^2$$

$$N_{55} = N_{70}(70/55) = 30(70/55) = 38$$

With a 1.5 m embedment into dense bearing sand, $L_b = 1.5$ m. We estimate the overburden unit weight $\gamma_s = 16.5\ \text{kN/m}^3$ since we have no N values or other data.

By Meyerhof's Eq. (16-8). From this we directly obtain

$$P_{\text{pu}} = A_p(40 \times N_{55})L_b/B = 0.136(40 \times 38)(1.5/0.361) = \mathbf{859}\ \text{kN}$$

The maximum recommended limit for the preceding equation is

$$P_{\text{pu}} = A_p 400 N_{55} = 0.136(380 \times 38) = 1964 > 859 \rightarrow \text{use } 859\ \text{kN}$$

We will also use the other equations for a comparison.

By Hansen's Eq. (16-6)

$$P_{\text{pu}} = A_p(cN_c d_c + \eta\bar{q}N'_q d_q + \tfrac{1}{2}\gamma' B_p N_\gamma)$$

For sand the cN_c term is 0. We can estimate for the medium coarse sand with $N_{70} = 30$ a value of $\phi \approx 36°$ (range from 36 to 50°) from Table 3-4 and in the tip zone $\gamma_{\text{sand}} = \mathbf{17.0}\ \text{kN/m}^3$. From Table 4-4 we obtain $N_q = \mathbf{37.7}$; $N_\gamma = \mathbf{40.0}$; depth factor = $\mathbf{0.247}$. We then compute

$$d_q = 1 + 0.247 \tan^{-1}(L/B) = 1 + 0.247 \tan^{-1}(25/0.361) = \mathbf{1.38}$$

$$\bar{q} = 5 \times 16.5 + 18.5(16.5 - 9.807) + 1.5(17.0 - 9.807)$$

$$= \mathbf{217.1}\ \text{kPa} \qquad (16.5\ \text{kN/m}^3 \text{ above tip zone and } 17.0\ \text{kN/m}^3 \text{ in tip zone})$$

$$P_{\text{pu}} = 0.136[217.1 \times 37.7 \times 1.38 + \tfrac{1}{2}(17.0 - 9.807)(0.361 \times 40)]$$

$$= 0.136(11\,295 + 52) = \mathbf{1543.2}\ \text{kN}$$

By Vesić's Method for N'_q, N'_γ. Estimate $K_o = 1 - \sin 36° = 0.412$:

$$\eta = \frac{1 + 2 \times 0.412}{3} = 0.61 \rightarrow \eta\bar{q} = 0.61 \times 217.1 = \mathbf{132.4}\ \text{kPa}$$

Based on using $I_{\text{rr}} = 100$, Eq. (16-7), and program FFACTOR (option 10), we obtain

$N'_q = 93.2$ (N'_c is not needed)

$N_\gamma = 40$ from Hansen equation (and Table 4-4)

$d_q = 1.38$, as before

Substituting values into Eq. (16-6), we obtain

$$P_{\text{pu}} = 0.136(132.4 \times 93.2 \times 1.38 + \tfrac{1}{2} \times 7.2 \times 0.361 \times 40)$$

$$= 0.136(17\,028.8 + 52.0) = \mathbf{2323}\ \text{kN}$$

By Janbu's method [Eq. (16-6) but using N'_q from Eq. (16-7*d*)]. Using program FFACTOR (option 10), for $\phi = 36°$ and estimating $\psi \approx 90°$, we obtain $N'_c = 37.4$; $d_q = 1.38$ as before; $\bar{q} = 217.1$ kPa (as before)

$N'_\gamma = 40.0$ as in Hansen equation also

Substituting values into Eq. (16-6), we obtain

$$P_{\text{pu}} = 0.136(217.1 \times 37.4 \times 1.38 + \tfrac{1}{2} \times 7.2 \times 0.361 \times 40)$$

$$= 0.136(11\,205.0 + 52.0) = \mathbf{1531}\ \text{kN}$$

By Terzaghi's method [$P_{pu} = 0.136(\bar{q}N_q + \frac{1}{2}\gamma' N_\gamma s_\gamma)$], **equation from Table 4-1.** Using $N_q = 47.2$; $N_\gamma = 51.7$; $s_\gamma = 0.8$; $L = 25$ m; $B = 0.361$ m; $A_p = 0.136$ m^2; $\bar{q} = 217.1$ kPa; $\gamma' = 17.0 - 9.807 = 7.2$, we obtain

$$P_{pu} = 0.136(217.1 \times 47.2 + \tfrac{1}{2} \times 7.2 \times 0.361 \times 51.7 \times 0.8)$$
$$= 0.136(10\,300.87) = \mathbf{1401}\ \text{kN}$$

A good question is what to use for P_{pu}. We could, of course, average these values, but there are too many computations involved here for a designer to compute a number of point resistances and obtain their average.

Let us instead look at a tabulation of values and see if any worthwhile conclusions can be drawn:

Method	P_{pu}, kN
Hansen	1543.2
Terzaghi	1401.0
Janbu	1531.0
Meyerhof	859.0
Vesić	2323.0

From this tabulation it is evident that the Meyerhof value is too conservative; the Vesić may be too large; but almost any value can be obtained by suitable manipulation of I_{rr} and, similarly with the Janbu equation, with manipulation of the ψ angle.

From these observations it appears that the Hansen equation from Chap. 4 using values from Table 4-4 provides as good an estimate of point capacity as the data usually available can justify. As a consequence that is the only method used in the rest of this text and is included as one of the point capacity contribution methods in the computer program PILCAPAC noted on your diskette and described further in the next section concerning skin resistance.

////

16-9 PILE SKIN RESISTANCE CAPACITY

The skin resistance part of Eq. (16-5) is currently computed using either a combination of total and effective, or only effective, stresses. Some evidence exists that use of only effective stresses gives a better correlation of prediction to load tests; however, both methods are widely used. Preference will depend on the data base of successful usage in a given locale/design office.

Three of the more commonly used procedures for computing the skin resistance of piles in cohesive soils will be given here. These will be called the α, λ, and β methods for the factors used in the skin resistance capacity part of Eq. (16-5). The β method is also used for piles in cohesionless soils. In all cases the skin resistance capacity is computed as

$$\sum_{1}^{n} A_s f_s \qquad \text{(in units of } f_s\text{)} \tag{16-10}$$

where A_s = effective pile surface area on which f_s acts; computed as perimeter × embedment increment ΔL. Refer to Fig. 16-11*a* for pile perimeters.

ΔL = increment of embedment length (to allow for soil stratification and variable pile shaft perimeters in the embedment length L)

f_s = skin resistance to be computed, using one of the three methods previously cited

Previous Page

By Terzaghi's method [$P_{pu} = 0.136(\bar{q}N_q + \frac{1}{2}\gamma' N_\gamma s_\gamma)$], **equation from Table 4-1.** Using $N_q = 47.2$; $N_\gamma = 51.7$; $s_\gamma = 0.8$; $L = 25$ m; $B = 0.361$ m; $A_p = 0.136$ m^2; $\bar{q} = 217.1$ kPa; $\gamma' = 17.0 - 9.807 = 7.2$, we obtain

$$P_{pu} = 0.136(217.1 \times 47.2 + \tfrac{1}{2} \times 7.2 \times 0.361 \times 51.7 \times 0.8)$$
$$= 0.136(10\,300.87) = \mathbf{1401}\ \text{kN}$$

A good question is what to use for P_{pu}. We could, of course, average these values, but there are too many computations involved here for a designer to compute a number of point resistances and obtain their average.

Let us instead look at a tabulation of values and see if any worthwhile conclusions can be drawn:

Method	P_{pu}, kN
Hansen	1543.2
Terzaghi	1401.0
Janbu	1531.0
Meyerhof	859.0
Vesić	2323.0

From this tabulation it is evident that the Meyerhof value is too conservative; the Vesić may be too large; but almost any value can be obtained by suitable manipulation of I_{rr} and, similarly with the Janbu equation, with manipulation of the ψ angle.

From these observations it appears that the Hansen equation from Chap. 4 using values from Table 4-4 provides as good an estimate of point capacity as the data usually available can justify. As a consequence that is the only method used in the rest of this text and is included as one of the point capacity contribution methods in the computer program PILCAPAC noted on your diskette and described further in the next section concerning skin resistance.

////

16-9 PILE SKIN RESISTANCE CAPACITY

The skin resistance part of Eq. (16-5) is currently computed using either a combination of total and effective, or only effective, stresses. Some evidence exists that use of only effective stresses gives a better correlation of prediction to load tests; however, both methods are widely used. Preference will depend on the data base of successful usage in a given locale/design office.

Three of the more commonly used procedures for computing the skin resistance of piles in cohesive soils will be given here. These will be called the α, λ, and β methods for the factors used in the skin resistance capacity part of Eq. (16-5). The β method is also used for piles in cohesionless soils. In all cases the skin resistance capacity is computed as

$$\sum_{1}^{n} A_s f_s \qquad \text{(in units of } f_s\text{)} \tag{16-10}$$

where A_s = effective pile surface area on which f_s acts; computed as perimeter × embedment increment ΔL. Refer to Fig. 16-11*a* for pile perimeters.

ΔL = increment of embedment length (to allow for soil stratification and variable pile shaft perimeters in the embedment length L)

f_s = skin resistance to be computed, using one of the three methods previously cited

The reader should note that the following equations for f_s are in general terms so that successful use will depend on how accurately the summation process is made and the soil parameters are identified.

16-9.1 The α Method

A general method for pile shaft skin resistance that was initially proposed by Tomlinson (1971) is

$$f_s = \alpha c + \bar{q} K \tan \delta \qquad \text{(units of } c, \bar{q}\text{)} \tag{16-11}$$

which includes both adhesion αc and friction. Equation (16-11) is not much used in this general form but rather simply as

$$f_s = \alpha c \qquad \text{or} \qquad \alpha s_u \tag{16-11a}$$

where α = coefficient from Fig. 16-14

c = average cohesion (or s_u) for the soil stratum of interest

$\bar{q}$ = effective average (or midheight) vertical stress $\gamma_s z_i$ on element ΔL (Fig. 16-11*a*)

K = coefficient of lateral earth pressure ranging from K_o to about 1.75, depending on volume displacement, initial soil density, etc. The author has found the following to work rather well:

$$K = \frac{K_a + F_w K_o + K_p}{2 + F_w}$$

where the K_i values are as previously defined and F_w = weighting factor for K_o ranging from 1.0 upward

δ = effective friction angle between soil and pile material (use either values from Table 11-6 or ϕ' = effective value); use $\delta = 0$ when $\phi = 0°$

Compute K_o using Eq. (2-18*a*) and adjust for OCR using Eq. (2-23).

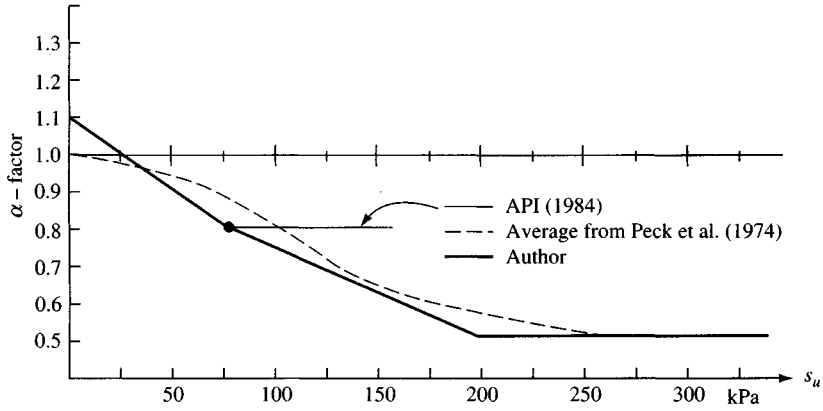

Figure 16-14 Relationship between the adhesion factor α and undrained shear strength s_u. (*From sources noted.*)

The API (1984) also suggests using the α method with factors as shown on Fig. 16-14 for normally consolidated clay. API recommends not more than 50 kPa for OCR > 1 or large L/B ratios.

Sladen (1992) derived an equation to compute α directly based on the undrained shear strength s_u and the effective overburden stress $\bar{q}$. It can be derived using the following:

$$f_s = \alpha s_u = \bar{q}_h \tan\delta \qquad \text{and} \qquad \bar{q}_h = \kappa K_{o,\text{nc}}\, \bar{q}$$

$$K_{o,\text{oc}} = \frac{\bar{q}_h}{\bar{q}} = K_{o,\text{nc}} \times \text{OCR}^n \qquad \text{[see Eq. (2-23)]}$$

$$\text{Also } s_u = A\bar{q}(\text{OCR})^m \quad \text{and } m \approx 1 - C_s/C_c$$

where C_s, C_c = compression indexes from Chap. 2

$A = s_u/p'_o$ (normally consolidated values) from Fig. 2-36

$\kappa > 1$ = for driven piles $\qquad \kappa < 1$ for bored piles

Making substitutions for f_s, q_h, and s_u and solving for α, we obtain

$$\alpha = \frac{\kappa K_{o,\text{nc}}}{A}\left(\frac{s_u}{Aq}\right)^{(n-m)/m} \tan\delta \tag{16-12}$$

If one assumes these values: $C_1 = \kappa \tan\delta = 0.40$ to 0.70; $A = 0.3$; $K_{o,\text{nc}} = 0.55$; $m \approx 0.8$; $n \approx 0.45$, the following approximation suitable for design use is obtained:

$$\alpha = C_1\left(\frac{\bar{q}}{s_u}\right)^{0.45} \tag{16-12a}$$

This equation shows that α depends upon both the effective vertical overburden stress $\bar{q}$ and the undrained shear strength s_u; use $C_1 = 0.4$ to 0.5 for bored piles/piers and ≥ 0.5 for driven piles.

16-9.2 The λ Method

Vijayvergiya and Focht (1972) presented a method of obtaining the skin resistance of a pile in overconsolidated clays and have claimed a correlation between design and load tests on the order of $\pm$ 10 percent. The original development was based primarily on pile load tests. These were on long piles used for offshore oil production structures and founded in clays located in or along the U.S. coastline of the Gulf of Mexico. This method has also been used in other marine installations with some success (e.g., North Sea oil production structures). In equation form the method is given as

$$f_s = \lambda(\bar{q} + 2s_u) \qquad \text{(units of } s_u\text{)} \tag{16-13}$$

where s_u = undrained shear strength of soil previously defined (kPa, ksf)

$\bar{q} = \gamma_s z_i$ effective overburden pressure to the average depth of pile segment or $\frac{1}{2}$ full depth. For tapered piles you may have to use element lengths ΔL and do a summation, $\sum$.

λ = coefficient, which can be obtained from Fig. 16-15, is pile length-dependent, and *applies over the total pile embedment depth*

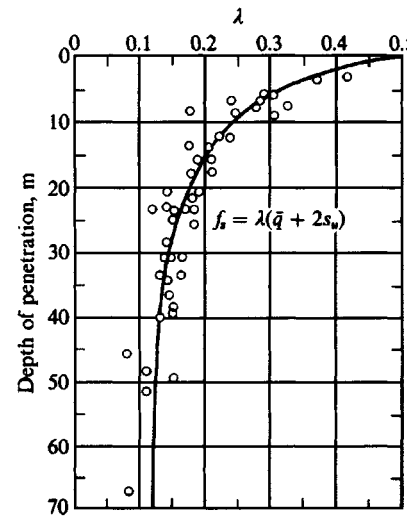

Figure 16-15 The dependence of λ coefficients on pile penetration. Data replotted and depths converted to meters by author from Vijayvergiya and Focht (1972).

The λ coefficient was obtained from a graphical regression (best-fit) analysis of a plot with a large number of pile-load tests. If we compare Eq. (16-13) to Eq. (16-11) it is evident the λ term includes both the α and the $K \tan \delta$ effects.

Kraft et al. (1981*a*) studied this method in some detail and made the following observations:

1. The method overpredicts the capacity for piles when their length L is less than about 15 m in both normally and overconsolidated clay. For piles in this length range it appears that $0.2 \leq \lambda \leq 0.4$.
2. The minimum value of $\lambda \geq 0.14$.
3. The reduction in λ appears attributable to the installation process, which produces more soil damage in the upper regions since more pile shaft passes a given depth and there is more likelihood of lateral movement or whip causing permanent pile-soil separation.

Where long piles penetrate into soft clay the λ values reflect both averaging for a single value and development of a somewhat limiting skin resistance so that $\bar{q}$ does not increase pile capacity without bound.

This method has one very serious deficiency—it assumes a single value of λ for the pile. A more correct procedure is to use Eq. (16-10) with several elements.

16-9.3 The β-Method

This method, suggested by Burland (1973), makes the following assumptions:

1. Soil remolding adjacent to the pile during driving reduces the effective stress cohesion intercept on a Mohr's circle to zero.
2. The effective stress acting on the pile surface after dissipation of excess pore pressures generated by volume displacement is at least equal to the horizontal effective stress (K_o) prior to pile installation.

3. The major shear distortion during pile loading is confined to a relatively thin zone around the pile shaft, and drainage of this thin zone either occurs rapidly during loading or has already occurred in the delay between driving and loading.

With these assumptions Burland (1973) developed a simple design equation [also the second term of Eq. (16-11)] written as

$$f_s = K\bar{q}\tan\delta \tag{16-14a}$$

Taking $\beta = K\tan\delta$, we can rewrite the equation for skin resistance as

$$f_s = \beta\bar{q} \tag{16-14b}$$

Since $\bar{q}$ = *effective* overburden pressures at z_i, we can modify Eqs. (16-14*b*) for a surcharge q_s to read

$$f_s = \beta(\bar{q} + q_s) \tag{16-14c}$$

As previously used, $\bar{q}$ = average (midheight) effective vertical stress for the ith element of length ΔL. The friction angle δ must be obtained from Table 11-6 or estimated by some other means. Since a ϕ angle (and $\delta = 0$ when $\phi = 0$) is needed, the author recommends this method *only for cohesionless soils*.

The lateral earth-pressure coefficient K may be designer-selected; however, K_o as defined for use in Eq. (16-11) is commonly used.

A particularly attractive feature of the β method is that if we use $K_o = 1 - \sin\phi$ and $\delta = \phi'$, the range of β is from about 0.27 to 0.30 in the practical range of ϕ' (range of 25° to 45°). That is, almost any reasonable estimate for ϕ' gives the same computed skin resistance; however, it still remains to be seen from a load test whether it is correct.

Figure 16-16 is a data plot from Flaate and Selnes (1977) that was obtained from back-computing a number of reported load tests using this method. Although there is substantial

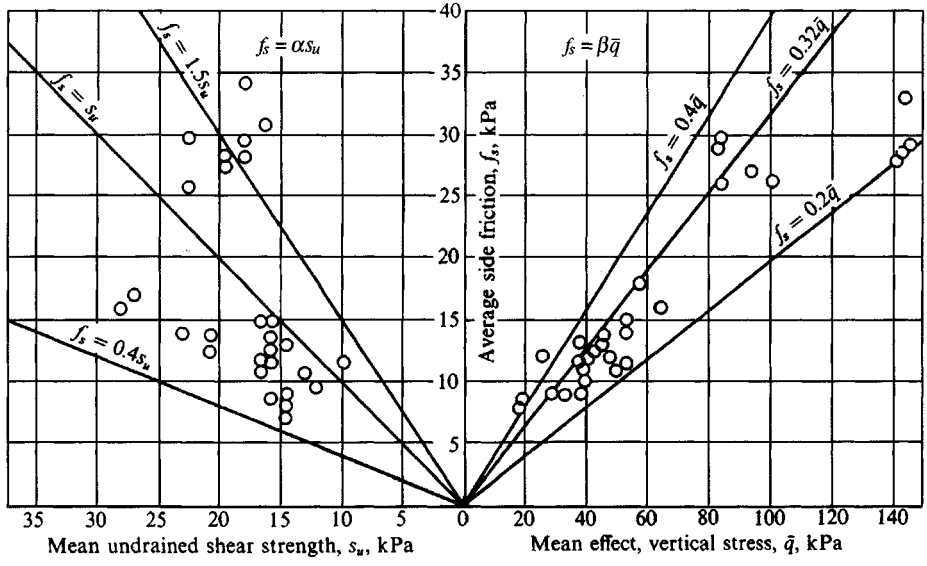

Figure 16-16 Plotting of average skin resistance f_s versus αs_u and $\beta\bar{q}$ to illustrate scatter. The $\beta\bar{q}$ plot seems to have somewhat less scatter than using α. [*After Flaate and Selnes (1977).*]

scatter it does not seem so great as in using other methods, including both the α and λ method, according to Esrig and Kirby (1979).

Most authorities agree that f_s in Eq. (16-11) does not increase indefinitely with depth but rather, beyond some critical L/B ratio, increases at an ever-decreasing rate. Bhushan (1982) suggests for large-displacement piles (closed-end pipe, solid concrete, possibly open-end pipe with a plug) that K and β can be estimated as follows:

$$\beta = K \tan \delta = 0.18 + 0.0065 D_r$$

and

$$K = 0.50 + 0.008 D_r$$

where D_r is the relative density (as a *percent*) previously defined in Chap. 2. We might use SPT correlations (see Table 3-4) to obtain D_r at increasing depths.

Zeitlen and Paikowsky (1982) suggest that the *limiting* f_s is automatically accounted for by the decrease in ϕ' with effective normal confining pressure. To obtain ϕ' at some depth of interest when a reference value of ϕ_o is available as from a triaxial test using an effective normal pressure of $\bar{q}_o$ (and refer to Fig. 2-31) the following equation is suggested

$$\phi' = \phi_o - 5.5 \log \frac{\eta \bar{q}}{q_o} \tag{16-15}$$

where ϕ' = angle of internal friction for design and is computed from the actual effective normal pressure $\eta \bar{q}$ existing at the depth of interest (along pile shaft or point). Use this angle in Eq. (16-6) and Eq. (16-6*a*).

ϕ_o = reference angle of internal friction measured at some effective normal pressure q_o in a laboratory test.

We must also make a decision on what to use for $\tan \delta$. Some persons suggest a maximum for δ on the order of 0.5 to $0.75\phi'$, whereas others routinely use the effective value ϕ'. It has already been pointed out that δ is dependent on the normal pressure at the interface of soil and pile.

Finally, there is a question of what to use for the lateral earth-pressure coefficient K that will give a consistent pile capacity estimation for design within, say, a $\pm$ 20 percent error. Several choices for K, given in the text, have been suggested by different authorities; however, although they tend to provide reasonable (after the fact) computations for their authors, for others they have the nasty habit of giving unpredictable results.

It appears that K values are very likely to be both site- and pile-type-specific. Table 16-3 tabulates a number of values of K found from several pile test programs. From this table one can readily see that there is not very good agreement on what to use for K.

It appears that the pile weight was not included in at least some of the pullout tests; and little to no consideration was given to stratification, to changes in the soil parameters with depth, or to effective normal confining pressure. Note, too, that a significant variation in K can be created by the assumption of how much of the load is carried by the point.

The major error in the foregoing back-computations for K was in obtaining a single value for the full pile depth rather than dividing the pile shaft into lengths of ΔL and using Eq. (16-5*a*) for compression and Eq. (16-5*b*) for tension tests.

TABLE 16-3
Summary of a number of pile tests for estimating the lateral earth-pressure coefficient *K*

	Pile type					
Source	H piles	Pipe	Precast concrete	Timber	Tapered	Tension tests
Mansur and Hunter (1970)	1.4–1.9	1.2–1.3	1.45–1.6	1.25		0.4–0.9 All types
Tavenas (1971)	0.5		0.7		1.25*	
Ireland (1957)						1.11–3.64†
API (1984)		1.0 or 0.8‡	1.0			

*Tapered timber

†Step-tapered tension; 3.64 not accepted (test was made in saturated soil and value may have resulted from water suction in point region).

‡Unplugged pipe; 1.0 for plugged or capped displacement

Residual driving stresses may be a significant factor; however, the mechanics are not fully understood nor are there any rational means to quantify them. Although there are claims that large values have been measured in some cases, it does not seem possible with modern driving equipment producing rapid hammer blows that large values could exist. In cohesionless soils the rapid driving impulses and resulting vibrations would create a viscous fluid in a zone several millimeters from the pile; a somewhat similar situation would develop in cohesive soils. Apparently, driving the pile point into rock would be more likely to create residual stresses since the point resistance would be so large that there could be significant axial compression from the hammer impact. Some of this compression might become locked in by lateral soil squeeze and produce compression stresses, which would add to those from the applied butt load. However, since these stresses are continuous acting there would be sufficient soil (and pile) creep to cause them to dissipate over a relatively short time.

In sand, on the other hand, other factors may cause an apparent negative skin resistance (or apparent increase in compressive load). These include driving other piles in the vicinity, heavy construction equipment in the area causing vibration-induced settlement, and the like.

One of the more serious errors in static pile capacity analyses has been the use of a single correlation factor or parameter for the full embedment depth. A trend is developing, however, to subdivide the estimated pile depth into a number of elements or segments, analyze these, and use their sum as in Eq. (16-10). This trend is accelerating because of computer programs such as PILCAPAC, so that computations considering the several strata in embedment length L are little more difficult than using a single skin resistance parameter.

Consideration of soil property variation in length L can make a substantial difference, particularly for long piles in clay where a pile of, say, $L/D = 30$ may fall entirely within an overconsolidated region, whereas with $L/D = 50$ perhaps one-third of the depth is in normally or underconsolidated clay. Similarly for sand, the upper depth may be recent and the lower one-third to one-half may be overconsolidated and/or cemented material. Making a static capacity prediction that compares favorably with a later load test is more a coincidence than the result of using a "good" equation in these circumstances. This observation is also

the most likely explanation of why the computed agreement with load tests on short piles is better than on long piles.

It is usually easier to back-compute a load test with considerable confidence of what the parameter(s) should be than to make a capacity forecast with little more than SPT numbers and possibly unconfined compression strength data from disturbed samples recovered in the SPT sampling procedure.

16-9.4 Other Methods to Compute/Estimate Skin Resistance

There are a number of other computational procedures for obtaining f_s for the skin resistance contribution of Eq. (16-5). Vesić (1970) used relative density D_r as follows:

$$f_s = \chi_v(10)^{1.54D_r^4} \qquad \text{(kPa)} \tag{16-16}$$

where χ_v = 8 for large-volume displacement piles
= 2.5 for bored, open-end pipe and for **HP** piles

According to Vesić (1975*a*) Eq. (16-16) may be a lower limit, and most load tests tend to produce average values at least 50 percent greater.

For SPT data, Meyerhof (1956, 1976) suggested obtaining f_s as

$$f_s = \chi_m N_{55} \qquad \text{(kPa)} \tag{16-17}$$

where χ_m = 2.0 for piles with large-volume displacement
= 1.0 for small-volume piles
N_{55} = statistical average of the blow count in the stratum (and with any corrections from Chap. 3)

Shioi and Fukui (1982) suggest the following:

For driven piles: $f_s = 2N_{s,55}$ for sand; $= 10N_{c,55}$ for clay (kPa)
For bored piles: $f_s = 1N_{s,55}$ for sand; $= 5N_{c,55}$ for clay (kPa)

where $N_{i,55}$ = average blow count in the material indicated for the pile or pile segment length

For cone penetration data, Meyerhof (1956) and Thorburn and MacVicar (1971) suggest

$$f_s = 0.005q_c \qquad \text{(kPa)} \tag{16-18}$$

where q_c = cone penetration resistance, kPa.

When a cone penetrometer is used and side friction q_s is measured, use

$f_s = q_s$ (small-volume displacement piles)
$f_s = (1.5 \text{ to } 2.0)q_s$ (large-volume piles)

16-9.5 Step-Taper and Tapered Piles

Most published pile tests have been made on straight shafts. Only a limited amount of data exists on tapered or step-taper piles in a form where one can reanalyze (easily or even

approximately) the work. The major sources seem to be D'Appolonia and Hriber (1963), Tavenas (1971), and a number of issues of *Foundation Facts*.[2] Generally, one may make the analysis on the basis of Fig. 16-17. Use the average pile shaft diameter in the length ΔL. This increment of shaft length may be either the stratum thickness or the total or partial pile segment. The additional bearing capacity (which may not be an "ultimate" value) from the bearing ledges or changes in diameter of the step-taper can be summed with the point resistance to obtain the total bearing contribution.

From Fig. 16-17 the skin resistance contribution [see Nordlund (1963)] is

$$P_s = \sum_1^n A_s K \bar{q} \frac{\sin(\omega + \delta)}{\cos\omega \cos\delta} \qquad \text{(units of } A_s\bar{q}\text{)} \tag{16-19}$$

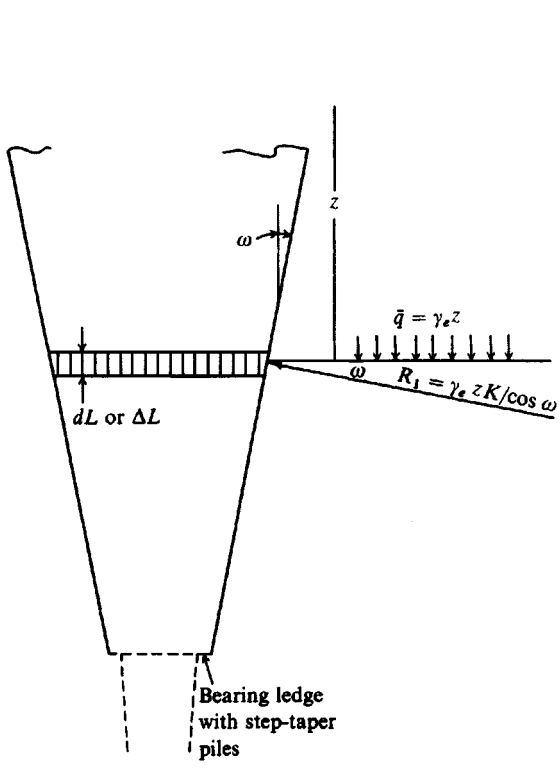

(*a*) Pile.

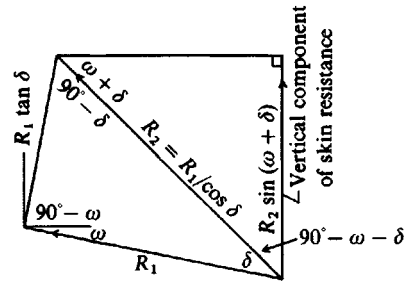

(*b*) Force polygon.

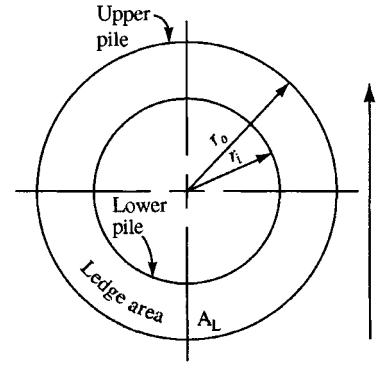

(c) Ledge bearing capacity

Figure 16-17 Geometry to obtain vertical component of skin resistance for tapered piles and for the bearing capacity when there are abrupt changes in shaft diameter producing resisting ledges.

[2]Published on occasion by Raymond International, Inc., P.O. Box 22718, Houston, TX 77026.

where K = earth-pressure coefficient. Tests reported and data analyzed by the author indicate $K = 1.7$ to $2.2K_o$ for tapered and step-tapered piles. Meyerhof (1976) suggests $K \geq 1.5$ and Blanchet et al. (1980) suggest $K = 2K_o$.

ω = angle of taper of pile shaft

Other terms have been previously defined.

For all practical purposes the trigonometric ratio in Eq. (16-19) is $\tan \phi'$ unless the taper is very large. This substitution produces Eq. (16-14*a*) except that load tests tend to indicate larger K values for tapered piles. The user must make some estimate for the limiting skin resistance in Eq. (16-19) since it is not unlimited with $\overline{q}$ regardless of taper.

16-9.6 Bearing Capacity of Pile/Pier Ledges

The step-taper pile has a ledge that contributes to the pile capacity. Few other pile types have this "ledge," but it is common with drilled piers (see Chap. 19) to drill the upper part at a larger diameter than the lower to produce a bearing ledge. There can be more than one ledge in a pile or pier. We may make an analysis as follows for the ledge contribution:

1. Referring to Fig. 16-17*c*, determine the bearing capacity q_L of a round footing of diameter $D_o = 2r_o$ using the Hansen bearing-capacity equation for pile points. Use $\overline{q}$ from ground surface to ledge and the soil properties ϕ, c below the ledge.
2. Compute the area of the ledge using r_o and r_i as

$$A_L = \pi(r_o^2 - r_i^2)$$

3. Compute the ledge resistance as

$$P_L = A_L q_L$$

which is summed with the other resistances P_i to obtain the total pile capacity.

16-10 PILE SETTLEMENTS

Pile settlements can be estimated as follows:

1. Compute the average pile axial force in each segment of length ΔL, average cross-section area A_{av}, and shaft modulus of elasticity E_p from the pile butt to point. That is,

$$\Delta H_{s,s} = \frac{P_{av} \Delta L}{A_{av} E_p}$$

and sum the several values to obtain the axial total compression

$$\Delta H_a = \sum \Delta H_{s,s}$$

2. Compute the point settlement using Eq. (5-16*a*) given below

$$\Delta H_{pt} = \Delta q D \frac{1 - \mu^2}{E_s} m I_s I_F F_1 \qquad (5\text{-}16a)$$

where $mI_s = 1.0$ (shape factor)

I_F = Fox embedment factor, with values as follows:

$$I_F = 0.55 \text{ if } L/D \leq 5$$
$$= 0.50 \text{ if } L/D > 5$$

D = diameter of pile point (or the bell diameter for belled piers), or the least lateral dimension for rectangular or **HP** sections

μ = Poisson's ratio (suggest using $\mu = 0.35$)

Δq = bearing pressure at point = input load/A_p. This is the pile load, not the point load

E_s = stress-strain modulus of soil below the pile point (may be obtained from Table 5-6 with the following as typical):

SPT: $E_s = 500(N + 15)$

CPT: $E_s = 3$ to $6q_c$ (use larger values 5, 6 if OCR > 1)

s_u: $E_s = 100$ to $500s_u$ ($I_p > 30$)

$= 500$ to $1500s_u$ ($I_p < 30$ or is stiff)

For OCR > 1: $E_{s,\text{OCR}} \approx E_s \sqrt{\text{OCR}}$

F_1 = reduction factor used as follows:

0.25 if the axial skin resistance reduces the point load $P_p \leq 0$

0.50 if the point load $P_p > 0$

0.75 if point bearing (there is always some skin resistance)

The factor F_1 is used to account for the tip zone moving down as a result of both actual point load (which is seldom known) and the point settlement from skin resistance along the shaft "pushing" the system down in some zone radiating from the shaft as indicated in Fig. 16-11*a*. This method uses the *total axial load*, which is known, and factor F_1, which is an estimate. You may have to use a local value or modify the F_1 suggested here for different stratification.

3. Sum the axial and point settlements to obtain the total as

$$\Delta H_p = \Delta H_a + \Delta H_{\text{pt}}$$

Note again the point settlement includes a side resistance contribution through the use of the F_1 factor.

How accurate is this settlement computation? Like most pile analyses, if it gives exactly the measured settlement it is more likely a happy coincidence from the equation and the user's choice of input. This method is incorporated into program PILCAPAC and has given quite good results compared with measured values. In any case it is better than just making a guess.

A more computationally rigorous solution is suggested by Randolph and Wroth (1979) and somewhat verified and extended by Lee (1993). The equation[3] for the settlement of a single pile ΔH_p with an embedment depth L_p is as follows:

$$\Delta H_p = \frac{G'_L r_o}{P}\left(\frac{1 + \dfrac{4}{\eta(1-\mu)}\dfrac{1}{\pi\lambda}\dfrac{L_p}{r_o} - \dfrac{\tanh \nu L_p}{\nu L_p}}{\dfrac{4}{\eta(1-\mu)} + \dfrac{2\pi\rho}{\zeta}\dfrac{L_p}{r_o}\dfrac{\tanh \nu L_p}{\nu L_p}}\right) \tag{16-20}$$

where, in consistent force and length units,

E_p = modulus of elasticity of pile material

G'_L = shear modulus at pile point; compute from E_s (see step 2 given earlier) using Eq. (*a*) of Sec. 2-14

$G'_{L/2}$ = shear modulus at pile embedment depth $L_p/2$

L_p = pile embedment length; $L_p/2$ = one-half embedment depth

r_o = effective pile radius in units of L_p. Use actual pile radius for round piles; for square or projected area of **HP** piles use $r_o = \sqrt{A_p/\pi}$.

$r_m = k\rho L_p(1-\mu)$, where
$k = 2.5$ for friction piles in soil where stratum thickness $H \geq 3L_p$; $= 2.0$ for $H < 3L_p$

$r_m = L_p(\frac{1}{4} + [2\rho(1-\mu) - \frac{1}{4}]\zeta)$ for *end-bearing* piles (and in this case use $\eta = 1$)

P = pile load (allowable, design, ultimate, etc.)

$\lambda = E_p/G'_L$

$$\nu L_p = \frac{L_p}{r_o}\sqrt{\frac{2}{\zeta\lambda}}$$

$$\rho = \frac{G'_{L/2}}{G'_L}$$

$\zeta = \ln(r_m/r_o)$

$\eta = r_o/r_{\text{base}} = 1$ unless $r_{\text{base}} > r_o$

16-11 STATIC PILE CAPACITY: EXAMPLES

The following examples will illustrate some of the methods given in the preceding sections.

Example 16-2. An **HP**360 × 132 (14 × 89) pile penetrates through 9 m of soft clay and soft silty clay into 1 m of a very dense, gravelly sand for a total pile length $L = 10$ m. The GWT is at 1.5 m below the ground surface. The pile was driven essentially to refusal in the dense sand. The SPT blow count prior to driving ranged from 3 to 10 in the soft upper materials and from 40 to 60 in the dense

[3]The equation has not been derived by the author, but the two references cited used the same general form, so it is assumed to be correct.

sand. On this basis it is decided to assume the pile is *point bearing* and receives no skin resistance contribution from the soft clay. We know there will be a considerable skin resistance contribution, but this design method is common. We will make a design using Meyerhof's Eq. (16-8) and using Eq. (16-6) with Vesić's N-factors but neglecting the N_γ term.

Solution.

By Meyerhof's method. Assuming the blow counts given are N_{70}, we need the N_{55} value. If we use an average blow count $N_{70} = 50$,

$$N_{55} = N_{70}(70/55) = 50(70/55) = \mathbf{64}$$

For an **HP**360 × 132 we obtain $b_f = 373 \times d = 351$ mm (using Appendix Table A-1). The projected point area $A_p = b_f \times d = 0.373 \times 0.351 = \mathbf{0.131}$ m^2.

The L_b/B ratio in the sand is

$$L_b/B = 1.000/0.351 = 2.85 \qquad \text{(use smallest dimension for } B\text{)}$$

Using Meyerhof's Eq. (16-8), we calculate

$$P_{pu} = A_p(40N_{55})L_b/B = 0.131 \times 40 \times 64 \times 2.85 = 956 \text{ kN}$$

Checking the limiting $P_{pu,m}$, we obtain

$$P_{pu,m} = A_p(380N_{55}) = 0.131 \times 380 \times 64 = 3186 \text{ kN} \gg 956$$

Tentatively use Meyerhof's $P_{pu} = \mathbf{956}$ kN.

By Eq. (16-6). Assume $\phi = 40°$ (from Table 3-4—range of 30 to 50°) and also the following:

$$\gamma_s = 16.5 \text{ kN/m}^3 \text{ for 9 m} \qquad \gamma' = 16.5 - 9.807 = 6.7$$
$$= 18.5 \text{ kN/m}^3 \text{ for 1 m} \qquad \gamma' = 18.5 - 9.807 = 8.7$$
$$\bar{q} = 16.5 \times 1.5 + 6.7(9.0 - 1.5) + 8.7 \times 1.0 = \mathbf{83.7} \text{ kPa}$$
$$\eta = \frac{1 + 2(1 - \sin 40°)}{3} = \mathbf{0.571}$$
$$\eta\bar{q} = 0.571 \times 83.7 = 47.8 \text{ kPa} \qquad \text{(for estimating } I_{rr}\text{)}$$

Note that I_{rr} is based on both D_r and the mean normal stress $\eta\bar{q}$, so we now assume $I_r = I_{rr} = 75$.

Using program FFACTOR (option 10) with $\phi = 40°$ and $I_{rr} = 75$, we obtain

$$N'_q = 115.8$$

For d_q obtain the 2 tan . . . term = 0.214 from Table 4-4 and compute

$$d_q = 1 + 0.214 \tan^{-1}(L/B) = 1 + 0.214 \tan^{-1}(10/0.351)$$
$$= 1.33$$

Substituting values, we see that

$$P_{pu} = A_p\eta\bar{q}N'_q d_q = 0.131 \times 0.571 \times 83.7 \times 115.8 \times 1.33 = \mathbf{964} \text{ kN}$$

We would, in this case, use $P_{pu} \approx \mathbf{950}$ kN.

////

Example 16-3. Estimate the ultimate pile capacity of a 300-mm round concrete pile that is 30 m long with 24 m driven into a soft clay soil of average $q_u = 24$ kPa. Assume $\gamma' = 8.15$ kN/m^3 for the soil. The water surface is 2 m above the ground line.

Solution. We will use both the α and λ methods. With the α method we will use a single value and then divide the pile into four 6-m lengths and use Eq. (16-12*a*) to compute the several α's.

Step 1. Find pile area and perimeter:

$$A_p = 0.7854(0.30)^2 = \mathbf{0.071}\ \text{m}^2$$

$$\text{Perimeter } p = \pi D = \pi \times 0.30 = 0.942\ \text{m}$$

Step 2. For any of the methods the point capacity $P_{pu} = 9 s_u A_p$ and $s_u = q_u/2 = 24/2 = 12\ \text{kPa} \rightarrow$ $P_{pu} = 9 \times 12 \times 0.071 = \mathbf{7.7}\ \text{kN}$.

Step 3. Using a single α and from Fig. 16-14 we obtain $\alpha = 1.05$ (Bowles' curve) and

$$\begin{aligned} P_u &= P_{pu} + \alpha s_u A_s \\ &= 7.7 + 1.05 \times 12 \times 0.942 \times 24 = 7.7 + 284.9 = \mathbf{292.6}\ \text{kN} \end{aligned}$$

Step 4. Using the λ method and a copier enlargement of Fig. 16-15, we obtain, at $D =$ 24 m, $\lambda \approx 0.16$. Also we must compute the average vertical stress in the 24-m depth:

$$\bar{q} = \gamma' L_p/2 = 8.15 \times 24/2 = 97.8\ \text{kPa}$$

Substituting into Eq. (16-13) with $A_s = 0.942 \times 24 = 22.6\ \text{m}^2$ gives

$$\begin{aligned} P_p &= P_{pu} + \lambda(\bar{q} + 2s_u)A_s \\ &= 7.7 + 0.16(97.8 + 2 \times 12)22.6 = 7.7 + 440.4 = \mathbf{448.1}\ \text{kN} \end{aligned}$$

Step 5. Using Eq. (16-12*a*) for α with four segments, we make the following computations:

$$\bar{q}_v = 8.15 \times 3 = \mathbf{24.5}\ \text{kPa}$$

Then with $s_u = 12$, we compute

$$\begin{aligned} \alpha &= 0.5(24.5/12)^{0.45} = \mathbf{0.69} \qquad (C_1 = 0.5) \\ A_s &= p\Delta L = 0.942 \times 6 = 5.65\ \text{m}^2 \\ f_s &= \alpha s_u = 0.69 \times 12 = 8.28 \\ f_s A_s &= 8.28 \times 5.65 = \mathbf{46.8}\ \text{kN} \end{aligned}$$

With the computation methodology established, set up the following table (not including top 2 m and using ground surface as the reference):

Element #	Depth, m	$\bar{q}_v$, kPa	α	$f_s = \alpha s_u$, kPa	$f_s A_s$, kN
1	3	24.5	0.69	8.28	46.8
2	9	73.4	1.13	13.56	76.6
3	15	122.2	1.42	17.04	96.3
4	21	171.2	1.65	19.8	111.9
				Total friction	= 331.6 kN
				+ point P_{pu}	= 7.7
				Total pile capacity P_u	= 339.3 kN

Summarizing, we write

	P_u, kN
Single α	292.6
Multiple α	339.3
The λ method	448.1

What would be a reasonable value of P_p to recommend for this pile capacity? A value of about **350** kN could be justified. The single α is too low (but conservative); the λ does not consider any depth variation.

Since the pile is concrete, its weight is (γ_c = 23.6 kN/m^3) = 0.071 × 23.6 × 30 = 50 kN, and the actual reported value should be

$$P_{p,\text{rep}} = P_p - W = 350 - 50 = \mathbf{300}\ \text{kN}$$

////

Example 16-4. Estimate the pile length required to carry the 670 kN axial load for the pile-soil system shown in Fig. E16-4. The 460-mm pipe is to be filled with concrete after driving.

Solution. We will make length estimates based on both the α and λ methods and use an average of the two unless there is a large difference.

By the α method. Use two depth increments since we have a soil variation that is clearly identified. If there were more data it would be prudent to use additional depth increments. From Fig. 16-14 we obtain

$$\alpha = 0.98 \text{ for first 6 m}$$
$$\alpha = 0.88 \text{ for remainder (stiffer soil)}$$

Use point N_c = 9.0. We then compute the following:

$$\text{Point area } A_p = 0.7854D^2 = 0.7854 \times 0.460^2 = 0.166\ \text{m}^2$$
$$\text{Pile perimeter } p = \pi D = \pi \times 0.460 = 1.45\ \text{m}$$

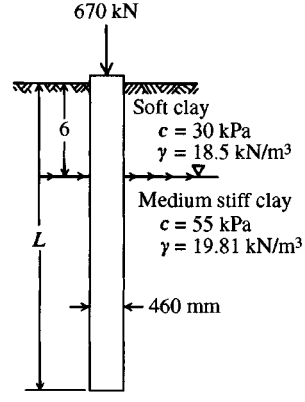

Figure E16-4

Skin resistance is usually neglected in the top 0.6 to 1 m of depth because of excessive soil damage from driving; we will not do this here since the upper soil is very soft and likely to flow back against the pile perimeter.

We can write the pile capacity as

$$P_u = P_1 + P_2 + P_p \qquad P_p = cN_cA_p \qquad dP = p(\alpha c)dL$$

giving

$$P_u = \int_0^6 p(\alpha_1 c_1)dL + \int_0^{L_1} p(\alpha_2 c_2)dL + c_2 9A_p \qquad \text{(note integration over 0 to } L_1 \text{ not 6 to } L_1\text{)}$$

Substituting, we find that

$$P_u = \int_0^6 (0.98 \times 30 \times 1.45)dL + \int_0^{L_1} (0.88 \times 55 \times 1.45)dL + 55 \times 9 \times 0.166$$

Clearing, we obtain

$$P_u = 29.4 \times 1.45 \times 6.0 + 48.4 \times 1.45L_1 + 82.0$$
$$P_u = 256 + 70.2L_1 + 82 = 70.2L_1 + 338$$

Using an SF = 3 and equating, we have

$$P_u \geq 3P_a$$

and replacing the $\geq$ with an equal sign, we have $P_u = 3 \times 670 = 2010$ kN, or

$$70.2L_1 + 338 = 2010$$

Solving for L_1, we find

$$L_1 = 1672/70.2 = 23.8 \text{ m} \qquad \text{(say, 24 m)}$$
$$\text{Total } L_t = 6.0 + L_1 = 6 + 24 = \mathbf{30} \text{ m}$$

By the λ Method. Find the equivalent s_u for the full stratum. Based on side computations, which indicate the required total depth may be around 32 m, we see that

$$s_{u,\text{av}} = \frac{6 \times 30 + 26 \times 55}{32} = 50 \text{ kPa} \qquad \text{(rounded)}$$

We also need an average effective unit weight for this soil depth in order to compute $\overline{q}$ to mid-depth of the pile:

$$\gamma'_{\text{av}} = \frac{6 \times 18.5 + 26(19.81 - 9.81)}{32} = 12.0 \text{ kN/m}^3 \qquad \text{(rounded)}$$

For an assumed $L = 32$ m, we obtain (using an enlargement of Fig. 16-15) $\lambda = 0.14$. The point capacity is the same as for the α method of $P_{\text{pu}} = 82$ kN. Thus,

$$P_s = A_s\lambda(\overline{q} + 2s_u) \qquad A_s = p \times L = 1.45L$$

Substituting values, we obtain a quadratic equation in L as

$$1.45L(0.14)[12 \times L/2 + 2 \times 50] + 82 = 3 \times 670$$
$$1.22L^2 + 20.3L = 1928$$

Solving for L, we obtain $L = 32.3$ m (use **32** m).

Summary.

By α method	$L = 30$ m	
By λ method	$L = 32$ m	
Use	$\boldsymbol{L = 32}$ m	(if the pile can be driven that deep)

////

Example 16-5. Find the required length of **HP**360 × 174 friction pile to carry an axial load of 675 kN using an SF = 2. The accompanying table is an abbreviated soil profile for use:

Depth, m	q_u, kPa	w_L, %	w_p, %	γ, kN/m^3	Computed I_p	
0–3	48	36	22	17.5	14	Water table
3–6	54	37	23	17.9	14	at 3 m
6–9	56	36	21	18.4	15	
9–12	59	38	24	18.6	14	
12–15	63	41	26	18.8	15	
15–18	66	38	25	18.6	13	
18–21	63	36	25	19.1	11	
21–24	60	42	28	19.2	14	
24–27	54	35	26	19.3	9	
27–30	48	37	25	19.5	12	
30–33	37	38	24	19.7	14	
	$\sum = 608$			$\sum = 206.6$	$\sum = 145$	

Solution. We will find the length using the α and β methods and then make a decision on what to use for the pile length L. Note the given conditions state a *friction pile,* so there is no point capacity to compute.

By the α method. First, let us average the q_u values to obtain

$$q_u = \frac{\sum q_u}{n} = 608/11 = 55.3 \qquad s_u = q_u/2 = 55.3/2 = \mathbf{28}\text{ kPa}$$

For $s_u = 28$ kPa use $\alpha = 0.98$ (Fig. 16-14)

The pile dimensions are $b = 378$ mm and $d = 361$ mm (Table A-1 in Appendix). Thus, the perimeter (assuming full plug) is

$$p = 2d + 2b = 2(0.361 + 0.378) = \mathbf{1.48}\text{ m (rounded)}$$

We will neglect the pile weight since we are also neglecting any point capacity. So with an SF = 2,

$$pL\alpha s_u = 2 \times 675 \qquad \text{and} \qquad L = \frac{1350}{1.48 \times 0.98 \times 28} = \mathbf{33.2}\text{ m}$$

By the β method. We must somehow estimate an effective angle of friction ϕ'. We can do this by using an average of the plasticity indexes to obtain

$$I_{P,\text{av}} = \sum \frac{I_{P,i}}{n} = 145/11 = 13.2$$

From Fig. 2-35 at $I_P = 13$ we obtain $\phi' = 32°$ ("undisturbed" clays). The pile friction is made up of two parts:

Soil-to-pile $\rightarrow \delta = 25°$ (see Table 11-6)—the two flanges
Soil-to-soil $\rightarrow \delta = 30°$ (not 32° as web soil may be somewhat disturbed)

We need an average soil unit weight, so with the GWT at −3 m depth we will average all the values as being sufficiently precise.

$$\gamma_{av} = (17.5 + 17.9 + \cdots + 19.7)/11 = 206.6/11 = 18.8 \text{ kN/m}^3$$

The effective unit weight $\gamma'_e = 18.8 - 9.8 = \mathbf{9.0}$ kN/m^3.

We will next compute the lateral pressure coefficient K:

$$K_a = 0.307 \qquad K_p = 3.255 \text{ (Rankine values from Tables 11-3, 11-4)}$$
$$K_o = 1 - \sin\phi = 1 - \sin 32° = 0.470$$

We will weight K_o using $F_w = 2$, giving

$$K = \frac{0.307 + 2 \times 0.470 + 3.255}{2 + 2} = 4.502/4 = \mathbf{1.13}$$

Now equating total skin resistance $P_{su} \geq$ SF × given load, obtain

$$P_{su} = p_1 L\bar{q}K \tan\delta_1 + p_2 L\bar{q}K \tan\delta_2 \geq 2 \times 675 = 1350 \text{ kN}$$

Now substituting (with $p_1 = 2b = 2 \times 0.378 = 0.756$ m; $p_2 = 2 \times 0.361 = 0.722$ m; $\bar{q} = qL/2$), we find

$$0.756L \times 9 \times \frac{L}{2} \times 1.13 \tan 25° + 0.722L \times 9 \times \frac{L}{2} \times 1.13 \tan 30° = 1350$$

Simplifying, we obtain

$$1.79L^2 + 2.12L^2 = 1350 \rightarrow 3.91L^2 = 1350$$
$$L = \sqrt{\frac{1350}{3.91}} = \mathbf{18.6} \text{ m}$$

Summary.

By the α method:	$L = \mathbf{33.2}$ m
By the β method:	$L = \mathbf{18.6}$ m

Which L do we use? There is too much difference to use an average of 25.9 m. It would be prudent here to use $L \geq 30$ m, particularly because too many "estimates" were used in the β method.

////

Example 16-6. We are given the following data for a step-taper pile (from *Foundation Facts,* vol. 1, no. 2, fall 1965, p. 17, and slightly edited). The pile capacity was estimated to be 227 kips. There was no water, and only SPT data were furnished. *Note:* This problem is worked in Fps units since those were the units of the original data.

Required. Estimate the pile capacity using Eq. (16-19) and include the ledge contributions based on bearing capacity.

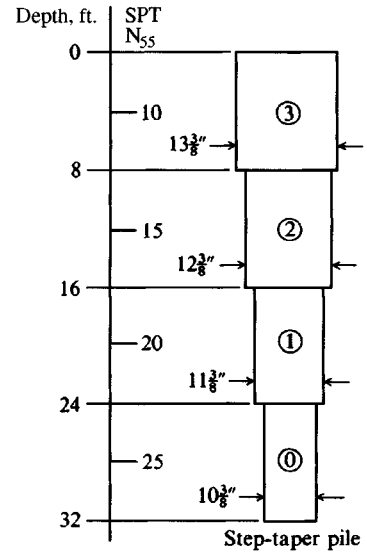

Figure E16-6

Solution. It is necessary to obtain the shaft diameters from Raymond International pile literature as shown on Fig. E16-6. From Table 3-4 estimate the ϕ angles given in the computation table following, which are based on the SPTs being N_{55} values.

We will have to compute the following:

$$A_L = 0.7854(r_o^2 - r_i^2),\ \text{ft}^2 \qquad \text{(ledge areas)}$$
$$A_s = \eta D L_s,\ \text{ft}^2 \qquad \text{(shaft area)}$$
$$K_o = 1 - \sin\phi \qquad \beta = 2K_o \tan\phi$$
$$P_u = \sum P_{\text{ledg}} + \sum P_{si} + P_{\text{pu}}$$

We will compute a "design" value for N_q that is an approximate average of the Terzaghi and Hansen values. We will use the following table and transfer the N_q values to Table E16-6. Refer to Table 4-5 for computing s_q, d_q.

$\phi°$	$N_{q,h}$	2 tan...	D/B	s_q	d_q	$N_{q,H}$	$N_{q,T}$	$N_{q,\text{des}}$
30	18.4	0.289	7	1.50	1.41	38.9	33.5	31*
32	23.2	0.276	16	1.53	1.42	50.4	29.0	40
34	29.4	0.262	25	1.56	1.40	64.2	36.5	50
34	29.4	0.262	37	1.56	1.40	64.2	36.5	50

*is close to ground surface (any value of 30 to 35 would be satisfactory)

A typical computation for the ledge resistance at the base of top section is

$$P = A_L \gamma L N_q = 0.14 \times 0.100 \times 8 \times 31 = \mathbf{3.5}\ \text{kips}$$

For side resistance we find that

$$P_s = A_s \bar{q} \beta = 28.01 \times 0.40 \times 0.58 = \mathbf{6.5}\ \text{kips}$$

TABLE E16-6

Section	$\phi°$	γ, kcf	$\bar{q}$, ksf	A_s	A_L	β	N_q	P_p, kips	P_s, kips
3	30	0.100	0.40	28.01	Top	0.58	31	—	6.5
2	32	0.105	1.22	25.92	0.140	0.59	40	3.5	18.3
1	34	0.110	2.08	23.82	0.130	0.59	50	8.5	29.2
0	34	0.110	2.96	21.73	0.119	0.59	50	15.0	37.9
Point			3.40		0.587			99.8	
								$\sum = \overline{126.8}$	$= \overline{92.3}$

Note that $\bar{q} = \gamma L/2 = 0.10 \times 8/2 = 0.40$. The next value is $\bar{q} = 0.10 \times 8 + 0.105 \times 4 = 1.22$ ksf, ..., etc. The N_γ term for the ledges and tip is ignored.

Both γ_s and ϕ have been estimated for this site. Experience will be a determining factor in what values probably should be used. From using Table 3-4 with the blow counts N as a guide, the values used are certainly not unreasonable—if anything, they are conservative. Why use an average of the Terzaghi and Hansen values for N_q? The reason is the Hansen values tend to be large when shape and depth factors are included but the Terzaghi values are too small since they have no means of adjustment. A logical progression is to compute the two and average them.

The sum of ledge, side, and point resistance is

$$27.0 + 99.8 + 92.3 = \mathbf{219.1} \text{ kips (vs. 227 measured)}$$

Questions.

1. Should SPT N have been corrected for overburden etc?
2. Is the range of 30 to 34° more realistic than perhaps 34 to 38°?
3. Is using $\beta = 2K_o \tan\phi$ preferable to using $\beta = 1.5$ to 2.0?

Clearly, the answer (now that the outcome is known) to these questions is no, yes, yes—but the designer seldom knows the outcome in advance.

////

Example 16-7. This example uses the computer program PILCAPAC that has been cited several times. From the output you can get an idea of how to write your own computer program (or obtain this one). To illustrate the versatility of the program and for your verification of methods given in this chapter to compute static pile capacity, we shall consider a load test from *ASCE Special Publication No. 23* [see Finno (1989)] on a 50-ft **HP** 14× 73 pile. The soil profile is shown in Fig. E16-7*a* together with selected other data. The soil properties were estimated from the given soil boring data and any supplemental data provided by Finno. The pile cross section and other data are in Appendix Table A-1 of this text. *Fps units are used in this example since the original source uses those units and it would be difficult to check results if the original parameters were converted to SI.*

Solution. A data file was created and named ASCEPL0, as shown on the output sheets (Fig. E16-7*b*). Most of the soil data are echoed in the table labeled "Soil Data for Each Layer." Although only layers 2 through 8 provide skin resistance, nine layers are shown. The ninth (bottom) layer is for computing point capacity. Both ϕ and δ are shown. The program checks whether this is an **H** pile and if so uses the given tan δ on the flanges and 1.2δ for the web, which is soil-to-soil.

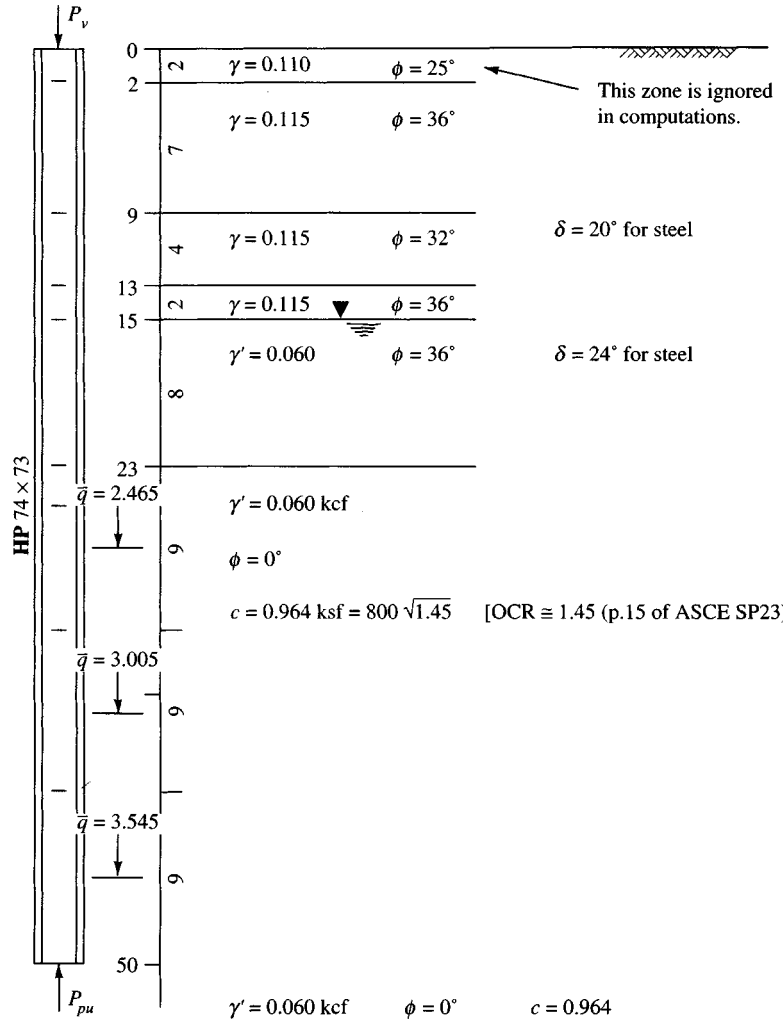

Figure E16-7a

The program computes K (K-FACT) on output sheets using

$$K = \frac{K_a + F_w K_o + K_p}{2 + F_w}$$

For the first value (the first layer is never used so, having the option of program computing or inputting a value) I input 0.9. The second layer has $\phi = 36°$, giving $K_a = 0.2596$; $K_p = 3.8518$; $K_o = 1 - \sin 36° = 0.4122$; and $K = (0.2596 + 0.4122 + 3.8581)/3 = \mathbf{1.5}$ (rounded). Other values are computed similarly.

The program has the option of using either (or both) the Hansen or Terzaghi point bearing-capacity method. The Hansen method was chosen as noted, and sufficient data were output for a hand check.

Next the program inquires whether to use the α or β method. The α method is selected as shown and the skin resistances for each element are computed and written for a hand check. Note the following when checking here:

```
+++++++++DATA FILE NAME FOR THIS EXECUTION:  ASCEPL0.DTA

 ASCE PILE TEST IN GT SP 23, H-PILE 14 X 73 FIG. 5, P11

NO OF SOIL LAYERS =     9          IMET (SI > 0) =  0

 PILE LENGTH FROM GROUND SURFACE TO POINT, PLEN =  50.000 FT
                                        PILE TYPE:  H-PILE

PILE DIMENSIONS B X H =  1.216  1.134 FT


       POINT X-AREA = 1.379     SQ FT

SOIL DATA FOR EACH LAYER:
LAY   EFF WT     PHI      DELTA     COHES                              THICK
NO    K/FT*3     deg        deg      KSF       ALPHA     K-FACT        FT
 1     .110     25.00         .0    1.000      .910       .900        2.00
 2     .115     36.00        24.0     .000      .000      1.500        7.00
 3     .115     32.00        20.0     .000      .000      1.300        4.00
 4     .115     36.00        24.0     .000      .000      1.500        2.00
 5     .060     36.00        24.0     .000      .000      1.500        8.00
 6     .060       .00          .0     .964      .910      1.000        9.00
 7     .060       .00          .0     .964     1.000      1.000        9.00
 8     .060       .00          .0     .964     1.080      1.000        9.00
 9     .060       .00          .0     .964     1.000      1.000       10.00

++++  HANSEN BEARING CAPACITY METHOD USED--IBRG = 1

          PILE POINT IS SQUARE W/AREA =  1.3789 SQ FT

PILE POINT AND OTHER DATA
 PILE LENGTH, PLEN =    50.00 FT       UNIT WT OF SOIL =     .060 K/FT*3
         PHI-ANGLE =     .000 DEG           SOIL COHES =     .96 KSF
       EFFEC OVERBURDEN PRESSURE AT PILE POINT QBAR =    3.81 KSF

EXTRA DATA FOR HAND CHECKING HANSEN
NC, NQ, NG =    5.140    1.000     .000
SC, SQ, SG =     .200    1.000     .600
DC, DQ, DOB =    .619  1.000  1.5481
COMPUTE QULT =  12.829             POINT LOAD PBASEH =   17.6903 KIPS



+++++ IN ROUTINE USING ALPHA-METHOD FOR SKIN RESISTANCE--IPILE =  1

I,QBAR =     2     .623    DEL ANGS D1,D2 =    24.00    28.80
 KFACT(I) = 1.5000                    FRIC FORCE SFRIC =    15.227


I,QBAR =     3    1.255    DEL ANGS D1,D2 =    20.00    24.00
 KFACT(I) = 1.3000                    FRIC FORCE SFRIC =    12.366


I,QBAR =     4    1.600    DEL ANGS D1,D2 =    24.00    28.80
 KFACT(I) = 1.5000                    FRIC FORCE SFRIC =    11.182


I,QBAR =     5    1.955    DEL ANGS D1,D2 =    24.00    28.80
 KFACT(I) = 1.5000                    FRIC FORCE SFRIC =    54.652
```

Figure E16-7*b*

Figure E16-7*b*(*continued*)

```
 IN ROUTINE ALPHAM FOR I =    6   H1 =   9.00
ALP1,ALP2 =      .910     1.000
PERIMETERS PER1,PER2 =   2.432   2.268          ADHES =    38.878

 IN ROUTINE ALPHAM FOR I =    7   H1 =   9.00
ALP1,ALP2 =     1.000     1.000
PERIMETERS PER1,PER2 =   2.432   2.268          ADHES =    40.777

 IN ROUTINE ALPHAM FOR I =    8   H1 =   9.00
ALP1,ALP2 =     1.080     1.080
PERIMETERS PER1,PER2 =   2.432   2.268          ADHES =    44.039

                    TOTAL ACCUMULATED SKIN RESISTANCE =  217.1221

 USING THE ALPHA METHOD GIVES TOTAL RESISTANCE, PSIDE =   217.122 KIPS
    WITH TOP   2.00 FT OMITTED

          TOTAL PILE CAPACITY USING HANSEN POINT LOAD =   225.97 KIPS


 SETTLEMENTS COMPUTED FOR AXIAL DESIGN LOAD =   226.0 KIPS
            USING SHAFT MODULUS OF ELAST ES = .4176E+07 KSF

LAYER    THICK   X-AREA     PTOP     SKIN R    PBOT     ELEM     SUM DH
 NO       FT     SQ FT     KIPS      KIPS     KIPS      DH        IN
   1     2.00    .1486      226.0       .0     226.0    .0087     .0087
   2     7.00    .1486      226.0      15.2    210.8    .0296     .0383
   3     4.00    .1486      210.8      12.4    198.4    .0158     .0541
   4     2.00    .1486      198.4      11.2    187.2    .0075     .0616
   5     8.00    .1486      187.2      54.7    132.6    .0247     .0863
   6     9.00    .1486      132.6      38.9     93.7    .0197     .1060
   7     9.00    .1486       93.7      40.8     52.9    .0128     .1188
   8     9.00    .1486       52.9      44.0      8.9    .0054     .1241

   SETTLEMENT DATA:     DQ, BMAX =    163.90       1.22
            SOIL THICKNESS HTOT =  50.00
            HTOT/BMAX & FOX FAC =   41.12     .500
      FOR MU = 0.35 AND SOIL Es =     450.0 KSF
  COMPUTED POINT SETTLEMENT, DP =  1.1659 IN
    TOTAL PILE/PIER SETTLEMENT (BUTT MOVEMENT) = DP + DH =    1.2901 IN
```

1. The top 2-ft element is not used because of driving damage.
2. The friction shows two "DEL ANGS" (24° and $1.2 \times 24° = 28.8°$) are used—24° for the flanges and 28.8° for the web. Pipe piles would use the input δ since the full perimeter is soil-to-steel.
3. The sum of skin resistance + point resistance gives 225.97 kips [the measured value was between 220 and 237 kips after 43 weeks—see page 345 of Finno (1989)]. For design you would divide this ultimate capacity by a suitable SF.

These values are also output to the screen, and the program inquires if a settlement estimate is desired. You can input either a design load here or the ultimate load just computed. I input 226 kips as shown on the output sheet since I wanted a check of the load test settlement. The program allows a number of materials (steel, concrete, wood) so it asks me for the modulus of elasticity of the pile and I input 4 176 000 ksf (for steel). For point settlement a modulus of elasticity of the ninth soil layer is required. I input 450 ksf (approximately $450 s_u$) on request as shown. The program then computed the point settlement and the accumulated side settlements. The point settlement uses the

modified Eq. (5-16*a*) as given in Sec. 16-10 with $I_F = 0.5$; the value DQ shown $= 226/A_p$ (point area is given earlier as 1.379 ft^2); and the largest point dimension is BMAX = 1.22 ft. These are used with $\mu = 0.35$ to compute the point settlement (with these data you can work backward to see what the program used for F_1). The total settlement is 1.29 in. (program converts feet to inches for this output). The measured value was in the range of 1.2 to 1.5 in.

////

16-12 PILES IN PERMAFROST

Piles are used in permafrost regions to control differential settlement from volume changes caused by freeze-thaw cycles. This is accomplished by isolation of the superstructure from the ice-rich soil by either an air space or a space filled with insulation material. The load capacity is usually obtained via the adfreeze[4] bond between the pile surface and a slurry of soil or other material used as a backfill in the cavity around the pile. Sometimes capacity is obtained by end bearing if competent strata are found at a reasonable depth. In most cases the pile-soil-ice interaction provides the significant portion of the load capacity, particularly where the pile penetrates ice-rich fine-grained soils.

Piles may be driven into the frozen ground; however, in remote areas transport of heavy equipment for driving is costly and alternative means are often preferred. The principal alternative is to auger a hole in which the pile is placed. The remaining cavity is backfilled with a slurry of water and coarse sand or with soil removed from the hole, which freezes to the pile to produce the adhesion used for load resistance. Often the loads to be carried are not large, so that small hand-powered auger equipment can be used to drill a hole of sufficient diameter and depth for the small piles required. Next upward in cost would probably be use of a truck-mounted auger. Low-energy driving equipment is sometimes used to insert piles into slightly undersized predrilled holes.

Care is necessary when adding the soil-water slurry (about 150-mm slump) if the temperature is below freezing so that an ice film with a greatly lowered skin resistance does not prematurely form on the pile shaft, from accidental wetting. Skin resistance can be significantly increased by adding shear connectors (rings, collars, or other) to the shaft. Certain of these devices may be used to circulate refrigerant [Long (1973)] where the mean ground temperature is close to freezing and the pile loads are large. In other cases the shear connectors can be added to steel piles by welding suitable protrusions to the shaft.

Principal pile materials in cold regions are timber, steel pipe, and **HP** shapes. Timber is probably the most economical in the remote regions of Canada and Alaska but may require weighting to avoid floating out of the hole when slurry is placed. Preservative may be painted on the pile but pressure treating is preferred; untreated piles have only a short service life (perhaps as little as two years), depending on wood quality, but may be adequate for certain installations. Cast-in-place concrete is not much used because of possible freezing prior to hydration, and precast concrete piling has a serious economic disadvantage from weight. Steel piles can be driven into fine-grained frozen soils using diesel and vibratory hammers if the air temperature is not much lower than −4°C. Rarely, steam jetting may be used to aid in pile insertion but the long resulting refreeze time is a serious disadvantage.

[4]Adfreeze is adhesion developed between pile and soil-water mixture as the water turns to ice (or freezes).

Pile Design

The principal design criteria are to control ice creep settlements and ensure adequate adfreeze skin resistance. Both of these factors are temperature-dependent. In turn, these require using very low adhesion stresses (high safety factor) in design and an assessment of the probable high temperature since adhesion increases (while creep decreases) with lower temperature.

The ultimate adfreeze stress is difficult to estimate but depends on at least the following:

1. Ground temperature (very important). Since the ground temperature varies from the active zone to the steady-state zone, the adfreeze varies similarly.
2. Initial (unfrozen) water content. Pure ice gives a lesser adfreeze than a frozen soil-water mixture.
3. Pile material. It appears from the limited test data available that wood and steel piles have approximately the same adfreeze resistance, with concrete slightly higher.
4. Soil (sand, silt, clay, etc.). Fine-sand- or silt-water mixtures seem to produce the highest adfreeze stresses. Gravels produce very low adfreeze—almost none unless saturated.
5. Soil density. Higher soil density increases adhesion and reduces creep.
6. Strain rate (low strain rates tend to lower adfreeze strengths).

Based on the work of Laba (1974), Tsytovich (1975), Penner and Irwin (1969), Penner and Gold (1971), Andersland and Anderson (1978), and Parameswaran (1978), the ultimate adfreeze f_{au} of several materials can be based on the following equation:

$$f_{au} = M_1 + M_2(T)^{0.7} \text{ kPa} \tag{16-21}$$

where T = degrees below 0°C
M_1 = 0 for pure ice; about 40 for silty soils and 70 for sand
M_2 = 75 for pure ice; about 80 for silty soils and gravel and about 150 for fine-to-medium sand

Orders of magnitude of f_{au} for ambient soil temperatures of -1 and -3°C seem to be as follows:

Soil	Wood	Steel	Concrete
		kPa	
Sand	400–1600	625–1000	500–3000
Silt	120–1000		
Clay	300–1200	100–1300	500–1300
Gravel	< 160		

There is a wide variation in the adfreeze values obtained and, of course, they depend somewhat on how the temperature variations have been accounted for. In general, the lower values just given would be applicable for temperatures close to 0°C. Below about -10 to -12°C the adfreeze reaches some limiting value.

The ultimate pile point stress in permafrost may be estimated [Long (1973)] at from 3 to 10 times the ultimate skin adfreeze stress. In any case a substantial safety factor should be applied and careful consideration should be given to whether to use any point contribution

since it is developed only after substantial adfreeze slip (and stress reduction) has occurred. Substantial slip may occur for skin resistance > 50 kPa [Nixon (1988)].

Creep is the second major factor for consideration in pile foundation design. Several researchers have addressed this problem, with recommendations being given by Morgenstern et al. (1980) and Biggar and Sego (1994). The general form of the creep equation is

$$\frac{\dot{u}_a}{B} = \frac{3^{(n+1)/2}(f_{ad})^n M_3}{n-1} \tag{16-22}$$

where $\dot{u}_a$ = creep rate per year
B = pile diameter
n = creep parameter—current value = 3
f_{ad} = design (actual) adfreeze stress, kPa
M_3 = creep parameter with following values:

T,° C	$M_3 \times 10^{-8}$, kPa^{-n}/year*
−1	4.5
−2	2.0
−5	1.0
−10	0.56

*Increase M_3 by 10 if salinity increases from 0 to 10 ppt. Increase M_3 by 100 if salinity increases from 20 to 30 ppt. (ppt = parts per thousand)

Pile Spacing

The latent heat of the soil-water slurry mixture and the additional heat loss required to reduce the slurry to the ambient temperature of the permafrost will control pile spacing. This spacing is based on the heat (calories) necessary to convert the water to ice at no change in temperature (latent heat) and then to lower the slurry temperature from that at placing to the ambient temperature (sensible heat). The latent heat of pure water is 778 Btu or approximately 79.7 g · cal. There are 4.185 joules (J) in 1 Btu or in 1 g · cal. For latent heat H_L of the water in the slurry in a unit volume (1 m^3) based on the slurry water content w_m (decimal) and dry density ρ_d in g/cm^3, and noting (100 cm)^3 gives m^3 and MJ, we can calculate the following:

$$H_L = 79.7 \times 4.185 \times \rho_d \times w_m = 333.6 \times \rho_d \times w_m \quad \text{MJ/m}^3 \tag{16-23}$$

The volumetric heat capacity (unit volume) is based on the heat capacity of the soil c_s and of the water in the slurry to obtain

$$c_{slurry} = \rho_d(c_s + c_w)4.185 = \rho_d(c_s + w_m)4.185 \quad \text{MJ/m}^3 \tag{16-24}$$

Values of heat capacity c_s for soils range from 0.15 to about 0.22 with most values around 0.16 to 0.18. Mitchell and Kao (1978) describe several methods that can be used to measure heat capacity or specific heat of soils.

Example 16-8. A timber pile is to carry 150 kN in a silty permafrost. The active zone is 2 m. Although the best data are obtained from a soil temperature profile, we will take the average ambient

temperature at −3°C for the soil below the active zone. The diameter of the pile will be taken as an average of 200 mm. This will be placed in a 310-mm predrilled hole and backfilled with a slurry at $w_m = 40$ percent and $\rho_d = 1.25$ g/cm^3. The slurry placement temperature is +3°C. The permafrost density is $\rho_d = 1.35$ g/cm^3 and $w_N = 35$ percent.

Required.

1. Find the approximate length of the pile if 1.0 m is above ground and there is no point contribution.
2. Find the approximate spacing needed to limit the permafrost temperature to −1.0° C (or less) when slurry is placed.
3. Check settlements at the end of two years.

Solution. *a.* Find the pile length. Based on Eq. (16-21),

$$f_{au} = M_1 + M_2(T)^{0.7} = 40 + 80(3)^{0.7} = 213 \text{ kPa}$$

From tests on several pile materials, the values for f_{au} range from 120 to 1000 for wood; use $f_{au} = 250$ kPa. For SF = 4 (arbitrary assumption),

$$f_{ad} = \frac{250}{4} = 62.5 \text{ kPa} \qquad \text{(say, 60 kPa)}$$

Now, find the length [using Eq. (16-10) with $f_s = f_{ad}$] and add 2 m for the active zone and 1 m for the above-ground projection,

$$\pi BL' f_{ad} = P_a$$

$$L' = \frac{150}{\pi(0.20)(60)} = 3.97 \text{ m} \qquad \text{(say, 4 m)}$$

$$L = 4 + 2 + 1 = \mathbf{7} \text{ m}$$

b. Find the approximate pile spacing. Using $c_s = 0.18$ g·cal and from Eq. (16-24), we calculate

$$c_{slurry} = \rho_d(c_s + w_m)4.185 = 1.25(0.18 + 0.40)4.185 = 3.03 \text{ MJ/m}^3$$

$$c_{permafrost} = 1.35(0.18 + 0.35)4.185 = 2.99 \text{ MJ/m}^3 \qquad \text{(same } c_s \text{ for both soils)}$$

The latent heat in slurry water from Eq. (16-23) is

$$H_L = 333.6\rho_d w_m = 333.6(1.25)0.40 = 1.67 \text{ MJ/m}^3$$

The average volume of slurry per meter of pile embedment is

$$V_s = 0.7854(0.31^2 - 0.20^2)(1) = 0.044 \text{ m}^3/\text{m}$$

We will assume the heat lost from the slurry equals the heat gain in the cylinder of permafrost surrounding the pile. The potential heat transfer to the permafrost per meter of embedment depth is

$$Q = V_s \times [H_L + (T_i - T_f)c_{slurry}]$$

$$= 0.044\{167 + [3 - (-1)]3.03\} = 7.88 \text{ MJ/m}^3$$

This Q is adsorbed based on a spacing s (diameter s of volume centered on a pile is also pile spacing) to give

$$Q = 0.7854s^2(T_f - T_i)c_{permafrost} = 7.88 \text{ MJ/m}^3$$

$$0.7854s^2[-1 - (-3)]2.99 = 7.88$$

$$s \geq \mathbf{1.29} \text{ m}$$

c. Estimate the settlement of the pile at the end of 2 years. We will use Eq. (16-22) and interpolate $M_3 \cong 1.5 \times 10^{-8}$ at $-3°C$ (no salt). Also $f_{ad} = 60$ kPa. Substituting values, we find

$$\frac{\dot{u}}{B} = \frac{3^2(1.5 \times 10^{-8})(60)^3}{3-1} = 1.5 \times 10^{-2} \text{ year}^{-1}$$

$$\Delta H = \frac{\dot{u}}{B} \times B \times \text{time, years} = \frac{0.015}{\text{yr}} \times 0.20 \times 2 \text{ yr} = \mathbf{0.006} \text{ m}$$

Summary.

$L = \mathbf{7}$ m (total length)

$s \geq \mathbf{1.3}$ m (center-to-center spacing)

$\Delta H = \mathbf{6}$ mm (estimated settlement)

////

16-13 STATIC PILE CAPACITY USING LOAD-TRANSFER LOAD-TEST DATA

The static capacity and settlement ΔH of a pile can be back-computed from load-transfer data obtained from one or more test piles that are sufficiently instrumented with strain gauges and/or telltales (see Fig. 16-18*b*). Telltales are rods used to measure accurately the movements of ledges welded a known distance from a reference point on the butt end of the pile. Sleeves are welded to the pile shaft above the ledge so a rod can be inserted to the ledge to measure the displacement after the pile has been driven and some load increment applied. Strain gauges, if used, can be calibrated to give the stress in the pile at the gauge location directly and corroborate the telltale.

The difference in measured load (or stress) between any two points is taken as the load transferred to the soil by skin resistance and is assumed constant in the segment length. The shear resistance is readily computed since the pile perimeter and segment length are known. The segment deformation can be computed using the average axial load in the expression PL/AE, and if the point displacement is known or assumed, the segment movement (termed slip) is known. A curve of slip versus shear resistance can then be plotted as in Fig. 16-18*c* for later use in estimating static capacity for surrounding piles. Note that several load increments must be applied to the pile in order to develop a load-transfer curve, and in general, more than one curve of the type shown in Fig. 16-18*c* is required to model the pile-soil response reasonably. A load transfer curve can be developed for each pile segment ΔL over the shaft length L_p. Segments are defined by strain gauges or telltales located at each end of the lengths ΔL. If adjacent segment curves are quite similar, a composite can be used; otherwise, one would use the individual curves.

The pile capacity computations can be made by hand [Coyle and Reese (1966)] or using a computer program [Bowles (1974*a*)]. Hand calculations are practical for no more than three to five pile segments (three are shown in Fig. 16-18*a*). Better results may be obtained using a larger number of segments if there are sufficient load-transfer curves and the data are of good quality.

Basically, the load-transfer method proceeds as follows:

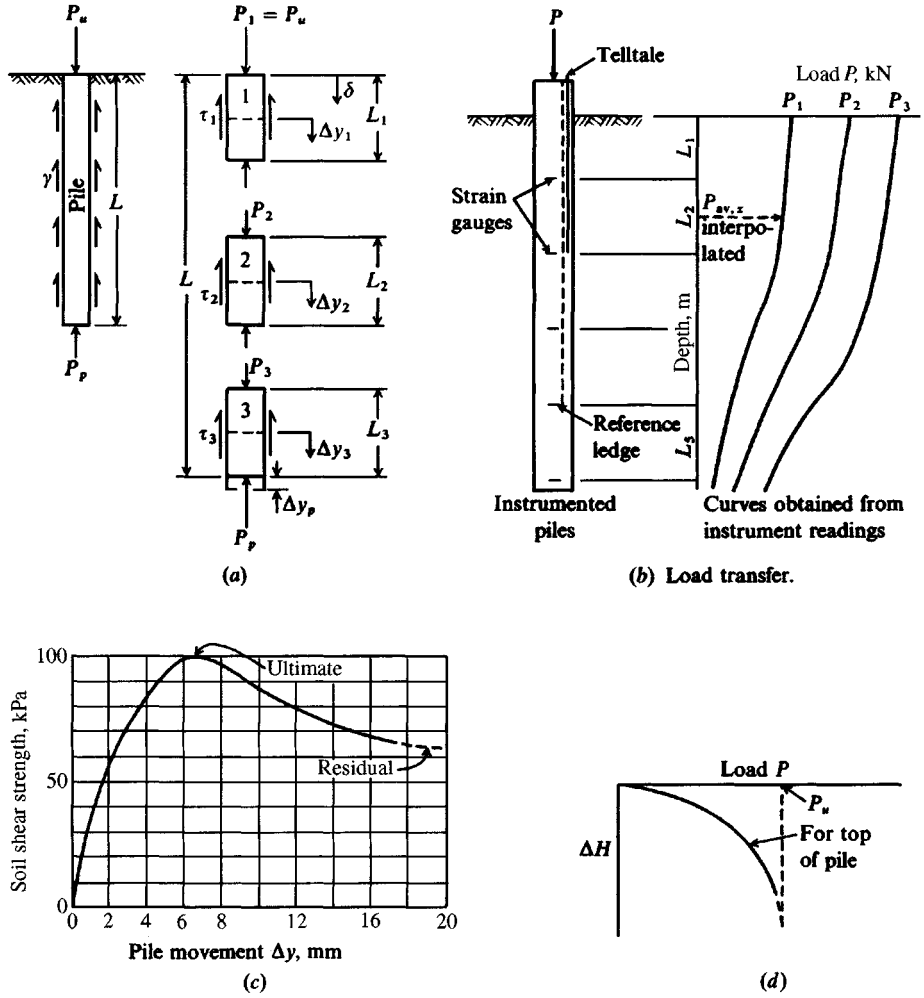

Figure 16-18 Method of computing load-settlement relationships for an axially loaded pile in clay. [*After Coyle and Reese (1966).*]

1. Divide the pile into a number of segments as shown in Fig. 16-18*a* using any stratification and shape of load-transfer curves as a guide.
2. Assume a small tip displacement Δy_p (zero may be used but generally the point will displace some finite amount unless it is on rock).
3. Compute the point resistance P_p from this assumed point displacement. One may apply a soil "spring" using an estimated k_s or use the Theory of Elasticity equation for ΔH given in Chap. 5 [Eq. (5-16*a*) see Sec. 16-10]. Using the modulus of subgrade reaction k_s, we may write

$$P_p = A_p k_s \Delta y_p$$

4. Compute the average movement (or *slip*) of the bottom segment. For a first approximation assume the movement is Δy_p. From the appropriate load-transfer curve of slip versus shear strength obtain the corresponding shear resistance for this value of Δy_p. For example

(Fig. 16-18*c*), if slip is $0.2 \times 10 = 2.0$ mm, the corresponding shear strength is 55 kPa. The axial load in the pile at the top of the segment (segment 3 in Fig. 16-18*a*) is the point load + load carried by skin resistance or

$$P_3 = P_p + L_3 \times \text{perimeter} \times \tau_3$$

Now recompute the element slip using

$$\Delta y_3 = \Delta y_p + \frac{(P_p + P_3)L_3}{2AE}$$

and obtain a new shear resistance. Recycle until slip used and slip computed are in satisfactory convergence. Note that absolute convergence is nearly impossible and would be of more computed accuracy than the data would justify.

5. With convergence in the bottom segment, proceed to the next segment above (segment 2 in Fig. 16-18*a*). A first estimate of slip in that segment is the last computed slip (Δy_3) of the element just below. From this slip obtain the corresponding shear resistance and compute the pile load (P_2) in the top of that segment. With values of P_2 (of this case) and P_3 obtain a revised slip as

$$\Delta y_2 = \Delta y_3 + \frac{(P_2 + P_3)L_2}{2AE}$$

Again recycle until suitable convergence is obtained and then go to the next above segment, etc.

6. The ultimate pile load (on top segment) is obtained as

$$P_u = P_1 = P_p + \sum L_i p_i \tau_i$$

We can see this is Eq. (16-5*a*) using the skin resistance given by Eq. (16-10) where we define $A_{si} = L_i p_i$ and $f_s = \tau_i$.

Obtain an estimate of pile settlement or vertical top movement ΔH as

$$\Delta H = \sum \Delta y_i$$

i.e., simply sum the displacements of the several pile segments (the point displacement is included in the lowest segment).

The shear versus pile slip curves of Fig. 16-18*c* are sometimes called *t-z* curves (*t* = tau = symbol sometimes used for shear stress *s* and *z* = slip of pile shaft with respect to adjacent soil). Kraft et al. (1981) proposed a semitheoretical procedure for obtaining the *t-z* curves. The procedure is best described as semitheoretical since the method is substantially theoretical yet, when it is reduced to the equation for curve development, it requires these assumptions:

a. Shear stress at pile-soil interface
b. G' the soil shear modulus (or somehow measuring it in situ)
c. An empirical parameter R_f
d. An estimate of peak shear stress ($s_{\max}$)
e. An estimate of the radius of influence r_m over which the shear stress ranges from a maximum at the pile shaft to zero at r_m from the pile

This number of assumptions is rather large; however, if one has pile tests that can be used and the method has been programmed, one can by trial obtain good agreement between predicted and measured values for the pile test under consideration.

Load test results are highly site-specific in the sense they are pile responses only for the pile in that location—and subject to interpretation. For this reason it is suggested that in the practical situation if we are able to obtain three or four load-transfer curve profiles we can then construct two or more trial shear transfer curves and use the simpler procedure outlined in Fig. 16-18.

16-14 TENSION PILES—PILES FOR RESISTING UPLIFT

Tension piles may be used beneath buildings to resist uplift from hydrostatic pressure. They also may be used to support structures over expansive soils. Overturning caused by wind, ice loads, and broken wires may produce large tension forces for power transmission towers. In this type of situation the piles or piers supporting the tower legs must be designed for both compressive and tension forces. In all these cases a static pile analysis can be used to obtain the ultimate tension resistance P_{tu} from Eq. (16-5*b*), slightly modified as

$$P_{tu} = \sum P_{si} + P_{pb} + W \tag{16-25}$$

where $\sum P_{si}$ = skin resistance from the several strata over the embedment depth L and is computed as

$$P_{si} = A_s f_s$$
$$f_s = c_a + \bar{q} K \tan \delta$$
$$A_s = \text{shaft perimeter} \times \Delta L$$

P_{pb} = pullout capacity from base enlargement (bell); may also be from suction but suction is usually transient

W = total weight of pile or drilled pier/caisson

The adhesion c_a is some fraction of the cohesion, $\bar{q}$ is the effective overburden pressure to middepth of element ΔL, and K is a lateral earth-pressure coefficient. The large majority of tension piles/piers are straight shafts, so the term P_{pb} is zero and the principal resistance to pullout is skin resistance and the shaft weight. For driven metal and precast concrete piles the same K for compression and tension would seem appropriate—or possibly with a slight reduction to account for particle orientation during driving and residual stresses. A value of K larger than K_o should be appropriate in sand since there is some volume displacement. The API (1984) suggests $K = 0.8$ for tension (and compression) piles in sand for low-volume displacement piles and $K = 1$ for displacement piles. For piles driven in clay one may use the same methods as for compression piles (α, λ, β methods).

For short drilled shafts (maximum depth = 5–6 m) that are filled with concrete, as commonly used for electric transmission tower bases and similar, we should look at the shaft diameter. The following is suggested [based on the author's analysis of a number of cases—the latest being Ismael et al. (1994) where K_{meas} was 1.45, and $K_{computed}$ was 1.46] for piles in *uncemented* sand:

K =	Shaft diameter, mm
K_a	$D \leq 300$ (12 in.)
$\frac{1}{2}(K_a + K_o)$	$300 < D \leq 600$
$\frac{1}{3}(K_a + K_o + K_p)$	$D > 600$ (or any D for slump > 70 mm)

In cemented sands you should try to ascertain the cohesion intercept and use a perimeter × cohesion × L term. If this is not practical you might consider using about 0.8 to $0.9K_p$.

The data base for this table includes tension tests on cast-in-place concrete piles ranging from 150 to 1066 mm (6 to 42 in.) in diameter. The rationale for these K values is that, with the smaller-diameter piles, arching in the wet concrete does not develop much lateral pressure against the shaft soil, whereas the larger-diameter shafts (greater than 600 mm) allow full lateral pressure from the wet concrete to develop so that a relatively high interface pressure is obtained.

16-15 LATERALLY LOADED PILES

Piles in groups are often subject to both axial and lateral loads. Designers into the mid-1960s usually assumed piles could carry only axial loads; lateral loads were carried by batter piles, where the lateral load was a component of the axial load in those piles. Graphical methods were used to find the individual pile loads in a group, and the resulting force polygon could close only if there were batter piles for the lateral loads.

Sign posts, power poles, and many marine pilings represented a large class of partially embedded piles subject to lateral loads that tended to be designed as "laterally loaded poles." Current practice (or at least in this textbook) considers the full range of slender vertical (or battered) laterally loaded structural members, fully or partially embedded in the ground, as *laterally loaded piles*.

A large number of load tests have fully validated that vertical piles can carry lateral loads via shear, bending, and lateral soil resistance rather than as *axially* loaded members. It is also common to use superposition to compute pile stresses when both axial and lateral loads are present. Bowles (1974*a*) produced a computer program to analyze pile stresses when both lateral and axial loads were present [including the $P - \Delta$ effect (see Fig. 16-21)] and for the general case of a pile fully or partially embedded and battered. This analysis is beyond the scope of this text, partly because it requires load-transfer curves of the type shown in Fig. 16-18*b*, which are almost never available. Therefore, the conventional analysis for a laterally loaded pile, fully or partly embedded, with no axial load is the type considered in the following paragraphs.

Early attempts to analyze a laterally loaded pile used the finite-difference method (FDM), as described by Howe (1955), Matlock and Reese (1960), and Bowles in the first edition of this text (1968).

Matlock and Reese (ca. 1956) used the FDM to obtain a series of nondimensional curves so that a user could enter the appropriate curve with the given lateral load and estimate the ground-line deflection and maximum bending moment in the pile shaft. Later Matlock and Reese (1960) extended the earlier curves to include selected variations of soil modulus with depth.

K =	Shaft diameter, mm
K_a	$D \leq 300$ (12 in.)
$\frac{1}{2}(K_a + K_o)$	$300 < D \leq 600$
$\frac{1}{3}(K_a + K_o + K_p)$	$D > 600$ (or any D for slump > 70 mm)

In cemented sands you should try to ascertain the cohesion intercept and use a perimeter × cohesion × L term. If this is not practical you might consider using about 0.8 to $0.9K_p$.

The data base for this table includes tension tests on cast-in-place concrete piles ranging from 150 to 1066 mm (6 to 42 in.) in diameter. The rationale for these K values is that, with the smaller-diameter piles, arching in the wet concrete does not develop much lateral pressure against the shaft soil, whereas the larger-diameter shafts (greater than 600 mm) allow full lateral pressure from the wet concrete to develop so that a relatively high interface pressure is obtained.

16-15 LATERALLY LOADED PILES

Piles in groups are often subject to both axial and lateral loads. Designers into the mid-1960s usually assumed piles could carry only axial loads; lateral loads were carried by batter piles, where the lateral load was a component of the axial load in those piles. Graphical methods were used to find the individual pile loads in a group, and the resulting force polygon could close only if there were batter piles for the lateral loads.

Sign posts, power poles, and many marine pilings represented a large class of partially embedded piles subject to lateral loads that tended to be designed as "laterally loaded poles." Current practice (or at least in this textbook) considers the full range of slender vertical (or battered) laterally loaded structural members, fully or partially embedded in the ground, as *laterally loaded piles*.

A large number of load tests have fully validated that vertical piles can carry lateral loads via shear, bending, and lateral soil resistance rather than as *axially* loaded members. It is also common to use superposition to compute pile stresses when both axial and lateral loads are present. Bowles (1974*a*) produced a computer program to analyze pile stresses when both lateral and axial loads were present [including the $P - \Delta$ effect (see Fig. 16-21)] and for the general case of a pile fully or partially embedded and battered. This analysis is beyond the scope of this text, partly because it requires load-transfer curves of the type shown in Fig. 16-18*b*, which are almost never available. Therefore, the conventional analysis for a laterally loaded pile, fully or partly embedded, with no axial load is the type considered in the following paragraphs.

Early attempts to analyze a laterally loaded pile used the finite-difference method (FDM), as described by Howe (1955), Matlock and Reese (1960), and Bowles in the first edition of this text (1968).

Matlock and Reese (ca. 1956) used the FDM to obtain a series of nondimensional curves so that a user could enter the appropriate curve with the given lateral load and estimate the ground-line deflection and maximum bending moment in the pile shaft. Later Matlock and Reese (1960) extended the earlier curves to include selected variations of soil modulus with depth.

Although the nondimensional curves of Matlock and Reese were widely used, the author has never recommended their use. A pile foundation is costly, and computers have been available—together with computer programs—for this type of analysis since at least 1960. That is, better tools are now available for these analyses.

THE *p–y* METHOD. The initial work on the FDM lateral pile solution [see McClelland and Focht (1958)] involved using node springs p and lateral node displacements y, so that users of this method began calling it the "p–y method." Work continued on this FDM computer program to allow use of different soil node springs along the pile shaft—each node having its own p–y curve [see Reese (1977)]. Since p–y curves were stated by their author to represent a line loading q (in units of kip/ft, which is also the unit of a soil spring), user confusion and uncertainty of what they represent has developed. This uncertainty has not been helped by the practice of actually using the p part of the p–y curve as a node spring but with a 1-ft node spacing so that it is difficult to identify exactly how p is to be interpreted. The product of node spring and node displacement y gives $p \cdot y$ = a node force similar to spring forces computed in the more recognizable form of force $= K \cdot X$.

The data to produce a p–y curve are usually obtained from empirical equations developed from lateral load tests in the southwestern United States along the Gulf Coast. In theory, one obtains a p–y curve for each node along the pile shaft. In practice, where a lateral load test is back-computed to obtain these curves, a single curve is about all that one can develop that has any real validity since the only known deflections are at or above the ground line unless a hollow-pipe pile is used with telltale devices installed. If the node deflection is not known, a p–y curve can be developed with a computer, but it will only be an approximation.

The FDM is not easy to program since the end and interior difference equations are not the same; however, by using 1-ft elements, interior equations can be used for the ends with little error. The equations for the pile head will also depend on whether it is free or either translation and/or rotation is restrained. Other difficulties are encountered if the pile section is not constant, and soil stratification or other considerations suggest use of variable length segments. Of course, one can account for all these factors. When using 1-ft segments, just shift the critical point: The maximum shift (or error) would only be 0.5 ft.

The FDM matrix is of size $N \times N$, where N = number of nodes. This matrix size and a large node spacing were advantages on early computers (of the late 1950s) with limited memory; however, it was quickly found that closer node spacings (and increases in N) produced better pile design data. For example, it is often useful to have a close node spacing in about the upper one-third of a pile.

The FDM would require all nodes to have equal spacing. For a 0.3-m spacing on a 36-m pile, 121 nodes would be required for a matrix of size $N \times N = 14\,641$ words or 58.6 kbytes (4 bytes/word in single precision). This size would probably require double precision, so the matrix would then use 117 kbytes.

THE FEM LATERAL PILE/PIER ANALYSIS. The author initially used the FDM for lateral piles (see first edition of this text for a program); however, it soon became apparent that the FEM offered a significant improvement. Using the beam element requires 2 degrees of freedom per node, but the matrix is always symmetrical and can be banded into an array of size

$$2 \times \text{number of nodes} \times \text{Bandwidth}$$

This array is always 2 × NNODES × 4, thus, a pile with 100 nodes would have a stiffness matrix of 2 × 100 × 4 = 800 words. This is 3200 bytes or 3.2k of memory and in double precision only requires 6.4k bytes.

One advantage of the FEM over the FDM is the FEM has both node translation and rotation, whereas the FDM only has translation. The elastic curve is somewhat better defined using both translation and rotation.

Another advantage is that the element lengths, widths, and moments of inertia can vary with only slightly extra input effort. One can even use composite piles. The pile modulus of elasticity is usually input as a constant since most piles are of a single material, but it is trivial to modify the moment of inertia for a composite section so that the program computes the EI/L value correctly. This value is determined by computing a modified moment of inertia I_m as in Eq. (13-4).

When using variable element lengths it is suggested that one should try to keep the ratio of adjacent element lengths (longest/shortest) < 3 or 4.

A major advantage of the FEM is the way in which one can specify boundary cases (nodes with either zero rotation or translation) and lateral loads. The FDM usually requires the load and boundary points be pre-identified; the FEM allows any node to be used as a load point or to have known translation or rotation—the known value is usually 0.0 but can be nonzero as well.

A final advantage is that the FEM for a lateral pile program can be used for a lateral pier (piles with a larger cross section) or beam-on-elastic-foundation design. It is only necessary to input several additional control parameters so the program knows what type of problem is to be solved. Thus, one only has to learn to use one fairly simple program in order to solve several classes of problems. Your sheet-pile program FADSPABW (B-9) is a special case of this method. It was separately written, although several subroutines are the same, because there are special features involved in sheet-pile design. These additional considerations would introduce unnecessary complexity into a program for lateral piles so that it would be a little more difficult to use. Many consider it difficult in any case to use a program written by someone else, so the author's philosophy has been to limit what a program does so that it is easier to use.

Refer to Sec. 9-8 for the derivation of the stiffness matrix and other matrices for the beam-on-elastic foundation and also used for the lateral pile. The only difference is that the beam-on-elastic foundation is rotated 90° clockwise for the lateral pile P–X coding and the end springs are not doubled (see Fig. 16-19). You must know how the finite-element model is coded and how the element force orientations (direction of arrowheads on force, moment, and rotation vectors) are specified either to order the input loads or to interpret the output element moments and node displacements.

USING THE FEM COMPUTER PROGRAM. The general approach to setting up an FEM model for using your diskette program FADBEMLP (B-5) to analyze lateral piles is this:

1. Divide the pile into a convenient number of elements (or segments) as in Fig. 16-19. From experience it has been found that the top third of the embedment depth is usually critical for moments and displacements, so use shorter element lengths in this region. Avoid very short elements adjacent to long elements; place nodes at pile cross-sectional changes, at soil strata changes, and where forces or boundary conditions are being applied. Generally 10 to 15 elements are adequate, with 4 to 8 in the upper third of the embedded shaft length.

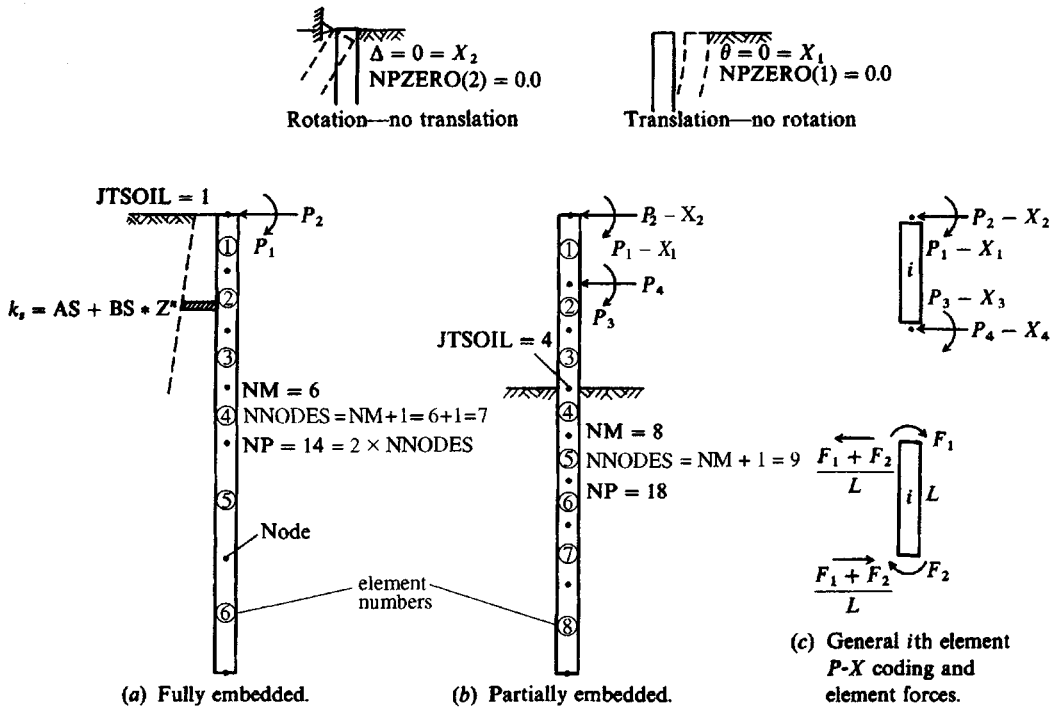

Figure 16-19 Laterally loaded pile using finite elements. Typical loadings shown in (*a*) and (*b*). Note that elements do not have to be same size or length. Generally use short elements near ground surface and longer elements near pile point where moments are less critical.

2. Partially embedded piles are readily analyzed by using JTSOIL equal to the node where soil starts (same as for sheet-pile wall). Use JTSOIL = 1 if ground line is at first pile node.
3. Identify any nodes with zero translation and/or rotation. NZX = number of *X*s of zero displacement. Use element coding to identify those *X* values that are input using NXZERO(I).
4. Make some estimate of the modulus of subgrade reaction and its depth variation (AS, BS, EXPO). Note that either AS or BS can be zero; EXPO = 0.5, 0.75, 1.0, or 1.5 may be appropriate; EXPO is the exponent of Z^n. You can also estimate a k_s-value [and XMAX(I)] for each node to input similar to the sheet-pile program.
5. Back-compute lateral load test data, if they are available, for the best estimate of k_s. One should not try to back-compute an exact fit since site variability and changes in pile type (pipe versus **HP**) preclude the existence of a unique value of k_s. The large number of pile tests reported by Alizadeh and Davisson (1970) clearly shows that great refinement in back computations is not required. One should, however, use in a load test the lateral load that is closest to the working load for best results.

WHAT TO USE FOR THE MODULUS OF SUBGRADE REACTION k_S.[5] The modulus of subgrade reaction is seldom measured in a lateral loaded pile test. Instead, loads and deflec-

[5]It should be understood that even though the term k_s is used in the same way as for the beam-on-elastic foundation, it is a vertical value here. The type (vertical or horizontal) is identified to the user by the context of usage.

tions are usually obtained as well as, sometimes, bending moments in the top 1 to 3 m of the embedded pile. From these one might work back using one's favorite equation for lateral modulus (or whatever) and obtain values to substantiate the design for that site.

Node values (or an equation for node values) of k_s are required in the FEM solution for lateral piles. Equation (9-10), given in Chap. 9 and used in Chap. 13, can also be used here. For convenience the equation is repeated here:

$$k_s = A_s + B_s Z^n \tag{9-10}$$

If there is concern that the k_s profile does not increase without bound use $B_s = 0$ or use B_s in one of the following forms:

$$B_s\left(\frac{Z}{D}\right)^n = \frac{B_s}{D^n}Z^n = B_s' Z^n \qquad \text{(now input } B_s' \text{ for } B_s\text{)}$$

or use $B_s(Z)^n$ where $n < 1$ (but not < 0)

where Z = current depth from ground surface to any node
D = total pile length below ground

The form of Eq. (9-10) for k_s just presented is preprogrammed into program FADBEMLP (B-5) on your diskette together with the means to reduce the ground line node and next lower node k_s (FAC1, FAC2 as for your sheet-pile program). You can also input values for the individual nodes since the soil is often stratified and the only means of estimating k_s is from SPT or CPT data. In this latter case you would adjust the ground line k_s before input, then input FAC1 = FAC2 = 1.0.

The program then computes node springs based on the area A_c contributing to the node, as in the following example:

Example 16-9. Compute the first four node springs for the pile shown in Fig. E16-9. The soil modulus is $k_s = 100 + 50Z^{0.5}$. From the k_s profile and using the average end area formula:

$$K_i = \frac{BL}{6}(2k_{s,i} + k_{s,i-1}) \quad \text{or} \quad \frac{BL}{6}(2k_{s,i} + k_{s,i+1})$$

$$K_1 = H(1) \times B(1)(2k_{s,1} + k_{s,2})/6 = 1.0 \times 0.45(2 \times 100 + 150)/6 = 26.3$$

$$K_2 = H(1) \times B(1)(2k_{s,2} + k_{s,1})/6 = 1.0 \times 0.45(2 \times 150 + 100)/6 = 30.0$$

$$K_2' = H(2) \times B(2)(2k_{s,2} + k_{s,3})/6 = 1.0 \times 0.45(2 \times 150 + 174.2)/6 = 42.7$$

$$K_3 = H(3) \times B(3)(2k_{s,3} + k_{s,2})/6 = 1.0 \times 0.45(2 \times 174.2 + 150)/6 = 44.9$$

$$K_3' = 1.0 \times 0.30(2 \times 174.2 + 189.4)/6 = 26.9$$

$$K_4 = 1.0 \times 0.30(2 \times 189.4 + 174.2)/6 = 27.7$$

Summary.

$$K_1 = \mathbf{26.3}\ \text{kN/m}$$

$$K_2 = K_2 + K_2' = 30.0 + 42.7 = \mathbf{72.7}\ \text{kN/m}$$

$$K_3 = K_3 + K_3' = 44.9 + 26.9 = \mathbf{71.8}\ \text{kN/m}$$

$$K_4 = 27.7 + 29.1 = \mathbf{56.8}\ \text{kN/m}, \ldots, \text{etc.}$$

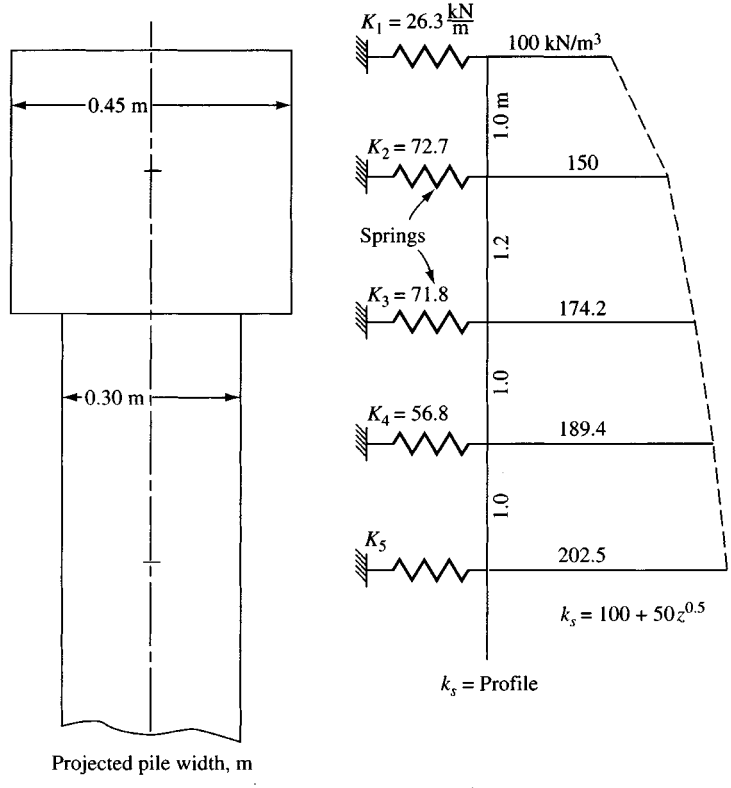

Figure E16–9

////

Example 16-9 illustrates a basic difference between this and the sheet-pile program. The sheet-pile section is of constant width whereas a pile can (and the pier or beam-on-elastic foundation often does) have elements of different width.

This program does not allow as many forms of Eq. (9-10) as in FADSPABW; however, clever adjustment of the BS term and being able to input node values are deemed sufficient for any cases that are likely to be encountered.

In addition to the program computing soil springs, you can input $k_s = 0$ so all the springs are computed as $K_i = 0$ and then input a select few to model structures other than lateral piles. Offshore drilling platforms and the like are often mounted on long piles embedded in the soil below the water surface. The drilling platform attaches to the pile top and often at several other points down the pile and above the water line. These attachments may be modeled as springs of the *AE/L* type. Treating these as springs gives a partially embedded pile model—with possibly a fixed top and with intermediate nonsoil springs and/or node loads—with the base laterally supported by an elastic foundation (the soil).

Since the pile flexural stiffness *EI* is several orders of magnitude larger than that of the soil, the specific value(s) of k_s are not nearly so important as their being in the range of 50 to about 200 percent of correct. You find this comparison by making trial executions using a k_s, then doubling it and halving it, and observing that the output moments (and shears) do not vary much. The most troublesome piece of data you discover is that the ground line displacement is heavily dependent on what is used for k_s. What is necessary is to use a pile stiff enough

and keep the lateral load small enough that any computed (or actual) lateral displacement is tolerable.

A number of persons do not like to use the modulus of subgrade reaction for anything—beams, mats or lateral piles. Generally they have some mathematical model that purportedly works for them and that they would like for others to adopt. In spite of this the k_s concept has remained popular—partly because of its simplicity; partly because (if properly used) it gives answers at least as good as some of the more esoteric methods; and, most importantly, because k_s is about as easy to estimate as it is to estimate the stress-strain modulus E_s and Poisson's ratio μ.

WHAT PILE SECTION TO USE. It is usual to use the moment of inertia I of the actual pile section for both **HP** and other piles such as timber and concrete. For reinforced concrete piles, there is the possibility of the section cracking. The moment of inertia I of a cracked section is less than that of the uncracked section, so the first step in cracked section analysis is to recompute I *based on a solid transformed section,* as this may be adequate.

It is suggested that it is seldom necessary to allow for section cracking. First, one should not design a pile for a lateral load so large that the tension stresses from the moment produce cracking—instead, increase the pile cross section or the number of piles. Alternatively, use steel or prestressed concrete piles.

The possibility of concrete pile cracking under lateral load is most likely to occur when partially embedded piles are used. The unsupported length above the ground line may undergo lateral displacements sufficiently large that the section cracks from the resulting moment-induced tension stresses. The unsupported pile length must be treated similarly to an unsupported column for the structural design, so a larger cross section may be required—at least in the upper portion of the pile.

16-15.1 Empirical Equations for Estimating k_s

Where pile-load tests are not available, some value of k_s that is not totally unrealistic must be estimated, one hopes in the range between ± 50 and ± 200 percent[6] of the correct value. The following equations can be used to make reasonable estimates for the lateral modulus of subgrade reaction.

An *approximation* proposed by the author is to *double* Eq. (9-9) since the soil surrounds the pile, producing a considerable side shear resistance. For input you obtain A_s, B_s values and multiply by two. Using the bearing-capacity components of Eq. (13-1) to give the needed parts of Eq. (9-9), we have

$$A_s = \text{AS} = C(cN_c + 0.5\gamma B_p N_\gamma)$$

$$B_s Z^n = \text{BS} * (\text{Z\^{}N}) = C(\gamma N_q Z^1)$$

where $C = 40$ for SI, 12 for Fps. It was also suggested that the following values could be used, depending on the actual lateral displacement:

[6]Two hundred percent is double the true value, and 50 percent is one-half the true value.

For ΔH,		C		
SI (m)	Fps (in.)	SI	Fps	$2C$
0.0254	1	40	(12)	80
0.006	$\frac{1}{4}$	170	(48)	340
0.012	$\frac{1}{2}$	80	(24)	160
0.020	$\frac{3}{4}$	50	(36)	100

16-15.2 Size and Shape Factors

The idea of *doubling* the lateral modulus was to account for side shear developed as the pile shaft moves laterally under load, both bearing against the soil in front and shearing the soil on parts of the sides as qualitatively illustrated in Fig. 16-20. Clearly, for piles with a small projected D or B, the side shear would probably be close to the face bearing (consisting of 1.0 for face $+2 \times 0.5$ for two sides $= 2.0$). This statement would not be true for larger D or B values. The side shear has some limiting value after which the front provides the load resistance. Without substantiating data, let us assume this ratio, two side shears to one face, of 1:1 reaches its limit at $B = D = 0.457$ m (18 in.). If this is the case then the *size factor* multiplier (or ratio) C_m should *for single piles* be about as follows (the 1.0 is the face contribution):

For	Ratio, C_m
Lateral loads of both P_x and P_y (face + 1 side)	$1.0 + 0.5$
$B = D \leq 0.457$ m	$1.0 + 2 \times 0.5$
$B = D > 0.457$	$1.0 + \left(\frac{457}{D, \text{mm}}\right)^{0.75} \geq 1.5$
	use $1.0 + 0.25$ for $D > 1200$mm

You should keep the foregoing contributing factors in mind, for they will be used later where the *face* and *side* contributions may not be 1.0 and 0.5, respectively.

Now with C_m, rewrite Eq. (13-1) as used in Sec. 16-15.1 to read

$$\left.\begin{aligned} A_s &= \text{AS} = C_m C(cN_c + 0.5\gamma B_p N_\gamma) \\ B_s Z^n &= \text{BS} * \text{Z\^{}N} = C_m C(\gamma N_q Z^n) \end{aligned}\right\} \tag{16-26}$$

It is also suggested that the BS term should use an exponent n that is on the order of 0.4 to 0.6 so that k_s does not increase without bound with depth.

Research by the author by back-computing k_s from piles in cohesionless soils at the same site indicates that Eq. (9-10) should be further rewritten to read

$$\left.\begin{aligned} A_s &= \text{AS} = F_{w1} C_m C(cN_c + 0.5\gamma B_p N_\gamma) \\ B_s Z^n &= \text{BS} * \text{Z\^{}N} = F_{w2} C_m C(\gamma N_q Z^n) \end{aligned}\right\} \tag{16-26a}$$

where $F_{w1}, F_{w2} =$ **1.0** for square and **HP** piles (reference modulus)

$F_{w1} = 1.3$ to 1.7; $F_{w2} = 2.0$ to 4.4 for round piles

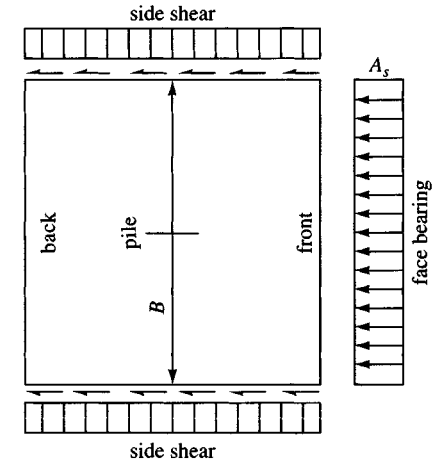

(*a*) Square of rectangular

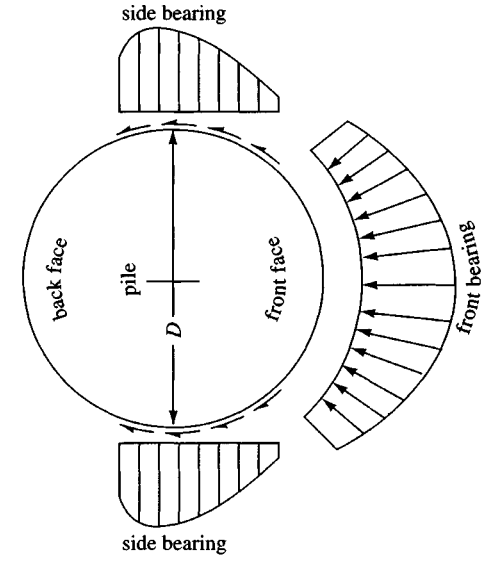

(*b*) Circular pile

Figure 16-20 Qualitative front and side resistances for a lateral pile.

One probably should apply the F_i factors only to the *face* term (not side shear) for round piles. Whether these shape factors actually result from a different soil response for round piles or are due to erroneous reported data from neglecting the distortion of the hollow pipe (laterally into an oblate shape) under lateral load is not known at this time. Gleser (1983) and others have observed that the response of a round pile is different from that of a square or **HP** pile, in general agreement with the foregoing except in a case where a comparison of a 100-mm **HP** pile to a 180-mm diameter pipe pile was claimed not to produce any noticeable difference.

Size and projection widths would make it very difficult to note any differences in this case, particularly if the pipe wall thickness was such that the diameter did not tend to oblate (flatten).

USING THE GIVEN BEARING CAPACITY. If we have only the allowable bearing pressure q_a, we can use Eq. (16-26) as follows (but may neglect the N_q term):

$$k_s = F_{w,1} \times \text{SF} \times C_m C \times q_a + F_{w,2} \times C_m C \gamma Z^n N_q \qquad (16\text{-}26b)$$

where SF = safety factor used to obtain q_a (usually 3 for clay; 2 for cohesionless soil)
N_q = value from Table 4-4 or from Eq. (16-7) or (16-7*d*)
n = exponent as previously defined; 1 is probably too large so use about 0.4 to 0.6 so k_s does not increase too much with depth

If you use either Eq. (16-26) or (16-26a) you should plot k_s for the pile depth using several values of exponent n to make a best selection.

It has been found that the use of Eq. (16-26) produces values within the middle to upper range of values obtained by other methods.

If we take $q_a = q_u$ (unconfined compression test) and omit the N_q term in Eq. (16-26*a*), the value of k_s in *Fps* units for a pile of unknown B is

$$k_s = C_m \times 12 \times \text{SF} \times q_u = 2 \times 3 \times 12 \times q_u = 72q_u$$

Davisson and Robinson (1965) suggested a value of $k_s \approx 67s_u$, which was about half of $72q_u$. Later Robinson (1978) found that $67s_u$ was about half the value of k_s indicated by a series of lateral load tests [that is, $72q_u$ (or $240q_u$, kPa) was about the correct value].

The API (1984) suggests that the lateral bearing capacity for soft clay ($c \leq 50$ kPa) be limited to $9c$ and for stiff clay from $8c$ to $12c$ [see Gazioglu and O'Neill (1985) for detailed discussion]. In soft clay this bearing capacity would give, according to Eq. (16-26*a*), the value

$$k_s = C_m(40)(9c) = 360C_m c \qquad (\text{kN/m}^3)$$

which does not appear unreasonable.

You may indirectly obtain k_s from the following type of in situ tests:

a. Borehole pressuremeter tests where E_{pm} = pressuremeter modulus

$$k_s = \frac{3.3E_{\text{pm}}}{B_p} \qquad (16\text{-}27)$$

For cohesionless soils [see Chen (1978)]:

$$k_s = \frac{3E_{\text{pm}}}{B} \qquad (16\text{-}27a)$$

And for cohesive soils:

$$k_s = \frac{1.6E_{\text{pm}}}{B} \qquad (16\text{-}27b)$$

b. Flat dilatometer tests:

$$k_s = \frac{E_d F_p}{3.7B} \tag{16-28}$$

where E_d = dilatometer modulus, kPa or ksf
F_p = pile shape factor: 1.5 to 4.0 for round piles; 1.0 for **HP** or square piles

For these values of k_s you would compute values as close to your pile nodes as possible and input the several node values, not just a single value for the full depth.

The stress-strain modulus E_s can be used in Eq. (16-31) following [or Vesić's Eq. (9-6), given earlier] to compute k_s. Estimate E_s from your equation or method or one of the following:

a. Triaxial tests and using the secant modulus E_s between 0 and 0.25 to 0.5 of the peak deviator stress. The initial tangent modulus may also be used. Do not use a plane strain E_s.

b. The standard penetration test [see Yoshida and Yoshinaka (1972)] to obtain

$$E_s = 650N \qquad \text{kPa} \tag{16-29}$$

This equation has a maximum error of about 100 percent with an average error of close to ± 20 percent. Assume that N in Eq. (16-29) is N_{70} (see under donut hammer of Table 3-3).

For CPT data convert to equivalent SPT N and use Eq. (16-29).

c. Use consolidation test data to obtain m_v to compute the stress-strain modulus by combining Eqs. (2-43) and Eq. (*f*) of Sec. 2-14 and noting

$$\frac{\Delta H}{\Delta pH} = \frac{1}{E_b}$$

to obtain

$$E_s = \frac{3(1 - 2\mu)}{m_v} \tag{16-30}$$

Any of these three values of E_s can be used to compute k_s in clay using any of the following three equations cited by Pyke and Beikae (1983):

$$k_s = \frac{0.48 \text{ to } 0.90E_s}{B} \tag{a}$$

where 0.48 is for **HP** piles; 0.9 for round piles (i.e., a shape factor $F_{w1} \approx 2$);

$$k_s = \frac{1.8E_s}{B} \tag{b}$$

and for sands

$$k_s = \frac{E_s}{B} \tag{c}$$

where in Eq. (*c*) E_s = triaxial test value at about $\epsilon \approx 0.01$. You may also use these stress-strain moduli values in the following equation [Glick (1948)] to obtain a modified k_s' that is then used in Eq. (16-32):

$$k_s' = \frac{22.4E_s(1-\mu)}{(1+\mu)(3-4\mu)[2\ln(2L_p/B)-0.433]} \quad \text{(units of } E_s\text{)} \tag{16-31}$$

where L_p = pile length, m or ft
B = pile width, m or ft

After computing k_s', convert it to the usual k_s using the following:

$$k_s = \frac{k_s}{B} \tag{16-32}$$

Since this value of k_s' has the same meaning as the Vesić value given by Eq. (9-6), we can use that equation with the following suggested modification:

$$k_s = \frac{k_{s,v}z^n}{B} \tag{16-32a}$$

The z^n term is suggested to allow some controlled increase in k_s with depth.

The *NAFAC* Design Manual DM7.2 (1982) suggests the following:

$$k_s = \frac{fz}{D} \tag{16-33}$$

where f = factor from following table, kN/m^3 or k/ft^3
D = pile diameter or width, m or ft
z = depth; m or ft gives $k_s = 0$ at ground surface and a large value for long piles at the tips. A better result might be had using $(z/D)^n$ where n ranges from about 0.4 to 0.7.

Values for f (use linear interpolation)

	q_u	D_r	f
Fine-grained:	20	0	200
	40		350
	60		550
	80	15	800
Coarse-grained:		30	800
	110	40	1400
	150	50	2000
	190	60	2800
	230	70	3400
	270	80	4200
	310	90	4900
	370		

TABLE 16-4
Representative range of values of lateral modulus of subgrade reaction (value of A_s in the equation $k_s = A_s + Bz^n$

Soil*	k_s, kcf	k_s, MN/m^3
Dense sandy gravel	1400–2500	220–400
Medium dense coarse sand	1000–2000	157–300
Medium sand	700–1800	110–280
Fine or silty, fine sand	500–1200	80–200
Stiff clay (wet)	350–1400	60–220
Stiff clay (saturated)	175–700	30–110
Medium clay (wet)	250–900	39–140
Medium clay (saturated)	75–500	10–80
Soft clay	10–250	2–40

*Either wet or dry unless otherwise indicated.

Table 16-4 gives ranges of k_s for several soils, which are intended as a guide for probable values using more precise methods—or at least using the site soil for guidance. They should be taken as reasonably representative of the $A_s + B_s$ terms at a depth from about 3 to 6 m and for pile diameters or widths under 500 mm.

16-15.3 Nonlinear Effects

It is well known that doubling the load on a lateral pile usually more than doubles the lateral displacement and increases the bending moment. The moment increase results from both the increase in δ_h and the greater depth in which lateral displacements occur. Both of these effects result from nonlinear soil behavior idealized by the curve shown in Fig. 2-43*c*, particularly at higher stress levels σ that result from larger lateral loads. Usually the lateral displacements in the load range of interest are in that part of the σ–δ curve that is approximately linear.

In the curve of Fig. 2-43*c* the modulus of subgrade reaction is taken as a "secant" line from the origin through some convenient stress value σ. Ideally one should have a curve such as this for each node point (see Fig. E13-1*e*) for a lateral pile. Then, as a displacement is computed one would enter the curve, obtain a revised secant modulus k_s, and recompute the displacements until the δ_h value used = δ_h value obtained.

This approach is seldom practical since these curves are difficult to obtain—usually a pipe pile must be used for the test so that lateral measurements can be taken at nodes below the ground line. A pipe pile, however, has a shape factor, so the results are not directly usable for other pile shapes.

Most lateral piles are designed on the basis of using penetration testing of some kind, supplemented with unconfined compression data if the soil is cohesive. For these cases the two-branch nonlinear model proposed by the author (see Fig. 9-9*c*) will generally be adequate.

The program FADBEMLP on your diskette allows you to model the two-branch nonlinear node displacement curve for the soil as you did in program FADSPABW. That is, you can input the maximum linear displacement at each node as XMAX(I) and activate a nonlinear check using the control parameter NONLIN > 0. Here a negative displacement is not a soil separation, but rather the pile has deflected forward such that the elastic line has produced

a displacement at a lower node against the soil behind the pile. An extensive discussion of XMAX(I) was given in Chap. 13 that will not be repeated here except to note that the nonlinear check is $|X(I)| \leq XMAX(I)$.

CYCLIC LOADING. The k_s for cyclic loading should be reduced from 10 to 50 percent of that for static loading. The amount of reduction depends heavily on the displacements during the first and subsequent cycles.

Quasi-dynamic analysis of offshore piles subject to wave forces can be obtained by applying the instant wave force on the nodes in the water zone for several closely spaced discrete time intervals.

DISPLACEMENTS FROM SOIL CREEP. Lateral displacement from long-term loading, producing secondary consolidation or creep, has not been much addressed for lateral piles. Kuppusamy and Buslov (1987) gave some suggestions; however, the parameters needed for the necessary equations are difficult to obtain. Although one could consult that reference, their equations are little better than simply suggesting that, if the lateral load is kept under 50 percent of the ultimate, the creep displacement for sand after several years is not likely to exceed 10 percent of the initial lateral displacement.

For clay, the creep will depend on whether it is organic or inorganic. The creep displacement may be as much as the initial displacement for an organic clay but only about 15 to 20 percent for an inorganic one. One might compute a lateral influence depth of approximately $5 \times$ projected width of pile/pier $= H_f$ and use Eq. (2-49) for a numerical estimate if you have a secondary compression coefficient C_α.

Laterally loaded piles in permafrost also undergo creep. Here the creep depends on the temperature, quantity and type of ice, and the lateral pressure, generally expressed as a "creep" parameter. Neukirchner (1987) claims to have a reasonable solution, but the creep parameter is so elusive that there is substantial uncertainty in any permafrost creep estimate.

When lateral piles undergo creep, the effect is to increase the lateral displacement and bending moment. The goal is an estimate of the final lateral displacement and bending moment. The bending moment might be obtained in any situation where creep is involved by simply measuring the displacements and, using the current lateral displacement as the specified displacement in program FADBEMLP, computing the moment produced by that displacement.

Alternatively since creep decreases approximately logarithmically it might be obtained by plotting the displacement at several time intervals (long enough to be meaningful) and numerically integrating the curve to find the anticipated total lateral displacement for input so as to compute the lateral pile bending moments.

16-15.4 Including the *P*–Δ Effect

The *P*–Δ effect can be included for lateral piles (refer to Fig. 16-21) in a straightforward manner as follows:

1. Draw the partially embedded pile to rough scale, code the nodes, and locate the node JTSOIL. We will use JTSOIL as the reference node.
2. Make an execution of the data with the horizontal force P_h located at the correct node above JTSOIL. This will generally be at the top of the pile where the vertical load P_v also

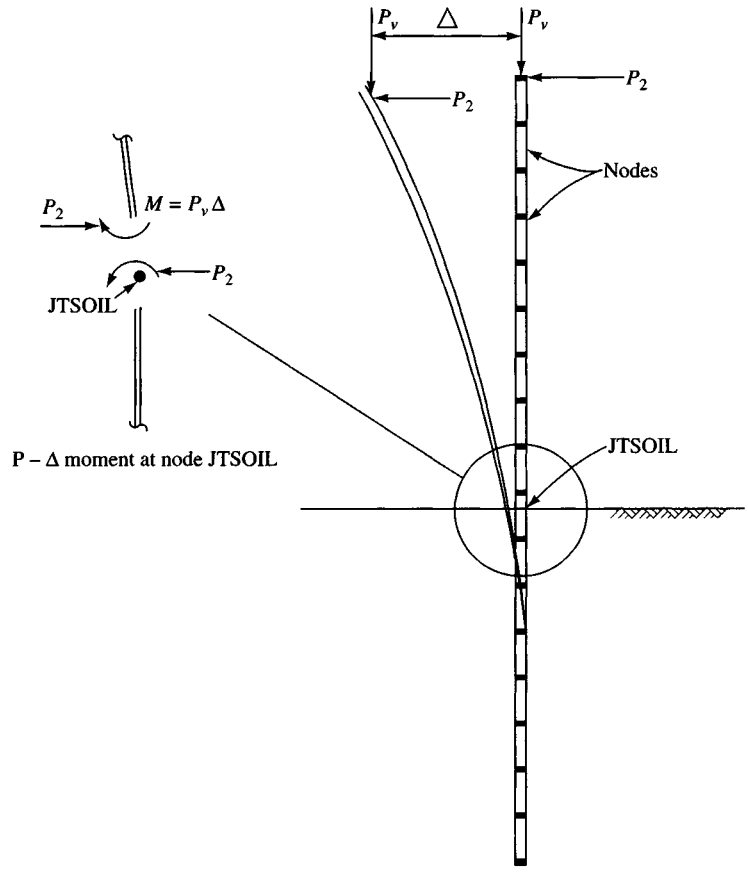

Figure 16-21 The geometric P–Δ effect for laterally loaded piles.

acts. Until you become familiar with program FADBEMLP you should use the pile and load geometry which corresponds to Fig. 16-21.

3. Inspect the output, and at the top node where P_v acts there will be a lateral displacement (let us use, say, $\Delta = 0.40$ m and a vertical force $P_v = 60$ kN). From the lateral displacement, which is with respect to the original position of node JTSOIL, a P–Δ moment can be computed (see inset of Fig. 16-21) of $60 \times 0.40 = 24$ kN·m.
4. Make a copy of the original data and change NNZP from 1 (for the horizontal force only) to 2 to include both the original horizontal force and the P–Δ moment just computed of 24 kN· m. If we assume JTSOIL = 11, the moment NP location is $2 \times 11 - 1 = 21$.
5. In the data file you can see the horizontal load and its NP number. Just below, enter 21 and the moment value of 24. Note from the inset, however, that the moment has a negative sign. The two load matrix entries would now read

Node	Load	
2	P_h	(this is the problem value)
21	−24.0	

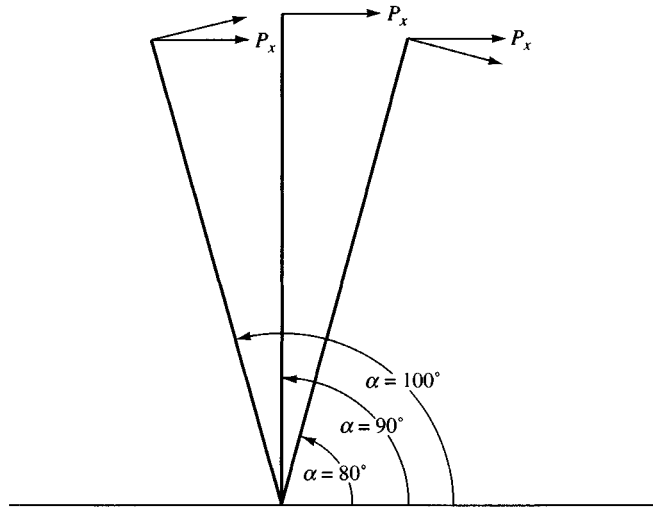

Given: $\phi = 32°$; $\beta = 0°$; $\delta = 20°$

unfactored $k_s = 200 + 40Z^n$; Coulomb $K_p = 6.89$ ($\alpha = 90°$)

$\alpha = 100° \rightarrow K_{pb} = 11.35$ (use prog. FFACTOR) $\alpha = 80° \rightarrow K_{pb} = 4.89$

$C_m = 11.35/6.89 + 2(0.5) = 2.65$ $C_m = 4.89/6.89 + 2(0.5) = 1.71$

$k_s = 2.65(200 + 400Z^n)$ $k_s = 1.71(200 + 400Z^n)$

$= 530 + 1060Z^n$ $= 342 + 684Z^n$

(a) Definition of batter angle α for adjustment of C_m for k_s.

Figure 16-22 Adjusting k_s factor C_m for pile batter and spacing and/or location in group.

6. Now execute this data set (if the sign is correct the top node displacement Δ will slightly increase). Obtain the displacements, and if the previous $\Delta_p - \Delta_{\text{current}} \leq$ some convergence (not in program but decided by the user), say, 0.005 m or less, stop. Otherwise continue to compute a new P–Δ moment and recycle.

Note that the second data set has two changes initially: (1) to increase NNZP by 1 and (2) to input the P–Δ moment. After this, the only change to that second data set is to reinput the new P–Δ moment until the problem converges.

The node JTSOIL will probably move laterally also, and the most critical P–Δ moment is not the difference between the top node and node JTSOIL but between the top node and some node farther down that does not move laterally. You could, of course, put the P–Δ moment at this location, but the foregoing suggested solution is generally adequate. You can also use the difference between the top translation and the computed translation at node JTSOIL, but this is less conservative.

16-15.5 Lateral Piles on Slopes

Laterally loaded piles are frequently sited on slopes, for example, power poles and bridge foundations. It is suggested that the same procedure be used to reduce the lateral k_s values as was used for the sheet-pile wall case. That is, use program WEDGE or FFACTOR to

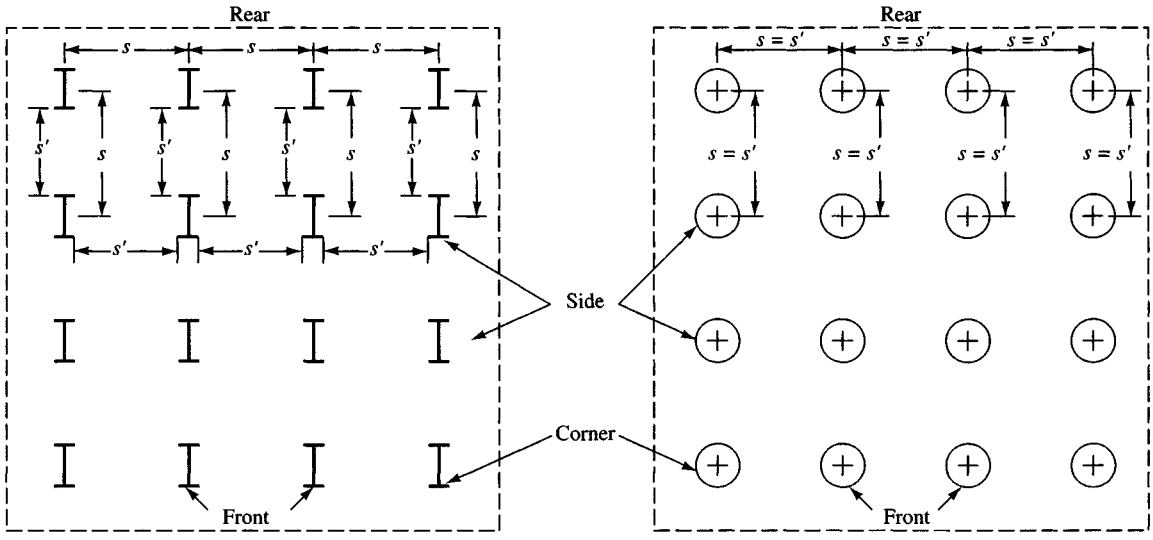

(*b*) Pile spacing s' and location for c_m adjustments for k_s.

compute the passive force (or coefficient K_p) case for the horizontal ground line and for the actual ground slope and use the ratio RF as in Eq. (13-3). Because the side shear part from factor C_m is not required to be reduced, you should apply the slope ratio RF *only to the face* (or bearing) part of k_s. For example, compute $k_s = 2000$ based on using $C_m = 2$; RF = 0.6. This calculation gives $k_{s1} = 2000/C_m = 1000 = k_{s2}$. The revised $k_s = k_{s2} + \text{RF} \times k_{s1} = 1000 + 0.6 \times 1000 = \mathbf{1600}$.

16-15.6 Battered Piles

The k_s for battered piles has not been addressed much in the literature. In the absence of substantiating data the author suggests (see Fig. 16-22*a*) the following:

1. Compute the Coulomb passive earth pressure coefficient K_p for a vertical wall ($\alpha = 90°$), including any slope angle β. A lateral pile is a "passive" earth-pressure case but requires including side shear effects since the Coulomb case is one of plane strain.
2. Next draw the battered pile and place a perpendicular load on the pile with the (+) direction as shown on Fig. 16-22*a*. The perpendicular load direction should correspond to that used to establish the batter direction [will be either (+) or (−)]. Draw a horizontal component line as, say, P_x as shown.
3. Now measure (or compute) the batter angle α. It is *counterclockwise* from a horizontal line at the pile tip for the (+) load perpendicular; it is *clockwise* for a (−) load perpendicular. For the (+) perpendicular shown on Fig. 16-22*a* we have $\alpha > 90°$ if the horizontal component is below and $\alpha < 90°$ if the horizontal component is above the perpendicular.
4. Compute a Coulomb passive pressure coefficient K_{pb} for the applicable batter angle α. Use program FFACTOR. You probably should include a pile-to-soil friction angle δ.

5. Compute a revised k_s as

$$k_s = \left(1.0 \times \frac{K_{pb}}{K_p}\right) + (2 \times 0.5)$$

This calculation should give the expected result of a larger k_s for $\alpha > 90°$ and a smaller k_s for $\alpha < 90°$ for the (+) case shown on Fig. 16-22*a*.

Note: We only adjust the face or bearing part of k_s because the side shear should be about the same for either a vertical or a battered pile.

16-15.7 Adjusting k_s for Spacing

It is generally accepted that there is a reduction in the lateral subgrade modulus k_s when piles are closely spaced. Poulos (1979) suggested using factors from curves developed using an elastic analysis of pile-soil interaction (i.e., E_s, μ), which are then combined to give a *group* factor. This method does not seem to be used much at present.

The following method (refer to Fig. 16-22*b*) is suggested as an easy-to-visualize alternative to obtain the lateral modulus for individual piles in a group:

1. Referring to the Boussinesq pressure bulb (Fig. 5-4) beneath a rectangular footing, we see that at a $D/B > 6$ the pressure increase on the soil is negligible. So, using a *clear* pile spacing s' for depth D and pile projected width for B, we can say that if $s'/B > 6$ no adjustment in k_s is necessary.
2. For spacings of $s'/B < 6$ use Fig. 5-4 ("Continuous") and multiply the face bearing term by (1.0 − interpolated pressure intensity factor). For example at $s'/B = 2$, we obtain 0.29, and the face term is $1.0 \times (1.0 - 0.29) = \mathbf{0.71}$ (here 0.29, or 29 percent, of the pressure is carried by the front pile). This is the *face factor* contribution to C_m (= 2 sides + face $= (2 \times 0.5) + 0.71 = \mathbf{1.71}$).
3. For the *side shear factor* contribution to C_m we have two considerations:
   a. Location (corner, front, side, interior, or rear)
   b. What reduction factor (if any) to use

Clearly for side and corner piles one side is not affected by any adjacent pile so for those we have some interior side interaction factor Ψ + an exterior factor of 0.5. For front, interior, and rear piles we have a side interaction factor of 2Ψ.

One option is to consider that any pile insertion increases the lateral pressure so that the use of $\Psi = 0.5$ is adequate. Another option is to consider that enough remolding takes place that the soil is in a residual stress state and to reduce the 0.5 side factor to

$$\Psi = 0.5 \frac{\text{Residual strength}}{\text{Undisturbed strength}}$$

16-15.8 Estimating Required Length of a Laterally Loaded Pile

The required length of a laterally loaded pile has not been directly addressed in the literature. Obviously, it should be long enough to provide lateral stability, and if there is an axial load, the pile must be long enough to develop the required axial capacity.

We can obtain the required pile embedment length for lateral stability (it was previously noted that usually the upper one-third of the pile actively resists the lateral loads) as follows:

1. Compute the embedment length required for any axial load. If there is no axial load initially, try some reasonable length, say, L'.
2. Use computer program B-5 with your lateral load P_h and obtain a set of output.
3. Inspect the horizontal displacement δ_{hp} at the pile base (or point). If the absolute value of $\delta_{hp} \approx 0.0$, the pile length is adequate. If $|\delta_{hp}| > 0.0$, you have to decide whether the length is adequate, since this amount of displacement may be indicative of a toe kickout (lateral soil failure). Also check that the active (zone of significant bending moment) depth is approximately $L'/3$. Now do two other checks:
   a. Depending on how you initialized L', you may want to increase it by 20 to 30 percent to allow for a modest stability number (SF).
   b. Make two additional program executions using 1/2 and 2 times the initial value of lateral subgrade modulus k_s. If both these executions give $\delta_{hp} \approx 0.0$, you have an adequate pile embedment depth L'. If $\delta_{hp} > 0.0$ (particularly for the $k_s/2$ case), you probably should increase L'.

   If you increase L' based on either (*a*) or (*b*), you should recycle to step 2. When you find an L' value that satisfies the toe-movement criteria, you have a suitable pile embedment depth. The total pile length is then $L_p = L'$ + pile length above soil line.

16-15.9 Pile Constants for Pile Group Analyses

The lateral pile program B-5 can be used to obtain the pile constants needed for the group analysis of Chap. 18. Figure 16-19 illustrates how the node displacements are specified in order to obtain the required computer output. Figure E16-13*c* illustrates how the output is plotted to obtain curve slopes that are the desired constants. The units of these constants produce either shear springs (translation for P/δ) or rotational springs (M/θ). The specific procedure for a given pile is outlined in Example 16-13 following. The general procedure is (*for either partially or fully embedded piles*) to select one of the two axes and do the following:

1. Fix the pile head against translation [NZX = 1 and NXZERO(1) = 2 since NP = 2 is the translation NP at node 1]. Apply a series of moments for NP = 1 (or only one moment if a linear model is assumed). The computer output gives the corresponding rotations at node 1, which are plotted versus M. Also plot the unbalanced force (required to restrain translation) versus M as in Fig. E16-13*c* curve *A*. The slopes of these two curves are two of the required pile constants.
2. Fix the pile head against rotation [NZX = 1, NXZERO(1) = 1]. Apply a series of lateral loads for NP = 2 (or a single load if a linear model is assumed). The computer outputs translations at node 1, which are plotted versus input load P. Also plot the "near" end moment in element 1 (the rotation-fixed node) versus P. These two plots are shown in Fig. E16-13*c* curve *B*. The slopes of these two curves are also two of the required pile constants.
3. If the pile is round, the preceding two items complete the necessary computer usage since either axis gives the same output. If the pile is rectangular or an **HP** pile, one set of data

(for four constants) uses the moment of inertia about the x axis and a second set (the other four constants) uses the moment of inertia about the y axis.

4. Strictly, there will be a set of constants for each of the corner, side, front, interior, and rear piles (including batter effects) in a pile group, although some of the constants may be the same for several piles depending on the group geometry. The reason is that the lateral soil modulus k_s will be different for the several piles (although many analyses have been done using a single k_s and set of pile constants for the group). A single k_s is used for Example 16-13 and for the group examples in Chap. 18 to save text space and make the examples easier to follow.

16-16 LATERALLY LOADED PILE EXAMPLES

The following several examples will illustrate computing k_s for a laterally loaded pile and using your program FADBEMLP to analyze lateral piles.

Example 16-10.

Given. A soft silty clay with average $q_u = 47.5$ kPa and, from a consolidation test, $m_v = 5.32 \times 10^{-5}$ m^2/kN. An **HP** 310 × 174 pile ($d = 324$; $b = 327$ mm; and $I_x = 394 \times 10^{-6}$ m^4) is to be used.

Required. What is the lateral k_s by Vesić's Eq. (9-6) and Bowles' method?

Solution.

a. Use Vesić's Eq. (9-6) and take $\mu = 0.45$. We find

$$E_s = \frac{3(1-2\mu)}{m_v} = \frac{3(1-2\times 0.45)}{0.000\,0532} = \mathbf{5639}\text{ kPa} \qquad \text{[from Eq. (16-30)]}$$

$$E_s \approx 200 s_u = 100 q_u = 100 \times 50 = 5000\text{ kPa}$$

Use $E_s = \mathbf{5300}$ kPa

Using Eq. (9-6) with $E_s = 5300$; $E_{\text{pile}} = 200\,000$ MPa; $B = 327$ mm (0.307 m), we obtain

$$k_s B = 2 \times 0.65 \sqrt[12]{\frac{E_s B^4}{E_p I_p}} \times \frac{E_s}{1-\mu^2} = 1.3 \sqrt[12]{\frac{5300.0 \times 0.327^4}{200 \times 394}} \times \frac{5300.0}{1-0.45^2}$$

$$= 1.3 \times 0.550 \times 5300/0.798 = 4749\text{ kPa}$$

$$k_s = 4749/0.327 = \mathbf{14\,520} Z^n \text{ kN/m}^3 \qquad \text{(slight rounding)}$$

b. Using Bowles' method and $q_a = q_u$ with an SF = 3, a square pile gives $F_{w,i} = 1.0$, and doubling for side shear, $C_m = 2.0$. Then

$$k_s = F_{w,1} \times 2 \times C \times \text{SF} \times q_u = 1 \times 2 \times 40 \times 3 \times 50 = \mathbf{12\,000} Z^n \text{ kN/m}^3$$

Note that C has units of 1/m.

Check the API method where $q_{\text{ult}} = 9c = 4.5 q_u$.

$$k_s = F_{w,1} \times 2 \times C \times q_{\text{ult}} = 1 \times 2 \times 40 \times 4.5 \times 50 = \mathbf{18\,000} Z^n \text{ kN/m}^3$$

If q_u is the average for the range of the embedment depth of the pile, one would use the exponent $n = 0$.

What would you recommend for k_s for this pile(s)? The author would be reluctant to use much over **10 000**Z^n kN/m based on the range of the three computed values shown.

////

Example 16-11. Given the soil profile of Fig. E16-6 containing average blow counts for each 2.4 m (8 ft) of depth as follows: 10, 15, 20, and 25. Compute a reasonable equation in the form of

$$k_s = \text{AS} + \text{BS} * Z^n$$

Solution. Using Eq. (16-29) and converting the N values given to N_{70}, we obtain k_s at these points:

−1.2	$650 \times N = 650 \times 10(55/70) = 5100$ (rounding)
−3.6	$650 \times 15 \times 0.786 = 7600$
−6.0	$650 \times 20 \times 0.786 = 10\,200$
−8.4	$650 \times 25 \times 0.786 = 12\,700$

These values are used to plot a curve of Z versus k_s, which is approximately linear. If we extend it to $Z = 0$, the intercept is AS = 4000. With this value and at $Z = 8.4$ we solve

$$\text{AS} + \text{BS} \times Z^1 = 12\,700 = 4000 + \text{BS} \times 8.4$$
$$\text{BS} = 1036 \quad \text{(rounded)}$$

The resulting equation is

$$k_s = 4000 + 1036Z$$

In using this equation we would want to use FAC1 and FAC2 on the first two nodes since sand would have little lateral capacity at $Z = 0$.

////

Example 16-12. This and Example 16-13 require that you use program FADBEMLP on your diskette. The data set for this example is EX1612.DTA. Its use illustrates using several load cases in a single execution—four in this example.

Given. The pile-soil geometry shown in Fig. E16-12*a*, which is from a series of lateral pile tests for a lock and dam on the Arkansas River in the mid-1960s. The approximate data can be found in Alizadeh and Davisson (1970) in Fps units, but the author had access to one of the original reports provided to the U.S. Army Corps of Engineers (who built the lock and dam). The 406-mm (16-in.) diameter pile test was selected for this example. The test used four loads as given in the table on Fig. E16-12*a*.

Solution.

Step 1. Divide the pile into a number of segments. The pile was loaded 0.03 m (0.1 ft) above the ground surface, but this will be neglected. We will take the top two elements as 0.335 m and 0.3 m and increase the lengths to 0.6 for four elements, etc. as shown on the output sheet Fig. E16-12*b*. The pile moment of inertia was given in the report as 0.3489×10^{-3} m^4 (838.2 in.^{4}). The pipe being steel, $E_{\text{pile}} = 200\,000$ MPa. The length was given as 16.12 m (52.8 ft). The width is the pipe diameter, or 0.406 m.

Step 2. Estimate k_s. Use Eq. (16-26*a*) with $C_m = 2.0$; and the shape factors $F_{w,1} = 1.5$ and $F_{w,2} = 3.2$. Obtain from Table 4-4 $N_q = 23.2$ and $N_\gamma = 20.8$; use no depth or shape factors.

$$k_s = 2 \times 40(F_{w,1}\tfrac{1}{2}\gamma' BN_\gamma + F_{w,2}\gamma' N_q Z^1)$$

Loading LC	P_h, kN	Node	M_{max}, kN•m Computed	Measured
1	93.4	5	81	81
2	140.1	5	128	115
3	191.3	5	166	163
4	249.1	5	216	206

*

Node 5 = –1.835 m.
Computed moments rounded.
*Only 2 cases for Fig. E16-12b.

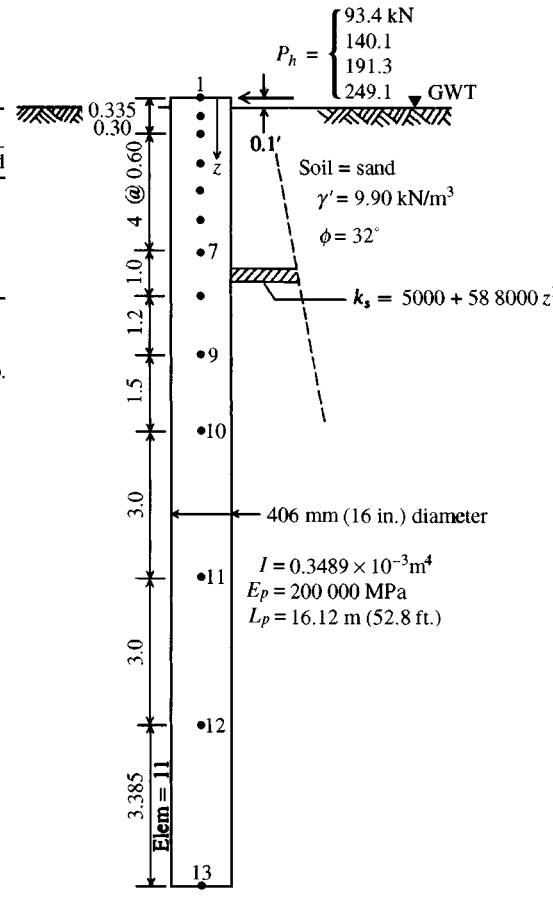

Figure E16-12a

Making substitutions ($\gamma' = 9.8$ kN/m^3), we obtain

$$k_s = 80 \times 1.5 \times 0.5 \times 9.9 \times 0.406 \times 20.8 + 80 \times 3.2 \times 9.9 \times 23.2Z^1$$

$$k_s = 5000 + 58\,800Z^1 \qquad \text{(using minor rounding)}$$

These values are input to the program (and shown on Fig. E16-12*b*). The modulus reduction factors FAC1, FAC2 = 1.0. For node 1 the lateral displacement $\delta_h = 0.00817$ m = 8.17 mm versus about 6.6 mm measured for the 140.1 kN load.

This output compares quite well both in displacements and maximum moment (and its location), and this aside from the fact the lateral modulus was computed only one time using the foregoing input. The results might be somewhat improved using an exponent of 0.4 or 0.6 instead of 0.5, but this supposition is left as a reader exercise. Certainly the output is well within the scatter one would expect in testing several piles at a site.

The file EX1612.DTA was edited to use only two load cases for text output; all four load cases are in the file for reader use.

You have a plot file option in this program by which you can save data to a disk file for later plotting using a CAD plotting program. The file contents are output to paper (but only if the plot

```
 ARKANSAS LOCK AND DAM TEST PILE NO. 2--406 MM (16-IN) PIPE
      +++++++++++++++++ THIS OUTPUT FOR DATA FILE:  EX1612.DTA

 SOLUTION FOR LATERALLY LOADED PILE--ITYPE = 1  ++++++++++

 NO OF NP =  26   NO OF ELEMENTS, NM = 12   NO OF NON-ZERO P, NNZP =  1
   NO OF LOAD CASES, NLC =  2                  NO OF CYCLES NCYC =  1
 NODE SOIL STARTS JTSOIL =  1
      NONLINEAR (IF > 0) =  0          NO OF BOUNDARY CONDIT NZX =  0
           MODULUS KCODE =  2                   LIST BAND IF > 0 =  0
                                                  IMET (SI > 0) =  1

MEMNO   NP1   NP2   NP3   NP4   LENGTH     WIDTH     INERTIA, M**4

    1     1     2     3     4      .335      .406     .34890E-03
    2     3     4     5     6      .300      .406     .34890E-03
    3     5     6     7     8      .600      .406     .34890E-03
    4     7     8     9    10      .600      .406     .34890E-03
    5     9    10    11    12      .600      .406     .34890E-03
    6    11    12    13    14      .600      .406     .34890E-03
    7    13    14    15    16     1.000      .406     .34890E-03
    8    15    16    17    18     1.200      .406     .34890E-03
    9    17    18    19    20     1.500      .406     .34890E-03
   10    19    20    21    22     3.000      .406     .34890E-03
   11    21    22    23    24     3.000      .406     .34890E-03
   12    23    24    25    26     3.385      .406     .34890E-03

 THE INITIAL INPUT P-MATRIX ENTRIES
 NP    LC     P(NP,LC)
  2     1       93.400
  2     2      140.100
 MOD OF ELASTICITY E =   200000. MPA
 GROUND NODE REDUCTION FACTORS FOR PILES, FAC1,FAC2 =    1.00    1.00
     EQUATION FOR KS =    5000.0 +    58800.0*Z**1.00

 THE NODE SOIL MODULUS, SPRINGS AND MAX DEFL:
 NODE    SOIL MODULUS    SPRING,KN/M   MAX DEFL, M
    1          5000.0          786.5         .0250
    2         24698.0         3095.3         .0250
    3         42338.0         8809.4         .0250
    4         77618.0        18907.7         .0250
    5        112898.0        27502.0         .0250
    6        148178.0        36096.2         .0250
    7        183458.0        62133.6         .0250
    8        242258.0       109943.1         .0250
    9        312818.0       174678.4         .0250
   10        401018.0       393186.8         .0250
   11        577418.0       703295.1         .0250
   12        753818.0       986845.7         .0250
   13        952855.9       609169.8         .0000
```

Figure E16-12*b*

BASE SUM OF NODE SPRINGS = 3134450.0 KN/M NO ADJUSTMENTS
* = NODE SPRINGS HAND COMPUTED AND INPUT

MEMBER MOMENTS, NODE REACTIONS, DEFLECTIONS, SOIL PRESSURE, AND LAST USED P-MATRIX FOR LC = 1

MEMNO	MOMENTS--NEAR END 1ST, KN-M		NODE	SPG FORCE, KN	ROT, RADS	DEFL, M	SOIL Q, KPA	P-, KN-M	P-, KN
1	-.001	29.855	1	4.28	-.00299	.00544	27.22	.00	93.40
2	-29.857	52.463	2	13.78	-.00292	.00445	109.93	.00	.00
3	-52.462	78.643	3	31.72	-.00274	.00360	152.44	.00	.00
4	-78.643	80.827	4	40.00	-.00217	.00212	164.19	.00	.00
5	-80.827	66.255	5	27.92	-.00149	.00102	114.63	.00	.00
6	-66.255	44.799	6	11.47	-.00086	.00032	47.10	.00	.00
7	-44.799	11.754	7	-2.71	-.00038	-.00004	8.02	.00	.00
8	-11.754	-4.037	8	-19.89	.00003	-.00018	43.82	.00	.00
9	4.037	-2.094	9	-14.45	.00009	-.00008	25.89	.00	.00
10	2.094	.523	10	.42	.00003	.00000	.43	.00	.00
11	-.523	-.101	11	1.08	-.00001	.00000	.89	.00	.00
12	.101	.000	12	-.24	.00000	.00000	.18	.00	.00
			13	.03	.00000	.00000	.05	.00	.00

SUM SPRING FORCES = 93.41 VS SUM APPLIED FORCES = 93.40 KN

(*) = SOIL DISPLACEMENT > XMAX SO SPRING FORCE AND Q = XMAX*VALUE ++++++++++++
NOTE THAT P-MATRIX ABOVE INCLUDES ANY EFFECTS FROM X > XMAX ON LAST CYCLE ++++++++++

MEMBER MOMENTS, NODE REACTIONS, DEFLECTIONS, SOIL PRESSURE, AND LAST USED P-MATRIX FOR LC = 2

MEMNO	MOMENTS--NEAR END 1ST, KN-M		NODE	SPG FORCE, KN	ROT, RADS	DEFL, M	SOIL Q, KPA	P-, KN-M	P-, KN
1	.001	44.782	1	6.42	-.00448	.00817	40.83	.00	140.10
2	-44.783	78.696	2	20.67	-.00437	.00668	164.90	.00	.00
3	-78.694	117.965	3	47.58	-.00411	.00540	228.66	.00	.00
4	-117.965	121.240	4	60.00	-.00326	.00317	246.29	.00	.00
5	-121.240	99.383	5	41.89	-.00223	.00152	171.95	.00	.00
6	-99.383	67.199	6	17.21	-.00129	.00048	70.65	.00	.00
7	-67.199	17.631	7	-4.07	-.00057	-.00007	12.02	.00	.00
8	-17.631	-6.056	8	-29.83	.00004	-.00027	65.73	.00	.00
9	6.056	-3.141	9	-21.68	.00014	-.00012	38.83	.00	.00
10	3.141	.784	10	.63	.00004	.00000	.65	.00	.00
11	-.784	-.151	11	1.62	-.00001	.00000	1.33	.00	.00
12	.151	.000	12	-.36	.00000	.00000	.27	.00	.00
			13	.04	.00000	.00000	.07	.00	.00

SUM SPRING FORCES = 140.12 VS SUM APPLIED FORCES = 140.10 KN

(*) = SOIL DISPLACEMENT > XMAX SO SPRING FORCE AND Q = XMAX*VALUE ++++++++++++
NOTE THAT P-MATRIX ABOVE INCLUDES ANY EFFECTS FROM X > XMAX ON LAST CYCLE ++++++++++

Figure E16-12*b* (*continued*)

file is created) with headings so you can identify the contents of the plot file. *You can use the paper output to plot shear and moment diagrams by hand if you do not have a plotting program.*

////

Example 16-13. This example illustrates how to obtain pile constants as required for the pile cap analysis using computer program FAD3DPG (B-10) or program B-28. For this analysis an **HP**360 × 174 is used with the required data of $d = 361$ mm; $b = 378$ mm; $I_x = 0.5080 \times 10^{-3}$ m^4; $I_y = 0.1840 \times 10^{-3}$ m^4. These and selected other data are shown in Fig. E16-13*a*, including the element lengths and number of nodes. The soil modulus is somewhat arbitrarily taken as

$$k_s = 200 + 50Z^{0.5}$$

partly to illustrate using an exponent less than 1.0. A spring taken as 0.9 × computed value is input for the cases of translation but no rotation (the first node spring can be anything since it is not used for the case of no translation but node rotation). The input of a spring here is to illustrate how it is done.

To obtain four sets of pile constants we must make two executions with respect to each principal axis of the pile. In one execution node 1 is fixed to allow rotation but no translation (data set EX1613A.DTA); in the second execution the node is fixed to allow translation but no rotation (EX1613B.DTA). You have this sample output set as Fig. E16-13*b*. Data sets EX1613C.DTA and EX1613D.DTA are similar but with respect to the *y* axis.

From execution of all the data sets one can plot the Curves *A* and *B* of Fig. E16-13*c*. The loads were somewhat arbitrarily chosen after making several trial runs using different values of k_s so that displacements and rotations would be large enough to produce easily identifiable data for the textbook user.

Pile input data: HP360 × 174 Obtain I_x, b_f; I_y, d from Table A-1
$E = 200\,000$ MPa
10 elements: 3 @ 1, 2 @ 1.5, 2 @ 2, and 3 @ 3 m
$K_x = 200 + 50Z^{0.5}$
REDFAC = 0.9

Comments. (see figures on pages following)

1. $P_h = 50.78$ kN is plotted versus $\delta = 0.06206$ m for one curve with respect to the *x* axis.
2. The fixed-end moment (from no rotation) of 208.483 kN · m is plotted versus $\delta = 0.06206$ m for a second curve, also with respect to the *x* axis.
3. The other two curves with respect to the *x* axis are obtained from executing data set EX1613A.DTA.

////

16-17 BUCKLING OF FULLY AND PARTIALLY EMBEDDED PILES AND POLES

The author, using a method presented by Wang (1967) for buckling of columns of variable cross section, developed a procedure that can be used to obtain the buckling load for piles either fully or partially embedded. The method is easier to use and considerably more versatile, if a computer program such as B-26 is available, than either the methods of Davisson and Robinson (1965) or those of Reddy and Valsangkar (1970). This method can be used to

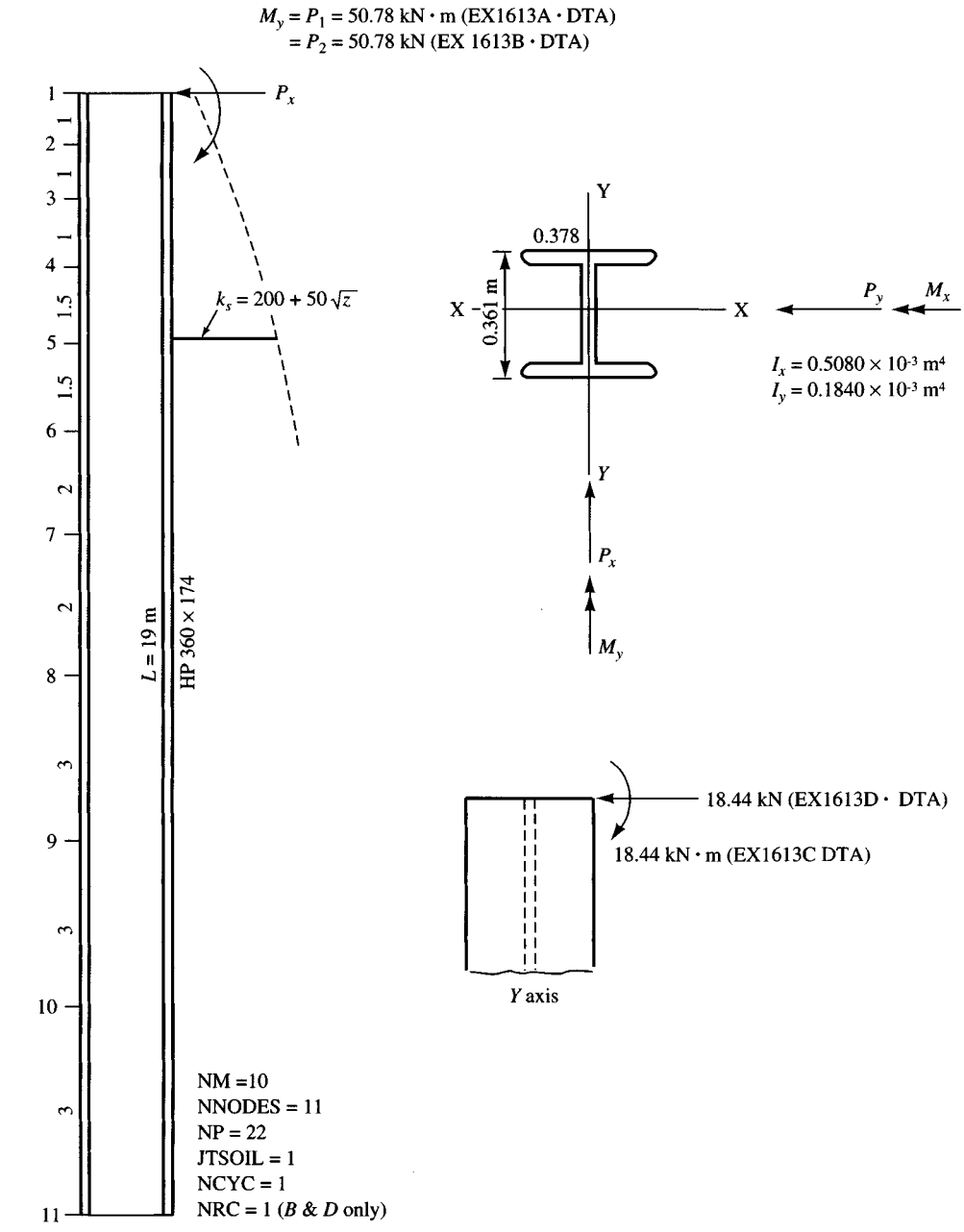

Figure E16-13*a*

```
 USING H360 X 174 TO OBTAIN PILE CONST FOR EXAM 18-7--TRANSL--NO ROTAT

     +++++++++++++++++ THIS OUTPUT FOR DATA FILE:  EX1613B.DTA


 SOLUTION FOR LATERALLY LOADED PILE--ITYPE = 1  ++++++++++


 NO OF NP =  22   NO OF ELEMENTS, NM = 10   NO OF NON-ZERO P, NNZP =  1
   NO OF LOAD CASES, NLC =  1                    NO OF CYCLES NCYC =  1
 NODE SOIL STARTS JTSOIL =  1
      NONLINEAR (IF > 0) =  0            NO OF BOUNDARY CONDIT NZX =  1
           MODULUS KCODE =  2                    LIST BAND IF > 0 =  0
                                                    IMET (SI > 0) =  1


MEMNO   NP1   NP2   NP3   NP4   LENGTH     WIDTH     INERTIA, M**4

    1     1     2     3     4     1.000      .378     .50800E-03
    2     3     4     5     6     1.000      .378     .50800E-03
    3     5     6     7     8     1.000      .378     .50800E-03
    4     7     8     9    10     1.500      .378     .50800E-03
    5     9    10    11    12     1.500      .378     .50800E-03
    6    11    12    13    14     2.000      .378     .50800E-03
    7    13    14    15    16     2.000      .378     .50800E-03
    8    15    16    17    18     3.000      .378     .50800E-03
    9    17    18    19    20     3.000      .378     .50800E-03
   10    19    20    21    22     3.000      .378     .50800E-03

 NX BOUNDARY CONDITIONS =     1

  BOUNDARY VALUES XSPEC =   .0000

 THE INITIAL INPUT P-MATRIX ENTRIES
 NP    LC      P(NP,LC)
  2    1         50.780
 MOD OF ELASTICITY E =   200000. MPA

 GROUND NODE REDUCTION FACTORS FOR PILES, FAC1,FAC2 =    1.00    1.00

     EQUATION FOR KS =     200.0 +       50.0*Z** .50

          +++++NUMBER OF NODE SPRINGS INPUT =  1
```

Figure E16-13*b*

THE NODE SOIL MODULUS, SPRINGS AND MAX DEFL:

NODE	SOIL MODULUS	SPRING,KN/M	MAX DEFL, M
1	200.0	36.8*	.0250
2	250.0	92.7	.0250
3	270.7	102.0	.0250
4	286.6	136.3	.0250
5	306.1	173.3	.0250
6	322.5	214.2	.0250
7	341.4	257.8	.0250
8	358.1	340.5	.0250
9	380.3	430.8	.0250
10	400.0	453.3	.0250
11	417.9	233.6	.0250

BASE SUM OF NODE SPRINGS = 2475.2 KN/M NO ADJUSTMENTS
* = NODE SPRINGS HAND COMPUTED AND INPUT

MEMBER MOMENTS, NODE REACTIONS, DEFLECTIONS, SOIL PRESSURE, AND LAST USED P-MATRIX FOR LC = 1

MEMNO	MOMENTS--NEAR END 1ST, KN-M		NODE	SPG FORCE, KN	ROT, RADS	DEFL, M	SOIL Q, KPA	P-, KN-M	P-, KN
1	208.483	-159.990	1	2.29	.00000	.06206	12.41	.00	50.78
2	159.988	-117.168	2	5.66	-.00181	.06112	15.28	.00	.00
3	117.161	-80.323	3	5.98	-.00318	.05859	15.86	.00	.00
4	80.320	-36.280	4	7.48	-.00415	.05489	15.73	.00	.00
5	36.281	-4.697	5	8.31	-.00501	.04794	14.67	.00	.00
6	4.698	20.219	6	8.60	-.00531	.04014	12.94	.00	.00
7	-20.218	29.876	7	7.63	-.00516	.02959	10.10	.00	.00
8	-29.876	24.209	8	6.72	-.00467	.01973	7.07	.00	.00
9	-24.209	9.535	9	3.00	-.00387	.00697	2.65	.00	.00
10	-9.535	.000	10	-1.71	-.00337	-.00378	1.51	.00	.00
			11	-3.18	-.00323	-.01361	5.69	.00	.00

SUM SPRING FORCES = 50.77 VS SUM APPLIED FORCES = 50.78 KN

(*) = SOIL DISPLACEMENT > XMAX SO SPRING FORCE AND Q = XMAX*VALUE ++++++++++++
NOTE THAT P-MATRIX ABOVE INCLUDES ANY EFFECTS FROM X > XMAX ON LAST CYCLE ++++++++++

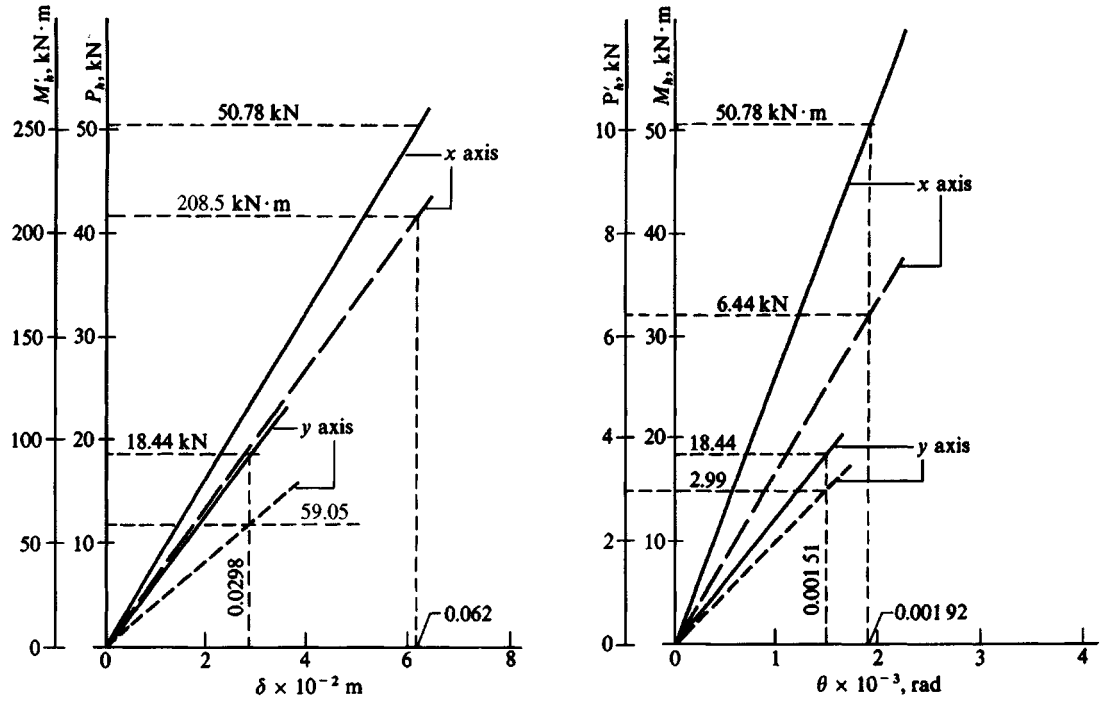

Curve A: translation but no rotation.

Curve B: rotation but no translation.

Figure E16-13*c*

analyze the buckling load of other pole structures such as steel power-transmission poles [see ASCE (1974) and Dewey and Kempner (1975)] or even columns of varying end conditions.

The method used in program B-26 consists in the following steps:

1. Build the $\mathbf{ASA}^T$ matrix and obtain the $\mathbf{ASA}^T$ inverse of the pile system for whatever the embedment geometry. It is necessary in this inverse, however, to develop the matrix such as shown in Fig. 16-23*a*. All the rotation *P–X* are coded first, then the translation *P–X* values. The resultant matrix can be partitioned as

$$\frac{P_m}{P_s} = \left|\begin{array}{c|c} A_1 & A_2 \\ \hline A_2 & A_3 \end{array}\right| \frac{X_R}{X_s}$$

2. From the lower right corner of the $\mathbf{ASA}^T$ inverse (Fig. 16-23*b*) take a new matrix called the *D* matrix (of size $NX_s \times NX_s$), identifying the translation or sidesway *X*'s as

$$X_s = \mathbf{D}P_s \qquad (a)$$

3. Develop a "second-order string matrix" considering one node deflection at a time as Fig. 16-24*b*:

$$P'_s = \mathbf{G}X_s P_{cr} \qquad (b)$$

4. Since P'_s must be equal to P_s, substitute (*b*) into (*a*), noting that P_{cr} is a critical load column matrix for which the placing order is not critical, to obtain

$$X_s = P_{cr}\{\mathbf{DG}\}X_s \qquad (16\text{-}34)$$

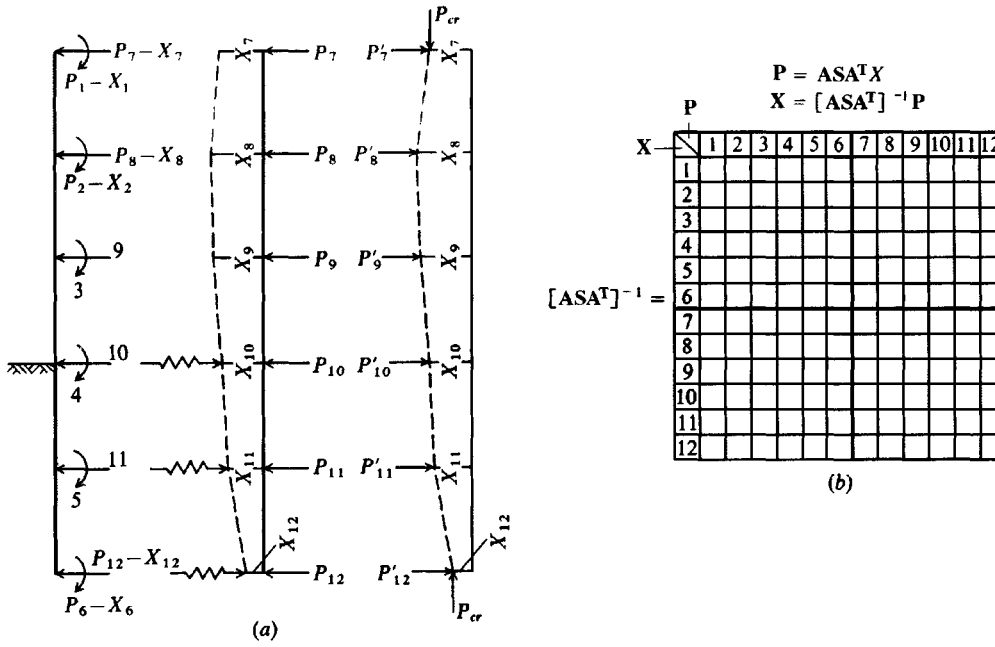

Figure 16-23 (*a*) General coding and notation used in the pile-buckling problem. The ground line can be specified at any node. Develop the $\mathbf{ASA}^T$, invert it, and obtain the **D** matrix from the location shown in (*b*).

This is an eigenvalue problem, which can be solved to some predetermined degree of exactness (say, $\Delta X = 0.000\,000\,1$) by an iteration process proposed by Wang as follows:

1. Calculate the matrix product of **DG** (size $NX_s \times NX_s$) and hold.
2. As a first approximation set the column matrix $X_s(i) = 1.00$.
3. Calculate a matrix $X'_s = \mathbf{DG}X_s$ using the value 1.00.
4. Normalize the X'_s matrix just computed by dividing all the values by the largest value.
5. Compare the differences of $X_s - X'_s \leq \Delta X$ and repeat steps 2 through 5 until the difference criterion is satisfied. On the second and later cycles the current matrix values of X_s are computed from the values of X_s from one cycle back.
6. When the convergence criterion has been satisfied, compute the buckling load using the largest current values in the X'_s and X_s matrix as

$$P_{\text{cr}} = \frac{X'_{s,\max}}{X_{s,\max}}$$

This step is simply solving Eq. (16-34) for P_{cr} with the left side being the current computation of X_s using the preceding cycle X'_s on the right side.

If higher buckling modes are desired, and one should always compute at least the first two since this method does not always give the lowest buckling load on the first mode (especially

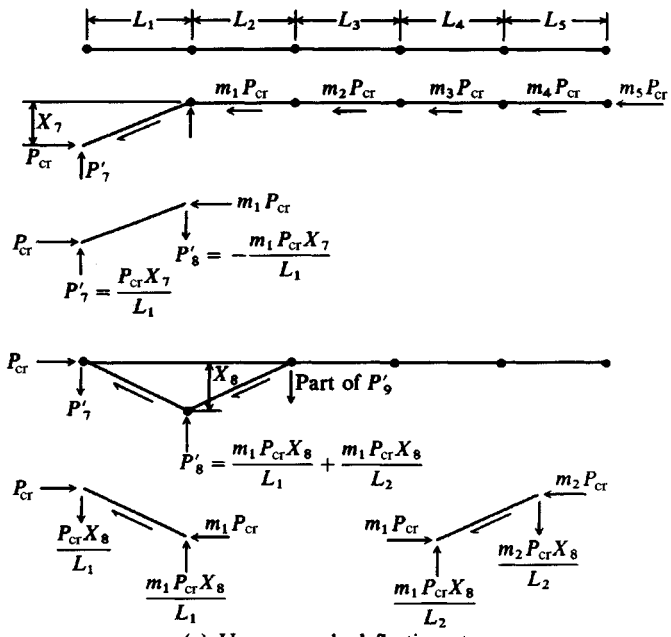

(*a*) Use one node deflection at a time to develop the G matrix.

[G] =

P'_s \ X'_s	7	8	9	10	11	12
7	$\frac{1}{L_1}$	$-\frac{m_1}{L_1}$				
8	$-\frac{1}{L_1}$	$\frac{m_1}{L_1}+\frac{m_2}{L_2}$	$-\frac{m_2}{L_2}$			
9		$-\frac{m_1}{L_2}$	$\frac{m_2}{L_2}+\frac{m_2}{L_3}$	$-\frac{m_3}{L_3}$		
10			$-\frac{m_2}{L_3}$	$\frac{m_3}{L_3}+\frac{m_3}{L_4}$	$-\frac{m_4}{L_4}$	
11				$-\frac{m_3}{L_4}$	$\frac{m_4}{L_4}+\frac{m_4}{L_5}$	$-\frac{m_5}{L_5}$
12					$-\frac{m_4}{L_5}$	$\frac{m_5}{L_5}$

(*b*) The G matrix for the number of elements given in (*a*).

Figure 16-24 The **G** matrix. For partially embedded piles m will be 1 until the soil line is encountered.

if the values are close together), one may continue steps 1 through 6 using a revised **DG** matrix for step 1 obtained from the following matrix operation:

$$\{\mathbf{DG}\}_{i+1} = \{\mathbf{DG}\}_i - \frac{1}{(P_{cr}X_s^T\mathbf{G}X_s)_i}(X_s\{\mathbf{G}X_s\}^T)_i \tag{16-35}$$

where i identifies the current mode and $i + 1$ is the next higher mode. For proof of the validity

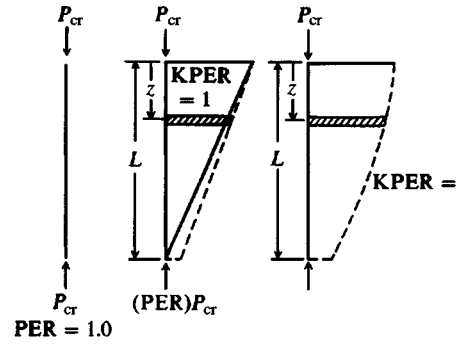

Figure 16-25 Variation of P_{cr} with depth of embedment of the pile or pole. PER = computer program variable used by the author relating the assumed amount of P_{cr} at the point. KPER = computer variable to specify type of skin resistance reduction as shown.

of Eq. (16-35) see Wang (1967). The values of P_{cr} and X are obtained as the values of the ith buckling mode.

Any variation of skin resistance to reduce P_{cr}, as illustrated in Fig. 16-25 to develop the string matrix, can be used. Note that no skin resistance is used in developing the $\mathbf{ASA}^T$ and corresponding **D** matrix since the assumption of small values of rotation and translation for vertical piles does not produce any skin-resistance effect. Note also that the lateral soil resistance effect is included only in the $\mathbf{ASA}^T$ matrix and not in the **G** matrix.

This solution can be readily compared with the theoretical solutions by applying one large soil spring at the top and bottom of the pile and no intermediate values (i.e., the pile becomes a beam column). It is possible to use a method (similar to that in your included computer program B-5) of zeroing boundary conditions, except that this will not work for the case of a fully embedded pile with top and bottom both specified zero. Satisfactory results can usually be obtained with 8 to 15 finite elements.

Example 16-14. To illustrate pile buckling and the effect of soil on buckling of piles, the following example will be presented. Its solution requires use of program FADPILB (B-26), but you can see how buckling loads are affected by the soil from careful study of the example.

Given. A 254-mm diam × 6.35-mm wall (10 × 0.25 in.) pipe pile that is 12 m in length. It is embedded 5 m in an extremely soft soil (average q_u for full depth is only 10 kPa) with the point on rock as shown in Fig. E16-14*a*. We would like to estimate the buckling load. Assume the point carries 50 percent of the buckling load (side friction carries a significant amount of the load of any pile in any soil—even though this is a point-bearing design). Assume further that the side friction distribution is parabolic (KPER = 2) as shown in Fig. 16-23. The first soil spring is reduced 25 percent for driving damage.

Solution. First draw a sketch and locate the pile nodes. Note the *P–X* coding here is automatically done as in Fig. 16-23. That is, the rotation *P–X* values are numbered first, then the translation *P–X* values. The program will also compute the moment of inertia of round solid, round pipe, tapered, and square piles so all you have to input (in this case) is the diameter and wall thickness.

We will have to input k_s, and we will use Eq. (16-26*b*) and not use the N_q-term, giving

$$k_s = F_{w,1} \times \mathrm{SFC}_m C \times q_a = 1.3 \times 3 \times 2 \times 40 \times 10 = \mathbf{3100}\ \mathrm{kN/m^3} \qquad \text{(rounded)}$$

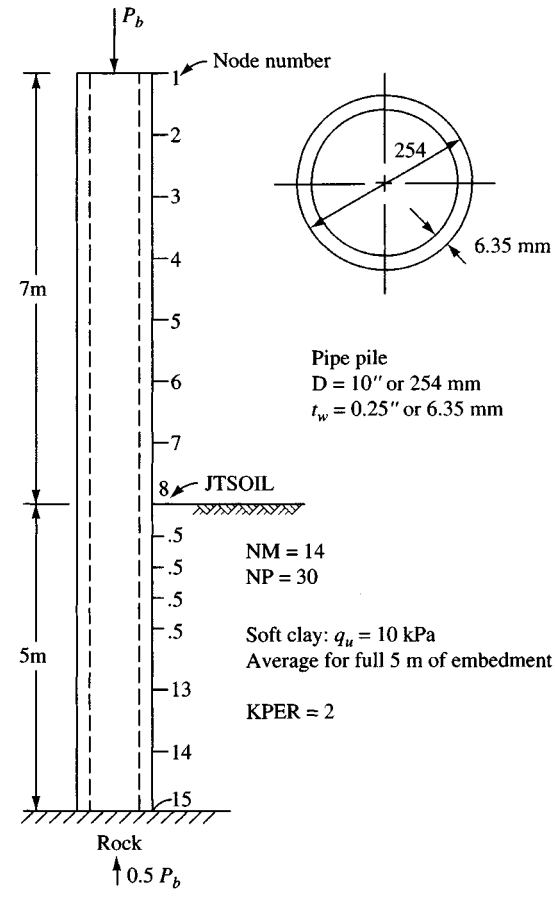

Figure E16-14*a*

The resulting computer output is shown on Fig. E16-14*b*. The *Euler load* shown is for a column fixed at the ground line (making the effective column length 14 m). The Euler equation used is

$$P_{cr} = \frac{\pi^2 EI}{kL^2}$$

where k = 1 for members pinned on each end; = 2 for members fixed on one end; = 0.5 for members fixed on both ends

L = length of column or member

Other terms have been previously defined.

The program uses JTSOIL; when it is 1 (fully embedded pile) the Euler critical load is computed for a column pinned at each end. Of course, if $k_s = 0$ the program inputs lateral node springs $K_i = 0$ so it is actually a column pinned at each end.

The program allows the user to specify boundary cases of fixing one or more nodes, however, in the case of columns one of the nodes should be fixed by inputting a very large spring.

An alternate Euler load for this example would be for a column that is fixed on one end but 12 m in length (effective length = 24 m). Inspection of the Euler load of 381.7 kN versus the computed buckling (or critical) load of 198.0 kN (first mode) seems reasonable. We would expect a partially

```
   254 MM X 6.35 MM TW 12 M L X 5 M EMBEDDED IN SOFT CLAY

          +++++++++ NAME OF DATA FILE USED FOR THIS EXECUTION:  EX1614.DTA

  DIAMETER OF ROUND SECTION =      .25400  M   WALL THICK =  .006350  M

     NO OF PILE ELEMENTS = 14
        NODE SOIL STARTS =  8                NO OF BUCKLING MODES REQD =  2
      PERCENT POINT LOAD =  50.00 %        NO OF NODES W/SPRINGS INPUT =  0
  GROUND LINE REDUCT FAC =   .750
   MODULUS OF ELASTICITY =    200000. MPA            TOTAL PILE LENGTH =   12.00  M

  PARABOLIC SKIN RESISTANCE REDUCTION--KPER = 2

  PILE EMBEDMENT DEPTH, DEMB =   5.00  M
    EMBED DEPTH SOIL MOD, KS =   3120.000 +       .000Z**1.000 KN/M**3

               +++++++EULER BUCKLING LOAD =        381.7   KN
                      BASED ON AVERAGE I =   .000038 M**4
             LENGTH (OR L ABOVE GROUND) USED =     7.00  M
```

MEMNO	NP1	NP2	NP3	NP4	ELEM L	WIDTH	I, M**4	NODE	SOIL MOD	SOIL SPRNG	ELEM FRIC
1	1	2	16	17	1.000	.000	.37900E-04	1	.0	.0	1.000
2	2	3	17	18	1.000	.000	.37900E-04	2	.0	.0	1.000
3	3	4	18	19	1.000	.000	.37900E-04	3	.0	.0	1.000
4	4	5	19	20	1.000	.000	.37900E-04	4	.0	.0	1.000
5	5	6	20	21	1.000	.000	.37900E-04	5	.0	.0	1.000
6	6	7	21	22	1.000	.000	.37900E-04	6	.0	.0	1.000
7	7	8	22	23	1.000	.000	.37900E-04	7	.0	.0	1.000
8	8	9	23	24	.500	.254	.37900E-04	8	3120.0	148.6$	1.000
9	9	10	24	25	.500	.254	.37900E-04	9	3120.0	396.2	.995
10	10	11	25	26	.500	.254	.37900E-04	10	3120.0	396.2	.980
11	11	12	26	27	.500	.254	.37900E-04	11	3120.0	396.2	.955
12	12	13	27	28	1.000	.254	.37900E-04	12	3120.0	594.4	.920
13	13	14	28	29	1.000	.254	.37900E-04	13	3120.0	792.5	.820
14	14	15	29	30	1.000	.254	.37900E-04	14	3120.0	792.5	.680
								15	3120.0	396.2	.500

```
  $ = NODE SPRING REDUCED BY FAC = .750

  THE BUCKLING MODE SHOWN ON OUTPUT IS USED AS A COUNTER--INSPECTION
   OF THE UNIT DEFLECTIONS WILL GIVE THE CURRENT BUCKLING MODE

  THE BUCKLING LOAD IS      198.0   KN FOR MODE  1 AFTER    8  ITERATIONS

  THE BUCKLING LOAD IS     1712.1   KN FOR MODE  2 AFTER   19  ITERATIONS

        NODE DISPLACEMENTS--MAXIMUM OF 3 OUTPUT
  MODE NO =          1                    2
  NODE       ACTUAL    NORMALIZED       ACTUAL    NORMALIZED
      1      .00505      1.00000        .00043       .51830
      2      .00424       .83892        .00054       .74109
      3      .00344       .68203        .00062       .91452
      4      .00269       .53341        .00065      1.00000
      5      .00200       .39693        .00062       .97812
      6      .00139       .27613        .00053       .85291
      7      .00088       .17416        .00040       .65099
      8      .00047       .09366        .00025       .41577
      9      .00031       .06211        .00018       .30146
     10      .00018       .03639        .00012       .19675
     11      .00008       .01605        .00006       .10472
     12      .00000       .00038        .00002       .02638
     13     -.00010      -.02046       -.00006      -.09345
     14     -.00017      -.03315       -.00011      -.17971
     15     -.00022      -.04303       -.00015      -.25211
```

Figure E16-14*b*

embedded pile in a very soft soil not to have a buckling load as large as the Euler load of the free-standing part fixed on one end. The computed buckling load of 198 kN should be larger than that of a 12-m column fixed on only one end. This idea is left for the reader to check.

The critical buckling load of 1712.1 kN for the second mode is larger than the first mode. This increase is generally the case, but if the second mode is smaller than the first, then the second buckling mode governs. You should always obtain two buckling modes using a program such as this.

////

PROBLEMS

Few answers are provided since a major part of pile design is selection of parameters. When parameters are provided all one does is solve a given equation.

16-1. A 460-mm diameter pipe pile is driven closed-end 15 m into a cohesionless soil with an estimated ϕ angle of 34°. The soil has a $\gamma_{wet} = 16.50$ kN/m^3 and $\gamma' = 8.60$ kN/m^3. The GWT is 6 m below the ground surface. Estimate the ultimate pile capacity P_u using the β method and friction angle $\delta = 22°$.

Answer: $P_u \approx 510$ kN (using $K = 1.5K_o$)

16-2. A **HP**360 × 152 pile is driven into a cohesionless soil with a ϕ angle = 34°. The soil has $\gamma_{wet} = 17.3$ kN/m^3; $\gamma' = 10.1$ kN/m^3 and the GWT is 3 m below the ground surface. Estimate the pile capacity P_u using a pile length of 16 m, the β method, and $\delta = 22°$ soil-to-steel and 26° soil-to-soil (in web zone). Use $K = 1.0$.

16-3. A pile is driven through a soft cohesive deposit overlying a stiff clay. The GWT is 5 m below the ground surface and the stiff clay is at the 8-m depth. Other data:

	Soft clay	Stiff clay
γ_{wet}	17.5	19.3 kN/m^3
γ'	9.5	10.6 kN/m^3
s_u	50	165 kPa

Estimate the length of a 550-mm diam pile to carry an allowable load $P_a = 420$ kN using an SF = 4 and the λ method.

Answer: $L \approx 13$ m

16-4. Redo Problem 16-3 using an **HP**360 × 109 pile.

Answer: $L \approx 16$ to 16.5 m

16-5. A **J** taper Union Monotube pile with a top diam of 457 mm and a taper of 1 : 48 and a length of 12.2 m is driven into a medium stiff clay deposit with an average $s_u = 67$ kPa. The pile will later be filled with concrete. Estimate the ultimate capacity P_u using the α method and the API value.

16-6. A Union Monotube **F** taper shell is driven into a cohesionless deposit with an average $\phi = 34°$. The $\gamma_{wet} = 17.8$ and $\gamma' = 9.8$ kN/m^3, and the GWT is 5 m below the ground surface. The pile top diam = 460 mm and the taper is 1 : 48. For a length of 20 m what is the ultimate pile capacity using Eq. (16-19)?

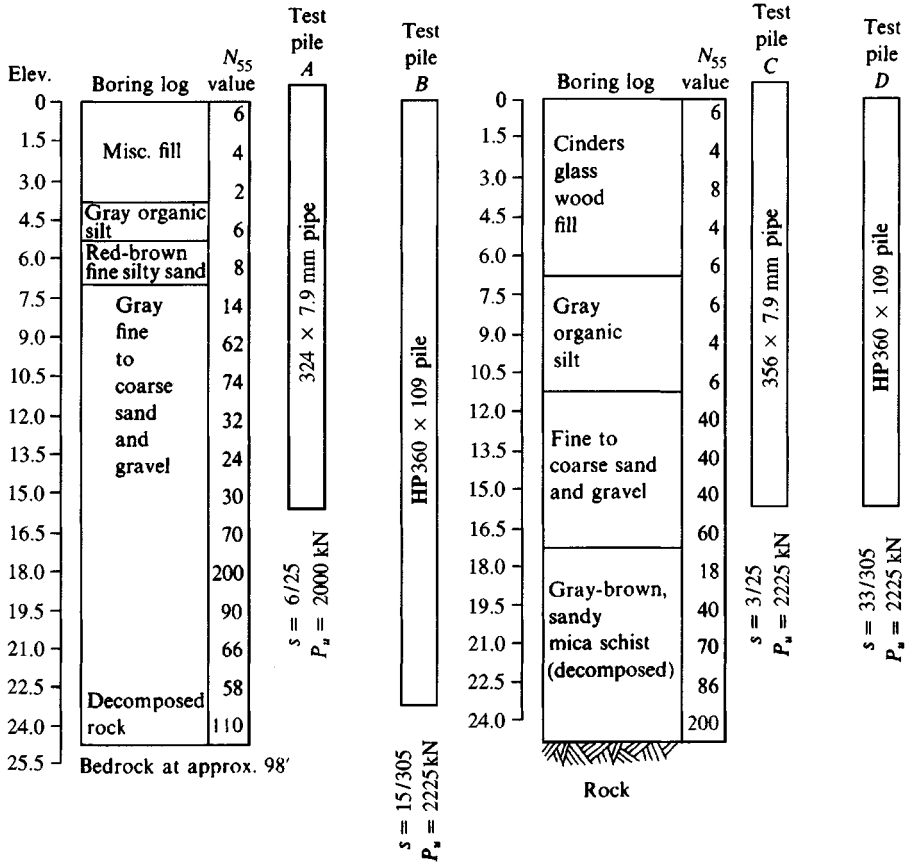

Figure P16-7

16-7. For the assigned boring log and pile (A, B, C, or D) of Fig. P16-7 estimate the pile capacity using Meyerhof's or Vesić's equations for skin resistance and point capacity. These are actual boring logs that have been converted to SI.

16-8. What is the approximate ultimate pullout resistance T_u for a tension pile in a medium dense sand with $\phi \approx 36°$, $\gamma = 18.2$ kN/m^3, and using an 800-mm diameter concrete pile with a length of 5 m (and no bell)?

16-9. For the same data of Prob. 16-8 what is T_u if the diameter is only 300 mm, both without *and* with a 1-m diameter bell?

16-10. Verify the skin resistance of the sand layers given on Fig. E16-7*b*.

16-11. Verify the skin resistance of the clay layers given on Fig. E16-7*b*. Recompute the α values. Also, what is the effect if you use a single 27-m layer with $\alpha = 1$ instead of the three layers of the example?

16-12. See if you can reproduce the settlement computed and shown on the output sheets of Fig. E16-7*b*.

16-13. Redo Example 16-8 for $P_a = 170$ kN and with $c_s = 0.22$ g·cal.

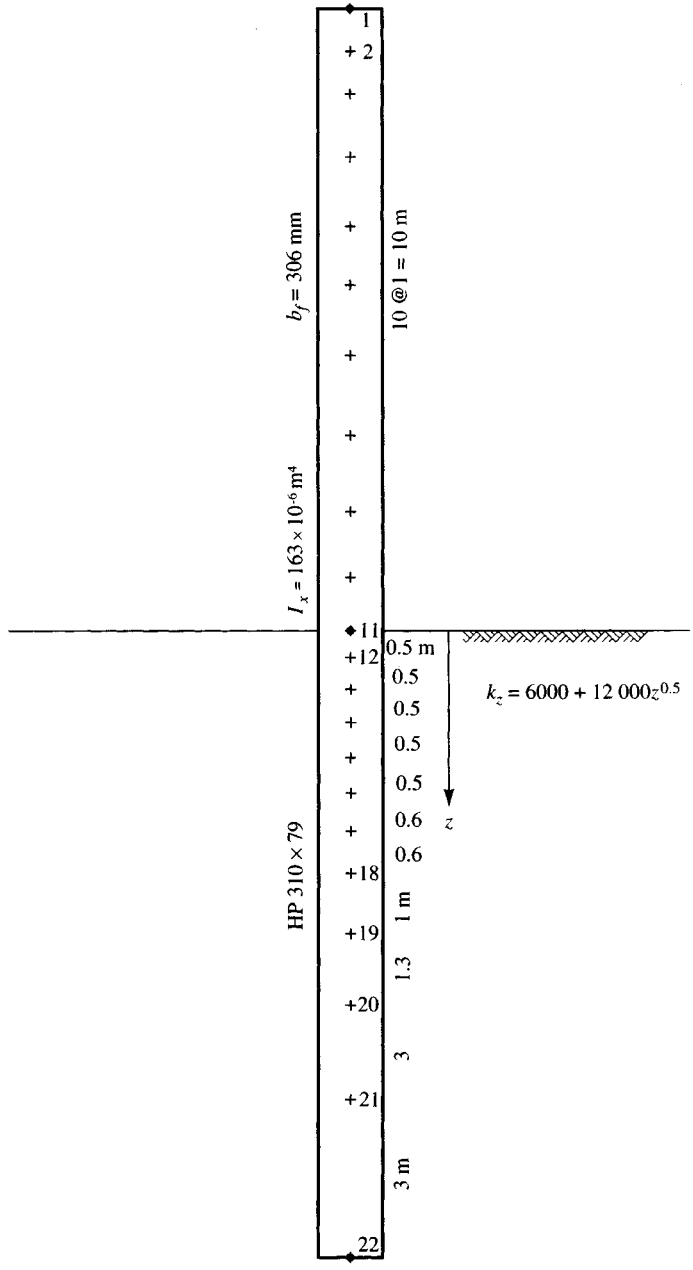

Figure P16-18

16-14. Check the side resistance of Example 16-8 and estimate if creep will be a problem. If creep is a problem, how can you reduce its effect?

16-15. What is P_u for Fig. 16-18 if the pile perimeter = 1.3 m; AE = 2600 MN; L_i = 2 m (for all three elements); and Δy_p = 3 mm? Assume the point load P_p = 40 kN.

Answer: $P_u \approx 657$ kN

16-16. Do Example 16-12 for the other two load cases and, together with those given on Fig. E16-12*b*, make a plot of P_h versus displacement δ. Also plot the shear and moment diagrams for the assigned load case. If the P_h versus δ plot is linear, what can be done to make it somewhat nonlinear since real plots of this type are seldom linear except near the origin?

16-17. Make a copy of data set EX1612.DTA as EX1612A.DTA and apply a lateral load of P_h = 40 kN at node 1. Then make a second copy and fix node 4 against translation; make a third copy and input a zero spring at node 4. Compare the results and answer the following:

a. What external cause could produce a fixed node 4?

b. What would reduce the spring at node 4 to 0?

16-18. Referring to Fig. P16-18 (see previous page), code and make an estimate of the P–Δ effect [i.e., solve with the horizontal load, then resolve where you input a moment (need a 2nd NZX) produced by the vertical load $P_v \times \Delta_{top}$ with respect to the dredge line, continue doing this until δ_{top} converges within about 0.01 m]. The two initial data sets are included as HP1619.DTA and HP1619A.DTA on your program diskette.

16-19. Redo Example 16-13 using loads as follows:

x-axis	y-axis
$P_h = M_y = 40$	$P_h = M_x = 20$ kN or kN · m

Plot the results and see if there is any difference in the computed curve slopes. Explain why there is or is not a difference.

16-20. Compute the Euler load for the pile of Example 16-14, assuming it is 14 m long and fixed at the end bearing on rock, and compare your result with the buckling load shown on Fig. E16-14*b*.

16-21. Verify that the moment of inertia for the concrete base of Problem 16-22 would be input as 1.744 ft^4 so that E_{st} = 30 000 ksi applies to all the pile elements. The E_c = 4000 ksi.

16-22. If you have the pile buckling program FADPILB (B-26) compute the buckling load for the tapered power transmission pole shown in Fig. P16-22. All element lengths are equal.

$$L = 10 \text{ ft (element lengths—use average diameter for } I)$$

$$E_{steel} = 30\,000 \text{ ksi} \qquad E_c = 4\,000 \text{ ksi}$$

Element I in order from top down:

0.07, 0.095, 0.125, 0.155, 0.190, 0.240
0.295, 0.350, 0.410, 0.475, 0.550, 0.640
0.735, 0.825, 1.744, 1.744

Use $k_s = 100 + 100Z^1$

Answer: P_{cr} = 216.5 kips (requires program B-26)

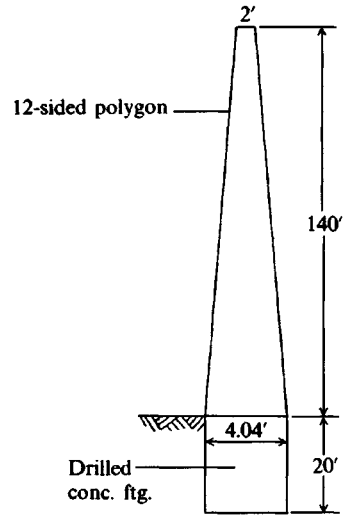

Figure P16-22

CHAPTER 17

SINGLE PILES: DYNAMIC ANALYSIS, LOAD TESTS

17-1 DYNAMIC ANALYSIS

Estimating the ultimate capacity of a pile while it is being driven into the ground at the site has resulted in numerous equations being presented to the engineering profession. Unfortunately, none of the equations is consistently reliable or reliable over an extended range of pile capacity. Because of this, the best means for predicting pile capacity by dynamic means consists in driving a pile, recording the driving history, and load testing the pile. It would be reasonable to assume that other piles with a similar driving history at that site would develop approximately the same load capacity. This chapter will examine some of the driving equations, the load test, and some of the numerous reasons why dynamic pile prediction is so poor. Some of the field problems associated with pile driving such as splicing, redriving, and heave will also be briefly examined. A brief introduction to the *wave equation* method of dynamic analysis will also be presented.

Probably one of the best sources of practical considerations in pile driving is given by Hal Hunt, *Design and Installation of Driven Pile Foundations,* published by the Associated Pile and Fitting Corp., Clifton, NJ, 1979 (217 pages).

17-2 PILE DRIVING

Piles are inserted into the ground using a pile hammer resting on or clamped to the top of the pile cap, which is, in turn, connected to the pile. The pile may contain a capblock between the cap and hammer as shown in Fig. 17-1. The cap usually rests on the pile and may be of, or contain, adequate geometry to effect a reasonably close fit. A pile cushion is sometimes used between the cap and pile (particularly concrete piles) to make the hammer impulses produce a more uniform driving pressure across the pile cross section. The pile and hammer are aligned vertically using leads suspended by a crane-type device except for the vibratory

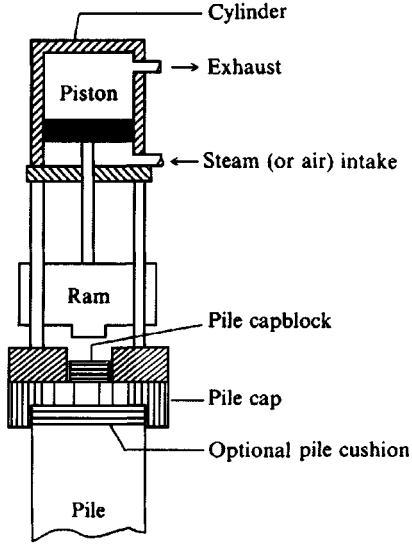

(*a*) Single-acting hammer. At bottom of stroke, intake opens with steam pressure raising ram. At top of lift steam is shut off and intake becomes exhaust, allowing ram to fall.

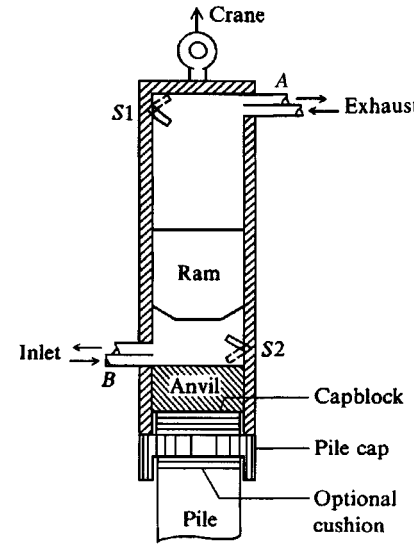

(*b*) Double-acting hammer. Ram in down position trips *S*2, which opens inlet and closes exhaust valves at *B* and shuts inlet and opens exhaust at *A*; hammer then rises from steam pressure at *B*. Ram in up position trips *S*1, which shuts inlet *B* and opens exhaust; valve *A* exhaust closes; steam enters and accelerates ram downward.

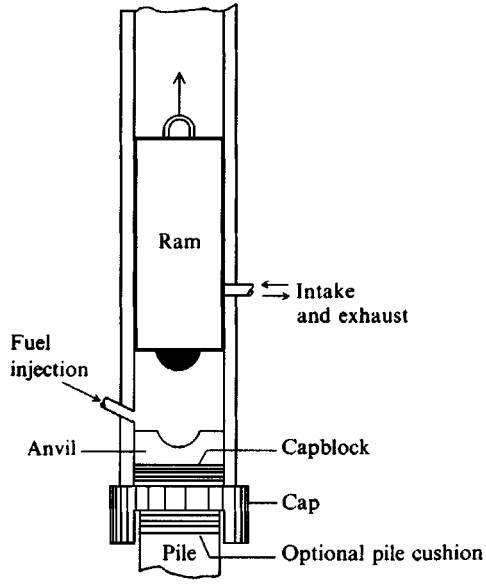

(*c*) Diesel hammer. Crane initially lifts ram. Ram is released and falls; at select point fuel is injected. Ram collides with anvil, igniting fuel. Resulting explosion drives pile and lifts ram for next cycle.

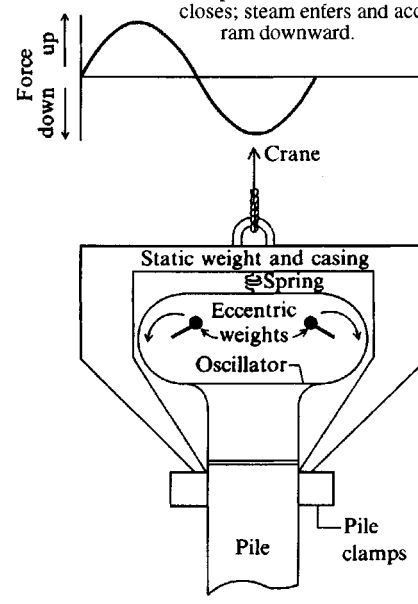

(*d*) Vibratory hammer. External power source (electric motor or electric-driven hydraulic pump) rotates eccentric weights in relative directions shown. Horizontal force components cancel—vertical force components add.

Figure 17-1 Schematics of several pile hammers.

hammers, which normally do not use leads. Piles may also be inserted by jetting or partial augering.

Leads provide free travel of the hammer as the pile penetrates the soil and are on the order of 6 m longer than the pile to provide adequate space for the hammer and other appurtenances.

Mandrels are used to assist in driving pipe piles. These devices fit inside the pipe and rest on the baseplate when the pipe is closed-end; they become the pile point for open-end piles. The mandrel becomes the driving element, which basically drags the pipe down with it during driving so that the thin pipe shell is not damaged.

Spuds are sometimes used in pile-driving operations to penetrate hard strata or seat the pile in rock. The spud may be a separate driving device or simply a massive point attached to the pile, especially for **HP** piles seated into rock. Seating a driven pile into sloping rock is a difficult task as the pile may tend to follow the rock slope. This tendency may not be readily detected without a load test. Special driving points may be required to assist in seating the point adequately into the rock slope.

Pile hammers are the devices used to impart sufficient energy to the pile so that it penetrates the soil. Several pile hammers are described in the following paragraphs.

Drop Hammers

Drop hammers are still occasionally used for small, relatively inaccessible jobs. The drop hammer consists of a metal weight fitted with a lifting hook and guides for traveling down the leads (or guides) with reasonable freedom and alignment. The hook is connected to a cable, which fits over a sheave block and is connected to a hoisting drum. The weight is lifted and tripped, freely falling to a collision with the pile. The impact drives the pile into the ground. Principal disadvantages are the slow rate of blows and length of leads required during the early driving to obtain a sufficient height of fall to drive the pile.

Single-Acting Hammers

Single-acting hammers are idealized in Fig. 17-1*a*. Steam or air pressure is used to lift the ram to the necessary height. The ram then drops by gravity onto the anvil, which transmits the impact energy to the capblock, thence to the pile. The hammer is characterized by a relatively slow rate of blows. The hammer length must be such as to obtain a reasonable impact velocity (h or height of ram fall), or else the driving energy will be small. The blow rate is considerably higher than that of the drop hammer. In general the ratio of ram weight to pile weight including appurtenances should be on the order of 0.5 to 1.0. Table A-2 in the Appendix gives typical lengths and other useful data.

Double-Acting Hammers

These hammers (Fig. 17-1*b*) use steam both to lift the ram and to accelerate it downward. Differential-acting hammers are quite similar except that more control over the steam (or air) is exerted to maintain an essentially constant pressure (nonexpansion) on the accelerating side of the ram piston. This increase in pressure results in a greater energy output per blow than with the conventional double-acting hammer. The blow rate and energy output are usually higher for double-acting or differential hammers (at least for the same ram weight), but steam consumption is also higher than for the single-acting hammer. The length may be a meter or more shorter for the double-acting hammer than for the single-acting hammer with length

ranges on the order of 2 to 4.5 m. The ratio of ram weight to pile weight should be between 0.50 and 1.

When compressed air instead of steam is used with single- or double-acting hammers, there is the additional problem of the system icing up at temperatures close to freezing.

Diesel Hammers

Diesel hammers (Fig. 17-1*c*) consist of a cylinder or casing, ram, anvil block, and simple fuel injection system. To start the operation, the ram is raised in the field as fuel is injected near the anvil block, then the ram is released. As the ram falls, the air and fuel compress and become hot because of the compression; when the ram is near the anvil, the heat is sufficient to ignite the air-fuel mixture. The resulting explosion (1) advances the pile and (2) lifts the ram. If the pile advance is very great as in soft soils, the ram is not lifted by the explosion sufficiently to ignite the air-fuel mixture on the next cycle, requiring that the ram be again manually lifted. It is thus evident that the hammer works most efficiently in hard soils or where the penetration is quite low (point-bearing piles when rock or hardpan is encountered) because maximum ram lift will be obtained.

Diesel hammers are highly mobile, have low fuel consumption (on the order of 4 to 16 L/hr), are lighter than steam hammers, and operate efficiently in temperatures as low as 0°C. There is no need for a steam or air supply generation unit and the resulting hoses. The diesel hammer has a length varying from about 3.5 to 8.2 m (4.5 to 6 m average). The ratio of ram weight to pile weight should be on the order of 0.25 to 1.0.

Jetting or Preaugering

A water jet is sometimes used to assist in inserting the pile into the ground. That is, a high-pressure stream of water is applied at the pile point to displace the soil. This method may be used to loosen sand or small gravel where for some reason the pile must penetrate to a greater depth in the material than necessary for point bearing. Care must be exercised that the jetting does not lower the point-bearing value. Some additional driving after the jet is halted should ensure seating the point on firm soil.

Preaugering is also sometimes used where a firm upper stratum overlies a compressible stratum, which in turn overlies firmer material into which it is desired to seat the pile point. Preaugering will reduce the driving effort through the upper firm material.

For both jetting and preaugering, considerable engineering judgment is required to model the dynamic pile capacity equations (and static equations) to the field system.

Pile Extraction

Piles may be pulled for inspection for driving damage. Sudden increases of penetration rate may be an indication of broken or badly bent piles. Pile *extractors* are devices specifically fabricated for pulling piles. Double-acting steam hammers may be turned upside down and suitably attached to the pile for the driving impulse and to a hoisting device (crane) to apply a pull at least equal to the weight of the hammer and pile. The hammer impacts loosen and lift the pile, and the crane provides a constant pull to hoist it from the hole. The lower broken part of a wooden pile (metal piles seldom break) is usually left in place, but may cause further driving problems.

Vibratory Drivers

Since about 1949 vibratory drivers have been used to insert piles. The principle of the vibratory driver is two counterrotating eccentric weights (Fig. 17-1*d*). The frequency (ranging from 0 to about 20 Hz) is readily computed using equations given in Chap. 20. The driver provides two vertical impulses of as much as 700^+ kN at amplitudes of 6 to 50 mm each revolution—one up and one down. The downward pulse acts with the pile weight to increase the apparent gravity force. The pile insertion (also for terraprobing) is accomplished by

1. The push-pull of the counterrotating weights— push (+pile weight) > pull upward
2. The conversion of the soil in the immediate vicinity of the pile to a viscous fluid

Best results using vibratory driving are obtained in cohesionless deposits. Results are fairly good in silty and clayey deposits. Impulse hammers are used in heavy clays or soils with appreciable numbers of boulders.

Three principal advantages of the vibratory driver (where soils are compatible) are these:

1. Reduced driving vibrations—the vibrations are not eliminated but they are less than using impact drivers.
2. Reduced noise.
3. Great speed of penetration—penetration rates of 50^+ mm/s are possible.

At present the ultimate pile capacity P_u for vibration-driven piles can only be estimated using static pile methods, although Davisson (1970) developed an equation that purports to estimate the capacity of the patented Bodine Resonant Driver (BRD) used principally by Raymond Concrete Pile company. Other vibratory drivers currently used include the patented vibro driver of the L. B. Foster company and a hydraulic-powered device available from McKiernan-Terry Corporation. The BRD equation (but not for tip on rock) is

$$P_u = \frac{A(\text{hp}) + Br_p}{r_p + \Omega \times S_L} \qquad \text{(lb or kN)} \tag{17-1}$$

A = 550 ft · lb/s (Fps); 0.746 kJ/s (SI)
B = hammer weight, 22 000 lb in Fps; 98 kN in SI for Bodine hammers
r_p = final rate of penetration, m/s or ft/s
Ω = frequency, Hz
S_L = loss factor, ft/cycle or m/cycle (see table following)
hp = horsepower delivered to the pile

	Loss factor for:	
	Closed-end pipe	HP piles
Soil at pipe tip	m/cycle × 10^{-3} (ft/cycle)	
Loose silt, sand, or gravel	0.244 (0.0008)	−0.213 (−0.0007)
Medium dense sand or sand and gravel	0.762 (0.0025)	0.762 (0.0025)
Dense sand or sand and gravel	2.438 (0.008)	2.134 (0.007)

Example 17-1. Use the BRD equation to estimate the dynamic pile capacity on p. 12 of *Foundation Facts* [the page following the Davisson (1970) reference]:

hp = 414 Final penetration r_p = 240 s/ft = 787.4 s/m = 0.001 27 m/s

Closed-end pipe pile 325 × 4.54 mm wall approximately 30.5 m long and filled with concrete after driving. Soil is dense coarse sand and gravel (based on SPT blow count); thus, $S_L = 2.44 \times 10^{-3}$ m/cycle from table, Ω = 126 Hz.

Substituting, and with Bodine driver, we find

$$P_u = \frac{0.746(414) + 98(0.001\,27)}{0.001\,27 + 126(0.002\,44)} = 1000 \text{ kN}$$

The load test (pipe filled with concrete) indicated P_u = 2450 kN. The pile insertion was terminated nearly on rock for which no S_L was given, and one may debate if that action affects the foregoing results. In pile driving, however, piles are often driven until the point reaches approximate refusal—this practice will always affect the final penetration rate used in Eq. (17-1). It is expected that the computed capacity of friction piles compared to load tests might be in closer agreement.

////

17-3 THE RATIONAL PILE FORMULA

Dynamic formulas have been widely used to predict pile capacity. Some means is needed in the field to determine when a pile has reached a satisfactory bearing value other than by simply driving it to some predetermined depth. Driving the pile to a predetermined depth may or may not obtain the required bearing value because of normal soil variations both laterally and vertically.

It is generally accepted that the dynamic formulas do not provide very reliable predictions. Predictions tend to improve by using a load test in conjunction with the equation to adjust the input variables. Predictions by persons with experience in a given area and using certain equipment and with a good knowledge of the input variables of weights, etc., are often considerably better than many of the predictions found in the literature where authors use the reported results of other writers in statistical types of analyses.

The basic dynamic pile capacity formula, termed the *rational pile formula,* will be derived in the following material. Nearly all the dynamic pile formulas currently used are based on this equation—generally by simplifying certain terms. The rational pile formula depends upon impulse-momentum principles.

For the derivation of the rational pile formulas, refer to Fig. 17-2 and the following list of symbols. Applicable symbols from this list are used also with the several pile formulas of the next section and in Table 17-1. The units for the symbol are in parentheses; e.g., (FTL) is the product of variables with units of force, time, and length.

A = pile cross-sectional area (L^2)
E = modulus of elasticity (FL^{-2})
e_h = hammer efficiency
E_h = manufacturer's hammer-energy rating (FL)
g = acceleration of gravity (LT^{-2})
h = height of all of ram (L)

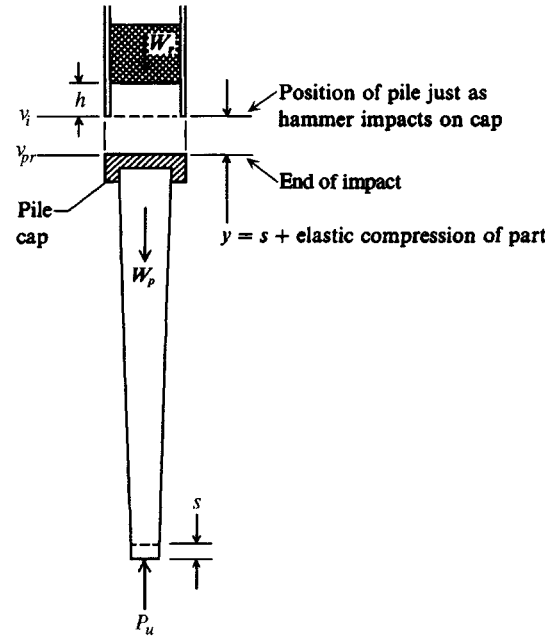

Figure 17-2 Significance of certain terms used in the dynamic pile-driving equations.

I = amount of impulse causing compression or change in momentum (FT)
k_1 = elastic compression of capblock and pile cap and is a form of P_uL/AE (L)
k_2 = elastic compression of pile and is of a form P_uL/AE (L)
k_3 = elastic compression of soil, also termed *quake* for wave equation analysis (L)
L = pile length (L)
m = mass (weight/g) (FT^2L^{-1})
M_r = ram momentum = $m_r v_i$ (FT)
n = coefficient of restitution
nI = amount of impulse causing restitution (FT)
P_u = ultimate pile capacity (F)
s = amount of point penetration per blow (L)
v_{bc} = velocity of pile and ram at end of compression period (LT^{-1})
v_i = velocity of ram at the moment of impact (LT^{-1})
v_{pr} = velocity of pile at the end of period of restitution (LT^{-1})
v_{rr} = velocity of ram at the end of the period of restitution (LT^{-1})
W_p = weight of pile including weight of pile cap, all or part of the soil "plug," driving shoe, and capblock (also includes anvil for double-acting steam hammers) (F)
W_r = weight of ram (for double-acting hammers include weight of casing) (F)

At impact, the ram momentum is

$$M_r = \frac{W_r v_i}{g}$$

TABLE 17-1

Several dynamic pile formulas (use any consistent set of units)

Many (of the more progressive) building codes no longer specify the pile-driving equation(s) to use to estimate pile capacity. A suitable equation is left to the designer (who may have to justify it to the local building official). Several other dynamic formulae are given in Young (1981).

Canadian National Building Code (use SF = 3) as used in Table 17-5 but C_3 simplified to that shown here

$$P_u = \frac{e_h E_h C_1}{s + C_2 C_3} \qquad C_1 = \frac{W_r + n^2(0.5W_p)}{W_r + W_p}$$

$$C_2 = \frac{3P_u}{2A} \qquad C_3 = \frac{L}{E} + C_4$$

$$C_4 = 0.0001 \text{ in.}^3/\text{k (Fps)}$$
$$= 3.7 \times 10^{-10} \text{m}^3/\text{kN (SI)}$$

Note that product of C_2C_3 gives units of s.

Danish formula [Olson and Flaate (1967)] (use SF = 3 to 6)

$$P_u = \frac{e_h E_h}{s + C_1} \qquad C_1 = \sqrt{\frac{e_h E_h L}{2AE}} \qquad \text{(units of } s\text{)}$$

Eytelwein formula (use SF = 6) [Chellis (1961)]

$$P_u = \frac{e_h E_h}{s + C(W_p/W_r)} \qquad C = 2.5 \text{ mm} = 0.1 \text{ in.}$$

Gates formula [Gates (1957)] (use SF = 3)

$$P_u = a\sqrt{e_h E_h}(b - \log s)$$

P_u = kips or kN $\qquad E_h$ = kips · ft or kN · m

	s	a	b
Fps	in.	27	1.0
SI	mm	104.5	2.4

e_h = 0.75 for drop and 0.85 for all other hammers

Janbu [see Olson and Flaate (1967), Mansur and Hunter (1970)] (use SF = 3 to 6)

$$P_u = \frac{e_h E_h}{k_u s} \qquad C_d = 0.75 + 0.15\frac{W_p}{W_r}$$

$$K_u = C_d\left(1 + \sqrt{1 + \frac{\lambda}{C_d}}\right) \qquad \lambda = \frac{e_h E_h L}{AEs^2}$$

Use consistent units to compute P_u. There is some disagreement of using e_h since it appears to be in C_d; however, a better statistical fit tends to be obtained by using e_h as shown.

TABLE 17-1
Several dynamic pile formulas (use any consistent set of units) *(continued)*

Modified ENR [ENR (1965)] formula (use SF = 6)

$$P_u = \left[\frac{1.25e_hE_h}{s + C}\right]\left[\frac{W_r + n^2W_p}{W_r + W_p}\right] \qquad C = 2.5 \text{ mm} = 0.1 \text{ in.}$$

AASHTO [(1990)[1]; Sec. 3.6.2 p. 251] $P_u \leq 1$ and SF = 6; primarily for timber piles]

$$P_u = \frac{2h(W_r + A_rp)}{s + C} \qquad C = 2.5 \text{ mm} = 0.1 \text{ in.}$$

For double-acting steam hammers take A_r = ram cross-sectional area and p = steam (or air) pressure; for single-acting and gravity, $A_rp = 0$. Use consistent units. Take $e_h \cong 1.0$. The above or other formulas may be used for steel and concrete piles. Set s = penetration of last 10 to 20 blows for steam hammers.

Navy-McKay formula (use SF = 6)

$$P_u = \frac{e_hE_h}{s(1 + 0.3C_1)} \qquad C_1 = \frac{W_p}{W_r}$$

Pacific Coast Uniform Building Code (PCUBC) (from Uniform Building Code,[2] Chap. 28) (use SF = 4)

$$P_u = \frac{e_hE_hC_1}{s + C_2} \qquad C_1 = \frac{W_r + kW_p}{W_r + W_p}$$

$k = 0.25$ for steel piles
$= 0.10$ for all other piles

$$C_2 = \frac{P_uL}{AE} \quad \text{(units of } s\text{)}$$

In general start with $C_2 = 0.0$ and compute value of P_u; reduce value by 25 percent; compute C_2 and a new value of P_u. Use this value of P_u to compute a new C_2, etc. until P_u used $\cong P_u$ computed.

[1]AASHTO (1990) allows any Department of Transportation–approved pile formula in addition to this one.

[2]Not in 1976 and later UBC editions; it can still be used, just not in code.

At the end of the compression period the ram momentum is

$$M_r = \frac{W_rv_i}{g} - I$$

with a velocity of

$$v_{bc} = \left(\frac{W_rv_i}{g} - I\right)\frac{g}{W_r} \tag{a}$$

If we assume at this instant the pile momentum $M_p = I$, the pile velocity is

$$v_{bc} = \frac{g}{W_p}I \tag{b}$$

Next, if we assume that the pile and ram have not separated at the end of the compression period, the instantaneous velocities of the pile and ram are equal; therefore, combining equations (*a*) and (*b*), we have

$$I = v_i\frac{W_rW_p}{g(W_r + W_p)} \tag{c}$$

At the end of the period of restitution, the momentum of the pile is

$$I + nI = \frac{W_p}{g} v_{pr} \tag{d}$$

and substituting Eq. (*c*) for I and solving for the pile velocity, we see that

$$v_{pr} = \frac{W_r + nW_r}{W_r + W_p} v_i \tag{e}$$

At the end of the period of restitution, the momentum of the ram is

$$\frac{W_r v_i}{g} - I - nI = \frac{W_r v_{rr}}{g} \tag{f}$$

Substituting for I and solving for v_{rr}, we obtain

$$v_{rr} = \frac{W_r - nW_p}{W_r + W_p} v_i \tag{g}$$

The total energy available in the pile and ram at the end of the period of restitution is

$$(\tfrac{1}{2} m v_{pr}^2)_{\text{pile}} + (\tfrac{1}{2} m v_{rr}^2)_{\text{ram}}$$

and substituting (*e*) for v_{pr} and (*g*) for v_{rr} and with some simplification one obtains

$$\frac{W_r}{2g} v_{rr}^2 + \frac{W_p}{2g} v_{pr}^2 = e_h W_r h \frac{W_r + n^2 W_p}{W_r + W_p} \tag{h}$$

If the system were 100 percent efficient, the ultimate load P_u multiplied by the point displacement s should be

$$P_u s = e_h W_r h$$

The instant pile top displacement is $s + k_1 + k_2 + k_3$, of which only s is permanent, and the actual input energy to the pile system is

$$e_h W_r h = P_u(s + k_1 + k_2 + k_3) = P_u(s + C)$$

Replacing the equivalent energy term with the equivalent from equation (*h*), we find

$$P_u = \frac{e_h W_r h}{s + C} \frac{W_r + n^2 W_p}{W_r + W_p} \tag{i}$$

Cummings (1940) correctly points out that Eq. (*h*) already includes the effects of the losses associated with k_i; however, the form of Eq. (*i*) is generally accepted and used.

The term k_2 can be taken as the elastic compression of the pile $P_u L/AE$ with the corresponding strain energy of $P_u^2 L/2AE$.

Rewriting Eq. (*i*) and factoring out $\frac{1}{2}$ from all the k terms for strain energy, the Hiley (1930)[1] equation is obtained:

$$P_u = \left[\frac{e_h W_r h}{s + \frac{1}{2}(k_1 + k_2 + k_3)} \right] \left[\frac{W_r + n^2 W_p}{W_r + W_p} \right] \tag{17-2}$$

[1]Cummings (1940) indicates that Redtenbacher (ca. 1859) may be the originator of this equation.

For double-acting or differential steam hammers, Chellis (1941, 1961) suggested the following form of the Hiley equation:

$$P_u = \left[\frac{e_h E_h}{s + \frac{1}{2}(k_1 + k_2 + k_3)}\right]\left[\frac{W + n^2 W_p}{W + W_p}\right] \tag{17-3}$$

According to Chellis, the manufacturer's energy rating of E_h is based on an equivalent hammer weight term W and height of ram fall h as follows:

$$E_h = Wh = (W_r + \text{weight of casing})h$$

Inspection of the derivation of the Hiley equation indicates the energy loss fraction should be modified to W as shown in Eq. (17-3) also.

A careful inspection of the Hiley equation or Eq. (*i*), together with a separation of terms, results in

$$\text{Energy in} = \text{work} + \text{impact loss} + \text{cap loss} + \text{pile loss} + \text{soil loss}$$

$$e_h W_r h = P_u s + e_h W h \frac{W_p(1 - n^2)}{W_p + W_r} + P_u k_1 + P_u k_2 + P_u k_3$$

Best results from the dynamic formula as a pile capacity prediction tool are obtained when a careful and separate assessment is made of the several loss factors.

There may be some question of the correctness of computing the strain energy k_2 based on a gradually applied P_u as $P_u^2 L/2AE$ when an impulse-type load is actually applied for which the strain energy is $P_u^2 L/AE$. Use of the given equation form seems to give an adequate estimate of the ultimate pile capacity; however, we might note that the k_2 term would not produce a great difference in P_u whether used as k_2 or the more correct value of $k_2/2$.

It is necessary to use consistent units in Eqs. (17-2) and (17-3) so that the value of P_u is obtained in the force units contained in W_r. For example, if h = ft and s = in., it is necessary to multiply by 12; if h = m and s = mm, it is necessary to multiply by 1000 to obtain the correct value of P_u.

17-4 OTHER DYNAMIC FORMULAS AND GENERAL CONSIDERATIONS

All of the dynamic pile-driving formulas except the Gates formula shown in Table 17-1 are derived from Eq. (17-2) or (17-3) by using various assumptions. The assumptions usually reflect the author's personal experiences and/or attempts to simplify the equation for practical use. Since interpretation of user experience is highly subjective and coupled with wide variability of soils and hammer conditions, the dynamic formulas do not have very good correlation with field experience—especially when used by others in different geographical areas or for statistical comparisons. Statistical comparisons are especially difficult owing to the scarcity of realistic input into the equations of hammer efficiencies, and weights of hammer and driving equipment such as caps, capblocks, and driving points and any soil "plug." For example, Chellis (1961) suggested that pile tips founded on rock or relatively impenetrable material should use a value for pile weight of $W_p/2$. This can make some, even considerable, difference in the loss factor. Also, where is the breakpoint for the factor 2? It would appear that for medium dense materials a factor of 0.75 might be used, gradually increasing to 1.00 for friction piles. Likewise, if the user does not adjust the Hiley equation to include correctly the ram and/or applicable portions of casing and anvil weights, considerable discrepancies

can result. Finally, the equations are heavily dependent on hammer efficiency, which must be estimated and which can change during driving operations on the same job.

If we define the impact term in the Hiley equation as

$$C_1 = \frac{W_r + n^2 W_p}{W_r + W_p}$$

and rearrange it to

$$C_1 = \frac{1 + n^2 W_r/W_p}{1 + W_r/W_p}$$

and take $n^2 W_r/W_p \cong 0$, we obtain

$$C_1 = \frac{1}{1 + W_r/W_p}$$

which becomes the starting point for the several formula factors.

The *Engineering News* (commonly, but incorrectly termed the ENR) formula was published in the *Engineering News* ca. 1888 (which merged with McGraw-Hill in 1917 to become the *Engineering News-Record*) and was developed for wood piles using a drop hammer with an approximate safety factor (SF) of 6. The formula has been modified for different driving equipment and is probably the most used of the several "dynamic" pile formulas. It was obtained by lumping all the elastic compression into a single factor $C = \mathbf{25}$ mm (1 in.) with $C_1 = \mathbf{1}$ to obtain for drop hammers (length units of s and h must be the same)

$$P_u = \frac{e_h W_r h}{s + 25} \tag{17-4}$$

and for steam hammers with $C = \mathbf{2.54}$ mm (0.1 in.) obtain

$$P_u = \frac{e_h W_r h}{s + 2.54} \tag{17-5}$$

Equations (17-4) and (17-5) will be called the ENR formulas.[2] A more recent ENR modification (and approximately as used in Table 17-5) is

$$P_u = \left(\frac{e_h W_r h}{s + C}\right)\left(\frac{W_r + n^2 W_p}{W_r + W_p}\right) \tag{17-6}$$

Values of k_1 for use in Eq. (17-2) or (17-3) are presented in Table 17-2. Values of hammer efficiency depend on the condition of the hammer and capblock and possibly the soil (especially for diesel hammers). In the absence of known values the following may be taken as representative of hammers in reasonably good operating condition:

Type	Efficiency e_h
Drop hammers	0.75–1.00
Single-acting hammers	0.75–0.85
Double-acting or differential	0.85
Diesel hammers	0.85–1.00

[2]The author will refer to these formulas as the ENR since this is its commonly used designation in nearly all of the technical literature on pile driving.

TABLE 17-2
Values for k_1—temporary elastic compression of pile head and cap*
For driving stresses larger than 14 MPa use k_1 in last column

Pile material	Driving stresses P/A on pile head or cap, MPa (ksi)			
	3.5 (0.5)	7.0 (1.0)	10.5 (1.5)	14 (2.0)
	k_1, mm (in.)			
Steel piling or pipe				
Directly on head	0	0	0	0
Directly on head of timber pile	1.0 (0.05)	2.0 (0.10)	3.0 (0.15)	5.0 (0.20)
Precast concrete pile with 75–100 mm packing inside cap	3.0 (0.12)	6.0 (0.25)	9.0 (0.37)	12.5 (0.50)
Steel-covered cap containing wood packing for steel **HP** or pipe piling	1.0 (0.04)	2.0 (0.05)	3.0 (0.12)	4.0 (0.16)
5-mm fiber disk between two 10-mm steel plates	0.5 (0.02)	1.0 (0.04)	1.5 (0.06)	2.0 (0.08)

*After Chellis (1961).

Chellis (1961) suggested increasing the efficiency 10 percent when using Eq. (17-2) or (17-3) to compute the driving stresses. Since the reliability of the equations is already with considerable scatter both (+) and (−), it does not appear necessary to make this adjustment.

Table 17-3 presents representative values of the coefficient of restitution n. Again the actual value will depend upon the type and condition of the capblock material and whether a pile cushion is used with concrete piles.

The term k_2 is computed as $P_u L/AE$, and one may arbitrarily take the k_3 term (quake) as

$$k_3 = 0.0 \text{ for hard soil (rock, very dense sand, and gravels)}$$
$$= 2.5 \text{ to } 5 \text{ mm } (0.1 \text{ to } 0.2 \text{ in.})$$

Equation (17-2) and following must be adjusted when piles are driven on a batter. It will be necessary to compute the axial pile component of $W_r h$ and further reduce this for the friction lost due to the normal component of the pile hammer on the leads or guide. A reasonable estimate of the friction coefficient f between hammer and leads may be taken as

$$f = \tan\theta = 0.10$$

TABLE 17-3
Representative values of coefficient of restitution for use in the dynamic pile-driving equations*

Material	n
Broomed wood	0
Wood piles (nondeteriorated end)	0.25
Compact wood cushion on steel pile	0.32
Compact wood cushion over steel pile	0.40
Steel-on-steel anvil on either steel or concrete pile	0.50
Cast-iron hammer on concrete pile without cap	0.40

*After ASCE (1941).

For small wood piles on the order of 100 to 150 mm used to support small buildings on soil with a water table at or very near the ground surface Yttrup et al. (1989) suggest using

$$P_u = \frac{0.4Wh}{s} \tag{17-7}$$

in kN when W = kN; h, s = m. This formula is applicable for drop hammers mounted on small conventional tractors.

PLUG WEIGHT. Open-end pipe piles always cut a soil plug. The plug usually does not fill the pipe when observed from above since it is much compressed both from vibration and from side friction on the interior walls. The plug weight can be estimated as

$$W_{\text{plug}} = \gamma' \times V_{\text{pipe}} \tag{17-8}$$

where V_{pipe} = internal pipe volume. This weight may be critical when the pile is nearly driven to the required depth since it is a maximum at that time.

HP piles will also have a plug of unknown dimensions; however, it would not be a great error to assume the plug length L_{plug} is one-half the embedded length of the pile (when blow counts are taken for pile capacity or for penetration resistance). The plug weight (refer also to Fig. 16-11*c*) in this case is

$$W_{\text{plug}} = 0.50L_{\text{pile}} \times b_f \times d \times \gamma' \tag{17-8a}$$

Equation (17-8*a*) includes the web t_w and flange thickness t_f in the soil volume but the plug length is an estimate, so the computation as shown is adequate.

Use effective unit weight γ' for the soil, as the water will have a flotation effect for both the soil and the pile.

The "pile" weight should be the actual weight W_p plus plug, or

$$W_p = W_p + W_{\text{plug}} \tag{17-9}$$

for use in any of the equations given that uses a pile weight term W_p.

The plug weight was not included in the past because few persons ever checked the derivation of the equations to see how the pile weight term was treated. Do not include the plug weight unless the equation you are using includes the pile weight in a term similar to the second term in the Hiley equation.

Example 17-2. Estimate the allowable pile capacity of test pile No. 1 reported by Mansur and Hunter (1970, Tables 2, 4, 5, and 6) by the *ENR, Janbu, Gates,* and *Hiley* equations (see Table 17-1) and Eq. (17-3). The data have been converted to SI for this edition. (The example in Fps is in the previous edition.)

Other data:

Hammer = Vulcan 140C	W_r = 62.3 kN (Table A-2 of Appendix)
Hammer E_h = 48.8 kN · m	e_h = 0.78 (efficiency table, this section)
Pile = 305 mm pipe	A = 11 045 mm^2 (incl. instrumentation)
Pile L_p = 16.76 m	E = 200 000 MPa $\quad \gamma_{st}$ = 77.0 kN/m^3

Pile set s = 305/16 = 19 mm/blow (given in reference)

Pile cap + capblock = 7.61 kN

Pile driven closed end—no plug

Load test: P_u = **1245.4** kN

Solution.

a. By the *ENR* equation [Eq. (17-5)] and using SF = 6:
Make a direct substitution:

$$P_{ult} = \frac{e_h W_r h}{s + 2.54} = \frac{0.78 \times 48.8 \times 1000}{19 + 2.54} = \mathbf{1245}\ \text{kN}$$

$$P_a = \frac{1245}{6} = \mathbf{295}\ \text{kN}$$

b. By the *Janbu* equation (see Table 17-1) and average SF = 4.5:

$$\text{Weight of pile (no plug)} = A_p \times \gamma_{st} \times L_p$$

$$= \frac{11\,045}{10^6} \times 77.0 \times 16.76 = \mathbf{21.86}\ \text{kN}$$

$$AE = 11\,045 \times 0.200 = 2209\ \text{MN} \qquad \text{(the } 10^6 \text{ terms cancel)}$$

$$C_d = 0.75 + 0.15 \times \frac{W_p}{W_r} = 0.75 + 0.15 \times \frac{21.86}{63.3} = 0.80$$

$$\lambda = \frac{e_h E_h L}{AE s^2} = \frac{0.78 \times 48.8 \times 16.76}{2.209 \times 19^2} = 0.80 \qquad \text{(the } 10^6 \text{ terms cancel)}$$

$$k_u = C_d\left(1 + \sqrt{1 + \frac{\lambda}{C_d}}\right) = 0.80\left(1 + \sqrt{1 + \frac{0.80}{0.80}}\right) = 1.93$$

Making the necessary substitutions, we find

$$P_u = \frac{e_h E_h}{k_u s} = \frac{0.78 \times 48.8}{1.93 \times 0.019} = \mathbf{1038}\ \text{kN}$$

$$P_a = \frac{1038}{4.5} = \mathbf{231}\ \text{kN}$$

c. By the *Gates* equation (see Table 17-1) with SF = 3:

$$P_u = a\sqrt{e_h E_h}(b - \log s) = 104.5\sqrt{e_h E_h}(2.4 - \log s)$$

Making substitutions, we obtain

$$P_u = 104.5\sqrt{0.78 \times 48.8}\,(2.4 - \log 19) = \mathbf{754}\ \text{kN}$$

$$P_a = \frac{754}{3} = \mathbf{251}\ \text{kN}$$

d. By the *Hiley* equation [Eq. (17-3)] with SF = 4:

$$P_u = \left[\frac{e_h E_h}{s + \frac{1}{2}(k_1 + k_2 + k_3)}\right]\left[\frac{W + n^2 W_p}{W + W_p}\right] \tag{17-3}$$

W = weight of hammer = 125 kN (see Table A-2 of Appendix)
Let us estimate k_1:

$$f_p = \frac{P}{A_p} = \frac{125 \times 10^3}{11\,045} = 11.3\ \text{MPa}$$

From Table 17-2 we have

k_1	f_p
3.0	10.5
5.0	14.0

Interpolating, we obtain $k_1 = 3.5$ mm.
The term $k_3 = 2.5$ mm [given in text following Eq. (17-6)]. Then we obtain k_s by trial. As a first trial, assume $P_u = 900$ kN:

$$k_2 = \frac{P_u L}{AE} = \frac{900 \times 16.76}{2209} = 6.8 \text{ mm} \qquad \text{(Note: The } 10^n \text{ terms cancel as used.)}$$

$s = 19$ mm (set per blow and given) $\qquad n = 0.5$ (Table 17-3)

Substituting values into Eq. (17-3) (1000 converts kN · m to kN · mm), we obtain

$$P_u = \left[\frac{0.78 \times 48.8 \times 1000}{19 + \frac{1}{2}(3.5 + 6.8 + 2.5)}\right]\left[\frac{125 + 0.5^2 \times 21.86}{125 + 21.86}\right]$$

$$= \frac{38\,064}{25.4} \times 0.888 = 1331 \text{ kN} \qquad \text{(rounded)}$$

Since we used $P_u = 900$ kN and computed 1331 kN, we must revise k_s to something between 900 and 1331. Try $P_u = 1260$ and by proportion obtain $k_2 = 6.8 \times 1260/900 = 9.5$ mm; again, substituting, we have

$$P_u = \frac{0.78 \times 48.8 \times 1000}{19 + \frac{1}{2}(3.5 + 9.5 + 2.5)} \times 0.888 = 1264 \text{ kN} \approx 1260 \text{ kN used} \qquad \text{(O. K.)}$$

Use $P_u = \mathbf{1260}$ kN

$P_a = 1260/4 = \mathbf{315}$ kN

Summary.

Method	P_u, kN	P_a, kN
ENR	1245	295
Janbu	1038	231
Gates	754	251
Hiley	1260	315
Measured	**1245**	

The Gates value of P_a for design would be recommended. It was developed for this range of pile capacities. It does not, however, give the best load test value. Both the ENR and Hiley equations give better values for this case. The ENR and Gates equations have the advantage of simplicity. From this spread of P_u it is evident that one should always use more than one equation to see if there are large differences. The agreement of the ENR and Hiley equations may be as much coincidence as equation accuracy.

////

Example 17-3. Estimate the ultimate pile capacity P_u of test pile No. 6 (**HP** pile) from the Mansur and Hunter (1970) reference. Use the *ENR, Janbu,* and *PCUBC* equations. The original Fps data

were soft-converted to SI by the author. Given:

HP360 × 109(14 × 73) (see Table A-1 of Appendix for pile section data)
Capblock = 5.4 kN (1220 lb) Pile length L = 12.18 m (40 ft)
Hammer: Vulcan 80C E_h = 33.12 kN · m γ' = 9.8 kN/m^3
W_r = 35.58 kN (see Table A-2 of Appendix)
Pile weight without plug = 109 × 9.807 × 12.18/1000 = 13.01 kN
Pile weight + capblock = W_p = 13.01 + 5.4 = 18.4 kN
Pile weight *with plug* = 18.4 + 0.5 × 12.18 × 0.346 × 0.371 × 9.8 = 26.2 kN
AE = 3 313 000 kN Take e_h = 0.84
Set = 17 blows/ft → 18 mm/blow Load test: **1245** kN

Solution.

a. By the *ENR* equation (Eq. 17-5), we can directly substitute C = 0.1 in. = 2.5 mm = 0.0025 m, s = 18 mm = 0.018 m, to find

$$P_u = \frac{e_h E_h}{s + C} = \frac{0.84 \times 33.12}{0.018 + 0.0025} = \mathbf{1357}\ \text{kN} > 1245$$

b. By the *Janbu* equation in Table 17-1 (but we will not use plug), we find

$$C_d = 0.75 + 0.15\frac{W_p}{W_r} = 0.75 + 0.15\frac{18.5}{35.58} = \mathbf{0.83}$$

$$\lambda = \frac{e_h E_h L}{AE s^2} = \frac{0.84 \times 33.12 \times 12.18}{3.313 \times 10^6 \times 0.018^2} = \mathbf{0.316}$$

$$k_u = C_d\left(1 + \sqrt{1 + \frac{\lambda}{C_d}}\right) = 0.83\left(1 + \sqrt{1 + \frac{0.316}{0.83}}\right) = 1.805$$

$$P_u = \frac{e_h E_h}{k_u s} = \frac{0.84 \times 33.12}{1.805 \times 0.018} = \mathbf{856}\ \text{kN} < 1245 \text{ measured}$$

c. By the *PCUBC* formula of Table 17-1, and using a pile plug, based on computation methods (*a*) and (*b*), $P_u \approx 900$ kN.

Also use k = 0.25 (from Table 17-1) to find

$$C_2 = \frac{P_u L}{AE} = \frac{900 \times 12.18}{3.313 \times 10^6} = \mathbf{0.00331}\ \text{m}$$

$$P_u = \left(\frac{e_h E_h}{s + C_2}\right)\left(\frac{W_r + kW_p}{W_r + W_p}\right) = \left(\frac{0.84 \times 33.12}{0.018 + 0.00331}\right)\left(\frac{35.58 + 0.25 \times 26.2}{35.58 + 26.2}\right)$$

$$= 1305.5 \times 0.682 = \mathbf{890}\ \text{kN} < 1245$$

Since the 900 kN assumed is sufficiently close to the 890 kN computed, we will use P_u = 890 kN.

Summary.

	P_u, kN
ENR	1357
Janbu	856
PCUBC	890
Measured	1245

The use of a soil plug for the *PCUBC* formula reduces the computed value from about 960 to 890 but appears (when compared with the other methods) to give a more reasonable value—or at least as good a value as not considering the plug.

////

17-5 RELIABILITY OF DYNAMIC PILE-DRIVING FORMULAS

Many attempts have been made to improve the reliability of the dynamic formulas. A most comprehensive pile-testing program was undertaken under the direction of the Michigan State Highway Commission (1965). In this program 88 piles were driven and tested as shown in Table 17-4 using the following hammers in the driving operations:

Vulcan No. 1, 50C and 80C
McKiernan-Terry DE30 and DE40
Raymond 15-M
Link-Belt 312 and 520
Delmag D12 and D22

From using the various dynamic formulas based on pile-load tests this study found that the true safety factors are as indicated in Table 17-5. The table indicates reasonable values for the Gates formula in the 0- to 1800-kN load range (range in which the formula was derived). The modified *Engineering News-Record* [Eq. (17-6)] formula is reasonably valid over the entire range of load tests. It was proposed from these tests that the modified *Engineering News-Record* formula as given in Eq. (17-6) be further modified as shown in Table 17-1. This study also brought to light that the amount of energy actually input to the pile for penetration is considerably different from the manufacturer's rating. The actual energy input was heavily

TABLE 17-4
Summary of piles driven in the Michigan State Highway Commission (1965) test program

Pile type	Dimensions, mm	Weight kN/m	Manufactured by	Approx. length range, m	Number driven
HP sections CBP124 (**HP** 12 × 53)	305 flange	0.773	US Steel	13.4–26.8	48
305mm OD pipe piles (mandrel-driven)	6.35 wall 5.84 wall 4.55 wall	0.458 0.433 0.330	Armco	13.4–54.3	16 6 11
Monotube piles, fluted tapered, F 12-7 (9.1 m taper section) and an N 12-7 entension	305 nominal	F 0.286 N 0.358	Union Metal Manufacturing Co.	16.8–24.4	5
Step-taper shell with 2.4 m sections	241 OD tip	Varies	Raymond International	17.7–20.4	2

TABLE 17-5
Summary of safety factor range for equations used in the Michigan Pile Test Program

Formula	Upper and lower limits of SF = P_u/P_d* Range of P_u, kips		
	0 to 900	900 to 1800	1800 to 3100
Engineering News	1.1–2.4	0.9–2.1	1.2–2.7
Hiley	1.1–4.2	3.0–6.5	4.0–9.6
Pacific Coast Uniform Building Code	2.7–5.3	4.3–9.7	8.8–16.5
Redtenbacher	1.7–3.6	2.8–6.5	6.0–10.9
Eytelwein	1.0–2.4	1.0–3.8	2.2–4.1
Navy-McKay	0.8–3.0	0.2–2.5	0.2–3.0
Rankine	0.9–1.7	1.3–2.7	2.3–5.1
Canadian National Building Code	3.2–6.0	5.1–11.1	10.1–19.9
Modified *Engineering News*	1.7–4.4	1.6–5.2	2.7–5.3
Gates	1.8–3.0	2.5–4.6	3.8–7.3
Rabe	1.0–4.8	2.4–7.0	3.2–8.0

*P_u = ultimate test load.
P_d = *design* capacity, using the safety factor recommended for the equation (values range from 2 to 6, depending on the formula).

dependent on hammer base, capblock, pile cap, and pile cap-pile interfacing. Energy input/E_h was found to range from about 26 to 65 percent—averaging less than 50.

Olson and Flaate (1967) performed a statistical analysis on some 93 other piles and concluded that the Hiley equation [Eq. (17-3)] and the Janbu and Gates formulas (Table 17-1) produced the least deviations and highest statistical correlations. This analysis was based largely on data reported in the literature; thus, some considerable estimating of pile weight, average penetration, pile cap weight, capblock weight, and condition (for n and use of a cushion for concrete piles) was required. The hammer condition, which would be particularly critical in obtaining either e_h or E_h, was generally not known.

An earlier statistical analysis of 30 piles of timber, steel, and concrete was presented by ASCE (1946, p. 28) from a previous discussion of a progress report [ASCE (1941)], which prompted Peck (1942) to propose a pile formula of $P_u = 810$ kN (91 tons). For the reported data it was statistically as good as any of the several dynamic equations used for computing the pile capacity.

A major problem with using statistical analyses primarily based on piles reported in technical literature is that although one can obtain a large data base it is not of much value. The reason is that there are not sufficient data given for the reader to make a reliable judgment of significant parameters to consider. Where the person making the analysis uses a self-generated data base (as in the case of Gates) results are generally more reliable.

17-6 THE WAVE EQUATION

The wave equation is based on using the stress wave from the hammer impact in finite-element analysis. This method was first put into practical form by Smith (1962) and later by others. A more detailed discussion of the principles and a reasonably sophisticated computer program are readily available [Bowles (1974*a*) or B-27] and will not be repeated here.

The wave equation has particular application for piling contractors in determining pile drivability with available equipment in advance of project bidding. It may also be used to estimate pile-driving stresses but does not have much application in prediction of pile capacity.

According to a pile practice survey reported by Focht and O'Neill (1985) the wave equation was used by about 30 percent of the practitioners at the time of the survey with most usage in the United States and Canada. The survey did not include contractors, so their usage is unknown. This lag between state-of-art and the state of practice is typical and results, in this case, partly from requiring both a computer and a computer program [although the latter may not be a valid reason, since this textbook included a program in 1968 as well as in Bowles (1974)]. Programs by others have been available for purchase for some time as well.

Uses of the Wave Equation

The wave equation is usually used to investigate the following problems:

1. *Pile capacity.* A plot of P_u versus set is made and the load test plotted on the curve to obtain the correct curve.
2. *Equipment compatibility.* Solutions are not obtained when the hammer is too big or too small for the pile.
3. *Driving stresses.* Plots of stress versus set can be made to ensure that the pile is not overstressed.

For the discussion to follow, refer to the list of symbols:

A = cross-sectional area of pile
C_m = relative displacement between two adjacent pile elements
D''_m = element displacement two time intervals back
D'_m = element displacement in preceding time interval DT (previous DT)
D_m = current element displacement
D_{sm} = plastic ground displacement
DT = time interval (Δt on Fig. 17-3*c*)
E_p = modulus of elasticity of pile material
F_m = element force = $C_m K_m$
F_{am} = unbalanced force in element causing acceleration ($F = ma$)
g = gravitation constant
J_i = damping constant; use J_s for side value, J_p = point value
K_m = element springs = AE/L for pile segments
K'_m = soil springs = R/quake
L_i = length of pile element (usually constant)
R_m = side or point resistance including damping effects
R'_m = amount of pile resistance (fraction of R_u) estimated to be carried by each element including the point j; for 100 percent of R_u on point j, the values of R_3 through R_{11} of Fig. 17-3*b* are zero, and $R_{12} = R_u$. Usually R_m of the first pile element is taken as zero for any assumed distribution of side and point resistance.
R_u = assumed ultimate pile capacity (same as P_u used previously)

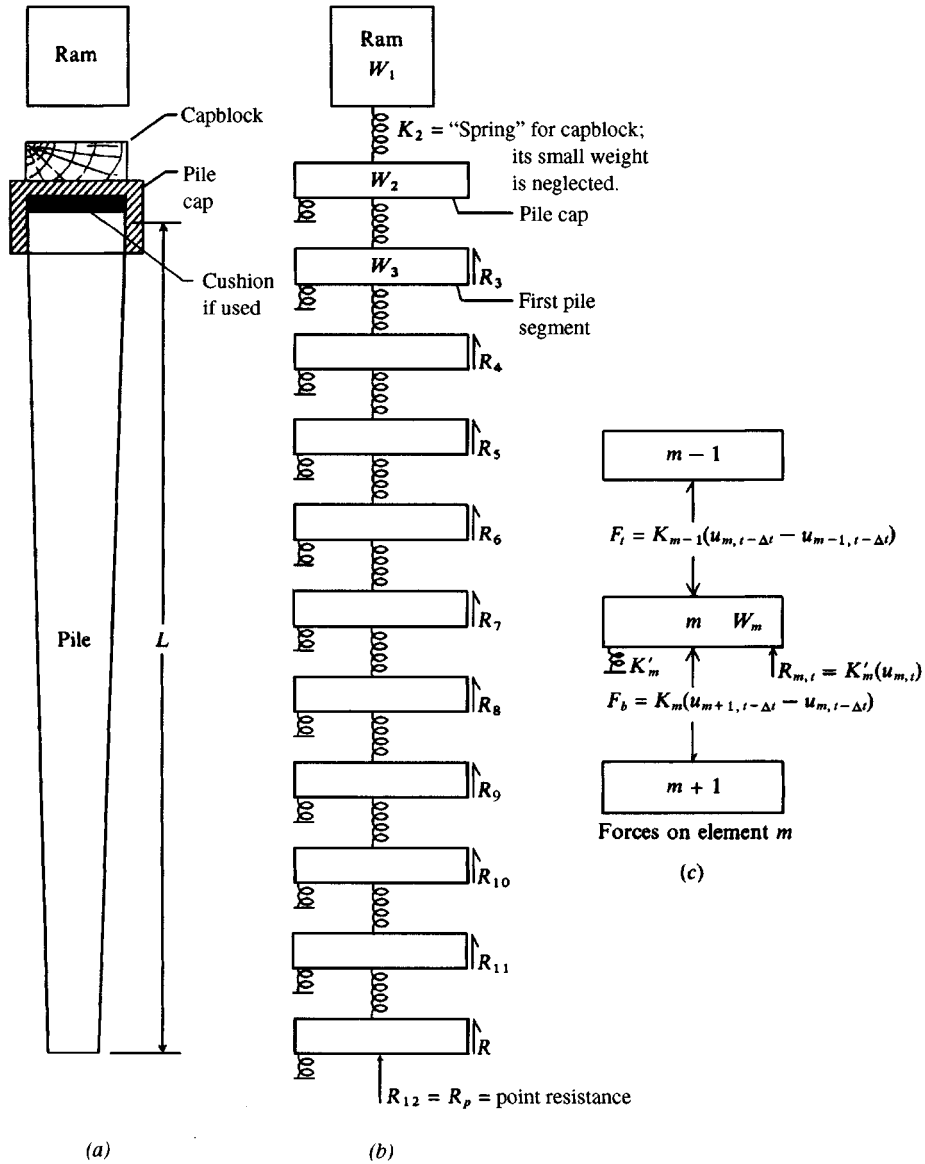

Figure 17-3 Formulation of pile into a dynamic model to solve the wave equation [*After Smith (1962)*].

t = current instant in time = number of iterations × DT
v_m = velocity of element m at DT
v'_m = velocity of element m at DT − 1
W_m = weight of pile segment m

A pile is formed into a set of discrete elements as shown in Fig. 17-3. The system is then considered in a series of separate time intervals DT chosen sufficiently small that the stress wave should just travel from one element into the next lower element during DT. Practically,

this time choice is not possible, and DT is taken as a value that usually works, as in the following table:

Element material	Length, m	Trial DT, s
Steel	2.4–3.1	0.000 25
Wood	2.4–3.1	0.000 25
Concrete	2.4–3.1	0.000 33

For shorter lengths, DT should be made correspondingly smaller. The actual time DT can be approximately computed as

$$\text{DT} = C\sqrt{\frac{W_m L_i}{AE_p g}},\ \text{s}$$

where C is 0.5 to 0.75; L_i = element length; g = 9.807 m/s^2 (in SI).

The finite-element form of the differential equation used in the wave analysis is

$$D_m = 2D'_m - D''_m + \frac{F_{am}g}{W_m}(\text{DT})^2 \tag{17-10}$$

It is not necessary to solve this equation directly, however, since the items of interest for each assumed value of ultimate pile capacity P_u are these:

1. Forces in each pile segment
2. Displacement (or set) of the pile point

The instantaneous element displacement is computed alternatively as

$$D_m = D'_m + v_m(\text{DT}) \tag{a}$$

With the instantaneous element displacements, the relative compression or tension movement can be computed between any two adjacent elements as

$$C_m = D_m - D_{m+1} \tag{b}$$

The force in segment m is

$$F_m = C_m\left(\frac{AE}{L}\right)_m = C_m K_m \tag{c}$$

The soil springs are computed as

$$K'_m = \frac{R'_m}{\text{quake}} \tag{d}$$

The side or point resistance term is obtained using damping with the side or point value of J and K' as appropriate:

$$R_m = (D_m - D_{sm})K'_m(1 + Jv_m) \tag{e}$$

The accelerating force in segment m is obtained by summing forces on the element to obtain

$$F_{am} = F_{m-1} - F_m - R_m \tag{f}$$

The element velocity is computed as

$$v_m = v'_m + \frac{F_{am}g}{W_m}(\text{DT}) \qquad (g)$$

The wave equation requires the following computation steps:

1. Compute the displacements of each element in turn using Eq. (*a*) and consistent units. At DT = 1 there is only a displacement in element $m = 1$; at DT = 2 there are two displacements; at DT = 3 there are three displacements; DT = m computes displacements in all m pile elements.
2. Compute the plastic ground displacements D_{sm}. Values will be obtained only when $D_m >$ quake or elastic ground displacement, i.e.,

$$D_{sm} = Q - D_m \qquad (\text{but } D_{sm} > 0)$$

   This step requires two subroutines—one for the point element and one using a loop for all the other pile elements.
3. Compute side and point resistance R_m (use p instead of m for point) using Eq. (*e*). Use J_s = side damping for all except the point element; use J_p = point damping for point element. This requires one equation in a DO loop and a separate point equation.
4. Compute the spring compression in each element C_m using Eq. (*b*).
5. Compute the forces in each element using C_m and the spring constant AE/L as Eq. (*c*). Forces in the capblock and pile cap are computed separately using subroutines because these elements are not usually carrying tension and because of restitution with the dissimilar materials in the capblock and cap cushion (if used).
6. Compute the velocity of each element using Eq. (*g*).
7. Set the computed D_m and v_m into storage and reidentify as one time interval back (i.e., become D'_m and v'_m so new values can be computed for D_m and v_m for the current (new) DT).
8. Repeat as necessary (generally not less than 40 and not more than 100 iterations unless a poor value of DT is chosen or the pile-hammer compatibility is poor) until
   a. All the velocities become negative, and
   b. The point-set value becomes smaller than on previous cycles(s).

The wave equation analysis requires input data as follows:

a. Height of ram fall and ram weight P (obtain from tables such as A-2). The height is either given or back-computed as $h = E_h/W_r$. This is needed to obtain the velocity of the pile cap at DT = 1 (instant of impact), which is computed as

$$v_1 = \sqrt{e_h(2gh)}$$

b. Weight of pile cap, capblock, pile segments, driving shoe, and modulus of elasticity of pile material.

c. Values of capblock and pile cushion spring constants. Table 17-6 gives values of modulus of elasticity E for several materials used for these elements for computing the spring as $K = AE/L$. Use Table 17-3 for coefficient of restitution.

TABLE 17-6
Secant modulus of elasticity values for several capblock and pile-cushion materials*

(Approximate A = 12 in. or 30 cm square and $L = A$ unless other data are available to compute spring constant of AE/L.)

Material	E, ksi	E, MPa
Micarta	450	3100
Hardwood, oak	45	310
Asbestos disks	45	310
Plywood, fir	35	240
Pine	25	170
Softwood, gum	30	205

*Data from Smith (1962) and Hirsch et al. (1970).

d. Soil properties:

Quake (same as k_3 used earlier)

Point damping J_p (PJ in computer program)

Side damping J_s (SJ in computer program)—usually about $J_p/3$

Sovinic et al. (1985) performed a number of load tests on pipe piles driven open-ended and concluded that the soil plug reduces the point and side damping values on the order of $J_p/5$ and $J_s/5$. Although they did not test any **HP** piles, it would be reasonable to apply a reduction for those as well—but not nearly so large. Smith (1962) initially did not consider soil plugs; he used an **HP**310 × 79 (**HP**12 × 53) pile as an example, but most of the pipe piles considered were apparently driven closed-end—some were mandrel-driven. It is quite possible, however, that the original Smith **HP** pile example was for illustration of the method and not one where there was a load test to compare with the computed capacity by the wave equation analysis.

Typical values (no plug) for quake and for both Q and J_p (use $J_s \cong J_p/3$) are as follows:

	Quake		Damping constant J_p*	
Soil	in.	mm	s/ft	s/m
Sand	0.05–0.20	1.0–5.0	0.10–0.20	0.33–0.66
Clay	0.05–0.30	1.0–8.0	0.40–1.00	1.30–3.30
Rock	> 0.20	> 5.0		

* Reduce damping constants when there is a soil plug.

e. Estimate of percentage of the ultimate load P_u carried by the pile point (0 to 100 percent). In general, no pile carries 100 percent of the load on the point, and one should not use more than 80 to 95 percent on the point. Placing 100 percent of the load on the point produces a discontinuity in computations, since side load from skin resistance will include damping as shown in Eq. (*f*), with no side resistance $K'_m = 0.0$.

Plots of P_u versus blows per centimeter (cm) (or inch) are made by assuming several values of P_u and using the wave equation computer program to obtain the set. The blows per centimeter N is obtained as

$$N = \frac{1}{s}$$

For any curve the percentage of P_u assumed to be carried by the pile point is held constant as, say, 25, 50, 75, 95 percent.

Plots of $1/s$ (or N) versus driving stress are obtained for any given P_u by obtaining from the computer output the maximum element force and the corresponding point set for some value of DT. Several other values of maximum element force (not necessarily in the same element) and set at other DTs are also selected so that enough points are obtained to draw a curve. This curve is somewhat erratic, owing to the mathematical model, and must be "faired" through the origin, since it is usually not possible to obtain $1/s$ values as low as 0.5, 1.0 and 1.5 or 2.0. In the region of large $1/s$ it is evident that the curve will approach some asymptotic value of driving stress. Curves of P_u versus blows per centimeter and driving stress versus blows per centimeter are shown in Fig. 17-4.

Figure 17-4 Output from the wave equation used to plot curves of $R_u = P_u$ versus 1/set and driving stresses versus 1/set for field use and using the pile data shown on the figure. *It is necessary to use cm units so that the blow/cm values are* > 1, *i.e.,* $1/2.5 = 0.4$ *but* $1/0.25 = 4$ *and can be plotted.*

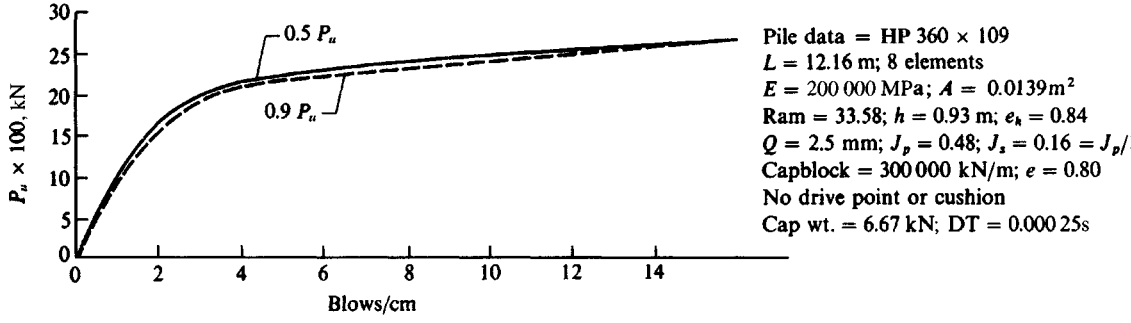

(*a*) Plot of P_u (assumed values) versus blows/cm (or 1/set, cm) for several assumed point values.

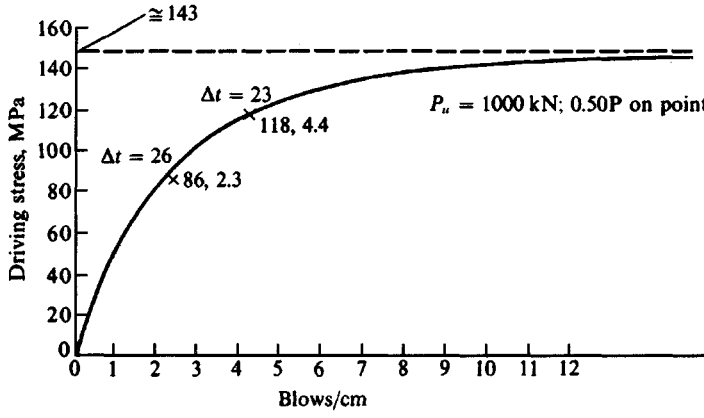

(*b*) Plot of driving stress versus blows/cm (or 1/set, cm) for the assumed value of P_u = 1000 kN at Δt values selected from the computer printout for that P_u.

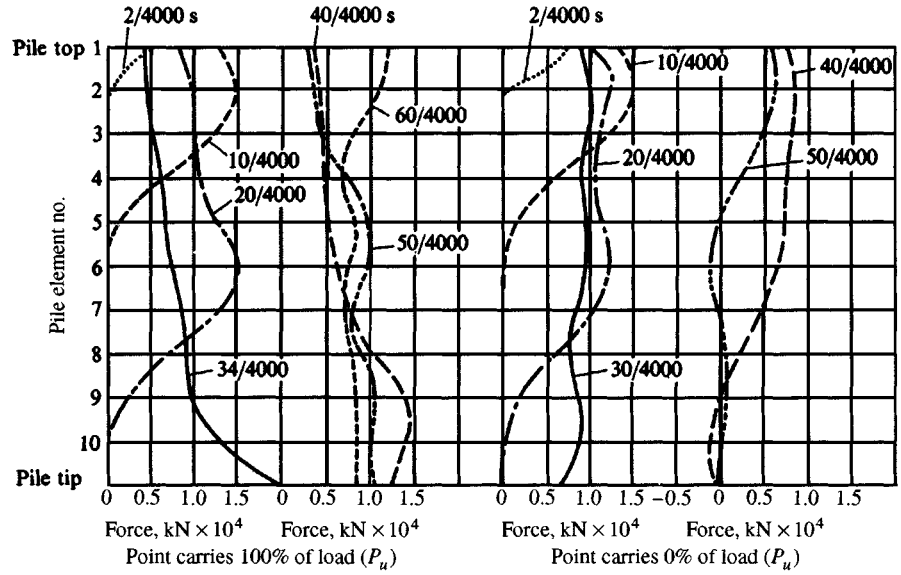

Figure 17-5 Plot of forces computed on pile elements by the wave equation using a **HP**310 × 79 pile. The plot is shown for selected time intervals. The purpose of the figure is to show in a somewhat quantitative manner the force distribution down the pile at the selected time intervals shown. The plot had to be reduced for text usage and is too small to obtain actual force values.

Traces of several stress waves down a pile are shown in Fig. 17-5 for a pile with the following data:

HP310 × 79 [**HP**12 × 53 as used by Smith (1962)]; $L_p = 30$ m;
Use 10 pile elements of 3 m each; Driving point = 0.44 kN;
Pile cap = 3.10 kN; pile cross section = 0.010 m^2;
Wt./m of pile = 0.774 kN/m (steel $\rho = 7850$ kg/m^3); $E = 200\,000$ Mpa;
Hammer: Ram = 22.2 kN; height of fall $h = 0.91$ m; $e_h = 0.80$;
$J_p = 0.50$ s/m; $J_s = 0.16$ s/m; $\Delta t = 0.00025$ s;
Capblock $n = 0.5$; capblock spring $K = 350\,000$ kN/m;
Point load = 100 and 0 percent; estimated pile load $R_u = 900$ kN

The program FADWAVE (B-27) has several output options: one is just the set and last set of computed pile element forces; a second option is that shown in Fig. 17-6; and a third option (not shown but used to plot Fig. 17-5) outputs the data of Fig. 17-6 plus the pile forces for each time increment DT (in program). The time values shown were selected, rounded, and plotted as shown in Fig. 17-5.

The output sheet of Fig. 17-6 echoes the input data (given above) and for each DT gives the set, point displacement D, maximum force in the pile F, and the element in which it occurs. For example, at time increment DT = 16 when the first point displacement occurs, the force in element 5 is 1240.3 kN. The point does not have any set until DT = 32, when it is 0.407 mm, with a point displacement $D = 2.907$ mm. The maximum pile force at this DT is in element 4 and is 964.3 kN. The maximum set = **10.417** mm and is the average of the last 6 DT computations (if you add the set values for DT = 57 through 62 and divide by 6 you

```
   TRIAL PILE HP310X79 X 30 M FOR FIG. 17-5 OF 5/E--SI

                    NAME OF DATA FILE FOR THIS EXECUTION:  FIG175A.DTA

  ++GENERAL INPUT DATA:                NCHECK = 1
          NO OF PILE SEGMENTS =  10
          LENGTH OF PILE ELEM =  3.000 M
 NO OF ELEMENTS INCL RAM & CAP =  12
        PILE MODULUS OF ELAST =  200000. MPA

                 WT/M  OF PILE =    .7740 KN      PILE X-SECT =    .0100 M **2
           ELEM WTS, KN   :   RAM =  22.200          PILE CAP =  3.1000
          WT BOT ELEM + DRIVE PT =  2.7620        WT DRIVE PT =   .4400
               HT OF RAM FALL =   .910 M          HAMMER EFF =   .80
           SIDE DAMP CONST,SJ =  .160   POINT DAMP CONST,PJ =  .500 S/M

  SPRING CONSTANT, KN/M:   CAPBLOCK =  350000.0   PILE CUSHION =        .0
                       1ST PILE SEG =  666666.6   2ND PILE SEG =  666666.6
        COEFF OF RESTIT:  CAPBLOCK =  .500         PILE CUSHION = 1.000
                          TIME INTERVAL, DT =  .0002500 SEC

   I      RU(I), KN      +++ ASSUMED ULT PILE RESIST RUTOT =    900.00 KN
   4         .000
   5       112.500
   6       112.500
   7       112.500
   8       112.500
   9       112.500
  10       112.500
  11       112.500
  12       112.500
  13         .000  ( % POINT =  .000)
    ++ SUM OF ABOVE RU(I) SHOULD =    900.00 KN


  NO OF ITERATIONS =  62    INPUT QUAKE =  2.500 MM
       AVERAGE SET = 10.417 MM   NO OF VALUES USED IN AVERAGE SET = 6

 DT=   1       2       3       4       5       6       7       8       9       10      11
SET=  .00000  .00000  .00000  .00000  .00000  .00000  .00000  .00000  .00000  .00000  .00000
 D=   .00000  .00000  .00000  .00000  .00000  .00000  .00000  .00000  .00000  .00000  .00000
 F=       .0   43.6   157.5   341.9   572.0   808.6  1013.9  1163.4  1250.3  1274.5  1260.0
 ELEM NO 13      3       3       3       3       3       3       3       3       3       4

 DT=  12      13      14      15      16      17      18      19      20      21      22
SET=  .00000  .00000  .00000  .00000  .00000  .00000  .00000  .00000  .00000  .00000  .00000
 D=   .00000  .00000  .00000  .00000  .00001  .00006  .00023  .00075  .00224  .00601  .01472
 F=  1331.0  1341.6  1302.1  1258.6  1240.3  1185.5  1171.5  1132.6  1097.5  1073.4  1075.7
 ELEM NO  4      4       4       5       5       5       6       6       7       7       4

 DT=  23      24      25      26      27      28      29      30      31      32      33
SET=  .00000  .00000  .00000  .00000  .00000  .00000  .00000  .00000  .00000  .40762 1.19905
 D=   .03326  .06968  .13620  .24950  .42996  .69938 1.07688 1.57391 2.18949 2.90762 3.69905
 F=  1074.0  1055.8  1029.8  1006.9   994.0   990.9   991.9   989.7   980.3   964.3   946.2
 ELEM NO  4      4       4       4       4       4       4       4       4       4       4

 DT=  34      35      36      37      38      39      40      41      42      43      44
SET= 2.02634 2.85062 3.63777 4.36279 5.01162 5.58071 6.07526 6.50681 6.89071 7.24339 7.57950
 D=  4.52634 5.35062 6.13777 6.86279 7.51162 8.08071 8.57526 9.00681 9.39071 9.74339 10.07950
 F=   931.1   921.3   915.8   910.7   902.7   890.3   875.0   859.4   845.5   833.0   819.0
 ELEM NO  4      4       4       4       4       4       4       4       4       4       4

 DT=  45      46      47      48      49      50      51      52      53      54      55
SET= 7.90916 8.23601 8.55677 8.86294 9.14414 9.39206 9.60339 9.78066 9.93055 10.06052 10.17556
 D= 10.40916 10.73601 11.05677 11.36294 11.64414 11.89206 12.10339 12.28066 12.43054 12.56052 12.67556
 F=   799.7   771.3   731.5   683.9   649.5   601.6   536.8   453.4   351.1   231.7   110.2
 ELEM NO  4      4       4       3       3       3       3       3       3       3       7

 DT=  56      57      58      59      60      61      62
SET= 10.27620 10.35895 10.41856 10.45084 10.45474 10.43253 10.38835
 D= 12.77620 12.85895 12.91856 12.95084 12.95474 12.93253 12.88835
 F=   126.3   121.9   133.9   136.1   116.2   195.5   279.9
 ELEM NO  7      7       6       6       6       4       4


   THE FORCES IN PILE SEGEMENTS ARE (3 = 1ST PILE SEGMENT)
 ELEM #  MAX ELEM FORCE   DT    LAST COMP FORCE, KN      LAST V(M,2), S/M
    2        1336.3        7              .0                -.981
    3        1274.5       10              .0                -.551
    4        1341.6       13            279.9               -.054
    5        1258.6       15            167.4               -.260
    6        1173.0       17             51.3               -.466
    7        1097.5       20             12.2               -.358
    8        1020.5       22            -20.3               -.229
    9         943.6       24              3.6               -.259
   10         873.2       27            -21.8               -.286
   11         782.8       29            -96.7               -.213
   12         538.6       29            -82.2               -.209
   13            .0       62              .0                -.250
```

Figure 17-6 Wave equation output (using program FADWAVE) for the **HP**310 × 79 given in TITLE line.

should obtain 10.417). An average is used based on the difference between the maximum set (occurs at DT = 60), and the program checks adjacent values and finds those within 0.12 mm of that value. All of these values are summed and divided by the number. Sometimes there are only three or four values—here there were six. The last six values are averaged for the set since these are so close that it is difficult to determine exactly what the set should be.

This large set (10.417 mm) occurs because the point is assumed not to carry any load. For the case of the point carrying 100 percent of the load the set = **4.881** mm. These are the two limiting cases—for the point carrying 20 to 80 percent of the load the point set would be somewhere between 4.881 and 10.417 mm.

To plot Fig. 17-4*a* one would need to obtain the set from several assumed values of R_u (900, 1200, 1500, ...) and for each execution obtain the blow/cm (as 1/1.0417 = 0.959). Since there is no such thing as a fraction of a blow, this should be rounded to 1 (an integer). The value would be 1/10.417 = 0.09 using mm; for the point load case we obtain 1/0.4881 = 2.04, which can be plotted as 2.0 (but not 1/4.881 = 0.20). Thus, it is necessary to plot these curves using 1/set with set in cm and not mm.

To plot the curve of Fig. 17-4*b* we must extract the set and corresponding F from calculations such as Fig. 17-6. We can use the list of maximum element forces versus DT to find worst cases, but there must be a "set" for the cases selected. For example, the maximum force in element 2 occurs at DT = 7 but at this time the set = 0. The first set of 0.407 mm = 0.0407 cm occurs at DT = 32 when the force F = 964.3 kN. This data locates a curve point at $\sigma = F/A$ = 964.3/0.0139 = 69.4 MPa versus 1/0.0407 = 24.6 → 25 (blows/cm). At DT = 43 we have σ = 833/0.0139 = 59.9 MPa versus 1/0.724 cm = 1.38 (blows/cm). We can plot the nonintegers, but the curve user can carry out only integer blow counts. The reader should obtain several additional points and draw a curve similar to Fig. 17-4*b*.

General Comments on the Wave Equation

There have been a number of modifications to the original wave equation to include what the programmer asserts to be better modeling of the soil effects on the shaft sides [$R(M)$], of the interface elements (ram, anvil, capblock, etc.) to the pile, and in the case of the diesel hammer, to model the fuel-mixture explosion. In all these cases the result is little better than the original Smith proposal (if proper allowances are made) for a number of reasons. The point and shaft resistances and quake are at best factors that make the program give a solution. The hammer impacts and resulting pile vibration will reduce the soil immediately adjacent to the pile shaft and point to a viscous fluid. The "viscosity" probably does increase with depth but this problem can be accounted for by inputting an $R(M)$ different for each pile segment. Since a wide range of quake gives solutions with not much difference, it is evident that this is a "make it work factor," although certain factors do work better than others. Those recommended by Smith work as well as any. A similar statement can be made for the side and point damping factors.

Modeling the pile-hammer interface is at best an exercise in computational tenacity. The different hammers have different anvil configurations (and dimensions), the driving cap varies widely, and the capblock "spring" varies widely (even during driving the same pile) depending on how much it has been used. Pile input energy is heavily dependent on the mechanical state of the hammer. Considering all these variables, it is suggested that the simplest

form of the wave equation is adequate. Any comparison between computer output and predicted pile capacity within a 30 percent deviation is likely to be a happy coincidence of input data [see also the comprehensive study by Tavenas and Audibert (1977)] rather than computer program sophistication. It is relatively easy with any of the wave equation programs to back-compute excellent correlation with a load test. It is less easy to predict the load test results in advance, however.

Since the wave equation is really concerned with the energy that the pile segments "receive," it should be evident that the energy input to the program is only an estimate unless it is directly measured via strain gauges or velocity- or acceleration-measuring devices attached to one or more of the upper pile segments. This approach is essentially that of Rausche and Goble (1979) where the force/acceleration measurements are then directly input into a wave equation type of program.

A number of programs purport to model the input energy of the diesel hammer using the "blast energy." Since the fuel-explosion energy is somewhat indeterminate and as previously stated the energy output depends on the mechanical condition of the hammer, it is evident that the earlier programs, which are much simpler, can as easily be used. It is only necessary to input the correct energy (i.e., adjust either ram weight or height of fall h) so that the energy output is the same as assumed for the blast force. The capblock "spring" can be adjusted to account for the interfacing of the diesel hammer elements, which might be different from a steam hammer. Again, the problem is solved if the first pile segment is instrumented to obtain the energy input.

A number of the early wave equation programs had an interface modeling error [in Smith's original paper; found by the author when developing a wave equation for the vibratory pile driver (unpublished)]. This error could affect the output by as much as 5 percent. This kind of error is difficult to find since minor variations in input and order of magnitude of the output forces are such that small errors are usually insignificant.

17-7 PILE-LOAD TESTS

The most reliable method to determine the load capacity of a pile is to load-test it. This consists in driving the pile to the design depth and applying a series of loads by some means. The usual procedure is to drive several of the piles in a group and use two or more of the adjacent piles for reactions to apply the load. A rigid beam spans across the test pile and is securely attached to the reaction piles. A large-capacity jack is placed between the reaction beam and the top of the test pile to produce the test load increments. The general setup (Fig. 17-7*c*) is similar to the plate load test shown in Fig. 4-8 with the plate being replaced by the pile. The test has been standardized as ASTM D 1143; however, local building codes may stipulate the load increments and time sequence. Somewhat similar means are used to test laterally loaded piles. Here the lateral load may be applied by jacking two adjacent piles apart or suitably connecting several piles for the lateral reaction.

Figure 17-7 illustrates typical data from a pile-load test. Figure 17-7*a* is the usual plot for a load test.

The ultimate pile load is commonly taken as the load where the load-settlement curve approaches a vertical asymptote as for the 2200 kN load shown in Fig. 17-7*a*, or as the load corresponding to some amount of butt settlement, say, 25 mm, based on the general shape of the load-settlement curve, design load of the pile, and local building code (if any). The

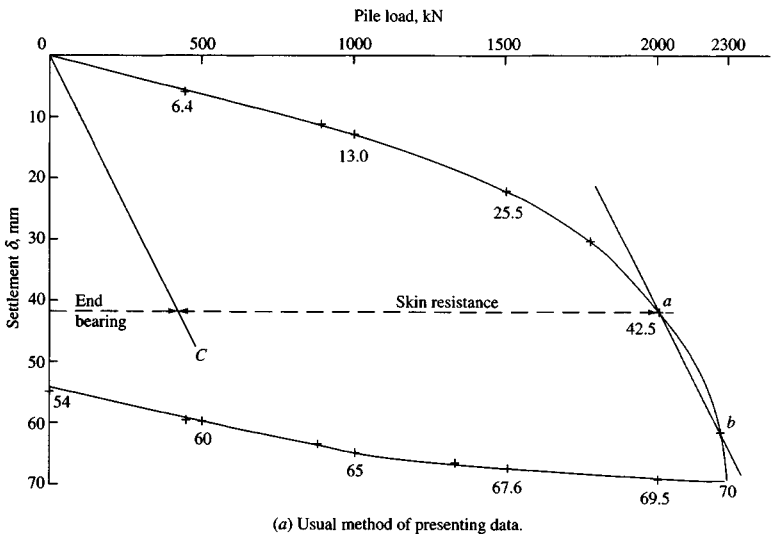

(*a*) Usual method of presenting data.

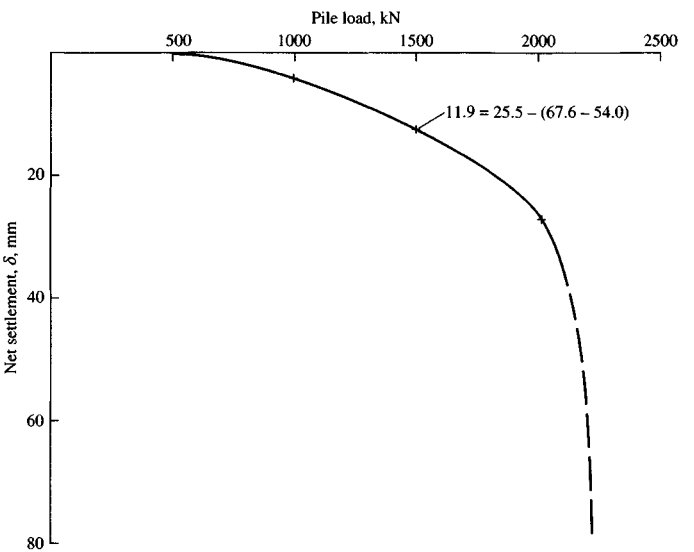

(*b*) Plot of load vs. net settlement computed as shown on the figure using data from (*a*).

Figure 17-7 Pile load-test data. This is the pile shown in Fig. P16-7 (356 diam × 7.9 mm wall × 15.24 m long). The method of estimating end bearing and side resistance shown in (*a*) was suggested by Van Weele (1957).

load-settlement curve must be drawn to a suitably large settlement scale so that the shape (and slope) is well defined. Referring to Fig. 17-7*a*, we see that reducing the vertical scale by a factor of one-half would make it very difficult to determine that the curve is becoming nearly vertical between the 2000 and 2200 kN load.

An alternative method of interpreting Fig. 17-7*a* is based on the concept that the load is carried mostly by skin resistance until the shaft slip is sufficient to mobilize the limiting value. When the limiting skin resistance is mobilized, the point load increases nearly linearly until the ultimate point capacity is reached. At this point further applied load results in direct settlement (load curve becomes vertical). Referring to Fig. 17-7*a*, these statements translate as follows:

1. From 0 to point *a* the capacity is based on the skin resistance plus any small point contribution. The skin resistance capacity is the principal load-carrying mechanism in this region. Point *a* usually requires some visual interpretation since there is seldom a sharp break in the curve.
2. From point *a* to *b* the load capacity is the sum of the limiting skin resistance (now a constant) plus the point capacity.
3. From point *b* the curve becomes vertical as the ultimate point capacity is reached. Often the vertical asymptote is anticipated (or the load to some value is adequate) and the test terminated before a "vertical" curve branch is established.

This concept was introduced by Van Weele (1957) and has since been used by others [e.g., Brierley et al. (1979), Leonards and Lovell (1979), among others]. According to Van Weele, if we draw the dashed line 0 to *c* through the origin and parallel to the point capacity region from *a* to *b*, the load-carrying components of the pile are as shown on Fig. 17-7*a*. In this figure we have at settlement $\delta = 25$ mm the load carried as follows:

Point	= 250 kN		
Skin resistance	= 1350 kN	= 1600 − 250 kN	
Total	= 1600 kN		shown on figure

Local building codes usually stipulate how the load test is to be run and interpreted and pile design loads above which a load test is required (usually $P_d > 200$ kN). For example, the Chicago building code stipulates the test as follows:

1. Apply load increments of 25 percent of the proposed working load.
2. Carry the loading to two times the proposed working load. This requires seven or eight load increments.
3. Apply the loads after a specified time lapse or after the settlement rate is some small value.
4. The allowable pile load is taken as one-half that load that causes a net settlement of not more than 1 mm/35 kN. For example, in referring to Fig. 17-7*b*, the allowable pile load is about 1100 kN (so $2 \times 1100/35 = 63$ mm versus about 70 mm measured).
5. The building codes limit the minimum value of hammer energy E_h.
6. The codes require a minimum number of test piles per project.

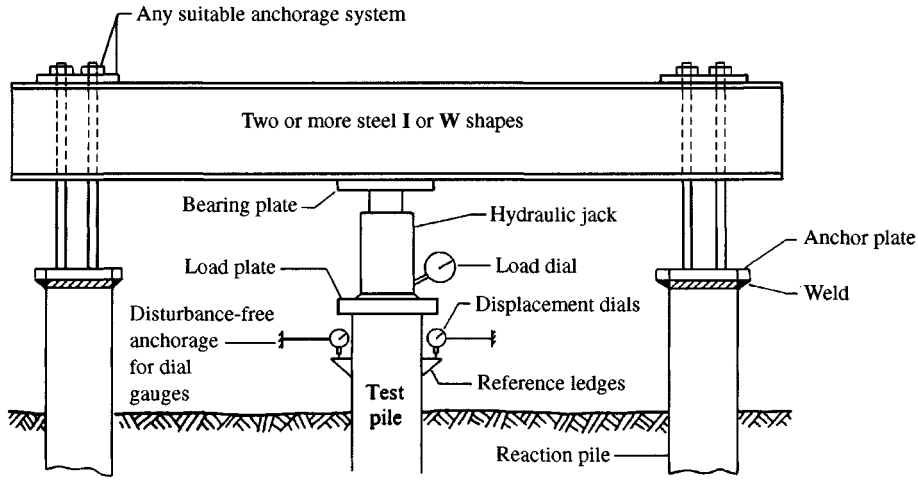

(*c*) **Typical pile load test setup using adjacent piles in group for reaction.**

Figure 17-7(*c*) Typical pile load test setup using adjacent piles in group for reaction.

Piles in *granular* soils are often tested 24 to 48 hr after driving when load test arrangements have been made. This time lapse is usually sufficient for excess pore pressures to dissipate; however, Samson and Authier (1986) show that up to a 70 percent capacity gain may occur if load tests are made two to three weeks after driving.

Piles in *cohesive* soils should be tested after sufficient lapse for excess pore pressures to dissipate. This time lapse is commonly on the order of 30 to 90 days giving also some additional strength gain from thixotropic effects.

In any soil sufficient time should elapse before testing to allow partial dissipation of residual compression stresses in the lower shaft and point load from negative skin resistance on the upper shaft caused by shaft expansion upward as the hammer energy is released. Residual stresses and/or forces have been observed in a number of reports and summarized by Vesić (1977). It appears that pile load testing of the load-unload-reload type is more likely to produce residual stresses than driving.

ASTM D1143 gives the "standard" pile load test procedure and outlines in considerable detail the data to be collected in addition to load versus butt displacement. It would, of course, be most worthwhile for the various organizations that publish technical papers (such as ASCE and CGJ) to establish a similar checklist of information that would be the minimum to be included for the paper to be accepted for publication. This would give readers sufficient information to verify or provide alternative conclusions as well as to create a useful data base for future correlations that are more reliable. This is particularly important for piles since, as noted in Chap. 16, such a large amount of conflicting test data have been published.

17-8 PILE-DRIVING STRESSES

A pile must be adequately sized to satisfy both the static and dynamic (or driving) stresses. The driving stresses are difficult to determine except as approximations. Stresses are computed as P_d/A, and the limitations inherent in the dynamic equations exist for computing the driving force P_d so that a stress can be computed.

The wave equation seems to provide the best means to estimate the driving force P_d, both for compression in all piles and tension in concrete piles, and to find compressive and tension loads in the pile elements.

Figure 17-6, which is a printout of a wave equation trial, shows that the maximum force $P_d = 1341.6$ kN; this occurred in element 4 at DT = 13. Because this was a metal pile we do not need tension forces, but the pile had some (with the proper option activated, the program would also collect the largest negative forces in the elements as well). The option should always be activated for concrete piles.

The pile element forces depend on two factors in a wave equation analysis:

1. The estimated ultimate load $P_u = R_u$ (used as RU in program)
2. The amount of load estimated to be carried by the point

For the pile of Fig. 17-5 we have 100 percent point load and 0.0 point load—the two extremes. In this case the maximum loads are these:

Point load	Pile element	P_d, kN	At DT
100%	10 (bottom)	1808.2	34 (of 59)
0% (Fig. 17-6)	4 (near top)	1341.6	13 (of 62)

Also DT = 1/4000 = 0.000 25 sec. These data are for an estimated $P_u = 900$ kN, so it appears that the driving stresses can be from 50 to 100 percent larger than the estimated ultimate load.

The dynamic equations (such as the ENR and Hiley types) can also be used to estimate driving stresses and set. The use of the Hiley equation is illustrated in Example 17-4 following.

Since the pile driving supervisor can only obtain blow counts in the field, it is useful to present the data as illustrated in Fig. 17-4 or in E17-4. It should be evident, however, that the curves in these two figures represent particular pile-hammer combinations. A change in either invalidates the curves.

It should also be evident that a measurement of "set" is not straightforward, rather it must be done indirectly. The reason is that there is both "set" and axial compression (PL/AE) during driving. This makes it necessary to attach some type of scribing device to the pile head (for measurements when the approximate design depth is reached) so that the scribe moves down at impact and back up but not to the original starting point. The difference between the starting point and the final point (below the initial) is assumed as the "set" for that blow.

There is a question of what the limit should be on driving stresses. Since they are temporary and always higher than the design load stresses, some leeway must be allowed. Driving on the order of $0.85f'_c$ has resulted in fracture of concrete piles, so it would appear that their stresses should be limited to about 0.5 to $0.6f'_c$.

Driving stresses for wood piles should also be limited to about 0.5 to $0.6f_{ult}$ because of knots and other interior flaws.

Steel piles can probably be limited to stresses on the order of 0.8 to $0.9f_y$. If steel piles are stressed into the yield zone the principal result is increased possibility of corrosion from flaking off of mill scale as Luder (or slip) lines form. There is also opinion that driving stresses for steel piles can be from f_y to as much as $1.15f_y$ because of strain-hardening. The author

suggests not over $0.9f_y$ as a reasonable compromise, knowing that we are being optimistic if the driving stresses are not over ±20 percent of the estimate.

Example 17-4. Make a set versus driving resistance curve using the Hiley equation [Eq. (17-2)] with the following data:

DE-30 hammer (get data from Table A-2, in Appendix)
$W_r = 12.45$ kN $\quad E_h = W_r h = 22\,700$ to $30\,400 \rightarrow 27\,000$ kN·m
Efficiency $e_h = 0.85$ (not 1.0); $n = 0.40$ (Table 17-3)
Pile and other data: 406-mm (16-in.) OD with $t_w = 4.8$ mm
$A_p = 0.006\,02$ m^2 $\quad E_p = 200\,000$ MPa; Pile length $= 18.3$ m
Driven open-end but later cleaned and filled with concrete
Design load $= 900$ kN $\quad \gamma_s' = 9.0$ kN/m^3 $\quad \gamma_{st} = 77$ kN/m^3
Take SF $= 1$ for driving stresses $\quad f_y = 250$ MPa

Solution. The Hiley equation [Eq. (17-2)] is as follows:

$$P_u = \left[\frac{e_h E_h}{s + \frac{1}{2}(k_1 + k_2 + k_3)}\right]\left[\frac{W_r + n^2 W_p}{W_r + W_p}\right] \qquad k_2 = \frac{P_u L}{AE}$$

$$AE = 0.00602 \times 200\,000 = \mathbf{1204}\ \text{MN}$$

(Where 10^3 values cancel they will not be shown.) Obtain $k_1 = 2.5$ mm (given). Estimate $k_3 = \mathbf{2.0}$ mm (in range of 0 to 5 mm given earlier). Compute pile weight including plug as

$$\text{ID area} = 0.7854(0.406 - 2 \times 0.0048)^2 = \mathbf{0.123}\ \text{m}^2$$

$$W_p = \text{Weight of steel + cap + soil plug}$$

$$W_p = 0.00602 \times 77 \times 18.3 + 2.67 + 0.123 \times 9.0 \times 18.3$$

$$= 8.5 + 2.7 + 20.3 = \mathbf{31.5}\ \text{kN}$$

Making substitutions into the Hiley equation, we obtain

$$P_u = \left[\frac{0.85 \times 27\,000}{s + 0.5(2.5 + 2.0 + P_u L/AE)}\right]\left[\frac{12.45 + 0.16 \times 31.5}{12.45 + 31.5}\right]$$

Collecting terms, we obtain

$$P_u = \left[\frac{22\,950}{s + 2.25 + P_u(18.3/2408)}\right]\left[\frac{17.49}{44.0}\right] = \frac{9123}{s + 2.25 + P_u(18.3/2408)}$$

In this form the equation was programmed (since P_u is on both sides of the equation) for selected values of "set" in millimeters with the following output (Table E17-4) for plotting curves of set versus P_u and number of blows N/cm versus f_s as in Fig. E17-4. Note again that it is necessary to use the set in centimeters (cm) to obtain meaningful values—that is, divide by mm but multiply by 10. Since this step is equivalent to using centimeters we should call it that.

Notes.

1. We must initialize P_u to start computations. I used $P_u = 900$ kN.
2. We must use the pile area as the area of steel (0.00602 m^2), since the pipe must be filled with concrete after it is driven.
3. Adequate convergence is taken as 10 kN. That is, the difference between computed and used P_u is not over 10 kN.
4. You can use program FFACTOR (Hiley option 12) for these computations.

TABLE E17-4

$k = \frac{1}{2}(2.5 + 2.0) = 2.25$ mm

Set s_s, mm (cm)	C, mm $k + k_3$	Current P_u	Previous P_u, kN	Blows/cm N	Driving stress $f_s = P_u/A_p$, MPa
.0	9.522	958.1	(956.9)	.0	159.1
1.0	9.120	901.4	(904.0)	10.0	149.7
2.0	8.735	849.8	(853.4)	5.0	141.2
4.0	8.032	758.2	(760.8)	2.5	125.9
6.0	7.436	679.0	(682.4)	1.7	112.8
8.0	6.925	611.3	(615.1)	1.3	101.5
10.0 (1.0)	6.486	553.4	(557.4)	1.0	91.9
25.0 (2.5)	4.632	307.9	(313.5)	.4	51.1
50.0 (5.0)	3.607	170.2	(178.5)	.2	28.3
60.0 (6.0)	3.403	143.9	To plot s, cm vs. P_u		
100.0 (10.0)	2.973	88.6			

at $s = 1.0$ mm: $C = 2.25 + 904(18.3)/2408 = 9.120$ mm $(904 - 901.4 = 2.6 < 10)$

$f_s = 901.4/(0.00602 \times 1000) = 149.7$ MPa

Blows/cm $= 1/s \times 10 = 1/1.0 \times 10 = 10.0\ldots$ etc.

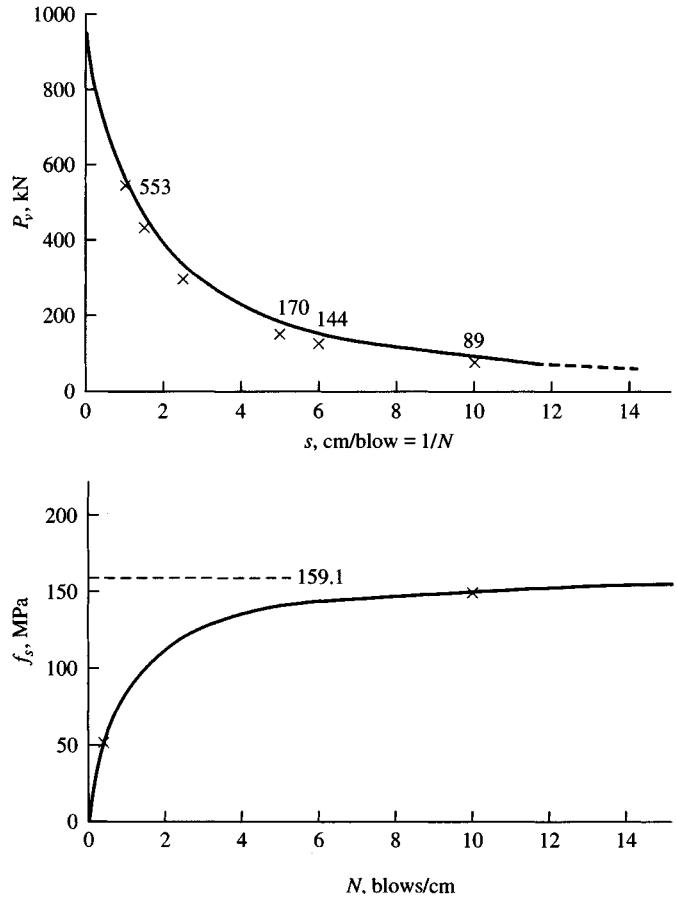

Figure E17-4

Question.
Would a better estimate of k_1 be 4 mm instead of the 2.5 used?

////

17-9 GENERAL COMMENTS ON PILE DRIVING

Alignment of piles can be difficult to get exactly correct, and often the driven piles are not exactly located in plan. A tolerance of 50 to 100 mm is usually considered allowable. Larger deviations may require additional substructure design to account for eccentricities, or more piles may have to be driven. Alignment of pipe piles may be checked by lowering a light into the tube. If the light source disappears, the alignment is not true. Pile groups should be driven from the interior outward because the lateral displacement of soil may cause excessively hard driving and heaving of already driven piles.

Damage to piles may be avoided or reduced by squaring the driving head with the energy source. Appropriate pile-driving caps and/or cushions should be used. When the required driving resistance is encountered, driving should be stopped. These driving resistances may be arbitrarily taken as

Timber piles	4–5 blows/25 mm
Concrete piles	6–8 blows/25 mm
Steel piles	12-15 blows/25 mm

Driving may require corrective action if the head of a timber pile becomes damaged; e.g., use a cap or metal band or cut the head of the pile more carefully. If during driving any pile changes direction, or the penetration becomes irregular or suddenly increases, the pile may already be broken or bent. Damaged piles will have to be pulled; pulling a broken timber pile is not a trivial task—particularly the lower broken part.

Pile driving may induce heave in saturated, fine-grained, non-quick-draining soils, where the displaced soil increases the pore water pressure so that the void ratio cannot rapidly change. As the pore pressure dissipates, the amount of heave may be reduced. Piles already driven in this material may be uplifted, the problem being especially aggravated if the piles are closely spaced [Klohn (1961)]. The problem may or may not be serious, depending on how the heave takes place [Nordlund (1962)], and may be more serious for point-bearing piles if they are driven to refusal and then heave takes place, since excessive settlements may result after the structure is built as the piles reseat themselves under load. If heave is anticipated, survey benchmarks should be established, and elevations taken on the piles after they are driven and as other piles are driven in the vicinity.

Since heave is caused by volume displacement, it can be somewhat controlled by using small-volume displacement piles (**HP** or open-end pipes). Heave can be controlled by predrilling an undersized hole for timber and closed-end pipe piles to reduce the volume displacement.

In granular soils a rearrangement of the soil structure from the driving vibrations may result in a subsidence of the adjacent area. Already driven piles may be preloaded to some extent by this phenomenon. A pile driven in a zone within about three pile diameters of an already driven pile will be more difficult to drive because the soil in this zone will be densified.

Continuity of cast-in-place piles is verified by computing the volume of concrete used to fill the pile cavity and comparing this with the theoretical cavity volume.

PROBLEMS

Pile hammer data are obtainable in Table A-2 of the Appendix.

17-1. A pile-load test provides the following data:

Pile = 406-mm diameter pipe L_p = 16.8 m
A = 0.015 39 m^2 E_{st} = 200 000 MPa wt = 1.2 kN/m
Weight includes attachments for instrumentation.
Hammer = Vulcan 140C e_h = 0.75
Set = 8 mm/blow for last 300 mm
Pile cap = 7.61 kN (driven open-end)

Find P_u and P_a by Hiley, ENR, and Gates equations.
Answer: P_u = 1735 kN (load test); by ENR P_u = 3485; Gates P_a = 340 kN

17-2. A pile-load test provides the following data:

Pile = 406 mm square concrete L_p = 13.7 m
A = 0.1648 m^2 E_c = 43 430 MPa
Weight/m = 3.89 kN/m
Hammer = Vulcan 140C e_h = 0.78
Set = 13.8 mm/blow
Pile cap (uses cushion) = 7.604 kN

Find P_u and P_a by Hiley, ENR, and Janbu equations.
Answer: P_u = 1512 kN (load test); by Janbu $P_u \cong$ 1400 kN

17-3. A pile-load test provides the following data:

Pile = 400 mm square concrete L_p = 16.0 m
E_c = 27 800 MPa (f_c' = 35)
Hammer = Vulcan 140C e_h = 0.85
Set = 6 mm/blow for last 300 mm
Weight of pile cap = 7.61 kN

Required: Compute ultimate and allowable pile capacity using the ENR equation [Eq. (17-5)].
Answer: P_u = 2130 kN (load test), ENR P_u = 3950 kN, P_a = 660 kN

17-4. A pile-load test provides the following data:

Pile = timber 0.116 m^2 butt, 0.058 m^2 tip L_p = 12.2 m
E_w = 11 000 MPa wood = 20.6 kN/m^3
Hammer = Vulcan 65C e_h = 0.76
Set = 13.3 mm/blow
Weight of pile cap = 4.23 kN

Required: Compute the ultimate and allowable pile capacity using the Gates and CNBC equations from Table 17-1.

Answer: P_u = 712 kN (load test); by Gates P_u = 627, by CNBC P_u = 477 kN

17-5. Plot a curve of P_u versus $1/s$ and stress versus $1/s$ for the pile of Prob. 17-3 using the equation from Table 17-1 as assigned by the instructor.

17-6. Plot a curve of P_u versus $1/s$ and stress versus $1/s$ for the pile of Prob. 17-4 using the Hiley equation.

17-7. What is the allowable load on the pile of Prob. 17-3 using the PCUBC equation?

17-8. What is the allowable load on the pile of Prob. 17-4 using the PCUBC equation?

17-9. Plot the assigned load-test data from the following two actual load tests, and select the allowable design load based on pile and load-test data.

	Test No. 1 HP 360 × 109, L = 15.2 m			**Test No. 2 324 × 8 mm pipe*, L = 16.8 m**	
P, kN	**Load, mm**	**Unload, mm**	**P, kN**	**Load, mm**	**Unload, mm**
0		0.6			25.4
445	5.0	20.3	445	03.0	29.2
890	9.0	25	890	05.6	31.8
1335	12.5	29	1330	10.2	34.3
1780	20.3	32	1780	16.5	37.8
2220	30.5		2000	31.8	
	33.0 (24 hr)			38.1 (24 hr)	

*Filled with concrete of f'_c = 28 MPa.

Use the building code in your area or the Chicago code method given in Sec. 17-7.

17-10. Compute P_u for the piles shown in Fig. P16-7 using a dynamic equation assigned by the instructor, and compare the solution to the load-test values of P_u shown. The driving hammer in all cases was a Vulcan No. 0 single-acting hammer.

17-11. Refer to Fig. 17-6 (wave equation output). Why is there no set at DT = 31 and how is the value of 0.40762 obtained for the "set" at DT = 32? What is the difference between total point displacement D and "set" at DT = 42? Can you draw any conclusions about the point displacement and set?

17-12. From the DT data of Fig. 17-6, make a plot of DT versus set and point displacement from DT = 10 to DT = 62.

17-13. What is the maximum stress (in MPa) in element 8 of the pile model of Fig. 17-6?

17-14. Verify that the first pile "spring" = 666 666.6 kN/m as shown on the output sheet (Fig. 17-6).

17-15. If the first pile element (element 4) were assumed also to carry an equal part of the 900 kN load, what would the side resistances be (they are 112.5 kN excluding the first pile element of Fig. 17-6)?

17-16. If you have access to a wave equation program, verify the output given in Fig. 17-6. Also verify that using 100 percent point load gives approximately the maximum load given in the textbook. Note that different programs may give slightly different answers. Also vary the point percent using 0.0, 0.25, 0.50, and 0.75 of P_u = 900 kN. The base data is on files FIG175.DTA and FIG175A.DTA on your diskette for using the Bowles program B-27.

CHAPTER 18

PILE FOUNDATIONS: GROUPS

18-1 SINGLE PILES VERSUS PILE GROUPS

The preceding two chapters have considered the soil and structural aspects of single piles in some detail together with a brief discussion of pile-driving operations. Rarely, however, is the foundation likely to consist of a single pile. Generally, there will be a minimum of two or three piles under a foundation element or footing to allow for misalignments and other inadvertent eccentricities. Building codes[1] may stipulate the minimum number of piles under a building element. The load capacity, settlement, and individual pile loads associated with pile groups are the concern of this chapter. Figure 18-1 presents some typical pile clusters, for illustrative purposes only, since the designer must make up the group geometry to satisfy any given problem.

18-2 VERTICALLY LOADED PILE GROUPS

When several piles are clustered, it is reasonable to expect that the soil pressures produced from either side friction or point bearing will overlap as idealized in Fig. 18-2. The superimposed pressure intensity will depend on both the pile load and spacing, and if sufficiently large the soil will fail in shear or the settlement will be excessive. The stress intensity from overlapping stressed zones will obviously decrease with increased pile spacing s; however, large spacings are often impractical since a pile cap is cast over the pile group for the column base and/or to spread the load to the several piles in the group.

[1]The Chicago Building Code (Sec. 13-132-120) states: "A column or pier supported by piles shall rest on not less than three piles . . . "

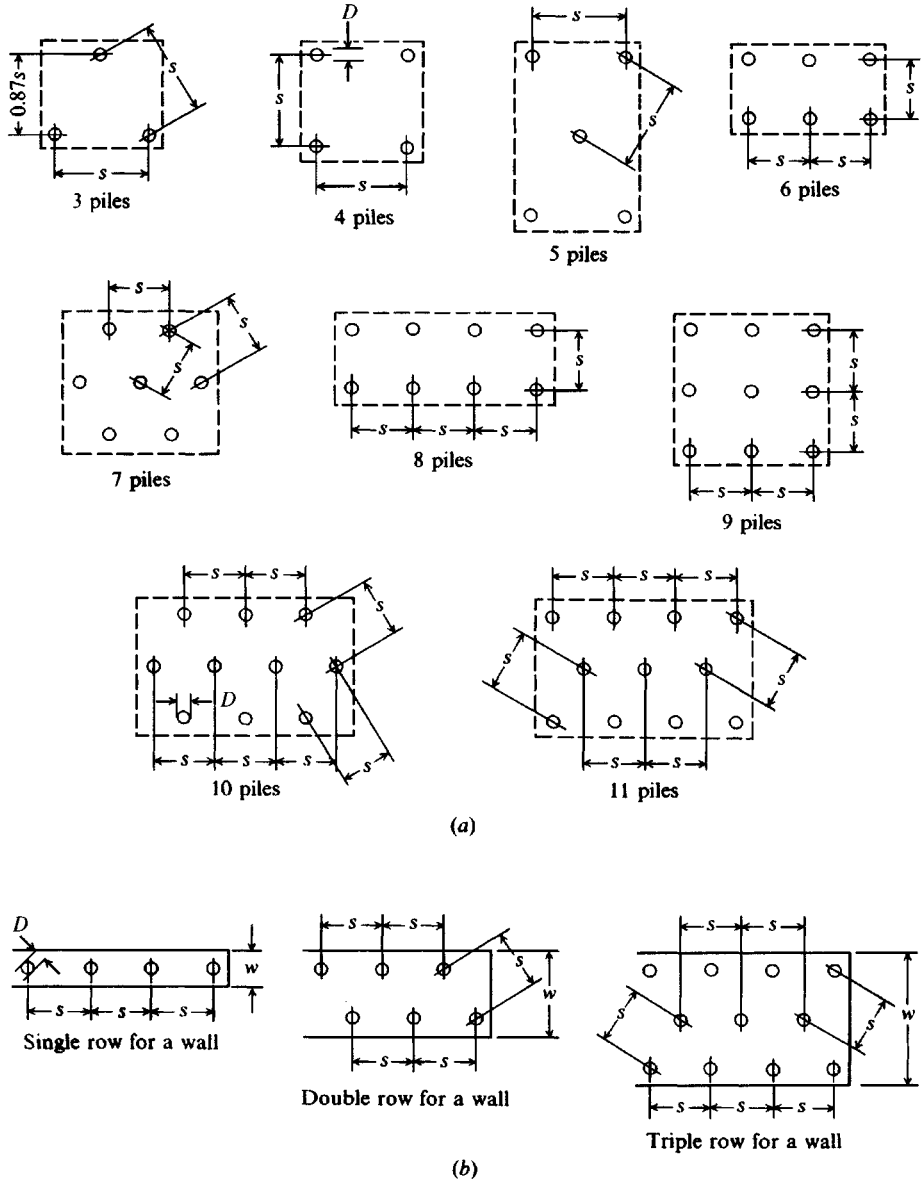

Figure 18-1 Typical pile-group patterns: (*a*) for isolated pile caps; (*b*) for foundation walls.

Suggested minimum center-to-center pile spacings by several building codes are as follows:

Pile type	BOCA, 1993 (Sec. 1013.8)	NBC, 1976 (Sec. 912.1*l*)	Chicago, 1994 (Sec. 13-132-120)
Friction	$2D$ or $1.75H \geq 760$ mm	$2D$ or $1.75H \geq 760$ mm	$2D$ or $2H \geq 760$ mm
Point bearing	$2D$ or $1.75H \geq 610$ mm	$2D$ or $1.75H \geq 610$ mm	

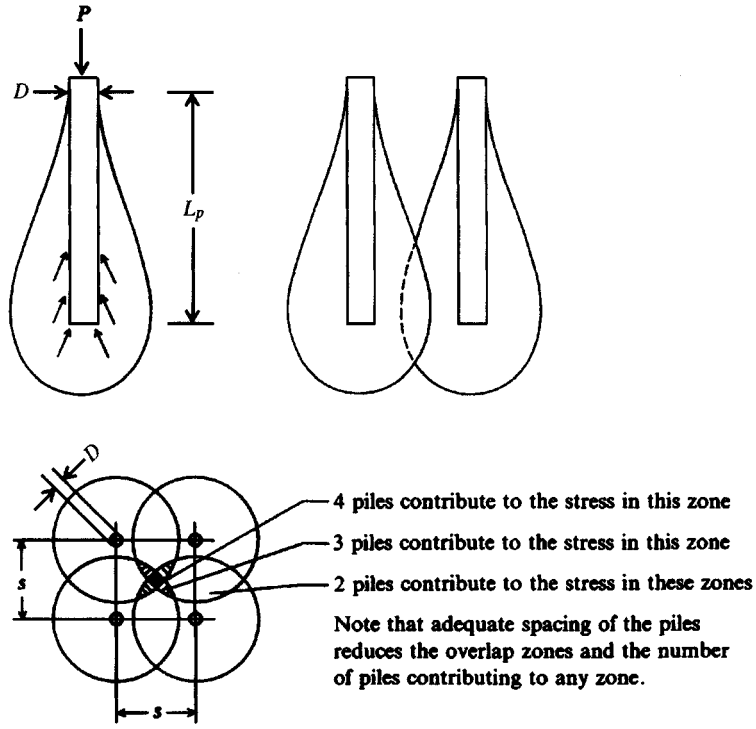

Figure 18-2 Stresses surrounding a friction pile and the summing effects of a pile group.

Here D = pile diameter; H = diagonal of rectangular shape or **HP** pile. The BOCA code also stipulates that spacing for friction piles in loose sand or loose sand-gravels shall be increased 10 percent for each interior pile to a maximum of 40 percent. Optimum spacing s seems to be on the order of 2.5 to 3.5D or 2 to 3H for vertical loads; for groups carrying lateral and/or dynamic loads, larger pile spacings are usually more efficient. Maximum pile spacings are not given in building codes, but spacings as high as 8 or 10D have been used on occasion.

18-3 EFFICIENCY OF PILE GROUPS

When several pile butts are attached to a common structural element termed a *pile cap* the result is a *pile group*. A question of some concern is whether the pile group capacity is the sum of the individual pile capacities or something different—either more or less. If the capacity is the sum of the several individual pile contributions, the group efficiency $E_g = 1.0$.

There are mixed opinions on pile group efficiency defined as

$$E_g = \frac{Q_o}{\sum Q_p}$$

where Q_o = group capacity as measured, kN or kips
$\sum Q_p$ = sum of individual pile capacities of group, kN or kips

None of the building codes seen by the author (including those just cited) provides guidance on group efficiency. The ASCE Committee on Deep Foundations report [CDF (1984)]

recommends not using group efficiency as a description of group action. This committee report was a synthesis of work from 1963 to its publication date, so it is probably a very realistic guideline. It suggests that friction piles in cohesionless soils at the usual spacings s of $s = 2$ to $3D$ will have a group efficiency $E_g \geq 1$. The reason given is that in cohesionless soil the pile displacement + driving vibrations increase the soil density (or γ_s) in a zone in the vicinity of the pile, which is further increased as other piles are driven nearby.

For friction piles in cohesive soils the block shear + point bearing of the group in plan is used as the group capacity, but in no case is the group capacity to be considered greater than the single pile capacity times the number of piles in the group. The block bearing capacity should only be included if the cap is in ground contact. If it is above the ground, the group capacity may be the block perimeter shear + the individual point capacities. When the cap is in contact with the ground it will settle with the soil since the piles will also settle that amount. Thus, the bearing capacity is that of a block the size of the cap.

The pile practice survey by Focht and O'Neill (1985) indicated essentially that the CDF recommendations were being used. About 6 percent used group spacing in group efficiency and about 30 percent considered E_g if a block shear failure controlled.

At present the Converse-Labarre equation [see Moorhouse and Sheehan (1968)], which at one time was widely used to compute group efficiency, is seldom used. The AASHTO (1990) bridge specifications still give it as a "suggestion" for friction piles. The Converse-Labarre equation is

$$E_g = 1 - \theta \frac{(n-1)m + (m-1)n}{90mn} \tag{18-1}$$

where m, n, and D are shown on Fig. 18-3 and $\theta = \tan^{-1} D/s$ in degrees. This equation is limited to rectangular groups with identifiable values of $m \times n$.

Recently Sayed and Bakeer (1992) introduced an efficiency equation of the form

$$E_g = 1 - (1 - \eta' K) \frac{\sum Q_s}{\sum (Q_s + Q_p)} \tag{18-1a}$$

where Q_s = shaft friction resistance for each pile in group, kN or kips
Q_p = point load for each pile in group, kN or kips

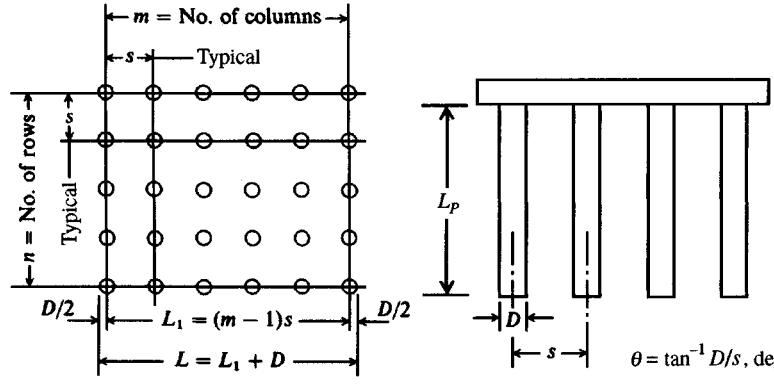

Figure 18-3 Pile group efficiency.

η' = geometric efficiency parameter, which can be computed using an equation similar to Eq. (18-1) giving values generally in the range of 0.6 to 2.5

K = group interaction factor (also to be estimated); ranges from 0.4 to about 9.0

For end-bearing piles the $\sum Q_s$ term is zero, giving $E_g = 1$ in Eq. (18-1*a*), which is, of course, the correct value. For other piles there is a lot of estimation (guessing) involved so Eq. (18-1*a*) should be used most cautiously, if at all.

When a concrete pile cap is poured directly on the ground, as is the most common case, the group capacity is at least the block capacity based on the shear around the perimeter of the group defined by the plan dimensions + the bearing capacity of the block dimension at the pile points. The only exception is point bearing piles founded in rock where the group capacity would be the sum of the individual point capacities.

When the pile cap is above ground, as is common for offshore structures, the group capacity will be the lesser of the following:

1. The smaller of the block capacity based on the group perimeter (see distance L_1 of Fig. 18-3) or the sum of the several pile perimeters making up the group. In either case the sum of the bearing capacity of the pile points is added. The group perimeter will be equal to the sum of the pile perimeters and for square piles, $s/D \geq \sqrt{n} + 1$; for round piles, $s/D \geq 0.7854\sqrt{n} + 1$.
2. Sum of the capacity of the individual piles. This usually controls for large s/D ratios.

There are very few full-scale pile group load tests reported in the literature. Vesić (1977) reported the results of five group load tests in clay and all gave an $E_g \approx 1$. Six full-scale load tests in sands gave $E_g > 1$. There are a large number of model group tests such as Barden and Monckton (1970); however, because of scale effects they are not considered to be reliable.

Vesić (1969*a*) reported on a series of vertically loaded group load tests using 100-mm diameter piles 1800 mm in length in sand. The groups consisted of four and nine piles. In the four-pile groups the vertical load was evenly distributed among the four piles; in the nine-pile group the interior pile carried a larger load than the corners (which carried the least) and the sides (which were intermediate). If we denote the interior pile as 100 percent efficient, then the corners carry about 60 to 70 percent of the interior and the side piles about 80 percent.

Example 18-1. Compute the efficiency of the group of friction piles shown in Fig. E18-1 by the Converse-Labarre equation [Eq. (18-1)] and using the CDF recommendation. Take $D = 400$ mm and spacing $s = 1000$ mm (both ways) and all cohesionless material in the pile embedment zone.

Solution. By inspection of Fig. E18-1 we see that $m = 5$ and $n = 3$.

$$\theta = \tan^{-1} D/s = \tan^{-1}(400/1000) = \mathbf{21.8}^\circ$$

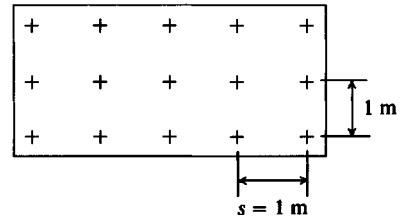

Figure E18-1

Directly substituting into Eq. (18-1), we find

$$E_g = 1 - 21.8\frac{(3-1)5 + (5-1)3}{90(5)(3)} = \mathbf{0.64} \text{ or } 64 \text{ percent}$$

$$\text{Group capacity:} \quad Q_g = N_p Q_p E_g = 15Q_p(0.64)$$

By CDF recommendations ($s = 1$ m $= 2.5D$ is in "usual" range of spacings)

$$\text{Group capacity} = \text{at least } 15 \times \text{single pile capacity.}$$

////

Example 18-2. Assume the pile group of Example 18-1 is in a clay soil for which the undrained shear strength $c = s_u = q_u/2 = 30$ kPa. The piles are 20 m in length (average). Estimate the ultimate group capacity Q_{ult} and assume there is a 250-mm cap projection beyond the outer piles.

Solution. This computation is for "block" capacity. Note pile diam. = 400 mm. Then the cap dimensions are these:

$$L = 4 \times 1 + 2 \times (0.200 + 0.250) = 4.9 \text{ m}$$

$$B = 2 \times 1 + 2 \times (0.200 + 0.250) = 2.9 \text{ m}$$

$$\frac{L}{B} = \frac{4.9}{2.9} = 1.7$$

$$\frac{D}{B} = \frac{20}{2.9} = 6.9 > 4 \qquad \text{Use } N_c = 9.0$$

$$\text{Block perimeter} = 2(4.9 + 2.9) = 15.6 \text{ m} \qquad \text{Block area } A_b = 4.9 \times 2.9 = 14.21 \text{ m}^2$$

Take $\alpha = 0.6$ from Fig. 16-14 using the API curve (soil-to-soil), but remember that driving of exterior piles 250 mm interior from cap edge may remold soil. Then

$$Q_{ult} = 9cA_b + \text{block shear} \qquad \text{Block shear} = \alpha s_u(\text{perimeter})(\text{length})$$

$$= 9(30)(14.21) + 0.6(30)(15.6)(20)$$

$$= 3807 + 5616 = \mathbf{9423} \text{ kN}$$

$$\text{Load for single pile} = \alpha c_u(\text{perimeter})L + \text{point bearing}$$

$$P_u = 0.6(30)(\pi \times 0.400)(20) + 9(30)(0.7854 \times 0.400^2)$$

$$= 452 + 34 = 486 \text{ kN/pile}$$

$$\text{For 15 piles } Q'_{ult} = 15 \times 486 = \mathbf{7290} \text{ kN}$$

Use $Q_{ult} = 7290$ kN although the apparent $E_g = 9423/7290 = 1.3$.

////

18-4 STRESSES ON UNDERLYING STRATA FROM PILES

The soil stresses on underlying strata produced by the several piles in a group are often required to make a strength or settlement estimate. These stresses are difficult to estimate for several reasons:

1. Influence of pile cap—usually in direct contact with ground except on expansive soils. This results in both the cap and the pile carrying the load with the interaction highly indeterminate.
2. The distribution of friction effects along the pile, which are generally not known; hence point load is also not known.

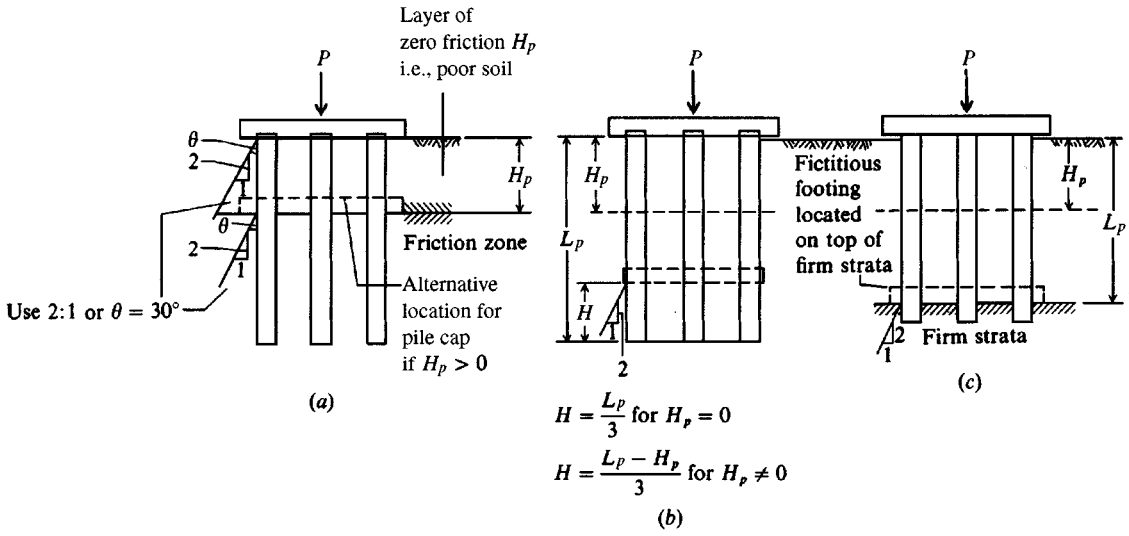

Figure 18-4 Simplified computation of soil stresses beneath a pile group: (*a*) friction piles; (*b*) alternative method for stress computations for friction piles; (*c*) point-bearing piles.

3. The overlap of stresses from adjacent piles, which is difficult to evaluate.
4. The influence of driving the piles on the adjacent soil.
5. Time-dependent effects such as consolidation, thixotropy, varying loads, and change in groundwater level.

Considering all these variables, it is common practice to simplify the stress computations, as illustrated in Fig. 18-4. For friction piles two cases may be considered. In case 1 (Fig. 18-4*a*) the load is assumed to spread from a fictitious rigid footing located at the top of the layer providing friction resistance at a 2:1 slope (or 30°). For a homogeneous stratum this is the ground surface. In case 2 the load is placed on a fictitious rigid footing located at $L_p/3$ from the bottom of the piles (average depth), with L_p as in Fig. 18-4*b*. The spread-out of load is also taken at either 2:1 or 30°. Case 1 or 2 should be used, whichever gives the larger computed stresses on underlying strata. Blanchet et al. (1980) report that this method is not very good for computing settlements and that an elastic solution might be preferred.

For point-bearing piles (case 3) in dense sand or sand-gravel deposits, the fictitious footing is placed on the deposit in which the piles penetrate. Again, the load is spread at a 2:1 or 30° slope, as shown in Fig. 18-4*c*.

These analyses are necessary to avoid overstressing the underlying strata. They are also necessary to compute immediate settlements on loose granular deposits or consolidation settlements in clay deposits. As can be seen, a pile group either transmits the load throughout a soil mass of depth L_p for friction piles or to the full depth for an end-bearing pile. The soil at or below these depths must carry the load without excessive deformation, or the load must be transmitted to deeper strata.

An analytical method of computing the stresses—and resulting settlements—in the strata underlying a pile group uses the author's extension of a method based on the Mindlin (1936*b*) solution, developed into a computer-programmable format by Geddes (1966), of a point load at the interior of an elastic solid. As with the Boussinesq analysis, this method assumes the soil is semi-infinite, isotropic, homogeneous, and elastic. Soil does not usually fit these assump-

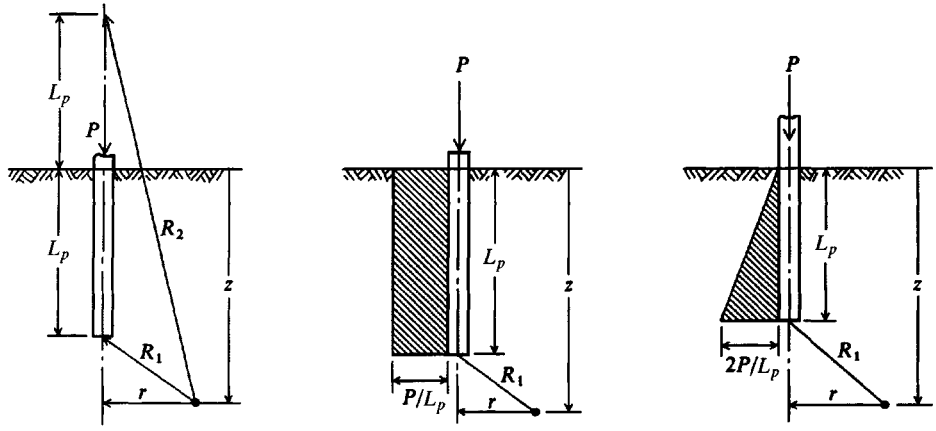

Figure 18-5 Pile-soil system for the evaluation of soil stresses using the Mindlin solution. [*After Geddes(1966).*]

tions; thus, the solutions are in error, but they should be as good as the Boussinesq solution, which is widely used for footing settlements.

Geddes (1969) later made solutions for the Boussinesq case for subsurface loadings. These are generally less accurate than the Mindlin solution. Poulos and Davis (1968) also used the Mindlin solution to predict settlements. Instead of presenting tables of stress coefficients, they presented charts for settlement-influence factors. Either the Geddes or the Poulos and Davis solutions should provide the same deflection if properly used, since they are both based on the Mindlin solution. The Geddes solution is included since one can easily compute deflections from stresses, but stresses are not so easily back-computed from deflections; stresses may be needed for consolidation settlements.

Geddes developed three cases, as shown in Fig. 18-5. As with the Boussinesq analysis, it is convenient to use stress coefficients that can be evaluated on an electronic computer. Four stresses can be evaluated for each case (vertical, shear, radial, and circumferential). For **case 1** the vertical stress is

$$\sigma_z = \frac{P}{8\pi(1-\mu)}\left\{-\frac{(1-2\mu)(z-L_p)}{R_1^3}+\frac{(1-2\mu)(z-L_p)}{R_2^3}-\frac{3(z-L_p)^3}{R_1^5}\right.$$
$$\left.-\left[\frac{3(3-4\mu)z(z+L_p)^2-3L_p(z+L_p)(5z-L_p)}{R_2^5}\right]-\frac{30zL_p(z+L_p)^3}{R_2^7}\right\} \tag{18-2}$$

The shearing stress is computed as

$$\tau = \frac{Pr}{8(1-\mu)}\left\{-\frac{1-2\mu}{R_1^3}+\frac{1-2\mu}{R_2^3}-\frac{3(z-L_p)^3}{R_1^5}\right.$$
$$\left.-\left[\frac{3(3-4\mu)z(z+L_p)-3L_p(3z+L_p)}{R_2^5}\right]-\frac{30zL_p(z+L_p)^2}{R_2^7}\right\} \tag{18-3}$$

$$R_1^2 = r^2+(z-L_p)^2$$
$$R_2^2 = r^2+(z+L_p)^2$$

The other equations are of similar form and will not be presented. For computer programming they may be expressed in dimensionless form by substituting the following (terms identified on Fig. 18-5):

$$n = \frac{r}{L_p} \qquad m = \frac{z}{L_p} \qquad F^2 = m^2 + n^2$$
$$A^2 = n^2 + (m-1)^2 \qquad B^2 = n^2 + (m+1)^2$$

and introducing a stress coefficient to obtain for the vertical stress

$$\sigma_z = \frac{P}{L_p^2} K_z \tag{18-4}$$

The stress coefficient K_z for **case 1** is

$$K_z = \frac{1}{8\pi(1-\mu)}\left[-\frac{(1-2\mu)(m-1)}{A^3} + \frac{(1-2\mu)(m-1)}{B^3} - \frac{3(m-1)^3}{A^5} - \frac{3(3-4\mu)m(m+1)^2 - 3(m+1)(5m-1)}{B^5} - \frac{30m(m+1)^3}{B^7}\right] \tag{18-5}$$

For the case of uniform skin friction (**case 2**) the vertical stress coefficient is

$$K_z = \frac{1}{8\pi(1-\mu)}\left[-\frac{2(2-\mu)}{A} + \frac{2(2-\mu) + 2(1-2\mu)\left(\frac{m}{n}\right)\left(\frac{m}{n} + \frac{1}{n}\right)}{B} - \frac{(1-2\mu)2\left(\frac{m}{n}\right)^2}{F} + \frac{n^2}{A^3} + \frac{4m^2 - 4(1+\mu)\left(\frac{m}{n}\right)^2 m^2}{F^3} + \frac{4m(1+\mu)(m+1)\left(\frac{m}{n} + \frac{1}{n}\right)^2 - (4m^2 + n^2)}{B^3} + \frac{6m^2\left(\frac{(m^4 - n^4)}{n^2}\right)}{F^5} + \frac{6m\left(mn^2 - \frac{1}{n^2}\right)(m+1)^5}{B^5}\right] \tag{18-6}$$

For the case of a linear variation of skin friction (**case 3**) the vertical stress coefficient is

$$K_z = \frac{1}{4\pi(1-\mu)}\left[-\frac{2(2-\mu)}{A} + \frac{2(2-\mu)(4m+1) - 2(1-2\mu)\left(\frac{m}{n}\right)^2 (m+1)}{B} + \frac{2(1-2\mu)\left(\frac{m^3}{n^2}\right) - 8(2-\mu)m}{F} + \frac{mn^2 + (m-1)^3}{A^3} + \frac{4\mu n^2 m + 4m^3 - 15n^2 m - 2(5+2\mu)\left(\frac{m}{n}\right)^2 (m+1)^3 + (m+1)^3}{B^3}\right]$$

$$+\frac{2(7-2\mu)mn^2-6m^3+2(5+2\mu)\left(\frac{m}{n}\right)^2 m^3}{F^3}$$

$$+\frac{6mn^2(n^2-m^2)+12\left(\frac{m}{n}\right)^2(m+1)^5}{B^5}-\frac{12\left(\frac{m}{n}\right)^2 m^5+6mn^2(n^2-m^2)}{F^5}$$

$$-2(2-\mu)\ln\left(\frac{A+m-1}{F+m}\frac{B+m+1}{F+m}\right)\Bigg] \tag{18-7}$$

Values are not shown in Table 18-1 for any $m = z/L_p < 1.00$ for any cases 1-3, as these represent a tension stress in the soil at depth z above the pile tip. Tension stresses would not likely form in this zone, because gravity effects would produce a downward flow of the soil mass to eliminate them. The inclusion of potential tension stresses would, however, implicitly include the soil weight, so computed settlements would be in error. Only compressive soil stresses in the strata below the soil tip cause settlement, although the pile cap settlement is actually the sum of both point settlement and elastic axial pile shaft deformation, which can be computed in the form of $e_s = \lambda' P_u L_p/AE$. Also it was necessary to use $n = 0.002^+$ when programming the case 2 and case 3 table output, since $n = 0.0$ would produce a discontinuity (divide-by-zero error) in the computations.

Table 18-1 lists values for K_z for various $m = z/D$ and $n = r/D$ values and three selected values of Poisson's ratio μ for all three cases. By superposition of effects, these three cases should provide a general solution for the vertical stress at a point for any reasonable type of stress distribution along a pile. To avoid interpolation use your program FFACTOR (option 11) for any of these 3 skin resistance cases.

This procedure is recommended to obtain a vertical stress profile for making consolidation (or elastic) settlement computations in the soil below the pile tips. As the following example illustrates, the "conventional" method, although quite simple, may substantially underestimate (assuming the theory of a load on the interior of a semi-infinite elastic solid is valid) the soil stress at a point. Unfortunately there are few pile group settlements measured and almost no stress measurements taken below pile groups to verify any theory.

Example 18-3. Compute the vertical stress at a point A of the four-pile group shown in Fig. E18-3. Take $\mu = 0.3$. Compare the results with what has been the conventional method of analysis.

Solution.

Step 1. Assume point-loaded piles.

$$r = 0.610\sqrt{2} = 0.863 \text{ m}$$

$$m = \frac{z}{L_p} = \frac{18.3}{16.8} = 1.09$$

$$n = \frac{r}{L_p} = \frac{0.863}{16.8} = 0.0514$$

From Table 18-1*a* [actually using program FFACTOR (option 11)] with input: $r = 0.863$, $L = 16.8$, $\mu = 0.3$, case 1, $z = 18.3 \rightarrow K_z = \mathbf{-12.41}$.

$$\sigma_z = 4\left[\frac{2000}{4(16.8)^2}\right](-12.4) = \mathbf{-87} \text{ kPa} \qquad \text{(compression)}$$

TABLE 18-1*a*

Stress coefficients for a point load as shown in case 1 of Fig. 18-5

(−) = compression; $m = z/D$; $n = r/D$

m	n = 0.0	0.1	0.2	0.3	0.4	0.5	0.75	1.0	1.5	2.0
					Poisson ratio = 0.20					
1.0		−0.0960	−0.0936	−0.0897	−0.0846	−0.0785	−0.0614	−0.0448	−0.0208	−0.0089
1.1	−17.9689	−3.7753	−0.6188	−0.2238	−0.1332	−0.0999	−0.0659	−0.0467	−0.0222	−0.0099
1.2	−4.5510	−2.7458	−1.0005	−0.3987	−0.2056	−0.1325	−0.0724	−0.0490	−0.0236	−0.0110
1.3	−2.0609	−1.6287	−0.9233	−0.4798	−0.2672	−0.1681	−0.0811	−0.0520	−0.0249	−0.0119
1.4	−1.1858	−1.0328	−0.7330	−0.4652	−0.2926	−0.1930	−0.0905	−0.0555	−0.0263	−0.0129
1.5	−0.7782	−0.7153	−0.5682	−0.4114	−0.2875	−0.2025	−0.0985	−0.0592	−0.0277	−0.0138
1.6	−0.5548	−0.5238	−0.4457	−0.3518	−0.2664	−0.1997	−0.1038	−0.0625	−0.0290	−0.0147
1.7	−0.4188	−0.4018	−0.3569	−0.2984	−0.2399	−0.1893	−0.1061	−0.0651	−0.0303	−0.0156
1.8	−0.3294	−0.3193	−0.2918	−0.2539	−0.2133	−0.1755	−0.1057	−0.0668	−0.0315	−0.0164
1.9	−0.2673	−0.2609	−0.2431	−0.2177	−0.1890	−0.1606	−0.1033	−0.0675	−0.0325	−0.0172
2.0	−0.2222	−0.2180	−0.2060	−0.1883	−0.1676	−0.1462	−0.0995	−0.0673	−0.0334	−0.0179
					Poisson ratio = 0.30					
1.0		−0.1013	−0.0986	−0.0944	−0.0889	−0.0824	−0.0641	−0.0463	−0.0209	−0.0087
1.1	−19.3926	−3.9054	−0.5978	−0.2123	−0.1287	−0.0986	−0.0668	−0.0475	−0.0222	−0.0097
1.2	−4.9099	−2.9275	−1.0358	−0.4001	−0.2027	−0.1303	−0.0722	−0.0493	−0.0235	−0.0106
1.3	−2.2222	−1.7467	−0.9757	−0.4970	−0.2717	−0.1687	−0.0808	−0.0519	−0.0247	−0.0116
1.4	−1.2777	−1.1152	−0.7805	−0.4891	−0.3032	−0.1974	−0.0908	−0.0555	−0.0260	−0.0125
1.5	−0.8377	−0.7686	−0.6070	−0.4356	−0.3012	−0.2098	−0.0999	−0.0594	−0.0274	−0.0134
1.6	−0.598	−0.5626	−0.4768	−0.3738	−0.2809	−0.2086	−0.1063	−0.0631	−0.0288	−0.0143
1.7	−0.4500	−0.4312	−0.3819	−0.3177	−0.2538	−0.1988	−0.1094	−0.0661	−0.0302	−0.0152
1.8	−0.3536	−0.3424	−0.3122	−0.2706	−0.2262	−0.1849	−0.1096	−0.0682	−0.0315	−0.0161
1.9	−0.2866	−0.2795	−0.2600	−0.2321	−0.2006	−0.1697	−0.1076	−0.0693	−0.0326	−0.0169
2.0	−0.2380	−0.2333	−0.2201	−0.2007	−0.1780	−0.1547	−0.1039	−0.0694	−0.0336	−0.0177
					Poisson ratio = 0.40					
1.0		−0.1083	−0.1054	−0.1008	−0.0947	−0.0876	−0.0676	−0.0483	−0.0212	−0.0083
1.1	−21.2910	−4.0788	−0.5699	−0.1970	−0.1228	−0.0970	−0.0680	−0.0486	−0.0223	−0.0093
1.2	−5.3884	−3.1699	−1.0829	−0.4020	−0.1989	−0.1274	−0.0720	−0.0496	−0.0233	−0.0102
1.3	−2.4373	−1.9040	−1.0455	−0.5200	−0.2776	−0.1695	−0.0804	−0.0519	−0.0244	−0.0111
1.4	−1.4002	−1.2179	−0.8438	−0.5208	−0.3173	−0.2032	−0.0913	−0.0554	−0.0256	−0.0120
1.5	−0.9172	−0.8395	−0.6587	−0.4678	−0.3194	−0.2196	−0.1017	−0.0596	−0.0270	−0.0129
1.6	−0.6527	−0.6143	−0.5181	−0.4033	−0.3001	−0.2205	−0.1095	−0.0638	−0.0284	−0.0138
1.7	−0.4915	−0.4705	−0.4152	−0.3435	−0.2724	−0.2116	−0.1138	−0.0675	−0.0300	−0.0147
1.8	−0.3858	−0.3732	−0.3393	−0.2929	−0.2433	−0.1976	−0.1148	−0.0701	−0.0314	−0.0156
1.9	−0.3123	−0.3044	−0.2825	−0.2512	−0.2161	−0.1818	−0.1133	−0.0717	−0.0328	−0.0166
2.0	−0.2590	−0.2537	−0.2390	−0.2173	−0.1919	−0.1659	−0.1098	−0.0722	−0.0340	−0.0174

TABLE 18-1*b*

Stress coefficients for constant skin friction as shown in case 2 of Fig. 18-5

(−) = compression; $m = z/D$; $n = r/D$

m	n = 0.00	0.02	0.04	0.06	0.08	0.10	0.15	0.20	0.50	1.0	2.0
					Poisson ratio = 0.20						
1.0		−6.4703	−3.2374	−2.1592	−1.6202	−1.2962	−0.8630	−0.6445	−0.2300	−0.0690	−0.0081
1.1	−1.7781	−1.7342	−1.5944	−1.4178	−1.2418	−1.0850	−0.7953	−0.6138	−0.2283	−0.0730	−0.0096
1.2	−0.9015	−0.8789	−0.8576	−0.8269	−0.7882	−0.7446	−0.6317	−0.5307	−0.2231	−0.0759	−0.0111
1.3	−0.5968	−0.5799	−0.5725	−0.5629	−0.5500	−0.5340	−0.4867	−0.4355	−0.2138	−0.0779	−0.0125
1.4	−0.4569	−0.4288	−0.4241	−0.4201	−0.4142	−0.4068	−0.3838	−0.3562	−0.2010	−0.0789	−0.0139
1.5	−0.3482	−0.3359	−0.3334	−0.3313	−0.3282	−0.3242	−0.3113	−0.2952	−0.1862	−0.0790	−0.0152
1.6	−0.2922	−0.2726	−0.2716	−0.2707	−0.2689	−0.2666	−0.2589	−0.2487	−0.1708	−0.0784	−0.0165
1.7	−0.2518	−0.2304	−0.2287	−0.2274	−0.2261	−0.2247	−0.2195	−0.2127	−0.1559	−0.0770	−0.0175
1.8	−0.1772	−0.1953	−0.1949	−0.1942	−0.1936	−0.1925	−0.1891	−0.1844	−0.1420	−0.0750	−0.0185
1.9	−0.1648	−0.1702	−0.1698	−0.1687	−0.1682	−0.1675	−0.1650	−0.1616	−0.1295	−0.0727	−0.0193
2.0	−0.1461	−0.1482	−0.1486	−0.1480	−0.1478	−0.1473	−0.1455	−0.1429	−0.1180	−0.0700	−0.0201
					Poisson ratio = 0.30						
1.0		−6.8419	−3.4044	−2.2673	−1.6983	−1.3567	−0.8998	−0.6695	−0.2346	−0.0686	−0.0076
1.1	−1.9219	−1.8611	−1.7072	−1.5134	−1.3211	−1.1503	−0.8368	−0.6419	−0.2335	−0.0728	−0.0091
1.2	−0.9699	−0.9403	−0.9166	−0.8825	−0.8400	−0.7922	−0.6688	−0.5588	−0.2292	−0.0760	−0.0105
1.3	−0.6430	−0.6188	−0.6099	−0.5992	−0.5850	−0.5675	−0.5157	−0.4597	−0.2207	−0.0782	−0.0120
1.4	−0.4867	−0.4558	−0.4507	−0.4461	−0.4396	−0.4316	−0.4063	−0.3761	−0.2082	−0.0796	−0.0134
1.5	−0.3766	−0.3561	−0.3533	−0.3510	−0.3476	−0.3432	−0.3291	−0.3115	−0.1834	−0.0800	−0.0148
1.6	−0.3339	−0.2895	−0.2878	−0.2863	−0.2843	−0.2817	−0.2732	−0.2621	−0.1777	−0.0796	−0.0160
1.7	−0.2664	−0.2438	−0.2414	−0.2399	−0.2384	−0.2369	−0.2313	−0.2239	−0.1623	−0.0784	−0.0172
1.8	−0.2025	−0.2065	−0.2054	−0.2044	−0.2038	−0.2026	−0.1989	−0.1938	−0.1479	−0.0766	−0.0182
1.9	−0.1847	−0.1794	−0.1785	−0.1777	−0.1768	−0.1760	−0.1733	−0.1696	−0.1347	−0.0744	−0.0191
2.0	−0.1634	−0.1565	−0.1561	−0.1556	−0.1551	−0.1545	−0.1525	−0.1498	−0.1229	−0.0718	−0.0199
					Poisson ratio = 0.40						
1.0		−7.2744	−3.6270	−2.4110	−1.8026	−1.4373	−0.9488	−0.7029	−0.2407	−0.0681	−0.0069
1.1	−2.0931	−2.0296	−1.8574	−1.6409	−1.4266	−1.2372	−0.8921	−0.6794	−0.2404	−0.0725	−0.0083
1.2	−1.0486	−1.0209	−0.9947	−0.9567	−0.9091	−0.8556	−0.7181	−0.5964	−0.2373	−0.0760	−0.0098
1.3	−0.6922	−0.6694	−0.6598	−0.6476	−0.6318	−0.6122	−0.5543	−0.4921	−0.2298	−0.0787	−0.0113
1.4	−0.5347	−0.4922	−0.4860	−0.4807	−0.4735	−0.4645	−0.4362	−0.4026	−0.2178	−0.0805	−0.0128
1.5	−0.4020	−0.3823	−0.3798	−0.3771	−0.3734	−0.3684	−0.3527	−0.3332	−0.2029	−0.0813	−0.0142
1.6	−0.3440	−0.3096	−0.3083	−0.3068	−0.3045	−0.3017	−0.2922	−0.2800	−0.1868	−0.0812	−0.0155
1.7	−0.2943	−0.2606	−0.2580	−0.2564	−0.2549	−0.2531	−0.2469	−0.2387	−0.1708	−0.0803	−0.0167
1.8	−0.2114	−0.2207	−0.2189	−0.2181	−0.2174	−0.2161	−0.2119	−0.2063	−0.1558	−0.0787	−0.0178
1.9	−0.1782	−0.1907	−0.1904	−0.1890	−0.1881	−0.1873	−0.1843	−0.1802	−0.1419	−0.0766	−0.0188
2.0	−0.1741	−0.1660	−0.1658	−0.1652	−0.1648	−0.1642	−0.1620	−0.1590	−0.1294	−0.0741	−0.0196

TABLE 18-1*c*

Stress coefficients for a linear variation of skin friction as shown in case 3 of Fig. 18-5

(−) = compression; $m = z/D$; $n = r/D$

m	n = 0.00	0.02	0.04	0.06	0.08	0.10	0.15	0.20	0.50	1.0	2.0
					Poisson ratio = 0.20						
1.0		−11.5315	−5.3127	−3.3023	−2.3263	−1.7582	1.0372	−0.7033	−0.1963	−0.0618	−0.0082
1.1	−2.8427	−2.7518	−2.4908	−2.1596	−1.8329	−1.5469	1.0359	−0.7346	−0.2074	−0.0656	−0.0096
1.2	−1.2853	−1.2541	−1.2158	−1.1620	−1.0930	−1.0162	0.8211	−0.6529	−0.2141	−0.0689	−0.0110
1.3	−0.7673	−0.7753	−0.7585	−0.7420	−0.7195	−0.6928	0.6142	−0.5312	−0.2139	−0.0717	−0.0123
1.4	−0.5937	−0.5450	−0.5343	−0.5267	−0.5181	−0.5063	0.4693	−0.4261	−0.2068	−0.0737	−0.0136
1.5	−0.4485	−0.4051	−0.4059	−0.4006	−0.3960	−0.3901	0.3704	−0.3460	−0.1947	−0.0750	−0.0148
1.6	−0.3635	−0.3201	−0.2326	−0.3183	−0.3154	−0.3123	0.3008	−0.2861	−0.1803	−0.0754	−0.0160
1.7	−0.3204	−0.2583	−0.2635	−0.2618	−0.2595	−0.2574	0.2503	−0.2408	−0.1652	−0.0750	−0.0170
1.8	−0.2533	−0.2222	−0.2239	−0.2206	−0.2181	−0.2166	0.2122	−0.2059	−0.1506	−0.0739	−0.0180
1.9	−0.2382	−0.1761	−0.1855	−0.1880	−0.1878	−0.1853	0.1827	−0.1782	−0.1371	−0.0722	−0.0188
2.0	−0.1767	−0.1643	−0.1648	−0.1630	−0.1631	−0.1614	0.1591	−0.1561	−0.1248	−0.0700	−0.0196
					Poisson ratio = 0.30						
1.0		−12.1310	−5.5765	−3.4591	−2.4320	−1.8346	1.0774	−0.7276	−0.1997	−0.0616	−0.0777
1.1	−3.0612	−2.9620	−2.6751	−2.3119	−1.9547	−1.6433	1.0908	−0.7680	−0.2115	−0.0654	−0.0090
1.2	−1.3821	−1.3465	−1.3052	−1.2465	−1.1706	−1.0864	0.8730	−0.6899	−0.2198	−0.0689	−0.0104
1.3	−0.8262	−0.8035	−0.8130	−0.7949	−0.7705	−0.7411	0.6548	−0.5639	−0.2212	−0.0720	−0.0117
1.4	−0.6194	−0.5827	−0.5722	−0.5630	−0.5540	−0.5410	0.5005	−0.4530	−0.2150	−0.0744	−0.0130
1.5	−0.5189	−0.4337	−0.4332	−0.4281	−0.4227	−0.4163	0.3946	−0.3679	−0.2033	−0.0760	−0.0143
1.6	−0.3841	−0.3415	−0.3449	−0.3395	−0.3361	−0.3327	0.3202	−0.3039	−0.1887	−0.0768	−0.0155
1.7	−0.3332	−0.2764	−0.2810	−0.2782	−0.2764	−0.2739	0.2660	−0.2556	−0.1732	−0.0767	−0.0166
1.8	−0.2837	−0.2268	−0.2381	−0.2347	−0.2319	−0.2300	0.2253	−0.2183	−0.1580	−0.0758	−0.0176
1.9	−0.2654	−0.1873	−0.1963	−0.1991	−0.1988	−0.1965	0.1937	−0.1887	−0.1439	−0.0742	−0.0186
2.0	−0.1872	−0.1730	−0.1744	−0.1732	−0.1725	−0.1714	0.1684	−0.1651	−0.1310	−0.0721	−0.0194
					Poisson ratio = 0.40						
1.0		−12.9304	−5.9282	−3.6683	−2.5729	−1.9365	1.1311	−0.7600	−0.2042	−0.0614	−0.0069
1.1	−3.3525	−3.2423	−2.9209	−2.5144	−2.1171	−1.7719	1.1641	−0.8125	−0.2170	−0.0652	−0.0083
1.2	−1.5030	−1.4712	−1.4255	−1.3588	−1.2742	−1.1800	0.9422	−0.7394	−0.2274	−0.0689	−0.0096
1.3	−0.8965	−0.9066	−0.8862	−0.8649	−0.8383	−0.8056	0.7089	−0.6076	−0.2308	−0.0723	−0.0109
1.4	−0.6753	−0.6350	−0.6222	−0.6120	−0.6018	−0.5874	0.5419	−0.4890	−0.2260	−0.0752	−0.0123
1.5	−0.5629	−0.4718	−0.4712	−0.4641	−0.4584	−0.4511	0.4270	−0.3971	−0.2147	−0.0773	−0.0136
1.6	−0.4198	−0.3701	−0.3730	−0.3672	−0.3642	−0.3600	0.3461	−0.3278	−0.1999	−0.0786	−0.0149
1.7	−0.3752	−0.2840	−0.3039	−0.3011	−0.2984	−0.2956	0.2870	−0.2754	−0.1838	−0.0788	−0.0161
1.8	−0.3158	−0.2496	−0.2575	−0.2530	−0.2497	−0.2479	0.2427	−0.2349	−0.1680	−0.0782	−0.0172
1.9	−0.2851	−0.2022	−0.2122	−0.2155	−0.2142	−0.2113	0.2083	−0.2028	−0.1530	−0.0769	−0.0182
2.0	−0.2012	−0.1929	−0.1878	−0.1854	−0.1850	−0.1837	0.1807	−0.1771	−0.1393	−0.0749	−0.0191

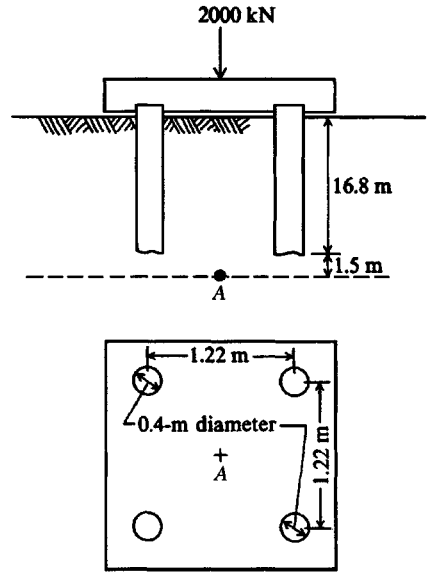

Figure E18-3

Step 2. Assume one-half of load carried by point and one-half carried by friction, as in result 1 preceding. For point,

$$\sigma_A = 4\left[\frac{2000}{2(4)(16.8)^2}\right](-12.4) = -44 \text{ kPa}$$

For constant variation of skin friction (case 2) and using program FFACTOR, we find that

$$\sigma_A = 4\left[\frac{200}{2(4)(16.8)^2}\right](-1.73) = -6 \text{ kPa}$$

$$\sum \sigma_A = -44 - 6 = \mathbf{-50} \text{ kPa} \qquad \text{(compression)}$$

Step 3. By conventional analysis, what is stress at A? Use Fig. 18-4*b*.

$$H = \frac{16.8}{3} = 5.6 \text{ m} \qquad \text{(above pile tip)}$$

Therefore, depth to $A = 5.6 + 1.5 = 7.1$ m and (using $2V$ to $1H$); total cap load = 2000 kN

$$\sigma_A = \frac{2000}{(1.22 + 7.1)^2} = \mathbf{29} \text{ kPa} \qquad \text{(compression)}$$

This compares with 86 kPa for point-load conditions and 50 kPa for one-half point, one-half skin friction. A possible value is $\sigma = (87 + 50 + 29)/3 \cong 50$ kPa.

////

18-5 SETTLEMENTS OF PILE GROUPS

The settlement of a pile group is exactly equal to the displacement of the pile point plus the elastic shortening of the pile shaft between cap and point as illustrated in Fig. 18-6. For point-bearing piles the point displacement is relatively small and the principal displacement is the elastic shortening of the pile. For friction piles the point displacement will be the

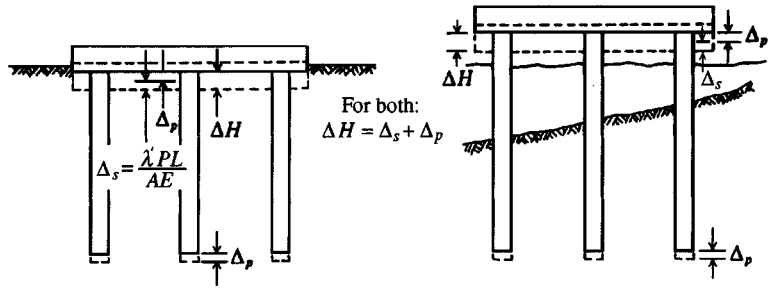

(*a*) **Pile cap in contact with ground.** (*b*) **Pile cap above ground.**

Figure 18-6 Pile cap/group settlement. In (*a*) the cap-soil interaction introduces considerable difficulty in evaluating the elastic shortening of the pile. In both cases the point-deflection computation is a considerable exercise in engineering judgment.

significant quantity causing settlement. Note, however, that the *total point displacement is due to both point load and settlement of the underlying soil from stresses from shaft friction or areal fill or ground subsidence.* The group settlement involves the following:

1. The problem of obtaining the stresses in the strata below the point and the correct elastic properties of those soils so that the point displacement can be computed. Currently the only practical means is to use some type of Boussinesq or Mindlin solution of Sec. 18-4.
2. The determination of the load carried by the piles in the group and the distribution of the load along the pile shaft so that the axial shortening can be computed. Vesić (1969*a*) found that when a pile group consists of more than just corner (3 and 4 pile groups) piles, the interior piles carry more load than side piles and corner piles carry less load than side piles. In numerical perspective we might say that if interior piles carry $P = 400$ kN, then side piles carry about 0.75 to $0.80P = 300$ to 320 kN and corner piles about 0.6 to $0.7P = 240$ to 280 kN. Now there is the question of whether this is a short-duration load test phenomenon or exists some time after the pile group is in service. Since soil tends to creep under sustained load, like concrete, it is reasonable to expect that the individual pile loads in a group will tend to more nearly equalize under sustained loading (the design load). When load equalization occurs, there are questions of how long it will take, whether the settlements change, how—if at all—they are influenced by the pile cap rigidity, whether the pile cap is in contact with the soil, and pile spacing. When the pile cap is above ground (or water as for offshore structures), the pile loads can be estimated reasonably well. When the cap is of concrete poured directly on the ground as is the usual case, except on expansive soil, the pile load is considerably indeterminate. According to Broms (1972) the modulus of elasticity of concrete piles is not a constant value but deteriorates with time as much as 10 percent. This decrease is not likely to affect the computations to any significant amount. First, this change is somewhat speculative for reinforced piles because the transformed section is rarely used. Second, concrete strength gradually improves with age.

   This latter modulus reduction, if deemed valid, would also apply equally for wood. The major problem for all pile materials is the distribution of load along the pile shaft.

To obtain the pile load (but not its distribution along the shaft—this must be estimated) for an estimate of pile shortening under load, use your FADMAT program or similar and

input a composite value of k_s for those mat elements contributing to computation of the soil "spring" at the given pile locations. This method appears to be similar to that of Butterfield and Banerjee (1971).

The composite k_s would be obtained by computing the pile constant for compression (as in Sec. 18-10), which may be of the form $\lambda' AE/L$. The contributory area of the mat for the soil "spring" at the node is obtained as $K_i = k_s ab$ as in Fig. 18-7. The equivalent soil modulus is computed by considering the pile and soil springs in parallel (as in Fig. 18-7*b*) with the same deflection to obtain

$$k_s abX + \frac{\lambda' AE}{L} X = K'X \qquad (a)$$

from which the equivalent spring $K' = k_s ab + \lambda' AE/L$.

The equivalent composite soil modulus at that node is $K_s' = K'/ab$. The computer output will give the total nodal force $K'X$, which can be separated into the pile and soil components using Eq. (*a*) above. Obviously, the solution will be only as good as the soil parameter k_s and the pile constant. The λ' term used in $\lambda' PL/AE$ is to make allowance for the type of pile and distribution of skin resistance. In any case the computer solution will give values of relative effects that may be useful in estimating pile-group response.

Larger pile groups should settle more than small groups for the same pile loads owing to the overlapping effect of stresses below the pile point from the additional piles. In addition

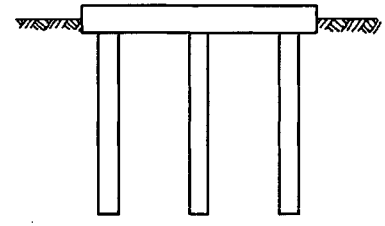

(*a*) Pile-cap–pile-soil interaction.

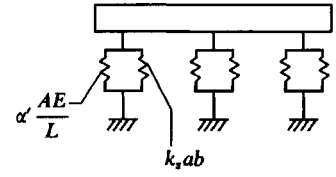

(*b*) Soil and pile springs in parallel

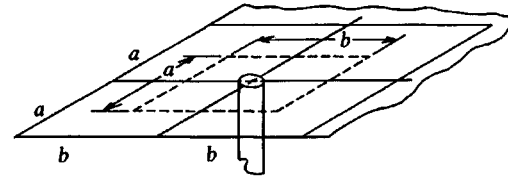

(*c*) Contributory soil area for computing soil "spring."

Figure 18-7 Method of obtaining equivalent soil modulus for input into mat computer program (B-6) to obtain an estimate of the effects of the interaction displayed in (*a*).

to the overlap effect the outer piles cause stresses to penetrate to a greater depth L_1 such that integration of strain effects

$$\delta = \int_{L_0}^{L_1} \epsilon \, dL$$

produces a larger deflection beneath the pile group.

It is usual (but usually not correct) to assume that the pile cap is rigid so that the cap movements can be described by rigid body translations and rotations.

Pile groups supported by clay soils may produce both elastic (or immediate) and consolidation settlements. The elastic settlements may be the major amount for preconsolidated clays; the consolidation settlements may be the principal value(s) for normally consolidated clays using friction or floating piles. The stress coefficients of Table 18-1 may be used to estimate the stress increase causing consolidation settlements using Eq. (5-22) for Δq and Eq. (2-44) or its equivalent for ΔH.

Pile groups supported by cohesionless soils will produce only immediate-type settlements, the principal problems being to obtain the correct evaluation of the stress increase in the underlying strata, the depth L_1 through which the stress increase acts, and the elastic properties so that Eq. (5-16*a*) or simply

$$\delta = \frac{\sigma L_1}{E_s} \tag{18-8}$$

can be used to obtain the downward point movement δ.

There are two basic approaches to computing pile-group settlements: empirical and theoretical. Either method involves estimating the settlement of a single pile ΔH_{pt} using one or another of the methods given in Sec. 16-10.

The pile-group settlement ΔH_g is usually larger than that obtained for a single pile (either computed or measured). In a general form, the group settlement of n piles is related to the settlement of a single pile as

$$\Delta H_g = F\alpha_g \cdot n \cdot \Delta H_{pt} \tag{18-9}$$

where α_g = a group interaction factor usually in the range of 0.3 to 0.7 (before any adjustment) with larger values for small numbers of piles n or small s/D spacing ratios; α_g is smaller for end-bearing piles, for large s/D or n, or if a very stiff layer (or rock) is in close proximity to the pile point. The pile length/width (L_p/D) ratio also modifies the group settlement, and we might obtain F values from the following table:

L_p/D	Adjustment factor F
5	0.75
10	0.80
100	1.25

The adjustment factor F is also dependent on the spacing ratio s/D. A theoretical approach originating with Dr. H. Poulos and his coworkers at the University of Sydney, Australia [see Poulos (1979)], gives Eq. (18-9) in the following slightly different form. This form uses single-pile settlement based on a unit load $\Delta H'_{pt}$ with an average pile load in the group of P' to obtain

$$\Delta H_g = \alpha'_g(P')\Delta H'_{pt} \tag{18-9a}$$

Poulos (1979) provides a number of tables and curves from which one can obtain α'_g = function of (L_p/D, s/D, E_s, μ, H_{stratum}/L_p). In most cases some interpolation will be required. This approach—while theoretical—requires soil properties that are usually "best estimates." Most engineers prefer simpler methodologies if the end result is only an estimate. For this reason several more simple methods are given here.

Vesić (1969*a*, 1977)—and others—have suggested computing the settlement of a pile group using using the settlement of a single pile as

$$\Delta H_g = \Delta H_{pt}\sqrt{B/D} \qquad \text{(units of } \Delta H_{pt}\text{)} \tag{18-10}$$

where B = least lateral group dimension, m or ft, and
D = pile diameter or effective width (and as used for the spacing ratio s/D), m or ft.

Here the $F \cdot \alpha_g \cdot n$ terms of Eq. (18-9) have been combined into a single group factor in Eq. (18-10) as

$$F \cdot \alpha_g \cdot n = \sqrt{B/D} \tag{18-10a}$$

Equation (18-10) is suggested for use by NAVAC (1982*b*), but only for cohesionless soils. Based on testing large-scale group models containing four and nine piles in sand, Vesić (1969*a*) found that using the group amplification factor of $\sqrt{B/D}$ gave a scatter of about ±50 percent.

Meyerhof (1976) gives some empirical equations for the settlement of pile groups ΔH_g using in situ penetration test data (usually about all that is available for many projects). He computes the settlement of a single pile similarly to the settlement of a shallow spread footing (adjusted for depth), so an estimate of the intensity of the vertical stress Δq at the pile tip is required. For a pile group a modification of Eq. (18-10*a*) is used, so the pile group width B (which is dependent on the s/D ratio) must be computed.

We can approximately derive Meyerhof's (1976) equation for the standard penetration test (SPT) as follows: Meyerhof (1956) gives $q_{\text{ult}} = N_{55}B$, ft/10 (tons/ft^2), which in SI becomes $q_{\text{ult}} = N_{55}B$, m/0.0318 (kPa). It is usual to assume that the ultimate bearing pressure q_{ult} occurs at a settlement of ΔH = 25 mm (1 in.). Meyerhof (1956) also suggested a depth factor = $1 + 0.33L_p/D \leq 1.33$. Meyerhof and others later found that this equation predicts q_{ult} about 50 percent too low. Making these adjustments, and using pile diameter or width D for footing width B, we obtain the ultimate bearing pressure as

$$q_{\text{ult}} = \frac{N_{55}D}{0.0318}1.33 \times 1.5 = 62.7N_{55}D, \text{ kPa} \tag{a}$$

Now for the actual pile point stress Δq, we can make a ratio to give the point settlement as

$$\frac{\Delta H_{pt}, \text{mm}}{25, \text{mm}} = \frac{\Delta q, \text{kPa}}{q_{\text{ult}}, \text{kPa}} \rightarrow \Delta H_{pt} = \frac{25\Delta q}{62.7N_{55}D}, \text{mm} \tag{b}$$

If we assume that Δq should be about 25 percent larger than the actual point bearing to allow for a skin resistance contribution, we can simplify Eq. (*b*) above to

$$\Delta H_{pt} = \frac{\Delta q}{2N_{55}D}, \text{mm} \tag{c}$$

Using the group factor of Eq. (18-10) of $F_g = \sqrt{B/D}$ in Eq. (*c*) to amplify single-pile settlement to a group value gives

$$\Delta H_g = \Delta H_{pt} F_g = \frac{\Delta q \sqrt{B/D}}{2N_{55}D}, \text{ mm} \tag{18-11}$$

Meyerhof's original form of Eq. (18-11) was in Fps units and did not include the D-term (he used $D = 1$). The above form should be used with SI units. Other terms are defined following:

B = pile-group width (and indirectly includes the s/D spacing ratio), m (you must use meters in this equation)

Δq = vertical pressure at pile tip (do not include any skin resistance contribution, as it was done in the simplification), kPa

$k_1 = 1 - \dfrac{L_p}{8B} \geq 0.5$ (L_p = pile length)—see Eq. (18-12)

N_{55} = average SPT N_{55} value in the zone from about group width B above to $2B$ below the pile tips

For the cone penetration test (CPT) we can estimate settlement of a pile group as

$$\Delta H_g = \frac{k_1 \Delta q B}{2q_c} \quad \text{(units of group width } B\text{)} \tag{18-12}$$

Use Δq, q_c in the same pressure units, and other terms are defined with Eq. (18-11). Obtain an average q_c for Eq. (18-12) using the same pile tip zone as used to obtain the average N_{55} used in Eq. (18-11).

The Focht and O'Neill (1985) pile survey reported that only about 18 percent of the respondents used the elastic settlement procedures as given in Poulos (1979) and earlier. The other 82 percent are using a variety of procedures—or nothing at all. The author has not included Poulos's methodology since it is essentially based on the Mindlin solution. The methodology presented here is more fundamental and gives the user some control over the analysis as illustrated in the previous examples and in the following example.

Example 18-4. One of the better-reported series of building and pile settlements available in geotechnical literature was made by Koerner and Partos (1974). From these data the soil profile and typical pile cap on two columns are shown in Fig. E18-4.

Other data: Pile load = 1070 kN (approx.)
Pile length = 7.62 m (cased and enlarged base)
Pile diameter = 406 mm f'_c = 35 mPa
E_s = 27.57 MPa (doubled by Koerner and Partos to allow for increased density)
$s = 2.7D$
Measured settlements 38 to 84 mm with an average ΔH = 65 mm

Required. Estimate settlement of a typical pile cap.

Solution. There are a number of ways to estimate settlement values for this building including Eq. (18-9). We will look at two of them. First we will need to find the point displacement, which is done as follows:

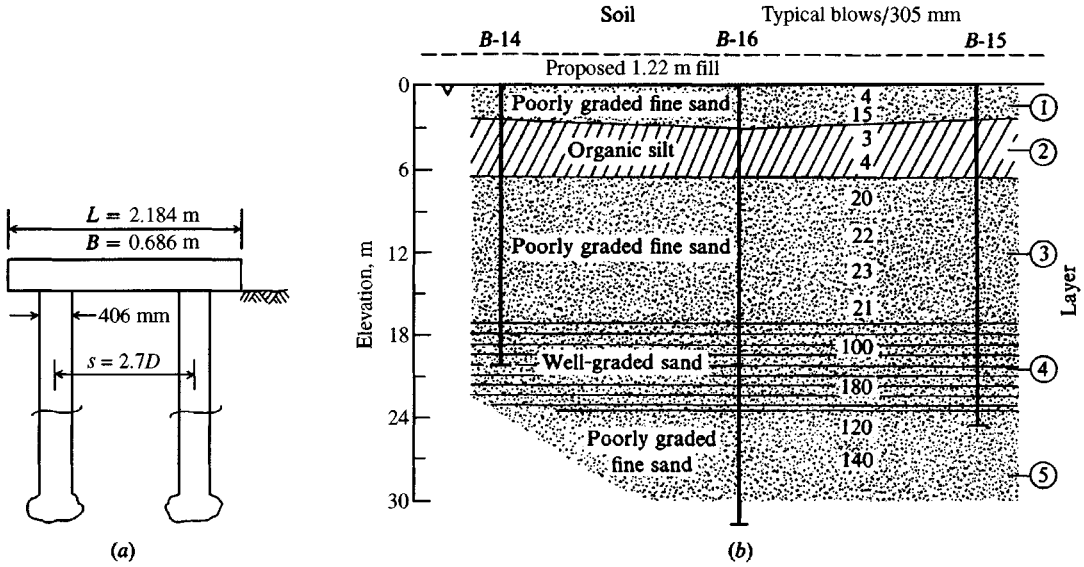

Figure E18-4

Step 1. Use Table 18-1*c*, case 3, since a load test indicates very little point movement for a working load of 1070 kN indicating the principal load mechanism must be skin resistance. Assume $\mu = 0.3$.

$$L_p = 7.62 \text{ m} \qquad s = 2.7D = 1.0962 \text{ m}$$

take $r = \frac{s}{2}$

$$n = \frac{r}{L_p} = \frac{1.0962}{2(7.62)} = 0.072 \qquad \text{(use 0.06 to avoid interpolation)}$$

With this n and several $m = z/L_p$ values we obtain the following table for K_z at a point midway between the two piles beneath the cap:

z/L_p	K_z
1.0	3.46
1.1	2.31
1.2	1.25
1.3	0.79
1.4	0.56
1.5	0.43
1.6	0.34
1.7	0.28
1.8	0.23
1.9	0.20
2.0	0.17

The average influence value in the zone L_p to $2L_p$ using the trapezoidal rule is

$$K_z = \left(\frac{3.46 + .17}{2} + 2.31 + 1.25 + 0.79 + \cdots + 0.20\right) = 8.205$$

$$K_{z,\text{av}} = \frac{8.205}{10} = 0.82$$

Step 2. Compute the average stress in depth L_p below pile and the corresponding settlement. Assume stress only from the two piles:

$$\sigma = \frac{2PK_{z,av}}{L_p^2} = \frac{2(1070)(0.82)}{7.62^2} = 30.2 \text{ kPa}$$

The point settlement based on $E_s = 190$ kPa is

$$\Delta H_{\text{pile}} = \frac{\sigma L}{E_s} = \frac{30.2(7.62)}{27.57} = \mathbf{8.4} \text{ mm}$$

which compares reasonably well with the value of 5.3 or 5.6 measured in the load test.

Method 1. Total settlement is settlement of cap plus point movement just computed. Use Eq. (5-16*a*) for cap settlement.

$$B = 0.686 \text{ m} \qquad L = 2.185 \text{ m} \qquad \text{(both given in reference)}$$
$$E_s = 27.57 \text{ mPa} \qquad \text{(given)}$$

Using Table 5-5 and N values given in the reference and weighting, one can obtain $E_s \cong 14\,300$ kPa. We will therefore use an average since the value of 27 570 was arbitrarily doubled and may be somewhat too large.

$$E_s = \frac{27\,570 + 14\,300}{2} = 20\,900 \text{ kPa} \qquad \text{(rounding)}$$

For $L/B = 2.19/0.69 = 3.17$ (use 3) and for $H = 23$ m from the boring log, we obtain $H/B' = 23(2)/0.686 = 67$ (use 100 to avoid massive interpolation). From Table 5-2 we obtain

$$I_s = 0.872 + \frac{1 - 2(0.3)}{1 - 0.3}(0.005) = 0.87 \qquad \text{Take } I_F = 1.0$$

$$\Delta H = \Delta q B' \frac{1 - \mu^2}{E_s} m I_s I_F \qquad \text{(Eq. 5-16}a\text{)}$$

$$\Delta q = \frac{2P}{BL} = \frac{2(1070)}{0.686 \times 2.19} = 1420 \text{k Pa} \qquad \text{(2 piles/cap)}$$

Using $m = 4$ contributing corners and 1000 to obtain mm

$$\Delta H_{\text{cap}} = 1420\left(\frac{0.686}{2}\right)\frac{1 - 0.3^2}{20\,900}(4 \times 0.87)(1.0)(1000) = 73.8 \text{ mm}$$

$$\text{Total } \Delta H = \Delta H_{\text{cap}} + \Delta H_{\text{pile}} = 73.8 + 8.4 = \mathbf{82.2} \text{ mm}$$

This compares quite well with 63.5 to 83.8 mm measured.

Method 2. Settlement is computed as elastic shortening of pile + $\Delta H_{\text{pile point}}$. For a linear variation of P at top to $P = P_{\text{top}} - \Delta P$ where $\Delta P = 0.5P$, we have

$$e = \int_0^{L_p} \epsilon \, dy = \frac{1}{AE}\int_0^{L_p}\left(P_o - \Delta P \frac{y}{L}\right) dy$$
$$= \frac{1}{AE}\left(P_o L_p - \frac{\Delta P L_p}{2}\right)$$
$$= \frac{L_p}{AE}\left(P_o - \frac{0.5}{2}P_o\right) = \frac{0.75 P_o L_p}{AE}$$

Taking $E_c = 27\,805$ MPa for $f_c' = 35$ MPa and $A = 0.1294$ m^2 for 0.406-m diameter pile, we have

$$e = \frac{PL_p}{AE} = \frac{0.75 \times 1070 \times 7.62}{0.1294 \times 27\,805} = 1.7 \text{ mm}$$

$$\Delta H_g = \Delta H_{\text{pile}} + e = 8.4 + 1.7 = \mathbf{10.1} \text{ mm}$$

It is evident that, although this method is correct for the stated assumptions, the measured deflections indicate something causing additional settlement. Probably the 1.22 m of fill is a major contributor.

////

18-6 PILE CAPS

Unless a single pile is used, a cap is necessary to spread the vertical and horizontal loads and any overturning moments to all the piles in the group. The cap is usually of reinforced concrete, poured on the ground unless the soil is expansive. Caps for offshore structures are often fabricated from steel shapes. The pile cap has a reaction that is a series of concentrated loads (the piles); and the design considers the column loads and moments, any soil overlying the cap (if it is below the ground surface), and the weight of the cap. It was usual, before the widespread use of personal computers and the availability of computer programs such as FAD3DPG on your diskette or B-28 listed on your diskette, to make the following assumptions for a conventional pile cap design:

1. Each pile carries an equal amount of the load for a concentric axial load on the cap; or for n piles carrying a total load Q, the load P_p per pile is

$$P_p = \frac{Q}{n} \tag{18-13}$$

2. The combined stress equation (assuming a planar stress distribution) is valid for a pile cap noncentrally loaded or loaded with a load Q and a moment, as

$$P_p = \frac{Q}{n} \pm \frac{M_y x}{\sum x^2} \pm \frac{M_x y}{\sum y^2} \tag{18-14}$$

where M_x, M_y = moments about x and y axes, respectively

x, y = distances from y and x axes to any pile

$\sum x^2, \sum y^2$ = moment of inertia of the group, computed as

$$I = I_0 + Ad^2$$

but the pile moment of inertia I_0 is negligible, and the A term cancels, since it is the pile load desired and appears in both the numerator and denominator of Eq. (18-14).

The assumption that each pile in a group carries an equal load may be nearly correct when the following criteria are all met:

1. The pile cap is in contact with the ground.
2. The piles are all vertical.
3. Load is applied at the center of the pile group.
4. The pile group is symmetrical and the cap is very thick (or rigid), usually about 1.8 to 2^+ m thick for plan dimensions of 2 to 3 m and depending on pile spacing.

In a practical case of a four-pile symmetrical group centrally loaded, each pile will carry one-fourth of the vertical load regardless of cap rigidity (or thickness). With a fifth pile directly under the load, cap rigidity will be a significant factor.

The structural design of pile caps is only minimally addressed in the literature but the following may be used as a guide:

1. Bending moments are taken at the same sections as for reinforced-concrete footings and defined in Art. 15-4 of the ACI Code (and as given in Chap. 8).
2. Pile caps must be reinforced for both positive and negative bending moments. Reinforcement should be placed so there is a minimum cover of 70 mm for concrete adjacent to the soil. When piles extend into the cap only about 70 mm, the bottom cap reinforcement should be 75 mm above the pile top to control concrete cracking around the pile head.
3. Pile caps should extend at least 150 mm beyond the outside face of exterior piles and preferably 250 mm. When piles extend into the cap more than 75 mm, the bottom rebars should loop around the pile to avoid splitting a part of the cap from pile head moments and shears.
4. When pile heads are assumed fixed, they should extend into the pile cap at least 300 mm. The minimum thickness of pile cap above pile heads is 300 mm (required by ACI 318- in Art. 15-7).
5. Some kind of tension shear connectors should be used on the pile heads if the piles are subjected to tension forces.
6. Pile cap shear is computed at critical sections as shown in Fig. 18-8.

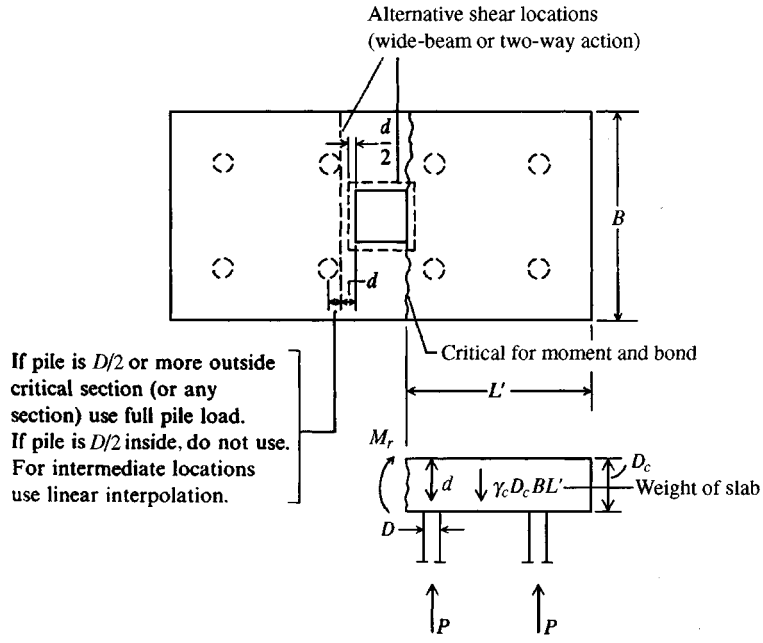

Figure 18-8 Critical pile cap locations for shear, moment, and bond computations according to Chap. 15 of ACI 318-.

Pile cap moments and shears for design are best obtained by using a FEM or a computer program such as B-6 based on the finite-grid method (FGM), or, preferably, B-28. When the cap load is at the centroid of both cap and group, the group is symmetrical, and the cap load is vertical, any computer program for plates will give node moments with adequate accuracy. The FGM can be used to obtain both the node moments and shears. In using these programs one replaces (or adds the vertical pile spring) the soil spring at the nodes where piles are located with a pile "spring" and produces a set of output. Since the pile spring is usually several orders of magnitude larger than the soil springs in the soft soils where piles are usually used, the model is *not significantly improved* by using soil springs at all nodes and with soil and pile springs in parallel at the pile nodes.

When there are battered piles and/or additional load degrees of freedom, one must use a special program to obtain a correct pile cap solution. This problem is considered in more detail in Sec. 18-11. In three- and four-pile groups centrally loaded with a vertical load, cap flexibility is not a factor as each pile carries P/n, where n = the three or four piles in the group. When there are more piles than this—particularly both interior and exterior—cap flexibility is a significant factor; e.g., in a centrally loaded five-pile group with four exterior and one central pile the central pile will carry most of the load until the cap becomes very rigid (thick). In a long-term case, the pile loads might tend to even out somewhat; however, the piles must be designed to support worst-case loading even if it is transient.

18-7 BATTER PILES

When large lateral loads are to be resisted by a pile group, it has been a common practice to use piles driven at a slope with the vertical, i.e., batter piles. It has also been common to assume that the batter piles carry all the lateral loads. All piles have some lateral load-carrying ability dependent on the pile width, the flexural rigidity (EI) of the pile, and the stiffness of the soil in which they are embedded. Early methods of pile-group analysis with both vertical and lateral loads were primarily graphical. These early methods also assumed that the piles were axially loaded, which precluded bending moments being developed. From combining graphical solutions and the assumptions of axial loading, it naturally followed that the lateral loads had to be carried by batter piles.

Modern methods of pile-group analysis use the computer, and additionally lateral pile-load tests have verified what the computer solutions illustrate, namely, that all the piles in a group carry lateral load. The graphical solutions are no longer used, since they are obviously incorrect. The computer method of group analysis, being the only practical way of analyzing a group, is the only method presented in this chapter.

Common pile batters range from $\frac{1}{12}$ (1 horizontal to 12 vertical) to $\frac{5}{12}$. When the batter exceeds $\frac{1}{4}$, the driving may require special equipment, with resulting increased costs.

18-8 NEGATIVE SKIN FRICTION

When a fill is placed on a compressible soil deposit, consolidation of the compressible material will occur. When a pile is driven through (or into) the compressible material (either before or after fill placement) before consolidation is complete, the soil will move downward relative to the pile. This relative movement will develop skin friction between the pile and the moving soil termed *negative skin friction*. According to measurements reported by Bjerrum et al. (1969), Bozozuk (1972), and Bozozuk et al. (1979), the negative skin friction can exceed the

allowable load for pile sections. Fellenius (1972) has also reported large values of measured negative skin resistance.

The principal effect of negative skin resistance is to increase the axial load in the lower fixed portion of the pile. It may result also in increased pile settlements due to the axial shortening and/or additional point penetration of the pile under the increased axial load. Note that in Fig. 18-9 the fill settlement may be such that a gap forms between the bottom of the pile cap and the soil. This will transfer the full cap weight to the piles and may change the bending stresses in the cap.

Negative skin friction can produce large tension stresses when the effect is from expansive soils—especially if no, or insufficient, gap is left between soil and pile cap and the soil expands against both the pile and the cap.

Negative skin friction can be developed from the following:

1. A cohesive fill placed over a cohesionless soil deposit. The fill develops shear resistance (adhesion) between the soil and pile from lateral pressure/flow effects, so that the pile, is pushed downward as the fill consolidates. Little effect is produced in the underlying cohesionless soil except that the weight of fill increases the lateral pressure. This provides additional skin resistance against further pile penetration and raises the center of resistance nearer the cohesive fill for point-bearing piles.
2. A cohesionless fill placed over a compressible, cohesive deposit. In this case there will be some downdrag in the fill zone, but the principal downdrag will occur in the zone of consolidation. For point-bearing piles any settlement of the group will be due to axial shortening of the pile. For floating piles, additional penetration with matching settlement will occur unless the pile is sufficiently long that the bottom portion can develop enough positive skin resistance to balance the additional load developed by negative (or downward) skin

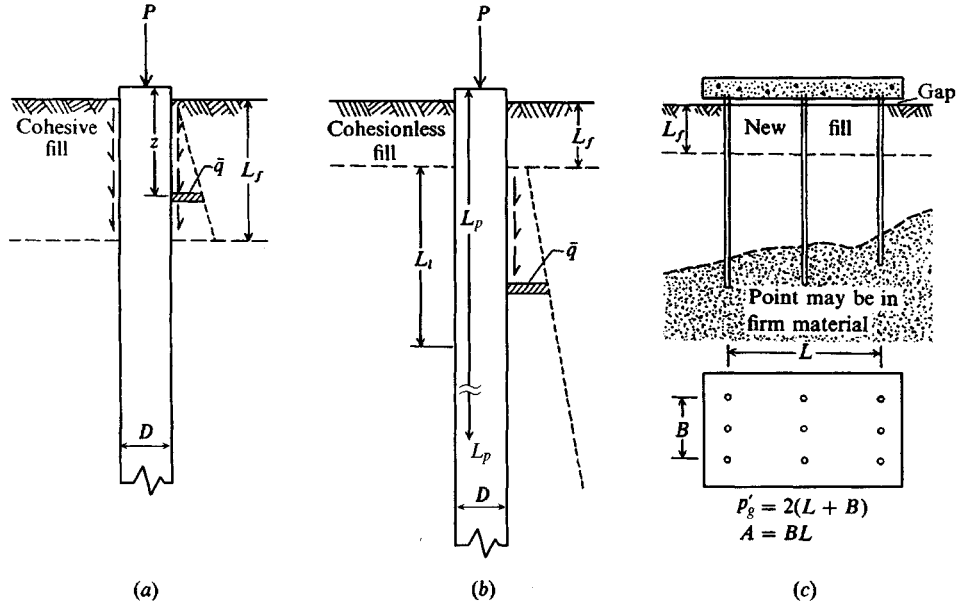

Figure 18-9 Development of negative friction forces on a single pile from a cohesive or cohesionless fill or on a pile group in a cohesive soil fill.

resistance. In this case an approximation of the location of the balance, or neutral, point can be made.

3. Lowering of the groundwater table with resulting ground subsidence.
4. Pile-driving (and load-test) operations that produce negative stresses in the upper shaft when the load is released and the pile shaft expands upward. The resulting slip and negative skin resistance must be balanced by a positive skin resistance in the lower shaft and/or point load [Vesić (1977)].

For negative skin resistance forces to develop significantly, a portion of the pile must be fixed against vertical movement, such as the point being on rock or the lower part being in a dense sand. If the entire pile moves down with the consolidation effect no negative skin resistance forces develop. For a single pile the negative skin resistance force can be estimated as follows:

1. For cohesive fill overlying cohesionless soils as in Fig. 18-9*a*:

$$P_{nf} = \int_0^{L_f} \alpha' p' \bar{q} K \, dz \tag{18-15}$$

where α' = coefficient relating the effective lateral pressure $\bar{q}K$ to the shearing resistance about the pile perimeter; $\alpha' = \tan\delta$ where $\delta \cong 0.5$ to 0.9ϕ; s_u is replaced by $\bar{q}K$ as this is somewhat of a drained case

p' = pile perimeter

K = lateral earth-pressure coefficient; use $K = K_o = 1 - \sin\phi$

$\bar{q}$ = effective overburden pressure at any depth z

Equation (18-12) could be written using the equivalent of f_s from any of Eqs. (16-14) to obtain the β method, which may be more reliable than the α method of Eq. (18-13) [see Indraratna et al. (1992)]. That is,

$$P_{nf} = \int_0^{L_f} r\beta \bar{q} \, dz$$

where r = reduction factor ranging from about 0.5 to 1.0.

2. For cohesive soil underlying cohesionless fill take the origin of coordinates at the bottom of the fill (see Fig. 18-9*b*):

$$P_{nf} = \int_0^{L_1} \alpha' p' \bar{q} K \, dz \tag{18-16}$$

Below the neutral point (refer to Fig. 18-10), if there is one, positive friction is developed to the bottom of effective pile length L:

$$P_{pf} = \int_{L_1}^{L} \alpha_2' p' \bar{q} K \, dz + P_{np} \tag{18-17}$$

where P_{np} = amount of negative skin resistance carried by the point where point-bearing piles are used and other terms as previously defined.

Note that the general form of $\bar{q}$ is

$$\bar{q} = \bar{q}_o + \gamma' z$$

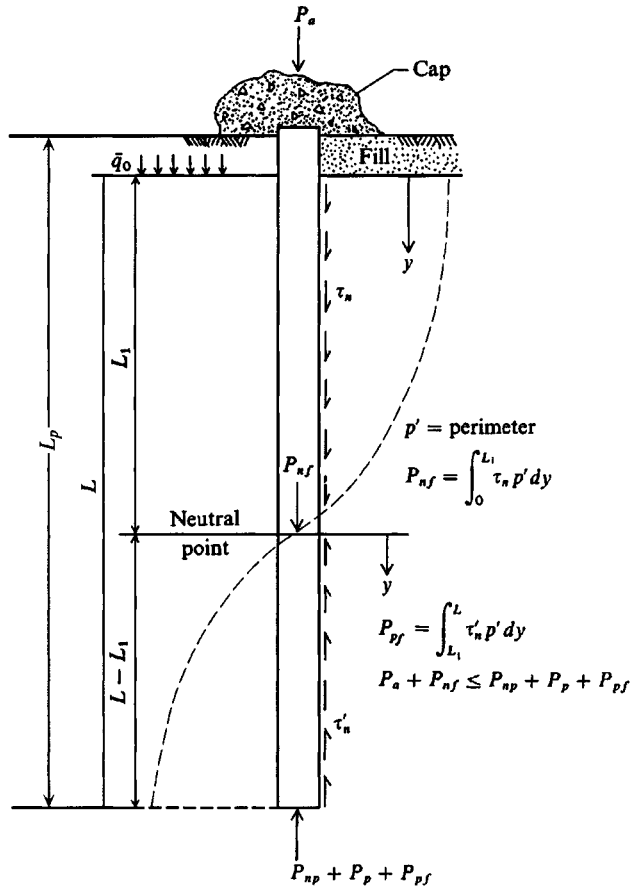

Figure 18-10 Location of neutral point to satisfy statics of vertical equilibrium with negative skin friction acting on pile.

Also it may be necessary to adjust the integration limits if the soil is stratified to obtain a summation of negative skin contributions.

If we take $\alpha' = \alpha'_2$, and a floating pile where $P_{np} \cong 0$, and if we equate Eqs. (18-16) and (18-17) after integration for the limits shown, we obtain

$$\alpha' p' \left(\bar{q}_o L_1 + \frac{\gamma' L_1^2}{2}\right) K = \alpha' p' \bar{q}_o (L - L_1) K + \alpha' p' \gamma' (L^2 - L_1^2) \frac{K}{2}$$

from which L_1, the distance to the neutral point, is

$$L_1 = \frac{L}{L_1}\left(\frac{L}{2} + \frac{\bar{q}_o}{\gamma'}\right) - \frac{2\bar{q}_o}{\gamma'} \tag{18-18}$$

which reduces for $\bar{q}_o = 0$ to

$$L_1 = \frac{L}{\sqrt{2}}$$

Note that L is the effective pile length in the embedment zone and usually is not L_p.

The P_{np} term of Fig. (18-10) requires estimation for either point-bearing piles or where it may be substantial for floating piles. The most recent attempt to refine the location of the neutral point and obtain a general quantification of the negative skin resistance is that of Matyas and Santamarina (1994). This work is not presented because in the author's opinion there are too many estimations (both yield and working load side and point displacements and point capacities—five values to estimate). From their work, however, it does appear that the neutral point is somewhere between $L/2$ and $L/3$ (of Fig. 18-10) measured upward from the pile point. The $L/3$ point seems particularly applicable when the point carries a substantial part of the design load.

If you have enough load test data to compute the neutral point directly, this method is preferable—but seldom likely to be carried out because of the expense. Alternatively, you might compute the neutral point using Eq. (18-18) and see where it locates along shaft zone L. Then arbitrarily compute the estimated axial load to this neutral point and also at depths of about $0.6L$ and $0.67L$ down the shaft length L. If the pile shaft can carry these loads using an SF on the order of 2 to 3, it is adequately sized. If the shaft is overstressed, then use a slightly larger pile cross section.

When the piles are spaced at small s/D ratios, the negative friction force may act effectively on the block perimeter rather than on the individual piles to obtain two modes of stressing requiring investigation:

1. The total group negative skin resistance as the sum from the individual piles,

$$Q_n = \sum P_{nf} \tag{18-19}$$

2. The "block" skin resistance based on shear resistance on the block perimeter + weight of block trapped between the piles,

$$Q_n = f_s L_f p'_g + \gamma L_f A \tag{18-20}$$

where γ = unit weight of soil enclosed in pile group to depth L_f
A = area of pile group enclosed in perimeter p'_g (Fig. 18-9*c*)
$f_s = \alpha' \bar{q} K$ = effective skin resistance on the group perimeter
p'_g = perimeter of pile group

The maximum from Eq. (18-19) or (18-20) should be used for the estimate of the negative skin resistance that could be developed. Some evidence exists [Baligh et al. (1978), Indraratna et al. (1992)] that coating the pile shaft downdrag zone with a special bitumen mixture will substantially reduce the negative skin friction force.

Example 18-5. Estimate the negative skin-friction effect for the pile group shown in Fig. E18-5. The group is square and the piles are driven through the fill after it has been placed and while the underlying soil is still in a consolidating state. The CD angle of internal friction of the fill is assumed as shown.

Solution. We will use Eq. (18-14) to obtain the single-pile increase:

$$P_{nf} = \frac{\alpha' p' \gamma' L_f^2 K}{2} \qquad \text{(after integration)}$$

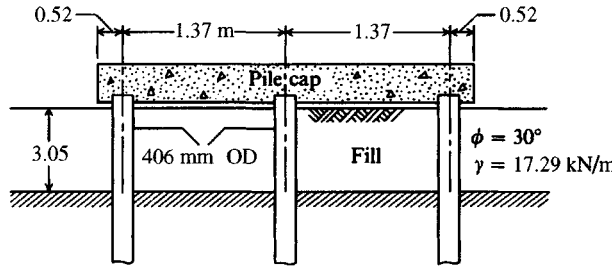

Figure E18-5

Obtain $\alpha' = 0.667 \tan \phi' = 0.667 \tan 30° = 0.385$. Then by inspection $\bar{q}_o = 0$. Take $K = K_o = 1 - \sin 30° = 0.5$, so that

$$P_{nf} = \frac{0.385(\pi \times 0.406)(17.29 \times 3.05^2)0.50}{2} = 20 \text{ kN}$$

Check the alternative possibility of block loading of the piles using Eq. (18-20). Take the effective perimeter of the group based on center-to-center pile spacing:

$$Q_n = f_s L_f p'_g + \gamma L_f A \qquad \text{[Eq. (18-20)]}$$

where $f_s = \dfrac{\alpha' \gamma L_f K}{2}$

$$p'_g = 2(2 \times 1.37) = 5.48 \text{ m}$$

Then

$$Q_n = \frac{0.385 \times 17.29 \times 3.05^2 \times 5.48 \times 0.5}{2} + 17.29 \times 3.05 \times (2 \times 1.37)^2$$

$$= 85 + 396 = 481 \text{ kN}$$

The increase per pile is $481/9 = 53 > 20$ kN and controls.

There is no certainty that the s/D is such as to allow this latter negative resistance to develop, but one will be on the safe side to assume this increase is due to negative skin resistance in the absence of a better limitation on s/D.

////

Example 18-6. Redo Example 18-5 as if the fill is only 1.5 m deep and the underlying soil is a soft clay. Assume the piles are $D = 400$ mm $\times$ 25 m long. The water table is at the top of the clay and $\gamma'_{\text{clay}} = 9.4$ kN/m³. Assume the piles are floating and the clay is normally consolidated with $\phi' = 30°(CD)$.

Required. Compute the location of the neutral point and the maximum load increase in the piles due to negative skin function.

Solution. We will use Eq. (18-18) and take an effective $L = 25 - 1.5 = 23.5$ m:

$$\bar{q}_o = 17.29 \times 1.5 = 26 \text{ kPa} \qquad \text{(on top of clay)}$$

$$L_1 = \frac{L}{L_1}\left(\frac{L}{2} + \frac{\bar{q}_o}{\gamma'}\right) - \frac{2\bar{q}_o}{\gamma'} = \frac{23.5}{L_1}\left(\frac{23.5}{2} + \frac{26}{9.4}\right) - \frac{2(26)}{9.4}$$

$$L_1 = \frac{341.1}{L_1} - 5.53$$

Solving by trial (programmable calculator), we find $L_1 = 15.9$ m. From the ground surface (or base of pile cap) $L_1' = 15.9 + 1.5 = 17.4$ m. The increase in pile load is the accumulation of negative friction from the fill base (distance of L_1) to the neutral point (see Fig. 18-10), or

$$P_n = \alpha' p' \left(\bar{q}_o + \frac{\gamma' L_1}{2}\right) L_1 K$$

Use $\alpha' = 0.667 \tan 30° = 0.385$; $K = 1 - \sin\phi = 0.50$; and $p' = \pi D = 0.40\pi = 1.26$ m to find

$$P_n = 0.385(1.26)\left(26 + \frac{9.4 \times 15.9}{2}\right)15.9 \times 0.50 = 388 \text{ kN}$$

Check positive resistance (no point load and $L = 23.5$ m) by Eq. (18-14)

$$P_{\text{pos}} = \alpha' p' \left[\bar{q}_o(L - L_1) + \frac{\gamma'(L^2 - L_1^2)}{2}\right] K$$

$$= 0.385 \times 1.26\left[26(23.5 - 15.9) + \frac{9.4(23.5^3 - 15.9^2)}{2}\right]0.50$$

$$= 389 \text{ vs. } 388 \text{ kN} \qquad \text{(within round-off and O.K.)}$$

The increase in pile load due to negative skin friction $\cong$ 388 kN.

////

18-9 LATERALLY LOADED PILE GROUPS

This topic has produced a quantity of conflicting literature—primarily concerning whether a group of, say, four piles would displace more with a lateral group load $P_{hg} = 40$ kN than a single pile with a load $P_{hs} = 10$ kN. For example, one case reported in the literature involved a nine-pile group consisting of 2134-mm pipe piles with $t_w = 57$ mm. The measured group $\delta_{hg} \approx 135$ mm versus a single pile $\delta_{hp} \approx 40$ mm. Ooi and Duncan (1994) report using a nine-pile group with a rigid cap; pile spacing on the order of $s/B = 3$; and **HP** 250 × 63 (10 × 42) piles. It was given that the group load $P_{hg} = 9P_{hs} = 400.5$ kN produced a lateral $\delta_{hg} = 3.4$ mm, whereas a single pile with $P_s = 44.5$ kN had a $\delta_{hp} = 1.7$ mm. Several other lateral pile tests have reported similar ratios of δ_{hg}/δ_{hp}.

Stating that a cap is "rigid" does not make it so, for pile cap computations including the flexural rigidity (EI) of the cap indicate that a cap on the order of 2 to 3 m in plan has to be between 1.8 and 2^+ m thick—most caps are considered "rigid" if they are from 0.6 to 1 m thick (see Sec. 18-6). If the cap is not truly rigid, in-plane plate distortion from both bending and shear may be measured as a part of the cap displacement; for small displacements, the percent error can be large, i.e., 1 mm in 4 mm is a 25 percent error.

There are only two tests reported in the literature (known to the author) in which one can have confidence that "rigid" caps were indeed used: by Kim and Brungraber (1976) and Beatty (1970). In both cases the caps were massive blocks of concrete. In the Kim-Brungraber case the group displacement δ_{hg} was about 50 percent of the single-pile displacement δ_{hs}. In the Beatty case it was difficult to draw any conclusions since they tested two-pile and six-pile groups. From two of the tests under nearly identical loading conditions—ground contact and no passive resistance—the two-pile group when loaded to 180 kN had a lateral displacement

$$L_1 = \frac{341.1}{L_1} - 5.53$$

Solving by trial (programmable calculator), we find $L_1 = 15.9$ m. From the ground surface (or base of pile cap) $L_1' = 15.9 + 1.5 = 17.4$ m. The increase in pile load is the accumulation of negative friction from the fill base (distance of L_1) to the neutral point (see Fig. 18-10), or

$$P_n = \alpha' p' \left(\bar{q}_o + \frac{\gamma' L_1}{2}\right) L_1 K$$

Use $\alpha' = 0.667 \tan 30° = 0.385$; $K = 1 - \sin\phi = 0.50$; and $p' = \pi D = 0.40\pi = 1.26$ m to find

$$P_n = 0.385(1.26)\left(26 + \frac{9.4 \times 15.9}{2}\right)15.9 \times 0.50 = 388 \text{ kN}$$

Check positive resistance (no point load and $L = 23.5$ m) by Eq. (18-14)

$$P_{\text{pos}} = \alpha' p' \left[\bar{q}_o(L - L_1) + \frac{\gamma'(L^2 - L_1^2)}{2}\right] K$$

$$= 0.385 \times 1.26\left[26(23.5 - 15.9) + \frac{9.4(23.5^3 - 15.9^2)}{2}\right]0.50$$

$$= 389 \text{ vs. } 388 \text{ kN} \qquad \text{(within round-off and O.K.)}$$

The increase in pile load due to negative skin friction $\cong$ 388 kN.

////

18-9 LATERALLY LOADED PILE GROUPS

This topic has produced a quantity of conflicting literature—primarily concerning whether a group of, say, four piles would displace more with a lateral group load $P_{hg} = 40$ kN than a single pile with a load $P_{hs} = 10$ kN. For example, one case reported in the literature involved a nine-pile group consisting of 2134-mm pipe piles with $t_w = 57$ mm. The measured group $\delta_{hg} \approx 135$ mm versus a single pile $\delta_{hp} \approx 40$ mm. Ooi and Duncan (1994) report using a nine-pile group with a rigid cap; pile spacing on the order of $s/B = 3$; and **HP** 250 × 63 (10 × 42) piles. It was given that the group load $P_{hg} = 9P_{hs} = 400.5$ kN produced a lateral $\delta_{hg} = 3.4$ mm, whereas a single pile with $P_s = 44.5$ kN had a $\delta_{hp} = 1.7$ mm. Several other lateral pile tests have reported similar ratios of δ_{hg}/δ_{hp}.

Stating that a cap is "rigid" does not make it so, for pile cap computations including the flexural rigidity (EI) of the cap indicate that a cap on the order of 2 to 3 m in plan has to be between 1.8 and 2^+ m thick—most caps are considered "rigid" if they are from 0.6 to 1 m thick (see Sec. 18-6). If the cap is not truly rigid, in-plane plate distortion from both bending and shear may be measured as a part of the cap displacement; for small displacements, the percent error can be large, i.e., 1 mm in 4 mm is a 25 percent error.

There are only two tests reported in the literature (known to the author) in which one can have confidence that "rigid" caps were indeed used: by Kim and Brungraber (1976) and Beatty (1970). In both cases the caps were massive blocks of concrete. In the Kim-Brungraber case the group displacement δ_{hg} was about 50 percent of the single-pile displacement δ_{hs}. In the Beatty case it was difficult to draw any conclusions since they tested two-pile and six-pile groups. From two of the tests under nearly identical loading conditions—ground contact and no passive resistance—the two-pile group when loaded to 180 kN had a lateral displacement

of $\delta_{h2} \approx 7.5$ mm, whereas a six-pile group loaded with 960 kN had a $\delta_{h6} \approx 29$ mm. These results give a pile-load ratio of 160/90 = 1.8 versus a displacement ratio of 29/7.5 = 3.9.

Apparently a laterally loaded pile group of n piles with the same nominal load per pile ($P_s = P_g/n$) might displace more than a single pile under the same loading conditions—at least for a pile spacing s to pile diameter D ratio (s/D) under about 6 to 8. There was some discussion in Sec. 16-15 of the necessity of adjusting the soil modulus k_s for spacing and other factors for piles in a group. With the lateral displacement very dependent on k_s it is clear that there may be load shedding to adjacent piles to produce a group displacement that is larger than for a single pile.

For the more common pile caps with both vertical and lateral load and poured directly on the soil, the lateral displacement is usually quite small. In the Beatty case one of the caps (no vertical load but with both ground friction and passive resistance developed) displaced $\delta_{hg} = 1.2$ mm versus approximately 29 mm for the same 960 kN load (with friction but no passive resistance). When the pile cap has a vertical load the lateral displacement will include a small P–Δ effect—that is, the lateral displacement will include a component for the lateral load and an additional amount from the moment produced by the vertical load $P_v \times \delta_h$.

What sometimes causes a group of n piles to produce $\delta_{hg} > \delta_{hs}$ when using identical apparent loadings, i.e., P_s and nP_s? The group certainly has a much larger effective moment of inertia ($I_{\text{piles}} + \sum A_p d^2$). To answer this question partially, let us assume we have a single fixed-head pile (set rotation $NX = 1$ to zero) and pile groups as follows (see also Fig. 18-11*a*):

Case I: One **HP** 360 × 174 fixed head against rotation and $P_s = 15$ kN.

Case II: Two **HP** 360 × 174 driven flange in contact with flange so that the effective face width $b_f = 0.378$ and the moment of inertia $I_g = 2 \times 0.000\,508 + 2A_p(d/2)^2 = 0.001\,016 + 0.001\,447 = \mathbf{0.002\,463}$ m^4. Use a $2 \times P_s = 30$ kN load.

Case III: Two-pile group with piles side by side, $I_g = 2 \times 0.000\,508 = 0.001\,016$ m^4. Use 30 kN load.

Case IV: Four-pile group—piles connecting both ways, giving a moment of inertia of $4 \times 0.000\,508 + 4A_p d_1^2 = 0.000\,4925$ m^4. Use a 60 kN load (4×15).

Case V: Four-pile group, piles stacked front to rear so the width is that of one (1) flange but a moment of inertia of $4 \times 0.000\,508 + 2A_1 d_1^2 + 2A_2 d_2^2 = 0.016\,50$ m^4. Also $P_g = 60$ kN.

Since the piles are grouped so that they can be visualized as a single laterally loaded pile, you can use program FADBEMLP on your diskette. The base $k_s = C_m(600 + 125Z^{0.5})$. We will use the following values (see Sec. 16-15.2) for C_m:

Case	C_m	Adjusted C_m
I	2	$1 + 2 \times 0.5 = 2$
II	2	$1 + (0.457/2 \times 0.378)^{0.75} = 1.69$
III	2	$1 + 4 \times 0.5 = 3$ (two extra sides)
IV	2	$1.69 + 2 \times 0.5 = 2.69$ (two extra sides)
V	2	$1 + 4 \times 2 \times 0.5 = 5$ (front + 8 sides)

The resulting computed displacements (data shown are self-explanatory except L_c', which is the "effective" length of a cantilever beam taken from the output sheets as the depth to where

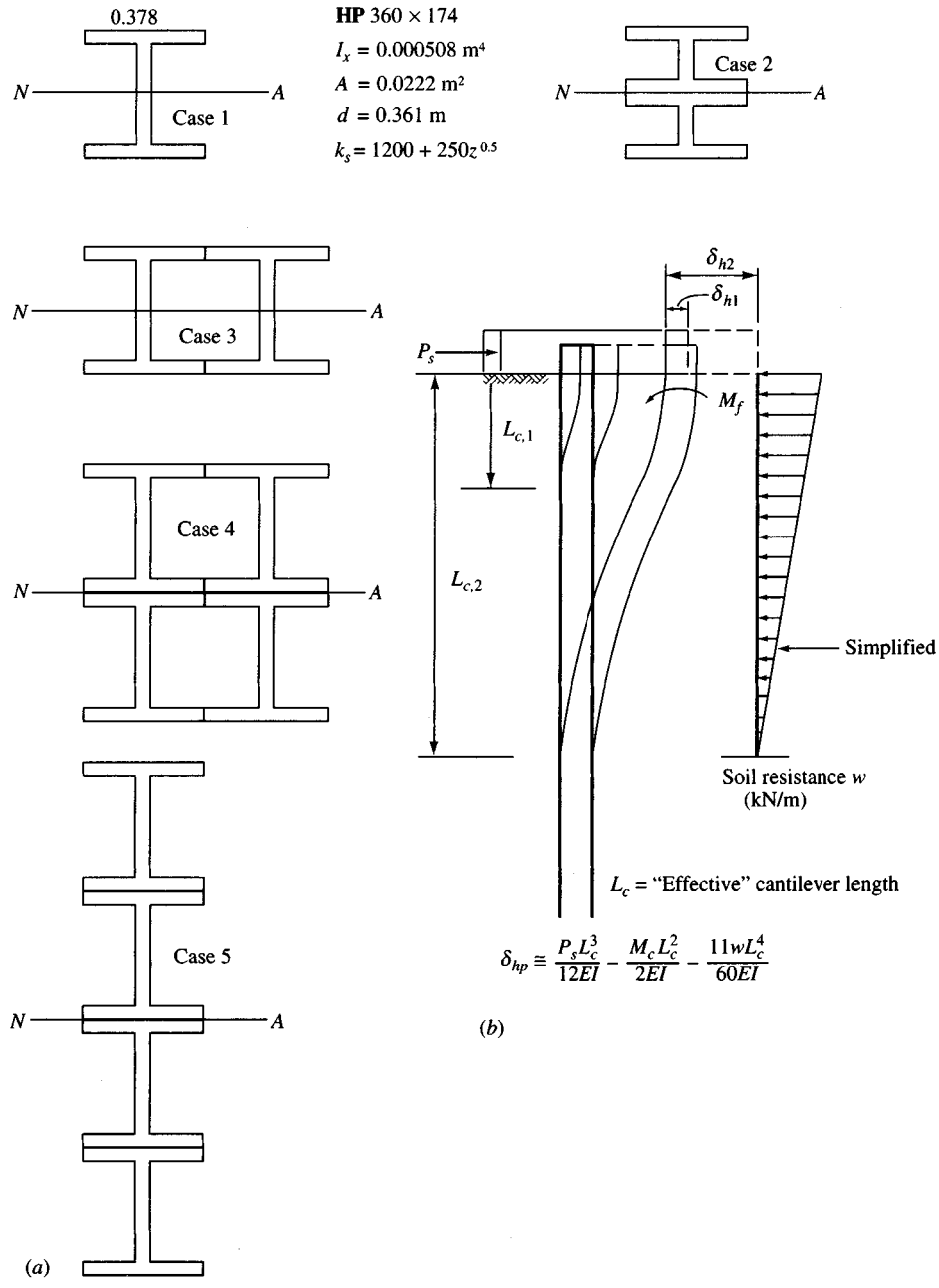

Figure 18-11 Laterally loaded pile groups: (*a*) several pile "groups" with an $s/D = 0$; (*b*) the approximation of an "equivalent" cantilever portion of a laterally loaded pile in a pile group.

$\delta_h \approx 0$) are as follows:

Case	Load, kN	I, m^4	I_g/I_p	C_m	L_c', m	δ_h, mm	Adj. C_m	L_c', m	δ_h, mm
I (1 × 1)	15	0.000 508	1.00	2.0	12	4.95	2.0	12	4.95
II (2 × 1)	30	0.001 016	2.00	2.0	12	4.95	1.69	13	5.59
III (1 × 2)	30	0.002 463	4.84	2.0	17	6.47	3.0	15	4.80
IV (2 × 2)	60	0.004 925	9.69	2.0	17	6.47	2.69	15	5.20
V (1 × 4)	60	0.016 500	32.48	2.0	20	8.24	5.0	20	4.07

Looking at the tabulation of displacements for these several cases, we see that one should "adjust" the size/shape factor C_m. Because of the group shape, it is clearly possible for group displacements to be either larger or smaller than those for a single pile. The reader should verify the computations for C_m for these five cases. The use of $C_m = 2.0$ is evidently valid only for the single pile of Case I.

If we consider any laterally loaded pile as a cantilever beam fixed at some depth L_c' in the soil as in Fig. 18-11*b*, the lateral displacement δ_{hp} is nonlinear, as shown by the approximate equations using L_c^n shown on the figure. From structural analysis methods the lateral force P_s produces a lateral displacement δ_{ps}, which is reduced by the head fixity moment M_{fh} effect of δ_{hm}; the lateral soil pressure q_s also reduces the lateral displacement by an amount δ_{hs}. The triangular lateral resisting pressure diagram should probably be closer to parabolic; however, there is not much difference in the computed lateral displacement from either type of pressure distribution. Both of these are as one would expect—data on the figure merely quantify these displacements somewhat approximately.

Since the laterally loaded "effective" cantilever produces a nonlinear δ_h, it is clear that even if the soil behaves linearly the group displacement will not be linear except for special cases.

The author did the foregoing analysis using k_s values as shown on Fig. 18-11*a* and also for $k_s = 200 + 50Z^{0.5}$. The displacements were considerably larger for the softer soil, but the displacement ratios remained about the same. These analyses show that the group I_g is a factor, but k_s is a very significant factor. The pile groups used here have $s'/D = 0$, so each pile carries P_g/m; this statement may not be true where $s'/D > 0$ and we have different values of C_m depending on the pile location in the group (front, corner, side, interior, rear). In any group, however, and for whatever pile orientation the net horizontal component of pile head displacement must be the same for every pile in the group unless the cap is not rigid and undergoes in-plane distortions.

Poulos (1971) produced a number of nondimensional curves for several pile stiffness values and the preceding table is somewhat instructive in the validation of those curves. For the two-pile case and interpolating for $s/D = 0$, we find his curves indicate the group displacement δ_{hg}/δ_{hs} should be about two times that of the single pile; but the author's ratio (and considering C_m) gives a maximum of about $\delta_{hg}/\delta_{hs} = 5.59/4.95 = 1.13$, or, depending on orientation, $4.80/4.95 = 0.97$.

For the four-pile case with a 2 × 2 arrangement, apparently there would be a lateral influence of about 1 and a front-to-rear influence of 1, giving about 4 times the displacement, which was computed as only $5.20/4.95 = 1.05$. The Poulos influence curves give reductions,

not increases, for piles that are side by side at spacings of $s/D = 2$ and 5, which do not seem correct.

Since some pile groups do apparently displace more than a single pile does that is similarly configured and loaded for s'/D ratios in the range of 2 to about 5 or 6, there must be some validity—particularly if the piles are not "fixed" to the pile cap—to the claim that the rear piles push their face soil into the back of the forward piles to increase the displacements further, as noted in Sec. 16-15.7. A pile with a pinned head may be able to rotate enough away from the cap load to shift a major portion of its soil load to the forward pile.

When the piles are securely attached to the pile cap, the rear piles must trail the forward piles with exactly the same δ_h. Their forward "push" is carried by soil resistance if the s'/D ratio is large or by a combination of soil resistance and forward pile stiffness at small s'/D. That is, if the "effective" group k_s is smaller than that of a single pile, the group displacement is larger than the single pile. If the "effective" group k_s is unchanged, the group displacement will be smaller since the group has a larger "effective" moment of inertia. When the rear piles push on the forward piles, the result is sometimes called soil-pile-soil interaction.

Depending on where the lateral load is applied to the group, a significant bending moment can be produced at the pile-cap interface of $P_{hg} \times T_{cap}$, with the direction depending on the direction of P_{hg}. This bending moment will tend to reduce the compression in some of the piles and increase it in others. In fact, the position of the lateral load may be a significant factor in the group behavior—whether it is at the forward or back edge or in the center of the cap.

Another question concerning group action is how the pile cap interacts with the soil. Pile caps are usually large concrete blocks poured directly on the soil after the piles for the group have been driven, so that the heads are at the desired elevation (or cut as required). The pile head elevation is designed to allow sufficient embedment into the cap that one can usually assume the heads are "fixed." Larger pile caps may be partially to fully embedded in the ground as well. The combined result is that a portion of the lateral load is carried by friction, a part by passive resistance, and the remainder by the piles. It is usual, however, to assume the piles carry all the lateral load via shear at the interface with the bottom of the pile cap. It should be evident that for the case as described it is very difficult to compute by any means what the actual lateral pile cap displacement will be.

We also have not answered the question of how much of the total group load P_{hg} each pile in a laterally loaded pile group carries. Statements have been made that some of the rear (or interior) piles may only carry about 25 percent of the lateral load. In using a computer program it is a trivial exercise to reduce the lateral soil stiffnesses of the interior piles and increase that of the exterior piles. If the lateral soil stiffness were sufficiently reduced, it may be possible to compute some rather small loads for the interior piles since the computer program only manipulates the numbers that are input. The author would suggest that if the program computes very small loads (and if you have confidence in the program), give consideration to removing some of the piles to increase the s/D (and actual s'/D) ratio.

Lastly, there is a question of how the use of battered piles in a group will affect the load distribution among the piles. From inspection of Fig. 16-22 we see that a battered pile is more efficient if the batter (pile on left) resists the load. It should also be evident that if the lateral load is reversible and battered piles are used, there will be variation in the pile constants since one load mode gives maximum efficiency and the other mode gives minimum. The maximum efficiency (batter resists load) may be reasonably analyzed and in the group analysis the pile constant components are correctly summed. In contrast, in the minimum efficiency mode the

batter is with the load and with the vertical load component carried by a combination of pile bending *and* shaft bearing on the soil. In this configuration obtaining a reliable set of pile constants would be very difficult.

Until there is some supporting field testing with results reported in a useful format, you will simply have to do the best you can with your group analysis. Use comments made here as a guide with your computer program to make your "best" estimates of what to use for pile constants.

If the lateral group displacement is much over two times (but depending on what that two times is—especially if it is only about 6–10 mm) that of the single pile *similarly loaded,* you probably should investigate increasing the s'/D; try to obtain some reliance on pile cap-to-ground friction; and see if it is possible to use passive pressure. Also check your computer data for input errors; have you inadvertently reduced the stiffness of one or more piles excessively?

In pile group design it is conventional practice, which seems to work reasonably well, to assume that in a group of n vertical piles each pile carries P_{hg}/n and/or P_{vg}/n. Nearly all groups carry vertical load, but not all groups carry a lateral load, and very few groups—primarily waterfront structures—carry only lateral load.

18-10 MATRIX ANALYSIS FOR PILE GROUPS

When pile-group loadings consist of vertical loads concentrically placed or with an eccentricity on the order of not more than $0.67s$ and with all vertical piles, the pile loads can be predicted with sufficient accuracy using Eq. (18-19) or Eq. (18-20) based on experience.

When the pile group is loaded with larger eccentricities, large bending moments, and/or horizontal forces and includes both vertical and batter piles, the analysis becomes quite complex. Approximate solutions were proposed by Culmann (simple force polygon) and Westergaard (using a center-of-rotation method). Neither of these solutions recognized that vertical piles can carry lateral loads and moments. Later Hrennikoff (1950) proposed a three-dimensional group solution, which he simplified to place major emphasis on two-dimensional pile groups. This method remained dormant until the early 1960s partly because these analyses are better performed on digital computers. Aschenbrenner (1967) introduced a method of group analysis using pinned pile caps. Saul (1968) introduced a general three-dimensional matrix solution, and Reese et al. (1970) published a similar matrix solution. Bowles (1974*a*) published a matrix solution similar to the one presented in this section; however, the orientation of the pile forces in the solution presented here makes computation of the direction cosines quite straightforward compared with Bowles' earlier solution.

The matrix solution consists in the use of the same matrix equations presented in Chap. 9:

$$\mathbf{P} = \mathbf{AF} \qquad \mathbf{e} = \mathbf{A}^T\mathbf{X} \qquad \mathbf{F} = \mathbf{Se} = \mathbf{SA}^T\mathbf{X} \qquad \mathbf{P} = \mathbf{ASA}^T\mathbf{X}$$

The essential difference in that solution and the pile-group solution is as follows:

1. The equation $\mathbf{P} = \mathbf{AF}$ is for a single (ith) pile; thus,

   $\mathbf{P}$ = that part of the total pile-cap force carried by the ith pile

   $\mathbf{A}$ = a complete matrix relating the ith pile forces to the part of the total pile-cap force carried by the ith pile (see Table 18-2)

2. The $\mathbf{S}$ matrix introduces the concept of pile constants instead of the familiar $4EI/L$, $2EI/L$, and soil "spring" terms K used in Chap. 9. Here it is necessary to solve a laterally loaded pile to obtain eight of the 10 $\mathbf{S}$-matrix entries and compute the S(1, 1) entry as $\lambda AE/L_p$;

TABLE 18-2
The A matrix

$\cos\theta\cos\beta$	$\sin\beta$	$\sin\theta\cos\beta$	0	0	0	F_u		P'_x
$-\sin\theta$	0.0	$\cot\theta$	0	0	0	F_v		P'_y
$\cos\theta\sin\beta$	$-\cos\beta$	$\sin\theta\sin\beta$	0	0	0	F_w		P'_z
$+Z\sin\theta$ $+Y\cos\theta\sin\beta$	$-Y\cos\beta$	$-Z\cos\theta$ $+Y\sin\theta\sin\beta$	$\cos\theta\cos\beta$	$\sin\beta$	$\sin\theta\cos\beta$	M_u	=	M'_x
$+Z\cos\theta\cos\beta$ $-X\cos\theta\sin\beta$	$+Z\sin\beta$ $+X\cos\beta$	$+Z\sin\theta\cos\beta$ $-X\sin\theta\sin\beta$	$-\sin\theta$	0	$\cos\theta$	M_v		M'_y
$-Y\cos\theta\cos\beta$ $-X\sin\theta$	$-Y\sin\beta$	$-Y\sin\theta\cos\beta$ $+X\cos\theta$	$\cos\theta\sin\beta$	$-\cos\beta$	$\sin\theta\sin\beta$	M_w		M'_z

the S(4, 4) entry as $\Omega G'J/L_p$ to produce a complete $S_{6,6}$ stiffness (or spring) matrix for each pile in the group. In these expressions the following terms appear:

E = modulus of elasticity of pile material

G' = shear modulus = $E/[2(1 + \mu)]$ of pile material

λ = axial adjustment factor (see values in later discussion)

Ω = torsion adjustment factor (see values in later discussion)

A = cross-sectional area of pile as used, but do not include any plug for open-end pipe or **HP** sections

J = torsion inertia, computed as

Round shapes $\quad J = \dfrac{\pi}{32}(d_o^2 - d_i^2)$ $\quad$ (hollow pipe)

HP piles $\quad J = \dfrac{d_w t_w^3 + 2b_f t_f^3}{3}$

3. The $\mathbf{ASA}^T$ is computed for each pile in the pile group *and summed* into a group (or global) $\mathbf{ASA}^T$ matrix. For a four-pile group, each $\mathbf{ASA}^T$ entry is the sum of four individual pile $\mathbf{ASA}^T$ values.
4. The pile-group $\mathbf{ASA}^T$ matrix (size 6×6) is inverted and the foundation displacements, or X's, are obtained.
5. With the X values the pile-head displacements (e's) are computed using

$$\mathbf{e} = \mathbf{A}^T\mathbf{X}$$

This calculation is necessary because the **A** matrix (and the $\mathbf{A}^T$) contains entries relating to the pile position with respect to the origin of coordinates, which disallows use of the equation $\mathbf{F} = \mathbf{SA}^T\mathbf{X}$.

6. With the pile displacements **e**, the pile forces can be computed as

$$\mathbf{F} = \mathbf{Se}$$

The matrix solution is completely general, in that six degrees of freedom are used—three translations, of x, y, and z, and three rotations, of α_x, α_y, α_z. The principal assumption is that the pile cap is **perfectly rigid** such that only rigid body displacements of body translation and rotation with respect to a set of body axes occur. It is assumed that no bending rotations or cap elongations between pile heads take place; e.g., for a given x translation, each pile head has an x component displacement of the same value, etc.

The **A** matrix (refer to Fig. 18-11 and Table 18-2) is built as follows:

1. Note F_v is always parallel to the xz plane.
2. β = angle of pile projection with x axis.
3. θ = slope of batter pile with horizontal.
4. Pile heads do not have to be at the same elevation.
5. Note that the pile forces act on the cap in the direction opposite to the positive directions shown for the pile.

The P_i' and M_i' values are related to the pile-cap forces as follows:

Pile force	Component part of	Pile force	Component part of
P_x'	P(1)	M_x'	P(4)
P_y'	P(2)	M_y'	P(5)
P_z'	P(3)	M_z'	P(6)
$\sum_1^n P_x' = \text{P(1)}$	$\sum_1^n P_y' = \text{P(2)}$ etc.		

The β angle is zero for vertical piles and varies from 0 to 360° (or 0 to ±180°) rotated clockwise about the vertical y axis of Fig. 18-12. The angle θ defines any pile batter as shown: For a vertical pile $\theta = 0°$.

The pile **S** matrix is as shown in Table 18-3 from the relationship of **F** = **Se**. Table 18-4 gives the correspondence of the **S** matrix and the corresponding pile constants input as C(I, J) and their method of computation. Also shown are the computations to produce the pile constants of Examples 18-7 and 18-8. Note that eight of the pile constants are obtained from a lateral pile analysis with four each from considering the pile x axis (strong) and four from the pile y axis (weak) resisting bending and displacement. When the pile is square or round, the eight constants reduce to four different values, as

$$\text{C}(1, 2) = \text{C}(1, 4)$$
$$\text{C}(1, 3) = \text{C}(1, 5)$$
$$\text{C}(1, 7) = \text{C}(1, 9)$$
$$\text{C}(1, 8) = \text{C}(1, 10)$$

The axial pile constant C(1, 1) can be computed from the displacement obtained from Sec. 16-13 if the computed pile axial force is close to the value that is obtained from the group output. We would obtain the displacement $\delta_p = e_p$ and axial force P_p from the computations of Sec. 16-13. Here

$$F = |\mathbf{Se}| = \frac{\lambda A E e_p}{L_p} = P_p = F$$

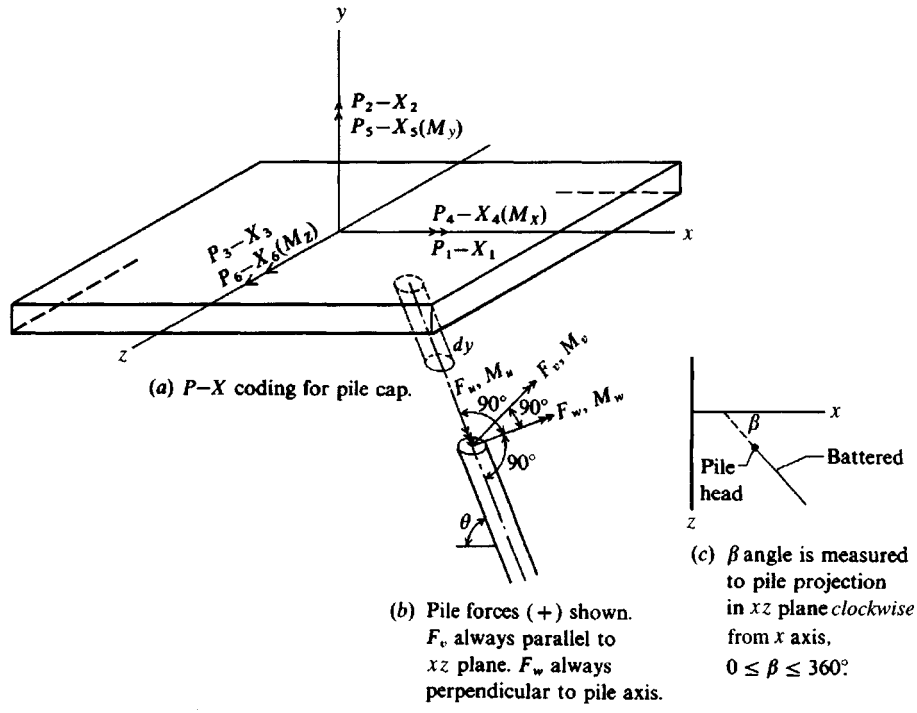

Figure 18-12 Coding and pile-force identification for building the A and S matrices. Note that F_w is perpendicular to pile axis, and is also perpendicular to F_u. Also F_w is perpendicular to F_v.

so that

$$\mathrm{C}(1,1) = \mathrm{S}(1,1) = \frac{P_p}{\delta_p}$$

More generally, we would estimate C(1, 1) using A = cross-sectional area of pile (no soil plug), which also may be composite using concrete with steel casing; E = modulus of elasticity; and L_p = pile length (total including any part not embedded). For friction piles we might take $\lambda = 2.0$ for the embedded part, but you will somehow have to include an adjustment if the pile is point-bearing and/or friction and/or partially embedded, for example, off-shore structures. For point-bearing piles use $\lambda \approx 1.2$ to 1.1, since any point-bearing pile

TABLE 18-3
The single-pile S matrix using S(I, J) entries of Table 18-4 for the pile head forces in the pile force matrix F = Se

$$\mathbf{S} = \begin{bmatrix} \mathrm{S}(1,1) & 0 & 0 & 0 & 0 & 0 \\ 0 & \mathrm{S}(2,2) & 0 & 0 & 0 & \mathrm{S}(2,6) \\ 0 & 0 & \mathrm{S}(3,3) & 0 & -\mathrm{S}(3,5) & 0 \\ 0 & 0 & 0 & \mathrm{S}(4,4) & 0 & 0 \\ 0 & 0 & -\mathrm{S}(5,3) & 0 & \mathrm{S}(5,5) & 0 \\ 0 & \mathrm{S}(6,2) & 0 & 0 & 0 & \mathrm{S}(6,6) \end{bmatrix} \begin{bmatrix} e_1 = \delta_u \\ e_2 = \delta_v \\ e_3 = \delta_w \\ e_4 = \alpha_u \\ e_5 = \alpha_v \\ e_6 = \alpha_w \end{bmatrix}$$

TABLE 18-4
Correspondence between S(I, J) and C(I, J) in Table 18-3

C values	S(I, J)	Computed as	For Example 18-7*
C(I, 1)	S(1, 1)	$\lambda AE/L_p$	$0.5(22.2 \times 10^{-3})(200\,000\,000)/19 = 116\,800$ kN/m
C(I, 2)	S(2, 2)	P_y/δ_y	$18.44/0.0298 = 618$
C(I, 3)	S(2, 6)	P'_x/θ_x	$2.99/0.001\,51 = 1980 \rightarrow 1981$†
C(I, 4)	S(3, 3)	P_x/δ_x	$50.78/0.0621 = 818$
C(I, 5)	S(3, 5)	P'_y/θ_y	$6.44/0.001\,92 = 3354 \rightarrow 3356$†
C(I, 6)	S(4, 4)	$\Omega G'J/L_p$	$2.5(75.2 \times 10^6)(3.0455 \times 10^{-6})/19 = 30.13$
C(I, 7)	S(5, 3)	M'_x/δ_x	$208.5/0.062 = 3357 \rightarrow 3356$†
C(I, 8)	S(5, 5)	M_x/θ_x	$50.78/0.001\,92 = 26\,448$
C(I, 9)	S(6, 2)	M'_y/δ_y	$59.05/0.0298 = 1982 \rightarrow 1981$†
C(I, 10)	S(6, 6)	M_y/θ_y	$18.44/0.001\,51 = 12\,212$

*Refer to Fig. E16-13c for values used to compute all but C(I, 1) and C(I, 6) in above table.

†Values should be equal in pairs [$S(2, 6) = S(6, 2)$]—use average.

In above: P_x = pile head force applied parallel to y axis shown here
M_x = moment applied to pile head about x axis
P_y = pile head force applied parallel to x axis
M_y = moment applied to pile head about y axis
M'_x = fixed head pile moment from P_x and rotation = 0
P'_x = pile head force parallel to y axis from M_x with zero head displacement
M'_y, P'_y = analogous to M'_x and P'_x
δ_x = lateral displacement of pile head when fixed against rotation
θ_x = pile head rotation for M_x when fixed against translation
HP360 × 174; $b_f = 0.378$; $t_f = t_w = 0.0204$; $d_w = 0.3202$

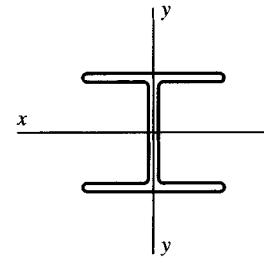

will carry some load in side friction. *Battered* piles will undergo more vertical displacement than vertical piles for the same vertical load component [see Kim and Brungraber (1976)]. Batter piles will also displace laterally under vertical load. Clearly, these latter two statements translate into some additional adjustment in the λ term to make the axial spring softer and a modification in the C_m term to make the lateral soil resistance more or less, as outlined in Sec. 16-15.6.

For the $\Omega G'J/L_p$ = C(I, 6) = S(4, 4) term, we must compute G' = shear modulus of the pile using the equation given earlier where Poisson's ratio is usually taken as 0.15 for concrete and 0.33 for steel. For steel compute

$$G' = \frac{200\,000}{2(1 + 0.33)} = 75\,200 \text{ MPa}$$

The torsion constant J is computed using the equation given earlier and, inserting values for the **HP**360 × 174, we obtain

$$J = \frac{d_w t_w^3 + 2b_f f_f^3}{3}$$

$$J = \tfrac{1}{3}[(0.361 - 2 \times 0.0204)0.0204^3 + 2 \times 0.378 \times 0.0204^3]$$

$$= \mathbf{3.0455} \times 10^{-6} \text{ m}^4$$

The value of Ω ranges from 2 to 4; unpublished research by the author using 8-ft model piles fitted with strain gauges indicates 2.5 is reasonable. Constant C(I, 6) is not very critical

since principal group torsion resistance is obtained from pile head shear. For several piles spaced around the load point, substantial torsion resistance can be obtained with little direct contribution for the individual pile torsion responses.

GENERAL COMMENTS ON PROCEDURE

1. Pile head constants reduce to C(I, 1), C(I, 2), and C(I, 4) for piles pinned to the cap—not a very realistic pile cap system. Pinned piles will produce cap moments depending on pile coordinates. Also round-off errors may indicate computed pile forces when they should be zero.
2. The y axis coordinate allows you to model a thick cap since the origin of coordinates is usually the top plane of the cap. A thick cap will produce a moment $P_h \times Y$ that tends to rotate the pile cap and increase some axial forces and decrease others. This moment cannot be avoided but is accounted for in the program by using a y coordinate for the pile head that is the cap thickness. The cap must be thick or else it is not rigid (but the computer program does not know this). Do not forget to include cap weight into the vertical cap load.
3. No methods currently exist that are practical to model batter piles for pile constants except to adjust k_s as outlined in Sec. 16-15.6. The method given by Bowles (1974*a*) allowed a batter pile analysis but did not provide any procedures to adjust k_s (assuming an adjustment is necessary) for the pile being battered. Depending on the lay of the batter, a lateral force will either cause it to rise and translate or lay and translate. With translation, however, there is axial movement which produces skin resistance that in turn requires load transfer curves.
4. For a linear analysis (small lateral displacements) it is only necessary to make a lateral pile analysis using a single load or moment about each axis (unless round) and make plots as shown in Fig. E16-13*c* for the eight pile constants. You can make a nonlinear analysis by adjusting for X > XMAX, but few designers want pile caps to translate more than 6 to 10 mm, where a linear analysis is likely to be nearly correct.
5. The pile cap displacements can be used to estimate cap movements if you have confidence in the pile constants. The pile forces output is used directly for a structural design of the cap. You can design the piles by reusing the pile data used to develop the curves such as Fig. E16-13*c*, taking the pile as having a free head, and applying the head moment and shear for each direction to see if a larger moment is obtained farther down the shaft. Usually, however, the fixed-head moment in this analysis is the largest and is suitable for design.
6. You can orient the principal axis of the pile parallel to the appropriate cap (or global) axis. You may orient different piles at different axis orientations when they are vertical; however, the pile axis rotates with angle β, so when you make a group layout be sure to take this into account.
7. Pile constants for partially embedded piles in a group are computed similar to fully embedded piles. It is necessary (assuming you use program FADBEMLP) to specify the node where the soil line starts JTSOIL but specify head fixities at node 1. These are: translation = 0.0 for one execution; rotation = 0.0 for one execution. The output is

plotted, and computations for the constants are made similar to that given by Example 16-13 where the pile was fully embedded.

The method will be illustrated by two problems with computer output listed. The first problem is a symmetrical pile group with an axial load and moment about the z axis. The second example is general in that the piles are given batters and the group is not symmetrical.

Example 18-7. Analyze the nine-pile group of Fig. E18-7*a* using a cap that is 0.6 m thick; this is not a "rigid" cap with the plan dimensions shown, but for purposes of illustration we will assume it is—the computer program does not know. Obtain the pile constants from Fig. E16-13*c* (as computed for Table 18-4) and for the loads shown on the output sheet of Fig. E18-7*b*. Carefully note that we are using a single set of pile constants for all nine piles; with an s/D ratio of about 2.25 it should be evident that there should be four sets of pile constants (piles 4, 5, 7, and 8); the others are similar

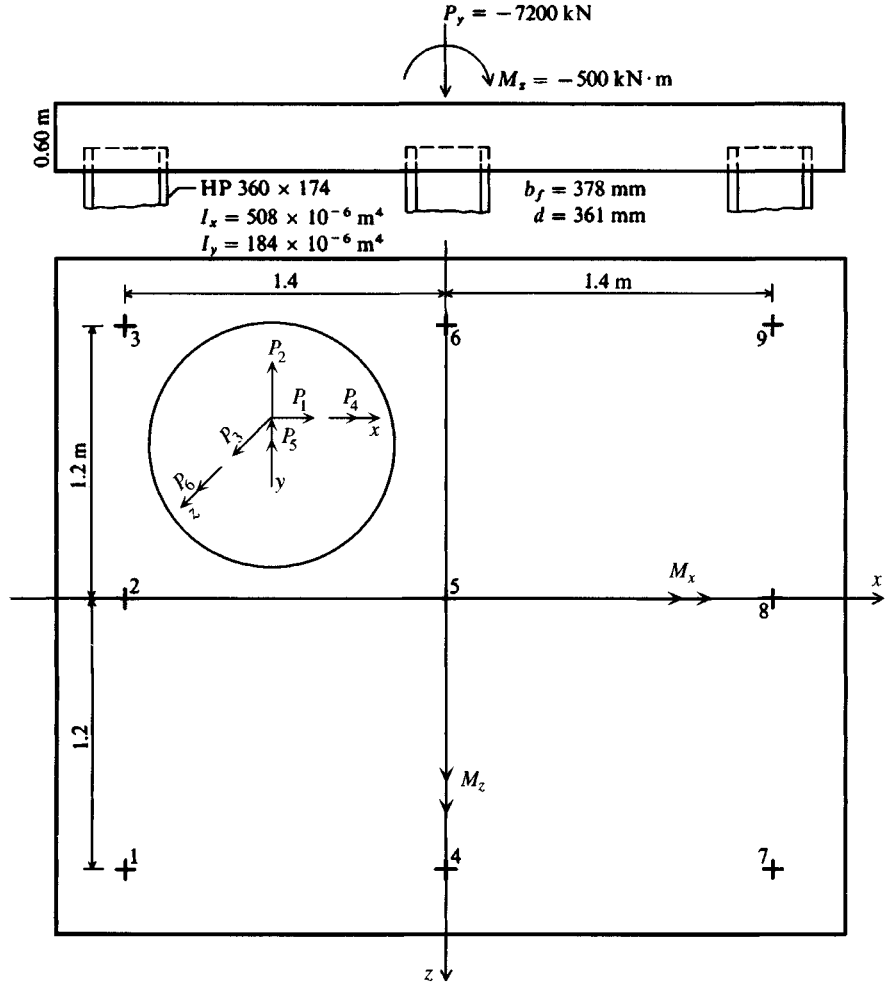

Figure E18-7*a*

EXAMPLE 18-7 FAD 5/E NINE PILE GROUP USING HP360 PILES

DISK FILE NAME FOR THIS DATA SET: EXAM187.DTA

GENERAL INPUT DATA

PILE NO	X	Z	Y	BETA	BATTER
1	-1.40	1.20	-.60	.00	.00
2	-1.40	.00	-.60	.00	.00
3	-1.40	-1.20	-.60	.00	.00
4	.00	1.20	-.60	.00	.00
5	.00	.00	-.60	.00	.00
6	.00	-1.20	-.60	.00	.00
7	1.40	1.20	-.60	.00	.00
8	1.40	.00	-.60	.00	.00
9	1.40	-1.20	-.60	.00	.00

THE PILE CONSTANTS ARE

PILE NO	C(1)	C(2)	C(3)	C(4)	C(5)	C(6)	C(7)	C(8)	C(9)	C(10)
1	116800.0	618.0	1981.0	818.0	3356.0	30.1	3356.0	26448.0	1981.0	12212.0
2	116800.0	618.0	1981.0	818.0	3356.0	30.1	3356.0	26448.0	1981.0	12212.0
3	116800.0	618.0	1981.0	818.0	3356.0	30.1	3356.0	26448.0	1981.0	12212.0
4	116800.0	618.0	1981.0	818.0	3356.0	30.1	3356.0	26448.0	1981.0	12212.0
5	116800.0	618.0	1981.0	818.0	3356.0	30.1	3356.0	26448.0	1981.0	12212.0
6	116800.0	618.0	1981.0	818.0	3356.0	30.1	3356.0	26448.0	1981.0	12212.0
7	116800.0	618.0	1981.0	818.0	3356.0	30.1	3356.0	26448.0	1981.0	12212.0
8	116800.0	618.0	1981.0	818.0	3356.0	30.1	3356.0	26448.0	1981.0	12212.0
9	116800.0	618.0	1981.0	818.0	3356.0	30.1	3356.0	26448.0	1981.0	12212.0

THE P-MATRIX FOR 1 LOAD CASES IS AS FOLLOWS:

1	PX =	.000
2	PY =	-7200.000
3	PZ =	.000
4	MX =	.000
5	MY =	.000
6	MZ =	-500.000

THE FOUNDATION (GLOBAL) ASAT MATRIX:

1	7362.0	.0	.0	.0	.0	34621.2
2	.0	1051200.0	.0	.0	.0	.0
3	.0	.0	5562.0	-21166.2	.0	.0
4	.0	.0	-21166.2	1142457.0	.0	.0
5	.0	.0	.0	.0	14606.4	.0
6	34621.2	.0	.0	.0	.0	1650495.0

THE PILE CAP DISPLACEMENTS FOR NLC = 1

X = .001581 Y= -.006849 Z= .000000 ALPHA X= .000000 ALPHA Y= .000000 ALPHA Z= -.000336

THE PILE DISPLACEMENTS AND PILE FORCES FOR LC = 1 ++

PILE	DU	DV	DW	ALPHA U	ALPHA V	ALPHA W	FU	FV	FW	MU	MV	MW
1	.0064	.0000	.0014	.0000	.0003	.0000	745.042	.000	.000	.000	4.261	.000
2	.0064	.0000	.0014	.0000	.0003	.0000	745.042	.000	.000	.000	4.261	.000
3	.0064	.0000	.0014	.0000	.0003	.0000	745.042	.000	.000	.000	4.261	.000
4	.0068	.0000	.0014	.0000	.0003	.0000	800.000	.000	.000	.000	4.261	.000
5	.0068	.0000	.0014	.0000	.0003	.0000	800.000	.000	.000	.000	4.261	.000
6	.0068	.0000	.0014	.0000	.0003	.0000	800.000	.000	.000	.000	4.261	.000
7	.0073	.0000	.0014	.0000	.0003	.0000	854.958	.000	.000	.000	4.261	.000
8	.0073	.0000	.0014	.0000	.0003	.0000	854.958	.000	.000	.000	4.261	.000
9	.0073	.0000	.0014	.0000	.0003	.0000	854.958	.000	.000	.000	4.261	.000

INDIVIDUAL PILE FORCE COMPONENTS TO CHECK SUM OF FORCES ALONG AXES

PILE NO	FX	FY	FZ	MX	MY	MZ
1	.0000	-745.0420	.0000	894.0504	.0000	1038.7970
2	.0000	-745.0420	.0000	.0000	.0000	1038.7970
3	.0000	-745.0420	.0000	-894.0504	.0000	1038.7970
4	.0000	-800.0000	.0000	960.0001	.0000	-4.2615
5	.0000	-800.0000	.0000	.0000	.0000	-4.2615
6	.0000	-800.0000	.0000	-960.0001	.0000	-4.2615
7	.0000	-854.9580	.0000	1025.9500	.0000	-1201.2030
8	.0000	-854.9580	.0000	.0000	.0000	-1201.2030
9	.0000	-854.9580	.0000	-1025.9500	.0000	-1201.2030
TOTAL =	.0000	-7200.0000	.0000	.0000	.0000	-500.0007
	(.000)(	-7200.000)(	.000)(	.000)(	.000)(	-500.000)

++

Figure E18-7*b*

from symmetry, i.e., 4 and 6; 8 and 2; 5; and corner piles 1, 3, 7, and 9. Four sets have not been used so as to simplify the input and output.

Cap input is +P = parallel to the + coordinate directions
+M = use right-hand rule based on double arrowheads shown in the inset of Fig. E18-7*a*

You may orient the x axis either horizontally as shown or down the page, but the z axis also rotates. If you rotate the axis be sure that the pile constants (or springs) are oriented correctly. Orientation is of no consequence for round piles but makes a substantial difference for **HP** piles.

This problem requires using computer program FAD3DPG (B-10) to obtain a solution; this data set is on your diskette as EXAM187.DTA.

Discussion of output.

1. The computer program outputs all critical input [x, y, z coordinates, angle β, pile batter ratios, and pile constants C(I, J) for each pile]. Note the program requires all 10 pile constants.
2. The global **ASAT** matrix is not always symmetrical, and with all vertical piles (as here) it contains a large number of zeros. It is not symmetrical because it contains both elastic entries and position vector entries from the lower left corner of the **A** matrix.
3. The cap displacements are listed, and we see that the principal displacement for this group configuration and loading of 7200 kN is vertical at 0.006 849 m (6.85 mm), which is not unexpected. The cap has a small α_z rotation of 0.000 336 rad from the M_z moment, which was input as (−) using the right-hand rule for the z axis. The sign is therefore correct for the moment direction. If the $\lambda AE/L$ is accepted as correct then the vertical group settlement under load is 6.85 mm, and no further settlement computations are required unless there is a consolidating layer of clay below the pile points. Horizontal displacements are 0.0 since there was no P_x or P_z.
4. There are only pile moments MV (= M_v) of 4.261 kN · m with a (+) sign, consistent with the applied moment $M_z = -500$ kN · m. The conventional $P/A \pm Mc/I$ analysis would not obtain these pile-head moments, which are caused by head fixity to the cap.
5. The moments MX are from position of the piles with respect to the x axis. The three piles on the axis (2, 5, 8) have MX = 0. Pile 1 has MX = FU × Z = 745.047 × 1.2 = 894.0504 as shown. The other MX values are computed similarly in making the $\sum$MX = 0 statics check.
6. Moments MZ are computed, e.g., for pile 1 as FU × X + MV = 745.042 × 1.4 − 4.261 = 1038.797 [−MV since a (+) pile moment acts in opposite direction on the cap]. Note the three piles on the z axis have no x moment arm so the MZ moment is −4.261. The $\sum$MZ = −500.0007 versus −500.0 input.
7. In the general case where the **A** matrix has a number of sine and cosine entries, it is most useful to have the program make the statics check as shown here.

////

Example 18-8. Analyze the nine-pile group of Fig. E18-8*a*, which is a general case of Example 18-7 using the same pile constants but also with batters and β angles on selected piles. To simplify input/output we will again use the same set of pile constants as in Example 18-7 even though this is not strictly correct.

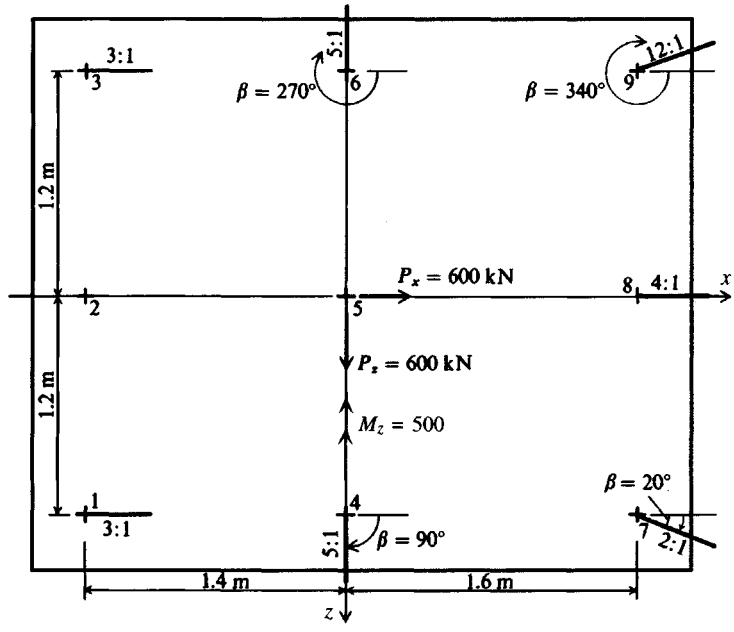

Figure E18-8*a*

Solution. Using computer program B-10, one can obtain the output shown in Fig. E18-8*b*.

Discussion of results. Because of the pile batters we will only look at pile 2, which is vertical. The computer program has facility to allow output of the pile **A** and $\mathbf{SA}^{\mathrm{T}}$ matrices, but this is left for the reader.

1. Pile 2 has a vertical axial force of 991.475 kN; a force FV parallel to the z axis of -38.998 kN; a force FW parallel to the x axis of -6.786 kN; and moments MU = 0.206 kN · m, MV = 25.11 kN · m, and MW = -137.814 kN · m. These values can be directly used for designing the pile. The signs for FU, FV, etc., are (−) when opposite to the (+) directions of the pile as shown in Fig. 18-12*b*.
2. The force component contribution (pile-head forces to cap results in a sign change):

   FX = -6.786 kN (shear parallel to x axis ←)

   FY = -991.475 kN (axial load↑ on cap)

   FZ = 38.9977 kN (shear parallel to z axis; note pile 4 carries most of 600 kN)

   MX = 161.2125 = 137.814 + 0.6 × 38.9977 (pile head is 0.6 m below xz plane)

   MY = 54.8030 = 38.9977 × 1.4 + 0.206

   MZ = -1358.8810 = 991.4748 × 1.4 − 25.112 − 6.786 × 0.6
3. Pile 5 has DU = 0.0082 m = y = -0.008187 m↓ cap settlement at load point. Other values include effect of pile head at 0.6 m below origin of coordinates and any rotations about the x and z axes.

////

EXAMPLE 18-8 FAD 5/E NINE PILE GROUP USING HP360 PILES--NONSYMMETRICAL LOADS

DISK FILE NAME FOR THIS DATA SET: EXAM188.DTA

GENERAL INPUT DATA

PILE NO	X	Z	Y	BETA	BATTER
1	-1.40	1.20	-.60	.00	3.00
2	-1.40	.00	-.60	.00	.00
3	-1.40	-1.20	-.60	.00	3.00
4	.00	1.20	-.60	90.00	5.00
5	.00	.00	-.60	.00	.00
6	.00	-1.20	-.60	270.00	5.00
7	1.60	1.20	-.60	20.00	12.00
8	1.60	.00	-.60	.00	4.00
9	1.60	-1.20	-.60	340.00	12.00

THE PILE CONSTANTS ARE

PILE NO	C(1)	C(2)	C(3)	C(4)	C(5)	C(6)	C(7)	C(8)	C(9)	C(10)
1	116800.0	618.0	1981.0	818.0	3356.0	30.1	3356.0	26448.0	1981.0	12212.0
2	116800.0	618.0	1981.0	818.0	3356.0	30.1	3356.0	26448.0	1981.0	12212.0
3	116800.0	618.0	1981.0	818.0	3356.0	30.1	3356.0	26448.0	1981.0	12212.0
4	116800.0	618.0	1981.0	818.0	3356.0	30.1	3356.0	26448.0	1981.0	12212.0
5	116800.0	618.0	1981.0	818.0	3356.0	30.1	3356.0	26448.0	1981.0	12212.0
6	116800.0	618.0	1981.0	818.0	3356.0	30.1	3356.0	26448.0	1981.0	12212.0
7	116800.0	618.0	1981.0	818.0	3356.0	30.1	3356.0	26448.0	1981.0	12212.0
8	116800.0	618.0	1981.0	818.0	3356.0	30.1	3356.0	26448.0	1981.0	12212.0
9	116800.0	618.0	1981.0	818.0	3356.0	30.1	3356.0	26448.0	1981.0	12212.0

THE P-MATRIX FOR 1 LOAD CASES IS AS FOLLOWS:

1	PX =	600.000
2	PY =	-7200.000
3	PZ =	600.000
4	MX =	.000
5	MY =	.000
6	MZ =	-500.000

THE FOUNDATION (GLOBAL) ASAT MATRIX:

1	38346.6	-114916.9	.4	3.0	.2	74495.2
2	-114916.9	1010660.0	1.0	-.5	-4.8	23589.5
3	.4	1.0	15117.7	31846.3	-2016.7	1.8
4	3.0	-.5	31846.3	1058967.0	127667.8	.4
5	.2	-4.8	-2016.7	127667.8	54054.8	-2.8
6	74495.2	23589.5	1.8	.4	-2.8	1795981.0

THE PILE CAP DISPLACEMENTS FOR NLC = 1

X = -.009308 Y= -.008187 Z= .045205 ALPHA X= -.002185 ALPHA Y= .006846 ALPHA Z= .000215

THE PILE DISPLACEMENTS AND PILE FORCES FOR LC = 1 ++

PILE	DU	DV	DW	ALPHA U	ALPHA V	ALPHA W	FU	FV	FW	MU	MV	MW
1	.0053	-.0561	-.0028	-.0072	-.0002	.0001	614.507	-34.487	-1.543	-.216	3.603	-110.008
2	.0085	-.0561	-.0092	-.0068	-.0002	-.0022	991.475	-38.998	-6.786	-.206	25.112	-137.814
3	.0050	-.0561	-.0200	-.0072	-.0002	.0001	588.662	-34.487	-15.650	-.216	61.477	-110.008
4	.0146	-.0010	.0445	-.0067	-.0022	.0016	1702.958	2.481	43.750	-.201	-207.194	17.060
5	.0082	-.0465	-.0092	-.0068	-.0002	-.0022	956.290	-33.075	-6.786	-.206	25.112	-118.828
6	.0015	.0174	-.0477	-.0068	.0022	.0011	172.512	12.993	-46.376	-.204	217.968	48.285
7	.0061	-.0337	.0108	-.0070	-.0009	-.0014	716.952	-23.637	12.008	-.211	-61.304	-84.000
8	.0054	-.0356	-.0108	-.0072	-.0002	-.0005	628.717	-22.887	-8.118	-.216	30.576	-76.057
9	.0081	-.0275	-.0293	-.0070	.0005	-.0016	941.528	-20.046	-25.782	-.211	112.687	-73.347

INDIVIDUAL PILE FORCE COMPONENTS TO CHECK SUM OF FORCES ALONG AXES

PILE NO	FX	FY	FZ	MX	MY	MZ
1	192.8602	-583.4608	34.4871	575.0295	245.1320	928.9580
2	-6.7859	-991.4748	38.9977	-161.2125	54.8030	1358.8810
3	171.3048	-563.4027	34.4871	-801.2067	-191.8661	830.0698
4	2.4912	-1661.3070	376.8779	1560.2480	6.5323	18.1897
5	-6.7859	-956.2897	33.0747	-138.6726	.2063	-29.1836
6	-12.9925	-178.2570	11.6440	-438.8661	25.2599	-55.0852
7	59.1099	-713.4780	46.6681	728.5278	-10.5031	-1077.1280
8	144.6109	-611.9138	22.8872	-87.5704	-54.8563	-922.8719
9	56.1874	-940.4171	.8763	-1236.2780	-74.7079	-1551.8300
TOTAL =	600.0001	-7200.0010	599.9999	-.0007	.0000	-499.9999
	(600.000)(	-7200.000)(	600.000)(	.000)(	.000)(	-500.000)

++

Figure E18-8*b*

18-11 PILE CAP DESIGN BY COMPUTER

The preceding section outlined pile group design for a rigid pile cap. The computer program outputs pile-head forces, which can be used in the structural design of the piles or, possibly, to relocate select piles for a better balance of pile forces and to limit cap rotation. The basic limitation was that the cap *be absolutely rigid,* but criteria defining a rigid cap were not given.

This section addresses the complete group cap and pile design as a cap-pile interaction process. This can be done [see Bowles (1983)] as follows:

1. Revise the mat program to use 6 degrees-of-freedom nodes so there is a direct relationship between the 6-d.o.f. pile head and the cap (or mat) node.
2. Slightly reorder the pile-group computer program to be a subroutine of the revised mat program.
3. Grid the pile cap so nodes occur at all pile-head locations.
4. Build the stiffness matrix (ASAT) for the cap as a plate or mat.
5. Build the stiffness matrix (ASAT) for each pile in turn and add the entries into the cap (or global) ASAT using superposition of effects. This step is similar to that for adding node soil springs. Here the pile stiffness matrix is effectively an array of "springs" that are added to the appropriate cap stiffness entries from use of Tables 18-2 and 3.
6. Invert the stiffness matrix (or reduce the band array), and obtain the cap moments and shears at nodes.
7. Using the pile "group" subroutine, compute the pile-head forces. The following precautions are required:
   a. The X, Y, and Z terms in the lower left corner of the pile **A** matrix of Table 18-2 *are not used* in building the pile ASAT to add to the cap ASAT since the pile-node location automatically includes the effects of the x and z coordinates. This will then give a symmetrical pile ASAT so the global cap matrix will remain symmetrical and can be banded.
   b. When computing the statics check for the piles, go back and use the full **A** matrix of Table 18-2.

Figure 18-13 illustrates the general case of 6-d.o.f. nodes and the corresponding forces on the beam-column element. Note that the AE/L term for element axial compression and bending about the y axis is not used in design of the cap but is necessary to allow the six general loadings at loaded nodes.

As previously stated, for only vertical piles and vertical cap loads, any 3-d.o.f. FEM (or the mat) program can be used. Where pile caps are loaded by vertical and horizontal loads and moments about one or more axes and with horizontal loads and/or moments the general 6-d.o.f. solution is necessary.

Figure 18-14 is an edited part of the 6-d.o.f. **A** matrix. The remainder can be developed using the element forces applied to the node in a manner similar to the 3-d.o.f case. The full 6-d.o.f. **S** matrix for any cap element is given in Fig. 18-15.

Solution by the author of a number of pile cap cases indicates that (depending on pile spacing s) a very thick cap is often required to produce a "rigid" cap.

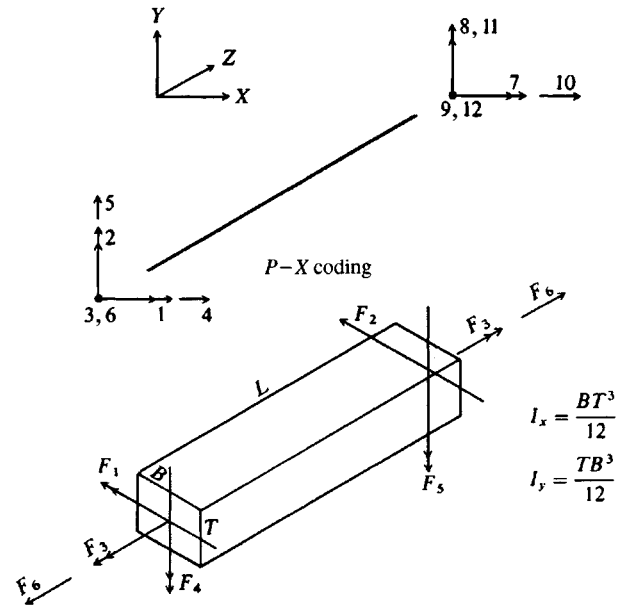

Figure 18-13 Typical finite grid element *P–X* coding for nodes and element moments and axial force (*F*6). Use right-hand rule for moment sign convention. Other coding can be used but that shown here corresponds to author's computer program. [*Bowles (1983).*]

The author's computer program for this analysis is FADPILCP (B-28) and makes use of a data generator program (B-28A) since there is a very large amount of element data to input—even for small pile caps.

To the author's knowledge there is currently no other general rational procedure available for use in the structural analysis/design of a pile cap taking flexibility of cap (and piles) into account. Apparently the CDF (1984, page 33 of report) in their extensive literature search also did not find any alternatives.

$A =$

P \ F	1	2	3	4	5	6
1	$-B$		E			
2	$-E$		$-B$			
3				1.0		
4				C	C	E
5				D	D	$-B$
6	$1/L$	$1/L$				
7						

$E = \sin\beta$
$B = \cos\beta$
$C = \frac{\cos\beta}{L}$
$D = \frac{\sin\beta}{L}$

Figure 18-14 Partial *A* matrix using Fig. 18-12. Far-end values (7–12) are obtained similarly by using equilibrium of node and element forces. Blank spaces shown are 0.0. [*Bowles (1983).*]

$S =$

F \ E	1	2	3	4	5	6
1	A'	$A'/2$				
2	$A'/2$	A'				
3			D			
4				B	$B/2$	
5				$B/2$	B	
6						C

$A' = 4EI_1/L$
$B = 4EI_2/L$
$C = AE/L$
$D = \Omega G'J/L$

E = modulus of elasticity of cap; G' = shear modulus of cap
I_1 = moment of inertia of element about horizontal axis
I_2 = moment of inertia of element about vertical axis
J = polar moment of inertia (allowing for rectangular shape)
A = cross-sectional area of element
L = element length
Ω = torsion adjustment factor dependent on width/thickness ratio of element. Currently $\Omega = 0.75B/t \leq 1.1$

Figure 18-15 The complete element S matrix for a 6-d.o.f. cap element. Only nonzero values shown. [*After Bowles (1983).*]

PROBLEMS

18-1. Compute the allowable group capacity Q_a using an SF = 3 for the six-pile group of Fig. 18-1*a* using the Converse-Labarre equation and compare with the CDF recommendation. Pile and group data include s = 1 m, pile length L = 25 m, and D = 400 mm. The piles are in a medium coarse sand with a computed single-pile capacity of 1200 kN.

18-2. Using the pile and group data of Prob. 18-1, assume the piles are in a cohesive soil of s_u = 75 kPa. Use the α method of Chap. 16 with the API value from Fig. 16-14 to compute ultimate pile capacity. With these data estimate the group capacity. What does the Converse-Labarre equation give for group capacity? As in Prob. 18-1 use an SF = 3 to obtain the design group capacity Q_a.

18-3. A pile group consists of three piles as in Fig. 18-1*a*. The piles are **HP**360 × 152, used as friction piles. The group is subjected to an axial load of 1700 kN. The pile spacing is 0.831 m. Take μ = 0.40 and case 2 (Table 18-1*b*) conditions.

a Compute the stress, using Table 18-1*b*, in the soil at the center of the group 1.8 m below the bottom of the piles, which are 18 m long.

b Compute the stress 1.8 m beneath one of the piles.
Answer: ≅ 29.8 kPa

c Compare the stress in (*a*) and (*b*) with that obtained using the Boussinesq theory of Chap. 5.

d Compare the stresses of (*a*) and (*b*) with that obtained from the method shown in Fig. 18-4*a* and *b*.

18-4. A clay stratum 4.6 m thick is located 2.5 m beneath the points of the pile group of Prob. 18-3. The soil overlying the clay consists of a sandy material with a unit weight of 18.1 kN/m^3 for the top immediate 3.6 m and γ' = 8.6 kN/m^3 (average) to the clay stratum. The clay has $\gamma \cong$ 19.81 kN/m^3 with w_N = 28.5, w_L = 36.2, and w_P = 17.4 percent. Compute the estimated consolidation settlement of this pile group. *Hint:* Assume G_s = 2.70 for clay and use one of the correlation equations of Chap. 2 for C_c.

18-5. A pile group consists of nine square concrete piles as in Fig. 18-1*a*. The piles are 300 × 300 mm with $E_c = 26\,500$ MPa. The pile lengths are 20 m. The ultimate group load $Q_{ult} = 10\,800$ kN. The soil has an undrained shear strength $c = 60$ kPa at −3 m to 90 kPa at −40 m. The water table is at elevation −5 m. The cap is poured on the ground. C_c at elevation −15 m is 0.45. The saturated unit weight is 17.53 kN/m^3. Estimate the total group settlement and αc in Eq. (16-12) used to obtain L.

18-6. Redo Example 18-3 for a linear (case 3) increase in skin friction.

Answer: ≅ 19.2 kPa

18-7. Estimate the settlement in Example 18-4 due to negative skin friction.

18-8. What width of fill would compute the measured settlement of Example 18-4?

18-9. The pile of Prob. 18-5 is assumed to be in parallel with the soil. The contributory cap area is 2 × 2 m. The existing modulus of subgrade reaction k_s is taken as 9500 kN/m^3. Estimate the equivalent soil modulus k_s' for the pile node so the node spring is $K = a \times b \times k_s'$.

Answer: Approx. 303 900 kN/m^3 using $\lambda = 2.0$ in the term $\lambda AE/L$

18-10. Assume in Example 18-6 the pile length is 36 m and other conditions are the same. What is the negative skin friction? Assume the pipe piles are filled with concrete of $f_c' = 35$ MPa. Can the piles carry this negative skin friction?

18-11. Do Example 18-8 if all but piles 7 and 9 are vertical.

18-12. Do Example 18-8 if piles 7, 8, and 9 are battered at 4:1 and piles 7 and 9 are skewed as in the example. All batter directions are to be taken as in example.

18-13. Verify the eight pile constants from Fig. E16-13*b* and *c*.

18-14. Do Example 18-7 using your estimation of λ and ψ in pile constants C(I, 1) and C(I, 4).

18-15. Form the remainder of the **A** matrix of Fig. 18-4. How many stiffness entries will the product of $E\mathbf{ASA}^T$ have for any element?

18-16. Compute the approximate pile loads of Example 18-7 using Eq. (18-9) adjusted for moment about only the z axis. Compare these computed pile loads to the computer output and make any appropriate comments.

Answer: $P_{max} = 860$ (vs. 853.1) using $I_z = 11.76$

18-17. Make two copies of data set EXAM187.DTA and set $M_z = 0$ so you only have a vertical load. Now execute one set and obtain a set of output axial pile forces.

Using the other data set copy, increase the AE/L springs for piles 2, 4, 6, and 8 by 20 percent (value × 1.2). Increase the AE/L springs for piles 1, 3, 7, and 9 by 30 percent (value × 1.3). Now make a second analysis and compare pile loads. Does the comparison have any resemblance to the Vesić comments that side and corner piles carry more load than the interior piles?

18-18. Make two copies of data set EXAM87.DTA and in both set the vertical force $P_y = 0$ (It is now −7200 kN) and $M_z = 0$ and input a $P_x = P_1 = +900$ kN (a single lateral force parallel to the x axis).

Make an execution and check the output to ensure you have done everything correctly for that data set.

Next take the second data set and reduce the horizontal pile springs for piles 4, 5, and 6 by 20 percent each and the back springs for piles 1, 2, and 3 by 15 percent (value × 0.85). The horizontal springs are the P_x/δ_x values of Table 18-4. If the results are not very good, consider reducing the off-diagonal terms of M_x'/δ_x as well. Can you draw any conclusions from these two executions about "soil-pile-soil" interaction?

CHAPTER 19

DRILLED PIERS OR CAISSONS

19-1 INTRODUCTION

The *drilled pier* is constructed by drilling a cylindrical hole of the required depth and subsequently filling it with concrete. The shaft may be straight or the base may be enlarged by underreaming. This structural member is also termed as follows:

a. Drilled shaft
b. Drilled caisson (or sometimes, simply, a caisson)
c. Bored pile (but usually restricted to $D < 760$ mm)

If the base is enlarged the member takes one of these names:

d. Belled pier (or belled caisson)
e. Underreamed foundation

These several configurations are shown in Fig. 19-1.

The term *caisson* is also used to describe large prefabricated box-type structures that can be sunk through soft ground or water at a site to provide a dry work space.

This chapter will focus primarily on the analysis and design of drilled piers.

19-2 CURRENT CONSTRUCTION METHODS

Early drilled piers were constructed by digging the shaft and/or bell by hand although drilling methods using horse power were in use in the early 1900s. Early methods include the Chicago and Gow methods shown in Fig. 19-2. In the Chicago method, workers excavated a circular pit to a convenient depth and placed a cylindrical shell of vertical boards or staves held in place by an inside compression ring. Excavation depth then continued to the next board length and a second tier of staves was set, etc., to the required shaft depth. The tiers could be set at a constant diameter or stepped in about 50 mm.

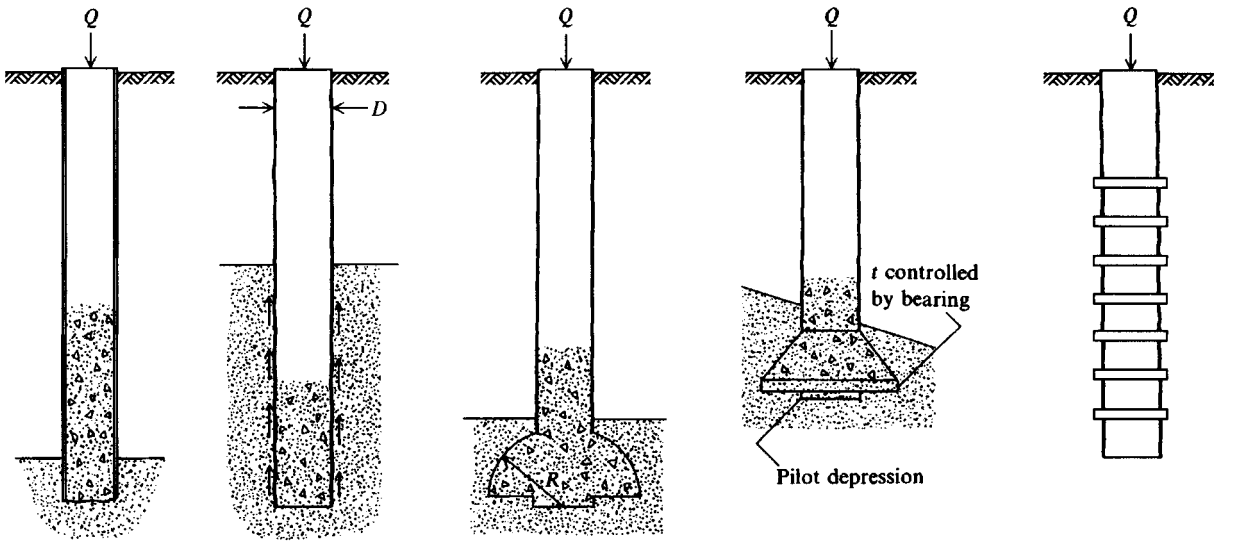

(*a*) End-bearing cased pier.

(*b*) End-bearing uncased with some skin resistance.

(*c*) Domed bell end-bearing.

(*d*) Angled bell (usually between 30 and 45°) end-bearing.

(*e*) Friction caisson using shear rings cut by auger during drilling to improve shear resistance.

Figure 19-1 Common drilled pier configurations. Such a structure is considered a pile if shaft diameter $D < 760$ mm; a pier if $D > 760$ mm.

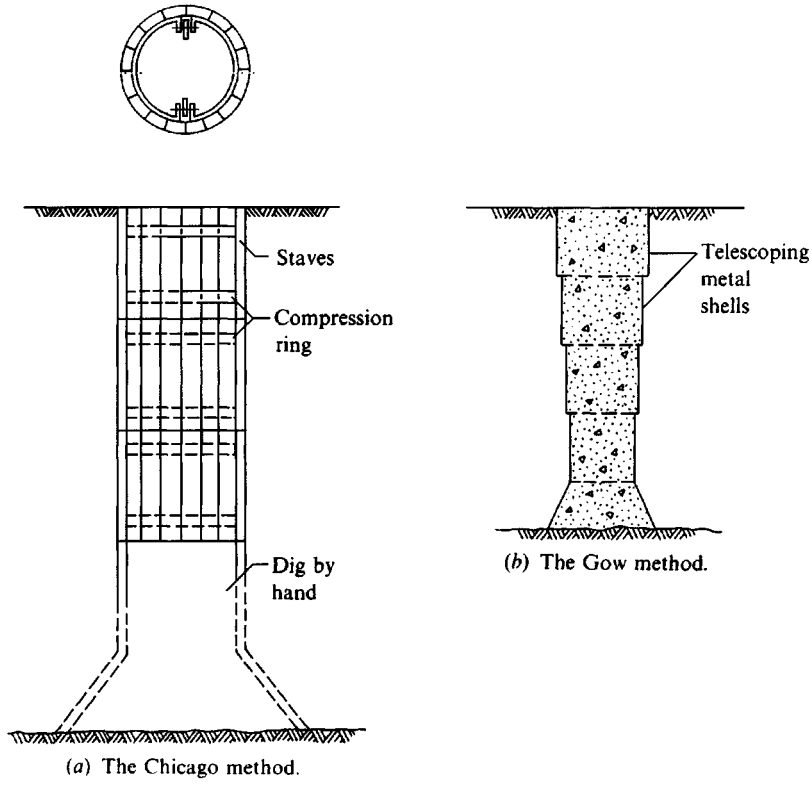

(a) The Chicago method.

(b) The Gow method.

Figure 19-2 Early methods of caisson construction.

The Gow method, which used a series of telescoping metal shells, is about the same as the current method of using casing except for the telescoping sections reducing the diameter on successive tiers.

The shaft base can be enlarged for additional bearing if the base soil does not cave (i.e., if founded in a fairly stiff nonfissured clay). Many of the early piers were founded on rock.

Drilled piers—particularly large-diameter ones—are not often used in groups. Most often a drilled pier interfaces with a single column carrying a very large superstructure load. Reinforcing bars may be required either for the full pier depth L_p or only in the upper moment-active zone (about $L_p/2$). The rebars—if used—are to carry any tensile Mc/I stress from shaft moment. Reinforcing bars may not be required in those cases where the pier requires steel casing that is filled with concrete to form a metal-encased shaft.

The shaft moment may result from using a fixed-base column, from accidental misalignment of the load-carrying column with the pier shaft (a P–Δ type effect not known at the time the pier is designed), or from lateral loads from the superstructure (which are usually known). Since the pier shaft is embedded in the soil, where its temperature is a relatively constant value, T&S steel is used only as a designer prerogative or if the local building official requires its use.

The reinforcing bars are usually prewired—including vertically spaced tie bars—into a designed pattern called a *rebar cage*, which can be set as a unit into the pier shaft cavity into about 1 m of previously poured concrete (so that the bars are not in contact with earth) and

the remaining space filled with concrete to form a vertically reinforced structural member. Where the rebars are not required for the full depth, some concrete is placed, the rebar cage is set, and then the shaft pour is continued.

The shaft supports for the Chicago and Gow methods were usually left in place since the pier did not rely on shaft friction. Furthermore, they were not very easy to remove after the concrete had been poured.

Currently, labor and insurance costs for hazardous conditions preclude hand digging shafts, so machine digging is universally used. There are three basic methods (site variables may require a mix of methods, however).

1. DRY METHOD. Here the production sequence is as in Fig. 19-3. First the shaft is drilled (and belled if required). Next the shaft is partly filled with concrete as in Fig. 19-3*b* with the rebar cage then set and the shaft completed. Note that the rebar cage should never go all the way to the bottom, for a minimum concrete cover is required, but it may extend nearly the full shaft depth rather than approximately one-half as shown here.

This method requires site soils be noncaving (cohesive) and the water table be below the base or the permeability so low the shaft can be drilled (pumped possibly) and concreted before it fills with sufficient water to affect the concrete strength.

2. CASING METHOD. This method is outlined in Fig. 19-4. Casing is used at sites where caving or excessive lateral deformation toward the shaft cavity can occur. It is also used where it is desired to seal the hole against groundwater entry but to do this requires an impermeable stratum below the caving zone into which the casing can be socketed. Note that until the casing is inserted, a slurry is used to maintain the hole. After the casing is seated the slurry is bailed out and the shaft extended to the required depth in the dry stratum. Depending on the site and project requirements the shaft below the casing will be decreased to at least the ID of the casing—sometimes 25 to 50 mm less for better auger clearance.

The casing may be left in place or pulled. If it is left in place the annular space between casing OD and soil (currently filled with slurry or drilling fluid) is displaced with pressure-injected grout (a cement + water + additives) mixture. By inserting a tube to the base of the slurry and pumping grout the slurry is displaced over the top so the void is filled with grout.

Alternatively, the casing can be pulled but with great care to ensure the following:

a. Concrete inside casing is still in a fluid state.
b. Concrete "head" is always sufficiently greater than the slurry head that concrete displaces slurry and not vice versa.

Pulling the casing may result in a substantially oversize top shaft zone—depending on how close the casing OD and initial shaft ID match. The oversize is seldom of consequence but may need to be known so that the total shaft volume can be compared to concrete volume used to ensure the shaft does not contain any accidental voids. The change in shaft diameters will produce an increase in capacity from the ledge-bearing Q_L.

3. SLURRY METHOD. This method is applicable for any situation requiring casing. It is required if it is not possible to get an adequate water seal with the casing to keep groundwater out of the shaft cavity. The several steps are outlined in Fig. 19-5. Note that it is essential in this method that a sufficient slurry head is available (or that the slurry density can be increased

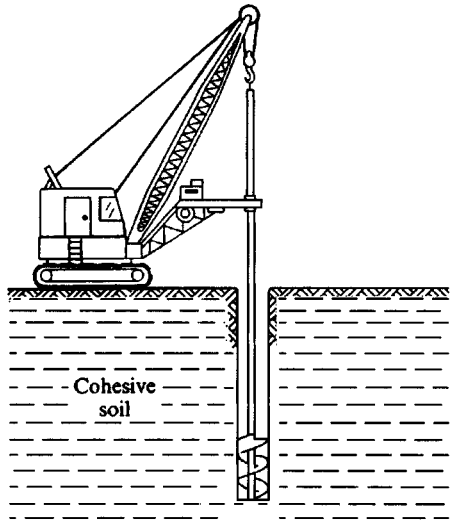

(*a*) Drill shaft to required depth.

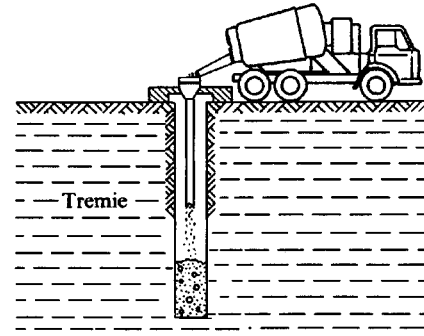

(*b*) Place concrete through tremie (and use limited free fall).

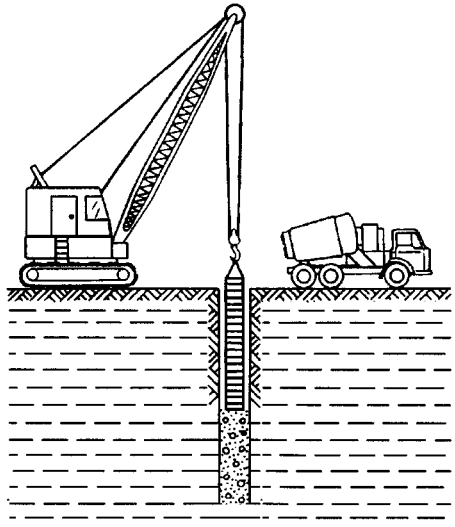

(*c*) Pull-out tremie and set rebar cage to depth required.

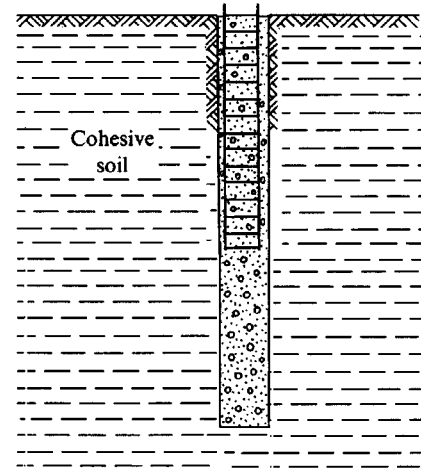

(*d*) Completed shaft.

Figure 19-3 Dry method of drilled pier construction.

as needed) so the inside pressure is greater than that from the GWT or from the tendency of the soil to cave. Many of the considerations of slurry trench construction discussed in Sec. 14-9 are equally applicable here.

Bentonite is most commonly used with water to produce the slurry ("bentonite slurry") but other materials (admixtures) may be added. Some experimentation may be required to obtain optimum percentage for a site, but amounts in the range of 4 to 6 percent by weight of admixture are usually adequate.

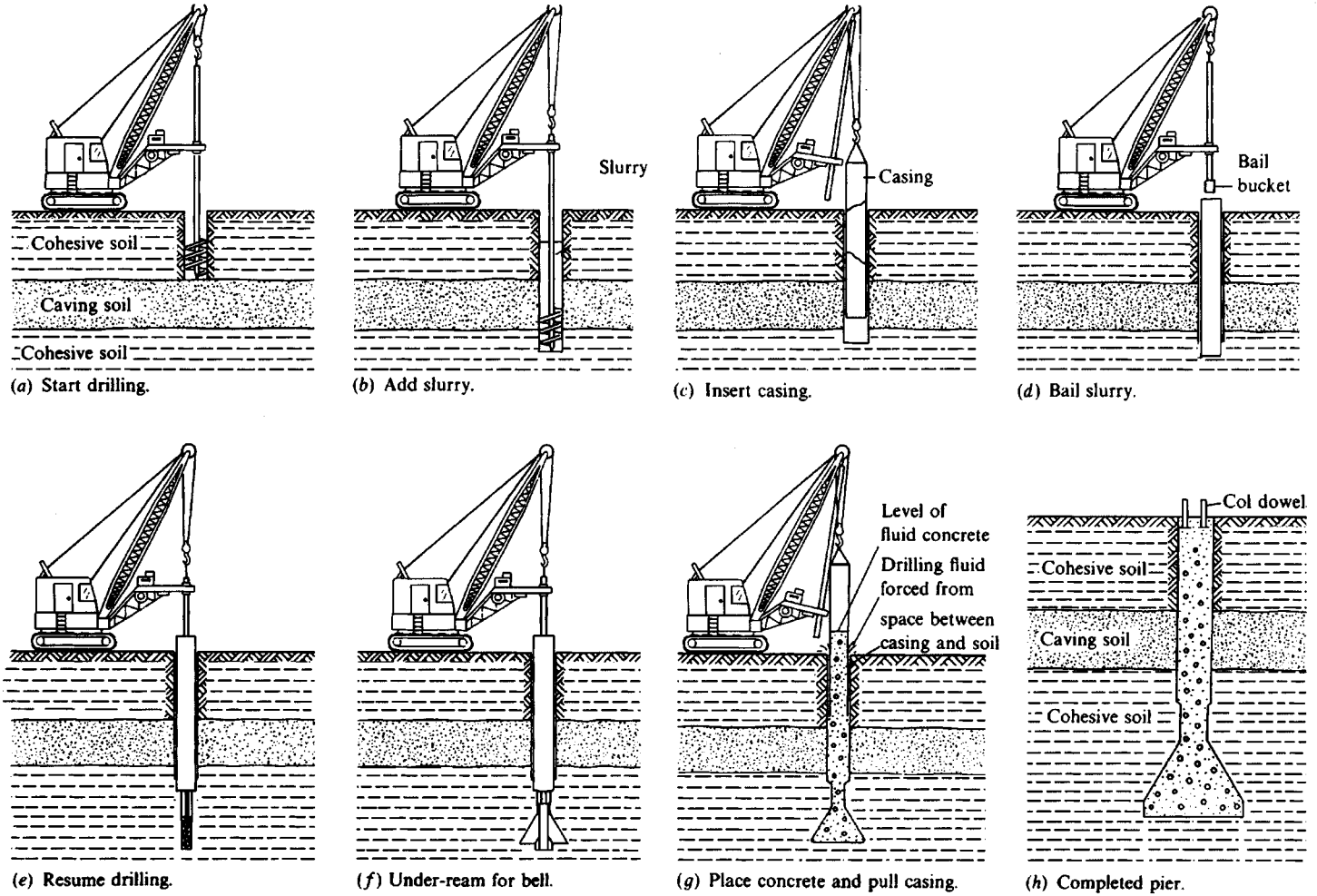

Figure 19-4 Casing method of drilled pier construction.

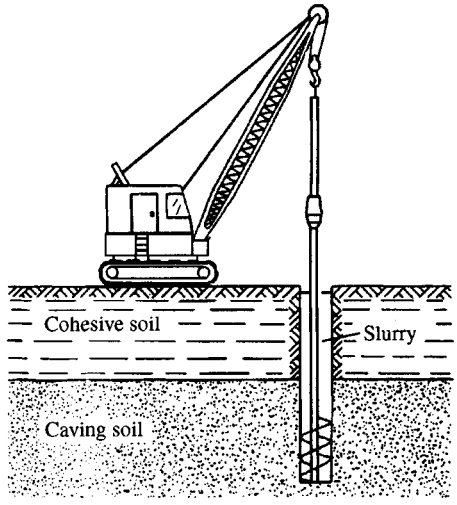

(*a*) Drill into caving soil and add slurry as necessary for adequate head and to required depth.

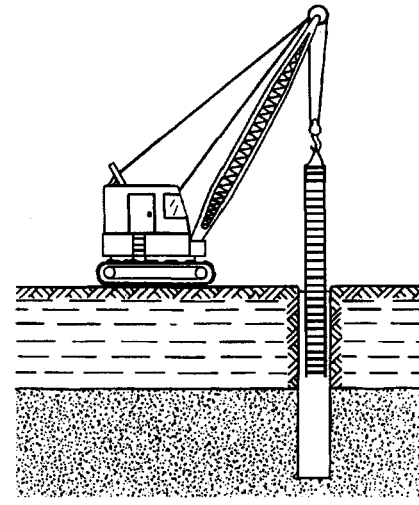

(*b*) Pull drill and insert rebar cage.

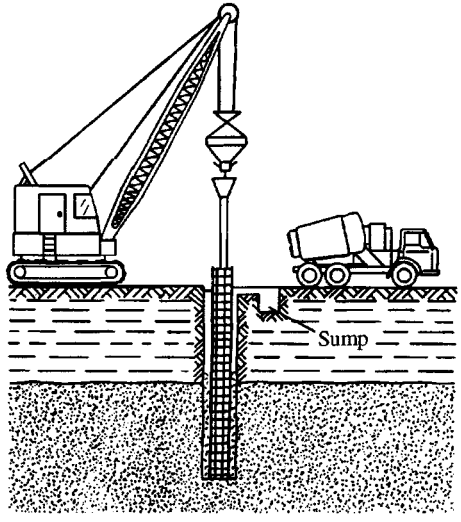

(*c*) Add tremie and pump cement. Catch displaced slurry in sump pit.

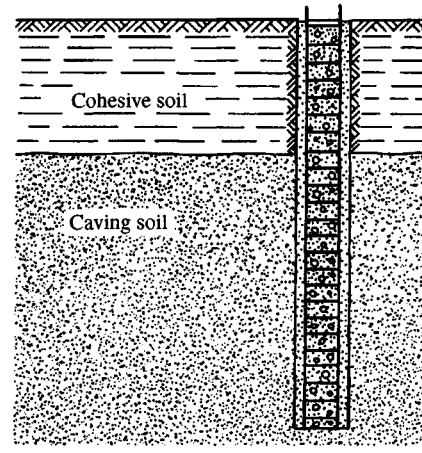

(*d*) Completed shaft.

Figure 19-5 Slurry method of drilled pier construction.

The bentonite should be well mixed with water so that the mixture is not lumpy. The slurry should be capable of forming a filter cake on the shaft wall and of carrying the smaller (say, under 6 mm) excavated particles in suspension. Sometimes if the local soil is very clayey it may be used to obtain an adequate slurry. The shaft is generally not underreamed for a bell since this procedure leaves unconsolidated cuttings on the base and creates a possibility of trapping slurry between the concrete base and bell roof.

With the slurry method the following are generally desirable:

a. Not have slurry in the shaft for such a long time that an excessively thick filter cake forms on the shaft wall; a thick cake is difficult to displace with concrete during shaft filling.
b. Have the slurry pumped and the larger particles in suspension screened out with the "conditioned" slurry returned to the shaft just prior to concreting.
c. Exercise care in excavating clay through the slurry so that pulling a large fragment does not cause sufficient negative pore pressure or suction to develop and collapse a part of the shaft.

When the shaft is complete the rebar cage is set in place and a tremie installed (this sequence is usually necessary so that the tremie does not have to be pulled to set the cage and then reinserted—almost certain to produce a slurry-film discontinuity in the shaft). Concrete made using small aggregate is pumped and great care is taken that the tremie is always well submerged in the concrete so a minimum surface area is exposed and contaminated with slurry. It appears that the concrete will adequately displace slurry particles from the rebar cage so a good bond can be obtained, and as previously noted, if the shaft is not open too long the filter cake is reasonably displaced as well.

19-3 WHEN TO USE DRILLED PIERS

Drilled piers can be used in most cases requiring pile foundations. Where the site soil requires use of deep foundations one should make a comparative analysis to determine whether piles or drilled piers are more economical.

Drilled piers have the following direct advantages:

a. They eliminate the need for pile caps, for dowels can be placed in the wet concrete at the required plan location (even if pier center is slightly misaligned) for direct column attachment.
b. They use fewer but with larger diameter shafts.
c. Their use eliminates much of the vibration and noise associated with pile driving.
d. They can go through a boulder soil where driven piles might be deflected. Boulders of size less than about one-third the shaft diameter can be directly removed. Others may be broken with special tools, or a temporary casing can be installed to give access for hand drilling and blasting larger rocks.
e. It is easy to enlarge the top portion of the pier shaft to allow for larger bending moments.
f. Almost any diameter shaft in the range of 0.460 to 3.5 m can be produced.
g. Larger-diameter shafts (if cased) allow direct inspection of bearing capacity and soil at shaft base.

There are a few disadvantages:

a. They cannot be used if a suitable bearing stratum is not close enough to the ground surface (and assuming that the soil to the competent stratum is unreliable for skin resistance).
b. Bad weather conditions may make drilling and/or concreting difficult.

c. There may be ground loss if adequate precautions are not taken.

d. One must dispose of soil from drilling ("spoil") and any slurry that is used.

19-4 OTHER PRACTICAL CONSIDERATIONS FOR DRILLED PIERS

Several practical considerations of importance in drilled pier construction include shaft alignment, disposal of slurry, concrete quality control, underreaming, and ground loss.

Shaft Alignment

It is often difficult to get a drilled pier perfectly aligned either in plan or elevation. If the plan location is within about 150 mm this is usually satisfactory. Much larger misalignment may require an adjustment in design for the additional moment resulting from eccentricity of the design load.

Maximum vertical misalignment as suggested by ACI Committee 336 (1988) is as follows:

Category A. Unreinforced shafts extending through materials offering minimal lateral restraint—not more than 0.125 × diameter

Category B. Same, but soil is competent for lateral restraint—not more than 0.015 × shaft length

Category C. Reinforced concrete shaft—to be determined on a site basis by the project engineer

Slurry Disposal

Slurry disposal is always a problem. One might use a (or several) large storage tank(s) on-site as temporary storage so the slurry can be reconditioned and reused to keep the total required volume to a minimum. One may construct a storage pit for the same purpose. Ultimately, however, the remaining residue must be hauled to a suitable disposal site.

Concrete Quality Control

Concrete is often specified in the 28 to 35 MPa range to reduce the shaft diameter. The slump should be in the range of 125 to 150 mm. Some persons suggest slumps in the range of 125 to 250 mm but one should check whether adequate (and reliable) strength can be obtained at slumps over 150 mm. Higher slumps are more necessary in slurry construction than for cased or uncased piers. Proprietary plasticizers are available to improve flowability (reason for large slumps) and eliminate arching. These might be appropriate for the dry method or with casing. Use of a plasticizer in the slurry method might be a viable solution, but there should be reasonable certainty that there will be no adverse chemical reactions with the slurry constituents.

To ensure reasonable shaft continuity, one should compare the shaft and concrete volumes for each pier. Several highly specialized nondestructive test procedures are available to measure shaft continuity (and quality, e.g., for voids) where a defective shaft is suspected [see Olson and Thompson (1985)] and the concrete has hardened. Sometimes a small-diameter core is taken from a suspect shaft.

Test cylinders are routinely taken to have a record of the concrete strength used. This aspect is usually set up by the project engineer using ACI guidelines. The top 1.5 m of the shaft should be vibrated to ensure adequate density.

Underreaming

Underreaming or belling can be done in noncaving soils to enlarge the base to increase the bearing capacity where the base is founded on soil. For bases on rock the bearing capacity of the rock is often at least as large as that of the shaft based on f_c' of the concrete.

Belling produces unconsolidated cuttings on the base soil. Some of these may be isolated into the reamer seat (pilot depression of Fig. 19-1*d*). Alternatively, a temporary casing can be installed and an inspector lowered to the base to remove the cuttings by hand and to check the soil strength with a pocket penetrometer.

Bells may enlarge the base up to about four times the shaft diameter. As there would be great difficulty in placing rebars, the enlarged base is seldom reinforced. By using a maximum slope on the underream of 45°, two-way action shear is usually adequate so that the shaft does not "punch" through the bell. Bending should not be of concern for the short moment arm of about $1.5D$ maximum. Also note the concrete is placed in a fluid state so that it flows to a substantial contact pressure against the soil from the hydrostatic head. After hardening the soil provides substantial "confinement" to the bell to aid in resisting bending and punching failure.

Ground Loss

When the shaft is drilled the loss of lateral support will allow the surrounding soil to squeeze into the hole, decreasing its diameter. The squeeze can result in surface subsidence in the vicinity of the hole. The amount, of course, is directly related to the reduction in hole volume. Lukas and Baker (1978) suggest that a convenient method of determining whether hole squeezing will be a problem depends on the squeeze ratio R_s, which is the inverse of the s_u/p_o' ratio of Sec. 2-11.9

$$R_s = p_o'/s_u \tag{19-1}$$

where p_o' = effective overburden pressure
s_u = undrained shear strength

If $R_s < 6$ squeezing may take place but usually it is slow enough that it is of no consequence.

If $R_s > 6$ squeezing is almost certain to take place, and if R_s is on the order of 8 to 9 it will occur so rapidly it will be taking place as the hole is being excavated.

The foregoing is based on experiences in Chicago clay, and the ratio may be somewhat different at other locations.

The ground loss can be controlled in the following ways:

1. Rapid shaft excavation and replacement with concrete
2. Use of a shaft liner
3. Use of the slurry method

Either of the two latter options increases project costs, and many contractors do not like to use the slurry method because of the resulting mess and cleanup.

19-5 CAPACITY ANALYSIS OF DRILLED PIERS

Drilled piers are widely used to carry compressive loads. They are also used to carry tension loads—particularly under power line and antenna tower legs. They may carry lateral loads or a combination of vertical and lateral loads. The tension load case as given for piles in Sec. 16-14 can be written (here using Q instead of P) as

$$Q_{\text{ult},t} = \sum Q_{si} + Q_b + W \tag{19-2}$$

where $\sum Q_{si}$ = sum of perimeter $\times f_s \times \Delta L$ of the several (or single) shaft elements making up total length L—ultimate value

Q_b = bell pullout resistance and/or any point suction. Similarly as for piles the point suction contribution is transient so is seldom used.

W = total pier weight including shaft and bell

Safety factors in the range of 2 to 4 are common, giving an allowable tension load of either

$$Q_{a,t} = \frac{Q_{\text{ult},t}}{\text{SF}}$$

or, preferably, but not much used,

$$Q_{a,t} = \frac{\sum Q_{si}}{\text{SF}_s} + \frac{Q_b}{\text{SF}_b} + \frac{W}{\text{SF}_w} \tag{19-2a}$$

The use of partial safety factors as in Eq. (19-2*a*) is preferable since we might use $\text{SF}_s = 3$ or 4 for the skin resistance component because of uncertainties, an $\text{SF}_b = 2$ to 5 on the bell if Q_b is included, and an SF_w of about 1.4 since the volume of concrete and resulting weight of the pier are reasonably well known. The structural design would require that the allowable concrete stress in tension plus rebar allowable tension stress be sufficient to carry the tension design load $Q_{d,t} \leq Q_{a,t}$.

19-5.1 Pier Capacity in Compression

The ultimate capacity of a drilled pier (see Fig. 19-6) in compression is the smaller of

$$Q_{\text{ult}} = \sum Q'_{si} + \sum Q_L + Q_p \tag{19-3a}$$

or

$$Q_{\text{ult}} = \sum Q_{si} + \sum Q_L + Q'_p \tag{19-3b}$$

where $\sum Q_{si}$ = ultimate skin resistance as defined in Eq. (19-2)

$\sum Q'_{si}$ = limiting skin resistance, generally $< Q_{si}$

Q_p = ultimate point bearing

Q'_p = point bearing just at transition from ultimate to limiting skin resistance, and is generally $< Q_p$

$\sum Q_L$ = bearing resistance from any ledges produced by changes in shaft diameter or shear rings

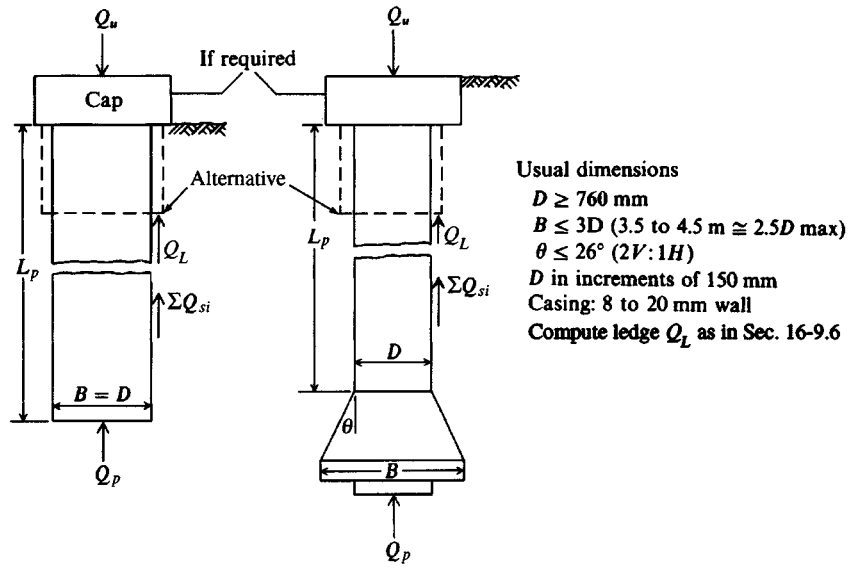

Figure 19-6 Capacity of straight- or stepped-shaft and belled piers. Commonly used dimensions are shown, but other dimensions can also be used.

The rationale for Eqs. (19-3) is based on load tests for both piles and drilled piers where the maximum skin resistance is developed at very small shaft movements on the order of about 3 to 10 mm. As a ratio the movements are on the order of $0.002D$ to $0.01D$. The movement necessary to develop ultimate bearing resistance is on the order of $0.005B$ to $0.05B$ where B = base diameter = D for straight shafts. The base displacement to develop maximum point resistance is much smaller for dense sand than for clay, which is often near 0.03 to $0.05B$.

The load test in Fig. 19-7 illustrates load resistance development as a combination of two separate effects. The pier is 762-mm diameter × 7.01-m long and was selected because of the particular clarity and the nearly ideal load-transfer curves that are developed. Most load tests produce similar results but less clearly. Here we have the following:

1. At application of the first load increment of approximately 110 kN, skin resistance develops along nearly the full shaft length. The skin resistance contribution Q_{si} for any segment length ΔL can be obtained as the difference in shaft load at the top and base of the element. The sum of all these Q_{si} contributions for this load increment is simply the load Q = 110 kN.
2. With the second load increment to approximately 285 kN the load-transfer curve shifts to the right, but we see again that the tip load of about 45 kN is negligible.
3. The third load increment (to 735 kN), however, appears to produce a "limiting" shaft skin resistance with a small increase in point load (from 45 to about 80 kN). Also note:
   a. The limiting skin resistance is analogous to the "residual" soil strength in a direct shear test.
   b. The limiting skin resistance is not constant. In the upper 1.5 m and the bottom 1.0 m there is almost no skin resistance (in these two zones the curve is nearly vertical).
   c. The point load is now the Q'_p of Eq. (19-3).
4. Next, the fourth load stage of 1250 kN is applied to develop what one could define as Q_{ult} for the pier. The point load has increased nearly the amount of the load increase (1250−

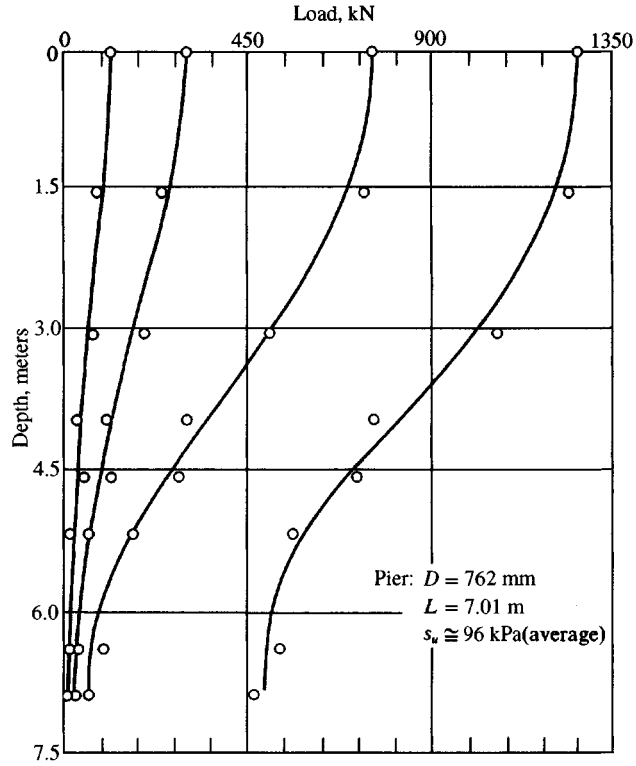

Figure 19-7 Load distribution for drilled pier. [*From Reese and O'Neill (1969)*; converted to SI by author.]

735 = 515 vs. 500 − 80 = 420). An inspection of the load-transfer curve for load stage 4 shows that it is nearly identical in shape to that from the 735-kN load stage 3 load. In comparing the last two load transfer curve shapes it is clear that the skin resistance only increases a small amount from load stage 3 to 4, with the major part of the load increment being carried directly by the point. The load transfer curve for load stage 4 approximates this by its lateral displacement to the right, so the shaft curve profile is similar to curve 3, but the bottom is shifted by very nearly the load increment.

Considering these load stages and again referring to Fig. 19-7, we see that we can define the following:

$$Q_{\text{ult}} = 1250 \text{ kN}$$

$$Q_p = 490 \text{ kN} \qquad \text{(read directly from the load-transfer curve at the tip level)}$$

from which the skin resistance component is computed as

$$\sum Q'_{si} = 1250 - 490 = 760 \text{ kN}$$

Since s_u in the 7.01 pier depth was about 96 kPa we can compute a full-depth α coefficient as

$$\alpha = \frac{\sum Q'_{si}}{L \times p' \times s_u}$$

$$= \frac{760}{7.01 \times \pi \times 0.762 \times 96} = 0.47$$

however, we probably should have used a length $L = 7.01 - 1.5 - 1.0 = 4.5$ m (and $\alpha \cong 0.73$) since the upper 1.5 m and lower 1 m of the shaft has negligible skin resistance at ultimate load.

If the pier load were increased to, say, 1560 kN or more, we may speculate that the load-transfer curve would become nearly vertical to a greater depth; and the point load would increase, with the settlement greatly increasing.

From this description of events in a load test, together with Eqs. (19-3*a*) and (19-3*b*), we see that estimating the capacity of a drilled pier—particularly without the guidance of a load test—is not a simple task in spite of the relatively simple format of the equations. Obviously, if ultimate values of skin resistance and point bearing occurred at about the same amounts of displacement the problem would be much simpler.

Because the shaft and point maximum load capacities are not developed simultaneously, many practitioners use either point bearing or skin resistance rather than a combination. This practice is common in the United States (and is not unduly conservative when the point is founded on rock or very dense bearing soil). Others, primarily in Europe, often try to use some kind of interaction to obtain the pier capacity as a combination of skin resistance and point bearing. This approach is also given by Reese et al. (1976) and later by Reese (1978) based on his extensive research. As given by Reese et al. (1976) the pier capacity *in clay* is

$$Q_{\text{ult}} = \sum Q_{si} + Q_p \tag{19-4}$$

where $\sum Q_{si} = \sum \alpha s_{us} \times p' \times \Delta L$

$Q_p = N_c c A_p = 9 s_{u,p} A_p$

α = reduction coefficient from Table 19-1 based on installation process

$s_{u,s}$ = average undrained shear strength *along shaft length* ΔL; use $s_{u,s}$ = cohesion in range of $0 \leq \phi \leq 10°$

p' = average pier perimeter in shaft length ΔL

ΔL = element length over which $s_{u,s}$ can be taken as a constant value

$s_{u,p}$ = average undrained shear strength from about $0.5B$ above base to about $3B$ below the base

TABLE 19-1
Average α values to estimate shaft skin resistance of drilled piers in clay

Method of pier construction	Limiting f_s*	
	α†	kPa
Dry or using lightweight drilling slurry	0.5	90
Using drilling mud where filter cake removal is uncertain	0.3	40
Belled piers on about same soil as on shaft sides		
By dry method	0.3	40
Using drilling mud where filter cake removal is uncertain	0.15	25
Straight or belled piers resting on much firmer soil than around shaft	0	0

*$f_s = \alpha s_u \cong f_{s(\text{limiting})}$.

†For soil-to-concrete; use values of 0.25 to 0.1 for cased piers where adhesion is to the steel shell. Use higher values for driven casing. After Reese et al. (1976)

A_p = area of base = $0.7854B^2$
B = base width

For the immediate settlement to be tolerable *in clay* it was recommended that the allowable design load be

$$Q_a = \frac{Q_{\text{ult}}}{\text{SF}} \geq Q_d \tag{19-5}$$

with the SF in the range of 1.5 to 4. Alternatively, or where the base is on clay with $OCR > 1$,

$$Q_a = \sum Q_{si} + \frac{Q_p}{3} \geq Q_d \tag{19-6}$$

The premise of Eq. (19-6) is that by reducing the base load by a factor of 3 the small slip necessary to mobilize Q_{si} is well within settlement tolerances. *Use the smaller* Q_a from *either* Eq. (19-5) or Eq. (19-6) above.

For piers in *sand* Reese et al. (1976) suggest using Eq. (19-4) with the terms separated as

$$\left.\begin{aligned} \sum Q_{si} &= \sum K\bar{p}_o \tan\delta(p' \times \Delta L) \\ \text{and} \qquad Q_p &= \frac{q_p}{\alpha_p} A_p \end{aligned}\right\} \tag{19-6a}$$

where the new variables are as follows:

K = shaft lateral pressure factor, conservatively taken as follows:

Depth to base, m	K
≤ 7.5	0.7
$7.5 < L \leq 12$ m	0.6
> 12	0.5

$\bar{p}_o$ = average effective overburden pressure to midheight of ΔL
δ = ϕ for pier shaft in sand because of the rough concrete interface
q_p = maximum point pressure for an assumed 5 percent point displacement which, based on load tests, is suggested as follows:

	q_p	
Sand state	kPa	ksf
Loose (not likely used)	0	0
Medium (possibly used)	1600	32
Dense (very likely used)	4000	80

α_p = base reduction factor to limit base settlement to 25 mm (1 in.) and given as

SI: $2.0B$ (base width B in meters)
Fps: $0.6B$ (B in feet)

SPT or CPT correlations may be used to estimate the angle of internal friction ϕ in Eq. (19-6*a*) unless better data is available, since the lateral pressure coefficient K as given above is considered to be conservative. One would never found a drilled pier base on loose sand and probably would not place the point on a medium dense sand unless a more competent stratum is at a substantially greater depth.

If Eq. (19-6*a*) is used, the immediate settlement should not be a problem, since it is based on a 25-mm maximum settlement through use of the α_p factor. The allowable pier design load Q_a is

$$Q_a = \frac{Q_{\text{ult}}}{\text{SF}}$$

It is recommended to use SF = 1.0 when Q_{ult} = point value from Eq. (16-6*a*) with $\Delta H_p \approx 25$ mm; use SF = 1.5 to 4 when skin resistance is included in Q_{ult} and with point settlement ΔH_p now somewhat less than 25 mm.

We should note that Eqs. (19-3) and (19-4) are theoretically correct and that Eqs. (19-6) are empirical. Any difference between the theoretical equations and load-test values are from using incorrect design parameters to estimate the skin resistance and point capacity, or an oversimplification of using L rather than ΔL in a summation process. The parameters suggested by Reese et al. (1976) are from a fairly limited data base + use of some reported load-test data of others, and the correlation is generally very good. As with any of the correlation-type data, however, the reader should expect some scatter as more test data are accumulated—either from errors or from natural variability in soils from different geographic regions. Further, locally obtained parameters in these equations may provide better designs than the use of global (of universal application) parameters.

The computation for the α coefficient for skin resistance illustrates how wide variations can be reported in the literature (ranging from about 0.15 to 1). Here with the simple load test discussed earlier we could obtain 0.47 or 0.60 depending on what is used for shaft length. It is common to use a single factor for the full shaft length. In a load test where data can easily be back-computed it might be better to use shaft segments of ΔL. Practice tends to simplify the computations by using the effective shaft length and average shear strength values. Practice also tends to use the effective shaft length and average soil parameters for piles in cohesionless soils as well. According to Reese et al. (1976) the effective shaft length for skin resistance should exclude the top 1.5 m (5 ft) and the bell perimeter or, for straight shafts, the bottom 1.5 m (or 5 ft).

19-5.2 Other Methods for Point Bearing Capacity

Besides using Eq. (19-6*a*), one can compute the pier base capacity using the Terzaghi bearing-capacity equations from Table 4-1 as

$$Q_a = \frac{Q_{\text{ult}}}{\text{SF}} = \frac{A_p}{\text{SF}}(1.3cN_c + L'\gamma N_q + 0.4\gamma B_p N_\gamma) \tag{19-7}$$

For the case of the base on either clay ($\phi = 0$) or sand ($c = 0$),

$$Q_a = \frac{A_p \times 9c}{\text{SF}} \qquad \text{(clay)}$$

$$Q_a = \frac{A_p}{\text{SF}}(L'\gamma N_q + 0.4\gamma B_p N_\gamma) \qquad \text{(sand)}$$

We can also use the Hansen equations, where

$$Q_a = \frac{A_p}{\text{SF}}(cN_c s_c d_c + L'\gamma N_q s_q d_q + 0.5B_p N_\gamma s_\gamma) \tag{19-7a}$$

or for $\phi = 0$

$$Q_a = \frac{A_p}{\text{SF}} 5.14 \times s_u(1 + s'_c + d'_c) + L'\gamma$$

where A_p = pier point area (bell area if one is used)
B_p = width of pier point [shaft or bell (if used)]
L' = about 15 × shaft diameter for Terzaghi equations, and effective length L_p for the Hansen equations

Meyerhof (1956) suggested equations using the SPT and CPT for the allowable bearing capacity for spread footings for a 25-mm settlement, *and* with the statement they should be *doubled* for pier bases. After doubling by the author these equations become

$$\text{SPT:} \qquad Q_a = A_p \frac{N_{55}}{0.052} \qquad \text{(kN)} \tag{19-8}$$

$$\text{CPT:} \qquad Q_a = A_p \frac{q_c}{40} \qquad \text{(kN)} \tag{19-9}$$

where q_c is given in kPa.

For drilled piers socketed into rock the allowable bearing capacity q_a can be computed as in Example 4-14 of Sec. 4-16 so that the allowable point

$$Q_a = A_p q_a$$

Drilled piers socketed into rock some depth D_r will have a substantial skin resistance capacity as well as point bearing. This may allow using a reduced shaft diameter in this region.

The socket skin resistance capacity [see Benmokrane et al. (1994)] can be expressed as

$$Q_s = \pi B_r D_r \lambda \sqrt{q_u} \qquad \text{(MN)}$$

where B_r = shaft diameter in rock socket at depth D_r
q_u = unconfined compression strength of the smaller of the rock or the pier shaft concrete, MPa
λ = adjustment factor, usually ranges between 0.2 for smooth-sided and 0.3 for rough-sided shafts. Others have suggested values of 0.45 for fairly smooth sides and 0.6 for rough sides.

19-5.3 General Capacity Analysis for Drilled Piers

For the usual case of a drilled pier in soil the analysis is essentially identical to that for a pile, and the computer program PILCAPAC can be used. The two basic differences are that the shaft is usually round (and larger than a pile) and some adjustment in the α factor must be made if the pier is constructed by the slurry method.

19-6 SETTLEMENTS OF DRILLED PIERS

The settlement of a pier is the axial shortening of the shaft + the point settlement, written as

$$\Delta H = \sum \Delta H_{si} + \Delta H_p$$

where $\sum H_{si}$ = accumulation of shaft axial compression, $\frac{P_i \Delta L}{AE}$

ΔH_p = point settlement due both to the point bearing pressure and to settlement caused by skin resistance

The computer program PILCAPAC in Example 16-7 and Example 19-1 (following) also computed pier settlement by this method.

If we do not have a computer program we can estimate that the settlement should not be more than 25 mm if the recommendations for Q_{pu} made by Reese (1978) are followed. The resulting design ΔH should be 25/SF since Q_{pu} = ultimate value and is always divided by an SF.

We may use Meyerhof's equations [Eqs. (19-8) and (19-9)] as alternatives, which are suggested not to give more than $\Delta H = 25$ mm for the allowable design pressure q_a.

We may also use the stress coefficients from Table 18-1 and our best estimate as to which of the three table cases (1, 2, or 3) applies. From the stress influence coefficients, compute a stress profile for a depth of influence $L_i \approx 4$ to $5B$ below the base and compute the average stress increase Δq_{av}. Next make some kind of estimate for the stress-strain modulus E_s in this depth and solve the following:

$$\Delta H_p = \epsilon \times D_i = \frac{\Delta q_{av} L_i}{E_s}$$

for the point settlement term.

The methodology of program PILCAPAC will be used to illustrate both capacity and settlement analysis in the following example.

Example 19-1. Use program PILCAPAC and compute the estimated ultimate pier capacity for the "slurry" pier [one of the four "piles" tested and reported in ASCE SP No. 23 (see Finno (1989)]. See Fig. E16-7*a* for the soil profile. This pier had a nominal 24-in. diameter shaft in the upper 9 ft and 18 in. below. Thus, there is one ledge [the program will allow any number—you have to specify the number of layers to the ledge and the upper and lower diameter in millimeters (or inches)]. The concrete $f'_c = 6000$ psi and the pier length is 50 ft. *Fps units are used in this example since the original source uses those units and it would be difficult to check results if converted to SI.*

Solution. A data file was created and named ASCEPL2.DTA as shown on the output sheets (Fig. E19-1). Most of the soil data are contained in the table labeled "Soil Data for Each Layer." Although only layers 2 through 8 provide skin resistance, nine layers are shown. The ninth (bottom) layer is for computing point capacity. Shown are both the assumed ϕ and δ angles of the soil. The K factor is computed as described in Example 16-7.

Note that for friction in the sand the friction angle $\delta = \phi$ since the concrete is poured against the soil—or at least flowed against the soil as the casing in the top depth was pulled.

The α factors are all 1.25 in the bottom three clay layers and are substantially larger than the Reese recommendations given earlier. The value of $\alpha = 1.25$ was selected for two reasons: (1) The soil is below the GWT; the contractor had some drilling problems, so this part of the shaft may have been enlarged somewhat (it was stated that the concrete volume was about 10 percent larger than the theoretical shaft volume). (2) The concrete had a slump between 9 and 10 in. (a very high value), so it would tend to give a large lateral pressure, which would in turn give a larger undrained cohesion

than that used. Rather than do a numbers shuffle (increase the shaft diameter, increase cohesion) it was easier just to increase α.

I elected to use the Terzaghi equation for point capacity since the Hansen equation had been used in Example 16-7. I had to stay with the computer during execution, for the program asks how many diameter changes occur for a drilled pier (ITYPE = 5) and the number of soil layers from the top down to the change (here 1 change and 2 layers down from the top).

Figure E19-1

```
      +++++++++DATA FILE NAME FOR THIS EXECUTION:  ASCEPL2.DTA


 ASCE DRILLED "SLURRY" PIER TEST IN GT SP-23, FIG. 4, P 9--ALPHA METHOD

NO OF SOIL LAYERS =    9          IMET (SI > 0) =  0

 PILE LENGTH FROM GROUND SURFACE TO POINT, PLEN =  50.000 FT
                                      PILE TYPE:  DRILL PIER

       PILE DIAMETER =  1.500 FT
    DRIVE POINT DIAM =   .000 FT

       POINT X-AREA = 1.767     SQ FT

SOIL DATA FOR EACH LAYER:
LAY  EFF WT    PHI      DELTA     COHES                          THICK    PERIMETR
NO   K/FT*3    deg        deg      KSF      ALPHA     K-FACT      FT        FT
 1     .110   25.00        .0    1.000      .907      1.000      2.00      6.283
 2     .115   36.00       36.0     .000      .000      1.600      7.00      6.283
 3     .115   32.00       32.0     .000      .000      1.400      4.00      4.712
 4     .115   32.00       32.0     .000      .000      1.400      2.00      4.712
 5     .060   36.00       36.0     .000      .000      1.700      8.00      4.712
 6     .060     .00         .0     .964     1.250      1.000      9.00      4.712
 7     .060     .00         .0     .964     1.250      1.000      9.00      4.712
 8     .060     .00         .0     .964     1.250      1.000      9.00      4.712
 9     .060     .00         .0     .964     1.000      1.000     10.00      4.712

THERE ARE  1 STEP CHANGES IN X-SECTION AND ALSO SHAFT MAY BE TAPERED


FOR ABRUPT X-SECT CHANGE =  1
   DIAM D1, D2 =   2.000   1.500
   NET AREA =   1.374      QULT USES D1 =      2.00
EXTRA DATA FOR CHECKING TERZAGHI STEP LOAD
NC, NQ, NG =  44.034  28.515  27.490
SC, SG, QBAR =  1.300   .600   1.025
COMPUTE QULT =  31.125              STEP LOAD PBASET =   42.7792 KIPS


++++TERZAGHI BEARING CAPACITY METHOD USED--IBRG = 2

          PILE POINT IS ROUND W/AREA =  1.7672 SQ FT
                      BASED ON DIAM =  1.500 FT

PILE POINT AND OTHER DATA
 PILE LENGTH, PLEN =   50.00 FT       UNIT WT OF SOIL =     .060 K/FT*3
        PHI-ANGLE =   .000 DEG            SOIL COHES =     .96 KSF
       EFFEC OVERBURDEN PRESSURE AT PILE POINT QBAR =    3.81 KSF

EXTRA DATA FOR HAND CHECKING TERZAGHI POINT LOAD
NC, NQ, NG =   5.700   1.000    .000
SC, SG, QBAR =  1.300   .600   3.815
COMPUTE QULT =  10.958              POINT LOAD PBASET =   19.3654 KIPS


+++++ IN ROUTINE USING ALPHA-METHOD FOR SKIN RESISTANCE--IPILE =  5
```

```
I,QBAR -     2     .623   DELTA ANG DELTA(I) =    36.00
 KFACT(I) = 1.6000                    FRIC FORCE SFRIC =     31.827

I,QBAR =     2     .623   DEL ANGS D1,D2 =    36.00      .00
 KFACT(I) = 1.6000                    FRIC FORCE SFRIC =     31.827

I,QBAR =     3    1.255   DELTA ANG DELTA(I) =    32.00
 KFACT(I) = 1.4000                    FRIC FORCE SFRIC =     20.694

I,QBAR =     3    1.255   DEL ANGS D1,D2 =    32.00      .00
 KFACT(I) = 1.4000                    FRIC FORCE SFRIC =     20.694

I,QBAR =     4    1.600   DELTA ANG DELTA(I) =    32.00
 KFACT(I) = 1.4000                    FRIC FORCE SFRIC =     13.192

I,QBAR =     4    1.600   DEL ANGS D1,D2 =    32.00      .00
 KFACT(I) = 1.4000                    FRIC FORCE SFRIC =     13.192

I,QBAR =     5    1.955   DELTA ANG DELTA(I) =    36.00
 KFACT(I) = 1.7000                    FRIC FORCE SFRIC =     91.029

I,QBAR =     5    1.955   DEL ANGS D1,D2 =    36.00      .00
 KFACT(I) = 1.7000                    FRIC FORCE SFRIC =     91.029

 IN ROUTINE ALPHAM FOR I =     6    H1 =    9.00
ALPHA(I) =      1.250
 SHAFT PERIMETER PER(I) =    4.712                ADHES =     51.106

 IN ROUTINE ALPHAM FOR I =     7    H1 =    9.00
ALPHA(I) =      1.250
 SHAFT PERIMETER PER(I) =    4.712                ADHES =     51.106

 IN ROUTINE ALPHAM FOR I =     8    H1 =    9.00
ALPHA(I) =      1.250
 SHAFT PERIMETER PER(I) =    4.712                ADHES =     51.106

                    TOTAL ACCUMULATED SKIN RESISTANCE =  310.0595

 USING THE ALPHA METHOD GIVES TOTAL RESISTANCE, PSIDE =    310.060 KIPS
    WITH TOP    2.00 FT OMITTED

        TOTAL PILE CAPACITY USING TERZAGHI POINT LOAD =    372.20 KIPS


 SETTLEMENTS COMPUTED FOR AXIAL DESIGN LOAD =    372.2 KIPS
            USING SHAFT MODULUS OF ELAST ES = .6358E+06 KSF

 LAYER     THICK    X-AREA      PTOP     SKIN R     PBOT      ELEM     SUM DH
   NO       FT      SQ FT      KIPS      KIPS      KIPS       DH        IN
     1     2.00     3.142      372.2        .0     372.2     .0045     .0045
     2     7.00     3.142      372.2       31.8     340.4     .0150     .0195
     3     4.00     1.767      340.4       20.7     319.7     .0141     .0336
     4     2.00     1.767      319.7       13.2     306.5     .0067     .0402
     5     8.00     1.767      306.5       91.0     215.5     .0223     .0625
     6     9.00     1.767      215.5       51.1     164.4     .0183     .0808
     7     9.00     1.767      164.4       51.1     113.2     .0133     .0941
     8     9.00     1.767      113.2       51.1      62.1     .0084     .1026

    SETTLEMENT DATA:     DQ, BMAX =     210.62       1.50
              SOIL THICKNESS HTOT =   50.00
             HTOT/BMAX & FOX FAC =    33.33     .500
       FOR MU = 0.35 AND SOIL Es =      450.0 KSF
    COMPUTED POINT SETTLEMENT, DP =   1.8482 IN
     TOTAL PILE/PIER SETTLEMENT (BUTT MOVEMENT) = DP + DH =    1.9507 IN
```

Figure E19-1 (*continued*)

The resulting output is shown on Fig. E19-1, and we can make the following comparison:

Computed	Load test
Q_u = 372 kips	340 (after 4 weeks) kips 413 (after 43 weeks)
ΔH = 1.95 in.	Between 2 and 2.5 in.

This comparison indicates that the estimated soil properties were fairly good (with aging not considered, both ϕ and α are too low); that aging is a factor; and that pile/pier loads are not easy to predict. The use of the computer program clearly indicates that the best predictions for capacity and settlement are made by considering the several soil layers making up a site profile rather than trying to obtain a single site parameter such as α or β. It is usually easier to back-compute from known values; however, note that the ϕ angles were not readjusted to obtain a better fit and the α factor was selected with some justification.

As a final comment, there were 24 predictors for these tests and not one got a quality value. One was about 30 percent over—the others ranged from about 50 to 60 percent of the load test. Most did not include a ledge contribution Q_L, which is larger (since it bears on the sand) than the point capacity Q_p, which is in clay.

////

19-7 STRUCTURAL DESIGN OF DRILLED PIERS

Since the pier shaft is supported by the surrounding soil, column slenderness effects do not have to be considered. Thus, the design is considerably simplified. Design requirements are usually met if the shaft diameter is large enough to carry the design load without exceeding the allowable concrete and steel (if used) stresses.

The bell dimensions should be adequate to resist a punching failure and have adequate bending resistance as a plain concrete member, because reinforcement would be difficult to place.

For unreinforced pier shafts the allowable concrete stress in a number of building codes is

$$f_c = 0.25 f_c' \tag{19-10}$$

For ordinary reinforced drilled piers we can design conservatively as

$$P = A_c f_c + A_s f_s \geq P_d \tag{19-11}$$

where A_i = cross-sectional areas of concrete and steel, respectively
f_i = allowable concrete and steel stresses, respectively
$f_c = 0.25 f_c'$
$f_s = 0.40 f_y$

In many cases the pier shaft must be designed for both bending and an axial load. This issue is not directly addressed in most building codes nor in the ACI 318- or by ACI Committee 336. If we use the ACI 318- as a guide, a reinforced pier shaft for axial load can be designed using the factored axial load P_u for tied rebars (usual case) as

$$P_u = 0.80\phi(0.85 f_c' A_c + f_y A_s) \tag{19-12}$$

For bending with axial load one should consult a textbook on reinforced concrete design of short columns with bending since strain compatibility between concrete and steel is necessary unless $P/A + Mc/I$ gives compressive stress everywhere on the cross section. A round column computer program is most useful for this analysis since it is a computationally intensive iterative process.

When the drilled pier casing is left in place it may be used to increase the shaft capacity either by using a transformed section ($A_t = A_g + nA_s$) or as

$$P = A_c f_c + A_s f_a$$

where A_s = effective area of casing steel (after reduction for corrosion has been made). Alternatively, the casing can be used to increase the allowable concrete stress f_c as follows:

$$f_c = 0.30 f_c' + \frac{1.5 t f_y}{D} \leq 0.40 f_c' \tag{19-13}$$

where t = casing thickness after deduction for corrosion, mm or in.
D = ID of casing, mm or in.
f_y = yield stress of casing steel, MPa or ksi

This recommendation is given by the Chicago Building Code (Sec. 13-132-400).

19-8 DRILLED PIER DESIGN EXAMPLES

We will illustrate some of the preceding design discussion with the following two design examples.

Example 19-2. For the soil profile given in Fig. E19-2 we must make a trial pier design in order to develop an economic comparison with piles. For the pier use $f_c' = 28$ MPa with a 150-mm slump. By inspection of the GWT elevation we see it will be necessary to use the slurry method since we could not seal the water out of the hole with a casing socketed into the sand. The upper part of the pier shaft will use an arbitrary 1 percent of rebars (a designer decision since only axial load is present).

The design axial load $P_d = 3000$ kN.

Required. Make a preliminary design recommendation.

Solution.

Step 1. Find the approximate shaft diameter based on the allowable concrete stress of $f_c = 0.25 f_c' = 0.25 \times 28 = \mathbf{7}$ MPa. Let us write

$$0.7854 D^2 f_c = P_d$$

Substituting and solving, we find

$$D = \sqrt{\frac{3}{0.7854 \times 7}} = \mathbf{0.74}\ \text{m}$$

Step 2. Estimate the pier length $L = 11$ m (into dense sand), and find the estimated point capacity neglecting any skin resistance as a first trial. Use the Reese (1978) recommendations:

$$q_p = 4000\ \text{kPa (dense sand)} \qquad A_p = 0.7854 B^2 \qquad \alpha_p = 2.0$$

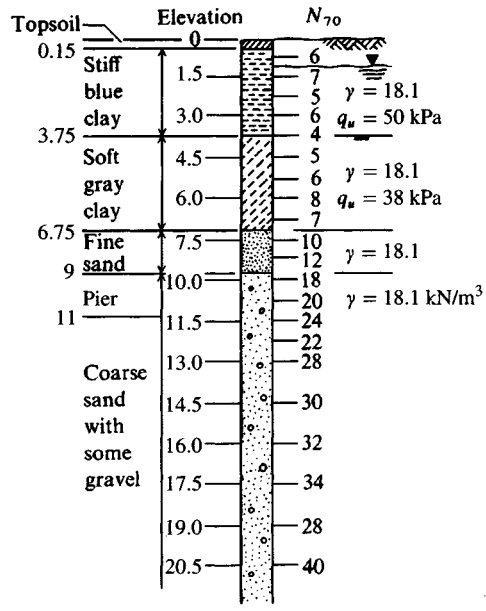

Figure E19-2

Substituting into Eq. (16-6*a*), we obtain

$$Q_p = \frac{q_p A_p}{\alpha_p} = \frac{4000 \times 0.7854B^2}{2B} = 1571B$$

Since this result is for a 25-mm settlement, we can use an SF = 1 and directly solve for pier diameter B, giving

$$B = \frac{Q_d}{Q_p} = \frac{3000}{1571} = 1.91 \text{ m (rather large)}$$

At this point it would appear that we must use either a large-diameter shaft or a bell. We cannot bell in sand, so let us look at alternatives. First, the Meyerhof equation [Eq. (19-8)] may help. Averaging N_{70} for the four values in the approximate influence depth below the base, we have 24 and $N_{55} = 24 \times 70/55 = 31$. Directly substituting into Eq. (19-8), we obtain

$$q_a = N_{55}/0.052 = 31/0.052 = 596 \rightarrow 600 \text{ kPa}$$

The required point diameter is

$$0.7854D^2 \times 600 = 3000 \rightarrow D = \sqrt{\frac{3000}{0.7854 \times 600}} = 2.52 \text{ m} \gg 1.91$$

We might be able to obtain some skin resistance from the clay and sand layers to reduce the point load. The L for layer 1 is $L \approx 3.75 - 0.15 = 3.60$ m; for layer 2, $L \approx 6.75 - 3.75 = 3.0$ m. Use $\alpha = 1$ for both layers (clay is both below GWT and soft). Also arbitrarily estimate the required pier shaft = 1.372 m.

$$\begin{aligned} \text{For layer 1:} \quad & \pi \times 1.372 \times 50 \times 3.60 = 775 \text{ kN} \\ \text{For layer 2:} \quad & \pi \times 1.372 \times 38 \times 3.0 = \underline{490 \text{ kN}} \\ & \text{Total} = Q_{sc} = \mathbf{1265} \text{ kN} \end{aligned}$$

For the sand, we estimate $\phi = 32° = \delta$; $\gamma' = 18.1 - 9.81 = 8.3$ kN/m^3; $\Delta L = 11.0 - 0.15 - 3.6 - 3.0 = 4.25$ m; $z_o = 11.0 - 4.25/2 = 8.8$ m; $K = 0.60$ (Reese value for $L < 12$ m). Then

$$\overline{q_o} = \gamma' z_o = 8.3 \times 8.8 = 73 \text{ kPa}$$

$$Q_{ss} = K\bar{q}_o \tan\delta(\pi \times D)\Delta L = 0.6 \times 73 \times \tan 32(\pi \times 1.372 \times 4.25) = \mathbf{501} \text{ kN}$$

Total side resistance $\sum Q_s = Q_{sc} + Q_{ss} = 1265 + 501 = \mathbf{1766}$ kN

Net point load $Q_p = Q_d - \sum Q_s = 3000 - 1766 = 1234$ kN

Shaft load (concrete $\gamma_c = 23.6$ kN/m^3) $= 0.7854 \times 1.372^2 \times 23.6 \times 11$

$= 384$ kN

Total point load $= 1234 + 384 = \mathbf{1618}$ kN

Using Eq. (19-6a) for a point settlement of 25 mm, we can write

$$Q_p = \frac{q_p A_p}{\alpha_p} = \frac{4000 \times 0.7854 \times 1.372^2}{2 \times 1.372} = 2155 > 1618 \qquad \text{(O.K.)}$$

We may be able to use a pier with dimensions as follows:

Shaft diameter $D = 1.372$ m

$L = 11$ m

The major question is whether an $\alpha = 1.0$ is valid. Note that the overall SF is rather small.

Comments.

1. This is a fairly large-diameter shaft—so is the load.
2. It would not be practical to use a bell in the clay—even if the base were on the sand, for that sand is somewhat loose and settlement would be a problem.
3. Piles may be a more viable option since they can be driven into the dense sand and their lengths would also be on the order of 11 m.
4. A lower f_c' could be used but may not be allowed by the local code.
5. One may consider a point-bearing pier on rock if the depth is not over 30 to 35 m down and the stratum is reasonably competent. The greater length is offset by a smaller-diameter shaft.

////

Example 19-3. Make a preliminary design for a drilled pier to be founded on the firm clay at depth −27 m of Fig. E19-3*a*. The top 3.5 m of depth is in a water-bearing sand-gravel stratum. The pier is to carry 10 500 kN, and we will use $f_c' = 35$ MPa. Use an SF = 2 on the skin resistance, and use a belled base if necessary.

Solution. From Fig. E19-3*a* estimate the base $s_u = 145$ kPa. Take the average shaft $s_u = 120$ kPa. We should actually divide the 27-m thick stratum into several layers and obtain $s_{u,av}$ for each.

The dry method (Fig. 19-3) of pier installation will be used. First, a casing will be socketed into the clay about 1 m below the sand-gravel, material for a water seal and then the shaft excavation will proceed.

Step 1. For $f_c' = 35$ MPa the allowable $f_c = 0.25 \times 35 = 8.750$ MPa. Also we have

$$0.7454D^2 f_c = 10\,500 \text{ kN}$$

Rearranging and solving for a trial shaft diameter, we find

$$D = \frac{10\,500}{0.7854 \times 8.750 \times 1000} = 1.23 \text{ m}$$

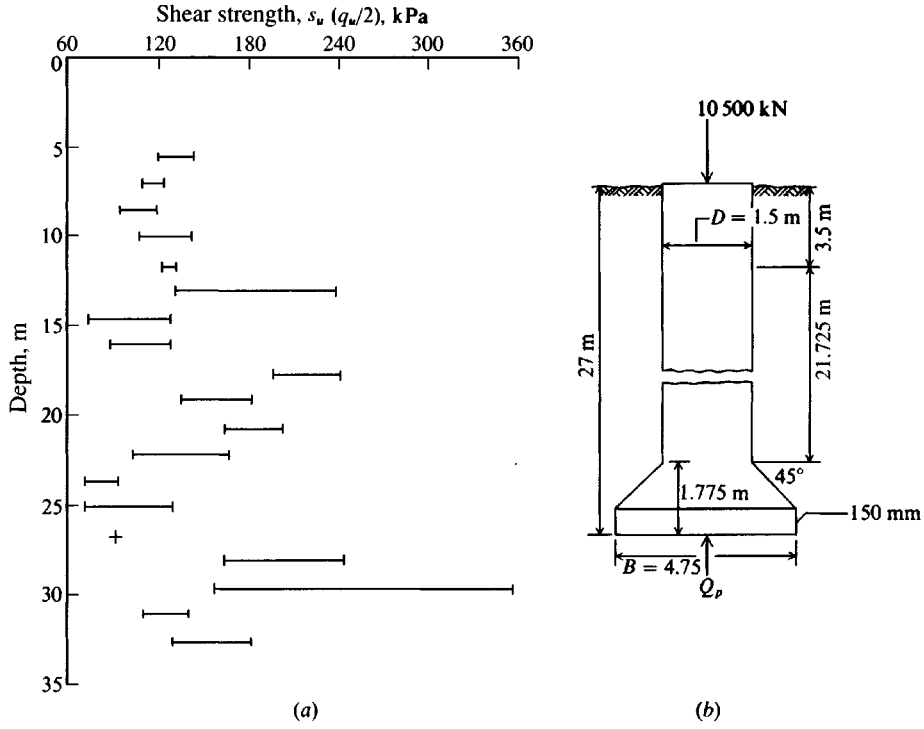

Figure E19-3

Step 2. Estimate the shaft friction resistance. We will try $D = 1.5$ m, giving a shaft perimeter $p' = \pi D = \mathbf{4.71}$ m. The effective shaft length for cohesive skin resistance is

$$L' = L - 3.5 \text{ m of sand-gravel} = 27 - 3.5 = 23.5 \text{ m}$$

From Table 19-1 obtain the Reese value of $\alpha = 0.5$, which is very conservative. From Fig. 16-14 we can obtain $\alpha = 0.7$ to 0.8. We should in a real case divide the 27-m shaft into several layers, with the top layer being about 1.5 m, the second layer 2.0 m (the sand-gravel), then layers based on the s_u profile; obtain an average s_u for each layer and an α for each layer using either Fig. 16-14 or Eq. (16-12*a*).

We could also use PILCAPAC for the analysis but obtain printouts whereby we analyze the skin resistance and point capacity and apply a suitable SF to see if the system is adequate. That program also allows a belled base. We would make the point layer thick enough that we could add any needed intermediate layers with minor adjustments to the data file.

To get the general idea of pier design/analysis we will *incorrectly* use a single $\alpha = 0.5$ for the full shaft length.

Check that $0.5 \times 120 = 60$ kPa < 86, the limiting value in Table 16-1. Then

$$\sum Q_{si} = \alpha \times s_u \times p' \times L' = 0.5 \times 120 \times 4.71 \times 23.5 = 6641 \text{ kN} \ll 10\,500$$

It is immediately evident that either we have to use a larger shaft, a larger α, or a bell. We will use a bell, which reduces the shaft length for friction resistance but creates a substantial gain in point bearing Q_p. Estimate a bell height of 1.75 m, giving $L' = 23.5 - 1.75 = 21.75$ m and a revised

$$\sum Q_{si} = 60 \times 4.71 \times 21.75 = \mathbf{6150}\ \text{kN}$$

Step 3. Compute bell dimensions. We will use an SF = 2 on the skin resistance. Noting that Reese suggests using $Q_p/3$ to provide a bearing value so the settlement $\Delta H \leq 25$ mm, we find

$$Q_{p,a} = \frac{s_u \times 9 \times A_p}{3} = \frac{145 \times 9 \times 0.7854 D_b^2}{3} = 341.65 D_b^2$$

The bell must carry $P_b = 10\,500 - 6150/2 = \mathbf{7425}$ kN. Equating these expressions, we find

$$341.65 D_b^2 = 7425 \rightarrow D_b = \sqrt{\frac{7425}{341.65}} = \mathbf{4.66}\ \text{m}$$

Use $D_b = 4.75$ m to find $D_b/D_s = 4.75/1.5 = 3.17$, which is close to the maximum allowed. The revised bell depth (see Fig. E19-3*b* for geometry) is

$$H_b = 0.15 + (4.75 - 1.50)/2 = 1.775\ \text{m} \approx 1.75\ \text{used} \qquad \text{(O.K.)}$$

Step 4. Check potential ground loss from possible "squeezing."

For this we will estimate $\gamma_{wet} = 19.8$ kN/m^3 and $\gamma' = 10$ kN/m^3 for full shaft length. Thus,

At 10 m depth: $p'_o = 10(\gamma') = 10(10) = 100$ kPa

$$s_u = 120, \text{ giving } \frac{p'_o}{s_u} = \frac{100}{120} = 0.83 \ll 6 \text{ to } 8$$

At 20 m depth: $p'_o = 25(10) = 250$ kPa

$$s_u = 120, \text{ giving } \frac{p'_o}{s_u} = \frac{250}{100} = 2.5 < 6 \text{ to } 8$$

It appears that ground loss from squeezing will not be a problem here.

Step 5. Check axial shortening—use the effective shaft length = $27 - 1.775 = 25.2$ m even though a part is the "bell." Assume the average shaft load $P = \sum Q_{si} = 6150$: Then

$$A_s = 0.7854 \times 1.5^2 = 1.767\ \text{m}^2$$

$$E_c = 4700\sqrt{f'_c} \qquad \text{(Table 8-3)}$$

$$= 4700(35)^{0.5} = 27\,800\ \text{MPa}$$

The axial shortening is

$$\Delta H_s = \frac{PL}{A_s E} = \frac{6150(25.2)}{1.767(27\,800)} = \mathbf{3.2}\ \text{mm}$$

Since the point should displace not more than 25 mm the total immediate ΔH of the pier should not exceed 30 mm; any consolidation settlement would be additional.

Summary.

Use the dry method with a casing to about 5 m depth.
Use $D = 1.50$ m (Fig. E19-3*b*).
Use $B = 4.75$ m.
Total settlement under 30 mm.
Squeezing or ground loss does not seem a problem.

////

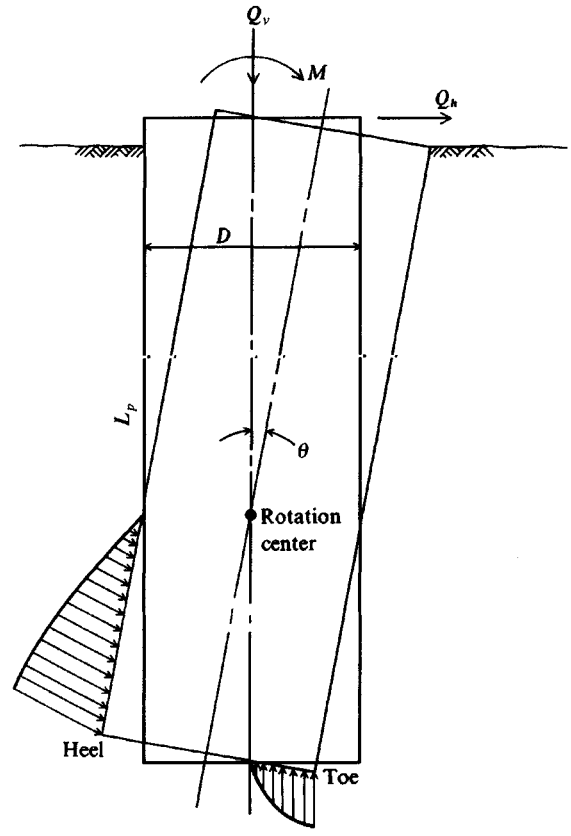

Figure 19-8 Idealization of rigid pier rotation with rotation angle θ greatly exaggerated. The toe and heel pressures will be highly indeterminate. Whereas toe pressure is nearly vertical, the heel pressure has both horizontal and vertical components, giving the slope shown.

19-9 LATERALLY LOADED DRILLED PIER ANALYSIS

Laterally loaded drilled piers can be analyzed using program FADBEMLP (B-5). There is some opinion that a short rigid pier is so stiff that the shaft will rigidly rotate about a point designated the center of rotation (see Fig. 19-8) and that a resisting moment will develop on the base from the toe and heel pressure profiles qualitatively shown. This moment is not accounted for in the usual FEM lateral pile program (unless we inspect the output from a trial run and arbitrarily select a possible base moment, which is input as an additional base node load on a subsequent trial).

It is immediately evident that if Fig. 19-8 is a correct representation of rigid pier-soil interaction, modeling it would be nearly impossible in any FEM/FD computer program unless one has a load test for a guide. In the author's opinion this model is not likely to develop unless the pier L_p/D ratio is less than about 2 except at lateral loads far in excess of the design load, e.g., lateral load tests are commonly taken to the limiting resistance of the pile or pier where the design load may only be one-fourth to one-half the ultimate load. Very short stub piers with L_p/D less than about 2 can probably be analyzed as footings with a passive pressure on the shaft about as accurately as trying to treat the stub pier as a rigid laterally loaded pier.

For larger L_p/D ratios the pier shaft, being substantially stiffer than the soil, will carry the lateral force similar to a laterally loaded pile. In any case, one can make a lateral pile-type analysis and inspect the output displacement of the bottom node. If there is a horizontal

displacement in the load direction much over 1 or 2 mm the analytical model *may* be inadequate *or* the lateral load is too large for the pier-soil system.

Lateral load tests on drilled piers of small L_p/D ratios tend to confirm that the base rotation of Fig. 19-8 is seldom of consequence. For example, Bhushan et al. (1978) report test results of a series of short drilled piers in the range of $L_p/D = 15/4 = 3.75$ to $22/4 = 5.5$. Some of the 1.22-m diameter shafts had 1.677-m diameter bells installed. They reported no discernible difference in capacity for shafts with bells versus no bells. Davisson and Salley (1968) reported the results of four laterally loaded test piers. For lateral loads up to about 450 kN the differences between the displacements of belled and straight-shaft piers were negligible. At near ultimate loads, however, the displacement differences were noticeable, with the bell tending to reduce the lateral displacement. Referring to Fig. 19-8 we see that in a rigid shaft rotation any bell should decrease rotation and increase the lateral load capacity of the pier.

To illustrate that the lateral pile FEM provides a reasonable solution, we will analyze a laterally loaded short drilled pier reported by Bhushan and Askari (1984). By citing a reference I do not use an excessive amount of text space for test details, and the reader can gain experience in trying to follow the work of others in developing his or her own experience base.

Bhushan et al. (1978) and Bhushan and Askari (1984) suggested that predicted displacements (that is, values computed in some manner) are in the range of two to six times measured values for laterally loaded piers. It should be noted in passing that a number of methods have been suggested in the *ASCE Geotechnical Journal*. Obviously if some of these give predictions in error by a factor of six [and most suggestions have been made since about 1960] they were worthless to begin with and should not have been published. The author readily concedes, however, that it is common at a site with similar piers (or piles) for lateral load test measurements to differ by ± 20 percent—sometimes more. The cause is the natural heterogeneity of the soil, which prompted the author to comment in Sec. 16-14 that one should not spend great effort in exactly matching a load test for site parameters. Any parameters obtained in this manner are strictly applicable for that test, and if they happen to match values for an adjacent test it is more a happy coincidence than computational rigor.

What one should try to do with load-test data is obtain average site parameters that are, one hopes, in an easy-to-use format so that changes can be made using commonly used soil parameters such as ϕ and s_u.

If you have a pier located on a slope refer to Sec. 16-15 for the necessary methodology to estimate the lateral modulus of subgrade reaction k_s.

Example 19-4. Use your computer program FADBEMLP and analyze pier No. 1 of Table 1 of Bhushan and Askari (1984). Figure E19-4*a* illustrates the general test setup as interpreted by the author. Figure E19-4*b* is the FEM used. The second node at 0.2 m from top was included since the lateral displacement of this node was given in Table 3 of the reference, which summarized the test results.

Solution. Obtain soil parameters as needed. The reference gave $\phi = 36°$ and an average $\gamma = 99$ pcf, which the author rounds to $\gamma = 16$ kN/m^3 since we will use all SI units. The load cases were given as follows:

LC	*P*(2), kN	*P*(1) = *P*(2) × 4.88m, kN· m
1	5.36	−5.36(4.88) = −26.16
2	9.00	−43.92
3	18.37	−86.64

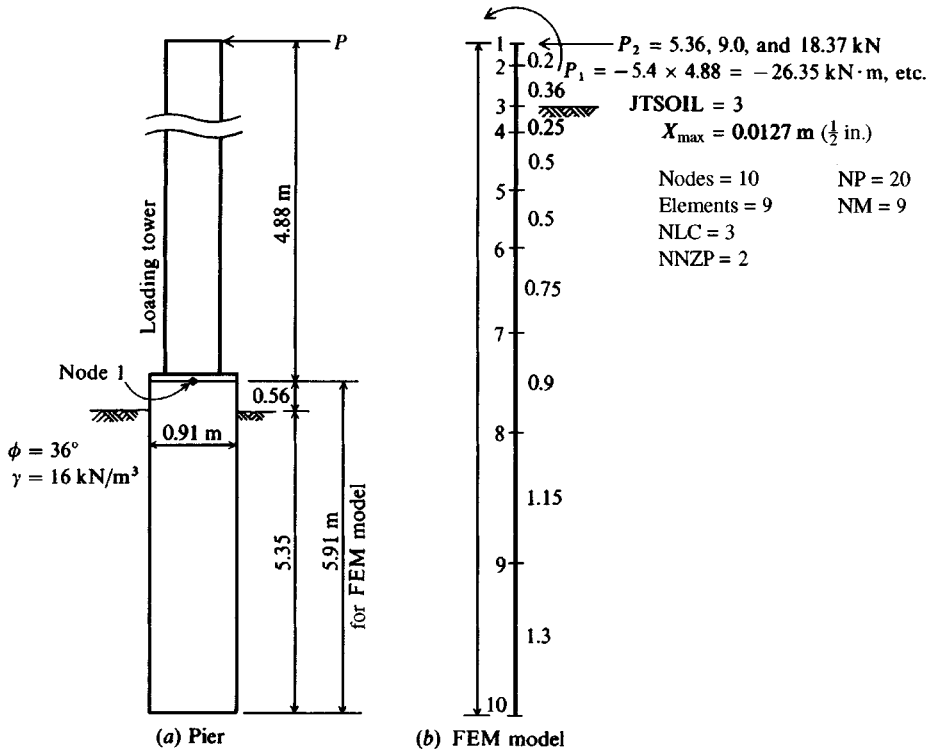

Figure E19-4*a, b*

Note that these are very small loads for piers of this size. We will use nine elements with lengths taken as shown in Fig. E19-4*b*. Use short elements in the upper region, grading into larger values. The ground line starts at node 3, giving JTSOIL = 3. Other data are as follows:

$$f_c' = 40 \text{ MPa} \qquad \text{(given)}$$

$$\text{Compute } E_c = 4700\sqrt{f_c'} = 4700\sqrt{40} = 29\,700 \text{ MPa}$$

$$\text{Estimate maximum } \delta_h = 1/4 \text{ in.} = 0.0254/4 \text{ m}$$

$$C = 1/(0.0254/4) = 160 \text{ m}^{-1} \qquad \text{(rounded)}$$

$$C_m = 1 + (460/910)^{0.75} = 1.6 \qquad \text{[see Eq. (16-26)]}$$

$$\text{Use shape factors } F_{w1} = 1.5 \text{ and } F_{w2} = 3 \qquad \text{[see Eq. (16-26}a\text{)]}$$

$$\text{For } \phi = 36° \text{ obtain } N_q = 38; \qquad N_\gamma = 40 \qquad \text{(Table 4-4)}$$

$$\text{AS} = F_{w1} \times C \times C_m(0.5\gamma B N_\gamma)$$

$$= 1.5 \times 160 \times 1.6(0.5 \times 16 \times 0.91 \times 40) = \mathbf{111\,820} \text{ kN/m}^3$$

$$\text{BS} = F_{w2} \times C \times C_m(\gamma Z^n N_q) = 3.0 \times 160 \times 1.6 \times 16 \times 38Z^n = 466\,994Z^n$$

$$\text{We will arbitrarily use } n = 0.5.$$

$$\text{The input } k_s = 112\,000 + 500\,000Z^{0.5} \text{ (some rounding)}$$

$$\text{The moment of inertia } I = \frac{\pi D^4}{64} = \frac{\pi \times 0.91^4}{64} = 0.033\,66 \text{ m}^4$$

$$\text{With drilled shafts take FAC1} = \text{FAC2} = 1$$

```
                DRILLED PIER FROM BHUSHAN & ASKARI IN ASTM STP 835--PP 140-156

                   +++++++++++++++++ THIS OUTPUT FOR DATA FILE:  EXAM194.DTA

               SOLUTION FOR LATERALLY LOADED PILE--ITYPE = 1  ++++++++++

               NO OF NP =  20   NO OF ELEMENTS, NM =  9   NO OF NON-ZERO P, NNZP =  2
                 NO OF LOAD CASES, NLC =  3                    NO OF CYCLES NCYC =  1
               NODE SOIL STARTS JTSOIL =  3
                    NONLINEAR (IF > 0) =  0            NO OF BOUNDARY CONDIT NZX =  0
                         MODULUS KCODE =  2                    LIST BAND IF > 0 =  0
                                                                  IMET (SI > 0) =  1

           MEMNO   NP1   NP2   NP3   NP4   LENGTH     WIDTH    INERTIA, M**4

               1     1     2     3     4      .200      .910    .33660E-01
               2     3     4     5     6      .360      .910    .33660E-01
               3     5     6     7     8      .250      .910    .33660E-01
               4     7     8     9    10      .500      .910    .33660E-01
               5     9    10    11    12      .500      .910    .33660E-01
               6    11    12    13    14      .750      .910    .33660E-01
               7    13    14    15    16      .900      .910    .33660E-01
               8    15    16    17    18     1.150      .910    .33660E-01
               9    17    18    19    20     1.300      .910    .33660E-01

               THE INITIAL INPUT P-MATRIX ENTRIES
               NP    LC      P(NP,LC)
                1     1       -26.160
                2     1         5.360
                1     2       -43.920
                2     2         9.000
                1     3       -86.640
                2     3        18.370
               MOD OF ELASTICITY E =     29700. MPA

               GROUND NODE REDUCTION FACTORS FOR PILES, FAC1,FAC2 =     1.00      .50

                   EQUATION FOR KS =  112000.0 +   500000.0*Z** .50

               THE NODE SOIL MODULUS, SPRINGS AND MAX DEFL:
               NODE     SOIL MODULUS     SPRING,KN/M    MAX DEFL, M
                  1              .0              .0         .0250
                  2              .0              .0         .0250
                  3         112000.0         15356.3         .0250
                  4         181000.0         86754.3         .0250
                  5         545012.7        229931.8         .0250
                  6         671017.0        388930.8         .0250
                  7         819106.8        617804.7         .0250
                  8         963469.3        905963.4         .0250
                  9        1118231.0       1249183.0         .0250
                 10        1268503.0        720690.9         .0250

               BASE SUM OF NODE SPRINGS = 4214616.0 KN/M NO ADJUSTMENTS
               * = NODE SPRINGS HAND COMPUTED AND INPUT
```

Figure E19-4c

MEMBER MOMENTS, NODE REACTIONS, DEFLECTIONS, SOIL PRESSURE, AND LAST USED P-MATRIX FOR LC = 1

MEMNO	MOMENTS--NEAR END 1ST, KN-M		NODE	SPG FORCE, KN	ROT, RADS	DEFL, M	SOIL Q, KPA	P-, KN-M	P-, KN
1	-26.160	27.232	1	.00	-.00008	.00011	,00	-26.16	5.36
2	-27.232	29.159	2	.00	-.00007	.00009	,00	.00	.00
3	-29.160	30.229	3	1.07	-.00006	.00007	7,84	.00	.00
4	-30.229	29.990	4	4.75	-.00006	.00005	9,92	.00	.00
5	-29.990	26.289	5	6.93	-.00004	.00003	16,42	.00	.00
6	-26.289	17.004	6	4.98	-.00003	.00001	8,58	.00	.00
7	-17.004	6.704	7	-.94	-.00001	.00000	1,24	.00	.00
8	-6.704	.211	8	-5.80	.00000	-.00001	6,17	.00	.00
9	-.211	.000	9	-5.48	.00000	.00000	4,91	.00	.00
			10	-.16	.00000	.00000	,29	.00	.00

SUM SPRING FORCES = 5.35 VS SUM APPLIED FORCES = 5.36 KN

(*) = SOIL DISPLACEMENT > XMAX SO SPRING FORCE AND Q = XMAX*VALUE ++++++++++++
NOTE THAT P-MATRIX ABOVE INCLUDES ANY EFFECTS FROM X > XMAX ON LAST CYCLE ++++++++++

MEMBER MOMENTS, NODE REACTIONS, DEFLECTIONS, SOIL PRESSURE, AND LAST USED P-MATRIX FOR LC = 2

MEMNO	MOMENTS--NEAR END 1ST, KN-M		NODE	SPG FORCE, KN	ROT, RADS	DEFL, M	SOIL Q, KPA	P-, KN-M	P-, KN
1	-43.920	45.720	1	.00	-.00013	.00019	,00	-43.92	9.00
2	-45.720	48.957	2	.00	-.00013	.00016	,00	.00	.00
3	-48.957	50.753	3	1.80	-.00011	.00012	13,16	.00	.00
4	-50.753	50.352	4	7.98	-.00010	.00009	16,66	.00	.00
5	-50.352	44.137	5	11.63	-.00007	.00005	27,56	.00	.00
6	-44.137	28.549	6	8.35	-.00005	.00002	14,41	.00	.00
7	-28.549	11.257	7	-1.57	-.00002	.00000	2,08	.00	.00
8	-11.257	.354	8	-9.73	.00000	-.00001	10,35	.00	.00
9	-.354	.000	9	-9.21	.00001	-.00001	8,24	.00	.00
			10	-.27	.00001	.00000	,48	.00	.00

SUM SPRING FORCES = 8.99 VS SUM APPLIED FORCES = 9.00 KN

(*) = SOIL DISPLACEMENT > XMAX SO SPRING FORCE AND Q = XMAX*VALUE ++++++++++++
NOTE THAT P-MATRIX ABOVE INCLUDES ANY EFFECTS FROM X > XMAX ON LAST CYCLE ++++++++++

MEMBER MOMENTS, NODE REACTIONS, DEFLECTIONS, SOIL PRESSURE, AND LAST USED P-MATRIX FOR LC = 3

MEMNO	MOMENTS--NEAR END 1ST, KN-M		NODE	SPG FORCE, KN	ROT, RADS	DEFL, M	SOIL Q, KPA	P-, KN-M	P-, KN
1	-86.636	90.313	1	.00	-.00027	.00037	,00	-86.64	18.37
2	-90.313	96.920	2	.00	-.00025	.00032	,00	.00	.00
3	-96.919	100.606	3	3.60	-.00021	.00023	26,24	.00	.00
4	-100.608	100.014	4	15.93	-.00019	.00018	33,24	.00	.00
5	-100.014	87.796	5	23.25	-.00014	.00010	55,11	.00	.00
6	-87.796	56.890	6	16.77	-.00009	.00004	28.93	.00	.00
7	-56.890	22.496	7	-2.99	-.00004	.00000	3.97	.00	.00
8	-22.496	.745	8	-19.30	.00000	-.00002	20.53	.00	.00
9	-.745	.000	9	-18.34	.00001	-.00001	16.42	.00	.00
			10	-.57	.00001	.00000	1.01	.00	.00

SUM SPRING FORCES = 18.34 VS SUM APPLIED FORCES = 18.37 KN

(*) = SOIL DISPLACEMENT > XMAX SO SPRING FORCE AND Q = XMAX*VALUE ++++++++++++
NOTE THAT P-MATRIX ABOVE INCLUDES ANY EFFECTS FROM X > XMAX ON LAST CYCLE ++++++++++

Figure E19-4c (*continued*)

With these data for input (see data set EXAM194.DTA on your diskette), we obtain the computer output shown on Fig. E19-4*c*. The displacements are summarized as follows:

LC	Measured δ_h, mm	Computed δ_h, mm	$R = \frac{\text{Computed}}{\text{Measured}}$
1	0.074	0.09	1.22
2	0.163	0.16	1.00
3	0.0351	0.32	0.91

Discussion of output

1. The computed output compares quite well with the load test values. The foregoing data represent some revisions to the execution given in the fourth edition; that is, k_s is adjusted for factor C_m, an improved (smaller) F_{wi} is used, and we have taken into account that the k_s should be representative of the small displacements (under $\frac{1}{4}$ in.) of this system.
2. With such a large shaft and such small lateral loads, the computed and measured δ_h are almost meaningless. What one generally hopes to avoid is a measured $\delta_h = 50$ mm when the computed value is only 20 or 25 mm.
3. The equation for k_s is not an "after the fact" development, so it can be used with reasonable confidence for other cases.
4. One might question if a shaft diameter this large should be considered a "deep" beam.
5. The program makes several self-checks, so it would seem it is making correct computations—or at least correct for this set of input.
6. The displacements at the bottom three nodes are either zero or so near zero that we can say they are. That is, the shaft– -at least in this load range—is behaving similarly to any laterally loaded pile.
7. The ground line moment (node 3) is readily checked for all three cases as simply the input moment $+0.56P_h$. For $LC = 3$ we obtain

$$M_{gl} = 86.64 + 0.56 \times 18.37 = \mathbf{96.92}\ \text{kN} \cdot \text{m}$$

as on the output sheet for node 3.

////

19-10 DRILLED PIER INSPECTION AND LOAD TESTING

The drilled pier (or caisson) usually carries a very large load, so structural integrity is an absolute necessity. This is partially achieved by an inspection of the shaft cavity. When the shaft is cased, a person may enter to check the base for loose material. If the base is in rock, it can be checked for cracks or voids and loose material; however, present technology is at a state where equipment is available to precondition the shaft sides and to clean the base of loose material. When the base is on soil, it is often desirable to check the bearing capacity manually (and visually), using a pocket penetrometer to obtain the unconfined compression strength q_u at a number of points similar to the testing illustrated in Fig. 3-9*a*. A visual comparison of the actual shaft soil with the original boring logs is of much value. Usually at this point it is not too late to make a rapid redesign if the shaft soil is found to be different from the original borings. When the shaft is not cased, the diameter is too small for an inspector to enter, or hazardous gas is being emitted, it may be possible to lower a video camera to obtain an indirect visual

check of shaft conditions. If a video camera is not available, it may be possible to get some indication of shaft condition and vertical alignment by lowering a light into the cavity. If the light disappears, the shaft is not vertical; soil crumbs may be visible on the pier base soil (if the shaft is vertical and not too deep); the condition of the shaft sides may be visible at least in the upper part.

It is usually specified that the inspector do at least the following:

1. Perform a specified number of slump tests on the wet concrete.
2. Take a specified number of concrete cylinders for later strength testing.
3. Observe and compare the volume of concrete placed in the pier shaft (and bell if used) to the shaft volume. It is self-evident that if less than the shaft volume of concrete is placed, there is some kind of discontinuity in the shaft. This is usually the first verification of pier integrity.

There are electronic test devices [see, for example, Lin et al. (1991)] that can measure a seismic wave down the shaft after the concrete has hardened (nondestructive testing, NDT) to ascertain whether any voids or discontinuities are present. A core sample is considered to be more reliable, but it is usually too costly (and permanently damages the pier some amount); it may be done if the concrete strength f_c' is suspect or if litigation is pending.

The ACI committee 336 has two current specifications, titled *Standard Specification for the Construction of Drilled Piers* and *Design and Construction of Drilled Piers*, which can be obtained from the ACI; they give a number of suggested inspection procedures to ensure the quality of the drilled pier.

Pier load testing. Load-testing a drilled pier for its capacity is a difficult task, since large piers carry substantial load and conventional testing, similar to that for piles, requires a large load frame (see Fig. 17-7*c*).

A recent development is to put a high-capacity hydraulic jack, termed an *O-cell,* onto a plate 1 on the base soil of the pier (shaft or bell), and an upper plate 2 against which the bell/shaft is poured. Hydraulic and electronic pickup lines are routed to the ground surface for later use. When the pier concrete hardens, the jack is activated to attempt to separate plates 1 and 2; the resistance can be related to point bearing. If the lower plate 1 has been referenced to a known elevation (a surface reference frame), the change in elevation caused by the jack load is related to point settlement and to side skin resistance. This pier load test is termed an *O-test* (also an *upside-down load test,* because the load is applied at the base and pier movement is upward) and has been in use since about 1985 [Goodwin (1993), Meyer and Schade (1995)].

PROBLEMS

In any economic analysis assume f_c' costs (\$100/7 MPa per m^3) over the base strength of 21 MPa—that is, 28 MPa costs \$100/m^3 more than 21 MPa strength concrete; 35 MPa is \$200/m^3 more, etc.

19-1. Compute α for the three 9-m ΔL increments of clay in Example 19-1.

19-2. In Example 19-1 what ϕ angle for the sand layers together with $\alpha = 0.5$ for the 27 m of clay and the computed point value would give the load test value $P_u \approx 410$ kN? Is this angle realistic (you should try to obtain a copy of the original source)?

19-3. Using the given ϕ angles and $\alpha = 0.5$, what s_u would you have to use to give the load test value of $P_u \approx 410$ kN for Example 19-1? Remember the point value also changes, so that Q_p must also be recomputed.

19-4. Verify the skin resistance computations shown on Fig. E19-1.

19-5. Compare the quantity of concrete required in Example 19-2 to that required if we extended the shaft to bedrock at 33 m below the ground surface and the rock $q_a = 28$ MPa.

19-6. What shaft diameter would be required for the drilled pier of Example 19-2 with the point at -21 m elevation?

19-7. For Example 19-3, what shaft length is required to eliminate the need for a bell? Would it be more economical to increase the shaft diameter D_S? Use a single α as in the example.

19-8. Redo Example 19-3 using at least four clay layers instead of one and compute α for each layer using Eq. (16-12*a*). Use $Q_p = Q_{ult}/3$ for the point contribution and skin resistance SF = 2 as in the example.

19-9. Would the drilled pier of Example 19-3 be more economical using $f'_c = 28$ MPa (example uses 35 MPa)?

19-10. Design a drilled pier for a column load of 4500 kN using the soil profile shown in Fig. P19-10. Soil data is from "undrained" tests.

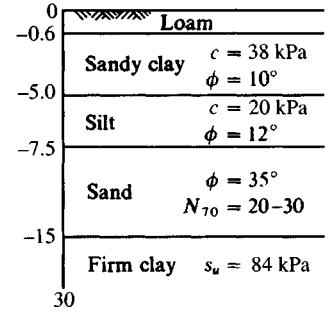

Figure P19-10

19-11. Design a drilled pier for the soil profile of Fig. P19-11 for a 5000-kN axial load. Use a bell if it will be more economical.

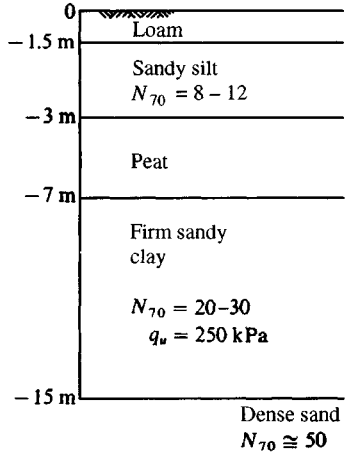

Figure P19-11

All of the following problems require use of your lateral pile/pier program FADBEMLP.

19-12. Verify the output of Fig. E19-4*c* using data set EXAM194.DTA on your program diskette.

19-13. Verify the c_m side resistance factor of 1.6 for Example 19-4. Do you think 1.6 or 2.0 is a better value for these piers?

19-14. Redo Example 19-4 using $I = 0.0370$ m^4 (a 10 percent increase from the example) to allow some increase in stiffness for the rebar cage. If we assume the pier contained 15 No. 20 rebars on a radius of 0.70 m, what is the computed moment of inertia I? How does this compare to the moment of inertia of the gross section actually used of 0.03366 m^4?

19-15. Redo Example 19-4 using the exponent $n = 0.4$, 0.75, and 1.0. Compare your results with the output given (which used $n = 0.5$). Plot P_h versus δ_h for each n value onto the same curve together with the measured values for a visual comparison.

19-16. Make a literature search for a laterally loaded drilled pier in a cohesive soil and see if you can back-compute the ground line displacements using your program FADBEMLP.

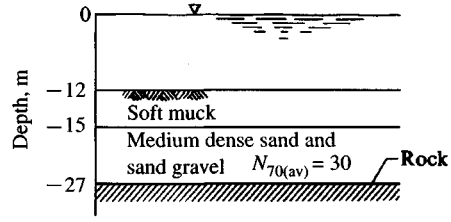

Figure P19-17

19-17. Outline considerations you think necessary to design a large-diameter pile or caisson/pier (whatever you want to call it) for a bridge pier for the water-soil-rock profile of Fig. P19-17. The pier top is 6 m above water and carries an axial load of 36 500 kN and a lateral load of 500 kN.

CHAPTER 20

DESIGN OF FOUNDATIONS FOR VIBRATION CONTROLS

20-1 INTRODUCTION

Foundations supporting reciprocating engines, compressors, radar towers, punch presses, turbines, large electric motors and generators, etc. are subject to vibrations caused by unbalanced machine forces as well as the static weight of the machine. If these vibrations are excessive, they may damage the machine or cause it not to function properly. Further, the vibrations may adversely affect the building or persons working near the machinery unless the frequency and amplitude of the vibrations are controlled.

The design of foundations for control of vibrations was often on the basis of increasing the mass (or weight) of the foundation and/or strengthening the soil beneath the foundation base by using piles. This procedure generally works; however, the early designers recognized that this often resulted in considerable overdesign. Not until the 1950s did a few foundation engineers begin to use vibration analyses, usually based on a theory of a surface load on an elastic half-space. In the 1960s the lumped mass approach was introduced, the elastic half-space theory was refined, and both methods were validated.

The principal difficulty in vibration analysis now consists in determining the necessary soil values of shear modulus G' and Poisson's ratio μ for input into the differential equation solution that describes vibratory motion. The general methods for design of foundations, both shallow and deep, that are subject to vibration (but not earthquakes) and for the determination of the required soil variables will be taken up in some detail in the following sections.

20-2 ELEMENTS OF VIBRATION THEORY

A solid block base rests in the ground as in Fig. 20-1. The ground support is shown replaced by a single soil spring. This is similar to the beam-on-elastic-foundation case except the beam uses several springs and the foundation base here only uses one. Also this spring is

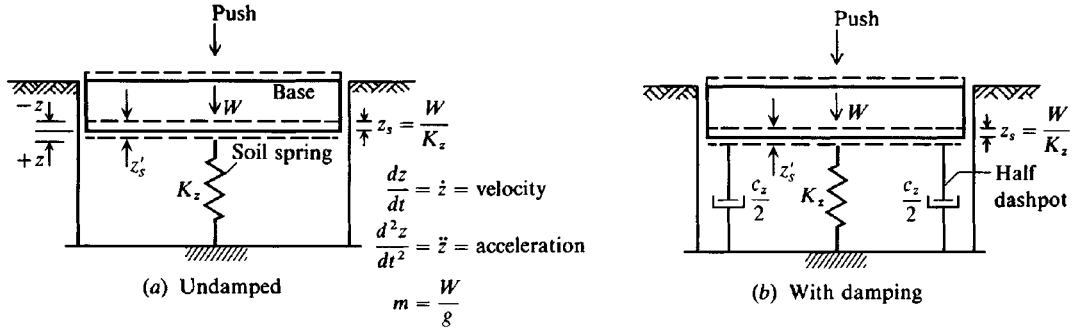

Figure 20-1 Foundation base in equilibrium position just prior to being displaced slightly downward by a quick push.

for dynamic loading and will be computed differently from the beam problem. As we shall later see, the spring will be frequency-dependent as well.

Here the soil spring has compressed under the static weight of the block an amount

$$z_s = \frac{W}{K_z} \tag{a}$$

At this time z_s and the spring K_z are both *static* values. Next we give the block a quick solid shove in the z direction with a quick release, at which time the block begins to move up and down (it vibrates). Now the z_s and soil K_z are *dynamic* values.

We probably could not see the movement, but it could be measured with sensitive electronic measuring equipment. After some time the block comes to rest at a slightly larger displacement z_s' as shown in Fig. 20-1. The larger displacement is from the vibration producing a state change in the soil (a slightly reduced void ratio or more dense particle packing).

We can write the differential equation to describe this motion [given in any elementary dynamics or mechanical vibration textbook (as Den Hartog (1952)], using the terms shown in Fig. 20-1*a* in a form of $\mathbf{F} = m\mathbf{a}$ to give, in one dimension,

$$m\ddot{z} + K_z z = 0 \tag{b}$$

Solving by the methods given in differential equation textbooks after dividing through by the mass term m and defining $\omega_n^2 = K_z/m$, we can obtain the *period* of vibration T as

$$T = \frac{2\pi}{\omega_n}$$

and the natural frequency f_n as any one of the following

$$f_n = \frac{\omega_n}{2\pi} = \frac{1}{2\pi}\sqrt{\frac{K_z}{m}} = \frac{1}{2\pi}\sqrt{\frac{K_z g}{W}} = \frac{1}{2\pi}\sqrt{\frac{g}{z_s}} \tag{20-1}$$

From Eq. (*b*) it would appear that the vibration will continue forever; we know from experience that this is not so. There must be some damping present, so we will add a damping device termed a *dashpot* (analog = automobile shock absorbers) to the idealized model. To maintain symmetry we will add half the dashpot to each edge of the base as in Fig. 20-1*b*.

Dashpots are commonly described as developing a restoring force that is proportional to the velocity ($\dot{z}$) of the mass being damped. With this concept for the dashpot force a vertical force summation gives the following differential equation

$$m\ddot{z} + c_z\dot{z} + K_z z = 0 \tag{c}$$

Solving this equation, we obtain the general form of the instantaneous dynamic displacement z as

$$z = C_1 e^{\beta_1 t} + C_2 e^{\beta_2 t} \tag{d}$$

where

$$\begin{Bmatrix} \beta_1 \\ \beta_2 \end{Bmatrix} = \frac{-c_z \pm \sqrt{c_z^2 - 4K_z m}}{2m} = \frac{-c_z}{2m} \pm \sqrt{\left(\frac{c_z}{2m}\right)^2 - \frac{K_z}{m}} \tag{e}$$

From the β values we note that the $\sqrt{\ }$ term is one of the following:

Case 1. No damping (< 0)—gives Eq. (20-1) when $c_z = 0$.
Case 2. Overdamped (> 0) with $c_z^2 > 4K_z m$ (see Fig. 20-2).
Case 3. Critically damped ($= 0$) with $c_z^2 = 4K_z m$. We define the critical damping as

$$c_{z,c} = 2m\omega_n = 2\sqrt{K_z m}$$

Figure 20-2 Plot of time-displacement curves for three types of damped movement. The plot is relative since the natural frequency is constant and ωt is to the same scale. The variable in the three plots is the damping factor.

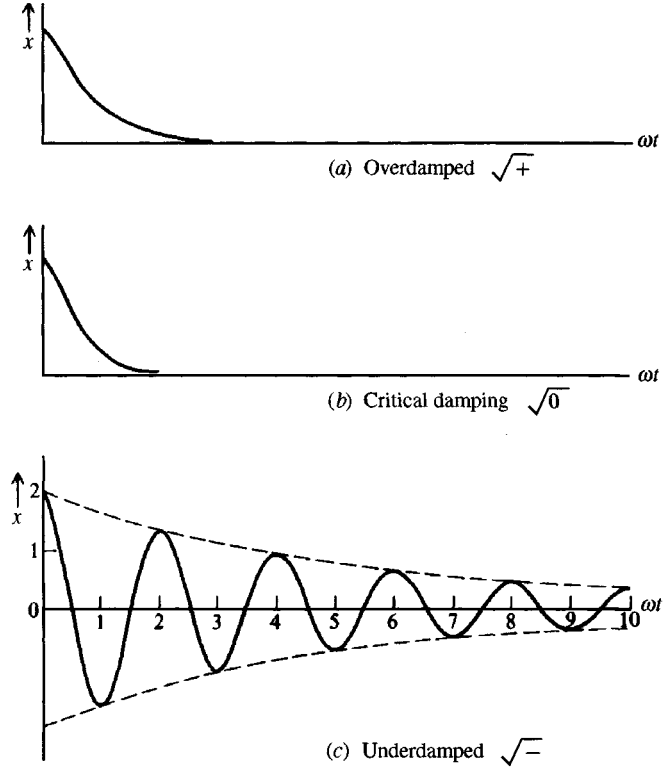

Case 4. Underdamped (< 0) when $c_z^2 < 4K_z m$. This is the usual case in foundation vibrations since case 1 is impossible (even the spring K_z will have some internal damping) and vibrations rapidly dissipate in cases 2 and 3 as shown in Fig. 20-2.

From case 3 we can define a damping ratio D_i as

$$D_z = c_z/c_{z,c} \qquad (\text{here } i = z) \tag{20-2}$$

and the damped circular frequency ω_d from a reordering of the $\sqrt{\ }$ term of Eq. (e)

$$\omega_d = \sqrt{-1}\sqrt{\frac{K_z}{m} - \left(\frac{c_z \omega_n}{c_{z,c}}\right)^2} \tag{20-3}$$

Since $\omega_n^2 = K_z/m$ and $c_z^2 = D_z^2 c_{z,c}^2$, we can obtain an alternative form as

$$\omega_d = \omega_n \sqrt{1 - D_z^2} \tag{20-3a}$$

The $\sqrt{-1}$ disappears, since $D_z \leq 1$.

In the general vibrating base case, however, we have a base load consisting of a large weight colliding with an anvil as in a punch press, a piece of rotating machinery, or an operating engine. The engine in turn may drive a piece of equipment such as a compressor or pump. Any of these latter can have the effect of an unbalanced force (or several forces) rotating about an axis such as a crankshaft (see Fig. 20-3). From elementary dynamics a mass m_e connected to a shaft with an arm of $\bar{y}$ rotating at a circular frequency of ω produces a force at any instant in time of

$$F_i = m_e \bar{y} \omega^2$$

If the operating frequency is ω_o it is evident that the force F_i is varying from zero to the maximum at the operating speed, after which it is a constant. It is also evident that along the particular axis of interest the foregoing force will vary as

$$F = F_o \sin \omega t \qquad \text{or as} \qquad F = F_o \cos \omega t$$

In these cases we rewrite Eq. (c) as

$$m\ddot{z} + c_z \dot{z} + K_z z = F(t) \tag{f}$$

Using the same methods as for Eqs. (b) and (c), we obtain the following for the case of $F = F_o \sin \omega t$—the maximum z occurs at $\omega t = \pm \pi/2$ radians $\rightarrow F_o \times 1 = F_o$:

$$z = \frac{F_o}{\sqrt{(K_z - m\omega^2)^2 + c_z^2 \omega^2}} \tag{20-4a}$$

After factoring K_z and making substitutions for m and c_z, we obtain the following:

$$z = \frac{F_o/K_z}{\sqrt{[1 - (\omega/\omega_n)^2]^2 + (2D_z \omega/\omega_n)^2}} \tag{20-4b}$$

Note that K_z is a static soil spring for $\omega = 0$ and is a dynamic value when $\omega > 0$—in other words, $K_z = f(\omega)$. If the radical in the denominator of Eq. (20-4b) is written as

$$A = (1 - a^2)^2 + (2D_z a)^2$$

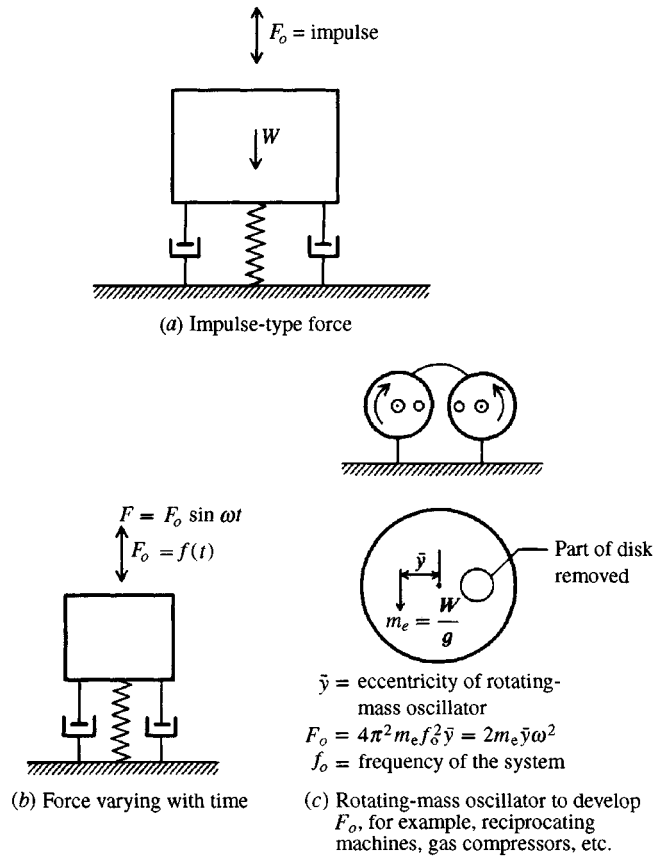

Figure 20-3 Types of foundation exciting forces.

then by setting the derivative $dA/da = 0$ we obtain the maximum value of dynamic z possible in the form (and using z_s = static displacement = F_o/K_z) as

$$z_{\max} = \frac{z_s}{2D_z\sqrt{1 - D_z^2}} \tag{20-5}$$

The resonant frequency f_r is obtained as

$$f_r = f_n\sqrt{1 - 2D_z^2} \tag{20-6}$$

where f_n is defined by Eq. (20-1). Here resonance is somewhat below the natural base frequency f_n. Use F_o = constant or $F_o = m_e\bar{y}\omega_o^2$ in these equations. When $F_o = m_e\bar{y}\omega^2$ the resonance frequency can be computed as

$$f_r' = \frac{f_n}{\sqrt{1 - 2D_z^2}} \tag{20-6a}$$

which gives a resonance frequency *above* the natural frequency f_n.

It is sometimes useful to obtain curves of relative displacement versus a frequency ratio as in Fig. 20-4. In this case we can rewrite Eq. (20-4*b*) to obtain an amplitude ratio of

$$\frac{z}{z_s} = N$$

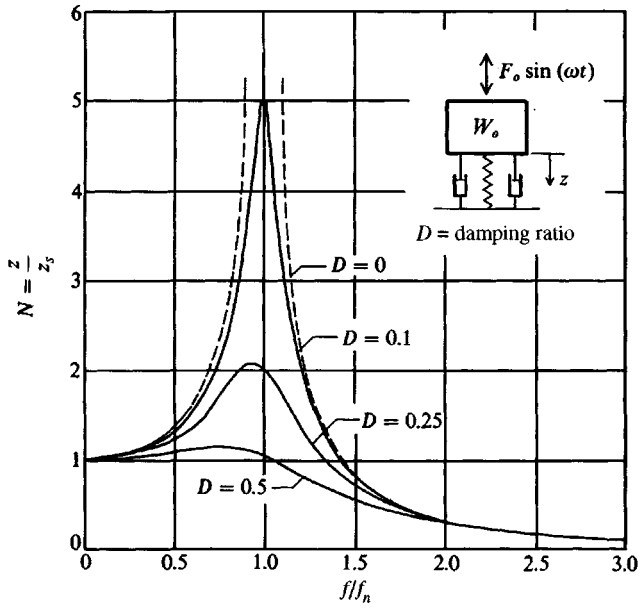

(*a*) Constant-amplitude exciting force (never larger than F_o)

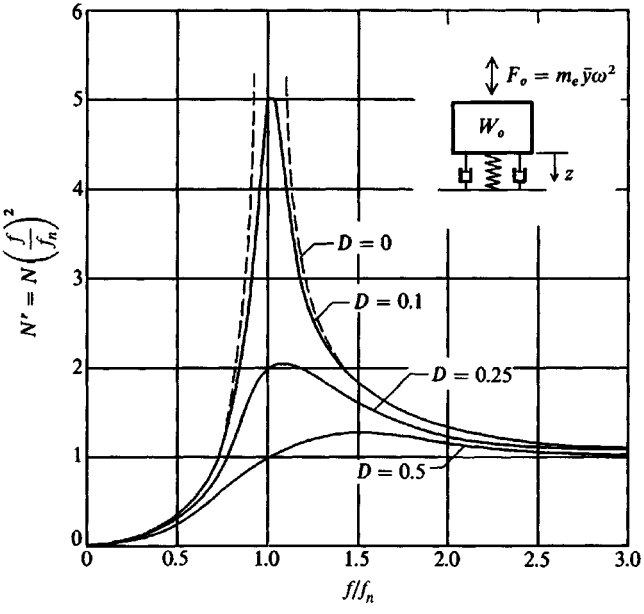

(*b*) Frequency-dependent exciting force f_o varies with ω^2

Figure 20-4 Plots of relative amplitude ratios versus frequency ratios.

where N equals 1/(square root terms) and is a magnification factor. When the exciting force F_o is frequency dependent (Fig. 20-3*c*) the amplitude ratio is

$$\frac{z}{z_s} = N\left(\frac{f}{f_n}\right)^2 = N'$$

It is about as easy, however, to program Eq. (20-4*a*), simply vary $F_o = m_e\bar{y}\omega^2$, and directly compute the z/z_s ratio—particularly since both K_z and c_z are frequency-dependent. The values of N and N' for a range of $f/f_n = 0$ to 3 and for several values of damping ratio $D = 0, 0.1$, etc. are shown in Fig. 20-4. The most significant feature is that N ranges from 1 to a peak at f/f_n slightly less than 1 and approaches zero at large f/f_n where a frequency-dependent force produces an N' that starts at zero, peaks slightly beyond $f/f_n = 1$, and then flattens toward 1 at large f/f_n.

For vibration analyses we can directly use Eq. (20-4*a*) if we have values of soil spring K_z and damping coefficient c_z and can reasonably identify the block mass (W/g) that includes the base and all permanent attachments. We also must have a value of F_o. We do not usually use the force $F = F_o \sin \omega t$ since we are interested in the maximum z and at some instant in time $\sin \omega t = 1$ so $F = F_o$, but we do have to be aware the vibration displacement oscillates at $\pm z$ from z_s.

Carefully note that within the terms f and ω in the frequency ratios are the frequencies of the machine that are developed by the unbalanced forces and depend on revolutions per minute or cycles per second (Hz); and f_n, ω_n, and ω_d are the natural (n) and damped (d) system frequencies.

20-3 THE GENERAL CASE OF A VIBRATING BASE

Figure 20-5 illustrates the general case of a foundation with 6 d.o.f. of vibration/excitation modes possible. From this figure we can have

Translations:	3 modes along the x, y, and z axes
Rotations:	3 modes about the x, y, and z axes

The rotations about the x and y axes are usually termed *rocking modes* and the z axis rotation is termed *yawing*.

Figure 20-5 Rectangular foundation block with 6 degrees of freedom.

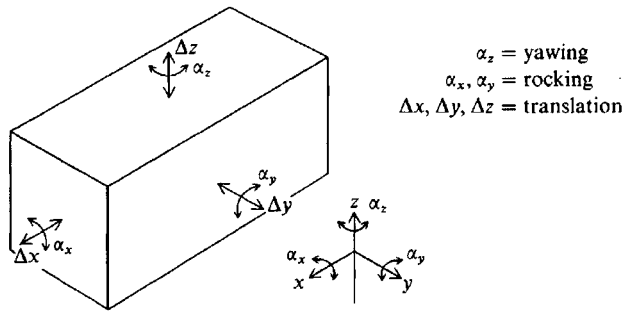

There are three procedures currently used to analyze these vibration modes:

a. Elastic half-space theory [outlined by Sung (1953)]
b. Analog methods [as given by Richart et al. (1970)]
c. Lumped mass or lumped parameter method (as given in the preceding section)

After an extensive literature survey and review of the several methods the author decided that the lumped mass approach is at least as reliable and substantially more general than any of the alternative procedures. Current state-of-art allows adjustments to the spring and damping constants for frequency. The same soil data are required as for any of the alternative procedures, and the method is rather simple, for it is only necessary to program Eq. (20-4*a*) to increment the frequency of the engine/machine to obtain the corresponding displacement amplitudes and see if any are too large for the particular equipment. Of course it is also necessary to obtain certain data, as subsequently noted, as input along with soil parameters. It is particularly helpful to use a computer program to do most of the work because this type of problem is computationally intensive—particularly when making parametric studies.

By direct analogy of Eq. (*f*) we can write differential equations as follows:

For sliding modes:

$$m\ddot{x} + c_x\dot{x} + K_x x = F_x(\text{time})$$
$$m\ddot{y} + c_y\dot{y} + K_y y = F_y(\text{time})$$

For rocking modes:

$$I_{\theta i}\ddot{\theta} + c_{\theta i}\dot{\theta} + K_{\theta i}\theta = F_{\theta i}(\text{time})$$

Since the differential equation is similar in form for all cases we have a general solution in Eq. (20-4*a*) with appropriate entries for K_z, c_z, and m as follows:

Axis	Spring	Damping	Mass, m_i =
	Translation modes		
x	K_x	c_x	$m_x = m$
y	K_y	c_y	$m_y = m$
z	K_z	c_z	$m_z = m = W/g$
	Rocking and yawing modes		
x	$K_{\theta x}$	$c_{\theta x}$	$I_{\theta x}$
y	$K_{\theta y}$	$c_{\theta y}$	$I_{\theta y}$
z	$K_{\theta z}$	$c_{\theta z}$	$I_{\theta z}$

where W = weight of base + all machinery and other attachments that will vibrate with the base; g = gravitation constant (9.807 or 32.2).

Values of $I_{\theta i}$ can be computed using formulas given in Table 20-1 or from methods given in most dynamics textbooks. The mass m used in these equations is the same for all translation modes. Most mass moments of inertia will be composites in which the transfer formula will be required; however, the total mass m will be the same in all the modes.

TABLE 20-1

Mass moments of inertia $I_{\theta i}$ for shapes most likely to be used for a vibrating base

Method of derivation is found in most dynamics textbooks. Units are mass × length^2 (for SI = kN·m·s^2). Use transfer formula to transfer to parallel axes for composite sections.

Slender rod	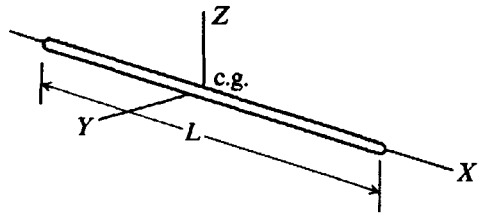	$I_{\theta y} = I_{\theta z} = \frac{1}{12}mL^2$
Circular cylinder	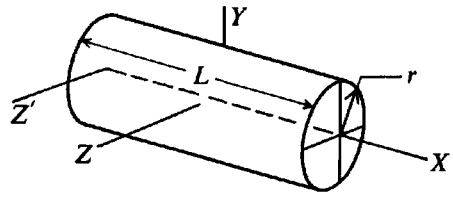	$I_{\theta x} = \frac{1}{2}mr^2$ $I_{\theta y} = I_{\theta z} = \frac{1}{12}m(3r^2 + L^2)$ $I_{\theta z'} = I_{\theta z} + mL^2/4$ (base)
Thin disk	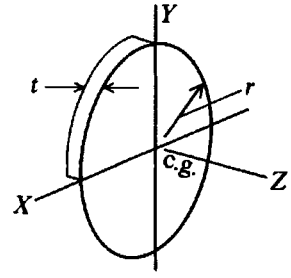	$I_{\theta z} = \frac{1}{2}mr^2$ $I_{\theta x} = I_{\theta y} = \frac{1}{4}mr^2$

The soil spring (K_i) and damping (c_i) terms can be computed by a number of procedures, all giving slight to major computed differences in vibration displacements. Fortunately the spring and damping effects are under the square root of Eq. (20-4) so the estimation effect is somewhat reduced. We would not like, however, to compute a displacement of, say, 0.001 mm and have the value be 0.01 mm, which results in the machine supported by the base becoming damaged from excessive base movements.

20-4 SOIL SPRINGS AND DAMPING CONSTANTS

Barkan (1962) is a frequently cited source for soil springs. Other references such as Richart et al. (1970) and Novak and Beredugo (1972) also give methods to compute spring values. Dobry and Gazetas (1986) made an extensive literature survey for methods to compute the spring and damping constants and plotted the values from the several sources versus a dimensionless frequency factor a_o and produced a series of best-fit curves. They then compared

TABLE 20-1 (*continued*)

Mass moments of inertia $I_{\theta i}$ for shapes most likely to be used for a vibrating base

Method of derivation is found in most dynamics textbooks. Units are mass × length^2 (for SI = kN·m·s^2). Use transfer formula to transfer to parallel axes for composite sections.

Thin rectangular plate	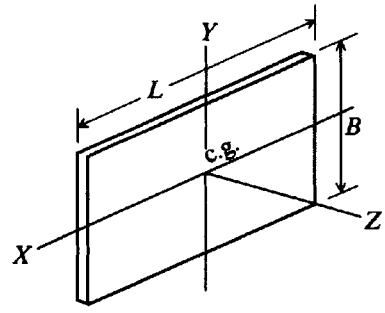	$I_{\theta z} = \frac{1}{12}m(L^2 + B^2)$ $I_{\theta x} = \frac{1}{12}mB^2$ $I_{\theta y} = \frac{1}{12}mL^2$
Rectangular prism	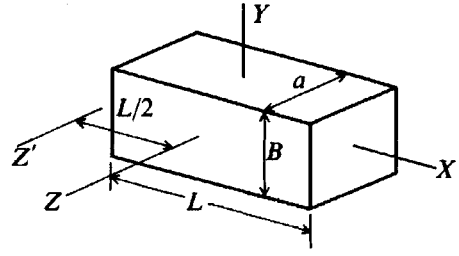	$I_{\theta x} = \frac{1}{12}m(a^2 + B^2)$ $I_{\theta y} = \frac{1}{12}m(a^2 + L^2)$ $I_{\theta z} = \frac{1}{12}m(B^2 + L^2)$ $I_{\theta z'} = I_{\theta z} + mL^2/4$ (base)
Sphere	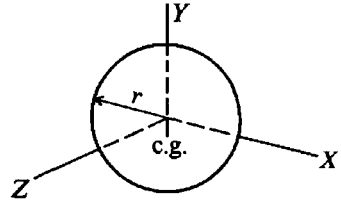	$I_{\theta x} = I_{\theta y} = I_{\theta z} = \frac{2}{5}mr^2$

Transfer formula: $I'_{\theta i} = I_{\theta i} + md^2$

predicted vibrations from these curves with measured values and found very good agreement in all cases. The dimensionless frequency parameter a_o is defined for a round base as

$$a_o = \frac{\omega r_o}{V_s} = \omega r_o \sqrt{\frac{\rho}{G'}}$$

where the shear wave velocity in the soil is defined by Eq. (20-15) with ρ = density of soil and G' = shear modulus defined in Sec. 20-5. The corresponding a_o used in the curves of spring versus a_o and damping versus a_o for rectangular bases is

$$a_o = \frac{\omega B}{V_s} \tag{20-7}$$

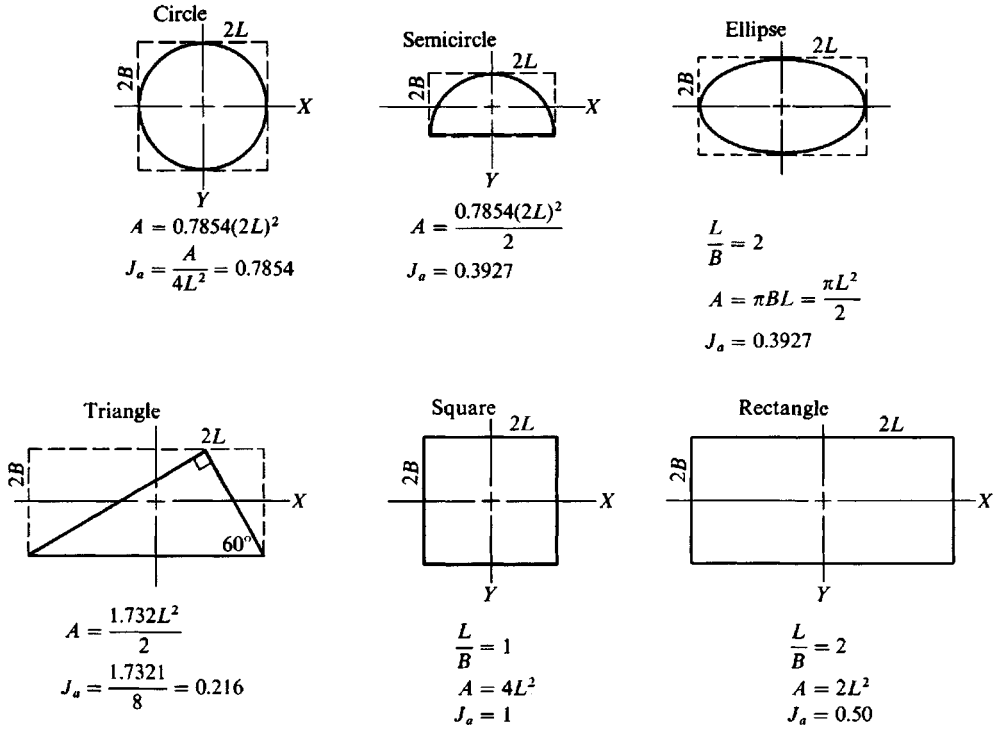

Figure 20-6 Factor $J_a = A/4L^2$ for several geometric shapes. Note axis orientation in all cases, and length = $2L$ and width = $2B$.

Carefully note that the base width defined in Fig. 20-6 is $2B$, so the B value used in this equation is half the base width (analogous to r_o for a round base). Here ω is the frequency of the machine and not the system natural frequency.

In most cases the foundation base being dynamically excited is not round with a radius r_o but, rather, is rectangular—often with an L/B of 2 to 5. The solutions generally published prior to those of Dobry and Gazetas required converting the rectangular (or other) shape to an equivalent round base, equivalent being defined as a round base with the same area in plan as in the actual base. Solution quality deteriorated as the L/B ratio increased as would be expected since the equivalent round foundation would become a poor model at larger L/B ratios. Observe that in using the Dobry and Gazetas method we would make a better model by converting a round base to an equivalent square than by converting a square to an equivalent round base.

This method uses a base of dimensions $2B \times 2L$ as shown on Fig. 20-6. Note very carefully that the circumscribed base width is $2B$ and the length is $2L$. This gives the plan area directly as $2B \times 2L$ only for solid rectangles. For all other bases one must obtain the circumscribed dimensions and then compute the actual base area by any practical means (perhaps by using the sum of several components consisting of squares, triangles, etc.).

Similarly in this method it may be necessary, in computing certain of the soil springs, to use the plan moment of inertia about the x, y, or z axes. This computation gives for a solid rectangle

$$I_x = 1.333LB^3 \qquad I_y = 1.333BL^3 \qquad \text{and} \qquad I_z = I_x + I_y = J$$

From Fig. 20-6 we see that $2L$ is always parallel to the x axis, giving $L/B \geq 1$. The factor $1.333 = \frac{16}{12}$ since we use $2B \times 2L$. When the circumscribed dimensions are not completely filled in, it is necessary to compute the moment of inertia about any axis (I_x is about the x axis, etc.) using the sum of the component parts and the transfer of axes formula as necessary.

Another constant used by this procedure is

$$J_a = \frac{\text{Area}}{4L^2} \qquad \text{(dimensionless)} \tag{20-8}$$

with several values of J_a shown on Fig. 20-6.

In using the method it is necessary first to compute the static spring values using the curve fit values given in Table 20-2 and, for damping, values from Table 20-4 to obtain

$$\text{Spring: } K_i \qquad \text{Damping: } c_i$$

These values are then multiplied by frequency-dependent factors η_i obtained from Fig. 20-7*a, b, c* (as appropriate) and by λ_i factors from curve-fitted equations in Table 20-4 (done by the author for computer programming convenience). These factors then give the dynamic springs and damping coefficients as

$$\text{Spring: } \overline{K}_i = \eta_i K_i \qquad \text{Damping: } \overline{c}_i = \lambda_i c_i$$

TABLE 20-2

Dynamic spring K_i for use in Eq. (20-4*a*). Obtain S_i factors from Table 20-3

Values shown are "static" values that must be multiplied by a factor η_i, which may be obtained from Fig. 20-7.* Note that $2L$ = base length and $2B$ = base width with L parallel to x axis and B parallel to y axis.

For rectangular bases	Round base	Strip
Vertical mode		
$K_z = S_z \dfrac{2LG'}{1-\mu}$	$K_z = \dfrac{4G'B}{1-\mu}$	$K_z = \dfrac{0.8G'(2L)}{1-\mu}$
Horizontal mode		
Parallel to y axis		
$K_y = S_y \dfrac{2LG'}{2-\mu}$	$K_y = \dfrac{8G'B}{2-\mu}$	$K_y = \dfrac{2.24G'(2L)}{2-\mu}$
Parallel to x axis		
$K_y = S_y \dfrac{2LG'}{2-\mu}$	$K_x = K_y$	
$K_x = S_y \dfrac{2LG'}{2-\mu} - \dfrac{0.21LG}{0.75-\mu}\left(1 - \dfrac{B}{L}\right)$	($n_x = 1$ for K_x so $\overline{K}_x = K_x$)	
Rocking mode		
About x axis		
$K_{\theta x} = S_{\theta x} \dfrac{G'}{1-\mu}(I_{\theta x})^{0.75}\left(\dfrac{B}{L}\right)^{-0.25}$	$K_{\theta x} = \dfrac{8G'B^3}{3(1-\mu)}$	$K_{\theta x} = \dfrac{\pi(2L)G'B^2}{2-2\mu}\left[1 + \left(\dfrac{\ln(3-4\mu)}{\pi}\right)^2\right]$
About y axis		
$K_{\theta y} = S_{\theta y} \dfrac{G'}{1-\mu}(I_{\theta y})^{0.75}$	$K_{\theta y} = K_{\theta x}$	
Torsion mode		
$K_t = S_t G'(J)^{0.75}$	$K_t = \dfrac{16G'B^3}{3}$	

*After Dobry and Gazetas (1986).

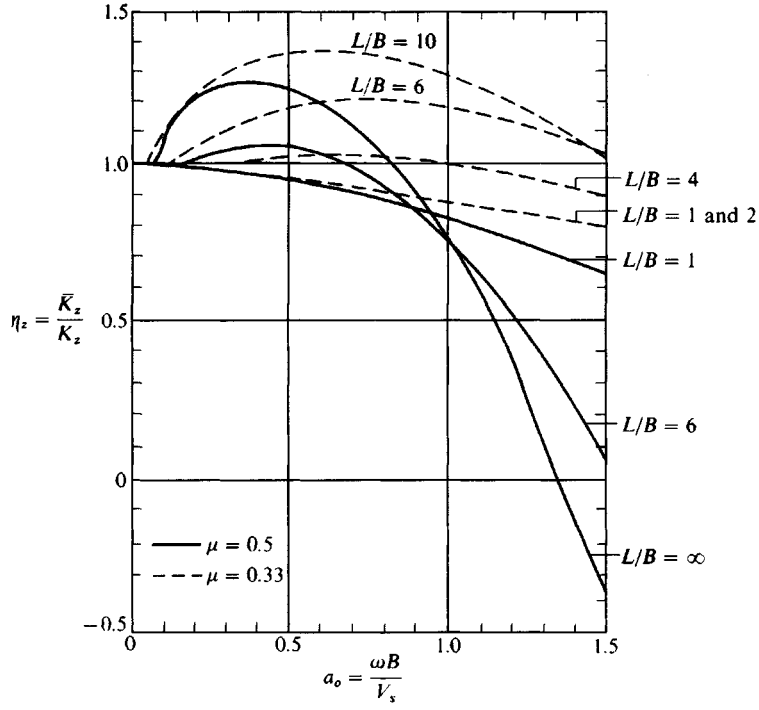

(*a*) Vertical η_z factors. Note these are dependent on Poisson's ratio μ. Use $\mu = 0.5$ for saturated clay and $\mu = 0.33$ for all other soil.

Fig. 20-7 The η_i factors to convert static springs of Table 20-2 to dynamic values as $\overline{K}_i = \eta K_i$. Curves condensed from Dobry and Gazetas (1985).

These dynamic spring $\overline{K}_i$ and damping $\overline{c}_i$ are based on a perfectly elastic soil with zero material damping. Experimental evidence indicates that even at very small strains soil exhibits a material (or hysteretic) damping. This is usually specified using a frequency-independent damping ratio D_i (see Eq. 20-2) that is used to adjust $\overline{K}_i$ and $\overline{c}_i$ further according to Lysmer as cited by Dobry and Gazetas (1986) as follows:

$$K_i = \overline{K}_i - \omega \overline{c}_i D_i \tag{20-9}$$

$$c_i = \overline{c}_i + \frac{2\overline{K}_i D_i}{\omega} \tag{20-10}$$

These values of K_i and c_i are used in Eq. (20-4) or its variations depending on whether there is translation or rocking.

Values of material damping D_i are considered in Sec. 20-5.3.

From the discussion to this point it is evident that the only really practical way to solve vibration problems is to use a computer program. In a computer program it is necessary to do the following:

1. Allow input of the problem parameters (base data, soil data, and dynamic force data).
2. Compute the static spring and damping and the dynamic factors η_i and λ_i as appropriate for that mode. Use Fig. 20-7 for the η_i factors.
3. Compute the dynamic spring and damping values using Eqs. (20-9) and (20-10).

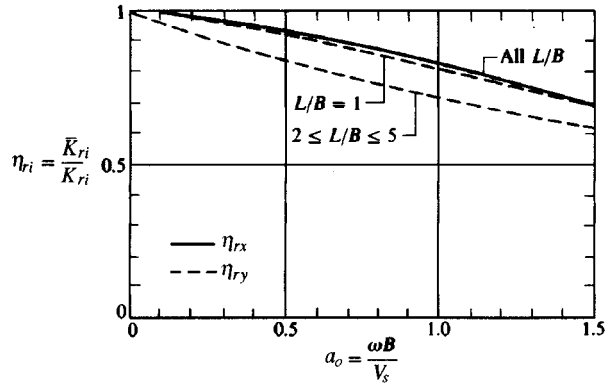

(*b*) Rocking η_{rx} and η_{ry} factors.

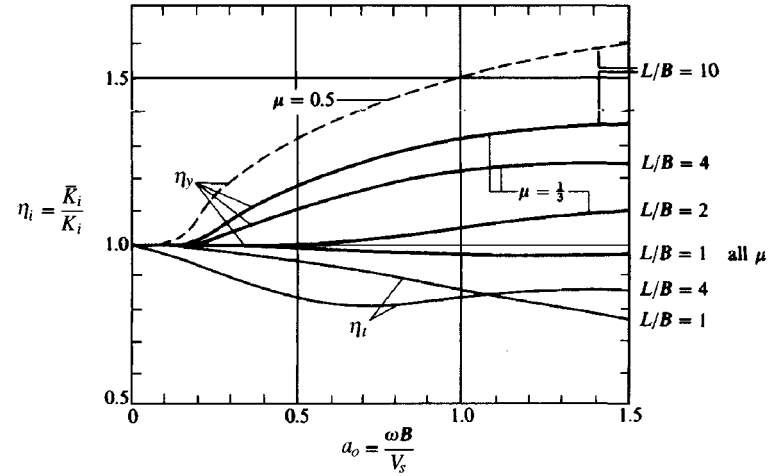

(*c*) Sliding η_y and torsion η_t factors. All torsion factors are $\eta_t < 1$.

Figure 20-7 (*continued*)

4. Solve Eq. (20-4*a*) for the displacement amplitude or Eq. (20-4*b*) for the magnification factor to apply to the static displacement.
5. Output sufficient results so a spot check for correctness can be made.

To accomplish these requirements, FADDYNF1 (B-11) is provided on your program diskette. This program directly uses the equations for a rectangular base given in Tables 20-2 and 20-3. A curve-fitting (regression-type) analysis was used to obtain a best fit of the curves of Fig. 20-7 with the coefficients directly programmed for the η_i values. A similar curve-fitting scheme was used to produce Table 20-4 from the cited reference (without providing the figures in the text to conserve space). The coefficients were then programmed in the several subroutines in the program so that λ_i could be obtained. A linear interpolation between curves is used for intermediate values of L/B.

TABLE 20-3
S_i factors for computing K_i of Table 20-2

Mode		Applicable
Vertical:	$S_z = 0.8$	$J_a \leq 0.02$
	$S_z = 0.73 + 1.54(J_a)^{0.75}$	$J_a > 0.02$
Horizontal:	$S_y = 2.24$	$J_a \leq 0.16$
	$S_y = 4.5(J_a)^{0.38}$	$J_a > 0.16$
Rocking:	$S_{\theta x} = 2.54$	$B/L \leq 0.4$
	$S_{\theta x} = 3.2(B/L)^{0.25}$	$B/L > 0.4$
	$S_{\theta y} = 3.2$	All B/L
Torsion:	$S_t = 3.8 + 10.7(1 - B/L)^{10}$	All B/L

J_a = area/$(4L^2)$ where $2L$ = length of base; area = $2B \times 2L$ for solid rectangle.

The program should generally be limited to $L/B \leq 5$. One should check the range of L/B given either in Fig. 20-7 or in Table 20-4 since certain vibration modes may allow a larger L/B. The range of a_o should be limited to between zero and 1.5 (usual range provided in most literature sources), which should cover nearly all likely base designs. For a_o to exceed 1.5 one would have a very high speed machine (large ω) and/or a small ground shear wave velocity V_s. In these cases some kind of soil strengthening or the use of piles may be necessary if vibration control is critical.

20-5 SOIL PROPERTIES FOR DYNAMIC BASE DESIGN

The soil spring constants shown in Table 20-2 directly depend on the dynamic soil shear modulus G' and Poisson's ratio μ. The unit weight γ_s is needed to compute the soil density ρ as

$$\rho = \gamma_s/9.807 \text{ kN} \cdot \text{s}^2/\text{m}^4 \qquad \text{(SI and } \gamma_s \text{ in kN/m}^3\text{)}$$

$$\rho = \gamma_s/32.2 \text{ k} \cdot \text{s}^2/\text{ft}^4 \qquad \text{(Fps and } \gamma_s \text{ in k/ft}^3\text{)}$$

It is usual to estimate μ in the range of 0.3 to 0.5 as done in Chap. 5 for foundation settlements. We note that the dynamic coefficients η_z and η_y also depend on μ; however, here only two values—0.333 and 0.50—can be used (as programmed in the computer program). These two values are probably sufficient for most problems since μ is estimated and not directly measured.

The unit weight of a cohesive soil can be directly measured using the procedures outlined in Example 2-1. In other cases it can generally be estimated with sufficient precision using Table 3-4 or simply be taken as between 17 and 20 kN/m^3 (or 110 to 125 lb/ft^3). Larger values for γ_s can be justified for a dynamic analysis as no one would place a base on loose soil. The soil would be either densified or stiffened with admixtures, soil-cement piles, or stone columns; or the base would be placed on piles.

20-5.1 Laboratory Determination of G'

The shear modulus can be estimated from resonant-column tests. These involve a laboratory apparatus consisting of a specially constructed triaxial cell capable of providing a very small

TABLE 20-4

Damping constants for computing the damping coefficient c_i

Obtained using curve fitting to enlarged figures from Dobry and Gazetas (1986). Values programmed in computer program. A = actual base area

For vertical damping in range of $0 \le a_o \le 1.5$

$$\lambda_z = \frac{c_z}{\rho V_{LA} A} = X_1 + (a_o R)X_2 + (a_o R)^2 X_3 + X_4 \exp(-a_o R)$$

$L/B = R$	X_1	X_2	X_3	X_4
1	0.9716	−0.0500	0.0520	−0.0660
2	1.2080	−0.1640	0.0385	−0.2515
4	1.0900	−0.0025	0.0012	0.0000
6	1.2285	−0.0359	0.0024	0.1515
10	1.3112	−0.0285	0.0011	0.4388

$$V_{LA} = \frac{3.4}{\pi(1-\mu)} V_s$$

For $R > 10$ use $\lambda_z = \lambda_{z(10)}(1 + 0.001R)$ For $a_o > 1.5$ use $c_z = \rho V_{LA} A$

For sliding damping parallel to y axis in range of $0 \le a_o \le 1.5$

$$\lambda_y = \frac{c_y}{\rho V_s A} = X_1 + (a_o R)X_2 + (a_o R)^2 X_3 + X_4 \exp(-a_o R)$$

$L/B = R$	X_1	X_2	X_3	X_4
1	1.5720	−0.6140	0.2118	−0.7062
2	1.0200	0.0000	0.0000	0.0000
4	1.7350	−0.2915	0.0288	−0.4950
10	1.8040	−0.1273	0.0051	0.7960

For $R > 10$ use $\lambda_{y(R)} = \lambda_{y(10)}(1 + 0.0025R)$ For $a_o > 1.5$ use $c_y = \rho V_s A$

For sliding damping parallel to x axis use the following

$0 \le L/B \le 3$ **use** $c_x = \lambda_{y(1)} \rho V_s A$ $L/B > 3$ **use** $c_x = \rho V_s A$

For rocking damping use

$$\lambda_{ri} = \frac{c_i}{\rho V_{LA} I_i} = a_o X_1 + a_o^2 X_2 + a_o^3 X_3 + a_o^4 X_4$$

	λ_{rx} = rocking about x axis				
$L/B = R$	X_1	X_2	X_3	X_4	
1 and 2	0.0337	1.1477	−1.0369	0.2849	
5	1.0757	−0.4492	−0.1621	0.1550	
≥ 10	1.6465	−1.5247	0.8516	−0.2046	
	λ_{ry} = rocking about y axis				
1	0.0337	1.1477	−1.0369	0.2849	(same as λ_{rx})
2	0.2383	1.6257	−1.6804	0.4895	
3	0.6768	1.5620	−2.0227	0.6382	
4 and 5	1.4238	0.5046	−1.5762	0.6052	

For $R \ge 100$ ($\cong \infty$) $\lambda_{ry} = 1$

(continued on next page)

TABLE 20-4 (*continued*)
Damping constants for computing the damping coefficient c_i

For torsion damping use

$$\lambda_t = \frac{c_t}{\rho V_s J} = a_o X_1 + a_o^2 X_2 + a_o^3 X_3 + X_4 \tan^{-1} \frac{R}{a_o}$$

$L/B = R$	X_1	X_2	X_3	X_4
1	−0.0452	0.5277	−0.1843	0.0214
2	0.8945	−0.2226	−0.0042	−0.0612
3	1.6330	−0.8238	0.1156	−0.0962
4	2.6028	−2.0521	0.5312	−0.1070
> 100	$\lambda_t = 1.0$			

amplitude vibration to a soil specimen. The technique is described in some detail in Cunny and Fry (1973) and in ASTM D 4015.

The value of dynamic shear modulus G' can be estimated using empirical equations presented by Hardin and Black (1968) as

$$G' = \frac{6900(2.17 - e)^2}{1 + e} \sqrt{\sigma_o} \quad \text{(kPa)} \tag{20-11}$$

for round-grained sands, where the void ratio $e < 0.80$.

For angular-grained materials, with $e > 0.6$, and clays of modest activity the estimate of G' is

$$G' = \frac{3230(2.97 - e^2)}{1 + e} \sqrt{\sigma_o} \quad \text{(kPa)} \tag{20-12}$$

Hardin and Drnevich (1972) included the overconsolidation ratio (OCR) into Eq. (20-12) to obtain

$$G' = \frac{3230(2.97 - e)^2}{1 + e} \text{OCR}^M \sqrt{\sigma_o} \quad \text{(kPa)} \tag{20-12a}$$

where, in Eqs. (20-11) through Eq. (20-13),

e = void ratio in situ or in laboratory test sample

σ_o = mean effective stress = $\dfrac{\sigma_1 + \sigma_2 + \sigma_3}{3}$ for laboratory sample

= $\dfrac{\sigma_1(1 + 2K_o)}{3}$ in situ, kPa

A more general form of Eq. (20-12a) is the following:

$$G' = C_o \frac{(2.97 - e)^2}{F(e)} \text{OCR}^M \sigma_o^n \quad \text{(kPa)} \tag{20-13}$$

where terms not previously defined for Eqs. (20-11) and (20-12) are

Item	Hardin & Drnevich (1972)	Kim & Novak (1981)
C_o	3230	440–1450, but use 770
n	0.5	0.51–0.73, but use 0.65
$F(e)$	$1 + e^\dagger$	$1 + e$

† Hardin and Blandford (1989) suggest $F(e) = 0.3 + 0.7e^2$.

TABLE 20-5
Representative values of shear modulus G'

Material	ksi	MPa
Clean dense quartz sand	1.8–3	12–20
Micaceous fine sand	2.3	16
Berlin sand (e = 0.53)	2.5–3.5	17–24
Loamy sand	1.5	10
Dense sand-gravel	10^+	70^+
Wet soft silty clay	1.3–2	9–15
Dry soft silty clay	2.5–3	17–21
Dry silty clay	4–5	25–35
Medium clay	2–4	12–30
Sandy clay	2–4	12–30

Values for the OCR exponent M in Eqs. (20-12a) and (20-13) are related to the plasticity index I_P of the soil as follows:

I_P, %	0	20	40	60	80
M	0	0.18	0.30	0.41	0.48

Anderson et al. (1978) and others indicate that Eqs. (20-12) and (20-12a) are likely to underpredict G' in situ by a factor from 1.3 to 2.5 since they do not include the stiffening effects from cementation and anisotropy. On the other hand, Kim and Novak (1981) found for several Canadian clays and silts that Eq. (20-12a) overpredicted G' by a factor of about 2. Typical values of G' as found by several researchers are given in Table 20-5 as a guide or for preliminary estimates of vibration amplitudes.

One cannot use static triaxial test values of E_s to compute dynamic values of G', since the strain ϵ_d for the dynamic G' is on the order of 0.002 to 0.00001 (or less) where triaxial strains ϵ_{tr} are usually recorded (and plotted) in the range of 0.01^+.

20-5.2 In Situ Determination of Dynamic Shear Modulus G'

In an elastic, homogeneous soil mass dynamically stressed at a point near the surface, three elastic waves travel outward at different speeds. These are as follows:

Compression (or P) wave
Shear (or secondary S) wave—usually wave of interest
Surface (or Rayleigh) wave

The velocity of the Rayleigh wave is about 10 percent less than that of the shear wave. For surface measurements it is often used in lieu of the shear wave owing to the complex waveform displayed on the pickup unit from these nearly simultaneous wave arrivals. The wave peaks on the waveform are used to indicate wave arrival so the time of travel from shock source to detection unit can be computed. Compression and shear wave velocities are related to the dynamic elastic constants of the soil according to Theory of Elasticity as follows:

Compression:
$$V_c = \sqrt{\frac{E_s(1-\mu)}{\rho(1+\pi)(1-2\mu)}} \tag{20-14}$$

Shear:
$$V_s = \sqrt{\frac{G'}{\rho}} \tag{20-15}$$

The relationship between shear modulus G' and stress-strain modulus E_s is the same as for static values and is given by Eq. (*b*) of Sec. 2-14, repeated here for convenience with a slight rearrangement:

$$E_s = 2(1 + \mu)G'$$

Dividing Eq. (20-15) by Eq. (2-14), squaring, substituting, and simplifying, we obtain

$$\left(\frac{V_s}{V_c}\right)^2 = \frac{1 - 2\mu}{2(1 - \mu)} \tag{20-16}$$

From Eq. (20-16) we see the shear wave ranges from

$$0 \leq V_s \leq 0.707V_c$$

depending on Poisson's ratio μ. From this it is evident the compression waves will arrive at the detection unit some time before the shear and surface waves arrive.

The shear modulus can be obtained by making field measurements of the shear wave velocity V_s and by using Eq. (20-15) to find

$$G' = \rho V_s^2$$

In addition to the direct measurement of the Rayleigh surface shear wave and using Eq. (20-15) to compute G', one can obtain the shear wave velocity V_s in situ using any one of a number of tests such as the up-hole, down-hole, cross-hole, bottom-hole, in-hole, and seismic cone penetration [see Robertson and Addo (1991), which includes a large reference list describing the tests in some detail]. More recently (ca. 1984) a modification of the surface wave method, termed the *spectral analysis of surface wave* (*SASW*) method, has been suggested.

The cross-hole and down-hole methods for the in situ shear wave velocity V_s are described in considerable detail by Woods (1986, with large number of references).

CROSS-HOLE METHOD. In the cross-hole method (see Fig. 20-8*a*) two boreholes a known distance apart are drilled to some depth, preferably on each side of the base location so that the shear wave can be measured between the two holes and across the base zone.

At a depth of about B a sensor device is located in the side or bottom of one hole and a shock-producing device (or small blast) in the other. A trigger is supplied with the shock so that the time for the induced shear wave can be observed at the pickup unit. The time of travel T_h of the known distance D_h between the two holes gives the shear wave velocity V_s (in units of D_h) as

$$V_s = \frac{D_h}{T_h}$$

DOWN-HOLE METHOD. The down-hole method is similar to the cross-hole but has the advantage of only requiring one boring, as shown on Fig. 20-8*b*. In this method, the hole is drilled, and a shock device is located a known distance away. A shock detector is located at some known depth in the hole and a shock applied. As with the cross-hole method, we can measure the time T_h for arrival of the shear wave and, by computing the diagonal side of the triangle, obtain the travel distance D_h. The detector device is then placed at a greater depth and the test repeated, etc., until a reasonably average value of V_s is obtained. Hoar and Stokoe

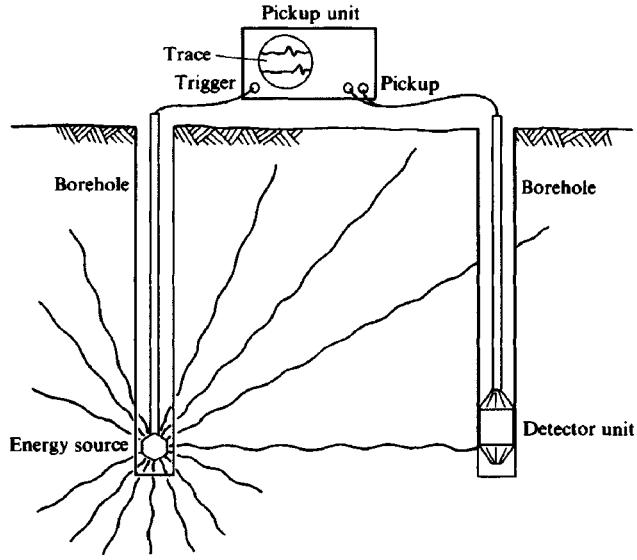

(*a*) Cross-hole method and test under way at some depth z_i.

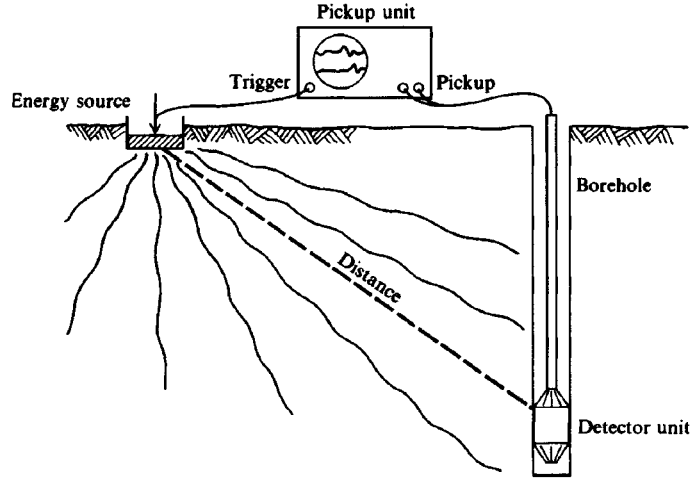

(*b*) Down-hole method with test at some depth z_i.

Figure 20-8 Two recommended in situ methods for obtaining shear modulus G'.

(1978) discuss in some detail precautionary measures to take in making either of these two tests so that the results can justify the test effort.

SEISMIC CONE METHOD. This method directly measures the shear wave velocity by incorporating a small velocity seismometer (an electronic pickup device) inside the cone penetrometer. Essentially, the test proceeds by pushing the seismic cone to some depth z and then applying a shock at the ground surface, using a hammer and striking plate or similar. This method seems to have been developed ca. 1986 [see Robertson et al. (1986)]. This device has the advantage of not requiring a borehole. It requires that the site soil be suitable for a CPT (fine-grained, with little to no gravel).

SPECTRAL ANALYSIS OF SURFACE WAVES (SASW) METHOD. This is a modification of the seismic surface method based on the dispersive characteristics of Rayleigh waves in layered media. It involves applying a vibration to the soil surface, measuring the wave speed between two electronic pickup devices a known distance apart, and then interpreting the data. The test procedure and early development is described in substantial detail by Nazarian and Desai (1993); the theory and use by Yuan and Nazarian (1993). An in-depth test program based on the SASW by Lefebvre et al. (1994) found that empirical correlations based on laboratory tests and using void ratio, OCR, and the mean effective stress σ_o as equation parameters may substantially underpredict the dynamic shear modulus G'.

The SASW has particular value in not requiring a borehole or a large amount of field equipment.

SHEAR WAVE–G' CORRELATIONS. Schmertmann (1978*a*) suggests that V_s may be related to the SPT N value or to the CPT q_c. From a plot of a large number of N values at a test site in sand, he suggested that $V_s \approx 15N_{60}$—for that site. From this it appears that

$$V_s = 10 \text{ to } 20N_{60} \qquad \text{(m/s)} \tag{20-17}$$

with the range to account for increasing density, fine or coarse sand and other variables. Use Table 20-5 as an additional guide.

Seed et al. (1986) and later Jamiolkowski et al. (1988) suggested that the shear velocity is approximately

$$V_s = C_1 N_{60}^{0.17} z^{0.2} F_1 F_2 \qquad \text{(m/s)} \tag{20-17a}$$

where C_1 = empirical constant; Seed et al. (1986) suggested 69; Jamiolkowski et al. (1988) suggested 53.5
z = depth in soil where blow count N_{60} is taken, m
F_1 = age factor:
= 1 for Holocene age (alluvial deposits)
= 1.3 for Pleistocene age (diluvial deposits)
F_2 = soil factor as follows:

	Clay	Fine sand	Med sand	Coarse sand	Sand & Gravel	Gravel
F_2 =	1.0	1.09	1.07	1.11	1.15	1.45

Yoshida et al. (1988) give an equation for V_s as follows:

$$V_s = C_1(\gamma z)^{0.14} N_{60}^{0.25} \qquad \text{m/s} \tag{20-17b}$$

where γz = average overburden pressure in depth z of interest, kPa
C_1 = coefficient depending on soil type as follows:

Soil	Fine sand	25% Gravel	50% Gravel	All soils
C_1 =	49	56	60	55

The V_s estimate from Eqs. (20-17) are then used together with an estimated (or measured) value of soil density ρ to back-compute G' using Eq. (20-15). With some attention to details the computed G' will probably not be in error more than ±25 percent—but it can be as much as 100 percent.

Mayne and Rix (1995) suggest a correlation using either a seismic cone or a piezocone with q_c corrected for pore pressure to q_T in the following form:

$$G' = \frac{99.5 \times p_a^{0.31} \times q_T^{0.69}}{e^n} \quad \text{(kPa)} \qquad (20\text{-}17c)$$

Here, p_a = atmospheric pressure, kPa. In most cases using p_a = 100 kPa (vs. actual value of about 101.4 kPa) is sufficiently precise; q_T and the in situ void ratio e have been previously defined. The n-exponent for e has a value ranging from 1.13 to 1.3. For p_a = 100 kPa, q_T = 180 kPa, $e^n = (wG_s)^n = 1.08^{1.13}$, Eq. (20-17$b$) gives G' = **13 683** kPa (13.7 MPa).

Alternatively, you may convert q_c from the CPT to an equivalent SPT N using Eq. (3-20); adjust this N to N_{60} and use Eqs. (20-17) to obtain V_s then use Eq. (20-15) to compute G'.

Poisson's ratio is more troublesome, however, since a difference between μ = 0.3 and 0.4 can result in about 16 percent error in computing the soil spring.

20-5.3 Soil or Material Damping Ratio D_i

Soil damping, defined here as the ratio of Eq. (20-3), i.e., actual damping, c_i/critical soil damping, c_{ci},

$$D_i = \frac{c_i}{c_{ci}} \times 100 \quad (\%)$$

is usually estimated in the range of 0 to about 0.10 (0 to 10 percent). This damping ratio range has been suggested by Whitman and Richart (1967), who compiled values from a number of sources available at that time including Barkan (1962).

The recent work of Stewart and Campanella (1993) reasonably validates the earlier range of values. However, they also suggested that although the damping ratio is frequency- (as well as material-) dependent, it can be estimated in about the following range:

	Damping D_z, %	
Soil Type	**S & C (1993)**	**Summary of Others**
Clay	1.0 to 5	1.7 to 7
Silt		2.5
Alluvium		3.5 to 12
Sand	0.5 to 2	1.7 to 6

The use of D_i, % is consistent with the S & C (1993) reference, but for use in such as Eq. (20-4), D_i is a decimal, i.e., 1.0/100 = 0.01, 5/100 = 0.05, etc. The values in the table above are suggested for the vertical-mode damping ratio D_z. Values will seldom be the same for sliding (D_x or D_y) and rotational (D_θ) modes.

20-6 UNBALANCED MACHINE FORCES

The unbalanced forces from the machinery, engines, or motors and their location with respect to some reference point from the machine base are required. The manufacturer must supply

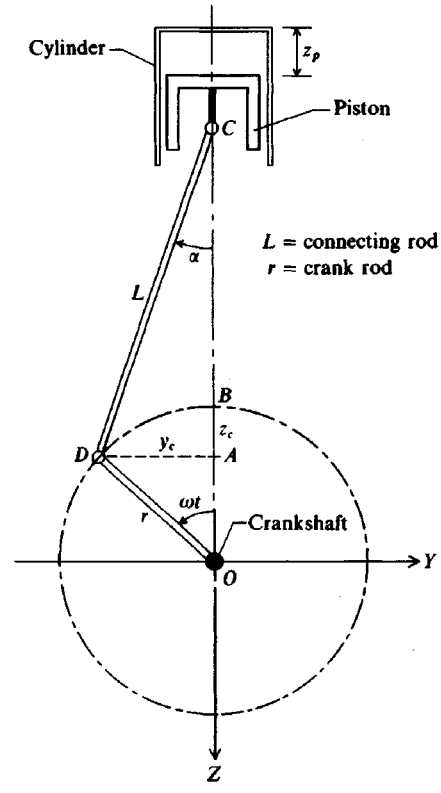

Figure 20-9 Moving parts of a single-cylinder engine producing unbalanced frequency-dependent forces.

this information for machinery and motors. The project engineer would have to obtain it in some manner if the vibrations are from wind gusts and such.

To illustrate the concept of an engine producing both primary and secondary forces we will briefly examine the single-cylinder engine idealized in Fig. 20-9. We define z_p = downward displacement of the piston from zero (when $\omega t = 0$) at top dead center; maximum z_p occurs at $\omega t = \pi$ rad counterclockwise. At any time t we have for ωt as shown

$$z_p = r(1 - \cos \omega t) + L(1 - \cos \alpha)$$

but $\alpha = f(\omega t)$ since y_c is common to both r and L so that

$$\sin \alpha = \frac{r}{L} \sin \omega t$$

Using a number of trigonometric relationships [see Den Hartog (1952)], we finally obtain

$$\left.\begin{aligned} z_p &= \left(r + \frac{r^2}{4L}\right) - r\left(\cos \omega t + \frac{r}{4L} \cos 2\omega t\right) \\ \dot{z}_p &= r\omega \left(\sin \omega t + \frac{r}{2L} \sin 2\omega t\right) \\ \ddot{z}_p &= r\omega^2 \left(\cos \omega t + \frac{r}{L} \cos 2\omega t\right) \end{aligned}\right\} \qquad (20\text{-}18)$$

A similar exercise can be done for the crank to obtain

$$\left.\begin{aligned} y_c &= -r\sin\omega t & z_c &= r(1-\cos\omega t) \\ \dot{y}_c &= -r\omega\cos\omega t & \dot{z}_c &= r\omega\sin\omega t \\ \ddot{y}_c &= r\omega^2\sin\omega t & \ddot{z}_c &= r\omega^2\cos\omega t \end{aligned}\right\} \tag{20.19}$$

Designating the mass of the piston plus a part of the connecting rod as the vertical reciprocating mass m_{rec} concentrated at point C and that of the crank plus the remainder of the connecting rod as the rotating mass m_{rot} concentrated at D, we obtain the unbalanced forces as

Vertical:
$$F_z = m_{\text{rec}}\ddot{z}_p + m_{\text{rot}}\ddot{y}_c$$
$$F_z = (m_{\text{rec}} + m_{\text{rot}})r\omega^2\cos\omega t + m_{\text{rec}}\frac{r^2\omega^2}{L^2}\cos 2\omega t \tag{20-20}$$

Horizontal:
$$F_y = m_{\text{rot}}\ddot{y}_c = m_{\text{rot}}r\omega^2\sin\omega t \tag{20-21}$$

From these forces we have in Eq. (20-20) two parts:

A primary force:
$$= (m_{\text{rec}} + m_{\text{rot}})r\omega^2\cos\omega t$$

A secondary force:
$$= m_{\text{rec}}\frac{r^2\omega^2}{L^2}\cos 2\omega t$$

These are vertical primary and secondary forces and are a maximum at $\omega t = 2\omega t = 0$ and multiples of π so that the cosine term $= 1$ with the same sign. Note that these forces are frequency-dependent, so the forces are larger at, say, 3000 r/min (rpm) than at 2000 rpm.

Equation (20-21) gives a horizontal primary force; there is no secondary force because there is only one term. This force is a maximum at $\omega t = \pi/4, 5\pi/4$, etc., and will be at some distance $\bar{y}$ above the center of the base-ground interface and will therefore produce a rocking moment about the x axis (which is perpendicular to the plane of the paper and passes through point O of Fig. 20-9). In this case the horizontal force produces both a sliding mode and a rocking mode. As we will see in the next section these two modes are generally interdependent or *coupled.*

Most motors have more than one cylinder, and manufacturers attempt to keep the unbalanced forces small (use small r and masses; have one crank rotate counterclockwise while another is rotating clockwise, etc.). Although it is possible to minimize the unbalanced forces and resulting rocking moments they are never completely eliminated.

Computational procedures can be used to obtain the unbalanced forces but as this simple example illustrates the work is formidable (for example, how does one allocate L between m_{rot} and m_{rec}?). For this reason equipment manufacturers use electronic data acquisition equipment such as displacement transducers and accelerometers located at strategic points on the machinery to measure displacements and accelerations at those points for several operational frequencies (or rpm's). These data can be used to back-compute the forces since the total machine mass can be readily obtained by weighing. Using these methods, we can directly obtain the unbalanced forces without using the mass of the several component parts.

These data should be requested from the manufacturer in order to design the equipment base for any vibration control. We should also note that in case the base does not function as intended (vibrations too large or machinery becomes damaged) it is usual to put displacement transducers and accelerometers on the installation to ascertain whether the foundation was improperly designed or whether the manufacturer furnished incorrect machinery data.

20-7 DYNAMIC BASE EXAMPLE

Now that we have identified the soil properties and machine forces and other data needed to solve Eq. (20-4*a*) or (20-4*b*) we can use this information for the following example.

Example 20-1. Use the computer program FADDYNF1 on your computer diskette and data set EXAM201.DTA and obtain the six displacements for the base as shown in Fig. E20-1*a*. Note that rocking modes will be about the center of area both in plan and elevation (B, L, $T_b/2$). The following data are given:

Soil:	$G' = 239\,400$ kPa	
Damping factor:	$D_i = 0.05$	(estimated—see Sec 20-5.3; same for all modes)
	$\gamma_s = 19.65$ kN/m^3	
	$\mu = 0.333$	(estimated)
Machine:	rpm = 900	(operating speed)

For purposes of illustration we will only use the primary forces.

$F_{ox} = 45$ kN $= F_{oy}$	(horizontal for sliding)
$F_{oz} = 90$ kN	(vertical)
$M_{ox} = 20.3$ kN · m	(about x axis)
$M_{oy} = 27.1$ kN · m	(about y axis)
$M_{oz} = 33.9$ kN · m	(about z axis)

Solution. Compute the remaining parameters. Note that we will only make a solution for the operating speed of 900 rpm for cases 2 through 7 (Example 20-1*a–f* on your diskette file EXAM201.DTA). The special case of Example 20-1*a* is provided to illustrate the case of frequency-dependent forces. In this case we have a frequency-dependent vertical force $F_o = 90$ kN at 900 rpm. In these examples we are not inputting any secondary forces or secondary moments—although they usually exist

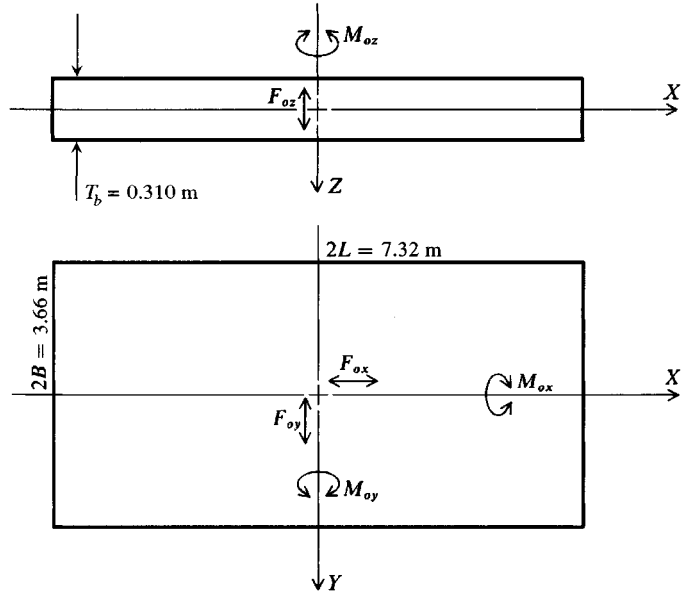

Figure E20-1*a*

```
    EXAMPLE 20-1A-A  VERTICAL MODE   FZ = 90 KN

          DISK DATA FILE USED FOR THIS EXECUTION:  EXAM201.DTA

 VIBRATION MODE = VERT
 FORCE TYPE (FO = 1; M*E = 2) = 1          IMET (SI > 0) = 1

 BASE DATA:
   DIMENSIONS:  B =     3.660   L =     7.320 M
   INERTIA:  IX =      29.9  IY =     119.6  JT =     149.5 M**4
   ACTUAL BASE AREA =   26.80 SQ M
 SOIL DATA:
   GS =  239400.0 KPA  XMU = .330
   SHEAR WAVE VELOCITY, VS =     346.0 M/S
   SOIL DENSITY ,RHO =  2.00000   KN-SEC**2/M**4
   SOIL MATERIAL DAMPING, BETA =  .05

 STARTING, ENDING AND RPM INCREMENT =  900.  900.    0.

 ROTATIONAL MASS MOMENT OF INERTIA OF BASE, IPSI =      .000   KN-SEC**2-M
 MASS OF BLOCK + MACHINE = 19.99000   KN-SEC**2/M

 INPUT PRIMARY AND SECONDARY FORCES, FORCP, FORCS =  90.000     .000   KN
 INPUT PRIMARY AND SECONDARY MOMENTS, MOPR, MOSEC =    .000     .000 KN-M


      STATIC SPRING =  .43049E+07 KN-M
    NATURAL FREQ WN =  464.064 RAD/SEC
CRITICAL DAMPING CC =  .18553E+05   KN-SEC/M
          MASS USED =    19.990   KN-SEC*2/M
          DR (C/CC) = 2.*SQRT(SPRING*MASS)/CC

 RPM    SPRING       DAMPING    FREQ W   W/WN     C/CC     YP/YS    YP,MM
900.  .39960E+07       34044.    94.2    .203     .963     .966   .20189E-01


     EXAMPLE 20-1A  VERTICAL MODE   FZ = 90 KN AT RPM = 900

          DISK DATA FILE USED FOR THIS EXECUTION:  EXAM201.DTA

 VIBRATION MODE = VERT
 FORCE TYPE (FO = 1; M*E = 2) = 2          IMET (SI > 0) = 1

 BASE DATA:
   DIMENSIONS:  B =     3.660   L =     7.320 M
   INERTIA:  IX =      29.9  IY =     119.6  JT =     149.5 M**4
   ACTUAL BASE AREA =   26.80 SQ M
 SOIL DATA:
   GS =  239400.0 KPA  XMU = .330
   SHEAR WAVE VELOCITY, VS =     346.0 M/S
   SOIL DENSITY ,RHO =  2.00000   KN-SEC**2/M**4
   SOIL MATERIAL DAMPING, BETA =  .05

 STARTING, ENDING AND RPM INCREMENT =  800. 1000.  100.

 ROTATIONAL MASS MOMENT OF INERTIA OF BASE, IPSI =      .000   KN-SEC**2-M
 MASS OF BLOCK + MACHINE = 19.99000   KN-SEC**2/M

 INPUT PRIMARY AND SECONDARY FORCES, FORCP, FORCS =  90.000     .000   KN
 INPUT PRIMARY AND SECONDARY MOMENTS, MOPR, MOSEC =    .000     .000 KN-M

      OPERATING MACHINE SPEED, RPMO =   900. RPM


      STATIC SPRING =  .43049E+07 KN-M
    NATURAL FREQ WN =  464.064 RAD/SEC
CRITICAL DAMPING CC =  .18553E+05   KN-SEC/M
          MASS USED =    19.990   KN-SEC*2/M
          DR (C/CC) = 2.*SQRT(SPRING*MASS)/CC

 RPM    SPRING       DAMPING    FREQ W   W/WN     C/CC     YP/YS    YP,MM
800.  .40415E+07       34606.    83.8    .181     .969     .972   .16057E-01
900.  .39960E+07       34044.    94.2    .203     .963     .966   .20189E-01
1000.  .39482E+07      33591.   104.7    .226     .958     .959   .24749E-01
```

Figure E20-1*a*

in most rotating equipment. If you have any, you would input them when asked by the program when the data file is first being built.

When F_o is of the form $F = F_o \sin \omega t$, it is only necessary to look at the maximum F_o that occurs at $\omega t = \pi/2$ and the program option control parameter IFORC = 1 (it is 2 for Example 20-1*a*).

In most real cases we would probably set the range of rpm from about 100 or 200 up to about 1200, which includes the operating speed. This is usually necessary since no machine suddenly starts spinning at 900 rpm with a constant force F_o; it is possible an rpm rate between 0 and 900 produces a larger displacement than one at 900 rpm (i.e., resonance with damping occurs). Note how the data were set up for Example 20-1*a*. One can write

$$F_o = 2m_e \bar{y} \omega^2$$

but this expression is equivalent to the following:

$$F_{o,i} = F_{o,\max} \left(\frac{\text{rpm}_i}{\text{rpm}_o} \right)^2$$

and the operating rpm are required input for this case (as is shown on the output sheet).

Foundation parameters.

Ratio $L/B = 2L/2B = 7.32/3.66 = 2.00$

(falls on all curves and equations for easy reader checking without interpolation)

$$B/L = 1.83/3.66 = 0.5$$

$$\text{Base area } A = 2B \times 2L = 3.66 \times 7.32 = 26.8 \text{ m}^2$$

$$J_a = \frac{A}{4L^2} = \frac{26.8}{4 \times 3.66^2} = \mathbf{0.5} \qquad \text{(as on Fig. 20-6)}$$

$$I_x = \frac{bh^3}{12} = \frac{7.32 \times 3.66^3}{12} = \mathbf{29.91} \text{ m}^4$$

$$I_y = \frac{hb^3}{12} = \frac{3.66 \times 7.32^3}{12} = \mathbf{119.6} \text{ m}^4$$

$$J = I_x + I_y = 29.91 + 119.6 = \mathbf{149.51} \text{ m}^4$$

We will use a concrete base ($\gamma_c = 23.6$ kN/m^3) with a thickness $T_b = 0.31$ m. Then

$$\text{Base mass } m_b = V_b \gamma_c / g = 3.66 \times 7.32 \times 0.31 \times 23.6/9.807 = \mathbf{19.99} \text{ kN} \cdot \text{s}^2/\text{m}$$

Moments. We must compute the rotational mass moments of inertia using equations from Table 20-1. About the x axis use dimensions perpendicular to axis; since these are through the geometric (and in this case the mass) center, all rocking will be with respect to the center of mass:

$$I_{\theta x} = \frac{m}{12}(a^2 + B^2) = \frac{19.99}{12}(0.31^2 + 3.66^2) = \mathbf{22.47} \text{ kN} \cdot \text{m}^3 \cdot \text{s}^2$$

$$I_{\theta y} = \frac{m}{12}(a^2 + L^2) = \frac{19.99}{12}(0.31^2 + 7.32^2) = \mathbf{89.42} \text{ kN} \cdot \text{m}^3 \cdot \text{s}^2$$

$$I_{\theta z} = \frac{m}{12}(B^2 + L^2) = \frac{19.99}{12}(3.66^2 + 7.32^2) = \mathbf{111.57} \text{ kN} \cdot \text{m}^3 \cdot \text{s}^2$$

We will use m and the just-computed $I_{\theta i}$ values in the mass term of Eq. (20-4*a*).

```
     EXAMPLE 20-1B  SLIDING MODE--PARALLEL TO X-AXIS  IDIRS = 1

          DISK DATA FILE USED FOR THIS EXECUTION:  EXAM201.DTA

 VIBRATION MODE = SLID
 FORCE TYPE (FO = 1; M*E = 2) = 1          IMET (SI > 0) = 1

 SLIDING PARALLEL TO LENGTH DIMENSION

 BASE DATA:
   DIMENSIONS:  B =     3.660   L =     7.320 M
   INERTIA:  IX =      29.9  IY =     119.6  JT =     149.5 M**4
   ACTUAL BASE AREA =   26.80 SQ M
 SOIL DATA:
   GS =  239400.0 KPA  XMU = .330
   SHEAR WAVE VELOCITY, VS =     346.0 M/S
   SOIL DENSITY ,RHO =  2.00000   KN-SEC**2/M**4
   SOIL MATERIAL DAMPING, BETA =  .05

 STARTING, ENDING AND RPM INCREMENT =  900.  900.    0.

 ROTATIONAL MASS MOMENT OF INERTIA OF BASE, IPSI =     .000   KN-SEC**2-M
 MASS OF BLOCK + MACHINE = 19.99000   KN-SEC**2/M

 INPUT PRIMARY AND SECONDARY FORCES, FORCP, FORCS =  45.000    .000   KN
 INPUT PRIMARY AND SECONDARY MOMENTS, MOPR, MOSEC =    .000    .000 KN-M


      STATIC SPRING =  .36291E+07 KN-M
   NATURAL FREQ WN =  426.079 RAD/SEC
CRITICAL DAMPING CC =  .17035E+05   KN-SEC/M
         MASS USED =    19.990   KN-SEC**2/M
         DR (C/CC) = 2.*SQRT(SPRING*MASS)/CC

 RPM     SPRING       DAMPING    FREQ W   W/WN     C/CC     YP/YS    YP,MM
900.  .33323E+07       20116.     94.2    .221     .958     .960   .11908E-01
```

Figure E20-1b

Soil parameters.

$$\rho = \frac{\gamma_s}{g} = \frac{19.65}{9.807} = 2.00 \text{ kN} \cdot \text{s}^2/\text{m}^4$$

The shear velocity [using Eq. (20-15)] is

$$V_s = \sqrt{\frac{G'}{\rho}} = \sqrt{\frac{239\,400}{2.0}} = \mathbf{346} \text{ m/sec}$$

Computations. The preceding computed items are required for input to create the data file EXAM201.DTA on your diskette, which is executed to produce Fig. E20-1*b* for the six different d.o.f.

The program computes the following frequency parameters but they are also computed here so you can see how the computations are made:

$$f = \frac{\text{rpm}}{60} = \frac{900}{60} = \mathbf{15} \text{ Hz}$$

$$\omega = 2\pi f = 2\pi \times 15 = \mathbf{94.3} \text{ rad/s}$$

$$a_o = \frac{\omega B}{V_s} = \frac{4.3 \times 1.83}{346} = \mathbf{0.4985} \qquad \text{(Note: } B = B/2 = 3.66/2 = 1.83 \text{ m)}$$

Let us check selected values shown on the output sheet for EXAMPLE 20-1A.

Figure 20-1*b* *(continued)*

```
      EXAMPLE 20-1C  SLIDING MODE--PARALLEL TO Y-AXIS  IDIRS = 2

            DISK DATA FILE USED FOR THIS EXECUTION:  EXAM201.DTA

 VIBRATION MODE = SLID
 FORCE TYPE (FO = 1; M*E = 2) = 1          IMET (SI > 0) = 1

 SLIDING PARALLEL TO WIDTH  DIMENSION

 BASE DATA:
   DIMENSIONS:  B =     3.660   L =     7.320 M
   INERTIA:  IX =      29.9  IY =     119.6  JT =     149.5 M**4
   ACTUAL BASE AREA =   26.80 SQ M
 SOIL DATA:
   GS =  239400.0 KPA  XMU = .330
   SHEAR WAVE VELOCITY, VS =     346.0 M/S
   SOIL DENSITY ,RHO =  2.00000   KN-SEC**2/M**4
   SOIL MATERIAL DAMPING, BETA =  .05

 STARTING, ENDING AND RPM INCREMENT =  900.  900.    0.

 ROTATIONAL MASS MOMENT OF INERTIA OF BASE, IPSI =     .000   KN-SEC**2-M
 MASS OF BLOCK + MACHINE = 19.99000   KN-SEC**2/M

 INPUT PRIMARY AND SECONDARY FORCES, FORCP, FORCS =  45.000    .000   KN
 INPUT PRIMARY AND SECONDARY MOMENTS, MOPR, MOSEC =    .000    .000 KN-M


      STATIC SPRING =  .36291E+07 KN-M
    NATURAL FREQ WN =  426.079 RAD/SEC
 CRITICAL DAMPING CC =  .17035E+05   KN-SEC/M
          MASS USED =    19.990   KN-SEC*2/M
          DR (C/CC) = 2.*SQRT(SPRING*MASS)/CC

 RPM    SPRING      DAMPING    FREQ W   W/WN     C/CC     YP/YS    YP,MM
900.  .35999E+07      22831.    94.2    .221     .996     .954   .11830E-01
     EXAMPLE 20-1D  ROCKING MODE--ABOUT Y-AXIS  IDIRR = 1

            DISK DATA FILE USED FOR THIS EXECUTION:  EXAM201.DTA

 VIBRATION MODE = ROCK
 FORCE TYPE (FO = 1; M*E = 2) = 1          IMET (SI > 0) = 1

 ROCKING RESISTED BY LENGTH DIMENSION

 BASE DATA:
   DIMENSIONS:  B =     3.660   L =     7.320 M
   INERTIA:  IX =      29.9  IY =     119.6  JT =     149.5 M**4
   ACTUAL BASE AREA =   26.80 SQ M
 SOIL DATA:
   GS =  239400.0 KPA  XMU = .330
   SHEAR WAVE VELOCITY, VS =     346.0 M/S
   SOIL DENSITY ,RHO =  2.00000   KN-SEC**2/M**4
   SOIL MATERIAL DAMPING, BETA =  .05

 STARTING, ENDING AND RPM INCREMENT =  900.  900.    0.

 ROTATIONAL MASS MOMENT OF INERTIA OF BASE, IPSI =   89.420   KN-SEC**2-M
 MASS OF BLOCK + MACHINE = 19.99000   KN-SEC**2/M

 INPUT PRIMARY AND SECONDARY FORCES, FORCP, FORCS =    .000    .000   KN
 INPUT PRIMARY AND SECONDARY MOMENTS, MOPR, MOSEC =  27.100    .000 KN-M


      STATIC SPRING =  .41352E+08 KN-M/RAD
    NATURAL FREQ WN =  680.035 RAD/SEC
 CRITICAL DAMPING CC =  .12162E+06   KN-SEC/M
          MASS USED =    89.420   KN-SEC*2/M
          DR (C/CC) = 2.*SQRT(SPRING*MASS)/CC

 RPM    SPRING      DAMPING    FREQ W   W/WN     C/CC     YP/YS    YP,RADS
900.  .33709E+08      82096.    94.2    .139     .903     .988   .64744E-06
```

Figure 20-1*b* *(continued)*

```
      EXAMPLE 20-1E  ROCKING MODE--ABOUT X-AXIS  IDIRR = 2

            DISK DATA FILE USED FOR THIS EXECUTION:  EXAM201.DTA

 VIBRATION MODE = ROCK
 FORCE TYPE (FO = 1; M*E = 2) = 1          IMET (SI > 0) = 1

 ROCKING RESISTED BY WIDTH  DIMENSION

 BASE DATA:
   DIMENSIONS:  B =     3.660   L =     7.320 M
   INERTIA:  IX =      29.9  IY =     119.6  JT =     149.5 M**4
   ACTUAL BASE AREA =   26.80 SQ M
 SOIL DATA:
   GS =  239400.0 KPA  XMU = .330
   SHEAR WAVE VELOCITY, VS =     346.0 M/S
   SOIL DENSITY ,RHO =  2.00000   KN-SEC**2/M**4
   SOIL MATERIAL DAMPING, BETA =  .05

 STARTING, ENDING AND RPM INCREMENT =  900.  900.    0.

 ROTATIONAL MASS MOMENT OF INERTIA OF BASE, IPSI =   22.470   KN-SEC**2-M
 MASS OF BLOCK + MACHINE = 19.99000   KN-SEC**2/M

 INPUT PRIMARY AND SECONDARY FORCES, FORCP, FORCS =    .000    .000   KN
 INPUT PRIMARY AND SECONDARY MOMENTS, MOPR, MOSEC =  20.300    .000 KN-M


      STATIC SPRING =  .10341E+08 KN-M/RAD
   NATURAL FREQ WN =  678.378 RAD/SEC
CRITICAL DAMPING CC =  .30486E+05   KN-SEC/M
         MASS USED =    22.470   KN-SEC*2/M
         DR (C/CC) = 2.*SQRT(SPRING*MASS)/CC

 RPM    SPRING      DAMPING    FREQ W   W/WN     C/CC     YP/YS    YP,RADS
900.  .95886E+07      16596.    94.2    .139     .963     .984   .19312E-05
     EXAMPLE 20-1F  TORSION MODE MODE--ABOUT Z-AXIS

            DISK DATA FILE USED FOR THIS EXECUTION:  EXAM201.DTA

 VIBRATION MODE = TORS
 FORCE TYPE (FO = 1; M*E = 2) = 1          IMET (SI > 0) = 1

 BASE DATA:
   DIMENSIONS:  B =     3.660   L =     7.320 M
   INERTIA:  IX =      29.9  IY =     119.6  JT =     149.5 M**4
   ACTUAL BASE AREA =   26.80 SQ M
 SOIL DATA:
   GS =  239400.0 KPA  XMU = .330
   SHEAR WAVE VELOCITY, VS =     346.0 M/S
   SOIL DENSITY ,RHO =  2.00000   KN-SEC**2/M**4
   SOIL MATERIAL DAMPING, BETA =  .05

 STARTING, ENDING AND RPM INCREMENT =  900.  900.    0.

 ROTATIONAL MASS MOMENT OF INERTIA OF BASE, IPSI =  111.570   KN-SEC**2-M
 MASS OF BLOCK + MACHINE = 19.99000   KN-SEC**2/M

 INPUT PRIMARY AND SECONDARY FORCES, FORCP, FORCS =    .000    .000   KN
 INPUT PRIMARY AND SECONDARY MOMENTS, MOPR, MOSEC =  33.900    .000 KN-M


      STATIC SPRING =  .39003E+08 KN-M/RAD
   NATURAL FREQ WN =  591.259 RAD/SEC
CRITICAL DAMPING CC =  .13193E+06   KN-SEC/M
         MASS USED =   111.570   KN-SEC*2/M
         DR (C/CC) = 2.*SQRT(SPRING*MASS)/CC

 RPM    SPRING      DAMPING    FREQ W   W/WN     C/CC     YP/YS    YP,RADS
900.  .35276E+08      69545.    94.2    .159     .951     .980   .85156E-06
```

Using Table 20-2, we obtain

$$K_z = s_z \frac{2LG'}{1-\mu}$$

and from Table 20-3

$$S_z = 0.73 + 1.54 J_a^{0.75}$$

Solving, we find $S_z = 0.73 + 1.54 \times 0.5^{0.75} = \mathbf{1.646}$. We were given that also $\mu = 0.333$; $G' = .23964E+6$; and $2L = 7.32$ m. By substitution,

$$K_z = 1.646 \times \frac{7.32 \times 239\,400}{1 - 0.333} = 0.432445\text{E+7 (output} = 0.43049\text{E+7)}$$

Large numbers will produce minor internal computer rounding errors, and with so many values having been estimated double precision is too much computational accuracy.

From Eq. (20-1) we compute

$$\omega_n = \sqrt{\frac{K_z}{m}} = \sqrt{\frac{.43245\text{E+7}}{19.99}} = 465 \text{ (output} = 464.06) \text{ rad/s}$$

We can also compute

$$c_c = 2\sqrt{K_z m} = 2\sqrt{.43245\text{E+7} \times 19.99} = .18595\text{E+5 (output} = .18553\text{E+5)}$$

From Eq. (20-2) we obtain the damping ratio $D_i = c/c_c$(= computer variable DR) using the computer-generated K_z for 900 rpm, giving

$$\text{DR} = \frac{c}{c_c} = \frac{2\sqrt{.39960\text{E+7} \times 19.99}}{.18553\text{E+5}} = \mathbf{0.963}$$

and

$$\frac{\omega_d}{\omega_n} = \frac{94.2}{464.06} = \mathbf{0.203}$$

$$Y_s = \frac{P_v}{K_{z,s}} = \frac{90.0}{.43049\text{E+7}} = .20906\text{E}-4 \text{ m}$$

$$= .020906 \text{ mm}$$

Dynamic displacement Y_p must be computed using Eq. (20-4*b*); dynamic springs, using $\overline{K}_z = \eta_i K_i$; and damping constants, using $\overline{c}_i = \lambda_i c_i$ [see Eqs. (20-9) and (20-10)]. These dynamic values are then used in Eq. (20-4*b*) to find $z_i/(F_o/K_z) = V = Y_p/Y_s$ and $Y_p = VY_s$, with both values shown on the output sheet.

If you check Fig. E20-1*b* for the output labeled Example 20-1A you will find that the several "constants" and the line of data for 900 rpm are exactly the same as in Example 20-1A-A even though the program computed first for 800 rpm. This small check demonstrates that the program is working correctly. Also since 1000 rpm gives a larger vertical displacement, it would appear the resonance frequency is above 900 rpm.

////

20-8 COUPLED VIBRATIONS

Figure 20-10*a* is a machine on a base with the *center of mass* (or center of gravity = cg) as shown. At the crankshaft a distance of z_o above the base we have a horizontal force $F_y =$

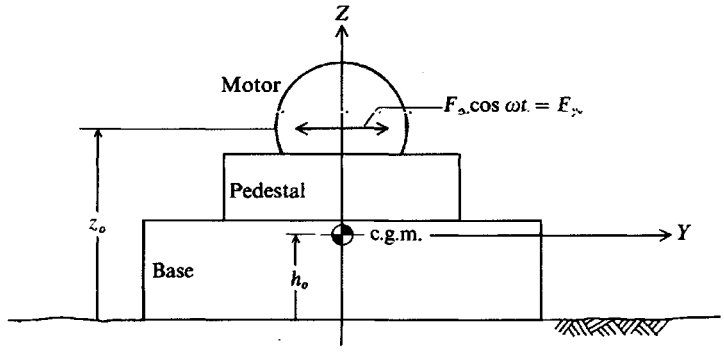

(*a*) Motor and base.

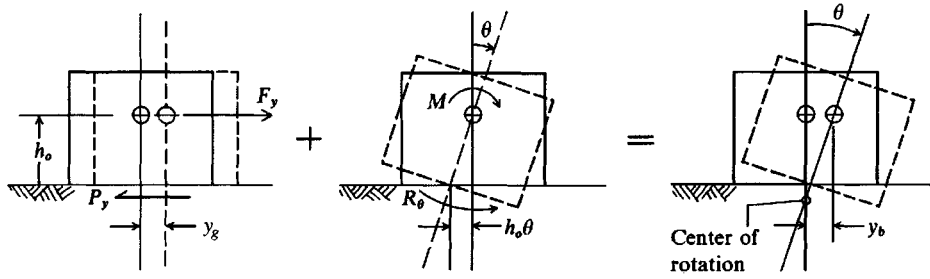

(*b*) The equivalent of (*a*) and using superposition of effects.

Figure 20-10 Coupled sliding and rocking.

$F_o \cos \omega t$. It is evident that this force produces both translation and rocking about the x axis through the c.g.m. From use of the transfer formula at the cg we have

$$F_y = F_o \cos \omega t$$
$$M = (z_o - h_o)F_y$$

The base is usually used as a reference (or the top of the base or the top of the pedestal) to locate the center of mass of the component parts and locate the unbalanced machine forces.

With the cg located and the forces F_y and M acting, we can replace the system with the block base of Fig. 20-10*b*. From the figure geometry we can write by inspection the base movement (needed since this is what develops base-to-soil resistance) y_b from the translation at the cg of y_g as

$$y_b = y_g - h_o\theta = \text{net base translation}$$
$$\dot{y}_b = \dot{y}_g - h_o\dot{\theta} \qquad (a)$$

The net base translation y_b produces a sliding resistance P_y as

$$P_y = c_y\dot{y}_b + K_y y_b \qquad (b)$$

The base rotational resistance (*and using single subscripts to simplify the equations but noting* θ *should be interpreted as* θ_y*, for example,* I_θ *is actually* $I_{\theta y}$) is as for uncoupled cases

$$R_\theta = c_\theta\dot{\theta} + K_\theta\theta \qquad (c)$$

Summing horizontal forces through the cg, we have

$$m\ddot{y}_g + P_y = F_y \tag{d}$$

Summing moments about the cg and noting the base resistance P_y produces an additional moment to consider, we obtain

$$I_\theta\ddot{\theta} + R_\theta - h_o P_y = M \tag{e}$$

Now substituting for P_y, R_θ, y_b, and $\dot{y}_b$, we obtain

$$my_g + c_y\dot{y}_g + K_y y_g - h_o(K_y\theta + c_y\dot{\theta}) = F_o\cos\omega t \tag{20-22}$$

$$I_\theta\ddot{\theta} + (c_\theta + h_o^2 c_y)\dot{\theta} + (K_\theta + h_o^2 K_y)\theta - h_o(c_y\dot{y}_g + K_y y_g) = M \tag{20-23}$$

Coupling can now be identified from all terms containing h_o. If $h_o = 0$ these two equations would reduce to the basic (or uncoupled) form of Eq. (*f*) of Sec. 20-2. Also note that a vertical force anywhere on the base is not coupled to rocking even if it produces a moment from eccentricity with respect to the cg. If the presence of h_o produces coupling, the effects evidently reduce with h_o and was the reason for analyzing Example 20-1 using a 0.31 m thick base giving $h_o \cong 0.155$ m.

Also note that the moment and F_y are always in phase (act so results are cumulative). In this case the center of rotation would always be below the cg. If they are out of phase the center of rotation will lie somewhere along a vertical line through the cg and may be above this point depending on the relative magnitude of the translation and moment forces.

With rocking taking place about the cg you will have to use the transfer formula (shown on Fig. 20-1) when computing $I_{\theta i}$ as necessary. For example, $I_{\theta y}$ and $I_{\theta x}$ of Fig. 20-10*b* will require use of the transfer formula component md^2, and it is possible that $I_{\theta z}$ will require its use as well. The axis subscript is *about* that axis, not parallel with it.

With reference to Eqs. (20-22) and (20-23) it is convenient to write the displacements in complex form ($e = 2.71828\ldots$) as follows:

Force	Rotation
$y_g = (X_1 + iX_2)e^{i\omega t}$	$\theta = (X_3 + iX_4)e^{i\omega t}$
$\dot{y}_g = \omega(iX_1 - X_2)e^{i\omega t}$	$\dot{\theta} = \omega(iX_3 - X_4)e^{i\omega t}$
$\ddot{y}_g = -\omega^2(X_1 + iX_2)e^{i\omega t}$	$\ddot{\theta} = -\omega^2(X_3 + iX_4)e^{i\omega t}$

The process of substituting these displacement functions into Eqs. (20-22) and (20-23), simplifying, and collecting real and imaginary terms for Eq. (20-22) gives two equations in the four values of X_i. Similarly, the real and imaginary terms of Eq. (20-23) give two equations in the four values of X_i. These equations are given as follows:

$$\left.\begin{aligned}
(K_y - m\omega^2)X_1 - c_y\omega X_2 - h_o K_y X_3 + h_o c_y\omega X_4 &= F_y \quad \text{(real part)}\\
c_y\omega X_1 + (K_y - m\omega^2)X_2 - h_o c_y\omega X_3 - h_o K_y X_4 &= 0 \quad \text{(imag. part)}\\
-h_o K_y X_1 + h_o c_y\omega X_2 + (h_o^2 K_y + K_\theta - I_\theta\omega^2)X_3 & \\
-(h_o^2 c_y\omega + c_\theta\omega)_4 &= M \quad \text{(real part)}\\
-h_o c_y\omega X_1 - h_o K_y X_2 + (h_o^2 c_y\omega + c_\theta\omega)X_3 & \\
+ (h_o^2 K_y + K_\theta - I_\theta\omega^2)X_4 &= 0 \quad \text{(imag. part)}
\end{aligned}\right\} \tag{20-24}$$

These equations can be programmed to give the unknowns X_i, which are then used to obtain the displacements (noting the complex definition of displacements) as

$$y_g = \sqrt{X_1^2 + X_2^2} \qquad \theta = \sqrt{X_3^2 + X_4^2} \tag{20-25}$$

Note X_1, X_2 = translations of m, ft, etc. and X_3, X_4 = rotations in radians. Since the springs and damping constants are frequency-dependent it is usually necessary to cycle the problem using the range of values of ω from 0 to somewhat above the operating frequency ω_o (or rpm) for the "worst" case.

Secondary forces that are out of phase will require a second computer analysis with the rotations and displacements summed with the primary values and giving careful attention to signs. In-phase secondary forces (or select in-phase values) can simply be added to the primary forces for direct analysis.

A Computer Program

The computer program used in Example 20-1 was modified (see B-29) with some effort for allowing a coupling analysis.

20-9 EMBEDMENT EFFECTS ON DYNAMIC BASE RESPONSE

The previous methods of analysis considered the dynamic base on the ground surface. Most bases supporting machinery will be embedded some depth into the ground so as to be founded on more competent soil below the zone of seasonal volume change.

It is generally accepted from both a theoretical analysis and field measurements that placing the base into the ground affects the system response to excitation forces. It appears that embedment tends to increase the resonant frequency and may decrease the amplitude.

Several methods to account for vertical vibration exist, including those of Novak and Beredugo (1972), Dobry and Gazetas (1985), and as attributed to Whitman by Arya et al. (1979). Those of Novak and Beredugo and in Arya et al. are for round bases and will not be used here since rectangular base response is substantially different.

The Arya et al. (1979) reference is the only one the author located purporting to allow for rocking and sliding as well as vertical excitation. It is suggested, however, that rocking and sliding spring adjustments for depth should be used cautiously—if at all—for these reasons:

1. Rocking of the base into the side soil may produce a gap over time.
2. Sliding of the base into the side soil may produce gaps over time.
3. The space around the base would have to be carefully backfilled and compacted to provide any appreciable side resistance unless the excavation was excavated and the base poured without using concrete forms.
4. It is not uncommon, where wooden concrete forms are used, to leave them in place.
5. A slight adjustment for depth is automatically accounted for since the effective normal stress at a depth is larger [see Eqs. (20-12) through (20-13)] so that G' is larger. This in turn increases the computed soil springs.

The method given by Dobry and Gazetas (1985) is suggested, however, for the vertical vibration mode spring, as it is both rational and applicable to rectangular- (and other-) shaped bases. Referring to Fig. 20-11, we may define the vertical dynamic spring as the product of

$$K_z' = K_z \times \kappa_{\text{tre}} \times \kappa_{\text{wall}} \tag{20-26}$$

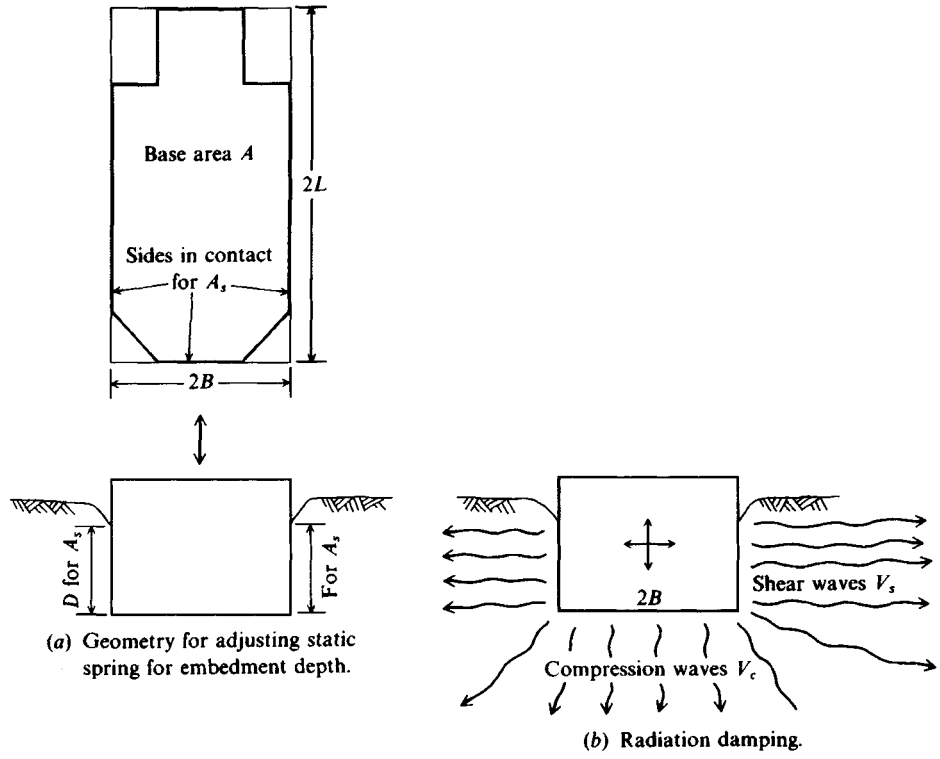

Figure 20-11 Adjustments for embedment springs and damping for vertical mode of vibration. Note: Part (*b*) may be applicable for all modes of vibration.

where K_z = static spring computed using the formula given in Table 20-2

κ_{tre} = factor > 1 from a curve-fitting scheme from the base being at the bottom of a trench (the excavation), given as

$$\kappa_{tre} = 1 + \frac{D}{21B}\left(1 + \frac{4}{3}J_a\right) \tag{20-27}$$

κ_{wall} = factor > 1 from contact of base sides against soil—either backfill or original ground given as

$$\kappa_{wall} = 1 + 0.19\left(\frac{A_s}{A}\right)^{0.67} \tag{20-28}$$

with A_s = area of sides of base in contact with side soil and gives for a rectangular base of $2B \times 2L \times T_b$

$A_s = 2T_b(2B + 2L)$ $\quad A = 2B \times 2L$

This is the more theoretical form given by the reference and is recommended as it allows adjustment in the side contact area A_s. For example, we might compute A_s and decide, based on a site study, to use only 0.25, 0.50, or some other fraction rather than the full value. For damping it is suggested to use the computed damping + addition of side damping as

$$c_z' = c_z + \rho V_s A_s \tag{20-29}$$

Example 20-2. Assume the base of Example 20-1 is 1 m in the ground. What are the revised values of the static spring and damping coefficient c_z' [which are then used to compute the dynamic value(s)]?

Solution. From the computer printout obtain the surface static spring as $K_z = .43049\text{E}+7$. Also $2B = 3.66$ m. $2L = 7.32$ m giving $J_a = 0.5$ (computed in example) and $A = 26.8$ m^2. $A_s = 2 \times 0.31 \times (3.66 + 7.32) = 6.8$ m^2. We will assume A_s is 50 percent effective so use $A_s = 3.4$ m^2.

Substituting into Eq. (20-27), we obtain for $D = 1$ m and $B = 3.66$ m

$$\kappa_{\text{tre}} = 1 + \frac{1.0}{21(3.66)}\left(1 + \frac{4}{3}(0.5)\right) = 1.02$$

Substituting into Eq. (20-28) gives

$$\kappa_{\text{wall}} = 1 + 0.19\left(\frac{3.4}{26.8}\right)^{0.67} = 1.05$$

from which the static spring adjusted for embedment is

$$K_z' = K_z \kappa_{\text{tre}} \kappa_{\text{wall}} = .43049E + 7(1.02)(1.05) = \mathbf{.46105E+7}\ \text{kN/m}$$

The damping constant, being directly additive, gives

$$\begin{aligned} c_z' &= c_z + \rho V_s A_s \qquad (\text{where } A_s = 3.4\ \text{m}^2 \text{ as previously used}) \\ &= .18553\text{E}+5 + 2 \times 346 \times 3.4 = \mathbf{.20906E+5} \end{aligned}$$

////

From Fig. 20-11 we note that the base sliding or rocking against the side soil could be similarly accommodated for damping as for the vertical mode. For spring adjustments we could do the following:

For sliding. This is equivalent to vertical vibration rotated 90°, so we might compute a horizontal spring using the vertical spring equations and place it (or a fraction) in parallel with the horizontal spring.

For rocking. This is equivalent to base rocking, so compute the side equivalent rocking value ($2B$ = base thickness rocking against side soil) and put this spring in parallel with the base rocking spring.

Springs in parallel are directly additive as

$$K_{\text{tot}} = K_1 + K_2 \tag{20-30}$$

Springs in series are

$$\frac{1}{K_{\text{tot}}} = \frac{1}{K_1} + \frac{1}{K_2} \tag{20-30a}$$

20-10 GENERAL CONSIDERATIONS IN DESIGNING DYNAMIC BASES

Experience has provided some guidelines for the analysis of foundation blocks to control vibrations. Other guides may be obtained from carefully analyzing Eq. (20-4*a*) or by making a series of parametric studies using the provided computer program. Some particular

considerations are as follows:

1. If a dynamic analysis predicts a resonance condition at the operating frequency f_o you must increase or decrease the mass or alter the spring constant. Even if the resonance amplitude is acceptable we do not want to have $f_o = f_r$. It is usually suggested to keep f_o at least ± 20 percent from f_r.
2. Try to adjust the base so the center of gravity of equipment and block are coincident. Doing this provides reasonably uniform soil pressure and static settlement.

   Proportion the base dimension for about half the allowable static soil bearing-capacity pressure. The static + dynamic pressure should not be much over 75 percent of the allowable static pressure.
4. Use as wide a base as possible to resist rocking. Try to use a width that is greater than or equal to z_o to $1.15z_o$ of Fig. 20-10*a*. Rocking about the narrow dimension will very likely produce vibration amplitudes that are too large. Also the edge pressures may be excessive, so the base eventually tilts.
5. Use a base thickness of at least 0.6 m to produce a "rigid" foundation, in line with the general theory used to develop Eq. (20-4*a*).
6. Use a machinery/block (W_m/W_b) mass ratio of 2 to 3 for centrifugal machinery and 3^+ for reciprocating equipment.
7. Try to provide a 300-mm clearance all around the machinery frame for any maintenance or other requirements.

It is seldom necessary to use high-strength concrete for vibrating bases since mass is usually more critical than strength; however, $f_c' < 21$ MPa is not recommended.

When a foundation is designed and put into service and problems develop, a question arises of what remedial action to take. Often a first step is to check if increasing the mass will solve the problem. A temporary mass increase can be made by use of sandbags placed on the block (symmetrically to maintain uniform soil pressure). Other alternatives consist in stiffening the base soil by drilling holes through the base (if not too thick) and injecting grout into the underlying soil in a zone up to about $3B$ in depth.

In many cases the problem can be solved by a combination of increasing the mass and the base area. This can be fairly easy to accomplish by simply pouring a perimeter enlargement that is well-bonded (using dowels) to the original base—often without having to take the machine out of service. Contrary to some opinion, concrete will harden while being vibrated (at low amplitudes)—and usually will have some strength gain from the greater resulting density and slightly lowered w/c ratio.

20-11 PILE-SUPPORTED DYNAMIC FOUNDATIONS

When the soil is loose or soft, or when it is necessary to alter the foundation frequency, piles may be used. Intuitively, one sees that piles provide a greater apparent soil stiffness; and for the same supported mass m it is evident from

$$\omega_n = \sqrt{\frac{K}{m}}$$

that an increase in K also increases the natural frequency ω_n of the foundation block.

The piles provide additional spring and damping contributions to the system, so some means is necessary to incorporate the significant properties of the two materials into equivalent springs and damping factors. When we do this we can then use Eq. (20-4*a*) to obtain the solution (or the coupling concepts) for that vibration mode.

There are few theories and even fewer reported data from field performance studies on full-scale dynamically loaded bases supported by pile foundations. For this reason the theories are substantially uncertain; however, rational estimates are better than simply guessing at the response.

It is generally accepted that using piles will:

1. Decrease geometric (or radiation) damping
2. Increase the resonant frequency f_r and may also increase f_n
3. Influence the amplitude near resonance
4. When laterally loaded, produce dynamic responses that are uncertain to estimate

The principal effort in dynamic pile analyses has been undertaken by and under the direction of the late Professor M. Novak at the University of Western Ontario, Canada. The basic theory is given by Novak (1974) and Novak and Howell (1977) for torsion. The dynamic pile equations of Novak (1974) are of the following general form using Novak's notation and noting $i = \sqrt{-1}$:

Horizontal and rocking: $$G'(S_{u,1} + iS_{u,2})u(z, t)dz = F(t)$$

Vertical: $$G'(S_{w,1} + iS_{w,2})w(z, t)dz = F(t)$$

The parameters $S_{i,j}$ depend on Poissons' ratio μ and $x_o = a_o\sqrt{q} = \left(r_o\omega\sqrt{q}\right)/V_s$. Terms are defined in the following list if not identified here. The term q is given as

$$q = \frac{1 - 2\mu}{2 - 2\mu}$$

From using $i = \sqrt{-1}$ we can see the $S_{u,j}$ factors are complex and in the original derivation include Hankel functions of the second kind of orders 0, 1, and 2 based on a_o and x_o.

The $S_{w,j}$ factors are also complex and include Bessel functions of order 0 and 1 based on a_o and x_o. It is convenient to program the Bessel and Hankel function computations as subroutines to obtain the $S_{i,j}$ functions without having to use charts, tables, or curve-fitting schemes. This step is done in computer program B-30.

The following list of variables are also significant problem parameters:

E_p = modulus of elasticity of pile

G' = shear modulus of soil (and depends on μ)

γ_p, γ_s = unit weights of pile material and soil, respectively

V_p, V_s = shear wave velocities in pile and soil respectively [for the pile compute $V_p = \sqrt{E_p/\rho}$; for the soil use Eq. (20-15)]

L_p/r_o = ratio of pile length L_p/effective radius of pile r_o

r_o = effective radius of pile = radius of round pile and the equivalent for a square or rectangular pile computed as $r_o = \sqrt{\text{area}/\pi}$

a_o = dimensionless frequency factor previously used but here defined as $a_o = \omega r_o \sqrt{q/V_s}$; q = Poisson ratio value previously defined; ω is same as used in Eq. (20-4)

One must use consistent units, and with a_o as a problem parameter it is evident the pile springs and damping constants will be frequency-dependent since a_o is used to obtain the $S_{i,j}$ factors.

The general solution is only practical by using a computer program to develop the necessary constants for use in the stiffness and damping constants. Novak (1974) provides a number of curves and a table of some values, but invariably a practical problem requires interpolation or falls out of the table range. The references give the necessary information so that one can produce a computer program, but it will have to be written in a computer programming language, which allows manipulation of complex variables.

Solutions are provided for all six degrees of freedom of the base with proper interpretation and for piles with the head fixed in the base and the lower end either pinned or fixed. It appears that for the pile lengths (in terms of the L_p/r_o ratio) likely to be used the fixed lower end case will occur for nearly all cases. The theoretical solutions for the fixed lower end and the pinned lower end converge at about $L_p/r_o = 25$ to 30. The solution produces factors $f_{i,i}$ that are multipliers to obtain the actual spring and damping constants. Generally these $f_{i,i}$ constants depend on the following:

Parameter	Amount of dependency
V_s/V_p	Considerable as illustrated in Table 20-6
L_p/r_o	Not much for $L_p/r_o > 25$
μ	Not much, e.g., for $V_s/V_p = 0.030$ and $L_p/r_o > 25$,

μ	$f_{18,1}$	$f_{7,1}$
0.25	0.0373	0.339
0.33	0.0373	0.345
0.40	0.0373	0.351

a_o	Substantial—particularly above 0.50

Table 20-7 lists the spring and damping constants computed using the $f_{i,i}$ constants given in Table 20-6 for a typical concrete pile.

When the spring and damping constants are computed for a single pile it is necessary somehow to concentrate the several piles to an equivalent total or global spring and damping coefficient that, together with the block mass m, are used in Eq. (20-4*a*) to compute displacement amplitudes and other data. There are conflicting opinions on how to make the summing process. Most persons agree that if the pile spacing ratio s/D is greater than 5 or 6 one can make a summation by simply adding the individual pile contributions (where the piles are all similar and there are n piles the global spring $= n \times K_{\text{pile}}$ and global damping $= n \times c_{\text{pile}}$). When the s/D ratio is less, there is opinion that corner piles contribute more than side piles and side piles contribute more than interior piles. A method suggested by Poulos (1979) has been noted by Novak (1974) and suggested by Arya et al. (1979). Others having used the Poulos (1979) method have found it does not predict

TABLE 20-6
Novak's $f_{i,i}$ values for an intermediate value of $\mu = 0.33$ for a concrete pile with $\rho_s/\rho_p = 0.7$

Values from author's computer program based on Novak (1974) and Novak and Howell (1977). Values $f_{12,i}$ are for torsion and use author's identification.
Fixed parameters: $L/r_o = 30$, $a_o = 0.3$ and for torsion $\beta = 0.10$, $\mu = 0.33$.

	Stiffness					Damping				
V_s/V_c	$f_{18,1}$	$f_{7,1}$	$f_{9,1}$	$f_{11,1}$	$f_{12,1}$	$f_{18,2}$	$f_{7,2}$	$f_{9,2}$	$f_{11,2}$	$f_{12,2}$
0.01	0.034	0.199	−0.019	0.004	0.045	0.002	0.136	−0.028	0.008	0.002
0.02	0.035	0.282	−0.038	0.010	0.072	0.007	0.198	−0.056	0.023	0.007
0.03	0.037	0.345	−0.057	0.018	0.105	0.016	0.245	−0.084	0.043	0.011
0.04	0.040	0.398	−0.076	0.027	0.139	0.027	0.283	−0.112	0.066	0.015
0.05	0.044	0.445	−0.095	0.038	0.174	0.041	0.314	−0.141	0.092	0.019
0.06	0.049	0.448	−0.114	0.050	0.208	0.055	0.346	−0.169	0.122	0.022

displacement amplitudes very well. The method does, however, consider interior piles to contribute less resistance than exterior and corner piles. Since the Poulos method does not predict very well and it is fairly computationally intensive, the author suggests either doing nothing but sum values or considering the following approach if s/D is less than about 3.5:

1. When displacement piles are driven the soil densifies in the vicinity of the pile. The densification is more concentrated at the interior of a pile group than around the exterior piles. This suggests that we should use a base factor G' for the soil (prior to the pile insertion

TABLE 20-7
Pile spring and damping constants [Novak (1974), Novak and Howell (1977)]

Mode	Spring K_1	Damping c_i
Vertical	$K_z = \frac{EA}{r_o} f_{18,1}$	$c_z = \frac{EA}{V_s} f_{18,2}$
Horizontal	$K_h = \frac{EI}{r_o^3} f_{11,1}$	$c_h = \frac{EI}{r_o^2 V_s} f_{11,2}$
Rocking	$K_\theta = \frac{EI}{r_o} f_{7,1}$	$c_\theta = \frac{EI}{V_s} f_{7,2}$
Cross-stiffness/damping		
	$K_{x\theta} = \frac{EI}{r_o^2} f_{9,1}$	$c_{x\theta} = \frac{EI}{r_o V_s} f_{9,2}$
	$K_{\theta x} = K_{x\theta}$	$c_{\theta x} = c_{x\theta}$
Torsion	$K_t = \frac{G'J}{r_o} f_{12,1}$	$c_t = \frac{G'J}{V_s} f_{12,2}$

Use consistent units for all
where E = modulus of elasticity of pile
A = cross-section as area of pile
G' = shear modulus of pile
I = moment of inertia of pile about axis to resist displacement
J = torsion (or polar) moment of inertia of pile

process) and increase it some amount for side piles (perhaps use a factor of 1.1 to 1.25). Interior piles might be increased by a factor of 1.25 to 1.5. Call this factor A.

2. Solve a typical interior pile of the group using $G'' = G'/A$, a side pile using the intermediate G'', and the corner piles using G'. Inspection of Table 20-7 indicates this action will give reduced springs and damping constants for the interior compared to the sides and corner piles.
3. Now make a summation by adding all the interior springs + all the side springs + all the corner springs to obtain the global spring. Make a similar sum for the damping.
4. Use this global spring and damping value with the block mass m in Eq. (20-4a) to obtain data for that frequency ω.

Piles also have internal damping β_d. As a first approximation we may estimate the damping ratio D on the order of 0.05 to 0.10 and use Eqs. (20-9) and (20-10) to adjust the spring and damping coefficients. A global adjustment is about the best the problem data can generally justify; however, you may make individual pile adjustments where reliable problem parameters are used.

Example 20-3. Compute the several single-pile spring and damping constants for the pile-supported block of Fig. E20-3. Use the vertical spring and damping values to compute the displacement in the vertical mode using Eq. (20-4a).

You are given these data:

Piles: precast concrete 300 × 300 mm square

$L_p = 9.1$ m (spacing s for s/D shown in Fig. E20-3)

$E_p = 27\,800$ MPa $\gamma_p = 23.6$ kN/m^3 $\mu_p = 0.15$

Soil: $G' = 17\,700$ kPa $\mu_s = 0.33$ $\gamma_s = 16.5$ kN/m^3

Other: $\omega = 179.2$ rad/sec (for current rpm)

Solution.

$$r_o = \sqrt{\frac{A_p}{\pi}} = \sqrt{\frac{0.3 \times 0.3}{\pi}} = \mathbf{0.169}\ \text{m}$$

$$L_p/r_o = 9.1/0.169 = 54 > 30 \qquad \text{(O.K. to use Table 20-6)}$$

$$V_s = \sqrt{G'/\rho_s} = \sqrt{17\,700 \times 9.807/16.5} = \mathbf{103}\ \text{m/sec}$$

$$V_p = \sqrt{E_p/\rho_p} = \sqrt{\frac{27.8\text{E+6} \times 9.807}{23.6}} = \mathbf{3400}\ \text{m/sec}$$

$$V_s/V_p = 103/3400 = 0.0303 \qquad \text{(use } \mathbf{0.030} \text{ for table)}$$

$$\rho_s/\rho_p = \gamma_s/\gamma_p = 16.50/23.60 = 0.70$$

$$I_p = bh^3/12 = \frac{0.30^4}{12} = \mathbf{.6750E-3}\ \text{m}^4$$

For torsion constant J use an equivalent round pile based on r_o, or

$$J = \frac{\pi r_o^4}{2} = \frac{\pi \times 0.169^4}{2} = \mathbf{.1281E-2}\ \text{m}^4$$

The dimensionless frequency factor a_o is computed as

$$a_o = \frac{\omega r_o}{V_s} = \frac{179.2 \times 0.169}{103} = 0.29$$

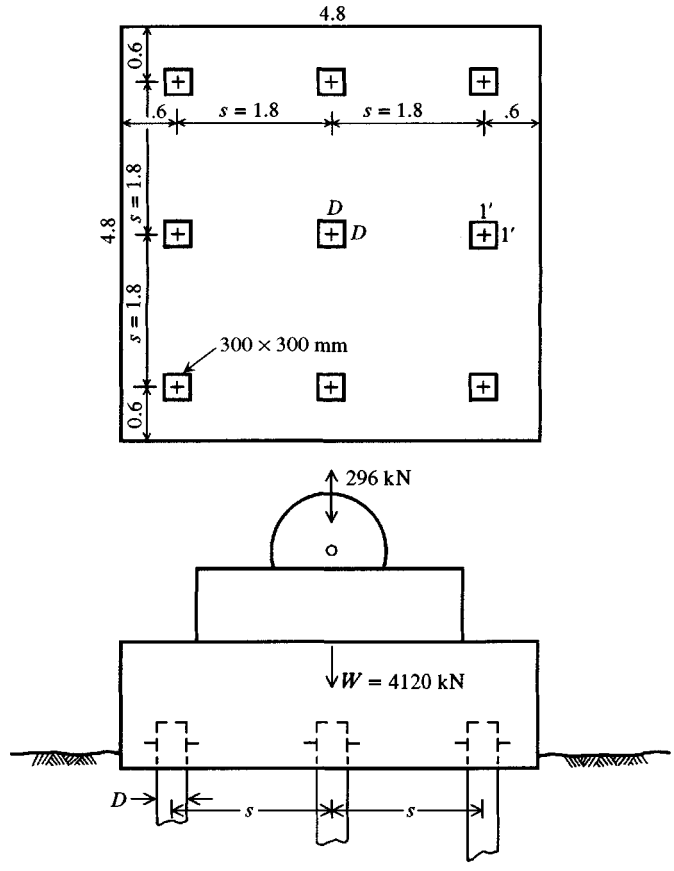

Figure E20-3

With these several data values computed, we can compute the several spring and damping constants using equations given in Table 20-7 with $f_{i,i}$ values from Table 20-6 (E, A, I, J are pile values):

Vertical.

$$K_z = \frac{EA}{r_o} f_{18,1} = \frac{27\,800 \times 0.3^2}{0.169} \times 0.037 = \mathbf{547.8}\ \text{MN/m}$$

$$c_z = \frac{EA}{V_s} f_{18,2} = \frac{27\,800 \times 0.09}{103} \times 0.016 = \mathbf{0.389}\ \text{MN} \cdot \text{s/m}$$

Horizontal.

$$K_h = \frac{EI}{r_o^3} f_{11,1} = \frac{17\,800 \times .6750\text{E}{-3}}{0.169^3} \times 0.018 = 44.8\ \text{MN/m}$$

$$c_h = \frac{EI}{r_o^2 V_s} f_{11,2} = \frac{12.015}{0.169^2 \times 103} \times 0.043 = 0.1756\ \text{MN} \cdot \text{s/m}$$

Rocking.

$$K_\theta = \frac{EI}{r_o} f_{7,1} = \frac{12.015}{0.169} \times 0.345 = 24.53 \text{ MN} \cdot \text{m}$$

$$c_\theta = \frac{EI}{V_s} f_{7,2} = \frac{12.015}{103} \times 0.245 = 0.02858 \text{ MN} \cdot \text{m} \cdot \text{s}$$

Torsion. For this we need

$$G'_p = \frac{E_p}{2(1 + \mu_p)} = \frac{27\,800}{2 \times 1.15} = \mathbf{12\,000} \text{ MPa}$$

Then

$$K_t = \frac{G'_p J}{r_o} f_{12,1} = \frac{12\,000 \times .1281\text{E}{-2}}{0.169} \times 0.105 = 9.55 \text{ MN} \cdot \text{m}$$

$$c_t = \frac{G'_p J}{V_s} f_{12,2} = \frac{15.372}{103} \times 0.011 = .00164 \text{ MN} \cdot \text{m} \cdot \text{s}$$

With these data and the large s/D ratio $= 1.8/0.3 = 6$, the vertical spring and damping constants will be summed to obtain a global value for the nine piles as

$$K_z = 9 \times 547.8 = \mathbf{4930.2} \text{ MN/m}$$

$$c_z = 9 \times 0.389 = \mathbf{3.501} \text{ MN} \cdot \text{s/m}$$

We can compute the block mass from the weight of block and machinery shown in Fig. E20-3 (in MN) to obtain

$$m = 4.12/9.807 = \mathbf{0.4201} \text{ MN} \cdot \text{s}^2/\text{m}$$

and, using Eq. (20-4*a*),

$$z = \frac{F_o}{\sqrt{K_z - (m\omega)^2)^2 + (c_z\omega)^2}} \tag{20-4a}$$

and making group substitutions for K_z, c_z and $\omega = 179.2$ we obtain

$$z = \frac{0.296}{\sqrt{[4930.2 - (0.4201 \times 179.2)^2]^2 + (3.501 \times 179.2)^2}}$$

$$= .3058\text{E}{-3} \text{ m} \rightarrow \mathbf{0.306} \text{ mm}$$

Comments.

1. The first term under the square root is negative, so it appears that the vertical displacement can be reduced most economically by either increasing ω or the damping c_z. Reducing the vertical force would also reduce the displacement, but this is probably not possible.
2. The soil velocity V_s should be reduced, but this approach is also not possible. Increasing the soil density ρ_s usually increases G'_s, so soil improvement does not appear to be a solution.
3. Adding piles does not appear to be a good solution, but increasing the base thickness to increase m may be of some aid. Increasing pile size to 600×600 mm would reduce the s/B to 3 and would not be of much help—even if it were possible to reduce pile length (so $L_p/r_o \approx 31$ or 32).
4. We do not know the static displacement; however, we may obtain coefficients at $a_o \rightarrow 0$ that would approximate "static" values for computing the natural system frequency and critical damping if that is desired.

////

GENERAL COMMENTS ON USING PILES.

1. Probably the best piles to use are concrete piles or pipe piles filled with concrete. Where wood piles are available they might be used to some advantage. **HP** piles are not a good choice for vibration control.
2. Use as large a pile spacing as possible—preferably $s/D \geq 5$ where D = pile diameter or width.
3. Use low pile stresses. A rule of thumb is to limit static stresses to not more than one-half the allowable design stress for the pile material. The pile stresses in Example 20-3 are quite low at $4.12/(9 \times 0.09) = 5.09$ MN.
4. Pile cap (or block) mass should be about 1.5 to 2.5 × mass of centrifugal machines and 2.5 to 4 × mass of reciprocating machines.
5. Arrange the centroid of the pile group to coincide with the centroid of the block mass as closely as practicable.
6. Consider batter piles with large horizontal dynamic forces. Here we could compute the axial spring of the batter pile and use the horizontal component together with the horizontal springs of the vertical piles in the group.
7. Be sure the cap is well anchored to the piles. Use shear connectors in combination with at least 300 mm of pile embedment.
8. The soil properties—particularly G'—after driving the piles will be substantially different from those obtained initially. Unless you can somehow determine the parameters after the piles have been installed for use in the equations given here, great refinement in spring and damping coefficients for use in Eq. (20-4*a*) is not necessary, and the equations and methodology given are satisfactory. Note, too, that it would be difficult to determine the parameters after driving by the down-hole or cross-hole method if the shear waves travel through both pile and soil to the detection unit.

PROBLEMS

20-1. Use your computer program FADDYNF1 and compute a value of F_z (refer to Example 20-1) that would increase the given displacement by a factor of 8. To do this, make a copy of data set EXAM201.DTA and then separate the several different vibration modes into separate disk files. Revise the set labeled EXAMPLE 20-1A-A and make several copies of the file with different forces F_z and make a plot of z versus F_z to find the resonant value.

20-2. Using your computer program, make a parametric study of the effect of G' on the vertical mode of Example 20-1. That is, make a plot of G' versus z for 50, 75, and 150 percent of the given $G' = 239\,400$ kPa.

20-3. Use your computer program as in Problem 20-2 but for the sliding mode parallel to the x axis.

20-4. Use your computer program as in Problem 20-2 but for the rocking mode about the z axis.

20-5. A single-cylinder engine weighs 24.15 kN. The unbalanced vertical forces are these: primary = 18.50 kN, secondary = 9.75 kN, at the operating speed of 1600 rpm. The soil is a very sandy clay with $q_u = 250$ kPa. Find the amplitude of vibration for the system using a concrete foundation block 1.2 × 2.4 × 1.0 m thick. Find the displacements in the range of rpm from 0 to 1800. (Assume this is a $m_e\bar{y}\omega^2$ type with the above vertical forces occurring at 1200 rpm.) Use increments of 100 rpm. If you find the resonance frequency is in the operating range, make a second run starting at 100 rpm before resonance to 100 rpm beyond, using increments of 25 rpm.

20-6. Estimate the revised lateral spring and damping for Example 20-2.

20-7. Compute the estimated horizontal displacement of Example 20-3 for a dynamic lateral force of 50 kN acting 1.5 m above the block base at ground line. Should coupling be considered in this case?

20-8. Referring to Example 20-3, we know that $V_s/V_p = 0.06$. Back-compute the corresponding soil G', recompute the vertical soil springs K_z and damping c_z, and compute the resulting vertical displacement z. Can you draw any conclusions about the effect of G' on this class of problems?

20-9. Redo Example 20-3 for the displacement mode assigned if the frequency is either 149.2 or 209.2 rad/sec (also as assigned). Compare the spring value to that in the example, which uses 179.2 rad/sec. Does frequency ω appear to have a significant effect on the displacements? *Hint:* Compare 1/square root term computed using the example springs and ω and your springs and ω.

20-10. Write a short computer program and verify Figs. 20-4.

APPENDIX A

GENERAL PILE-DATA AND PILE HAMMER TABLES

Representative steel and prestressed pile data are provided for the book user. The **HP** pile data are similar to those in the AISC *Steel Construction Manual* except for the addition of Algoma sections. The sheetpiling data are generally representative of those available both in the United States and elsewhere. The pipe piling data are only a partial list of available diameters and wall thicknesses. The prestressed pile data are a partial list of available sections.

The SI conversions have been made by the author based on the best currently available data on nominal section sizes and rounding. The European sections dimensions are as given by them except where values have been provided in *centimeters*—a non-SI term. Generally the use of section values in meters (m) with a 10^{-n} where $n = 3$ or 6 is the best format since the exponential term can usually be canceled without even having to write it down. Using millimeters gives numbers too large to write, and decimal shifting is difficult.

Because of the great difficulty in finding sources (some trade organizations charge for a list of manufacturers), I have elected to provide addresses for pile hammer manufacturers and the address of at least one producer of **HP** piles, sheet piles, pipe piles, and concrete piles. Although these addresses are correct at the time of publication (I did not include any representatives' addresses), no warranty can be made that they will remain correct for the life of this publication.

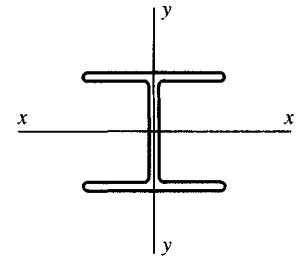

TABLE A-1

HP pile dimensions and section properties

Metric units in dark type, Fps units in light type.

Designation nominal size/wt, in. × lb/ft mm × kg/m	Area, in.^{2} m$^2 \times 10^{-3}$	Depth, in. mm	Flange Width, in. mm	Flange Thick, in. mm	Web, in. mm	Section properties I_x, in.^{4} m$^4 \times 10^{-6}$	S_x, in.^{3} m$^3 \times 10^{-3}$	I_y, in.^{4} m$^4 \times 10^{-6}$	S_y, in.^{3} m$^3 \times 10^{-3}$
HP 14 × 117	34.4	14.21	14.89	0.805	0.805	1220	172	443	59.5
HP360 × 174	**22.2**	**361**	**378**	**20.4**	**20.4**	**508**	**2.817**	**184**	**0.975**
HP 14 × 102	30.0	14.01	14.78	0.705	0.705	1050	150	380	51.4
HP360 × 152	**19.4**	**356**	**376**	**17.9**	**17.9**	**437**	**2.458**	**158**	**0.842**
HP 14 × 89	26.1	13.83	14.70	0.615	0.615	904	131	326	44.3
HP360 × 132	**16.9**	**351**	**373**	**15.6**	**15.6**	**373**	**2.147**	**136**	**0.726**
HP 14 × 73	21.4	13.61	14.59	0.505	0.505	729	107	261	35.8
HP360 × 108	**13.9**	**346**	**371**	**12.8**	**12.8**	**303**	**1.753**	**109**	**0.587**
HP 13 × 100	29.4	13.15	13.20	0.765	0.765	886	135	294	44.5
HP330 × 149	**19.0**	**334**	**335**	**19.4**	**19.4**	**369**	**2.212**	**122**	**0.729**
HP 13 × 87	25.5	12.95	13.10	0.665	0.665	755	117	250	38.1
HP330 × 129	**16.5**	**329**	**333**	**16.9**	**16.9**	**314**	**1.917**	**104**	**0.624**
HP 13 × 73	21.6	12.75	13.01	0.565	0.565	630	98.8	207	31.9
HP330 × 109	**13.9**	**324**	**330**	**14.4**	**14.4**	**262**	**1.619**	**86.2**	**0.522**
HP 13 × 60	17.5	12.54	12.90	0.460	0.460	503	80.3	165	25.5
HP330 × 89	**11.3**	**319**	**328**	**11.7**	**11.7**	**209**	**1.315**	**68.7**	**0.417**
*HP 12 × 117	34.3	12.77	12.87	0.930	0.930	946	148	331	51.4
HP310 × 174	**22.2**	**324**	**327**	**23.6**	**23.6**	**394**	**2.43**	**138**	**0.843**
*HP 12 × 102	30.0	12.55	12.62	0.820	0.820	812	129	275	43.6
HP310 × 152	**19.4**	**319**	**321**	**20.8**	**20.8**	**338**	**2.120**	**115**	**0.716**
*HP 12 × 89	26.2	12.35	12.33	0.720	0.720	693	112	226	36.7
HP310 × 132	**16.7**	**314**	**313**	**18.3**	**18.3**	**287**	**1.830**	**93.7**	**0.599**
HP 12 × 84	24.6	12.28	12.30	0.685	0.685	650	106	213	34.6
HP310 × 125	**15.9**	**312**	**312**	**17.4**	**17.4**	**271**	**1.737**	**88.7**	**0.566**
HP 12 × 74	21.8	12.13	12.22	0.610	0.605	569	93.8	186	30.4
HP310 × 110	**14.1**	**308**	**310**	**15.5**	**15.4**	**236**	**1.537**	**77.4**	**0.498**
HP 12 × 63	18.4	11.94	12.13	0.515	0.515	472	79.1	153	25.3
HP310 × 93	**11.9**	**303**	**308**	**13.1**	**13.1**	**196**	**1.296**	**63.7**	**0.415**
HP 12 × 53	15.5	11.78	12.05	0.435	0.435	393	66.8	127	21.1
HP310 × 79	**10.0**	**299**	**306**	**11.0**	**11.0**	**163**	**1.095**	**52.9**	**0.346**
HP 10 × 57	16.8	9.99	10.22	0.565	0.565	294	58.8	101	19.7
HP250 × 85	**10.8**	**254**	**260**	**14.4**	**14.4**	**122**	**0.964**	**42.0**	**0.323**
HP 10 × 42	12.4	9.70	10.08	0.420	0.415	210	43.4	71.7	14.2
HP250 × 62	**8.0**	**246**	**256**	**10.7**	**10.5**	**87.4**	**0.711**	**29.8**	**0.233**
HP 8 × 36	10.6	8.02	8.16	0.445	0.445	119	29.8	40.3	9.88
HP200 × 53	**6.84**	**204**	**207**	**11.3**	**11.3**	**49.5**	**0.488**	**16.8**	**0.162**

*From Algoma Steel Co. (Canadian); all others available in both United States and Canada.

All shapes not designated with an * are available from:

Bethlehem Steel Corp.
501 East 3rd Street
Bethlehem, PA 18016-7699

TABLE A-2

Typical pile-driving hammers from various sources

Consult manufacturers' catalogs for additional hammers, later models, other details.

Model no.	Type*	Max. rated energy, kips · ft	Max. rated energy, kN • m	Working weight, kips	Working weight, kN	Ram weight,¶ kips	Ram weight,¶ kN	Stroke ft	Stroke m	Blow rate/min	Approx. length, m
	Drop hammers	**Variable**		0.50–10	**2.2–45**			**Variable‡**		**Very few**	
Vulcan Iron Works											
West Palm Beach, FL 33407											
400C	SA	113.5	**153.86**	83	**369**	40	**177.9**	1.37	**0.42**	100	**5.1**
200C	DA	50.2	**68.05**	39	**174**	20	**89.0**	1.29	**0.39**	98	**4.0**
140C	DA	36.0	**48.80**	28	**125**	14	**62.3**	1.29	**0.39**	103	**3.7**
80C	DA	24.45	**33.14**	18	**80**	8	**35.58**	1.37	**0.42**	111	**3.7**
65C	DA	19.2	**26.03**	15	**67**	6.5	**28.91**	1.29	**0.39**	117	**3.7**
1–106	SA	15.0	**20.33**	9.7	**43**	5.0	**22.24**	3.0	**0.91**	60	**4.0**
7	DA	4.15	**5.63**	5.1	**22.7**	0.8	**3.56**	0.78	**0.24**	225	**1.8**
4N100	D	43.4	**58.8**	12.8	**56.9**	5.3	**23.5**	8.13	**2.48**	50–60	
IN100	D	24.6	**33.4**	7.6	**33.8**	3.0	**13.3**	8.13	**2.48**	50–60	
0	SA	24.38	**33.04**	16.0	**71.2**	7.5	**33.4**	3.25	**0.99**	50	**4.6**
McKiernan-Terry, Koehring-MKT Division											
Dover, NJ 07801											
MBRS–7000	SA	361.15	**489.57**	161	**712**	88.0	**391.4**	4.10	**1.25**	40	**8.5**
OS–30	SA	90.0	**122.0**	50.5	**225**	30.0	**133.4**	3.0	**0.91**	60	**6.4**
S–20	SA	60.0	**81.34**	39.0	**173**	20.0	**88.9**	3.0	**0.91**	60	**4.6**
S–8	SA	26.0	**35.25**	18.3	**81.4**	8.0	**35.6**	3.25	**0.99**	53	**4.3**
S–5	SA	16.25	**22.03**	12.5	**55.4**	5.0	**22.2**	3.25	**0.99**	60	**4.0**
IHI-J44	D	79.4	**107.63**	21.5	**95.6**	9.7	**43.2**	8.17	**2.49**	42–70	**4.6**
DA55B	D	38.0	**51.51**	19.6	**87.3**	5.0	**22.2**	8.0	**2.44**	48	**5.1**
DE40	D	32.0	**43.38**	11.2	**49.9**	4.0	**17.8**	10.7	**3.26**	48	**4.6**
DE30	D	22.4	**30.37**	9.1	**40.4**	2.8	**12.4**	10.7	**3.26**	48	**4.6**
Raymond International, Inc.											
2801 South Post Road, Houston, TX 77027											
30X	DA	75.0	**107.67**	52.0	**231.2**	30.0	**133.4**	2.5	**0.76**	70	**5.8**
5/0	SA	56.9	**77.10**	26.5	**117.6**	17.5	**77.8**	3.25	**0.99**	44	**5.1**
150C	DA	48.8	**66.09**	32.5	**144.5**	15.0	**66.7**	1.50	**0.46**	95–105	**4.8**
2/0	SA	32.5	**44.06**	18.8	**83.4**	10.0	**44.5**	3.25	**0.99**	50	**4.6**
80C	DA	24.5	**33.14**	17.9	**79.5**	8.0	**35.6**	1.38	**0.42**	95–105	**3.7**
65C	DA	19.5	**26.43**	14.7	**65.3**	6.5	**28.9**	1.33	**0.41**	110	**3.7**
1	SA	15.0	**20.33**	11.0	**48.9**	5.0	**22.2**	3.0	**0.91**	60	**4.0**
The Foundation Equipment Corp. (distributor of Delmag Hammers)											
New Commerstown, OH 43832											
D55	D	117.175†	**158.84**	26.3	**116.9**	11.9	**52.8**		‡	36–47	**5.5**
D44	D	87.0	**117.94**	22.4	**99.6**	9.5	**42.1**			37–55	**4.8**
D36	D	73.78	**100.02**	17.8	**79.1**	7.9	**35.3**			37–53	**4.8**
D30	D	54.2	**73.47**	12.4	**55.1**	6.6	**29.4**			40–60	**4.3**
D22	D	39.78	**53.93**	11.1	**49.4**	4.8	**21.5**			40–60	**4.3**
D5	D	9.05	**12.27**	2.7	**12.0**	1.1	**4.9**			40–60	**4.0**

TABLE A-2

Typical pile-driving hammers from various sources (*continued*)

Consult manufacturers' catalogs for additional hammers, later models, other details.

Model no.	Type*	Max. rated energy, kips · ft	Max. rated energy, kN • m	Working weight, kips	Working weight, kN	Ram weight,¶ kips	Ram weight,¶ kN	Stroke ft	Stroke m	Blow rate/min	Approx. length, m
Link Belt											
Link Belt Speeder Division, FMC Corp., Cedar Rapids, IA 52406											
520	D	26.3	**35.65**	12.6	**56.0**	5.07	**22.55**	5.18	**1.58**	80–84	
440	D	18.2	**24.67**	10.3	**45.8**	4.0	**17.79**	4.35	**1.39**	86–90	
312	D	15.0	**20.33**	10.4	**46.2**	3.86	**17.15**	3.89	**1.18**	100–105	
180	D	8.1	**10.98**	4.6	**20.5**	1.72	**7.67**	4.70	**1.43**	90–95	
L. B. Foster Co. (distributor for Kobe Diesel Hammers)											
7 Parkway Center, Pittsburgh, PA 15220											
K150	D	281.3	**381.33**	80.5	**358.0**	33.1	**147.2**	8.5	**2.59**	45–60	**8.5**
K45	D	91.1	**123.51**	25.6	**113.8**	9.9	**44.0**	9.17	**2.80**	39–60	**5.8**
K42	D	79.0	**107.09**	24.0	**106.7**	9.26	**41.2**	8.5	**2.59**	45–60	**5.8**
K32	D	60.1	**81.47**	17.8	**79.2**	7.1	**31.4**	8.5	**2.59**	45–60	**5.5**
K25	D	50.7	**68.73**	13.1	**58.2**	5.5	**24.5**	9.17	**2.80**	39–60	**5.5**
K13	D	24.4	**33.08**	8.0	**35.6**	2.9	**12.7**	8.5	**2.59**	45–60	**5.1**
Berminghammer Corp., Ltd.											
Hamilton, Ontario (Canada)											
B500	D	75.0	**101.67**	16.5	**73.4**	6.9	**30.7**	12.0	**3.66**	40–60	
B225	D	25.0	**33.89**	6.8	**30.2**	2.9	**12.7**	9.7	**2.96**	40–60	
Mitsubishi International Corp.											
875 North Michigan Avenue, Chicago, IL 60611											
MB70	D	137.0	**185.72**	46.0	**204.6**	15.84	**70.5**	8.5	**2.59**	38–60	**6.1**
M43	D	84.0	**113.87**	22.6	**100.5**	9.46	**42.1**	8.5	**2.59**	40–60	**4.8**
M33	D	64.0	**86.76**	16.9	**75.2**	7.26	**32.3**	8.5	**2.59**	40–60	**4.8**
M23	D	45.0	**61.00**	11.2	**49.8**	5.06	**22.5**	8.5	**2.59**	42–60	**4.3**
M14	D	26.0	**35.25**	7.3	**32.5**	2.97	**1.32**	8.5	**2.59**	42–60	**4.3**

*SA = single-acting; DA = double-acting or differential-acting; D = diesel.

†Energy varies from maximum shown to about 60 percent of maximum depending on stroke and soil.

‡Variable stroke; stroke = energy out/weight of ram.

¶ Ram weight or weight of striking part.

TABLE A-3*a*

Steel sheetpiling sections produced in the United States*

	Section index	Depth *d*, in. mm	Driving distance, in. mm	Weight lb/ft kg/m	Weight lb/ft² kg/m²	Section modulus* per pile, in.³ m³ × 10⁻³	Moment of inertia per pile, in.⁴ m⁴ × 10⁻⁶
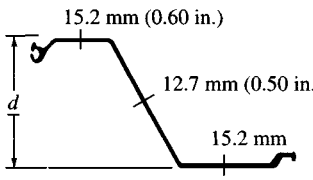	PZ40	16.1 **410**	19.69 **500**	65.6 **97.6**	40.0 **195.3**	99.6 **1.632**	805.4 **335.23**
	PZ35	14.9 **380**	22.64 **575**	66.0 **98.2**	35.0 **170.9**	91.4 **1.498**	681.5 **283.7**
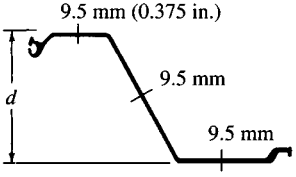	PZ27	12 **305**	18 **460**	40.5 **60.3**	27.0 **131.8**	45.3 **0.742**	276.3 **115.0**
	PZ22	9 **230**	22 **560**	40.3 **60.0**	22.0 **107.4**	33.1 **0.542**	154.7 **64.39**
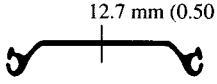	PS31	—	19.69 **500**	50.9 **75.7**	31.0 **151.4**	3.3 **0.054**	5.3 **2.206**
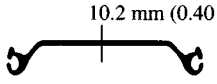	PS27.5	—	19.69 **500**	45.1 **67.1**	27.5 **134.3**	3.3 **0.054**	5.3 **2.206**
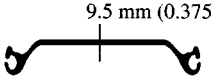	PSA23	—	16.00 **405**	30.7 **45.7**	23.0 **112.3**	3.2 **0.052**	5.5 **2.290**
	Box pile	31.0 **787**	45.28 **1150**	261.2 **388.7**	— —	480.7 **7.877**	7618 **3170.9**

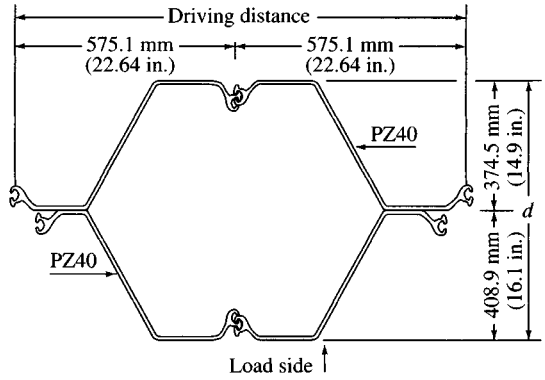

*These sections are now available only from Bethlehem Steel Corporation.

Steel grades: A328 with F_y = 270 MPa (39 ksi)
A572 with F_y = 345 and 415 MPa (50 and 60 ksi)
A690 with F_y = 345 MPa (50 ksi) for marine environments

TABLE A-3*b*

Steel sheetpiling sections produced in Europe

	Section index	Depth *d*, mm	Driving distance, mm	Weight kg/m	Weight kg/m²	Section modulus per pile, $m^3 \times 10^{-3}$	Moment of inertia per pile, $m^4 \times 10^{-6}$
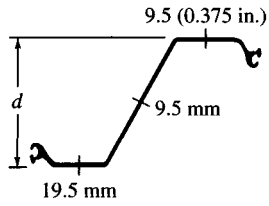	AZ 13	303	670	72.0	107	0.870	132.0
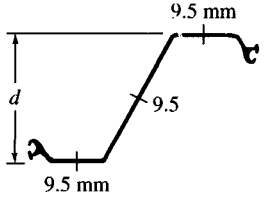	AZ 18	380	630	74.4	118	1.135	215.40
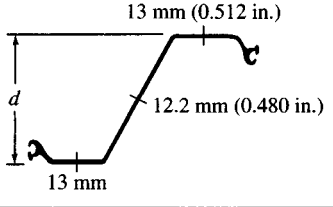	AZ 26	427	630	97.8	155	1.640	349.70
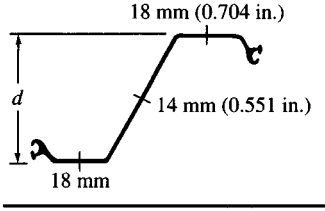	AZ 36	460	630	122.2	194	2.270	521.60
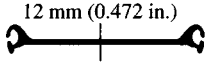	AS500-12.0	—	500	72.3	145	0.047	1.80

TABLE A-3*b* (*continued*)

12.5 mm (0.492 in.) 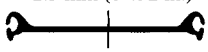								
12.7 mm (0.500 in.)  Driving distance 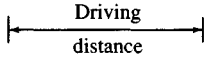	AS500-12.7	—	500	75.2	150	0.047	1.80
Combination 10/13 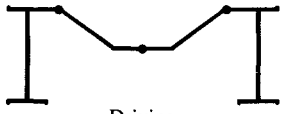 Driving distance 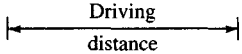	HZ775A / ZH9.5	775	1585	184	222	4.80	1859.9

Sheetpiling produced by International Sheet Piling Group
ARBED Group
3-7, rue Schiller
L-2930 Luxemburg, Tel.: (352)-5550-2060

TABLE A-4

Typical available steel pipe sections used for piles and caisson shells

In spiral welded pipe almost any wall thickness and diameter can be produced.
[Courtesy Skyline Steel Corporation, Pipe Division, Peachtree Industrial Boulevard, Duluth, GA, Tel.: 404-623-6200]

Nominal OD, mm (in.)	Wall thickness		Weight, kg/m	Area, $m^2 \times 10^{-3}$	
	mm	in.		Concrete	Steel
254	4.78	0.188	29.2	46.9	3.75
(10)	5.56	0.219	34.0	46.3	4.35
	6.35	0.250	38.7	45.9	4.94
273	4.78	0.188	31.5	54.5	4.03
($10\frac{3}{4}$)	6.35	0.250	41.7	53.2	5.32
	7.79	0.307	51.0	52.1	6.50
	9.27	0.365	60.3	50.9	7.68
305	4.78	0.188	35.2	68.5	4.49
(12)	5.56	0.219	41.0	67.7	5.23
	6.35	0.250	46.7	67.0	5.97
325	4.78	0.188	37.4	77.6	4.79
($12\frac{3}{4}$)	6.35	0.250	49.7	76.0	6.34
	7.92	0.312	61.8	74.5	7.86
	9.53	0.375	73.8	73.0	9.41
	12.70	0.500	97.3	69.9	12.41

TABLE A-4 (*continued*)

In spiral welded pipe almost any wall thickness and diameter can be produced.
[Courtesy Skyline Steel Corporation, Pipe Division, Peachtree Industrial Boulevard, Duluth, GA, Tel.: 404-623-6200]

Nominal OD, mm (in.)	Wall thickness		Weight, kg/m	Area, $m^2 \times 10^{-3}$	
	mm	in.		Concrete	Steel
356	5.56	0.219	47.9	93.2	6.12
(14)	6.35	0.250	54.6	92.3	6.97
	7.92	0.312	68.0	90.6	8.66
	9.53	0.375	81.3	89.0	10.35
	12.70	0.500	107.3	85.6	13.68
410	4.78	0.188	41.2	123.7	6.03
(16)	6.35	0.250	62.7	121.7	7.98
	7.92	0.312	78.0	119.8	9.92
	9.53	0.375	93.2	117.8	11.88
	12.70	0.500	123.2	114.0	15.71
460	5.56	0.219	61.8	156.3	7.89
(18)	6.35	0.250	70.5	155.2	8.99
	7.92	0.312	87.8	153.0	11.19
	9.53	0.375	105.1	150.8	13.39
510	6.35	0.250	78.4	192.6	10.01
(20)	7.92	0.312	97.8	190.3	12.45
	9.53	0.375	117.0	187.7	14.92
	12.70	0.500	154.9	182.9	19.76
610	6.35	0.250	94.3	279.8	12.06
(24)	7.92	0.312	117.7	276.9	14.97
	9.53	0.375	140.8	273.9	17.94
	12.70	0.500	186.8	268.1	23.81
760	9.53	0.375	176.6	433.5	22.52
(30)	12.70	0.500	234.4	426.1	29.87
915	9.53	0.375	212.4	629.5	27.10
(36)	12.70	0.500	282.2	620.7	36.00
1070	9.53	0.375	248.1	862.2	31.61
(42)	12.70	0.500	329.8	851.7	42.06
1220	9.53	0.375	283.8	1131.2	36.19
(48)	12.70	0.500	377.5	1119.4	48.13
1370	9.53	0.375	320.0	1436.8	40.76
(54)	12.70	0.500	424.1	1423.4	54.19

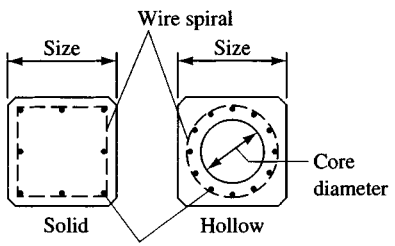

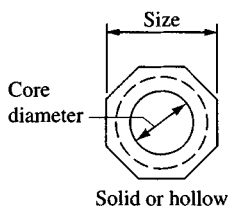

TABLE A-5

Typical prestressed-concrete pile sections—both solid and hollow-core (HC)*

Nominal pile size		Area concrete,	Approx. weight,	Minimum pre-stress	No. of strands in pile,¶	Mom. of inertia I,	Perimeter,
mm	(in.)	$m^2 \times 10^{-3}$	kN/m	force, ‡ kN	11.1/12.7 mm	$m^4 \times 10^{-6}$	m
250	(10)	64.5	1.52	311	4/4	346.7	1.02
300	(12)	92.9	2.19	449	6/5	719.2	1.22
360	(14)	126.5	2.99	610	8/6	1332.4	1.42
410	(16)	171.0	4.04	830	11/8	2273.0	1.63
460	(18)	209.0	4.93	1010	13/10	3641.2	1.83
510	(20)	258.1	6.09	1250	16/12	5549.6	2.03
560	(22)	312.3	7.37	1500	20/15	8125.3	2.24
610	(24)	371.6	8.77	1790	23/18	11 508.0	2.44
510	(20)HC†	196.7	4.64	950	13/10	5250.8	2.03
560	(22)HC	226.5	5.35	1095	14/11	7504.8	2.24
610	(24)HC	257.4	6.07	1245	16/12	10473.6	2.44
250	(10)	53.5	1.26	260	4/4	231.0	0.84
300	(12)	76.8	1.81	370	5/4	472.0	1.02
360	(14)	104.5	2.47	500	7/5	876.2	1.17
410	(16)	136.8	3.23	660	9/7	1495.1	1.35
460	(18)	172.9	4.08	835	11/8	2374.6	1.52
510	(20)	213.5	5.04	1030	14/10	3650.3	1.68
560	(22)	258.7	6.11	1250	16/12	5343.2	1.85
610	(24)	307.7	7.26	1485	19/15	7567.1	2.03
510	(20)HC	132.3	3.12	735	10/8	3350.7	1.68
560	(22)HC	172.9	4.08	835	11/8	4761.7	1.85
610	(24)HC	193.5	4.57	835	12/9	6533.2	2.03

*Additional data available from Prestressed Concrete Institute, 20 North Wacker Drive, Chicago, IL 60606.

†Voids in 510-, 560-, and 610-mm diameter HC piles are 279-, 330-, and 381-mm diameter, respectively, to provide a minimum 115-mm wall thickness.

‡Minimum prestress force based on f_p = 4.8 MPa after losses.

¶Uses 11.1 ($\frac{7}{16}$-in.) and 12.7 ($\frac{1}{2}$-in.) stress-relieved strands with P_{ult} = 138 and 184 kN, respectively.

REFERENCES

To simplify and condense the reference list, the following abbreviations are used:

AASHTO		American Association of State Highway and Transportation Officials, 444 N. Capitol St., N.W., Washington, DC 20001.
ACI		American Concrete Institute, PO Box 19150, Detroit, MI 48219.
	JACI	*Journal of American Concrete Institute* (monthly)[now *ACI Structural Journal* (ca. vol. 80)]
ASCE		American Society of Civil Engineers, New York, NY
	JGED	*Journal of Geotechnical Engineering Division* (1974–)
	JSMFD	*Journal of Soil Mechanics and Foundation Division,* ASCE (1955–1973, inclusive)
	SMFE	*Soil Mechanics and Foundation Engineering*
	PSC	*Proceedings of Soil Mechanics and Foundation Division,* ASCE, specialty conferences as follows: 1st PSC: Shear Strength of Cohesive Soils (1960) 2nd PSC: Design of Foundations for Control of Settlement (1964) 3rd PSC: Placement and Improvement of Soil to Support Structures (1968) 4th PSC: Lateral Stresses in the Ground and Design of Earth Retaining Structures (1970) 5th PSC: Performance of Earth and Earth Supported Structures (1972) 6th PSC: Analysis and Design in Geotechnical Engineering (1974) 7th PSC: In Situ Measurements of Soil Properties (1975)

8th PSC: Rock Engineering for Foundations and Slopes (1976)
9th PSC: Geotechnical Practice for Disposal of Solid Waste Materials (1977)
10th PSC: Earthquake Engineering and Soil Dynamics (1978)
11th PSC: Grouting in Geotechnical Engineering (1982)
12th PSC: Engineering and Construction in Tropical and Residual Soils (1982)
13th PSC: Geotechnical Practice in Offshore Engineering (1983)
14th PSC: Use of In Situ Tests in Geotechnical Engineering (1986)

After 1986 ASCE produces Geotechnical Special Publications (Geotech. SP).

	JSD	*Journal of Structural Division*, ASCE
ASME		American Society for Mechanical Engineers
ASTM		American Society for Testing and Materials, 1916 Race Street, Philadelphia, PA
	STP	*ASTM Special Technical Publication* (with appropriate number)
	GTJ	*Geotechnical Testing Journal*
AWPI		American Wood Preservers Institute, 2600 Virginia Avenue, Washington, DC
	CGJ	*Canadian Geotechnical Journal,* Ottawa, Canada
	ENR	*Engineering News-Record,* New York (weekly)
ICE		Institution of Civil Engineers, London
	PICE	*Proceedings of Institution of Civil Engineers*
	ESOPT	*European Symposium on Penetration Testing* 1st: Stockholm, Swedish Geotechnical Society (1974) 2nd: Amsterdam, Balkema Publishers (1982)
	ISOPT	*International Symposium on Penetration Testing* 1st: Orlando, FL, Balkema Publishers (1988)
	ICSMFE	*Proceedings of International Conference on Soil Mechanics and Foundation Engineering* 1st: Harvard University, USA (1936) 2nd: Rotterdam, Holland (1948) 3rd: Zurich, Switzerland (1953) 4th: London, England (1957) 5th: Paris, France (1961) 6th: Montreal, Canada (1965) 7th: Mexico City, Mexico (1969) 8th: Moscow, USSR (1973) 9th: Tokyo, Japan (1977) 10th: Stockholm, Sweden (1981)—US$995

11th: San Francisco, USA (1985)—US$995
12th: Rio de Janeiro, Brazil (1989)—US$995
13th: New Delhi, India (1994)—US$750

The proceedings of *ICSMFE* are not much cited, because they are extremely expensive (if available—usually by A. A. Balkema, P.O. Box 1675, Rotterdam, Netherlands) and are available only at a few university libraries, if they are not out of print. Most material of much importance usually gets published in less expensive ASCE conference publications or in ASCE *JGED* or the *CGJ*.

Geotechnique, published quarterly by the Institution of Civil Engineers, London.

Highway Research Board (HRB), Highway Research Record (HRR), etc., published by National Academy of Sciences, Washington, DC.

In the following references, *et al.* is used with the senior author when there are more than two co-authors.

AASHTO (1990), *Standard Specifications for Highway Bridges,* 14th ed., 420 pp.

ACI (1991), "Standard Practice for Design and Construction of Concrete Silos and Stacking Tubes for Storing Granular Materials and Commentary," *ACI Committee 313,* 22 pp.

ACI (1989), *Building Code Requirements for Reinforced Concrete* (ACI 318-89), American Concrete Institute, Detroit, MI, 353 pp. (with commentary).

ACI (1977), "Recommended Practice for Design and Construction of Concrete Bins, Silos and Bunkers for Storing Granular Materials," *ACI Committee 313 Report* (revised 1983, 1991 now *MCP 4*), 39 pp.

ACI Committee 336 (1988), "Suggested Analysis and Design Procedures for Combined Footings and Mats," *ACI Committee 336 Report,* 21 pp. See also the "discussion" and "closure" in the *ACI Structural Journal,* vol. 86, no. 1, Jan–Feb, 1989, pp. 111–16.

ACI Committee 351 (1992), "Grouting for the Support of Equipment and Machinery," *ACI Committee 351 Report,* in the *ACI Structural Journal,* vol. 89, no. 6, Nov–Dec, pp. 721–737.

AISC (1992), *Metric Properties of Structural Shapes,* American Institute of Steel Construction, 400 N. Michigan Ave., Chicago, IL 60611, Publication No. S340, 97 pp.

——(1989), *Steel Construction Manual (ASD),* 9th ed., American Institute of Steel Construction, 400 N. Michigan Ave., Chicago, IL 60611.

AISI (1975), *Steel Pile Load Test Data,* American Iron and Steel Institute, Washington, DC, 84 pp.

API (1984), *API Recommended Practice for Planning, Designing and Constructing Fixed Offshore Platforms,* 15th ed., API RP2A, American Petroleum Institute, 115 pp.

ASCE (1987), *Soil Improvement—A Ten Year Update,* Geotech. SP No. 12, 331 pp.

ASCE (1974), "Design of Steel Transmission Pole Structures," *JSD,* ASCE, vol. 100, ST 12, Dec, pp. 2449–2518 (Committee Report).

ASCE (1966), "Revised Bibliography on Chemical Grouting," *JSMFD,* ASCE, vol. 92, SM 6, Nov, pp. 39–66.

ASCE (1962), *Symposium on Grouting,* a series of papers published in *JSMFD,* ASCE, vol. 87, SM 2, April, pp. 1–145.

ASCE (1959), *Timber Piles and Construction Timbers,* ASCE Manual of Practice No. 17, 48 pp.

ASCE (1957), *Chemical Grouting,* Progress Report on Chemical Grouting..., *JSMFD,* vol. 83, SM4, Nov, pp. 1426-1 to 1426-106.

ASCE (1946), *Pile Foundations and Pile Structures,* ASCE Manual of Practice No. 27, 72 pp. (reprinted in 1959).

ASCE (1941), "Pile-Driving Formulas," *Proceedings ASCE,* vol. 67, no. 5, May, pp. 853–866.

ASTM (1988), "Vane Shear Strength Testing in Soils," *ASTM STP* No. 1014, 378 pp.

ASTM (1971), "Underwater Soil Sampling, Testing and Construction Control," *ASTM STP* No. 501, 241 pp.

AWPI (1981), AE Concepts in Wood Design (Piling Issue), vol. 1, no. 4, Jan–Feb, 33 pp.

AWPI (1969), *Pile Foundations Know-How,* 66 pp.

AWPI (1967), *Pressure Treated Timber Foundation Piles for Permanent Structures,* 98 pp.

AWPI (1966), *Timber Pile Foundation Pile Study,* 46 pp.

Aas, G., et al. (1986), "Use of In Situ Tests for Foundation Design on Clay," *14th PSC,* ASCE, pp. 1–30.

Abdelhamid, M. S., and R. J. Krizek (1976), "At-Rest Lateral Earth Pressure of a Consolidating Clay," *JGED,* ASCE, vol. 102, GT 7, July, pp. 721–738.

Acar, Y. B., et al. (1982), "Interface Properties of Sand," *JGED,* ASCE, vol. 108, no. 4, April, pp. 648–654.

Aldrich, H. P. (1965), "Precompression for Support of Shallow Foundations," *JSMFD,* ASCE, vol. 91, SM 2, March, pp. 5–20.

Al-Khafaji, A. W., and O. B. Andersland (1992), "Equations for Compression Index Approximation," *JGED,* ASCE, vol. 118, no. 1, Jan, pp. 148–153.

Alizadeh, M., and M. T. Davisson (1970), "Lateral Load Tests on Piles—Arkansas River Project," *JSMFD,* ASCE, vol. 96, SM 5, Sept, pp. 1583–1604.

Alpan, I. (1967), "The Empirical Evaluation of the Coefficient K_o and $K_{o,OCR}$," *Soils and Foundations,* Tokyo, vol. 7, no. 1, Jan, pp. 31–40.

Andersland, O. B., and D. M. Anderson (1978), *Geotechnical Engineering for Cold Regions,* McGraw-Hill, New York, 576 pp.

Anderson, D. G., et al. (1978), "Estimating In Situ Shear Moduli at Competent Sites," *10th PSC,* ASCE, vol. 1, pp. 181–187.

Anderson, J. N., and P. V. Lade (1981), "The Expansion Index Test," ASTM, *GTJ,* vol. 4, no. 2, June, pp. 58–67.

Anderson, K. H, et al. (1994), "Estimation of Hydraulic Fracture Pressure in Clay," *CGJ,* Vol. 31, No. 6, Dec, pp. 817–828.

Anderson, T. C. (1982), "Discussion: Cam-Clay Predictions of Undrained Strength," *JGED,* ASCE, vol. 108, GT 1, Jan, pp. 176–178.

Arman, A., et al. (1975), "Study of the Vane Shear," *7th PSC,* ASCE, vol. 1, pp. 93–120.

Arthur, J. R., and B. K. Menzies (1972), "Inherent Anisotropy in Sand," *Geotechnique,* vol. 22, no. 1, March, pp. 115–128.

Arya, S., et al. (1979), *Design of Structures and Foundations for Vibrating Machines,* Gulf Publishing Co., Houston, TX, 191 pp.

Aschenbrenner, R. (1967), "Three Dimensional Analysis of Pile Foundations," *JSD,* ASCE, vol. 93, ST 1, Feb, pp. 201–219.

Azzouz, A. S., et al. (1976), "Regression Analysis of Soil Compressibility," *Soils and Foundations,* Tokyo, vol. 16, no. 2, pp. 19–29.

BOCA (1993), *The BOCA Basic National Building Code,* Building Officials and Code Administrators International, Inc., Country Club Hills, IL, 60477, two volumes.

BRAB (1968), "Criteria for Selection and Design of Residential Slabs-on-Ground," Building Research Advisory Board, FHA Report 33, Washington, DC, 289 pp.

Baguelin, F., et al. (1974), "Self-Boring Placement Method of Soil Characteristics Measurement," *Proceedings, Conference on Subsurface Exploration for Underground Excavation and Heavy Construction,* ASCE, pp. 312–322.

Baldi, G., et al. (1986), "Flat Dilatometer Tests in Calibration Chambers," *14th PSC,* ASCE, pp. 431–446.

——, et al. (1981), "Cone Resistance in Dry NC and OC Sands," *Proceedings Session: Cone Penetration Testing and Experience,* ASCE, pp. 145–177.

Baligh, M. M., et al. (1978), "Downdrag on Bitumen-Coated Piles," *JGED,* ASCE, vol. 104, GT 11, Nov, pp. 1355–1369.

Balla, A. (1961), "The Resistance to Breaking Out of Mushroom Foundations for Pylons," *5th ICSMFE,* vol. 1, pp. 569–576.

Barden, L. (1962), "Distribution of Contact Pressure under Foundations," *Geotechnique,* vol. 18, no. 1, March, pp. 1–24.

——, and M. F. Monckton (1970), "Tests on Model Pile Groups in Soft and Stiff Clay," *Geotechnique,* vol. 20, no. 1, March, pp. 94–96.

Barkan, D. D. (1962), *Dynamics of Bases and Foundations,* McGraw-Hill, New York, 434 pp.

Barksdale, R. D., and T. Takefumi (1991), "Design, Construction and Testing of Sand Compaction Piles," *ASTM STP* No. 1089, pp. 4–18.

Beatty, C. I. (1970), "Lateral Tests on Pile Groups," *Foundation Facts,* published by Raymond Concrete Pile Division of Raymond International, Inc., Houston, TX, pp. 18–21.

Becker, D. E., et al. (1987), "Work as a Criterion for Determining in Situ and Yield Stresses in Clays," *CGJ,* vol. 24, no. 4, Nov, pp. 549–564.

Begemann, H. (1974), "General Report: Central and Western Europe," *ESOPT,* Stockholm, vol. 2.1, pp. 29–39.

Bell, A. L. (1915), "The Lateral Pressure and Resistance of Clay, and the Supporting Power of Clay Foundations," in *A Century of Soil Mechanics,* ICE, London, pp. 93–134.

Benmokrane, B., et al. (1994), "Laboratory Investigation of Shaft Resistance of Rock-Socketed Piers Using the Constant Normal Stiffness Direct Shear Test," *CGJ,* vol. 31, no. 3, June, pp. 407–419.

Benoit, J., and G. W. Clough (1986), "Self-Boring Pressuremeter Tests in Soft Clay," *JGED,* ASCE, vol. 112, no. 1, Jan, pp. 60–78.

Berry, P. L., and B. Vickers (1975), "Consolidation of Fibrous Peat," *JGED,* ASCE, vol. 101, GT 8, Aug, pp. 741–753.

Bhatacharya, R. K. (1968), "Stresses and Displacements in Cross-Anisotropic Layered, Elastic Half-Space Due to Axi-Symmetric Loadings on the Top Surface," Ph.D. Dissertation, University of Wisconsin, Madison, 162 pp.

Bhushan, K. (1982), "Discussion: New Design Correlations for Piles in Sands," *JGED,* ASCE, GT 11, Nov, pp. 1508–1510.

——, and F. Boniadi (1988), "Settlement of a Ring Foundation Using Cone Data," *Proc. 1st ISOPT,* vol. 2, pp. 681–685.

——, and S. Askari (1984), "Lateral-Load Tests on Drilled Pier Foundations for Solar Plant Heliostats," *ASTM STP* No. 835, pp. 140–156.

——, et al. (1978), "Lateral Load Tests on Drilled Piers in Stiff Clays," ASCE Spring Convention, Pittsburgh, PA, Preprint No. 3248, 28 pp.

Biggar, K. W., and D. C. Sego (1994), "Time-Dependent Displacement Behaviour of Model Adfreeze and Grouted Piles in Saline Frozen Soils," *CGJ,* vol. 31, no. 3, June, pp. 395–406.

Bjerrum, L. (1972), "Embankments on Soft Ground," *5th PSC,* ASCE, vol. 2, pp. 1–54.

——, and O. Eide (1956), "Stability of Strutted Excavations in Clay," *Geotechnique,* vol. 6, no. 1, March, pp. 32–47.

——, and R. Kirkedam (1958), "Some Notes on Earth Pressures in Stiff Fissured Clay," *Proc., Brussels Conference on Earth Pressure Problems* (2nd European Conference on Soil Mechanics and Foundation Engineering, Brussels), pp. 15–27.

——, and N. E. Simons (1960), "Comparison of Shear Strength Characteristics of Normally Consolidated Clays," *1st PSC,* ASCE, pp. 711–726.

——, et al. (1969), "Reduction of Negative Skin Friction on Steel Piles to Rock," *7th ICSMFE,* vol. 2, pp. 27–34.

Blanchet, R., et al. (1980), "Behavior of Friction Piles in Soft Sensitive Clays," *CGJ,* vol. 17, no. 2, May, pp. 203–224.

Bolton, M. D., and C. K. Lau (1993), "Vertical Bearing Capacity Factors for Circular and Strip Footings on Mohr-Coulomb Soil," *CGJ,* vol. 30, no. 6, Dec, pp. 1024–1033.

Borowicka, H. (1936), "Influence of Rigidity of a Circular Foundation Slab on the Distribution of Pressures over a Contact Surface," *1st ICSMFE,* vol. 2, pp. 144–149.

Bowles, J. E. (1992), *Engineering Properties of Soils and Their Measurement,* 4th ed., McGraw-Hill, New York, 241 pp.

——(1987), "Elastic Foundation Settlements on Sand Deposits," *JGED,* ASCE, vol. 113, no. 8, Aug, pp. 846–860.

——(1986), "Mat Design," *JACI,* vol. 83, no. 6, Nov–Dec, pp. 1010–1017.

——(1984), *Physical and Geotechnical Properties of Soils,* 2nd ed., McGraw-Hill, New York, 578 pp.

——(1983), "Pile Cap Analysis," *Proc. 8th Conf. on Electronic Computation,* ASCE, pp. 102–113.

——(1974*a*), *Analytical and Computer Methods in Foundation Engineering,* McGraw-Hill, New York, 519 pp.

——(1974*b*), "Foundations for Family Housing," *Technical Report D-20: Systems Approach to Site Development,* Construction Engineering Research Laboratory, Champaign, IL, 107 pp.

Bozozuk, M. (1974), "Minor Principal Stress Measurements in Marine Clay with Hydraulic Fracture Tests," *Proc., Conf. on Subsurface Exploration for Underground Excavation and Heavy Construction,* ASCE, pp. 333–349.

——(1972), "Downdrag Measurements on a 160-ft Floating Pipe Test Pile in Marine Clay," *CGJ,* vol. 9, no. 2, May, pp. 127–136.

——et al. (1979), "Analysis of Load Tests on Instrumented Steel Test Piles in Compressible Silty Soil," *ASTM STP* No. 670, pp. 153–180.

Brand, E. W., et al. (1972), "Load Tests on Small Foundations in Soft Clay," *5th PSC,* ASCE, vol. 1, part 2, pp. 903–928.

Brandon, T. L., et al. (1990), "Hydrocompression Settlement of Deep Fills," *JGED,* ASCE, vol. 116, GT 10, Oct, pp. 1536–1548.

Briassoulis, D. (1991), "Limitations in the Range of Applicability of the Classic Silo Theories," *ACI Structural Journal,* vol. 88, no. 4, July–Aug, pp. 437–444.

Briaud, J. L., and R. M. Gibbens (1994), *Predicted and Measured Behavior of Five Spread Footings on Sand,* ASCE, Geotech. SP No. 41, 255 pp.

——, and M. Gambin (1984), "Suggested Practice for Drilling Boreholes for Pressuremeter Testing," *GTJ,* ASTM, vol. 7, no. 1, March, pp. 36–40.

Brierley, G. S., et al. (1979), "Interpreting End-Bearing Pile Load Test Results," *ASTM STP* No. 670, pp. 181–198.

Broms, B. (1972), "Settlements of Pile Groups," *5th PSC,* ASCE, vol. 3, pp. 181–199 (with extensive reference list).

Brooker, E. W., and H. O. Ireland (1965), "Earth Pressures at Rest Related to Stress History," *CGJ,* vol. 2, no. 1, Feb, pp. 1–15.

Brown, A. (1968), "A New Look at Tower Foundation Design," *Hydrocarbon Processing and Petroleum Refiner,* vol. 47, no. 4, April, pp. 174–180.

Brown, J. D., and G. G. Meyerhof (1969), "Experimental Study of Bearing Capacity in Layered Clays," *7th ICSMFE,* vol. 2, pp. 45–51.

Burland, J. B. (1973), "Shaft Friction Piles in Clay—A Simple Fundamental Approach," *Ground Engineering,* vol. 6, no. 3, pp. 30–42.

Butterfield, R., and P. K. Banerjee (1971), "The Problem of Pile Group–Pile Cap Interaction," *Geotechnique,* vol. 21, no. 2, June, pp. 135–142.

Button, S. J. (1953), "The Bearing Capacity of Footings on a Two-Layer Cohesive Subsoil," *3rd ICSMFE,* vol. 1, pp. 332–335.

CDF (1984), "Practical Guidelines for the Selection, Design, and Installation of Piles," *Report of ASCE Committee on Deep Foundations,* 105 pp.

Campanella, R. G., and P. K. Robertson (1988), "Current Status of the Piezocone Test," *1st ISOPT,* vol. 1, pp. 93–116.

——, et al. (1986), "Seismic Cone Penetration Test," *14th PSC,* ASCE, pp 116–130.

Caquot, A., and J. Kerisel (1948), *Tables for the Calculation of Passive Pressure, Active Pressure and Bearing Capacity of Foundations* (trans. by M. A. Bec, London), Gauthier-Villars, Paris.

Carrier, W. D. (1993), "Discussion: Hyperbolic Method for Consolidation Analysis," *JGED,* ASCE, vol. 119, no. 1, Jan, pp. 186–190.

——(1985), "Consolidation Parameters Derived from Index Tests," *Geotechnique,* vol. 35, no. 2, pp. 211–213.

Casagrande, A. (1936), "The Determination of the Preconsolidation Load and Its Practical Significance," *1st ICSMFE,* vol. 3, pp. 60–64.

——(1948), "Classification and Identification of Soils," *Trans. ASCE,* vol. 113, pp. 901–991.

——, and N. Carrillo (1944), "Shear Failure of Anisotropic Materials," *Boston Society of Civil Engineers: Contributions to Soil Mechanics 1941–53,* pp. 122–135.

Caspe, M. S. (1966), "Surface Settlement Adjacent to Braced Open Cuts," *JSMFD,* ASCE, vol. 92, SM 4, July, pp. 51–59.

Chandler, R. J. (1988), "The In-Situ Measurement of the Undrained Shear Strength of Clays Using the Field Vane," *ASTM STP* No. 1014, pp. 13–44.

Chang, C. Y., and J. M. Duncan (1970), "Analysis of Soil Movement around a Deep Excavation," *JSMFD,* ASCE, vol. 96, SM 5, Sept, pp. 1655–1681.

Chang, M. F. (1991), "Interpretation of Overconsolidation Ratio from In Situ Tests in Recent Clay Deposits in Singapore and Malaysia," *CGJ,* vol. 28, no. 2, April, pp. 210–225.

Chellis, R. D. (1961), *Pile Foundations,* 2nd ed., McGraw-Hill, New York, 704 pp.

——(1941), "Discussion: Pile Driving Formulas," *Proc. ASCE,* vol. 67, no. 8, Oct, pp. 1517–1537.

Chen, W. W. (1978), "Discussion: Laterally Loaded Piles: Program Documentation," *JGED,* GT 1, Jan, pp. 161–162.

Chicago, City of, Building Code (1995), Index Publishing Corp., 415 N. State St., Chicago, IL 60610. Published annually.

Chiwanga, M., and A. J. Valsangkar (1988), "Generalized Beam Element on Two-Parameter Elastic Foundation," *JSD,* ASCE, vol. 114, no. 6, June, pp. 1414–1427.

Chowdhury, R. N. (1972), "Deformation Problems in Anisotropic Soil—Application of the Finite Element Method," *Conference on Finite Element Method in Civil Engineering,* Montreal, pp. 653–675.

Chu, K. H., and O. F. Afandi (1966), "Analysis of Circular and Annular Slabs for Chimney Foundations," *JACI,* vol. 63, no. 12, Dec, pp. 1425–1446.

Clayton, C. R. I., et al. (1991), "The Pressure of Clay Backfill against Retaining Structures," *CGJ,* vol. 28, no. 2, April, pp. 282–297.

Clemence, S. P., and A. O. Finbarr (1981), "Design Considerations for Collapsible Soils," *JGED,* ASCE, vol. 107, GT 3, March, pp. 305–317.

Clough, G. W., and T. D. O'Rourke (1990), "Construction Induced Movements in Insitu Walls," Geotech. SP No. 25, ASCE, pp. 439–470.

——, and Y. Tsui (1974), "Performance of Tied-Back Walls in Clay," *JGED,* ASCE, GT 12, Dec, pp. 1259–1273.

——, et al. (1972), "Design and Observation of a Tied-Back Wall," *5th PSC,* ASCE, vol. 1, part 2, pp. 1367–1389.

Coyle, H. M., and R. Ungaro (1991), "Improved Design Procedures for Vertically Loaded *H*-Piles in Sand," *JGED,* ASCE, vol. 117, GT 3, March, pp. 507–528.

——, and R. R. Castello (1981), "New Design Correlations for Piles in Sand," *JGED,* ASCE, vol. 107, GT 7, July, pp. 965–986.

——, et al. (1972), "Field Measurements of Lateral Earth Pressures on a Cantilever Retaining Wall," TTI Research Report 169-2, College Station, TX, 58 pp.

——, and L. C. Reese (1966), "Load Transfer of Axially Loaded Piles in Clay," *JSMFD,* ASCE, vol. 92, SM 2, March, pp. 1–26.

Crawford, C. B., and K. N. Burn (1962), "Settlement Studies on the Mt. Sinai Hospital," *Engineering Journal of Canada,* Ottawa, vol. 45, no. 12, Dec.

——, and R. G. Campanella (1991), "Comparison of Field Consolidation with Laboratory and In Situ Tests," *CGJ,* vol. 28, no. 1, Feb, pp. 103–112.

Cummings, A. E. (1940), "Dynamic Pile Driving Form ulas," *The Boston Society of Civil Engineers: Contributions to Soil Mechanics 1925–40,* pp. 392–413.

Cummings, E. M. (1960), "Cellular Cofferdams and Docks," *Trans. ASCE,* vol. 125, pp. 13–45.

Cunny, R. W., and Z. B. Fry (1973), "Vibratory In Situ and Laboratory Soil Moduli Compared," *JSMFD,* ASCE, vol. 99, SM 12, Dec, pp. 1055–1076.

Cushing, J. J., and R. M. Moline (1975), "Curved Diaphragm Cellular Cofferdams," *JGED,* ASCE, vol. 101, GT 10, Oct, pp. 1055–1059.

DCDMA (1991), *Technical Manual,* Diamond Core Drill Manufacturers' Association, 3008 Millwod Avenue, Columbia, SC. 29205, Tel. 1-803-252-5646, Fax. 1-803-765-0860. 100 pp.

Dahlberg, R. (1974), "Penetration Testing in Sweden," *Proc. 1st ESOPT* Stockholm, Sweden, vol. 1, pp. 115–131.

——(1974a), "Penetration, Pressuremeter, and Screw-Plate Tests in a Preloaded Natural Sand Deposit," *Proc. 1st ESOPT,* Stockholm, Sweden, vol. 2.2, pp. 71–87.

Dakshanamurthy, V., and V. Raman (1973), "A Simple Method of Identifying an Expansive Soil," *Soils and Foundations,* Tokyo, vol. 13, no. 1, March, pp. 97–104.

Daniel, D. E., and R. E. Olson (1982), "Failure of an Anchored Bulkhead," *JGED,* ASCE, GT 10, Oct, pp. 1318–1327.

D'Appolonia, D. J., et al. (1970), "Closure: Settlement of Spread Footings on Sand," *JSMFD,* ASCE, vol. 96, SM 2, pp. 754–762.

——, et al. (1968), "Settlement of Spread Footings on Sand," *JSMFD,* ASCE, vol. 94, SM 3, May, pp. 735–760.

D'Appolonia, E. (1968), "Load Transfer-Pile Clusters," *Proc. Lecture Series on Foundation Engineering,* Northwestern Univ., Evanston, IL, pp. 93–152.

——, and J. A. Hribar (1963), "Load Transfer in a Step-Taper Pile," *JSMFD,* ASCE, vol. 89, SM 6, Nov, pp. 57–77 (also Discussion July 1964).

——, and J. P. Romualdi (1963), "Load Transfer in End Bearing Steel H-Piles," *JSMFD,* ASCE, vol. 89, SM 2, March, pp. 1–26.

Davies, T. G., et al. (1986), "Passive Pressure during Seismic Loading," *JGED,* ASCE, vol. 112, no. 4, April, pp. 479–483.

Davis, E. H., and J. T. Christian (1971), "Bearing Capacity of Anisotropic Cohesive Soil," *JSMFD,* ASCE, vol. 97, SM5, May, pp. 753–769.

Davisson, M. T. (1970), "BRD Vibratory Driving Formula," *Foundation Facts,* published periodically by Raymond Concrete Pile Division of Raymond International, Inc., Houston, TX, vol. 6, no. 1, pp. 9–11.

——, and K. E. Robinson (1965), "Bending and Buckling of Partially Embedded Piles," *6th ICSMFE,* vol. 2, pp. 243–246.

——, and J. R. Salley (1972), "Settlement Histories of Four Large Tanks on Sand," *5th PSC,* ASCE, vol. 1, part 2, pp. 981–996.

——, and J. R. Salley (1968), "Lateral Load Tests on Drilled Piers," *ASTM STP* No. 444, pp. 68–83.

Dawson, R. F. (1959), "Modern Practices Used in the Design of Foundations for Structures on Expansive Soils," *Quarterly of the Colorado School of Mines: Theoretical and Practical Treatment of Expansive Soils,* Golden, CO, vol. 54, no. 4, pp. 66–87.

Dayal, V., and J. H. Allen (1973), "Instrumented Impact Cone Penetrometer," *CGJ,* vol. 10, no. 3, Aug, pp. 397–409.

De Beer, E. E. (1970), "Experimental Determination of the Shape Factors and the Bearing Capacity Factors of Sand," *Geotechnique,* vol. 20, no. 4, Dec, pp. 387–411.

——(1965), "The Scale Effect on the Phenomenon of Progressive Rupture in Cohesionless Soils," *6th ICSMFE,* vol. 2, pp. 13–17.

Demartinecourt, J. P., and G. E. Bauer (1983), "The Modified Borehole Shear Device," *Geotech. Test. J.,* ASTM, vol. 6, no. 1, March, pp. 24–29.

De Mello, V. F. (1971), "The Standard Penetration Test," *4th Pan-American Conf. on SMFE,* San Juan, Puerto Rico (published by ASCE), vol. 1, pp. 1–86 (with 353 references).

Den Hartog, J. P. (1952), *Mechanical Vibrations,* 4th ed., McGraw-Hill, New York, 436 pp.

Denver, H. (1982), "Modulus of Elasticity for Sand Determined by SPT and CPT," *2nd ESOPT,* Amsterdam, vol. 1, pp. 35–40.

Desai, C. S. (1979), *Elementary Finite Element Method,* Prentice-Hall, Englewood Cliffs, NJ, 434 pp.

Dewey, F. B., and L. Kempner, Jr. (1975), "Discussion: Design of Steel Transmission Pole Structures," *JSD,* ASCE, vol. 101, ST 41, Nov, pp. 2439–2441.

Dismuke, T. D. (1975), "Cellular Structures and Braced Excavations," Chap. 14, *Foundation Engineering Handbook,* 1st ed., Van Nostrand Reinhold, New York, 751 pp.

——(1970), "Stress Analysis of Sheet Piling in Cellular Structures," *Proc. Conference: Design and Installation of Pile Foundations and Cellular Structures,* Lehigh University, Bethlehem, PA, pp. 339–365.

Dobry, R., and G. Gazetas (1986), "Dynamic Response of Arbitrary Shaped Foundations," *JGED,* ASCE, vol. 112, no. 2, Feb, pp. 109–135 (see errata July, p. 747).

——, and G. Gazetas (1985), "Dynamic Stiffness and Damping of Foundations Using Simple Methods," *Proc. Symposium: Vibration Problems in Geotechnical Engineering,* ASCE, pp. 75–107.

Drannikov, A. M. (1967), "Construction on Loess of Small Thickness," *3rd Asian Regional Conference on SMFE,* Haifa, Israel, vol. 1, pp. 3–4.

Drozd, K. (1974), "The Influence of Moisture Content in Sand on Penetration Results," *Proc. ESOPT,* Stockholm, vol. 2.1, pp. 162–164.

Duncan, J. M. (1993), "Limitations of Conventional Analysis of Consolidation Settlement," *JGED,* ASCE, vol. 119, no. 9, Sept., pp. 1331–1359. See also "Discussion," *JGED,* vol. 121, no. 6, June 1995, pp. 513–518. This paper was based on the 1993 annual Terzaghi Lecture.

——, and C. Y. Chang (1970), "Nonlinear Analysis of Stress and Strain in Soils," *JSMFD,* ASCE, vol. 96, SM 5, pp. 1629–1653.

ENR (1965), "Michigan Pile Test Program Test Results Are Released," *Eng. News-Record,* May 20, pp. 26–28, 33–34.

Edil, T. B., and A. W. Dhowian (1981), "At-Rest Lateral Pressure of Peat Soils," *JGED,* ASCE, vol. 107, GT 2, Feb, pp. 201–217.

Endley, S. N., et al. (1979), "A Study of Axial Pile Load Tests," *Symposium on Deep Foundations,* ASCE, pp. 101–121.

Esrig, M. I., and R. C. Kirby (1979), "Soil Capacity for Supporting Deep Foundation Members in Clay," *ASTM STP* No. 670, pp. 27–63.

Fadum, R. E. (1948), "Influence Values for Estimating Stresses in Elastic Foundations," *2nd ICSMFE,* vol. 3, pp. 77–84.

Fang, Y., and I. Ishibashi (1986), "Static Earth Pressures with Various Wall Movements," *JGED,* ASCE, vol. 112, No. 3, March, pp. 317–333.

Feda, J., et al. (1995), "Physical Similitude and Structural Collapse in K_o Compression of Soils," *JGED,* ASCE, vol. 121, no. 2, Feb, pp. 210–215.

Feld, J. (1965), "Tolerance of Structures to Settlement," *JSMFD,* ASCE, vol. 91, SM 3, May, pp. 63–67.

Fellenius, H. H. (1972), "Down-Drag on Piles in Clay Due to Negative Skin Friction," *CGJ,* vol. 9, no. 4, Nov, pp. 323–337.

Finno, R. J. (1989), ed. *Predicted and Observed Axial Behavior of Piles,* Geotech. SP No. 23, ASCE, 385 pp.

Fischer, J. A., et al. (1972), "Settlement of a Large Mat on Sand," *5th PSC,* ASCE, vol. 1, part 2, pp. 997–1018.

Flaate, K. (1972), "Effects of Pile Driving in Clays," *CGJ,* vol. 9, no. 1, Feb, pp. 81–88.

———, and P. Selnes (1977), "Side Friction of Piles in Clay," *9th ICSMFE,* vol. 1, pp. 517–522.

Flint, R. F. (1971), *Glacial and Quaternary Geology,* John Wiley & Sons, New York, 892 pp.

Focht, J. A., Jr., and L. M. Kraft (1977), "Progress in Marine Geotechnical Engineering," *JGED,* ASCE, vol. 103, GT 10, Oct, pp. 1097–1118.

———, and M. W. O'Neill (1985), "Piles and Other Deep Foundations," *11th ICSMFE,* vol. 4, pp. 187–209.

Foott, R., et al. (1980), "Embankments Through Cross River Swamp," *JGED,* ASCE, vol. 106, GT 3, March, pp. 219–234.

Fox, E. N. (1948*a*), "The Mathematical Solution for the Early Stages of Consolidation," *2nd ICSMFE,* vol. 1, pp. 41–42.

———(1948*b*), "The Mean Elastic Settlement of a Uniformly Loaded Area at a Depth below the Ground Surface," *2nd ICSMFE,* vol. 1, pp. 129–132.

Fox, P. J., et al. (1992), "C_α/C_c Concept Applied to Compression of Peat," *JGED,* ASCE, vol. 118, GT 8, Aug, pp. 1256–1263.

Francis, A. J. (1964), "Analysis of Pile Groups with Flexural Resistance," *JSMFD,* ASCE, vol. 90, SM 3, May, pp. 1–32.

———, et al. (1961), "The Behavior of Slender Point Bearing Piles in Soft Soil," *Symp. on Design of Tall Buildings,* University of Hong Kong, pp. 25–50.

Fredlund, D. G., and H. Rahardjo (1993), "An Over view of Unsaturated Soil Behaviour," Geotech. SP No. 39, ASCE, pp. 1–31. (See also *CGJ,* vol. 1, 1979.)

Frydman, S., and I. Keissar (1987), "Earth Pressure on Retaining Walls near Rock Faces," *JGED,* ASCE, vol. 113, no. 6, June, pp. 586–599.

Garbe, C. W., and K. Tsai (1972), "Engineering Improvements in Reclaimed Marshland for Housing Project," *Proc. 2nd International Symposium on Lower-Cost Housing Problems,* University of Missouri—Rolla, pp. 153–157.

Garga, V. K., and M. A. Khan (1992), "Interpretation of Field Vane Strength of an Anisotropic Soil," *CGJ,* vol. 29, no. 4, Aug., pp. 627–637.

Gates, M. (1957), "Empirical Formula for Predicting Pile Bearing Capacity," *Civil Engineering,* ASCE, vol. 27, no. 3, March, pp. 65–66.

Gaylord, E. H., and C. N. Gaylord (1972), *Design of Steel Structures,* 2nd ed., McGraw-Hill, New York, pp. 480–482 (may be out of print).

Gazetas, G., et al. (1985), "Elastic Settlement of Arbitrarily Shaped Foundations Embedded in Half-Space," *Geotechnique,* vol. 35, no. 3, Sep, pp. 339–346.

Gazioglu, S. M., and M. W. O'Neill (1985), "Evaluation of *p–y* Relationships in Cohesive Soils," *Symp. on Analysis and Design of Pile Foundations,* ASCE, pp. 192–213.

Geddes, J. D. (1969), "Boussinesq-Based Approximations to the Vertical Stresses Caused by Pile-Type Subsurface Loadings," *Geotechnique,* vol. 19, no. 4, Dec, pp. 509–514.

———(1966), "Stresses in Foundation Soils Due to Vertical Subsurface Loading," *Geotechnique,* vol. 16, no. 3, Sep, pp. 231–255.

Gibbs, H. J., et al. (1960), "Shear Strength of Cohesive Soils," *1st PSC,* ASCE, pp. 33–162.

———, and W. Y. Holland (1960), "Petrographic and Engineering Properties of Loess," *Engineering Monograph No. 28,* U.S. Bureau of Reclamation, Denver, CO, 37 pp.

———, and W. G. Holtz (1957), "Research on Determining the Density of Sands by Spoon Penetration Testing," *4th ICSMFE,* vol. 1, pp. 35–39.

Gill, S. A. (1980), "Applications of Slurry Walls in Civil Engineering," *Journal of Construction Division,* ASCE, vol. 106, CO 2, pp. 155–167.

Gleser, S. M. (1983), "Generalized Behavior of Laterally Loaded Piles," *ASTM STP* No. 835, pp. 72–96 (see also Discussion, p. 240).

Glick, G. W. (1948), "Influence of Soft Ground in the Design of Long Piles," *2nd ICSMFE,* vol. 4, pp. 84–88.

Gogoll, F. H. (1970), "Foundations on Swelling Clay beneath a Granular Blanket," *Proc., Symp. on Soils and Earth Structures in Arid Climate,* Institution of Engineers (Australia), Adelaide, May, pp. 42–48.

Golder, H. Q., et al. (1970), "Predicted Performance of Braced Excavation," *JSMFD,* ASCE, vol. 96, SM 3, May, pp. 801–815.

Goodwin, J. W. (1993), "Bi-Directional Load Testing of Shafts to 6000 Tons," Geotech. SP No. 38, ASCE, pp. 204–217.

Grant, R., et al. (1974), "Differential Settlement of Buildings," *JGED,* ASCE, vol. 100, GT 9, Sept, pp. 973–991.

Grayman, R. (1970), "Cellular Structure Failures," *Proc. Conference: Design and Installation of Pile Foundations and Cellular Structures,* Lehigh University, Bethlehem, PA, pp. 383–391.

Greenwood, D. A., and G. H. Thomson (1984), *Ground Stabilization: Deep Compaction and Grouting,* ICE Works Construction Guides, Thomas Telford Ltd., London, 47 pp. (available through ASCE).

Gromko, G. J. (1974), "Review of Expansive Soils," *JGED,* ASCE, vol. 100, GT 6, June, pp. 667–687.

Haliburton, T. A. (1968), "Numerical Analysis of Flexible Retaining Structures," *JSMFD,* ASCE, vol. 94, SM 6, Nov, pp. 1233–1251.

Hall, E. B., and B. B. Gordon (1963), "Triaxial Testing with Large-Scale High Pressure Equipment," *ASTM STP* No. 361, pp. 315–328.

Hamouche, K. K., et al. (1995), "In Situ Evaluation of K_o in Eastern Canada Clays," *CGJ,* vol. 32, no. 4, Aug., pp. 677–688.

Handy, R. L. (1986), "Borehole Shear Test and Slope Stability," *14th PSC,* ASCE, pp. 161–175.

——, (1985), "The Arch in Soil Arching," *JGED,* ASCE, vol. 111, no. 3, March, pp. 302–318.

——et al. (1982), "In Situ Stress Determination by Iowa Stepped Blade," *JGED,* vol. 108, GT 11, Nov, pp. 1405–1422.

Hansen, J. B. (1970), "A Revised and Extended Formula for Bearing Capacity," *Danish Geotechnical Institute,* Copenhagen, Bul. No. 28, 21 pp. (successor to Bul. No. 11).

——(1967), "The Philosophy of Foundation Design: Design Criteria Safety Factors, and Settlement Limits," *Proc., Symp. on Bearing Capacity and Settlement of Foundations,* Duke University, Durham, NC, pp. 9–13.

——(1961), "A General Formula for Bearing Capacity," *Danish Geotechnical Institute,* Copenhagen, Bul. No. 11, 46 pp.

Hardin, B. O., and W. L. Black (1968), "Vibration Modulus of Normally Consolidated Clay," *JSMFD,* ASCE, vol. 94, SM 2, March, pp. 27–42.

——, and G. E. Blandford (1989), "Elasticity of Particulate Materials," *JGED,* ASCE, vol. 115, No. 6, pp. 788–805.

——, and V. P. Drnevich (1972), "Shear Modulus and Damping in Soils: Design Equations and Curves," *JSMFD,* ASCE, vol. 98, SM 7, July, pp. 667–692.

Hetenyi, M. (1946), *Beams on Elastic Foundations,* The University of Michigan Press, Ann Arbor, MI, 255 pp.

Hiley, A. (1930), "Pile-Driving Calculations with Notes on Driving Forces and Ground Resistances," *The Structural Engineer,* London, vol. 8, pp. 246–259, 278–288.

Hirsch, T. J., et al. (1970), "Pile Driving Analysis by One-Dimensional Wave Theory: State of the Art," *Highway Research Record No. 333,* pp. 33–54.

Hoar, R. J., and K. H. Stokoe II (1978), "Generation and Measurement of Shear Waves In Situ," *ASTM STP* No. 654, pp. 3–29.

Holtz, R. D., and W. D. Kovacs (1981), *An Introduction to Geotechnical Engineering,* Prentice-Hall, Englewood Cliffs, NJ, 733 pp.

——, et al. (1986), "Lessons from Oedometer Tests on High Quality Samples," *JGED,* ASCE, vol. 112, GT 8, Aug, pp. 768–776.

Holtz, W. G. (1973), "The Relative Density Approach—Uses, Testing Requirements, Reliability, and Shortcomings," *ASTM STP* No. 523, pp. 5–17.

——(1959), "Expansive Clays—Properties and Problems," *Quarterly of the Colorado School of Mines: Theoretical and Practical Treatment of Expansive Soils,* Golden, CO, vol. 54, no. 4, pp. 89–125.

——, and J. W. Hilf (1961), "Settlement of Soil Foundations Due to Saturation," *5th ICSMFE,* vol. 1, pp. 673–679.

Hoshiya, M., and J. N. Mandal (1984), "Metallic Powders in Reinforced Earth," *JGED,* ASCE, vol. 110, no. 10, Oct, pp. 1507–1511.

Housel, W. S. (1929), "Discussion of: 'The Science of Foundations'," *Trans. ASCE,* vol. 93, pp. 322–330.

Howe, R. J. (1955), "A Numerical Method for Predicting the Behavior of Laterally Loaded Piling," *Exploration and Production Research Division Publ. No. 412,* Shell Oil Co., Houston, TX.

Hrennikoff, A. (1950), "Analysis of Pile Foundations with Batter Piles," *Trans. ASCE,* vol. 115, pp. 351–389.

Hughes, J. M., et al. (1975), "A Field Trial of the Reinforcing Effect of a Stone Column in Soil," *Geotechnique,* vol. 25, no. 1, March, pp. 31–44.

Hvorslev, M. J. (1949), "Subsurface Exploration and Sampling of Soils for Civil Engineering Purposes," *Waterways Experiment Station* (may still be available from Engineering Foundation, NY), 521 pp.

Indraratna, B., et al. (1992), "Development of Negative Skin Friction on Driven Piles in Soft Bangkok Clay," *CGJ,* vol. 29, no. 3, June, pp. 393–404; Also "Discussion" in vol. 30, no. 5, Oct, 1994, pp. 886–888.

Ingold, T. S. (1982), *Reinforced Earth,* Thomas Telford Ltd., London, 141 pp.

——(1979), "The Effects of Compaction on Retaining Walls," *Geotechnique,* vol. 29, no. 3, Sep, pp. 265–283.

Ireland, H. O. (1957), "Pulling Tests on Piles in Sand," *4th ICSMFE,* vol. 2, pp. 43–45.

Ismael, N. F., et al. (1994), "Tension Tests on Bored Piles in Cemented Desert Sands," *CGJ,* vol. 31, no. 4, Aug, pp. 597–603.

——, and A. M. Jeragh (1986), "Static Cone Tests and Settlement of Calcareous Desert Sands," *CGJ,* vol. 23, no. 3, Aug, pp. 297–303.

Jaky, J. (1948), "Pressure in Silos," *2nd ICSMFE,* vol. 1, pp. 103–107.

James, R. G., and P. L. Bransby (1970), "Experimental and Theoretical Investigations of a Passive Earth Pressure Problem," *Geotechnique,* vol. 20, no. 1, March, pp. 17–37.

Jamiolkowski, M., et al. (1988), "New Correlations of Penetration Tests for Design Practice," *Proc. 1st ISOPT,* vol. 1, pp. 263–296 (huge number of references cited).

——, et al. (1985), "New Developments in Field and Laboratory Testing of Soils," *11th ICSMFE,* vol. 1, pp. 57–153.

Janbu, N. (1976), "Static Bearing Capacity of Friction Piles," *Proc. 6th European Conference on SMFE,* vol. 1.2, pp. 479–488.

——(1957), "Earth Pressures and Bearing Capacity Calculations by Generalized Procedure of Slices," *4th ICSMFE,* vol. 2, pp. 207–212.

Janes, H. W. (1973), "Densification of Sand for Drydock by Terra-Probe," *JSMFD,* ASCE, vol. 99, SM 6, June, pp. 451–470.

Jaworski, G. W., et al. (1981), "Laboratory Study of Hydraulic Fracturing," *JGED,* ASCE, vol. 107, GT 6, June, pp. 713–732.

Jenike, A. W., and J. R. Johanson (1968), "Bin Loads," *JSD,* ASCE, vol. 94, ST 4, April, pp. 1011–1041.

Jewell, R. A., and M. J. Pedley (1992), "Analysis of Soil Reinforcement with Bending Stiffness," *JGED,* ASCE, vol. 118, no. 10, Oct, pp. 1505–1528.

Johnson, L. D., and D. R. Snethen (1979), "Prediction of Potential Heave of Swelling Soil," *GTJ,* ASTM, vol. 1, no. 3, Sept, pp. 117–124.

Johnson, S. D. (1975), "Analysis and Design Relating to Embankments," *6th PSC,* ASCE, vol. 2, pp. 1–48.

Johnson, S. J. (1970), "Precompression for Improving Foundation Soil," *JSMFD,* ASCE, vol. 96, SM 1, Jan, pp. 73–110.

Jose, B. T., et al. (1989), "Log-Log Method for Determination of Preconsolidation Pressure," *GTJ,* ASTM, vol. 12, no. 3, Sept, pp. 230–237.

Jumikis, A. R. (1962), *Soil Mechanics,* D. Van Nostrand, NJ, 791 pp.

Juran, I., et al. (1990), "Design of Soil Nailed Retaining Structures," Geotech. SP No. 25, ASCE, pp. 644–659.

Kanja, M. A., and C. M. Wolle (1977), "Residual Strength—New Testing and Microstructure," *9th ICSMFE,* vol. 1, pp. 153–154.

Kantey, B. A. (1965), "Session 5: Shallow Foundations and Pavements," *6th ICSMFE,* vol. 3, pp. 453–455.

Karlsson, R., and L. Viberg (1967), "Ratio c/p′ in Relation to Liquid Limit and Plasticity Index with Special Reference to Swedish Clays," *Proc. Geotechnical Conference,* Oslo, Norway, vol. 1, pp. 43–47.

Kay, J. N., and R. L. Cavagnaro (1983), "Settlement of Raft Foundations," *JGED,* ASCE, vol. 109, no. 11, Nov, pp. 1367–1382.

Keaveny, J. M., and J. K. Mitchell (1986), "Strength of Fine-Grained Soils Using the Piezocone," Geotech. SP No. 6, ASCE, pp. 668–685.

Kezdi, A. (1972), "Stability of Rigid Structures," *Proc. 5th European Conf. on SMFE,* vol. 2, pp. 105–130.

Kim, J. B., and R. J. Brungraber (1976), "Full-Scale Lateral Load Tests of Pile Groups," *JGED,* ASCE, vol. 102, GT 1, Jan, pp. 87–105.

Kim, T. C., and M. Novak (1981), "Dynamic Properties of Some Cohesive Soils of Ontario," *CGJ,* vol. 18, no. 3, Aug, pp. 371–389.

Kjellman, W. (1948), "A Method of Extracting Long Continuous Cores of Undisturbed Soil," *2nd ICSMFE,* vol. 1, pp. 255–258.

Klohn, E. J. (1961), "Pile Heave and Redriving," *JSMFD,* ASCE, vol. 87, SM 4, Aug, pp. 125–145.

Ko, H. Y., and L. W. Davidson (1973), "Bearing Capacity of Footings in Plane Strain," *JSMFD,* ASCE, vol. 99, SM 1, Jan, pp. 1–23.

Koerner, R. M. (1990), *Designing with Geosynthetics,* 2nd ed., Prentice-Hall, Englewood Cliffs, NJ, 652 pp.

——, and A. Partos (1974), "Settlement of Building on Pile Foundation in Sand," *JGED,* ASCE, vol. 100, GT 3, March, pp. 265–278.
Komornik, A., and D. David (1969), "Prediction of Swelling Pressure of Clays," *JSMFD,* ASCE, vol. 95, SM 1, Jan, pp. 209–225.
Kondner, R. L. (1963), "Hyperbolic Stress-Strain Response: Cohesive Soils," *JSMFD,* ASCE, vol. 89, SM 1, pp. 115–143.
Koppula, S. D. (1986), "Discussion: Consolidation Parameters Derived from Index Tests," *Geotechnique,* vol. 36, no. 2, June, pp. 291–292.
——(1981), "Statistical Estimation of Compression Index," *GTJ,* ASTM, vol. 4, no. 2, June, pp. 68–73.
Koutsoftas, D. (1980), "Undrained Shear Behavior of a Marine Clay," *ASTM STP* No. 740, pp. 254–276.
——, and J. A. Fischer (1976), "In-Situ Undrained Shear Strength of Two Marine Clays," *JGED,* ASCE, vol. 102, GT 9, Sept, pp. 989–1005.
Kovacs, W. D., and L. A. Salomone (1982), "SPT Hammer Energy Measurement," *JGED,* ASCE, GT 4, April, pp. 599–620.
Kraft, L. M., Jr., et al. (1981*a*), "Friction Capacity of Piles Driven into Clay," *JGED,* ASCE, GT 11, Nov, pp. 1521–1541.
——, et al. (1981), "Theoretical *t–z* Curves," *JGED,* ASCE, GT 11, Nov, pp. 1543–1561.
Kuhn, S. H., and A. B. Williams (1961), "Scour Depth and Soil Profile Determinations in River Beds," *5th ICSMFE,* vol. 1, pp. 487–490.
Kumbhojkar, A. S. (1993), "Numerical Evaluation of Terzaghi's N_γ," *JGED,* ASCE, GT 3, March, pp. 598–607.
Kuppusamy, T., and A. Buslov (1987), "Elastic-Creep Analysis of Laterally Loaded Piles," *JGED,* ASCE, vol. 113, GT 4, April, pp. 351–365.

Laba, J. T. (1974), "Adfreezing of Sands to Concrete," *Transport. Research Board,* TRR No. 497, Washington, DC, pp. 31–39.
——, and J. B. Kennedy (1986), "Reinforced Earth Retaining Wall Analysis and Design," *CGJ,* vol. 23, no. 3, Aug, pp. 317–326.
Lacasse, S., and T. Lunne (1986), "Dilatometer Tests in Sand," *14th PSC,* ASCE, pp. 686–699.
Lacroix, Y., et al. (1970), "Design, Construction, and Performance of Cellular Cofferdams," *4th PSC,* ASCE, pp. 271–328.
Ladanyi, B. (1972), "In-Situ Determination of Undrained Stress-Strain Behavior of Sensitive Clays with/nl the Pressuremeter," *CGJ,* vol. 9, no. 3, Aug, pp. 313–319.
——(1963), "Evaluation of Pressuremeter Tests in Granular Soils," *2nd Pan-American Conf. on SMFE,* Brazil, vol. 1, pp. 3–20.
Ladd, C. C., and R. Foott (1974), "New Design Procedure for Stability of Soft Clays," *JGED,* ASCE, vol. 100, GT 7, July, pp. 763–786.
——, et al. (1977), "Stress-Deformation and Strength Characteristics," *State-of-Art Report, 9th ICSMFE,* vol. 2, pp. 421–494.
Lade, P. V., and K. L. Lee (1976), "Engineering Properties of Soils," *Engineering Report,* UCLA-ENG-7652, Los Angeles, CA, 145 pp.
Lagasse, P. F., et al. (1995), "Guarding Against Scour," *Civil Engineering,* ASCE, vol. 65, no. 6, June, pp. 56–59.
Lambe, T. W. (1970), "Braced Excavations," *4th PSC,* ASCE, pp. 149–218.
——(1967), "Stress Path Method," *JSMFD,* ASCE, vol. 93, SM 6, pp. 309–331.
——(1964), "Methods of Estimating Settlement," *2nd PSC,* ASCE, pp. 47–71.
——, and R. V. Whitman (1979), *Soil Mechanics,* 2nd ed., John Wiley & Sons, New York, 553 pp.
——, et al. (1970), "Measured Performance of Braced Excavations," *JSMFD,* ASCE, vol. 96, SM 3, May, pp. 817–836.
Landau, R. E. (1978), "Sand Drain Theory and Practice," *Transport. Research Board,* TRR No. 678, Washington, DC, pp. 22–31.
——(1966), "Method of Installation as a Factor in Sand Drain Stabilization Design," *Highway Research Board,* HRR No. 133, Washington, DC, pp. 75–96.
Landva, A. O., and P. E. Pheeney (1980), "Peat Fabric and Structure," *CGJ,* vol. 17, no. 3, Aug, pp. 416–435.
Larew, H. G., and G. A. Leonards (1962), "A Repeated Load Strength Criterion," *Proc. Highway Research Board,* vol. 41, pp. 529–556.
La Russo, R. S. (1963), "Wanapum Development—Slurry Trench and Grouted Cutoff," *Proc. Symp.: Grouts and Drilling Muds in Engineering Practice,* Butterworths, London, pp. 196–201.
Laursen, E. M. (1962), "Scour at Bridge Crossings," *Trans. ASCE,* vol. 127, part 1, pp. 166–209.
——, and A. Toch (1956), "Scour around Bridge Piers and Abutments," *Iowa Highway Research Board Bull. No. 4,* Ames, IA, May, 60 pp.
Lavielle, C. C., et al. (1985), "Arctic Foundation Selection: A Decision Matrix," *Proc., Conf. Session on Foundations in Permafrost and Seasonal Frost,* ASCE, pp. 1–14.
Law, K. T. (1979), "Triaxial-Vane Tests on a Soft Marine Clay," *CGJ,* vol. 16, no. 1, Feb, pp. 11–18.
——, and K. Y. Lo (1976), "Analysis of Shear Induced Anisotropy in Leda Clay," *Proc., Conf. on Numerical Methods in Geomechanics,* ASCE, vol. 1, pp. 329–344.

Lawton, E. C., et al. (1989), "Collapse of Compacted Clayey Soil," *JGED,* ASCE, vol. 115, GT 9, Sept, pp. 1252–1267.

Lee, C. Y. (1993), "Settlement of Pile Groups—Practical Approach," *JGED,* ASCE, vol. 119, no. 9, Sept, pp. 1449–1461.

Lee, H. C., and W. K. Wray (1992), "Evaluation of Soil Suction Instruments," *7th International Conference on Expansive Soils,* Dallas, TX, published by Texas Tech. Univ., Lubbock, TX, vol. 1, pp. 307–312.

Lee, K. L. (1970), "Comparison of Plane Strain and Triaxial Tests on Sand," *JSMFD,* ASCE, vol. 96, SM 3, May, pp. 901–923.

Leet, L. D. (1950), *Earth Waves,* John Wiley & Sons, New York, 122 pp.

Lefebvre, G., et al. (1994), "Laboratory and Field Determination of Small-Strain Shear Modulus for a Structured Champlain Clay," *CGJ,* vol. 31, no. 1., Feb., pp. 61–70.

——, et al. (1991), "Evaluating K_o in Champlain Clays with Hydraulic Fracture Tests," *CGJ,* vol. 28, no. 3, June, pp. 365–377.

——, et al. (1988), "Comparison of Field Vane and Laboratory Undrained Shear Strength on Soft Sensitive Clays," *ASTM STP* No. 1014, pp. 233–246.

Leonards, G. A. (1968), "Predicting Settlement of Buildings on Clay Soils," *Proc., Lecture Series on Foundation Engineering, Northwestern University,* published by Illinois Institute of Technology, Chicago, IL, pp. 41–51.

——, and D. Lovell (1979), "Interpretation of Load Tests on High-Capacity Driven Piles," *ASTM STP* No. 670, pp. 388–415.

——, et al. (1980), "Dynamic Compaction of Granular Soils," *JGED,* ASCE, vol. 106, GT 1, Jan, pp. 35–44.

Leroueil, S., et al. (1988), "Direct Determination of Permeability of Clay under Embankment," *JGED,* ASCE, vol. 114, GT 6, June, pp. 645–657.

Li, K. S. (1989), "Discussion: Work as a criterion . . . ," *CGJ,* vol. 26, no. 2, May, pp. 324–326.

Liao, S. S., and T. L. Neff (1990), "Estimating Lateral Earth Pressures for Design of Excavation Support," Geotech. SP No. 25, ASCE, pp. 489–509.

——, and R. V. Whitman (1986), "Overburden Correction Factors for Sand," *JGED,* vol. 112, no. 3, March, pp. 373–377.

Lin, Y., et al. (1991), "Impact-Echo Response of Concrete Shafts," *GTJ,* ASTM, vol. 14, No. 2, June, pp. 121–137.

Linnel, K. A., and G. H. Johnston (1973), "Engineering and Design and Construction in Permafrost Regions: A Review," *North American Contribution to 2nd Int. Conf. on Permafrost,* National Academy of Sciences, Washington, DC, pp. 553–575.

Lo, K. W., et al. (1990), "Dynamic Replacement and Mixing of Organic Soils with Sand Charges," *JGED,* vol. 116, no. 10, Oct, pp. 1463–1482.

Loganathan, N., et al. (1992), "Strength Correlation Factor for Residual Soils," *JGED,* ASCE, vol. 118, GT 4, April, pp. 593–610.

Long, E. L. (1973), "Designing Friction Piles for Increased Stability at Lower Installed Cost in Permafrost," *Proc., 2nd International Conference on Permafrost,* National Academy of Sciences, Washington, DC, pp. 693–698.

Lorenz, H. (1963), "Utilization of a Thixotropic Fluid in Trench Cutting and the Sinking of Caissons," *Proc. of Symposium on Grouts and Drilling Muds in Engineering Practice,* Butterworths, London, pp. 202–205.

Lukas, R. G., and C. N. Baker (1978), "Ground Movement Associated with Drilled Pier Installations," *ASCE Spring Convention,* Pittsburgh, PA, Preprint No. 3266, 16 pp.

Lun, P. T., and A. K. Parkin (1985), "Consolidation Behaviour Determined by the Velocity Method," *CGJ,* vol. 22, no. 2, May, pp. 158–165.

Lunne, T., and O. Eide (1976), "Correlations between Cone Resistance and Vane Shear Strength in Some Scandinavian Soft to Medium Stiff Clays," *CGJ,* vol. 13, no. 4, Nov, pp. 430–441.

Luttenegger, A. J., and D. A. Timian (1986), "In Situ Test with K_o Stepped Blade," *14th PSC,* ASCE, pp. 730–751.

MacDonald, D. H., and A. W. Skempton (1955), "A Survey of Comparisons between Calculated and Observed Settlements of Structures on Clay," *Conf. on Correlation of Calculated and Observed Stresses and Displacements,* ICE, London, pp. 318–337.

Mackey, R. D., and D. P. Kirk (1967), "At Rest, Active and Passive Earth Pressures," *Proc., Southeastern Asian Regional Conf. on Soil Engineering,* Bangkok, pp. 187–199.

——, and P. A. Mason (1972), "Pressure Distribution during Filling and Discharging a Silo," *5th European Conf. SMFE,* Madrid, vol. 1, pp. 55–62.

Mahar, L. J., and M. W. O'Neill (1983), "Geotechnical Characteristics of Desiccated Clay," *JGED,* ASCE, vol. 109, GT 1, Jan, pp. 56–77.

Maitland, J. K., and W. L. Schroeder (1979), "Model Study of Circular Sheetpile Cells," *JGED,* ASCE, vol. 105, GT 7, July, pp. 805–821.

Makhlouf, H. M., and J. J. Stewart (1965), "Factors Influencing the Modulus of Elasticity of Dry Sand," *6th ICSMFE,* vol. 1, pp. 298–302.

Mana, A. I., and G. W. Clough (1981), "Prediction of Movements for Braced Cuts in Clay," *JGED,* ASCE, vol. 107, GT 6, pp. 759–777.

Mansur, C. I., and A. H. Hunter (1970), "Pile Tests—Arkansas River Project," *JSMFD,* ASCE, vol. 96, SM 5, Sept, pp. 1545–1582.

Marchetti, S. (1980), "In Situ Tests by Flat Dilatometer," *JGED,* ASCE, vol. 106, GT 3, March, pp. 299–321.

Massarsch, K. R. (1975), "New Method for Measurement of Lateral Earth Pressure in Cohesive Soils," *CGJ,* vol. 12, no. 1, Feb, pp. 142–146.

———, et al. (1975), "Measurement of Horizontal In-Situ Stresses," *7th PSC,* ASCE, vol. 1, pp. 266–286.

Matlock, H., and L. C. Reese (1960), "Generalized Solutions for Laterally Loaded Piles," *JSMFD,* ASCE, vol. 86, SM 5, Oct, pp. 63–91.

Matsuzawa H., et al. (1985), "Dynamic Soil and Water Pressures of Submerged Soils," *JGED,* ASCE, vol. 111, GT 10, pp. 1161–1176.

Matyas, E. L., and J. C. Santamarina (1994), "Negative Skin Friction and the Neutral Plane," *CGJ,* vol. 31, no. 4, Aug, pp. 591–596.

Mayne, P. W. (1984), "K_o–c_u/σ'_{vo} Trends for Overconsolidated Clays," *JGED,* ASCE, vol. 110, no. 10, Oct, pp. 1511–1516.

———(1982), "Cam-Clay Predictions of Undrained Strength: Discussion" *JGED,* ASCE, vol. 108, GT 2, Feb, pp. 327–330.

———(1980), "Cam-Clay Predictions of Undrained Strength," *JGED,* ASCE, vol. 106, GT 11, Nov, pp. 1219–1242.

———, et al. (1984), "Ground Response to Dynamic Compaction," *JGED,* ASCE, vol. 110, no. 6, June, pp. 757–774 (with 86 references).

———, and F. H. Kulhawy (1982), "K_o-OCR Relationships in Soil," *JGED,* ASCE, vol. 108, no. 6, June, pp. 851–872 (with 77 references).

Mayne, P., and G. R. Rix (1995), "Laboratory and Field Determination of Small-Strain Shear Modulus for a Structured Champlain Clay: Discussion," *CGJ,* vol. 32, no. 1, Feb., pp. 193–194.

McClelland, B., and J. A. Focht, Jr. (1958), "Soil Modulus for Laterally Loaded Piles," *Trans. ASCE,* vol. 123, pp. 1049–1086.

McGill Conference (1972), *Proc. Conf. Finite Element Method in Civil Engineering,* McGill University, Montreal, Canada, 1254 pp.

McKeen, R. G. (1992), "A Model for Predicting Expansive Soil Behavior," *Proc. 7th Internat. Conference on Expansive Soils,* Dallas, TX, published by Texas Tech. Univ., Lubbock, TX, vol. 1, pp. 1–6.

McLean, F. G., et al. (1975), "Influence of Mechanical Variables on the SPT," *7th PSC,* ASCE, vol. 1, pp. 287–318.

McManis, K. L., and A. Arman (1986), "Sampling and Testing in Stiff Crusted Clays," Geotech. SP No. 2, ASCE, pp. 1–13.

McRoberts, E. C. (1982), "Shallow Foundations in Cold Regions: Design," *JGED,* ASCE, vol. 108, GT 10, Oct, pp. 1338–1349.

Ménard, L. (1956), "An Apparatus for Measuring the Strength of Soils in Place," M. Sc. Thesis, University of Illinois, Urbana, IL.

———, and Y. Broise (1975), "Theoretical and Practical Aspects of Dynamic Consolidation," *Geotechnique,* vol. 25, no. 1, March, pp. 3–18.

Mesri, G. (1986), "Discussion: Postconstruction Settlement of an Expressway Built on Peat by Precompression," *CGJ,* vol. 23, no. 3, pp. 403–407.

———, and T. M. Hayat (1993), "The Coefficient of Earth Pressure at Rest," *CGJ,* vol. 30, no. 4, Aug, pp. 647–666.

———, et al. (1990), "Postdensification Penetration Resistance of Clean Sands," *JGED,* ASCE, vol. 116, GT 7, pp. 1095–1115.

———, and P. M. Godlewski (1977), "Time- and Stress-Compatibility Interrelationship," *JGED,* ASCE, vol. 103, GT 5, May, pp. 417–430.

Meyer, B. J., and P. R. Schade (1995), "Touchdown for the *O*-Cell Test," *Civil Engineering,* ASCE, vol. 65, no. 2, Feb, pp. 57–59.

Meyerhof, G. G. (1976), "Bearing Capacity and Settlement of Pile Foundations," *JGED,* ASCE, vol. 102, GT 3, March, pp. 195–228 (Terzaghi Lecture).

———(1974), "General Report: Outside Europe," *1st ESOPT,* Stockholm, vol. 2.1, pp. 40–48.

———(1972), "Stability of Slurry Trench Cuts in Saturated Clay," *5th PSC,* ASCE, vol. 1, part 2, pp. 1451–1466.

———(1970), "Safety Factors in Soil Mechanics," *CGJ,* vol. 7, no. 4, Nov, pp. 349–355.

———(1965), "Shallow Foundations," *JSMFD,* ASCE, vol. 91, SM 2, March, pp. 21–31.

———(1963), "Some Recent Research on the Bearing Capacity of Foundations," *CGJ,* vol. 1, no. 1, Sept, pp. 16–26.

———(1959), "Compaction of Sands and the Bearing Capacity of Piles," *JSMFD,* ASCE, vol. 85, SM 6, Dec., pp. 1–29

———(1957), "Discussion on Sand Density by Spoon Penetration," *4th ICSMFE,* vol. 3, p. 110.

———(1956), "Penetration Tests and Bearing Capacity of Cohesionless Soils," *JSMFD,* ASCE, vol. 82, SM 1, pp. 1–19.

———(1953), "The Bearing Capacity of Foundations under Eccentric and Inclined Loads," *3rd ICSMFE,* vol. 1, pp. 440–445.

———(1951), "The Ultimate Bearing Capacity of Foundations," *Geotechnique,* vol. 2, no. 4, pp. 301–331.

——, and J. I. Adams (1968), "The Ultimate Uplift Capacity of Foundations," *CGJ,* vol. 5, no. 4, Nov, pp. 225–244.

——, and J. D. Brown (1967), "Discussion: Bearing Capacity of Footings on Layered Clays," *JSMFD,* ASCE, vol. 93, SM 5, part 1, Sept, pp. 361–363.

Michigan State Highway Commission (1965), "*A Performance Investigation of Pile Driving Hammers and Piles,*" Lansing, MI, 338 pp.

Mikhejev, V. V., et al. (1961), "Foundation Design in the USSR," *5th ICSMFE,* vol. 1, pp. 753–757.

Milović, D. M. (1965), "Comparison between the Calculated and Experimental Values of the Ultimate Bearing Capacity," *6th ICSMFE,* vol. 2, pp. 142–144.

Mindlin, R. D. (1936*a*), "Discussion: Pressure Distribution on Retaining Walls," *1st ICSMFE,* vol. 3, pp. 155–156.

——(1936*b*), "Force at a Point in the Interior of a Semi-Infinite Solid," *J. Amer. Inst. Physics (Physics),* vol. 7, no. 5, May, pp. 195–202.

Mitachi, T., and S. Kitago (1976), "Change in Undrained Shear Strength Characteristics of Saturated Remolded Clay Due to Swelling," *Soils and Foundations,* Tokyo, vol. 16, no. 1, March, pp. 45–58.

Mitchell, J. K., and W. S. Gardner (1975), "In-Situ Measurement of Volume Change Characteristics," *7th PSC,* ASCE, vol. 2, pp. 279–345.

——, and T. C. Kao (1978), "Measurement of Soil Thermal Resistivity," *JGED,* ASCE, GT 10, Oct, pp. 1307–1320.

Mitchell, P. W., and D. L. Avalle (1984), "A Technique to Predict Expansive Soil Movements," *5th Int. Conf. on Expansive Soils,* Adelaide, Australia, pp. 124–130.

Moe, J. (1961), "Shearing Strength of Reinforced Slabs and Footings under Concentrated Loads," *Portland Cement Association Bull. No. D47,* 135 pp.

Moorhouse, D. C., and J. V. Sheehan (1968), "Predicting Safe Capacity of Pile Groups," *Civil Engineering,* ASCE, vol. 38, no. 10, Oct, pp. 44–48.

Morgan, J. R., and C. M. Gerrard (1971), "Behavior of Sands under Surface Loads," *JSMFD,* ASCE, vol. 97, SM 12, Dec, pp. 1675–1699.

Morgenstern, N. R., et al. (1980), "The Behavior of Friction Piles in Ice and Ice-Rich Soils," *CGJ,* vol. 17, no. 3, Aug, pp. 405–415.

Morin, P. (1988), "Discussion: Work as a criterion . . . ," *CGJ,* vol. 25, no. 4, Nov, pp. 845–847.

Morrison, A. (1982), "The Booming Business in Wick Drains," *Civil Engineering,* ASCE, March, pp. 47–51 (lists 3 technical references and sources for 5 wicks common in the United States).

Motta, E. (1994), "Generalized Coulomb Active-Earth Pressure for Distanced Surcharge," *JGED,* ASCE, vol. 120, GT 6, June, pp. 1072–1079.

Muhs, H., and K. Weiss (1969), "The Influence of the Load Inclination on the Bearing Capacity of Shallow Footings," *7th ICSMFE,* vol. 2, pp. 187–194.

Munfakh, G. A. (1990), "Innovative Earth Retaining Structures: Selection, Design and Performance," Geotech. SP No. 25, ASCE, pp. 85–118.

Murff, J. D. (1987), "Pile Capacity in Calcareous Sands: State of the Art," *JGED,* ASCE, vol. 113, no. 5, May, pp. 490–507.

NAVFAC (1982), "DM7.1, *Soil Mechanics,*" U.S. Department of the Navy, Naval Facilities Engineering Command, 200 Stovall Street, Alexandria, VA 22332, p. 7.1-237 (Fig. 16).

NAVFAC (1982*a*), "DM7.2, *Foundations and Earth Structures,*" U.S. Department of the Navy, Naval Facilities Engineering Command, 200 Stovall Street, Alexandria, VA 22332, p. 7.2-209.

NBC (1976), *National Building Code,* Engineering and Safety Service, 85 John Street, New York, NY, 10038.

NBS (1962), "Corrosion of Steel Pilings in Soils," Monograph 58, National Bureau of Standards, U.S. Department of Commerce, Washington, DC, 22 pp.

NCHRP (1970), Scour at Bridge Waterways, *Synthesis of Highway Practice No. 5,* National Academy of Sciences, Washington, DC, 37 pp.

Nagaraj, T. S., and B. R. Srinivasa Murthy (1986), "A Critical Reappraisal of Compression Index," *Geotechnique,* vol. 36, no. 1, March, pp. 27–32.

——(1985), "Prediction of the Preconsolidation Pressure and Recompression Index of Soils," *GTJ,* ASTM, vol. 8, no. 4, pp. 199–202.

Nakase, A., et al. (1988), "Constitutive Parameters Estimated by Plasticity Index," *JGED,* ASCE, vol. 114, GT 7, July, pp. 844–858.

Nash, J., and G. K. Jones (1963), "The Support of Trenches Using Fluid Mud," *Proc. of Symposium: Grouts and Drilling Muds in Engineering Practice,* Butterworths, London, pp. 177–180.

Nazarian, S., and M. R., Desai (1994), "Automated Surface Wave Method: Field Testing," *JGED,* ASCE, vol. 119, no. 7, July, pp. 1094–1110.

Neukirchner, R. J. (1987), "Analysis of Laterally Loaded Piles in Permafrost," *JGED,* ASCE, vol. 113, no. 1, Jan, pp. 15–29.

Newmark, N. M. (1943), "Numerical Procedure for Computing Deflections, Moments and Buckling Loads," *Trans. ASCE,* vol. 108, pp. 1161–1234.

——(1942), "Influence Charts for Computation of Stresses in Elastic Foundations," *University of Illinois Engineering Experiment Station Bull. No. 338,* Urbana, IL, 28 pp.

——(1935), "Simplified Computation of Vertical Pressures in Elastic Foundations," *University of Illinois Engineering Experiment Station Cir. No. 24,* Urbana, IL, pp. 5–19.

Nishida, Y. (1956), "A Brief Note on Compression Index of Soils," *JSMFD,* ASCE, vol. 82, SM 3, pp. 1027-1–1027-14.

Nixon, J. F. (1988), "Pile Load Tests in Saline Permafrost at Clyde River, Northwest Territories," *CGJ,* vol. 25, no. 1, Feb, pp. 24–32.

Nordlund, R. L. (1963), "Bearing Capacity of Piles in Cohesionless Soils," *JSMFD,* ASCE, vol. 89, SM 3, May, pp. 1–36 (see also "Closure," July 1964).

——(1962), "Discussion: Pile Heave and Redriving," *JSMFD,* ASCE, vol. 88, SM 1, Feb, p. 77.

Novak, M. (1974), "Dynamic Stiffness and Damping of Piles," *CGJ,* vol. 11, no. 4, Nov, pp. 574–594.

——, and Y. O. Beredugo (1972), "Vertical Vibration of Embedded Footings," *JSMFD,* ASCE, vol. 98, SM 12, Dec, pp. 1291–1310.

——, and J. F. Howell (1977), "Torsional Vibration of Pile Foundations," *JGED,* ASCE, vol. 103, GT 4, April, pp. 271–285.

Ohio (1947), "Investigation of the Strength of the Connection between a Concrete Cap and the Embedded End of a Steel H-Pile, *Department of Highways Research Report No. 1,* Columbus, OH.

Olsen, H. W., et al. (1986), "Piston Core Properties and Disturbance Effects," *JGED,* ASCE, vol. 112, no. 6, June, pp. 608–625.

Olson, L. D., and R. W. Thompson (1985), "Case Histories Evaluation of Drilled Pier Integrity by the Stress Wave Propagation Method," *Drilled Piers and Caissons II,* ASCE, pp. 28–42.

Olson, R. E. (1986), "State of the Art: Consolidation Testing," *ASTM STP* No. 892, pp. 7–68.

——, et al. (1974), "Finite Difference Analysis for Sand Drain Problems," *6th PSC,* ASCE, vol. 1, pp. 85–110.

——, and K. S. Flaate (1967), "Pile Driving Formulas for Friction Piles in Sand," *JSMFD,* ASCE, vol. 93, SM 6, Nov, pp. 279–296.

O'Neill, M. W., and O. I. Ghazzaly (1977), "Swell Potential Related to Building Performance," *JGED,* ASCE, vol. 103, GT 12, Dec, pp. 1363–1379.

——, and L. C. Reese (1972), "Behavior of Bored Piles in Beaumont Clay," *JSMFD,* ASCE, vol. 98, SM 2, pp. 195–213.

Ooi, P. S., and J. M. Duncan (1994), "Lateral Load Analysis of Groups of Piles and Drilled Shafts," *JGED,* ASCE, vol. 120, GT 6, June, pp. 1034–1050.

Oosterbaan, M. D., and D. G. Gifford (1972), "A Case Study of the Bauer Earth Anchor," *5th PSC,* ASCE, vol. 1, part 2, pp. 1391–1401.

Orrje, O., and B. Broms (1967), "Effects of Pile Driving on Soil Properties," *JSMFD,* vol. 93, SM 5, Sept, part 1, pp. 59–74.

Ovesen, N. K. (1962), "Cellular Cofferdams, Calculation of Methods and Model Tests," *Danish Geotech. Bull. No. 14,* Copenhagen.

PCA (1955), "Design of Concrete Airport Pavement," Portland Cement Association, Chicago, IL, 47 pp. (especially see p. 44).

PCA (1951), "Concrete Piles: Design, Manufacture, Driving," Portland Cement Association, Chicago, IL, 80 pp.

PCI (1974), "Tentative Recommendations for Prestressed Rock and Soil Anchors," Prestressed Concrete Institute, Chicago, IL, 32 pp.

Paikowsky, S. G., and R. V. Whitman (1990), "The Effects of Plugging on Pile Performance and Design," *CGJ,* vol. 27, no. 4, Aug, pp. 429–440.

Palmer, D. J., and J. G. Stuart (1957), "Some Observations on the Standard Penetration Test and a Correlation of the Test with a New Penetrometer," *4th ICSMFE,* vol. 1, pp. 231–236.

Pandian, N. S., et al. (1993), "Tropical Clays. I: Index Properties and Microstructural Aspects, and II: Engineering Behavior," *JGED,* ASCE, vol. 119, GT 5, May, pp. 826–839, 840–861.

Parameswaran, V. R. (1978), "Adfreeze Strength of Frozen Sand to Model Piles," *CGJ,* vol. 15, no. 4, Nov, pp. 494–500.

Parkin, A. K. (1978), "Coefficient of Consolidation by the Velocity Method," *Geotechnique,* vol. 28, no. 4, Dec, pp. 472–474.

Parry, R. H. G. (1977), "Estimating Bearing Capacity of Sand from SPT Values," *JGED,* ASCE, vol. 103, GT 9, Sept, pp. 1014–1019.

Patrick, A., et al. (1980), "Screw Plate Testing of a Soft Clay," *CGJ,* vol. 17, no. 4, Nov, pp. 465–472.

Payne, D. C., et al. (1992), "Two Computer Models for 3D Raft Slab Back-Analysis," *Proc. 7th Int. Conference on Expansive Soils,* Dallas, TX, vol. 1, pp. 78–83.

Peck, R. B. (1969), "Deep Excavations and Tunneling in Soft Ground," *7th ICSMFE, State-of-Art Volume,* pp. 225–290.

——(1965), "Pile and Pier Foundations," *JSMFD,* ASCE, vol. 91, SM 2, March, pp. 33–38.

——(1943), "Earth Pressure Measurements in Open Cuts," *Trans. ASCE,* vol. 108, pp. 1008–1058.

——(1942), "Discussion: Pile Driving Formulas," *Proc. ASCE,* vol. 68, no. 2, Feb, pp. 323–324.

——, et al. (1974), *Foundation Engineering,* 2nd ed., John Wiley & Sons, New York, 514 pp.

——, and H. O. Ireland (1961), "Full-Scale Lateral Load Test of a Retaining Wall Foundation," *5th ICSMFE,* vol. 2, pp. 453–458.

Penner, E., and L. W. Gold (1971), "Transfer of Heaving Forces by Adfreezing to Columns and Foundation Walls in Frost-Susceptible Soils," *CGJ,* vol. 8, no. 4, Nov, pp. 514–526.

——, and W. W. Irwin (1969), "Adfreezing of Leda Clay to Anchored Footing Columns," *CGJ,* vol. 6, no. 3, Aug, pp. 327–337.

Plantema, G. (1957), "Influence of Density on Sounding Results in Dry, Moist and Saturated Sands," *4th ICSMFE,* vol. 1, pp. 237–240.

Polshin, D. E., and R. A. Tokar (1957), "Maximum Allowable Non-Uniform Settlement of Structures," *4th ICSMFE,* vol. 1, pp. 402–405.

Poulos, H. G. (1979), "Group Factors for Pile-Deflection Estimation," *JGED,* ASCE, vol. 105, GT 12, Dec, pp. 1489–1509.

——(1971), "Behavior of Laterally Loaded Piles: II—Pile Groups," *JSMFD,* ASCE, vol. 97, SM 5, May, pp. 733–751.

——(1968), "The Settlement Behaviour of Single Axially Loaded Incompressible Piles and Piers," *Geotechnique,* vol. 18, no. 3, Sept, pp. 351–371.

——, and E. H. Davis (1974), *Elastic Solutions for Soil and Rock Mechanics,* John Wiley & Sons, New York, 411 pp.

Prescott, D. M., et al. (1973), "Field Measurements of Lateral Earth Pressures on a Pre-Cast Panel Retaining Wall," *Texas Transport. Institute,* Research Report No. 169-3, College Station, TX, 57 pp.

Purushothamaraj, P., et al. (1974), "Bearing Capacity of Strip Footings in Two Layered Cohesive-Friction Soils," *CGJ,* vol. 11, no. 1, Feb, pp. 32–45.

Pyke, R., and M. Beikae (1983), "A New Solution for the Resistance of Single Piles to Lateral Loading," *ASTM STP* No. 835, pp. 3–20.

Ramaswamy, S. D., et al. (1982), "Pressuremeter Correlations with Standard Penetration and Cone Penetration Tests," *2nd ESOPT,* vol. 1, pp. 137–142.

Randolph, M. F., and C. P. Wroth (1979), "A Simple Approach to Pile Design and the Evaluation of Pile Tests," *ASTM STP* No. 670, pp. 484–499.

Rausche, F., and G. G. Goble (1979), "Determination of Pile Damage by Top Measurements," *ASTM STP* No. 670, pp. 500–506.

Raymond, G. P. (1970), "Discussion: Stresses and Displacements in a Cross-Anisotropic Soil," *Geotechnique,* vol. 20, no. 4, Dec, pp. 456–458.

Reddy, A. S., and A. J. Valsangkar (1970), "Buckling of Fully and Partially Embedded Piles," *JSMFD,* ASCE, vol. 96, SM 6, Nov, pp. 1951–1965.

Reese, L. C. (1978), "Design and Construction of Drilled Shafts," *JGED,* ASCE, vol. 104, GT 1, Jan, pp. 95–116 (Terzaghi Lecture).

——(1977), "Laterally Loaded Piles—Program Documentation," *JGED,* ASCE, vol. 103, GT 4, April, pp. 287–305.

——, and M. W. O'Neill (1969), "Field Tests of Bored Piles in Beaumont Clay," *ASCE Annual Meeting,* Chicago, Preprint No. 1008, 39 pp.

——, et al. (1976), "Behavior of Drilled Piers under Axial Loading," *JGED,* ASCE, vol. 102, no. 5, May, pp. 493–510.

——, et al. (1970), "Generalized Analysis of Pile Foundations," *JSMFD,* ASCE, vol. 96, SM 1, Jan, pp. 235–250.

Rehnman, S. E., and B. B. Broms (1972), "Lateral Pressures on Basement Wall: Results from Full-Scale Tests," *Proc. 5th European Conf. SMFE,* vol. 1, pp. 189–197.

Rendon-Herrero, O. (1983), "Closure: Universal Compression Index Equation," *JGED,* ASCE, vol. 109, GT 5, May, pp. 755–761.

Richardson, A. M., Jr., and R. V. Whitman (1963), "Effect of Strain-Rate upon Undrained Shear Resistance of Saturated Remolded Fat Clay," *Geotechnique,* vol. 13, no. 4, Dec, pp. 310–324.

Richart, F. E. (1948), "Reinforced Wall and Column Footings," *JACI,* vol. 45, Oct–Nov, pp. 97–127, 237–260.

Richart, F. E., Jr. (1959), "Review of the Theories for Sand Drains," *Trans. ASCE,* vol. 124, pp. 709–736.

——, et al. (1970), *Vibrations of Soils and Foundations,* Prentice-Hall Inc., Englewood Cliffs, NJ, 414 pp.

Riggs, C. O. (1986), "American Standard Penetration Test Practice," *14th PSC,* ASCE, pp. 949–967.

——, et al. (1983), "Reproducible SPT Hammer Impact Force with an Automatic Free Fall SPT Hammer System," *GTJ,* ASTM, vol. 6, no. 4, Dec, pp. 201–209.

Robertson, P. K., and K. O. Addo (1991), "Recent In-Situ Method to Determine Seismic Velocity Profiles," *Geotechnical News,* Canadian Geotechnical Society, BiTech Publishers, Grand Forks, ND, vol. 9, no. 3, Sept, pp. 26–30.

——, et al. (1986), "Seismic *CPT* to Measure In Situ Shear Wave Velocity," *JGED,* ASCE, vol. 112, GT 8, Aug, pp. 791–803.

——, and R. E. Campanella (1983), "Interpretation of Cone Penetration Tests. Part I: Sand," *CGJ,* vol. 20, no. 4, Nov, pp. 718–733.

——, and R. E. Campanella (1983*a*), "Interpretation of Cone Penetration Tests. Part II: Clay," *CGJ,* vol. 20, no. 4, Nov, pp. 734–745.

——, et al. (1983), "SPT-CPT Correlations," *JGED,* ASCE, vol. 109, no. 11, pp. 1449–1459.

Robinson, K. E. (1978), "Horizontal Subgrade Reaction Estimated from Lateral Loading Tests on Timber Piles," *ASTM STP* No. 670, pp. 520–536.

——, and H. Taylor (1969), "Selection and Performance of Anchors for Guyed Transmission Towers," *CGJ,* vol. 6, no. 2, May, pp. 119–137.

Rogers, P. (1952), "Design of Large Coal Bunkers," Trans. ASCE, vol. 117, pp. 579–595.

Rollins, K. M., and G. W. Rogers (1991), "Stabilization of Collapsible Alluvial Soil Using Dynamic Compaction," ASCE, Geotech. SP No. 27, vol. 1, pp. 322–333.

Rosenfarb, J. L., and W. F. Chen (1972), "Limit Analysis Solutions of Earth Pressure Problems," *Fritz Engineering Laboratory Report 355.14,* Lehigh University, Bethlehem, PA, 53 pp.

Rossow, M. P. (1984), "Sheetpile Interlock Tension in Cellular Cofferdams," *JGED,* ASCE, vol. 110, no. 10, Oct, pp. 1446–1458.

Rowe, P. W. (1957), "Sheet-Pile Walls in Clay, " *PICE,* vol. 7, July, pp. 629–654.

——(1952), "Anchored Sheet-Pile Walls," *PICE,* vol. 1, part 1, pp. 27–70.

——, and K. Peaker (1965), "Passive Earth Pressure Measurements," *Geotechnique,* vol. 15, no. 1, March, pp. 57–78.

Rowe, R. K., and H. H. Armitage (1987), "A Design Method for Drilled Piers in Soft Rock," *CGJ,* vol. 24, no. 1, Feb, pp. 126–142.

Roy, S. K., and S. D. Ramaswamy (1983), "Measurement of Underground Corrosion of Steel," *GTJ,* ASTM, vol. 6, no. 2, June, pp. 96–99.

Saada, A. S., and F. C. Townsend (1981), "State of the Art: Strength Laboratory Testing of Soils," *ASTM STP* No. 740, pp. 7–77.

Safarian, S. S. (1969), "Design Pressures of Granular Material in Silos," *JACI,* vol. 66, no. 8, Aug, pp. 647–655.

Samson, L., and J. Authier (1986), "Change in Pile Capacity with Time: Case Histories," *CGJ,* vol. 23, no. 2, May, pp. 174–180.

Sarac, Dž, and M. Popović (1982), "Penetration Tests for Determination of Characteristics of Flood Dike Materials," *2nd ESOPT,* vol. 1, pp. 147–152.

Saran, S., et al. (1989), "Bearing Capacity of Footings Adjacent to Slopes," *JGED,* ASCE, vol. 115, GT 4, April, pp. 553–573.

Saul, W. E. (1968), "Static and Dynamic Analysis of Pile Foundations," *JSD,* ASCE, vol. 94, ST 5, May, pp. 1077–1100.

Sayed, S. M., and R. M. Bakeer (1992), "Efficiency Formula for Pile Groups," *JGED,* ASCE, vol. 118, GT 2, Feb, pp. 278–299.

Sayles, F. H. (1985), "Creep of a Strip Footing on Ice-Rich Permafrost," *Proc. Conf. Session: Foundations in Permafrost and Seasonal Frost,* ASCE, pp. 29–51.

Schaap, L., and H. Zuidberg (1982), "Mechanical and Electrical Aspects of the Electric Cone Penetrometer Tip," *2nd ESOPT,* vol. 2, pp. 841–851.

Schmertmann, J. H. (1986), "Dilatometer to Compute Foundation Settlement," *14th PSC,* ASCE, pp. 303–321.

——(1979), "Statics of SPT," *JGED,* ASCE, vol. 105, GT 5, May, pp. 655–670.

——(1978), "Guidelines for Cone Penetration Test: Performance and Design," FHWA-TS-78-209 (report), U.S. Dept. of Transportation, 145 pp.

——(1978*a*), "Use of the SPT to Measure Dynamic Soil Properties—Yes But . . . !" *ASTM STP* No. 654, pp. 341–355.

——(1975), "The Measurement of In-Situ Shear Strength," *7th PSC,* ASCE, vol. 2, pp. 57–138.

——(1970), "Static Cone to Compute Static Settlement over Sand," *JSMFD,* ASCE, vol. 96, SM 3, May, pp. 1011–1043.

——(1955), "The Undisturbed Consolidation Behavior of Clay," *Trans. ASCE,* vol. 120, pp. 1201–1233.

Schroeder, W. L., and P. Roumillac (1983), "Anchored Bulkheads with Sloping Dredge Lines," *JGED,* ASCE, vol. 109, no. 6, June, pp. 845–851.

Schultze, E. (1961), "Distribution of Stress beneath a Rigid Foundation," *5th ICSMFE,* vol. 1, pp. 807–813.

Schwab, E., and B. Broms (1976), "Bottom Heave in Soft Soils," *Proc. 6th European Conf. SMFE,* vol. 1.2, pp. 647–650.

Seed, H. G., et al. (1986), "Moduli and Damping Factors for Dynamic Analysis of Cohesionless Soils," *JGED,* ASCE, vol. 112, GT 11, Nov, pp. 1016–1032.

——, and I. M. Idriss (1971), "Simplified Procedure for Evaluating Soil Liquefaction Potential," *JSMFD,* ASCE, vol. 97, SM 9, Sept, pp. 1249–1273.

——, and R. V. Whitman (1970), "Design of Earth Retaining Structures for Dynamic Loads," *3rd PSC,* ASCE, pp. 103–147.

——, et al. (1985), "Influence of SPT Procedures in Soil Liquefaction Resistance Evaluations," *JGED,* ASCE, vol. 111, no. 12, Dec, pp. 1425–1445.

Sellmeijer, J. B., et al. (1995), "Hydraulic Resistance of Steel Sheet Pile Joints," *JGED,* ASCE, vol. 121, no. 2, Feb, pp. 105–110.

Senneset, K., et al. (1988), "Piezocone Tests in Silty Soils," *Proc. 1st ISOPT,* vol. 2, pp. 955–966.

——, et al. (1982), "Strength and Deformation Parameters from Cone Penetration Tests," *Proc. 2nd ESOPT,* vol. 2, pp. 863–870.

Sheeler, J. B. (1968), "Summarization and Comparison of Engineering Properties of Loess in the United States," *Highway Research Board,* HRR No. 212, pp. 1–9.

Sherif, M., et al. (1982), "Earth Pressures against Rigid Retaining Walls," *JGED,* ASCE, vol. 108, GT 5, May, pp. 679–695.

Shields, D. H., and A. Z. Tolunay (1973), "Passive Pressure Coefficients by Method of Slices," *JSMFD,* ASCE, vol. 99, SM 12, Dec, pp. 1043–1053.

——, et al. (1977), "Bearing Capacity of Foundations Near Slopes," *9th ICSMFE,* vol. 1, pp. 715–720.

Shioi, Y., and J. Fukui (1982), "Application of *N*-Value to Design of Foundations in Japan," *2nd ESOPT,* vol. 1, pp. 159–164.

Shukla, S. N. (1984), "A Simplified Method for Design of Mats on Elastic Foundations," *JACI,* vol. 81, no. 5, Sept–Oct, pp. 469–475.

Silvestri, V., and M. Aubertin (1988), "Anisotropy and In-Situ Vane Tests," *ASTM STP* No. 1014, pp. 88–103.

——, et al. (1986), "Controlled-Strain, Controlled-Gradient, and Standard Consolidation Testing of Sensitive Clays," *ASTM STP* No. 892, pp. 433–450.

Simons, N. E. (1960), "Effect of Overconsolidation on the Shear Strength Characteristics of an Undisturbed Oslo Clay," *1st PSC,* ASCE, pp. 747–763.

Singh, S., et al. (1982), "Undisturbed Sampling of Saturated Sands by Freezing," *JGED,* ASCE, vol. 108, GT 2, Feb, pp. 247–264.

Skempton, A. W. (1986), "Standard Penetration Test Procedures . . . ," *Geotechnique,* vol. 36, no. 3, pp. 425–447.

——(1951), "The Bearing Capacity of Clays," *Proc. Building Research Congress,* vol. 1, pp. 180–189. (Also in "Selected Papers on Soil Mechanics," published by Thomas Telford, Ltd., London.)

——, and D. J. Henkel (1953), "The Post-Glacial Clays of the Thames Estuary at Tilbury and Shellhaven," *3rd ICSMFE,* vol. 1, pp. 302–308.

——, and R. D. Northey (1952), "Sensitivity of Clays," *Geotechnique,* vol. 3, no. 1, pp. 40–51.

Sladen, J. A. (1992), "The Adhesion Factor: Applications and Limitations," *CGJ,* vol. 29, no. 2, April, pp. 322–326.

Smith, E. A. (1962), "Pile Driving Analysis by the Wave Equation," *Trans. ASCE,* vol. 127, part 1, pp. 1145–1193.

Smith, J. E. (1957), "Tests of Concrete Deadman Anchorages in Sand," *ASTM STP* No. 206, pp. 115–132.

Smith, J. W., and M. Zar (1964), "Chimney Foundations," *JACI,* vol. 61, no. 6, June, pp. 673–700.

Snethen, D. R. (1980), "Characteristics of Expansive Soils Using Soil Suction Data," *4th Int. Conf. on Expansive Soils,* ASCE, vol. 1, pp. 54–75.

——, and G. Huang (1992), "Evaluation of Soil Suction-Heave Prediction Methods," *7th Int. Conf. on Expansive Soils,* vol. 1, pp. 12–17.

Soderman, L. G., et al. (1968), "Field and Laboratory Studies of Modulus of Elasticity of a Clay Till," *Highway Research Board,* HRR No. 243, pp. 1–11.

Sokolovski, V. V. (1960), *Statics of Soil Media,* 2nd ed., Butterworth, London, 237 pp.

Sorota, M., and E. B. Kinner (1981), "Cellular Cofferdam for Trident Drydock: Design," *JGED,* ASCE, vol. 107, GT 12, Dec, pp. 1643–1655 (see also companion paper pp. 1657–1676).

——, et al. (1981), "Cellular Cofferdam for Trident Drydock: Performance," *JGED,* ASCE, vol. 107, GT 12, Dec., pp. 1657–1676.

Sovinc, I., et al. (1985), "Loading Tests on Closed and Open Ended Piles," *11th ICSMFE,* vol. 3, pp. 1475–1478.

Sowers, G. F. (1979), *Introductory Soil Mechanics and Foundations: Geotechnical Engineering,* 4th ed., Macmillan, New York, Chap. 2.

——(1968), "Foundation Problems in Sanitary Land Fills," *Jour. Sanitary Eng. Div.,* ASCE, vol. 94, SA 1, pp. 103–116.

Spangler, M. G. (1936), "The Distribution of Normal Pressure on a Retaining Wall Due to a Concentrated Surface Load," *1st ICSMFE,* vol. 1, pp. 200–207.

——, and R. L. Handy (1982), *Soil Engineering,* 4th ed., Harper and Row, New York, 819 pp.

——, and J. Mickle (1956), "Lateral Pressure on Retaining Walls Due to Backfill Surface Loads," *Highway Research Board,* HRB Bull. No. 141, pp. 1–18.

Sridharan, A., and K. Prakash (1985), "Improved Rectangular Hyperbola Method for the Determination of Coefficient of Consolidation," *GTJ,* ASTM, vol. 8, no. 1, March, pp. 37–40.

——, and S. Rao (1981), "Rectangular Hyperbola Fitting Method for One Dimensional Consolidation," *GTJ,* ASTM, vol. 4, no. 4, Dec, pp. 161–168.

——, et al. (1991), "Improved Method for Estimation of Preconsolidation Pressure," *Geotechnique,* vol. 41, no. 2, June, pp. 263–268.

Stagg, K. G., and O. C. Zienkiewicz (1968), *Rock Mechanics in Engineering Practice,* John Wiley & Sons, New York (with 12 contributing authors), 442 pp.

Steinbrenner, W. (1934), "Tafeln zur Setzungsberechnung," *Die Strasse,* vol. 1, Oct, pp. 121–124.

Stewart, W. P., and R. G. Campanella (1993), "Practical Aspects of In Situ Measurements of Material Damping with the Seismic Cone Penetration Test," *CGJ,* vol. 30, no. 2, April, pp. 211–219.

Stinnette, P. (1992), "Engineering Properties of Florida Organic Soils," Master's Thesis, Department of Civil Engineering and Mechanics, University of South Florida, Tampa, 50 pages with 200 page Appendix and very large number of references.

Sully, J. P., et al. (1988*a*), "Interpretation of Penetration Pore Pressures to Evaluate Stress History in Clays," *Proc. 1st ISOPT,* vol. 2, pp. 993–999.

——, et al. (1988), "Overconsolidation Ratio of Clays from Penetration Pore Pressures," *JGED,* ASCE, vol. 114, no. 2, Feb, pp. 209–216.

——, et al. (1990), "Closure: Overconsolidation Ratio of Clays from Penetration Pore Pressures," *JGED,* ASCE, vol. 116, no. 2, Feb, pp. 340–342.

Sung, T. Y. (1953), "Vibrations in Semi-Infinite Solids Due to Periodic Surface Loading," *ASTM STP* No. 156, pp. 35–68.

Swatek, E. P., Jr. (1970), "Summary: Cellular Structure Design and Installation," *Proc. Conf. Design and Installation of Pile Foundations and Cellular Structures,* Lehigh University, Envo Publishing Co., pp. 413–435.

——(1967), "Cellular Cofferdam Design and Practice," *Jour. Waterways and Harbors Div.,* ASCE, vol. 93, WW 3, Aug, pp. 109–132.

——, et al. (1972), "Performance of Bracing for Deep Chicago Excavation," *5th PSC,* ASCE, vol. 1, part 2, pp. 1303–1322.

Swiger, W. F. (1974), "Evaluation of Soil Modulii," *6th PSC,* ASCE, vol. 2, pp. 79–92.

TVA (1966), "Cofferdams on Rock," *Technical Monograph 75,* Tennessee Valley Authority, Knoxville, TN, 281 pp.

Taki, O. (1992), "Soil-Cement Columns for Building Foundations," Paper presented at the 17th Annual Deep Foundations Institute, Oct, 10 pp.

——, and D. S. Yang (1991), "Soil-Cement Mixed Wall Technique," Geotech. SP No. 27, ASCE, vol. 1, pp. 298–309.

Tan, T., et al. (1991), "Hyperbolic Method for Consolidation Analysis," *JGED,* ASCE, vol. 117, no. 11, Nov, pp. 1723–1737.

Tavenas, F. A. (1971), "Load Test Results on Friction Piles in Sand," *CGJ,* vol. 8, no. 1, Feb, pp. 7–22.

——, and J. M. Audibert (1977), "Application of Wave Equation Analysis to Friction Piles in Sand," *CGJ,* vol. 14, no. 1, Feb, pp. 34–51.

——, and R. Audy (1972), "Limitations of the Driving Formulas for Predicting the Bearing Capacity of Piles in Sand," *CGJ,* vol. 9, no. 1, Feb, pp. 47–62.

Taylor, D. W. (1948), *Fundamentals of Soil Mechanics,* John Wiley & Sons, New York, 700 pp.

Taylor, P. W. (1967), "Design of Spread Footings for Earthquake Loadings," *Proc. 5th Australia-New Zealand Conf. on SMFE,* pp. 221–229 (also p. 215).

Tekinsoy, A., and T. Haktanir (1990), "One-Dimensional Consolidation of Unsaturated Fine-Grained Soils," *JGED,* ASCE, vol. 116, no. 5, May, pp. 838–850.

Terzaghi, K. (1955), "Evaluation of Coefficient of Subgrade Reaction," *Geotechnique,* vol. 5, no. 4, Dec, pp. 297–326.

——(1954), "Anchored Bulkheads," *Trans. ASCE,* vol. 119, pp. 1243–1280.

——(1945), "Stability and Stiffness of Cellular Cofferdams," *Trans. ASCE,* vol. 110, pp. 1083–1202.

——(1943), *Theoretical Soil Mechanics,* John Wiley & Sons, New York, 510 pp.

——(1934), "Large Retaining Wall Tests," *Engineering-News Record,* Feb. 1, pp. 136–140; Feb. 22, pp. 259–262; Mar. 8, pp. 316–318; Mar. 29, pp. 403–406; Apr. 19, pp. 503–508.

——(1929), "The Science of Foundations," *Trans. ASCE,* vol. 93, pp. 270–405 (with large number of discussions and closure).

——, and R. B. Peck (1967), *Soil Mechanics in Engineering Practice,* 2nd ed., John Wiley & Sons, New York, 729 pp.

Tettinek, W., and F. Matl (1953), "A Contribution to Calculating the Inclination of Eccentrically Loaded Foundations," *3rd ICSMFE,* vol. 1, pp. 461–465.

Thorburn, S., and R. MacVicar (1971), "Pile Load Tests to Failure in the Clyde Alluvium," *Conference on Behaviour of Piles,* ICE, pp. 1–8.

Thornton, W. A. (1990), "Design of Base Plates for Wide Flange Columns—A Concatenation of Methods," *Engineering Journal,* AISC, vol. 27, no. 4, pp. 173–174. (See also vol. 27, no. 3, pp. 108–110.)

Timoshenko, S., and J. N. Goodier (1951), *Theory of Elasticity,* 2nd ed., McGraw-Hill, New York, 506 pp.

——, and S. Woinowsky-Krieger (1959), *Theory of Plates and Shells,* 2nd ed., McGraw-Hill, New York, 580 pp.

Tomlinson, M. J. (1971), "Some Effects of Pile Driving on Skin Friction," *Proc. Conference on Behaviour of Piles,* ICE, London, pp. 107–114.

Townsend, F. C., and M. C. McVay (1990), "SOA: Large Strain Consolidation Predictions," *JGED,* ASCE, vol. 116, GT 2, Feb, pp. 222–243. (See also "Discussion," GT 1, Jan, 1992, pp. 168–171.)

Tschebotarioff, G. P. (1973), *Foundations, Retaining and Earth Structures,* 2nd ed., McGraw-Hill, New York, 642 pp.

——(1962), "Retaining Structures," in *Foundation Engineering,* McGraw-Hill, New York, pp. 466–468.

——(1949), "Large Scale Earth Pressure Tests with Model Flexible Bulkheads," Final Report to Bureau of Yards and Docks U.S. Navy, Princeton University, 112 pp. plus figures.

Tsytovich, A. (1975), *The Mechanics of Frozen Ground,* McGraw-Hill, New York, 426 pp.

UBC (1994), *Uniform Building Code,* Published by International Conference of Building Officials, 5360 S. Workman Mill Road, Whittier, CA, 90601.

Ueda, T., B. Stitmannaithum, and S. Matupayont (1991), "Experimental Investigation on Shear Strength of Bolt Anchorage Group," *Structural Journal,* ACI, vol. 88, no. 3, May–June, pp. 292–300.

Ulrich, E. J., Jr. (1989), "Internally Braced Cuts in Overconsolidated Soils," and "Tieback Supported Cuts in Overconsolidated Soils," *JGED,* ASCE, vol. 115, No. 4, pp. 504–520, 521–545.

Underwood, L. B. (1967), "Classification and Identification of Shales," *JSMFD,* ASCE, vol. 93, SM 6, Nov, pp. 97–116.

Valsangkar, A. J., and G. G. Meyerhof (1979), "Experimental Study of Punching Coefficients and Shape Factor for Two-Layered Soils," *CGJ,* vol. 16, no. 4, Nov, pp. 802–805.

Van Weele, A. A. (1957), "A Method of Separating the Bearing Capacity of a Test Pile into Skin-Friction and Point Resistance," *4th ICSMFE,* vol. 2, pp. 76–80.

Vesić, A. S. (1977), "Design of Pile Foundations," *NCHRP Synthesis of Practice No. 42,* Transportation Research Board, Washington, DC, 68 pp.

——(1975*a*), "Principles of Pile Foundation Design," *Soil Mechanics Series No. 38,* School of Engineering, Duke University, Durham, NC, 48 pp. plus figures.

——(1975*b*), Chap. 3: *Foundation Engineering Handbook,* 1st ed., ed. Winterkorn and Fang, Van Nostrand Reinhold, 751 pp.

——(1973), "Analysis of Ultimate Loads of Shallow Foundations," *JSMFD,* ASCE, vol. 99, SM 1, Jan, pp. 45–73.

——(1970), "Tests on Instrumented Piles, Ogeechee River Site," *JSMFD,* ASCE, vol. 96, SM 2, March, pp. 561–584.

——(1969), "Discussion: Effects of Scale and Compressibility on Bearing Capacity of Surface Foundations," *7th ICSMFE,* vol. 3, pp. 270–272.

——(1969*a*), "Experiments with Instrumented Pile Groups in Sand," *ASTM STP* No. 444, pp. 177–222.

——(1961*a*), "Bending of Beams Resting on Isotropic Elastic Solid," *Jour. Eng. Mech. Division,* ASCE, vol. 87, EM 2, April, pp. 35–53.

——(1961*b*), "Beams on Elastic Subgrade and the Winkler's Hypothesis," *5th ICSMFE,* vol. 1, pp. 845–850.

——, and G. W. Clough (1968), "Behavior of Granular Materials under High Stresses," *JSMFD,* ASCE, vol. 94, SM 3, May, pp. 661–688.

——, and W. H. Johnson (1963), "Model Studies of Beams Resting on a Silt Subgrade," *JSMFD,* ASCE, vol. 89, SM 1, Feb, pp. 1–31.

Vidal, H. (1969), "The Principle of Reinforced Earth," *Highway Research Board,* HRR No. 282, Washington, DC, pp. 1–16.

Vijayvergiya, V. N., and J. A. Focht, Jr. (1972), "A New Way to Predict Capacity of Piles in Clay," *OTC Paper 1718,* 4th Offshore Technology Conference, Houston, TX.

Villet, W. C., and J. K. Mitchell (1981), "Cone Resistance, Relative Density and Friction Angle," *Proc. Symposium: Cone Penetration Testing and Experience,* ASCE, St. Louis, MO, pp. 178–208.

Vitone, D. M., and A. J. Valsangkar (1986), "Stresses from Loads over Rectangular Areas," *JGED,* ASCE, vol. 112, no. 10, Oct, pp. 961–964.

Volterra, E. (1952), "Bending of Circular Beams on Elastic Foundations," *J. Appl. Mechanics,* ASME, vol. 19, no. 1, March, pp. 1–4.

——, and R. Chung (1955), "Constrained Circular Beams on Elastic Foundations," *Trans. ASCE,* vol. 120, pp. 301–310.

Wahls, H. (1981), "Tolerable Settlement of Buildings," *JGED,* ASCE, vol. 107, ET 11, Nov, pp. 1489–1504.

Walker, W. L. (1986), "Vane Shear Testing for Staged Construction," *14th PSC,* ASCE, pp. 1108–1118.

Wang, C. K. (1970), *Matrix Methods of Structural Analysis,* 2nd ed., Intext Educational Publishers, Scranton, PA, 406 pp.

——(1967), "Stability of Rigid Frames with Non-Uniform Members," *JSD,* ASCE, vol. 93, ST 1, Feb, pp. 275–294.

Ware, K. R., et al. (1973), "Tieback Wall Construction—Results and Controls," *JSMFD,* ASCE, vol. 99, SM 12, Dec, pp. 1135–1152.

Watkins, L. L. (1969), "Corrosion and Protection of Steel Piling in Seawater," TM No. 27, U.S. Army Corps of Engineers, Coastal Engineering Research Center, 52 pp. plus several appendices.

Webb, D. L., and A. L. Melvill (1971), "Discussion: Static Cone to Compute Static Settlement over Sand," *JSMFD,* ASCE, vol. 97, SM 3, March, pp. 587–589.

Wesley, L. D. (1990), "Influence of Structure and Composition on Residual Soils," *JGED,* ASCE, vol. 116, GT 4, April, pp. 589–603.

Westergaard, H. M. (1948), "New Formulas for Stresses in Concrete Pavements of Airfields," *Trans. ASCE,* vol. 113, pp. 425–439. (See also "Discussion," pp. 443–444—particularly p. 444.)

——(1938), "A Problem of Elasticity Suggested by a Problem in Soil Mechanics: Soft Material Reinforced by Numerous Strong Horizontal Sheets," in *Contributions to the Mechanics of Solids,*

Stephen Timoshenko 60th Anniversary Volume, Macmillan, New York.

——(1933), "Water Pressures on Dams during Earthquakes," *Trans. ASCE,* vol. 98, pp. 418–472.

Whitaker, T., and R. W. Cooke (1966), "An Investigation of the Shaft and Base Resistances of Large Bored Piles in London Clay," *Proc. Conference: Large Bored Piles,* ICE, London, pp. 7–49.

White, L. S. (1953), "Transcona Elevator Failure: Eye-Witness Account," *Geotechnique,* vol. 3, pp. 209–214. (See also Peck and Bryant in same volume, pp. 201–208.)

Whitman, R. V. (1990), "Seismic Design and Behavior of Gravity Retaining Walls," Geotech. SP No. 25, ASCE, pp. 817–842.

——, and F. E. Richart, Jr. (1967), "Design Procedures for Dynamically Loaded Foundations," *JSMFD,* ASCE, vol. 93, SM 6, Nov, pp. 169–193.

Williams, C. C. (1929), "Discussion of 'The Science of Foundations'," *Trans. ASCE,* vol. 93, pp. 306–313.

Williams, K. O. H. (1989), "Geostatic Wall Pressures," *JGED,* ASCE vol. 115, no. 9, Sept, pp. 1321–1325.

Wineland, J. D. (1975), "Borehole Shear Device," *7th PSC,* ASCE, vol. 1, pp. 511–522.

Winter, E. (1982), "Suggested Practice for Pressuremeter Testing in Soils," *GTJ,* ASTM, vol. 5, no. 3/4, Sept, pp. 85–88.

——, and A. Rodriguez (1975), "Evaluation and Friction Angle in Granular Soils Using the Pressuremeter," *6th PSC,* ASCE, vol. 1, pp. 523–535. (Also see vol. 2, pp. 271–273.)

Woods, R. D. (1986), "In Situ Tests for Foundation Vibrations," *14th PSC,* ASCE, pp. 336–375.

Wright-Patterson AFB (1965, 1968, 1971), *Proceedings (1st, 2nd, 3rd) Conferences on Matrix Methods in Structural Mechanics,* Dayton, OH (available from NTIS, Springfield, VA).

Wroth, C. P. (1984), "The Interpretation of In Situ Tests," *Geotechnique,* vol. 34, no. 4, Dec, pp. 449–489.

——(1975), "In-Situ Measurement of Initial Stresses and Deformation Characteristics," *6th PSC,* ASCE, vol. 2, pp. 181–230,

——, and G. T. Houlsby (1985), "Soil Mechanics—Property Characterization and Analysis," *11th ICSMFE,* Vol. 1, pp. 1–56.

Yamada, Y., and K. Ishihara (1979), "Anisotropic Deformation Characteristics of Sand under Three Dimensional Stress Conditions," *Soils and Foundations,* Tokyo, vol. 19, no. 2, June, pp. 79–94.

Yen, B. C., and B. Scanlon (1975), "Sanitary Landfill Settlement Rates," *JGED,* ASCE, vol. 101, GT 5, May, pp. 475–487.

Yong, R. N., and V. Silvestri (1979), "Anisotropic Behaviour of a Sensitive Clay," *CGJ,* vol. 16, no. 2, May, pp. 335–350.

Yoshida, I., and R. Yoshinaka (1972), "A Method to Estimate Modulus of Horizontal Subgrade Reaction for a Pile," *Soils and Foundations,* Tokyo, vol. 12, no. 3, Sept, pp. 1–17.

——, et al. (1988), "Empirical Formulas of SPT Blow Counts for Gravelly Soils," *1st ISOPT,* vol. 1, pp. 381–387.

Young, F. E. (1981), *Piles and Foundations,* Thomas Telford, Ltd, London (a collection of 33 papers on piles and pile foundations presented to the ICE from 1967 to 1979), pp. 329.

Yttrup, P. J., et al. (1989), "Small Diameter Piling System Used in Australia," *Proceedings: Piling and Deep Foundations,* A. A. Balkema, Netherlands, vol. 1, pp. 155–162.

Yuan, D., and S. Nazarian (1994), "Automated Surface Wave Method: Inversion Technique," *JGED,* ASCE, vol. 119, no. 7, July, pp. 1112–1126.

Zeitlen, J. G., and S. Paikowsky (1982), "Discussion: New Design Correlations for Piles in Sands," *JGED,* ASCE, vol. 108, GT 11, Nov, pp. 1515–1518.

Zienkiewicz, O. C. (1977), *The Finite Element Method,* 3rd ed., McGraw-Hill, New York, 787 pp.

AUTHOR INDEX

This author index is a user convenience for quickly locating where the work is cited. The subject index does not contain authors' names, and this index does not include the page number in the "References" list where the reference work is identified. I have used the following notation:

(*aa*) = *single author;*
(bb) = two or more authors;
xx-z = citation on pages xx, xy, and xz

Index

This page has been reformatted by Knovel to provide easier navigation.

This page has been reformatted by Knovel to provide easier navigation.

This page has been reformatted by Knovel to provide easier navigation.

This page has been reformatted by Knovel to provide easier navigation.

This page has been reformatted by Knovel to provide easier navigation.

This page has been reformatted by Knovel to provide easier navigation.

This page has been reformatted by Knovel to provide easier navigation.

This page has been reformatted by Knovel to provide easier navigation.

This page has been reformatted by Knovel to provide easier navigation.

This page has been reformatted by Knovel to provide easier navigation.

This page has been reformatted by Knovel to provide easier navigation.

This page has been reformatted by Knovel to provide easier navigation.

This page has been reformatted by Knovel to provide easier navigation.

This page has been reformatted by Knovel to provide easier navigation.

This page has been reformatted by Knovel to provide easier navigation.

This page has been reformatted by Knovel to provide easier navigation.

This page has been reformatted by Knovel to provide easier navigation.

This page has been reformatted by Knovel to provide easier navigation.

Index terms **Links**

This page has been reformatted by Knovel to provide easier navigation.

This page has been reformatted by Knovel to provide easier navigation.

This page has been reformatted by Knovel to provide easier navigation.

This page has been reformatted by Knovel to provide easier navigation.

This page has been reformatted by Knovel to provide easier navigation.

This page has been reformatted by Knovel to provide easier navigation.

This page has been reformatted by Knovel to provide easier navigation.

This page has been reformatted by Knovel to provide easier navigation.

This page has been reformatted by Knovel to provide easier navigation.

This page has been reformatted by Knovel to provide easier navigation.

This page has been reformatted by Knovel to provide easier navigation.

This page has been reformatted by Knovel to provide easier navigation.

This page has been reformatted by Knovel to provide easier navigation.

This page has been reformatted by Knovel to provide easier navigation.

This page has been reformatted by Knovel to provide easier navigation.

This page has been reformatted by Knovel to provide easier navigation.

This page has been reformatted by Knovel to provide easier navigation.

This page has been reformatted by Knovel to provide easier navigation.

This page has been reformatted by Knovel to provide easier navigation.

This page has been reformatted by Knovel to provide easier navigation.

Z

This page has been reformatted by Knovel to provide easier navigation.